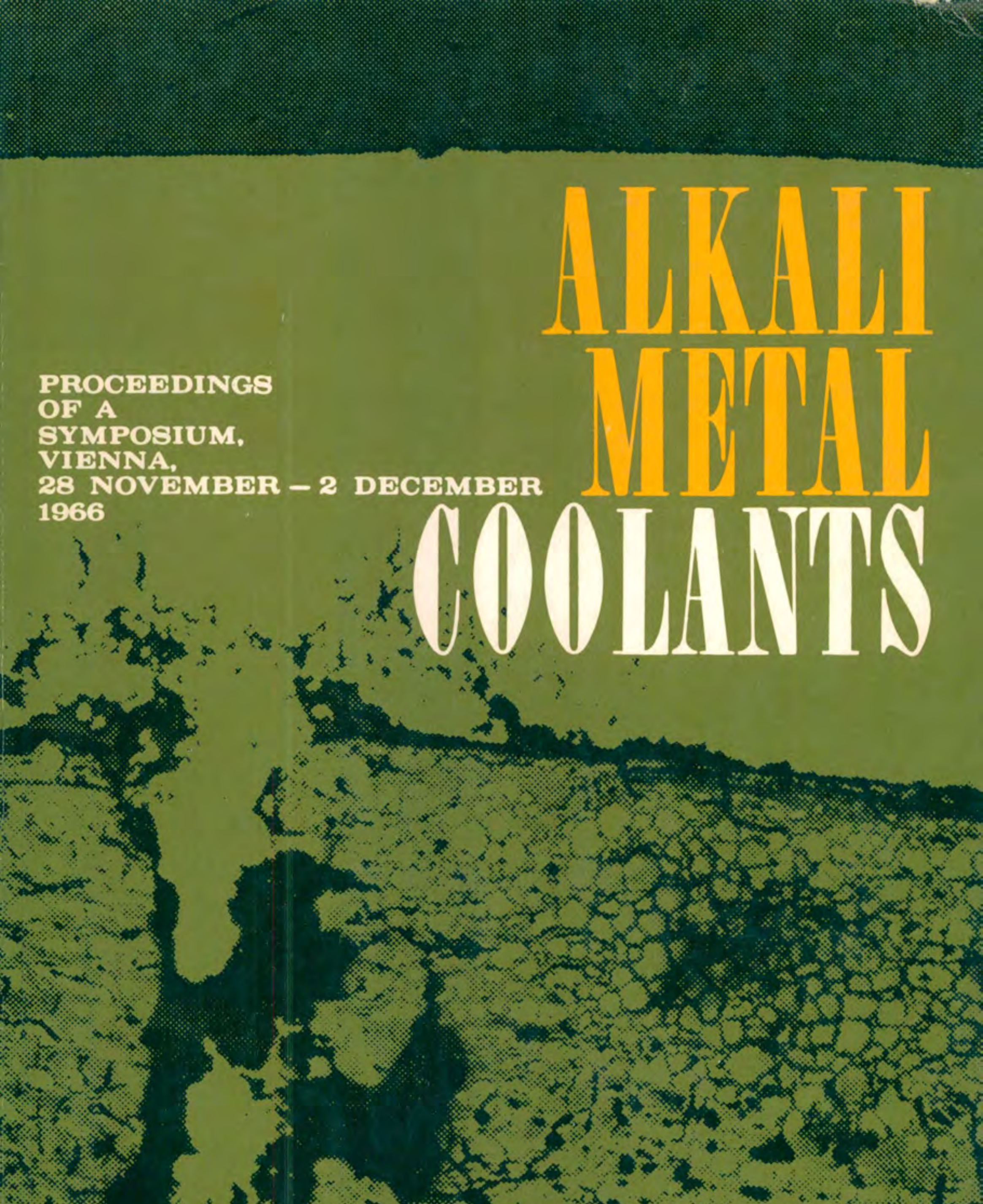

ALKALI METAL COOLANTS

PROCEEDINGS
OF A
SYMPOSIUM,
VIENNA,
28 NOVEMBER – 2 DECEMBER
1966

INTERNATIONAL ATOMIC ENERGY AGENCY, VIENNA, 1967

ALKALI METAL COOLANTS

CORRIGENDA

Because they have been reduced in size in the press, five illustrations in the book give magnification numbers that are misleading. The correct information is as follows:

Page No.	Fig. No.	Original magnification	Remarks
94	5	× 200	Reduced to 50% in the press
112	9	×200	Reduced to 60% in the press
206	9	× 250	Reduced to 75% in the press
206	10	× 100	
222	8	× 65	Reduced to 50% in the press

ALKALI METAL COOLANTS

CORRIGENDUM

A portion of the paper by L. Champeix et al. (SM-85/7) has been printed out of order: namely, the text from p. 57, line 15 (zirconium et le titane . . .) to p. 59, line 11 (produits d'oxydation . . .) inclusive, should be read after p. 61, line 2 (nettement supérieure...).

ALKALI METAL COOLANTS

The following States are Members of the International Atomic Energy Agency:

AFGHANISTAN
ALBANIA
ALGERIA
ARGENTINA
AUSTRALIA
AUSTRIA
BELGIUM
BOLIVIA
BRAZIL
BULGARIA
BURMA
BYELORUSSIAN SOVIET SOCIALIST REPUBLIC
CAMBODIA
CAMEROON
CANADA
CEYLON
CHILE
CHINA
COLOMBIA
CONGO, DEMOCRATIC REPUBLIC OF
COSTA RICA
CUBA
CYPRUS
CZECHOSLOVAK SOCIALIST REPUBLIC
DENMARK
DOMINICAN REPUBLIC
ECUADOR
EL SALVADOR
ETHIOPIA
FINLAND
FRANCE
GABON
GERMANY, FEDERAL REPUBLIC OF
GHANA
GREECE
GUATEMALA
HAITI
HOLY SEE
HONDURAS
HUNGARY
ICELAND
INDIA
INDONESIA
IRAN
IRAQ
ISRAEL
ITALY
IVORY COAST
JAMAICA
JAPAN
JORDAN
KENYA
KOREA, REPUBLIC OF
KUWAIT
LEBANON
LIBERIA
LIBYA
LUXEMBOURG
MADAGASCAR
MALI
MEXICO
MONACO
MOROCCO
NETHERLANDS
NEW ZEALAND
NICARAGUA
NIGERIA
NORWAY
PAKISTAN
PANAMA
PARAGUAY
PERU
PHILIPPINES
POLAND
PORTUGAL
ROMANIA
SAUDI ARABIA
SENEGAL
SINGAPORE
SOUTH AFRICA
SPAIN
SUDAN
SWEDEN
SWITZERLAND
SYRIAN ARAB REPUBLIC
THAILAND
TUNISIA
TURKEY
UKRAINIAN SOVIET SOCIALIST REPUBLIC
UNION OF SOVIET SOCIALIST REPUBLICS
UNITED ARAB REPUBLIC
UNITED KINGDOM OF GREAT BRITAIN AND NORTHERN IRELAND
UNITED STATES OF AMERICA
URUGUAY
VENEZUELA
VIET-NAM
YUGOSLAVIA

The Agency's Statute was approved on 26 October 1956 by the Conference on the Statute of the IAEA held at United Nations Headquarters, New York; it entered into force on 29 July 1957. The Headquarters of the Agency are situated in Vienna. Its principal objective is "to accelerate and enlarge the contribution of atomic energy to peace, health and prosperity throughout the world".

Printed by the IAEA in Austria
June 1967

PROCEEDINGS SERIES

ALKALI METAL COOLANTS

PROCEEDINGS OF THE SYMPOSIUM ON
ALKALI METAL COOLANTS – CORROSION STUDIES AND
SYSTEM OPERATING EXPERIENCE – HELD BY THE
INTERNATIONAL ATOMIC ENERGY AGENCY
IN VIENNA, 28 NOVEMBER - 2 DECEMBER 1966

INTERNATIONAL ATOMIC ENERGY AGENCY
VIENNA, 1967

ALKALI METAL COOLANTS
(Proceedings Series)

ABSTRACT. Proceedings of a Symposium organized by the IAEA and held in Vienna, 28 November - 2 December 1966. The meeting was attended by 107 participants from 16 countries and two international organizations.

Contents: Review papers (2 papers); Corrosion of steels and metal alloys (6 papers); Mass transfer in alkali metal systems, behaviour of carbon (5 papers); Effects of sodium environment on mechanical properties of materials (3 papers); Effect of water leakage into sodium systems (2 papers); Design and operation of testing apparatus (6 papers); Control, measurements and removal of impurities (13 papers); Corrosion by other alkali metals: NaK, K, Li, Cs (6 papers); Behaviour of fission products (3 papers).

Each paper is in its original language (32 English, 6 French and 8 Russian) and is preceded by an abstract in English and one in the original language if this is not English. Discussions are in English.

(786 pp., 16 x 24 cm, paper-bound, 375 figures) Sales Price: US $16.00; £5.13.0
(1967)

ALKALI METAL COOLANTS
IAEA, VIENNA, 1967
STI/PUB/143

FOREWORD

One of the major aims of the International Atomic Energy Agency in furthering the peaceful uses of atomic energy is to encourage the development of economical nuclear power. The potentially low fuel cycle cost, very high utilization of nuclear fuels and other well-known advantages of fast reactors are attracting increasing interest. Several sodium-cooled fast reactors and a number of test rigs and loops have been in operation in different countries.

However, before fast breeder reactors can reach the stage of industrial and commercial applications it is necessary to develop supporting technologies, of which an important one is alkali metals technology. Certainly, the excellent properties of alkali metals as heat-transfer media make them very suitable for use as coolants in fast reactors. There are, however, a number of basic problems, including corrosion of reactor materials by such metals, which have to be studied and resolved.

Recognizing the importance of these problems, the International Atomic Energy Agency convened in Vienna from 28 November to 2 December 1966, a Symposium on Alkali Metal Coolants – Corrosion Studies and System Operating Experience, in order to exchange information and experience on a wide international basis. More than 100 specialists from 16 countries and two international organizations took part.

The Agency wishes to thank the scientists who attended the symposium for their contributions and for the many spirited discussions, a sure sign of a successful meeting. The scientific information contained in these proceedings should help to quicken the pace of progress in alkali metal coolants technology, and it is hoped that their publication will be found useful to all workers in this and related fields.

EDITORIAL NOTE

The papers and discussions incorporated in the proceedings published by the International Atomic Energy Agency are edited by the Agency's editorial staff to the extent considered necessary for the reader's assistance. The views expressed and the general style adopted remain, however, the responsibility of the named authors or participants.

For the sake of speed of publication the present Proceedings have been printed by composition typing and photo-offset lithography. Within the limitations imposed by this method, every effort has been made to maintain a high editorial standard; in particular, the units and symbols employed are to the fullest practicable extent those standardized or recommended by the competent international scientific bodies.

The affiliations of authors are those given at the time of nomination.

The use in these Proceedings of particular designations of countries or territories does not imply any judgement by the Agency as to the legal status of such countries or territories, of their authorities and institutions or of the delimitation of their boundaries.

The mention of specific companies or of their products or brand-names does not imply any endorsement or recommendation on the part of the International Atomic Energy Agency.

CONTENTS

REVIEW PAPERS (Session I)

CORROSION OF STEELS AND METAL ALLOYS (Session II)

MASS TRANSFER IN ALKALI METAL SYSTEMS:
BEHAVIOUR OF CARBON (Session III)

EFFECTS OF SODIUM ENVIRONMENT ON MECHANICAL PROPERTIES OF MATERIALS (Session IV, Part 1)

EFFECT OF WATER LEAKAGE INTO SODIUM SYSTEMS (Session IV, Part 2)

DESIGN AND OPERATION OF TESTING APPARATUS (Session V)

CONTROL, MEASUREMENT AND REMOVAL OF IMPURITIES (Sessions VI and VII)

CORROSION BY OTHER ALKALI METALS: NaK, K, Li, Cs (Session VIII)

BEHAVIOUR OF FISSION PRODUCTS (Session IX)

REVIEW PAPERS
(Session I)

CORROSION BY THE ALKALI METALS

J.R. WEEKS, C.J. KLAMUT AND D.H. GURINSKY
BROOKHAVEN NATIONAL LABORATORY,
UPTON, NEW YORK,
UNITED STATES OF AMERICA

Abstract

CORROSION BY THE ALKALI METALS. This is a review of the state of the art of corrosion testing of materials by the alkali metals, the models proposed to explain the observed corrosion results, and the status of materials selection for application in alkali metal-cooled systems. Corrosion of structural and fuel cladding materials by liquid Na and NaK has been studied intensively, but intermittently for the last 18 years. These studies and the liquid-metal-cooled reactors in operation demonstrate that stainless steels can be considered for structural and cladding applications below 650°C. Above this temperature increased corrosion and radiation-induced embrittlement make them unsatisfactory.

Corrosion models are reviewed and their inability to explain all the experimental observations discussed. An alternate model is proposed which qualitatively is in agreement with experimental observations. In this model, the rate-controlling step is either the surface reaction of Fe with "available oxygen" (dissolved Na_2O) to form an Fe-O-Na complex or the rate at which "available oxygen" can reach the surface to form the complex; which process is rate controlling depends on the temperature, Na velocity and oxygen concentration in the Na.

The solution chemistry of oxygen, carbon and alkali metal-oxygen-transition metal complexes dissolved in the alkali metals is reviewed. "Molecular" complexes appear unlikely to exist in solution in the alkali metals, although the thermodynamic tendencies for them to form suggest that stable bonds exist in solution between oxygen, the transition and the alkali metals. The insolubility of carbon in "oxygen-free" sodium indicates that carbon transfer may be associated with oxygen in sodium down to very low oxygen levels, although experimental data do not generally confirm this postulate.

Corrosion of refractory metals by boiling alkali metals at temperatures above 1000°C is markedly affected by impurities in either the liquid or refractory metal; the addition of Ti, Zr or Hf as "getters" to the refractory alloys and proper heat treatment to make the "getter" addition react with oxygen, nitrogen, carbon and hydrogen in the alloys are required to prevent their corrosion by the alkali metals at these temperatures.

INTRODUCTION

The corrosion of materials by the alkali metals has been the subject of intermittent but intensive work for the past eighteen years in support of reactor and space power programs. This review paper[1] attempts to assess the present status of the development work in this broad field. Special emphasis will be given to the studies of the corrosion of structural and cladding materials by sodium (Na) because of their importance to the liquid metal fast breeder programs. The authors will also discuss the current theories or models which have been proposed to explain the corrosion data, present yet another corrosion model, and suggest a direction for future materials development.

Na CORROSION OF IRON, NICKEL AND COBALT-BASE ALLOYS

Corrosion studies in the early 50's showed that reasonably pure (~20 ppm oxygen) Na could be contained in stainless steels almost indefinitely at 538°C. More recent studies in the U.K. and the U.S. have established

---

[1] Other recent reviews are listed in references [1-6]

corrosion rates of various steels at temperatures up to 725°C. The effects on the corrosion rate of variables such as temperature, temperature differential, velocity and oxygen concentration in Na have also been evaluated.[7-8]

Type 316 stainless steel[2] (SS), 2 1/4Cr-1Mo steel, and 5Cr-1/2Mo-1/2Ti steel have been tested in the U.S. in forced convection circuits at temperatures up to 705°C, oxygen levels of 10 and 50 ppm, and velocities of 2 and 6 m/s.[7] The corrosion rate of all these steels was essentially the same. It varied with velocity, was proportional to oxygen level in the Na, was unaffected by temperature differential, and increased threefold with an increase of 55°C in the maximum temperature. Typical rates at 650°C for these steels fall between 0.013-0.038 mm/yr in Na containing 10-15 ppm oxygen flowing at 6 m/s. This is apparently the rate at which Fe is dissolving in the solution, since Ni and Cr are leached from the stainless steels leaving a ferritic surface exposed to the Na. A statistical analysis of the data has been used to develop an empirical corrosion equation[7] in which the rate is a function of velocity to the 0.88 power and oxygen to the 1.16 power.

Results on similar tests recently reported in the U.K. are in general agreement with the observations presented above.[8] In this work, however, a velocity effect on the corrosion rate was found below 3 m/s, but above this velocity (up to 8 m/s) there was no effect in a system containing 10 ppm oxygen operated at 650°C. There may not actually be a difference in the results since the U.S. data (at 2 and 6 m/s) straddle the transition velocity (3 m/s) reported in the U.K. work. The significance of these findings is discussed in the mechanisms section of this paper.

The corrosion rate of stainless steels in 650°C Na containing 10 ppm oxygen should be acceptable for reactor systems. However, the reported two to threefold increase in the corrosion rate for every 55°C temperature increase and the effect of oxygen excursions[9] limits the use of the stainless steels to 650°C. Nettley's results[8] with <5 ppm oxygen in the sodium suggest that the maximum temperature limit could possibly be raised at extremely low oxygen levels if strength is not limiting. Maintaining a large reactor system at the required low oxygen concentrations may be difficult, unless new methods of control are used.

Nickel-base alloys tested in Na and NaK at 816°C and higher show the corrosion rates to be several times greater than for stainless steels tested under similar conditions.[10] Corrosion of these alloys is characterized by leaching of Ni and to a lesser degree, Cr. A nickel alloy, Nimonic 80A[3] was tested at 650°C at various velocities and oxygen levels in Na.[8] Its corrosion rate was dependent on velocity and independent of oxygen concentration. At temperatures and flow rates of interest in reactors, unacceptable corrosion rates were obtained.

Cobalt-base alloys have not been evaluated in Na or NaK in the 650-760°C temperature range. Tests at higher temperatures (900-980°C) show the corrosion rate of Co-base alloys to be approximately equivalent to those of Ni-base alloys.[10-11] These tests however, were conducted with high (50-100 ppm) concentrations of oxygen in the Na (~50-100 ppm). Since corrosion of Co is probably sensitive to oxygen these results are not definitive.[12]

---

[2] Type 316 SS: 17%Cr, 12%Ni, 3%Mo, 0.08% maximum carbon, bal. Fe.
[3] Nimonic 80A: 19.4Cr, 1.2Al, 2.3Ti, bal. Ni.

Refractory metals and their alloys have been used and are still being considered for core components, primarily because of their compatibility with various fuels. The affinity of most refractory metals for oxygen, nitrogen, carbon and hydrogen, which are frequently present in Na, results in an increased corrosion rate or a reduction in mechanical properties. Unless the Na is purified to low oxygen levels with "getters", excessive weight losses are experienced with all the refractory metals with the exception of Mo. Excellent resistance of Mo to Na containing up to 110 ppm oxygen has been reported at 900°C and velocities of 2 m/sec. Under similar test conditions Nb samples are completely destroyed.[4] Vanadium and niobium have been used in the DFR; however, the operating temperature had to be limited to 480°C due to the oxygen level in the NaK.[13] Recently there has been some success in developing V alloys which have improved corrosion resistance in well cold-trapped Na. The promising alloys contain Ti and Cr.[14]

CARBON TRANSFER

Carbon transfer has been observed in liquid metal-cooled systems and is of concern because of possible effects on the mechanical properties of structural and cladding materials. Carbon transport occurs in an alkali metal-cooled system in which carbon activity differences exist between alloys in the same system, or if carbon is accidentally introduced into the system. Many studies are now in progress to evaluate the effect of carburization and decarburization on mechanical properties of stainless steels and low alloy steels.[7,15,16] Significant decreases in room temperature ductility, impact strength, fatigue life and increased notch sensitivity could reduce the useful life of type 316 SS exposed for extended times in Na containing C.[15] [4] No effects of velocity or oxygen concentration below 50 ppm on the rate of carburization have been reported.

The significance of carbon transfer on the mechanical properties of stainless and low alloy steels is unresolved. Generally the carbon source is the low alloy steel used in the low temperature portions of many systems. Several investigators have demonstrated that carbon in these alloys can be stabilized to prevent carbon transfer to stainless steel located in hot portions of the system, by adding niobium, vanadium and titanium to low alloy steels.[7,8,17] Transfer of carbon to refractory metals has been controlled by using a Nb- or Ti- stabilized stainless steel.[18,19]

CHEMICAL ANALYSIS

The above sections have discussed the important role that impurities (O, C, N and H) play in the corrosion of materials by the alkali metals. The analysis and control of these elements is necessary to ensure acceptable performance of structural and cladding materials.

Methods of analysis of these elements have been reviewed.[20] For oxygen in Na, the Hg amalgamation and the distillation methods have gained the greatest acceptance. Precision of ±1 ppm in the 5 ppm level is reported for the amalgamation procedure.[21] Recent results obtained by the distillation procedure indicate excellent precision in the 1-10 ppm range.[22,23] Although both procedures yield results with good precision at apparently low oxygen levels, they still suffer from the lack of a "standard" with which to determine the absolute quantity of oxygen. At least two techniques currently under development, neutron activation at General Atomic[24] and ORNL[25] and

---

[4] However, carburization has little effect on its mechanical properties at 650°C.

isotopic dilution at the authors' laboratory,[5] measure the oxygen concentration directly rather than the Na with which it was combined. The available oxygen analytical procedures, however, are adequate for monitoring Na in stainless-steel systems.

The wet combustion method for elemental carbon and the dry oxidation method for total carbon are the currently accepted techniques for C determination in Na. "Round robin" analyses for C in Na (14 laboratories participated) produced mean values which varied from 20 to 200 ppm for total carbon and 10 to 50 ppm for elemental carbon.[26] There was no apparent difference in either the total or elemental carbon detected in the prepared "high", "low" and "medium" samples. These results clearly point to the need for further work on the development of techniques to measure carbon in Na, and to a lack of an understanding of the chemical state of the carbon in Na.

HIGH-TEMPERATURE LIQUID METAL CORROSION

Interest in the development of high-performance space power systems has stimulated extensive corrosion testing of materials in liquid and boiling alkali metals at temperatures up to 1350°C. The extensive data generated in this area are reported in a recent survey.[1] The results of recent work at BNL are described in another session of this meeting.[27]

At these high temperatures only the refractory metals and their alloys have been tested because of their strength and apparent low solubility in the alkali metals. Corrosion of Nb and Ta by the alkali metals is markedly affected by impurities in either the liquid metal or the refractory metal. Oxygen in Na in high concentration accelerates corrosion of these alloys. Oxygen as an interstitial impurity in pure Nb and Ta causes rapid penetration by high purity[6] Li,[28,29] Na,[30] and K.**[31] The penetration by Li occurs along grain boundaries and {110} crystallographic planes. A threshold concentration of oxygen of 200-500 ppm in solid solution in the alloy is required to initiate corrosion by Li with the depth of attack increasing with increasing oxygen. Similar results are obtained with Na and K but the threshold oxygen levels in the alloy have not been determined. Addition of elements, such as Zr, Ti or Hf, which form very stable oxides, to the refractory metal essentially eliminates this penetration. Enough of these "getter" elements must be added to react stoichiometrically with all the oxygen present. Also in order to ensure complete protection against this penetration it is necessary to heat-treat the alloys to ensure precipitation of the "getter oxide". Analysis of data obtained from experiments with K and Na in refractory metals in which a limited amount of oxygen is available suggests corrosion occurs by the formation of complex refractory metal alkali metal oxides,[32,33] which have, in some instances, been identified.[31,34]

Recently several large forced-convection boiling liquid metal loops fabricated completely of refractory metals have been operated to assess the resistance of refractory metal alloys to high velocity vapor impingement. No detectable erosive effect was detected on molybdenum alloy TZM[7]

---

[5] In the isotopic dilution method a known amount of O^{18} is introduced into a sample of Na in which O^{16} is to be determined. The Na is distilled off. The Na_2O^{16}, Na_2O^{18} mixture is reacted with C to form CO^{16}, CO^{18}. The CO^{16}/CO^{18} ratio is determined mass spectrographically.

[6] High purity alkali metal is here defined as that which has been contacted with Zr above 650°C.

[7] TZM: 0.5%Ti, 0.08%Zr, bal. Mo.

exposed to K vapor up to 1100°C and velocities up to 405 m/s.[35] Molybdenum alloys were also resistant to Cs vapor at 840°C and 245 m/s. However, in the latter tests deposits of loop container material were found adhering to the impingement samples.[27]

PRESENT STATUS

Available corrosion data indicate that stainless steels can be used for structural and cladding applications in a reactor cooled by Na if the maximum metal temperature does not exceed 650°C. There remain, however, two problems which must be solved before stainless steel can be used with confidence: radiation embrittlement, which becomes pronounced at 650°C and above,[36] and the reduction in mechanical properties due to carburization. It has been shown that carbon transfer can be minimized practically by controlling the carbon source. Study of radiation embrittlement of stainless steel suggests it can be controlled by modifying the composition and by a proper heat treatment.[36] It will be necessary to determine whether these modifications affect the corrosion resistance of stainless steel.

Increasing the reactor operating temperature to improve the economics results in unacceptably higher rates of corrosion of stainless steels. Some design studies propose 650°C as the mixed mean Na outlet temperature. This mixed mean temperature requires operation of fuel cladding at 760-815°C. In this temperature range neither the stainless steels nor the nickel alloys appear to have adequate corrosion resistance to Na and the stainless steels may not have adequate strength.

Refractory metal alloys, although they may not have as favorable nuclear properties as stainless steels, do have excellent corrosion resistance to high purity Na at temperatures as high as 1300°C. However, as has been shown in the DFR, their practical use is limited by the ability to purify Na to very low levels of oxygen, carbon and hydrogen. Whether the oxygen content of the Na coolant of a large power plant can be lowered, maintained and monitored at such low levels is, at present, questionable. One approach, currently underway, is to develop refractory metal alloys which have acceptable corrosion rates in Na containing 10 ppm oxygen.[14]

Cobalt-base alloys have not been sufficiently studied in cold-trapped Na to eliminate them as cladding materials for use at 750-815°C. At these temperatures they have a distinct strength advantage over the stainless steels. The use of Co alloys has been under investigation at the authors' laboratory. Cobalt alloy H.A. 25[8] is known to lose room temperature ductility upon aging in the 650-870°C temperature range. This embrittlement can be minimized by making compositional adjustments which, however, produce a loss in the high temperature strength.[37] Currently further alloy modifications are being made to develop non-embrittling, high-strength Co alloys. In this program, elements with high nuclear cross-section, especially W, are being kept to a minimum.[38] A possible objection to using Co as a cladding material is its cross-section. Calculations made at BNL show Co alloys require a slightly greater critical mass and give a lower breeding gain compared to stainless steel. The results are shown in Table I. However, Co is comparable to or more attractive than some of the refractory metals. Perhaps the greatest objection to the use of Co alloys is the radioactivity transferred to out-of-reactor components. The activity transferred from Co-base alloys is about 15 times greater than that from stainless steel; the isotopes also have longer half-lives.

---

[8] H.A.25: 20%Cr, 10%Ni, 15%W, bal. Co.

TABLE I. EFFECT OF CLADDING MATERIAL IN Na COOLED FAST REACTOR*

Cladding Material	Critical Mass in kg	Breeding Ratio
316 SS	2000	1.25
Incoloy 800 (45Fe-35Ni-20Cr)	1991	1.26
S-1 (Co-20Cr-10Ni-6Mo-2Fe)	2077-2159	1.19-1.22
Mo	2264	1.15
V-20Ti	2062	1.24

*Fuel is PuO_2-UO_2 with a density of 11.1 gm/cm^3 representing 29% of core volume. Core: Diam. = 11.7 ft., H = 2 ft., structure and clad each ≈9% of core volume.

Other areas where studies are required include the following: (1) the control of the Na purity because of its marked effect on corrosion rate of stainless steels and refractory metals;(2) the design of hot and cold traps for large systems because the kinetics of impurity removal are not well understood; and(3) the effect of the addition of soluble getters to Na. The experiments in which Ba and Ca were added to Na demonstrated that they reduced mass transfer.[12] Calculations based on typical fast reactors have shown that about 25 ppm Mg will be produced from the decay of Na^{24} in one year. Since Mg will be present in the Na, its effect on corrosion and mass transfer should be studied as part of a larger program in which other getters such as Li, Ba, etc. are also being evaluated. Results obtained from capsule tests at our laboratory indicate corrosion of stainless steel by Na containing 15 at.% Li to be equivalent to that by "gettered" Na. Chemical analysis of the Na-Li alloy showed that the oxygen was associated with Li.

The effect of accidental introduction of H_2O to the Na coolant stream needs to be studied. The current state of steam generator technology is such that failures and introduction of water into the Na must be expected. The combined effect of the products of the reaction such as Na_2O, NaOH, etc. on the corrosion must be determined. Also sporadic introduction of high concentrations of oxygen in NaK produces accelerated corrosion rates.[9] It is therefore most important to evaluate the effect of accidental introduction of impurities on the corrosion rates of proposed reactor materials.

MECHANISM OF CORROSION OF STEELS BY LIQUID Na OR NaK

Until quite recently, very few experimental programs were specifically aimed at obtaining information on the mechanisms of corrosion by liquid Na. Consequently the corrosion models that have been proposed had to be based on corrosion data obtained in engineering tests. In this section, we present these corrosion models and propose an alternate model which is qualitatively in agreement with the corrosion data.

The corrosion of stainless steel by liquid Na is accompanied by structural and compositional changes at the steel-sodium interface, as noted previously. Nettley et al.[8] have pointed out that the steady-state corrosion rate of stainless steels, which develops after an initial preconditioning period, is linear with time. The surface of the steel becomes enriched in Fe due to selective leaching of Ni, Cr and Mn (except in Na containing 50 ppm or more oxygen). This suggests that solid-state diffusion of the more soluble alloying elements in the steel is not the rate-controlling step. In the following, therefore, the steady-state overall corrosion rate of a stainless steel will be assumed to be controlled by the rate of dissolution of Fe into the sodium.[9] The solid-state diffusion phenomena which take place during corrosion have been discussed by Brush.[39]

The General Corrosion Equation

All liquid metal corrosion phenomena arise from a difference in the chemical activity, a_x, of a species x between the liquid and the solid metals. This difference can arise from several sources, the most common being (1) the temperature dependence of the solubility of species x in the liquid metal, (2) variations in the activity of species x between several solid alloys in contact with the same liquid, and (3) the temperature dependence of the activity of species x in an alloy. The rate of dissolution of species x into liquid sodium at any point i in a corroding system can therefore be written

$$R_i(x) = k_x[a_{x(s)} - a_{x(\ell)}] \qquad (1)$$

in which the subscripts (s) and (ℓ) refer to solid and liquid; and k_x is the solution rate constant of species x. If $a_{x(\ell)}$ is greater than $a_{x(s)}$ a negative corrosion (precipitation) of species x will occur.

If we substitute Fe for species x, we can rewrite (1) as

$$R_i(\mathrm{Fe}) = \frac{d(\mathrm{Fe})}{dt}(i) = k_{\mathrm{Fe}}[a_{\mathrm{Fe}(s)} - a_{\mathrm{Fe}(\ell)}] \; . \qquad (2)$$

Further, since we have assumed that the corroding surface is Fe, $a_{\mathrm{Fe}(s)}=1$. Also, $a_{\mathrm{Fe}(\ell)} = S_i/S_o$, where S_i represents the concentration of Fe in solution at point i and S_o the solubility of Fe in the liquid at the same point. Equation (2) becomes, on substitution,

$$\frac{d(\mathrm{Fe})}{dt}(i) = k_{\mathrm{Fe}}\left(\frac{S_o - S_i}{S_o}\right) . \qquad (3)$$

The term S_o in the denominator of equation (3) can be included into the overall rate constant, so that equation (3) becomes

$$\frac{d(\mathrm{Fe})}{dt}(i) = k'_{\mathrm{Fe}}(S_o - S_i) \; . \qquad (4)$$

Applying equation (4) to an actual system requires a detailed knowledge of the factors that influence the rate constant k'_{Fe} at all points in the system as well as the solubility, S_o of Fe in Na throughout the temperature range in the circuit. The concentration, S_i(Fe) in Na can then be estimated at each point from the sum of the corrosion that occurred at each point upstream of point i. Such an analysis, however, cannot be made at present, since the factors that influence the rate constant are often interdependent and have not in all cases been unequivocally established.

---

[9] The ferritic layer, however, reaches a steady-state thickness, at which migration of Ni and Cr through the ferritic layer equals the rate of corrosion.[39]

The Solubility of Fe in Na

Before reviewing the corrosion models and the observations which they must explain, the available determinations of the solubility of Fe in Na will be discussed. The results of three measurements made before 1955 are summarized in Table II. Epstein's[40] determinations were made by dipping samples out of sodium contained in an Fe crucible located in an inert-gas-filled bell jar. Bogard[41] distilled Na into a stainless-steel crucible in which a small specimen of irradiated Fe was suspended. He made the questionable assumption that during a four-hour period the Fe^{59} activity had equilibrated by exchange between the surfaces of the specimen and the steel crucible. He repeated the experiment after intentionally saturating the Na with, first, Na_2O and, then, Na_2O and NaOH, and found an order of magnitude increase in the apparent solubility after the addition of each impurity. Rodgers et al.[42] equilibrated Na with stainless steel both in a pot and in a pumped loop, and detected no difference in the apparent Fe solubility at oxygen concentrations in Na from ~30 to 150 ppm.

TABLE II. "SOLUBILITY" OF Fe in Na AT 500°C

	Bogard[41]	Epstein[40]	Rodgers et al.[42]
"Pure" Na	0.008	~12	10-13
Na + Na_2O	0.033[1]	12	10-13[2]
Na+Na_2O+NaOH[3]	0.28		

[1] Saturated with Na_2O

[2] 30-150 ppm oxygen

[3] Saturated with Na_2O + NaOH

No results have been published since 1955. Mottley[43] and Parkman[44] have pointed out that substituting the low data of Bogard into equation (4) and a value for the rate constant similar to that obtained from most liquid metal corrosion models gives reasonable agreement with the measured corrosion rates. However, samples of Na taken from operating loops have all contained ~2-5 ppm Fe.

A recent attempt by Thorley and his co-workers[45] to measure the Fe solubility in Na was inconclusive, but suggested the solubility was close to the higher values. An earlier attempt at Harwell[46] indicated it was less than the limit of detection, 1 ppm at 500°C. Two efforts, one at Atomics International, the other at Brookhaven National Laboratory, are underway to reinvestigate this equilibrium.

Corrosion Rate Models

At present an acceptable model must explain the following observations: (1) the low corrosion rates of steels by Na, (2) the concentrations of Fe (2-5 ppm) found in samples of circuit Na, (3) the first order dependence of the corrosion rate on the oxygen concentration of the Na, (4) the known and postulated complexes of Fe with oxygen and Na, (5) the velocity dependence of the rate of corrosion of steels by Na, and (6) the downstream effect.

Early models for corrosion were required to explain only the first three observations. In 1950 Epstein and Weber[47] concluded that the dissolution of Fe into Na was more nearly approximated by a surface-controlled dissolution reaction than by liquid boundary layer diffusion. They derived equation (5) for the corrosion in an ideal circuit in which the temperature profile along its length was represented by a sine wave:

$$R = -\frac{\alpha}{2}\frac{dS}{dT}\Delta T \qquad (5)$$

in which α is the mean rate constant for dissolution of Fe into the Na, and dS/dT is the average temperature coefficient of solubility over the temperature differential, ΔT, in the circuit. Their derivation required the ΔT to be small. The rate constant α in this equation was found to be a linear function of the oxygen concentration in the Na; also, α extrapolated to zero at zero oxygen concentration.

To explain why the dissolution of Fe into Na should be controlled by a surface reaction rather than by a liquid boundary layer diffusion (as is the case in its dissolution into most other liquid metals such as Hg, Bi and Pb) the authors[48] and, independently, Horsley[49] suggested that the rate-controlling step was the interaction of Fe with Na_2O dissolved in Na:

$$Fe_{(s)} + Na_2O_{(\ell)} \rightleftharpoons FeO_{(\ell)} + 2Na \ . \qquad (6)$$

Horsley contacted Fe with sodium containing several percent Na_2O and identified a complex sodium ferrite, $(Na_2O)_2 \cdot FeO$. He suggested that this, or a similar complex, was the state in which Fe existed in sodium. Such a mechanism satisfactorily explains how a surface-reaction could be rate-controlling, and how the solution rate could have a high activation energy (which is required to predict the low solution rates). However, the inability of two of the three experimenters to find an effect of oxygen on the solubility of Fe in Na, and the radiochemical techniques of the third[10] suggest that the dissolution process is not this simple. The authors[50] have pointed out, however, that the oxygen-dependence of the solubility data of Bogard are in reasonable agreement with a thermodynamic calculation of reaction (6); this calculation also suggested that the free energy change of the reaction

$$2Na_2O_{(Na)} + FeO_{(Na)} \rightleftharpoons (Na_2O)_2 \cdot (FeO)_{(Na)} \qquad (7)$$

should be of the order of -9 kcal/g-atom Fe at 753°K. Subsequently, the Fulmer Research Institute measured ΔH_{298} of reaction (7) to be -24.8 kcal/gm-atom[51] Fe, and ΔF_{923} to be -3.3 kcal/gm-atom Fe[52] From these values, assuming ΔH is independent of temperature, we calculate that $\Delta F_{753} = -7.3$ kcal/gm-atom Fe.

Present models for corrosion have to take into account the recently observed velocity and geometry effects[7,8] A velocity-dependent corrosion process is incompatible with the dissolution-surface reaction control previously assumed. Further, the "downstream effect" suggests that whatever species is controlling the dissolution rate approaches saturation as the sodium passes through the hot zone: the term $(S_0 - S_i)$ in equation (4) approaches zero. It is difficult to reconcile these observations with the low, oxygen-dependent corrosion rates, and the 2-5 ppm concentrations of Fe in circuit Na.

Mottley[43] suggested that the rate-controlling step is the migration of a dissolved complex through the boundary layer. He developed a heat-

---

[10] Bogard's "oxygen-dependent solubility" could be due to the oxygen-dependent kinetics of exchange of Fe^{59} between the radioactive specimen and the crucible.

transfer analog which accounts semi-quantitatively for all of the corrosion observations in the G.E. loops.[7] He assumed that Bogard's solubility of Fe in Na saturated with oxygen represented the solubility of the Fe-Na-O complex. The G.E. loops, however, contained very much less oxygen than the Na in Bogard's tests. Mottley implied that the majority of the Fe present in Na samples taken from these loops exists as elemental Fe, which is presumed to be soluble to several parts per million. Inherent in Mottley's treatment is the implication that oxygen in small amounts in sodium is actually a corrosion inhibitor: in oxygen-free Na, Fe should corrode by simple dissolution. Since the Fe solubility is assumed to be several hundred-fold greater than Bogard's data, steels should corrode several hundred-fold faster in oxygen-free Na than in Na containing small amounts of oxygen. Such corrosion rates have not been observed either in loops containing Zr hot traps,[8] or Li,[9] or alkaline-earth additions[12] to reduce the oxygen activity. Thus we must conclude that Mottley's treatment fails to explain the high solubility and low solution rate paradox. Tyzack[52] has suggested that a ferrite may form as a stable surface layer. This model also implies either that small amounts of oxygen in sodium act as a corrosion inhibitor or that the surface ferrites are not reduced by hot-trapped Na or by Li, Ca or Mg dissolved in Na.

The U.K. observation of a transition at 3 m/s from a velocity-dependent to a velocity-independent corrosion rate at 650°C in Na containing 10 ppm oxygen suggests an alternative model for the rate controlling step which, at least qualitatively, is consistent with all the experimental observations. The overall corrosion rate is, of course, controlled by the slowest step in the corrosion process. The evidence cited above suggests that the majority of the dissolved Fe is present in Na as an Fe-O-Na complex. There are three possible rate-controlling steps in the dissolution process: (1) the migration of Na_2O through the boundary layer to the Fe (or steel) surface, (2) the chemical reaction of the Na_2O and Fe at the interface to form the complex, and (3) the migration of the complex away from the surface through the boundary layer to the flowing stream of Na. Mottley assumed step (3) control and could not satisfactorily explain all the experimental observations. However, if the rate-controlling process is considered to be a competition between steps (1) and (2), the experimental observations can be explained.

The activation energy for step (1) should be of the order of a few thousand calories per mole, whereas the activation energy for, and, the temperature dependence of step (2), should be considerably greater. Of the two, only step (1) is expected to be a function of the velocity of sodium. Both steps are first-order dependent on the oxygen concentration of the sodium. The lower temperatures and higher oxygen concentrations of the pre-1955 experiments lie within the region of step (2) control. The more recent G.E. and U.K. experiments, with their higher temperatures and lower oxygen content, suggest that the rate of the surface reaction (2), with its higher temperature dependence, has exceeded the rate at which oxygen can migrate to the corroding surface at low Na velocities, so that diffusion of Na_2O to the surface becomes the rate-controlling step. At higher velocities, the diffusion path (boundary layer) for the Na_2O becomes shorter, so that Na_2O can reach the surface more rapidly than it is removed by reaction (2), and the corrosion rate becomes velocity independent. Rowland et al.[7] have tabulated the rate of hot leg metal loss, corrected to zero downstream, at temperatures ranging from 538 to 705°C, 6 m/s Na flow, and oxygen levels of 10-15 ppm and 45-50 ppm. Figure 1 shows these data plotted, according to absolute reaction rate theory, as log (R/T) vs (1/T). The apparent activation energies calculated from all four sets of data are 26 ± 1 kcal per mole of Fe, suggesting that the corrosion rate

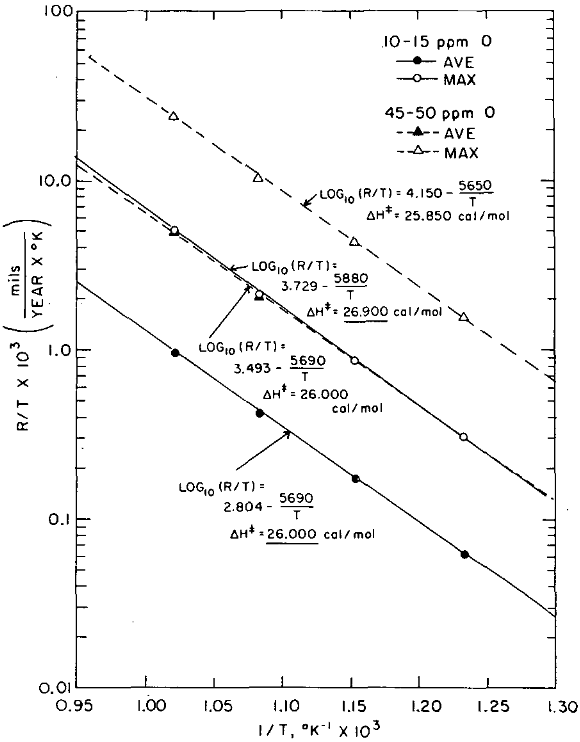

FIG. 1. Temperature dependence of the corrosion of Type 316 stainless steel in Na flowing at 6 m/s [7]

is controlled by a chemical reaction.[11] Similar tabulation of their low-velocity data was not available from which to estimate the activation energy under conditions in which the liquid velocity is likely to be rate controlling.

The two most difficult observations to explain by the proposed model are the low corrosion rates and the downstream effects. In fact, the model suggests that, in the velocity-dependent region, the corrosion rate depends only on the diffusion of Na_2O through the boundary layer. In sodium containing an Fe-O-Na complex, most of the oxygen must be tied up as the complex, leaving a low concentration of available oxygen for migration to the corroding surface. The downstream effect in the velocity-dependent region requires that the available oxygen be depleted upstream of the downstream specimens.

It should be pointed out that the reverse of the dissolution step, decomposition of the complex into metallic (solid) Fe and available oxygen, also has a high activation energy, and, since the removal of Fe occurs at an appreciably lower temperature, it has a much lower rate than the dissolution of Fe by this reaction. Thus, in a normal pumped circuit only a small percentage of the dissolved complex decomposes during passage through the cold leg. Therefore, the cold leg process governs the

---

[11] It should be noted that the calculated "activation energies" are for k .

overall corrosion rate in the circuit, according to this model. This model suggests that the velocity dependence of the corrosion rate is complex, and not the simple $v^{0.88}$ reported by G.E.,[7] and that the apparent Fe solubility in Na is oxygen-dependent. Further the corrosion rate in the hot leg of a loop will increase as the residence time of the Na in the cold leg increases.

SODIUM SOLUTION CHEMISTRY

The above description of the corrosion of steels by Na implies that a major part of the Fe dissolved in Na exists there as a complex with sodium and oxygen. The evidence for the existence of such complexes between the alkali metals, oxygen and the transition metals will now be discussed. The state of nonmetals (primarily oxygen and carbon) dissolved in the alkali metals will be described.

Alkali Metal-Oxygen-Transition Metal Complexes

The existence in alkali metal solutions of complexes between the solvent, oxygen and a transition metal solute has not been substantiated by direct observation. They have been observed after precipitation from the alkali metal solution or on surfaces contacted with these solutions; also, their existence has been inferred from the effects of oxygen on the corrosion behavior of materials in the alkali metals.

The reaction to form these complexes can be written as below, for the example of Fe in Na:

$$x\,Fe_{(s)} + yNa_2O_{(\ell)} + Na \rightarrow Fe_x \cdot O_y \cdot Na_{z(\ell)} + Na_{(\ell)} \qquad (8)$$

which can be broken down into two simple equations which can be analyzed by the application of thermodynamics:

$$Fe_{(s)} + Na_2O_{(\ell)} \rightleftarrows FeO_{(\ell)} + 2Na_{(\ell)} \qquad (8a)$$

$$x\,FeO_{(\ell)} + yNa_2O_{(\ell)} = (FeO)_x \cdot (Na_2O)_y \qquad (8b)$$

The probability that reaction (8a) will occur to a finite extent in a dilute solution is directly related to the free energy change for this reaction.

The activity of oxygen in the alkali metal at some temperature T can be approximated as follows:

$$[a_{O\ \mathrm{in\ L.M.}}]_T = [(\mathrm{ppm\ O\ in\ L.M.})/(\mathrm{ppm\ O\ soluble\ in\ L.M.})]_T \qquad (9)$$

and the free energy of oxygen in solution (i.e. $Na_2O_{(\ell)}$ in equation 8) becomes

$$\Delta F[O]_T = \Delta F + RT \log (a_{O\ \mathrm{in\ L.M.}}) \qquad (10)$$

where ΔF is the standard free energy of formation of the alkali metal oxide at temperature T. Thus the solubility of oxygen in the alkali metal has a considerable influence on whether a reaction such as (8a) will occur.

TABLE III. THERMODYNAMIC PROPERTIES OF THE ALKALI METAL OXIDES AND THEIR DILUTE SOLUTION IN LIQUID ALKALI METALS AT 900°K

Alkali Metal Oxide	ΔF°, 900°K (kcal/g-atom O)[65]	Estimated Solubility of O, 900°K (ppm)	ΔF°(O), 900°K (100 ppm O dissolved in the alkali metal) (kcal/g-atom O)
Li_2O	-113.8	3390[66]	-120.0
Na_2O	- 69.0	1580[67]	- 74.5
K_2O	- 53.8	23,000[68]	- 64.0
Rb_2O	- 49.0		~ 60
Cs_2O	- 42.0	56,800*[69]	- 53.3

*56,800 ppm = 100% Cs_2O

TABLE IV. FREE ENERGY OF FORMATION AT 900°K (627°C) OF OXIDES OF METALS COMMONLY STUDIED AS CONTAINERS OF THE ALKALI METALS[65]

Oxide*	ΔF° O at 900°K (kcal/g-atom O)
NiO	- 37.3
CoO	- 40.6
FeO	- 49.4
1/2 WO_2	- 49.9
1/2 MoO_2	- 50.2
1/3 Cr_2O_3	- 71.7
1/4 Nb_2O_4	- 75.8
1/5 Ta_2O_5	- 78.7
VO	- 81.0
TiO	-103.2
1/2 ZrO_2	-110.2

*When more than one oxide exists, the lowest oxide state is given, unless one of the higher oxides is more stable.

Table III lists the free energies of formation of the oxides of the alkali metals at 900°K (627°C), the estimated (extrapolated) solubilities of oxygen in each metal, and the free energy of oxygen in a 100 ppm solution in each alkali metal. Table IV lists free energies of formation at 900°K of the oxides of the metals frequently considered for containment of the alkali metals, in order of increasing stability.

The corrosion of Fe, Cr, Mn, Nb and Ta by liquid Na is a function of the oxygen concentration of the Na, whereas the transfer of Ni is not. The free energies of formation of the oxides of all of these elements, except Ni, fall within 25 kcal of the free energy of oxygen in a solution of 100 ppm oxygen in Na. Nickel oxide is more than 37 kcal less stable. Thermodynamic calculations of equation (8a) and (b) have been previously discussed by the authors[50] The lower free energy of formation of NiO indicates that its concentration in Na from equation (8a) would $\sim 10^{-3}$ times the FeO concentration, which quantity can probably be neglected. Similarly, the equilibrium Na_2O concentration in Na in the presence of solid Ti or Zr can be calculated to be vanishingly small at this temperature.

Lithium oxide is sufficiently stable in Li that it is unlikely to interact to form complexes with any of the metals listed except possibly Ti or Zr. Lithium will, however, reduce the oxides of these metals, and, in the case of Nb or Ta, penetrate into the solid metal to interact with the oxygen dissolved in these metals.[53] It is not known at present whether a double oxide of Li with Nb or Ta is formed; the existence of such oxides has been postulated but their composition has not been identified. Mixed oxides of Li with Ti or Zr have also not been identified.

Oxygen in the alkali metals heavier than Na has a strong tendency to interact with all the metals above Ti (except, possibly Ni) to form complex oxides. The failure to obtain the predicted oxygen distribution between liquid K and the refractory metals, especially Zr, has been explained to be due to the presence of stable, complex oxides which may be substantially soluble in liquid K.[31,54]

The existence of a complex in solution in molecular form in a liquid metal is difficult to rationalize with our understanding of the atomic nature of liquid metal solutions. However, the tendency for interaction between the oxygen, the alkali metal and the transition metal atoms must still exist in solution. Iron atoms and sodium atoms, for example, should be more strongly bonded to oxygen atoms than to each other; otherwise iron should be much more soluble in sodium than it has been reported to be. Units such as Na-O-Cr or Na-O-Fe, as distinct from complexes such as $(Na_2O)_2 \cdot FeO$, should have a high probability of existing in the liquid solution; the dissolved transition metals, especially Cr, should therefore have a measurable effect on the activity of oxygen in Na.

Since oxygen is known to lower the surface tension of liquid sodium, it has a preference to adsorb at the interface between Na and its container. Thus, a bond such as Fe|-O-Na could readily form at a solid-liquid interface. The rate-controlling process in step 2 of the kinetic argument would then be the breaking away of the surface complex which dissolves in the liquid phase.

The Nature of Dissolved Nonmetals in the Alkali Metals

By far one of the least understood aspects of liquid metal solution chemistry is the nature of the dissolved nonmetals, especially oxygen and carbon.

Oxygen in Sodium

The oxygen dissolved in sodium is generally considered to be present as dissolved Na_2O, except for oxygen present in the ternary complexes noted above. Also, it is Na_2O that precipitates from supersaturated solutions of oxygen in sodium. However, Nevsorov[55] has suggested from electromigration studies on oxygen-bearing sodium that Na_2O is at least partially ionized to Na and oxygen ions; they correlated their electromigration results with a thermally activated ionization of the Na_2O. Further development of the electrochemical meter for oxygen in Na may throw additional light on this subject.[56]

Carbon in Sodium

The mechanism by which carbon transfers through sodium becomes increasingly more difficult to explain as more information is obtained. The transfer of carbon through an alkali metal occurs according to predictable thermodynamic driving forces; consequently, carbon behaves as though it were soluble in Na. Some years ago Gratton[57] published a solubility curve of carbon in sodium, and showed an oxygen-dependence of this solubility which suggested that at least some of the carbon exists in Na as a C-O-Na complex. Corrosion tests with sodium containing >50 ppm oxygen have shown that carbon transfer is a function of the oxygen concentration of the sodium,[58,59] as have the electromigration studies of Lyashenko and Nevsorov.[60] Carbon transfer in Na with <50 ppm oxygen has generally been found to be oxygen-independent;[7,8] however, a recalculation of the data in Table IV of the paper by Nettley et al[8] suggests, as seen in Table V, that carbon transfer may be a function of the oxygen concentration in sodium down to below 5 ppm oxygen.

TABLE V. CARBON INCREASE AFTER TEST[8]

Steel wt.%C	T_{Na}	O_2	Time (Months)	Carbon Increase After Test* Mean	Carbon Increase After Test* 0.01cm Surface Layer
321	650	<5	6	.003	.016
0.07		5	3	.013	.017
		10	4	.012	.028
		25/30	6	.010	.040
316	650	<5	6	.003	-
0.05		5	3	.010	.017
		10	4	.007	.023
		25/30	6	.007	.023

*wt.%/month.

Recent attempts to measure the carbon solubility in oxygen-free Na have failed to disclose any measurable solubility.[61] An attempt by the same authors to zone-refine Na to remove C also failed, suggesting that C may be present in sodium as a dispersion rather than as a true solution. It is quite possible that C present in as-received Na could be finely dispersed, having originated either from C electrodes used in the reduction of the metal, or from traces of oils that reacted with the Na during subsequent handling. However, it is difficult to imagine that carbon transfer from low to high alloy steels could occur with suspended rather than dissolved carbon as the intermediary state in the sodium. Recent studies by Sinclair et al.,[62] Addison,[63] and Pulham[64] suggest that carbon-sodium bonds without intermediate oxygen atoms are highly unlikely; and, if carbon is soluble in Na without reaction with oxygen, its solubility must be <3 ppm. Perhaps, therefore, carbon transfer is a function of the oxygen concentration of Na down to very low levels.

CONCLUSIONS

1. The stainless steels should be adequate container materials for liquid sodium if the maximum temperature in the circuit does not exceed 650°C and the oxygen levels in the sodium are maintained at approximately 10 ppm.

2. The importance of the irradiation embrittlement and loss of high temperature ductility of these steels has not been evaluated at the present time.

3. Stainless steels with compositions modified to reduce their embrittlement by irradiation require corrosion testing to demonstrate their adequacy for fuel cladding and structural applications.

4. The development of new alloys for fuel cladding applications at temperatures above 650°C needs to be vigorously investigated.

5. The effects of radiogenic Mg on the corrosion process need to be studied.

6. The effects of intentional additions of soluble oxygen "getters" to Na on the corrosion behavior of steels in this liquid need further study as a method of reducing corrosion and as a test of the several proposed corrosion mechanisms.

7. The effect of residence time in the heat exchanger on the corrosion process needs to be evaluated.

8. Careful studies of the mechanism of carbon transfer are needed.

9. The relationship between the Fe solubility and the oxygen content of Na requires resolution.

10. There is a need for a general corrosion equation which can be used to predict the corrosion in a large system.

ACKNOWLEDGEMENTS

The authors would like to thank all those workers who made available their unpublished papers, especially P. T. Nettley of the U.K.A.E.A. Reactor Materials Laboratory, V. M. Sinclair of the Dounreay Experimental Reactor Establishment and H. E. Feder of Argonne National Laboratory. The trip report of L. F. Epstein of the General Electric Corporation on the Nottingham Conference on the Alkali Metals made available to the authors much of the pertinent material that will be included in Special Report #22 of the Chemical Society of London. The careful reading of this manuscript and pertinent suggestions of B. Minushkin are greatly appreciated. The patience of our secretary, Mrs. Lois Norman, was invaluable in assisting in the preparation and many revisions of this manuscript.

REFERENCES

[1] STANG, J. H., SIMONS, E. M., DeMASTRY, J. A., and GENCO, J. M., Compatibility of liquid and vapor alkali metals with construction materials, U.S. Government Report DMIC-227 (1966).

[2] GOLDMANN, K., and MINUSHKIN, B., Sodium technology, Reactor Technology, Selected Reviews (1965) 321.

[3] TYZACK, C., The behaviour of materials in liquid sodium, Advances in Materials 239, The Institution of Chemical Engineers, London (1964).

[4] NEVSOROV, B. A. et al., Corrosion resistance of constructional materials in alkali metals, Third United Nations International Conference on the Peaceful Uses of Atomic Energy, Geneva, Paper A/Conf. 28/P/343 (1964).

[5] GURINSKY, D. H., WEEKS, J. R., KLAMUT, C. J., ROSENBLUM, L., and DeVAN, J. H., Corrosion in liquid metal systems, Third United Nations International Conference on the Peaceful Uses of Atomic Energy, Geneva, Paper A/Conf. 28/P/244 (1964).

[6] FROST, B. R. T., Advances in liquid metal technology, J. Nuclear Materials 7 #2 (1962) 109.

[7] ROWLAND, M. C., PLUMLEE, D. E., and YOUNG, R. S., Sodium mass transfer:XV behavior of selected steels in flowing sodium test loops, USAEC Report GEAP-4831 (1965).

[8] NETTLEY, P. T., BELL, I. P., BAGLEY, K. W., HARRIES, D. R., THORLEY, A. W., and TYZACK, C., Problems in the selection and utilization of materials in sodium cooled fast reactors, Paper 5B/3 presented at the London Conference on Fast Breeder Reactors [May 1966].

[9] SAVAGE, H. W., COMPERE, E. L., HUNTLEY, W. R., FLEISCHER, B., MacPHERSON, R. E., and TABOADA, A., SNAP-8 Corrosion Program Summary Report, USAEC Report ORNL-3898 (1965).

[10] FRYE, J. H., Jr., et al., Metallurgy Division Progress Report for Period Ending October 10, 1957, USAEC Report ORNL-2422 (1957).

[11] SCHENCK, G. F. and CLEARY, R. E., Alkali metal corrosion, I. Maximum temperature application of sodium-NaK/stainless steel, USAEC Report CNLM-5359 (1964).

[12] HAAG, F. G., Material transport in sodium systems - Part I, Chem. Eng. Prog. Symp. Ser. 53 (1957) 20.

[13] MATHEWS, R. R., et al., Performance and operation of the Dounreay fast reactor, Third United Nations International Conference on the Peaceful Uses of Atomic Energy, Geneva, Paper A/Conf. 28/P/130 (1964).

[14] GREENBERG, S., RUTHER, W. E., and LEVIN, H. A., Corrosion of vanadium-base alloys in sodium at 550-750°C, Paper SM-85/20 this conference (1966).

[15] ANDREWS, R. C., et al. Results of mechanical properties tests of 316 SS specimens in 1200°F sodium contaminated with oxygen (~300 ppm), USAEC Report MSAR 66-78 (1966).

[16] WEBER, C. E., Program plan - stability of cladding and structural alloys in a high temperature, liquid metal, fast neutron environment, USAEC Report NAA-SR-Memo-11871 (1966).

[17] ANDERSON, W. J., SHEFFIELD, G. S., and BIRKLE, A. J., Development of ferritic steels for high temperature sodium service (part II) USAEC Report NAA-SR-7544 (1963).

[18] HARRISON, R. W., Stabilization of carbon and nitrogen in stainless steel and its effect on mass transfer in a stainless steel--Cb-1Zr--potassium system, NASA Report R66SD3009 (1966).

[19] GOLDMANN, K. et al., Carbon and nitrogen transfer in a type 316 stainless steel Cb-1Zr, liquid potassium system, USAEC Report UNC-SPLM-94 (1965).

[20] DUTINA, D., The current state of the art of alkali metal analysis, AEC-NASA Liquid Metals Information Meeting, USAEC Report Conf. 650-411 (1965).

[21] NEWMAN, L., Brookhaven National Laboratory, private communication (1966).

[22] WALKER, J. A. J., FRANCE, E. D., and EDWARDS, W. T., The determination of oxygen in sodium, Analyst 90 (1965) 727.

[23] BERGSTRESSER, K. S., WATERBURY, G. R., and METZ, C. F., Determination of trace amounts of oxygen added to metallic sodium, USAEC Report LA-3343 (1965).

[24] GUINN, V. P., Determination of oxygen by fast neutron activation analysis, paper presented at Sodium Components Development Program Information Meeting, Hollywood, California (1964).

[25] DeVAN, J. H., Oak Ridge National Laboratory, private communication (1965).

[26] LOCKHART, R. W., et al., Results of the USAEC round robin analysis for carbon impurity in sodium, USAEC Report GEAP-4602 (1964).

[27] ROMANO, A. J., FLEITMAN, A. H., KLAMUT, C. J., "Behavior of refractory metals and alloys in boiling sodium and other boiling alkali metals", these Proceedings.

[28] HOFFMAN, E. E., Effects of oxygen and nitrogen on the corrosion resistance of columbium to lithium at elevated temperatures, USAEC Report ORNL-2675 (1959).

[29] FREED, M. S., and KELLY, K. J., Corrosion of columbium base and other structural alloys in high temperature lithium, USAEC Report PWAC-355 (1961).

[30] ROMANO, A. J., KLAMUT, C. J., and GURINSKY, D. H., Vapor liquid corrosion of refractory metals and their alloys by sodium, NASA-AEC Liquid Metals Corrosion Meeting, Report NASA SP-41 (1963) 182.

[31] LITMAN, A. P., The effect of oxygen on the corrosion of niobium by liquid potassium, USAEC Report ORNL-3751 (1965).

[32] SCHEUERMANN, C. M., and BARRETT, C. A., Compatibility of columbium and tantalum tubing alloys with refluxing potassium, NASA TND-3429 (1966).

[33] ROMANO, A. J., FLEITMAN, A. H., KLAMUT, C. J., The evaluation of Li, Na, K, Rb, and Cs boiling and condensing in Nb-1Zr capsules. To be published in Nuclear Applications (1967).

[34] TYZACK, C., Applications of sodium chemistry in fast nuclear reactors, Special Publication No. 22 of The Chemical Society of London, to be published (1966).

[35] HOFFMAN, E. E. Private communication. Space Power and Propulsion Section, General Electric Co., Evendale, Ohio, Contract NAS 3-2547 (1966).

[36] MARTIN, W. R. and WEIR, J. R., Solutions to the problems of high-temperature irradiation and embrittlement, USAEC Report ORNL-TM-1544 (1966).

[37] FRANK, R. G., Private communication, Space Power and Propulsion Section General Electric Co., Evendale, Ohio, Contract NAS 3-2547 (1966).

[38] FLEITMAN, A. H., Private communication, Brookhaven National Laboratory, Upton, N. Y. (1966).

[39] BRUSH, E. G., Sodium mass transfer:XVI the selective corrosion component of steel exposed to liquid sodium, USAEC Report GEAP-4832 (1965).

[40] EPSTEIN, L. F., Preliminary studies on the solubility of iron in sodium, Unpublished paper; abstract: Science 112 (1950) 426.

[41] BOGARD, A. D., The solubility of iron in sodium metal, sodium-sodium oxide, and sodium-sodium oxide-sodium hydroxide, U.S. Report N.R.L. 4131 (1953). Data included in BAUS, R. A., BOGARD, A. D., GRAND, J. A., LOCKHART, L. B., Jr., MILLER, R. R., and WILLIAMS, D. D., Proceedings of the First International Conference on the Peaceful Uses of Atomic Energy 9 United Nations, N. Y. (1956) 356.

[42] RODGERS, S. J., MAUSTELLER, J. W., and BATUTIS, E. F., USAEC Report N.P. 5247 (1954).

[43] MOTTLEY, J. D., Sodium mass transfer:VIII corrosion of stainless steel in isothermal regions of a flowing sodium system, USAEC Report GEAP-4313 (1964).

[44] PARKMAN, M. F. (Eimac Division of Varian Associates, San Carlos, Calif.) Private communication (1962).

[45] THORLEY, A. W., U. K. A. E. A. Reactor Materials Laboratory, Culcheth. Private communication (1965).

[46] WYATT, L. M., A. E. R. E. Harwell, private communication (1954).

[47] EPSTEIN, L. F., and WEBER, C. E., USAEC Report KAPL 362 (1950).

[48] WEEKS, J. R., A possible effect of oxygen on mass transfer by liquid sodium, in BNL Metallurgy Memo #414 (1953) and 414A (1955). Also WEEKS, J. R. and GURINSKY, D. H., Solid-liquid reactions in bismuth and sodium, in Liquid Metals and Solidification (Ed. B. Chalmers) Am. Soc. Metals, Cleveland (1958) 106.

[49] HORSLEY, G. W., J. Iron and Steel Inst. 182 (1956) 43. Originally U.K. Report A.E.R.E. M/R 1441 (1954).

[50] WEEKS, J. R., and KLAMUT, C. J., Liquid metal corrosion mechanisms in Corrosion of Reactor Materials Vol. 1 IAEA, Vienna (1962) 105.

[51] TYZACK, C., UKAEA Reactor Materials Lab., Culcheth, Letter to J. R. Weeks, Nov. 26, 1964.

[52] TYZACK, C., Application of sodium chemistry in fast nuclear reactors, in Special Report #22 of The Chemical Society of London, to be published (1966).

[53] DiSTEFANO, J. R., and HOFFMAN, E. E., Relation between oxygen distribution and corrosion in some refractory metal-lithium systems, in Corrosion of Reactor Materials Vol. 2 IAEA Vienna (1962) 431.

[54] LITMAN, A. P., and PRADOS, J. W., The partitioning of oxygen between zirconium and liquid potassium, Electrochemical Technology 3 (1965) 228.

[55] NEVZOROV, B. A., The nature of oxygen in liquid sodium,Corrosion of Reactor Materials,Vol. II IAEA, Vienna (1962) 271, English translation, USAEC-TR-5412.

[56] MINUSHKIN, B., Development of a continuous electrochemical meter for oxygen in sodium, USAEC Report UNC 5131 (1966).

[57] GRATTON, J. G., Solubility of carbon in sodium at elevated temperatures, USAEC Report KAPL-1807 (1957).

[58] KOENIG, R. F., and BRUSH, E. G., Behavior of materials in nonaggressive liquid metals, Nuclear Metallurgy, IMD Special Report Series #2, Am. Inst. Min. and Met. Engrs., New York (1956) 21.

[59] LYASHENKO, V. S., ZOTOV, V. V., and IVANOV, V. A., Resistance to corrosion of austenitic and ferro-pearlitic steels in a stream of liquid sodium at temperatures of 600°C and 700°C, Corrosion of Reactor Materials,Vol. I, IAEA, Vienna (1962) 297, English translation, AEC-TR-5409.

[60] LYASHENKO, V. S., and NEVZOROV, B. A., Mechanism of carbon transfer in liquid sodium, Corrosion of Reactor Materials II, IAEA, Vienna (1962) 373, English translation, AEC-IR-5408.

[61] LUNER, C., COSGAREA, A., and FEDER, H. M., "Solubility of carbon in sodium," these Proceedings.

[62] SINCLAIR, V. M., DAVIES, R. A., and DRUMMOND, J. L., Reaction of carbon monoxide with sodium, Special Report #22 of The Chemical Society of London, to be published (1966).

[63] ADDISON, C. C., Liquid metals as reaction media, Special Report #22 of The Chemical Society of London, to be published (1966).

[64] PULHAM, R. J., Reaction of acetylene with sodium, Special Report #22 of The Chemical Society of London, to be published (1966).

[65] COUGHLIN, J. P., U.S. Bur. Mines Bulletin 542 (1954).

[66] HOFFMAN, E. E., Symposium on Newer Metals, A.S.T.M. Spec. Tech. Pub. 272 (1959) 195.

[67] SALMON, O. N. and CASHMAN, T. J., Jr., KAPL-1653 (1956).

[68] WILLIAMS, D. D., GRAND, J. A. and MILLER, R. R., J. Phys. Chem. 63 (1959) 68.

[69] ELLIOTT, R. P., Constitution of Binary Alloys, First Supplement, McGraw-Hill, N.Y. (1965) 368.

DISCUSSION

C. TYZACK: In general, do you think that further development of refractory metals is likely to be the most profitable course, or should more effort be put into nickel-cobalt materials, e.g. nimonics, or nimonics modified with high-strength cobalt?

J.R. WEEKS: I think the answer must depend to a considerable extent on the spectrum in the reactor, and on whether the oxygen content can in time be kept sufficiently low in large reactor systems. Apart from some of the special vanadium alloys, there are no materials I know of at present that do not require this. At Brookhaven we are interested in the cobalt alloys partly because we wish to determine whether there is not perhaps after all some alternative to these very low oxygen levels.

C. TYZACK: Did I understand you to suggest that the mass transport properties of cobalt and cobalt-rich alloys might be sensitive to oxygen levels in sodium? If this is your assumption, I wonder whether it is based on experimental evidence; in view of the fact that cobalt is chemically similar to nickel, I should say it is less than certain. Has anyone studied compounds in the sodium-oxygen-cobalt system?

J.R. WEEKS: There is a slight misunderstanding here. Haag (Ref. [12] in our paper) found the transfer of radioactive cobalt from stainless-steel fuel element claddings to the non-radioactive part of a circuit to be a function of the oxygen content of the sodium. In fact, however, the thermodynamic data presented in Tables III and IV of our paper suggest that the corrosion of cobalt may not be dependent on oxygen in the sodium. I know of no studies in which compounds in the sodium-oxygen-cobalt system have been identified. It may be worth recalling that Haag also thought the transfer of nickel isotopes was a function of the oxygen content of the sodium, something we now believe not to be true; so his observations on cobalt transfer might well be in error also. At the relatively low temperatures of his experiments, the corrosion and mass transfer of all minor constituents of the stainless steels may have been controlled by the oxygen-sensitive corrosion rate of the major element, namely iron.

L.F. EPSTEIN: I think you have perhaps put too much emphasis in your oral presentation on our early work in connection with the "solution rate" mechanism. This work was based on sodium systems with a high oxygen content, in which the rate was found to be nearly independent of velocity. More recent work at General Electric has shown a velocity dependence, and the model formulated previously must be revised accordingly.

Another point: it does not seem to me necessarily to follow that the solubility of iron in sodium must be dependent on oxygen content; a variation of the solution rate constant appears to be compatible with the corrosion data. Such a variation was in fact observed in early KAPL[1] work.

J.R. WEEKS: Your first comment is, I agree, quite right; the point was actually made in our paper.

With regard to your second point, our reason for suggesting that an oxygen-dependent solubility of iron in sodium is required is simply that we had difficulty in explaining how a high barrier to dissolution of iron into sodium could exist without a surface oxide film of some type at the interface. If the iron solubility at 650°C is about 20 ppm and is independent of oxygen, as the KAPL and MSA[2] solubility data imply, then the dissolution rate of iron in the absence of oxygen should be many times the rates observed in ordinary sodium circuits. It should then be controlled by diffusion of the iron through the liquid boundary layer, as is the dissolution of iron in mercury, bismuth and lead (and of nickel in sodium, as well

---

[1] Knollys Atomic Power Laboratory.

[2] MSA Research Corporation.

as in these other metals). This is, of course, simply a restatement of the premise set out in our paper, namely that if solubility in sodium were not dependent on oxygen content, the oxygen would necessarily act as a corrosion inhibitor — an effect which to my knowledge has never been observed.

Let me add, finally, that the solubility data in the literature, and the rate constant data noted by Mr. Epstein, were also obtained under the "high oxygen" conditions prevailing in the older work.

E. L. ZEBROSKI: I think perhaps the first of the conclusions stated at the end of your paper needs some qualification. While there may be few problems with regard to average weight loss, localized (intergranular) attack still remains a serious pitfall.

I should also like to comment on two other points in your conclusions. In the third conclusion you say that stainless steels with compositions modified to reduce radiation embrittlement will need corrosion testing, and so on; but I think the close similarity in rates for a wide range of iron-base alloys, ferritic and austenitic, suggests that this will be only a second-order effect. As to the fourth conclusion, I agree it is naturally of some importance to continue searching for a practical refractory alloy cladding. Even so, it is not at all certain that there is an urgent need for refractory materials in the early generations of fast reactors. It seems to me that a conclusion implied throughout much of your paper is that a great deal of important work, of high practical priority, still needs to be done if we are to get the best possible performance from the austenitic iron-base alloys.

СОСТОЯНИЕ И РАСПРЕДЕЛЕНИЕ ПРИМЕСЕЙ, ИХ КОНТРОЛЬ И УДАЛЕНИЕ В ЦИРКУЛИРУЮЩИХ ЩЕЛОЧНО-МЕТАЛЛИЧЕСКИХ ТЕПЛОНОСИТЕЛЯХ

А.И.ЛЕЙПУНСКИЙ, В.И.СУББОТИН, М.Н.ИВАНОВСКИЙ
ФИЗИКО-ЭНЕРГЕТИЧЕСКИЙ ИНСТИТУТ, ОБНИНСК
СССР

Abstract — Аннотация

CONDITION AND DISTRIBUTION OF IMPURITIES, THEIR CONTROL AND DISPOSAL IN CIRCULATING ALKALI METAL COOLANTS. This survey, drawing mainly on the work of Soviet authors, discusses the present status of research on questions related to impurities in circulating liquid-metal coolants.

СОСТОЯНИЕ И РАСПРЕДЕЛЕНИЕ ПРИМЕСЕЙ, ИХ КОНТРОЛЬ И УДАЛЕНИЕ В ЦИРКУЛИРУЮЩИХ ЩЕЛОЧНОМЕТАЛЛИЧЕСКИХ ТЕПЛОНОСИТЕЛЯХ. В докладе представлен обзор современного состояния вопросов, связанных с примесями в циркулирующих жидкометаллических теплоносителях. Обзор составлен преимущественно по материалам советских авторов.

1. ПРИМЕСИ В ЖИДКОМЕТАЛЛИЧЕСКИХ ТЕПЛОНОСИТЕЛЯХ

В процессе эксплуатации установок и реакторов с охлаждением щелочнометаллическими теплоносителями установлено, что одним из основных условий надежной эксплуатации является высокая и контролируемая чистота жидкометаллического теплоносителя.

Примеси, особенно неметаллические, могут существенно снизить эксплуатационные характеристики теплоносителя по следующим основным причинам:

1. Наличие концентрации примесей в потоке теплоносителя большей, чем концентрация насыщения при минимальной температуре контура, может привести к осаждению взвесей в активной зоне реактора, к частичной или полной закупорке трубопроводов в относительно холодной зоне и нарушению циркуляции теплоносителя в теплообменниках, парогенераторах, а также к закупорке мест входа в перекрытые байпасные линии. Осевшие примеси могут вызвать заклинивание подвижных элементов жидкометаллической аппаратуры.

2. Присутствие взвешенных примесей в жидкометаллическом теплоносителе приводит к возникновению контактного термического сопротивления. Контактное термическое сопротивление обусловлено тем, что взвешенные примеси скапливаются вблизи горячей стенки в низкотеплопроводный слой, толщина которого зависит от местной скорости в потоке [1].

В результате теплоотдача уменьшается почти вдвое в условиях нагрева теплоносителя. В каналах сложной формы, образованных пучком стержневых элементов, примеси должны высаживаться неравномерно. В основном они будут концентрироваться в зонах касания тепловыделяющих элементов, где скорость теплоносителя меньше. Это приведет к увеличению неравномерности температуры по периметру элемента [2].

Высаждение твердой фазы примесей на горячих и холодных поверхностях приводит к ухудшению и гидродинамики установки.

3. Коррозионное воздействие теплоносителя на конструкционные материалы зависит от содержания таких коррозионно-активных примесей, как кислород, азот, углерод, водород.

Повышение количества коррозионно-активных примесей приводит к увеличению растворимости и к увеличению переноса масс элементов конструкционных материалов, к интенсификации процессов коррозии [3].

4. Примеси в теплоносителе, циркулирующем в контуре ядерного реактора, могут явиться источником наведенной радиоактивности, приводят к увеличению периода спадания активности. Они могут ухудшить использование нейтронов в реакторе.

2. ИСТОЧНИКИ ПРИМЕСЕЙ

С точки зрения постоянства содержания примеси могут быть разделены на две группы. К первой группе относятся примеси, источники которых отсутствуют в установках, использующих жидкометаллические теплоносители. От примесей этой группы можно заранее избавиться в процессе производства теплоносителя.

Вторую группу составляют примеси, содержание которых определяется условиями эксплуатации циркуляционного контура. Основное содержание этой группы примесей и основную опасность при эксплуатации установок представляют неметаллические примеси – кислород, углерод, азот, водород.

Одним из основных источников этих примесей являются элементы воздушной атмосферы, проникающие в контур через неплотности и вследствие диффузии через конструкционные материалы при повышенной температуре.

Особенно высокой диффузионной подвижностью обладают водород и азот [4]. При температуре $\sim 700°C$ через железную стенку толщиной 1 мм проникает ~ 5 гр N_2 в час через поверхность в 1 $м^2$ при перепаде давлений в 1 $кг/см^2$. Еще большей проницаемостью обладает водород. Интенсивным источником кислорода и водорода может служить течь парогенератора и попадание воды или пара в теплоноситель. Значительное количество примесей попадает в контур с исходным теплоносителем. В процессе транспортировки и подготовки к заполнению теплоноситель взаимодействует с воздухом, влагой и элементами консервирующих веществ – масел, парафина, керосина. В результате в исходном натрии технической чистоты может содержаться до $1 \cdot 10^{-2}$ вес % кислорода, $5 \cdot 10^{-2}$ вес% углерода, 0,1 вес % водорода. Некоторые щелочнометаллические теплоносители восстанавливают окисную пленку конструкционных материалов.

По нашим расчетам количество кислорода, поступающего в теплоноситель за счет восстановления окисной пленки нержавеющей стали, составляет $\sim 5 \cdot 10^{-2}$ $г/см^2$.

Газы, адсорбированные внутренней поверхностью контура,вносят пренебрежимо мало загрязнений. Относительно мало кислорода вносится и с недостаточно очищенным инертным газом, если установка герметична и расход газа невелик. Однако азота может быть внесено заметное количество.

Неглубокий вакуум (0,1 мм рт.ст.) при первичном заполнении контура дает малое загрязнение.

Постоянно действующие источники примесей приводят к изменению равновесного содержания примесей в контуре и в условиях непрерывной очистки теплоносителя.

Источники примесей и их мощность необходимо знать для выбора метода очистки, расчета производительности и времени очистки, расчета равновесной глубины очистки, для расчета количества геттеров в устройствах химической очистки. Оценивать мощность источников примесей можно из анализа конструкции и условий эксплуатации данной установки на основе опыта эксплуатации других установок с жидкими металлами. Окончательно определить все возможные источники примесей и их мощность для конкретной установки в настоящее время, по-видимому, можно только опытным путем.

3. СОСТОЯНИЕ ПРИМЕСЕЙ В ТЕПЛОНОСИТЕЛЯХ

Примеси могут находиться в жидкометаллических теплоносителях в различном химическом состоянии – в свободном виде; в виде простых соединений, являющихся окисями, нитридами и др.; в виде сложных соединений и комплексов.

Выбор методики очистки теплоносителя зависит от формы существования примесей. Так удаление сложных соединений или комплексов приводит к одновременной очистке сразу от нескольких примесей. Химическая очистка теплоносителя в принципе основана на переводе примесей из одной формы в другую.

Форма существования примесей влияет на физические свойства теплоносителей. Так, перераспределение кислорода между теплоносителем и его примесями (например натрием, кальцием, магнием и т.д.) при изменении температуры натриевого или натрий-калиевого теплоносителя приводит к изменению его электросопротивления при неизменности полного содержания кислорода.

Знание формы существования примесей в жидкометаллических теплоносителях необходимо для понимания процессов очистки и контроля чистоты, для понимания поведения примесей при изменении температурных и концентрационных условий теплоносителя.

Разработанные и практически применяющиеся в настоящее время методы физико-химического анализа теплоносителей часто не позволяют определить в каком виде находится тот или другой элемент.

Предварительное суждение о состоянии примесей в теплоносителях можно составить, используя аппарат, разработанный в химической термодинамике. Несмотря на упрощения, связанные с отсутствием в большинстве случаев необходимых эмпирических констант, с помощью термодинамических расчетов можно получить представление о характере системы теплоноситель – примеси, о взаимосвязях между отдельными элементами и об основных закономерностях, которым эта взаимосвязь подчиняется при изменении температуры и других условий.

С помощью химико-термодинамических расчетов можно получить приближенные значения концентрации форм существования тех или иных примесей в различных условиях, если известны величины, характеризующие термодинамическую стабильность соединений, вступающих во взаимодействие друг с другом. Такими величинами являются изменения изобарно-изотермических потенциалов реакций ΔZ°_T. Методики расчетов ΔZ°_T общеизвестны. Значения ΔZ°_T позволяют вычислить константы равновесия реакций. Как правило, в теплоносителях одна примесь одновременно может существовать в различных формах. Количественное соотношение между этими формами определяется равновесным состоянием одновременно протекающих реакций взаимодействия между примесями, находящимися в различных формах, поэтому особенностью расчетов состояния примесей в теплоносителях является необходимость совместного решения уравнений, выражающих равновесие для нескольких одновременно протекающих реакций взаимодействия, реакций термической диссоциации и так далее.

Количественным выражением равновесия являются термодинамические константы равновесия соответствующих реакций взаимодействия. Для обобщенной реакции взаимодействия окислов металла-теплоносителя (Me_T) с металлами-примесями ($Me_п$)

$$(Me_T)_2O + \frac{x}{y} Me_п \rightleftarrows \frac{1}{y} (Me_п)_x O_y + 2\, Me_T$$

константа равновесия записывается в виде

$$K_a = \frac{a^2_{Me_T} \cdot a^{1/y}_{(Me_п)O_y}}{a^{x/y}_{Me_п} \cdot a_{(Me_T)_2O}} \qquad (1)$$

Реакции взаимодействия протекают в избытке теплоносителя. Это позволяет с достаточной точностью считать величину активности теплоносителя равной единице

$$a_{Me_T} = 1$$

Для растворов с ограниченной растворимостью, таких как растворы примесей в расплавленных металлах активность может быть выражена формулой:

$$a_i = \frac{N_i}{N_i^н},$$

где N_i и $N_i^н$ соответственно мольные концентрации i-ой примеси в жидком металле и ее концентрации насыщения при данной температуре. Арнольдовым и др. разработана указанная выше методика и были рассчитаны концентрации неметаллических примесей в различных формах в щелочнометаллических теплоносителях – натрии, калии, сплаве натрий-калий, литии, цезии [5]. При расчетах полагалось, что исходные количества примесей соответствуют теплоносителю, очищенному от этих примесей с помощью холодных ловушек.

Соотношение между количеством окислов (и других соединений) теплоносителя и металлических примесей в нем определялось путем совместного решения соответствующих уравнений равновесия и баланса примеси при различной температуре и исходной концентрации.

В результате термодинамических расчетов получено, что в наиболее простой форме неметаллические примеси содержатся в расплавленном литии. Это связано с тем, что литий имеет по сравнению с другими щелочнометаллическими теплоносителями наиболее прочную молекулу окиси, нитрида, карбида и гидрида.

Установлено, что кислород в литии находится практически весь только в виде окиси лития и окисей металлических примесей – Са и Ве, кислород перераспределяется между ними в зависимости от концентрации и температуры. При увеличении температуры возрастает равновесное количество окиси лития и окиси бериллия за счет уменьшения количества окиси кальция. При увеличении содержания кислорода в литии вначале происходит увеличение содержания окиси кальция, затем окиси бериллия. Окись лития появляется лишь после того, когда кальций и бериллий почти полностью израсходованы.

Сложные соединения лития с кислородом, также как гидроокись $LiOH$ и карбонат Li_2CO_3 в расплавленном литии отсутствуют ($N_{Li_2CO_3} \cdot N_{LiOH} \ll 10^{-10}$). Экспериментально подтверждено, что гидроокись лития полностью разлагается при избытке расплавленного лития [6].

Азот в литии технической чистоты в подавляющей части находится в форме нитрида лития. В литии, содержащем порядка 10^{-3} вес % азота количество нитридов Ве, Са, Ti, Zr может стать соизмеримым с количеством Li_3N.

Весь углерод в литии должен существовать в форме карбида лития. Водород в литии находится только в форме гидрида лития. Гидрид лития является сравнительно легко диссоциирующей примесью. Поэтому над поверхностью раствора гидрида лития в литии всегда имеется свободный водород. Количество свободного водорода зависит от температуры, концентрации гидрида и от соотношения объемов газовой и жидкой фазы. Давление азота и особенно кислорода в газовой фазе несоизмеримо меньше давления водорода при заданной температуре.

В отличие от лития натрий имеет менее прочную термодинамически молекулу окиси. В натрии более кислородоактивными примесями являются кальций, бериллий, литий, титан, цирконий, ниобий и т.д. При увеличении содержания кислорода прежде образуются окиси более активных элементов примесей. Окись натрия образуется только после полного израсходования этих элементов на образование своих окисей. При изменении температуры содержание одних окисей увеличивается за счет других.

В расплавленном натрии кислород может находиться и в форме гидроокиси натрия. Гидроокись может образоваться при попадании воды в натрий. Расчет равновесных продуктов для системы реакций взаимодействия показал, что при малых количествах введенной воды будут в равновесии преобладать окись и гидрид натрия [7]. При количествах воды или кислорода и водорода превышающих процент, в равновесии количества гидроокиси превышает количества окиси или гидрида.

В ряде работ гидроокись была экспериментально обнаружена в расплавленном натрии [8]. Термодинамический анализ показывает, что кислород, по-видимому, может находиться в натрии и в форме карбоната Na_2CO_3.

Анализ образца натрия, циркулировавшего в контуре из нержавеющей стали при температуре 350°С показал, что 10% из обнаруженного в техническом натрии $4{,}4 \cdot 10^{-3}$ углерода находится в виде карбоната натрия.

Равновесная концентрация карбида-натрия в натрии мала. Возможно существование карбидов Са, Ве, Mn, U, V, Th, Zr, Ti, Nb и др. Однако часть этих металлических примесей с большей вероятностью образует окиси. В [9] указывается на возможность присутствия в Na ацетилидов $NaHC_2$ и метанидов CH_3Na натрия в значительных количествах. Однако эти соединения термически непрочны.

Соединения натрия с азотом неустойчивы. Однако возможно существование молекулярного раствора азота в натрии. В [10] указывается на присутствие в натрии значительного количества ионов типа CN. По данным [9] азот вместе с кислородом и углеродом может образовывать в натрии сложные комплексы.

Азот может существовать в натрии в форме соединений металлических элементов примесей. Одной из основных форм существования водорода в натрии является гидрид натрия NaH. Часть водорода может находиться в виде гидридов кальция, лития, бериллия и др.

Однако более вероятно, что эти металлы-примеси практически будут находиться в натрии в форме окисей, а водород в форме гидрида и гидроокиси натрия.

Гидрид натрия – одна из наиболее легко диссоциирующих примесей. Давление водорода над насыщенным гидридом раствором натрия при температуре 420°С составляет 1 кг/см^2. Равновесное парциальное давление свободного водорода над натрием определяется температурой, концентрацией гидрида в натрии и соотношением между объемом газовой фазы над натрием и количеством натрия [11].

В расплавленном калии кислород находится в виде гидроокиси калия. Окись калия K_2O может существовать только если содержание кислорода превышает стехиометрическое количество, необходимое для образования гидроокиси и если многочисленные более активные по отношению к кислороду металлы – примеси израсходованы на образование своих окисей. Водород в калии находится также в основном в форме гидроокиси калия и гидридов металлов-примесей и наконец, при избыточном содержании, в виде гидрида, калия. Так же как и в натрии над калием имеется равновесное давление свободного водорода за счет диссоциации гидрида и гидроокиси. Значительные количества газообразного водорода над калием были экспериментально обнаружены в опытах по конденсации калия [12, 13].

Преимущественной углеродосодержащей формой в калии и сплаве натрий-калий является карбонат калия K_2CO_3.

Азот в калии и сплаве натрия с калием, по-видимому, может находиться в форме молекулярного раствора, или в форме соединений с другими примесями.

Термодинамический анализ показывает, что в отличие от натрия в калии наиболее устойчивым кислородосодержащим соединением является карбонат калия, за ним следует гидроокись и затем окись калия.

В сплаве натрия с калием присутствие тех или иных соединений определяется в значительной степени температурой. При низких температурах возможно присутствие карбоната, гидроокиси и окиси натрия. При увеличении температуры сплава резко возрастает и становится преобладающей доля карбоната и гидроокиси калия.

Таким образом, в отличие от распространенного мнения, в сплаве в широком температурном интервале преобладают калиевые соединения и лишь в узком низкотемпературном интервале возможно существование наряду с калиевыми и натриевых соединений.

Состояние примесей в цезии, используемом в термоэлектронном преобразователе энергии рассмотрено в работе [5]. На основании химико-термодинамических расчетов показано, что при наступлении равновесного состояния кислород находится в термоэлектронном преобразователе в форме окисей элементов, использованных в качестве конструкционных материалов электродов, а также в форме водяных паров. В цезиевом резервуаре кислород находится в форме окиси и гидроокиси цезия, водород – в форме гидроокиси цезия и в свободном виде.

4. РАСПРЕДЕЛЕНИЕ ПРИМЕСЕЙ В ЦИРКУЛИРУЮЩЕМ В КОНТУРЕ ТЕПЛОНОСИТЕЛЕ

При концентрации примесей, превышающей растворимость, часть примесей находится в теплоносителе в виде взвесей. Нерастворенные примеси осаждаются на горячих поверхностях контура в виде слоя и в несколько раз снижают теплопроводность пристенного слоя потока [4].

Решение дифференциального уравнения баланса на единицу поверхности пристенного слоя примесей показывает, что предельная толщина пристенного слоя примесей зависит от скорости потока (Re) и не зависит от концентрации примеси в потоке. Этот результат подтверждается исследованиями теплообмена при контролируемом содержании примесей [1].

Экспериментальное исследование распределения примесей в потоке щелочнометаллического теплоносителя (лития) позволило установить следующее. В случае, когда примеси (азот) полностью растворены в теплоносителе, их концентрация постоянна по всему контуру и по сечению потока с точностью ±1% при чувствительности регистрации $1{,}6 \cdot 10^{-4}$ вес%.

При наличии нерастворенных примесей их концентрация в потоке на различных участках циркуляционного контура может быть разной. Различно количество примесей, осевших на стенках, и полная концентрация примесей в различных участках контура. Количество примесей в данном участке контура зависит от температурных и гидродинамических условий в нем и от условий работы других узлов контура. Примеси перераспределяются между всеми участками контура при изменении режима работы всего контура или части его.

На относительно холодных стенках контура происходит накапливание примесей за счет кристаллизации. При этом, после установления стационарного режима, концентрация примеси в потоке соответствует концентрации насыщения при данной температуре теплоносителя.

Если в контуре включаются стоки примесей (зоны выкристаллизации примесей в холодных ловушках или на сильно охлаждаемых поверхностях), то происходит постепенная очистка теплоносителя. Если при этом отсутствуют источники примесей, то в потоке вначале достигается содержание примесей, близкое к насыщению при температуре в данном участке. После переноса примесей со стенок участков контура в зону выкристаллизации, в потоке устанавливается концентрация, соответствующая концентрации насыщения при температуре выкристаллизации.

В случае изотермического контура и в случае когда отсутствуют стоки примесей, или имеются источники примесей, компенсирующие стоки, то в потоке могут постоянно находиться взвешенные примеси.
К появлению взвешенных примесей приводит снижение температуры теплоносителя ниже температуры насыщения, диффузия газов через стенки контура, прогрев холодных ловушек и др.

Накапливание примеси может происходить не только на холодных стенках и не только за счет кристаллизации. В случае изотермического контура и в случае нагрева теплоносителя нерастворенные примеси скапливаются и у горячих стенок и в застойных зонах с малой скоростью теплоносителя. При этом устанавливается определенное соотношение между количеством примеси в потоке и на стенке. Примеси перераспределяются между турбулентным ядром потока и пристенной областью в зависимости от скорости теплоносителя. Как показали наши измерения и анализы, вблизи горячей стенки нерастворенные примеси скапливаются в слой, представляющий почти плотную упаковку кристаллов примеси. В турбулентном ядре потока концентрация взвешенных примесей невелика и полная концентрация примеси близка к концентрации насыщения.

Увеличение скорости потока теплоносителя приводит к уменьшению слоя осевших на стенке нерастворенных примесей и к уносу их потоком. Унесенные потоком взвеси откладываются в других участках контура, пока не наступит новое стационарное распределение примеси между участками контура. Увеличение скорости потока приводит к увеличению стационарного содержания взвешенных в нем примесей [15].

Пробы жидкого металла, взятые для химанализа из потока теплоносителя, содержащего нерастворенные примеси, имеют концентрацию примесей, близкую к концентрации насыщения при температуре потока и зависящую от скорости потока теплоносителя в участке и от направления теплового потока на его стенке. В действительности полное содержание примеси в участке может быть значительно большим (в сотни раз). Анализ теплоносителя, взятый из данного участка контура, может не соответствовать содержанию примесей в других участках контура, особенно если они отличаются температурой и скоростью теплоносителя в них.

Все это необходимо учитывать при создании представительных методов отбора проб, создании ловушек примесей, при изучении теплоотдачи и ее зависимости от чистоты теплоносителя, при изучении процессов коррозии и массообмена.

Неучет законов распределения примесей приводит к серьезным ошибкам при контроле чистоты теплоносителей, при исследовании установок с жидкометаллическими теплоносителями.

5. МЕТОДЫ КОНТРОЛЯ ПРИМЕСЕЙ В ЦИРКУЛИРУЮЩИХ ЖИДКОМЕТАЛЛИЧЕСКИХ ТЕПЛОНОСИТЕЛЯХ

Контроль содержания примесей в теплоносителях совершенно необходим как при разработке методов очистки теплоносителей, так и при эксплуатации установок с жидкими металлами. Особенно четкий контроль должен быть в том случае, когда источник примеси возникает внезапно и накопление примеси приводит к аварийной ситуации. К такому случаю относится, например внезапная течь воды в парогенераторе с натриевым теплоносителем.

Особый интерес для контроля чистоты теплоносителей непосредственно на циркуляционном контуре представляют физические методы, так как часть из них может быть использована для непрерывного и дистанционного контроля чистоты жидкометаллического теплоносителя.

Известно, что присутствие примесей отражается на различных физических свойствах металлов. Изменение этих свойств может послужить сигналом изменения содержания примесей.

В литературе описывается целый ряд возможных методов контроля содержания газовых примесей в жидкометаллических теплоносителях. Это эффект Холла, ядерный магнитный резонанс, электрон-спиновый резонанс, инфракрасные и ультрафиолетовые поглощения отраженного или проходящего излучения примесями, изменение температуры плавления, кипения, изменение давления паров, потенциал реакции с геттером, изменение свойств или веса геттера после реакции с примесями, полярография расплавленных солей, органическая полярография, измерение количества электричества, масс-спектрометрия, спектрография дуговой эмиссии, хромотография, радиоактивация примесей, концентрационная ячейка, пробковый индикатор, термоэлектродвижущая сила, электросопротивление и др.

Несмотря на внушительные размеры, перечень разнообразных методов далеко не исчерпывает всех возможных и применяющихся в практике (лабораторий или полупромышленной) методов контроля содержания примесей, основанных на измерении физических свойств жидкометаллических теплоносителей.

По нашему мнению из перечисленных методов наиболее перспективными и распространенными являются радиоактивационный метод, метод концентрационной ячейки, метод пробкового индикатора, метод термоэлектродвижущей силы, метод диффузии примеси через мембрану, метод электросопротивления. Эти методы могут обеспечить непрерывное и дистанционное измерение содержания примесей в циркулирующем теплоносителе.

Так измерения термоэлектродвижущей силы литиевого теплоносителя, проведенные авторами доклада дали значения уменьшения коэффициента термоэлектродвижущей силы в диапазоне температур 250 – 500°С в среднем на 0,04 мкв/°С при измерении концентрации кислорода на $1 \cdot 10^{-3}$ вес % и на 0,02 мкв/°С при изменении концентрации азота на $1 \cdot 10^{-3}$ вес %.

Более подробно рассмотрим два последних метода контроля. Один метод [16] основан на диффузии контролируемой примеси через мембрану в вакуумную полость. По степени изменения вакуума можно судить о интенсивности диффузионного потока, который, в свою очередь, определяется концентрацией примеси в теплоносителе.

Известно, что коэффициент диффузии вещества и его растворимость в материале мембраны определяют диффузионный поток в твердой стенке. Наиболее подвижной в диффузионном отношении газовой примесью в теплоносителях является водород.

Метод был исследован применительно к контролю течи воды в натриевую полость в парогенераторах атомных электростанций. В качестве материала мембран использовался никель, отличающийся хорошей проницаемостью для водорода и достаточной коррозионной устойчивостью в среде натрия.

Датчик, изготовленный из никелевой трубки с толщиной стенки 1 мм, размещается в газовой полости над поверхностью натрия или непосредственно в потоке натрия.

Величина потока водорода определялась путем измерения роста давления водорода в камере известного объема за мембраной вакуумметра с термопарной лампой ЛТ-2.

Эксперименты [16] показали, что поток водорода через никель в датчике, расположенном в натрии, пропорционален концентрации водорода в натрии.

Величина потока возрастает с увеличением температуры и не зависит от скорости течения натрия, омывающего датчик.

Это означает, что скорость процесса целиком определяется диффузией водорода через никелевую мембрану. Чувствительность определения содержания водорода в натрии при температуре 450°С в работе [16] составляет $(3 \div 4) \cdot 10^{-4}$ вес%. Второй метод основан на измерении изменения электросопротивления жидкометаллического теплоносителя с изменением уровня загрязненности.

В литературе описан прибор, основанный на измерении электросопротивления. С помощью этого прибора осуществлялся контроль чистоты протекающего в контуре ядерного реактора сплава натрий-калий [7]. Результаты измерений указывают на зависимость электросопротивления сплава от степени его очистки с помощью холодных ловушек. Однако в этой работе не было приведено никаких доказательств, что изменение электросопротивления сплава связано с изменением содержания только кислорода.

Напротив, в работе [18] указывается, что контроль содержания кислорода в натрии и сплаве методом электросопротивления невозможен.

С другой стороны в работе [19] обнаружена существенная зависимость электросопротивления натрия от концентрации кислорода.

В докладе [20], представленном на настоящей конференции, приводятся данные по непосредственному измерению зависимости электросопротивления литиевого и натриевого теплоносителей от содержания газовых примесей. Исследуемый металл циркулировал через трубку диаметром 9/8,2 мм из нержавеющей стали, помещенной в термостат, где постоянство температуры трубки поддерживалось с точностью 0,05°С. Измерительная трубка соединена с циркуляционным контуром, снабженным устройствами для дозированного ввода газов в металл и для анализов металла.

Количество введенных газов согласуется с данными систематических химанализов теплоносителей.

В работе показано, что во всем диапазоне концентраций вплоть до концентраций насыщения имеется линейная зависимость примесной добавки электросопротивления от концентрации примесей.

Обнаружена сильная зависимость электросопротивления литиевого теплоносителя от содержания азота и водорода, составляющая соответственно 3,6 момсм/вес% N_2 и 25 момсм/вес% H_2, и натриевого теплоносителя от содержания водорода 60 момсм/вес% H_2. Это позволяет обеспечить чувствительность определения азота и водорода в литии и водорода в натрии на уровне $2 \cdot 10^{-4}$, $3 \cdot 10^{-5}$ и $1 \cdot 10^{-5}$ вес% соответственно при использовании в качестве вторичного прибора стандартного моста постоянного тока.

В процессе ввода кислорода как в виде газа так и в виде перекиси натрия не было обнаружено влияния примеси кислорода на электросопротивление натрия. (Погрешность в определении электросопротивления не превышает 0,01 процента). Электросопротивление лития также очень слабо зависит от содержания кислорода. Возможно это связано с относительно высокой прочностью молекул окисей лития и натрия.

При измерении электросопротивления натрия, загрязненного водородом, следует иметь в виду возможное изменение содержания водорода за счет диссоциации гидрида при изменении температуры или давления в системе, а также за счет изменения объема газовой полости над поверхностью натрия. При быстром изменении этих параметров происходит вспенивание и связанное с ним увеличение объема натрия.

Рассматривая перечисленные выше методы контроля содержания примесей, можно заметить, что некоторые методы пригодны для непрерывного контроля.

Другие методы пригодны лишь для анализа отобранной пробы жидкого металла. К таким относятся метод масс-спектрометрического анализа остатка после дистилляции пробы и т.д.

Выбор тех или иных средств контроля качества теплоносителя определяется прежде всего пригодностью его к использованию в данных условиях и желательной точностью. Часто бывает целесообразно комплексное применение нескольких методов.

6. НЕПРЕРЫВНАЯ ОЧИСТКА ТЕПЛОНОСИТЕЛЕЙ С ПОМОЩЬЮ ПРОТОЧНЫХ ХОЛОДНЫХ ЛОВУШЕК

Очистка циркулирующего в контуре теплоносителя производится в основном с помощью так называемых "горячих" и "холодных" ловушек примесей. Горячие или геттерные ловушки основаны на использовании химических реакций, переводящих примесь в малорастворимую в теплоносителе форму соединения с металлом-геттером. Горячие ловушки применяются на специальных высокотемпературных установках в основном в тех случаях, когда допустимое содержание примесей в теплоносителе не может быть обеспечено холодными ловушками. Например, при очистке натрия от углерода. На большинстве эксплуатируемых в настоящее время ядерных реакторах одним из основных средств непрерывной и периодической очистки от примесей циркулирующих жидкометаллических теплоносителей являются холодные ловушки проточного типа.

В докладе [21] отражены результаты изучения проточных холодных ловушек и процессов, происходящих в них. Основная задача исследования была направлена на увеличение полезной емкости ловушек и на выбор параметров и режимов, при которых распределение примесей "окислов" в ловушке было бы равномерным по объему.

Ловушка, как правило, состоит из трех зон: зоны охлаждения, отстойника и зоны фильтрации. Изучение распределения окислов по зонам проводилось на экспериментальных участках, моделирующих в определенной степени эти части ловушки.

С помощью дистилляционно-газового метода анализа определялось распределение кислорода по длине в замороженных после опыта участках.

Установлено, что в зоне охлаждения осаждение окислов на стенки начинается практически в том месте, где температура натрия достигнет температуры насыщения. По-видимому, пересыщения незначительны. Однако специально величина пересыщения не измерялась. Например, для лития, охлаждаемого от температуры 290°C, переохлаждение, необходимое для начала кристаллизации, составляет 20°C, а охлаждаемого от температуры 350°C – 30°C [22]. Высаждение примесей происходит не равномерно по длине участка охлаждения, а в узкой зоне. Это является причиной преждевременного увеличения гидравлического сопротивления ловушки. Уже при содержании 15 – 20% примесных соединений в среднем по всему объему ловушки, она начинает закупориваться. Такое местное накапливание примесей является причиной преждевременного забивания ловушки, которое происходит особенно быстро, если в результате какой-либо аварийной ситуации повысится концентрация примесей в контуре и на входе в ловушку.

Увеличение скорости натрия в зоне охлаждения даже до 10 м/сек только ускоряет процесс высаждения примесей на стенках зоны охлаждения и не позволяет избежать неравномерного высаждения окислов. Максимальная местная концентрация окислов (в пересчете из количества кислорода) составляет 80% проанализированного осадка. Такое высокое содержание кислорода означает по нашему мнению, что на холодной поверхности происходит кристаллизация примеси из раствора, а не высаждение взвеси.

Преждевременное увеличение гидравлического сопротивления можно исключить, если через ловушку некоторое время прокачивать чистый натрий. Такой режим приводит к переносу и перераспределению примесей в ловушке и делает ее способной к дальнейшей работе. В результате такой операции емкость по окислам стендовой ловушки была повышена до 40 %.

Следует отметить, что осаждение окислов в зоне охлаждения в опытах [21] нестабильно. Наблюдается большой разброс экспериментальных данных. Одну из причин нестабильности авторы [21] видят в появлении газов в участке охлаждения. Присутствие газа влияет на массообмен.

В отстойнике концентрация окислов при малых накоплениях экспоненциально убывает от дна отстойника, при больших накоплениях – концентрация почти равномерна по высоте. Максимальная концентрация окислов в осадке у дна отстойника около 25%. Это указывает на малую плотность осадка, состоящего в основном из осевшей взвеси.

В зоне фильтра максимальная местная концентрация окислов в осадке достигает 65%. Распределение окислов по глубине фильтра зависит от скорости натрия и плотности набивки. Фильтр рекомендуется делать небольшой протяженности с плотностью набивки из нержавеющей стружки, возрастающей по глубине от 100 до 400 кг/м^3, а скорость натрия иметь порядка 1 – 3 мм/сек.

При испытаниях ловушек на максимальную емкость концентрация кислорода в натрии изменялась в относительно узком интервале $(1 \div 5) \cdot 10^{-3}$ вес %, как вырастание гидравлического сопротивления в режиме накопления окислов всегда происходило из-за закупорки в зоне охлаждения. Концентрация примеси на входе в зону охлаждения должна быть ниже, чем концентрация насыщения при температуре входа в ловушку и, тем более, при температуре в рекуператоре.

При этих условиях была достигнута емкость ловушки по окислам 40 вес% (при применении режима прокачки через ловушку чистого натрия).

При объемной доле зоны охлаждения, отстойника и фильтра соответственно доля 0,3 0,4 и 0,3 доляуловленных окислов составила 0,35, 0,30 и 0,35 и средняя концентрация окислов $23 \div 33$ вес%, 18 вес% и $26 \div 33$ вес % (в опытных участках, моделирующих ловушку).

Фильтрационные характеристики ловушек вполне удовлетворительны при времени пребывания натрия в ловушке 15 – 20 минут. При этом происходит практически полное удержание окислов. При увеличении скорости (время пребывания 9 мин) наблюдается пронос окислов.

Концентрация кислорода в натрии, достижимая с помощью холодной ловушки, равна растворимости кислорода при минимальной температуре натрия в ловушке.

Авторами настоящего обзора проводились исследования переходных режимов работы холодных ловушек. Установлено, что увеличение скорости потока через ловушку приводит к немедленному резкому возрастанию концентрации примесей в контуре за счет вымывания их из проточной холодной ловушки. К возрастанию концентрации примесей в контуре приводит также увеличение температуры на входе в ловушку.

После замораживания ловушки, накопившей некоторое количество примесей, ее последующий запуск может производиться без выброса примесей в контуре только следующим способом. При открытых вентилях ловушка медленно разогревается. Как только появится расход, включается охлаждение на ловушку. Только такой режим пуска позволил избежать выброса примесей из ловушки. Таким образом холодная проточная ловушка позволяет очищать натрий от окислов вплоть до концентрации, соответствующих насыщений при минимальной температуре ловушки и при соответствующих режимах работы имеет значительную емкость по отношению к примесям (окислам). Ловушки такого типа успешно эксплуатируются на реакторе с натриевым охлаждением. Некоторые недостатки проточной холодной ловушки являются следствием протекающих в ловушках процессов. Так из химической кинетики известно, что наиболее эффективно примеси улавливаются, если выкристаллизация и улавливание примесей происходит в одном месте. В аппаратах химтехнологии стараются не допускать слишком больших скоростей охлаждения, при которых раствор переохлаждается, происходит зарождение центров кристаллизации в объеме и кристаллизация на этих центрах. Появившуюся взвесь твердой фазы гораздо труднее уловить, чем выкристаллизовать эту фазу из молекулярного раствора. К тому же коэффициенты молекулярной диффузии на несколько порядков больше коэффициентов броуновской диффузии взвеси.

Кристаллы взвеси могут иметь форму, в какой-то мере напоминающую снежинки, и осажденный слой такой примеси имеет относительно малую плотность. Осевшая в отстойнике и в объеме фильтрующей насадки взвесь может при увеличении скорости быть выброшена опять в контур.

В проточной холодной ловушке имеется специальная зона охлаждения, в которой снижается температура теплоносителя, раствор становится пересыщенным и примеси выпадают в виде взвеси. Однако они также кристаллизуются и на стенках участков охлаждения, причем не равномерно по длине зоны, а в том месте, где достигнуто необходимое для кристаллизации пересыщение. Это приводит к преждевременному закупориванию проточной ловушки, особенно если концентрация примесей в контуре заметно повышена вследствие аварийного загрязнения.

7. НЕПРЕРЫВНАЯ ОЧИСТКА ТЕПЛОНОСИТЕЛЯ С ПОМОЩЬЮ ДИФФУЗИОННОЙ ХОЛОДНОЙ ЛОВУШКИ

По сравнению с проточными диффузионные ловушки отличаются простотой конструкцией, меньшими размерами и весом, отсутствием необходимости в специальном ответвлении от циркуляционного контура, относительно малой мощностью, требуемой на их охлаждение и значительно меньшей чувствительностью к колебаниям расхода теплоносителя и концентрации примеси в нем.

Диффузионная ловушка представляет собой кусок трубы, приваренный одним концом к циркуляционному трубопроводу и заглушенный с другого конца, который охлаждается. На внутренней поверхности охлаждаемого конца трубы-ловушки выкристаллизовываются из раствора теплоносителя примеси. Новые порции примесей поступают из контура в холодный тупик ловушки посредством молекулярной или турбулентной диффузии.

Существует мнение, изложенное в работе [23], согласно которому диффузионные ловушки имеют малую емкость по отношению к примесям и поэтому не получили распространения.

Авторами доклада [24] были исследованы условия, при которых диффузионные ловушки имеют эффективность, во всяком случае не меньшую, чем проточные ловушки. К параметрам, определяющим эффективность, относятся емкость ловушки по накопляемым примесям, скорость очистки и минимально достижимая концентрация примеси в контуре.

В докладе экспериментально показано, что диффузионные ловушки позволяют организовывать процесс таким образом, что достигается практически полное заполнение холодной ловушки примесями. Примеси кристаллизуются в сплошную и твердую неразмываемую кристаллическую массу, состоящую более чем на 90% из основной удаляемой примеси.

При этом ловушки мало чувствительны к изменениям расхода теплоносителя в линиях, на которых они установлены, не выбрасывают примеси обратно в контур при любом повышении скорости потока теплоносителя. Диффузионные ловушки не закупориваются примесями на входе при любых практически существующих концентрациях примесей на входе в ловушку, в том числе и при концентрациях существенно превышающих концентрацию насыщения, а также при резком изменении концентрации.

На основании теоретического анализа процесса переноса примесей в диффузионной холодной ловушке и экспериментального ее исследования установлено, что для эффективной работы ловушки необходимо, чтобы поле температур "t" по длине ловушки "x" удовлетворяло условию $d^2t/dx^2<0$. *При этом примеси выкристаллизовываются на дне ловушки.* Если это условие не соблюдается, примеси выкристаллизовываются во входном сечении ловушки, закупоривают вход в ловушку и существенно уменьшают ее емкость.

Условие $d^2t/dx^2<0$ обеспечивается автоматически, если охлаждается только нижняя часть ловушки. По мере накопления примесей на дне ловушки необходимо непрерывно или периодически перемещать зону охлаждения ближе к входной части ловушки, т.е. необходимо перемещать сечение с минимальной температурой жидкого состояния теплоносителя вместе с фронтом кристаллического слоя примеси, растущего от дна ловушки.

Опыты по очистке натрия показали, что минимальная концентрация примеси в контуре соответствует концентрации насыщения при минимальной температуре ловушки и составляет в натрии $5 \cdot 10^{-4}$ вес% кислорода и $1 \cdot 10^{-4}$ вес% водорода.

При исследовании гидродинамики диффузионных ловушек, проведенном авторами [24] на натрии и на подкрашенной воде, установлено, что между потоком жидкости в трубопроводе и зоной выкристаллизации в холодной ловушке осуществляется интенсивный конвективный обмен.

Относительная глубина зоны перемешивания пропорциональна логарифму числа Рейнольдса потока теплоносителя в трубопроводе и практически не зависит от соотношения между диаметрами трубопровода и ловушкой. При ламинарном течении жидкости в трубопроводе перемешивание жидкости в изотермической ловушке отсутствует. При изменении числа Re от $2 \cdot 10^3$ до $0{,}25 \cdot 10^5$ глубина зоны интенсивного перемешивания изменяется от 1,5 до 8 диаметров ловушки. Дополнительная турбулизация потока в трубопроводе перед ловушкой путем установки шайбы с отверстием в 0,6 диаметра трубы увеличивает глубины перемешивания в 2 раза при $\mathrm{Re} = 2 \cdot 10^4$.

Так как молекулярная диффузия, термодиффузия и т.п. процессы характеризуются малыми значениями коэффициентов переноса, для эффективной работы диффузионной ловушки необходимо, чтобы в трубопроводе, к которому ловушка подключена, режим течения был турбулентным.

Скорость очистки с помощью диффузионной ловушки достаточно высока. Это обеспечивается турбулентным подносом примесей к зоне выкристаллизации и высокой интенсивностью кристаллизации примесей из молекулярного раствора на кристаллах плотного осадка. Скорость очистки в опытах увеличивается с ростом числа Рейнольдса, однако при росте числа Re сверх $20 \cdot 10^3$ вплоть до $70 \cdot 10^3$ коэффициент скорости очистки практически не изменился.

С помощью холодной диффузионной ловушки осуществлялась одновременная эффективная очистка от кислорода, водорода и продуктов коррозии и эррозии. В одном из экспериментов по очистке намеренно сильно загрязненного неметаллическими примесями теплоносителя было обнаружено, что на дне ловушки концентрация осажденного железа превышает 10 вес% состава осажденной примеси.

Таким образом холодная диффузионная ловушка является высокоэффективным устройством для очистки теплоносителя.

В заключение следует отметить, что в настоящее время имеются основные сведения и методы, необходимые для создания устройств, обеспечивающих контроль и очистку циркулирующих жидкометаллических теплоносителей. При создании устройств для пробоотбора, контроля и очистки теплоносителя необходимо знать форму существования данной примеси и законы ее распределения.

ЛИТЕРАТУРА

[1] СУББОТИН В.И., ИВАНОВСКИЙ М.Н., ОРЛОВ Ю.И. Контактное термическое сопротивление при охлаждении каналов жидкими металлами. Ж. "Теплофизика высоких температур" (в печати).

[2] СУББОТИН В.И., ИВАНОВСКИЙ М.Н. Минимальные значения коэффициентов теплоотдачи к жидким металлам. Доклад на симпозиуме в Гренобле (Франция), ноябрь 1966 г (в печати).

[3] ГУРИНСКИЙ Т.Х. и др. Коррозия в жидкометалличеких системах. Доклад США 28R/244 на III конференции по мирному использованию атомной энергии. Женева, 1964 г. Proc. 3rd UN Int. Conf. PUAE, 9 (1965) 550.

[4] МИРСКИЙ Л.М. Процессы диффузии в сплавах. Оборонгиз, М., 1959.

[5] АРНОЛЬДОВ М.Н., ИВАНОВСКИЙ М.Н., СУББОТИН В.И. Состояние примесей в цезии, используемом в термоионном преобразователе. Ж. "Теплофизика высоких температур" (в печати).

[6] МЮЛЛЕР, БЕССОН, C.r. Lebd. Seanc. Acacb. Sci., Paris, 247, 25 (1958) 2370.

[7] ИВАНОВСКИЙ М.Н., КОЗЛОВ Ф.А. Термодинамический расчет реакции натрия с водой для парогенератора типа натрий-вода. Журнал "Атомная энергия", 17, (1964) 406.

[8] МИТКЕВИЧ Э.М., ШИХОВ Б.А. Журнал "Прикладная химия", №3 (1966).

[9] KELLY H.J. et al., Nucl. Sci. Abstr. 19, 20 (1965) 39157.

[10] HOBART E.W. et al., Nucl. Applicat., 1 5 (1965).

[11] АРНОЛЬДОВ М.Н., ИВАНОВСКИЙ М.Н., СУББОТИН В.И., ШМАТКО Б.А. Зависимость удельного электросопротивления щелочных металлов от содержания примесей. Доклад на конференции в г.Новосибирске, 1966 г. (в печати).

[12] ИВАНОВСКИЙ М.Н., МИЛОВАНОВ Ю.В., СОРОКИН В.П., СУББОТИН В.И., ЧУЛКОВ Б.А. Теплообмен при пленочной и капельной конденсации металлов. Доклад на конференции в Гренобле (Франция), ноябрь 1966 (в печати).

[13] СУББОТИН В.И., ИВАНОВСКИЙ М.Н., СОРОКИН В.П., БАКУЛИН Н.В. Интенсивность теплообмена при пленочной конденсации натриевого пара. Журнал "Теплофизика высоких температур" (в печати).

[14] ИВАНОВСКИЙ М.Н., СУББОТИН В.И., ОРЛОВ Ю.И. Теплопроводность пристенного слоя потока жидких металлов. Доклад на конференции в Новосибирске, июль 1966 (в печати).

[15] ИВАНОВСКИЙ М.Н., ОРЛОВ Ю.И., СУББОТИН В.И. Исследование распределения взвешенных примесей в потоке. Доклад на конференции МАГАТЭ, Австрия, ноябрь 1966. См. в данном издании SM-85/52.

[16] СУББОТИН В.И., КОЗЛОВ Ф.А., КУЗНЕЦОВ Э.К., ИВАНОВСКИЙ М.Н. Контроль за содержанием кислорода и водорода в натрии. Доклад на конференции МАГАТЭ, Австрия, ноябрь 1966. См. в данном издании SM-85/49.

[17] BLAKE R.N., Nucleonics, 19 5 (1961).

[18] CLAXTON K., J. nucl. Energy, Part A/B, 19 11 (1965).

[19] КОЗЛОВ Ф.А. и др. "Теплофизика высоких температур", 3, 1 (1965).

[20] АРНОЛЬДОВ М.Н., ИВАНОВСКИЙ М.Н., СУББОТИН В.И., ШМАТКО Б.А. Исследование возможностей контроля примесей в жидкометаллических теплоносителях путем измерения электросопротивления. Доклад на конференции МАГАТЭ, Австрия, ноябрь 1966 г. См. в данном издании SM-85/46.

[21] СУББОТИН В.И., КОЗЛОВ Ф.А. Осаждение окислов из потока натрия. Доклад на конференции МАГАТЭ, Австрия, 1966. См. в данном издании SM-85/48.

[22] ИВАНОВСКИЙ М.Н., АРНОЛЬДОВ М.Н., ШМАТКО Б.А. О кинетике выкристаллизации примеси азота из расплавленного лития. Журнал "Теплофизика высоких температур" (в печати).

[23] ПАРКИНС В. Экспериментальный натриевый реактор. Доклад №499 (США) на I Женевской конференции по мирному использованию атомной энергии, 1956 г. Proc. UN Int. Conf. PUAE, 3 (1956) 295.

[24] АРНОЛЬДОВ М.Н., ИВАНОВСКИЙ М.Н., СУББОТИН В.И., ШМАТКО Б.А. Исследование процесса очистки натрия с помощью высокоэффективных холодных ловушек диффузионного типа. Доклад на конференции МАГАТЭ, Австрия, ноябрь 1966 г. См. в данном издании SM-85/47.

DISCUSSION

C. TYZACK: What was the form of the iron found in your diffusion cold traps? Was it present as metallic iron, as an iron-sodium-oxide complex, or as a mixture of both?

M.N. IVANOVSKY: I cannot reply to that, unfortunately, because only the quantity of iron was determined, not the form.

L.P. VAUTREY: You indicated that you could get the same degree of purity with the diffusion cold traps as with circulation cold traps. Could you perhaps give us a somewhat more detailed comparison of these two devices, particularly as regards the rate of purification, i.e. the evolution of purity when you start with a certain degree of oxygen contamination?

M.N. IVANOVSKY: In comparable flow conditions there is not a great deal of difference between the purification rates obtained with the two traps. The rate of purification can become especially important in accident conditions, when serious contamination of the liquid-metal coolant ensues. In these circumstances the circulation trap as a rule becomes plugged in the cooling zone or in the recuperator; the diffusion trap on the other hand purifies more rapidly as the concentration of impurity rises, and does not become plugged even when the coolant is seriously contaminated.

CORROSION OF STEELS AND METAL ALLOYS
(Session II)

CORROSION DU VANADIUM ET DE SES ALLIAGES DANS LE SODIUM LIQUIDE

L. CHAMPEIX, R. DARRAS ET J. SANNIER
CEA, CENTRE D'ETUDES NUCLEAIRES DE SACLAY, FRANCE

Abstract — Résumé

CORROSION OF VANADIUM AND VANADIUM ALLOYS IN LIQUID SODIUM. The corrosion of vanadium and its binary alloys V-20% Ti, V-10% Al, V-6% Cr, V-5% Nb, V-1.5% Zr and V-0.8% Si has been studied at 600° C under experimental conditions representative of the conditions liable to be encountered in a fast neutron reactor. The circuits were fitted with electromagnetic pumps providing a sodium flow of about 2 m/s as well as bypass clean-up systems utilizing cold or hot traps.

When sodium purification is performed by hot trap the positive and negative variations of weight are invariably very slight - about 0.1 mg/cm^2 month. Neither the structure nor the hardness of the alloys are modified appreciably. A slight surface hardening does however occur in the case of the titanium and zirconium alloys.

In the case of cold trap sodium purification the vanadium suffers considerable weight losses (about 7 mg/cm^2 month) as a result of the erosion of oxidation products by the flow of sodium.

A straight line representing weight losses as a function of time does not pass through the point of origin. It is probable that the metal is initially enriched in oxygen, and that this results in lower weight losses at the start of the exposure period and favours the subsequent formation of oxidation products leading to accelerated metal degradation. In the non-alloyed vanadium very pronounced core hardening occurs.

Of the additives investigated titanium and zirconium do not seem very favourable as the weight losses for the relevant alloys are at least equal to those occurring with non-alloyed vanadium.

Aluminium and molybdenum additives, which give rise to increases in weight, seem better. However, considerable surface hardening occurs with the V-Al alloy whereas a considerable increase occurs in the core hardness of the V-Mo alloy.

On the basis of weight losses it would seem that silicon, niobium and chromium reduce the susceptibility of vanadium to oxidization by a factor of 3; however, these substances also undergo considerable core hardening. Chromium can nevertheless be considered as one of the most valuable additives since it forms a relatively adhesive oxide layer on the corresponding alloys which could result in a long-term slowing up of corrosion kinetics.

CORROSION DU VANADIUM ET DE SES ALLIAGES DANS LE SODIUM LIQUIDE. La corrosion du vanadium et des alliages binaires V-20% Ti, V-10% Al, V-6% Cr, V-5% Nb, V-1,5% Zr et V-0,8% Si a été étudiée à 600°C dans des conditions expérimentales représentatives de celles susceptibles de régner dans un réacteur à neutrons rapides: les circuits utilisés disposaient de pompes électromagnétiques assurant un débit du sodium d'environ 2 m/s, ainsi que de systèmes de purification par piège froid ou piège chaud placés en dérivation.

Dans le cas d'une purification du sodium par piège chaud, les variations de poids, positives ou négatives, restent très faibles dans tous les cas: environ 0,1 mg/cm^2.mois. Les alliages ne subissent aucune modification notable, ni quant à leur structure, ni quant à leur dureté. Seuls les alliages au titane et au zirconium manifestent un léger durcissement superficiel.

Par contre, dans le cas d'une purification du sodium par piège froid, le vanadium subit des pertes de poids importantes (environ 7 mg/cm^2 . mois) dues à l'érosion des produits d'oxydation par le courant de sodium.

La droite représentative des pertes de poids en fonction du temps ne passe pas par l'origine. Il est probable que le métal s'enrichit initialement en oxygène, ce qui se traduit, d'une part par des pertes de poids plus faibles au début de l'exposition et, d'autre part favorise la formation ultérieure de produits d'oxydation, accélérant ainsi la dégradation du métal. D'autre part, le vanadium non allié manifeste un durcissement à cœur très important.

Parmi les éléments d'addition étudiés, le titane et le zirconium se révèlent plutôt défavorables, les pertes de poids relatives aux alliages correspondants étant au moins égales à celles du vanadium non allié.

Les additions d'aluminium et de molybdène, qui conduisent à des augmentations de poids, semblent plus favorables; toutefois, l'alliage V-Al subit un durcissement superficiel important, alors que l'alliage V-Mo voit sa dureté à cœur augmenter notablement.

Le silicium, le niobium et le chrome diminuent d'un facteur 3 la susceptibilité du vanadium à l'oxydation, si on se réfère aux pertes de poids; mais ils subissent également une augmentation importante de dureté à cœur. Le chrome peut néanmoins être considéré comme un élément d'addition des plus intéressants: il se forme en effet, sur les alliages correspondants, une couche d'oxyde relativement adhérente, qui pourrait conduire à un ralentissement de la cinétique de corrosion à long terme.

I - INTRODUCTION

Dans le domaine nucléaire, et en particulier dans le contexte de la filière des réacteurs à neutrons rapides, le vanadium possède certains avantages potentiels. En effet, il présente d'une part de bonnes caractéristiques mécaniques à chaud, propres aux métaux réfractaires, et d'autre part des propriétés neutroniques favorables ; ainsi sa section de capture pour les neutrons rapides (réaction n, α) se limite à 0,035 millibarn, en regard de 0,45 millibarn pour le fer par exemple [1] .

Malheureusement, le vanadium non allié, comme le niobium [2], montre un taux de corrosion inacceptable dans le sodium normalement purifié par piège froid. La corrosion de ces deux métaux dans ces conditions repose d'ailleurs sur un processus d'oxydation, dont la vitesse dépend essentiellement de la teneur en oxygène du sodium et du débit de ce dernier; en effet, l'oxyde formé étant peu adhérent, il ne se constitue pas de couche protectrice capable de limiter la corrosion.

Précisément, DAVIS et DRAYCOTT [3] indiquent que seule une teneur en oxygène inférieure à 5 ppm dans le sodium permet de maintenir un taux de corrosion admissible en pratique ; toutefois les pertes de poids constatées en présence de sodium purifié seulement par piège froid seraient nettement plus faibles pour le vanadium que pour le niobium [4] [5] .

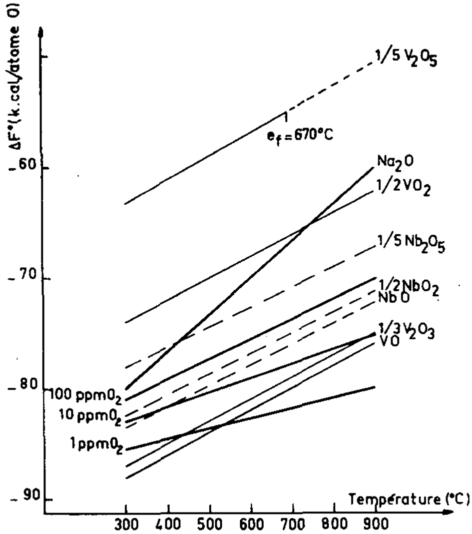

FIG. 1. Variations d'énergie libre de formation des oxydes de vanadium et de niobium, comparées à celles relatives à l'oxyde Na_2O et à diverses activités de l'oxygène en solution dans le sodium

La comparaison des valeurs des changements d'énergie libre de formation des oxydes correspondants n'explique pas cette différence (fig. 1). Mais il convient de noter que la "tendance" à former des oxydes inférieurs (VO et V_2O_3) est plus forte pour le vanadium que pour le niobium. D'autre part la formation de l'oxyde V_2O_5 ne serait pas possible, le milieu étant trop peu oxydant, ce qui constitue une circonstance favorable, étant donné la température de fusion relativement faible de cet oxyde (670°C).

En ce qui concerne les alliages à base de vanadium, des travaux ont été effectués aux Laboratoires d'ARGONNE (Etats-Unis), à partir de matériaux élaborés par Armour Research Foundation. Certains alliages contenant du titane, du chrome ou du molybdène ont été cités comme résistant mieux que le vanadium à la corrosion dans le sodium [6] . Des études sur de tels matériaux sont également en cours au Kernforchungszentrum de KARLSRUHE (Allemagne Fédérale).

De notre côté, nous avons entrepris une étude visant à déterminer ou à préciser l'influence de divers éléments d'addition sur la résistance du vanadium à la corrosion par le sodium liquide. A cet effet, des essais systématiques ont été effectués à 600°C sur les matériaux suivants :

- vanadium non allié
- alliages vanadium-aluminium à 10 % Al (en poids)
- alliages vanadium-silicium à 0,5 % Si
- alliages vanadium-titane à 20 % Ti
- alliages vanadium-chrome à 6 % Cr
- alliages vanadium-zirconium à 1,5 % Zr
- alliages vanadium-niobium à 5 % Nb
- alliages vanadium-molybdène à 5 % Mo

Ces alliages ont été élaborés à four à arc, sous forme de boutons,par la Société Imphy-Kuhlmann. Ces derniers étaient ensuite forgés à 1 100°C, puis laminés à froid en largets de 1 mm d'épaisseur, qui subissaient finalement un recuit sous vide à 1 000°C pendant 1 heure.

Le présent texte regroupe les premiers résultats de cette étude, qui constituent une base d'orientation pour un développement ultérieur.

II - CONDITIONS OPERATOIRES

Les essais ont été réalisés dans deux circuits munis de pompes électromagnétiques, la vitesse du sodium au niveau des échantillons étant de l'ordre de 1,5 mètre par seconde. La purification du sodium était assurée soit par un piège froid soit par un piège chaud,placés sur des circuits dérivés. La température du piège froid était maintenue à 105°C ; le piège chaud, constitué par des copeaux de zirconium, était porté à 650°C.

Par ailleurs, en vue de permettre la détermination des cinétiques de corrosion, les deux circuits utilisés disposaient chacun d'une chambre d'essai pouvant recevoir trois séries d'échantillons. Un sas autorisait l'introduction ou la sortie de chaque série indépendamment des autres.

Les échantillons étaient constitués par des plaquettes présentant une surface totale d'environ 7 cm^2. Leurs variations de poids étaient déterminées après lavages àl'alcool puis à l'eau, dans le but de les débarrasser du sodium résiduel et des produits superficiels non adhérents.

III - RESULTATS

Les comportements des divers matériaux dans le milieu considéré sont essentiellement caractérisés par les mesures gravimétriques d'une part, et des observations micrographiques d'autre part.

Les variations de poids sont évidemment faciles à mesurer et à comparer ; il convient toutefois d'être prudent dans leur exploitation . En effet, dans le cas du vanadium ou de ses alliages, elles résultent toujours de plusieurs processus dont les effets peuvent se compenser, au moins en partie : d'une part les processus de dissolution dans le sodium et surtout d'entraînement d'oxyde non adhérent, d'autre part la fixation d'oxygène, avec formation d'oxydes plus ou moins bien déterminés ou simplement dissolution dans la phase métallique. Par ailleurs, l'importance relative de chacun de ces phénomènes varie souvent avec le temps, comme le montre la figure 2 concernant des échantillons de vanadium non allié : l'allure de cette courbe semble bien indiquer que les variations de poids négatives et sensiblement proportionnelles au temps n'apparaissent qu'après une période initiale durant laquelle elles seraient quasiment nulles ou plus probablement de signe contraire.

Il s'ensuit que, sur la seule base des mesures gravimétriques, les comparaisons entre les divers alliages n'ont qu'une signification qualitative. Compte tenu de cette réserve, les mesures gravimétriques constituent néanmoins des critères qu'il convient de prendre en considération, mais qui doivent être complétés par d'autres observations plus détaillées et plus spécifiques.

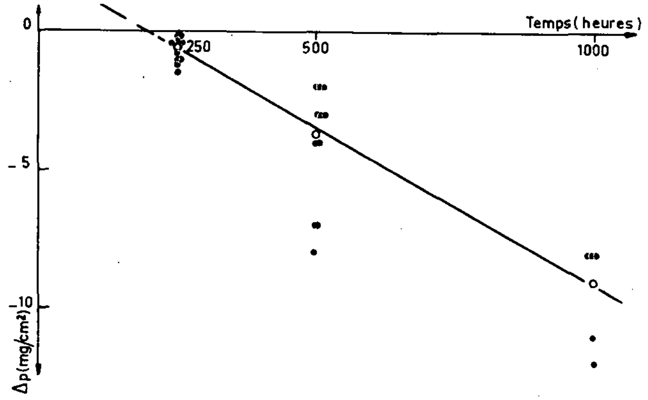

FIG.2. Variation de poids en fonction du temps du vanadium non allié exposé à 600°C dans le sodium purifié par piège froid

1. Mesures gravimétriques

Dans le cas d'une purification du sodium par piège chaud, les variations de poids de tous les matériaux étudiés sont très faibles, à la limite de sensibilité des mesures (tableau I). Par contre, dans le cas d'une purification par piège froid, elles sont toujours notables et le plus souvent négatives.

TABLEAU I. VARIATIONS DE POIDS DE DIVERS ALLIAGES DE VANADIUM, APRES SEJOUR PENDANT 1000 h DANS LE SODIUM DYNAMIQUE PURIFIE PAR PIEGE CHAUD

Métal ou alliage	Variations de poids (mg/cm^2)
V non allié	+ 0,2
V-10 % Al	- 0,02
V-0,5 % Si	+ 0,1
V-20 % Ti	+ 0,2
V-6 % Cr	+ 0,1
V-1,5 % Zr	+ 0,1
V-5 % Nb	+ 0,2
V-5 % Mo	- 0,02

Deux séries d'essais ont été effectuées en utilisant cette dernière technique de purification ; malheureusement, en ce qui concerne la première série, par suite du contrôle imparfait de la teneur en oxygène du sodium, la corrosion s'est révélée anormalement élevée ; de sorte que les résultats des deux séries doivent être considérés séparément.

Les résultats relatifs à la première série sont représentés sur la figure 3 : après une période initiale d'environ 250 heures, qui correspond très probablement à la présence d'une concentration anorma-

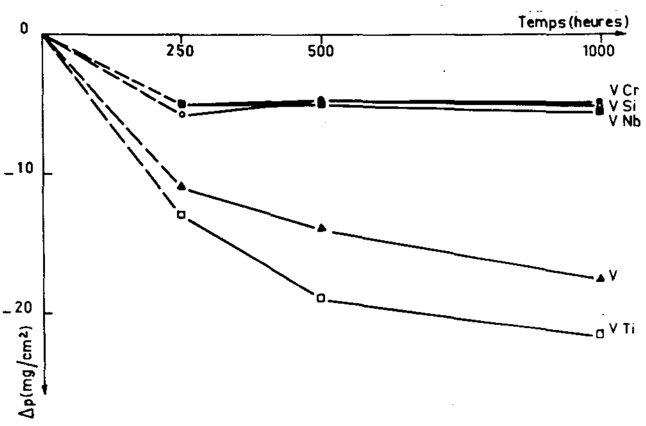

FIG. 3. Variation de poids en fonction du temps d'alliages de vanadium exposés à 600°C dans le sodium purifié par piège froid ($1^{ère}$ série d'essais, où la concentration en oxygène dans le sodium était plus élevée pendant les 250 premières heures)

lement élevée en oxygène dans le sodium, les alliages V-Cr, V-Si et V-Nb ne présentent plus que des variations de poids négligeables, alors que l'alliage V-Ti continue au contraire à subir des pertes de poids notables, comme le vanadium non allié.

Les résultats relatifs à la seconde série, représentés sur la figure 4, confirment les pertes de poids importantes subies par l'alliage V-Ti et, à un degré moindre, par le vanadium non allié. L'alliage V-Zr présente un comportement analogue à celui du vanadium non allié. Par contre, les alliages V-Al et V-Mo subissent des augmentations de poids, d'ailleurs croissantes jusqu'à 1 000 heures.

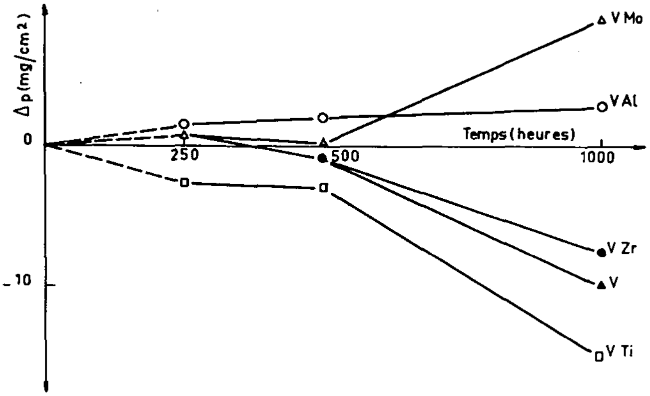

FIG.4. Variation de poids en fonction du temps d'alliages de vanadium exposés à 600°C dans le sodium purifié par piège froid (2^{e} série d'essais)

Ainsi, du seul point de vue gravimétrique, les alliages considérés peuvent être classés en trois groupes :

- les alliages au titane et au zirconium subissent des pertes de poids supérieures ou équivalentes à celles du vanadium non allié,

- les alliages au silicium, au chrome et au niobium sont nettement moins affectés que le vanadium non allié,

- les alliages à l'aluminium et au molybdène présentent au contraire des augmentations de poids.

2. Examens micrographiques

Les examens micrographiques en coupe, complétés par des mesures de microdureté, fournissent des précisions intéressantes quant à la nature des mécanismes mis en jeu.

Dans le cas des échantillons ayant séjourné dans le sodium purifié par piège chaud, le caractère très limité de la corrosion se confirme : il n'apparaît pas de nouvelle phase, telle qu'une couche superficielle distincte, et la dureté à coeur ne subit aucune modification par rapport à sa valeur initiale. Toutefois les alliages V-Ti et V-Zr accusent un léger durcissement strictement superficiel.

Par contre, dans le cas des échantillons exposés dans le sodium purifié par piège froid, les variations de dureté à coeur deviennent en général sensibles, et doivent de toute évidence correspondre à un enrichissement en oxygène ; d'autre part, sur certains alliages, il apparaît des zones superficielles perturbées.

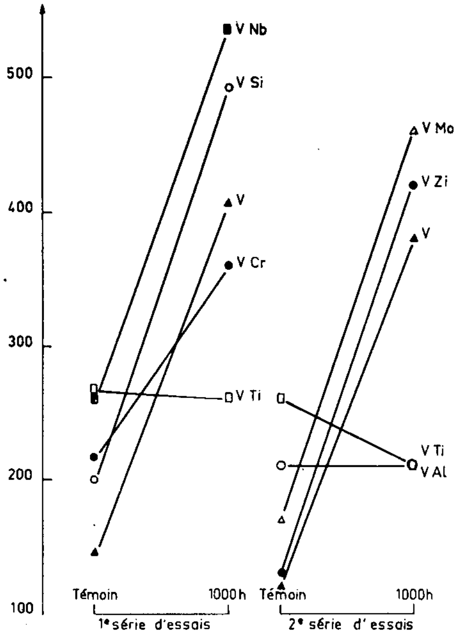

FIG. 5. Microdureté Vickers (sous charge de 50 g) de divers alliages de vanadium avant et après séjour de 1000 h à 600°C dans le sodium purifié par piège froid

FIG. 6. Examen micrographique en coupe de l'alliage V-5% Cr, après exposition à 600°C pendant 1000 h dans le sodium purifié par piège froid (X 355)

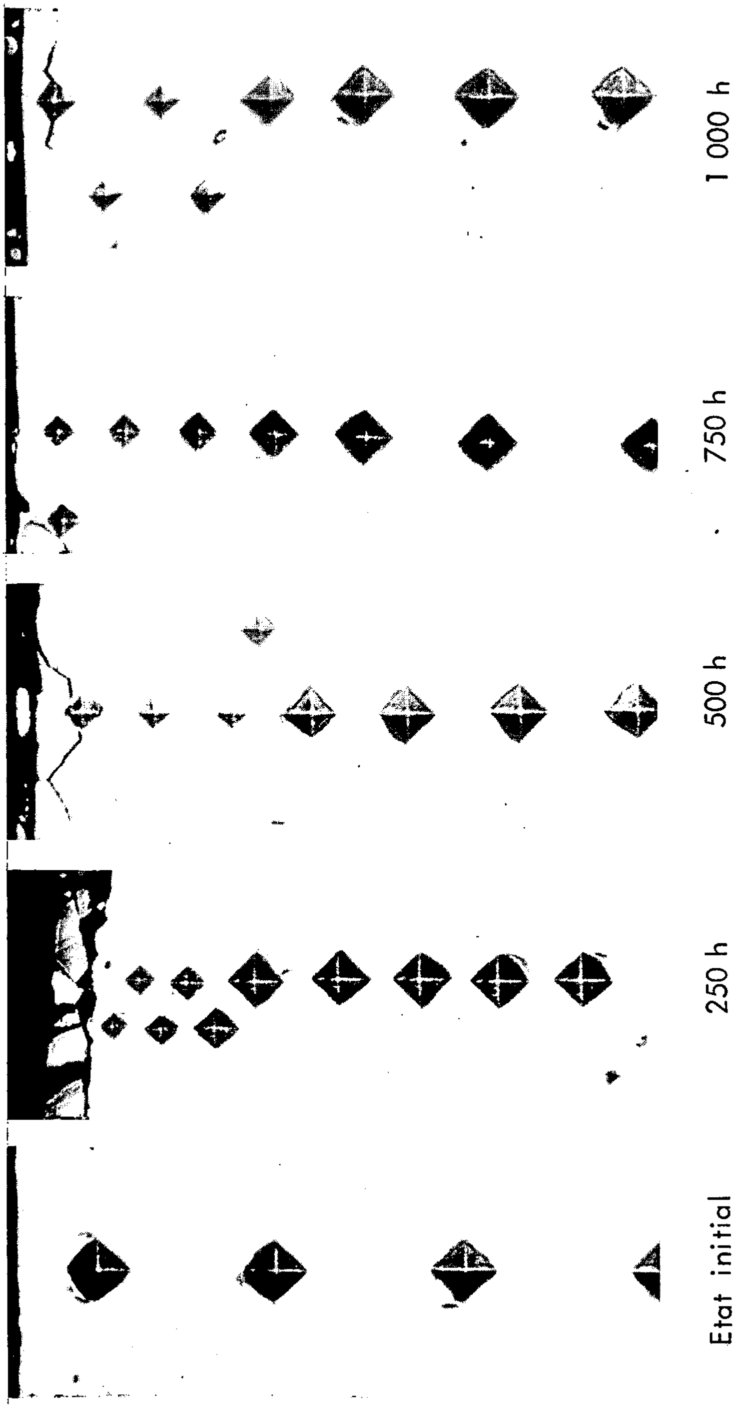

FIG.7. Evolution de la dureté de l'alliage V-10% Al en fonction du temps de traitement à 600°C dans le sodium purifié par piège froid.
Empreintes de microdureté sous charge de 50 g (X 425)

Ainsi, la figure 5 permet de comparer les mesures de microdureté Vickers sous charge de 50 g, effectuées sur témoins d'une part et sur échantillons de même nature traités pendant 1 000 heures d'autre part. On constate un durcissement important à coeur pour le vanadium non allié, ainsi que pour les alliages V-Si, V-Nb, V-Mo et V-Zr ; ce durcissement est plus faible pour l'alliage V-Cr, alors que les alliages V-Ti et V-Al conservent pratiquement leur dureté initiale.

Par ailleurs, au voisinage de la surface, des couches perturbées apparaissent sur les trois alliages V-Cr, V-Ti et V-Al ; toutefois elles présentent des caractères particuliers pour chacun de ces alliages :

a) l'alliage V-Cr est recouvert d'une couche oxydée adhérente et relativement régulière (fig. 6) ; son épaisseur, qui est d'environ 5 microns au bout de 250 heures, passe à 15 microns après 1 000 heures d'exposition. Dans cette couche, la diffraction de rayons X n'a pas mis en évidence d'oxyde défini, mais seulement la phase bêta (ordonnée) du diagramme V-VO. Il n'est d'ailleurs pas exclu que cette phase renferme du chrome en solution.

b) les alliages V-Al et V-Ti, de leur côté, ne montrent pas de couche d'oxyde proprement dite, mais présentent chacun une zone métallique superficielle extrêmement dure (de 800 à 1 200 Vickers) (fig. 7 et 8). L'épaisseur de ces zones perturbées, évidemment enrichies en oxygène, augmente avec le temps, comme le montre le tableau II. Cependant les deux phases correspondantes ont des morphologies sensiblement différentes (fig. 9) : sur l'alliage au titane, la zone considérée présente un caractère friable, ce qui explique les pertes de poids observées précédemment, tandis que sur l'alliage à l'aluminium elle reste cohérente, également en accord avec les augmentations de poids alors enregistrées.

TABLEAU II. VARIATION DE L'EPAISSEUR DE LA ZONE SUPERFICIELLE DURCIE FORMEE SUR LES ALLIAGES V-Al ET V-Ti, EN FONCTION DE LEUR TEMPS DE SEJOUR DANS LE SODIUM EPURE PAR PIEGE FROID

Temps (heures)	Epaisseur de la zone durcie (microns)	
	V-10 % Al	V-20 % Ti
250	50	30
500	70	-
750	80	-
1 000	80	70

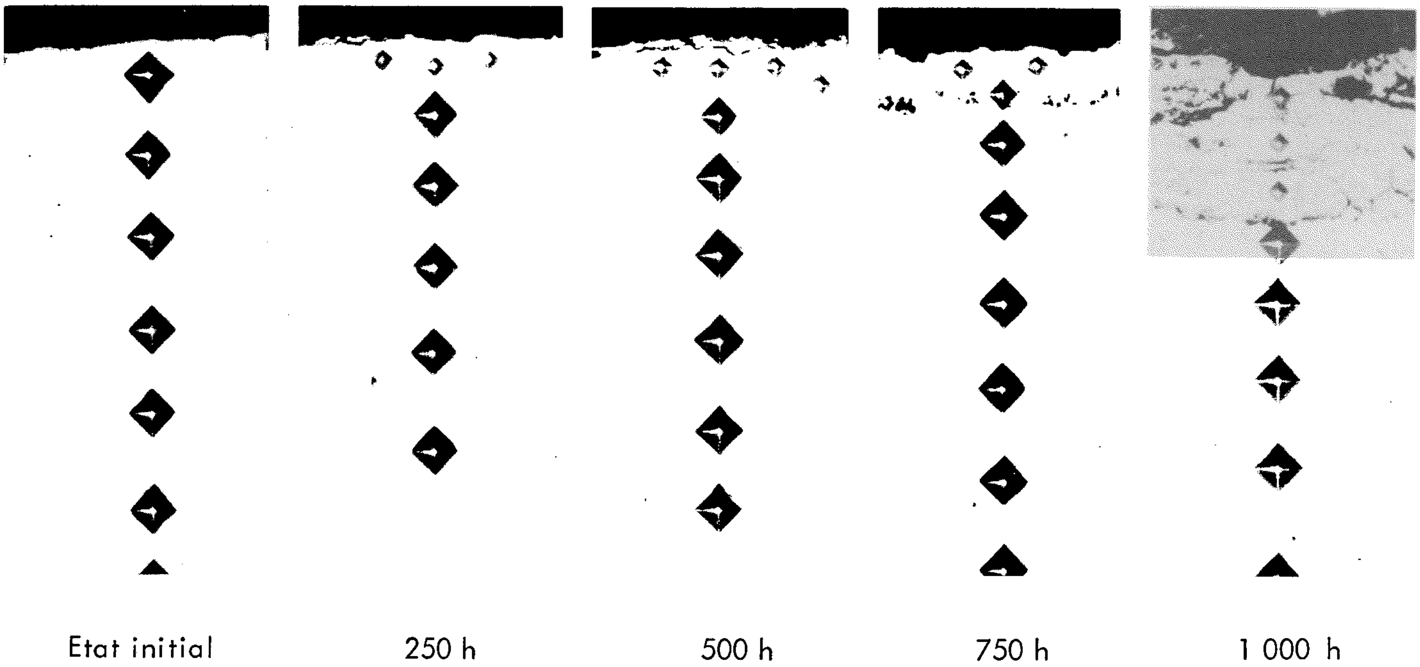

FIG. 8. Evolution de la dureté de l'alliage V-20% Ti en fonction du temps de traitement à 600°C dans le sodium purifié par piège froid.
Empreintes de microdureté sous charge de 50 g (X 355)

I

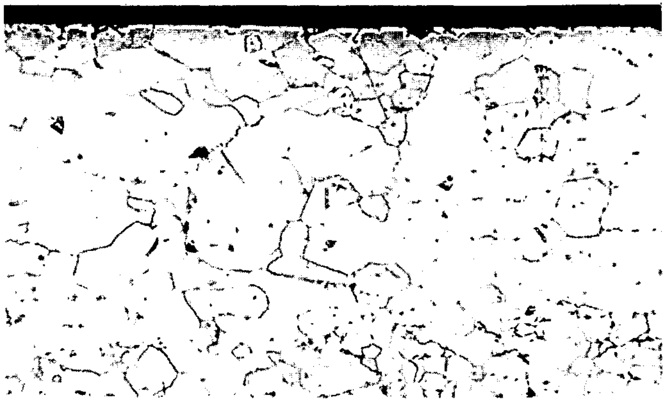

II

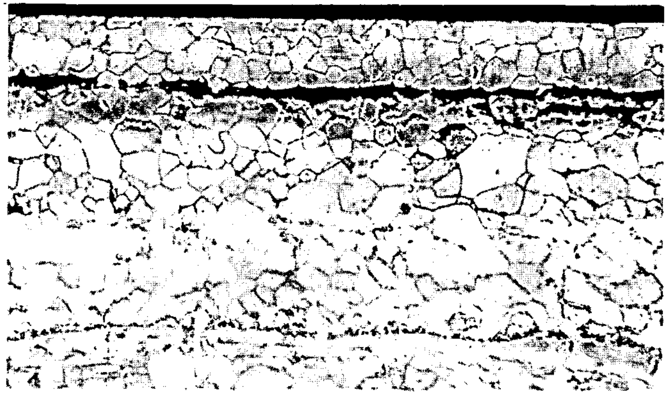

III

FIG. 9. Examen micrographique en coupe de l'alliage V-10% Al, attaque chimique au mélange glycérine (60%), acide fluorhydrique (20%), acide nitrique (20%). (X 180):

I Etat initial

II Après exposition pendant 1000 h à 600°C dans le sodium purifié par piège chaud

III Après exposition pendant 1000 h à 600°C dans le sodium purifié par piège froid

I

II

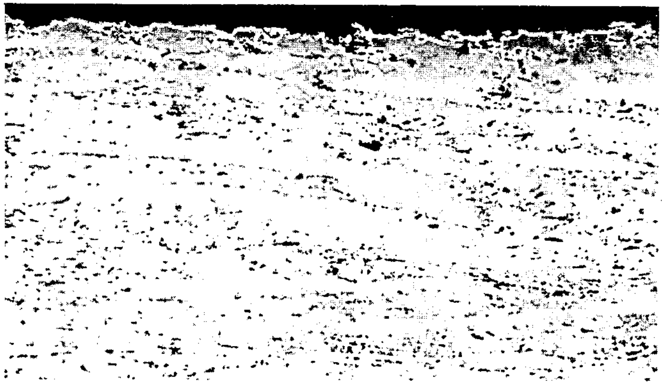

III

FIG. 10. Examen micrographique en coupe de l'alliage V-1,5% Zr (X180):

I Etat initial

II Après exposition pendant 1000 h à 600°C dans le sodium purifié par piège chaud

III Après exposition pendant 1000 h à 600°C dans le sodium purifié par piège froid

Enfin, et d'une manière générale, il n'a pas été relevé de corrosion intergranulaire, ni de modification notable de structure à coeur, éventuellement dues au séjour dans le sodium. En particulier les hétérogénéités observées, notamment quant aux dimensions des grains, préexistaient dans les états initiaux. On note seulement, pour la plupart des alliages, une certaine "organisation" de la structure, que l'on doit simplement attribuer au traitement thermique prolongé subi par les échantillons au cours des essais de corrosion. En effet, les conditions du recuit systématique préalable, soit une heure à 1 000°C sous vide, sont probablement insuffisantes pour stabiliser définitivement les structures (fig. 10 et 11).

IV - DISCUSSION

Les diverses observations qui viennent d'être relatées appellent quelques commentaires, d'une part quant à l'influence de la teneur en zirconium et le titane, seul le zirconium ne provoque pas la formation d'une zone superficielle distincte, susceptible de limiter la diffusion de l'oxygène. Cet élément, dont l'alliage subit un durcissement à coeur aussi important que le vanadium non allié, ne paraît donc avoir aucun rôle favorable : bien au contraire, sa présence risque plutôt d'augmenter la sensibilité du vanadium à l'enrichissement en oxygène.

Le titane et l'aluminium s'opposent au durcissement à coeur, en donnant naissance à une zone métallique superficielle très dure. Mais si cette zone apparaît relativement adhérente et compacte, bien que fragile, dans le cas de l'alliage à l'aluminium, elle se révèle friable et ne paraît pas pouvoir jouer de rôle protecteur efficace en ce qui concerne l'alliage au titane, comme le confirment d'ailleurs les pertes de poids importantes subies par cet alliage.

Le titane qui, par ailleurs, a un effet bénéfique sur l'aptitude à la mise en forme, ne peut donc être considéré comme un élément d'addition favorable du point de vue de la résistance à la corrosion. Si l'on désirait néanmoins conserver cette addition pour des raisons métallurgiques, il conviendrait donc d'envisager des alliages au moins ternaires.

Le rôle de l'aluminium est à peu près opposé ; s'il peut, dans une certaine mesure, être considéré comme un élément inhibiteur de la corrosion, par contre les mauvaises propriétés mécaniques de l'alliage V-10 % Al semblent exclure son utilisation pratique. Cette addition d'aluminium ne doit donc pouvoir être envisagée qu'en proportion relativement faible, et notamment sous forme de tiers élément dans un alliage binaire qui possèderait des propriétés mécaniques favorables, mais serait encore trop oxydable.

Parmi les éléments présentant, vis-à-vis de l'oxygène, une affinité équivalente ou inférieure à celle du vanadium, le chrome paraît occuper une position privilégiée : en effet, il se forme, sur l'alliage correspondant, une couche oxydée relativement adhérente et d'une dureté voisine de celle de la matrice, qui pourrait conduire à un ralentissement de la vitesse de corrosion à long terme.

I

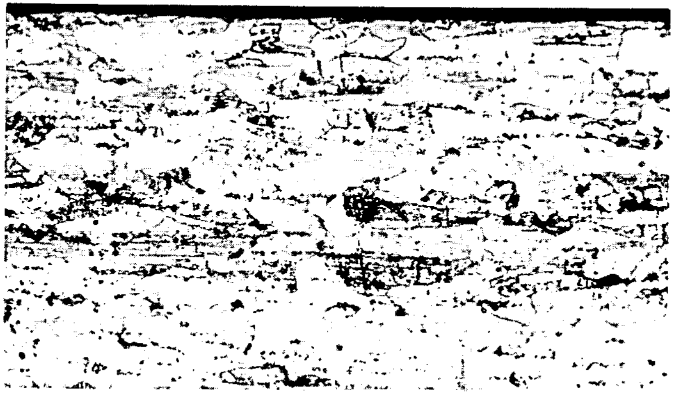

II

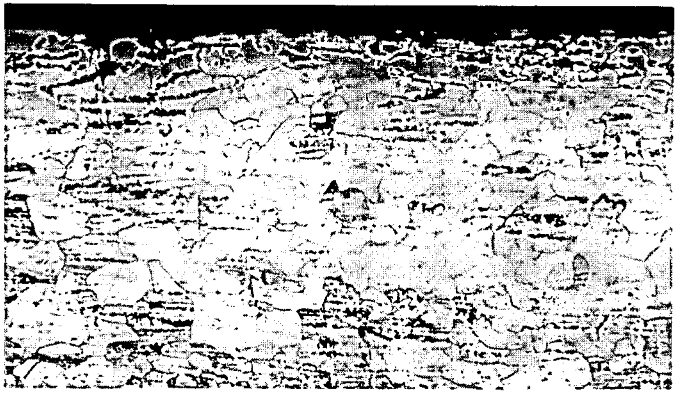

III

FIG. 11. Examen micrographique en coupe de l'alliage V-5% Mo (X180):

I Etat initial

II Après exposition pendant 1000 h à 600°C dans le sodium purifié par piège chaud

III Après exposition pendant 1000 h à 600°C dans le sodium purifié par piège froid

Enfin, les alliages au molybdène, au niobium et au silicium manifestent des comportements assez voisins : en particulier, ils apparaissent moins sensibles à la corrosion que le vanadium non allié, mais ne développent aucune couche d'oxyde superficielle, et subissent tous un durcissement notable à coeur. Il s'avère en fait difficile d'émettre un jugement relativement sûr quant à l'effet de ces dernières additions, vu les résultats trop restreints actuellement disponibles. Les formules au molybdène pourraient peut-être bénéficier d'un léger avantage, en raison de leur tendance à augmenter de poids, contrairement aux deux autres formules, ce qui laisse supposer que les phénomènes de dissolution ou d'entraînement des produits d'oxydation sont atténués par cette addition.

oxygène du sodium, et d'autre part quant au rôle des divers éléments introduits dans le vanadium.

1. En vue de préciser le mode d'action du piège chaud dans l'amélioration de la résistance à la corrosion du vanadium et de ses alliages en présence de sodium, des analyses d'oxygène ont été effectuées par la méthode d'amalgamation sur des échantillons prélevés à divers stades des essais. Leurs résultats sont rassemblés dans le tableau III.

TABLEAU III. ANALYSES D'OXYGENE DANS LE SODIUM

Conditions de purification du sodium	Origine du prélèvement	Teneur en oxygène (ppm)	
		Valeurs obtenues	Moyenne
Piège froid	Au début de la 2ème série d'essais	5-7-8-9	7
Piège froid	A la fin de la 2ème série d'essais	7-10-10-10	9
Piège chaud	Au début de l'essai	3-4-4-6-7-8	5

On constate d'une part une reproductibilité satisfaisante des divers résultats relatifs à chaque échantillon de sodium, ce qui peut être considéré comme un indice de la validité des techniques de prélèvement et d'analyse, et d'autre part une différence peu significative entre les teneurs en oxygène correspondant aux deux types de purification du sodium, c'est-à-dire par piège chaud et par piège froid.

Ainsi, comme cela avait été déjà observé dans le cas du niobium [2], la différence importante de comportement du vanadium et de ses alliages suivant le mode de purification du métal liquide ne se reflète pas nettement dans les résultats des dosages d'oxygène. L'existence d'une erreur systématique inhérente à la méthode d'analyse étant hautement improbable [7], il semble donc permis de penser que le mécanisme d'action du piège chaud ne consiste pas nécessairement en une simple fixation quantitative de l'oxygène par le zirconium utilisé dans ce piège. Il se pourrait que l'activité de l'oxygène se trouve seulement diminuée -jusqu'à un seuil inférieur où le vanadium devient "inoxydable" -soit à la suite d'une fixation partielle sur le zirconium du piège chaud, soit en raison de la formation dans le sodium de composés solubles du type zirconate, les deux phénomènes pouvant du reste intervenir simultanément.

D'ailleurs la subsistance de traces d'oxygène dans le sodium purifié par piège chaud est confirmée par le durcissement superficiel des alliages V-Ti et V-Zr, signalé plus haut.

2. En ce qui concerne la comparaison entre les comportements des divers alliages de vanadium considérés, c'est-à-dire l'influence des divers éléments d'addition correspondants, il est certainement prématuré de tirer des conclusions définitives. En effet, le nombre restreint des essais effectués, de même que l'anomalie constatée dans le déroulement de la première série d'essais avec piège froid, limitent les possibilités de recoupement. Quelques faits précis se dégagent cependant dès maintenant.

a) En présence de sodium purifié par piège chaud, aucune influence particulière des divers éléments d'addition n'a été mise en évidence ; tous les alliages considérés, de même que le vanadium non allié, présentent une résistance excellente à la corrosion dans ce milieu.

b) En présence de sodium simplement épuré par piège froid, si tous les alliages expérimentés subissent une corrosion notable, on relève cependant des différences significatives dans leurs comportements respectifs, qui sont résumées dans le tableau IV.

TABLEAU IV. CARACTERISTIQUES DES COMPORTEMENTS DES DIVERS ALLIAGES BINAIRES ETUDIES DANS LE SODIUM PURIFIE PAR PIEGE FROID

Elément d'addition	Signe des Variations de poids	Durcissement à coeur	Présence ou non d'une couche superficielle, et caractéristiques
Al	+	non	Importante ; zone dure et adhérente, mais très fragile
Zr	-	oui	non
Ti	-	non	Importante ; zone dure et friable
Si	-	oui	non
Nb	-	oui	non
Cr	-	oui	Zone de faible épaisseur, semblant adhérente
Mo	+	oui	non

Parmi les éléments d'addition ayant une affinité pour l'oxygène nettement supérieure à celle du vanadium, c'est-à-dire l'aluminium, le

V - CONCLUSION

Le vanadium ou ses alliages sont tout à fait compatibles avec le sodium liquide, à condition que ce dernier soit soigneusement désoxygéné au moyen d'un piège chaud.

Par contre, aucun des alliages binaires présentement étudiés ne semble utilisable à long terme en présence de sodium liquide seulement épuré par piège froid. Parmi les éléments d'addition les plus favorables, on peut cependant retenir le chrome, l'aluminium et éventuellement le molybdène. L'intérêt du titane ne peut être que d'ordre métallurgique.

En définitive, la solution à ce dernier problème, si elle existe, semble devoir être recherchée dans la voie d'alliages complexes, c'est-à-dire comportant plusieurs éléments d'addition, de manière à conjuguer au mieux les effets spécifiques de chacun d'eux , à la fois du point de vue de la résistance à la corrosion et de celui des propriétés mécaniques.

REMERCIEMENTS

Les auteurs tiennent à remercier Messieurs J. Kraft, W. Graff et P. Juste, de la Société Ugine, qui ont eu la lourde charge de mettre en oeuvre les circuits à sodium liquide utilisés dans cette étude et de réaliser les essais de corrosion, ainsi que Monsieur R. Dominget, du CEN Saclay, qui a effectué les examens micrographiques particulièrement délicats.

REFERENCES

[1] ALTER, H., WEBER, C.E., J. nucl. Mater. 16 (1965) 68.
[2] CHAMPEIX, L., SANNIER, J., DARRAS, R., Rapport CEA 3028 (1966).
[3] DAVIS, M., DRAYCOTT, A., Proc. 2nd UN Int. Conf. PUAE 7 Geneva (1958) 94.
[4] MACHERY, R.E., SIMMONS, W.R., NOLAND, R.A., "Materials for Argonne National Laboratory sodium cooled reactors", Nucl. Metall. AIME 9 (1963).
[5] GURINSKY, D.H., WEEKS, J.R., KLAMUT, C.J. et al., Actes 3^{e} Conf. int. util. EAFP 9, Nations Unies (1964) 550.
[6] ARGONNE NATIONAL LABORATORY, ANL 6944 (1964) 9.
[7] SANNIER, J., CHAMPEIX, L., ces comptes rendus, SM-85/8.

CORROSION OF VANADIUM-BASE ALLOYS IN SODIUM AT 550° TO 750°C*

S. GREENBERG, W.E. RUTHER AND H.A. LEVIN
ARGONNE NATIONAL LABORATORY,
ARGONNE, ILL.,
UNITED STATES OF AMERICA

Abstract

CORROSION OF VANADIUM-BASE ALLOYS IN SODIUM AT 550° TO 750°C. Vanadium alloys are being investigated as fuel cladding materials for sodium-cooled fast reactors. The requirement for compatibility with metallic fuel as well as coolant, has, until recently, restricted the choice of materials to the refractory metal alloys. Considerations of physics further limit the choice of materials.

In exploratory tests in low velocity sodium, vanadium-titanium alloys were clearly superior to niobium-base alloys. Vanadium-20 wt.% titanium was chosen as the tentative reference alloy and basis for comparison. It is being studied in detail under both static and dynamic conditions, these studies having a dual objective: (1) the understanding of the corrosion mechanism as a function of the impurity content, temperature and velocity of the sodium; and (2) the development of usable alloy-environment combinations.

The corrosion behaviour is particularly sensitive to the oxygen concentration of the sodium. In static systems at low concentrations (2-6 ppm) the alloy gains weight in a protective manner, and above about 10 ppm weight loss proportional to exposure time is observed.

Under the low oxygen conditions for times up to 475 h, and over the temperature range 550° to 750°C, most of the experimental results can be expressed in terms of the parabolic rate law, $(\Delta w/A)^2 = K_pt$. The observed weight gains are due to the solution of oxygen in the metal rather than to the formation of a surface oxide. The variation of the parabolic rate constant with temperature follows an Arrhenius-type relationship. Microhardness traverses indicate that the solution of oxygen is confined to a very shallow depth.

In a dynamic system (velocity of 6.1 m/s) at 650°C and oxygen concentrations of approximately 10 ppm, protective kinetics are also observed. After 139 d exposure, the weight gain may be described by the empirical equation $\Delta w = 0.26\,t^{0.24}$ (Δw in mg/cm^2 and t in days). The quantitative difference in the rate laws observed in the two types of experiments cannot yet be explained.

Alloy development work is continuing, and alloy with corrosion resistance superior to vanadium-20 wt.% have been developed. Based solely upon considerations of metal penetration, several alloys suitable for use in cold-trapped flowing sodium systems at 650°C have been developed.

1. INTRODUCTION

The liquid-metal-cooled fast-breeder reactor programme at Argonne National Laboratory has, in the past, emphasized the use of metallic fuels. The fuel alloys under consideration in 1962 and 1963 were not compatible with ferrous (stainless-steel) and nickel alloys. It was, therefore, logical to consider the use of refractory metals and alloys as fuel cladding materials. This corrosion study is part of an over-all effort to develop refractory metal cladding.

Nuclear considerations, as summarized by Okrent [1], indicated the desirability of vanadium as a cladding material for large central station power reactors. Smith and Van Thyne [2] had also noted the desirability of vanadium alloys as a cladding material and presented an

---

* Work performed under the auspices of the United States Atomic Energy Commission.

evaluation based chiefly on metallurgical, physical and mechanical considerations. Molybdenum has excellent mechanical and corrosion-resistant properties, but its nuclear characteristics make it much less desirable as cladding for large fast reactors [1]. It was decided therefore to investigate the potential of vanadium alloys as cladding materials for sodium-cooled reactors.

The corrosion behaviour of vanadium and niobium in sodium and NaK had been studied by Davis and Draycott [3] and by Evans and Thorley [4] at temperatures of interest in the Argonne programme. It had been concluded that both materials were suitable for use in sodium in the range of 600°C only under conditions of very low oxygen concentration, i.e. those conditions for which hot-trapping was probably necessary. There were also indications that niobium had greater corrosion resistance than vanadium.

Nevertheless, because of the needs of the Argonne programme, it was decided to investigate the behaviour of both vanadium and niobium[1] alloys in sodium of relatively low oxygen concentration, including concentrations achievable in cold-trapped systems. Screening tests [5] clearly demonstrated the superior corrosion resistance of vanadium and vanadium alloys compared with niobium and niobium alloys at 650°C. As a result of the screening tests, V-20Ti[2] was chosen for continued intensive study.

2. EXPERIMENTAL EQUIPMENT AND PROCEDURES

Oxygen refreshed, static autoclave systems of the type shown in Fig.1 were used for corrosion exposures when the desired oxygen content of the sodium was more than about 8 ppm. The sodium was circulated slowly by a diaphragm pump through a cold trap previously loaded with an excess of sodium oxide; the controlled temperature of the cold trap thus established the oxygen level of the system. The system was constructed of Type 304 stainless steel with Type 316 fittings and valves.

A small dynamic test facility was also constructed of Types 318 and 316 stainless steel (Fig.2). An adjustable temperature cold trap loaded with excess sodium oxide was also used for oxygen control in this equipment. Commercially available electromagnetic pumps and flowmeters were used with 2.54-cm O.D. tubing.

In all tests the vanadium alloy specimens were added and removed, and the sodium samples for oxygen analysis taken with the system at operating temperature, usually 650°C. Analytical samples of the sodium were removed in electropolished stainless-steel or chemically polished nickel tubes. A plunger within the sampling tube, actuated from outside the autoclave, permitted the inside of the tube to be flushed several times with bath sodium before retrieving a specimen. The sodium sample was extruded, amalgamated, and washed with mercury under vacuum

---

[1] Niobium alloys were included in exploratory tests as a basis for comparison because niobium alloys were considered as preliminary reference alloys for use in smaller reactors in which their nuclear properties were acceptable. Such relatively small reactors were considered of importance in 1962 and 1963.

[2] All compositions in this paper are given in weight per cent.

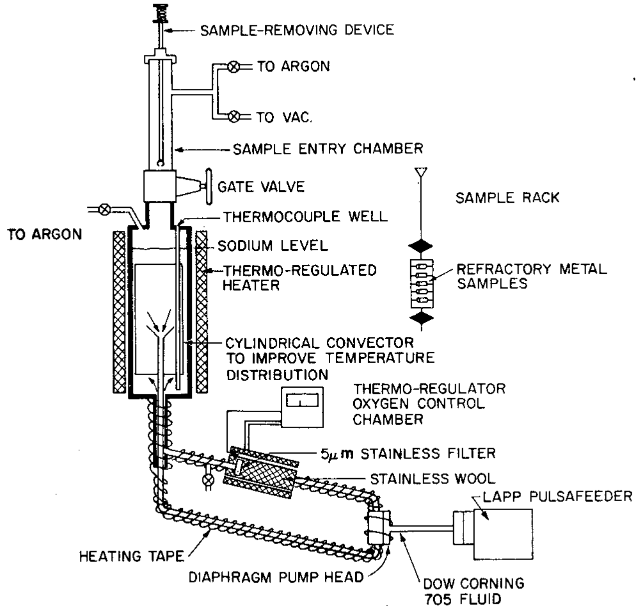

FIG. 1. Static sodium corrosion equipment with oxygen control

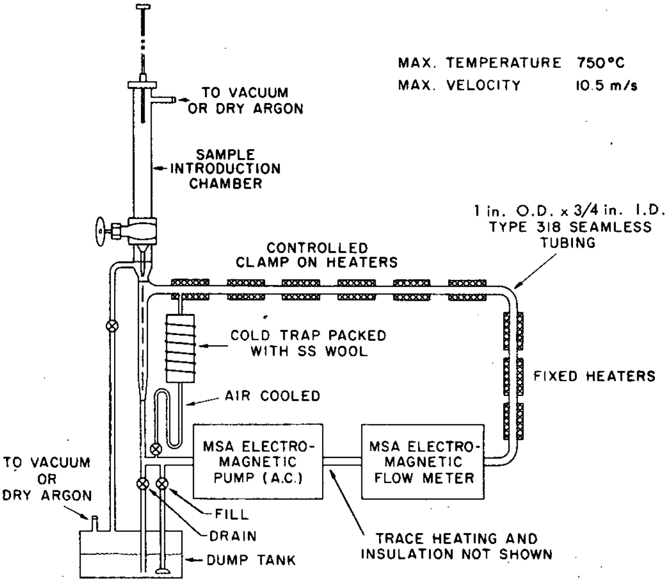

FIG. 2. Liquid sodium test loop

(~ 4×10^{-6} mm). Precautions were taken to minimize contamination during the analysis. Because of the high sampling temperature (650°C), sodium monoxide was assumed to be the sole source of the alkalinity determined by titration.

As can be inferred from the data presented in the body of this paper, the precision of the mercury amalgamation technique is adequate for our purposes. However, the accuracy is unknown, and recent work by other members of our group indicates that the technique may be sensitive to other sodium compounds in addition to the oxide. The reported values may therefore be somewhat high. Distillation analysers are being incorporated as integral components in all our test equipment, but conclusions based on the use of cold-trapped sodium are independent of the method of analysis.

The Type 304 stainless-steel equipment used for experiments with sodium of low oxygen content (< 6 ppm) is shown in Fig. 3. Individual vanadium alloy specimens could be removed or added to a rotating rack in the sodium through a vacuum-gas transfer lock without interrupting the test or contaminating the sodium. The sample rack was rotated during the tests resulting in an effective flow past the samples of 2.5 cm/s.

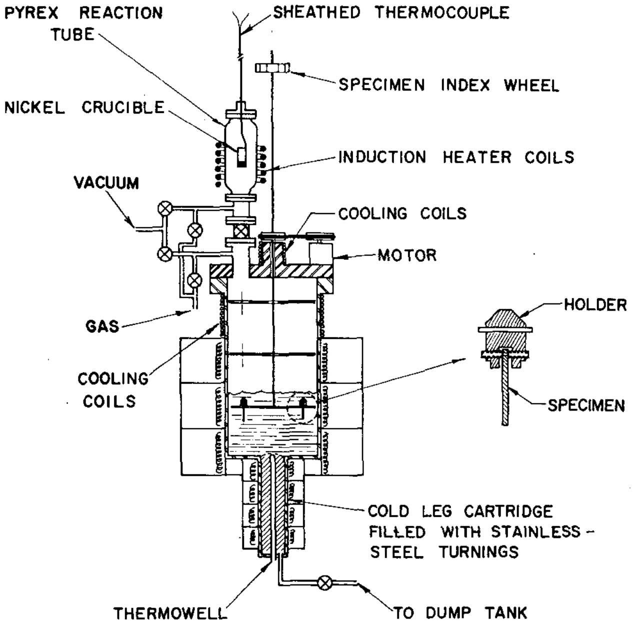

FIG. 3. Low oxygen static sodium corrosion equipment

The helium gas used over the sodium and in the transfer lock was purified by passing it over a chilled (-75°C) molecular sieve and through a hot (700°C) zirconium trap. About 2.9 litres of filtered (5 μm) sodium at 150°C was required to fill the equipment. It was then hot gettered with zirconium to the required oxygen level.

Analysis for oxygen of the sodium was accomplished by attaching a vacuum distillation apparatus to the top of the experimental system. A nickel crucible was vacuum annealed in place and then used to sample the sodium. Distillation of the sodium was completed at 325-350°C and the residue titrated as Na_2O.

Alloys were made by levitation melting (small ingots) or by multiple-arc melting. The levitation melts were tested in the "as chill cast" condition with machined, lightly etched surfaces. The larger arc-melted castings were fabricated into sheet by the ANL Metallurgy Fabrication Group and tested with various heat treatments. Most of the samples were wet ground (240 grit) and lightly etched before corrosion testing; those specimens used in low oxygen sodium (< 6 ppm) were wet ground to 600 grit.

Standard metallographic mounting and polishing methods were used to prepare the corroded specimens for microhardness traverses. This procedure provided a valuable method of measuring the extent of the internal penetration of oxygen into the specimens.

3. RESULTS

3.1. V-20Ti

V-20Ti was exposed to sodium containing 1-6 ppm oxygen over the temperature range of 550-750°C for times up to 475 h. The specimens gained weight in this range of conditions and the process initially followed a parabolic rate law, $\Delta w^2 = K_p t$. Any subsequent deviations from parabolic behaviour were in the direction of lower weight gains.

The data are summarized in Table I. It is quite apparent that the parabolic rate constant depended to a large extent on the oxygen level in the sodium. To approximate the behaviour of the alloy in "hot-gettered" sodium (1-6 ppm oxygen), the average value of the rate constant at each temperature is plotted as a function of temperature (Fig.4), resulting in an activation energy of 22.8 kcal/mole.

A photomicrograph of a sample exposed to sodium containing 6 ppm oxygen for 40 h at 650° is shown in Fig.5. The appearance is typical for all the exposed V-20Ti samples exposed to low oxygen sodium. No surface oxide is present on the specimens. The observed weight gains are the result of the solution of oxygen in the alloy rather than of the formation and growth of a protective oxide film[3].

The solution of oxygen at the surface results in an oxygen concentration gradient and inward diffusion of oxygen. Oxygen enters the lattice interstitially, causing solid solution hardening. The extent of this hardening is graphically illustrated in Fig.5 by the decrease in size of the Knoop microhardness indentations (15 g load) as the surface is approached.

Microhardness profiles taken from samples exposed under various conditions are shown in Fig.6. The large variation in the extrapolated surface hardness is significant. In general, at any given temperature of exposure, the higher the surface hardness, the larger the parabolic rate constant. It should also be noted that, at a given temperature and time of exposure, a higher surface hardness (i.e. oxygen concentration)

---

[3] The behaviour of sodium-exposed samples in nitric-hydrofluoric acid solution may be of interest. A non-uniform rate of removal of the oxygen-rich zone results upon etching (i.e. thin plates of material are removed). Unexposed material dissolves uniformly. This phenomenon emphasizes the need for precision in use of descriptions such as film.

TABLE I. EXPOSURE OF V-20Ti IN SODIUM OF LOW OXYGEN CONCENTRATION (HOT-GETTERED)

Temperature (°C)	Length of exposure (h)	Rate constant $K_p \left(\frac{mg}{cm^2}\right)^2 h^{-1}$	Surface hardness[a] KHN (15 gm load)	Oxygen content in Na (ppm)
550	85	3.8×10^{-4}		
550	475	1.5×10^{-4}	2600	
600	32	4.9×10^{-4}	1300	1.2
650	333	2.7×10^{-4}	1600	
650	32	6.2×10^{-4}	1500	3.8
650	32	18.8×10^{-4}	1950	4.5
650	40	30.0×10^{-4}	2600	6.3
700	32	5.2×10^{-4}	700	2.3
700	32	13.2×10^{-4}	800	2.3
750	32	17.0×10^{-4}	1000	4.6
750	32	43.0×10^{-4}	2000	4.4

[a] Extrapolated value, see Fig. 6.

resulted in a thicker diffusion zone. At approximately the same surface hardness the hardness of the diffusion zone increases with time. This is illustrated for samples exposed for 32 h and for 333 h.

More protective kinetics were observed (Fig. 7) in a long-term dynamic (6.1 m/s) corrosion exposure of V-20Ti in sodium at 650°C containing approximately 10 ppm oxygen. No dimensional changes were observable and only a slight staining of the samples was noted. A typical hardened zone approximately 50 μm thick was measured at 139 d.

As the oxygen concentration of the sodium is increased above the range of approximately 10 ppm, a striking change in corrosion behaviour is observed. Roughly linear corrosion kinetics were observed in short tests at oxygen levels of 20-25 and 45-50 ppm (Fig. 8) and in one longer exposure at approximately 15 ppm (Fig. 9). All the specimens removed from these tests (adhering sodium dissolved in ethyl alcohol) were covered with a flaking, gun metal grey coating. This outer layer was completely removed by vigorous scrubbing exposing a black adherent corrosion product. Sizeable weight losses were recorded at this point. X-ray identification

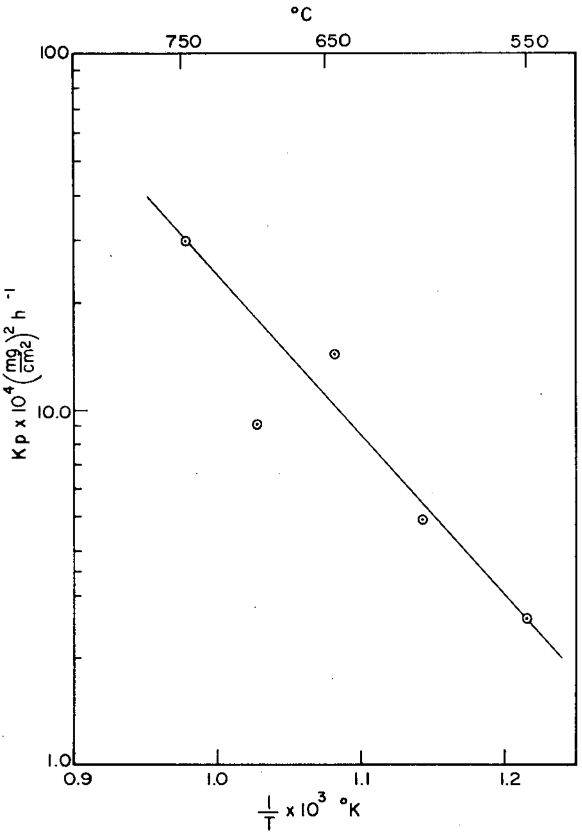

FIG.4. Variation of the parabolic rate constant of V-20 wt.% Ti in sodium containing 1-6 ppm oxygen with temperature

of this dark layer indicated a $VO_{0.9}$ structure with faint lines of TiO. Micro examination of polished sections indicated that this dark layer was only a few microns thick. A hardened band was located immediately beneath the surface film. The depth of this diffusion zone beneath the surface tended to remain roughly constant with time (Table II) when the corrosion kinetics were linear.

A few short (7-d) dynamic experiments at 650°C, 6.1 m/s velocity, showed that the corrosion process was also velocity sensitive above 15 ppm oxygen. For example (Fig.10), erosive effects and significant thinning (100 μm per side) of the specimens occurred in a one-week test at 20-28 ppm. Exposure in a refreshed static system at the same oxygen level would be expected to lead to only about 30-40 μm thinning. The difference between static and dynamic corrosion results was sharply reduced as the oxygen content of the system was lowered. For example, at 15 ppm oxygen, the dynamic test specimens lost only 10-18 μm per side in a one-week test, while static exposure samples lost ~10 μm at the same oxygen level during a one-week exposure.

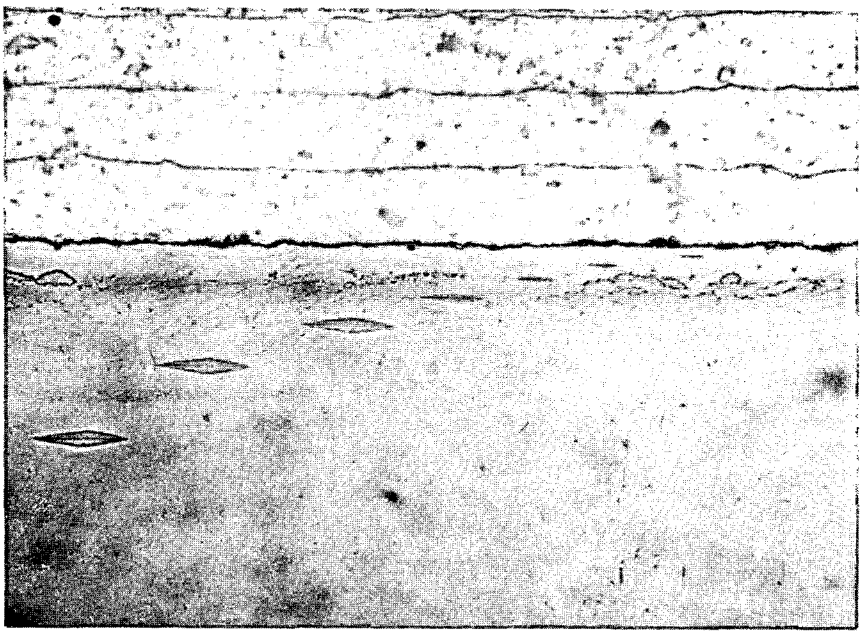

FIG. 5. V-20Ti exposed for 40 h to sodium at 650°C containing 6 ppm oxygen

3.2. Vanadium-titanium binary alloys

While V-20Ti corrodes with acceptable kinetics in sodium containing approximately 10 ppm or less of oxygen, it could not be used satisfactorily in a fast reactor operating much above this oxygen level. A search was therefore made for alloys which might show greater resistance to more highly oxygenated (> ~ 10 ppm) sodium. Initial testing was performed at 650°C and at about 50 ppm oxygen concentration in an effort to accentuate differences in alloy performance. Recent testing has been conducted at somewhat lower oxygen levels, as we have become more familiar with system behaviour and with reactor performance[4].

Only the V-Ti system was studied over a wide range of compositions (Table III). The average total metal penetration decreased with increasing titanium content, resulting in a minimum penetration at about 70-80 wt.% Ti. However, starting at about 40 wt.% Ti, stringers of a second phase appeared with the same etching characteristics as the oxygen-hardened zone near the surface. These stringers extended much further into the metal than the average depth of the hardened surface zone,

---

[4] A few very recent tests (not discussed in this paper) have shown that the order of corrosion resistance of vanadium alloys in sodium at 650°C differs for the regions above and below a dividing line at approximately 10-15 ppm oxygen. This suggests that it would be prudent to re-evaluate the behaviour of some of the alloys in sodium at oxygen concentrations below 15 ppm.

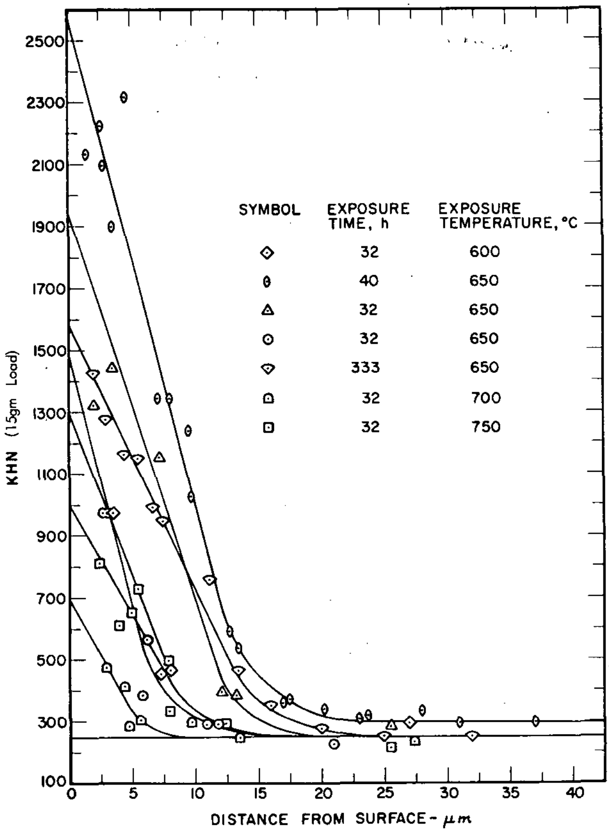

FIG.6. Hardness profiles for V-20Ti exposed to sodium under various conditions of time and temperature

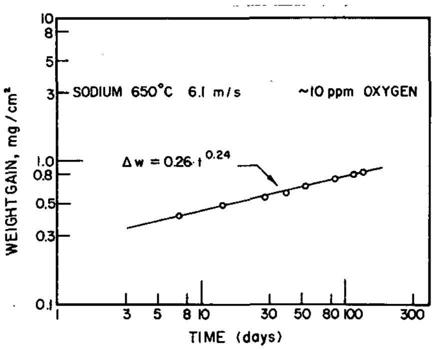

FIG.7. Corrosion of V-20Ti in flowing sodium at 650°C

and would represent a potential cracking hazard in many practical applications. Considering this factor, the region of practical titanium content would seem to be 0-40 wt.%. The V-Ti alloy systems also showed a distinct effect of annealing on corrosion resistance as indicated in Table IV.

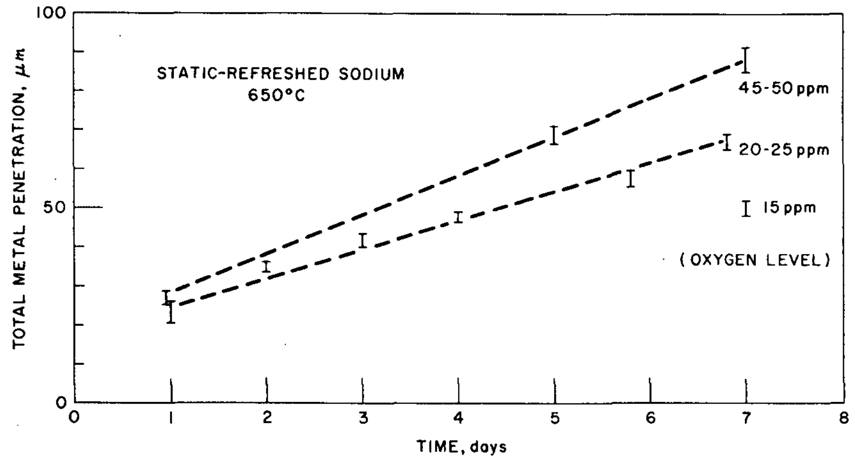

FIG. 8. Effect of oxygen level on corrosion of annealed V-20 wt.% Ti alloy

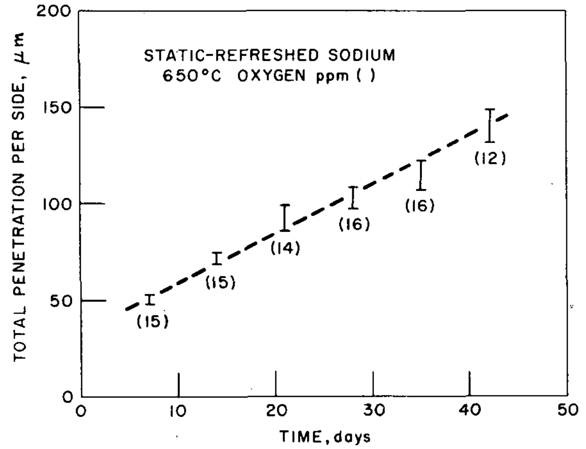

FIG. 9. Behaviour of V-20 wt.% Ti (annealed sheet) in oxygenated sodium

3.3. Other binary alloys

A group of selected binary alloys was prepared and tested with the results shown in Table V. In general, alloying elements were selected with the idea of increasing the oxidation resistance of the vanadium.

In addition to the controlled oxygen tests summarized in Table V, a number of preliminary tests in a non-refreshed autoclave indicated by relative metal penetration of oxygen that V-10Zr, V-5Y, V-5Si and V-10Mo were substantially poorer alloys than the V-Al, V-Cr and V-Ti types. It is interesting that every addition has had the effect of reducing the penetration of oxygen somewhat compared with pure vanadium, which suffers penetration of over 1000 μm under the conditions of the tests summarized in Table V.

TABLE II. EFFECT OF TITANIUM CONCENTRATION ON CORROSION BEHAVIOUR IN STATIC-REFRESHED SODIUM AT 650°C CONTAINING 45-50 ppm OXYGEN

Alloy	External loss per side (μm)	Δw mg/cm²	Depth hardened layer[a] (μm)	Total metal penetration (μm)
V-10Ti	77	-51.7	68-72	145-149
V-30Ti	39	-20.0	12-15	51-54
V-50Ti	27	-12.4	12-15	39-42
V-70Ti	17	-7.6	7-10	24-27[b]
V-90Ti	13	-5.3	50-55	63-68[b]

[a] Including adherent oxide.
[b] Not including stringer penetration.
7.0-d exposure; alloys tested as levitation melted, chill cast and machined.

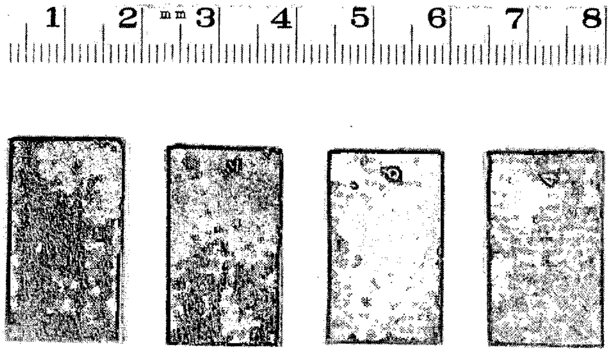

20-28 ppm oxygen 15 ppm oxygen

FIG.10. Effect of high oxygen concentration on corrosion of V-20Ti in sodium at 650°C

Of the binary systems studied, all suffered a weight loss due to loss of corrosion product. As with V-20Ti, at least a portion of the weight loss resulted from the loss of a poorly adherent coating when the samples were separated from clinging sodium by washing in ethyl alcohol. As described previously, the V-Ti alloys form a thin (< 50 μm) hardened layer at the exposed surface. No hardened layer was detected on V-5Cr exposed under identical conditions (650°C-15 ppm oxygen – 7 d).

TABLE III. DEPTH OF HARDENED LAYER ON V-20Ti CORRODED IN SODIUM AT 650°C

Time (d)	Oxygen level (ppm)	Layer (μm)
7.0	15	38-42
14.0	15	49-55
21.1	14	45-58
28.1	16	44-57
35.1	16	45-60
42.1	12	50-65

TABLE IV. EFFECT OF HEAT TREATMENT ON CORROSION OF VANADIUM-TITANIUM ALLOYS EXPOSED TO STATIC-REFRESHED SODIUM AT 650°C: 7 d, 45-50 ppm OXYGEN (ROLLED SHEET)

Alloy	External loss (μm per side)	Internal penetration (μm)	Total metal penetration (μm)
V-20Ti Control (annealed, 900°C - 1 h in vac.)	42	43-46	85-88
V-30Ti Cold worked[a]	52	23-27	75-79
V-30Ti Annealed[b]	33	15-17	48-50
V-40Ti Cold worked[a]	28	13-16	41-44
V-40Ti Annealed[b]	14	13-16	27-30
V-50Ti Cold worked[a]	25	12-18	37-43

[a] As cold rolled.

[b] Annealed in the same way as V-20Ti.

TABLE V. CORROSION BEHAVIOUR OF VANADIUM BINARY ALLOYS EXPOSED 7.0 d IN STATIC-REFRESHED SODIUM AT 650°C

Alloy composition	Oxygen concentration in sodium (ppm)	Weight loss (mg/cm^2)	External loss (μm per side)
V-20Ti[a]	15	9.7	-
V-20Ti[a]	42-50	28.4	34
V-10Al[b]	42-50	51.2	93
V-10Cu[b]	42-50	104	180
V-5Cr[c]	15	9.1	-
V-10Cr[b]	42-50	61.4	100
V-10Cr[c]	15	9.3	-
V-20Cr[b]	42-50	27.5	32
V-10Fe[b]	42-50	88.5	129
V-20Fe[b]	42-50	91.8	64
V-10Ni[b]	42-50	93.8	146
V-20Ni[b]	42-50	115	189
V-2Si[b]	42-50	82.5	133

[a] Rolled and annealed at 900°C.
[b] Levitation melted, chill cast and machined.
[c] As rolled.

Some of the experimental alloys were also exposed in flowing sodium at 650° (~ 10 ppm oxygen concentration) with interesting results. For example, the V-5Cr alloy samples gained only 0.02 and 0.05 mg/cm^2 after 57 d. The corresponding value for V-20Ti is about 0.69 mg/cm^2.

3.4. Ternary alloys

A number of ternary alloys were also exposed to sodium. Quite a large fraction of these were of the V-Ti-X type. Better fabricability and/or increased high temperature mechanical properties, as well as possible improvements in corrosion resistance, were factors considered in many of the alloys tested. The results of corrosion testing of some of

TABLE VI. EFFECT OF ALLOY COMPOSITION ON CORROSION IN 650°C STATIC-REFRESHED SODIUM CONTAINING ABOUT 45 ppm OXYGEN (ROLLED SHEET)

Alloy	External loss (μm per side)	Δw (mg/cm^2)	Depth hardened layer (μm)	Total metal penetration (μm)
V-5Ti-15Cr	9	-9.2	60-70	69-79
V-15Ti-5Cr	24	-14.7	40-45	64-69
V-15Ti-7½Cr	21	-15.6	34-38	55-59
V-20Ti-5Cr	23	-19.5	32-35	55-58
V-30Ti-5Cr	14	-13.1	20-22	34-36
V-30Ti-10Cr	18	-14.1	15-18	33-36
V-20Ti-2Mo	17	-8.5	40-45[a]	57-62
V-20Ti-2Ta	34	-11.2	35-40[a]	69-74
V-20Ti-2Nb	34	-14.7	40-50[a]	74-84
V-20Ti (Reference)[b]	42	-16.3	30-35	72-77

[a] Longitudinal surface cracks in hardened layer 10-20 μm deep.

[b] Reference: V-20Ti rolled and annealed at 900°C.

7.0-d test; samples tested with about 50% cold work.

TABLE VII. EFFECT OF ALLOY COMPOSITION ON CORROSION IN 650°C STATIC-REFRESHED SODIUM CONTAINING ABOUT 30 ppm OXYGEN (ROLLED SHEET)

Alloy composition	External loss (μm per side)	Δw (mg/cm^2)
V-20Ti (Reference)[a]	22	-17.3
V-40Ti-10Cr	16	-9.8
V-40Ti-10Mo	14	-9.0
V-15Ti-7½Mo	37	-25.6

[a] Reference: V-20Ti rolled and annealed at 900°C.
7.0-d exposure; alloys tested with about 50% cold work.

these materials are given in Table VI for the 40-50 ppm oxygen tests, and in Table VII for the 20-30 ppm tests. The results suggest that at this oxygen level titanium content is most significant in these ternary alloys in determining the corrosion resistance, with chromium serving to reduce the external loss more effectively than titanium. While many of these alloys showed improved corrosion resistance compared with the reference V-20Ti samples included in the same experiment, none of them offered an order of magnitude improvement. The V-15Ti-7½Cr alloy had about 65% of the weight gain of V-20Ti after 89-d exposure in flowing (6.1 m/s) sodium at 650° containing approximately 10 ppm oxygen.

Because of the film retention properties shown by the V-Cr binary, some ternary alloys were made with chromium as the major addition. The better alloys showed more than an order of magnitude improvement in corrosion resistance compared with V-20Ti (Table VIII). In addition, the internal hardening is sharply reduced. A few of the V-Cr-Al ternaries were exposed for a longer time to determine if their relatively greater corrosion resistance would be maintained. The results (Table IX) show a consistent improvement over V-20Ti.

Unfortunately, the ternary V-Cr-Al alloys were very difficult to fabricate. An effort was made to modify V-20Cr-10Al with Zr (1 wt.%) or Y(0.5 wt.%), but no marked improvement in fabrication resulted. The corrosion resistance in 25-30 ppm oxygenated sodium at 650°C was not altered by the modifying additions.

One further attempt to improve the fabricability involved adding sizeable amounts of titanium to the ternary. As shown in Table X, the titanium additions increased somewhat the weight loss of the V-20Cr-10Al composition. In addition, the presence of titanium re-introduced the subsurface hardened band. No serious attempt was made to fabricate the alloys in view of the latter development.

TABLE VIII. CORROSION BEHAVIOUR OF V-Cr-Al TERNARY ALLOYS IN STATIC-REFRESHED SODIUM AT 650°C

Alloy	Oxygen concentration in sodium (ppm)	Weight change (mg/cm²)
V-10Cr-10Al	25-35	-10.7
V-20Cr-5Al	25-35	-20.7
V-20Cr-7½Al	25-35	-13.0
V-20Cr-10Al	25-35	-1.8, -2.2
V-25Cr-5Al	25-35	-15.8
V-30Cr-5Al	25-35	-6.0
V-30Cr-7½Al	25-35	-5.1
V-30Cr-10Al	25-35	-1.8
V-20Ti (Reference annealed sheet)[a]	25-35	-19.0, -20.9
V-30Cr-5Al	15-18	-4.0
V-30Cr-7½Al	15-18	-1.8
V-40Cr-10Al	15-18	-0.2
V-20Ti (Reference annealed sheet)[a]	15-18	-8.4

[a] Rolled and annealed at 900°C.

7.0-d exposure; alloys tested as levitation melted, chill cast and machined.

4. DISCUSSION

In sodium containing less than approximately 10-15 ppm oxygen, V-20Ti gains weight by solution and diffusion of oxygen into the metal rather than through the formation and growth of a protective oxide film. This mechanism is consistent with the observed parabolic kinetics. For the case of solution and diffusion of oxygen into the metal for our sample

TABLE IX. CORROSION OF TERNARY VANADIUM ALLOYS IN STATIC-REFRESHED SODIUM AT 650°C CONTAINING 15-18 ppm OXYGEN

Alloy	Weight loss (mg/cm^2)				
	7.0 (d)	21.0 (d)	44.3 (d)	58.1 (d)	72.1 (d)
V-25Cr-10Al	1.29	3.61	7.0	10.0	14.6
V-20Cr-10Al	2.40	4.30	11.9	17.1	22.7
V-20Cr-15Al	0.46	1.09	3.32	4.78	5.55
V-20Ti (Reference annealed sheet)[a]	9.70	27.3	47.9	64.7	74.7

[a] Rolled and annealed at 900°C.
Alloys tested as levitation melted, chill cast and machined.

TABLE X. CORROSION OF V-20Cr-10Al-Ti ALLOYS IN STATIC-REFRESHED SODIUM AT 650°C CONTAINING ~16 ppm OXYGEN

Alloy	Weight loss (mg/cm^2)
V-20Cr-10Al	1.54
V-20Cr-10Al-5Ti	2.15
V-20Cr-10Al-10Ti	1.64
V-20Cr-10Al-15Ti	2.77
V-20Cr-10Al-20Ti	3.13
V-20Ti[a]	7.14

[a] Rolled and annealed at 900°C.
7.0-d; alloys tested as levitation melted, chill cast and machined.

geometry and for the case where diffusion of oxygen to the centre of the sample had not occurred, the samples would be expected to gain weight according to the following relationship:

$$\left(\frac{\Delta w}{A}\right)^2 = An(C_s - C_0)^2 Dt$$

where $K_p = An(C_s - C_0)^2 D$ and An is a numerical constant.

According to the above expression, increasing the concentration of oxygen in the solid at the surface should result in an increased rate constant. An increase in the rate constant with an increase in surface hardness has been observed. The increase in surface hardness (surface concentration of oxygen) is a direct result of an increase in the oxygen concentration of the sodium. In the range of surface hardnesses found the variation of hardness with oxygen concentration is not quantitatively known. Therefore, quantitative verification of the above dependence of the rate constant on the surface concentration cannot be accomplished.

At a fixed oxygen level in the sodium and for $C_s >> C_0$ the temperature dependence of the rate constant is as follows:

$$\frac{d \ln K_p}{d(1/T)} = 2 \frac{d \ln C_s}{d(1/T)} - \frac{\Delta H_{diff.}}{R}$$

This expression is the sum of the activation energy for diffusion of oxygen in the alloy and of the rate of change of the surface concentration with temperature. Depending on the thermodynamics of the system, $d \ln C_s/d(1/T)$ can be positive or negative. In the absence of thermodynamic and diffusion data for the V-Ti system, the relative effect of each quantity on the observed activation energy of 22.8 kcal/mole cannot be determined.

Above the approximately 10-15 ppm oxygen concentration range, a drastic change in the kinetics occurs. The parabolic behaviour at the lower oxygen levels is replaced by linear kinetics accompanied by a loss of corrosion product. Above 10-15 ppm, the oxygen level in the sodium is high enough so that $VO_{0.9}$ does form. This forms a spalling non-protective oxide. The corrosion rate increases with increasing oxygen content of the sodium and with increasing velocity, suggesting that the rate is controlled by the arrival of oxygen to the surface.

5. CONCLUSIONS

Economic, as well as operating considerations make it desirable that a sodium-cooled fast reactor be operated with a cold trap rather than a hot trap for maintenance of sodium purity. It has been demonstrated that, based upon considerations of metal loss and/or penetration, V-20Ti, V-15Ti-7½Cr and V-5Cr have satisfactory behaviour in flowing sodium at 650°C containing oxygen at concentration levels achievable by cold trapping, i.e. in the range 10 ppm or less.

Unfortunately, no practical alloys were developed which relax the oxygen concentration requirements sufficiently to permit satisfactory operation at levels appreciably above 10 ppm. (Such a characteristic would, for example, greatly decrease the consequences of an oxygen excursion.) Above 10 ppm oxygen concentration most of the alloys corroded at unacceptably high rates comparable to that of V-20Ti. Only the V-Cr-Al ternary system offered significant corrosion improvement and these alloys were not fabricable by the techniques developed for other vanadium alloys.

It is encouraging that several vanadium alloys have shown acceptably low corrosion rates in cold-trapped flowing sodium at 650°C. A final selection for a fuel cladding alloy may thus be able to be made on the basis of high temperature strength and fabricability from among a group of corrosion-resistant materials.

REFERENCES

[1] OKRENT, D., Nuclear considerations in the selection of materials for fast power reactors, Nucl. Metall. (A.I.M.E.) 9 (1963) 1; see also OKRENT, D., Nuclear physics considerations in large fast reactors, Pwr React. Technol. 7 (1964) 128.

[2] SMITH, K.F., VAN THYNE, R.J., Selected properties of vanadium alloys for reactor application, USAEC Rpt ANL-5661 (1957).

[3] DAVIS, M., DRAYCOTT, A., "Compatibility of reactor materials in flowing sodium", Proc. UN Int. Conf. PUAE 7 (1956) 94; also available as U.K.A.E.A. Rpt IGR-TN/C-857 (1958).

[4] EVANS, J.W., THORLEY, A., *Corrosion of niobium and vanadium in liquid sodium*, U.K.A.E.A. Rpt IGR-TN/C-1019 (1958).

[5] LEVIN, H.A., GREENBERG, S., *An exploratory study of the behaviour of niobium and vanadium base alloys in oxygen contaminated sodium*, USAEC Rpt ANL-6982 (to be published).

DISCUSSION

A.V. CAMPISE: You mention the formation of protective layers on the cladding surfaces. What effect do you think a very high fast-neutron flux would have on such a layer in an operating reactor?

S. GREENBERG: There are no "protective layers" as such formed at oxygen concentrations of interest. As I have pointed out in the paper, a thin region close to the surface exposed to the sodium may become enriched in oxygen.

Many aspects of the behaviour of materials may be modified by exposure to fast neutrons. Several alloys of interest are now being exposed in the core sodium of EBR-II, but no results are yet available.

H.U. BORGSTEDT: There seems to be a critical concentration of oxygen in liquid sodium above which the vanadium alloys are affected very seriously. Have you ever observed any definite relationship between the composition of particular vanadium alloys and the magnitude of this critical oxygen concentration?

S. GREENBERG: As I have indicated, we believe that the critical concentration for vanadium alloys is approximately 10 ppm of oxygen (as determined by our mercury amalgamation technique). We have not observed any variation of this concentration with different alloy compositions, but no experiments specifically designed for this purpose have been conducted; and if there are small variations around 10 ppm I am not sure that our present technique is sensitive enough to detect them. However, the behaviour of the V-Cr-Al alloys described in the paper suggests that alloy composition may in fact have some effect on the "critical" oxygen concentration.

L. CHAMPEIX: Is it really the same sample that is taken out, weighed and then replaced in the sodium? Does this not result in undesirable perturbations?

S. GREENBERG: In most of the experiments I have discussed the same sample was removed from test, examined and replaced. Experiments specifically designed for the purpose revealed no perturbations as a result of this method. Samples with the same total exposure – whether one continuous exposure or the sum of several shorter exposures, including removals for examination – gave the same results.

L. CHAMPEIX: I have a further question about these dynamic tests. You indicated that the temperature of the cold trap was about 120°C. I should like to know how you checked the oxygen content of the sodium during these experiments – at what point you withdrew samples. What intrigues me particularly is the fact that you should have found increases in weight where I find weight losses.

S. GREENBERG: This has us puzzled too. The sodium samples were removed periodically throughout the experiment for analysis by amalgamation, and our results almost invariably fell, to within 1 or 2 ppm, around this level of 10 ppm. This is what I mean in fact when I say that the precision is satisfactory but the accuracy unknown. Another thing that concerns us is that the oxygen solubility which we measured is not at all what others report as the solubility of sodium oxide at these temperatures, even if we allow for a slightly higher cold-trap temperature than what we get by measuring on the outside wall. The only explanation I can think of for this is some inherent systematic error in our amalgamation technique which leads us to overestimate the oxygen content. We are in fact, as I have tried to emphasize, dealing with a reproducible system of unknown oxygen concentration. Later we hope to find out exactly what the oxygen concentration is.

L. CHAMPEIX: I think you have probably hit on the answer. Everything takes place in your system as though the actual oxygen content were lower than your amalgamation tests indicate, and this would explain, moreover, the difference between your results and ours.

S. GREENBERG: Yes, this is very likely true. As I mentioned, we are now putting integral distillation apparatus on all our equipment, and the errors which we think may have been made in the amalgamation measurements will no longer occur. We should soon have a more accurate answer for the oxygen concentration. Let me add one thing, however: while I do not want to underrate the importance of knowing the exact oxygen concentration – it is essential for many reasons – I do want to emphasize that we have demonstrated the technological feasibility of using vanadium alloys in cold-trapped systems. This is a claim which I think we can make now, whatever the exact oxygen concentration turns out to be.

R. RADEBOLD: If you get this oxygen-enriched layer, which you mentioned in replying to Mr. Campise, I wonder whether you have observed any wetting by the sodium. And, secondly, do you think that the formation of this layer provides some sort of protection against corrosion?

S. GREENBERG: We have not investigated wetting specifically as yet, though it could be a very important aspect of the corrosion mechanism. The appearance of the samples does suggest, however, that they were wet by the sodium in every case.

In reply to your second question I think that the layer – whether a solution of oxygen in the metal or a conventional corrosion layer – probably does afford some protection.

A. W. THORLEY: I should like to make a few comments about the behaviour of vanadium alloys in cold-trapped sodium. Our experience at Culcheth with an alloy of vanadium and 20% titanium seems to confirm the results of the French work rather than the American. High corrosion rates were found during short exposures at 650°C in cold-trapped sodium with an oxygen content of about 10 ppm. The hard brittle layer already discussed was observed to a depth of 20 μm (hardness: 1100-1200 DPN). However, the outer surface of the specimens had a brittle friable layer which would not support the hardness indenter, and this layer is easily removed by flowing sodium. In view of all this, I think your assertion that vanadium-titanium alloys can be used in cold-trapped sodium at high temperatures should perhaps be qualified somewhat: the cold-trapping must be highly efficient and the trap itself at as low a temperature as possible. Finally, our experience suggests that in operating sodium circuits cold-trap temperatures must be measured on the trap filter or in the trap itself rather than on the wall of the vessel, a technique that must almost certainly lead to errors in measuring the solubility of oxygen in sodium.

S. GREENBERG: I certainly agree that efficient cold-trapping is needed. When we built this system we were comparative novices; moreover, we were working at rather high oxygen concentrations and made no attempt to develop a very efficient cold trap, although we apparently got one by good luck.

As to your experience with sodium containing 10 ppm of oxygen, we found identical alloy behaviour at oxygen concentrations which were, to judge by the results of our analyses, rather different. This is no doubt due to differences in measurement technique: the results may have been distorted by errors in one or both of the analyses.

You are also quite right about the measurements of trap temperature. The position we chose for our measuring and controlling thermocouple unquestionably leaves a lot to be desired if an accurate measurement of trap temperature is needed. It is, however, apparently quite acceptable as a means of control. As we all know, the corrosion of these materials is very sensitive to oxygen concentration, which in turn is a function of the cold-trap temperature. Using this method of control, which is easy and efficient for our apparatus, we are able to reproduce our results, which is what we set out to do. Our intention was to depend on analysis to find the oxygen concentration, and, apart from the improvements we expect from the integral distillation apparatus, this is still our aim.

L. P. VAUTREY (Chairman): It appears from the two papers we have just heard that the use of vanadium alloys would be perfectly feasible in extremely pure sodium, i. e. sodium purified by hot traps and not by cold-trapping alone. Could anyone comment on the practical use of these two methods of purification (cold and hot traps) in large loops such as reactor circuits?

S. GREENBERG: In the first place I do not agree that vanadium alloys can be used only with "very pure" (that is, hot-trapped) sodium. On the contrary, our work, as I have already argued, indicates that they can give satisfactory performance in sodium that is efficiently cold-trapped. If hot-trapping is considered necessary, however, you might construct and maintain a very tight system, purifying the sodium charge initially with cold traps to the limit of their capability, then removing the last traces of impurity (e. g. oxygen) and maintaining high purity with hot traps.

One other point is perhaps worth making. I think we shall all find that in large reactor systems the sodium quality can be maintained far more easily than in small laboratory loops. The samples of EBR-II sodium which we have received and analysed in amalgamation apparatus could perhaps serve as an illustration of what I mean, because after shipment and comparatively crude handling they still reveal only 6 to 13 ppm of oxygen; and they come from a system in which the cold trap is not even being used.

ПОВЕДЕНИЕ НЕРЖАВЕЮЩИХ СТАЛЕЙ В НАТРИИ В ОБЛАСТИ ТЕМПЕРАТУР 600 – 900°

Н.П.АГАПОВА, А.Г.ИОЛТУХОВСКИЙ, В.В.РОМАНЕЕВ
ОРДЕНА ЛЕНИНА ИНСТИТУТ АТОМНОЙ ЭНЕРГИИ
им. И.В.КУРЧАТОВА, МОСКВА
СССР

Abstract — Аннотация

THE BEHAVIOUR OF STAINLESS STEELS IN SODIUM AT TEMPERATURES BETWEEN 600° AND 900°C. The interaction of steel with a molten sodium flow has been studied in experimental loops with forced coolant circulation.

During a first stage of the work, the behaviour in sodium of the basic components of the steel – iron, nickel and chromium – was studied. The tests showed that nickel reacts particularly sharply to any change in (experimental) conditions: its stability is markedly affected by increases in temperature and sodium velocity.

When the oxygen content of the sodium is increased to 5×10^{-2} wt.% the stability of iron and chromium is reduced while that of nickel is improved. Further, the manner in which variations of the iron, nickel and chromium balance can affect the stability of different steels and alloys is considered. It is shown that changes in the chromium content (from 12 to 20 wt.%) have little effect on the stability of steels (with constant nickel content of 15 wt.%), but that the stability depends basically on the ratio of iron to nickel: high nickel steels behave in sodium much as unalloyed nickel, and low nickel steels much as unalloyed iron.

The effect on steel stability of alloying with certain other elements (e.g. C, N, Mn, Si, Nb, Ti, Mo, W) has also been studied. It was shown that if austenitic or 13% chromium steel does not contain enough of a strong carbide-forming element (Nb or Ti), considerable decarbonization occurs at 650°C and higher. Alloying of steels with elements such as Si, Mn and N substantially worsens their structural stability and mechanical properties, whereas alloying with Mo or W gives better stability.

On the basis of these findings an attempt is made to formulate the characteristics of a steel of optimum composition, designed for use in contact with reactor-grade sodium ($3\text{-}5 \times 10^{-2}$ wt.% of oxygen, temperature 600-900°C).

Further, the stability of type Х16Н15М3Б austenitic steel and type 1Х13М2БФ chromium steel (13% Cr) is considered in relation to variations in experimental conditions. It is shown that temperature increases up to 800-900°C and increases in the oxygen content of the sodium (up to 5×10^{-2} wt.%) sharply reduce the stability of the steel. Increases in sodium velocity (to 5 m/s) reduce the stability of the steel only when the oxygen concentration is high.

Experiments on tubular samples filled with argon under pressure showed that sodium of reactor grades (in respect to oxygen content) has virtually no effect on the creep rate of type Х16Н15М3Б and type 1Х13М2БФ steels at 650°C.

ПОВЕДЕНИЕ НЕРЖАВЕЮЩИХ СТАЛЕЙ В НАТРИИ В ОБЛАСТИ ТЕМПЕРАТУР 600 – 900°С. Взаимодействие стали с потоком расплавленного натрия изучалось в испытательных стендах с принудительной циркуляцией теплоносителя.

Предварительно было изучено поведение в натрии основных компонентов стали – железа, никеля и хрома. Испытания показали, что никель особенно резко реагирует на изменение условий; его стойкость заметно снижается с повышением температуры и скорости потока натрия.

Увеличение концентрации кислорода в натрии до $5 \cdot 10^{-2}$ вес% вызывает снижение стойкости железа и хрома и улучшение стойкости никеля. Далее рассматривается влияние содержания железа, никеля и хрома на стойкость сталей и сплавов. Показано, что изменение концентрации хрома (от 12 до 20 вес%) мало сказывается на стойкости сталей (с постоянным содержанием никеля – 15 вес%), а стойкость стали, в основном, зависит от соотношения между железом и никелем, причем высоконикелевые сплавы ведут себя в натрии также, как и нелегированный никель, а стали с низкой концентрацией никеля – как нелегированное железо.

Изучалось также влияние на стойкость сталей легирование их такими элементами, как C, N, Mn, Si, Nb, Ti, Mo, W и др. Показано, что, если аустенитная или 13% хромистая сталь не содержит в достаточном количестве сильного карбидообразующего элемента (Nb или Ti), то при 650°С и выше наблюдается заметное обезуглероживание стали. Легирование стали такими элементами как Si, Mn и N вызывает существенное снижение стабильности структуры и механических свойств стали. Легирование стали Mo или W существенно улучшает ее стойкость.

На основании изучения влияния легирования на стойкость стали сформулированы требования к примерному оптимальному составу стали, предназначенной для работы в контакте с натрием реакторной чистоты по кислороду ($3 \div 5 \cdot 10^{-3}$ вес%) и температуре 600 – 900°.

Далее рассматриваются стойкости в натрии аустенитной стали Х16Н15М3Б и 13%-ной хромистой стали 1Х13М2БФ в зависимости от изменения условий испытаний. Показано, что повышение температуры испытания до 800 – 900°С и концентрации кислорода в натрии (до $5 \cdot 10^{-2}$ вес%) вызывает резкое снижение стойкости стали. Увеличение скорости потока (до 5 м/сек) вызывает снижение стойкости стали только при повышенной концентрации кислорода в натрии.

Испытания на трубчатых образцах, заполненных аргоном под давлением, показали, что натрий реакторной чистоты по кислороду при 650° практически не оказывает влияния на скорость ползучести сталей Х16Н15М3Б и 1Х13М2БФ.

При выборе реакторных материалов приходится оценивать их с самых различных сторон, в том числе и по поведению их в теплоносителе.

Необходимость выбора сталей для натриевых аппаратов заставила исследовать коррозионную стойкость сталей в зависимости от легирония и условий испытаний. В настоящем сообщении приводится ряд сведений, полученных в результате некоторых из проведенных работ.

Взаимодействие стали с потоком расплавленного натрия изучалось преимущественно на испытательных стендах с принудительной циркуляцией теплоносителя.

Принципиальная схема типового стенда дана на рис.1, а в табл. 1 приведены основные рабочие параметры трех высокотемпературных стендов. В горячую зону стенда №3 дополнительно ставилась циркониевая ловушка.

Перед загрузкой в стенд натрий дистиллировался. Содержание кислорода на заданном уровне (от 10^{-4} до 10^{-2} вес%) поддерживалось с помощью холодной и горячей ловушек, а контроль за содержанием кислорода осуществлялся дистилляционным методом анализа. Одновременно с испытаниями в натрии в тех же стендах проводились испытания в аргоне.

Оценка стойкости материалов производилась по изменению структуры, веса (образцы 30 × 10 × 0,4 мм), механических свойств (образцы 49 × 10 × 0,4 мм), химического состава (образцы толщиной 0,4 и 0,1 мм).

Для изучения коррозии под напряжением использовались нагруженные плоские образцы (49 × 6 × 0,4 мм) – одноосное напряженное состояние и трубчатые образцы, заполненные аргоном под давлением ($\varnothing$ 14 × 0,35; $\ell = 65$ мм) – двухосное напряженное состояние.

Предварительно было изучено поведение в натрии основных параметров стали – железа, никеля и хрома. В качестве исследуемых материалов в данной работе были выбраны: железо-армко, электролитический никель и литой деформированный хром. Испытания в натрии показали, что поведение всех этих материалов в значительной степени определяется условиями испытаний (рис 2), и никель особенно резко реагирует на изменение этих условий. Так, его стойкость заметно снижается с повышением температуры и скорости потока натрия.

Стойкость хрома и особенно железа в меньшей степени зависит от изменения указанных факторов. Увеличение содержания кислорода в натрии до $5 \cdot 10^{-2}$ вес% вызывает снижение стойкости железа и хрома и улучшение стойкости никеля (рис.2).

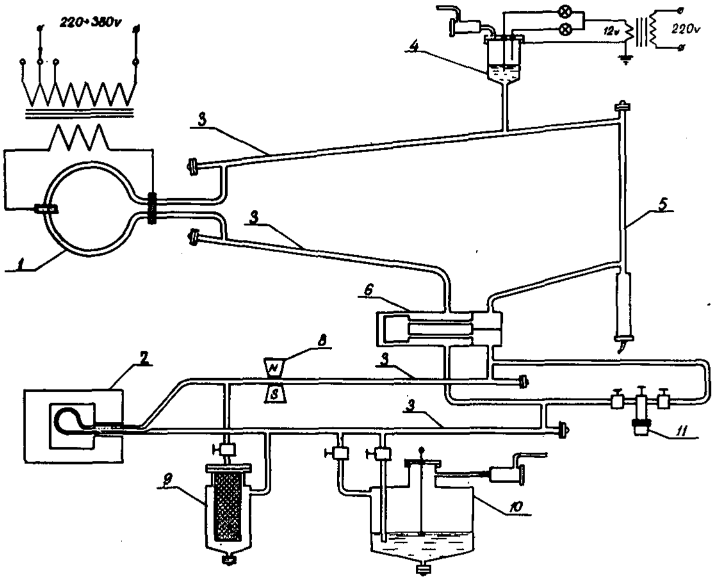

Рис.1. Принципиальная схема натриевого стенда:
1 – нагреватель; 2 – электромагнитный насос; 3 – камера с образцами; 4 – расширительный бак; 5 – камера для испытания под напряжением; 6 – рекуператор; 7 – вентиль; 8 – магнитный расходомер; 9 – холодная ловушка; 10 – сливной бак; 11 – пробоотборник-дистиллятор.

Полученные результаты позволяют предположить, что соотношение между железом, никелем и хромом в сталях и сплавах в значительной степени будет определять их поведение в натриевом теплоносителе.

Исследование ряда промышленных сплавов с различным содержанием железа и никеля при постоянном содержании хрома и других элементов убедило в правильности этого предположения. Исследования показали, что с увеличением содержания никеля в сплавах стойкость их в натрии будет приближаться к стойкости чистого никеля, а при снижении содержания никеля – к стойкости железа (рис. 3).

Повышение скорости потока и температуры испытания вызывает полное заметное снижение стойкости высоконикелевых сплавов, чем аустенитных сталей, а увеличение концентрации кислорода в натрии вызывает улучшение стойкости высоконикелевых сплавов и снижение стойкости аустенитных сталей.

Однако одновременное повышение температуры испытания ($T > 800$°C) и скорости потока ($V > 3$ м/сек) приводит к катастрофическому разрушению образцов высоконикелевых сплавов даже в случае повышенного ($3 \div 5 \cdot 10^{-2}$ вес%) содержания кислорода в натрии.

Исследование стойкости в натрии сталей с различным соотношением между железом и хромом при постоянном содержании никеля и других

ТАБЛИЦА 1. ПАРАМЕТРЫ НАТРИЕВЫХ ИСПЫТАТЕЛЬНЫХ СТЕНДОВ

№ п/п	Температура горячей зоны, °C	Температура холодной зоны, °C	Скорость потока натрия м/сек	Расход натрия, л/сек	Способ очистки натрия от кислорода	Температура холодной ловушки, °C	Температура горячей ловушки, °C
1	650	380	0,8+9,0	0,8	Холодная ловушка	110+130[a]	–
2	875	600	0,6+5,0	0,7	Холодная ловушка	110+130[a]	–
3	900	650	0,6+5,0	0,7	Холодная + горячая ловушки	110+130	900

Примечание: При испытании в натрии с повышенным содержанием кислорода ($3 \div 5 \cdot 10^{-2}$ вес%) температура холодной ловушки повышалась до ~300°C.

элементов показало, что увеличение содержания хрома в стали от 12 до 20 вес% практически не сказывается на результатах испытания, и лишь при достаточно высокой температуре – 800°С и высоком кислороде ($3 \div 5 \cdot 10^{-2}$ вес %) отмечается незначительное снижение стойкости стали (рис. 4).

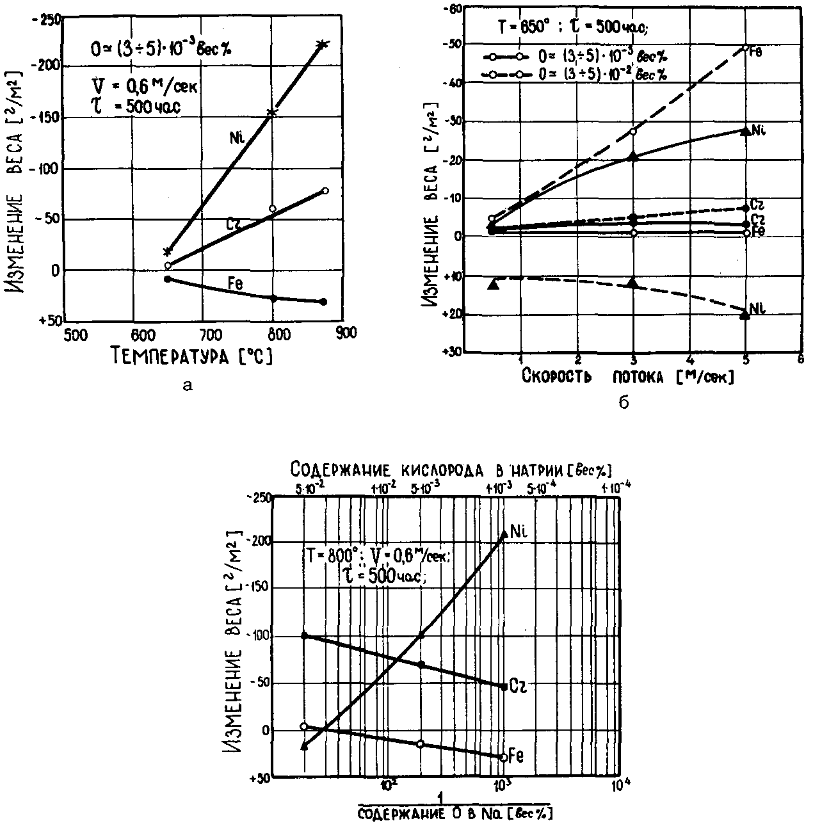

а

б

в

Рис.2. Влияние условий испытаний на стойкость железа, никеля и хрома в потоке натрия: а) влияние температуры (0 ~ $3 \div 5 \cdot 10^{-3}$ вес %; v = 0,6 м/сек; τ = 500 час); б) влияние скорости потока (T = 650°С; τ = 500 час); в) влияние содержания кислорода в Na (T = 800°С; v = 0,6 м/сек; τ = 500 час).

Выдержка аустенитных хромникелевых сталей в натрии сопровождается селективным уносом из поверхностных слоев образцов железа, никеля и хрома, причем с увеличением содержания кислорода в натрии возрастает унос железа, а с понижением содержания кислорода – унос никеля. Унос хрома происходит и в том, и в другом случае и величина его практически не зависит от содержания кислорода в натрии. Продукты селективного удаления основных компонентов стали, оседая на металлических поверхностях, вступают с ними при повышенных температурах во взаимодействие с образованием твердых растворов и новых фаз.

Так, на поверхности железа и хромистых сталей может появляться слой с решеткой γ-железа, а на поверхности аустенитных сталей – слой с решеткой α-железа, на хроме – σ-фаза и так далее.

В работе было изучено влияние на коррозийную стойкость в натрии большого числа других легирующих элементов (C, N, Si, Mn, Mo, W, Nb, Ti и др.).

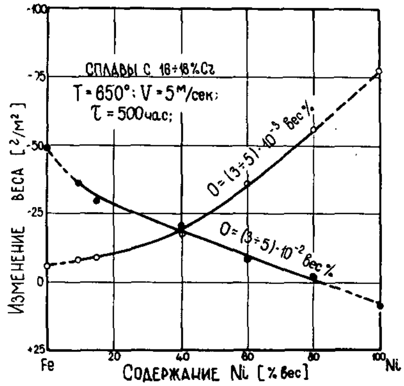

Рис.3. Влияние содержания никеля в сплавах с ~16% Cr на их стойкость в натрии (T = 650 °C; τ = 500 час).

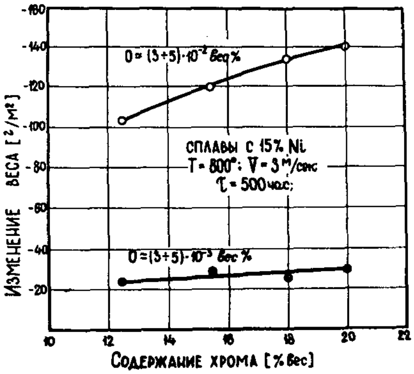

Рис.4. Влияние содержания хрома на стойкость аустенитной стали с 15% никеля.

Обнаружено, что при контакте с натрием происходит значительное обезуглероживание нестабилизированных нержавеющих сталей. Этот процесс ускоряется с повышением температуры (T > 800°C), но имеет место и при 650°C. Для заметного протекания этого процесса необходим определенный уровень кислорода в натрии $- 3 \div 5 \cdot 10^{-3}$ вес%. Унос углерода не наблюдается в сталях, легированных в достаточной степени ниобием или титаном (табл. 2). Установлено, что из аустенитных сталей, легированных азотом, последний уносится при температурах более 650° C, причем этот процесс не зависит от содержания кислорода в натрии (табл. 2).

Аустенитные стали, легированные кремнием до 2,5 вес% или марганцем (до 30 вес%), имеют значительно худшую стойкость в натрии, чем другие стали данного класса, из-за значительного уноса этих элементов из стали и связанного с этим снижения их механических свойств, особенно при температурах более 650°C (см. табл. 2 и 3).

Отрицательное влияние кремния на стойкость стали возрастает с повышением содержания кислорода в натрии, а действие марганца не зависит от концентрации кислорода.

Удаление из стали углерода, азота, кремния и марганца при взаимодействии с потоком расплавленного натрия отмечается и в хромистых нержавеющих сталях. В последнем случае, благодаря большим скоростям диффузии в α-решетке, процессы переноса массы развиваются более интенсивно.

При контакте с натрием в интервале температур 600 – 900°С в структуре нержавеющих сталей могут происходить существенные изменения – рост зерна, выпадение новых фаз, изменение состава твердого раствора, межкристаллитная коррозия (рис. 5а, б).

Как видно из рис.5 и табл.3, изменения в структуре стали могут приводить к резкому снижению механических свойств. Введение в состав стали молибдена (до 4 вес%) или вольфрама (до 3 вес%) улучшало коррозионную стойкость в натрии при всех условиях испытаний.

На основании изучения влияния легирования на стойкость в натрии нержавеющих сталей были сформулированы требования к примерному оптимальному составу стали, предназначенной для службы в контакте с натриевым теплоносителем, имеющим реакторную чистоту по кислороду – $3 \div 5 \cdot 10^{-3}$ вес%, при повышенных температурах (более 650°С):

1. Содержание никеля в стали должно быть минимальным, но обеспечивающим стабильность структуры и механических свойств.

2. Сталь должна быть стабилизирована сильными карбидообразующими элементами (ниобием или титаном) для связывания углерода в стойкие карбиды и предотвращения обезуглероживания в процессе контакта с натрием.

3. Содержание марганца и кремния в стали должно быть минимальным. Специальное легирование стали азотом также недопустимо.

4. Желательно введение в состав стали молибдена или вольфрама.

В работе было изучено влияние условий испытания на стойкость сталей. Показано, что повышение температуры (от 650°С до 875°С) и увеличение содержания кислорода в натрии (от $<1 \cdot 10^{-3}$ вес% до $3 \div 5 \cdot 10^{-2}$ вес%) вызывает заметное снижение стойкости как аустенитных хромоникелевых, так и 13%-ных хромистых нержавеющих сталей (рис. 6а).

Увеличение скорости потока натрия до $3 \div 5$ м/сек вызывает снижение стойкости как аустенитных, так и 13%-ных хромистых сталей только при повышенном содержании кислорода в натрии (рис. 6б).

Изучение кинетики этого процесса показало, что коррозия в натрии носит затухающий характер (рис. 6в). Изучена была также коррозия в натрии под напряжением. Испытания, проведенные на образцах аустенитной и 13%-ной хромистой сталей, показали, что как одноосные, так и двухосные растягивающие напряжения не оказывают существенного влияния на ползучесть и изменение механических свойств при выдержке в натрии реакторной чистоты ($0 \approx 3 - 5 \cdot 10^{-3}$ вес%) по сравнению с испытаниями в аргоне (рис. 7).

Однако, если натрий загрязнен кислородом ($0 \approx 3 \div 5 \cdot 10^{-2}$ вес%), то приложение одноосного растягивающего напряжения вызывает охрупчивание (снижение относительного удлинения δ% и повышение условного предела текучести σ 0,2) (см. табл. 4).

Для стали Х16Н15М3Б, содержащей 3% молибдена, потеря пластичности заметно ниже, чем для стали Х18Н10Т, что указывает на эффективность введения молибдена в сталь с целью стабилизации свойств и повышения коррозионной стойкости в натрии.

ТАБЛИЦА 2. ИЗМЕНЕНИЕ ХИМИЧЕСКОГО СОСТАВА СПЛАВОВ ПОСЛЕ ВЫДЕРЖКИ В НАТРИИ

№ п/п	Обозначение сплава	Темп. испытания, °C	Содержание кислорода в натрии, вес %	Длительность испытаний, часы	Содержание элементов, вес %			
					C	Si	Mn	N
1	Х20Н14С2 (20Cr – 14Ni – 2Si)	Исх.	–	–	0,078	2,26	1,45	н.о.
		650	$(3 \div 5) \cdot 10^{-3}$	350	0,072	2,26	1,44	н.о.
		730	$(3 \div 5) \cdot 10^{-3}$	350	0,067	0,72	1,17	н.о.
		875	$(3 \div 5) \cdot 10^{-3}$	350	0,024	0,58	0,78	н.о.
		875	$<1 \cdot 10^{3}$	350	0,080	1,20	0,73	н.о.
		875	$(3 \div 5) \cdot 10^{-2}$	500	0,021	<0,10	0,81	н.о.
2	Х20Н14С2Б (20Cr – 14Ni – 2Si– Nb) Nb/C = 10	Исх.	–	–	0,07	2,2	1,08	н.о.
		875	$<1 \cdot 10^{-3}$	350	0,12	1,2	н.о.	н.о.
		875	$(3 \div 5) \cdot 10^{-2}$	500	0,11	0,10	н.о.	н.о.
3	Х18Н15Г30 (18Cr – 15Ni – 30Mn)	Исх.	–	–	0,035	0,65	30,1	н.о.
		800	$(3 \div 5) \cdot 10^{-3}$	500	0,034	0,12	6,1	н.о.
		800	$(3 \div 5) \cdot 10^{-2}$	500	н.о.	н.о.	4,4	н.о.
4	Х16Н15М3 с азотом (16Cr– 15Ni– 3Mo – N)	Исх.	–	–	0,03	0,61	0,045	0,146
		720	$<1 \cdot 10^{-3}$	500	н.о.	н.о.	н.о.	0,090
		720	$(3 \div 5) \cdot 10^{-2}$	500	н.о.	н.о.	н.о.	0,085
		875	$<1 \cdot 10^{-3}$	500	н.о.	н.о.	н.о.	0,021
		875	$(3 \div 5) \cdot 10^{-2}$	500	н.о.	н.о.	н.о.	0,025
5	1Х13М2С2 (13Cr – 2Mo – 2Si)	Исх.	–	–	0,14	1,60	0,56	н.о.
		730	$<1 \cdot 10^{-3}$	350	0,07	1,40	н.о.	н.о.
		730	$(3 \div 5) \cdot 10^{-3}$	350	0,07	1,00	н.о.	н.о.
		875	$(3 \div 5) \cdot 10^{-3}$	350	0,054	0,80	н.о.	н.о.

Примечание: н.о. – *не определялось; толщина исследованных образцов* – 0,1 мм.

ТАБЛИЦА 3. ИЗМЕНЕНИЕ МЕХАНИЧЕСКИХ СВОЙСТВ ПОСЛЕ ИСПЫТАНИЯ В НАТРИИ И ВЫДЕРЖКИ В АРГОНЕ (T = 800°C; τ = 500 час)

№ п/п	Обозначение сплава	Условия испытаний		Механические свойства при 20°		
		Среда	Содержание кислорода, вес %	Предел прочности $\sigma_в$, кг/мм^2	Предел текучести $\sigma_{0,2}$, кг/мм^2	Удлинение δ, %
1	Х18Н15Г30 (18Cr – 15Ni – 30Mn)	Исх.	–	68	29	47
		Ar	–	70	35	22
		Na	$(3 \div 5) \cdot 10^{-3}$	38	27	2
			$(3 \div 5) \cdot 10^{-2}$	42	29	3
2	Х20Н14С2 (20Cr – 14Ni – 2Si)	Исх.	–	70	28	39
		Ar	–	75	30	31
		Na	$(3 \div 5) \cdot 10^{-3}$	69	26	37
			$(3 \div 5) \cdot 10^{-2}$	64	25	17
3	1Х13М2С2 (13Cr – 2Mo – 2Si)	Исх.	–	75	51	18
		Ar	–	47	34	23
		Na	$(3 \div 5) \cdot 10^{-3}$	49	32	25
			$(3 \div 5) \cdot 10^{-2}$	14	13	2

Примечание. Испытания проводились на разрывных образцах 49 × 6 × 0,4 мм.

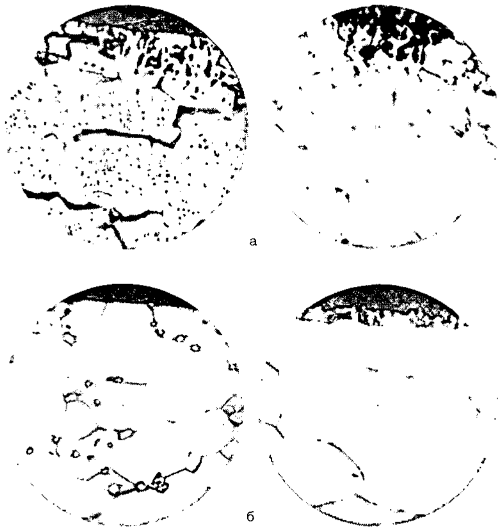

Рис.5. Структурные изменения под действием натрия в аустенитных и 13%-ных хромистых сталях (увел. 200 раз):

а) Межкристаллитная коррозия, шлиф не травлен (T = 800°C; $\tau = 500$ час; v = 3 м/сек; $0 \sim 3 \div 5 \cdot 10^{-2}$ вес%; слева – Х18Н15Г30 (180 Cr – 15 Ni – 30 Mn), справа – 1Х13М2С2 (13 Cr – 2 Mo - 2 Si).

б) Рост зерна (T = 800°C; $\tau = 500$ час; v = 3 м/сек; $0 \sim 3 \div 5 \cdot 10^{-2}$ вес%); слева – 1Х13 (13 Cr – 0,1 C (старение); справа – 1Х13 (13 Cr – 0,1 C) (Na).

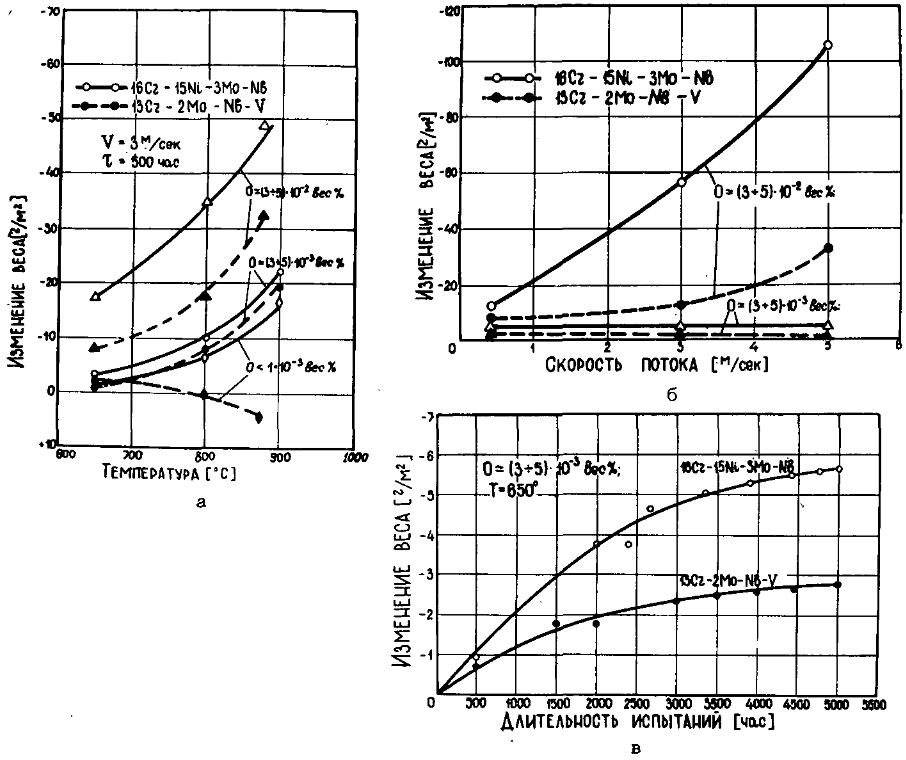

Рис.6. Влияние условий испытаний на стойкость в натрии аустенитной и 13%-ной хромистой сталей.

а) Влияние температуры (v = 3 м/сек; $\tau = 500$ час).

б) Влияние скорости потока (T = 650°C; $\tau = 1500$ час).

в) Влияние длительности испытаний (T = 650°C; $0 \sim 3 \div 5 \cdot 10^{-3}$ вес%; v = 3 м/сек).

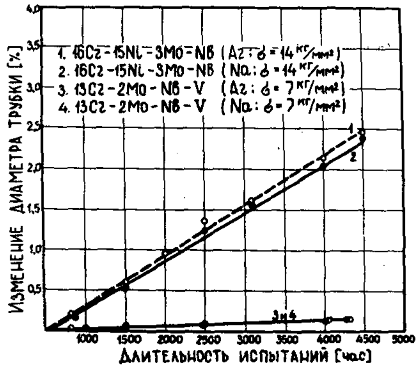

Рис.7. Сопротивление ползучести аустенитной и 13%-ной хромистой сталей в натрии (T = 650°C; 0 ÷ 3 – 5·10⁻³ вес %; v = 1 м/сек) и аргоне (T = 650°C).

ТАБЛИЦА 4. ИЗМЕНЕНИЕ МЕХАНИЧЕСКИХ СВОЙСТВ АУСТЕНИТНЫХ СТАЛЕЙ ПОСЛЕ ВЫДЕРЖКИ В НАТРИИ, ЗАГРЯЗНЕННОМ КИСЛОРОДОМ (ОДНООСНОЕ НАПРЯЖЕННОЕ СОСТОЯНИЕ, $\tau = 500$ час, $T = 600°C$, $O \sim 3 \div 5 \cdot 10^{-2}$ вес%)

Обозначение сплава	Уровень напряжений, кгс/мм²	Механические свойства	
		$\sigma_{0,2}$, кгс/мм²	δ, %
Х18Н10Т (18Cr – 10Ni – Ti)	0 2	19 32	40 10
Х16Н15М3Б (16Cr – 15Ni – 3Mo – Nb)	0 2	25 38	36 19

ЛИТЕРАТУРА

[1] HORSLEY, G.W., J. Iron Steel Inst. 182 (1956).
[2] DISTEFANO, J.R., HOFFMAN, E.E., Corrosion of Reactor materials II, IAEA, Vienna (1962) 431.

DISCUSSION

J. BEAUFRERE: Have you considered copper as one of the possible additives in your steels? What in your opinion would be the behaviour of a copper-bearing steel in sodium?

A.G. IOLTUKHOVSKY: We have investigated the effect of copper on the stability of austenitic steel in sodium at 650°C. We found that copper introduced into Type 18-8 steel has no effect on the stability of the steel if it is separated out by heat treatment (quenching and tempering) as an excess phase of the Cu-Ni type. If copper remains in the solid solution, however, the stability of the steel is somewhat reduced.

A. W. THORLEY: I should be interested to hear how you managed to maintain 500 ppm of O_2, as it is extremely difficult (owing to outside contamination effects) to maintain these levels in stainless-steel circuitry.

A. G. IOLTUKHOVSKY: To obtain the higher oxygen levels we inserted sodium peroxide at various points on the circuit before beginning the experiment. The cold-trap temperature was, correspondingly, raised to 300°C. Our analyses then showed 0.03-0.05 wt.% of oxygen.

A. W. THORLEY: And what values did you obtain with zirconium hot-trapping?

A. G. IOLTUKHOVSKY: Unfortunately our distillation method of analysis was not perfectly developed at the start of the work. Our results varied, depending partly on the material of the sampling container, from 0.001% to 0.0004%, but to be on the safe side we always based ourselves on the 0.001% value; this is of course for hot-trapping in every case.

H. O. BÖHM: You mentioned at the end of your talk that sodium appeared to have no effect on the secondary creep rate. Did you find that it affected the rate of tertiary creep?

A. G. IOLTUKHOVSKY: No, in low-oxygen sodium we observed no appreciable effect compared with what we observed in the experiments using argon.

M. N. IVANOVSKY: I should like to make a few general remarks which concern not only this but also papers SM-85/7 and 20. Oxygen, we should remember, is only one of many corrosion-producing impurities in sodium. Thus, in conditions more nearly approximating those encountered in actual reactor operation, when not only oxygen but other impurities as well are present, corrosion may differ from what we find in our test loops. In the presence of carbon or hydrogen, oxygen may take the form of Na_2CO_3, NaOH, or other compounds. If there is nitrogen in the sodium, this too can result in the formation of relatively unstable complex compounds which foster corrosion and mass transfer. In these circumstances the effect of oxygen, and the variation in its effect with changes of temperature and other factors, may be quite different from what we find in experimental loops where oxygen is the only impurity.

CORROSION BEHAVIOUR OF STEELS AND NICKEL ALLOYS IN HIGH-TEMPERATURE SODIUM

A.W. THORLEY AND C. TYZACK
U.K. ATOMIC ENERGY AUTHORITY,
REACTOR MATERIALS LABORATORY,
CULCHETH, WARRINGTON, LANCS.,
UNITED KINGDOM

Abstract

CORROSION BEHAVIOUR OF STEELS AND NICKEL ALLOYS IN HIGH-TEMPERATURE SODIUM. Our findings are summarized on the corrosion behaviour of low-alloy steels, austenitic steels and nickel alloys when exposed to sodium under flowing conditions in a pumped loop. The effects of altering various parameters on the rate of mass transfer from steel specimens in the highest temperature portion of the loops have been studied. These include the effect of temperature in the range 450 to 725°C, the effect of oxygen content of the liquid metal up to a level of approximately 30 ppm by weight (by adjustment of cold-trapping temperature), the effect of sodium velocity in the range 0.5 to 40 ft/s, the effect of specimen position, i.e. any downstream effects, and material variables such as the effect of alloying content in stainless steels and metallurgical conditions, i.e. cold work.

A discussion is included of the nature of complex oxide films formed on the surface of steels on initial exposure to sodium, and indications are given of selective loss of alloying elements from the surface of austenitic steels on exposure to liquid metal, as determined by microprobe, chemical and X-ray analysis.

Differences between the behaviour of iron-rich and nickel-rich alloys are discussed, particularly with respect to different responses to the effect of liquid metal velocity and oxygen level in the sodium. This leads to a general discussion of possible mechanisms of mass transfer and likely rate-determining processes, in particular why the mass transfer rate of iron should be sensitive to the level of oxygen in the the sodium. Also discussed are possible reasons for the very sharp fall in mass transfer rate of steel above a certain limiting velocity in the loop system in use. Much more remains to be done before a full understanding of the process is gained, and possible experiments are outlined.

1. INTRODUCTION

The sodium compatibility work at the Reactor Materials Laboratory in support of the fast reactor fuel cladding programme has pursued the following objectives:

(1) Study of mass-transfer by solution or oxidation processes at various temperatures and velocities.

(2) Study of the effect of loss of metal section and carbon pick-up upon mechanical properties.

(3) Study of the effect of imposed stresses on the clad material in a corrosive and carburizing environment.

In addition, work has been carried out on the evaluation of various braze alloys in sodium, as these may be used for joining components in future design.

TABLE I. LIST OF MATERIALS TESTED IN LIQUID SODIUM

Stainless steel	Composition (%)	Condition
Type 321	18Cr, 9Ni, 0.5Ti, 0.07C, Bal. Fe	Annealed (½h 1050°C Vac.)
316	18Cr, 11Ni, 3Mo, 0.06C, Bal. Fe	Annealed (½h 1050°C Vac.)
316L	17Cr, 12.5Ni, 2.8Mo, <0.03C, Bal. Fe	Annealed (½h 1050°C Vac.)
M316L	17.3Cr, 2.5Mo, 14Ni, 0.01C, Bal. Fe	As above, also 20% cold-worked
M316	17.3Cr, 2.5Mo, 14Ni, 0.04C, Bal. Fe	As above, also 20% cold-worked
FV548	16.5Cr, 11.5Ni, 1.5Mo, 1.0Nb, 0.08C	H.T. 1h 1150°C Vac. also 20% 3h 850°C cold-worked

Nickel alloys	Composition (%)	Condition
Solid solution strengthened		
Inconel 600	77Ni, 6Fe, 16Cr, 0.02C	940°C 2h Vac.
Nilo. 50	50Ni, 50Fe, 0.03C	900°C 1h Vac.
Nilo. K	53Fe, 29Ni, 16Co, 0.03C	950°C 1h Vac.
Precipitation hardening		
Nimonic 80A	75Ni, 20Cr, 2.3Ti, 1.4Al. 0.06C	Soft 1100°C 10 min. W.Q. O.P. 1050°C 8h 700°C 16h
PE 11	35Fe, 38Ni, 18Cr, 5.2Mo, 2.2Ti, 0.9Al, 0.07C	20 min 1020°C + 700°C 16h
PE 16	34Fe, 43Ni, 16.5Cr, 1.2Al, 1.2Ti, 0.06C	1020°C ½h AC + 800°C 2h AC + 700°C 16h AC also cold-worked

2. MATERIALS INVESTIGATED

The cladding materials investigated include stainless steel and nickel alloys, and are detailed in Table I. Braze materials examined have been restricted to four alloys:

Nichrobaz 30, 10% Si, 19% Cr, balance Ni
Nichrobaz 50, 10% P, 13% Cr, balance Ni
Coast NP, 3.5% P, 11% Si, 5.4% Mo, 30% Fe, balance Ni
Coast 57 S, 47% Fe, 11% P, balance Ni

3. PARAMETERS INVESTIGATED

The effects of varying the following parameters on the behaviour of fuel cladding materials are being investigated:

(1) Sodium temperature in the range 600 - 750°C.
(2) Oxygen content of the liquid metal up to levels of approximately 30 ppm (by varying cold-trap temperature)
(3) Sodium velocity in the range $\frac{1}{2}$ - 40 ft/s. Certain static tests are also being carried out. Reynolds number evaluations are also being made.
(4) Effect of internal pressure over the range 0 - 3000 lb/in^2 on the carburization rate of sealed capsules exposed in sodium at 650°C and 700°C.

4. EXPERIMENTAL METHODS

The design and operation of the electro-magnetic pumped loops has been described previously [1]. In general the test specimen is so designed that both corrosion values and mechanical property changes can be evaluated after exposure to sodium. Test pieces are in the form of hollow bore tensile specimens of wall thickness 0.040 in. or 0.015 in.

Once the desired test conditions have been established in the loop six or eight of these specimens arranged consecutively in a holder are located in the hot zone of the pumped sodium loop. During the total exposure period of six or nine months, specimens are removed periodically from the sodium to evaluate weight and diametral changes, carbon pick-up and tensile properties. In addition, certain specimens are sectioned for subsequent X-ray, chemical and microprobe analysis of the surfaces which have been in contact with sodium.

The oxygen level of the main circuit is maintained by the cold trap which dispenses oxygen to the circuit at a level dependent upon its temperature, and steady oxygen levels are established before specimens are inserted in the loop. More recently, experiments have been carried out in which the oxygen level has been changed during a test to assess whether the changes in corrosion rates observed are in line with rates obtained previously at the pre-set levels (Figs 1 and 2).

The carburization studies involve the determination by chemical analysis of carbon picked up by the specimens during the exposure period. The carbon levels are taken either as an average bulk value across the gauge length, or by machining layers from the exposed surfaces to

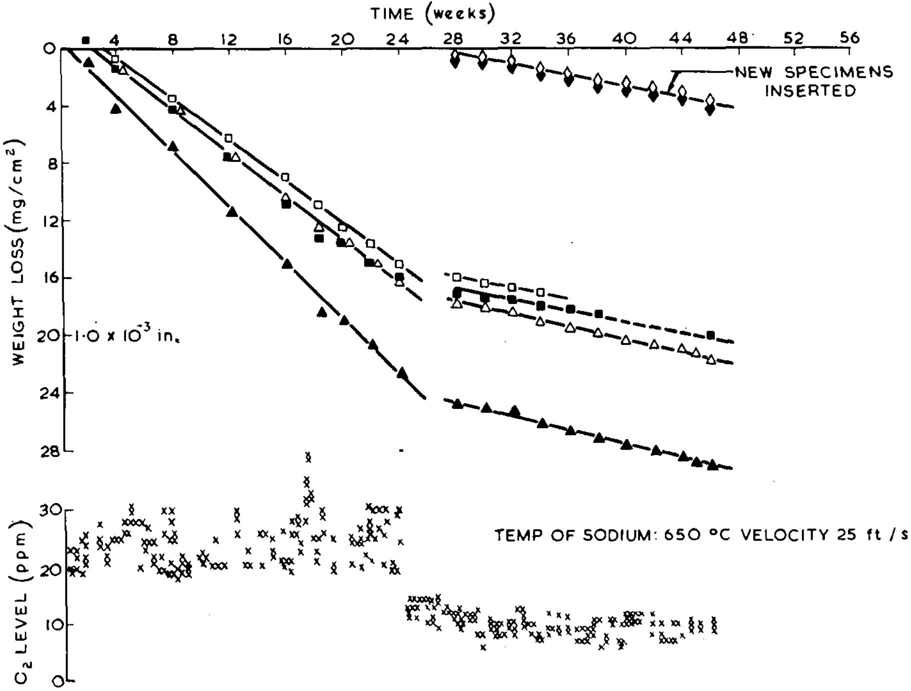

FIG. 1. The effect of changing the oxygen level of liquid sodium on the rate of metal loss of M316 stainless-steel specimens in situ during change

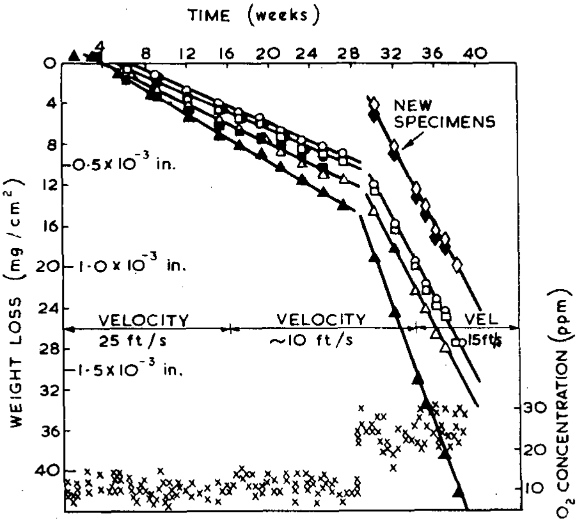

FIG. 2. The effect of changing velocity and oxygen level of liquid sodium on the rate of metal loss from 316 stainless steel, temp. 725°C specimens in situ during change

establish a carbon gradient. In addition to the high velocity specimens, similar specimens, together with thinner plate tensile specimens (0.028 in. thick) are also exposed to the same sodium environment by immersing these materials in the near-static sodium in the well of the loop, adjacent to the high velocity test section. Test pieces are fractured after sodium exposure, some in tensile tests at room temperature and others at the sodium test temperature. For comparison, mechanical tests are also carried out on control specimens which have been exposed in argon with a similar thermal history to those exposed in sodium.

To assess the effect of imposed stress on stainless steel while it is being subjected to carburizing and corrosive processes a tube-burst rig has been constructed in which pre-pressurized cans can be suspended in high-temperature flowing sodium. The study is aimed at determining whether the rate of corrosion and carburization of the cladding material is enhanced under stress in comparison with results obtained on unstressed specimens. In addition an attempt is being made to follow diametral changes during the exposure period. A test run has been completed on annealed and 20% cold-worked M316 material at 650°C with sodium containing oxygen about 10 ppm with varying can pressures up to 3000 $lb/in.^2$

5. EXPERIMENTAL RESULTS

5.1. Corrosion data on stainless steels

Long-term corrosion data are now available for the range of Type 316 alloys, together with some preliminary values for FV548.

The majority of the materials when first exposed to sodium show a small initial weight gain, but after periods which are somewhat variable, weight losses are measured and thereafter steady linear metal loss rates are recorded (see Fig. 3). The extrapolated weight losses given in thousandths of an inch per year, and illustrated in Fig. 4, are derived from this latter part of the curve. From the collected data and illustrations, the following points may be noted in relation to the corrosion of stainless steels.

5.1.1. The effect of temperature

Figure 4 summarizes the results obtained in the form of a plot of corrosion rate (in./yr) against reciprocal temperature at oxygen levels of 10 and 25 ppm. The corrosion rate at the higher oxygen levels is related to the absolute temperature, T, in the temperature range 450 - 725°C by the equation

$$S = 2.3 \times 10^{-6} \, (\exp) - \frac{17\,500}{RT} \; \mathrm{cm\ s^{-1}}$$

5.1.2. The effect of oxygen level

One of the most important parameters in determining corrosion rate is the oxygen content of the sodium. This is illustrated in Figs 1, 2 and 4. Reducing the level from 25 to 10 ppm reduces the rate by a factor of about

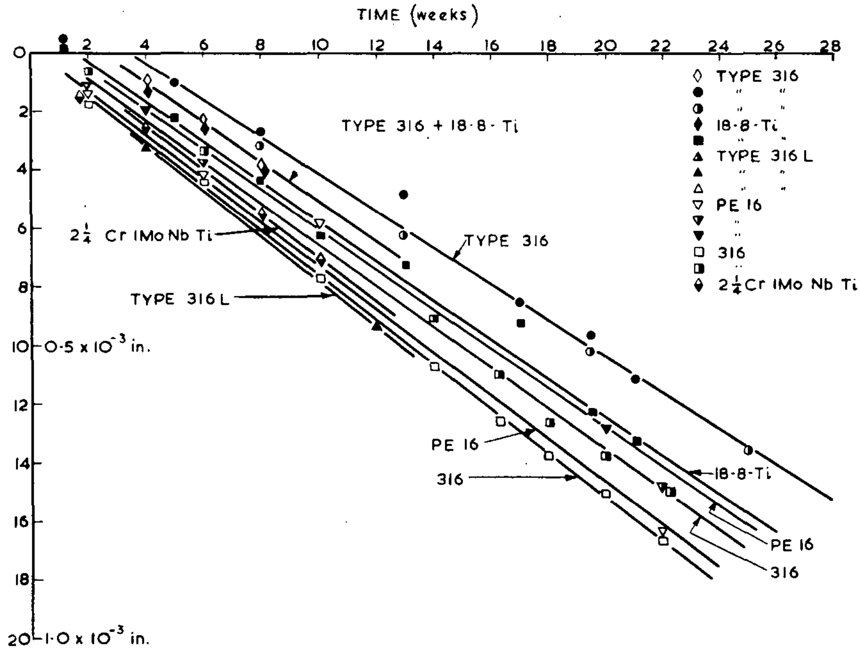

FIG.3. A comparison of the behaviour of various steels in flowing sodium at 650°C,O_2 level ~25 ppm central specimens taken for comparison purposes

2 at 650°C. At < 5 ppm oxygen corrosion rates are markedly reduced and over the short term are more or less negligible. It has been established that a roughly linear relationship exists between metal loss rate and oxygen level at 650°C.

5.1.3. Effect of specimen position

Over the short length of specimen holder (~8 in.) the "positional-effect" is not very marked (see Figs 1 and 2) although enhanced corrosion is observed on the first specimen, e.g. with stainless steel at 650°C and sodium containing ~25 ppm O_2 the corrosion rate on the first specimen is about 2.1×10^{-3} in./yr compared with 1.8×10^{-3} in./yr on the remainder. In the tube burst experiments (see later) a marked positional-effect is observed over the length of the specimen assembly, which is ~36 in.

5.1.4. Effect of velocity

This effect is currently being assessed at the 25 ppm O_2 level at 650°C on M316 material (see Fig. 5). Values so far obtained up to 10 ft/s show a more or less linear increase of corrosion with velocity in this lower range. However, it is thought that a point of inflexion occurs somewhere in the range 10 to 15 ft/s, above which velocity has very little effect on the rate of metal loss. At the lower oxygen levels, 10 ppm and < 5 ppm O_2, velocity changes have been investigated up to 40 ft/s. Here again very little change in corrosion rate is recorded in the range

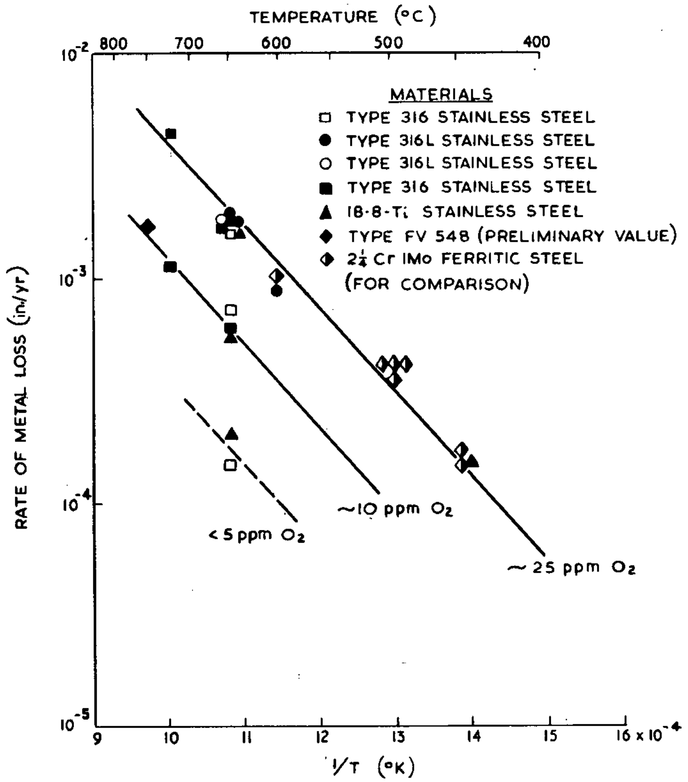

FIG.4. Effect of temperature and O_2 level on rate of metal loss of various steels in flowing sodium

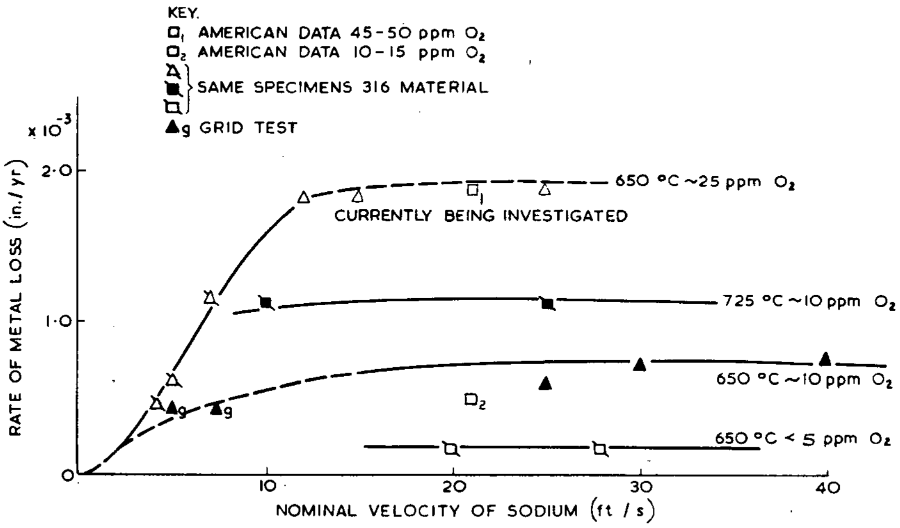

FIG.5. Effect of velocity on the rate of metal loss from various stainless steels (bore dia constant)

15 - 40 ft/s for Type 316 materials. It is noteworthy that the substantially velocity-independent rate established is a function of oxygen content of the liquid metal.

5.1.5. Effect of alloying content

Within the over-all specification embracing the stainless steels tested, the effect of slight variations in, say, nickel-chromium contents, plays no detectable part in altering corrosion rates. The same can be said for small additions of carbon stabilizing elements such as niobium or titanium. It is not until nickel contents are appreciably raised that changes in rate and processes become radically altered (see corrosion of nickel alloys). It is also of interest to note in Fig. 4 that the steady-state corrosion rate of $2\frac{1}{4}$ Cr 1 Mo steel shows essentially similar rates as the stainless steel.

5.1.6. Effect of metallurgical condition

Results to date suggest that material condition (i.e. whether annealed or 20% cold-worked) does not affect the rate of metal loss.

5.2. Corrosion of pre-pressurized 316 tubes

The specimen holder, which is ~36 in. long, consists of a cluster of four tubes, each containing a stringer of pre-pressurized tubes. Specimens in two of the tubes are exposed to flowing sodium, while the other two contain static sodium. There are twelve tubes per stringer covering a range of pressures from 0 - 3000 lb/in.^{2} at 650°C. The tubes have been exposed for nine months at 650°C (O_2 level - 10 ppm) and most of the earlier conclusions in the paper are relevant. Briefly, these and other points relevant to the tube burst programme can be summarized as follows:

(1) No tubes burst during the test period of nine months.
(2) The corrosion rates of both 20% cold-worked and annealed materials were the same.
(3) The corrosion rate did not appear sensitive to applied stress.
(4) Changing the velocity of the sodium over the specimens from 7 to 15 ft/s during the test increased the corrosion rate. Above 15 ft/s the change was not marked up to 25 ft/s.
(5) The corrosion rate was sensitive to any oxygen changes made during the test.
(6) The corrosion rate was sensitive to position. A change in rate of approximately 4 : 1 occurred over the specimen length.
(7) The highest rate of metal loss observed was equivalent to a maximum value of 0.4×10^{-3} in./yr.
(8) The specimens were extremely clean looking and to all intents and purposes looked matte chromium plated.

The tubes are currently being assembled for bursting to assess pressures required for failure. This will be followed by carbon analysis. Diametral changes have not yet been compared with those of pre-pressurized thermal controls.

5.3. Observations on corrosion processes

In the majority of runs it is found that the weight change-time curve for stainless steels consists of two parts. The first is a period of weight increment associated with the formation of either green or black oxide films on the surface of the material. This is eventually superseded by a linear weight loss regime where the film has disappeared, and the specimen surface is either matte-grey metallic or shiny metallic, depending upon the oxygen level of the sodium.

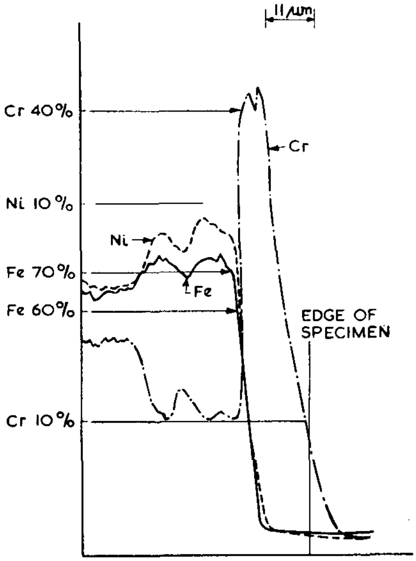

FIG. 6. Element depletion in 18-8-Ti stainless steel due to formation of oxide film in liquid sodium

Microprobe, chemical and X-ray analyses [2, 3] have been carried out on specimen sections and surfaces contacted by the liquid sodium from both the weight gain and weight loss regimes. In the first instance X-ray and chemical analysis have shown that the film formed on the specimen surface is of the sodium chromite type ($NaCrO_2$) and this results in a denudation of chromium in the substrate material (see microprobe trace Fig. 6). Secondly, once the film is removed by the flowing sodium further modification of the steel's surface occurs, due this time to the selective removal of nickel from the alloy (see Fig. 7). This produces a layer of ferrite which is then in contact with the liquid sodium for the remainder of the test period. In the light of these findings it is not perhaps surprising that the high-temperature stainless-steel results agree reasonably well with corrosion values obtained on ferritic steels tested at lower temperatures (see Fig. 4).

5.4. Corrosion of nickel rich materials

A preliminary examination of the behaviour of certain nickel-rich alloys of the Nimonic type showed that with increasing nickel content the rates of metal loss increased to values which were probably unacceptable

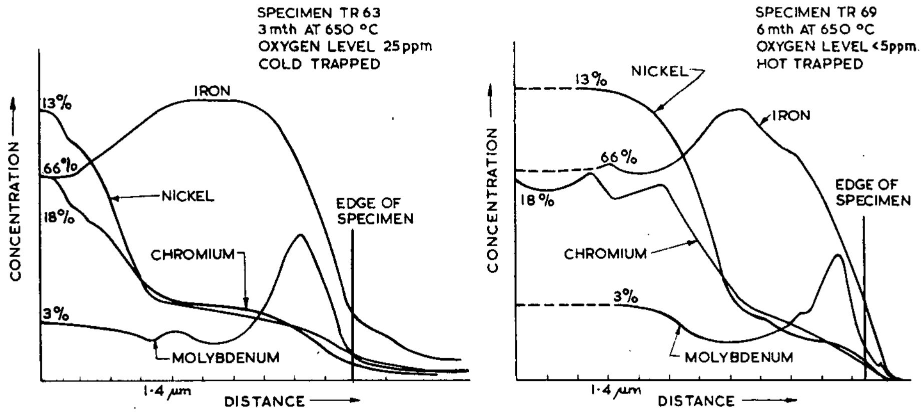

FIG. 7. Element depletion in Type 316 stainless steel after exposure to liquid sodium

for a fuel-cladding application. The short-term results obtained from two-month exposures at 650°C in sodium containing ~25 ppm oxygen and flowing at a velocity of 30/40 ft/s past the specimens are summarized in Table II. However, as Nimonic 80A has good high-temperature strength and is readily available in tube form, additional tests were carried out to establish whether the extent of corrosion could be reduced by lowering the oxygen content, or the velocity, of the sodium. It was found that over the velocity range 5 - 40 ft/s the material was relatively insensitive to oxygen level in the range investigated, namely, less than 10 ppm and

TABLE II. DATA OBTAINED FROM MATERIALS EXPOSED TO DYNAMIC SODIUM (30 - 40 ft/s) CONTAINING 25 - 30 ppm OF OXYGEN AT 650°C FOR 8 WEEKS

Material	Extrapolated loss in metal section (thousandths of an inch per year)
Inconel 600 (soft)	6.1
Nimonic 80A	4.9
Nickel	3.9
PE 11 (soft)	2.9
PE 16 (soft)	2.8
Nilo 50 (soft)	2.5
18/8/1 Ti	2.4
PE 16 (opt. props.)	2.3
316 S.S.	1.8
PE 11 (opt. props.)	1.8
Nilo K (soft)	0.95

approximately 25 ppm, but that there was a marked dependence on velocity in this range, in contrast to austenitic steels. The corrosion rate observed at 650°C at a linear velocity of 17.5 ft/s was in line with that observed in stainless steels in sodium containing 25 ppm of oxygen at high velocities (see Fig. 8).

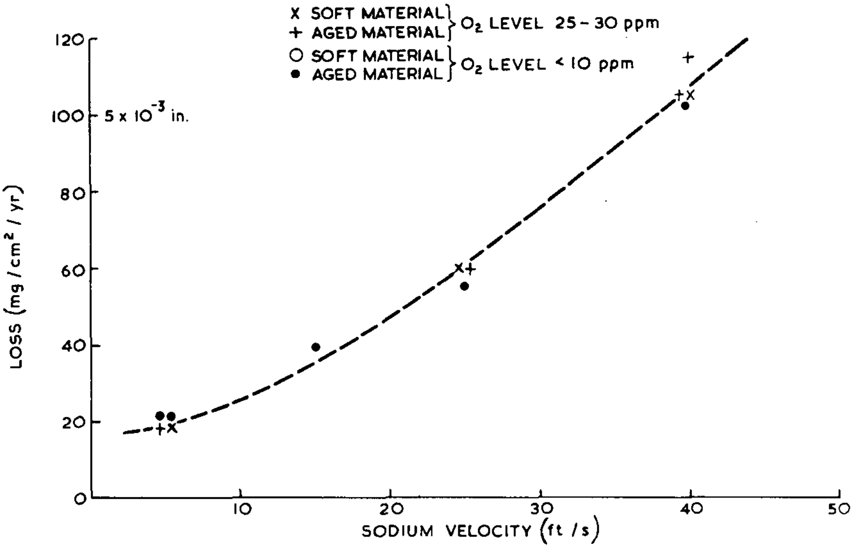

FIG. 8. Effect of velocity on the rate of metal loss from nimonic 80A at 850°C

From the metallographic appearance of the specimens after test it would appear that the corrosion of this material is primarily by the solution of nickel from the specimen surfaces. The insensitivity of the corrosion rate to oxygen level is in line with the findings of workers at Fulmer that no complex nickel sodium oxides can exist in the presence of sodium at unit activity [3]. The reported solubility of nickel in sodium at 650°C [4] is about 23 ppm, and it would appear that the amount removed from the hot side surfaces to be precipitated in the cold is markedly dependent on the velocity of the liquid metal, which indicates a diffusion-controlled process.

PE16, on the other hand, because of its lower nickel content, has shown a reduced corrosion rate at velocities of about 30 - 40 ft/s. The corrosion value is approximately half that of Nimonic 80A exposed under comparable conditions at 650°C, O_2 level ~25 ppm. However, whether the corrosion behaviour of PE16 is more characteristic of a nickel- or iron-rich material has yet to be established, and work is in hand to investigate the behaviour of the alloy in flowing sodium over a range of velocities at oxygen levels of < 5, 10 and 25 ppm at 650°C. The material is also being investigated at a possible hot-spot temperature of 750°C at 10 ppm O_2.

Preliminary values so far obtained (see Table III) suggest that the material is not drastically affected by velocity or oxygen changes of the liquid metal (compared with iron-or nickel-rich materials) although there does appear to be some decrease in rate when either variable is reduced. On the other hand, there are indications of a gradual decrease

TABLE III. CORROSION OF PE 16 AT 650°C

O_2 level of sodium (ppm)	Velocity of sodium	
	+15 ft/s[a]	30 - 40 ft/s
~10		1.5×10^{-3} in./yr (1-month test) 1.6×10^{-3} in./yr (Repeat 2-month test)
~25	1.8×10^{-3} in./yr (6-month test)	2.3×10^{-3} in./yr (2-month test)

[a] This is a down-rated velocity value caused by failure of a loop component. It is the minimum value finally measured. During the experiment it is considered the velocity was higher than 20 ft/s.

in corrosion rate as a function of time suggesting gradual enrichment of the surface with respect to iron. It will be interesting to check whether the material becomes oxygen sensitive at this stage.

5.5. Carburization of stainless steels

Carbon picked up by stainless steel from liquid sodium has been shown previously to reduce the room temperature ductility of both 18/8/Ti and Type 316 stainless steel. A similar drop has now been found with both M316L, M316 and PE16 alloys after continuous exposure to sodium. Results taken from the six-months and eight-months loop tests at 650°C for M316L and M316 materials respectively show that average carbon levels in both materials had increased to 0.06 and 0.3% (starting values 0.01 and 0.05% respectively) and to 0.10% carbon in PE16 (starting level 0.05%). In all materials carbon gradients existed through cross-sections of the specimens, and surface levels of 0.2 and 0.3% carbon in M316L and PE16 respectively were recorded. Although there was again some effect on the room temperature ductility, it was established that these levels did not materially affect the high temperature (650°C) ductility (see Table IV). The type of carbide resulting from the carburization of the steel surfaces has been identified as $M_{23}C_6$ type, which is dispersed both intra- and inter-granularly in the steel matrix. More recently examination of black deposits formed on M316 surfaces at 650°C during exposure to sodium has shown these to be M_6C type carbides which, from a comparison with standards, appear to be of the composition Fe_4Mo_2C.

It has been found that after approximately nine-months loop exposure at 725°C, M316 specimens of 0.015-in. wall thickness have picked up carbon to an average level of 0.37%. Room temperature ductility values of 24% have been measured after exposure, against control values of 40%. On the other hand, high-temperature (725°C) control and sodium-treated tensile values are comparable, 28 and 23% respectively being recorded.

In order to establish the sort of carbon level required to promote brittleness in stainless steels and nickel alloys certain materials have been exposed in static sodium to a carburizing source of 0.36% carbon steel. The experiment, which represents more arduous carburizing conditions than might be expected in practice, utilizes plate tensile specimens 0.028 in. thick which are exposed to sodium on both faces, so that the carbon diffusion path is not too dissimilar from the practical fuel cladding case. Mechanical property values are being obtained over a range of temperatures (500 - 800°C) after various periods of exposure up to six months for the 316, FV548 and Nimonic alloys. However, for the purpose of this review, ductility values obtained at 650°C for different carbon levels are taken as being demonstrative of the sort of carbon levels required to promote loss of ductility in these materials. The results are summarized in Table V.

5.6. Corrosion of braze materials in sodium

A certain amount of work has been carried out on the behaviour of braze alloys in liquid sodium. Materials were tested as either butt- or fillet-brazed joints where the braze was used to join M316L materials. Corrosion testing was started on four materials: Nichrobraz 30, Nichrobraz 50, Coast NP and Coast 57 S. However, Coast 57 S was eliminated from the studies because of its inferior as-brazed structure resulting from corrosion or erosion of the base stainless steel during the brazing operation.

Sodium exposures of two-months duration in both static and dynamic sodium (velocity 40 ft/s) at 650°C, O_2 level ~10 ppm, were carried out on both types of joint. The butt-brazed joints were tested "as-brazed" whereas the fillet-brazed materials were given a homogenization treatment of 1500 h at 750°C before exposure to sodium.

In relation to corrosion values determined on both specimen geometries it must be appreciated that the amount of braze surface exposed to the sodium in the case of butt-brazed joints is small compared with the remainder of the specimen (stainless-to-braze area 100 : 1), and, secondly, fillet-brazed materials were not comparable specimen to specimen because of the spreading of braze material on to other surfaces. However, in the case of butt-brazed assemblies, the weight-change values were no worse than the accompanying unbrazed M316L specimens, and metallographically they showed no obvious signs of erosion at the surfaces contacted by the sodium. Fillet-brazed joints, on the other hand, were more difficult to assess but from the data obtained Coast NP brazed specimens were comparable with unbrazed stainless steel whereas Nichrobraz 30 and 50 showed higher corrosion losses, 2×10^{-3} in./yr and $>1 \times 10^{-3}$ in./yr respectively. Unbrazed M316L over the same period was about 0.8×10^{-3} in./yr.

Microprobe analysis [5] and metallographic examination of the joints after test gave more informative results and these can be summarized as follows:

(1) Phosphorus is more or less completely removed from Nichrobraz 50 in both static and dynamic sodium (see Fig. 9). Homogenization of the braze before sodium testing does not prevent this occurring.

(2) Silicon is removed from Nichrobraz 30 to a depth of 0.0025 in. in both dynamic and static sodium tests.

TABLE IV. CARBURIZATION OF STAINLESS STEELS AND NIMONIC PE 16 IN SODIUM AND ITS EFFECT UPON DUCTILITY

Material and original carbon level (wt. %)	Type of specimen	Sodium temperature (°C)	Oxygen level (ppm)	Time (months)	Carbon level after test (wt. %)		Room temperature elongation (%)			Elongation at the sodium temperature (%)		
					Mean	In a surface layer 0.01 cm thick	Original	In argon	In sodium	Original	In argon	In sodium
Annealed 18/8/Ti 0.07	0.040 in. wall annular	650	25/30	6	0.13	0.31	59	57	25			
Annealed 316 0.05	0.040 in. wall annular	650	25/30	6	0.09	0.19	67	51	33			
Annealed M316L 0.01	0.040 in. wall annular	650	25/30	6	0.055	0.18	78	72	62	40	37.5	37.5
Annealed M316 0.05	0.015 in. wall annular	650	25/10	8	0.29	-	64	37	27	33	32	28
Annealed M316 0.05	0.015 in. wall annular	750	25/10	6½	0.32	-	52	40	31			
				9	0.38	0.60	52	40	24			
				9½	0.38	-				36	25	23
PE. 16 0.05 Aged	0.040 in. wall annular	650	25/30	6	0.1	0.40	25/32	23	10	23/30	22	22

TABLE V. EFFECT OF CARBON CONTENT ON THE DUCTILITY OF VARIOUS MATERIALS

Material	Temperature (°C)	Original elongation (%)	C level required to give 50% reduction in original ductility (%)	C level required to give 75% reduction in original ductility (%)	C level required to give 100% reduction in original ductility (or zero ductility) (%)
316L	R. T.	65 - 70	0.2 - 0.3	0.4	~1.0
annealed	650	33	0.4	0.6	>1.1[a]
18/8/Ti	R. T.	50 - 55	0.2	0.3 - 0.5	~1.0
annealed	650	30	0.7	1.0	>1.3
Nim. 80A	R. T.	15 - 17	0.1 - 0.2	0.1 - 0.2	>0.7
Aged	650	6 - 8	0.7	0.6	
PE 16	R. T.	20 - 22	0.1 - 0.2	~0.4	>0.4
Aged	650	20	0.5 - 0.7	0.7	>0.6
FV 548	R. T.	50 - 55	0.3	0.4	~1.0
annealed	650	25 - 30	0.5	0.4	>0.9

[a] Where the > sign is used this is the recorded value after 6 months exposure; complete embrittlement is still not observed.

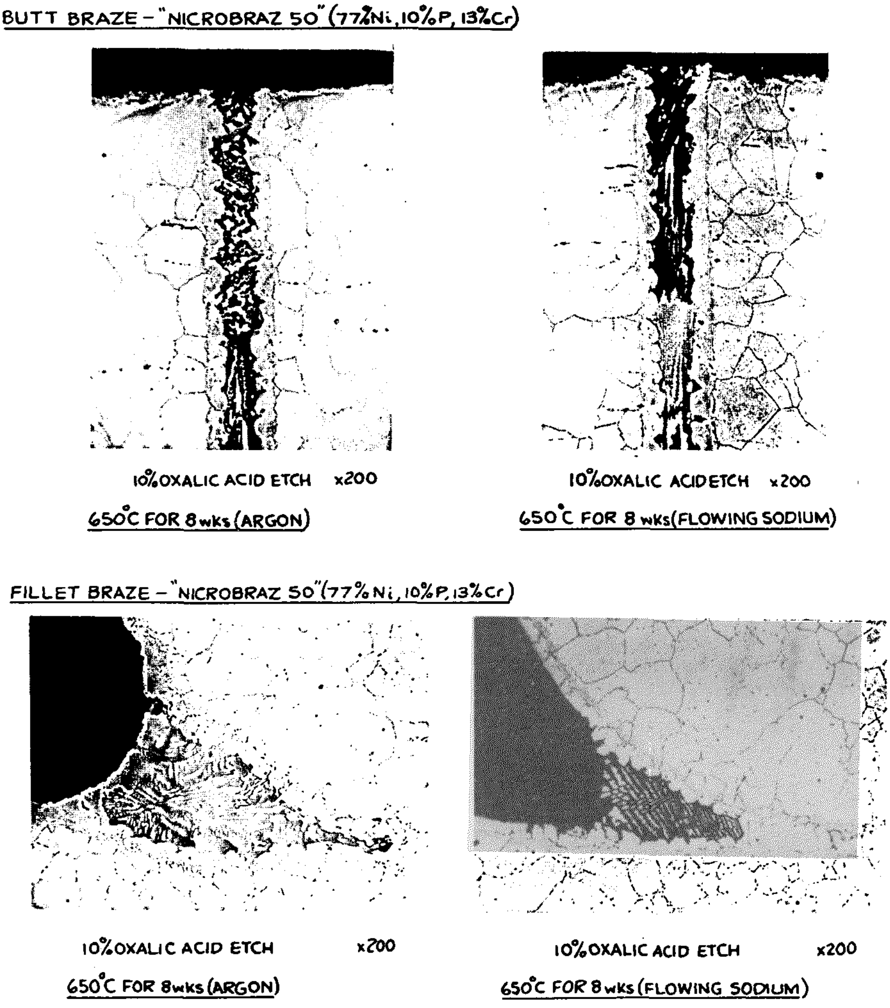

FIG. 9. Photomicrographs showing removal of phosphorus from the braze structure

(3) Phosphorus and silicon are depleted to a depth of 0.001 - 0.002 in. in Coast NP brazed materials.

(4) In all tests there was no marked erosion of the braze material due to localized turbulence around such things as brazed wires. Some surface attack was observed, but this was possibly a result of surface cleaning by the sodium.

(5) In the sodium-treated specimens the braze-steel interface was good, and within the optically defined limits of the braze area there was little or no diffusion of braze elements into the steel matrix, although in Nichrobraz 50 material there was still evidence of small isolated phosphorus-rich regions in existence at the edge of the braze adjacent to the stainless steel. However, a certain amount of iron (levels not recorded) was found in both

Nichrobraz 30 and 50 braze structures. From previous experience it seems that this could have resulted from pick-up during the actual brazing operation.

In the light of the above information, and with knowledge of the behaviour of certain nickel-rich materials, it is possible to hazard some guesses about the likely behaviour of these materials in sodium. For example, both Nichrobraz 30 and 50, because of sodium exposure, become basically an alloy not far removed from Nimonic 80A, and Coast NP, because of its iron content (30%), becomes very similar to PE 16. For this reason it would be expected that of the three alloys Coast NP would be the most corrosion resistant in flowing sodium. However, how far this view may have to be modified in the light of iron pick-up in the braze is not known until chemical analyses of the iron content of the brazes have been established.

6. DISCUSSION

6.1. Mass transfer of austenitic steel and nickel alloys in sodium

The steady-state corrosion rates of steel observed in experiments in our loops are generally more than two orders of magnitude lower than would be expected from a process involving diffusion control across a bonding layer at the solid-liquid metal interface. In the simplest treatment the rate of metal loss R at a given temperature should be given by

$$R = K(\bar{N}_{Fe} - N_{Fe})$$

where $\bar{N}_{Fe}$ is the mol fraction of iron dissoved in sodium at saturation
N_{Fe} is the mol fraction of iron in the main sodium stream
K is the constant for a given temperature.

If the process is diffusion controlled K should be dependent on the diffusion coefficient of iron in sodium, and on the velocity of the liquid metal past the specimens. If, on the other hand, the slowest step is some process occurring at the interface, then K may be independent of diffusion coefficient and velocity.

One reason for the discrepancy between calculated and observed mass transfer rates may be that the steady-state level of iron in the main sodium stream is close to saturation. If we consider an idealized loop composed of two equal areas, one area at temperature T_2 and the other at temperature T_1, where $T_2 > T_1$, on the assumption that the dissolution and deposition reactions are identical in that they involve the same species and are reversible, then the steady-state level of iron N_{Fe} in the circuit would be given by

$$N_{Fe} = \frac{K_{T_2}}{K_{T_2} - K_{T_1}} \bar{N}_{Fe_{T_2}} - \frac{K_{T_1}}{K_{T_2} - K_{T_1}} \bar{N}_{Fe_{T_1}}$$

where K_{T_2} and K_{T_1} are the constants of the dissolution reaction at temperature T_2, and of the deposition reaction at temperature T_1 respectively, and $\bar{N}_{Fe_{T_2}}$ and $\bar{N}_{Fe_{T_1}}$ are the terminal solubilities of iron at the two temperatures.

Clearly the more sluggish the back reaction, the closer the steady-state level of iron approaches the terminal solubility at the higher temperature. In practice in a loop no such ideal situation exists, nevertheless the following points may be significant.

In our stainless-steel loops the area of the specimens exposed in relation to the total loop area at high temperature is relatively small, consequently there will be a sizeable contribution of dissolved iron from these surfaces; secondly, measured iron contents of the sodium in the loops are in the range of a few ppm, which is an appreciable fraction of terminal solubility at the highest loop temperature; thirdly, the operation of the loop at a given oxygen level gives similar mass transfer rates whether or not the cold trap (taking approximately 1% of the flow) is valved in or out, arguing that at this small fractional flow the cold trap itself is not a major sink for iron.

It was suggested in an earlier paper [6] that the discrepancy between observed and calculated mass transfer rates for ferritic alloys might be explained if one took the figures of Baus et al. [7] for the solubility of iron in sodium (obtained by radiochemical techniques) which are 400 times smaller than those given by Epstein in the Liquid Metals Handbook [8]. This view is now thought to be erroneous as measurements at the Reactor Materials Laboratory of terminal solubilities of iron (at a range of temperatures) have shown that the values at 650°C, around 10 ppm, are in broad agreement with the Epstein KAPL figures.

One of the most clearly substantiated features of the work reported here is the dependence of the mass transfer rate on the oxygen level of the sodium, summarized in Figs 1, 2 and 4. This has also been observed in the United States of America [9], and any satisfactory mass transport theory must take cognizance of this fact. We have also observed this sensitivity to oxygen in the corrosion of pure iron in sodium, and so it is not peculiar to chromium-containing materials.

In trying to understand this phenomenon it is perhaps worthwhile first of all to examine whether any binary iron-sodium oxygen compounds exist in the low oxygen content sodium environments which could play a role in the corrosion process. Workers at the Fulmer Research Institute have carried out, under contract to us, thermochemical measurements on this system, and these will be reported in detail elsewhere.

Briefly, the reactions of sodium oxide with iron and its oxides have been studied at 500° and 600°C. The existence of a double oxide of composition $FeO(Na_2O)_2$ originally reported by Horsley [10] has been confirmed by mass balance and chemical analysis. The heat of solution of FeO and Na_2O to form this double oxide has been determined by measuring the heat of solution of samples containing the compound in hydrochloric acid and comparing this with the heats of solution of the constituent oxides. A value for the heat of combination has been determined as ΔH^0_{298} = -24.8 kcal per mole of FeO. The free energy of the reaction

$$Na_2O + Fe = FeO + 2\,Na \quad (1)$$

is given by $\Delta G^0 = 36.0 - 16.8\ T = 21.5$ kcal at 923°K.

This reaction combined with

$$FeO + 2\,Na_2O = FeO(Na_2O_2)$$

with $\Delta G^0 = DH^0 = -24.8$ kcal
gives $\Delta G^0 = -3.3$ kcal for the reaction

$$3\,Na_2O\ (\text{in Na}) + Fe\ (S) = FeO(Na_2O)_2\ (\text{in Na}) + 2\,Na\ (L)$$

This indicates, as was discussed in an earlier paper [6], that for the formation of the double oxide as a separate phase at 650°C it is necessary for the sodium oxide activity to be in excess of 0.55. As the solubility of oxygen in sodium at 650°C ~1585 ppm (extrapolated value) then it was argued that the oxide complex would only be present at unit activity at 650°C when the oxygen content of the sodium is in excess of about 870 ppm, and thus one would not expect it to be present as a discrete phase in our loop investigations where the maximum level of oxygen in the sodium is about 30 ppm. However, this argument overlooks one important fact, namely, that although the free energy of formation of the complex oxide decreases with decreasing temperature, nevertheless its formation may be favoured in the cold parts of the circuit, in the vicinity of the cold trap, because the oxygen activity of the sodium is close to unity, as is the iron activity. Hence, kinetics permitting, conditions in the sodium issuing from the cold trap may be favourable for nucleation of the double oxide. Once nucleated, the material may have a measurable life in the main circuit and the possible significance of this on the over-all mass transfer process will be discussed later.

On the assumption that the mass transfer process is diffusion controlled there would appear to be a number of ways in which oxygen might affect the process. One is by altering the value of the diffusion content of iron in sodium, about which we can say nothing at present; a second is by altering the terminal solubility at a given temperature. An examination of how oxygen as a dilute solute could alter the activity coefficient of iron in the ternary sodium-oxygen system, expressed in terms of the Chipman interaction parameter, was given in an earlier paper [6]. However, experimental measurements in our laboratories on the solubility of iron in sodium containing 10 and 100 ppm by weight of oxygen at 650°C indicated only ~50% increase from ~7 to ~10 ppm Fe, between the two levels, and this is insufficient to account for the major part of the increase in mass transfer rate with increasing oxygen level, as we know that an increase of only 10 to 25 ppm oxygen can double the rate of loss of metal.

As discussed by Dunn et al. [11] and Epstein [12] some success in the analysis of mass transfer data has been achieved by noting the physical parallelism between mass and heat transfer. Thus for turbulent forced convection flow through pipes the Chilton-Colburn equation for heat transfer can be modified for mass transfer to give

$$j_D = (K_D/v)\,(Sc)_f^{\frac{2}{3}} = 0.023\,(Re)_f^{-0.2}$$

where j_D is the j factor for mass transfer, K_D is the mass transfer coefficient, v is the linear velocity, Sc_f is the Schmidt number and Re_f

is the Reynolds number across the film. Whence it follows that the rate of metal loss, R, in a diffusion-controlled process is given by

$$R = 0.023\ (D/d)\ (\bar{N}_{Fe}^{ox} - N_{Fe})\ (Re)^{0.8}\ (Sc)^{0.33}$$

where D is the diffusion coefficient of iron in sodium and d is the pipe diameter. (Reynolds number is given by $dv\rho/\mu$ where d is diameter, v velocity, ρ density and μ viscosity. Schmidt number is given by $\mu/\rho D$.)

Thus in a diffusion-controlled process one would expect a plot of metal loss rate against $V^{0.8}$ or $(Re)^{0.8}$ to be linear where the concentration gradient across the barrier was not too large (corresponding to the section of the metal loss rate/velocity curve up to about 12 ft/s in Fig. 5). Where, however, the concentration gradient might be expected to be large, as in the case of nickel specimens exposed in a stainless-steel loop, the liquid metal immediately adjacent to the nickel would have nickel in solution at unit activity, while the nickel activity in the bulk sodium probably would not exceed that of the stainless-steel pipework, then one might expect to have a positive deviation from the $(V)^{0.8}$ or $(Re)^{0.8}$ relationship, as has been found experimentally and is shown in Fig. 8.

As can be seen from Fig. 5, stainless steels have shown deviations in the opposite direction. (This has also been observed with ferritic steels.) Most of our experiments to date have been made by varying mass flow of liquid metal (and hence linear velocity) through specimens of constant bore diameter. This work has shown that there is a linear dependence of mass transfer rate on $(Re)^{0.8}$ up to a certain limiting value of the Reynolds number beyond which the rate flattens off and tends to become independent of liquid metal velocity. The height of the "plateau" is a function of the oxygen level in the sodium, increasing with oxygen level (see Fig. 5). Latterly some experiments have been started in which the bore diameter of specimens has been altered in different runs while the mass flow has been kept constant. The results from the very limited number of experiments carried out so far are not inconsistent with the picture of a diffusion-controlled process at lower velocities probably with a fairly small concentration gradient across the film, but much further confirmatory work needs to be done.

At higher velocities it is clear that some other limiting process is coming into operation, and in view of the high level of iron in the sodium it seems likely that this slowest process is the deposition of iron in the cooler parts of the circuit, and/or some chemical process involving iron removal from the sodium via the double oxide. There seems no very obvious reason why increase in oxygen level should increase the rate of deposition of metallic iron in the cooler parts of the circuit; on the other hand if we allow for the possibility of the formation of double oxide in the cooler parts of the circuit (e.g. immediately after the cold trap) then the effect of increasing the oxygen level would be to reduce the concentration of soluble iron in the sodium purely through the law of mass action, and this should give the observed increased rate of dissolution in the hot zone through an increase in the concentration gradient of iron. If precipitation of double oxide were the dominating process for iron removal compared with metal deposition then we might expect that the rate of mass transfer in the hottest zone of the loop should be roughly proportional to the cube of the oxygen concentration. This is not observed in our experiments where the oxygen levels are low, and a roughly linear dependence of mass transfer on oxygen level is observed, perhaps suggesting that double oxide precipitation is not the dominating process in relation to metal deposition. However, it is of interest to note the results of French workers who have investigated sodium mass transfer of stainless steel at rather higher oxygen levels [13]. Their results are summarized in Table VI. They have investigated corrosion rate at ~50 ppm and 100 - 300 ppm oxygen, and if one takes the lower limit of the range quoted, then they find that doubling the oxygen level changes the rate of mass transfer by an order of magnitude; this is roughly in line with a cube dependence on oxygen concentration. It is perhaps worth noting that in addition to higher oxygen levels, their lower maximum temperature 550°C and cooler part of the circuit, 250°C, might tend to favour stability of the double oxide.

TABLE VI. INFLUENCE OF OXYGEN IN SODIUM ON CORROSION OF STAINLESS STEEL [13]
Specimen temperature 550°C; Minimum circuit temperature 250°C; Flow-rate 1800 litres/h; Duration of test 2700 h

Concentration of oxygen in sodium (ppm)	Weight loss (mg/cm^2/month)	Calculated penetration (μm/y)
~ 50	0.35	6
100 - 300	4.0	60

We have, from our work, some indications that factors other than pure metal dissolution and deposition could be operative in the mass transport process; thus we find non-metallic constituents in addition to metallic particles in the low velocity portions of the secondary side of the heat exchangers in our loops. It is also of interest to note that where corrosion specimens have been exposed downstream of the main corrosion specimen holders at a temperature approximately 20 degC cooler (630°C as against 650°C), then in addition to the expected reduced rate of metal loss due to the downstream effect, there was evidence for the deposition of brown film the nature of which is not yet known, but is being investigated.

7. CONCLUSIONS

Our tentative conclusions at this stage are that while the mass transfer processes of high nickel materials exposed in stainless-steel loops circulating sodium are fairly insensitive to oxygen levels within the limits investigated, but sensitive to liquid metal velocity implying diffusion control, the rate of mass transfer of ferritic and austenitic materials is sensitive to oxygen level and is proportional to velocity only up to some limiting Reynolds number. At higher velocities some other factor limiting mass transfer is operative, and in view of the fairly high measured iron content of the sodium in the loops it is believed that this is a combination of the processes limiting iron removal from the system, namely metal deposition and possibly precipitation of iron to form sodium ferrate $2\,Na_2OFeO$ in the cooler parts of the circuit where the oxygen activity is high. Where the latter process is dominant we might expect that the rate of mass transfer is proportional to the cube of the oxygen content; this has not been observed in our lower oxygen content tests, but may have been observed by French workers working with high oxygen levels, and lower temperatures.

REFERENCES

[1] THORLEY, A.V., TYZACK, C., "The embrittlement of niobium in hydrogen-contaminated NaK", Thermodynamics of Nuclear Materials, IAEA, Vienna (1962) 365.

[2] B.S.A. Research Centre, Private communication.

[3] Fulmer Research Institute, Private communication.

[4] Liquid Metals Handbook, A.E.C. Washington D.C.

[5] BRADSHAW, R.P., Reactor Fuel Laboratories, U.K.A.E.A., Private communication.

[6] TYZACK, C., "Applications of Sodium Chemistry in Fast Nuclear Reactors", International Symposium on the Alkali Metals, Nottingham, 1966.

[7] BAUS, R.A., BOGARD, A.D., GRAND, J.A., LOCKHART, L.B., Jr., MILLER, R.R., WILLIAMS, D.D., "The solubility of structural materials in sodium", Proc. UN Int. Conf. PUAE 9 (1956) 356.

[8] EPSTEIN, L.F., KAPL, Private communication; Liquid Metals Handbook, Sodium (NAK) Supplement (1955).

[9] MARABITO, J.J., et al., Paper 5B/4, British Nuclear Energy Society, London Conference on Fast Breeder Reactors (1966).

[10] HORSLEY, G.W., J. Iron Steel Inst. 182 (1956) 43.

[11] DUNN, W.E., BONILLA, C.F., FERSTENBERG, C., GROSS, B., Mass transfer in liquid metals, A.I. Ch. E. Journal 2 (1956) 184.

[12] EPSTEIN, L.F., Liquid Metal Technology Chemical Engineering Progress, Symposium Series No. 20, 53, 67.

[13] CHAMPLEIX, L., DARRAS, R., Bull. Infs scient. tech. Commt Energ. atom., 104 (1966) 93.

DISCUSSION

R.I. HODGE: What is the stress in the tube during test exposure when it is pre-pressurized to 3000 lb/in^2?

C. TYZACK: The maximum stress (loop stress) is 25 000 lb/in^2.

E.L. ZEBROSKI: I have two comments to make about your "double oxide" thermodynamic data for $(FeO)\,(Na_2O)_2$. When this compound is found in the solid state in loop systems much of it will take the form of a surface film, and a surface free-energy effect may overshadow, for practical calculations, the very small measured free energy for the solid compound.

Secondly, with regard to the "double oxide" in solution at less than unit activity, it is not clear from your paper why it should be necessary to postulate a complex; a trend such as this in the oxygen level could be described more simply in terms of a trace level of dissolved FeO (solvated).

INFLUENCE OF THE SURFACE QUALITY ON THE LIQUID SODIUM CORROSION OF NICKEL ALLOYS*

H. U. BORGSTEDT, G. DRECHSLER AND G. FREES
KERNFORSCHUNGSZENTRUM KARLSRUHE,
FEDERAL REPUBLIC OF GERMANY

Abstract

INFLUENCE OF THE SURFACE QUALITY ON THE LIQUID SODIUM CORROSION OF NICKEL ALLOYS. Our dynamic tests on the corrosion resistance of nickel alloys in liquid sodium have been a part of the canning material development within the Karlsruhe Fast Breeder Project. The influence of different surface qualities on the liquid sodium corrosion of two types of Inconel X has been studied. For this purpose five different metal finishing methods were used to get defined surfaces of the alloys. The test coupons of the dimensions 80 × 20 × 0.5 mm were annealed at 1050°C. As a surface treatment pickling with nitric acid, electropolishing in an H_3PO_4/H_2SO_4 mixture, grinding with grit paper 600, sandblasting, and mechanical polishing were used. All methods except pickling resulted in a metal surface of very low roughness.

The specimens were exposed to the flowing sodium in the test sections of a sodium loop built up of 18/8 CrNiTi steel. The temperature of the sodium in the three test sections was 500, 550 and 600°C, the velocity of the sodium flow at the specimens amounted to 0.5 m/s, and the concentration of Na_2O was less than 10 ppm.

After a run of more than 1000 h the nickel alloys were tested by microgravimetric, microscopic and microprobe analysis techniques.

The corrosion rates and their dependence on temperature are strongly influenced by the quality of the specimen surfaces. At 500°C the measured reaction rates have higher positive values after mechanical polishing of the metal surfaces than after chemical finishing. At 600°C higher negative corrosion rates in the mechanically polished alloys were found. The corrosion of the mechanically treated metals has a stronger temperature dependence than that of chemically finished ones.

This behaviour can be understood as a consequence of the formation of a Beilby layer during mechanical finishing. This layer takes part in the reaction of the specimens with the liquid sodium. At 500°C the coating layer seems to react with a positive weight gain; however, it seems to be dissolved in the liquid sodium and to increase the corrosion reaction at 600°C.

By microscopic study mass transfer products were found to be deposited on electropolished surfaces of specimens. The deposits are preferably placed along the grain boundaries, their quantity increasing with the temperature of the liquid sodium. No deposits were found on the specimens with mechanically polished surfaces. These surfaces show a change in colour and brightness due to the action of the liquid sodium. The Beilby layer isolates the metallic surface from the liquid sodium, and seems to hinder the crystal nucleation or the adhesion of the deposits on the specimen surfaces.

The chemical composition of mass transfer deposits was examined by X-ray microprobe study. By this analytical technique changes in the element concentrations in the surface layers of the specimens caused by selective solution of alloying elements were also observed.

Within the canning material selection programme for a sodium-cooled reactor of the Karlsruhe Fast Breeder Project we have been interested in resistance of austenitic stainless steels, nickel alloys and vanadium alloys against liquid sodium corrosion. We started the series of dynamic tests on the corrosion behaviour of nickel alloys by testing two types of commercial Inconel X that are precipitation-hardenable alloys of good high-temperature strength.

---

* Work performed as part of the joint programme in fast reactors of the European Atomic Energy Community and the Gesellschaft für Kernforschung, Karlsruhe.

The precipitation-hardened nickel alloys showed an extraordinary high-temperature embrittlement after neutron irridation of relative low integrated fluxes [1]. These alloys, therefore, are not in favour as cladding materials for a fast reactor. However, the observed effects of the surface quality on the liquid metal corrosion seem to be more common. They should occur in the liquid sodium reactions of matrix-hardened nickel alloys, too, as they do in part with austenitic stainless steels.

In our dynamic corrosion tests we wanted to obtain some information on the effects of the composition of the alloys, and on the influence of the different surface qualities which were varied by different surface treatment methods. We also wanted to see if a cold-working effect due to the mechanical finishing of the metal surfaces would decrease the corrosive action of the liquid sodium as it does in the case of water and steam corrosion of the same group of materials [2, 3].

1. THE SPECIMENS

1.1. Chemical composition

The chemical composition of the alloys Inconel X 750 and X 550 was controlled by chemical analysis. According to the nominal composition, the contents of nickel were determined to 73% and of chromium to 15%. Precipitation hardening of the alloys was due to the precipitation of Ni_3Al and Ni_3Ti phases. Both materials contained 2.5% Ti and 1% Al.

1.2. Shape and thermal state of the specimens

The test coupons of 20 X 80 mm were stamped from 0.5-mm thin sheets. They were marked by mechanically printed numbers. We annealed the specimens at 1050°C in the high vacuum and cooled them quickly to avoid local cold-work effects from the stamping and marking. We controlled the grain size of the alloys in this thermal state by metallographic study.

1.3. Surface treatment

We wanted to test the specimens in a well-defined surface state. We therefore tried to approximate the real surfaces to the exact geometrical surface by application of various surface-finishing methods. A comparison of the applied electrochemical and mechanical processes is given in Table I.

We were able to measure the resulting magnitudes of surface roughness with the aid of an electro-mechanical profile recorder and metallography. Surface profiles over a length of 1 mm of specimen surfaces of Inconel X 750 after the five different treatments are shown in Fig. 1.

The surfaces treated by pickling and sandblasting had the roughest structures, as is shown by the reflection of light of the different specimens. This was confirmed by the surface roughness measurement and metallographic study. The original surface roughness was not affected by pickling in a nitric acid/hydrofluoric acid mixture. Sandblasting led to surfaces of a low degree of polish, but the surface areas were affected strongly and showed cold-work effects, as was indicated by measurements

TABLE I. APPLIED METHODS OF SURFACE TREATMENT

Finishing method	Pickling I	Electro-polishing II	Grinding III	Mechanical polishing IV	Sandblasting V
Conditions of treatment	HNO_3/HF-water-mixture 60-80°C 10-15 min	H_3PO_4 / H_2SO_4 - water-mixture 60°C 15 min, 0. 6 A/cm²	SiC paper 600, water-cooled	Rotating brushes, polishing paste	Al_2O_3 grains 0. 1-0. 2 mm ϕ 4 atm
Effects on metal surfaces	Chemical descaling and cleaning	Electro-chemical oxidation of surface peaks	Mechanical smoothing	Mechanical smoothing	Effects of blows on small surface segments
Resulting surface roughness (μm)	8. 6	2. 2	0. 15 in the direction of working	1. 5	2. 4
Effect on specimen materials	No effect	No effect	Small cold-work effect	Small cold-work effect	Considerable cold-work effect

of the microhardness in the cross-section of the specimens. The least surface roughness could be obtained by grinding with SiC 600 paper, when the surfaces lost their grain structure. Electrolytic and mechanical methods resulted in a good polishing of micro areas, which led to a high reflection of light. However, there remained a considerable surface structure. Except for the pickled specimens the maximum surface roughness did not exceed 2.5 μm.

2. CORROSION TESTS

2.1. The corrosion loop

The specimens were exposed to the flowing sodium in a sodium loop built up of 18/8 Cr Ni Ti steel. The sodium of 350 - 400°C was kept flowing by an electromagnetic pump. A fraction of the flowing sodium passed a cleaning bypass, the chief component of which was a cold trap of relatively large dimensions. The concentration of sodium oxide was determined in another bypass by a plugging meter. While studying steels and nickel alloys we did not need the hot trap for further oxygen trapping.

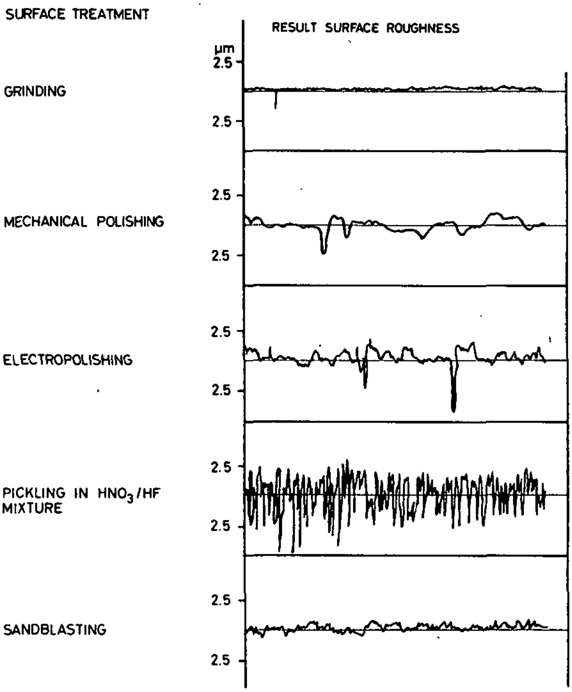

FIG.1. Surface roughness of Inconel X 750 specimens

The three test sections possessed heating elements with separate energy regulation. The temperatures of the sodium passing the test sections were set to 500, 550 and 600°C. The construction of the test sections resulted in the zone of the highest temperature being nearly identical with the place of the specimens. A test section with heating elements, specimen holders and the economizing heat exchanger is shown in Fig. 2.

The sodium leaving the pumped circuit was preheated in the outer part of the heat exchanger. Entering the test sections it had to pass six heat pockets of 2 kW each. At the head of the test section the heated sodium entered the central valve which contained 30 of the specimens described in Sub-section 1.2. We measured the velocity of the sodium flow in the loop with the aid of an electromagnetic flowmeter. From the measured values we calculated the velocity of the sodium flow to 0.5 m/s in the central valve of the test sections containing the specimens. We controlled the temperatures of the sodium before and after the specimens by thermocouples.

2.2. Evaluation of the corrosion tests

We found very low corrosion effects after a run of about 1000 h. Therefore the weight gains had to be determined very sharply to calculate corrosion rates [mg/cm^2 yr] of high accuracy. Our microbalance had a

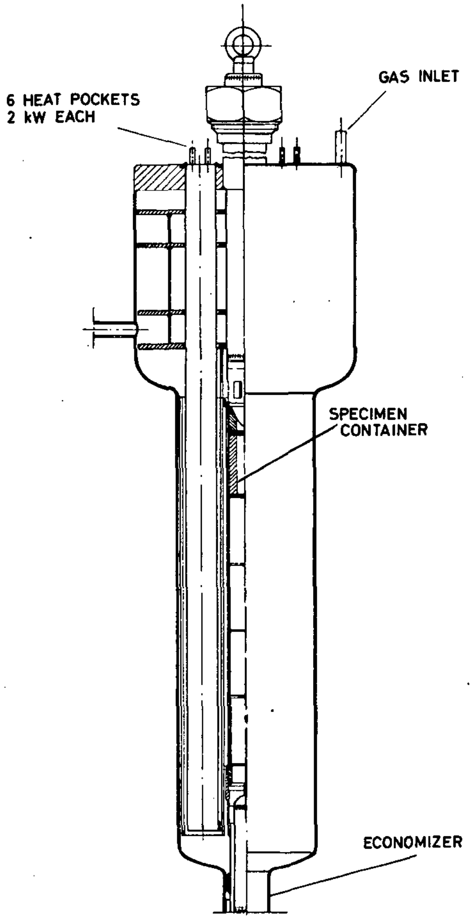

FIG.2. Test section of the sodium loop

sensitivity of 10^{-6} gm and a reproducibility of $\pm 4.10^{-6}$ gm. The minimum effects had values of $5 \cdot 10^{-5}$ gm for one specimen. Thus, the uncertainty of the weight gain was less than 10%.

The specimens were also examined by their appearance and by microscope study. In some cases we used X-ray microprobe analysis for detecting sodium mass transfer deposits and selective solution of alloy components in the surface zones. The studies were carried out by metallographic observations and by electro-mechanical measurements of the surface profiles, which gave information about changes from the action of liquid sodium.

3. RESULTS

3.1. Influence of the surface quality on the corrosion rates at different temperatures

The results of our measurement and observations of liquid sodium corrosion effects on the nickel alloy specimens are listed in Table II. The

TABLE II. CORROSION RATES AND OBSERVED CORROSION EFFECTS

Surface quality	Sodium temperature (°C)	Corrosion rates mg/cm^{2}yr	Visible corrosion effects	Mass transfer deposits
		Inconel X 750		
Pickled	500	+ 0.065	No changes	Not detectable
	550	- 0.147	No changes	Not detectable
	600	- 0.759	No changes	Not detectable
Electropolished	500	+ 0.019	No changes	Slight
	550	- 0.168	No changes	Considerable
	600	- 0.972	No changes	Strong
Ground	500	+ 0.153	Colour, brightness	No deposits
	550	- 0.173	Colour, brightness	No deposits
	600	- 1.062	Colour, brightness	No deposits
Polished	500	+ 0.150	Colour, brightness	No deposits
	550	- 0.207	Colour, brightness	No deposits
	600	- 1.117	Colour, brightness	No deposits
Sand-blasted	500	+ 0.076	Colour, brightness	No deposits
	550	- 0.336	Colour, brightness	No deposits
	600	- 1.662	Colour, brightness	No deposits
		Inconel X 550		
Pickled	500	+ 0.095	No changes	Not detectable
	550	- 0.100	No changes	Not detectable
	600	- 0.638	No changes	Not detectable
Electropolished	500	- 0.012	No changes	Slight
	550	- 0.138	No changes	Considerable
	600	- 0.624	No changes	Strong
Ground	500	+ 0.128	Colour, brightness	No deposits
	550	- 0.216	Colour, brightness	No deposits
	600	- 1.074	Colour, brightness	No deposits
Polished	500	+ 0.148	Colour, brightness	No deposits
	550	- 0.115	Colour, brightness	No deposits
	600	- 0.798	Colour, brightness	No deposits
Sand-blasted	500	+ 0.076	Colour, brightness	No deposits
	550	- 0.288	Colour, brightness	No deposits
	600	- 1.429	Colour, brightness	No deposits

influence of the physical and chemical state of the specimen surfaces is obvious after a simple comparison of the corroded metals. However, the different effects can be better evaluated by microscope study and by comparison of the corrosion rates as a function of temperature and surface treatment. In Figs 3 and 4 the corrosion rates are plotted against the sodium temperature for the two nickel alloys.

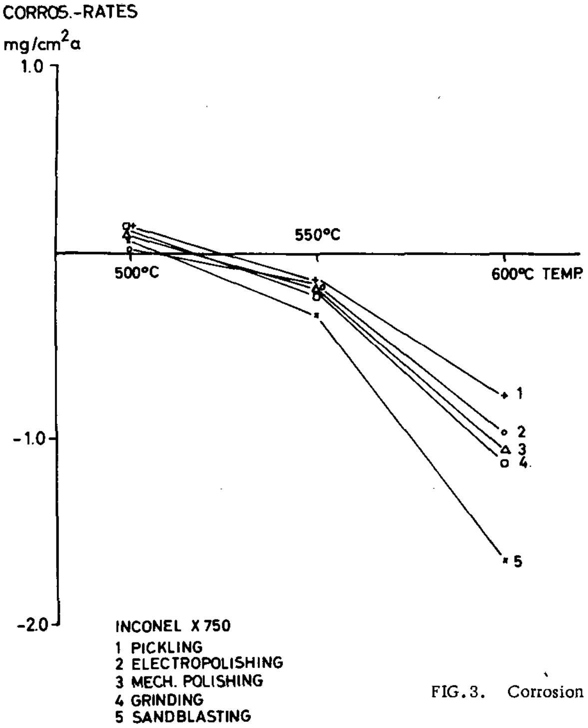

FIG.3. Corrosion rates in liquid sodium (a)

The dependence of the corrosion rates on temperature after chemical or electrochemical treatment of the specimen surfaces is less than after one of the mechanical polishing processes. The mechanically treated specimens have suffered more severe weight losses at 600°C. However, at 500°C we find positive weight changes caused by corrosion reactions. The positive values of the corrosion rates are accompanied by changes in colour and brightness of the polished metal surfaces (see Table II). The surfaces of the sandblasted specimens with the greatest roughness on the mechanically polished surfaces are attacked by the liquid sodium with the highest corrosion rates. At 600°C the nickel alloys react with the liquid sodium with rates the values of which are 2,5 to 4.0 higher than in the stainless steels.

3.2. Influence of the surface quality on some corrosion effects

The effects of the surface state on the liquid metal corrosion cause some phenomena which have been studied by microscope techniques.

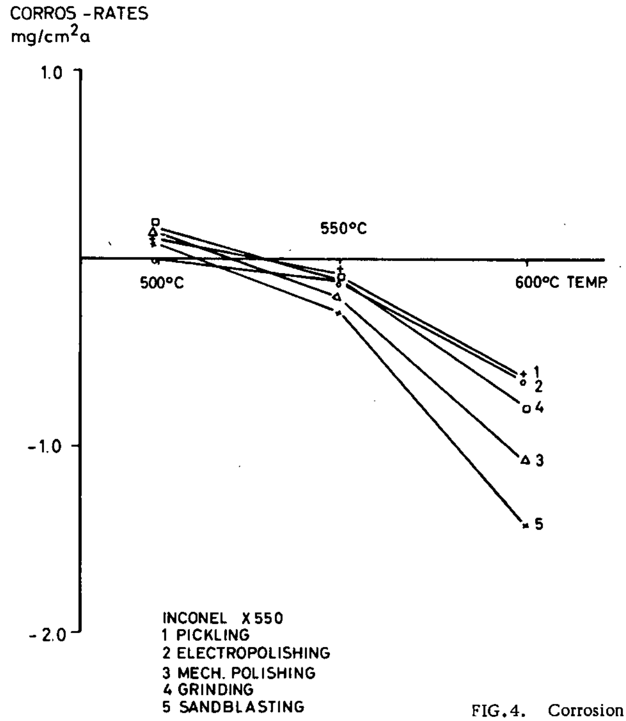

FIG.4. Corrosion rates in liquid sodium (b)

There is quite an obvious difference between the mechanically and the chemically treated metal surfaces. After the corrosion reaction we find that the mechanically polished and ground specimens are covered by a thin coloured layer which is uniform and without any structure all over the surface. A similar layer seems to cover the sandblasted surfaces. However, the pickled and the electropolished metal surfaces retain their metallic brightness despite the action of the corrosive medium.

On the surfaces of the electropolished specimens we find metallic deposits of microscopic dimensions. These are preferably placed along grain boundaries, only a small number being deposited on grain faces. The quantity of these deposits increases with the temperature of the flowing sodium. In the polarization microscope the deposits appear to be illuminated on the dark ground of the original surface. Electron microscope studies show the deposits to have a crystalline character.

We do not find any metallic deposits on the electropolished surfaces of 18/8 Cr Ni stainless-steel specimens after 1000-h corrosion tests in the same loop.

The deposited metallic phase covers the original surface of the nickel alloys in the region of the grain boundaries. The covered area has a width of 2 - 3 μm, the thickness of the deposits amounting to 0.3 μm as measured by the surface roughness measurement method. In the diagrams of the surface roughness recorded after the corrosion tests the deposits appear as small pins not previously detectable. The profiles of the original surfaces show decreased values of roughness as a consequence of the liquid metal corrosion.

We studied the composition of the deposits by microprobe analysis. They contain very much chromium, while the elements nickel and iron are contained in much lower concentrations than in the materials of the specimens. Some of the deposited particles are very rich in titanium. We decided not to analyse the particles quantitatively, because the formed surface relief hinders the exact focussing of the X-ray beams. Therefore the results of quantitative studies have a considerable uncertainty.

After the 1000-h corrosion test we did not find any traces of an intercrystalline attack of the liquid sodium on both nickel alloys by metallographic study. However, the evaluation of the metallographic studies gives further evidence for the existence of the deposited metallic phase in the grain boundary areas.

We detected slight changes in the composition of the zone in the neighbourhood of the metal surface by microprobe analysis. In a layer of 3 - 5 μm thickness the content in nickel and iron is enriched while the concentration of chromium is reduced slightly.

4. DISCUSSION

The tested nickel alloys Inconel X 750 and X 550 have good corrosion resistivity against flowing sodium of temperatures up to 600°C and of low sodium oxide content of about 5 ppm. From measured corrosion rates one can calculate the loss of thickness under the assumption that the reaction may follow a linear corrosion rate law. In two years the loss thickness will be less than 10^{-5} cm.

The strength of a fuel element may also be affected by the formation of a diffusion layer (see Sub-section 3.2). With tests lasting only 1000 h the depth of these layers after a long period of penetration cannot be estimated. However, after several 1000 h of test in a loop of ferritic steel 18/8 Cr Ni stainless steel has a diffusion zone with a diminished chromium content of 10 μm depth [4]. We do not know the effects of a zone poor in chromium on the mechanical properties of the canning materials.

The reaction of the tested alloys with the liquid sodium takes place at the surface of the solid phase. Therefore, that the physical and chemical state of the specimen surfaces will have an effect on the corrosion reaction can be supposed a priori. These reactions are technically interesting, too. They are of importance for the heat flux from the fuel element to the coolant, the hydrodynamic properties of the fuel element in the coolant flow, and the possibility of nucleate boiling or cavitation of the liquid at the can surface.

The results of our corrosion tests lead to the conclusion that there are two groups of surface qualities that show different behaviour in liquid metal corrosion. The chemically treated surfaces show the higher corrosion resistivity and a smaller temperature coefficient of the corrosion rates. The mechanically finished specimens have corrosion rates with relative high temperature coefficients and show changes in colour and brightness.

The corrosion rates of the nickel alloys with pickled or electropolished surfaces in sodium of 500, 550 and 600°C have nearly the same values (see Figs 3 and 4). However, the surface roughness and therefore the effective surface size of both are very different. Thus, the corrosion attack on the unit of the effective surface of the pickled specimens is less than on the electropolished ones. We think that the differing capacity to be wetted by the liquid sodium may be the reason for this different behaviour. The pickled surface is rich in inequalities (see Fig. 1). It may be wetted only at its elevated parts, and only these parts of the surfaces are attacked by the liquid metal. The poor capacity to be wetted may cause a decrease in the heat flux.

The uniform distribution of deposits along the grain boundaries all over the specimen surfaces gives evidence of perfect wetting by the liquid sodium at the test temperature. Therefore, the corrosive action of the sodium should be equal on all parts of the specimen surfaces except the grain boundary areas. In the case of electropolished surfaces the corrosion rates represent the reaction of the effective phase boundary between the solid and liquid. Thus, this state of the surface is the one best defined for sodium corrosion tests.

The deposits on the electropolished specimen surfaces are similar to those we found on the surfaces of similar alloys after static corrosion tests [5, 6]. In these tests the deposits are due to isothermal mass transfer. Their composition, differing from that of the specimen materials, shows that there has been a mass transfer of iron from the stainless-steel wall of the container to the tested alloys. We assume the deposits on Inconel X 750 and X 550 to be products of mass transfer too. This mass transfer may have taken place between the 18/8 Cr Ni Ti stainless steel of the components of the test sections and the tested nickel alloys. The favoured nucleation of crystals in the grain boundary areas seems to be the reason for the preferential deposition on these regions.

There is some evidence of a participation of the nickel alloys in the production of the new metallic phase by contributions of materials for the crystal growth. Indeed, we find changes in the chemical composition of the alloys in the surface layer.

Since the test sections represent nearly isothermal systems, the deposition of mass transfer products must be caused by chemical forces.

The liquid metal corrosion effects on mechanically polished specimens seem to be strongly influenced by the properties of a thin invisible layer produced by the different polishing processes, known as the Beilby layer [7]. In sodium of 500°C this layer reacts with the liquid metal or the impurities in it with a positive weight gain. We observe changes in colour and brightness of the originally invisible layer. We believe, therefore, that the polishing layer may have absorbed sodium or sodium oxide. This reaction may be the first step in the dissolution of the Beilby layer by the liquid metal. At higher temperatures we observe that the coloured layer is partially dissolved. At a sodium temperature of 600°C the reaction and the destruction of the Beilby layer accelerate the liquid sodium corrosion as does an increased content in oxygen in the corrosive medium.

The formation of coloured surfaces on polished specimens was previously observed, but the authors did not connect this observation with the polishing process [8]; the change in colour of austenitic stainless steel surfaces was reported in those cases in which positive weight gains were measured in sodium of 550°C and with a content of 400 - 500 ppm Na_2O.

Cold-work effects in the surface layers due to the mechanical finishing processes do not increase the resistivity of the alloys against the liquid metal corrosion. The surfaces are covered with thin layers which seem to grow because of the reaction with the corrosive agent. At relatively low temperatures the layers are able to decrease the corrosion rates. However, these layers isolate the metal from the coolant and restrict the heat flux from the fuel can to the liquid metal. They also prevent the formation or adhesion of the mass transfer products on the specimen surfaces. The effects of the applied mechanical polishing processes on the corrosion behaviour of the tested nickel alloys seem to be disadvantageous.

5. CONCLUSIONS

The resistivity of the tested nickel alloys against the liquid sodium attack at temperatures of 500, 550 and 600°C is excellent. The corrosion effects are strongly influenced by the physical and chemical state of the surface. Mechanical finishing processes produce Beilby layers on the specimen surfaces, which increase the corrosion rates at 600°C and affect the physical properties in the phase boundary of the solid phase.

Anodic polishing generates a very well-defined surface which is completely wetted by the liquid sodium at the test temperatures. The corrosion rates of these electropolished specimens represent the reaction of the whole surface with the liquid metal.

The construction of the core of a sodium-cooled reactor has to take into consideration the possibility of chemical mass transfer. The combination of the canning and construction materials should be chosen in such a way that the origin of deposits and diffusion zones poor in one or more components of the alloys due to the chemical mass transfer could be kept within a tolerable degree.

REFERENCES

[1] BÖHM, H., DIENST, W., HAUCK, H., J. nucl. Mater. 19 (1966) 59.
[2] RUTHER, W.E., GREENBERG, S., J. electrochem. Soc. 111 (1964) 1116.
[3] WARZEE, M., HENNAUT, J., MAURICE, M., SONNEN, C., WATY, J., BERGE, P., J. electrochem. Soc. 112 (1965) 670.
[4] BRUSH, E.G., Rpt GEAP-4832 (1965).
[5] BORGSTEDT, H.U., Werkstoffe Korros., Mannheim (to be published).
[6] BORGSTEDT, H.U., HEIN, W., Werkstoffe Korros., Mannheim (to be published).
[7] YAMAGUSHI, S., SAWAMURA, H., Werkstoffe Korros., Mannheim 16 (1965) 465.
[8] ILINCHEV, G., Atomn. Energ. 14 (1963) 375.

DISCUSSION

A. HATTERER: Corrosion by irreversible processes must fulfil a relation $A.v > 0$ which links a positive thermodynamic affinity, A, and a positive velocity, v (according to internationally accepted usage, a free enthalpy variation $\Delta G^{\circ}_{T} = -A$). Physical and chemical evolution may well be affected by an anomalous value for the surface energy of the polycrystalline solid (which would be difficult to estimate), particularly as a result of disturbances at grain boundaries and perturbations following superficial mechanical treatment. To explain the different types of corrosion behaviour that have been observed, do you not think that energy phenomena (defects, stress and even adsorption) are just as important as geometric or kinetic factors (surface size, wetting, diffusion)?

H. U. BORGSTEDT: We believe that the observed differences in corrosion behaviour are caused, on the whole, by the presence or absence of a surface layer. Differences in the corrosion rate may be due to variations in the size of the effective surface. However, we cannot exclude the possibility that corrosion behaviour may be influenced by solid surface energy phenomena; sandblasting, for example, has produced large deformation effects on the surfaces.

ВЛИЯНИЕ НЕКОТОРЫХ ФАКТОРОВ НА КОРРОЗИЮ КОНСТРУКЦИОННЫХ МАТЕРИАЛОВ В ЖИДКОМ НАТРИИ

Г.ИЛИНЧЕВ
ГОСУДАРСТВЕННЫЙ НАУЧНО-ИССЛЕДОВАТЕЛЬСКИЙ
ИНСТИТУТ ЗАЩИТЫ МАТЕРИАЛОВ, ПРАГА
ЧССР

Abstract — Аннотация

THE EFFECT OF CERTAIN FACTORS ON THE CORROSION OF STRUCTURAL MATERIALS IN LIQUID SODIUM. Special experimental loops for the study of corrosion and mass transfer in liquid sodium up to temperatures of approximately 800°C are described. Dynamic and convection loops were used. The amount of oxygen in the sodium was maintained at low concentrations (up to 3×10^{-3} %) in some experiments and at relatively high concentrations (approximately 4×10^{-2} %) in others.

The effect of a number of basic alloying elements (e.g. Ni, Cr, Mo, Ti, Nb and V) on the corrosion of about 30 types of steel in sodium was studied, as was their effect on mass transfer and carbon transfer. Corrosion in certain other pure metals (Ni, Mo and Ti) was also studied. The experiments showed that steels alloyed with Ni and Cr acquire increased resistance to corrosion in sodium with a high oxygen content. Steels with a low or medium content of Cr and Mo show, under the same conditions, a degree of corrosion several times greater; but in liquid sodium with a very low oxygen content these alloy elements have the opposite effect, i.e. corrosion increases with increasing Ni and Cr content, and is slightest in low-alloy steels.

Mass transfer in structural steels increases as the oxygen content of the sodium is increased; this is due to the transfer of Fe from hot to cold sections of the material.

Carbon can be eliminated from the system by a method similar to that used with oxygen (cold traps), but there is the difference that carbon tends to float on the surface of the sodium to a greater extent.

How sodium (and its degree of purity) can affect changes in the mechanical properties of the basic structural steels (austenitic and ferritic steels) is also described. The mechanical properties of stabilized ferritic steels and steels of the Cr and Ni type undergo virtually no change.

Attention is given to the influence of temperature on the corrosion of steels in pure sodium and the effect of basic alloying elements (Ni, Cr and Mo) in this connection. The relationship between decarbonization of steels and their composition - particularly the content of Cr and other carbide-forming elements (Ti and Nb) - is considered.

The experiments show that low-alloy steels (with Cr, Mo and V) are decarbonized to a substantial degree even at a temperature of 400°C. The degree of decarbonization in steels alloyed with 3-5% chromium is several times less. Ferritic steels stabilized with Ti or Nb undergo virtually no decarbonization and corrode very little in pure sodium.

A comparison is made of the kinetics of the corrosion of structural steels in liquid sodium and in heavy liquid metals (Pb, Bi and Pb-Bi). The experiments showed that the rate of corrosion in heavy liquid metals is influenced hardly at all by circulation velocity (from 1 to 100 cm/s), and we can therefore assume that the rate is not determined by diffusion processes. We assume that diffusion processes have no effect on corrosion in pure liquid sodium either. Certain experiments in liquid sodium with a high oxygen content suggest, however, that diffusion processes considerably affect the corrosion of low and medium alloy steels.

ВЛИЯНИЕ НЕКОТОРЫХ ФАКТОРОВ НА КОРРОЗИЮ КОНСТРУКЦИОННЫХ МАТЕРИАЛОВ В ЖИДКОМ НАТРИИ. В докладе описаны некоторые специальные опытные аппаратуры (контуры) для исследования коррозии и переноса массы в жидком натрии до температур приблизительно 800°С. Для изучения коррозии использовали динамические и конвекционные контуры. Кислород в натрии поддерживали на низкой (до $3 \cdot 10^{-3}$ %) и высокой (приблизительно $4 \cdot 10^{-2}$ %) концентрации.

Исследовали влияние основных легирующих элементов (например, Ni, Cr, Mo, Ti, Nb, V и других) на коррозию приблизительно 30 родов сталей в натрии и влияние приведенных легирующих элементов на перенос массы и углерода. Исследовали коррозию также некоторых чистых металлов (Ni, Mo, Ti). Проведенные опыты показывают, что на коррозию в натрии с повышенным содержанием кислорода имеет благоприятное влияние легирование сталей именно Ni и Cr. Стали с низким и средним содержанием Cr и Mo имеют при одинаковых условиях в несколько раз большую коррозию, но в жидком натрии с низким содержанием кислорода влияние приведенных легирующих элементов обратное, это значит, что коррозия растет с повышающимся содержанием Ni и Cr и самая малая – у низколегированных сталей.

Перенос массы конструкционных сталей растет с повышающимся содержанием кислорода в натрии и вызывается именно переносом Fe из теплых на холодные участки установок.

Углерод можно удалять из системы подобно кислороду (в холодных ловушках), но с тем различием, что углерод в большой мере плавает на поверхности натрия.

Описано влияние натрия и его чистоты на изменение механических свойств основных конструкционных сталей (аустенитных и ферритических). Механические свойства стабилизированных ферритических сталей и сталей типа Cr – Ni практически не изменяются.

Приводится температурная зависимость коррозии сталей в чистом натрии и влияние основных легирующих элементов (Ni , Cr и Mo), а также зависимость обезуглероживания сталей на их составе, именно на содержании Cr и других карбидообразующих элементов (Ti и Nb).

Опыты показывают, что низколегированные стали Cr, Mo и V значительно обезуглероживаются и при температуре 400°C. Стали, легированные хромом 3 – 5% несколько раз, меньше обезуглерожены. Феррические стали, стабилизированные Ti или Nb, которые практически не подвергаются обезуглероживанию, вызывают в чистом натрии самую малую коррозию.

В докладе дальше сравнивается кинетика коррозии конструкционных сталей в жидком натрии и в тяжелых металлах (Pb, Bi и Pb – Bi). Из проведенных опытов вытекает, что скорость коррозии приведенных материалов в тяжелых жидких металлах в зависимости от их скорости циркуляции (от 1 до 100 см/сек) практически не изменяется и поэтому можно предположить, что она не управляется диффузионными процессами. В чистом жидком натрии тоже предполагается, что на коррозию не оказывают влияния диффузионные процессы. Некоторые опыты в жидком натрии с повышенным содержанием кислорода, однако, показали, что диффузионные процессы имеют значительное влияние на коррозию низко- и среднелегированных сталей.

1. ВВЕДЕНИЕ

Как известно на коррозию конструкционных материалов в жидком натрии влияет много факторов, в частности температура, перепад температуры, чистота жидкого металла, а также род и химический состав конструкционных материалов. Известную роль могут играть также и дальнейшие факторы, как, например, скорость потока жидкого металла, структура материалов, наличие различных видов конструкционных материалов в одном контуре, влияние радиации, термической устойчивости и т.д.

Для выбора конструкционных материалов и определения оптимальных условий эксплуатации установок, охлаждаемых жидким натрием, необходимо изучать влияние коррозионных факторов в значительной широте. Это необходимо делать как с теоретической точки зрения, так и с точки зрения возможных аварийных состояний и их последствий на состояние установок.

Поэтому наши исследования были направлены на изучение влияния некоторых главных коррозионных факторов. Одновременно мы стремились установить некоторые более общие зависимости.

Для получения не только сравнительных данных о стойкости материалов, но и результатов, которые значительно приближаются к величинам коррозии натурных энергетических установок, крупное значение имеет выбор методики испытаний и способ проведения коррозионных испытаний. Поэтому методика испытаний должна по крайней мере учитывать наиболее важные коррозионные факторы и позволять их широкие исследования.

2. ИСПЫТАТЕЛЬНАЯ АППАРАТУРА

В качестве испытательной аппаратура для исследования коррозионной стойкости материалов использовались относительно простые контуры с конвекционным потоком или более крупные контуры с принудительной циркуляцией жидкого металла. Нам представляется, что пониженная скорость циркуляции не уменьшает значения конвекционных петель, в частности в тех случаях, если они приспособлены для поддержания концентрации кислорода, углерода и других примесей натрия на требуемой величине.

2.1. Конвекционная петля

Один из вариантов, применяемых у нас конвекционных петель, приведен на рис. 1. Такой тип конвекционных петель позволяет проведение коррозионных испытаний при весьма высоких температурах, примерно 800 – 900°C, и при перепаде температур между высокотемпературной (9) и низкотемпературной (10) испытательными ветвями, примерно 50 ÷ 300°C. Скорость циркуляции жидкого натрия в контуре может достигнуть 10 ÷ 15 см/сек. Требуемый температурный перепад между испытательными ветвями получается путем поворота круговой рамы, на которой закреплена вся петля.

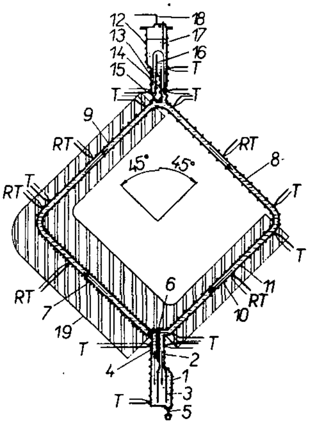

Рис.1. Конвекционная петля:
1 – холодная ловушка; 2 и 3 – подводящая трубка; 4 – отводящая трубка; 5 – вентиль для заполнения и выпуска натрия из петли; 6 и 15 – регулировочные вентили; 7 – ветвь нагрева; 8 – ветвь охлаждения; 9 – высокотемпературная испытательная ветвь; 10 – низкотемпературная испытательная ветвь; 11 – электрический нагрев сопротивления; 12 – расширительный бак; 13 и 14 – подводящая и отводящая трубки; 16 – перегородка; 17 – уровнемер; 18 – линия аргон-вакуум; 19 – тепловая изоляция; T – регистрирующие термоэлементы; RT – регулировочные термопары.

Приведенный тип конвекционной петли снабжен двумя добавочными контурами с соответствующими сосудами. На участке между высокотемпературной испытательной и охлаждающей ветвями расположен расширительный бак, используемый одновременно в качестве сепаратора большего количества углерода, растворенного в натрии в течение коррозионных испытаний. Удаление углерода основано на наблюдениях [1], согласно которым углерод в большинстве случаев плавает на поверхности жидкого натрия, так что таким способом можно регулировать его концентрацию в натрии. Регулировка температуры и количества жидкого металла, протекающего через этот бак, осуществляется посредством вентилей (15). На участке между низкотемпературной испытательной ветвью имеется добавочный контур с холодной ловушкой (1). С ее помощью содержание кислорода в натрии поддерживается на желаемой концентрации. Через упомянутую ловушку проходит лишь часть общего количества натрия, протекающего по контуру. Температура регулируется с помощью вентиля (6).

Конвекционные петли изготовляются в большинстве случаев из аустенитной хромоникелевой стали. Испытанные стали в виде плоских полосок, размещенных в специальных кассетах, помещаются на испытательной ветви (9, 10). По всей длине упомянутых выше ветвей поддерживается постоянная температура путем возмещения тепловых потерь вспомогательными, регулируемым отоплением.

Достоинство конвекционных петель заключается в том, что они не требуют непрерывного надзора. Система регуляторов обеспечивает их работу при требуемых параметрах. Другим преимуществом петель является то, что на них можно исследовать влияния различных коррозионных факторов в весьма широких пределах, можно их либо сменять совсем, либо изменять конструкцию в зависимости от исследуемых факторов. Температура в контуре поддерживается в пределах примерно ± 5°C требуемых значений; изменения температуры осуществляется посредством термопар из Ni – Ni – Cr, приваренных к трубопроводу.

На конвекционной петле сходного типа проводились коррозионные испытания с повышенным содержанием кислорода ($5 \cdot 10^{-2}\%$) при температуре высокотемпературной ветви 600°C и низкотемпературной ветви – 500°C в течение 1000 часов. Исследовали влияние кислорода на коррозию различных конструкционных сталей и на перенос масс. На конвекционных петлях изучалась также и коррозия в натрии с низким содержанием кислорода вплоть до температуры 760°C.

2.2. Контур с принудительной циркуляцией натрия

Испытания, проведенные в динамических контурах, значительно приближаются к условиям работы крупных установок, где, помимо температуры, температурного перепада и поддержания натрия на желаемой концентрации неметаллических загрязнений (O и C), достигается значительная скорость потока. Один из динамических контуров, применяемых у нас для исследования коррозионной стойкости конструкционных материалов в натрии, приведен на рис. 2. Контур имеет два испытательных участка – высокотемпературный (14) и низкотемпературный (5), где температура поддерживается на постоянном уровне; на этих участках размещены исследуемые образцы. На приведенном выше контуре обследуется главным образом коррозионная стойкость материалов в условиях,

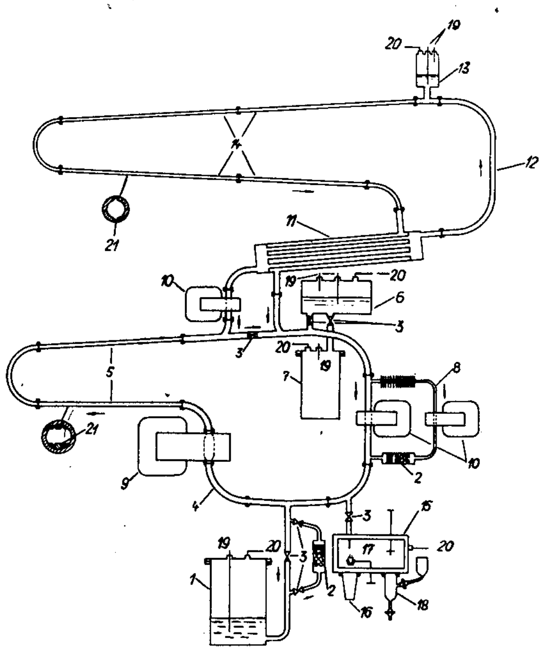

Рис.2. Контур с принудительной циркуляцией натрия:
1 – сосуд заполнения и выпуска; 2 – фильтры; 3 – вентили; 4 – низкотемпературная петля; 5 – низкотемпературный испытательный участок; 6 – расширительный бак; 7 – запасной выпускной сосуд; 8 – холодная фильтрационная ветвь; 9 – электромагнитный насос; 10 – электромагнитные расходомеры; 11 – регенеративный теплообменник; 12 и 13 – подогреватель и уравнительный бак высокотемпературной петли; 14 – высокотемпературный испытательный участок; 15 и 18 – рт. анализатор содержания кислорода и натрия и его части; 19 – уравномеры; 20 – аргон-вакуум; 21 – канавки для размещения испытуемых образцов.

приближающихся к оптимальным. Испытания в динамических контурах проводились вплоть до температуры 600°С и перепада температуры примерно 150°С в течение нескольких тысяч часов. Содержание кислорода поддерживалось на низкой концентрации (ниже $3 \cdot 10^{-3}$ %) посредством холодной фильтрационной ветви (8); количество кислорода определялось по методу амальгамации.

3. ВЛИЯНИЕ СОСТАВА КОНСТРУКЦИОННЫХ СТАЛЕЙ НА ИХ КОРРОЗИОННУЮ СТОЙКОСТЬ

Исследовалось влияние главных легирующих элементов – никеля и хрома на коррозию и изменения механических свойств жаростойких и жаропрочных сталей и сплавов. Значительное внимание уделялось низко- и среднелегированным сталям, стабилизированным титаном или ниобием. Обследовались также конструкционные стали низко- и среднелегированные хромом и молибденом и некоторые чистые металлы, как, например, никель, титан и молибден. Коррозионная стойкость оценивалась на основании как весовых изменений, по результатам металлографического анализа, так и изменений механических свойств. В качестве исходного состояния структуры и механических свойств материалов было принято их состояние после термического старения при одной и той же температуре в аргонной атмосфере.

3.1. Нержавеющие хромистые и хромоникелевые стали и сплавы на основе никеля

Проведенные коррозионные испытания в жидком натрии с низким содержанием кислорода (ниже $3 \cdot 10^{-3}$ %) в течение 1500 часов при наличии перепада температуры примерно 150°С показали, что скорость коррозии сталей и сплавов как при температуре 760°С при конвекционном потоке, так и при температуре 600°С с принудительной циркуляцией натрия повышается почти линейно с увеличением количества никеля (1). Скорость коррозионного нападения, например нимоника-80, при температуре 760°С составляет около 40 мк/год, а при температуре 600°С – примерно в десять раз меньше. При температуре 760°С было также установлено, что коррозия линейно возрастает с увеличением количества хрома в стали, однако скорость коррозионного нападения примерно в два раза ниже скорости, вызываемой наличием того же количества никеля. Это приводит к заключению, что железо в относительно чистом натрии обладает наименьшей растворимостью, и поэтому низко- и среднелегированные стали, стабилизированные сильно карбидообразующими элементами, не подвергающимися обезуглероживанию, имеют значительные перспективы применения. Аналогичные результаты относительно влияния никеля, хрома и железа получили также и другие авторы [2]. Интересно отметить, что они обнаружили у ферритных или нержавеющих сталей весьма близкие скорости коррозии при одних и тех же условиях. По всей вероятности, это вызвано тем, что после удаления хрома и никеля с поверхностного слоя, общая коррозия уже управляется коррозией ферритного поверхностного слоя. Точно такое же явление обнаружил автор при коррозии аустенитных хромоникелевых сталей и в тяжелых жидких металлах, например в эвтектическом сплаве свинец – висмут. После первоначального усиления коррозии вплоть до достижения равновесия между диффузией никеля и хрома через обедненный слой и коррозией этого ферритного слоя скорость коррозии стабилизировалась с наклоном, приблизительно параллельным скорости коррозии ферритных сталей. Однако общая коррозия была примерно на 50% выше. Нам думается, что повышенная коррозия аустенитных хромоникелевых сталей вызывается увеличением поверхности, образовавшегося ферритного слоя, вследствие его некомпактности. Одновременно было установлено, что по мере повышения температуры испытаний существенно уменьшалась толщина такого ферритного слоя, причем, однако, общая коррозия далее повышалась. Равновесие между диффузией никеля и хрома и коррозией ферритного слоя было достигнуто в течение нескольких суток.

Можно считать, что достижение такого равновесия в натрии будет относительно длительным процессом, зависимым в значительной степени от количества кислорода в натрии и таким образом и от общей коррозии. В течение коррозионных испытаний, длившихся 1500 часов, в относительно чистом натрии, по всей вероятности, не было достигнуто равновесия и поэтому коррозия при постоянной температуре возрастала почти линейно с повышением количества никеля и хрома в сталях и сплавах.

На понижение скорости коррозии аустенитных сталей в натрии с низким содержанием кислорода известное влияние оказывает также их легирование молибденом [1, 2]. Было установлено, что молибден в количестве примерно 2%, при температуре 760°С, снижает их коррозию примерно в 1,5 ÷ 2 раза. При температурах в пределах 550 ÷ 600°С влияние молибдена, вследствие малой коррозии, обнаружено не было.

Температурная зависимость коррозии некоторых аустенитных хромоникелевых сталей и нимоника приведена на рис. 3. На упомянутом рисунке можно заметить, что коррозия с температурой возрастает быстрее у материалов с большим количеством никеля. На это явление частичное влияние может оказывать постепенное образование ферритного слоя на поверхности аустенитных сталей, вследствие чего их общая коррозия по мере возрастания температуры замедлялась.

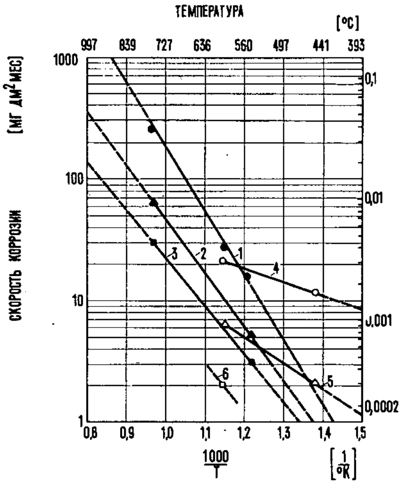

Рис.3. Температурная зависимость коррозии некоторых материалов в потоке натрия с содержанием кислорода ниже $3 \cdot 10^{-3}$ % (перепад темп. – 150°С): 1 – нимоник; 2 – сталь типа 1Cr23Ni18Si2; 3 – 1Cr18Ni9; 4 – низколегированные стали типа 1CrMoV; 5 – стали типа 1Cr3 ÷ 5 Mo; 6 – ферритные стали, стабилизированные титаном и ниобием.

Влияние увеличения содержания кислорода в натрии на коррозию нержавеющих хромистых и хромоникелевых сталей уже исследовалось [3]. Последние исследования подтвердили основные сведения, полученные в то время. Было установлено, что на коррозию сталей и сплавов в натрий при температурах 600°С, температурном перепаде 100°С и концентрации кислорода $5 \cdot 10^{-2}$ % благоприятное влияние оказывает главным образом никель и частично хром. Испытания проводились на конвекционных петлях. Скорость коррозии стали типа 18/8, установленная после 1000 часовых испытаний, составляла примерно 0,1 мм/год. Стали, содержащие 13 ÷ 24% хрома, подверглись большей коррозии – вплоть до 0,3 мм/год. Образцы приведенных выше материалов имели оксидированную поверхность. Хромистые стали были почти черного цвета, а хромоникелевые – скорее зеленого. Такие слои по истечении некоторого времени полностью растворялись в воде. Аналогичные оксидные слои были рассмотрены некоторыми другими авторами [2, 4], и приведены их составы, как, например, хромит натрия.

3.2. Стали с содержанием хрома до 5%

Приведенные выше стали обычно легируются еще молибденом или ванадием, а также другими элементами. Такие стали в натрии с низким содержанием кислорода подвергаются весьма малой коррозии. Основной их недостаток заключается в том, что они подвергаются обезуглероживанию [1, 3, 6], так что если в том же контуре находятся нержавеющие хромоникелевые стали, то может иметь место их науглероживание и ухудшение механических свойств. На рис. 3, где приведены зависимости изменения веса упомянутых сталей от температуры, показано, что стали типа 1CrMoV подвергаются значительному обезуглероживанию уже при температуре 400°С. Стали с содержанием 3 – 5% хрома претерпевают также частичное обезуглероживание, однако в относительно меньшей степени. Опираясь на изменения приведенных выше зависимостей, можно сказать, что изменения веса упомянутых сталей вызваны главным образом обезуглероживанием образца, а не растворимостью железа, так как концентрация кислорода в натрии поддерживалась низкой. На активность углерода в сталях большое влияние оказывает устойчивость карбидов, в которых он связан. Стали с карбидами типа цементита претерпевают весьма быстрое обезуглероживание. Относительно более устойчивы карбиды хрома типа Me_7C_3, а еще более устойчивы – карбиды типа $Me_{23}C_6$. Однако при повышенных температурах и такие карбиды неустойчивы в натрии с низким содержанием кислорода и углерода; поэтому стали постепенно обезуглероживаются.

Стали низко- и среднелегированные хромом в натрии с повышенным содержанием кислорода (примерно $5 \cdot 10^{-2}$%) при температуре 600°С подвергаются значительной коррозии. Скорость их коррозии при конвекционном потоке достигает примерно 0,5 мм/год.

3.3. Ферритные стали, стабилизированные титаном или ниобием

Потери веса у стабилизированных сталей при всех температурах испытаний в натрии с низким содержанием кислорода были ниже, чем у всех остальных сталей (см. рис. 3). Приведенные выше стали не подвергаются обезуглероживанию и поэтому не являются источником углерода [1, 3, 7]. Вследствие этого они применимы в одном контуре и в комбинации с нержавеющими хромоникелевыми сталями. Стабилизация сталей осуществляется с помощью сильно карбидообразующих элементов, как, например, титана и ниобия; в качестве же элементов, повышающих прочность и частично жаростойкость, применяются хром, молибден и возможно вольфрам. Стабилизирующие элементы применимы либо в отдельности, либо в комбинациях, однако их чрезмерная или недостаточная стабилизация – нежелательны. Влияние повышенного содержания кислорода на коррозию стабилизированных сталей аналогично влиянию на коррозию низко- и среднелегированных сталей хромом. Поэтому и такие стали не пригодны для систем, в которых содержание кислорода в натрии не поддерживается на низкой концентрации.

3.4. Коррозионная стойкость некоторых чистых металлов

Исследовалась коррозия металлического никеля, молибдена и титана. Было установлено, что титан при 600°С и скорости потока натрия с низким содержанием кислорода, равной примерно 1,5 м/сек, корродирует со скоростью примерно 3 мм/год. Его коррозия в натрии с повышенным содержанием кислорода также значительна даже при наличии конвекционного потока.

О коррозии никеля в чистом натрии было уже сказано в параграфе 3.1. Однако металлический никель и сплавы на его основе при температуре 600°С в натрии с повышенным содержанием кислорода обнаружили даже привес, соответствующий слою примерно 60 мк. Аналогичные слои были установлены и раньше [1, 3] в составе никель-железо и хром. Такое явление по всей вероятности вызвано выравниванием активностей различных металлов. Этот вопрос будет предметом дальнейших исследований.

Исследовалась также коррозия металлического молибдена. У такого молибдена при всех концентрациях кислорода в натрии какая-либо коррозия обнаружена не была. Точно также и в тяжелых жидких металлах металлический молибден обнаруживал самые малые коррозионные потери веса.

3.5. Влияние натрия на механические свойства испытанных сталей

Натрий с низким содержанием кислорода и углерода вплоть до температуры 760°С не вызывает заметных изменений механических свойств нержавеющих хромоникелевых сталей. Нержавеющие хромистые стали так же не обнаруживают заметных изменений. При различных температурах испытаний у некоторых хромоникелевых сталей наибольшие изменения были обнаружены при температуре примерно 600°С. Так например, относительное удлинение сталей 1Cr18Ni9 и 1Cr18Ni9Ti были на примерно 10 – 15% ниже, чем у таких же образцов после изотермического отжига. Такие изменения механических свойств по всей вероятности связаны с некоторыми диффузионными процессами по границам зерен, как например, диффузия углерода или даже внутреннее окисление кислородом.

Равным образом и у ферритных низко- и среднелегированных стабилизированных сталей при различных температурах испытаний значительные изменения механических свойств, вызываемые влиянием натрия, обнаружены не были.

Стали с низким и средним содержанием хрома в пределах температур 400 ÷ 500°С подвергаются заметному обезуглероживанию, их механические свойства ухудшаются и могут служить источником углерода для науглероживания аустенитных сталей, в особенности если углерод не был выделен из натрия.

Повышенное содержание кислорода в натрии оказывает неблагоприятное влияние как на коррозию, так и на изменение механических свойств главным образом нержавеющих аустенитных сталей. Влияние повышенного содержания кислорода на ухудшение их механических свойств, вероятно, связано с уже упомянутым внутренним окислением [5]. Наши испытания пока указывают на возможность такого объяснения процесса, так как межкристаллитное нападение само по себе по нашим наблюдениям столь существенных изменений вызвать не может.

3.6. Перенос масс

Перенос масс у всех конструкционных сталей значительно повышается по мере увеличения содержания кислорода в натрии. Однако он в значительной степени зависит от состава материалов. Но по мере увеличения содержания никеля и частично хрома общая коррозия аустенитных сталей по сравнению с низко- и среднелегированными сталями хромом, молибденом, титаном и ниобием существенно ниже. Так например, при испытаниях в натрии с содержанием кислорода $5 \cdot 10^{-2}$ % при температуре 600°С и перепаде температуры 100°С в результате неизотермического переноса масс значительно уменьшилось полезное сечение трубки циркуляции в низкотемпературной ветви. Металлические ферромагнитные кристаллы, выделенные там, содержали примерно 96% железа, 2% никеля и небольшое количество кремния, титана и молибдена. Изотермический перенос масс при вышеприведенных условиях наблюдали в высокотемпературной ветви, но лишь на образцах с содержанием никеля, превышающим 75%.

Однако же неизотермический перенос масс в натрии с низким содержанием кислорода вызван главным образом переносом никеля и хрома. Изотермический перенос масс вызывается также главным образом никелем и хромом, осаждающимися на сталях с низким содержанием легирующих элементов.

Из сказанного выше можно сделать следующий вывод. Неизотермический или изотермический перенос масс зависит от количества растворенных элементов; выделение осуществляется примерно в соотношении, соответствующем соотношению коррозии примененных материалов. Выделение перенесенных масс осуществляется главным образом в атомарном виде.

4. ВЛИЯНИЕ НЕКОТОРЫХ ФАКТОРОВ НА СКОРОСТЬ КОРРОЗИИ

Некоторые авторы [2, 4] считают, что скорость коррозии повышается со скоростью потока натрия. Приведенные данные касаются по большей мере относительно чистого натрия. Они также [2] указывают на возможности насыщения железом "по направлению потока" в высокотемпературных ветвях значительной длины. Коррозионные испытания, проведенные у нас в натрии с низким содержанием кислорода (ниже $3 \cdot 10^{-3}$%, определяли по методу амальгамации), как в динамических контурах при температуре 600°С, скорости потока натрия примерно 1,5 м/сек и длине испытательной ветви примерно 3 м, так и на конвекционных петлях при температуре вплоть до 760°С не только ничего не говорят в пользу насыщения "по направлению потока", но и не было обнаружено влияния скорости потока на коррозию.

Путем исследования коррозии конструкционных сталей в тяжелых жидких металлах было также установлено, что коррозия материалов протекала почти с одной и той же скоростью по всей длине испытательной ветви в конвекционных и динамических контурах и что их коррозия в свинце-висмуте при той же насыщенности железом по мере повышения циркуляции в пределах 2 – 100 см/сек повышалась весьма мало. Скорость коррозии сталей в зависимости от температуры при максимальном температурном перепаде (рис.4) имеет экспоненциальный ход изменений и в значительной степени зависит от растворимости железа в отдельных жидких металлах.

На основании сказанного выше можно считать, что коррозия в чистых жидких металлах, главным образом щелочных, не управляется процессами диффузии, даже при относительно малых скоростях потока. Скорость коррозии в таких случаях, главным образом, зависит от скорости перехода атомов растворенного металла в жидкий металл.

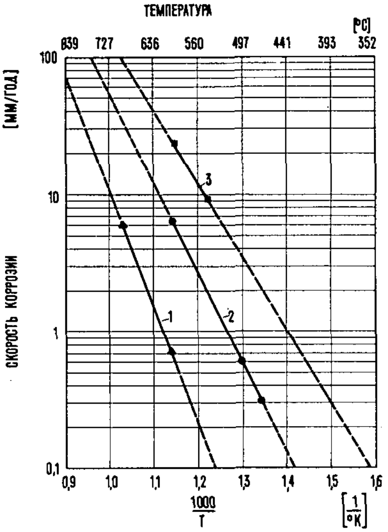

Рис.4. Температурная зависимость скорости коррозии углеродистых и низколегированных сталей в жидком свинце (1), в эвтектическом сплаве свинец-висмут (2) и в висмуте (3) при конвекционном потоке ($v = 1{,}5 \div 2$ см/сек, $\Delta t > 150\,°C$). Жидкие металлы раскислялись посредством добавки 0,05% магния.

Однако механизм и кинетика коррозии сталей в натрии с повышенным содержанием кислорода имеют иной характер. Испытания, проведенные на конвекционной петле с содержанием $5 \cdot 10^{-2}$ % кислорода, указывают на значительное влияние процессов диффузии. Поэтому мы считаем, что по мере увеличения содержания кислорода в натрии зависимость скорости коррозии от скорости потока будет повышаться. В таком случае коррозия будет управляться либо подачей кислорода на поверхность материала, либо растворимостью или разрушением продуктов реакции с его поверхности. Разъяснение таких вопросов является предметом дальнейших исследований.

Путем изучения влияния величины температурных перепадов между высокотемпературной и низкотемпературной ветвями установки на коррозию сталей в тяжелых жидких металлах было установлено, что скорость коррозии в высокотемпературной ветви при той же температуре с увеличением температурного перепада выше 150°С весьма мало отличается. Мы считаем, что коррозия конструкционной стали в чистом натрии будет определяться теми же закономерностями.

5. ЗАКЛЮЧЕНИЕ

Проведенные исследования коррозионной стойкости материалов показывают, что, чем чище будет жидкий натрий, тем меньшей будет коррозия конструкционных сталей. Коррозионная стойкость низко- и среднелегированных сталей в натрии с низким содержанием кислорода – если они не подвергаются обезуглероживанию – выше, чем у нержавеющих сталей и сплавов, легированных никелем и хромом. И, наоборот, в жидком натрии коррозия у низколегированных сталей по мере увеличения содержания кислорода возрастает скорее, чем у нержавеющих сталей и относительно более значительна.

Коррозионную стойкость конструкционных материалов можно исследовать как на динамических, так и на конвекционных петлях, в частности в жидких металлах с низким содержанием загрязнений.

ЛИТЕРАТУРА

[1] ILINČEV G., Jaderná Energ. 10, 8 (1964) 271.

[2] NETTLEY P.T., BELL I.P., BAGLEY K.Q., HARRIES D.R., THORLEY A.W., TYZACK C., London Conference on Fast Breeder Reactors, Ref. 5B/3 (1966).

[3] ILINČEV G., Jaderná Energ. 10, 1 (1964) 2.

[4] MORABITO J.J., DICKINSON R.W., JONES R.H., SAVAGE H.W., London Conference on Fast Breeder Reactor, Ref. 5B/4 (1966).

[5] НИКИТИН В.И., "Физико-химическая механика материалов", 3 (1965) 361.

[6] НЕВЗОРОВ Б.А., ЗОТОВ В.В. и др., Третья международная конференция ООН по использованию атомной энергии в мирных целях, Proc. 3rd UN Int. Conf. PUAE 9 (1965) 561.

[7] GURINSKY D.H. et al. Третья международная конференция ООН по использованию атомной энергии в мирных целях, Proc. 3rd UN Int. Conf. PUAE 9 (1965) 550.

DISCUSSION

A. HATTERER: I have a general comment to make regarding the oxide layers formed during corrosion of stainless steel and other alloys in liquid alkaline metals. The mixed oxides $NaCrO_2$, $NaFeO_2$ and Na_4FeO_3 have already been mentioned several times. There are however other ternary compounds of the $A_xB_yO_2$ form, where element A can be Li, Na, K, Rb or Cs, and element B can be Ti, Zr, V, Nb, Ta, Cr, Mo, Fe or W. These are produced by various types of reaction: $A_2O + B$, or $A + B_mO_n$, or $A_2O + B_mO_n$. Some of these compounds are poorly crystallized and relatively unstable (being sensitive to heat, oxygen and water). It is therefore still a tricky problem to detect them on metal surfaces, but nevertheless a problem that should engage our attention.

MASS TRANSFER IN ALKALI METAL SYSTEMS: BEHAVIOUR OF CARBON

(Session III)

DEVELOPMENT OF A LOW-ALLOY FERRITIC STEEL FOR HIGH-TEMPERATURE SODIUM SERVICE WITH SPECIAL REGARD TO CARBON TRANSPORT

E. BAERLECKEN, K. LORENZ, E. KRANZ
AND D. SCHLEGEL
THYSSEN RÖHRENWERKE AG,
METALLURGISCHE ABTEILUNG,
DÜSSELDORF, FEDERAL REPUBLIC OF GERMANY

Abstract

DEVELOPMENT OF A LOW-ALLOY FERRITIC STEEL FOR HIGH-TEMPERATURE SODIUM SERVICE WITH SPECIAL REGARD TO CARBON TRANSPORT. The design and construction of heat exchangers, especially in reactor engineering, with metal melts such as sodium or sodium/potassium used as a heat transfer medium brings up the problem of carbon transport between various materials through this medium.

If the conventional ferritic and austenitic chrome-nickel steels are used side by side, carburization of the austenitic steels will take place whereby structural elements, such as the fuel element and moderator jackets, are adversely affected. This phenomenon is due to different activities of the carbon contained in the ferrite and austenite, and it is sufficiently known from the use of welded joints of the ferritic-austenitic type. It was therefore necessary to determine whether a suitable ferritic material with an adequately low carbon activity could be developed for sodium circuits. Compared with austenite, such a material has the advantage of a higher rate of economy, a fact to be taken into account along with the low material costs and also with its higher thermal conductivity and lower thermal expansion.

Proceeding from the heat-resistant 2¼% chrome and 1% molybdenum steel, the effect of carbide-forming elements upon the decarburization tendency when brought into contact with chrome-nickel austenite was studied at temperatures up to 700°C. Additions of niobium and titanium prevent decarburization, if the concentration is sufficient to stabilize the entire carbon and nitrogen. Diffusion tests showed that this condition is satisfied if the titanium or niobium content corresponds to the stoichiometrical composition of the respective carbides and nitrides.

It was surprising to find that the carbide-forming element, vanadium, even at very high concentrations, *did not effectively prevent carbon diffusion*. Subsequently, preference was given to the Nb-stabilized material because niobium is much more suitable than titanium to obtain a sufficiently high stress-rupture strength.

Because of the association of carbon with niobium and of the ferrite-forming effect of the latter element, it was expected that the properties of the conventional 2¼% chrome-molybdenum steel would be altered. Examinations were therefore made to determine the influence of rising niobium contents on the transformation and precipitation properties. First, a quasi-binary section of the iron-carbon-chromium-molybdenum-niobium system was established. This quasi-binary section, which by itself does not allow any conclusions to be drawn regarding the time-dependence of the transformation processes, was supplemented by a continuous TTT-diagram that helped to investigate fully the heat treatment characteristics of various cross-sections.

Next, detailed examinations were carried out to determine the influence of niobium concentration on the technological properties. A close relationship was found to exist between the precipitation of Nb-carbide or iron-niobide and, in particular, the impact properties and yield strength. As the niobium acts unfavourably upon impact properties of this type of steel, limitation of the Nb-content and additions of suitable alloying elements, such as manganese or nickel, are necessary to ensure a sufficient degree of resistance to brittle fracture.

Having due regard to all these factors, a ferritic material was produced with a sufficiently low carbon activity to meet the requirements of sodium-cooled reactors, as has been borne out by the processing of commercial melts into tubes, sheet metal and forgings. The properties essential for the manufacture and application of this steel are indicated, such as notched-bar impact strength, yield point at elevated temperature, stress-rupture strength and scaling properties in air and steam, as well as weldability when using electrodes made of a material identical with the parent metal.

1. INTRODUCTION

When planning and constructing heat exchangers in reactor engineering with metal melts such as sodium or sodium/potassium used as a heat transfer medium, special care has to be taken in the selection of materials. Since steels of various properties and therefore different analysis will be used, the problem of carbon transport by decarburization and carburization of the different materials must be duly considered. The carburization effects induced by the metal melts acting as a carbon transport medium are comparable with those taking place under gas atmospheres such as CO/CO_2 or CH_4/H_2.

If the conventional ferritic and austenitic chromium-nickel steels are used together, the austenitic steels will be carburized, causing structural elements, such as fuel elements and moderator jackets, to be adversely affected. This carbon migration is due to the different activities of the carbon contained in the ferrite and austenite respectively, and is well known in weld joints between ferritic and austenitic steels, which are used at elevated temperatures [1].

It was necessary to develop a ferritic material suitable for sodium circuits, having not only an adequately low carbon activity, but also good mechanical properties, and perfect workability and weldability. Compared with austenitic steels, such a ferritic material has the advantage of a higher thermal conductivity and a lower thermal expansion [2]. Furthermore, a higher rate of economy can be expected because of the lower cost of material.

For the carbon diffusion which takes place in the direction of the activity gradient the carbon activity of the diffusion partners is of decisive importance. In the most simple cases, the activity is proportional to the difference of the carbon content. In multi-component systems, especially where alloy steels are concerned, the influence of the constitution of the structure and of the alloying constituents on the carbon activity must also be considered. Thus the carbon activity may be changed to such a degree that a carbon diffusion can take place contrary to the concentration gradient, the so called "up-hill diffusion" [3].

It is well known that the carbon activity of iron alloys with an austenitic lattice is lower than that of a ferritic one. In addition this activity is lowered by alloying elements with a carbon affinity higher than iron, whereas elements with a lower affinity have an effect to the contrary. Thus it becomes possible to lower a high carbon activity by the addition of suitable carbide-forming elements to such a degree that carbon diffusion between materials of a different type of lattice can also be avoided.

2. CARBON DIFFUSION

The present work deals in the first place with the problem of how in the case of a low-alloy ferritic steel the carbon activity, owing to the addition of suitable carbide-forming elements, can be lowered to such an extent that carbon diffusion in contact with austenitic steel will be avoided. On the basis of the conventional 2 ¼% chromium/1% molybdenum boiler steel, a study was made of how the elements niobium, titanium and vanadium, when in contact with the austenitic material X 8 Cr Ni Nb 16 13, influence the decarburization tendency. Table I shows the concentration ranges in wt. % of the tested materials

TABLE I. COMPOSITION OF TESTED 25-kg INDUCTION HEATS (Concentration ranges in wt. %)

Heat No.	% C	% Si	% Mn	% Cr	% Mo	% N	% Nb	% Ti	% V
1	0.05	0.20	0.43	2.02	1.06	0.009	-	-	-
2 - 16	0.02 0.10	0.20 0.46	0.39 0.58	2.11 2.36	0.91 1.10	0.009	0.21 1.95	-	-
17 - 21	0.04 0.06	0.24 0.41	0.48 0.54	2.19 2.25	1.01 1.07	0.009	-	0.18 0.37	-
22 - 27	0.05 0.06	0.20 0.31	0.43 0.52	2.27 2.60	0.96 1.15	0.009	-	-	0.45 2.63

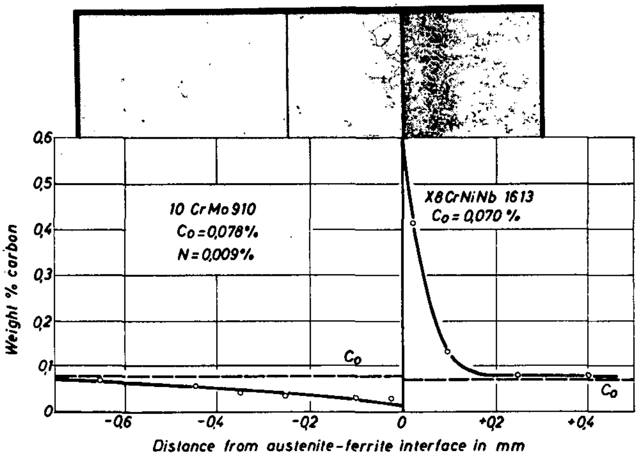

FIG.1. Change of carbon content after treatment for 10^3 h at 700°C; microstructure and trend of carbon concentration

which were available in the form of 25 kilo induction heats. A diffusion temperature of 700°C was chosen, a temperature above the expected reactor operating range. This was done in order to be able to transfer the results obtained from the tests of about 1000-h periods to the much longer service conditions encountered in practical reactor operations.

The diffusion partners were in direct contact with each other, without sodium as a carbon transport medium; the specimens were either welded or pressed under diffusion temperature. Both test methods led to the same results.

From a metallographic point of view the carbon diffusion was studied for the depth of carburization in the austenite and partly also for the pattern of carbon concentration, measured on layers of about 0.1-mm thickness. Examples significant for the carbon diffusion between ferrite and austenite with various alloying elements are shown in Figs 1-3. The decarburization of the ferrite and the intensive carburization of the austenite during contact of the unstabilized ferrite with chromium-nickel-austenite, according to Fig. 1, is already reduced by a small addition of niobium as shown in Fig. 2. As shown in Fig. 3, this is completely avoided by a higher niobium content.

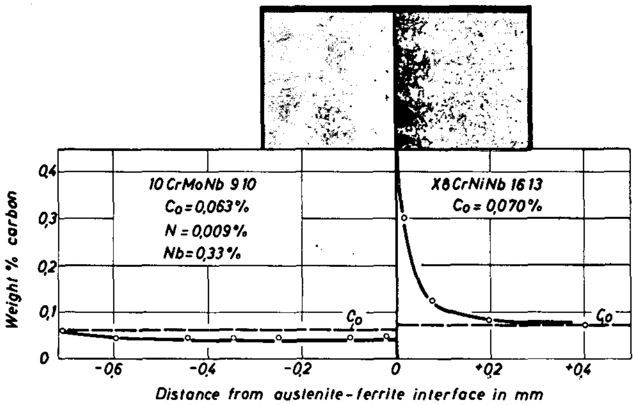

FIG. 2. Change of carbon content after a treatment for 10^3 h at 700°C; microstructure and trend of carbon concentration

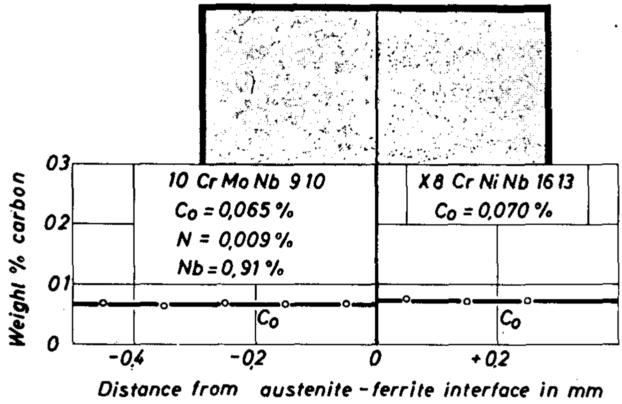

FIG. 3. Change of carbon content after treatment for 10^3 h at 700°C; microstructure and trend of carbon concentration

The effect of the contents in the ferrite of the carbide-forming elements niobium, titanium and vanadium on carbon diffusion is illustrated in Fig. 4. The difference between the total quantities of the alloying elements and those calculated in the stoichiometrical way for a complete stabilization of carbon and nitrogen to form Nb (C, N), Ti (C, N) or V (C, N) is marked "free content". As can be seen, the depth of the carburization zone in the austenite decreases with the increase in the alloying elements. To completely avoid the diffusion a niobium or titanium content will be sufficient that corresponds to the concentration calculated for a complete stabilization of carbon and nitrogen. The following formula is to be applied:

$$N^{Ti,Nb} \geq N^{C} + N^{N} \quad \text{in at.\%}$$

when N is the molar concentration of the elements. The conversion of this formula into wt. % results in the following simplified formula:

$$\text{Wt. \% Nb} \geq 8 \times \text{wt. \% } (C + N)$$

$$\text{Wt. \% Ti} \geq 4 \times \text{wt. \% } (C + N).$$

These results agree very well with experiments regarding the carbon transport between the niobium-alloyed 2 ¼% chromium/1% molybdenum steel and austenitic steels in static and flowing sodium systems made in co-operation with INTERATOM.

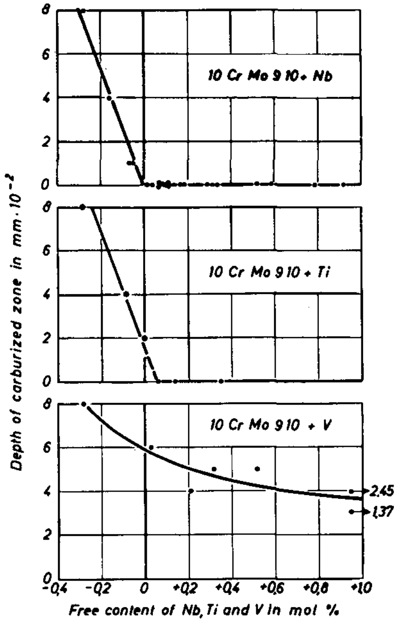

FIG.4. Carbon pick-up in austenite X 8 Cr Ni Nb 16 13 versus free content of Nb, Ti and V in ferrite after treatment for 500 h at 700°C

By additions of vanadium the carbon diffusion could not be completely avoided even with very high concentrations at the testing conditions specified. This result differed from the statements set out in literature [3]. According to these an addition of 0.94 wt. % vanadium at a temperature of 700°C and a (C + N) content of 0.05 wt. % is sufficient to avoid carbon diffusion. In our investigation, however, it was found that a vanadium content of up to 2.63 wt. % could not prevent diffusion completely.

During subsequent investigations carried out to develop a ferritic steel for sodium-cooled circuits, preference was given to the Nb-stabilized material, as niobium is much more suitable than titanium to get a sufficiently high-stress rupture strength [4, 5]. The vanadium-alloyed type was ruled out because of its decarburization when in contact with austenite.

3. TRANSFORMATION AND PRECIPITATION

Because of the affinity of niobium to carbon and nitrogen, and of the well-known ferrite-forming effect of niobium [6], it was to be expected that the behaviour of the conventional $2\frac{1}{4}\%$ chromium/1% molybdenum steel, in particular the transformation and precipitation, would be considerably altered.

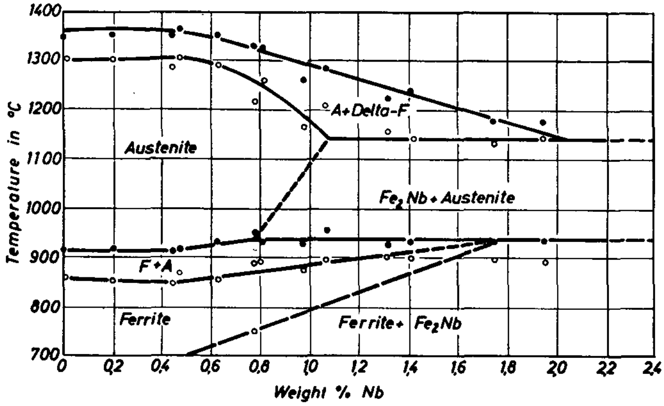

FIG. 5. Quasi-binary section in the phase diagram (Fe-Cr-Mo-C)-Nb in the composition of 10 Cr Mo 9 10 with 0.05% C, 2.25% Cr, 1.0% Mo, 0.25% Si, 0.45% Mn, bal. Fe.

For the phase diagram iron-chromium-molybdenum-carbon-niobium a quasi-binary section on the composition of the steel type 10 Cr Mo 9 10 could be established, as shown in Fig. 5; this was according to the results obtained by means of a thermomagnetic balance [7]. With increasing niobium contents the austenitic field was restricted. Restriction, however, was not complete even up to the highest concentrations examined, because of the formation of the intermetallic phase Fe_2Nb. This means that even in the case of high niobium concentrations this material retains its full transformation behaviour.

On the other hand, it was to be expected that the properties of the niobium-alloyed $2\frac{1}{4}\%$ chromium/1% molybdenum steel were influenced by the formation of new phases like Fe_2Nb and Nb(C, N). Therefore the precipitation behaviour of the material was studied after a normalizing and tempering treatment by X-ray investigations of electrolytic residues. The results are shown in Fig. 6.

The chromium and molybdenum carbide formation is reduced by niobium additions from the formation of Nb (C, N). A free niobium content of more than about 0.25 wt. % leads to the formation of the intermetallic phase Fe_2Nb as well as the formation of Nb (C, N).

4. MECHANICAL PROPERTIES

Figure 6 represents the correlation between the precipitation behaviour and the mechanical properties of the material, and shows the effect of the niobium content on the impact properties, proof stress and tensile strength. When the formation of niobium carbide increases there is first a rise of the impact strength, followed by a sudden drop as soon as the formation of niobide begins. With increasing formation of niobium carbide the proof stress is strongly and the tensile strength slightly lowered, while the increasing formation of Fe_2Nb has a visible effect only on the tensile strength. While the decrease of proof stress is inevitable because of the carbon stabilization, the decline in the impact strength could be avoided by a close limitation of the niobium content.

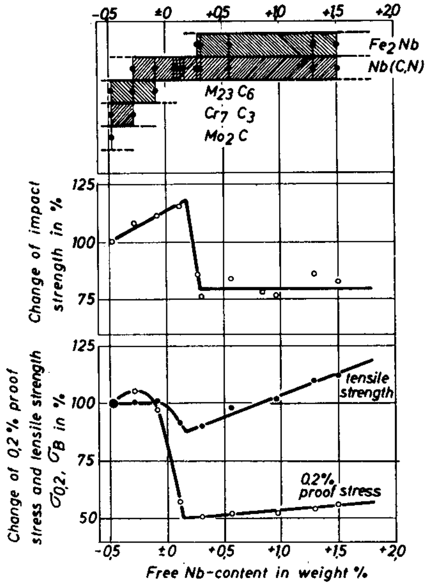

FIG. 6. Effect of precipitations on the 0.2% proof stress, tensile strength and impact properties versus free Nb-content of 10 Cr Mo Nb 9 10; heat treatment 30 min 1020°C AC+2 h 750°C AC

Additional investigations of the impact properties of plates, tubes and forgings made of 10-ton-electric-steel heats revealed that the impact strength is also dependent upon distribution and size of the precipitations. In the results shown in Fig. 6 these factors have been kept constant. As shown in Fig. 7, the optimum impact properties are gained with small particle sizes and homogeneous distribution of precipitations in the matrix. Increasing precipitation sizes and irregularities in distribution, which are particularly evident in the case of rolled material and forgings with a relatively low amount of deformation, favour the decrease of the impact strength. This undesirable effect on the niobium-alloyed 2 $\frac{1}{4}$% chromium/1% molybdenum steel could be avoided by appropriate technical measures, in particular by a small addition of nickel. Figure 8 shows by way of comparison the accumulative frequency curves of the notch impact values for the materials 10 Cr Mo Nb 9 10 and 10 Cr Mo Ni Nb 9 10 with the concentration ranges as shown in Table II. In Fig. 8 the DVM-transverse notched-bar impact strength has been evaluated at room temperature for plate material up to 130-mm thickness after normalizing and tempering. The result is that the nickel-alloyed type is certainly superior to the nickel-free type. Figure 9 shows impact-transition curves for plate material 16 and 22 mm thick of the nickel-alloyed type with different carbon contents and different proof stresses at room temperature. The minimum value for the Charpy-V-notch-impact test at room temperature is 4 mkg/cm^2, for the DVM-test 11 mkg/cm^2.

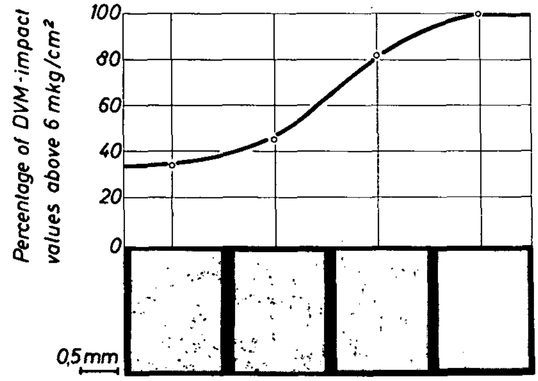

FIG. 7. Effect of size and distribution of niobium precipitations on the DVM impact properties at room temperature

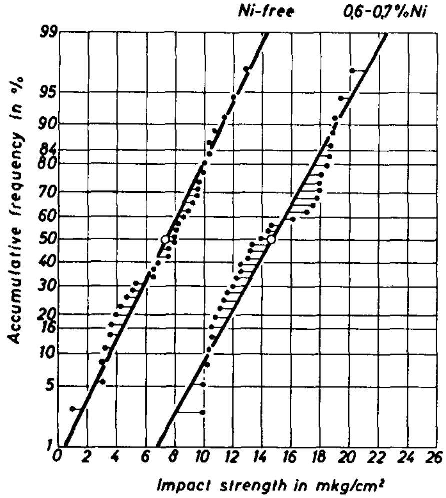

FIG. 8. Impact properties at room temperature of 10 Cr Mo Nb 9 10 without and with Ni addition, plate material up to 130-mm thickness; accumulative frequency curves

Further investigations were made to study the influence of the niobium addition on the mechanical properties of the conventional boiler steel. In this way a change is brought about in the time-temperature-transformation behaviour after the normalizing treatment.

TABLE II. COMPOSITION OF TESTED 10-t ELECTRIC-STEEL PRODUCTION HEATS
(Concentration ranges in wt. %)

Material	% C	% Si	% Mn	% Cr	% Mo	% Ni	% N	% Nb
10 CrMoNb 9 10	0.08 0.09	0.25 0.40	0.48 0.55	2.25 2.36	0.90 0.99	-	0.005 0.006	0.89 1.25
10 CrMoNiNb 9 10	0.05 0.07	0.20 0.36	0.64 0.85	2.09 2.46	0.97 1.07	0.60 0.72	0.008 0.014	0.56 1.02

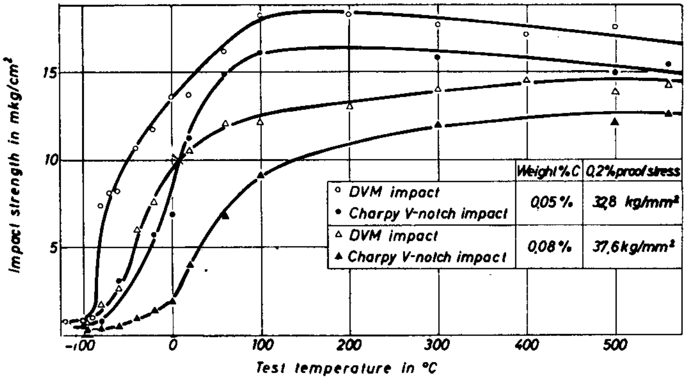

FIG. 9. Impact transition curves for 10 Cr Mo Ni Nb 9 10, plate material with different carbon contents and 0.2% proof stress; heat treatment 30 min 1020°C AC + 2 h 750°C AC

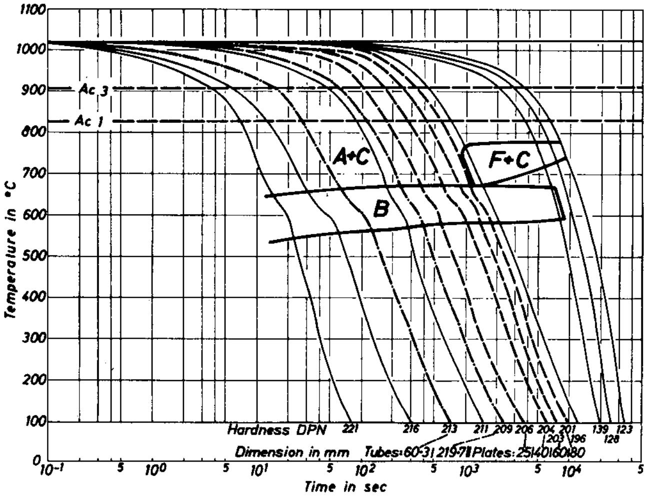

FIG. 10. T-T-T-diagram for 10 Cr Mo Ni Nb 9 10; normalized 30 min at 1020°C

The results are given in a continuous T-T-T-diagram in Fig. 10. The bainitic field compared with material free from niobium is being shifted towards higher temperatures and shorter periods as the stability of the austenite is reduced through the stabilized carbon content. Increasing normalization of temperature results in a higher solution of niobium carbides and reduces this effect accordingly. Likewise the beginning of ferrite-formation is shifted towards shorter periods.

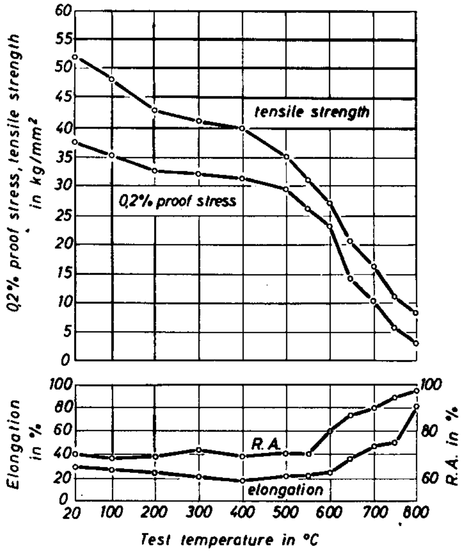

FIG. 11. Mechanical properties at elevated temperatures of 10 Cr Mo Ni Nb 9 10, plate material 16 mm thick; heat treatment: 30 min 1020°C AC + 2 h 750°C AC

A comparison with the typical dimensions of cooling curves in heat exchanger tubes, of line pipes and of plate material from 25-80-mm thickness at air cooling shows that these products get transformed in the bainitic structure without passing the proeutectoid ferrite field. Accordingly the yield strength and tensile strength of such products with the same chemical compositions only spread in a small field.

The dependence of the proof stress, tensile strength, elongation and reduction of area on the test temperature between 20°C and 800°C is shown in Fig. 11.

The stress rupture strength of the niobium-alloyed ferritic steel as calculation basis for operating temperatures above approximately 480°C is indicated in Fig. 12 for testing temperatures of 550°C and 600°C. The given scatterband results from experiments with laboratory and production heats. The testing times of more than 10^4 h reached so far allow for a quite reliable extrapolation of the stress rupture strength for long time service.

The given scatterband is plotted out for forged and rolled materials of different dimensions with a proof stress from 18.9 to 43.4 kp/mm^2 at room temperature. The tested plates with the highest wall thickness were transformed in the ferritic and bainitic field in the T-T-T-diagram. It was found, however, that this different transformation behaviour and the different proof stresses had no essential influence on the stress rupture strength.

Apart from the strength characteristics the resistance to scaling is a further criterion of the maximum service temperature of the material. Comparative investigations into the oxidation resistance of the niobium-free and niobium-alloyed steel types, when exposed to dry air within the scheduled application range near 600°C, revealed compatible results. As an example, scaling curves for a temperature of 610°C, based upon continuous gravimetric measurements, are shown in Fig. 13, the pattern of which follows to a satisfactory degree of approximation a parabolic rate law.

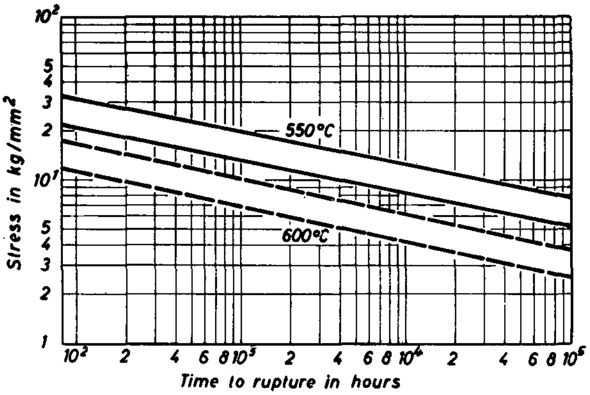

FIG. 12. Stress rupture properties (scatter band) of 10 Cr Mo Ni Nb 9 10 at 550°C and 600°C

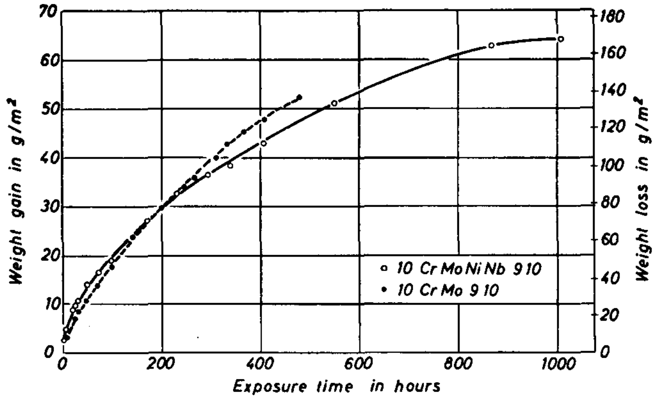

FIG. 13. Weight gain versus time of exposure for 10 Cr Mo Ni Nb 9 10 and 10 Cr Mo 9 10 exposed in dry air; temperature 610°C

5. WELDABILITY AND WORKABILITY

For welding the material 10 Cr Mo Ni Nb 9 10, a parent metal-like electrode was developed, mechanical and impact properties of which are nearly equivalent to those of the parent metal. Figure 14 illustrates a weld joint of 16-mm plate material with the typical structure of the parent metal, the fusion line with the heat-affected zone, and the weld deposit. Figure 15 shows the hardness through the weld joint. The

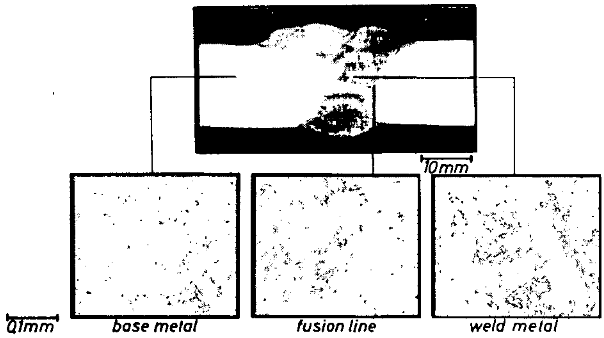

FIG.14. Welded macro- and microstructures of a weld joint of 10 Cr Mo Ni Nb 9 10, plate material 16 mm thick, 4 mm parent-like electrodes, welded without preheating; heat treatment of base metal: 30 min 1020°C AC +2 h 750°C AC

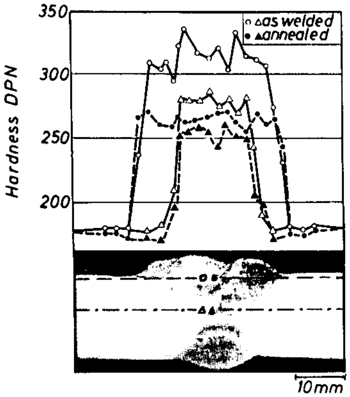

FIG.15. Hardness through a parent-like weld joint of 10 Cr Mo Ni Nb 9 10 before and after annealing for 1 h at 750°C; plate material, 16 mm thick

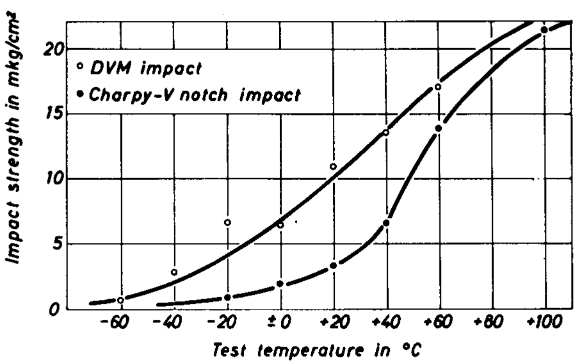

FIG.16. Impact transition curves for welded 10 Cr Mo Ni Nb 9 10, plate material 16 mm thick; welding process manual, Electrode 4 mm, parent-like V-type weld joint; tempered for 1 h at 750°C

maximum hardness of 335 DPN in the weld deposit has been reduced to a maximum of 270 DPN after annealing for 1 h at 750°C.

The impact properties of the weld deposit are shown in Fig. 16 by impact-transition-curves, obtained by Charpy-V-notch- and DVM-specimens. It is thus proved that the weld deposit has sufficient impact properties also.

The niobium-alloyed 2 $\frac{1}{4}$% chromium/1% molybdenum steel has excellent hot and cold working properties, as has been widely confirmed by practical experience when processing production heats into tubes, plates and forgings. Because the niobium-alloyed steel is more susceptible to carbon pick-up compared with the niobium-free steel, special care must be taken during the fabrication. The surface has to be free from lubricants, and a reducing atmosphere during heat treatment must be avoided to prevent the pick-up of carbon.

6. SUMMARY

On the basis of the conventional 2 $\frac{1}{4}$% chromium/1% molybdenum boiler steel, by adding the carbide- forming element niobium it was possible to achieve a low-alloy ferritic steel suitable for use in sodium-cooled reactors. The material has a sufficiently low carbon activity which prevents carbon diffusion when it comes into contact with austenitic steels. The test revealed satisfactory mechanical properties, and sound hot and cold working characteristics as well as good weldability.

REFERENCES

[1] BAERLECKEN, E., Mitt.Verein.Großkesselbesitzer 26 (1953) 569.
[2] MOTZ, J., Z.Metallk. 55 (1964) 489.
[3] WEVER, H., FLENDER, H., Arch. EisenhüttWes. 35 (1964) 65.
[4] PETER, W., FISCHER, W.A., Arch. EisenhüttWes. 19 (1948) 161.
[5] OPPENHEIM, R., LENNARTZ, G., DEW Techn.Ber. 4 (1964) 1.
[6] HANSEN, M., Constitution of Binary Alloys, Mc Graw-Hill, New York (1958) 676.
[7] LORENZ, K., FABRITIUS, H., Arch. EisenhüttWes. 33 (1962) 269.

DISCUSSION

J. W. SEMMEL: I should like to draw your attention to the fact that a programme to modify a ferritic alloy of the 2$\frac{1}{4}$ chromium-1% molybdenum type with carbide-forming elements has also been carried out at Atomics International. Some of the reports on that work are cited as Refs [8] and [9] in the paper I am presenting at this symposium[1]. Briefly, it was found that the addition of suitable carbide-forming elements resulted in resistance to carbon mass transfer in flowing sodium at 1200°F.

---

[1] These Proceedings (SM-85/36).

A PRELIMINARY MODEL FOR THE CARBURIZATION OF STAINLESS STEEL AT HIGH TEMPERATURES IN SODIUM CONTAINING CARBON AT UNIT ACTIVITY

C.S. CAMPBELL AND C. TYZACK
U.K. ATOMIC ENERGY AUTHORITY,
REACTOR MATERIALS LABORATORY,
CULCHETH, WARRINGTON, LANCS.,
UNITED KINGDOM

Abstract

A PRELIMINARY MODEL FOR THE CARBURIZATION OF STAINLESS STEEL AT HIGH TEMPERATURE IN SODIUM CONTAINING CARBON AT UNIT ACTIVITY. The problem of mass transport of carbon due to carbon activity gradients in sodium systems where part of the circuit is constructed in stainless steel and part in ferritic steel is one of practical importance. The use of low-alloy steels in the evaporator section of secondary circuits is attractive from the cost point of view, and should give freedom from worry on stress corrosion phenomena on the water side. Loss of carbon from an unstabilized low-alloy steel would, however, modify its mechanical properties, and lead to carburization of high-temperature austenitic components of the circuit, again with possibly adverse effects on mechanical properties.

No satisfactory model of the kinetics of carburization of stainless steel exists, and this paper is a preliminary attempt to provide one. It is assumed that at the surface of the specimen exposed to sodium the equilibrium level of carbon will be set by the carbon activity of the external medium, and that there will be a carbon activity gradient extending inwards to the as yet unaffected matrix, with the growth of the thickness of the carburizing zone being controlled by the diffusion of carbon down the activity gradient. Within this zone, chromium-rich carbide will tend to precipitate to bring the local level of dissolved chromium into equilibrium with the local carbon activity, as required by the composition of the carbide, and the law of mass action. A simple diffusion model is set up on this basis and, with the aid of experimental data on carbon pick-up, values for the diffusion coefficient of carbon are calculated which are in reasonable agreement with extrapolated values for carbon diffusion in chromium-free austenite. Earlier models have tacitly assumed homogeneous carbon diffusion through the affected layer and this is believed to be incorrect for reasons that are stated.

On a number of counts there would be advantages in being able to utilize low alloy steels for the construction of both primary and secondary circuits in sodium-cooled fast reactors. Major advantages include lower costs and freedom from worry on stress corrosion phenomena on the water side, and the disadvantages of joining problems for dissimilar materials. The major obstacles preventing the use of conventional low alloy steels are insufficient high temperature strength and susceptibility to loss of carbon.

Transport of carbon via sodium in a circuit containing different steels is potentially of importance as it leads to decarburization of materials such as ferritic steels of high carbon activity, and carburization of high chromium materials of lower carbon activity such as stainless steels and high nickel-chromium alloys. Changes of this nature may affect the strength, tensile creep and fatigue properties, and ductility of constructional materials. It is therefore of technological as well as scientific importance to attempt to understand the mechanics and thermodynamic concepts governing the transport of carbon in carburization and decarburization phenomena.

Data on these problems have and are being accumulated in a number of laboratories but no satisfactory quantitative treatment of carburization of stainless steel has emerged. Thus, while the experimental results of Anderson and Sneesby [1] are in general confirmed by subsequent work [2], the diffusion coefficient for carbon derived by them from these results is very much lower (4.12×10^{-11} cm^2/s at 650°C) than is compatible with that determined by the usual methods (c. 10^{-9} cm^2/s)[3, 4]. No explanation for this discrepancy has been put forward but the treatment used has ignored carbide precipitation. This present work is therefore a preliminary attempt to devise a model for the carburization of an austenitic steel by sodium containing carbon at or approaching unit activity as derived from carbon steel sources taking such precipitation into account.

Even in the absence of a stabilising element such as titanium or niobium the carbon activity of an austenitic steel is less than that of a plain carbon steel by what can be shown to be at least two orders of magnitude. In an isothermal system containing mild and austenitic steels bridged by sodium, carbon will therefore tend to be transferred to the stainless steel in an attempt to bring the carbon activities into equilibrium. The initial carbon content of the usual unstabilized austenitic stainless steels is of the same order as the carbon solubility limit, which is $\leqslant 0.04$ wt.% even at 700°C [5, 6]. Any transfer of carbon at such temperatures should therefore supersaturate the austenite virtually immediately and carbide precipitation should follow limiting the immediate rise in carbon activity. This carbide, however, will be chromium-rich ($Cr_{23}C_6$) and will lower the level of chromium in solution. If carbon continues to be made available, precipitation will therefore continue until the lowered chromium activity gives a sufficient rise in carbon activity to bring the system into equilibrium.

From the surface, where this equilibrium level will be set by the carbon activity of the external medium, there will be a carbon activity gradient extending inwards to the as yet unaffected matrix, with the growth of the thickness of the carburising zone being controlled by the diffusion of carbon down the activity gradient. Within this zone chromium-rich carbide will tend to precipitate to bring the local level of dissolved chromium into equilibrium with the local carbon activity, and as the zone increases in thickness and the local carbon activity at any point rises, precipitation will continue and the dissolved chromium level readjust to the new carbon activity. At the same time there may be some readjustment of the composition of precipitate already formed, e.g. to a lower chromium/iron ratio. These processes will involve some diffusion of chromium (and iron) but over distances which can be very small compared with the thickness of the diffusion zone. As an indication that these diffusion processes need not be unduly sluggish, Blanter [7] has shown that a ferritic steel containing 8.72 wt.% Cr and 1.05 wt.% C reached a steady precipitate composition in about 30 min at 600°C, and that an 11.2 wt.% Cr, 0.47 wt.% C steel did likewise in about an hour at the same temperature. Indeed, the result of any appreciable lag in precipitation, by reducing the amount of carbide precipitated, would be to reduce the carbon flux particularly at lower carbon activities thereby giving a greater rather than a reduced depth of carburized zone.

These changes in equilibrium-dissolved chromium content, and the local carbon activity, will be related to the carbide composition according to the law of Mass Action. Thus a plot of the logarithm of the chromium activity against the logarithm of carbon activity will have a slope at any point which is given by the chromium/carbon ratio of the carbide with which equilibrium has been established. Hence a curve relating chromium and carbon activities could be constructed from a suitable starting point, the slope of the curve following the changes in carbide composition with chromium (or carbon) activities, and in this way Fig. 1 has been constructed from available data.

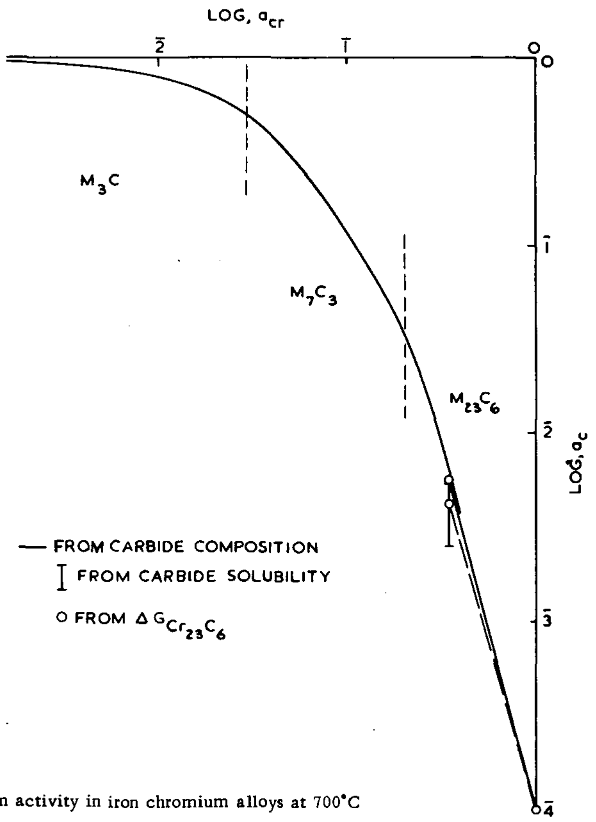

FIG. 1. Carbon activity in iron chromium alloys at 700°C

The information on carbide composition has been taken from the work of Shaw and Quarrell [8] who studied, by chemical analysis and X-ray techniques, carbides extracted from a range of steels annealed at 700°C containing 0.2% carbon and up to 12 wt.% chromium (and up to 2 wt.% vanadium). If allowance is made for the chromium present in the carbide, they found $M_{23}C_6$ down to about 5.7 wt.% dissolved chromium with an increasing substitution of chromium in the carbide by iron, M_7C_3 between this and 0.4 wt.% dissolved chromium, and M_3C below this again. These results are presented as a plot of chromium/carbon ratio against dissolved chromium level in Fig. 2.

Chromium activities in binary non-chromium alloys have been measured at somewhat higher temperatures (1040-1360°C) by Kubaschewski and Heymer [9] and by Jeannin, Mannerskantz and Richardson [10], and are in good agreement. Activities at lower temperatures have been estimated from these measurements on the assumption of a regular solution [10], i. e.

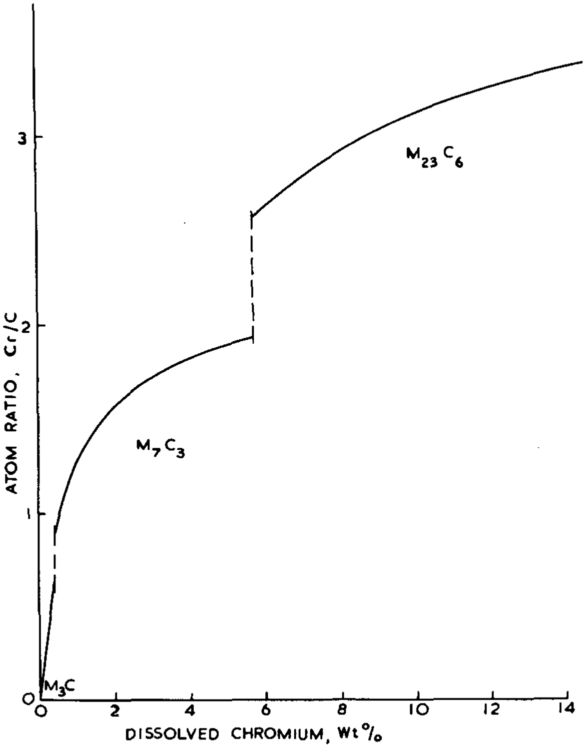

FIG.2. Chromium/carbon ratio of equilibrium carbides at 700°C (derived from Shaw and Quarrell.[8])

$$\log a_{Cr_1} = \log N_{Cr} + T_2/T_1 \log \gamma_2$$

The results of Shaw and Quarrell extend to chromium levels that are sufficiently low for an extrapolation to be made to an infinitely dilute chromium solution, i. e. a carbon activity corresponding to pure Fe_3C. This can accordingly be taken as a starting point and would give a value for $\log a_{C_{700°C}} = -2.2$ for an 18/8 steel in equilibrium with chromium carbide. This value may be compared with estimates derived by two other methods. The first gives from the free energy of formation of chromium carbide values of $\log a_C$ between -2.24 and -2.35 depending on the allowance made for iron substitution. In the second method, an estimate of $\log a_C$ between -2.25 and -2.58 is obtained from the ratio of the solubility of carbon in an 18/8 steel compared with the extrapolated solubility in unalloyed austenite, allowance then being made for the combined effect of chromium, nickel and carbon on the activity of carbon [11] (see Appendix).

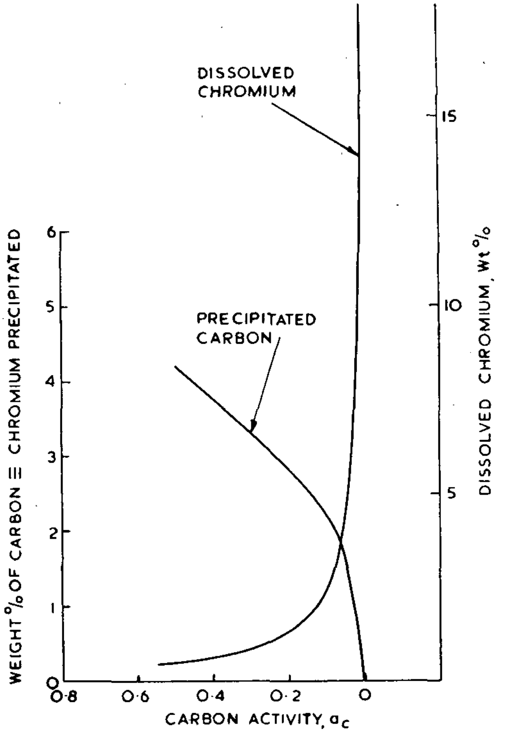

FIG.3. Dependence of precipitated carbon and dissolved chromium on carbon activity

Using Fig. 1 a similar curve may now be drawn (Fig. 3) giving the equilibrium-dissolved chromium level against carbon activity. As chromium is relatively immobile, the difference between the dissolved and the original chromium levels gives the amount of chromium which can be precipitated as carbide, and together with the chromium/carbon ratio of the precipitated carbide would give the amount of carbon in the carbide precipitated (Fig. 3). Making allowance for the amount of carbon in solution, which is relatively small even at high carbon activities, a curve can then be drawn giving total carbon against carbon activity. As the carbon activity gradient depends on the diffusion coefficient and the local carbon flux, it should now be possible in principle to construct curves for the carbon activity and total carbon profiles, and compare for example the expected increase in average carbon level of a specimen with that observed.

This procedure would, however, at best be somewhat tedious and some simplification is desirable, at least for a preliminary examination of the position.

It will be seen from Fig. 3 that at a carbon activity of 0.1 the equilibrium-dissolved chromium content remaining is only about 2 wt. % or less, i.e. all but a relatively minor fraction of an original 18 wt. % chromium could be precipitated before the carbon activity has risen to any great extent. Moreover, it would appear from our own experimental work and from others [2] that M_3C does not readily nucleate at high carbon activities in a carburizing stainless steel, presumably because of the presence of the other pre-existing carbides. Similarly, at intermediate carbon levels, $M_{23}C_6$ may persist at chromium/carbon ratios below the limit found by Shaw and Quarrell, i.e. implying lower dissolved chromium levels in the matrix. Such conditions are probably metastable and would not invalidate the computations on which Fig. 1 is based. Calculations on precipitation to about the 5 wt. % dissolved chromium level would not be affected, but beyond this level a formal solution would not be possible. However the additional carbon required for re-equilibration would be reduced below that indicated in Fig. 3, and could well be relatively modest. If then virtually all the chromium has been precipitated by a carbon activity of 0.1 and major changes in carbon flux are limited to this zone, some approximation in these calculations might be attempted.

Some change in diffusion coefficient of carbon may perhaps be expected across the carburizing zone reflecting the change in dissolved-chromium level. Data specifically on the effect of chromium is limited [12, 13], but would indicate a reduction in the diffusion coefficient. In general, however, the effects of such a third component are minimized if the gradient is expressed as one of activity rather than concentration. With a substantially constant carbon flux across the major part of the carburizing zone at any given time, the carbon activity gradient might then be approximately linear to a degree which would justify the use of a simple preliminary model.

At the temperatures of interest, the carbon activity of the uncarburized matrix is of the order of 10^{-2} or less, and the carbon activity difference between the matrix and the surface, where it is set by the carbon sources of the system, can therefore be taken as unity. If the diffusion for a given activity difference is assumed for present purposes to be unaffected by alloying and the depth of the carburized zone is x, the activity gradient $\frac{da_C}{d_L} = \frac{1}{x}$, and the carbon transport will be equal to $\frac{D \times C_{vFe}}{x}$, where C_{vFe} = carbon saturation concentration in g/cm^3 for a binary Fe-C alloy, and D is the mean diffusion coefficient for C in Fe between zero concentration and saturation.

The rate of increase in thickness would then be $\frac{D \times C_{vFe}}{x \times C_{vSS}}$ cm/s, where C_{vSS} is the increase in total carbon concentration in g/cm^3 of carburized stainless steel. Changing to weight concentrations the rate of increase in thickness is given by

$$\frac{dx}{dt} = \frac{D \times C_{wFe}}{x \times C_{wSS}}$$

$$\text{Hence}\quad x \times dx = \frac{D \times C_{wFe}}{C_{wSS}} \times dt$$

$$\therefore\quad \frac{x^2}{2} = \frac{Dt \times C_{wFe}}{C_{wSS}}$$

$$\text{or}\quad x^2 = 2\,Dt \times \frac{C_{wFe}}{C_{wSS}}$$

If the stainless steel is sheet of thickness 2L and carburized from both faces, and $\bar{C}_{wSS}$ is the increase in average carbon level of the sheet,

$$\text{then}\quad \frac{\bar{C}_{wSS}}{C_{wSS}} = \frac{x}{L}$$

$$\text{and}\quad \frac{(\bar{C}_{wSS})^2}{(C_{wSS})^2} = \frac{x^2}{L^2} = \frac{2Dt}{L^2} \times \frac{C_{wFe}}{C_{wSS}}$$

$$\text{i.e.}\quad \frac{2Dt}{L^2} = \frac{(\bar{C}_{wSS})^2}{C_{wSS} \times C_{wFe}}$$

This may be compared with the approach adopted by Anderson and Sneesby to their data. Although they recognised that carbide was precipitating extensively in the carburizing zone, they tacitly assumed a homogeneous diffusion model, i.e. carbon was assumed to be in solution up to the maximum concentration found on the surface and that the carbon profile followed the usual Gaussian error curve. Using the previous notation and rearranging for direct comparison leads to

$$\frac{2Dt}{L^2} = \frac{\pi}{2}\,\frac{(\bar{C}_{wSS})^2}{(C_{wSS})^2}$$

At 650°C their results indicated a surface carbon level of 3.20 wt.%; extrapolation of the solubility of carbon in γ iron gives a value of 0.48 wt.% at this temperature. Their figure for D (at 649°C) of 4.12×10^{-11} cm^2/s would therefore be increased by a factor of $\frac{2}{\pi} \times \frac{3.20}{0.48}$ to give 1.75×10^{-10} cm^2/s on the present model.

At present there is no direct experimental evidence on the carbon profile of the carburizing zone to check the assumptions of the model. Anderson and Sneesby have attempted to do so from hardness profiles but this is open to the serious objection that the extent of hardening depends on the degree of coherency of the precipitate.

As some indication of the possible effects of assuming other total carbon profiles, one may calculate the rate of carburization on the assumption that the total carbon profile is linear from the surface value to the uncarburized matrix, i.e.

$$\frac{\bar{C}_{wSS}}{C_{wSS}} = \frac{x}{2L}$$

TABLE I. CARBON DIFFUSION COEFFICIENTS IN IRON-CHROMIUM AUSTENITES CONTAINING 0.4% CARBON AT 1000°C (AFTER BLANTER [12, 13])

Reference	[13]	[13]	[13]	[13]	[15]		[12]	[12]	
Wt.% Cr	D_0 cm²/s	Q cal	$D_{1000°C}$ cm²/s × 10⁷	$\frac{D_{Fe}}{D_{alloy}}$	γ_C^{Cr}	Cr-effect remaining $\gamma_C^{Cr} \times \frac{D_{Fe}}{D_{alloy}}$	$D_{1000°C}$ cm²/s × 10⁷	$\frac{D_{Fe}}{D_{alloy}}$	Cr-effect remaining $\gamma_C^{Cr} \times \frac{D_{Fe}}{D_{alloy}}$
0	0.07	31 350	2.88	-	1	1	3.3	1	1
1	0.11	34 300	1.41	2.04	0.89	1.82	1.7	1.94	1.73
2.5	0.14	37 000	0.62	4.65	0.75	3.5	0.6	5.5	4.1
7	0.18	38 900	0.37	7.8	0.44	3.4	0.25	13.2	5.8

It can be shown that in this case

$$\frac{2\,Dt}{L^2} = \frac{4}{3}\,\frac{(\bar{C}_{wSS})^2}{C_{wSS} \times C_{wFe}}$$

so that despite a drastic change in profile increasing the thickness of the carburizing zone by a factor of $\sqrt{3}$, the rise in average carbon level would be reduced by 25%. On this somewhat arbitrary model the results of Anderson and Sneesby would therefore rise slightly from 1.75×10^{-10} cm^2/s to 2.33×10^{-10} cm^2/s.

Irrespective of the carbon profile to be taken, some allowance should be made, however, for the increased difficulty of diffusion due to the decreased cross-sectional area available for diffusion, and the tortuosity of the diffusion path. For much of the carburizing zone the volume occupied by carbide precipitate could approach 40 vol. %. No completely satisfactory theoretical treatment or experimental results are available for this range but the work of Francl and Kingery [14] on the thermal conductivity of porous solids would suggest an effective decrease in the apparent diffusion coefficient of about 50%. If such a correction is made the calculated true diffusion coefficient would be increased to the order of 4×10^{-10} cm^2/s at 600°C, but this is still appreciably less than values of the order of 11×10^{-10} cm^2/s indicated by extrapolation of the experimental results of other workers for diffusion of carbon in iron at higher temperatures [3, 4].

It is possible, however, that the effects of chromium on the diffusion of carbon are not entirely accounted for by the effects of chromium in reducing carbon activity, i.e. in reducing the carbon activity difference for any given carbon concentration difference. The only available data on the effect of chromium on the diffusion constant of carbon is that of Blanter [12, 13]. This work does not appear to have been published in full, but at 1000°C there was a reduction in diffusion rate in 0.4% carbon steels with increasing chromium content, amounting to an order of magnitude at 7 wt. % chromium (Table I).

This is rather more than the effects found on the activity of carbon at this temperature. Thus Brigham and Kirkaldy [15] found by equilibration with CO/CO_2 mixtures an interaction given by $\ln \gamma_C^{Cr} = -10.7\ N_{Cr}$ in good agreement with an earlier figure of $\ln \gamma_C^{Cr} \simeq -10\ N_{Cr}$ found by Kirkaldy et al. [16] by transient equilibrium carbon diffusion measurements. These would give reductions in carbon activities (and hence activity gradients) of only 1.33 and 2.3 for 2.5 wt. % and 7 wt. % Cr, where Blanter reports a drop by factors of about 5 and 10 respectively in diffusion coefficient. Moreover, the increases in activation energy for diffusion reported by Blanter [1 3] with increasing chromium level would outweigh the smaller effect of the interaction energies and greater differences might be expected at lower temperatures, e.g. the lack of compensation of the 7 wt. % Cr steel would at least double by 650°C. On this evidence, therefore, it would seem that the remaining difference between the diffusion coefficient as calculated and that obtained by extrapolation of high-temperature data might be due to uncompensated effects of chromium both in the zone close to the uncarburized matrix where the chromium content is still appreciable, and more generally in the carburized zone where the level of dissolved chromium, though lower, may still be significant in this respect.

This aspect requires further examination but it would seem possible that the simplified model examined based on carbide precipitation could reasonably account for the observed rates of carburization.

APPENDIX

Measurements evaluated by Richardson [17] give a value for the free energy of the reaction

$$C + 23/6\,Cr = 1/6\,Cr_{23}C_6$$

of (-16 380 - 1.54 T)cal. Accordingly at 973°K (700°C)ΔG = -17 880 cal and the equilibrium constant

$$K = \frac{[Cr_{23}C_6]^{\frac{1}{6}}}{[C]\ [Cr]^{\frac{23}{6}}}$$

is given by $\log_{10} K = \frac{-\Delta G}{4.573 \times 973} = 4.02$.

Kubaschewski and Heymer [9] by vapour pressure measurements, and Jeannin, Mannerskantz and Richardson [10] by equilibration of H_2/H_2O mixtures have determined chromium activities in iron-chromium binary alloys at higher temperatures (1040-1360°C). Their results are in reasonable agreement, and while a plot of log γ against $(N_{Fe})^2$ suggests that the solution is not entirely regular, the results have been averaged and the chromium activity at 700°C of an 18/8 composition ($N_{Cr} = 0.191$) estimated as 0.344 or $\log a_{Cr} = -0.464$, taking $\log \gamma_1/\log \gamma_2 = T_2/T_1$. In the absence of data on the effect of nickel it is assumed that the chromium activity in nickel-containing austenite is not greatly different from that in nickel-free ferrite.

If there is no substitution of chromium in the carbide by iron, then in the two-phase system

$$\log a_C + 23/6 \log a_{Cr} + \log K = 0$$

or

$$\log a_C = -\log K - 23/6 \log a_{Cr}$$

At 700°C a chromium activity of unity (pure Cr/C) will therefore give $\log a_C = -\log K = -4.02$, and this will increase at a chromium activity of 0.344 to $\log a_C = -4.02 + 23/6\,(0.464) = -2.24$.

Substitution of the chromium in the carbide by iron should, however, reduce the increase in carbon activity. On the other hand an estimate based on the composition of the carbide in equilibrium with stainless steel equally should underestimate the increase in carbon activity (Fig. 1). If this carbide composition is taken as $Cr_{3.5}\,Fe_{0.33}C$ then

$$\log a_C + 3.5 \log a_{Cr} + 0.33 \log a_{Fe} + \log K = 0$$

By the Gibbs-Duhem relationship $a_{Fe} \simeq 0.83$ and $0.33 \log a_{Fe} = -0.027$. Hence, at 700°C on this basis $\log a_C = -\log K - 3.5 \log a_{Cr}$ and 0.33 $\log a_C = -\log K - 3.5 \log a_{Cr} - 0.33 \log a_{Fe} = -4.02 + 1.63 + 0.03 = -2.38$. Whence it is concluded

$$-2.38 < \log a_{C_{700°C}} < -2.24$$

depending on the degree of iron substitution in the carbide.

A separate check of the carbon activity in stainless steel can be made using the estimated terminal solubilities of carbon in 18/8 and unalloyed austenite, and multiplying by the respective activity coefficients for carbon at the same temperature to give the required activity ratio.

From the estimates of Keating [6] a value of about 0.041 wt.% C is obtained by interpolation for the solubility of carbon in 18/8 steel at 700°C. A somewhat lower figure of about 0.019 wt.% C would, however, be inferred from the work of Buck et al. [5]. These estimates are to be compared with an extrapolated value of 0.58 wt.% from the carbon (graphite) solubility curve of the carbon-iron binary system, i.e. factors of 14.2 and 30.5 giving values of $(\log_{10} N_{C_{SS}} - \log_{10} N_{C_{Fe}})$ of -1.15 and -1.48 respectively.

The activity coefficient of carbon in 18/8 can be estimated from results summarized by Brown and Kirkaldy [11] for the individual effects of chromium, nickel and, as their interaction factors are referred to infinite carbon dilution, carbon itself. For an 18/8 steel (19.1 at.% Cr, 7.5 at.% Ni, 0.1 at.% C) and an unalloyed steel containing 0.58 wt.% carbon (2.68 at.%) the ratio of carbon activity coefficients would be given by

$$(\ln \gamma_{SS} - \ln \gamma_{Fe}) = (-10.7 \times 0.191 + 4.6 \times 0.075 - 8.9 \times 0.026)$$

$$= -1.93$$

or $\log_{10} \gamma_{SS}/\gamma_{Fe} = -0.84$ (at 1000°C).
If regular solutions can be assumed, then at 700°C $\log_{10} \gamma_{SS}/\gamma_{Fe}$

$$= -0.84 \times 1273/973 = -1.10$$

$\text{Log}_{10}\, a_{C_{700°C}} = (\log_{10} N_{C_{SS}} - \log_{10} N_{C_{Fe}}) + (\log_{10} \gamma_{SS} - \log_{10} \gamma_{Fe})$, hence two possible values for $\log a_{C_{700°C}}$ would be obtained, $(-1.15 - 1.10) = 2.25$ (solubility estimate of Keating) or $(-1.48 - 1.10) = -2.58$ (Buck et al.).

REFERENCES

[1] ANDERSON, W.J., SNEESBY, G.V., Atomics International Rpt NAA-SR-5282 (1960).

[2] ANDREWS, R.K., BARKER, K.R., M.S.A. Research Coporation, Evans City, Pa., MSAR 66-71 (1966), and unpublished work, U.K.A.E.A. Reactor Materials Laboratory.

[3] WELLS, C., BATZ, W., MEHL, R.F., Trans.Am.Inst.Min.metall.Engrs 188 (1950) 553.

[4] STEINER, W., KRISEMENT, O., Arch.EisenhüttWes., 30 (1959) 637.

[5] BUCK, D.C. et al., A.S.T.M. Special Publication 93 (1949).

[6] KEATING, F.H., Chromium-Nickel Austenitic Steels, Butterworth, London (1956) 8.

[7] BLANTER, M.E., Zh.tekh.Fiz. 18 (1948) 529.

[8] SHAW, S.W.K., QUARRELL, A.G., J.Iron Steel Inst. 185 (1957) 10.

[9] KUBASCHEWSKI, O., HEYMER, G., Acta.metall. 8 (1960) 416.
[10] JEANNIN, Y., MANNERSKANTZ, C., RICHARDSON, F.D., Trans.metall.Soc.A.I.M.E. 227 (1963) 300.
[11] BROWN, L.C., KIRKALDY, J.S., Trans.metall.Soc.A.I.M.E. 230 (1964) 223.
[12] BLANTER, M.E., Dokl.Akad.Nauk. SSSR 67 (1949).
[13] UMANSKY, Ya. S., FINKELSTEIN, B.N., BLANTER, M.E., Fizicheskie Osnovy Metallovedeniya Moscow (1955) 404 (Table 47).
[14] FRANCL, J., KINGERY, W.D., J.Am.Ceram.Soc. 37 (1963) 538.
[15] BRIGHAM, R.J., KIRKALDY, J.S., Trans.metall. Soc.A.I.M.E. 227 2 (1963) 538.
[16] KIRKALDY, J.S., DESTINON-FORSTMANN, J. VON, BRIGHAM, R.J., Can.Metall. Q.1 (1962) 59.
[17] RICHARDSON, F.D., J.Iron Steel Inst. 175 (1953) 33.

SOLUBILITY OF CARBON IN SODIUM

C. LUNER, A. COSGAREA, Jr., AND
H.M. FEDER
ARGONNE NATIONAL LABORATORY,
ARGONNE, ILL.,
UNITED STATES OF AMERICA

(Presented by S. Greenberg)

Abstract

SOLUBILITY OF CARBON IN SODIUM. The investigation reported here was undertaken to obtain a better understanding of the nature of carbon in sodium systems. The solubility of carbon in sodium has been reported by Gratton (KAPL-1807 (1957)). Because of the uncertainties in the data, an effort was made to redetermine this solubility. Two sets of experiments were performed: one employed essentially the same experimental procedure used by Gratton, but with an improved analytical determination of total carbon; the other involved ^{14}C as a tracer. In contrast to the earlier work, our results showed that the true solubility of elemental carbon in sodium is less than 0.005 ppm up to 450°C. The experiments indicated that liquid sodium usually contains significant amounts of dispersed carbon capable of passing through a 5 μm stainless-steel filter. The amount of carbon passing through such a filter depends, among other factors, on the previous history of the sodium. Measures of the degree of dispersion of carbon in sodium were furnished by ultra-centrifugation and filtration experiments. The distribution of carbon among its various forms, i.e. dispersed elemental carbon, carbonate, carbide, etc., are discussed.

INTRODUCTION

It has been established that various metals may be significantly carburized or decarburized when in contact with liquid sodium [1]. This phenomenon presents a potentially serious objection to the use of sodium in nuclear reactors because undesirable changes in the mechanical properties of structural materials, such as steel, may result even from small changes in carbon content. Various proposals [2,3] have been set forth regarding the mechanism of carbon transport in the presence of liquid sodium, but none has been generally accepted. It seemed likely that a better understanding of carbon transport might commence from a better understanding of the nature of carbon species in sodium.

Gratton [4] has reported the solubility of elemental carbon in sodium. His results were interpreted as showing a large ($>$ 10 ppm), temperature- and oxygen-concentration-dependent, reversible solubility. However, detailed consideration of the experimental techniques used led us to question these conclusions. In particular, his experiments seemed inadequate to distinguish between dissolved carbon and small suspended particles, or to reveal significant trends in carbon content above the blank of 10-20 μg per analysis. In the present work, an attempt was made to repeat Gratton's experiments with somewhat improved techniques. When these experiments failed to yield significant solubility data, an entirely different approach involving the use of ^{14}C-labeled carbon was taken. Finally, experiments were done which give some insight into the chemical and physical nature of carbon in one well-characterized source of sodium.

SOLUBILITY OF ELEMENTAL CARBON (Series A)

The apparatus and general procedures for obtaining filtered samples of sodium were generally similar to those described by Gratton [4]. A high-carbon sodium (Reagent Grade, Baker and Adamson Co.) was added to a charging tank under a helium atmosphere; it was then melted and transferred by pressurization through a 5μ-porosity stainless steel (SS) filter into a graphite crucible contained within an airtight SS vessel. (The crucible had been machined to a smooth finish from reactor-grade [ATJ] graphite, and had been outgassed at 1000°C prior to use.) Purified helium at a pressure of 700 torr above atmospheric was maintained over the melt at all times to prevent oxidation. The melt was stirred continuously, except just before and during sampling, and was heated to selected temperatures for various periods of time. Samples were obtained from time to time by lowering a tantalum or SS sampling tube (lower end closed by a 5μ-porosity SS frit) into the melt and forcing liquid through the frit by application of an external pressure of about 3 atm. The sample tube was then raised and isolated from the vessel in a sampling apparatus. The sampling apparatus was disconnected from the vessel at a Cenco coupling and transferred to a glovebox without exposure to the atmosphere. All further manipulations were made in this glovebox under helium containing < 10 ppm oxygen and about 1 ppm water vapor.

The filtered samples were analyzed for total carbon by the combustion method described in Appendix A. The results are shown in Figure 1. All the individual replicate analyses are indicated. Because of the duration of the experiment and the difficulty of repeated sampling without slight air contamination, the oxygen content of the sodium is believed to be at or near saturation at each temperature.

In contrast to Gratton's results, the carbon content of our filtered samples scatters considerably for a given condition and shows no smooth variation with temperature or time. If there is, in fact, any systematic increase in the carbon content with temperature or time, it is concealed by other sources of variability. It seemed unlikely that the scatter of our results was analytical in origin because the method used had a smaller and less variable blank and a better overall precision than the Van Slyke method used by Gratton. We were, therefore, led to a tentative hypothesis that particulate carbonaceous matter, capable of passing through a 5μ-porosity filter, was present in the sodium charged to the crucible and also occasionally arose from mechanical action on the graphite crucible; the heterogeneity of the dispersion would account for the scatter of the results.

To check whether carbonaceous particulates could be readily formed so as to pass through a 5μ filter, graphite which had been pulverized with a mortar and pestle in a helium-atmosphere glovebox was added (2.5 w/o C) to fresh sodium in a graphite crucible, and the mixture was maintained at a constant temperature of 316°C.

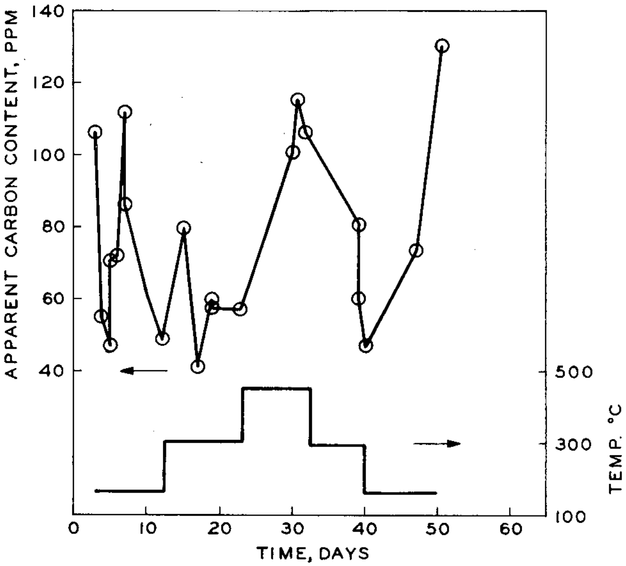

FIG.1. Apparent carbon content of sodium in contact with a graphite crucible

The results were revealing. Although the charged sodium had a total carbon content of 220 ppm prior to the addition, a filtered sample obtained after eight days of quiescent contact, followed by one hour of stirring and one hour of settling, contained 760 ppm of carbon. After six additional days of settling, two more filtered samples were taken; these showed 70 and 230 ppm of carbon. It was evident from this simple experiment that pulverized graphite was readily dispersed in sodium, that a small and variable fraction of the dispersion was in the form of particles small enough to pass through a 5μ-porosity filter, and that the amount of carbon which contaminates any given sample of liquid sodium probably depends in some complex way on its previous history. It was concluded from these experiments that the true solubility of graphite in sodium was probably not measured in our own or in Gratton's experiments; and that because of the difficulty of filtering fine, carbonaceous particles from sodium, measured values are invariably higher than the equilibrium solubility.

SOLUBILITY OF ELEMENTAL CARBON (Series B)

It was apparent, therefore, that to determine the true solubility of carbon in sodium, it would be necessary to differentiate between carbon which dissolves and carbon which pre-exists in sodium as nonfilterable carbonaceous material. Such a discrimination was accomplished by the use of amorphous carbon labeled with ^{14}C. The use of a radioactive tracer also increased the sensitivity of the measurements manyfold; concentrations of ^{14}C-labeled carbon as low as 5 parts in 10^9 of sodium could be detected. The radioactive carbon was obtained from New England Nuclear Corporation in the form of a pressed pellet with a specific activity of 2.4×10^6 dpm/mg. It was outgassed in vacuo at 1000°C before being used. The pellet (135 mg) was added to 300 g of liquid sodium (Reactor Grade, U. S. Industrial Co.) in a SS container. The total carbon content of the sodium charge was 32 ± 5 ppm, as determined by a lengthy series of analyses.

Filtered samples of sodium were withdrawn periodically at various temperatures over a period of four months from the stirred and settled melt. The samples were analyzed for total carbon and radiocarbon.

The total carbon content of the filtered sodium was found to be 9.8 ± 3.2 ppm. No trend with time or temperature was apparent; thus, two-thirds of the total carbon in this particular grade of sodium was ascertained to be particulate material which cannot pass through a 5μ filter. The remaining third of the carbon, which did pass through the filter, was either dissolved or submicron-sized. In either case, this material was not in equilibrium with solid carbon because radiochemical analyses (Appendix A) of the filtered samples indicated the absence of any significant amounts of radiocarbon at all temperatures investigated, even after four months of contact. It thus appears that the true solubility of elemental carbon in liquid sodium is less than 0.005 ppm at temperatures up to 450°C.

CARBON-BEARING CHEMICAL SPECIES IN SODIUM

(a) Chemical Characterization

Although it was realized that the nature of the carbon-bearing chemical species in sodium, as well as their amount, would vary with prior history, an effort was made fully to characterize one fairly uniform, large source of reactor-grade sodium (U.S.I.).

A sample of sodium was vaporized at a temperature of about 300°C into the vacuum chamber of a time-of-flight mass spectrometer. Peaks from volatile species other than Na^+ and Na_2^+ could be detected above the background by opening and closing the shutter. These peaks were in the light hydrocarbon region; however, this test was not considered to be conclusive.

More quantitative experiments, involving the dissolution of sodium in water and examination of the reactions products, were made despite the obvious disadvantage that only indirect information is thus obtained about the species originally present. Reactor-grade sodium was dissolved in distilled water and the gas evolved from the alkaline solution was pumped through a trap to remove water and then through a silica gel absorption bed cooled with liquid nitrogen; the absorbate was then analyzed by gas chromatography. Methane (0.7 to 1.6 ppm equivalent carbon) was the only identifiable off-gas evolved, other than hydrogen. It is surmised that methane was present in the sodium, dissolved as such, or as sodium methyl, or as certain metal carbides. When the alkaline solution was acidified and the evolved gas analyzed similarly, carbon dioxide (∿ 6 ppm equivalent carbon) was found. Filtered, reactor-grade sodium also gave the same amount of carbon dioxide. The carbon dioxide is presumed to originate from sodium carbonate in the sodium. Carbon monoxide, acetylene, ethylene, or ethane were not detected (< 1 ppm) as off-gases from either alkaline or acid solution.

The aqueous solution was examined specifically for two other carbon-containing compounds likely to be present in sodium: the sodium salt of hexahydroxybenzene, $Na_6(CO)_6$, which is known to be an end-product of the reaction between liquid sodium and carbon monoxide [5], and sodium cyanide, NaCN, which can be formed at high temperatures by the reaction of sodium, carbon compounds, and nitrogen [6]. When the clear aqueous solution was examined spectrophotometrically, no significant absorption was found in either the ultraviolet or visible regions (2150 - 7000 Å). The sensitivity of detection was such that sodium hydroxide solutions containing hexahydroxybenzene equivalent to about one ppm of carbon in sodium gave discernible absorption peaks in the ultraviolet. It was concluded that reactor-grade sodium contains less than one ppm of carbon as $Na_6(CO)_6$ or similar aromatic compounds.

A colorimetric analysis [7] capable of detecting as little as 0.75 ppm of cyanide ion was performed on the alkaline solution. No cyanide ion was detected.

On careful observation, a residue of dark particles could be seen after dissolution of reactor-grade sodium in distilled water. This residue was collected on a fine-porosity (10-15μ) quartz frit and analyzed for carbon by combustion. In a typical experiment, the residue from an 8-g sample was found to contain 112 μg of carbon, equivalent to 14 ppm. Because of the physical appearance of the residue, and because none of the suspected species of combined carbon - - Na_2CO_3, Na_2C_2, NaCN, $Na_x(CO)_y$, $NaCH_3$, $NaCO_2Na$ - - are known to hydrolyze to give insoluble materials, there is a strong but unproven presumption that the residue is elemental carbon. However, it need not represent all of the suspended, elemental carbon originally present because of the unlikelihood that all of the latter would aggregate sufficiently during dissolution to become filterable. By the same token, the size distribution of the filterable residue was not considered representative of the size distribution of the original suspension.

(b) Physical Characterization

The experiments discussed above indicated that various carbon-bearing species are dispersed in reactor-grade sodium. Approximate calculations showed that unless the density difference between the suspended particles and liquid sodium were very small, segregation of the suspended material should be achievable by centrifugation at reasonable speeds. Under favorable conditions, the actual size distribution could be determined.

Experiments to test the feasibility of centrifugal segregation of carbon were performed. However, it was decided to use a Na-44 w/o K alloy (m.p. 19°C) as an expedient substitute for sodium because of the temporary unavailability of a high-speed centrifuge capable of operation at temperatures above the melting point of sodium.

The alloy, which contained 52 ± 9 ppm total carbon, was sealed in stainless-steel centrifuge tubes in a helium-atmosphere glovebox. The tubes were then centrifuged either (1) at 17 000 rpm ($\sim$ 35 000 g) for 40 minutes while at an angle of 34° to the rotor axis, then incrementally slowed to a stop during the next 20 minutes, or (2) at 40 000 rpm ($\sim$ 130 000 g) for 3 3/4 hours while at an angle of 20° to the rotor axis. In the latter experiment, the centrifuge was cooled to 0°C during the last 1 1/2 hours in order to freeze the alloy while it was still spinning. After centrifugation, the tubes were cooled by immersion in liquid nitrogen in order to prevent remixing, and were transferred to the glovebox and opened. The tubes were held at the same angle as during centrifugation, and the alloys were allowed to warm slowly to room temperature and liquefy. Samples were withdrawn by pipette from the top of the liquid and analyzed for carbon. After centrifugation at either speed, the top layers contained 26 ± 3 ppm of carbon. Statistical analysis of the results based on eight samples indicate that, at the 95% confidence level, there was a significant segregation of suspended carbon-bearing material; the direction was that expected for a solid which is denser than the suspending liquid. The segregation attained does not represent the maximum achievable; some redistribution of small particles by convection and vibration probably occurred during the melting and sampling steps. Nevertheless, the results are sufficiently encouraging to warrant further investigation of size distribution of particles in liquid sodium by means of a heated, high-speed centrifuge.

Other examples of segregation of carbon in sodium have also been observed. For example, when reactor-grade liquid sodium was drawn up into clean quartz or SS tubes (10 mm I.D.) and allowed to freeze, the sodium adjacent to the tube walls was found to contain significantly greater (> 3X) concentrations of carbon than the central cores. The connection between this segregation and the size distribution of the particulate matter is being further examined.

SUMMARY

An earlier determination of the solubility of carbon in sodium is in error. The true solubility of elemental carbon in sodium is less than 0.005 ppm up to 450°C. The carbon usually found as a contaminant in all commercial grades of sodium consists of a variety of species whose amounts depend on the manufacture and subsequent history of the sample. In a typical case, reactor-grade sodium furnished by one manufacturer contained a total of 32 ± 5 ppm of carbon which was distributed as follows: $\sim$ 6 ppm as Na_2CO_3, either in solution

or as particles fine enough to pass through a 5μ filter; ∿ 1 ppm as CH_4 or $NaCH_3$ or metal carbide; less than 1 ppm as NaCN, $Na_6(CO)_6$ or Na_2C_2; and at least 14 and possibly as much as 25 ppm elemental carbon, most (but not all) of which is removable by a 5μ filter.

ACKNOWLEDGMENTS

We wish to thank Paul Hunt, Mrs. G. Lutz, and Karl Anderson for technical assistance, and Dr. I. Johnson for useful discussions.

APPENDIX A

Determination of Total Carbon in Sodium by Dry Oxidation Method

Most of the analytical techniques described in the literature are based on the oxidation of carbon to carbon dioxide and subsequent measurement of the latter. The principal variations occur in the oxidant employed and the method of liberation and measurement of carbon dioxide. For example, the oxidation of carbon may be carried out dry, by direct combustion with oxygen [8,9], or wet by use of a strong aqueous oxidizing agent, such as Van Slyke reagent [10]. The wet oxidation method with Van Slyke reagent was rejected because of the reported high blank levels, 10 to 20 μg of carbon.

The combustion tube was loaded in a helium-atmosphere glovebox to avoid exposure of the sample to air. Oxygen of "ultra high purity" was further purified by passage through two furnaces containing platinum and copper oxide at 950°C, two Ascarite traps, and a trap containing a molecular sieve (Linde 5A). The sample was burned in low-pressure (150 torr) purified oxygen to form a mixed residue of sodium oxide and sodium carbonate. Two variants were examined for the succeeding procedure. In the first, the residue, which was contained in a silica boat, was heated to 1100°C in oxygen [8]. The carbon dioxide liberated by the reaction of sodium carbonate and silica was condensed in a liquid-nitrogen-cooled trap and subsequently measured either manometrically or by gas chromatography. After each analysis, the combustion tube was tested with phenolphthalein solution to ensure that no sodium oxide had deposited in the cold zone where it could re-absorb the liberated carbon dioxide.

In the second variant, which was itself a modification of a method reported by Kallman and Liu [9], the sodium was burned in an alumina crucible. After the combustion tube had cooled, carbon dioxide was released from the residue by the addition of 2N sulfuric acid ("wet finish"), and the liberated gas was measured either manometrically or by gas chromatography. Reagent blanks for both variant methods were less than 3 μg.

The unavailability of suitable standard reference samples made it difficult to evaluate the accuracy of the methods as extensively as desired. However, the results obtained for the recovery of accurately known quantities of graphite thread in the presence and absence of added sodium, indicated that both the above variants are capable of accuracies of about 15% relative for the range 10 - 100 μg of carbon. A comparison of the two variants was made by analysis of various samples withdrawn within a short interval of time from a container of liquid sodium; the agreement between the averages of the two sets of results indicated the general equivalence of the methods. The reproducibility of the analytical method was established by repeatedly analyzing aliquots of various sizes from the same batch of sodium. Both variants showed the relative standard error of the mean of a series of determinations to be ± 15%. The variant with the "wet finish" is now used routinely in this laboratory; it is simpler to carry out than the "dry finish", and larger samples (up to 2 g) can be employed for analysis.

Precaution: The entire sodium specimen in a sample tube must be melted out and taken for analysis for carbon. Sodium frozen in a sample tube exhibits regions of carbon segregation near the tube walls.

Determination of Radiocarbon in Sodium.

The determination of radiocarbon proceeded just like the determination of total carbon up to the collection of carbon dioxide. For the radiocarbon determination, the gas was flushed with helium through two counting vials connected in series. Each vial contained 2 cm^3 of Hyamine-10X[1] which absorbed the $^{14}CO_2$-$^{12}CO_2$ mixture [11]. Fifteen cm^3 of toluene-scintillator solution[2] was then added, and the solutions were counted in a Packard Tri-Carb Model 2211 Liquid Scintillation Spectrometer. The background count was low and reproducible. The counting efficiency was about 75%.

REFERENCES

[1] LOCKHART, R.W., BILLURIS, G., IMD Special Report, Series No.12, Nucl.Metall. A.I.M.E. IX (1963) 207.

[2] HAYES, W.C., SHEPARD, O.C., Rpt NAA-SR-2973 (1958).

[3] LYASHENKO, V.S., NEVZOROV, B.A., "The mechanism of carbon transfer in liquid sodium", Corrosion of Reactor Materials, IAEA, Vienna, 2 (1962) 373.

[4] GRATTON, J.G., Rpt KAPL-1807 (1957).

[5] MILLER, H.C., U.S. Patent No.2 858 194 (1958).

[6] HOBART, E.W., BJORK, R.G., Nucl.Applicat.1 (1965) 490.

[7] NUSBAUM, I., SKUPEKO, I., Metal Finish. 49 (1951) 61.

[8] MUNGAL, T.G., MITCHEN, J.H., JOHNSON, D.E., Analyt.Chem. 36 (1964) 70.

[9] KALLMAN, S., LIU, R., Analyt.Chem. 36 (1964) 590.

[10] PEPKOWITZ, L.P., PORTER, J.T., Analyt.Chem. 28 (1956) 1606.

[11] PASSMAN, J.M., RADIN, N.S., COOPER, J.A.D., Analyt.Chem. 28 (1956) 484.

---

[1] Registered trademark of Rohm & Haas, Inc.: p-(diisobutylcresoxyethoxyethyl)-dimethylbenzyl-ammonium hydroxide.

[2] 4.90 g of 2,5-diphenyloxazole (PPO) and 0.10 g of 1,4-bis-2-(5-phenyloxazolyl)-benzene (POPOP) diluted with toluene to one litre.

DISCUSSION

R. DAVIES: A colleague of mine at the Dounreay Establishment, V. M. Sinclair, has carried out similar experiments with ^{14}C-labelled iron carbide in a stainless-steel capsule. No ^{14}C was detected in the sodium itself but some was found on the walls of the capsule. A similar experiment was carried out with a nickel capsule and in this case ^{14}C was detected in the sodium and a black deposit containing ^{14}C was obtained on the walls of the capsule. It was not clear whether the ^{14}C in the sodium was the result of contamination produced by particles from the walls. On the whole, I think it is doubtful whether the use of ^{14}C-labelled graphite is a particularly good method for measuring carbon solubility. If the rate of dissolution is less than the rate of deposition on the walls, no ^{14}C will be detected in the sodium. This will be the case whether true solubility is involved or not.

A. HATTERER: I found this paper most interesting and I think that, as a result of your findings, it should now be possible to eliminate free and combined carbon more effectively than in the past. In general, do you think that a hot trap combined with a cold filter is still the best means of purification?

S. GREENBERG: There is nothing in this paper specifically relating to the development of methods for removing carbon from sodium, but I would think that hot traps probably are among the most efficient means for the purpose.

CARBON MASS TRANSFER IN MULTIMETALLIC SYSTEMS CONTAINING POTASSIUM

J.W. SEMMEL, Jr., L.B. ENGEL, Jr.,
R.G. FRANK AND R.W. HARRISON
GENERAL ELECTRIC COMPANY,
SPACE POWER AND PROPULSION SECTION,
CINCINNATI, OHIO,
UNITED STATES OF AMERICA

Abstract

CARBON MASS TRANSFER IN MULTIMETALLIC SYSTEMS CONTAINING POTASSIUM. Carbon usually occurs in alkali metal containment materials as an impurity or alloying addition, and is a major constituent of carbide cermets used for bearings and valve seating and sliding components. Under certain conditions, carbon can transfer and result in deleterious changes associated with carburization and decarburization. Experiments were conducted to examine carbon transfer between pertinent materials, and demonstrate that it is reduced significantly by utilizing carbides of greater thermodynamic stability than those typically found in commercial materials.

To determine whether carbon transfer from ferrous alloys would be impeded by alloying with titanium, which forms a relatively stable carbide, companion capsules of Type 316 (Fe-17Cr-12Ni-2Mo-0.04C) and Type 321 (Fe-17Cr-12Ni-0.07C-0.46Ti) stainless steels containing potassium were heated for 1000 h at 1400°F. Both capsules contained Cb-1Zr alloy specimens which are readily carburized when carbon is present in potassium. The Cb-1Zr specimens were carburized significantly in Type 316SS capsules but not in Type 321SS capsules, demonstrating that the titanium addition impeded carbon depletion, and that bimetallic systems of Type 321SS and Cb-1Zr are more attractive for reducing carbon transfer effects. (Nitrogen transfer was similarly impeded by titanium in Type 321SS.) The effects of carburization and nitriding on the mechanical properties of Cb-1Zr are described.

Carbon transfer from carbide cermet bearing materials was investigated with isothermal capsules for 1000 h with potassium at 800°, 1200° and 1600°F. Decarburization of the cermets was determined by weight change, X-ray diffraction and chemical analysis of the Cb-1Zr capsule material for evidence of carburization. With commercial, cobalt-bonded WC and other materials containing WC to achieve high hardness, decarburization was observed at 1200° and 1600°F, but not 800°F. This was accompanied by carburization of the Cb-1Zr capsule material and Mo-TZM specimens located near the cermets. X-ray diffraction of the cermets identified new phases, especially elemental tungsten in the surface region, which would alter friction, wear and diffusion bonding characteristics. Conversely, TiC cermets bonded with columbium, tungsten or molybdenum were not decarburized.

These results are consistent with expectations based on the relative thermodynamic stabilities of the carbides involved.

INTRODUCTION

Carbon mass transfer has been observed in various systems at temperatures above approximately 1000°F. For example, with monometallic loops of iron (Type 316SS), cobalt (Haynes Alloy No. 25), and nickel (Inconel) alloys, extensive decarburization of hot regions and carburization of cold regions have been noted after exposure to potassium.[1] When isothermal capsules were used to expose dissimilar materials to potassium or sodium, several investigators observed the transfer of carbon from the same iron,[2] cobalt,[3] and nickel[4] alloys to zirconium or columbium alloys. More recently, the transfer of carbon (and nitrogen) from Type 316SS to Cb-1Zr in potassium[5] and NaK-78[6,7] has been described for bimetallic loop tests. In the cited experiments, the iron, cobalt, and nickel alloys contained no significant amounts of an alloying element that could form a carbide phase of high thermodynamic stability. Although the 2 1/4Cr-1Mo type of ferritic steel is usually subject to carbon transfer in monometallic loops and also transfers carbon to austenitic steels in bimetallic loops, several experiments conducted with sodium have shown that the addition of a relatively stable carbide-forming element to this type of ferritic steel can reduce or eliminate carbon transfer at temperatures up to 1200°F.[8,9]

The experiments reported here were conducted to determine if a relatively stable carbide-forming element in an austenitic steel would significantly affect the transfer of carbon. It was found that the tendency for carbon transfer to Cb-1Zr in potassium at 1400°F can be reduced greatly by forming a highly stable carbide such as TiC in stainless steel. Additional testing of WC and TiC cermets, candidates for application in bearings and valve seating and sliding components, also demonstrates that carbon will transfer more readily from WC than from the more stable TiC cermets. These results are consistent with expectations based on the relative thermodynamic stabilities of the carbides involved.

EXPERIMENTAL PROCEDURES

Two sets of capsules were used to conduct isothermal exposures to potassium. The first set of capsules was prepared from Type 321 and 316SS seamless tubing and contained specimens of Cb-1Zr sheet to compare the extent of carbon and nitrogen transfer from the stainless steels to the columbium alloy (Fig. 1). Duplicate capsules of each stainless steel were partially filled with potassium, sealed under vacuum, and heated in a furnace in air for 1000 h at 1400°F under essentially identical conditions.

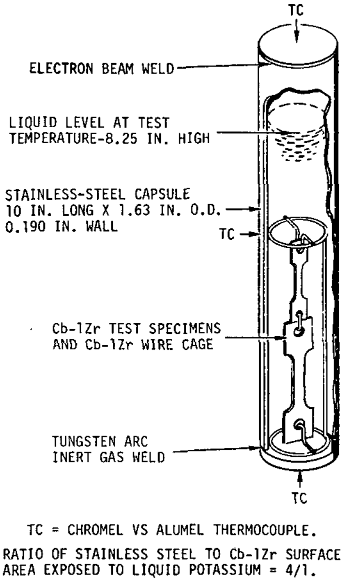

FIG.1. Design of the stainless-steel capsule and Cb-1Zr specimen arrangement used for exposures to potassium

The second set of capsules was made from Cb-1Zr seamless tubing and contained various carbide cermets to permit a comparison of the extent of carbon transfer from each type of carbide specimen to the Cb-1Zr capsule wall (Fig. 2). Three capsules of each material combination were partially filled with potassium, sealed under vacuum, and heated in a vacuum environment for 1000 h at 800°, 1200°, and 1600°F. Groups of six Cb-1Zr capsules were heated by placing each capsule in a peripheral hole in a cylindrical, molybdenum block that was heated centrally by radiation from a 0.003-in. thick tantalum foil resistance heater. The use of three of these units permitted testing of 18 capsules simultaneously in a 24-in. diameter x 54-in. high vacuum system capable of pressures in the 10^{-10} torr range at room temperature. After initial outgassing upon heating, a 1000 liter/sec getter ion pumping system maintained the pressure in the 10^{-8} torr range, which precluded significant reaction of the Cb-1Zr capsules with the external environment at elevated temperatures.

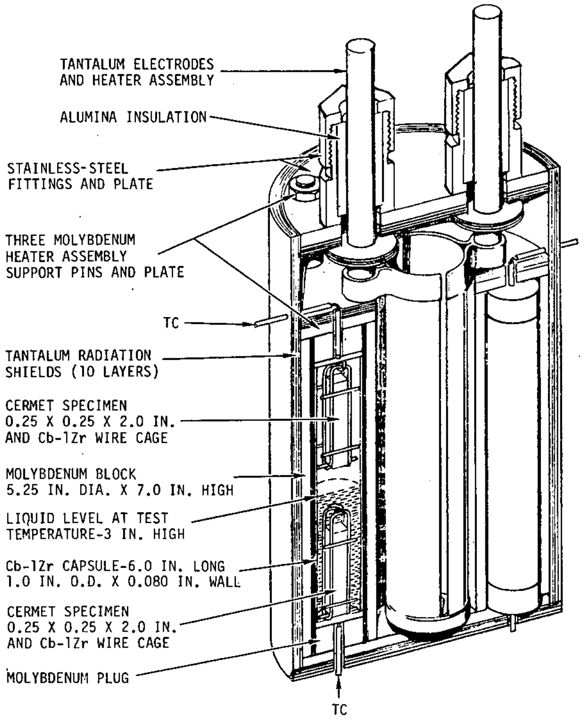

TC = ALUMINA-INSULATED Pt VS Pt+10%Rh THERMOCOUPLE.

RATIO OF Cb-1Zr TO CERMET SURFACE AREA EXPOSED TO LIQUID POTASSIUM = 4/1.

FIG. 2. Design of the facility used for exposing carbide cermets to potassium in Cb-1Zr capsules. The heated molybdenum block provided for isothermal testing of a group of six capsules

The chemical composition of the test materials is provided in TABLE I. For the present purposes, it was important to obtain Type 321SS material with a carbon content at least equal to that of the Type 316SS and also to assure that there was sufficient titanium present to combine with all the carbon as TiC (TABLE I). The TiC cermet materials contained approximately 5% WC as an impurity, introduced during pulverization of the TiC in a commercial WC ball mill. The amount of this impurity could, of course, be reduced by special procedures, but its presence was not significant in these corrosion experiments.

TABLE I. MATERIAL COMPOSITIONS

Material	Composition, Weight Per Cent
Type 321SS	17Cr-12Ni-0.46Ti-0.069C-0.013N-0.009 O-0.0008H-Bal. Fe
Type 316SS	17Cr-12Ni-2.2Mo-0.041C-0.017N-0.008 O-0.0004H-Bal. Fe
Cb-1Zr Sheet(a)	1Zr-0.003C-0.003N-0.014 O-0.001H-Bal. Cb
Cb-1Zr Tube(a)	1Zr-0.004C-0.010N-0.018 O-0.001H-Bal. Cb
Mo-TZM(a)	0.5Ti-0.08Zr-0.020C-0.0003N-0.0001 O-0.0002H-Bal. Mo
Carboloy 907	74WC-20TaC-6Co
Carboloy 999	97WC-3Co
Grade 7178	85.6W-6.9Mo-1.8Cb-0.3Ti-5.7C
K601	84.5W-10Ta-5.5C
TiC	94TiC-4.25WC-0.9Ni-0.1Fe-0.68Co
TiC+5%W	90TiC-4.79WC-5W-0.36Fe
TiC+10%Mo	85.4TiC-10.5Mo-3.99WC-0.13Fe
TiC+10%Cb	83.6TiC-9.54Cb-5.85WC-0.73Co-0.33Fe

(a) Average of several values for C, N, O, and H.

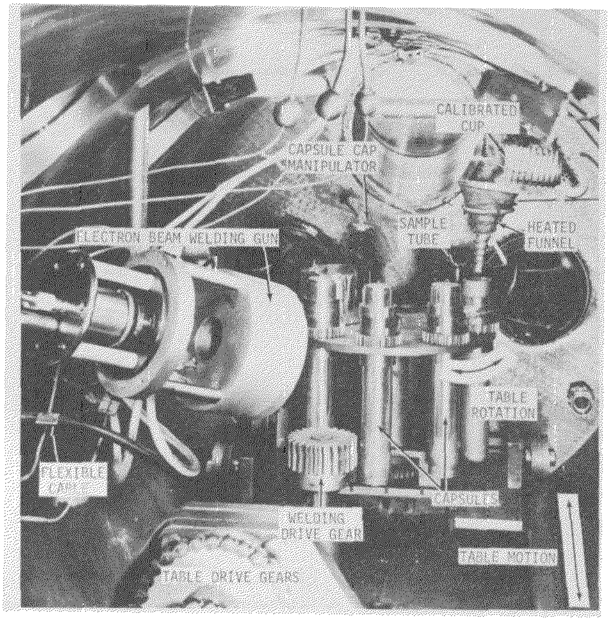

FIG.3. View of the vacuum chamber interior showing the arrangement used for filling capsules with potassium and sealing by electron beam welding

The potassium was purified by filtration, vacuum (10^{-5} torr) distillation at 500°-600°F. and hot trapping with zirconium and titanium for more than 24 h at 1200°-1400°F. Capsule filling and sealing by electron-beam welding was conducted under a 10^{-5} torr vacuum, as illustrated in Fig. 3. Argon was used to pressurize the hot trapping vessel and transfer liquid potassium, at approximately 200°F, into a calibrated cup within the evacuated chamber. The desired amount of potassium was poured into the capsule through a heated funnel. Using a bellows sealed manipulator, the capsule cap was positioned over the capsule. The capsule support table was then moved to engage the welding drive gear which located the capsule under the 30KV electron beam gun, and a variable speed motor permitted adjustment of the welding speed. Provision was made in the capsule support table for a chemical analysis sample tube and six capsules which could be filled consecutively during one evacuation. The following chemical analysis of the potassium sample taken while filling the stainless steel capsules is also typical of the results obtained while filling the Cb-1Zr capsules:

Element:	Ag	Al	Ca	Cb	Co	Cr	Cu	Fe	Mg	Mn	Mo	Na	Ni	Si	Sn	Ti	Zr
ppm:	<2	2	50	<10	<2	<2	<2	2	2	<2	2	50	2	10	<10	<2	<10

The oxygen content determined by the amalgamation method was less than 5 ppm for the stainless steel capsules and varied from less than 5 to 25 ppm for the Cb-1Zr capsules. Purification, transfer, and analytical procedures have been described in detail,[10,11] and there is considerable evidence that very pure potassium was contained in the capsules.

After testing, the capsules were opened in an argon atmosphere and drained of potassium at 200°F. Residual potassium was vacuum (10^{-5} torr) distilled from the Cb-1Zr capsules by heating at approximately 500°F for 2 h. Ethyl alcohol in hexane was used to remove the residual potassium from the stainless steel capsules. Standard metallographic techniques were used to evaluate the materials. Chemical analyses of Cb-1Zr specimens for carbon were performed by the combustion conductometric method, and analyses for oxygen, nitrogen, and hydrogen were performed by the vacuum fusion technique. Phase identification at the surface region of test specimens was performed using an X-ray diffractometer and copper K_α radiation.

EXPERIMENTAL RESULTS

Stainless Steel Capsules and Cb-1Zr Specimens

The Cb-1Zr specimens exposed in the Type 316SS capsules were discolored and revealed a weight gain of 0.03%, whereas the specimens exposed in Type 321SS capsules were not discolored and were essentially unchanged in weight. Chemical analyses of Cb-1Zr specimens were performed for carbon, oxygen, nitrogen, and hydrogen (TABLE II). Negligible changes in nitrogen and carbon contents were noted in the Cb-1Zr alloy specimens exposed in Type 321SS capsules compared to the highly significant transfer of carbon and nitrogen that occurred in the Type 316SS capsules. Considering possible variations in the chemical analyses and the chemical inhomogeneity of the material, no significant change in the oxygen and hydrogen content of the Cb-1Zr alloy specimens is attributed to the exposure in either the Type 316SS or the Type 321SS capsules. Qualitative spectrographic and electron microprobe analyses revealed that small amounts of iron and chromium transferred to the Cb-1Zr specimens contained in both types of capsules. Carburization and nitriding of the Cb-1Zr alloy specimens tested in Type 316SS capsules significantly affected the room temperature tensile properties as evidenced by the higher yield strength and the lower tensile elongation (TABLE III).

No change in metallurgical structure was observed in the Cb-1Zr specimens tested in Type 321SS capsules, whereas two distinct layers that have been reported as CbC and Cb2N in similar investigations[2] were observed on the Cb-1Zr alloy specimens tested in Type 316SS capsules (Fig. 4). In

TABLE II. POST-TEST CHEMICAL ANALYSES OF 0.040-INCH THICK Cb-1Zr ALLOY SPECIMENS EXPOSED FOR 1000 HOURS AT 1400°F IN POTASSIUM CONTAINED IN TYPE 321SS AND TYPE 316SS CAPSULES

Capsule Material and Capsule No.	Chemical Analyses of Cb-1Zr Alloy Specimens, ppm			
	C	N	O	H
Type 316SS-1	210	206	258	23
Type 316SS-2	280	336	156	7
Type 321SS-3	50	21	147	13
Type 321SS-4	35	16	114	14
Unexposed Cb-1Zr Specimen[(a)]	10	14	75	6
Unexposed Cb-1Zr Specimen[(b)]	50	50	200	24

(a) Conducted for quality control purposes prior to exposure.

(b) Conducted as a companion analysis at the same time the analyses were performed on the specimens exposed to potassium.

TABLE III. ROOM TEMPERATURE TENSILE PROPERTIES OF 0.040-INCH THICK Cb-1Zr ALLOY SPECIMENS EXPOSED FOR 1000 HOURS AT 1400°F IN POTASSIUM CONTAINED IN TYPE 321SS AND TYPE 316SS CAPSULES

Capsule Material and Capsule No.	0.2% Yield Strength[(a)], lb/in^2	Ultimate Tensile Strength, lb/in^2	Elongation Per Cent
Type 316SS-1	46 700	56 000	20
Type 316SS-2	40 300	57 000	15
Type 321SS-3	29 600	49 300	30
Type 321SS-4	25 300	42 800	36
Unexposed Cb-1Zr Specimen	23 300	40 000	37

(a) Strain rate was 0.005 in./in. of gauge length/min through 0.2% strain, and the gauge length was 0.50 in.

addition to forming these surface layers, carbon and nitrogen can diffuse into the Cb-1Zr alloy matrix and, thereby, have a pronounced effect on mechanical properties. Nitrogen has been found to diffuse more rapidly than carbon[2] and probably has the greater effect.

The metallurgical structure of the Type 321SS capsule material appeared unchanged; however, sigma phase (and possibly chi phase) formation as well as gross sensitization occurred in the Type 316SS capsule material (Fig. 5). The reduced amount of chromium carbide precipitate and the increased amount of iron-chromium sigma phase present at the capsule surface result from the depletion of carbon due to the mass transfer reaction.

Although the majority of the sigma phase was pulled out during metallographic preparation of this specimen, some selective removal of this phase at the surface by liquid potassium may be possible. Similar microstructural effects were observed in an investigation of a Type 316SS boiling potassium test loop.[1]

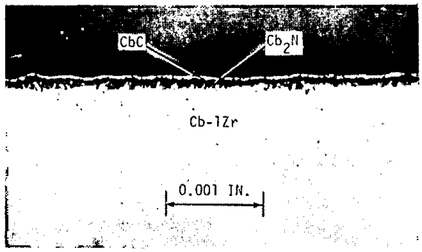

FIG.4. Cross-section of a Cb-1Zr specimen exposed to potassium for 1000 h at 1400°F in a Type 316SS capsule. Etchant: As-polished

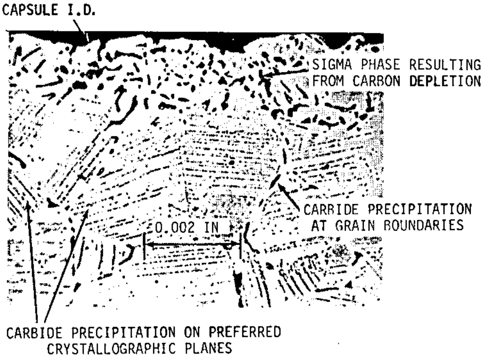

FIG.5. Cross-section of a Type 316SS capsule that contained Cb-1Zr specimens and potassium for 1000 h at 1400°F. Etchant: Electrolytic, oxalic acid

Cb-1Zr Capsules and Carbide Cermet Specimens

Visual examination revealed a discoloration of only the Cb-1Zr capsule surfaces which contained potassium and Carboloy 907 and Carboloy 999 at 1600°F. Otherwise, the appearance of the materials was essentially unchanged. Dimensional measurements and weight change determinations were not particularly definitive of corrosion reactions, and there was little or no evidence of major corrosion effects other than carbon transfer. A slight weight decrease in some of the WC cermets was consistent with the carbon transfer to the Cb-1Zr capsule which was defined by the evaluation techniques described below.

Chemical analysis of a 0.020-in. thick layer machined from the Cb-1Zr capsule wall that was in contact with liquid potassium clearly demonstrated cases of carbon transfer. Similar analyses indicated no change in oxygen, nitrogen, and hydrogen concentration. The carbon analysis data in TABLE IV show that the specimens containing substantial amounts of WC lost carbon to the Cb-1Zr capsule at the higher temperatures, whereas the TiC cermets did not. As expected, the increase in carbon content of the Cb-1Zr diminished with decreasing temperature, and there was essentially no carbon pickup

TABLE IV. CARBON CONTENT OF 0.020-INCH THICK LAYERS FROM THE WALLS OF Cb-1Zr CAPSULES THAT CONTAINED LIQUID POTASSIUM AND CARBIDE CERMETS FOR 1000 HOURS AT 800°, 1200° AND 1600°F

Carbide Cermet Contained in Capsule	Capsule Test Temperature, °F		
	1600	1200	800
	Carbon Content of Cb-1Zr, ppm(a)		
Carboloy 999	390,390	--	--
Carboloy 907	190,200	80,110	60,60
Grade 7178	110,130	80,100	30,30
K601	20,50	--	--
TiC	40,60	--	--
TiC+5%W	20,30	--	--
TiC+10%Mo	40,40	--	--
TiC+10%Cb	10,80	--	--
Unexposed Cb-1Zr Specimen	30,50,50,70		

(a) Duplicate analyses.

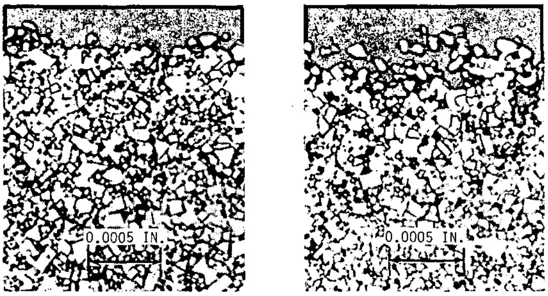

UNEXPOSED

EXPOSED AT 1600°F
NOTE APPARENT SURFACE ATTACK
TO A DEPTH OF 0.0004 IN.

FIG. 6. Cross-section of Carboloy 999 specimens before and after exposure to liquid potassium for 1000 h at 1600°F in a Cb-1Zr capsule. Etchant: Electrolytic, 10% NaOH

from the WC cermets at 800°F. (The apparent exception with K601 will be discussed presently.) Metallographic examination of the Cb-1Zr capsule material revealed the presence of CbC in the surface regions only when discoloration was evident and only when chemical analysis indicated an increase in carbon content after the exposures of WC cermets at 1600°F. The metallographic appearance was similar to that shown in Fig. 4, except that the nitride layer was absent.

In some cases after exposure at 1600°F, metallographic examination of the carbide cermets revealed subtle changes in the surface region to a depth of 0.001 in. or less, as illustrated by Carboloy 999 in Fig. 6. For the present considerations, however, examination at magnifications up to 2000X

TABLE V. PHASE CHANGES IN THE SURFACE REGION OF CARBIDE CERMETS AFTER EXPOSURE TO POTASSIUM LIQUID AND VAPOR FOR 1000 HOURS AT 1600°F IN Cb-1Zr CAPSULES

	Unexposed Specimens		Specimens Exposed in Liquid		Specimens Exposed in Vapor	
Material	Major	Minor	Major	Minor	Major	Minor
Carboloy 999	WC	--	W	WC Co_2W_4C $(Co,W)_xC$	WC	--
Carboloy 907	WC	TaC	W	TaC Co_2W_4C $(Co,W)_xC$	WC	TaC Co_2W_4C $(Co,W)_xC$
Grade 7178	WC	$(Mo,Cb)_2C$	W	$(Mo,Cb)_2C$ WC	WC	$(Mo,Cb)_2C$
K601	WC $(W,Ta)_2C$	--	W	WC $(W,Ta)_2C$	WC $(W,Ta)_2C$	W
TiC	TiC	--	TiC	--	TiC	--
TiC+5%W	(Ti,W)C	--	(Ti,W)C	--	(Ti,W)C	--
TiC+10%Mo	(Ti,Mo)C	--	(Ti,Mo)C	--	(Ti,Mo)C	--
TiC+10%Cb	(Ti,Cb)C	--	(Ti,Cb)C	--	(Ti,Cb)C	--

did not clearly define the occurrence of carbon transfer. X-ray diffraction of the surface revealed carbon transfer more effectively, inasmuch as the formation of elemental tungsten was readily observed. As indicated in TABLE V, tungsten was formed as a major phase in the surface of all WC cermets exposed to liquid potassium at 1600°F, but not in those specimens exposed to the vapor; the formation of minor phases was also detected. Conversely, no changes in the TiC cermets were detected. After exposure to liquid potassium at 1200°F, tungsten was detected as a minor phase in all of the WC cermets. No evidence of tungsten formation was obtained for the WC cermets exposed to potassium at 800°F, which is consistent with the carbon analysis data in TABLE IV.

The case of K601 exposed at 1600°F is interesting because carburization of the Cb-1Zr capsule wall was not observed by metallographic examination or by chemical analysis (TABLE IV), but the change from WC to tungsten was detected by X-ray diffraction (TABLE V), indicating that the latter technique was most sensitive for detecting carbon transfer under the present circumstances. This material is also somewhat unusual because of its lesser tendency for carbon depletion compared to other materials containing substantial amounts of WC. Although no detailed explanation will be attempted here, it should be noted that its processing, which is proprietary to the Kennametal Corporation, is reported to be significantly different from the procedures used to prepare the other WC cermets.

An additional group of similar capsule tests was conducted employing a slightly different specimen arrangement. A Mo-TZM specimen of the same dimensions as the cermet specimen was placed next to the cermet specimen with a 0.020-in. space between the two. This type of test was performed to permit a comparison of the interactions between these two classes of materials which are pertinent to bearing applications. Three of the carbide cermets were chosen for evaluation in separate tests for 1000 h at 800°, 1200°, and 1600°F, comprising a group of nine capsules. The transfer of carbon from the WC cermets to the adjacent Mo-TZM surface resulted in the formation of a uniform layer (Fig. 7) identified as Mo_2C by X-ray diffraction. It is important to note that Mo_2C formed only on the Mo-TZM surface adjacent to the WC cermet and not on the other surfaces of the same Mo-TZM specimen. The exposure of Mo-TZM and Carboloy 907 to liquid potassium resulted in the growth of a 0.0003-in. thick layer of Mo_2C at 1600°F and a 0.00003-in. layer at 1200°F; no layer was detected after exposure at 800°F. In the case of Mo-TZM and Grade 7178, the layer was 0.00015-in. thick after exposure at 1600°F; no layer resulted from the exposures at 1200° and 800°F. Testing of Mo-TZM with TiC+10%Cb did not result in the formation of a Mo2C layer at 1600°F. X-ray diffraction revealed the formation of tungsten in the surface of the Carboloy 907 and Grade 7178 specimens exposed at 1600°F. No phase changes in the TiC+10%Cb cermet were apparent.

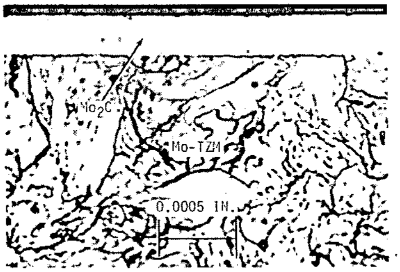

FIG. 7. Cross-section of the Mo-TZM specimen surface that was adjacent to Carboloy 907 during an exposure to liquid potassium for 1000 h at 1600°F in a Cb-1Zr capsule. Etchant: Murakami solution

DISCUSSION

The combined results obtained from metallographic examination, weight determination, chemical analysis, and tensile testing clearly demonstrate that carbon and nitrogen transfer from stainless steel to Cb-1Zr in potassium at 1400°F can be greatly reduced or eliminated when the stainless steel contains titanium (Type 321SS) which can form a relatively stable carbide and nitride. In the absence of titanium (Type 316SS), carburization and nitriding decrease the ductility of the Cb-1Zr alloy, and carbon depletion alters the morphology of the stainless steel surface region. The importance of these effects on engineering systems is dependent upon the specific operating requirements; in some cases they could be trivial and in other cases they could be of major significance. For critical engineering applications, it would be important to determine if the benefits derived from the titanium addition are obtained in dynamic systems with thermal gradients, at higher operating temperatures, and with other alkali metals. To a considerable extent, this has been done for the 2 1/4 Cr-1Mo and 5Cr-1/2Mo ferritic steels, and a titanium addition has provided resistance to carbon transfer in flowing sodium at temperatures up to 1200°F. [8,9]. It may also be anticipated that the amount of carbon transfer observed in several other monometallic systems[1] could be reduced by modifying the iron, cobalt and nickel alloys with an addition of titanium or other constituent capable of forming a relatively stable carbide.

Considering the candidates for bearing applications, the TiC cermets are more stable than the WC cermets with respect to carbon transfer to Cb-1Zr and Mo-TZM alloys. These alloys were definitely carburized in the presence of WC and potassium at 1200° and 1600°F and were essentially unaffected in the presence of TiC. As a result of carbon depletion, elemental tungsten could be observed by X-ray diffraction of the surfaces of WC cermets exposed at 1200° and 1600°F. Carbon transfer from WC cermets at 800°F was apparently too slow to be observed by any of the techniques employed. The engineering significance of these observations depends primarily on the particular application. For example, a disturbed surface layer and the formation of elemental tungsten on WC cermets could be damaging to friction, wear, and diffusion bonding characteristics which are pertinent to the application of these materials in bearings and valve seating and sliding components. At temperatures near 800°F, the commercial WC cermets appear quite stable and corrosion resistant for general usage, but the experimental TiC cermets offer advantages with respect to carbon transfer effects at the higher temperatures.

Considering the experiments with stainless steels and carbide cermets together, it is evident that all of the cases of carbon transfer are consistent with expectations based on the relative thermodynamic stabilities of the carbides involved (TABLE VI). It is interesting to note that carbon transfers from tungsten to molybdenum, even though the difference in the free energies of formation of the pertinent compounds is relatively small, and that carbon is retained by titanium even in the presence of columbium which also forms relatively stable carbides. This suggests that the thermodynamic properties of the carbides can be used to predict the occurrence of carbon transfer in multimetallic systems with some certainty at high temperatures where the reaction rates are likely to be fast.

SUMMARY AND CONCLUSIONS

1. The formation of a relatively stable carbide in stainless steel by the addition of titanium greatly reduced or eliminated the transfer of carbon to Cb-1Zr in potassium at 1400°F; nitrogen transfer was also reduced or eliminated. In the absence of titanium, the stainless steel surface region was altered by carbon depletion and the ductility of the Cb-1Zr was reduced by carburization and nitriding.

2. Carbon transferred from WC cermets to Cb-1Zr and Mo-TZM in the presence of potassium at 1200° and 1600°F, but this was not detected at 800°F. No transfer of carbon from the TiC cermets was observed after similar exposures up to 1600°F. At high temperatures, carbon depletion of the WC cermets resulted in the formation of elemental tungsten in the surface region which could affect friction, wear, and diffusion bonding characteristics important to the performance of these materials in bearings and valve seating and sliding components. At temperatures near 800°F, however, the commercial WC cermets appear quite stable and corrosion resistant for general usage, but the experimental TiC cermets offer advantages with respect to carbon transfer effects at higher temperatures.

3. All of the observed cases of carbon transfer are consistent with expectations based on the thermodynamic stabilities of the compounds involved, indicating that the tendency for carbon transfer in multimetallic systems may be predicted from thermodynamic properties with reasonable confidence.

TABLE VI. STANDARD FREE ENERGY OF FORMATION OF SELECTED CARBIDES AT VARIOUS TEMPERATURES

		Temperature, °F			
		800	1200	1400	1600
Carbide	Source	Free Energy, -kcal/g-atom of Carbon			
Fe_3C	(a)	-2.3	-1.0	-0.4	0.1
WC	(b)	4.7	5.6	6.0	6.4
Mo_2C	(c)	13.0	13.4	13.6	13.8
$1/6Cr_{23}C_6$	(d)	17.6	17.8	18.0	18.1
CbC	(e)	30.8	30.7	30.7	30.6
TaC	(a)	37.6	37.4	37.2	37.0
TiC	(a)	42.0	41.5	41.2	40.9
ZrC	(a)	42.6	42.2	41.8	41.5

(a) Smithells, C.J., Metals Reference Book, Vol. II, 3rd Edn, Butterworths, Washington (1962) 633.

(b) Alekseev, V.I., Shvartsman, L.A., Izvest. Akad. Nauk. SSSR, Met. i. Gornoe. Delo (1963) 9196.

(c) Gleiser, M., Chipman, J., J. Phys. Chem. 66 8 (1962) 1539.

(d) Samsonov, G.V., Plenum Press Handbooks of High Temperature Materials, No. 2, Properties Index, Plenum Press, New York (1964) 86.

(e) Worrell, W.L., Chipman, J., J. Phys. Chem. 68 4 (1964) 860.

4. It is suggested that the carbon transfer observed in several monometallic systems may be reduced by modifying the alloys with an addition of titanium or other constituent capable of forming a relatively stable carbide.

ACKNOWLEDGMENT

This work was performed under NASA Contracts NAS 3-2534 and NAS 3-6012. Technical contributions by R.L. Davies and T.A. Moss of the NASA-Lewis Research Center are gratefully acknowledged.

REFERENCES

[1] Jansen, D.H., Hoffman, E.E., Type 316 Stainless Steel, Inconel, and Haynes Alloy No. 25 Natural-Circulation Boiling Potassium Corrosion Test Loops, Oak Ridge National Laboratory Report No. ORNL-3790 for USAEC Contract No. W-7405-eng-26 (1965).

[2] DiStefano, J.R., Hoffman, E.E., "Corrosion mechanisms in refractory metal-alkali metal systems," pp. 257-288, The Science and Technology of Tungsten, Tantalum, Molybdenum, Niobium and their Alloys (Promisel, N.E., Ed.), Pergamon Press, Oxford (1964).

[3] Semmel, J.W., Jr., "Liquid metal investigations," pp. 69-86, NASA-AEC Liquid Metals Corrosion Meeting, December 14-15, 1961, Brookhaven National Laboratory, USAEC Report No. TID-7626 (Pt. 1) (1962).

[4] Jansen, D.H., private communication, Oak Ridge National Laboratory.

[5] Goldmann, K., Hyman, N., Kostman, S., McKee, J., Trans Am. nucl. Soc. 8 2 (1965) 396.

[6] Lloyd, D.B., Taboada, A., Trans Am. nucl. Soc. 8 2 (1965) 406.

[7] Lymperes, C.J., Chapman, J.D., Schenck, G.F., Interactions in a Type 316 Stainless Steel-NaK-Cb-1Zr Alloy System, Pratt and Whitney Aircraft-CANEL Report No. TIM-896 for USAEC Contract No. AT(30-1)-2789 (1965).

[8] Hetzler, F.J., Young, R.S., Sodium Mass Transfer: II Screening Test Data and Analysis, Volume 2-Metallurgy, General Electric Co. Report No. GEAP-3726 for USAEC Contract No. AT(04-3)-189 (1962).

[9] Anderson, W.J., Sheffield, G.S., Birkle, A.J., Development of Ferritic Steels for High Temperature Sodium Service. Part II, Atomics International Report No. NAA-SR-7544 for USAEC Contract No. AT(11-1)-GEN-8 (1963).

[10] Harrison, R.W., *Stabilization of Carbon and Nitrogen in Stainless* Steel and Its Effect on Mass Transfer in a Stainless Steel-Cb-1Zr-Potassium System, General Electric Co. Report No. R66SD3009 for NASA Contract No. NAS 3-6012 (1966).

[11] Frank, R.G., Miketta, D.N., Kearns, W.H., Young, W.R., Hand, R.B., Material and Process Specifications for Refractory Alloy and Alkali Metals, General Electric Co. Report No. R66SD3007 for NASA Contract No. NAS 3-2547 (1965).

EFFECTS OF MASS TRANSFER, AND OF CHANGES IN PROPERTIES, ON AUSTENITIC STEELS IN FLOWING SODIUM

E.L. ZEBROSKI, R.S. YOUNG, F.A. COMPRELLI
AND D. DUTINA
ADVANCED PRODUCTS OPERATION,
GENERAL ELECTRIC COMPANY,
SAN JOSE, CALIF.,
UNITED STATES OF AMERICA

Abstract

EFFECTS OF MASS TRANSFER, AND OF CHANGES IN PROPERTIES, ON AUSTENITIC STEELS IN FLOWING SODIUM. Corrosion and mass transfer effects have been investigated over a range of temperature, flow, velocity and sodium compositions believed to be typical of reactor coolant systems. Previous published results have been extended to a total of 1.4×10^5 h of small-scale loop operations, at temperatures up to 1300°F (700°C). Good agreement has been found by Thorley et al. for the dependence of mass transfer on temperature and oxygen level, but some unresolved differences remain in velocity and mass flow dependences. The effects of velocity and geometry in larger systems are under investigation in loops designed to mock-up mass transfer effects of large systems. Preliminary results on Types 304, 316 and Incoloy 800 indicate varying velocity dependence at moderate and low velocities with pronounced entrance and saturation effects.

Intergranular attack has been observed at specific locations in loop austenitic steel piping. Subsequent studies indicate a dependence on oxygen level and stress level.

The effectiveness of materials in sodium service depends on the changes in mechanical properties due to compositional and structural modifications, as well as the loss or gain of material by mass transfer. Where thin sections are required (fuel cladding, some control elements, instrumentation leads, pump ducts, etc.), surface effects, such as the compositionally disturbed layers, changes in precipitation kinetics due to carbon transport, or highly localized corrosion, can have gross effects on the useable properties of the material. Techniques for systematically determining the influence of such conditions on several critical alloy properties (while exposed to representative flowing sodium environments) have been developed and are described.

The possible effect of large heat fluxes on quantitative mass transfer rates is hypothesized and initial results of short-term experiments are discussed.

The analysis of trace impurities in sodium continues to pose problems because of the limited correlations found so far between elemental trace analysis and the behaviour of coupons of samples. Progress in methods to attain high sensitivity and identification of trace compounds using three improved methods is reported. Observations on the relationship of localized carbon analysis to the behaviour of plugging meters is reported.

The occasional occurrence of severe localized attack of austenitic steels during in-reactor tests is noted, and some of the observations and hypotheses are discussed.

INTRODUCTION

The effects of a sodium environment on austenitic steels have been under investigation for some years in out-of-pile dynamic test loops simulating a range of conditions of interest to fast reactor applications.[1]

---

[1] Mass Transfer Program, Investigations in Liquid Metal Systems at Moderately High Temperatures, USAEC Contract AT(04-3)-189, P.A. 15; also some data on irradiated materials from Contract AT(04-3)-189, P.A. 10

The primary objective of this work is to obtain systematic information on corrosion and changes in properties, as needed to establish the operating limits for several materials which are candidates for service in sodium-cooled fast reactors. Related subordinate objectives include the establishment of reproducible means of routine measurement and control of oxygen levels in sodium, and the detection and identification of the chemical species involved in the rate-determining steps of the mass transfer of iron, nickel, chromium, and carbon. Phase I of this program was started in 1959 with the following intended range of test variables:

(1) Maximum system temperatures; (tmax) 593 to 704°C (1100 to 1300°F) (local sample temperatures 482 to 704°C (900 to 1300°F).
(2) The maximum temperature difference from hot region to cold region of the loops ("system ΔT") was adjusted by varying the minimum cold leg temperatures from 139 to 278°C below Tmax (250 to 500°F ΔT)
(3) Sodium oxide level; from 10 to 50 ppm (expressed as ppm of oxygen)
(4) Sodium velocity; from 2.1 to 6.3 m/sec average in test sections
(5) Materials; austenitic and ferritic steels

Six loops have been operated, for a current cumulative total of 150,000 loop hours, using combinations of ferritic and austenitic steels as shown in Table I. For completeness, several other loops constructed subsequently are also listed.

Typical commercial alloys were used both for loop construction and for specimens with nominal compositions given in Table II.

TABLE I. LOOP MATERIALS

Loop No.	Heated Area ("hot leg")	Cooled Area ("cold leg")
1	Type 316 SS	Type 316 SS
2	" 316 "	2-1/4 Cr ferritic
3	" 316 "	2-1/4 Cr ferritic
4	" 316 "	5 Cr ferritic
5	2-1/4 Cr ferritic	2-1/4 Cr ferritic
5R	Type 304, 316** SS	Type 304, 316** SS
6	5-Cr ferritic	5-Cr ferritic
6R	Type 304, 316** SS	Type 304, 316** SS
7	Type 304 SS	Type 304 SS
8	Type 304, 316* SS	Type 304, 316* SS
9	Type 304, 316* SS	Type 304, 316* SS

* Piping Type 304 SS; heater and cooler sections and test section Type 316 SS
** Economizers and heaters only of Type 316 SS.

TABLE II. NOMINAL ALLOY COMPOSITIONS USED

Alloy	C max	Fe	Cr	Ni	Mn	Mo	other
Type 316 SS	.08	bal.	17	12	2	3	
Type 304 SS	.08	"	19	10	2		
2-1/4 Cr ferritic	.15	"	2.25	-	.45	1.0	
5-Cr ferritic	.12	"	5.0	-	.58	.5	.55 Ti
Incoloy 800	.06	"	21	32	1		(Al + Ti 0.6 max)

The six original loops were identical in mechanical design, each providing for four sample positions in the hot legs and three in the cold legs. Details of the design and construction of these loops have been reported.(1) An isometric drawing of one of these loops (Fig. 1) gives a map of sample location and an example of temperature distributions.

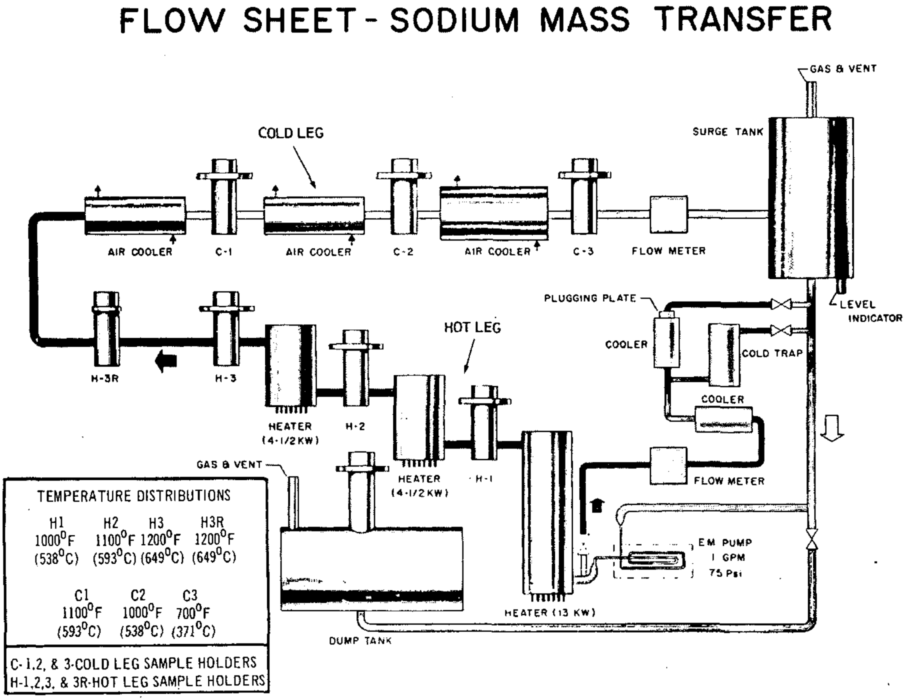

FIG. 1. Loop schematic, loops 1 to 6

The general results of the metallurgical examinations and statistical analysis of the corrosion data have been published.(2) Following is a brief summary of the main results, together with more recent results and analysis of the data to date.

COMPOSITION AND VELOCITY EFFECTS

The surface composition changes resulting from the mass transfer process were most pronounced for the austenitic stainless steel. At the lower oxygen level (~12 ppm oxygen) chromium and nickel were transported from the higher temperature regions to cold leg regions at a greater rate than iron. Accompanying this effect was the transport of carbon to 316 SS regions in the hot leg from unstabilized ferritic steel (2 1/4 Cr-1 Mo) in the cold leg. This occurred generally at temperatures over 400°C. The depletion of nickel and chromium from the surface of the austenitic steel results in a surface layer of ferrite, which attains a limiting steady-state thickness of about 0.01 mm (about 0.4 mil). The pickup of carbon in the stainless steel is evidenced by the increased density of carbide precipitates underneath the surface layer of ferrite (Fig. 2). During an initial period of several months, relatively high but decreasing corrosion rates are observed (as determined by weight changes) predominantly due to loss of nickel and chromium while a surface layer, progressively more depleted in nickel and chromium is formed. Eventually a constant and low corrosion rate is observed (for constant sodium conditions) and a thin layer, rich in iron at the surface, maintains a constant composition profile of iron, nickel and chromium. The initial high rates of loss of nickel and chromium (relative to iron) are reduced at the steady state by the added impedence of diffusion through the ferrite layer. At the steady state low-corrosion rate condition, the rates of loss of iron, nickel and chromium are proportional to the average weight percent of each in the alloy. E. G. Brush has analyzed the kinetics of the initial selective leaching transient effect.(3)

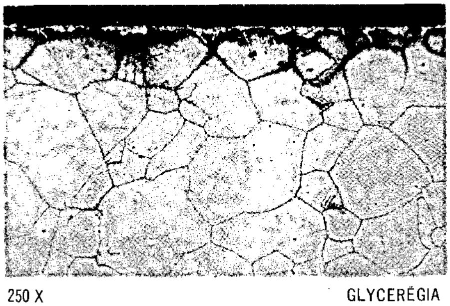

SAMPLE NO. 3403
EXPOSED 2813 HRS

NOTE: ALL SAMPLES
WERE EXPOSED IN LOW
VELOCITY SODIUM (~8 fps)
AT 650°C

FIG. 2. Carbide precipitates underneath ferritic surface layer on Type 316 stainless steel

After the initial transient period of several months or less, no significant differences in the steady state corrosion rates were found between the austenitic and ferritic steels at a given oxygen level and temperature. This result is in keeping with the observation that the exposed surface is over 90% iron at steady state, irrespective of whether the initial material is an austenitic or ferritic alloy. The observed steady state rates are shown in Table III. The data for the rate of loss of weight in flowing sodium is correlated by the expression:

$$R = V^{0.884} C_o^{1.156} \exp\left[12.845 - \frac{13,300}{T + 273} - 0.00676 \frac{L}{D} + \frac{2.26}{(t + 1)}\right] \quad \text{equation (1)}$$

where

R = rate of metal removal in mg/dm^2/month

V = sodium velocity in ft/sec

C_o = concentration of oxygen in the sodium in ppm

t = time in months

T = sample temperature °C

L = distance from inlet to a given isothermal and constant velocity region

D = hydraulic diameter

The constants were derived by a statistical analysis of 25 different runs covering the range of conditions listed in the introduction. Because of the sparsity of data at 700°C the region of greatest accuracy is from 600 to 650°C.

TABLE III. AVERAGE STEADY-STATE CORROSION RATES, MILS PER YEAR IN SODIUM AT 6.1 METERS/SEC

Specimen Temp. (hot leg)	Oxygen Content of the Sodium 10-15 ppm Ave.	Max.	45-50 ppm Ave.	Max.
538°C (1000°F)	0.05	0.25	0.25	1.25
593°C (1100°F)	0.15	0.75	0.75	3.75
649°C (1200°F)	0.39	1.95	1.9	9.5
704°C (1300°F)	0.95	4.95	4.7	23.5

General agreement on the trend effects of temperature and oxygen parameters is found by Nettley, et al.(4) with the exception of the velocity term. Nettley concludes there is little or no velocity dependence above 3-meter/sec for type 316 at 725°C, slightly less than linear dependence on velocity for a nickel-base alloy Nimonic 80A.

Recent data from larger test loops designed to simulate mass transfer processes of large systems confirm the corrosion rates and general trends with velocity and temperature observed in our prior work.

Due to limitations of our previous test section and "hockey-stick" sample design, it was not possible to separate the velocity dependence and "downstream" effect unequivocally. While the parameters given above represent the experimental data adequately for the limited range of values tested, the relative values of the velocity and "downstream" coefficients (in the first term and the L/D term, respectively of equation 1) are not uniquely determined. The test sections now in use employ a series of ring samples on a mandrel in a concentric flow annulus. More quantitative determination of entrance effects and "downstream" effect is now possible and preliminary results have been obtained at 704°C (1300°F) and times to 2000 hours. The design schematic of the new test loops is shown in Fig. 3. Velocities up to 7.6 meters/sec (25 fps) are being studied.

Initial results from a 2000-hour run in loop 8 (designed to observe the velocity and downstream effects) show a corrosion pattern which could not be observed quantitatively in prior tests. Higher than average corrosion rates were measured at the entrances of test sections after each change in velocity.

To take the entrance effect into account, the L/D term in equation (1) was replaced by two terms; the first term is a linear function of L/D along an isothermal region. This term measures the degree of saturation of the driving force for corrosion (at constant temperature). The other term is a log function of L/D measured along each isothermal region after a change in velocity. This term corresponds to the entrance effect. An example of the effect of these downstream factors is illustrated in Fig. 4.

The combination of the two terms fits the observed average shape of the decay curves from 11 sets of samples at 704°C. Taking into account the recent data and the revised (L/D) terms, there is a trend to lower values of the velocity coefficient and to a larger temperature coefficient than the values given in equation 1. Revised values of the coefficients will be published when sufficient statistical data has been accumulated for the new range of conditions.

The current program includes a variety of stainless steels which are candidates for core and cladding materials because of expected differences in properties under irradiation. Preliminary corrosion results indicate that types 304 and 316 stainless steel and Incoloy 800 exhibit similar corrosion rates generally in accord with the equation given previously. For example, the corrosion rate observed for Incoloy 800 was 4×10^{-3} mm/yr in 650°C (1200°F) sodium at 2.1 meters/sec (7 fps) and times to 3000 hours (10 ppm oxygen).

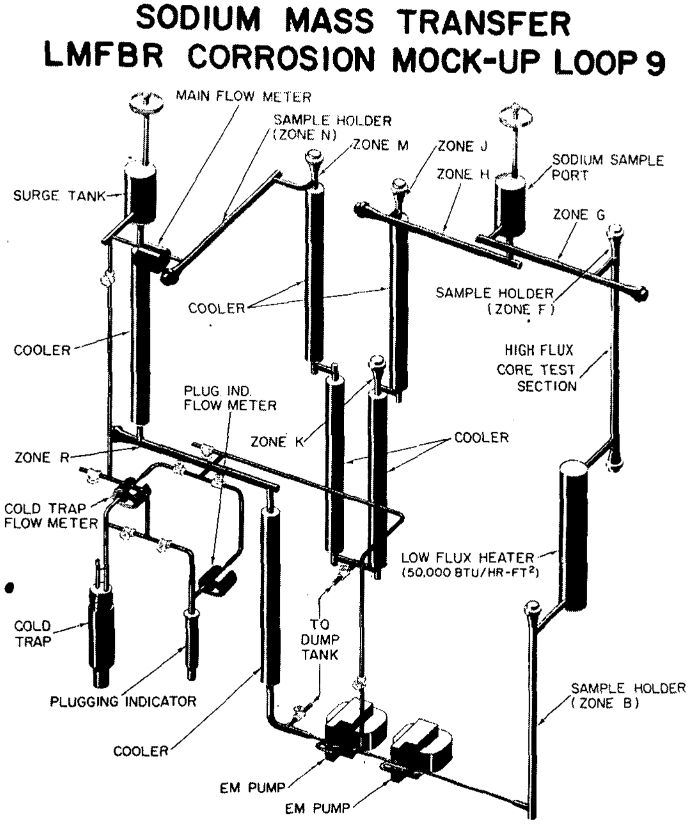

FIG.3. New test loop design (loops 8 and 9)

One complication in the apparent velocity dependence was noted in some runs with the small scale loops. Evidence of deposition of material and weight gains of hot-leg specimens, rather than the usual weight losses, were observed when a low-oxygen run (~10 ppm) was preceded by a high-oxygen run (~50 ppm), of 4300 hours. In this case, no velocity effect in the rate of weight changes was observed over the range of 2.1 meters/sec to 6.3 meters/sec sodium velocity, and for times to 2400 hours. Apparently the deposition effect is due to the changing nature of the oxide film on loop surfaces which persists for some months after a change in oxygen level.

SURFACE COMPOSITION CHANGES IN FERRITIC ALLOYS

The ferritic steels (2 1/4 Cr-1 Mo, and 5 Cr-1/2 Mo-1/2 Ti) studied in the first phase of the program experienced systematic composition changes in surfaces exposed to sodium. The changes were dependent on the oxygen content of the sodium. The effect was measured by x-ray fluorescent analysis of surface layer compositions of hot-leg and cold-leg samples. Surface analyses yielding average elemental composition changes in the outermost 12-micron layer of the surface showed that chromium was selectively removed from the hot-leg regions and deposited in cold-leg regions during runs with 10-15 ppm oxygen. Fig. 5 shows the typical distribution of chromium found on specimens located throughout the ferritic steel loops when operated at low oxygen. Manganese tended to show the same effect as chromium while molybdenum remained relatively inert to selective movement.

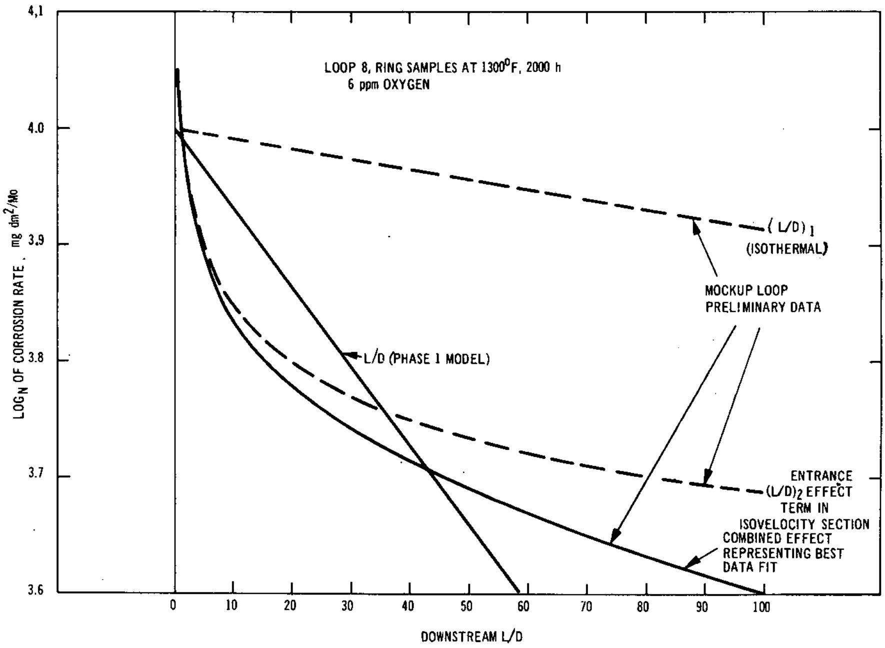

FIG. 4. Entrance and downstream effect analysis for Type 316 S S at 1300°F (704°C)

In contrast to the above behavior, runs at 50 ppm oxygen showed a reversal in relative mobility. The loss of iron in hot regions and deposition in cold regions exceeded the transport of chromium.

The studies of general corrosion or mass transfer have indicated that for temperatures of 650°C or lower and oxygen levels ~10 ppm, the uniform corrosion rates of any of the austenitic stainless steels tested are low enough to permit assurance of structural integrity of piping systems for anticipated lifetimes of the order of 20 years. Before this can be regarded as definitive, however, it is necessary to insure against possible occurance of pitting or intergranular attack.

INTERGRANULAR ATTACK

Recent examinations of the piping from the sodium mass transfer test loops have revealed the occurrence of localized intergranular penetrations in addition to general corrosion effects. This effect was observed in a type 316 piping which operated at 650°C (1200°F) maximum, for approximately 30,000 hours. The grain-boundary penetrations, to a maximum depth of .18 mm (7 mils) were almost always found only in the piping between the last hot-leg test section and first cooler (neither of which exhibited localized attack). The extent of penetration observed would be of little concern in thick-walled regions of a sodium system (unless also subjected to appreciable strain cycling). For thin members, such as fuel cladding, such penetration would define a serious limit on useful lifetime. There is, accordingly, considerable interest in determining the nature of the attack and the parameters which control or influence it.

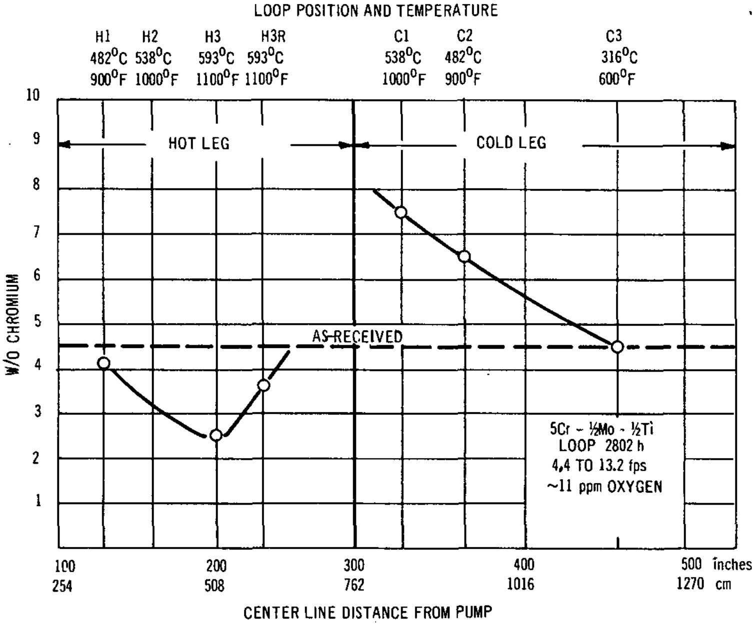

FIG. 5. Chromium distribution on ferritic steel loop surfaces

STRUCTURAL OBSERVATIONS OF INTERGRANULAR ATTACK

A section of loop piping from the attacked region was examined metallographically and revealed extensive intergranular penetration (see Fig. 6). Since the attack was characteristically intergranular, the differences in topology and precipitate morphology between the attacked and unattacked grain boundaries were examined.

A fractographic analysis, utilizing both two-step carbon and carbon extraction replicas, was carried out and yielded the following observations:

(a) The fracture surface away from the attacked area was typical of intergranular fracture and showed sensitization in the form of continuous sheets of minute, angular particles, identified by electron diffraction as $Cr_{23}C_6$.

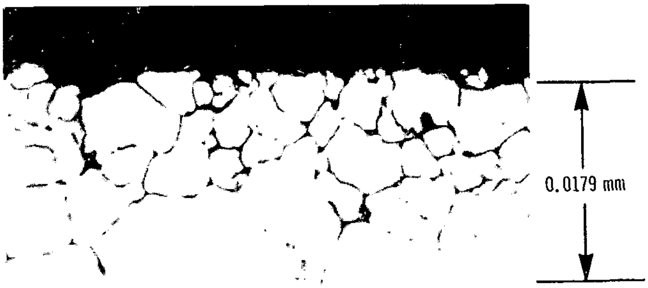

FIG. 6. Intergranular attack of Type 316 S S after ~30 000 h in sodium at 1200°F

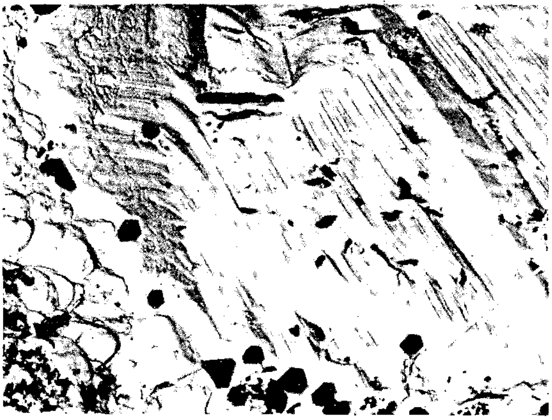

FIG. 7. Grain surface after attack by high-temperature sodium

(b) Examination of the attacked intergranular surfaces (Fig. 7) revealed "steps" or "serrations" which were not present on the original unexposed surface and are typical of a heavily etched surface. This suggests that the corrosive environment preferentially attacked and exposed certain crystallographic facets of the grains.

(c) The distribution of carbides on the attacked surfaces was substantially different than on the unattacked surfaces. The presence of large angular carbides indicated that the carbide particles themselves were not chemically attacked. The smaller carbide particles were probably dislodged from the surface during the fracture process after the carbide-matrix bonding had been weakened and disrupted by the corrosive attack.

(d) No positive evidence of any corrosion reaction product in the grain boundary could be established. Particles of different sizes and shapes were observed and examined by electron diffraction, but no positive identification could be made.

Considering a potential analogy with caustic stress corrosion, a possible reaction mechanism would require: (1) the existence of a continuous structural path along which the chemical reactivity is high relative to the surrounding matrix; (2) the existence of a normal stress across the path of high chemical reactivity.

Since the observed attack appears to be a selective and localized phenomenon, many variables within the material structure may assume importance, such as orientation effects, coherent precipitates, stacking faults, and other dislocation barriers. Relatively low macrostresses may induce locally high microstresses to initiate and propagate intergranular attack.

The opportunity for substantial stresses to develop in the loop piping was present during loop startup. During the inititial stages of the preheat cycle, a circumferential temperature gradient of about 145°C (260°F) maximum is calculated resulting from electrical heaters attached to the piping, The calculated thermal stress on the ID surface of the piping is of the order of 35,000 psi. As the temperature of the piping approached an equilibrium level of 371°C (700°F), the thermal stresses decrease to an insignificant level. During normal loop operation at 649°C (1200°F), the temperature differential across the piping wall was approximately 10 to 15°F, producing minimal thermal stresses.

A study of the procedures of loop operation indicated that during loop shut-down for removal and replacement of samples, the internal piping surfaces, coated with a residual sodium film, were potentially subjected to limited atmospheric contamination due to air back-diffusion into argon cover gas used. Under these conditions the residual sodium film would react to form Na_2O and some NaOH. The combination of this corrosive film, the presence of thermal stresses, and elevated temperature during the preheat and startup cycle are postulated to provide an environmental condition favorable for rapid intergranular attack.

Effects of a generally similar type have been observed previously under two slightly different sets of circumstances; (a) when sodium escapes from a leak and subsequently undergoes atmospheric oxidation, the leak region usually exhibits severe intergranular attack. (b) When steel samples (or fuel elements) are withdrawn from a sodium system and stored in a supposedly inert atmosphere without thorough cleaning to remove the surface film of sodium, air inleakage in time produces a white layer of Na_2O on the sample, beneath which intergranular penetration is observed upon subsequent examination.

Published data show that intergranular attack can occur in unstressed metal beneath a layer of Na_2O even at room temperature, and also in dilute to medium-strength solutions of NaOH at temperatures of 250-300°C (482-572°F) with sressed specimens. Only during loop startup can substantial thermal stresses and Na_2O or NaOH be present. When sodium flow is established, the pipe walls become essentially isothermal, and a thin layer of Na_2O-NaOH would be rapidly carried away. Therefore, prolonged attack during high-temperature operation is unlikely. It would then appear that the penetration occurred in steps with an increment in penetration during each startup period.

To extend the prior observations made on loop piping, further experiments are in progress which permit the application of static and dynamic stress patterns of varying intensities.

Initial observations suggest that intergranular penetrations, similar to those observed on loop piping, can be reproduced. Tubing specimens of solution-annealed type 316 SS were exposed in the hot leg exit region (test loop No. 3) under two sets of conditions. The first exposure was made over a period of 2200 hours at 593°C with the sodium oxide level at 50 ppm oxygen, and the second was for 2400 hours at 649°C with the oxide level reduced to 10 ppm. The specimens were pressurized to produce an approximate loop stress of 11 000 psi. Specimens exposed during the first high oxygen period showed evidence of initiation of intergranular attack while those exposed only during the low oxygen period revealed no evidence of intergranular attack. This is taken to support, but not conclusively, the mechanism suggested above. Further data with varying material and stress levels are being obtained in an attempt to establish the nature of the intergranular attack and the factors which can influence its initiation and prevention.

CLAD INTERACTION WITH FUEL

A survey of the fuel-cladding interface of irradiated mixed oxide fuel pins clad with 347 SS has been reported.(5) Specimens examined covered a burnup range of 52 to 77 000 MWD/T with fast neutron exposures up to 3.1×10^{20} nvt. The most prominent effect observed was the enhanced precipitation of intergranular carbides at and adjacent to the fuel-cladding interface. This interaction has been noted in specimens selected from both extremes in the burnup range studied and appears to be associated with regions in which there is intimate fuel-to-cladding contact.

The $M_{23}C_6$, previously established as the probable precipitative phase by electron microscopy, was examined by electron microprobe analysis which identified the cation constituents as predominantly iron and chromium (Fig. 8). The same type of analysis also showed that the niobium was homogeneously distributed throughout the cladding as NbC. No measurable concentration gradients of Fe, Cr or Ni were found in the region of enhanced precipitation.

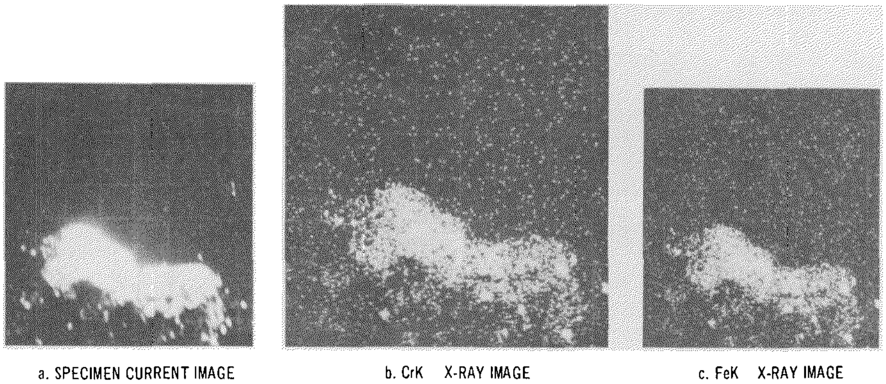

a. SPECIMEN CURRENT IMAGE b. CrK X-RAY IMAGE c. FeK X-RAY IMAGE

FIG. 8. Electron-beam scanning displays of grain boundary carbide precipitates in irradiated 347 stainless-steel cladding. Carbon extraction replica

The compatibility of $(U\text{-}20Pu)O_2$ fuel and FCR cladding materials was evaluated in a short-term (100 hour) anneal at 757°C (1400°F). Fuel of three stoichiometries -- 1.98, 2.00, and 2.04 -- and discs of type 304, 316, 321, 347, and

Incoloy 800 were held in intimate contact by differential expansion in an inert gas environment. No evidence of chemical instability or diffusion zones could be detected at any fuel-cladding interface. With type 316 SS only, Fig. 9, the typical layer of carbide precipitation was observed adjacent to the contact surface for each stoichiometry.

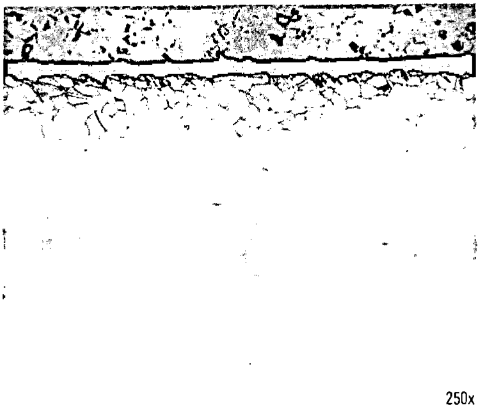

FIG. 9. Reaction interface between mixed oxide fuel and Type 316 S.S. after 100 h at 1400°F

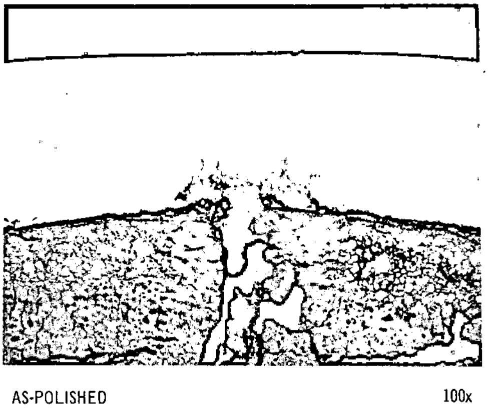

FIG. 10. Metallic phase attack of 347 stainless steel in a mixed oxide fuel and NaK environment

An unusual fuel-cladding interaction was observed in a fuel pin which experienced a peak burnup of 18 000 MWD/T in GETR followed by unscheduled overpower operation which produced gross failure. The interaction was characterized by local clad degradation at the inner diameter surface adjacent to radial cracks in the fuel. A metallic-appearing phase was observed to be in contact with attacked cladding into the adjoining fissure, as shown in Fig. 10. This phase exhibited a high chemical reactivity and did not exhibit the etching characteristics of the clad material.

HEAT FLUX EFFECTS

Most of the information on corrosion of materials in flowing sodium has been obtained to date by varying the bulk sodium stream temperature. Methods for heating the sodium have involved low heat flux heaters, typically generating about 30 000 to 50 000 Btu/hr/ft^2. Examinations have been made of type 316 SS heater thimble surfaces after service life times up to 19 000 hours heating bulk streams to about 650°C (1200°F). Comparison of this heat transfer surface with a nearby surface which did not transfer heat and which experienced the same bulk stream temperatures, revealed no systematic differences. (6)

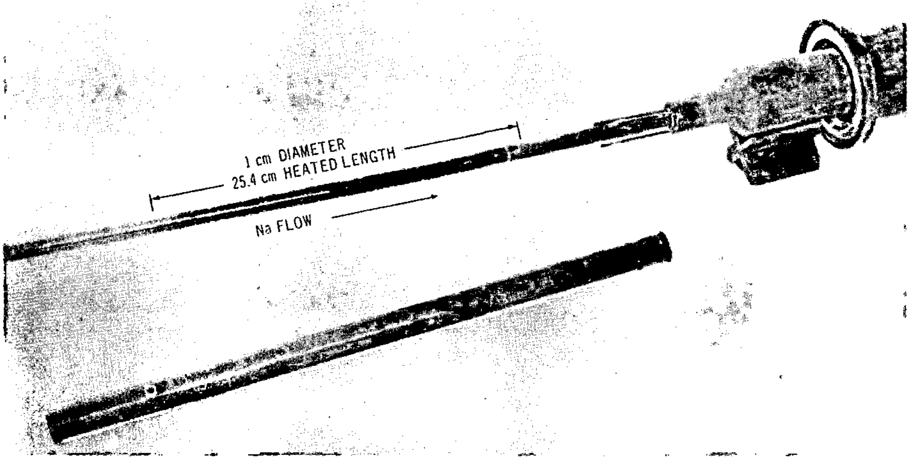

FIG. 11. Electron-bombardment heater

Peak heat fluxes on the order of 10^6 Btu/hr/ft^2 are specified for the current designs of fuel for large fast reactors. Due to film coefficients in sodium, the maximum temperatures of cladding surfaces will vary from 28 to 56°C (50 to 100°F) above the bulk stream temperatures. The isothermal corrosion rate data suggest a resultant increase in local corrosion rates of 2 to 3 times relative to the rate at the bulk sodium temperature.

There is also a temperature gradient in the cladding itself, of the order of 1250°C/cm (6000°F/in.). To the extent to which any of the corrosion rates or precipitation processes are limited by diffusion in the cladding or surface film, for example the diffusion of nickel and chromium in the ferritic surface layer, it is of interest to look for possible differences in corrosion rates relative to the equivalent isothermal case.

Tests are being run on an electron bombardment heater designed to simulate fuel rod heat flux. The heater (Fig. 11) has an effective heated length of 25.4 cm and is 1 cm in diameter. It has recently operated for a total of 478 hours in a sodium stream with 85 hours at heat fluxes of 680 000 to 800 000 Btu/hr/ft^2.

The sodium flow along the heater was at a velocity of approximately 10 ft/sec with a bulk sodium temperature increase along the heated length averaging

370°F. The outlet temperature was 566 to 621°C (1050 to 1150°F) during high power operation. Type 316SS specimens are shown in place on the heater after removal of the assembly from the loop and removal of residual sodium. An effect of increasing temperature is shown by the difference in surface appearance. Surfaces at the sodium entrance end have a lighter, metallic appearance in contrast to a darkened surface in the downstream areas at higher temperatures.

Other high heat flux heater designs which have been tried include graphite rod resistance heaters with a heated length of 5 cm and an annular induction-coupled high frequency heater with a uniformly heated length of 15 cm. The latter approach at present appears to be the most convenient and is being used for long duration tests at about 350 watts/cm^2.

METHOD FOR TESTING MECHANICAL PROPERTIES OF TUBES IN FLOWING SODIUM.

As noted in a previous section on intergranular attack, the useable mechanical properties of the material (strength, elongation, creep rupture life) can be very significantly affected under conditions which lead to relatively low corrosion rates for unstressed material. This is especially true for thin sections such as fuel cladding, typically about 0.4 mm (.016"), compared with usual tensile coupons which may be 1.6 mm or greater in thickness. Previous limited use of statically pressurized tube specimens for stress-rupture tests under carburizing conditions(7) has been extended to simulate more generally some of the stress patterns which may be present in fuel cladding.

A test technique utilized to study the effect of flowing high-temperature sodium on mechanical performance of materials is schematically illustrated in Fig. 12. The technique has been selected to incorporate the critical stress patterns -- primary and secondary, membrane and bending -- which are imposed upon fuel cladding during reactor exposure. The primary consideration in these tests is the ability of the material to support deformation, both localized and uniform, without fracture under the action of these stress patterns in the corrosive environment.

In order to achieve these conditions, pressurization techniques and specimens, typically shown in Fig. 13, have been built. In some cases the fatigue specimens also incorporate a wire wrap to simulate localized strains which can result from the use of wire spacers in a fuel assembly.

SODIUM CHEMISTRY

The analysis for and identification of trace impurities in sodium has received increasing attention. Despite development of sensitive techniques for determination of many of the elemental impurities there has been limited direct correlation between these analyses and the observed carburization and mass transfer rates. Elemental analyses have not led to the identification of the material responsible for the non-oxide breaks observed in plugging indicator curves. It has been concluded that more discriminating techniques are needed to correlate trace species with the observed effects.

In order to identify and determine such chemical species at low (parts per million) concentrations, unusually large samples have been used, 1 kg. X-ray methods are used for the initial examination of material after removal of sodium. Special care is taken to avoid contamination of the sample.

The basic methods for sodium removal which have been modified are liquid ammonia dissolution, vacuum distillation, and amalgamation. It was recognized that the chemical form of some, but not necessarily the same, impurity species may change during these separation procedures. Consequently all three techniques were chosen for study in order to complement each other and thus guard against loss of some species.

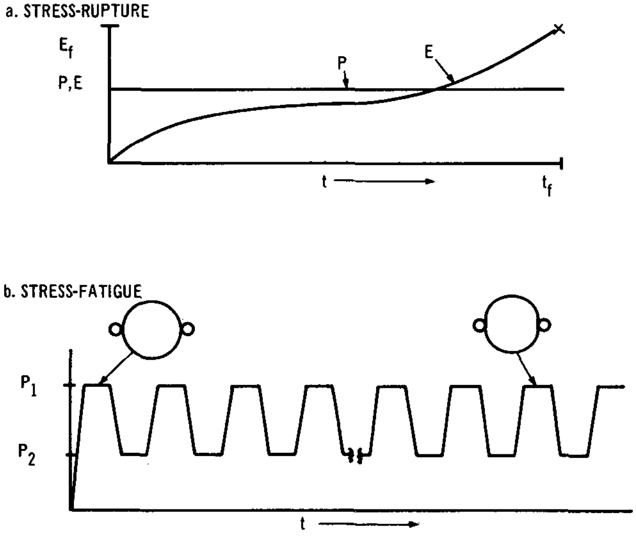

FIG. 12. Test techniques to study effects on mechanical properties

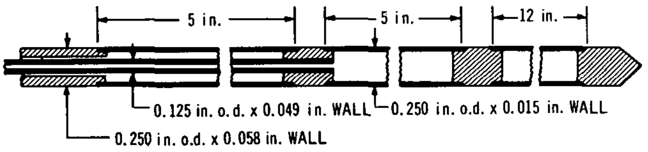

FIG. 13. Stress-rupture specimen design

In the liquid ammonia separations apparatus purified ammonia gas, condensed by means of circulating cooled acetone, dissolves the sodium sample situated on a perforated plate in the reaction vessel. The sodium solution flows to a sump while the impurities deposit on a filter. Recoveries of Fe and Ni at 1.5 ppm and Cr at .3 ppm were within 0.1 ppm for each element.

Distillation of molten sodium is carried out at 380°C (716°F) and an initial pressure of 7×10^{-7} torr. When distillation is complete, the residue is loaded into silica capillaries for X-ray analysis. A comparison of the concentration levels of several elemental impurities present in sodium before and after distillation has shown the separation to be over 80% efficient for all species tested except carbon, as shown in Table IV.

TABLE IV. RECOVERY DATA, DISTILLATION SEPARATION

Element	Sodium before Distillation (ppm)	Sodium after Distillation (ppm)
Fe	4.6 ± 0.1	0.5 ± 0.5
Ni	2.5 ± 0.1	0.5 ± 0.5
Cr	0.6 ± 0.1	0.1 ± 0.1
C	30.0 ± 5.0	15.0 ± 5.0
Ca	1.2 ± 0.2	0.1 (not detected)

REFERENCES

[1] LOCKHART, R.W., BILLURIS, G., LANE, M.R., Rpt GEAP 3725 (1962).

[2] JAECK, J.L., DUNN, E.L., STEWART, K.B., Rpt GEAP 4830 (1965). LOCKHART, R.W., BILLURIS, G., Nucl.Metall. AIME IX (1963) 207.

[3] BRUSH, E.G., Trans.Am.nucl.Soc. 8 (1965) 412.

[4] NETTLEY, P.T. et al., British Nuclear Energy Society, Conference, May 1966.

[5] COMPRELLI, F.A., HETZLER, F.J., LAURITZEN, T.A., Proc.Conf. on Fast Reactors, ANL 7120, October 1965, 366.

[6] ROWLAND, M.C., PLUMLEE, D.E., Rpt GEAP 3848 (1965) 180.

[7] HETZLER, F.J., LAURITZEN, T.A., Trans.Am.Nucl.Soc. 8 (1965) 412.

DISCUSSION

A. V. CAMPISE: I should like to ask a question in connection with the intergranular attack on cladding surfaces mentioned in your paper. Do you think that this intergranular phenomenon could be affected by the presence of He gas at the grain boundaries in highly irradiated samples?

E. L. ZEBROSKI: I know of no evidence either for or against this possibility. It is worth noting, however, that extreme cases of intergranular attack have sometimes been observed on the inner surface of irradiated fuel cladding.

K. T. CLAXTON: In view of the information given in Table III and other corrosion rate data appearing in your paper, I am somewhat doubtful about the accuracy of the exponent on the velocity term in corrosion rate equation (1). Do you have any information on the statistical significance, if any, of the difference between your conclusions regarding velocity dependence and those of Nettley, Thorley, Tyzack, etc? I am also rather sceptical about the accuracy of the exponent on the oxygen concentration term in this same equation. It strikes me as being far too optimistic.

E. L. ZEBROSKI: The statistical reliability is good but the difficulty is that one is averaging the entrance effect and a velocity effect around the perimeter of a sample. For this reason we have not taken the problem of comparing the exponent values very seriously. In the two short runs of 2000 h each carried out so far, we took the two correction terms I mentioned into account and obtained an exponent of about 0.5 for the velocity term. I think this involved a variance of 17%.

C. TYZACK: Figure 5 of your paper shows the increment of chromium in the 5 Cr-$\frac{1}{2}$Mo-$\frac{1}{2}$Ti steel on the cold leg. Does this refer to the average increment over the whole wall thickness or in a thin surface layer? If the latter is the case, what is the thickness involved?

E. L. ZEBROSKI: The X-ray fluorescence method used gives an average composition to a depth of about 12 μm below the surface. This method is used because it is convenient for surveying a large number of samples. Where necessary, confirmation can be obtained by means of microprobe traverses of sample sections.

A. W. THORLEY: I have a brief comment on the subject of nickel deposition on cold leg specimens. I notice that the data given in your paper on this subject are consistent with findings made by Babcock and Wilcox in the United States of America. Microprobe analysis carried out in the course of the Babcock and Wilcox investigations revealed nickel pick-up on the cold side of one of the loops which had run for long periods at low levels of oxygen.

I should also like to ask a question on Table IV of your paper. Is the inference in this table that element loss occurs during distillation?

E. L. ZEBROSKI: The table indicates concentrations in the distillate; chromium retention in the still bottoms was quantitative to within the accuracy of the measurement.

EFFECTS OF SODIUM ENVIRONMENT ON MECHANICAL PROPERTIES OF MATERIALS

(Session IV, Part 1)

EFFECT OF SODIUM EXPOSURE ON THE MECHANICAL PROPERTIES OF POTENTIAL FUEL JACKET ALLOYS AT 550-700°C*

F.L. YAGGEE AND E.R. GILBERT
ARGONNE NATIONAL LABORATORY,
ARGONNE, ILL.,
UNITED STATES OF AMERICA

(Presented by S. Greenberg)

Abstract

EFFECT OF SODIUM EXPOSURE ON THE MECHANICAL PROPERTIES OF POTENTIAL FUEL JACKET ALLOYS AT 550-700°C. Stainless steel, niobium-base and vanadium-base alloys have been considered as fuel jacket materials for sodium-cooled fast reactors. The popularity of stainless steel is associated with its reasonable cost and availability, whereas the potential of niobium-base alloys lies in their high-temperature strength and favourable nuclear properties. However, the need for an acceptable degree of compatibility between the jacket and the fuel has eliminated both stainless steel and niobium alloys as candidates for use with some metallic fuels. Thus vanadium-base alloys have the greatest interest of the refractory metal alloys as fuel jacket materials. They are stronger than stainless steel and are compatible with metallic fuels. They also show promise of being corrosion-resistant in low oxygen sodium.

The continuing interest in stainless steel for use with nonmetallic fuels is based on its good resistance to corrosion by impure sodium. Likewise the potential of niobium alloys for use with nonmetallic fuels is based on the possibility of achieving acceptable corrosion resistance in low oxygen sodium.

In uniaxial and biaxial creep tests stainless steel was less affected by prior sodium exposure than either vanadium-20 wt.% titanium or niobium-1 wt.% zirconium. After sodium exposure stainless steel (Type 304) exhibited a higher creep rate and a higher rupture ductility. This behaviour may be associated with decarburization. Vanadium-20 wt.% titanium exhibited a much higher creep rate after sodium exposure but no significant change in rupture ductility. This effect on creep strength decreased markedly as the sodium purity improved, being related to a visible reduction in specimen load-bearing area resulting from the formation of a brittle surface oxide layer. Niobium-1 wt.% zirconium was drastically affected by exposure to sodium containing 20 ppm oxygen resulting in a nil rupture ductility.

Bend tests in molten sodium at 300°C were conducted on Type 304 stainless steel, vanadium, vanadium-20 wt.% titanium and vanadium-15 wt.% titanium-7.5 wt.% chromium to determine the predisposition of these materials to stress corrosion cracking under conditions of rapid loading. No evidence of stress corrosion cracking was observed.

1. INTRODUCTION

The mechanical property studies of potential fuel jacket materials being reported were carried out in support of the Liquid Metal Cooled Fast Breeder Reactor Program at Argonne National Laboratory. The overall aim of this program was the development of a high temperature metallic fuel posessing all of the attributes associated with metal fuels (favorable thermal conductivity, breeding ratios, etc.) and a suitable jacket material to use with it. Toward this end parallel studies were also undertaken in the areas of fuel-jacket compati-

---

* Work performed under the auspices of the United States Atomic Energy Commission.

bility and jacket-coolant corrosion. Iron-base (stainless steel) and nickel-base alloys were found to be incompatible with the early U-Pu-Fs[1] type metallic fuels and the search for jacket materials was directed toward the refractory metals and their alloys. The potential refractory metal jacket materials were further narrowed to the alloys of chromium, niobium and vanadium largely on the strength of nuclear considerations.[1] Niobium (Nb-1w/o Zr[2]) has lost ground as a serious contender because of its unacceptable corrosion resistance to oxygen-contaminated sodium,[2] and chromium base alloys (Cr > 50 percent) present a difficult fabrication problem. In contrast the vanadium-base alloys are fabricable, they possess desirable nuclear properties and are potentially corrosion resistant to low oxygen sodium. The early work on fabricability[3] [4] and mechanical properties[5] of vanadium alloys has been substantiated and expanded.[6][7][8] Current work on the corrosion resistance of vanadium alloys is being reported at this meeting.

The two mechanical properties considered of greatest importance to fuel jacket materials are high temperature creep strength and ductility. Both exhibit a sensitivity to sodium exposure. The mechanical property studies of vanadium-base alloys are directed at the following objectives:

a) a quantitative evaluation and understanding of the effect of sodium exposure on creep strength and ductility, and

b) the development of vanadium alloys with greater creep strength and ductility consistent with the requirement for sodium corrosion resistance.

The work being reported includes data on Type 304 stainless steel, Nb-1Zr and V-20Ti. Of these V-20Ti commands the greatest interest as a fuel jacket material. Work on Type 304 stainless steel and Nb-1Zr was undertaken to provide the base line data necessary to the failure analysis of experimental fuel alloy irradiations where these materials were used as jackets. Both sheet and tube specimens have been used in the mechanical property studies. The sheet specimens are more easily available and easier to test, but the tubular specimens have a closer relationship to the actual fuel jackets.

V-Ti-Cr alloys have been developed with high temperature creep strengths superior to that of V-20Ti. Work on the effect of sodium exposure on their mechanical properties is still in progress.

2. EXPERIMENTAL EQUIPMENT AND PROCEDURE

2.1 Uniaxial Creep Tests on V-20Ti

The sheet specimen design is shown in Figure 1. The indicated specimen size was chosen for its ability to support a range of creep loads while maintaining a surface-to-volume ratio capable of detecting possible deleterious effects resulting from sodium exposure. The specimen thickness (0.04 cm) is comparable to the wall thickness of fuel

---

[1] Fs designates a collection of elements including Zr, Mo, Ru, Rh and Pd generated during nuclear fission.

[2] All alloy compositions are given in weight percent.

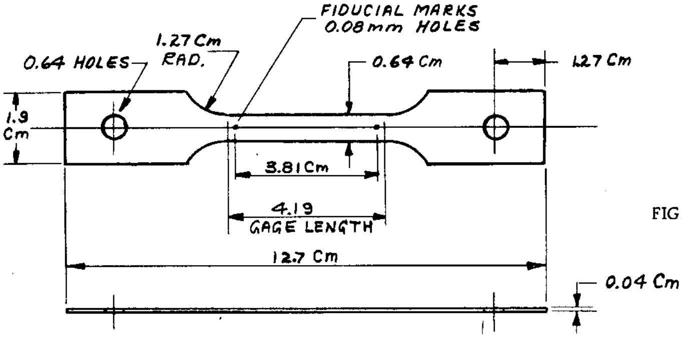

FIG. 1. Sheet specimen design

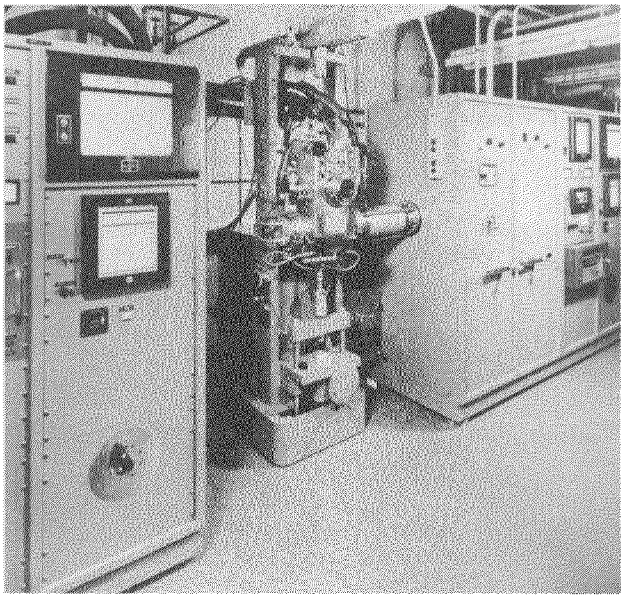

FIG. 2. Uniaxial creep testing apparatus

jackets being used in experimental fuel irradiations at Argonne National Laboratory.

The uniaxial creep tests were conducted in vacuum (4 x 10^{-7} to 5 x 10^{-6} mm Hg) at 650°C and stresses of 15 and 30 kg/mm^2. Creep tests were conducted on a conventional creep frame equipped with a vacuum tensile furnace and dead weight lever arm system for specimen loading. Strain measurements were recorded autographically in some tests with a mechanical extensometer (ASTM Class B-1) and obtained visually in other tests by using precision dial indicators to sense pull-rod displacement. In both instances the recorded specimen strain was checked against the measured strain between fiducial marks and found to be in good agreement. A typical dead weight loaded, lever arm, vacuum creep apparatus is shown in Figure 2.

Specimens were given a one-hour anneal (3 to 5 x 10^{-6} mm Hg) at 900°C and then exposed to flowing sodium at 650°C for periods of 7-21 days. Other annealed specimens were exposed to sodium under stress by a stress-relaxation loading method,[3] which takes advantage of the difference in linear thermal expansion of the stressing fixture (stainless steel) and the specimen. The resulting specimen strain after sodium exposure was 1.3 percent. Specimens exposed to sodium in the annealed condition showed no perceptible dimensional changes. Exposures were made in sodium containing 18 to 20 ppm oxygen (velocity 15 cm/sec) and 10 ppm (velocity <2 cm/sec). In each case the sodium sample was taken at temperature (650°C) at the conclusion of the exposure period and analyzed for oxygen by either the vacuum distillation or mercury amalgamation methods.

The creep data for the sodium-exposed specimens were compared with the creep data for appropriate control specimens tested under the same conditions of temperature and stress. Control specimens were given a vacuum anneal at 650°C for a period of seven days following the standard vacuum anneal of one hour at 900°C.

2.2 Biaxial Stress Creep Tests on Type 304 Stainless Steel, V-20Ti and Nb-1Zr

The tube specimen design used in the biaxial stress creep tests is shown in Figure 3. The specimen diameter ranged from 0.71 to 0.76 cm and the wall thickness ranged from 0.38 to 0.51 mm depending upon the material. For each of the three materials tested the variation in specimen diameter was about 0.3 percent and the variation in wall thickness was less than 0.1 percent. A 10 to 1 length-to-diameter ratio was maintained to avoid end effects. The gage length is defined between the reinforcing collars (about 7.6 cm) whose inside edges are machined with a smooth radius to avoid local stress raising conditions at large radial strains.

The biaxial stress creep tests were conducted in vacuum (4×10^{-7} to 1×10^{-6} mm Hg) at 550, 650 and 700°C and stresses between 25 and 31.5 kg/mm^2. The tube creep apparatus is shown in Figure 4. Specimens are stressed by an internal gas pressure (argon or helium) which is maintained constant to failure. Both the gas pressure and the temperature are continuously indicated throughout the creep test and controlled within 1 percent. A volume displacing plug is inserted into the specimen to minimize specimen damage immediately after failure by the kinetic energy of the pressurized gas. The apparatus is electronically interlocked to shut down automatically after specimen failure. The specimen diameter is measured at room temperature with a blade micrometer at periodic intervals. Several diameter measurements are taken at five points along the gage length from which the true tangential strain is calculated.

Multiple specimen lengths of V-20Ti and Nb-1Zr tubing were exposed to flowing sodium (velocity 15 cm/sec) at 650°C for seven days following the usual one hour vacuum anneal (3 to 5×10^{-6} mm Hg) at 900°C. Duplicate oxygen analyses for the sodium were 18 and 20 ppm. The tube lengths were exposed both under stress and as-annealed using a stress relaxation method similar to that described for V-20Ti sheet specimens. The longitudinal strain after sodium exposure was about 1.3 percent for V-20Ti and less than 1/2 percent for Nb-1Zr. Type 304 stainless steel specimen lengths were exposed without stress for seven days at 650°C to sodium containing 10 ppm oxygen (velocity <2 cm/sec) in the as-annealed condition. The V-20Ti and

---

[3] In service the fuel jacket experiences a relaxing thermal stress.

Nb-1Zr tubes passed inspections (eddy current and ultrasonic) for defects greater than 10 percent of the wall thickness. The Type 304 stainless-steel tubes passed a similar inspection to a 5 percent defect level.

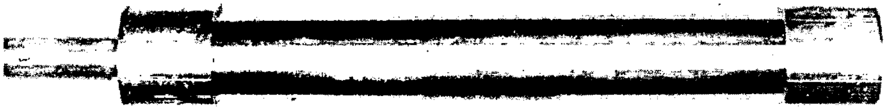

FIG.3. Tube specimen design (0.7 cm diameter × 10.2 cm long × 0.4 mm wall)

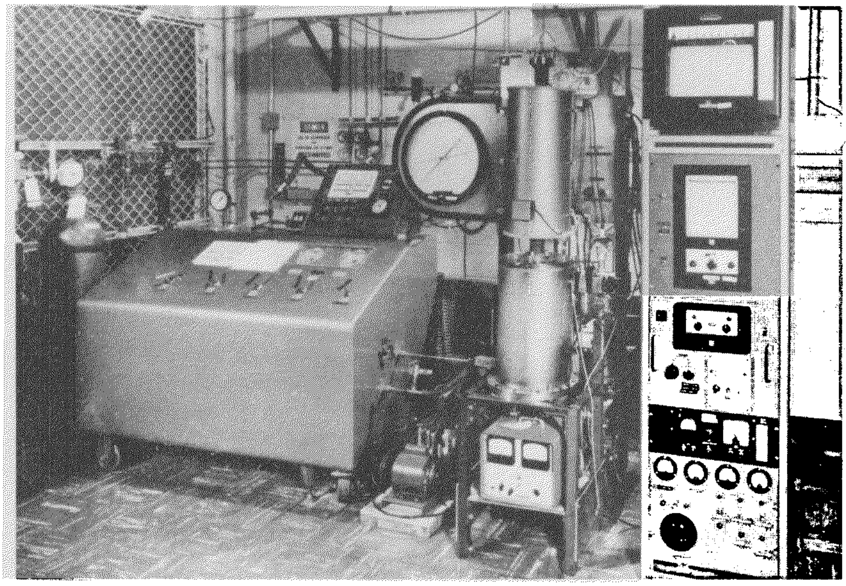

FIG.4. Biaxial creep testing apparatus

Creep data for sodium-exposed specimens were compared with creep data for appropriate control specimens tested at the same temperature and stress. Control specimens were given a vacuum anneal at 650°C for seven days following the usual vacuum anneal of one hour at 900°C.

The stainless steel specimens were creep tested at 550°C because of their relatively low creep strength above 600°C. The V-20Ti specimens were creep tested at 650°C for comparison with V-20Ti sheet specimens. The Nb-1Zr specimens were creep tested at 700°C because of difficulty in obtaining reasonable creep data at lower temperatures.

2.3 Bend Tests on Type 304 Stainless Steel, V-20Ti, V-15Ti-7.5Cr

The bend test specimens were 6.4 cm long by 1.3 cm wide and of two thicknesses (0.7 and 1.5 mm). The V-20Ti was the only 1.5-cm thick specimen used. Specimens were given a vacuum anneal before the bend test.

The bend tests were conducted in molten sodium (O_2>>20 ppm) at 300°C in accordance with the procedures outlined in report MAB-192M of the Materials Advisory Board. A 4T bend radius was used. The bent specimens were cleaned in alcohol and visually inspected for evidence of stress corrosion cracking.

3. RESULTS

3.1 Creep of V-20Ti Sheet Specimens

The calculated stress-time curve for the stress relaxation loading of V-20Ti sheet specimens during exposure to sodium is shown in Figure 5a. The applied stress begins at a value that is above the 650°C yield stress for this alloy then relaxes with time as specimen deformation occurs. The corresponding strain-time curve is shown in Figure 5b. The specimen strain approaches a limiting value of 1.3 percent during the period of its exposure under stress in sodium. It should be noted that this limiting value of strain is approached very quickly.

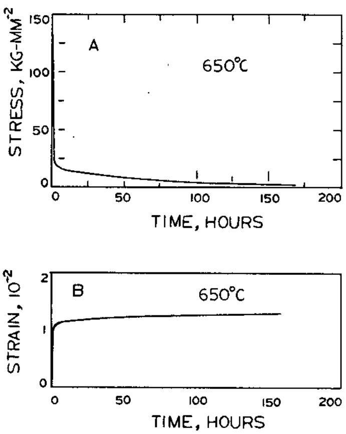

FIG. 5. Stress relaxation of V-20Ti sheet specimen at650°C: (a) Stress versus time; (b) Strain versus time

The effect of specimen exposure to high oxygen sodium (20 ppm O_2) on the creep strength of V-20Ti sheet at 650°C and 15 kg/mm^2 stress is illustrated in Figure 6. A similar comparison is made in Figure 7 for specimens exposed to sodium under stress and subsequently creep tested at 650°C and 30 kg/mm^2 stress. It is evident that the combination of stress with sodium exposure degrades the creep resistance of V-20Ti sheet more than sodium exposure alone.

The physical effect of sodium exposure on V-20Ti sheet (20 ppm O_2) at 650°C under stress is illustrated in Figure 8. The severe surface cracking in the vicinity of the fracture (Figure 8a) extends over the entire specimen gage length. Surface layer thickness and crack depth can be seen in Figure 8b. Formation of the surface layer decreases the load-bearing cross-section of the specimen resulting in the observed decrease in creep resistance shown in Figure 6.

Creep curves for V-20Ti tested at 650°C and 15 kg/mm^2 stress after exposure to 650°C sodium containing 10 ppm oxygen are given in

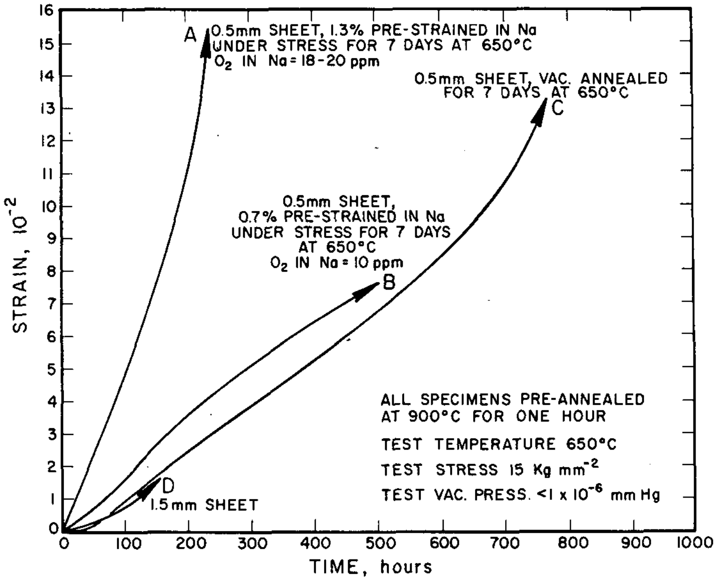

FIG. 6. Creep of V-20Ti sheet specimens at 650°C and 15 kg/mm^2 stress after exposure in sodium (20 ppm O_2)

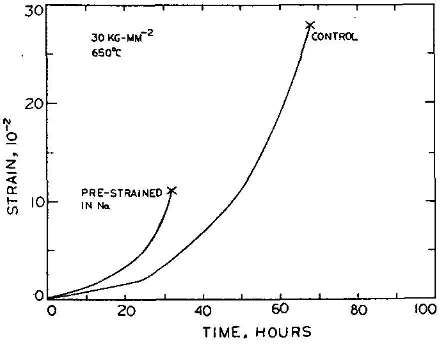

FIG. 7. Creep of V-20Ti sheet specimens at 650°C and 30 kg/mm^2 stress after exposure in sodium (20 ppm O_2)

Figure 9. The specimens were exposed to sodium under stress. The difference between the control and specimens exposed to sodium for two different times is not as dramatic as the difference shown in Figure 6 for specimens exposed to sodium containing 20 ppm oxygen. The degrading influence on the creep resistance of exposure to high oxygen containing sodium is again illustrated in Figure 10 for specimens tested at 650°C and 30 kg/mm^2 stress.

3.2 Creep of Type 304 Stainless Steel Tubes

Pre-exposing Type 304 stainless steel for seven days at 650°C to sodium containing 10 ppm oxygen has the effect of increasing ductility and decreasing the creep resistance. This is shown in Figure 11 for tube specimens creep tested at 550°C and stresses of 25.5 kg/mm^2

and 28.1 kg/mm^2, respectively. Both control specimens exhibited a rupture strain slightly more than 12 percent. A typical rupture in stainless steel tube specimens is shown in Figure 12. After sodium exposure the rupture ductility is increased approximately 2 1/2 times in specimens creep tested at 28.1 kg/mm^2 stress.

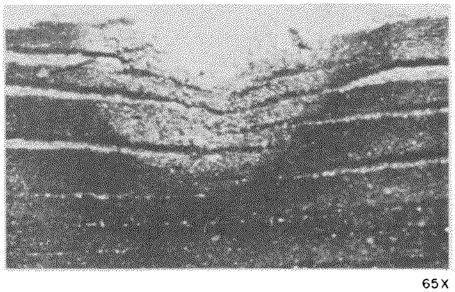

a. SURFACE CRACKS IN CASE IN VICINITY OF FRACTURE AFTER 0.11 STRAIN

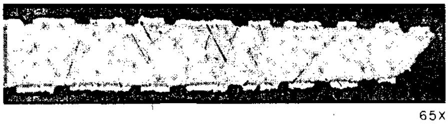

b. SPECIMEN THICKNESS PROFILE SHOWING CRACK DEPTH

FIG. 8. Surface oxide formation on V-20 Ti sheet specimen during sodium exposure (20 ppm O_2)

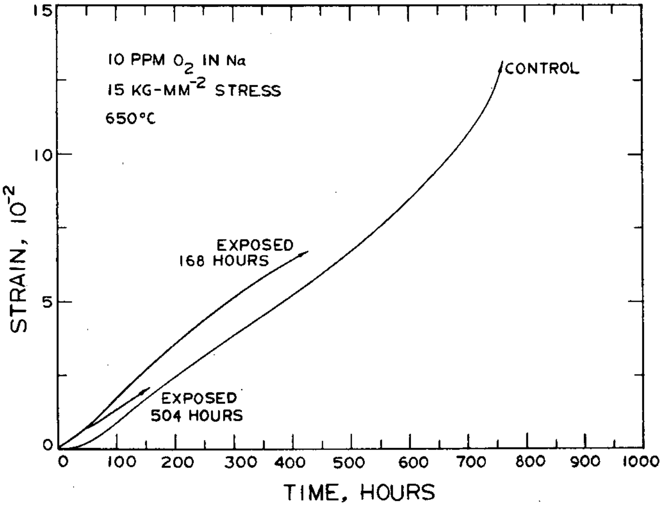

FIG. 9. Creep of V-20 Ti sheet specimens at 650°C and 15 kg/mm^2 stress after exposure in sodium (10 ppm O_2)

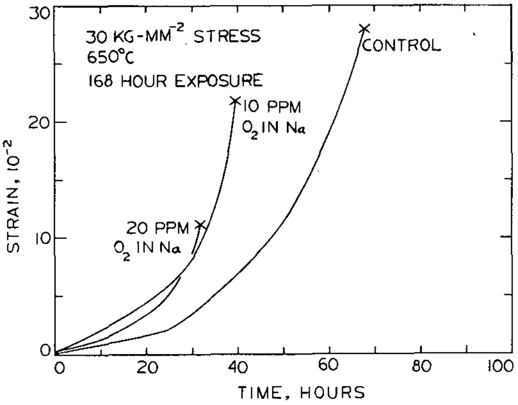

FIG.10. Effect of sodium purity on creep of V-20 Ti sheet specimens at 650°C and 30 kg/mm^2 stress (20 versus 10 ppm O$_2$)

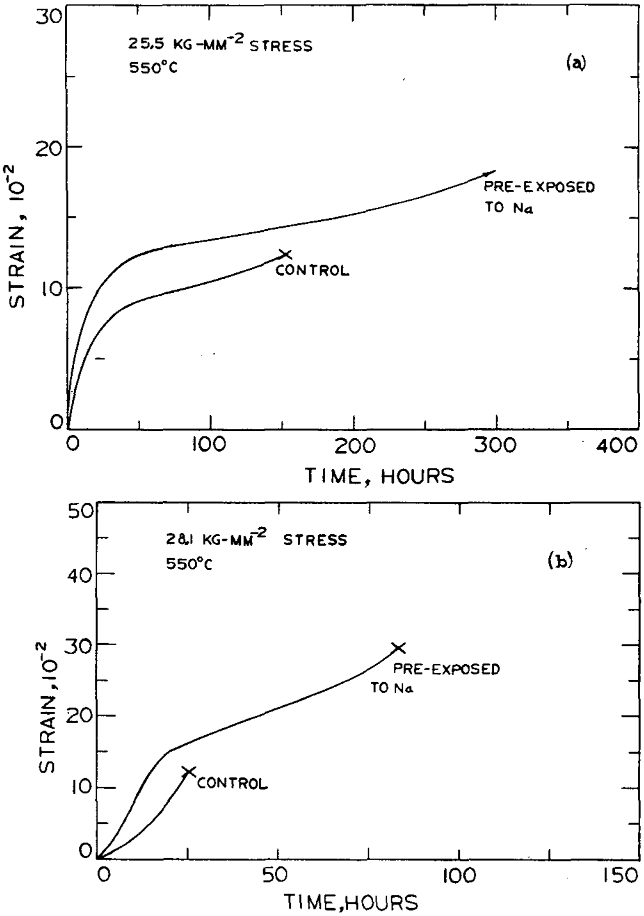

FIG.11. Creep of stainless-steel (Type 304) tube specimens at 550°C after exposure in sodium (10 ppm O$_2$): (a) 25.5 kg/mm^2 stress; (b) 28.1 kg/mm^2 stress

3.3 Creep of V-20Ti Tubes

The rupture strain of V-20Ti tube specimens exposed seven days at 650°C in sodium containing 20 ppm oxygen increases approximately 30 percent and the time to failure decreases as shown in Figure 13.

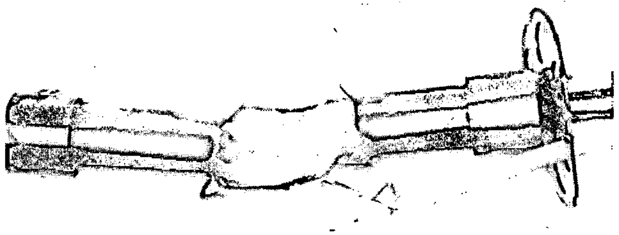

FIG. 12. Ruptured stainless-steel (Type 304) tube specimen tested at 550°C and 28.1 kg/mm^2 stress

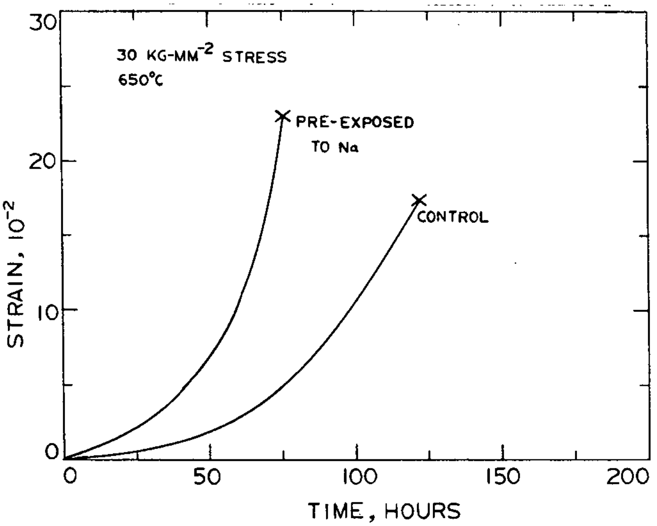

FIG. 13. Creep of V-20 Ti tube specimens at 650°C and 30 kg/mm^2 stress after exposure in sodium (20 ppm O_2)

Specimens were creep tested at 650°C and 30 kg/mm^2 stress. This creep behavior compares with that observed for V-20Ti sheet specimens under similar sodium exposure and creep test conditions. Ruptured V-20Ti tube specimens are shown in Figure 14. The short exposure (seven days) at 650°C to sodium containing 20 ppm oxygen results in the formation of a brittle surface oxide layer as shown in Figure 15. This surface oxide layer contains numerous cracks.

3.4 Creep of Nb-1Zr

The Nb-1Zr tube specimens exhibited a greater sensitivity to stress and sodium exposure than either stainless steel (Type 304) or V-20Ti. The creep curves for Nb-1Zr specimens tested at 700°C and stresses of 30 kg/mm^2 and 31.5 kg/mm^2 are shown in Figure 16. Control specimens tested at 700°C and stresses of 30 kg/mm^2 and 31.5 kg/mm^2

showed rupture strains of 7 percent and 2.7 percent, respectively. Specimens pre-exposed for seven days at 650°C to sodium containing 20 ppm oxygen (unstressed) ruptured in less than two hours at strains of 0.1 percent or less.

a. CONTROL SPECIMEN (0.16 RUPTURE STRAIN--119 hr RUPTURE TIME)

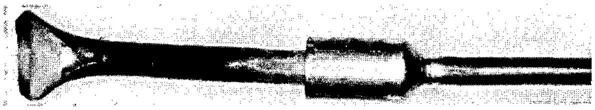

b. EXPOSED TO SODIUM (20 ppm O_2) FOR 7 days AT 650°C (0.24 RUPTURE STRAIN--74 hr RUPTURE TIME)

FIG. 14. Ruptured V-20 Ti tube specimens tested at 650°C and 30 kg/mm² stress

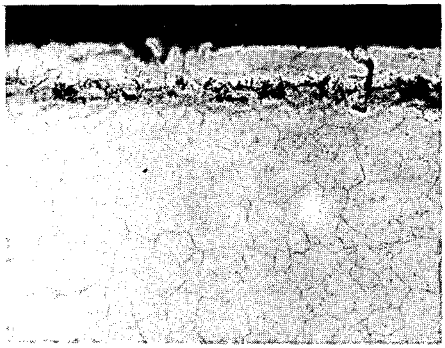

240 x

FIG. 15. Surface oxide formation on V-20 Ti tube specimen during sodium exposure (20 ppm O_2)

Ruptured Nb-1Zr tube specimens are shown in Figures 17 and 18. The sodium exposed specimen creep tested at a stress of 30 kg/mm² failed in 1.5 hours by crack propagation as illustrated in Figure 17. A similarly exposed specimen tested at a stress of 31.5 kg/mm² failed catastrophically in 1.7 hours as shown in Figure 18. The surface oxide layer formed during the sodium exposure can be seen in Figure 19. This layer has a heavily textured appearance and numerous cracks.

3.5 Bend Tests in Sodium

Type 304 stainless steel, V-20Ti and V-15Ti-7.5Cr showed no evidence of stress corrosion cracking when bent over a 4T radius in sodium at 300°C. The final bend angles were between 90 and 140 degrees.

4. DISCUSSION

The results of this study show that exposure of V-20Ti, Nb-1Zr, and Type 304 stainless steel to sodium containing greater than 10 ppm O_2 has a significant effect on the subsequent mechanical properties. The

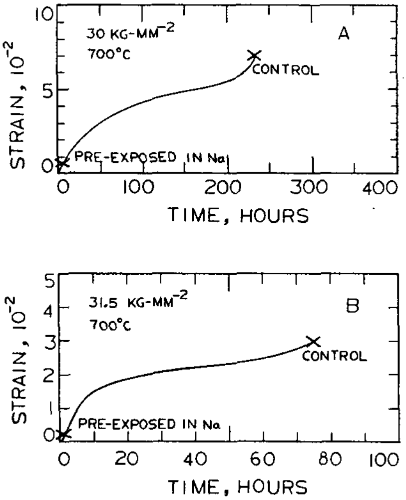

FIG. 16. Creep of Nb-1Zr tube specimens at 700°C and 30 and 31.5 kg/mm^2 stress

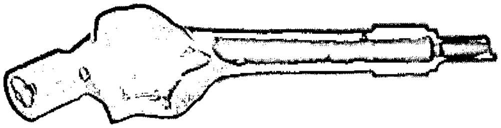

a. CONTROL SPECIMEN (0.07 RUPTURE STRAIN--231 hr RUPTURE TIME)

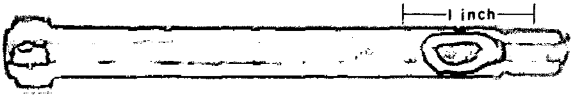

b. EXPOSED TO SODIUM (20 ppm O_2) FOR 7 days AT 650°C (0.001 RUPTURE STRAIN--1.5 hr RUPTURE TIME)

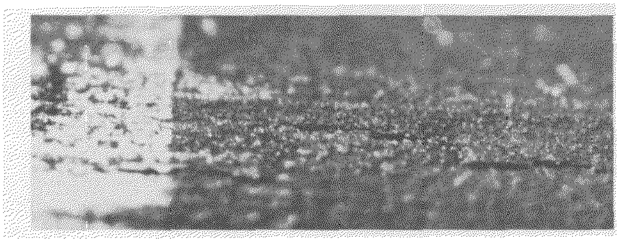

c. FAILURE BY CRACK PROPAGATION

FIG. 17. Ruptured Nb-1Zr tube specimens tested at 700°C and 30 kg/mm^2 stress

creep results of each alloy are affected differently. V-20Ti has a higher creep rate, shorter rupture time, but essentially unchanged ductility. Nb-1Zr is very severely embrittled. Type 304 stainless steel has a higher creep rate, greater ductility, and a longer rupture time. These results are reproducible on all three alloys.

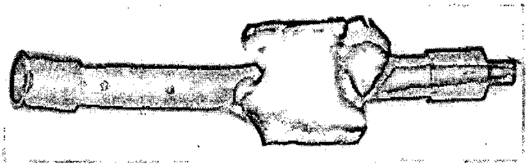

a. CONTROL SPECIMEN (0.027 RUPTURE STRAIN--75.2 hr RUPTURE TIME)

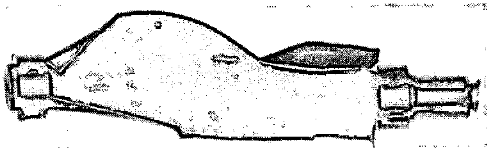

b. EXPOSED TO SODIUM (20 ppm O_2) FOR 7 days AT 650°C (RUPTURE STRAIN NOT MEASURED--1.7 hr RUPTURE TIME)

FIG. 18. Ruptured Nb-1Zr tube specimens tested at 700°C and 31.5 kg/mm^2 stress

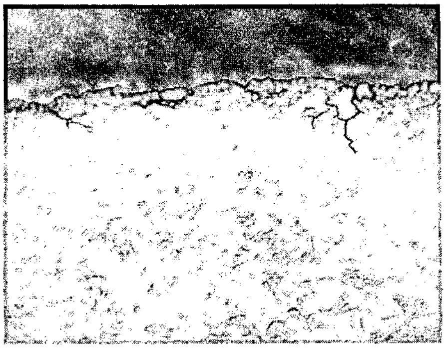

240 x

FIG. 19. Surface oxide formation on Nb-1Zr tube specimen during sodium exposure (20 ppm O_2)

These results can be explained from the creep data presented, the tensile tests on V-20Ti, and metallography. Both V-20Ti and Nb-1Zr getter oxygen from the sodium. The oxygen forms a hardened case about 30 microns thick, which is brittle and cracks when strained. The ductile core in V-20Ti is able to resist the propagation of cracks and the total elongation is unaffected; however, the load-bearing area is reduced resulting in a high effective stress and an increased creep rate. The Nb-1Zr core is unable to resist crack propagation and fractures at very low strain. The results on Type 304 stainless steel are explained on the basis of decarburization during sodium exposure. Decarburization results in greater ductility but less creep resistance. Even though the creep rate is higher for exposed specimens, the increased ductility permits the specimens to sustain stress for a longer time before rupture.

Short time tensile tests at 650°C were conducted on control-and sodium-exposed V-20Ti specimens to supplement the creep tests. Exposure to sodium containing 20 ppm O_2 resulted in a negligible change in yield stress from 34.6 to 33.5 kg/mm^2; however, the ultimate tensile stress was decreased from 46.3 to 42.3 kg/mm^2. The 0.002 offset strain is too low to cause extensive crack propagation in the hardened case and therefore an appreciable reduction in yield stress was not observed. The ultimate tensile stress is measured at 0.1 to 0.15 strain where extensive crack propagation has resulted. Very little change was observed in the yield stress (35 kg/mm^2) and ultimate tensile stress (45.7 kg/mm^2) of V-20Ti specimens exposed to sodium (10 ppm O_2) as compared to the control tests. The 10 percent decrease in the ultimate tensile stress (exposure in sodium containing 20 ppm O_2) is consistent with the reduction of load-bearing area observed by metallography. The relationship between strain rate and stress for control specimens was established to be exponential ($\dot{\varepsilon} \propto e^{0.23\sigma}$ where σ is expressed in kg/mm^2). If the stress in this exponential relationship is changed by 10 percent, then the calculated increase in creep rate is in agreement with the experimental observations.

5. CONCLUSIONS

The experimental data presented tend to support the following conclusions:

a) The application of stress during sodium exposure has a large influence on the mechanical properties of V-20Ti.

b) V-20Ti, Nb-1Zr and Type 304 stainless steel are affected differently by exposure to sodium. V-20Ti exhibits a higher creep rate and a shorter rupture life, but an essentially unchanged ductility. Nb-1Zr is severely embrittled. Type 304 stainless steel is more ductile, creeps at a faster rate and has a longer rupture life.

c) V-20Ti exhibits a much higher resistance to crack propagation than Nb-1Zr.

d) V-20Ti and Nb-1Zr form a brittle oxide case during exposure to oxygen contaminated sodium. This case cracks during specimen strain.

e) Sheet and tube specimens show the same general creep behavior after exposure to oxygen-contaminated sodium.

6. ACKNOWLEDGEMENT

The authors gratefully acknowledge the assistance of the following Argonne National Laboratory personnel: the Foundry and Fabrication Group in providing the alloys and fabricated shapes; the Engineering Corrosion Group in conducting the specimen exposures to low oxygen sodium and the sodium analyses and the Reactor Engineering Sodium Group in conducting the specimen exposures to high oxygen sodium. Sincere appreciation is also expressed to J.W. Styles and A.R. Brown for conducting the mechanical property tests and to R.H. Gebner for the metallography.

REFERENCES

(1) OKRENT, D., Nuclear physics considerations in large fast reactors, Power Reactor Technology 7 (2) 128-133 (1964)

(2) LEVIN, H.A. and GREENBERG, S., An exploratory study of the behavior of niobium and vanadium base alloys in oxygen contaminated sodium, USAEC Rep. ANL-6982 (to be published)

(3) ROSTOKER, W., McPHERSON, D.J. and HANSEN, M., Exploration of vanadium base alloys, U.S. Rep. WADC-TR-52-145, Part 2, p. 25

(4) YAMAMOTO, A.S. and ROSTOKER, W., Exploration of vanadium base alloys, U.S. Rep. WADC-TR-54-312

(5) SMITH, K.F. and VAN THYNE, R.J., Selected properties of vanadium alloys for reactor application, USAEC Rep. ANL-5661 (1957)

(6) BURT, W.R., Jr., KRAMER, W.C., McGOWAN, R.D., KARASEK, F.J., and MAYFIELD, R.M., Consolidation and fabrication techniques for V-20w/oTi, USAEC Rep. ANL-6928 (1965)

(7) BURT, W.R., Jr., KRAMER, W.C., KARASEK, F.J., and MAYFIELD, R.M., Improvements in consolidation and fabrication techniques for V-20w/oTi, USAEC Rep. ANL-7127 (1966)

(8) KRAMER, W.C., BURT, W.R., Jr., KARASEK, F.J., and MAYFIELD, R.M., Vanadium alloy screening studies and fabrication of V-15w/oTi-7.5w/oCr tubing for nuclear fuel cladding, USAEC Rep. ANL-7206 (to be published)

DISCUSSION[1]

A. G. IOLTUKHOVSKY: I was particularly interested in the tests carried out on tube samples under pressure and I should like to ask a few questions on this subject. Were the samples tested completely independent or were they associated with a gas system?

F. L. YAGGEE: The tube specimens tested under biaxial stress were physically connected to a 5-litre supply of high-pressure gas throughout the test. The relative volumes of the specimen and the high-pressure gas supply were chosen in such a way as to enable the specimen to strain to rupture without affecting the total pressure in the system.

A. G. IOLTUKHOVSKY: At what intervals during the sodium tests were the samples removed for the diameter and length measurements needed to establish creep curves?

---

[1] Replies supplied in writing by F. L. Yaggee.

F. L. YAGGEE: Creep tests were not conducted in molten sodium. What we did was to subject the specimens to a longitudinal stress during sodium exposure before creep-testing them in a vacuum environment. After sodium exposure the specimens were cleaned up. The longitudinal stress was applied to the specimens during sodium exposure by making use of the difference in thermal expansion between a stainless-steel fixture and the specimen material. During the early stages of creep under biaxial stress, specimen diameter measurements were made at approximately 2-, 4-, 6- and 10-h intervals. After steady-state creep had been established, diameter measurements were extended to 30-, 60- and 100-h intervals. The number and spacing of measurements is based on the progress of the creep test.

A. G. IOLTUKHOVSKY: Was tertiary creep observed in these investigations?

F. L. YAGGEE: Tertiary creep was not observed at all stresses. For example, it was not observed at the 30 kg/mm^2 stress in tubular specimens. At stresses of 15 and 20 kg/mm^2 it was usually of short duration and the tertiary strain-to-rupture was often low.

A. G. IOLTUKHOVSKY: Was any increase observed in the absorption of impurities (C, O, H, N) from the sodium when testing refractory metals and their alloys under stress?

F. L. YAGGEE: An increase in the interstitial impurities (C, O, H, N) was noticed as a result of sodium exposure. The amount of this increase was dependent on the oxygen content of the sodium.

650°C SODIUM FREE-SURFACE, STRESS AND WEAR EFFECTS ON REACTOR-COMPONENT METALS*

F.A. SMITH, E.S. SOWA, E.L. KIMONT
AND C.R. SUTTON
REACTOR ENGINEERING DIVISION,
ARGONNE NATIONAL LABORATORY,
ARGONNE, ILL.,
UNITED STATES OF AMERICA

Abstract

650°C SODIUM FREE-SURFACE, STRESS AND WEAR EFFECTS ON REACTOR-COMPONENT METALS. Reactor-component materials, mainly 304 SS shafts, piping and bellows, as well as bearings made of various materials, have been exposed to the 1200-1500°F sodium environment of interest for future fast reactors. This paper presents the data and describes the test apparatus. These preliminary tests show that at these sodium temperatures certain properties of structural materials behave in a significantly more complex manner than they do in the 900°F sodium environment of present fast-breeder reactors.

Severe sensitization of the 304 SS, as indicated by a modified Strauss test, shows extensive carbide precipitation in the grain boundaries. This is confirmed by changes in microstructure, increased electrical resistivity and microhardness, and reduced tensile strength, fatigue strength, and reduced impact resistance. In some cases, evidence has been found of sodium-induced absorption into grain boundaries of the structural material – a complex phenomenon related to temperature, stress, and chemical reactivity effects of surface adsorption. A nitride surface layer, which may adversely affect long-time metal strength but might also discourage intergranular attack, has also been found.

Evidence of "bath line" attack on Type 304 SS was noted in a shaft in the region where the shaft penetrated the free surface between 1200°F sodium and an inert-gas cover blanket. The existence of this effect at the sodium surface seems consistent with previously unexplained reactor-component failures at lower temperatures. Related effects at lower temperatures but for longer exposures are being investigated, as are the influences of complex environments and other alloys.

Studies of the mechanical properties of a bellows that failed in 1200°F sodium vapour indicate crack propagation and failure as functions of temperature range and applied stress.

The wear characteristics of bearing materials and their satisfactory performance in a 1200°F sodium environment are related both to the environment (loading, temperature, sliding velocity) and to the physical characteristics of the material, which determine the response of the material to the imposed conditions. Properties such as hardness, coefficient of friction, and modulus of elasticity are significant. The relative effects of these properties have been explored in preliminary screening tests in 1200°F inert gas, and will be followed by tests in sodium at the same temperature.

INTRODUCTION

Recent references [1-2] indicate the need to obtain more information of an engineering nature directed toward the use of 304 SS in 650°C sodium. The data contained in this report should be considered as complementary to other current US research in this field directed toward sodium-cooled fast reactors [3-6]. This paper shall not attempt to interpret our results, as, perhaps, related to the various programs referenced above.

---

* Work performed under the auspices of the United States Atomic Energy Commission

Once 304 SS was established as a reference material, it was very appropriate to consider a limited number of test devices and tests which would mock up engineering conditions expected in 650°C sodium. For the tests conducted, the data presented here provide a new insight as to sodium environmental conditions affecting engineering geometries without the presence of irradiation effects. The effects of irradiation on these specific engineering configurations of materials, in detail, may become an important part of the experimental work related to any fast reactor program of temperatures higher than EBR-II or FERMI.

Our work is presented, not as a guide to 650°C sodium reactor materials choice, but as an attempt to comply with the spirit of this meeting in the interchange of current fast reactor materials work.

CONCLUSION

For expediency we will state our conclusion before presentation of the data. Our conclusions are:

a. The analysis of a bellows failure in 650°C sodium gives evidence that, under specific but incompletely determined conditions of environment, the deterioration of the sodium side of the bellows must be attributed to the interaction with, or the infusion of, sodium at the grain boundaries.

b. The analysis of a section of pipe removed from a high-temperature sodium system, with an operating history over a range of temperatures, indicates surface effects on the sodium side of the pipe which are not consistent with surface effects noted on "new" tubular products of the same alloy and exposed to the same environment. This inconsistency of empirical data indicates that the full effects of time, temperature, and stress on the physicochemical mechanics [7] of these systems need further study.

BEARINGS: SLOW SPEED, ATMOSPHERIC EFFECTS TO INCLUDE SODIUM

Low-speed bearing surfaces will have to operate in a 650°C sodium atmosphere when applied to reactor control rod drives or fuel handling mechanisms. To evaluate the principal parameters of 650°C sodium low speed bearing application, a modified Falex wear tester was constructed. This device is shown in Fig. 1. Modifications to a conventional Falex wear tester provide for 650°C sodium atmosphere testing of a conventional Falex test V-block and shaft and yet retain the ability to record wear as small as 4.57×10^{-4} mm/division of chart record.

Consideration has been made of the basic equation for adhesive wear [8]. And consideration has been taken of a fluid, such as sodium, and the dependence of its ability to influence the boundary lubrication between contact surfaces.

The single penetration model [8] of lubrication relates the frictional coefficients for the lubricated and unlubricated cases. And therefore the evaluation of materials may be made most effective by comparison of wear rates and frictional coefficients under inert gas and sodium respectively. One of the factors that serves to complicate the classical behavior of bearings is the ultimate effect of the environment, sodium, upon the properties of the bearing materials.

Preliminary operation of the modified Falex tester, was conducted to determine the ability of the device to indicate measured wear using a carbon steel shaft rotating between blocks of 304 SS. Tests were conducted at room temperature with oil and water as the lubricants.

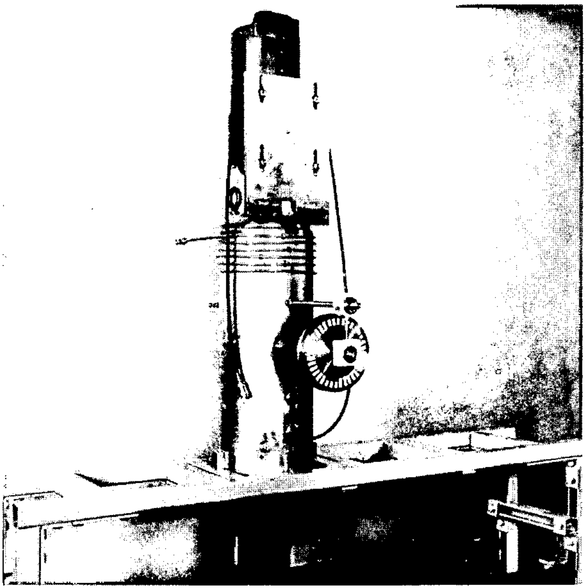

FIG. 1. Modified Falex wear test fixture

Results of these preliminary tests indicate the success of the modified wear tester to indicate accurately the small changes in wear for which the conventional Falex tester is designed.

A carbon steel shaft and 304 V-blocks were tested in argon gas at 650°C, loaded to 70 kg/cm^2, and a rotating velocity of 239 cm/min resulted in only 60mm of movement before galling terminated the test. Next, in argon at 650°C the load was decreased to 19.35 kg/cm^2, rotating velocity was decreased to 59.5 cm/min and these conditions resulted in a shaft movement of 660 cm before galling terminated the test.

These tests indicated the need to choose harder, more wear-resistant materials before start of initial sodium atmosphere testing. An initial wear resistant material couple consisted of a Haynes Stellite #19 "V"-block and a Carboloy 78B (83% WC, 8% TiC, 9% Co) test shaft. Test conditions were 650°C argon, 46.4 kg/cm^2, a sliding velocity of 65.5 cm/min. The test was arbitrarily concluded after 14 hours. During this time the measured wear was 0.406 mm entirely in the surface of the stellite blocks. Seizing and galling were entirely absent.

Testing of these and other metal pairs in sodium is to follow in the near future.

Even without benefit of sodium testing data, the high attrition of 304 SS and carbon steel at high temperature suggests that these materials are not suitable for use in bearing materials even for a low speed, relatively low load application. Concentration of tests on other materials is an indicated direction for future work.

ROD; MECHANICAL PROPERTIES AND MICROSTRUCTURE, SHORT TIME, 650°C SODIUM AND SODIUM VAPOR

A test fixture (Fig. 2) developed to measure "self welding" forces in 650°C sodium features a 16-mm OD 304 SS rod to transmit a static load to metal pairs. The results of self-welding studies are not yet reported.

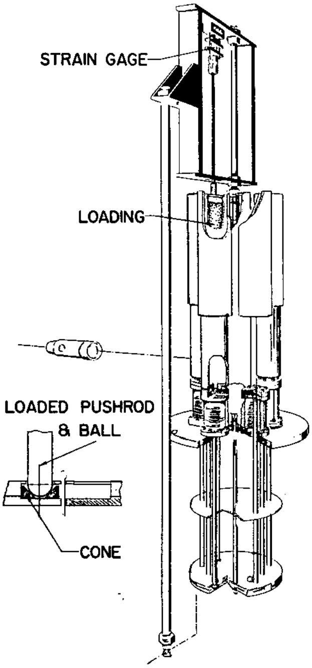

FIG. 2. Self-welding test fixture

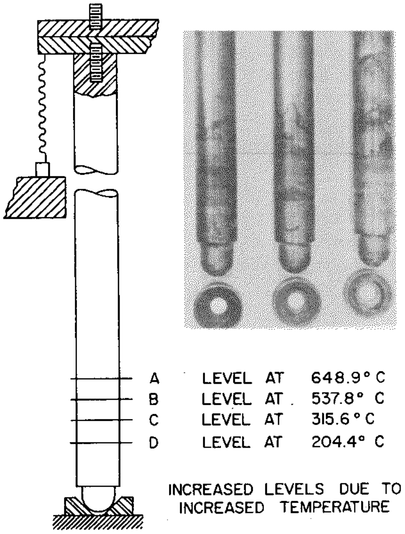

FIG. 3. "Bath Line" effect

However, a macro examination of the rods used to transmit the various loads indicated a surface effect on these rods at the "bath line" (Fig. 3) of sodium at 650°C.

The sodium exposure leading to the above "bath line" effect was relatively short, 856 hours. It should be emphasized that in previous engineering tests related to a number of EBR-I (350°C) and EBR-II (510°C) components, evidence of "bath line" corrosion was not observed.

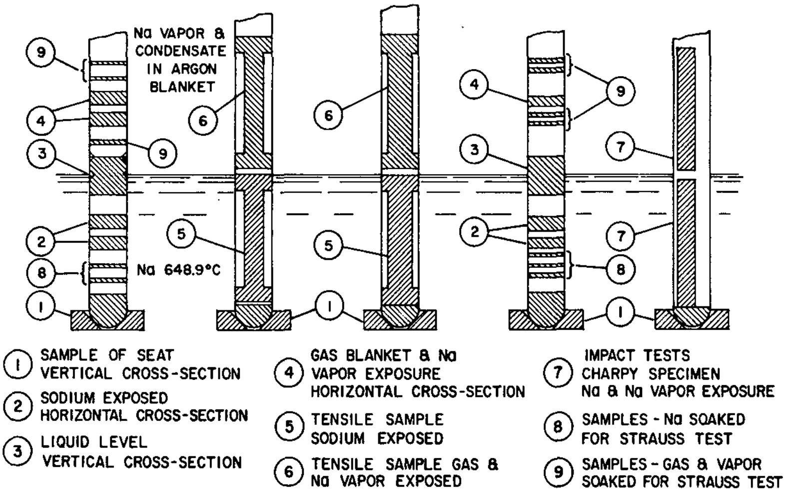

FIG.4. Schematic location of metallurgical specimens

In order to evaluate the nature and importance of the observed "bath line" effect, the rods were systematically identified and fabricated into specimens for studies of mechanical and metallurgical properties. Fig. 4 illustrates the volume of the rod and the position in the environment from which various metallurgical specimens were obtained.

These specimens were then machined into appropriate configurations to conduct measurements and observations of hardness, impact, tensile strength and microstructure in general accord with ASTM standards.

Of the tests conducted, hardness tests associated with the surface effects of sodium exposure have produced the most interesting data. Hardness tests, Rockwell "C" on the OD surface only, and superficial tests were conducted. The superficial tests were made on the curved surface OD and a machined flat 0.25 mm below the surface.

Results of Rockwell "C", 150 kg load, test are shown in Fig. 5. It can be noted that for the Rockwell "C" scale the hardness of the rod decreases from a nominal hardness no. of 24.5 to 15.2 with only a slight change, reduction, at the "bath line".

Results of superficial hardness tests are described in Fig. 6. These hardness measurements indicate that the greatest change in hardness takes place at the liquid level with a general reduction of surface hardness and a wide scatter of data.

Removal of 0.25 mm of surface of the rod results in the data of Fig. 7. Measurements indicate a persistent reduction in hardness and that the scatter of data is reduced from that observed on surface measurements.

The typical rod microstructure, associated with the hardness measurements, is shown in Fig. 8. These photos are etched and heat tinted [9].

The nonuniform surface indicated in the micro photo, resulting from effects of sodium and temperature, explain the wide scatter as measured in superficial hardness data.

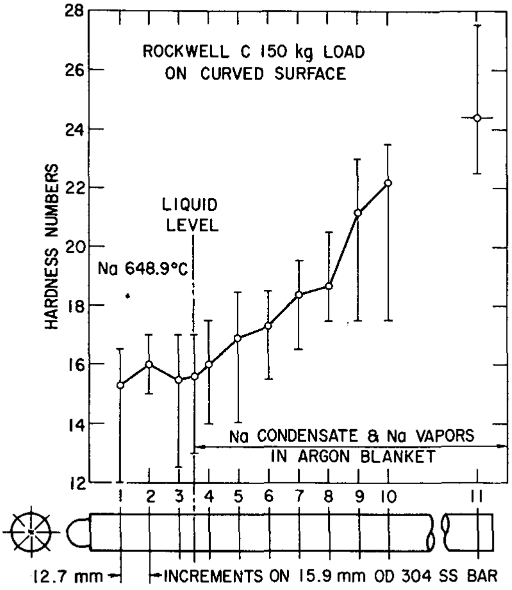

FIG. 5. Rod-surface vertical hardness traverse

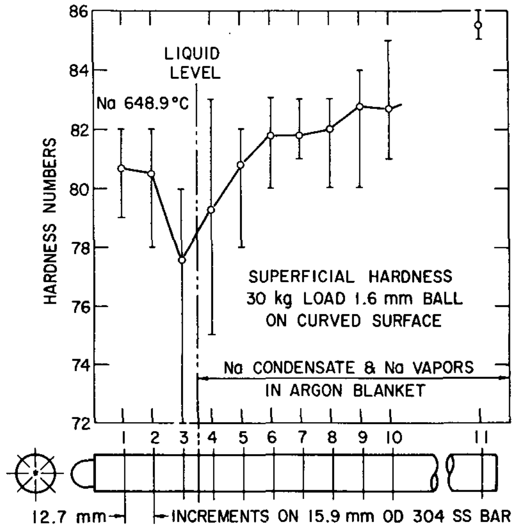

FIG. 6. Rod-surface superficial vertical hardness traverse

In addition to hardness tests, impact and tensile tests were conducted. The data from these tests do not indicate, for the time of sodium exposure chosen, measurable differences in properties to warrant a detailed description of the results at this time.

PIPE: CHEMICAL AND METALLURGICAL ANALYSIS, LONG TIME, 870°C-300°C, SODIUM

An engineering 304 SS pump test loop of 50-mm pipe size was built and operated from January 1958 as a part of EBR-II development [10]. This system was slowly brought to 600°C in 40°C increments and, then, in 20°C increments reached 808°C where it operated without reducing the temperature below 650°C for a significant period of time.

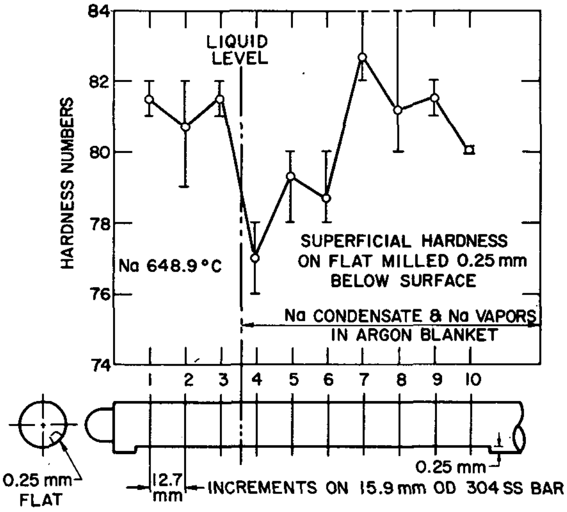

FIG. 7. Rod superficial vertical hardness traverse — 0.25 mm below surface

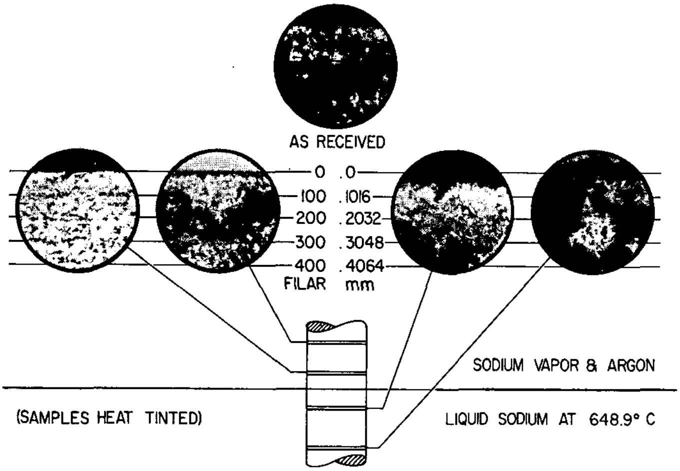

FIG. 8. Rod microstructure

This system is described schematically in Fig. 9. Of considerable interest to the subject of this paper is that six 50-mm pipe size bellows seal expansion joints accommodate the thermal expansion of the system. The system is in operation without failure of the relatively thin pump duct and stressed bellows assemblies.

The recent interest in 650°C effects of sodium, on especially 304 SS, has led to the completion of a report [11] describing the chemical composition and the metallurgical nature of a 150-mm length of pipe physically removed from the loop. A 150-mm length of as received pipe from the same heat was also made available for study.

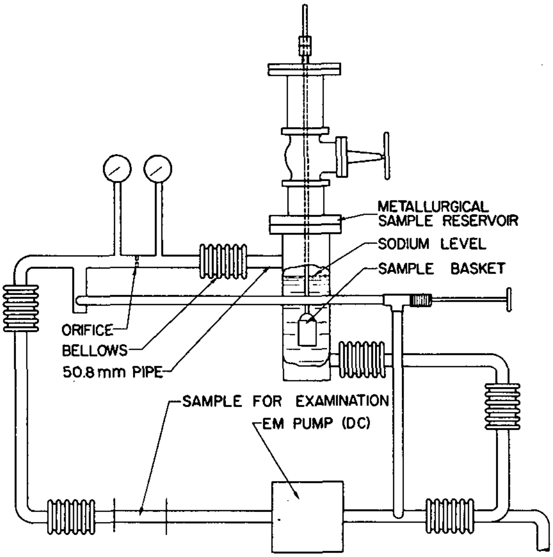

FIG. 9. Schematic of pump test loop

The results of chemical analysis, for 15 elements, of the exposed and unexposed pipe were compared. Except for nitrogen, and possibly sodium, no marked change in chemical composition occurred. Nitrogen of the OD of the pipe (air side) increased from 0.06 to 0.14 percent; the ID (sodium side) increased from 0.06 to 0.24 percent. In addition no carburization occurred during this exposure to sodium.

The yield strength of the sodium-exposed sample was lower and the tensile strength and elongation were slightly lower than those of the "as received" pipe sample. The tensile strength of the sodium-exposed sample was above the minimum values specified by ASTM. Standard flattening tests indicated flattening without cracking. However, a reverse flattening test produced some 0.1-mm cracks which appear to be associated with the nitride layer of the sodium side of the pipe. Metallographic inspection indicates a typical sensitized austenitic structure normally associated with this temperature of operation.

TABLE I. ENGINEERING LOOP SODIUM CHEMISTRY

No.	Loop Operating Condition	Al	Cu	Fe	Ni	Cr
0	As received sodium	8	2	2	2	-
1	Before Na drained to dump tank	40-24	750	15	8	-
2	Dump tank Na sample	2	3	40	-	-
3	Loop sample after dumping	3	4	40	-	-
4	Loop sample after operation	25	100	16	4	-

Prior to pipe sample removal from the engineering loop several samples of sodium were taken for spectrochemical analysis. The results of this work are presented in Table I.

The sample #1 contains an increase in all elements. The increase in aluminum and copper is detected as the probable solubility in sodium of these trace elements as contained in stainless steel. And finally the slight accumulation of Fe and Ni found in the sodium appears to confirm the lack of measured values for depletion of Fe and Ni as measured by chemical analysis of the pipe by other methods. A reasonable "mass balance" appears to be achieved.

BELLOWS: METALLURGICAL ANALYSIS, SHORT TIME, 650°C SODIUM VAPOR, AND AIR

A bellows seal provides a vacuum-tight closure for a solid rod, drilled for passage of inert gas, and used as the upper gripper for a tensile machine test application. Sodium vapor is contained in the OD of the bellows and air is in the ID. The test apparatus is illustrated in Fig. 10. The fixture described is used to provide internal pressure to produce bi-axial stress on a tubular product in a 650°C sodium atmosphere. Results of cyclic stress range studies on tubes are not reported here. A failure of the bellows assembly provided an opportunity to perform microstructural studies on the bellows assembly in order to determine the nature of failure.

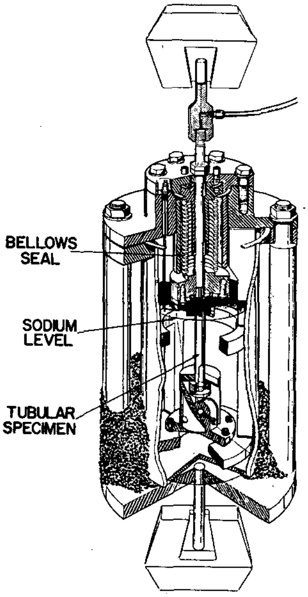

FIG. 10. Tensile test fixture

Metallographic sections were taken for three vertical elevations from the lower end of the bellows which is about 12 mm above the 650°C sodium level, to the upper end of the bellows which is about 200 mm above the sodium level.

In addition at each elevation a metallographic section was taken from an outer convolution, an inner convolution, and the "flat" of the bellows.

A typical set of microphotos near the sodium level is shown in Fig. 11. It can be seen that for this elevation the sodium-exposed side of the bellows undergoes a greater degradation of grain boundaries than does the air side. In addition the "flat" of the bellows, under less strain than the inner or outer convolution, has less degradation than the convolutions under higher stress. The deterioration of the sodium-vapor side of the bellows decreases as one goes from the 650°C sodium-inert gas interface or liquid level to the upper end of the bellows which is furthest removed from the sodium level.

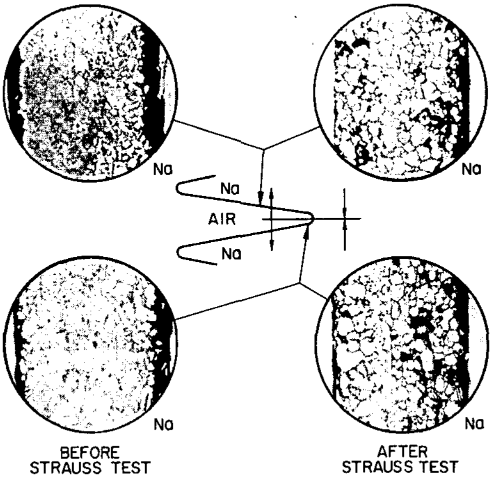

FIG.11. Microstructure of failed bellows

An additional macrophoto of the fracture, Fig. 12, indicates the greater amount of sound material remaining intact, after fracture, on the air side.

To verify the observed microstructure effects, sensitization tests and bend tests were conducted on samples from two vertical levels, one near the gross failure and one about 25 mm above the failure. See Table II.

The total significance of these laboratory measurements and observations may be evaluated in more detail by reference to recent analytical work of W. M. Robertson [12].

The electrical resistance measurement has its limitation [13] and cannot differentiate between a sodium side effect and an air side effect. However, the Strauss test exposes both the sodium and air side of the test section of the bellows for the same time in the same solution. The observed deterioration of the sodium side must be attributed to the horphilic or horophobic [14] reaction of sodium within the grain boundaries.

TUBING: METALLURGICAL ANALYSIS, SHORT TIME, SODIUM, AIR, AND VACUUM ATMOSPHERE, VARIOUS TEMPERATURES

A basic material tested was 304 SS tubing of 12.57-mm OD and 0.457-mm wall with a carbon content of 665 ppm. Additional samples of 347 SS tubing of 30.8-mm OD x 0.278-mm wall were tested for a basis of comparison. The objective of these tests was to correlate electrical resistivity measurements and microphotographs to the microstructure changes as affected by time, temperature, and environment. The environments of test were air, vacuum, and sodium and sodium vapor so that the observed and measured metallurgical changes in tubing due to sodium and sodium vapor could be quantitatively measured.

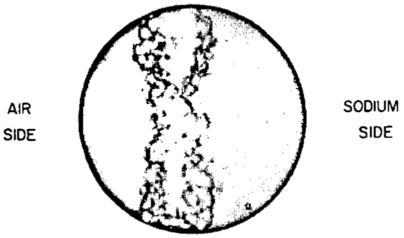

FIG. 12. Macrophoto of fracture of failed bellows

TABLE II. RESISTIVITY AND BEND TESTS FOR TWO ELEVATIONS OF A FAILED BELLOWS ASSEMBLY

Location	% Change in Resistivity	Fracture Bends (180°)	Bends for Complete Failure (180°)
25 mm above failure	50	5	9
Near the failure	215	12	23

The tubing samples for electrical resistance measurements were longitudinally sectioned into four quadrants and sized to strips 6.35 mm wide x 0.457 mm thick x 50 mm long.

Resistance measurements were made with a Kelvin Bridge using a special probe, whose contact points are separated by 8.0 mm and therefore the voltage drop across these two points is always associated with a constant length of specimen. Resistance measurements are converted into resistivity values where each term in the general resistivity formula is a measured quantity. For all tubular samples, resistance measurements were made for each of the following conditions:

a) as received tube

b) after environmental (air, vacuum, sodium and sodium vapor) exposure

c) after a modified 15-min Strauss test [13]

The effects of temperature, time and environment on the resistance of the tubes were controlled and identified by separate tests.

With temperature constant at 650°C the effects of sodium, air, and vacuum environments on electrical resistivity of 304 SS are shown in Table III. To be noted is the increase of resistivity from 80 micro-ohms-cm, as received, to as high as 267 micro-ohms-cm for the sodium-exposed sample after Strauss test. This 300% increase in resistivity indicates a high degree of change of microstructure. In contrast, air and vacuum samples indicate only reduced resistivity, slightly less than as received 304 SS. The creditability of the large change in resistivity of sodium-treated samples is substantiated by the observed differences in microstructure shown in Fig. 13.

TABLE III. ELECTRICAL PROPERTIES OF 304 STAINLESS STEEL
Temperature Constant - Time Variable

650°C (days)	Treated in Liquid Sodium		Treated in Air Furnace		Treated in Vacuum (5-10 microns)	
	Before Strauss Test	After Strauss Test	Before Strauss Test	After Strauss Test	Before Strauss Test	After Strauss Test
1	-	-	71	71	-	-
2	-	-	69	66	-	-
3	70	100	-	-	57	57
5	69	127	67	67	66	61
7	73	267	73	73	65	65
62	-	-	73	75	-	-

As Received		Published Value Allegheny Ludlum Steel Corporation
Before Strauss Test	After Strauss Test	
80	80	72 @ 20°C

Electrical Resistivity in microhms-cm @ Room Temperature.

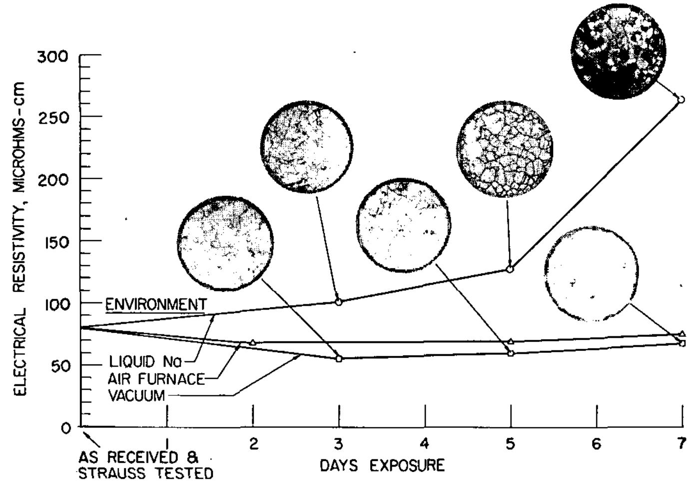

FIG. 13. Correlation of microstructures and changes in electrical resistivity at 650°C

In addition, relating potential difference as the driving force leading to corrosion [15], one can explain the large increase in electrical resistivity after sodium exposure and Strauss solution testing, if one accepts the hypothesis that sodium has penetrated the grain boundaries as a metal or a complex compound.

From the above data, seven days were chosen as the time of environmental exposure as a constant for subsequent measurements of electrical resistance of 304 SS at temperatures of 480°C to 760°C. Data for the vacuum and air exposures was obtained only at 650°C since data for vacuum and air exposures at other temperatures is of marginal interest. The effect of temperature on electrical resistivity is shown in Table IV. To be noted is the maximum increase of resistivity at 650°C, after Strauss test, of the sodium exposed sample. In contrast the resistivity changes, due to vacuum and air exposure, are negligible. Of importance, resistivity values

TABLE IV. ELECTRICAL PROPERTIES OF 304 STAINLESS STEELS
Time Constant – Temperature Variable

	Treated in Liquid Sodium		Treated in Sodium Vapors		Treated in Vacuum (5-10 microns)		Treated in Air Furnace	
7 days (°C)	Before Strauss Test	After Strauss Test	Before Strauss Test	After Strauss Test	Before Strauss Test	After Strauss Test	Before Strauss Test	After Strauss Test
480	73	68	-	-	-	-	-	-
540	59.7	105	59.5	66.7	-	-	-	-
590	65.6	126	62.2	68.6	-	-	-	-
650	68	201 ave.	65	65	65	65	73	73
700	74	78	64.7	112/211	-	-	-	-
760	65	70.4	66	66/92.5	-	-	-	-

As Received		Published Value Allegheny Ludlum Steel Corporation
Before Strauss Test	After Strauss Test	
80	80	72 @ 20°C

Electrical Resistivity in microhm-cm @ Room Temperature.

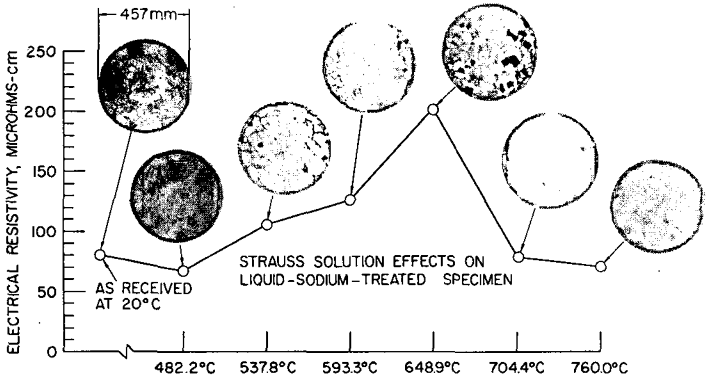

FIG. 14. Correlation of microstructures and changes in electrical resistivity at variable temperatures

at 700°C and at 760°C sodium exposure decrease to resistivity values normally associated with 304 SS. Both the increased resistivity values from 480°C to 650°C and the subsequent decrease in resistivity values from 650°C to 760°C is substantiated by the observed differences in microstructure shown in Fig. 14.

In addition, samples of 347 SS were treated at the same time and in the same sodium environment as the 304 SS samples discussed above. The results of electrical resistivity measurements for a temperature range of 480°C to 760°C are shown in Table V. Of interest is that the maximum resistivity measurements, after Strauss test, increase only about 15% compared to an increase of about 300% for 304 SS. These resistivity measurements are in agreement with the known effects of the stabilization of austenitics steels by the addition of titanium and columbium. Our work supports a view [16] that the added effect of sodium environment in the temperature range of sensitization accelerates the sensitization process compared to the environment of air and vacuum.

To further evaluate the effects of time, temperature, and sodium environment a perforated tubular component (sample basket) from the loop described in the Section concerning "pipe" was removed from the system and its electrical resistance measured as described above. The resistivity of this 18-8 component, held in 650°C-760°C sodium for ∿ 8000

TABLE V. ELECTRICAL PROPERTIES OF 347 STAINLESS STEEL
Time Constant – Temperature Variable

	Treated in Liquid Sodium			Treated in Liquid Sodium	
7 days (°C)	Before Strauss Test	After Strauss Test	7 days (°C)	Before Strauss Test	After Strauss Test
480	87	96.6	650	84	140
540	76	127	700	85	125
590	79	105	760	93	118

As Received		Published Value Allegheny Ludlum Steel Corporation
Before Strauss Test	After Strauss Test	
89.6	90.6	73 @ 20°C

Electrical Resistivity in microhms-cm @ Room Temperature.

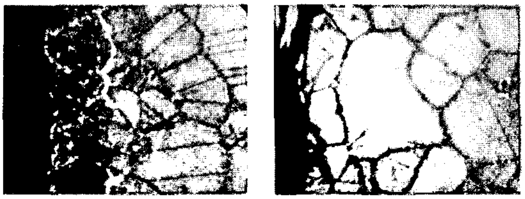

SODIUM TREATED & ETCHED BUT NOT STRAUSS TESTED

SODIUM TREATED STRAUSS TESTED 1.75 HOURS AND THEN ETCHED

FIG.15. Long-term sodium exposure 650°C to 870°C

hours, changed from 67 micro-ohm-cm to 85 micro-ohm-cm after a 1.75-hour Strauss test. As received 304 SS has a measured resistivity of 80-micro-ohm-cm. Since the loop has recently operated at or near 650°C for the past 2000 hours of service, the presodium or heat treatment which preclude this sample from having resistivity values associated with 650°C are not understood. The microstructure of this specimen is shown in Fig. 15.

Current work is directed toward a further understanding of these diverse effects of sodium on structural engineering shapes and geometries.

REFERENCES

[1] SHAW, M., Fast breeder reactor program in the United States, London Conference on Fast Breeder Reactors, May 17-19, 1966, pp. 6-10.

[2] KELMAN, L. R., DUNWORTH, R. J., Selection of structural material for the FARET liquid metal systems, USAEC Rep. ANL-6939 (December 1964) 14, 18-19.

[3] Effect of high temperature sodium on austenitic and ferritic steels, USAEC Rep. MSAR-66-78, Quarterly Report, April-June (1966).

[4] ROWLAND, M. C., PLUMLEE, D. E., YOUNG R. S., Sodium mass transfer, XV, behavior of selected steels exposed in flowing sodium test loops, USAEC Rep. GEAP-48-31 (March 1965).

[5] MACHEREY, R. E., SIMMONS, W. R., NOLAND, R. A., "Materials for Argonne National Laboratory sodium cooled reactors", Nuclear Metallurgy, Vol. IX, AIME (1963).

[6] HAYES, W. C., ANDERSON, W. J., ELKINS, P. E., JOHNSON, D. L., "Materials for sodium graphite reactors", Nuclear Metallurgy, Vol. IX, AIME (1963).

[7] LIKHTMAN, V. I., SHCHUKIN, E. D., REBINDER, P. A., Physicochemical Mechanics of Metals, Izdatel' stvo Akademii Nauk SSSR, Moskva (1962) Translated from Russian by Israel Program for Scientific Translation (1964).

[8] RABINOWITZ, E., Friction and Wear of Materials, John Wiley & Sons, Inc. (1965) 125-165.

[9] CROUSE, R. S., "Metallography", Course 4, American Society for Metals (1964).

[10] SMITH, F. A., Sodium handling at Argonne National Laboratory, Advances in chemistry, Proc. Amer. Chem. Soc. 19 (1957) 42-59.

[11] RATZ, G. A., BRICKNER, K. G., Examination of welded AISI type 304 stainless steel pipe exposed to liquid sodium, US Steel Company (to be published).

[12] ROBERTSON, W. M., Propagation of a crack filled with liquid metal, 95th Annual AIME Meeting, New York, New York (March 1965).

[13] RUTHERFORD, J. J. B., ABORN, R. H., KEARNY, N. J., A Quantitative Method for the Estimation of Intercrystalline Corrosion in Austenitic Stainless Steels, American Institute of Mining and Metallurgical Engineers 100 (1932).

[14] LEVIN, I. A., Intercrystalline Corrosion and Corrosion of Metals Under Stress, Consultant's Bureau, New York, New York (1962).

[15] MONDOLFO, L. F., ZMESKAL, O., Engineering Metallurgy, McGraw-Hill (1955) 286-294.

[16] KINZEL, A. B. FRANKS, R., The Alloys of Iron and Chromium, Vol. II, McGraw-Hill (1940) 400.

EFFECTS OF SODIUM ON THE METALLURGICAL AND MECHANICAL PROPERTIES OF CANDIDATE IMFBR ALLOYS*

K.E. HORTON
UNITED STATES ATOMIC ENERGY COMMISSION,
WASHINGTON, D.C., UNITED STATES OF AMERICA
R.C. ANDREWS, R.C. WERNER
MINE SAFETY APPLIANCE RESEARCH CORPORATION,
EVANS CITY, PA., UNITED STATES OF AMERICA
D.F. ATKINS
ATOMICS INTERNATIONAL,
CANOGA PARK, CALIF., UNITED STATES OF AMERICA

Abstract

EFFECTS OF SODIUM ON THE METALLURGICAL AND MECHANICAL PROPERTIES OF CANDIDATE LMFBR ALLOYS. The USAEC Liquid Metal Fast Breeder Reactor Program is currently expending considerable effort on the characterization of candidate structural and fuel cladding alloys. The alloy bases at present include iron, nickel, vanadium, niobium and cobalt. However, this paper will be concerned with austenitic and ferritic steel properties, the alloys including in-sodium, stress effects on metallurgical structure, creep and fatigue strengths, and also the heat-to-heat variation in properties.

The sodium effect studies were performed in isothermal loops constructed of Type 316 stainless steel. These instrumented loops permitted monitoring and control of sodium impurity contents. Creep, creep rupture and bend-fatigue specimens were fabricated from 0.065-in. thick sheet stock.

Tests performed at 593°C on a ferritic, 2¼% Cr-1Mo steel in clean sodium (less than 30 ppm oxygen), and sodium containing 300 ppm oxygen resulted in similar effects relative to air; stress rupture strengths were slightly decreased, creep rates were slightly increased, and fatigue life was increased an order of magnitude. Tests performed on 304 and 316 austenitic stainless steels at 649°C in high oxygen sodium did not show an appreciable effect on stress rupture life compared with air values. High oxygen sodium tests did, however, cause loss of ductility in these steels. Conversely, carbon-saturated sodium improved the stress rupture life of 316 steel while having no effect on fatigue strength. The most striking effect of these carbon tests was the substantial loss in material ductility due to carburization.

High-temperature stress rupture tests in helium on 304 and 316 steels have shown that a factor of eight difference in strength can exist from heat to heat. This difference may be a result of the steel's interstitial content or possibly the amount of precipitate. The variation clearly points out the caution which must be exercised in the cataloguing of design information for materials for use in reactors.

Further in- and out-of-sodium testing will be performed to delineate completely the synergisms between stress and corrosion.

INTRODUCTION

The U. S. Liquid Metal Fast Breeder Reactor program is currently exploring, among others, two important parameters: bulk sodium outlet temperatures up to 649°C, and ceramic fuel burnup up to 100,000 mwd/t. The expected maximum fuel clad temperature could approach 760°C, where the creep strength of the more conventional reactor materials are distressingly low, and plastic flow is concentrated at the grain boundaries. The high temperature operating conditions will also enhance corrosion and diffusion of radiation-induced defects and gases to sinks, such as precipitates and grain boundaries. In total then, most of the operating parameters are working against us. It would be dangerous to overlook the possibility of synergisms existing among these property degrading parameters.

---

* Work performed under the auspices of the United States Atomic Energy Commission.

This paper discusses the effect of corrosion and mass transport on the mechanical properties of reactor steels. The change of strength brought about by a sodium environment on the particular steels used in this study must logically be considered in light of the variation of properties within a given type of steel, and therefore, the heat to heat variation of properties is discussed first. This is followed by an ennumeration of the effects of pure and impure sodium on tensile, creep, and fatigue properties of steels. Clearly, however, the final story will not be known until the added parameter of irradiation is applied to the combined stress and corrosion tests.

1. HEAT VARIATION

The effect of chemistry on the tensile properties of austenitic stainless steels has been well documented in an ASTM publication of the early 1950 s [1]. A more recent program was instigated at Atomics International (AI) to study the creep and fatigue properties of types 304 and 316 stainless steel as a function of heat chemistry, with particular attention directed to the interstitial (C,N,P,S) content and the amount and form of carbide precipitate. The analysis of the AI heats is given in Table I, together with the analysis for the Mine Safety Appliance Research Corporation (MSAR) steels used in the in-sodium tests described in Section 2. The microstructures of the AI steels are shown in Figures 1 and 2 for the strongest and weakest heats, respectively. Grain sizes for all austenitic steels were similar.

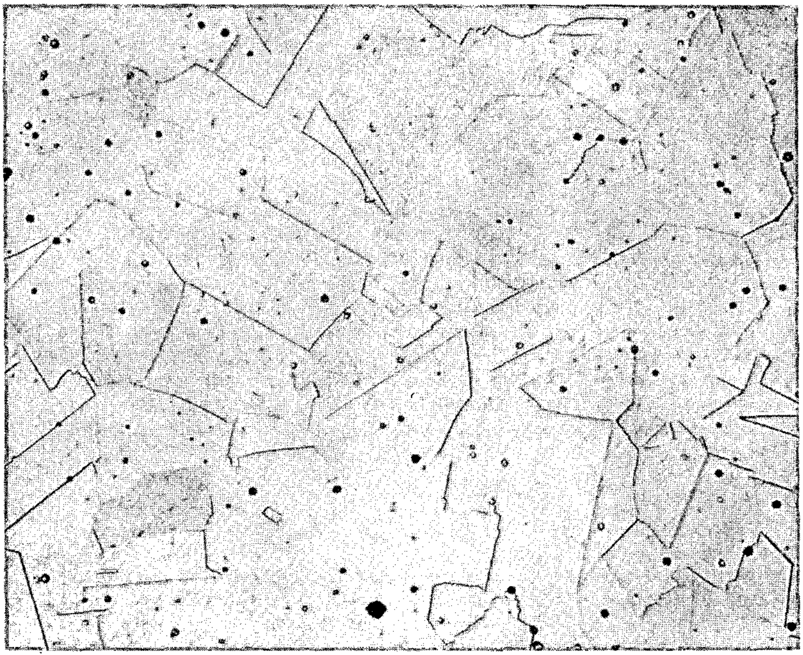

FIG.1. Photomicrograph of Heat F. Note amounts of inclusions. 500x

Creep-rupture test specimens were made from 29.3-cm long tubes, 1.27 cm in diameter and 0.0254 cm thick. Tubes were ultrasonically cleaned but the surface was left in the as-received condition. Helium gas was used as a pressurizing medium and a zirconium foil was placed in each specimen to ensure a continuously pure helium environment. The tests were performed in a helium environment.

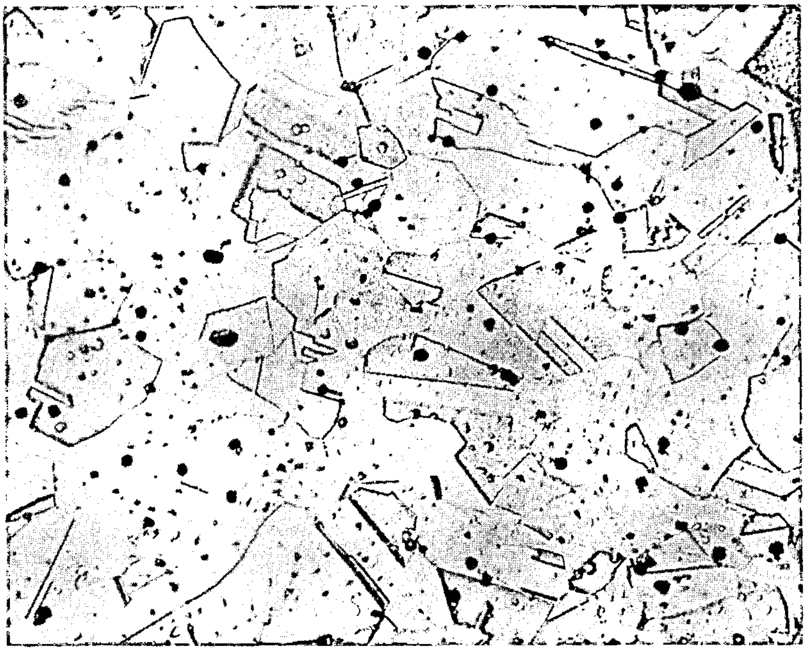

FIG.2. Photomicrograph of Heat E. Note increased amount of inclusion relative to Heat F (Fig.1). 500x

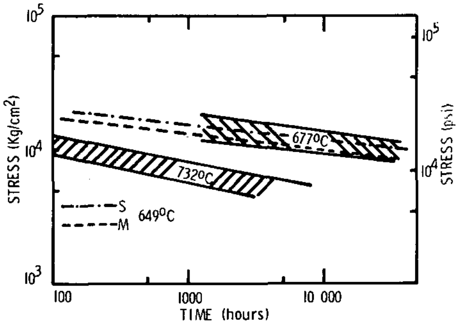

FIG.3. Creep rupture data for stainless steels at 649, 677 and 732°C (see Table I). Data plotted in band form (Heats A-H) was from biaxial stress tests. Other data from uniaxial stress tests

Early creep rupture test results for the steels indicated a close correlation between the total carbon plus nitrogen content and rupture time at a given stress. A similar correlation was noticed by Monkman [2] although he used considerably higher strain rates than used in the study reported herein. Later, more complete test results however did not bear out the interstitial strength correlation, except in the weakest and strongest heats (heats E and F, respectively, in Table I).

The creep rupture properties of the steels studied are shown in Figure 3. There is a clear spread in data, as expected, with a life variation factor-of-eight depending on heat composition. In all cases the strain

TABLE I. CHEMICAL COMPOSITION OF TEST SPECIMENS

Heat	Code	Type	C	N	Mn	P	S	Si	Ni	Cr	Mo
AI	A	304	0.06	0.060	1.67	0.021	0.011	0.50	10.41	18.93	
AI	B	304	0.06	0.056	1.64	0.022	0.025	0.39	9.82	18.54	
AI	C	304	0.06	0.047	1.84	0.023	0.009	0.44	9.79	18.54	
AI	D	304	0.05	0.052	1.77	0.023	0.021	0.55	9.70	18.55	
AI	E	304	0.05	0.037	1.68	0.018	0.021	0.45	9.67	18.47	
AI	F	304	0.06	0.059	1.68	0.027	0.013	0.66	10.27	18.71	
MSAR	M	304	0.06	0.09	1.20	0.023	0.010	0.52	9.36	18.26	
AI	G	316	0.03	0.027	1.54	0.003	0.021	0.30	13.39	17.01	2.28
AI	H	316	0.04	0.043	1.68	0.022	0.017	0.51	13.63	17.33	2.32
MSAR	S	316	0.04	0.048	1.94	0.019	0.012	0.45	12.84	18.00	2.33
MSAR		2¼ Cr-1Mo	0.09		0.64	0.010	0.024	0.33		2.19	0.99

to rupture increased with decreasing rupture time and increased with increasing strain rate. The heats having the least amounts of precipitate in the untested condition proved to have the greatest creep strengths.

It is commonly observed [3] that a continuous grain boundary precipitate lowers creep rupture strength in comparison to a steel with a discontinuous grain boundary precipitate. The metallography performed on the AI steel indicated both continuous and discontinuous precipitates, as illustrated in Figure 4 and 5, respectively. Unfortunately, the conclusion reached in Reference 3 could not be verified. For example, the continuous precipitates evident in Figure 4 were taken from a steel which had a better creep rupture life than the steel with the structure shown in Figure 5, in apparent contradiction to Reference 3. However, the elongated grains shown in Figure 4 are probably a result of tertiary creep and are not, therefore, indicative of a material operating below the equicohesive temperature during creep.

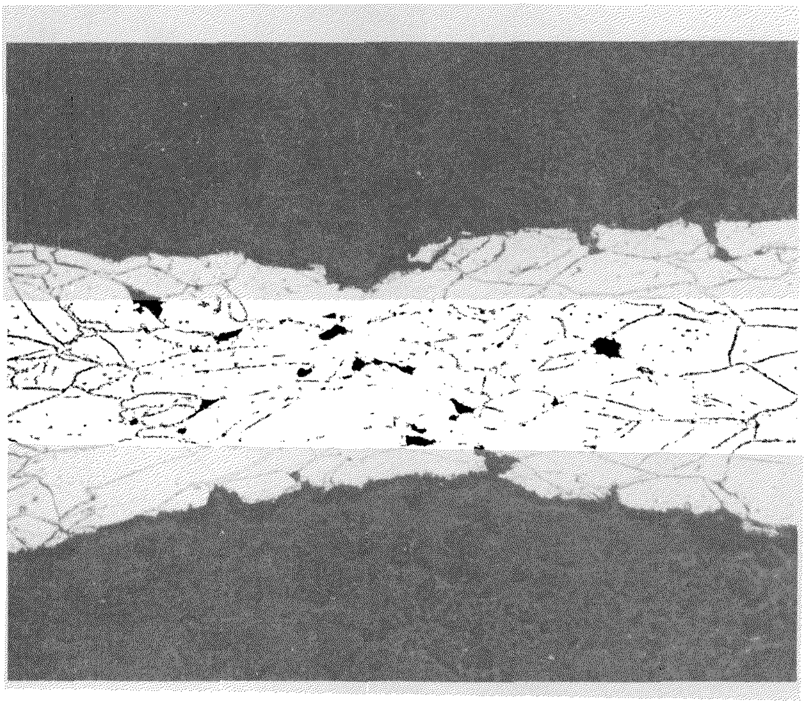

FIG.4. Photomicrograph of Heat F creep-rupture specimen. Life: 60 h at 732°C. Diametral strain: 28%. Note continuous precipitate. 250x

While it is not evident in Figure 3, 316 stainless steel was generally stronger than 304 stainless steel. This is true of both the AI and MSAR steels. The 649°C uniaxial stress, creep strength of the MSAR heats was approximately equal to the 677°C biaxial creep strength for the AI heats, thus suggesting that the heats used by these companies were equivalent prior to testing. Although it is generally predicted that a biaxial stress test should fail at approximately 15% less stress than a uniaxial stress test, this difference is small enough to neglect. The chemical analysis values given in Table I further predict test equality. The creep-rupture data of Reference 1 closely approximates the data plotted in Figure 3.

2. MECHANICAL PROPERTIES IN SODIUM

This section describes the mechanical properties and metallurgical changes resulting from exposure of austenitic and ferritic steels to pure and impure sodium. The three liquid metal exposure conditions were:

1. Pure sodium (less than 30 ppm oxygen);
2. High oxygen sodium (approximately 300 ppm oxygen);
3. High carbon sodium (continuous carbon source maintained at 649°C).

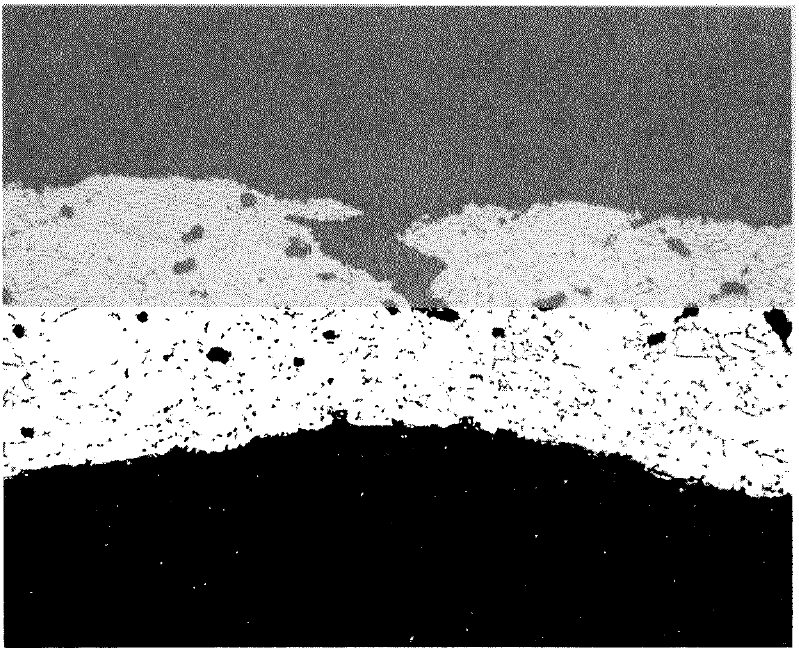

FIG. 5. Photomicrograph of Heat D creep-rupture specimen. Life: 15 h at 732°C. Diametral strain: 30%. Note discontinuous precipitate and equiaxed grains. 250x

The sodium tests were monitored by a plugging meter and controlled by a cold trap. Cold trap temperatures were at or below 150°C for the "pure" sodium tests, and at 360°C for the 300 ppm oxygen, sodium tests. The apparent carbon content of the pure sodium ranged primarily between 40 and 60 ppm, with excursions to 150 ppm, as determined by a dry oxidation process.

The sodium loop arrangement is shown schematically in Figure 6. The total sodium content in the circulating system was 138 liters and the total sodium -- 316 stainless steel contact area, exclusive of specimens, was 7.1 square meters.

The creep, tensile, and fatigue test specimens for each alloy studied were fabricated from 0.165-cm thick sheet, all material for each alloy being from one mill heat. Final machining operations were performed by wet grinding with a maximum of 0.013 cm removed per pass. The resulting surface was thus stress-free. Gage lengths for the tensile and creep rupture tests specimens were 6.35 cm and 2.54 cm, respectively. The bending fatigue test specimens were cycled over machined mandrels with radii of curvature fixed to give strain-controlled fatigue tests. Fatigue failure was determined by sudden changes in the bending force as measured by load cells.

In all loop mechanical property tests, the sodium velocity over the test specimens was low. The maximum velocity over the creep-rupture specimens was 0.014 m/sec and only one tenth this value in the fatigue tests.

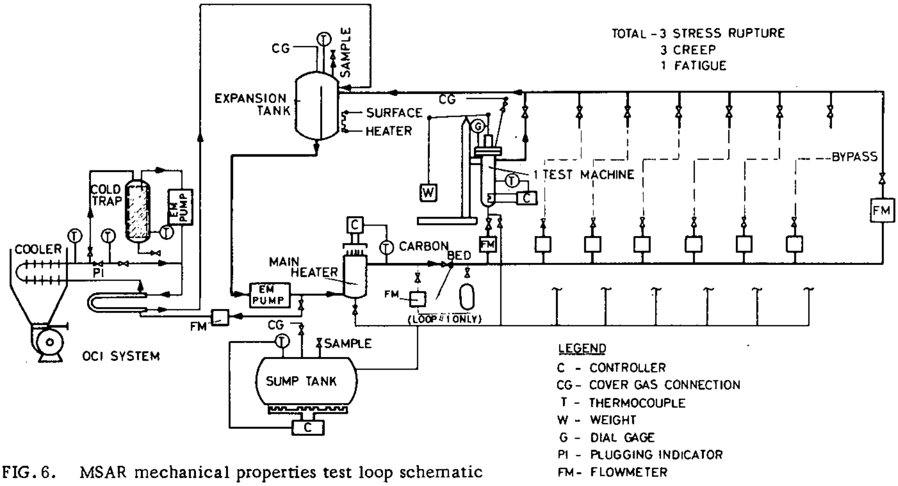

FIG. 6. MSAR mechanical properties test loop schematic

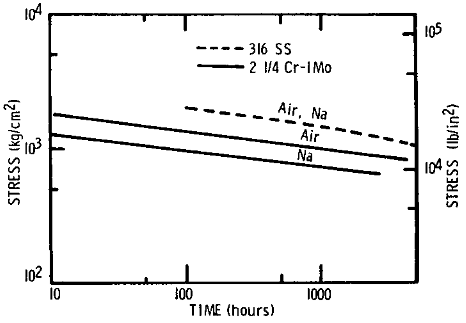

FIG. 7. Creep-rupture data for 2¼ Cr-1 Mo at 593°C and for 316 SS at 649°C in less than 30 ppm oxygen sodium. All specimens pre-exposed 4000 h to low oxygen sodium

2.1 "Pure" Sodium Test Results

2.1.1 Creep-Rupture

The results of creep rupture tests for air and low oxygen sodium are shown in Figure 7. While sodium had no effect on the creep rupture strength of 316 SS, it did significantly decrease the strength of 2 1/4 Cr-1Mo. Ductility changes were not noticeable in the 316 SS tests except at the higher stresses, where a 10-20% increase was recorded. On the other hand, large ductility increases, particularly at the low stress-long time test conditions, were found for the ferritic 2 1/4 Cr-1Mo alloy. It is natural, therefore, to expect a difference in metallurgical structure or composition for 2 1/4 Cr-1Mo specimens exposed to pure sodium, whereas no changes would be anticipated in the 316 SS. Metallographic and chemical examination confirms this hypothesis in that a significant loss in carbon content occurred in the 2 1/4 Cr-1Mo. The only change detected in some of the 316 SS specimens was a three-micron (maximum) thick carburization layer. Ruptured specimens exhibited voiding at grain boundaries in tests lasting more than 3000 hours due to plastic flow concentration in these regions, and ruptures were largely intercrystalline. Shorter term tests did not show voiding and fractures were transcrystalline.

2.1.2 Strain Cycling Fatigue

The fatigue test results for 316 SS and 2 1/4 Cr-1Mo are shown in Figure 8. For both steels the fatigue strength is increased in pure sodium. This trend is exactly opposite to that noted for the creep rupture tests.

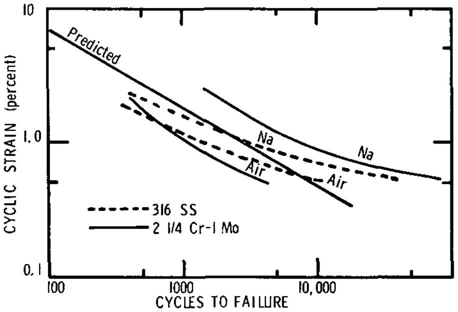

FIG.8. Fatigue life for 2 1/4 Cr-I Mo at 593°C and 316 SS at 649°C in less than 30 ppm oxygen sodium. No specimen pre-exposure

It is not possible to determine if a ductility change also occurred in these tests since the measurement techniques did not permit the extraction of plastic strain from the total measured (elastic + plastic) strain. Metallography of tested specimens showed no structural changes had occurred as a result of exposure to stress and sodium. Fractures and surface cracks were transcrystalline.

The lack of microstructural changes may be attributed in part to the relatively short duration of fatigue tests. The cycling rate was three per minute and consequently a 10 000 cycle life was equivalent to only a 50-hour exposure.

It is interesting to compare the results of actual fatigue tests with those predicted from tensile test data. A technique of Manson [4] based on "universal" slopes for elastic and plastic strain in a fatigue test was tried and gave the curve shown in Figure 8 for 2 1/4 Cr-1Mo. The predicting equation is:

$$\text{total strain range} = 3.5 \frac{\sigma}{E} N^{-.12} + \left[\ln\left(\frac{1}{1-RA}\right)\right]^{.6} N^{-.6}$$

where σ = ultimate tensile strength
E = modulus of elasticity
RA = reduction of area
N = cycles to failure

and the values used for the parameters were those values at 593°C in pure sodium. The prediction was clearly of surprising accuracy and also conservative.

2.1.3 Tensile Tests

The tensile properties of the steels exposed to low oxygen sodium per se are not significantly different from the properties in air, even though sodium exposures were for 4000 hours. For example, the tensile and yield strengths and ductility of 316 SS were unchanged by sodium exposure. On the other hand, the tensile strength properties of 2 1/4 Cr-1Mo were decreased, and the ductility increased, after 4000-hour sodium exposure but the same change in properties occur after a similar length exposure to 593°C helium. It is apparent then that the tensile property changes for this alloy are due to loss of carbide strengthening with both thermal aging (carbide spheroidization) and decarburization contributing to the effect.

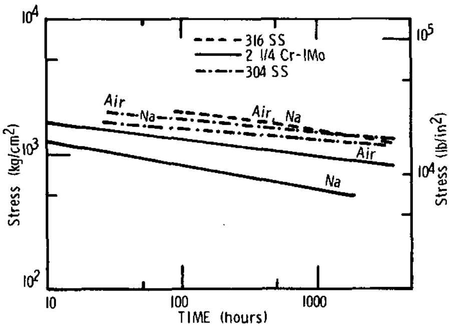

FIG. 9. Creep-rupture tests on 2¼ Cr-I Mo at 593°C and 304 and 316 stainless steels at 649°C in 300 ppm oxygen sodium. All sodium test specimens pre-exposed 4000 h in high oxygen sodium

2.2 High Oxygen Sodium Test Results

2.2.1 Creep Rupture

The results of creep rupture tests in air and high (300 ppm) oxygen sodium are shown in Figure 9. These test results are similar to those observed in low oxygen sodium. The major strength effect occurs in the ferritic alloy, with only slight sodium weakening in 304 SS. Conversely, ductility changes were significant in both 316 SS (decreased) and 2 1/4 Cr-1Mo (increased). A particularly disturbing finding was the less than 9% elongation manifested in the long-time creep rupture tests on 316 SS. Oxide was found in cracks in such tests and failures were, as expected, intercrystalline.

2.2.2 Strain Cycling Fatigue

The strain-controlled, fatigue test results for high oxygen sodium exposure are shown in Figure 10. The fatigue life of 2 1/4 Cr-1Mo was essentially the same in both low and high oxygen sodium and clearly superior to that found in air. In both air and sodium tests, the failures were transcrystalline, with oxidation occurring in cracks of specimens tested in air. This "oxide filling" of cracks contributed to early specimen failure since stress concentration would be particularly severe during the compressive portion of the fatigue cycle.

The fatigue life curves for 304 and 316 SS in high oxygen sodium are concave downward, which obviously could not be predicted from the equation in Section 2.1.2 and is presently unexplainable. The reason for the convergence of the 316 SS air and sodium curves at the low cycle end of

Figure 10 could be the short exposure times experienced by the specimens in these tests. The cross-over in the 304 SS air and Na data may be due to data scatter since no logical explanation exists for this observation. Failures occurred by transcrystalline cracking in all these tests, as it did in the low oxygen sodium tests.

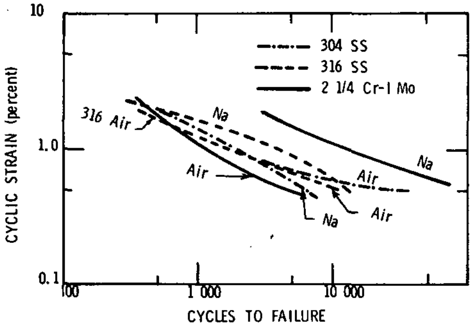

FIG.10. Fatigue life of 2¼ Cr-I Mo at 593°C and 304 and 316 stainless steels at 649°C and 300 ppm oxygen sodium. No specimen pre-exposure

2.2.3 Tensile Tests

The short-time tensile properties of 316 SS were relatively unaffected by exposure to high oxygen sodium, except for a significant (~50%) loss in ductility. However, failures were ductile with over 20% elongation occurring despite a slight surface oxidation. This embrittling oxidation reaction produced a typical effect of a small increase in yield strength but a decreased tensile strength and ductility.

The tensile properties of 2 1/4 Cr-1Mo were substantially more perturbed than those discussed above. Tensile and yield strengths were decreased 40% and 50%, respectively, and the ductility was increased 20%. This change in short-time properties is due largely to spheroidization and decarburization. The expected decarburization of the 2 1/4 Cr-1Mo occurred to an extent somewhat greater than that found in the low oxygen sodium exposures.

2.3 High Carbon-Sodium Tests

2.3.1 Creep-Rupture Tests

The tests performed in high carbon sodium were interesting due to the prominent effects a carburizing environment has on stainless steels. However, during the high carbon test runs it was impossible to analytically detect a carbon concentration higher than that which existed in the pure sodium and high oxygen sodium runs. The sodium carbon content was initially higher than the 649°C saturation value of 60 ppm [5] in all tests (both pure and impure sodium) but would decrease with time to a value below this amount. High carbon sodium exposures were performed by placing a 649°C pellet bed which contained 5.4 kg of 0.63-cm diameter by 0.63-cm long spectrographic grade carbon cylinders in stream. That high carbon sodium did indeed exist in these tests was manifested by heavy carburization of surveillance tabs, although the carbon bed appeared intact at the end of the test runs. As a result of performing these tests, a new carbon analysis technique was devised which consists of hydrolysis at 0°C, acidification, dehydration, and finally combustion of the dried salt at 649°C in pure oxygen.

Creep rupture test results for 304 SS and 316 SS are plotted in Figure 11. Only 316 SS showed an increased resistance to rupture in this carburizing medium. However, a 50-75% loss in ductility accompanied these tests, with elongation values going down to 13% in both steels.

The carburization which has occurred during these tests is shown in Figure 12. The structure consists of an austenite matrix surrounded by ferritic material containing carbides of the type $M_{23}C_6$ and M_7C_3. The saturation carbon content of these stainless steels appears to be in the range of 3.5 - 3.8 $^{w}/o$. The diffusion of carbon was greater in the 304 SS than in the 316 SS, as was the total amount of carbon absorbed. Due to the carbon gradient set up in specimens tested in high C sodium, a gradient in ductility is also found. The surface layers of both 316 and 304 SS are extremely brittle and many intercrystalline surface cracks are formed during stress application. In all cases failures were also primarily intercrystalline.

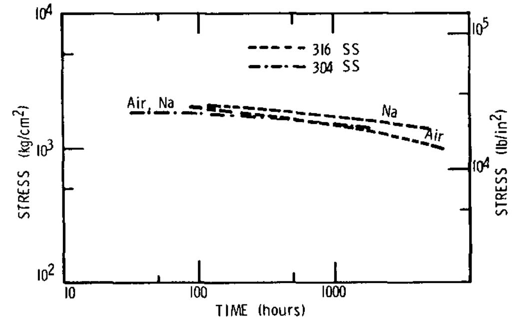

FIG.11. Creep-rupture data for 304 and 316 stainless steels at 649°C in high-carbon sodium. Specimens pre-exposed 4000 h in high-carbon sodium

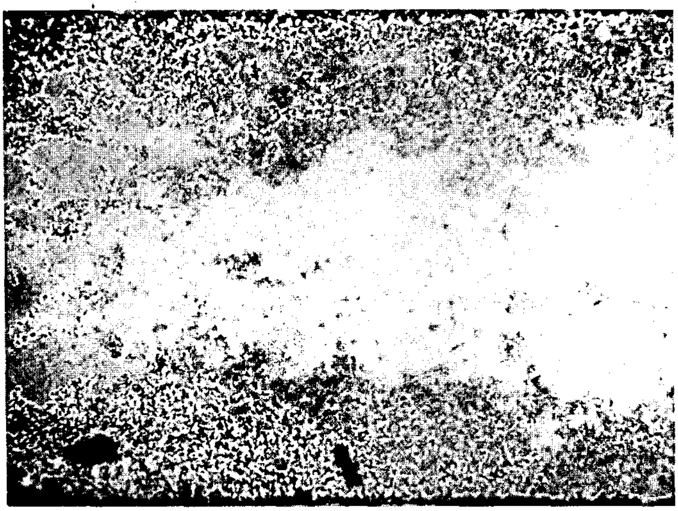

FIG.12. Photomicrograph of 0.0127-cm thick tab of Heat M. Held at 649°C for 1035 h in high carbon. 533x

2.3.2 Strain Cycling Fatigue

The results of high carbon fatigue testing are plotted in Figure 13 and are relatively uninteresting when there is no prior exposures to contaminated sodium. Conversely, the results of high strain fatigue tests on specimens pre-exposed for a few hundred hours in high carbon sodium show significant decrease in fatigue life. In this case, the data lie between curves 1 and 2, but are not plotted in Figure 13. The result of low strain fatigue tests on pre-exposed specimens is not known but it is surmised that it would fall close to curve 2. It is interesting to note that in all low strain fatigue tests the specimens tested in sodium last longer than those tested in air, a result opposite to the low and high oxygen sodium fatigue tests. It is also noted, at least in the 316 SS tests, that failure becomes more predominantly transcrystalline at the low strain range test conditions. This may signify a strengthening of the grain boundaries. The carbide morphology at the grain boundaries is not continuous and thus this data favors the observations of Garofalo [3] described in Section 1.

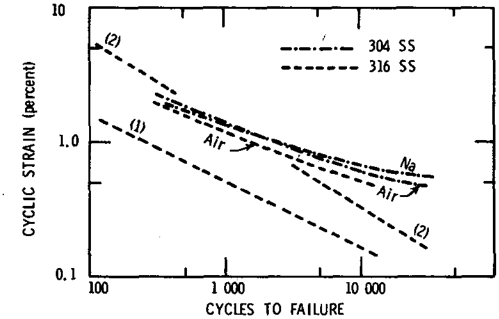

FIG. 13. Fatigue life of 304 and 316 stainless steels at 649°C in high carbon sodium. No specimen pre-exposure. Curves 1 and 2 predicted from 316 SS tensile data. Note: 316 SS sodium curve coincides with the 304 SS air curve

The prediction of fatigue life from tensile data for 316 SS has also been plotted in Figure 13. Curve 1 in the figure is a result of using tensile data obtained from specimens pre-exposed for 4000 hours in high carbon sodium. Curve 2 results from data taken from air tests on unexposed specimens. All tensile data was, of course, obtained at 649°C. It may be concluded that curve 1 is a fair prediction of actual fatigue life of specimens pre-exposed to sodium and certainly lies within the accuracy range stated by Manson [4].

2.3.3 Tensile Tests

The tensile test data of specimens exposed to high carbon sodium showed changes (as compared to air) somewhat greater than those discussed in earlier sections of this paper. Thus, 316 SS and 304 SS exhibited a 20% increase in tensile strength after 4000 hours exposure to high carbon sodium at 649°C as compared to no change for high and low oxygen sodium tests. Similarly, the yield strength of 316 and 304 SS increased 50% at 649°C. Ductility decreased 80% for 304 SS and 96% for 316 SS (down to 2% elongation). Failures in all high carbon sodium tests were intercrystalline.

3. DISCUSSION

From the various tests performed on the austenitic and ferritic steels in sodium of varying impurity content, it is apparent that mechanical properties may be enhanced or degraded from those measured in an atmospheric environment. Perhaps the greatest concern for material degradation arises in the area of ductility, particularly in view of the further ductility decrease manifested in post-irradiation tests. It seems probable that a material partially embrittled by sodium would become fully embrittled by a lower integrated neutron dose than an irradiated material not exposed to sodium.

The relative strength of the grain boundaries with and without continuous (carbide) precipitates was not fully delineated in these tests, nor was it evident that the higher temperature-longer term creep tests were undergoing significant grain boundary sliding. Plots of rupture time versus temperature were linear for heats A-H over the temperature range of 649°C to 760°C whereas one would normally expect a non-linear curve across this temperature range [3], where the region of plastic flow concentration changes from within the grains to the grain boundaries.

Another significant point is the low sodium velocity used in these tests. It is known that corrosion rate of austenitic steels varies approximately linearly with sodium velocity [6], particularly when the velocity is less than 3 m/sec [7]; thus the corrosion effect on mechanical properties could be far more important than manifested in these tests which experienced sodium velocities less than 0.02 m/sec.

In all in-sodium tests there was never any indication of sigma phase formation, although large amounts of carbides and ferrite were formed. Clearly, the very large amount of carbide formation which can result from sodium carburization must be considered. As carburization occurs there is, at first, a solid solution and fine carbide precipitation strengthening which is followed by a weakening due to ferrite formation and carbide coalescence [8]. Further microstructural changes can occur after the carbon source is removed, especially in 304 SS. Thus the problem of material changes after a carbon impurity excursion is not immediately removed by hot trapping the sodium.

The tests performed in these two studies do not permit the prognosis that mechanical properties of stainless steels in sodium would change as much or as little as indicated in the previously discussed graphs. However, the out-of-sodium tests data comparison indicates that the heats studied were not unusual with respect to one another, nor were they unusual with respect to the properties referenced in earlier studies [1]. Therefore, it is logical to expect a minimum sodium effect as delineated herein. The maximum effect would possibly arise in tests performed in-pile, in high velocity, impure sodium.

In creep tests wherein strength was relatively unaffected, but ductility was decreased (e.g., 316 SS, high oxygen sodium tests), the minimum creep rate was measurably smaller, as expected. Furthermore, Charpy keyhole impact data closely parallels the change in measured creep ductility in that impact energy decreased with decreasing ductility. Conversely, changes in fatigue life in sodium were directly opposite to changes in creep rupture life. That is, an increase in fatigue life at a given cyclic strain in a particular sodium environment would correspond to a decrease in creep rupture life in a similar environment -- both in respect to air environment tests. This experimental fact is probably a result of a strain being the independent variable in the bend fatigue tests and stress being the independent variable in the creep rupture tests. If the fatigue tests had been of the stress-controlled type then similar changes in fatigue and creep rupture would no doubt have been observed.

4. CONCLUSIONS

1. Heat to heat variation of creep properties out-of-sodium vary by a factor of eight, depending on heat composition and precipitate form. This same variation would be expected for properties in-sodium.

2. A "pure" sodium environment is just as effective in producing mechanical property changes as is a high oxygen sodium, possibly as a result of the low sodium velocity and corrosion rates operative during the 4000-hour exposures.

3. A high carbon sodium environment increases material strength but is detrimental to ductility.

4. Further testing is necessary to fully delineate the in-sodium properties of materials, particularly when stress and high corrosion rates are both present.

REFERENCES

[1] Simmons, W. F., and Cross, H. C., "The elevated temperature properties of stainless steels", ASTM-STP-#124 (1952).

[2] Monkman, F. C., Price, P. E., and Grant, N. J., "The effects of composition and structure on the creep-rupture properties of 18-8 stainless steels", Trans. ASM, Vol. 48 (1956), 418.

[3] Garofalo, F., "Fundamentals of Creep and Creep-Rupture in Metals", Macmillan Company., New York (1956).

[4] Manson, S. S., "Fatigue: a complex subject -- some simple approximations", Exp. Mechanics, July 1965, 193.

[5] Gratton, J. G., "Solubility of carbon in sodium at elevated temperatures", KAPL 1807 (1957).

[6] Young, R. S., and Lockhart, R. W., "Proceedings of Sodium Components Development Program", Conf. 650620, June 1965, pp. 18-35.

[7] Nettley, P. T., et. al., "Problems in the selection and utilization of materials in sodium cooled fast reactors", London Conference on Fast Breeder Reactors, May 1966.

[8] Hiltz, R. H., "Effect of carburization on the phases in austenitic stainless steels", MSA Research Corporation Report #66-119, June 1966.

DISCUSSION

A. G. IOLTUKHOVSKY: How good is the agreement between your curves for creep and fatigue life, which relate to tubular samples, and the corresponding curves obtained on the basis of standard cylindrical samples? Is there agreement between the ductility values for the two types of sample?

K. E. HORTON: The fatigue tests performed in this project were of the strain-controlled, reversed-bending type, and use was made of a flat, sheet specimen. As for the relation between the creep data for the tubular and cylindrical specimens, it is pointed out in the paper that there is little difference between the results quoted in Ref. [1] and the data plotted in Fig. 3. The strength values given in Ref. [2] are generally higher than those plotted in Fig. 3, at least for rupture times of 1000 h and less. I cannot give you any data on the correlation that exists in regard to creep rupture elongation since this information was not given in Refs [1] and [2].

EFFECT OF WATER LEAKAGE INTO SODIUM SYSTEMS
(Session IV, Part 2)

CORROSION OF STEELS IN THE VICINITY OF A SODIUM-WATER REACTION

R. A. DAVIES, J. A. BRAY AND J. M. LYONS
U. K. ATOMIC ENERGY AUTHORITY,
DOUNREAY EXPERIMENTAL REACTOR ESTABLISHMENT,
THURSO, CAITHNESS,
UNITED KINGDOM

Abstract

CORROSION OF STEELS IN THE VICINITY OF A SODIUM-WATER REACTION. Rapid corrosion of steels in the vicinity of a sodium-water reaction could lead to a major reaction in a sodium-water heat exchanger. An investigation of the magnitude of the corrosion problem has been carried out under conditions simulating both a small water leak and a full size pipe burst, and further tube failures have been obtained. These experiments were carried out on a sodium rig which could accommodate simple full-scale models of sections of heat exchanger, and up to 70 lb of water was injected into 700 lb of sodium in 9.0 s.

The corrosion phenomena have also been investigated on a small scale under more controllable conditions by pumping water at normal pressures into a pot of sodium. With a flow-rate of 1 ml/min corrosion rates in excess of 0.005 in./min have been obtained. The effect of various parameters on the corrosion rate has been studied, and a comparison has been made of the corrosion rates obtained with a variety of steels. The corrosion appears to be a direct result of conditions during the reaction, and the appearance of the specimen and pattern of damage suggests that the main effect is concentrated where the sodium water reaction front impinges on the metal surface.

The corrosion rates are very much lower with stainless steel and nickel alloys than with ferritic materials, and suggest that the phenomena are associated with the formation of $(Na_2O)_2FeO$. Iron powder has also been observed in the vicinity of the reaction which would suggest that this is reduced at a later stage, either as a result of the hydrogen produced during reaction, or by thermal cycling.

INTRODUCTION

The possibility of extensive damage arising from a leak between the two sides of a sodium-water heat exchanger has presented a serious problem in assessing the safety and design specifications of this system since its inception. A number of studies have been carried out since about 1950 to determine the magnitude of this problem. These tests have been mainly concerned with the mechanical damage which would occur from a sodium-water reaction, and the first observation of corrosion of steel in the vicinity of a water leak into sodium arose from an examination of the secondary heat exchanger of the Enrico Fermi Reactor after the incident in December 1962 [1]. It was found that considerable thinning of the water tubes had taken place in the region of the failure. It was thought that the corrosion had occurred during the reaction, and it was suggested that the original hole was probably small but had quickly enlarged until the resulting reaction became violent. The corrosion probably took place over less than an hour.

This observation was of obvious importance, and investigations have been carried out since in a number of countries interested in sodium-cooled reactors. The present paper describes some of the work carried out in the United Kingdom on this problem; these investigations have included both rig tests in a model heat exchanger facility and small-scale laboratory studies.

CORROSION DURING TESTS ON THE SODIUM-WATER REACTION RIG (NOAH)

Description of the rig

The sodium-water reaction rig at the Dounreay Experimental Reactor Establishment was originally intended to be a simple one-sixth scale model of an early P. F. R. 250 MW heat exchanger design. It consisted of a cylindrical mild steel pressure vessel, approximately 8 ft high and 2 ft in diameter. This was filled with approximately 700 lb of sodium. It was possible to circulate the liquid metal with a downward flow at temperatures of up to 400°C by an electro-magnetic pump. The water tube section was contained in a square duct within the main vessel, with most of the tubes being represented by a number of perforated metal plates packed in a spaced rack in the duct (Fig. 1). This provided similar flow resistance and pressure drop characteristics to those in the actual heat exchanger. One water pass was fitted at the base of the duct assembly where it was looped in the design layout and surrounded by a group of solid wire dummy water tubes arranged in the same way. Water injection into the sodium was initiated by shearing a blanked-off tee piece with a blade operated mechanically from outside the vessel. The duration of the water injection was controlled by a programmed timer actuating a stop valve in the water feed line.

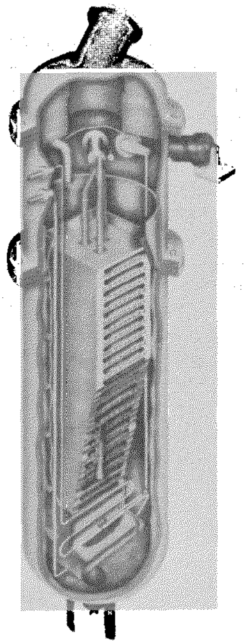

FIG. 1. Cutaway view of the sodium-water reaction test vessel

Water was circulated by convection through the loop from an electrically heated "boiler" beside the sodium vessel. The circuit was designed to allow the water temperature and pressure to approach values of approximately 300°C and 2000 lb/in^2 abs.

Temperature and pressure changes within the test vessel caused by the sodium-water reaction were measured and, together with strain gauge readings from the outer shell, were printed out on multi-channel high speed recorders. Excess gas pressure in the vessel was relieved by means of a bursting disc, operating at 100 lb/in^2 abs., and the reaction products were vented into a large surge vessel.

After a number of tests, changes in the P. F. R. heat exchanger design caused the small-scale model to be abandoned. The test vessel was then adapted to accommodate simple full-scale models of sections of heat exchanger tube banks so that the effects of a full bore tube failure could be investigated. A small water header tank inside the test vessel was arranged to carry 26 full size boiler tubes. The top ends of the 52-in. long tubes were connected to the header tank and the bottom ends were blanked off with welded caps. An injection tube of similar bore (0. 59 in.) could be arranged to conduct water at full pressure and temperature in the required position in relation to the test section. Reaction was initiated by a bursting disc.

Reaction tests

A total of 15 tests was carried out with the NOAH facility. A summary of the experimental conditions for the tests is given in Table I. The main object was to study the mechanical damage which could arise from a full bore tube failure but the tube bank was also examined after each test to assess the extent of corrosion. Three tests were specifically carried out to investigate the corrosion that could occur from a small water leak.

The first three tests used the one-sixth scale model. In the first approximately 2 lb of water were injected in 2 s through a 0. 125-in. diameter jet. The sodium was circulated during the test at a temperature of 350°C. The mechanical damage resulting from the reaction was negligible but severe corrosion occurred. This affected the mild steel wire bundles and plates lying in a cone-shaped section immediately above the centre of injection where the diameter (0. 125 in.) of the wire was reduced to half its value at some places (Fig. 2). Less damage was observed on the 18/8/1 stainless-steel water return, but the corrosion was sufficient to cause failure of the 0. 020-in. thick tube wall above the jet (Fig. 3). Metallurgical examination of items from inside the test vessel showed that there was pitting and intergranular attack of material in the corroded regions.

In the further two tests carried out with the one-sixth scale model the jet size was increased to simulate a full-size tube to determine whether the corrosion rate would be enhanced. The sodium was not circulated during these tests and the temperatures were 300°C and 270°C. Although the quantity and rate of addition of water was much greater and there was some mechanical damage resulting from the reaction, no corrosion was observed.

Nine tests were performed with the full-scale models of sections of heat exchanger. In these tests 35-70 lb of water at initial temperatures

TABLE I. EXPERIMENTAL CONDITIONS FOR SODIUM-WATER RIG TESTS

No.	Description	Injection time	Type and size of orifice
1	1/6th scale model of steam generator mild steel and 18/8/1	2 s	1/8 in. vertical
2		4.5 s	½ in. vertical
3		4.5 s	½ in. vertical
4	Pressurized tubes 2¼ Cr - 1 Mo	4.5 s	½ in. vertical with deflector
5	Pressurized tubes 2¼ Cr - 1 Mo	4.5 s	½ in. vertical with deflector
6	9 Cr - 1 Mo	4.5 s	½ in. right angles to axis of bundle
7	2¼ Cr - 1 Mo	9.0 s	½ in. right angles to axis of bundle
8	9 Cr - 1 Mo pre-weakened	9.0 s	½ in. right angles to axis of bundle
9	Corrosion test mild steel	9.0 s	2 × 1/8 in. and 2 × 1/16 in.
10	Pressurized tubes 9 Cr - 1 Mo	4.5 s	½ in. at angle of 45° to axis of bundle
11	Corrosion test (unpressurized tubes) mild steel	(a) 30 s (b) 30 s	1/16 in. at right angle to tubes
12	Pressurized tubes 316 stainless steel	9.0 s	½ in. at right angle to axis of bundle
13	Corrosion test pressurized tubes 9 Cr - 1 Mo	3.6 s	Pin-hole defect at right angles to axis of bundle
14	Pressurized tubes 316 stainless steel	9.0 s	½ in. at right angle to axis of bundle
15	Pressurized tubes inert gas 9 Cr - 1 Mo	9.0 s	½ in. at right angle to axis of bundle

in the region of 300°C were injected over periods between 4.5-9.0 s into the centre of the tube bundle. In the first test of this series the injection was upwards and a deflection plate was fitted 2 in. above the bursting disc used to initiate the reaction. The plate was intended to simulate the effect of a support grid and thus ensure that water impinged on the surrounding tubes. Later tests used positive guide tubes to direct the angle of the jet. The tube materials tested were $2\frac{1}{4}$ Cr - 1 Mo, 9 Cr - 1 Mo ferritic steels and Type 316 stainless steel.

FIG.2. Corrosion of 1/6 th scale dummy water tubes (mild steel wire)

In three of the tests (Nos 5, 8, 10) failure of one of the pressurized tubes occurred. One of the failures (No. 10) was thought to have been caused by high temperatures leading to over-pressurization of the tubes, in both the other tests severe thinning due to corrosion appeared to be a contributory cause of failure (Fig. 4). One of the tubes was $2\frac{1}{4}$ Cr - 1 Mo steel and the other 9 Cr - 1 Mo. The stainless-steel tube bundles did not show any failures, but some swelling was observed and the surface was polished in the reaction zone. Temperature measurements taken during the tests indicated transient maxima of up to 1350°C for periods of several seconds. These values have confirmed the deductions made from metallurgical examinations on the tube specimens.

Three tests were carried out to simulate small leak conditions. In the first of these tests (No. 9), two pairs of jets were fed from the water line; the jet diameters were 0.125 in. and 0.062 in. and water was injected for 9.0 s. The specimens were mild steel wires. No corrosion was observed but it was later thought that this may have been due to the

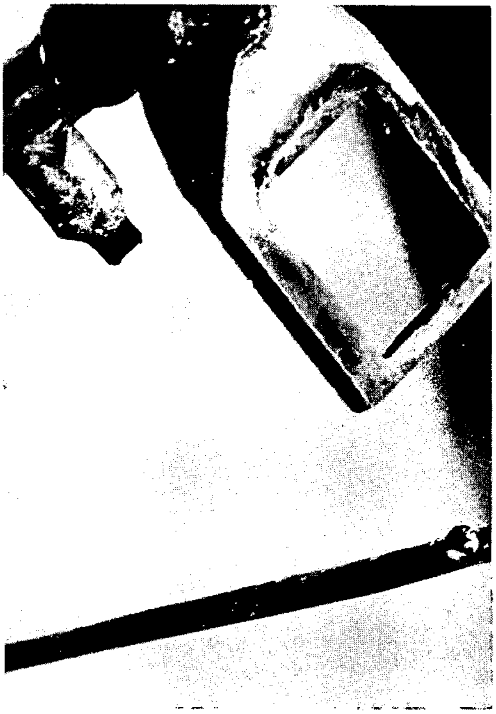

FIG.3. Failure of 18/8/1 water tube adjacent to sheared tee-piece

FIG.4. Pressurized tube bundle ($2\frac{1}{4}$ Cr-I Mo) showing bowing and rupture due to tube wastage

close proximity (0.125 in.) of the specimens to the injection orifice. In the second experiment a 0.062-in. orifice was used and 17 lb of water were injected in 30 s. An attempt was made to follow this by a second injection making use of the heat from the first reaction to raise the sodium temperature. The initial temperature was 370°C; this was raised to 390°C by the first injection. Only 2 lb of water could be added in a further 30 s in this injection, presumably due to blockage of the jet. Marked corrosion of the unpressurized mild steel tubes was observed in a similar pattern to that observed in the first one-sixth scale model test. The tube directly in line with the jet showed a distinct hollow at the orifice level, and above and below were regions of thinning and pitting aligned with similar regions on adjacent tubes. In the third corrosion study a specimen tube which had developed a small hole in one of the pressurized tube bundle tests was used as the injection tube. The specimens were pressurized 9 Cr - 1 Mo tubes. The point of injection was arranged at right angles to the axis of the bundle, and $2\frac{1}{2}$ lb of water were injected over 1 h. Some slight polishing of the specimen tubes was observed but no serious corrosion.

SMALL-SCALE TESTS

In view of the effort required to carry out a full investigation on the size of model used in the tests described above, an attempt was made to reproduce the corrosion in small-scale experiments. If this could be accomplished it was thought that it might be possible to use the technique to investigate some of the corrosion parameters and obtain information which would help to elucidate the corrosion mechanism.

In these experiments water was pumped using a metering pump into a stainless-steel pot containing about 3 lb of sodium. The pot was wound with electrical heating tapes and temperatures of up to 700°C could be obtained. All reactions were carried out under an argon blanket and build-up of pressure was avoided by venting the pot at intervals. The reaction proceeded smoothly but, for safety, the pot was shielded by concrete blocks.

The ability to simulate the corrosion on a small scale was well illustrated by an experiment in which seven rings of $2\frac{1}{4}$ Cr - 1 Mo steel were threaded on to a 0.1-in. capillary tube. The assembly was immersed in sodium at 500°C and 120 ml of water were injected into the sodium over a period of 2 h through a hole in the wall of the capillary tube halfway down its length. Extensive corrosion of the steel rings occurred in the region adjacent to the point of injection, and the walls of two of the specimens were completely penetrated, corresponding to a corrosion rate in excess of 0.5×10^{-3} in./min.

Some difficulty was encountered in obtaining reproducible results in these experiments and several different arrangements were tried. Initially it was thought that the specimens could be directly compared by distributing them symmetrically around the point of injection but large differences in corrosion rate were obtained even after considerable care had been taken to keep the conditions identical. This was believed to be due to difficulty in controlling the path of the steam. During these experiments a 0.5-mm thermocouple was attached to the needle and the output connected to a $\frac{1}{4}$-s recorder. A microphone was attached to one of the fixing bolts on the lid of the vessel and connected to an amplifier loudspeaker system. During injection the noise of steam bubbling into the sodium could be clearly heard. The reaction generally proceeded smoothly but, occasionally, crackles suggested that water rather than steam was being injected. Brief temperature increases of up to 200°C were recorded during these periods.

In the arrangement which gave the most reproducible results, the specimen was bent into an L-shape and attached directly to the water needle so that the jet impinged directly on to the specimen surface. To dry the steam more thoroughly and avoid the occasional violent injections of water, a simple heat exchanger was incorporated into the water-feed line and immersed in the sodium. In three experiments with this arrangement using mild steel specimens, weight losses of 0.631, 0.647 and 0.598 g were obtained with a water-injection rate of 1 ml/min for 30 min. The corrosion was concentrated into a small area at the point of impingement of the jet and a crater was formed; in some cases an accretion of iron powder was deposited around the corroded area. The maximum penetrations of the specimens were 0.016, 0.016 and 0.023 in. The jet diameter was 0.1 in. and it was clamped 0.1 in. from the specimen.

Using this assembly the corrosion of a range of steels was compared, and a study was made of the effect of sodium temperature and the specimen jet distance. As before 30 ml of water were injected over 30 min and the standard temperature was 500°C. The results of these tests are summarized in Table II.

TABLE II. SUMMARY OF SMALL-SCALE EXPERIMENTS

Experiment			Total weight loss (g)	
Comparison of various materials	18-8-1	Stainless steel	0.018	
	316	Stainless steel	0.015	
	2¼ Cr - 1 Mo	Ferritic steel	0.436	
	9 Cr - 1 Mo	Ferritic steel	0.203	
	12 Cr - 1 Mo	Ferritic steel	0.347	
	Incoloy 800		0.004	
Effect of temperature	350°C)	2¼ Cr - 1 Mo Ferritic steel	0.002	
	400°C)		0.050	
	450°C)		0.323	
	500°C)		0.436	
	550°C)		0.349	
				Maximum penetration (in.)
Effect of specimen-jet spacing	1/16 in.	Mild steel	0.6219	> 0.045
	1/8 in.		0.6284	0.035
	1/4 in.		0.9511	0.006

The corrosion of Incoloy 800 and stainless steel was clearly less than that of the ferritic alloys. Increasing the chromium content of the latter appeared to have little effect, but the chromium alloys do appear to be slightly superior to mild steel.

The sodium temperature has a marked effect on the corrosion and the weight loss increased rapidly on increasing the temperature from 350°C - 450°C. This is surprising in view of the probable high local temperature, and is most likely to be associated with the decomposition of sodium hydroxide. Increasing the temperature above 450°C had little further effect.

Increase in the jet-to-specimen spacing decreased the penetration although the total weight loss on the specimen did not change very much and may even have increased with increase in spacing. This resulted in a change in the corrosion pattern with an increase in the over-all area affected. A smaller jet, 0.45 mm in diameter, was used in these tests. It is likely that with a pressurized water system at very close spacing of the specimen to the jet the corrosion would again fall off. This appeared to occur in the corrosion test on the sodium water rig but could not be reproduced in these low pressure tests.

To determine the magnitude of the corrosion which could arise solely as a result of the specimens being heated in sodium containing the reaction products, a further series of experiments was carried out. In these, water was added to the sodium, and the specimens were immersed and heated for up to 24 h. With sodium to which 2 wt.% water had been added the weight losses on specimens heated at 500°C for 24 h were generally less than 5 $mg/cm^{-2}/d$. This was uniformly distributed over the surface and could be neglected in comparison with the rates occurring during the reaction.

FEATURES OF THE CORROSION PROCESS

While it cannot be suggested that the corrosion process is completely understood some features can be deduced from the results so far.

The wastage appears to be a direct result of the conditions during the reaction. The appearance of the specimens and the pattern of damage under small leak conditions suggests that the corrosion is localized to the path of the water-steam jet with the main damage being concentrated where the sodium-water reaction front impinges on a metal surface.

In the rig tests simulating full-scale tube failures the conditions at the point of injection are rather different, and a well-formed jet giving a clearly defined corrosion pattern would no longer be expected to form. Instead rapid displacement of sodium from the injection region should occur. Under these conditions any corrosion would be expected to be small and distributed over a wide area. This is confirmed by the lack of visible corrosion in the majority of the tests, and by observations reported from a study carried out at Atomic Power Development Associates where no corrosion was obtained at injection rates greater than 1.5 lb/s [1].

Tests 5 and 8 showed that even with a full-bore tube failure considerable thinning of tubes in the region of the leak can occur. The corrosion was sufficiently extensive to suggest that if the second burst had been connected to a back-up water supply there may have been further failures.

The reason for the difference in behaviour is not clear but it is probably associated with a disturbance of conditions at the point of injection which allowed a partial jet to form. Under some circumstances it may be possible for either the simultaneous failure of a number of tubes to occur giving a more violent reaction, or for the corrosion to cause a succession of tubes to burst with the rapid imposition of a series of shock waves on the outer shell. It is unlikely that optimum conditions for corrosion were fully reproduced in the large-scale tests. If the corrosion mechanism were more fully understood, and the effect of various parameters could be specified, it should be possible to define the optimum conditions more clearly.

The maximum corrosion damage was observed in the one-sixth scale model test but from the high weight loss per gram of water in the small tests it appears likely that the extent of corrosion could be increased by reducing the rate of addition of water.

The effect of temperature observed in small-scale tests is of particular interest, and would suggest that a rapid increase in the damage will occur if the sodium temperature is raised to 450°C. No large-scale tests have been reported at temperatures above 400°C, and very few experiments have been carried out above 300°C to substantiate this.

The corrosion of iron in oxygen-contaminated sodium has been associated with the formation of a double oxide $(Na_2O)_2FeO$. The rate of corrosion increases rapidly with increase in temperature, and the high local temperatures together with the constant supply of oxygen may be sufficient to account for the high rates. It has also been suggested that the stability of this compound depends upon the oxygen activity in the sodium, and it would therefore be expected to vary with temperature. Thermal cycling in a sodium-oxygen system may result in repeated formation and reduction of the double oxide leading to enhanced corrosion. Conditions during a sodium-water reaction with large temperature excursions and high local concentrations of sodium oxide appear to be particularly favourable for this process. The presence of iron powder in the corrosion region lends further support to this mechanism since it can be formed by reduction of $(Na_2O)_2FeO$ in a sodium-rich environment.

At low levels the corrosion of nickel is independent of the oxygen level and a similar double oxide of nickel has not been isolated. While it is nevertheless possible that compounds of this form exist they appear to be more difficult to form, and this may account for the lower corrosion with stainless steel and Incoloy 800.

REFERENCE

[1] MORABITO, J. J., SAVAGE, H. W., Major Components and Test Facilities for Sodium Systems, USAEC Rpt ANS-100 (1965) 308.

AN INVESTIGATION OF TUBE WASTAGE CAUSED BY SMALL LEAKS OF WATER IN SODIUM-HEATED STEAM GENERATORS

H.O. MUENCHOW AND W.L. CHASE
ATOMIC POWER DEVELOPMENT ASSOCIATES, INC.,
DETROIT, MICH.,
UNITED STATES OF AMERICA

Abstract

AN INVESTIGATION OF TUBE WASTAGE CAUSED BY SMALL LEAKS OF WATER IN SODIUM-HEATED STEAM GENERATORS. Examination of the results from a sodium-water reaction that occurred in a steam generator in the Enrico Fermi Plant revealed a generalized corrosion in the area of the reaction, producing failure of some of the adjacent tubes. The questions raised by this experience clearly indicated that the problem of small leaks causing general tube wastage should be investigated.

An experimental programme was designed and divided into two categories: (1) basic studies to establish the mechanisms of wastage, including wasted surface temperature measurements, chemical attack and hot erosion; (2) studies to establish the effect of design and operating parameters on wastage occurring in a test rig that simulates the dynamics of a commercial steam generator.

A small test rig supporting a 4-ft-high reaction vessel containing 5 gal of sodium was constructed. Wasted surface temperatures measured in this rig using thermocouples as the target for the sodium-water reaction have indicated temperatures in excess of 2200°F.

Corrosion studies, using the reaction products NaOH and Na_2O, have shown severe attack on 2¼ Cr-1 Mo steel tabs in 1 h under an argon atmosphere from 2200°F to 2400°F. Evidence indicates that corrosion is (1) minimal in the gas space above the reaction products, (2) extremely severe at the gas-liquid interface, and (3) less severe in the molten reaction products.

A 101-ft-high support structure was constructed to house a test rig designed to simulate the conditions in a commercial sodium-heated steam generator. The test rig circulates 5700 lb of sodium at 400 gal/min through a 16-ft-high reaction vessel. Tests conducted in this rig have shown that the circulating water coil, which served as the target tube during the sodium-water reaction, was wasted to the point of rupturing, causing a large secondary reaction and additional damage to surrounding material. The temperature recorder went off scale at 2200°F, indicating higher temperatures. In addition, large quantities of hydrogen, resulting from the reaction, were vented to the atmosphere without incident through a 2-in. pipe and an oil-filled reaction products trap.

1. INTRODUCTION

On December 21, 1962, the large sodium-water reaction in the No. 1 steam generator of the Enrico Fermi Atomic Power Plant (EFAPP) changed the thinking of engineers concerned with the design of sodium-heated steam generators. Prior to this event, engineers were primarily concerned with the handling of a large leak that was known to produce high surge pressures of fairly short duration, i.e., usually a leak resulting from the severing of one water tube. To handle this, the engineers designed the walls of the steam generators to withstand these surge pressures and included certain safety factors that would take care of any pressures not predicted by the experimenters.

Although large leaks were of some concern, small leaks were not. The existing philosophy prior to December 1962 seemed to be: "Small leaks will be detected early, and the steam generator will be shut down and repaired before any damage occurs." The incident at Fermi changed this. After the bundle had been removed and cleaned, a visual inspection showed that a small initiating leak had produced gross removal of metal by corrosion, erosion, or some unknown process. This process of metal removal, now called wastage, was severe enough to weaken other tubes to the point of rupture. This type of wastage can lead to many conjectures: It is possible that a chain reaction can be triggered in a steam generator during which a small initiating leak might waste holes in other tubes which, in turn, could cause other leaks. Eventually all tubes could be leaking, resulting in a very large reaction. Another possibility is that a small leak or leaks could insidiously waste away other tubes in a fairly large area of the steam generator. The final result might be that all the thinned tubes could rupture simultaneously, resulting in a very large surge pressure. In short, the Fermi incident proved that, in steam generator design, much more must be considered than the classical severed tube. A small leak of water in sodium must be considered.

As a result of the incident at Fermi and problems at other sites, the steam generator has been described as one of the weakest links in the heat transport chain in sodium-cooled reactors.(1) This impression must and will change when adequate design knowledge and successful operating experience are available. The fast reactor program must have reliable components. One approach to reliability in steam generators was the use of multiple-walled tubes which resulted in higher cost and did not provide long-term reliability in all cases. In at least one case, a leak occurred through both tubes, causing a sodium-water reaction.(2) Therefore, it is essential for engineers to understand sodium-water reactions and how to handle small and large leaks in the design of a steam generator. To help provide this knowledge APDA, under contract to the USAEC, is investigating the effect of small leaks of water into sodium in a sodium-heated steam generator. The specific objectives of this investigation are to:

(a) Determine the actual mechanism or mechanisms of wastage
(b) Establish a means of estimating the extent of tube wastage during a small leak of water into sodium
(c) Determine the dominant parameters of tube wastage during a small leak of water so that they may be applied to the design of a unit
(d) Determine suitable procedures for operating a steam generator after detection of a small leak.

It is the purpose of this paper to discuss the program, to present the results to date, and to indicate the future work in this area. Basically, the experimental program is divided into two categories:

(a) Experiments designed to provide a basic understanding of the phenomena which may contribute to rapid wastage. In these tests the effect of temperature, corrosion, erosion, etc., are measured without the presence of other variables.
(b) Experiments to show the effect of all variables combined with the dynamic characteristics of a large sodium-heated steam genera-

tor. These tests show what would happen should a small leak develop in a sodium-heated steam generator. The work in this category is concentrated on the safety aspects of the sodium-water reaction to determine the parameters to be considered in the design of a sodium-heated steam generator.

2. DESCRIPTION OF TEST EQUIPMENT

In the discussion to follow, reference will be made to Rig 10, Rig 43, and the corrosion test equipment. Rig 10 is a large test rig for examining small leaks of water into sodium under conditions simulating the environment of a steam generator. Rig 43 is a small rig designed to provide an environment for studying specific phenomena (i.e., temperature, erosion, etc.) associated with small leaks of water into sodium. As implied in its name, the corrosion test equipment is designed to permit the study of one aspect of sodium-water reactions--corrosion of steel by the products of a sodium-water reaction at high temperature.

2.1 Rig 10

The schematic flow diagram for Rig 10 is shown in Figure 1a. This rig consists of five main systems:

(a) the sodium system
(b) the circulating water system
(c) the reaction water system
(d) the reaction products system
(e) the nitrogen cover gas system.

The sodium system consists of the test unit, the filter tank, the centrifugal pump, and the dump tank. Also included in the system is a cold trap and a plugging indicator system. During a test, sodium is circulated by the pump down through the bundle in the test unit, through the filter tank, and back to the pump. After the completion of a test, the sodium is dumped through the filter tank to the dump tank. Should the filter tank become plugged with reaction products, the filter tank bypass may be used for dumping; this bypass is also used for filling the system.

The circulating water system contains a pressurizer, an air-cooled heat dump, and two rapid response valves for emergency isolation. The pressure for this system is provided by a 6000-psi bottled nitrogen station.

During operation, the high-purity boiler feedwater flows by gravity to the test coil where it is heated, then to the air-cooled heat dump where it is cooled prior to returning to the pressurizer.

Since the quantity of water in the reaction water system is rigidly controlled, this system is separate from the circulating water system and consists of the reaction water storage tank and a quick closing valve to shut off the water in an emergency. During operation, these are

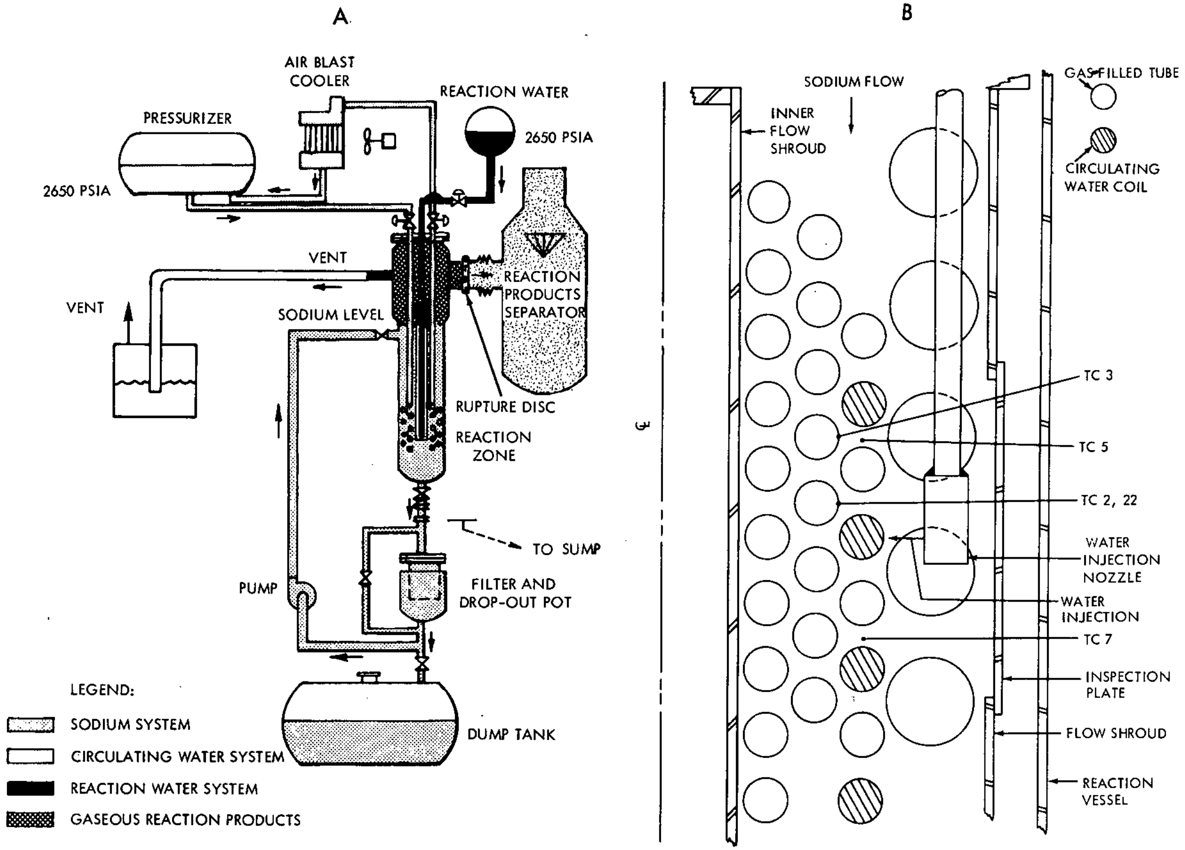

FIG. 1. Rig 10
(a) Flow diagram
(b) Elevation cross-section of tube bundle assembly

connected to the reaction water trigger tube. When the system is triggered, the water flows through the orifice toward the target area.

Reaction products from a sodium-water reaction are vented through two systems. The primary vent system consists of a pressure control valve, a two-inch pipe to an oil reservoir, and a vent on the reservoir. During operation, the gas flows into the oil, bubbles through the oil and vents to the atmosphere. Particulate matter and sodium droplets are left in the oil. Should the flow rate be too great for the primary vent system, the gas pressure will rise, and at about 50 psi the rupture disk in the back-up system will burst to relieve the reaction products. These reaction products are vented to the atmosphere through a centrifix separator which removes the particulates and droplets. This system has not operated because the primary vent system has been entirely adequate to this date.

The nitrogen cover gas system provides an inert atmosphere over the various sodium surfaces and in the two vent systems. Nitrogen is supplied through pressure control valves to the various components as needed.

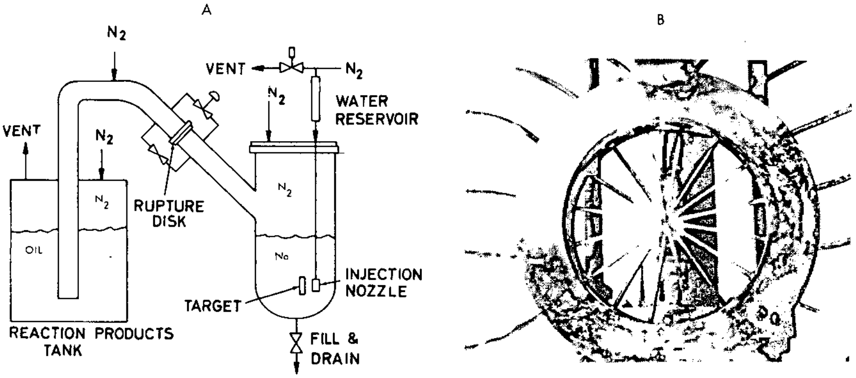

FIG. 2. Rig 43
(a) Schematic diagram
(b) Hub-and-wheel thermocouple array

The relative location of two pieces of equipment should be understood before discussion of the tests. As can be seen from Figure 1b, the injection nozzle is located about halfway down the tube bundle and is oriented to direct the reaction water at the circulating water coil. This figure also shows the location of various thermocouples in the reaction zone and positions of the flow shrouds, the inspection plate, and the wall of the reaction vessel.

2.2 Rig 43

Rig 43 is designed to study only one variable of the sodium-water reaction at a time; therefore, it has been made much smaller and less complex than Rig 10. Rig 43 is essentially a small test vessel (12 inches in diameter by 42 inches high) containing stagnant sodium (Figure 2a).

Attached to the vessel are appropriate nitrogen systems and a double vent system, one through a pressure control valve and one through a rupture disk. As on Rig 10, the rupture disk is a backup for the primary vent system. Both vent systems release the reaction products under oil.

The initial series of tests in Rig 43 is concerned with the temperature resulting from a small leak of water into sodium. Therefore, the target for these tests is composed of sixteen 1/16-inch-diameter stainless steel sheathed thermocouples swaged down to 0.040 inch at the hot junction. These are arranged like the spokes of a wheel with one thermocouple at the center and the rest arranged radially about 3/4 inch from the center (Figure 2b). This target of thermocouples is so arranged that it may be moved from 1/4 inch to 4 1/2 inches from the front of the injection nozzle.

2.3 Corrosion Test Equipment

The corrosion test equipment is basically quite simple consisting of small test tubes, 5/8-inch outside diameter by about 4 inches long with a 0.086-inch wall, made of 2 1/4 Cr-1 Mo steel containing sodium hydroxide (Figure 3). The tube is supported in a field of an induction heating coil under an inert atmosphere. In some of the tests, small

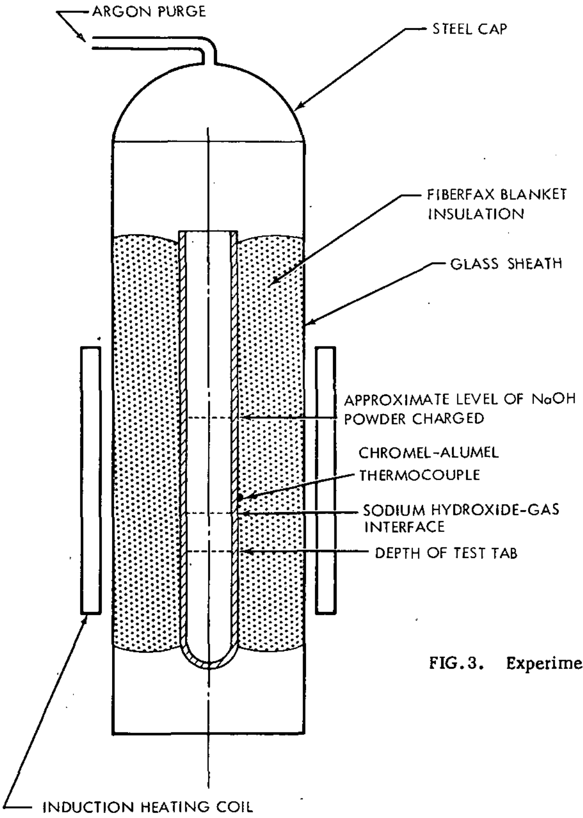

FIG.3. Experimental apparatus used in corrosion studies

tabs of 2 1/4 Cr-1 Mo steel have been inserted in the test tube to provide additional data.

3. EXPERIMENTAL RESULTS

3.1 Rig 10

To date, only two tests have been completed in Rig 10. The conditions for these two tests were essentially the same, as shown in Table I, except for the reaction water injection point to target tube spacing and the target.

TABLE I - RIG 10 TEST CONDITIONS

Conditions	Test 1	Test 2
Sodium flow rate, gpm	400	400
Bulk sodium temperature, °F	632	618
Sodium plugging temperature, °F	380	335
Sodium cover gas pressure, psig, N_2	10	10
Circulating water		
Flow rate, gpm	~1	~1
Temperature, °F	632	618
Pressure, psia	2650	2650
Reaction water		
Weight injected, lbs	0.88	0.88
Flow rate, lbs/sec	$\sim 2.9 \times 10^{-3}$	2.9×10^{-3}
Temperature, °F	632	618
Pressure, psia	2650	2650
Injection orifice ID, in.	0.008	0.008
Injection point to target spacing, in.	~1-1/4	1
Target	carbon steel plate	2 1/4 Cr-1 Mo tube 1 in. OD X 0.120 in. wall

3.1.1 Test 1, Rig 10

During the first test, the maximum local temperature increase recorded was 21°F; the cover gas pressure increased slightly from 10 to 13 psig. When the tube bundle was removed, samples of the material adhering to the surfaces were taken at various locations for analysis. The bundle was quite clean with only a thin coating of white material covering the surfaces. After steam cleaning, the section of the flow baffle which contained the wastage area was cut out for a more detailed dimensional inspection and metallurgical analysis. Inspection of the target area indicated that the metal surface was wasted away to a maximum depth of 16 mils below the original surface. The wastage area exhibited a highly polished surface and, upon magnification, showed many hills and valleys. Metallurgical examination of the wasted area revealed a more uniform and undisturbed grain structure; a microhardness survey of a cross-section through the wasted area indicated no significant change in hardness from that of the parent material.

3.1.2 Test 2, Rig 10

The second test was more dynamic. Within one minute after water injection, the sodium temperature in the target area reached 760°F. The temperature then decreased slightly to about 740°F at the end of two minutes, increasing to a maximum of 800°F for the 300-second injection period. At approximately 320 seconds, a disturbance occurred in the system which was first noted on the high-speed temperature recorders. Within one second after initiation of the disturbance, temperatures in the vicinity of the target area went off scale (2000°F). Other indications that the target tube had ruptured and circulating water was being injected into the sodium were:

(a) The reaction vessel cover gas pressure increased from 10 to 18.5 psig.
(b) The circulating sodium flow decreased from 400 gpm to about 140 gpm.
(c) The hydrogen detector went off scale, maximum range 5000 ppm, about 30 seconds after the large disturbance began.
(d) The reaction products tank vent line spewed a mixture of gases and visible material (probably oil vapor) at a very high velocity.
(e) The circulating water pressure decreased from 2650 psia to 1850 psia.

Two minutes after the initiation of the disturbance, the circulating water system was isolated. A plugging run was attempted and the system plugged immediately with the plugging valve wide open. Prior to draining, the sodium was circulated for a two-hour period. After the flow returned to normal, the sodium was dumped into the storage tank.

When the system had cooled, the tube bundle was pulled and inspected. When the inspection plate was removed, there appeared to be a brown glaze covering all visible tubes. Heavy, hard, brown, glass-type stalactities covered the tubes adjacent to the injection area, and white deposits adhered to the nozzle assembly and the inspection plate. The skirt supports had hard, heavy deposits that looked like concrete. The entire top of the tube bundle was covered with oxide material which, in some areas, was about 4 inches deep. Closer examination disclosed that the injection water wasted the 0.120-inch wall of the target tube to the point of rupture. In addition, about one-half of the left support of the trigger assembly was wasted, and a slit was cut through the 1/8-inch-thick inspection plate by the circulating water issuing from the target tube.

After tube bundle disassembly and steam cleaning, the wastage area on the target tube was found to have a circular hole which had pressure-ruptured outward. Inspection of the nozzle assembly after removal indicated that the nicrobraze material had melted around the capillary, and the high-pressure nitrogen inside the nozzle assembly had ejected the capillary. This probably happened after the high-pressure water from the slit in the target tube squirted back onto the nozzle and the temperature exceeded the melting point of the nicrobraze (approximately 1650°F). In addition, wastage along one side of the nozzle had taken place to a depth of 25 mils. The only visual wastage to the tubes occurred on the water target tube and the gas tube directly above it. The Type 304 stainless steel and 316 stainless steel gas-filled tubes located behind the target tube suffered no visual damage.

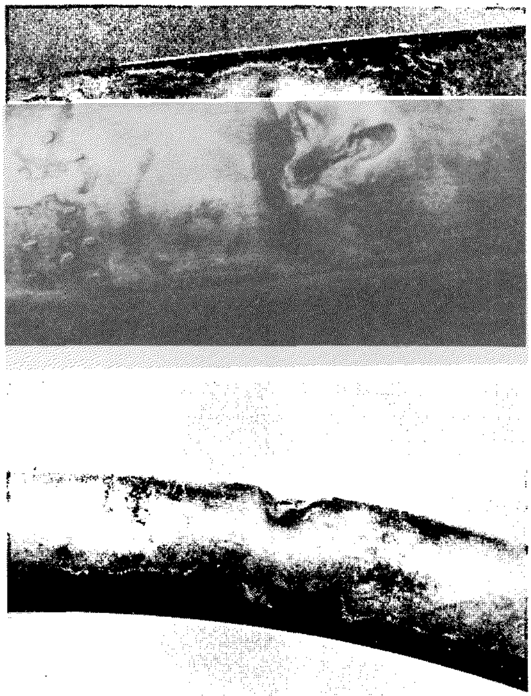

FIG. 4. Wasted portion of target tube, Test 2, Rig 10

The wasted portion of the target tube, shown in Figure 4, was sectioned into sixteen 3/16-inch pieces to facilitate microstructural examination and microhardness survey. Figure 5a shows a schematic diagram of the area where photomicrographs and hardness measurements were taken. Figure 5b is an axial hardness plot on a line through the center of the wasted area and at 20 degrees from it. This indicates some hardening of the material near the wasted area and a softening trend on either side of it, indicating a subcritical anneal at temperatures of 1350°F or below. The hardness data also shows the nonuniformity of the structure. High hardness, 220-270 Knoop, was associated with a darkened surface layer. This effect was not found on both sides of the wasted area in a given sample, indicating that one side had been cleanly wasted away leaving no trace of hardening.

In general, the photomicrographs taken in support of the microhardness measurement showed microstructural modifications indicating

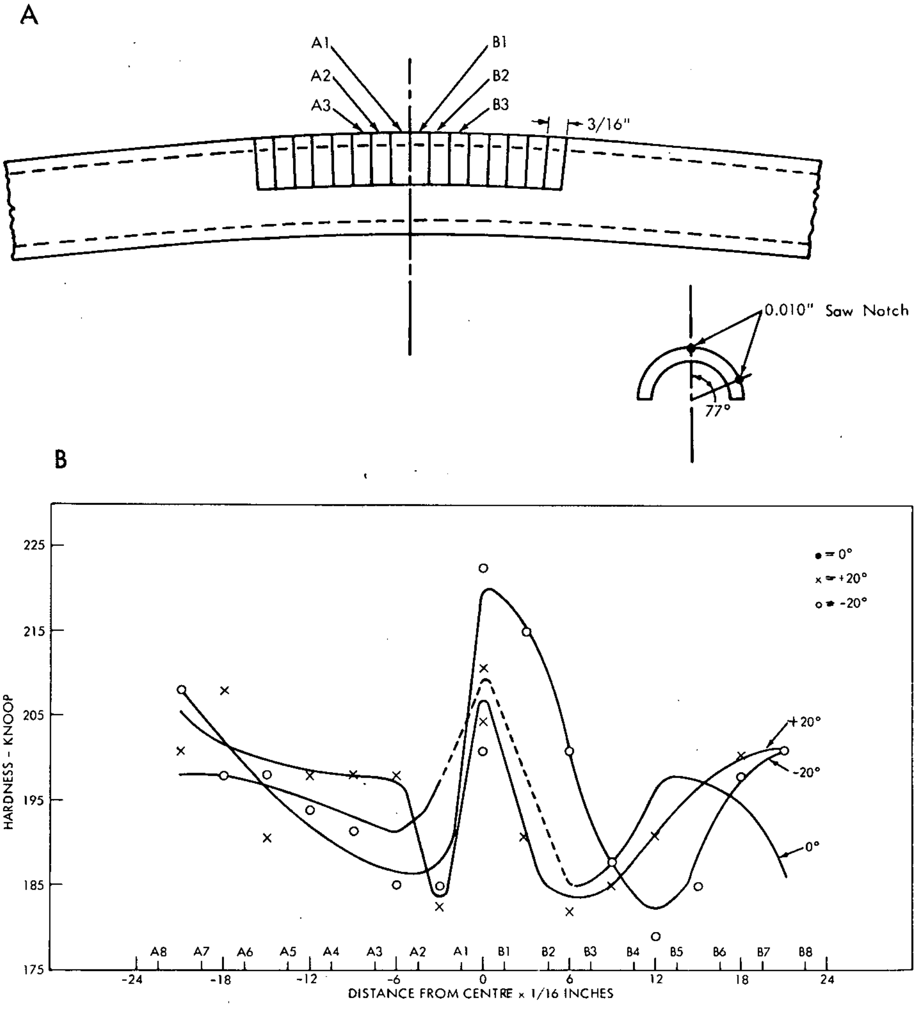

FIG. 5. Results from Test 2, Rig 10

(a) Sample identification of 2½ Cr-1 Mo tube

(b) Axial hardness transverse, 0.003-in. depth

that the wasted region reached temperatures above the 1400°F transformation temperature. Changes similar to these have been observed in Croloy specimens where they were subjected to temperatures of 1500 to 1550°F for approximately one minute. However, similar changes could also be produced in shorter periods of time by higher temperatures, or in longer periods of time by temperatures slightly in excess of 1400°F.

Two samples of the reaction products directly under the target tube were analyzed by X-ray diffraction. The results revealed the presence of alpha iron (ferritic) and gamma Fe_2O_3 (maghemite). The maghemite may have been produced by oxidation of the parent metal by steam. The ferritic iron could have been produced by direct mechanical abrasion caused by a high-velocity stream consisting of a combination of water, steam, and reaction products. It also could have been produced by reduction of the maghemite by sodium or hydrogen in the presence of localized high temperatures.

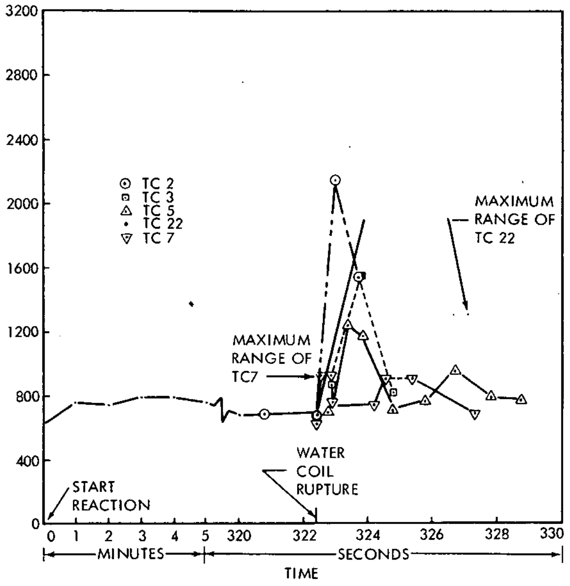

FIG.6. Temperature in reaction zone, Test 2, Rig 10

Figure 6 is a temperature history in the reaction zone during the test. A cross-sectional view of the tube bundle assembly, shown in Figure 1b, indicates the location of the thermocouples that provided the data plotted on Figure 6. Assuming the reaction produces sodium monoxide and hydrogen, heat balance calculations have shown that for a total weight of 5693 pounds of circulating sodium to sustain a bulk temperature rise of 75°F, 31.5 pounds of water must be injected into the system.

The water flow through the injection nozzle was found to be two-phase, critical flow due to the high temperature of the surrounding sodium and the high pressure drop across the capillary tube. Using two-phase, single component critical flow theory, the flow rate was calculated to be 2.9×10^{-3} lb/sec, resulting in a total calculated injection time interval of 300 seconds. The calculated velocity of the two components was 275 ft/sec for the liquid and 1250 ft/sec for the vapor. The calculated quality of the steam at the capillary exit was 14.6%.

3.1.3 Discussion of Results

An attempt was made to explain the difference in wastage experienced between Test 1 and Test 2 in Rig 10. The first significant fact con-

TABLE II - RIG 43 TEST SUMMARY

Test No.	Injection Point to Target Spacing, in.	Water Injected, pounds	Starting Bulk Sodium Temperature, °F	Injection Time, seconds	Water Injection Rate, lb/sec	Maximum Temperature, °F
1	1	0.11	612	41	2.68×10^{-3} (a)	1464
2	18/32	0.11	607	34	3.23×10^{-3}	1382
3	1-1/2	0.11	607	35	3.14×10^{-3}	693
4	3/4	0.11	600	33	3.34×10^{-3}	1545
5	3/4	0.11	600	(b)	(b)	1494
6	3/4	0.11	610	32	3.44×10^{-3}	1337
7	3/4	0.11	600	34	3.23×10^{-3}	910(c)
8	3/4	0.11	612	33	3.34×10^{-3}	1464
9	3/4	0.11	595	36	3.05×10^{-3}	1420
10	1-1/4	0.11	608	(d)		1279
11	1-1/2	0.11	605	(d)		709
12	1	0.11	600	(d)		706(c)

(a) Nozzle size - 0.008-inch ID nominal

(b) Temperature recorder was not turned on until reaction had commenced.

(c) Injection capillary partially obstructed causing a spray injection and probably reducing the maximum temperature

(d) Not recorded

sidered was the difference in distance between the water injection point and the target in the two tests. In the first test, the wasted area on the plate was about two inches away from the injection point (apparently the jet sprayed at an angle), while in the second test the wasted area on the target tube was one inch away from the injection point. In the case of the first test, the distance involved could have led to a more diffuse reaction at the wasted area since the water jet had more time to react with the sodium prior to reaching the metal surface. Also, the longer path would provide more resistance to the water flow and, therefore, allow less water to reach the surface, resulting in a less severe reaction at the surface.

The calculated sodium velocity in the wasted area of the plate was 0.8 ft/sec, while the velocity in the target tube area was 0.3 ft/sec. This might cause a more rapid dissipation of heat in the wasted area of the plate and tend to minimize wastage. These hypotheses will be resolved as the data from future tests become available.

3.2 Rig 43

A program involving the use of the small test apparatus, Rig 43, was formulated to study the primary mechanisms of metal wastage. Rig 43 was designed to fulfill the requirements of an apparatus that can be used in the basic support and variable screening tests for the Rig 10 program. The test vessel and trigger tube were constructed to reduce turn-around time and to make the rig applicable to varying types of tests.

It has been concluded that the possible mechanisms of wastage are largely dependent on the temperature of the metal surface at the wasted area during a sodium-water reaction. As a result, a series of tests is being run using thermocouples as the target. To date 12 tests have been conducted in Rig 43 to determine wastage surface temperatures during a sodium-water reaction. Table II and Figure 7 are a summary of the test results.

In Test 1, wastage occurred on 2 of the 16 target thermocouples; only insignificant wastage has occurred in the subsequent tests.

Figure 7 indicates that the maximum metal temperature occurred when the target was between 3/4 and 1 1/4 inches from the injection orifice. However, none of these tests have approached the 2000°F temperature indicated in Rig 10. It is postulated that the heat transfer characteristics established in the Rig 43 reaction are essentially isothermal. The relatively small amount of heat input, resulting from the reaction of the 0.11 pound of water, does not overtax the heat removal capability of the reaction surroundings. In contrast, when the target tube ruptured in the Rig 10 test, the heat input rate, resulting from the comparatively large water leak rate, was sufficiently great to overcome the heat removal capabilities of the reaction zone surroundings. Thus, conditions approached those of an adiabatic system and the reaction temperature may have approached the stoichiometric, adiabatic maximum of 3000°F, as indicated in Figure 6.

A significant observation was made during the test series. Inspection of the target after the third and eleventh test revealed that a much heavier coating of solid oxide reaction products had been deposited than had been deposited after the other tests. It would appear that most of the reaction had taken place before the target was reached, and the solid reaction products were carried and deposited on the target 1 1/2 inches distant. These products tended to insulate the target from the heat generated which resulted in the much lower temperature recorded.

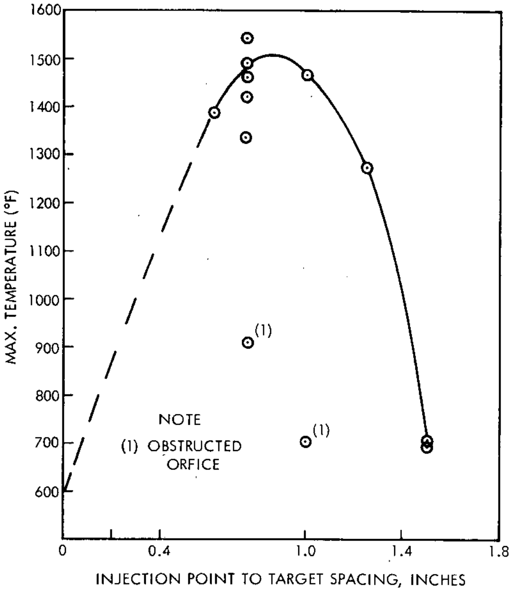

FIG. 7. Wasted surface temperature versus target spacing, Rig 43

Tests 7 and 12 did not reproduce the higher temperatures experienced in earlier tests having the same target spacings, 3/4 and 1 inch, respectively (Table II). The target was heavily coated with reaction products as in the tests with the 1 1/2-inch target spacing, again indicating that the reaction had taken place prior to hitting the target. When the injection nozzles were inspected by squirting water through their orifices into air, it was found that partial obstructions had caused the water to form a spray rather than the liquid jet exhibited by the other nozzles. It is postulated that the spray allowed better reactant mixing, resulting in more reaction products forming ahead of the target and depositing on the target than had been experienced with comparable tests. Again this insulating effect caused the lower temperature readings.

From this observation, the following statements can be made:

(a) It is evident that the most severe condition of leak geometry is being simulated by using an orifice which produces a jet. In the actual operation of a steam generator, no leak geometry may be expected to be more severe than that obtained in the test programs. It is generally accepted that small leaks occurring in tubing will come from irregular, rough fissures through which the water pressure drop will be sufficiently great to cause water drops or a spray.

(b) It is possible to reduce the reaction temperature which a target will experience by causing a jet leak to become a spray prior to reaching the target, essentially causing the reaction to occur at a location other than the tube surface. This is significant because a steam generator tube bundle may be designed incorporating a jet guard which protects small sections of the tube bundle. In this way, should a jet leak occur, only a small segment of the total number of tubes would be endangered before detection.

3.3 Caustic Corrosion Studies

The mechanism of metal wastage in a sodium-water reaction zone is not known. Knowledge of the mechanism should be very useful in interpreting the results of such reactions in a steam generator. Therefore, it is important to develop the qualitative understanding of the mechanism of tube wastage, and the effect of the parameters of sodium, water, and hydrogen concentrations, and metal reaction temperature on the rates observed.

Sodium water reactions are extremely difficult to control and reproduce. Since sodium hydroxide is one of the solid reaction products of the sodium-water reaction, it seems likely that quantitative studies of caustic corrosion of metals at the temperatures expected in sodium-water reactions will yield reproducible information on this one mechanism of tube wastage.

It has been shown that sodium water reactions generate temperatures in excess of 2000°F. The work of D.D. Williams(3) indicated that significant attack on iron starts at approximately 1100°F, and that the rate of attack and the nature of the reaction products are related to the rate of removal of the sodium metal and volatile hydrogen generated during the reaction. However, no information appears in the literature on the rate of attack of sodium hydroxide on Croloy at temperatures above 1500°F.

The experimental apparatus shown in Figure 3 was designed and constructed to determine the corrosion rates of metals of interest in sodium hydroxide. The first test specimens were 5/8-inch, 2 1/4 Cr-1 Mo steel tubes partially filled with sodium hydroxide and heated from 2200 to 2400°F using an induction heater. Figure 8 is a plot of the data from recent preliminary screening tests which have been made using the solid reaction products sodium hydroxide and sodium monoxide.

The results are presently being analyzed; however, some general observations may be made at this time. The specimens exhibited severe intergranular corrosion where the Croloy was submerged in sodium hydroxide. Above the sodium hydroxide surface, intergranular corrosion was also evident, but not as severe as that below the hydroxide surface. At the sodium hydroxide-argon interface, the corrosion was very high compared to the other two regions. In this zone, some material has been removed.

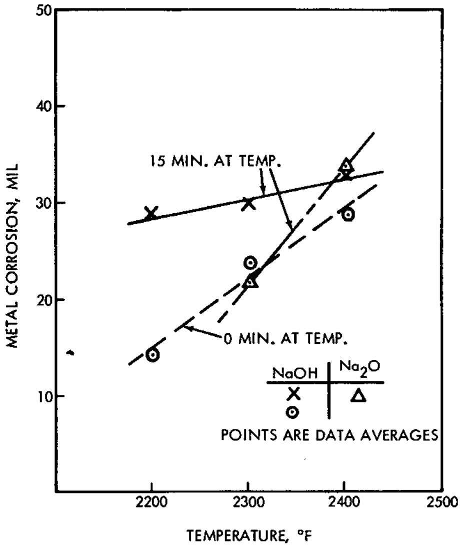

FIG. 8. Caustic corrosion of Croloy

4. GENERAL CONCLUSIONS

(a) It was determined that large quantities of hydrogen could be vented to the atmosphere through a pressure control valve and an oil bath. It is very significant that this method of operation prevented a high pressure buildup that could rupture the 24-inch rupture disk in Rig 10. Future steam generators may design such a vent system into the unit, thus reducing the shell design requirements and the necessity of a massive reaction product system similar to that of the Fermi units.

(b) Simple design innovations may be made to the tube bundles to prevent tubes or small groups of tubes adjacent to a small leak from experiencing higher reaction temperatures at their surface. Thus, the possibility of a small leak propagating into a chain reaction involving a great portion of the tube bundle before detection is practically eliminated.

5. FUTURE WORK AT APDA

The original test series outlined for Rig 10, the large unit, will be continued. The work will be expanded to investigate leaks occurring in the steam portion of the tube bundle and correlating leak detection indications with sodium-water reaction. The rig will then be used to investigate the effects of large leaks into sodium.

Rig 43 will be used to investigate steam oxidation of tube material, hot inert gas erosion of tube material, and variable scoping tests for Rig 10.

Work will continue on the basic caustic corrosion studies to determine the effect of sodium-water reaction products on Croloy and other metals.

REFERENCES

[1] GIAMBUSSO A., WENSCH, G.W., The USA fast breeder reactor program, VIII Nuclear Congress, Rome, Italy (1963).

[2] LOCKHART, R.W., KUKFA, R.S., MILLER, D.R., ROBB, W.L., KAPL-1450 (1955).

[3] WILLIAMS, D.D., J.Am.chem.Soc. 78 (1956) 5150.

DISCUSSION

(on the foregoing two papers)

N. LIONS: I should like to ask the authors how, in their opinion, the initial sodium velocity is liable to affect the corrosion due to reaction products. Do they think the results of these tests, particularly those carried out with static sodium, present an unduly gloomy picture of the corrosion effects likely to be found in an actual steam generator?

R.A. DAVIES: I do not think that the velocity of the sodium matters when the leak is above a certain size since the amount of turbulence caused will outstrip any velocity effects. I would not like to say offhand, however, how big the leak has to be. As some at least of the experiments described in the other paper under discussion were carried out under flowing-sodium conditions, perhaps Mr. Chase could say whether he thinks there is any great difference between flowing and non-flowing conditions.

W.L. CHASE: In our case the results were similar for both systems, viz. for static and flowing sodium. Since the large rig (Rig 10) simulated an actual steam generator with flowing sodium and since the results obtained were similar to those obtained in static systems, I do not think that the results present too gloomy a picture. It should also be remembered that the incident at Fermi on 12 December 1962 occurred in a flowing system and that the results were the same.

E.L. ZEBROSKI: What was the time constant of the thermocouples used in these investigations? Is it perhaps possible that rapid oscillations above the melting temperatures of the tube wall occurred but were not detected?

R.A. DAVIES: We used thermocouples of about 7 mm. The trouble with small thermocouples is that they are liable to get lost. We have actually observed peak temperatures of 1300°C and, while I do not believe that the melting mechanism is the only possibility, surface melting could perhaps occur here and there. I must add, however, that the actual ruptures we have had did not look as though they had been caused by melting.

W.L. CHASE: In our small rig we used rapid-response French thermocouples. I cannot remember what the diameter and response time of these thermocouples are but one of the French participants may know this. As for the question of melting, if the melting temperature does occur, it must occur extremely rapidly. We have seen no evidence for it on the tube surfaces.

N. LIONS: I imagine these thermocouples are the same as the ones we have been using in our tests on sodium-water reactions. The diameter of our thermocouples is 0.25 mm and the response time is about 30 ms.

B. KULPIN: Mr. Chase, how do you explain the fact that the thermocouple target indicated a temperature of ~ 800°F for the first three minutes and 2200°F after that?

W.L. CHASE: In the experiment in which we obtained temperatures above 2000°F, the target was not a thermocouple but a tube containing water at high pressure. The temperature of ~800°F was determined during the injection of the primary water. The high temperature value was obtained after the secondary rupture of the water tube and the secondary injection of water, which involved larger quantities and greater flow rates than the primary injection. Information on this is given in the temperature plot of Test 2, Rig 10 (Fig. 6).

B. KULPIN: Since there are three zones in the reaction jet (a water zone, the reaction zone proper and a reaction product zone), the rate of target wastage must vary depending on which zone the target comes into contact with. Have you studied target wastage in the different zones of the jet?

W. L. CHASE: In Rig 43 we measured the variation in temperature as a function of the distance of the target from the injection point. Indirectly, we also measured the variation of wastage since there is some wastage on the thermocouples. In previous work, which has been reported, by having two different impingement distances we got two sets of wastage variation data.

C. WERNER: Has any attempt been made in these investigations to determine what theoretical temperatures are possible in the case of ideal mixtures of sodium and water obtained at the supply temperatures?

W. L. CHASE: We have not measured the ideal temperatures in our investigations. This value has been determined at 3000-3300°F in work carried out by Atomics International. In our tests we do not produce ideal mixtures and so we do not expect to obtain ideal temperatures. It has to be borne in mind, of course, that sodium is a good coolant, and since it flows past the reaction zone, this should somewhat reduce the temperature in this zone. Another limiting factor is the boiling point of sodium at the test pressure.

R. A. DAVIES: We have measured temperatures as high as 1350°C and it is probable that higher values do occur. The tube damage does not appear, however, to be due to melting, and metallurgical examinations indicated that the wall temperature was about 950°C in the region of the damage.

C. WERNER: About 15 years ago we carried out a large number of sodium-water experiments for the United States Navy, and we found reaction temperatures to be possible which were above the melting point of the steels used in the experiments.

A. G. IOLTUKHOVSKY: I should be interested to hear the views of Mr. Davies and Mr. Chase on the prospects for work on materials other than low-chromium steels, e. g. high-nickel alloys.

W. L. CHASE: There were actually other materials present in the tube bundle shown in Fig. 1b of the paper. Although our present programme deals primarily with ferritic materials, the higher alloys may be tested later.

R. A. DAVIES: Our experiments suggest that high-nickel alloys may have a greater corrosion resistance than ferritic alloys but they may be too expensive for general use. Naturally, any material chosen would have to be compatible with the water side of the heat exchanger.

A. M. SOENEN: Could either of the authors give some information on possible methods for studying the influence of the reaction products formed on the velocity of the water injected?

W. L. CHASE: In our case we calculated the time required for the injection of the water on the basis of the amount of water injected and the size of the orifice. The experimentally determined value agreed with this calculated value. We assume, therefore, that our calculated velocity is approximately correct. It would, of course, be useful to measure this flow rate during the tests but it is very difficult to make precise measurements of flows of about 3×10^{-3} lb/s.

E. L. ZEBROSKI: An important question affecting the choice of one's experimental parameters is the rapidity with which one expects to be able to detect and isolate small leaks in a practical situation. Have either of the authors any comments on this?

W. L. CHASE: This is a very difficult question although, from the point of view of practical situations, there is no doubt that it is extremely desirable to make adequate provision for rapid leak detection and isolation of the steam generator. The difficulty is that speed of detection depends on so many factors, e.g. size and configuration of steam generator, rate of sodium flow, method of detection, time lags in the detector. In addition, one has to bear in mind the possibility of differences between the Fermi steam generator and the large 1000-MW steam generators.

R. A. DAVIES: As far as full-size leaks are concerned, I think there is little hope of devising a detection system capable of operating at the speed of $4\frac{1}{2}$ s or so that it takes to inject the water. At the moment we are studying injection systems and response times but, in view of the time required for dumping, I do not think that periods of much less than 30 s would be of much practical interest. It would probably take as long as that to get rid of the water side.

DESIGN AND OPERATION OF TESTING APPARATUS

(Session V)

EXPERIENCE GAINED WITH THE IN-PILE SODIUM LOOP FOR FAST NEUTRON IRRADIATION AFTER THE FIRST RUN IN THE BR-2 REACTOR *

M. SOENEN
CENTRE D'ETUDE DE L'ENERGIE NUCLEAIRE,
MOL, BELGIUM

Abstract

EXPERIENCE GAINED WITH THE IN-PILE SODIUM LOOP FOR FAST NEUTRON IRRADIATION AFTER THE FIRST RUN IN THE BR-2 REACTOR. A high performance in-pile sodium loop has been built for irradiation of fuel pins under fast neutron conditions in the high flux test reactor BR-2 (Mol, Belgium).

A description is given of the in-pile section of the loop after the irradiation, the dismantling in the high-activity hot cell, and the visual examination of the sodium circuit during cutting.

The first section gives a general description of loop circuitry, control, materials, inspection and the testing programme. Also described are the operational characteristics of the major items to illustrate possible working conditions of the loop.

The second section describes some important technological problems and their solutions in the design and construction of the in-pile section of the loop, more particularly the sodium-water reaction, sodium activation, fission products' detection, neutron screening, and also the heating, compactness and regulation of the loop. The use of a water mock-up to study some particularities of the design and development work done for an efficient sodium vapour-overflow trap are described.

The third section describes the general dismantling procedure followed in the BR-2 high-activity hot cell to recuperate the fuel pins and to permit adequate evacuation of the sub-assemblies and the scrap.

The fourth section presents a visual examination of the sodium circuit during cutting. Cleaning with alcohol and recuperation of some equipment are described.

I. GENERAL DESCRIPTION OF LOOP CIRCUITRY, CONTROL, MATERIALS, INSPECTION AND TESTING PROGRAMME

1. General principle of the loop

One of the principal aims of the irradiation programme to be followed with the in-pile sodium loop is to study the behaviour and performance of one or several pins of fissile materials in conditions as near as possible to those in a liquid-metal-cooled fast reactor.

The loop is designed for the French "Commissariat à l'Energie Atomique; Association CEA-EURATOM – Fast Breeder Project" to be irradiated in a large through channel in the high flux materials testing reactor BR-2 (Association CEN-EURATOM; Groupe d'exploitation du réacteur BR-2 et de ses installations connexes; MOL – Belgium). A certain amount of flexibility is possible in the operating conditions from the point of view of hydraulic and thermal conditions and also from that of the geometry of the test section.

---

* A large part of this work has been performed by the Association CEN-EURATOM for the exploitation of the BR-2 reactor and its auxiliary installations (Contract No. 006-60-5/BRAB).

The entire sodium circuit is contained in an envelope in the form of a leaktight cylindrical vessel which occupies the central 200-mm channel of the reactor (see Fig. 1).

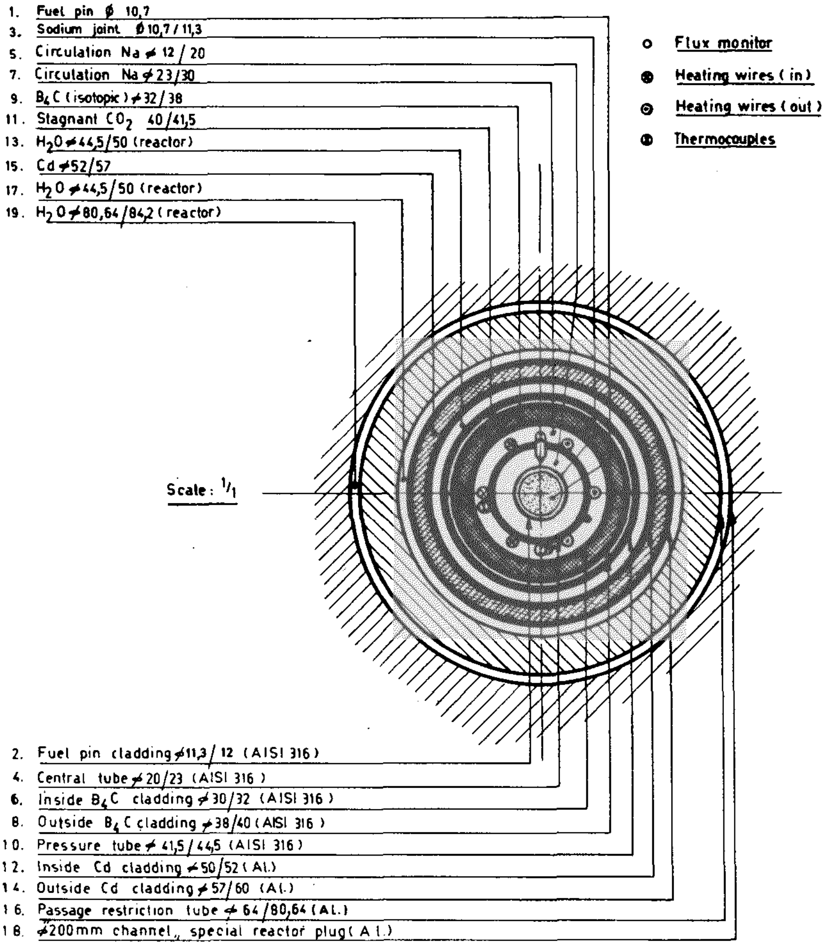

Note: thermocoax and thermocouples schematic.

FIG.1. Cross-section – at reactor mid-plane – through experiment centred in 200-mm diameter channel

At its lower end the envelope thins down to a finger which protrudes into the reactor core. This finger houses the fuel and the sodium coolant entrance and return circuits, surrounded by a B4C screen. Another similar neutron screen, in the form of a cold co-extruded "sandwich" tube of cadmium clad in aluminium, is situated around the finger. The inner cladding of the B4C screen is cooled by the sodium; the cadmium screen is cooled directly by the primary cooling water of the reactor. The heat generated in the primary circuit is removed to a secondary coolant, pure carbon dioxide gas, by means of a sodium-CO_2 heat exchanger inside the envelope. The cross-section of the reactor core configuration is shown in Fig. 2.

The aims of the design are to make an in-pile section as compact as possible, to reduce to a minimum the loading and unloading procedures in the reactor, optimizing the number and type of connections with the

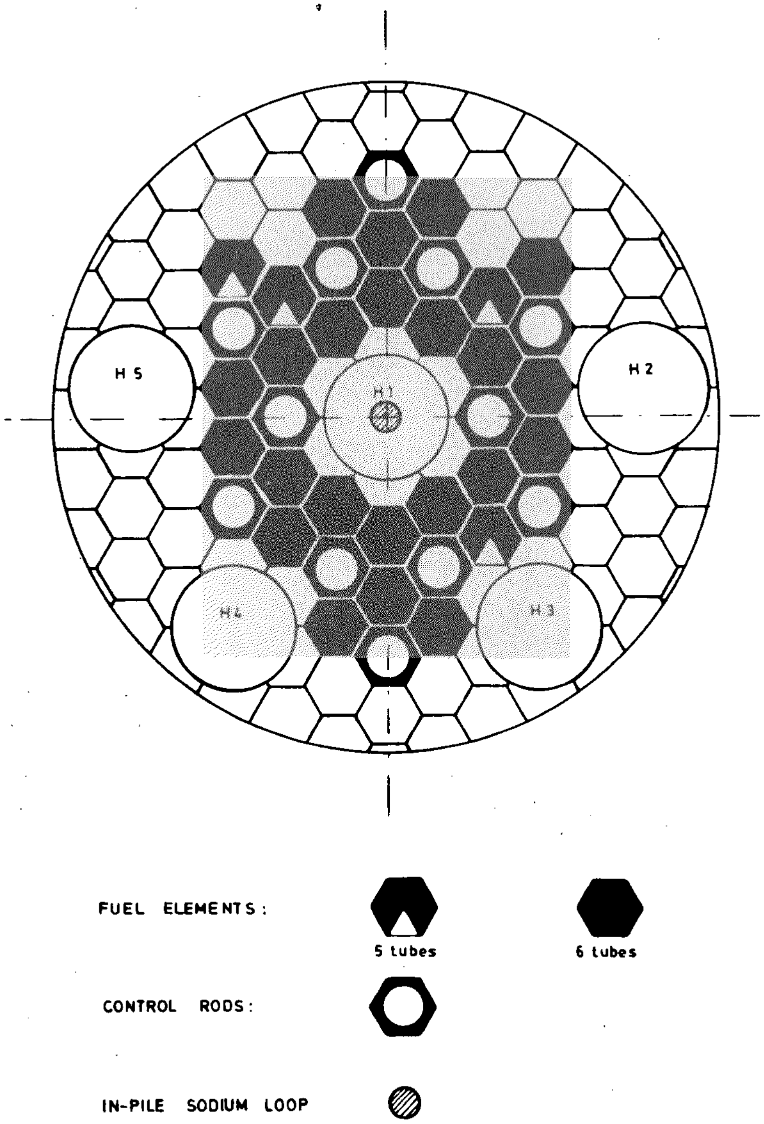

FIG. 2. Cross-section (at reactor mid-plane) of reactor core configuration

out-of-pile control and cooling circuitry, and to arrange that all out-of-pile work would be possible in the high activity hot cell connected to the reactor building.

The concept of an entirely contained primary circuit gives the following advantages: the activated sodium is entirely contained within the envelope, reducing the shielding problem to a minimum; the loop primary circuit can be completely assembled, filled with sodium and tested before loading in the reactor.

2. Primary circuit

The primary circuit contains the system for circulating the sodium coolant and hence the heat removal from the fissile material. The principal components of the primary circuit, arranged in a closed loop, in the order in which the coolant flows, are: two sodium pumps assembled in one unit, one flowmeter, the sodium level reduction tank, the test section and the heat exchanger. From top to bottom the components are placed in the following order: pump unit, flowmeter, heat exchanger, reduction tank and test section. This order has the following advantages: the pump is furthest from the core, the coldest sodium is at the top, the reduction tank is in a favourable position to store the sodium from the upper in-pile section during reactor shutdown periods, when it is necessary to work on the reactor top cover, or during loading and unloading of the in-pile section.

The primary circuit is suspended inside the envelope by means of the secondary coolant exit tubes from the heat exchanger, thus allowing free thermal expansion of the primary circuit. All pipework and equipment, with the exception of the pump unit, are equipped with electrical heating elements held in close contact to the outer surfaces by spot-welded stainless-steel clips.

The upper portion of the envelope extends above the nozzle on the reactor cover and is closed at its upper end by a welded cover through which all connections with the primary circuit pass. All electrical penetrations are provided with double seals to ensure pressure tightness of the envelope. The envelope is attached to the nozzle on the top cover of the reactor by means of a collar bolted to the nozzle with a loose flange. The whole protruding section is covered by a fixed lead shielding "hat". The middle portion of the envelope occupies the whole available volume above the reactor core of the central 200-mm channel of the vessel. The lower part of the envelope narrows down to fit inside a cadmium screen mounted in the control hole of a special 200-mm channel plug made of aluminium. Inside the envelope finger, the primary coolant passages are concentric with no thermal insulation between the two concentric tubes. Cold sodium flows down the annulus, and is inverted up the inside tube to flow over the fuel to remove the fission heat generated. The test section is shown in Fig. 3.

The connections leaving the envelope and passing through its top cover are:

(a) Two tubes, inlet and outlet of secondary coolant CO_2; except for the connections these tubes are double-walled where they are in contact with the pool water.

(b) Two tubes for the supply of helium to the reduction tank; these tubes together with their connections are doubled-walled where they are in contact with the pool water.

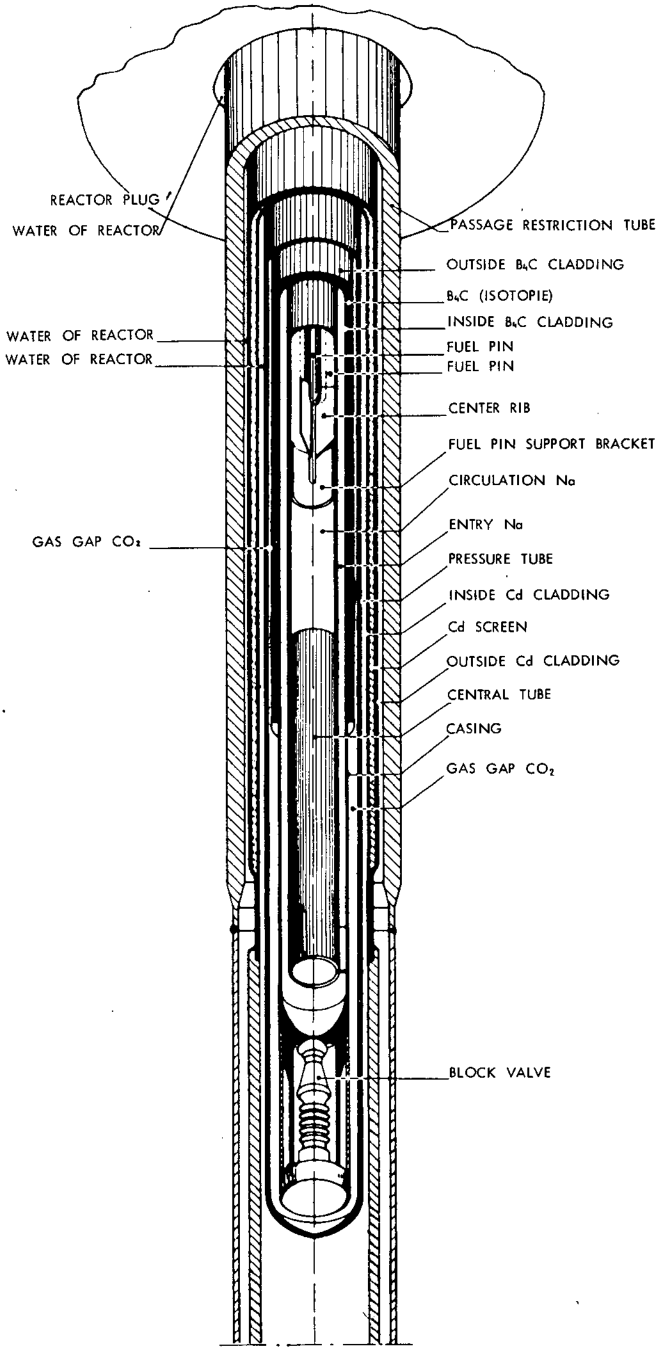

FIG. 3. Exploded view of test section

(c) A box with doubly sealed outlets for 6 cables for electrical supply of pump unit, 2 cables for flowmeter signals, 22 cables for thermocouples, 26 cables for electrical heater supplies (13 independent heaters), 1 tube for envelope pressure indication, 1 tube for leaktightness check between double-sealed outlets, and 1 tube for pneumatic command of release valve on the reduction tank.

The thermocouples in the envelope, 22 in number, are arranged as 6 thermocouples situated in the sodium in the core region (3 thermocouples downstream of the fuel and inside the central flow tube, 2 thermocouples at the mid-plane of the fuel one inside the central tube and one outside, 1 thermocouple at the lower end of the central tube). The other thermocouples are placed as 1 thermocouple in the B4C screen, 1 thermocouple in the sodium vapour trap, 3 thermocouples in the sodium reduction tank, 4 thermocouples in the pump windings (2 per pump), 2 thermocouples at the CO_2 inlet in the envelope, 5 thermocouples in the sodium circuit proper which monitor the inlet to heat exchanger (2 thermocouples), the outlet heat exchanger (1 thermocouple), the inlet to pump unit (1 thermocouple), and inlet to the sodium reduction tank (1 thermocouple).

The 13 electrical heaters are arranged as 3 on the central concentric sodium flow tube, 3 on the sodium reduction tank, 2 on the heat-exchanger Na/CO_2, which in reality has four heating elements arranged in pairs in parallel, 2 on the pipe connecting the heat exchanger to the pumps, 2 on the piping connecting the pumps to the sodium reduction tank, 1 on the piping in the grooved spaces in the upper cover of the reduction tank and on the sodium vapour trap.

The leaktight passages for the 6 thermocouples and the 3 electrical heaters on the central concentric sodium flow tube of the in-core region are made by two joints in series. Each joint consists of a stainless-steel bush brazed to the outside surface of the cladding of the wires. The leaktight passages for the connections leaving the envelope and passing through the box on its top cover are also made by two joints in series, each joint consisting of a stainless-steel bush brazed with silver to the outside surface of the cladding of the wires.

The connections to the out-of-pile control and cooling circuitry are made as follows:

(i) All connections (see (c) above) are grouped in one connection box joint by a flexible tube which runs to the reactor pool parapet. Rapid disconnection is possible at the connection box on top of the envelope or at the pool parapet. The length of the flexible tube is such as to permit the transfer of the in-pile section under water from the reactor channel to the storage cask in the deep pool of the reactor, or vice versa, without any decoupling.

(ii) The connections, according to (a) and (b) above, are also provided with flexible tubing. A special plug fitted into the pool wall carries all these tubes. Rapid disconnection is possible at the top of the envelope or at the pool side of the special pool wall traverse.

The reason for using flexible connections throughout is to facilitate handling in the pool and to permit good access to the reactor top cover for other experiments.

During operation of the loop, the reduction tank acts as expansion tank for the sodium, and during shutdown, when the reactor cover must be available for maintenance, as drain tank into which the sodium can be drained to reduce the radiation dose in the vicinity of the top reactor cover. Drainage is effected by applying vacuum to the primary-circuit pressurizing tube.

In the event of plugging of this tube, a stand-by tube, normally isolated from the reduction tank by a pneumatic release valve, is available. The fact of having two tubes for the supply of helium to the reduction tank allows the flushing of the blanket gas of this tank to detect a rupture of the fuel cladding and to adsorb the fission products released to an active charcoal adsorber.

The pressure of the blanket gas of the primary circuit is set at 6 kg/cm^2 gauge.

3. Secondary circuit

Pure CO_2 gas is circulated in the secondary circuit to remove the heat produced in the primary circuit; the pressure in the envelope is close to the reactor water pressure (12 kg/cm^2 gauge nominal). The CO_2 also serves to cool the primary circuit components in the envelope over which it is made to flow before entering the Na-CO_2 heat exchanger. Since the major resistance to heat transfer is in the CO_2, the heat transfer can effectively be controlled by regulating the CO_2 flow rate. The CO_2 inlet temperature to the envelope is set above the melting point of sodium to avoid sodium freezing in the primary circuit during operation of the loop.

The major components of the secondary circuit are two electrical motor-driven reciprocating compressors with dry pistons, one in normal operation, one in stand-by condition; two heat exchangers, one sodium gas for the heat transfer from primary to secondary coolants (this unit is also part of the primary circuit), the other gas water dissipates the heat to the cooling water system for experiments installed in the reactor; two flowmeters, one for total mass flow and one for the mass flow to the in-pile section; gas pressurization and supply; gas evacuation by means of a storage tank before discharge towards the stack; a connection to vacuum system; three water content meters; two electrolytic hygrometers; two activity detectors; a system of gas purification with molecular gas driers (operation is permanent and automatic); four filters (one upstream of each compressor, one upstream of the reactor pool, and one downstream of the reactor pool); and elecrical heater to heat the CO_2 and to carry out tests to simulate the heat exchanger performance of the primary circuit to the secondary circuit; and various bellow-sealed manual and automatic valves.

4. Auxiliary circuits

Several auxiliary circuits are necessary to enable the loop to function. These are the tertiary circuit containing de-mineralized water from the reactor experimental cooling circuit, and evacuating the heat contained in the CO_2 to the cooling tower; the gas purification cooling circuit, which is also connected to the reactor experimental cooling circuit; the compressor cooling water circuit (to minimize leakage of eventual active CO_2, the compressor cooling water circuit is closed with a heat exchanger cooled by an open lagoon water circuit); and the gaseous fission products adsorption system.

5. Loop control

The principal operating parameters of the loop are automatically controlled; all information on the state of the loop is transmitted to the main control panel.

6. Materials, inspection, testing and commissioning

As far as materials, inspection, testing and commissioning are concerned, only the in-pile section will be discussed here, since it is the most critical part of the loop in connection with the safety of the reactor.

6.1. Materials choice

The material for the primary and secondary sodium containment is chosen to satisfy the conditions of good corrosion resistance to sodium, good weldability (no carbide precipitation), good high temperature strength, and easy availability.

All the 18/8 austenitic stainless steels have excellent corrosion resistance to sodium, and all can be considered for long time use with sodium at temperatures up to 800°C. They are also suitable for normal welding procedures, provided they do not contain more than 0.06% carbon.

The high temperature strength and availability of the stainless steel therefore were the major considerations in the choice of materials.

The following materials were chosen:

(a) Primary sodium containment.

For the primary circuit a stainless steel with good high temperature strength is essential because of the compact nature of the in-core section. Stainless-steel AISI 316 has therefore been specified. Its percentage composition limits are shown in Table I. AISI 316 stainless steel will creep 1% in 10 000 h at 600°C under a tension of 11 kg/mm^2.

(b) Secondary sodium containment (envelope tube).

TABLE I. PERCENTAGE COMPOSITION LIMITS OF STAINLESS STEEL AISI 316

C	Si (max)	Mn (max)	P (max)	S (max)	Cr	Ni	Mo
0.04 - 0.06	1.00	2.00	0.04	0.03	16 - 18	10 - 14	2.00 - 3.00

Since the envelope tube is always in contact with the reactor primary cooling water, temperatures much higher than 100°C are not likely to arise and the material can be selected on the basis of availability of standard tubes. It should be noted that the envelope is designed solely to provide secondary containment for the sodium and is not stressed by the experiment during normal operation. The envelope is thermally insulated by the CO_2 gas from the primary circuit.

AISI 304 ELC has been chosen for the upper wide portion of the tube, and AISI 321 for the in-core finger. The percentage composition limits for these materials are shown in Table II. All joints in the primary circuit and envelope tube are welds. The in-line assembly of the fuel pins is shown in Fig. 4.

TABLE II. PERCENTAGE COMPOSITION LIMITS OF STAINLESS STEEL AISI 304 ELC AND AISI 321

Type	C	Mn (max)	Si (max)	P (max)	S (max)	Cr	Si	Ti
304 ELC	0.03 (max)	2.00	1.00	0.04	0.03	18 - 20	8 - 11	
321	0.04 - 0.06	2.00	1.00	0.04	0.03	17 - 19	8 - 11 Ti	5 × C(min)

6.2. Inspection

The circuits are constructed to established codes of practice coupled with high standards of fabrication. It is useful to mention here some of the inspection on the various items of equipment; the list is not, however, complete in every detail.

The following general inspection procedure must be carried out during construction and assembly: inspection for defects and certificates of chemical analysis of constructional materials, with particular emphasis on the primary system and its containment envelope; welds to be made by a qualified welder under supervision; dye penetration tests to be performed on all welds; radiographs of welds to be taken where required by safety considerations and to be accepted by a qualified organization; all assembly to be carried out in clean surroundings to meet reactor cleanness specifications; helium leaktightness with a mass spectrometer of 10^{-8} l torr/s sensitivity on the primary circuit and its containment envelope; all circuits to be pressure tested to 1.5 times design pressure.

6.3. Testing and commissioning

Allowing for the complex nature of the loop, it was decided to follow, in parallel with the design study and the construction of the circuits, a test and commissioning programme along the general lines as shown below.

6.3.1. Theoretical nuclear calculations. The calculations are done with the aid of a multigroup diffusion programme (Modic 25 energy groups) fed into a "Mercury" digital computer for several cases and geometrical configurations. A typical plot of the neutron spectrum obtained without fuel pins in the test section considering only the neutron screens is given in Fig. 5.

The radial distortion defined by

$$\frac{\text{maximum heat production - minimum heat production}}{\text{mean heat production}}$$

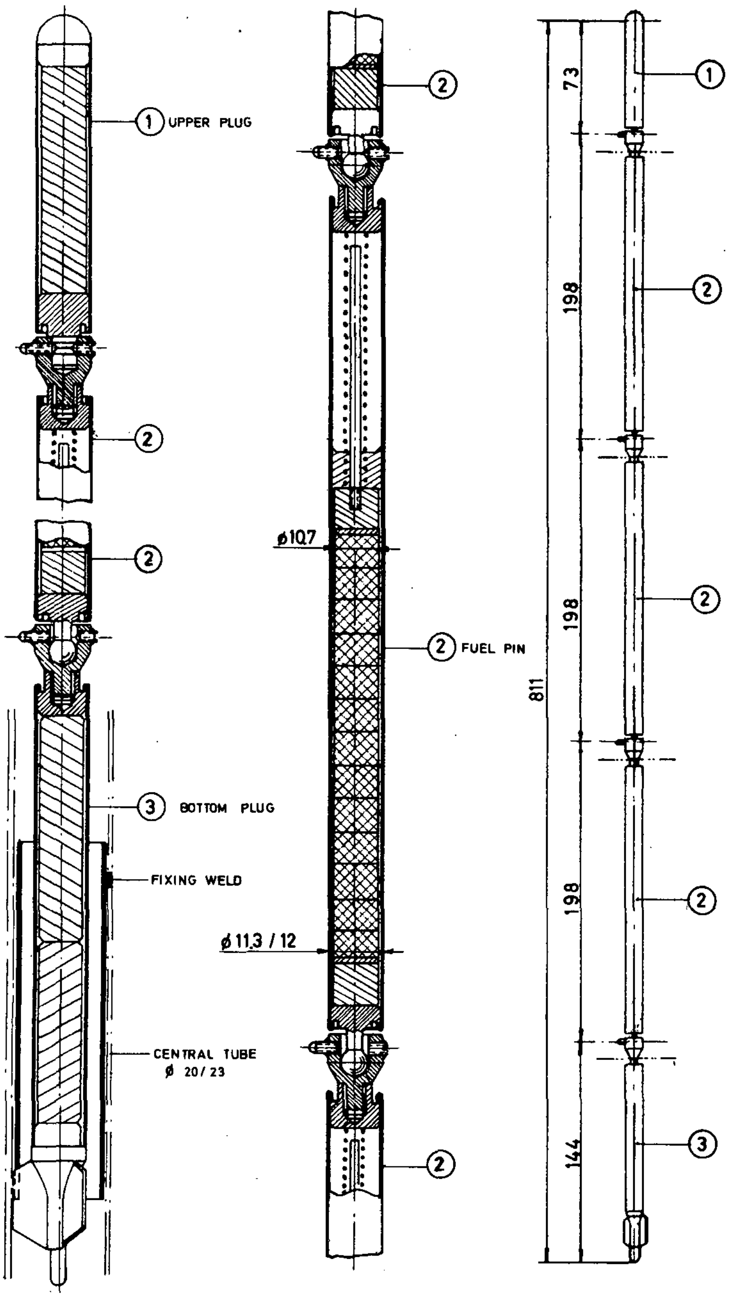

FIG.4. In-line assembly of fuel pins

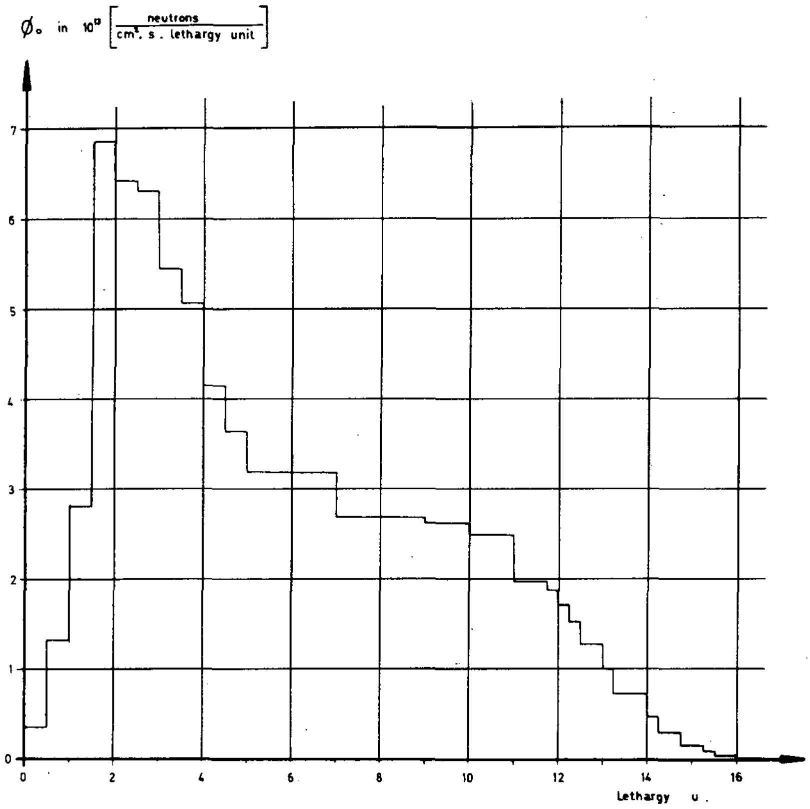

Note : the neutron spectrum is given for the following conditions :

- the fuel pin and the sodium are replaced by aluminium.
- the maximum heat flux at the outersuface of the BR_2 fuel plates is 400 W / cm^2.

FIG. 5. Neutron spectrum without fuel pins in the test section taking into consideration only the neutron screens

and the depression defined by

$$\frac{\text{mean heat production - minimum heat production}}{\text{mean heat production}}$$

calculated for two cases obtained the following values:

(a) Mixed Pu-U oxide fuel pin; diameter: 5.8 mm; distortion: 9%; depression: 4.5%.

(b) Mixed Pu-U carbide fuel pin; diameter: 8.9 mm; distortion: 31%; depression: 14%.

6.3.2. Dosimetry of the in-pile section. An extensive programme for the dosimetry using a nuclear mock-up of the experiment is worked out. These studies are done to support the theoretical nuclear calculations to obtain an understanding of the over-all and eventually detailed flux distributions, in particular along the axis of the fuel section. A typical plot of the specific power averaged over the reactor cycle time along the axis of the fuel section can be obtained in relative units.

Other objectives of the dosimetry programme comprise the formation of a core configuration which will satisfy at the same time the requirements of the operation of the reactor and the desiderata of other in-pile experiments; the determination of the anti-reactivity effect of the in-pile section and the surrounding neutron screens; and the supply of a suitable flux detector to give the degree of burn-up in the fuel section after irradiation.

6.3.3. Hydraulic conditions in the primary circuit. A "hydraulic" model representing the primary circuit of the loop is constructed; this model using water as circulating fluid has the same geometrical characteristics as the sodium circuit. Light glasses placed at certain points, having flow discontinuities, allowed observation of the conditions at these points. The main objectives of the tests done with the hydraulic model are explained in the second part of this document.

6.3.4. Final cleaning and filling of primary circuit. The cleaning of the primary circuit is done using the sodium itself. To achieve adequately clean conditions, three operation cycles are made, each one consisting of:

(a) Static conditions.
Filling of the circuit with sodium through a filter: this operation is done with sodium at 125°C, circuit at about 150°C.
Increasing the sodium temperature up to 400°C (by electrical heating).
Emptying the circuit at a temperature of 400°C.
Complete solidification of the sodium in the dump tank.

(b) Dynamic conditions.
Filling of the circuit with sodium through a filter; this operation is done with sodium at 125°C, circuit at about 150°C.
Increasing the sodium temperature up to 200°C (by electrical heating).
Circulating the sodium for at least a half an hour at 200°C.
Emptying the circuit at a temperature of 200°C.

To check the sequence of operations in the filling and cleaning procedures as mentioned above a mock-up similar to the primary circuit is built and tried out with sodium. The mock-up is also used for establishing the technique of emptying and cleaning of the circuit in the high activity hot cells.

6.3.5. Out-of-pile tests. The complete loop is tested out-of-pile to define the best operating conditions of all control items. The test is divided into four principal sections.

(a) Tests on the primary circuit outside the envelope.

The tests with the primary circuit out of the envelope are done to establish the procedures of filling and cleaning of the primary circuit, to check the correct operation of the primary circuit and the components such as electromagnetic pumps, flowmeter, electrical heating, thermocouples, thermal expansion bellows and leaktight passages, and to check the lowering of the sodium level from the upper section of the loop by means of the reduction tank.

(b) Tests on the primary circuit in the envelope, with the envelope in a water loop.

The tests with the primary circuit in the envelope, the latter being cooled in the flow channel of a water loop with the same geometrical and hydraulic characteristics of the reactor channel, allowed the following tests to be done: the correct operation of the primary circuit in the envelope, the pressure test and leaktightness of the envelope, the fitting of the envelope in the large channel hole, the adequate cooling of the cadmium screen, and the fitting of the support for the special aluminium in-core plug.

(c) Tests on the secondary circuit.

The tests on the secondary circuit are operation of the circuit to check the compressors, flowmeter, valves and filters, the purification of the CO_2 by the automatic molecular driers, pressurization of the circuit from CO_2 bottles, and all instrumentation with control and safety circuits.

(d) Over-all tests.

These tests on the loop are CO_2 pressure losses in the envelope (difficult to estimate precisely by calculation), the adequate cooling of the primary pumps and flowmeter, the performance of all connections and flexible tubes, and setting of operating limits of the instrumentation control and operation of the loop.

Figures 6 and 7 show the in-pile sodium loop flowsheet and the general disposition of the loop in the reactor channel.

6.3.6. Out-of-pile tests in the reactor building. After all the tests described above have been carried out, the equipment is transferred to the reactor building and installed in the space allotted to the loop. The loop equipment in the reactor building is shown in Fig. 8. When the installation is completed an over-all operational test of short duration is done before the loading of the in-pile section in the reactor.

II. OPERATING CONDITIONS

The operational characteristics of the major items of the loop are described. The characteristics are given in general to illustrate possible working conditions on the loop. Results from an over-all thermal balance with sodium and CO_2 temperature distribution during irradiation of the loop are given.

1. Electromagnetic pump unit

The principal characteristics of the electromagnetic pump unit are as follows:

1.1. Flow and pressure head with constant input voltage for the electromagnetic pump unit containing two type 1 1/1.07 kg annular linear induction pumps permanently coupled together.

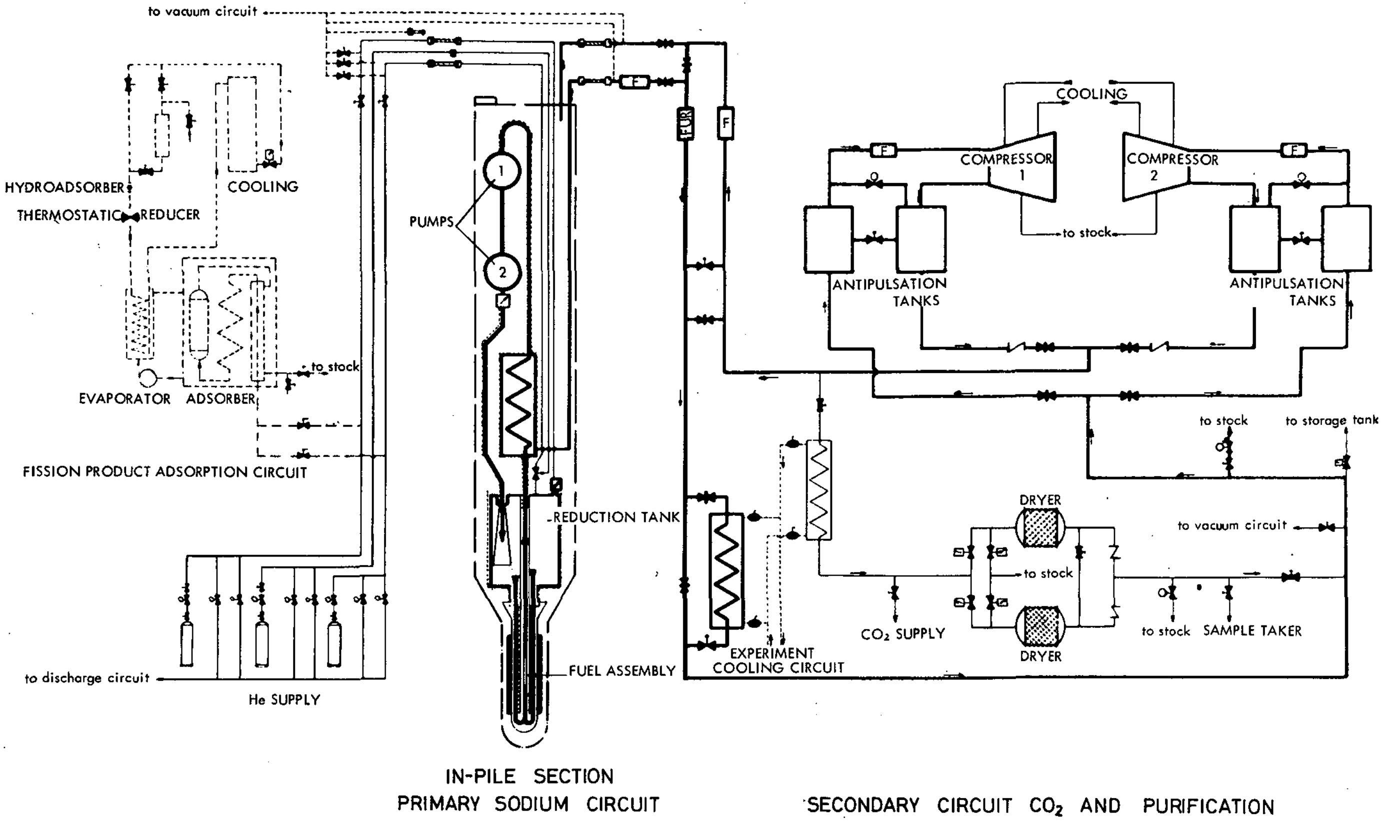

FIG.6. In-pile sodium loop, flowsheet

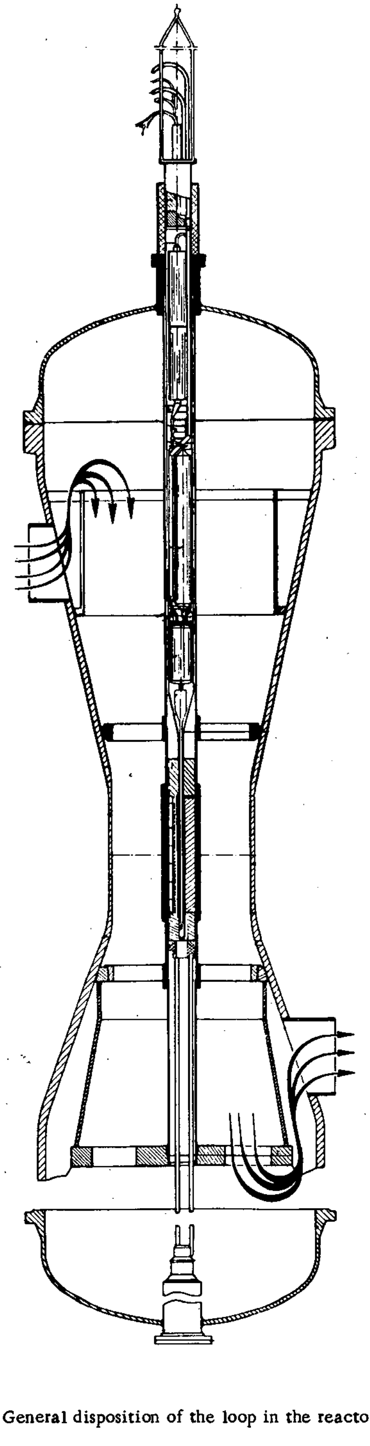

FIG. 7. General disposition of the loop in the reactor channel

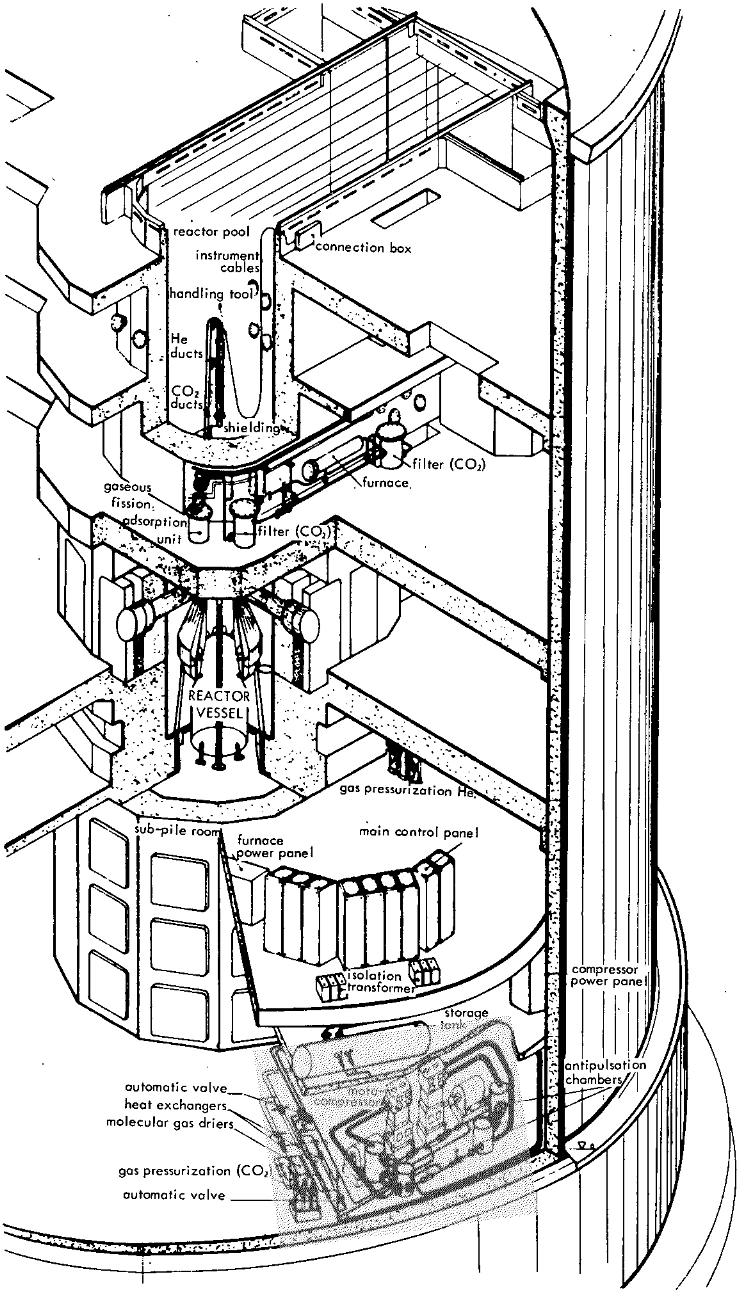

FIG. 8. Schematic disposition of the loop equipment in the reactor building

(a) For "one pump" at 100% output:

flow	l/s	(0)	1	2
maximum output pressure	kg/cm^2	(1.56)	1.07	0.33

(b) For the "pump unit" at 70% output:

flow	l/s	(0)	1	2
maximum output pressure	kg/cm^2	(2.1)	1.5	0.6

1.2. Electrical input

(a) For "one pump" at 100% output	1.6 kW or 3.2 kVA
(b) for the "pump unit" at 70% output	2.4 kW or 3.6 kVA

1.3. Functional relationship

Figures 9 and 10 indicate sodium flow as a function of line tension for both pumps and each pump separately based on measurements made on the loop.

2. Electromagnetic flowmeter

Figure 11 indicates the calibration curve for the flowmeter for sodium temperatures between 260 and 350°C.

3. CO_2 compressors Type K 105-1A with dry position

The principal characteristics of the CO_2 motor-compressor unit are obtained from constructor's information; they can be put on graphs indicating functional relationship of the different parameters: flow, pressure, temperature and electrical input.

4. Primary Na-CO_2 heat exchanger

The function of the Na-CO_2 heat exchanger is determined by the following parameters: CO_2 flow, Na flow, CO_2 inlet temperature, Na inlet temperature, CO_2 outlet temperature, Na outlet temperature, and total heat output.

If one determines four of the seven parameters above, the values of the three remaining parameters will be fixed. In determining the parameters, the following limiting factors must be kept in mind:

(a) The maximum sodium temperature in the pumps without CO_2 and Na flow may not exceed the value of 300°C.

(b) The inlet CO_2 temperature to the envelope lies in the limits 110 to 135°C.

The lower temperature limit is fixed to keep the sodium liquid at all times during irradiation.

The upper temperature limit is forced on by the outlet temperature of the compressor fixed at 140°C.

(c) The temperature gradients in the concentric tubes of the test section are limited because of thermal tensions in the range from 125 to 150°C with working sodium temperature from 600 to 400°C.

The admissible limits of the sodium temperature at the downstream end of the fuel assembly at normal operating conditions of the loop is given in Tables III and IV for two fixed heat transfer rates in the heat exchanger 130 kW and 70 kW respectively.

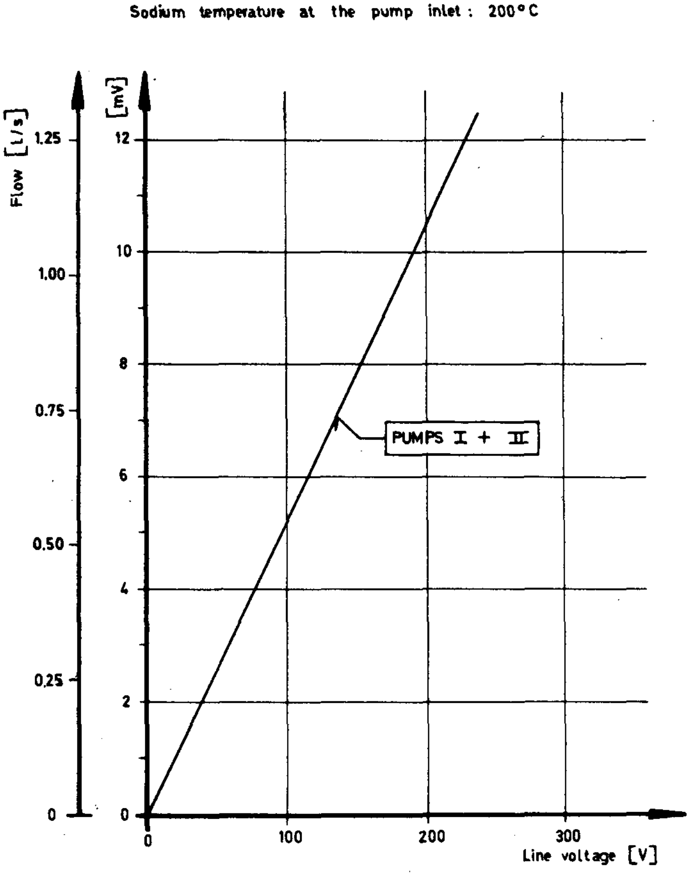

FIG.9. Sodium flow as a function of line tension for both pumps

5. Fuel assembly

Some characteristics of the fuel assembly that can be considered for irradiation in the loop are as follows:

5.1. Assembly

(a) A single fuel pin
(b) An in-line assembly of fuel pins (one on top of each other)
(c) A set of three to seven fuel pins in a given pitch (e.g. a triangular pitch)

5.2. Geometry

The outside diameter of the pin can vary from 5 to 15 mm; the active length of the fuel is limited to 700 mm.

A vented fuel pin can also be considered.

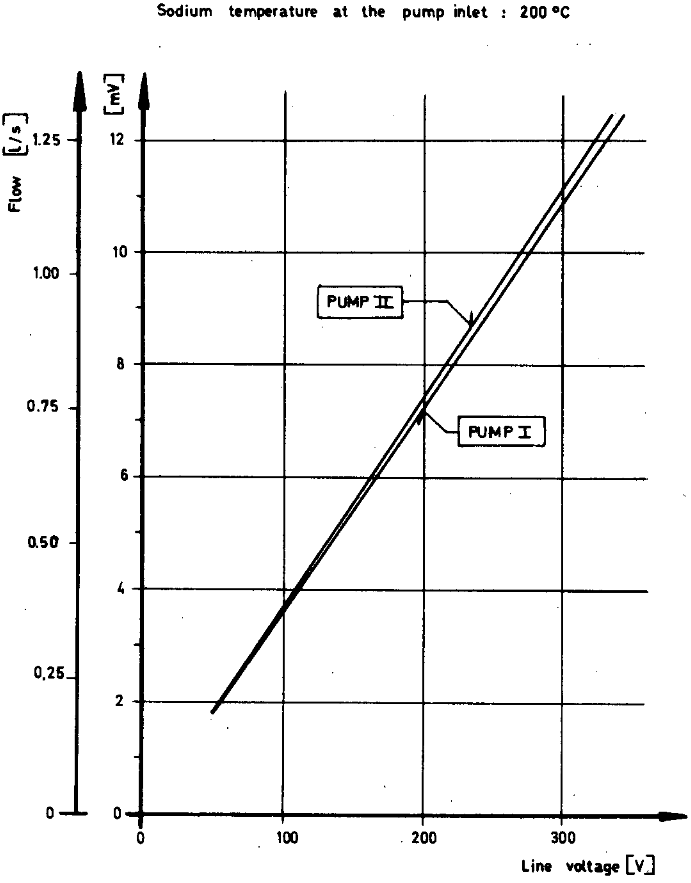

FIG.10. Sodium flow as a function of line tension for each pump

5.3. Specific power

Combined nuclear calculations, dosimetry measurements in BR0-2 (nuclear mock-up of BR-2) and BR-2, and results from an over-all thermal balance during operations of the loop in the reactor indicate that a maximum specific power of 2200 W/cm^2 in the fuel pin can be obtained using the BR-2 core configuration as shown in Fig. 2.

Another configuration of the reactor core with special fuel elements placed round the test finger in the 200-mm channel aluminium plug is considered to satisfy some operating requirements of the reactor.

An irradiation in which the boron carbide screen is omitted will allow maximum specific power in the fuel pins of about 4000 W/cm^3 to be obtained.

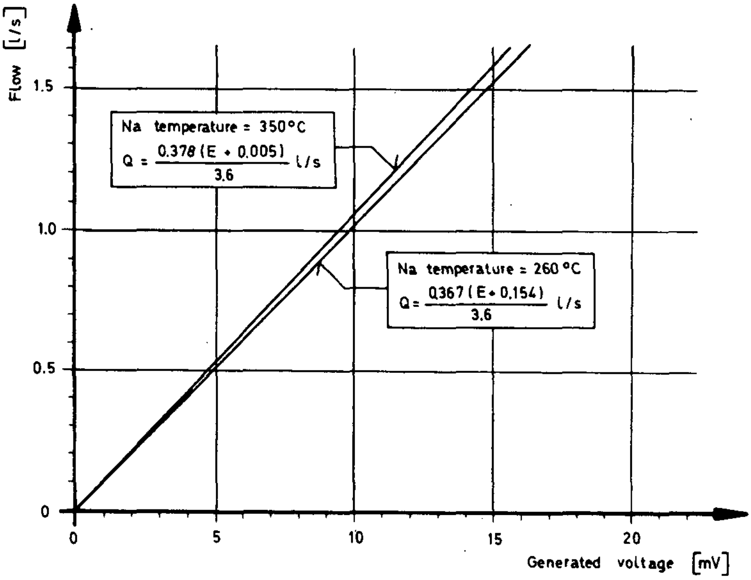

FIG. 11. Calibration curve for the flowmeter

6. Results obtained during the irradiation

Thermal results obtained during the first irradiation of an assembly of three fuel pins are presented.

6.1. Heat production in the materials

Results from an over-all thermal balance during irradiation of the loop give the following heat production figures:

Total in the three fuel pins	42 kW
Total in the boron carbide screen by neutron absorption	10 kW
Total by gamma heating in the materials of construction (except the fuel), about	8 kW.
Total heat dissipation, about	60 kW

The above figures lead to the following values:

Maximum specific heat production in the fuel pins at the start of the reactor cycle: 2200 W/cm^3

Maximum specific heat production in the boron carbide screen by neutron absorption: 200 W/cm of length

Maximum gamma heating in the materials of construction: 4 W/g.

6.2. Temperature distribution

The sodium and CO_2 temperature distributions in the envelope during the irradiation of the loop are shown in Fig. 12.

Figure 13 shows a typical data sheet indicating all measurements performed every two hours on the loop.

III. IMPORTANT TECHNOLOGICAL PROBLEMS AND THEIR SOLUTIONS

This section provides a summary of some of the important technological problems encountered during the conception, realization and exploitation of the loop and the solutions given.

The following problems are considered:

1. Sodium-water reaction
2. Sodium activation
3. Fission product detection and adsorption
4. Neutron screening
5. Electrical heating of the sodium circuit
6. Size of sodium circuit
7. Principal loop regulation
8. CO_2 activation
9. Development of an efficient sodium vapour-overflow trap

1. Sodium-water reaction

1.1. Problem

The in-pile section of the loop is introduced into a reactor that is moderated and cooled by light water. The primary water circuit of the reactor operates at about 12 kg/cm^2 gauge pressure. The reactor vessel is immersed in a water pool. In order to have access to the top cover of the reactor, the pool water must be lowered to the working grid during shutdown. Contact between the reactor water and sodium must be avoided. A sodium-water reaction with explosion of the resultant hydrogen in the air has been considered in the maximum credible accident study of the loop.

1.2. Adopted solution

Sodium and water are rigorously separated by double containment. The following details apply to both containers:

(a) All joints in the primary circuit and the envelope tube are welds.

(b) The envelope is pressurized by the secondary CO_2 gas to about the same pressure as the primary water circuit of the reactor.

(c) Moisture in the envelope is measured by two electrolytic hygrometers and three humidity detectors on the secondary circuit.
Two coincident indications on the humidity detectors provoke a "Slow Set Back" of the reactor.

(d) The blanket pressure in the sodium circuit is fixed for normal operation at 6 kg/cm^2 gauge, about half the CO_2 pressure in the

TABLE III. ADMISSIBLE LIMITS TO OPERATE THE LOOP WITH TOTAL POWER DISSIPATION OF 130 kW

	SODIUM			CARBON DIOXIDE			THERMAL GRADIENTS	
Temperature upstream of fuel pins (°C)	Flow (g/s)	Temperature entrance heat exchanger (°C)	Temperature outlet heat exchanger (°C)	Flow (g/s)	Temperature entrance heat exchanger (°C)	Temperature outlet heat exchanger (°C)	Test section (°C)	Heat exchanger entrance Na entrance CO_2 (°C)
420	725	345	220	1000	110	235	125	235
320	900	270	170	2000	110	170	100	160

TABLE IV. ADMISSIBLE LIMITS TO OPERATE THE LOOP WITH TOTAL POWER DISSIPATION OF 70 kW

	SODIUM			CARBON DIOXIDE			THERMAL GRADIENTS	
Temperature upstream of fuel pins (°C)	Flow (g/s)	Temperature entrance heat exchanger (°C)	Temperature outlet heat exchanger (°C)	Flow (g/s)	Temperature entrance heat exchanger (°C)	Temperature outlet heat exchanger (°C)	Test section (°C)	Heat exchanger entrance Na entrance CO_2 (°C)
450	400	330	215	460	110	250	115	220
220	900	195	145	2000	110	140	50	85

CHARACTERISTICS

- Heat production in the fuel pins { upper pin : 10.4 kW; centre pin: 18.5 kW; lower pin : 12.8 kW
- Total heat production in the pile section: 60 kW
- Heat removal in the heat exchanger Na - CO_2: 55 kW
- CO_2 flow: 0.58 kg/s
- Na flow: 0.42 kg/s

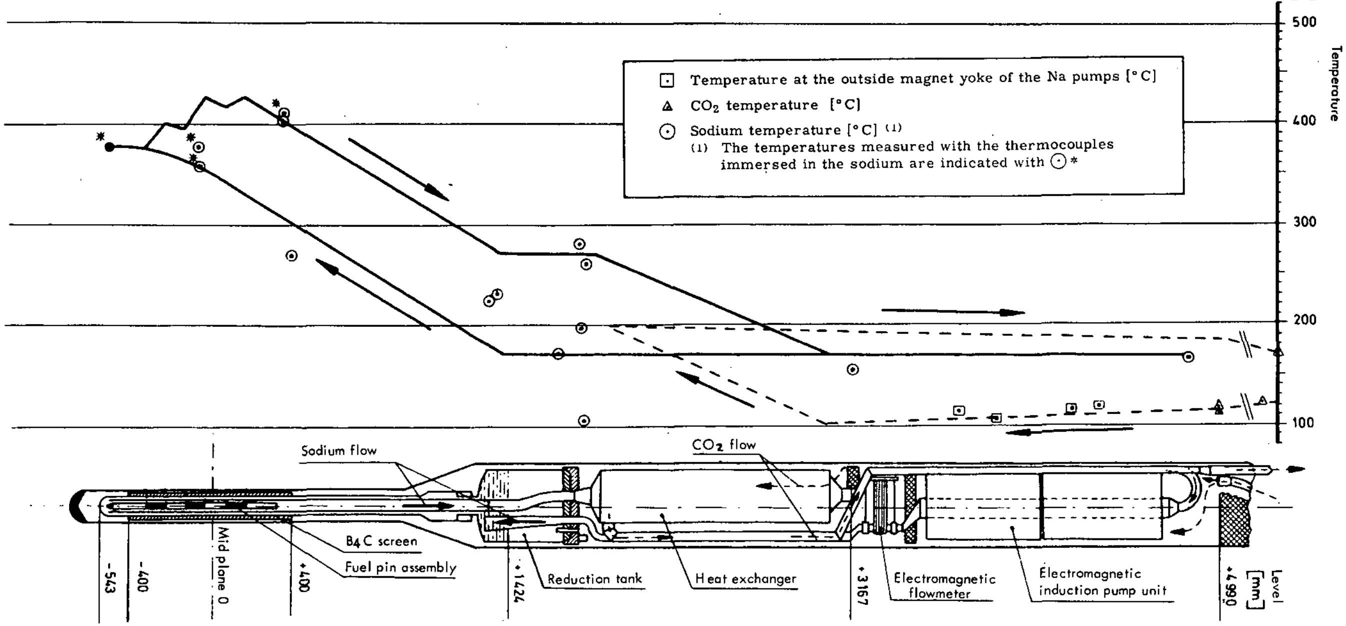

FIG. 12. Sodium and CO_2 temperature distribution in the envelope during irradiation of the loop

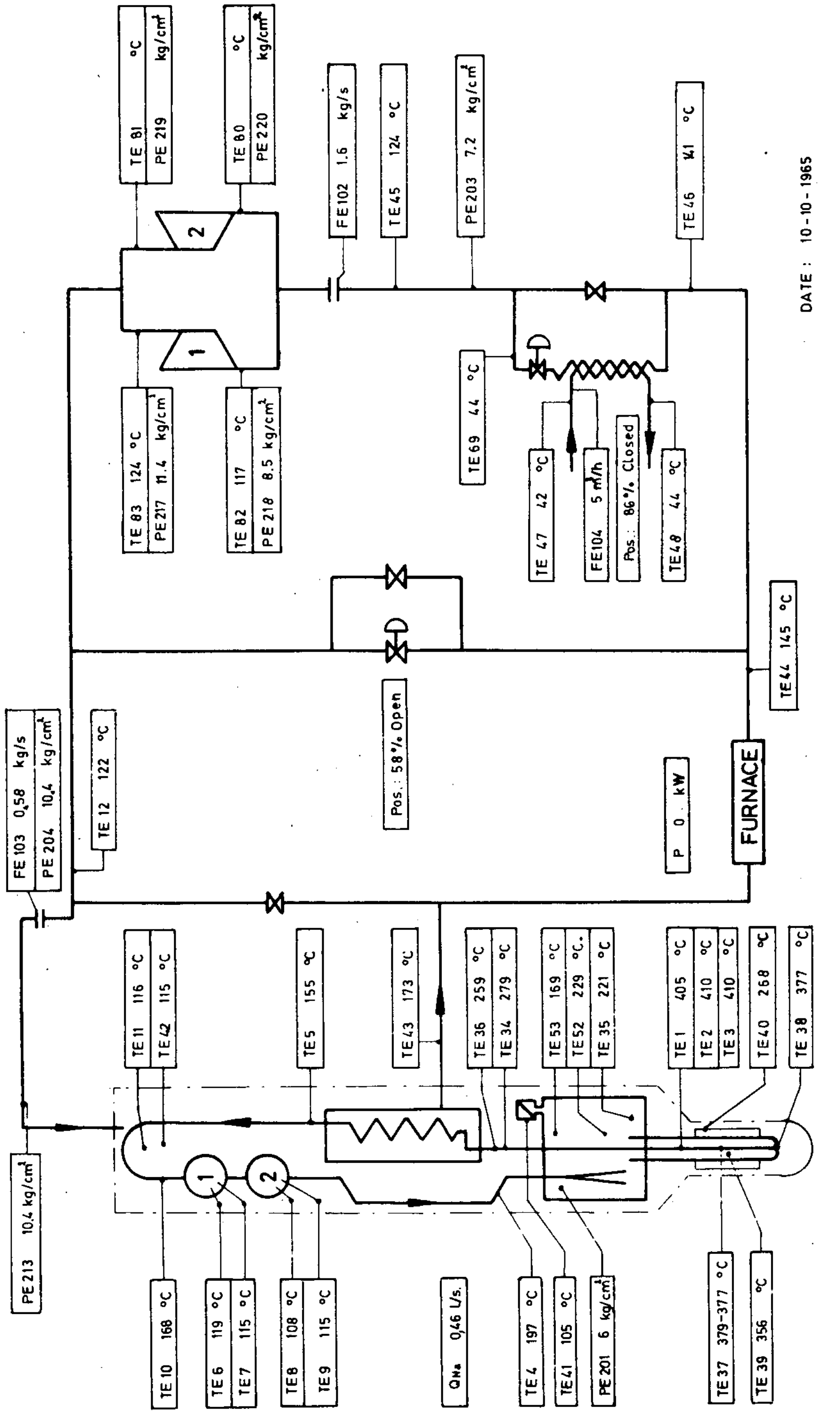

FIG. 13. Typical sheet indicating principal measurements made every 2 h on the loop

envelope. An alarm is set at 7 kg/cm^2 gauge. A safety valve opens at 10 kg/cm^2 gauge to communicate with the stack.

(e) The gas leaktight passage through which in-pile instrumentation is passed to the top flange of the envelope is made by two joints in series. A pressure indicator with alarm between the two joints is provided to detect any leaks. The set-up of the passages is indicated in Fig. 14.

(f) The sodium and gas leaktight passages through which pass the in-core instrumentation at the conical enlargement on the concentric in-core tubes just above the reactor core are also made by two joints in series. A pressure test fitting between the two joints is provided to detect any leaks. The set-up of the passages is indicated in Fig. 15.

(g) The helium flexible ducts to pressurize the sodium circuit are double-walled in the pool. A pressure indicator with an alarm between the flexibles is provided to detect any leaks.

2. Sodium-activation

2.1. Problem

In a neutron flux activation of sodium is brought about by one of the processes indicated below:

(a)	$11\ {}^{23}\mathrm{Na}\ (n, \gamma)\ 11\ {}^{24}\mathrm{Na}$	half-life :	15 h
		principal gamma:	2.75 MeV
(b)	$11\ {}^{23}\mathrm{Na}\ (n, 2n)\ 11\ {}^{22}\mathrm{Na}$	half-life :	2.6 yr
		principal gamma:	1.38 MeV

The activation due to ^{24}Na is estimated to be negligible because of the short duration of irradiation, the high threshold energy for reaction (neutrons higher than 13 MeV), and the small activation cross-section (inferior to 0.006 mb).

With the upper portion of the sodium circuit extending up in the nozzle on the reactor top cover a shielding problem has to be solved to ensure access to the top cover during shut-down of the reactor.

2.2. Adopted solution

To ensure access on the reactor top cover the sodium from the upper section of the circuit is drained into the "reduction tank". Drainage is effected by applying vacuum on the tank. The tank is situated in the lower part of the middle portion of the envelope. The inside diameter of the tank is 165 mm and the top cover fits into a tungsten shield.

Should normal lowering of the sodium level be impossible a lead shield is provided inside and outside the portion of the envelope extending above the nozzle on the reactor top cover to allow uncoupling of all connections fitted at the pool wall traverse.

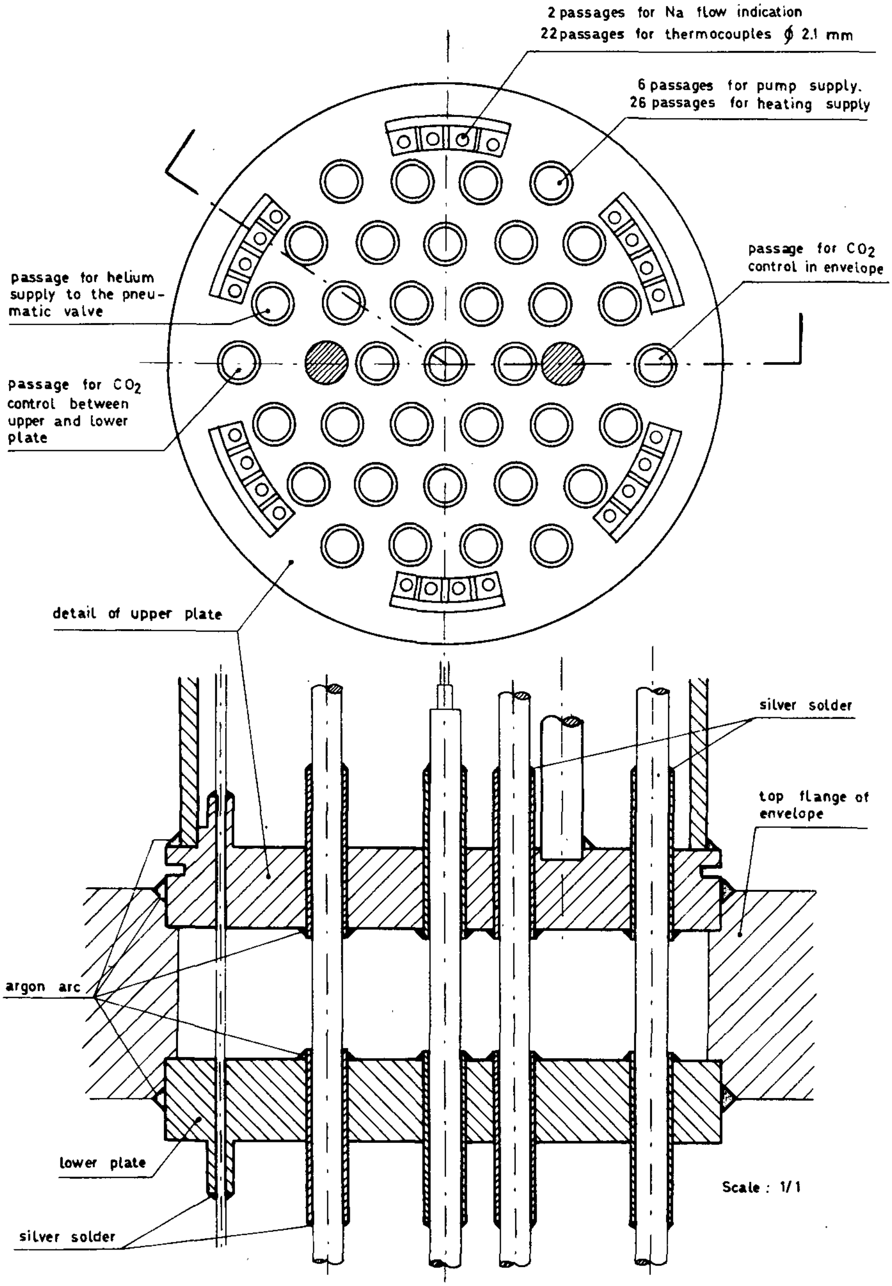

FIG. 14. Gas leak-tight passages to bring out in-pile instrumentation. Passages located at the top flange of the envelope

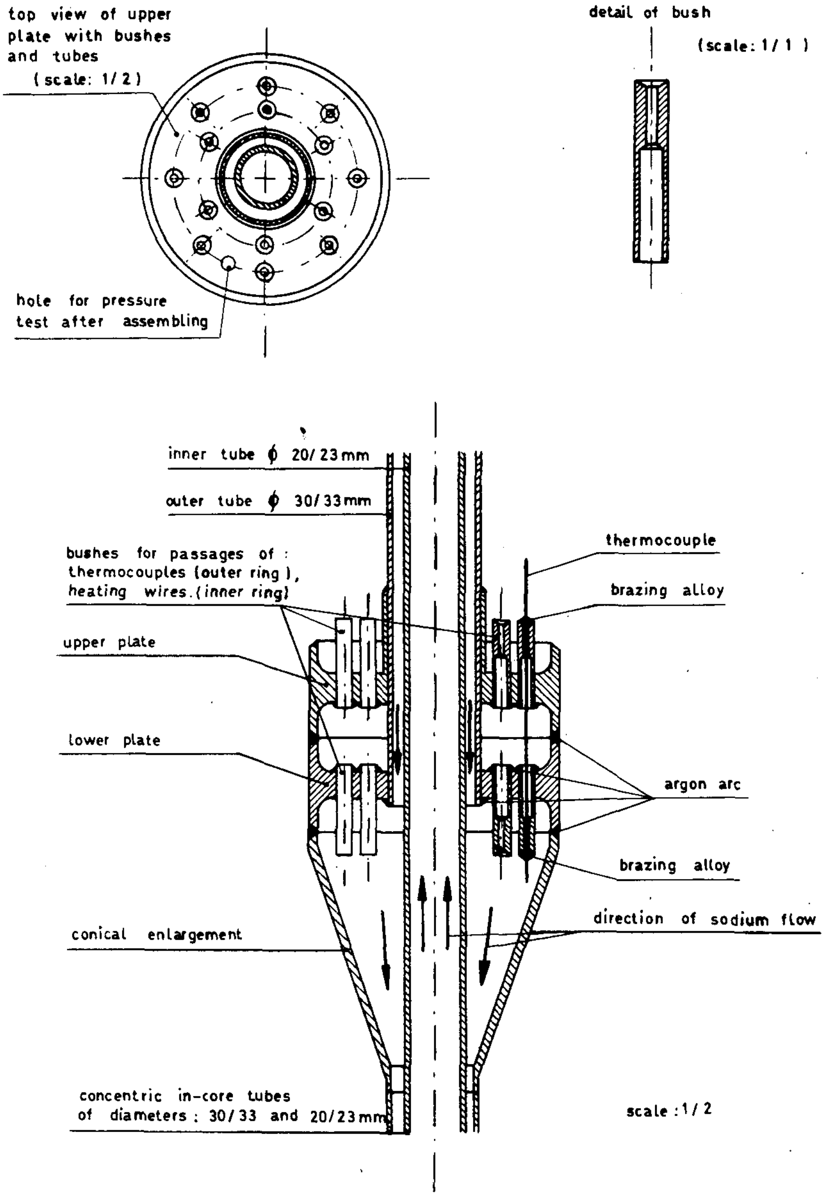

FIG.15. Sodium and gas leak-tight passages to bring out in-core instrumentation. Passages located at the conical enlargement on the concentric in-core tubes just above the reactor core

3. Fission product detection and adsorption

3.1. Problem

The irradiation is done with prototype elements containing, for instance, mixtures of carbides and nitrides. A rupture of the cladding material of these prototype elements is not a priori excluded.

3.2. Adopted solution

A system has been developed to detect and adsorb the fission gases continuously if they diffuse in the blanket gas, and discontinuously when they do not diffuse.

When the fission gases do not diffuse, their detection and adsorption after each reactor shut-down will be as follows:

(a) Expansion of the blanket gas through the active coal adsorber; this expansion is done along the normal helium duct containing the sodium vapour-overflow trap.
(b) Flushing of the blanket gas through the active coal adsorber; this flushing is done by means of the extra helium duct containing the pneumatic close-off valve at the top of the reduction tank.

The active coal adsorber is designed for krypton, the most difficult element to adsorb, and must provide a minimum reduction by a factor of 2.35×10^{-4} of the concentration of fission products in the reduction tank atmosphere.

The measuring devices are:

(a) A NaI crystal at the entrance of the absorber. This detector will indicate fission gases during irradiation if they diffuse in the blanket.
(b) A Geiger counter at the outlet of the adsorber to indicate the effectiveness of the adsorber.

The active coal adsorber is operated at -15°C with a freon refrigeration unit. To avoid radiolyse of the freon, ethylene glycol is used as an intermediate coolant medium. The adsorber can be completely isolated with close-off valves behind a lead shield.

4. Neutron screening

4.1. Problem

One of the principal aims of the irradiation programme is to study the behaviour and performance of fuel pins in conditions as near as possible to those in a liquid-metal-cooled fast reactor. To obtain a complete screening of thermal and epithermal neutrons the following problems have to be considered:

(a) Choice of absorbant material.
(b) Rigorous homogeneity of absorbant material.
(c) Thermal tensions in the cladding of absorbant material.
(d) Good contact between cladding and absorbant material.

4.2. Adopted solution

To meet the above specifications two concentric neutron screens are used:

(a) The exterior screen, a cold co-extruded "sandwich" tube of cadmium clad in aluminium, will retain all thermal neutrons (cut-off at 0.5 eV). This screen is completely cooled by the reactor primary water circuit. The cadmium used in the co-extrusion process is alloyed with 3.5% silver to give it the same hardness as aluminium.

(b) The interior screen, made of an annulus of boron carbide clad in stainless steel, will retain most of the epithermal neutrons (especially the epicadmium neutrons) and neutrons thermalized by the reactor cooling water in the gap between the Cd filter and envelope. The inside cladding of the screen is cooled by the sodium. The outside cladding is immersed in the CO_2 gas of the envelope. The top closure of the screen has holes to permit degassing of the helium towards the CO_2.

The use of two separated concentric screens has the following advantages:

The heat generated is distributed in the two screens, so that excessive thermal stresses are avoided in the screen;

Through leakage of neutrons with two concentric screens is less probable than with a single screen;

The in-pile section can be made nuclear safe by arranging the screens in such a way that both screens cannot be removed from the reactor core at the same time.

It is important that the screening materials be homogeneous and free from cracks and voids to avoid unacceptable local overheating of the test specimen. To verify that there are no regions in the screens transparent to thermal neutrons a collimated beam of neutrons is tapped from the graphite moderator of a reactor (BR-1) in the following test set-up:

The tubular screens are moved over a BF3 gas-filled detector tube (BF3 60% enriched in B^{10}) in such a way that every section of its surface consecutively intercepts the beam.

The cross-section of the beam is approximately 1 cm^2 and the flux is about 10^5 n/cm^2 s. The tests are done with the cadmium screen only, with the B4C screen only, and with both screens placed concentrically.

A typical plot for the neutron transmission of the B4C screen and the Cd screen at 60° is shown in Fig. 16, indicating that the fabrication of the screens and their metallurgical problems are well resolved.

5. Electrical heating of the sodium circuit

5.1. Problem

The electrical heating of the sodium circuit is done by means of thermocoax wires. The problems of this kind of heating wires are the fixation of the wires on the sodium circuit, the junction between the heating wires and the compensating wires, and the arrangement of the heating circuits with maximum control to heat up the sodium loop.

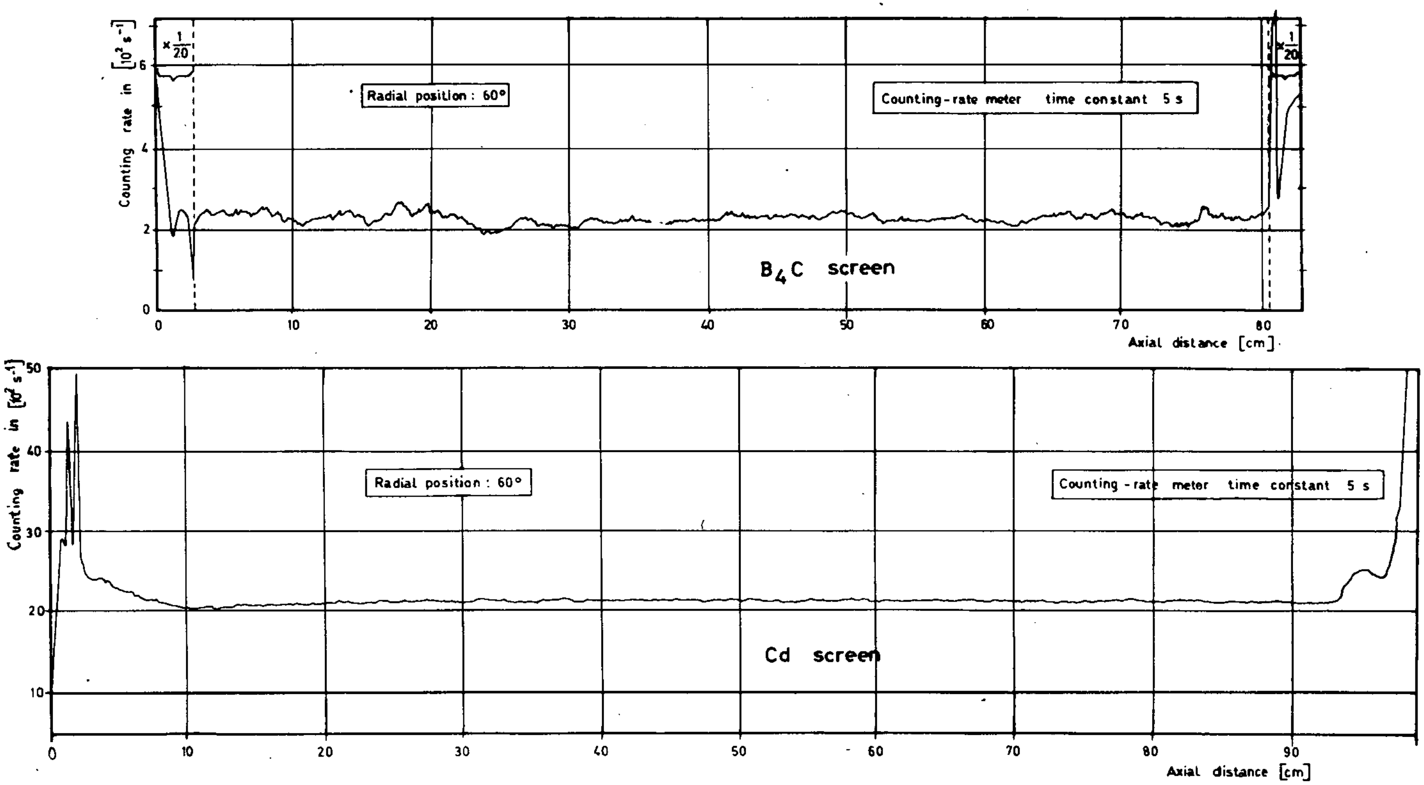

FIG. 16. Typical neutron transmission curve for the B_4C screen and the Cd screen at 60° C

5.2. Adopted solution

The following solutions have been adopted to solve these problems:

(a) The heating wires are fixed to the sodium circuit by means of 0.1-mm thick bands of stainless steel formed to the shape of the wires and spot welded to the surfaces.

(b) The junctions between the heating wire and the compensating wire are made of a sleeve of ceramic and a ruby disc. The junctions can operate up to 13 A (8 W/cm^2). A detail of a junction is shown in Fig. 17.

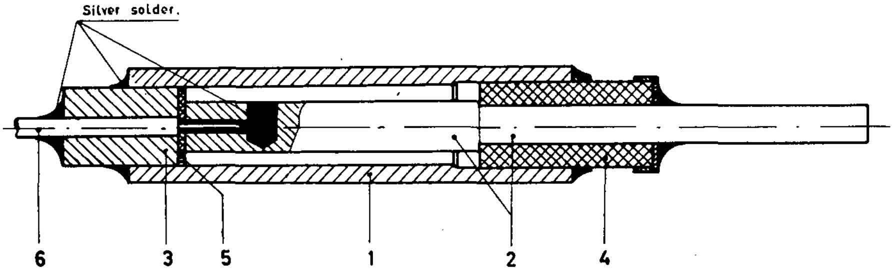

Piece N°	Material
6	THERMOCOAX Sodern 1 Nc Ac 20
5	RUBIS
4	CERAMIC
3	COPPER
2	COPPER
1	STAINLESS STEEL

FIG. 17. Detail of a junction between a heating wire and a compensating wire

(c) The electrical heaters on the sodium circuit, 13 in number, are arranged as indicated in Sub-section I.2 describing the primary circuit.

The reduction tank and the in-core test section of the loop are both provided with three independent electrical heaters because these parts cannot be heated with the secondary CO_2 gas. The other parts of the sodium circuit are provided with two independent electrical heaters only because these parts can be heated up by the flowing CO_2 gas.

All the electrical heaters are able to work at very low intensities. Each heating circuit is isolated from the network by means of isolating transformers.

6. Size of primary circuit

6.1. Problem

A. The parts of equipment of the sodium circuit are arranged one on top of the other in the envelope tube. Their size is such that they can be placed in the 200-mm channel of the reactor.

B. The in-core envelope finger is of such a size that it can be put inside a two-plate concentric tubes type fuel element.

6.2. Adopted solution

A. The equipment of the sodium circuit.

(a) The pump unit is of the annular induction type having small dimensions. The unit has two pumps coupled together in series. In normal operation both pumps are in service. To limit the current intensity and heating up of the windings the pumps deliver the flow and pressure head required with only 70% of their nominal output. If one pump fails the pilot is warned by an alarm on the sodium flow and is able to adjust the required flow and pressure head by the other pump.

(b) The flowmeter has magnets of a size to fit inside the middle portion of the envelope tube. As it is impossible to maintain the necessary stabilization lengths the flowmeter has been calibrated on a circuit with the same hydraulic performance as the loop.

(c) The heat exchanger is of the tube-shell type, with the advantage that it is a common type of construction. In this particular case, where the heat exchanger is immersed in the secondary CO_2 gas, this type of construction could be used to solve the problem of dilatation between the tubes and the shell by leaving one end of the tube bundle plate free in the shell. Special care is taken to have good penetration welds of the inner tubes to the tube plates. The use of bar material for the tube plates is prohibited and suitable plate material for these items is specified.

(d) As the reduction tank is not installed at the top of the circuit the performance of the circuit has been verified by using a hydraulic mock-up. The main objects of the tests done with the hydraulic model are experimental verification of the calculations of the pressure losses in the whole circuit, in the test section and in the heat exchanger; the accurate determination of the relative position(s) between the end of the central flow divider tube and the bottom of the outer tube where the sodium makes a 180° change of direction (a typical plot of pressure drop for different relative positions and flow rates is shown in Fig. 18); the testing of the fixing arrangements for the heating-wires and thermocouples on the test section and their influence on the pressure losses; the testing of the fittings through which the heating wires and the thermocouples pass; the determination of the geometric characteristics of the reduction tank aimed at preventing the entrainment of blanket gas by the primary fluid; and verification of the performance of the circuit without a header tank in the upper section.

(e) The vapour-overflow trap on the normal helium duct towards the reduction tank must be provided for condensation of the sodium vapour and back flow of the condensed sodium to the vapour source to avoid freezing of sodium in the duct. To obtain these conditions the vapour-overflow trap has the following characteristics:

Installation:	the installation is on the helium duct where it leaves the reduction tank.
Filling:	the trap is filled with a wire mesh to enlarge the condensation surface and to enhance vapour removal.

Function: the function of the trap as an overflow trap is assured by holes downstream from the entrance tube of the trap connecting the trap to the reduction tank. An independent electrical heater maintains the trap at the desired liquid sodium temperature.

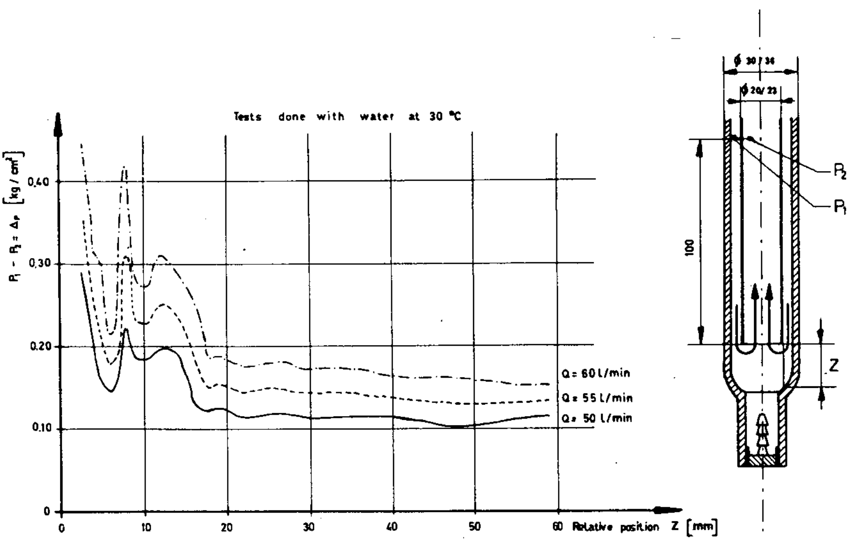

FIG. 18. Pressure drop for different relative positions between the end of the central flow divider tube and the bottom of the outer tube

B. The in-core envelope finger with fuel section.

Inside the in-core envelope finger, the sodium coolant passages are concentric with no thermal insulation between. Cold sodium flows down the annulus, cooling the boron carbide screen, and is inverted up the inside tube to flow over the fuel, removing the fission heat generated. Such an arrangement is necessary to fit the in-core envelope finger inside a fuel element. The envelope finger is thermally insulated from the sodium circuit by an annular CO_2 gap between. The determination of this gap is difficult because:

(i) A big gap is an important thermal barrier when the sodium is lowered in the reduction tank leading to bad heat conduction to the reactor water. Circulation of the CO_2 gas in the gap will lead to better heat convection but will enhance the activation of the CO_2 gas.

(ii) A small gap will lead to high heat conduction to the reactor water, especially in the case of a reactor reverse creating eventual boiling of the reactor water. A small gap may also jam the sodium circuit in the envelope finger avoiding free thermal expansion of the sodium circuit suspended at the top cover of the envelope.

To have an idea of the size of the annular gap a test set-up is used having the same geometry and heat transfer characteristics as the in-core section of the loop. Tests are done with "no" contact, "simple" contact and "pressed" contact between the sodium circuit and the envelope finger. Based on these tests the diametrical gap is fixed at 1.5 mm.

7. Principal loop regulation

7.1. Problem

The sodium temperature at the down-stream end of the fuel and the CO_2 temperature at the entrance of the envelope must be held constant.

7.2. Adopted solution

(a) Sodium temperature set point.

The sodium temperature set point at the down-stream end of the fuel is held constant by regulating the CO_2 flow through the primary heat exchanger. The flow rate is regulated by a motorized valve receiving the signal from the set point temperature. The parameters are fixed so that the control range of the valve is maximum when starting at the nominal conditions.

(b) CO_2 temperature set point.

The CO_2 temperature set point at the entrance to the envelope is held constant by by-passing the CO_2 flow through the secondary heat exchanger. The by-passing is regulated by a motorized valve receiving the signal from the set point temperature. Both regulations are tried out using the electrical heater on the CO_2 gas and there is no interference.

8. CO_2 activation

8.1. Terms of the problems

The CO_2 gas circulates in the upper and middle portions of the envelope tube, and is almost stagnant in the lower part of the envelope that narrows down to fit in the reactor core.

Impurities, especially iron oxides from the out-of-pile circuit built in steel, may constitute the major cause of CO_2 activation.

8.2. Adopted solution

To resolve the problems related to the CO_2 activation the following measures are taken:

(a) Gas filtration:

(i) One filter upstream of the reactor pool avoiding the impurities that enter the in-pile section.

(ii) One filter downstream of the reactor pool to retain the eventually activated particles.
A Geiger counter is installed on the last filter to detect the accumulated activity. Another Geiger counter is installed more downstream in the circuit to detect a dispersion of any activated particles in the circuit.

(b) Leaktightness of the circuit. The leaktightness of the circuit is assured by using:

(i) Special reciprocating compressors with dry pistons.

(ii) Bellows valves.

(iii) A limited number of special joints made of "Garlock" or "Larciet".

(c) The isolation of the circuit. The isolation of the circuit with respect to the other circuits in the loop is obtained by using:

(i) A closed circuit (reactor experimental cooling circuit) to evacuate the heat transferred to the secondary CO_2-H_2O heat exchanger, and to cool the CO_2 gas purification system.
(ii) A closed circuit to cool the compressors.
(d) Gas storage and evacuation.

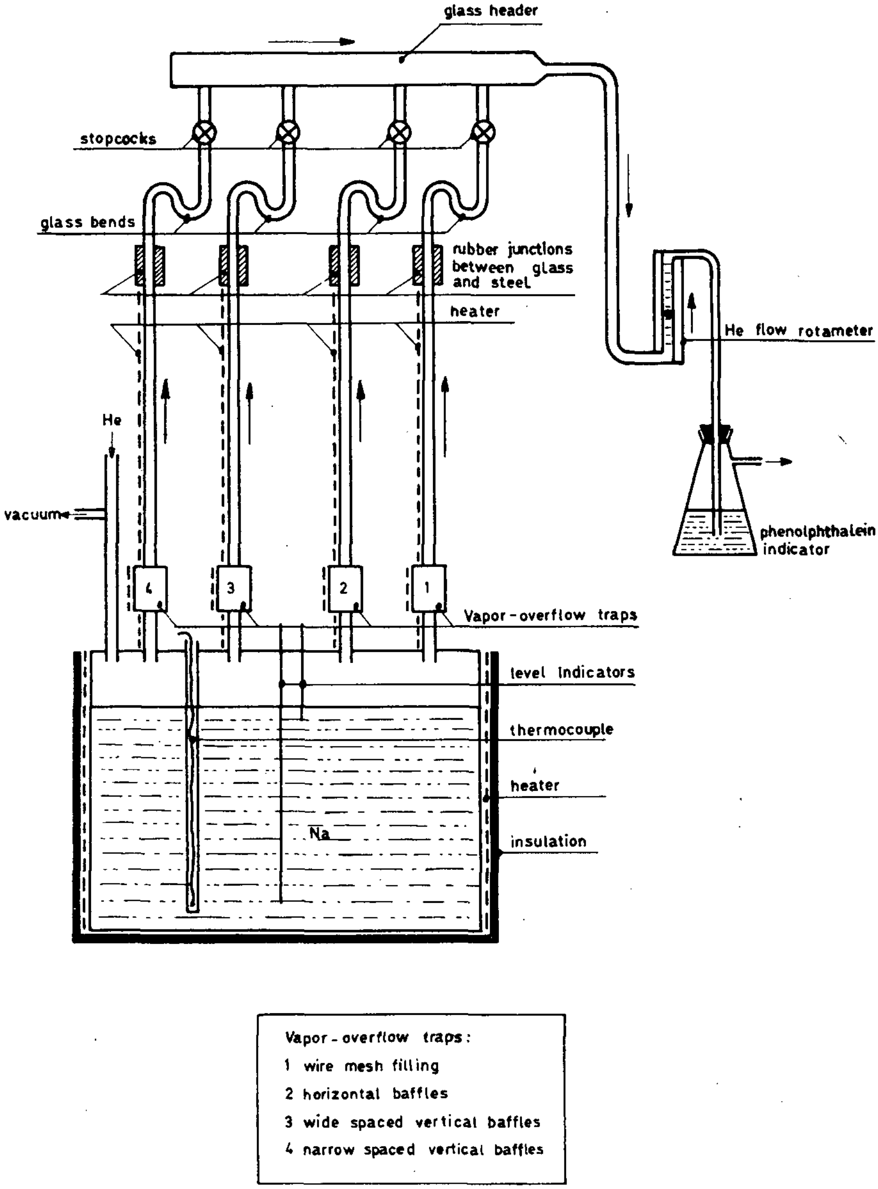

FIG.19. Test set-up for sodium-vapour overflow traps

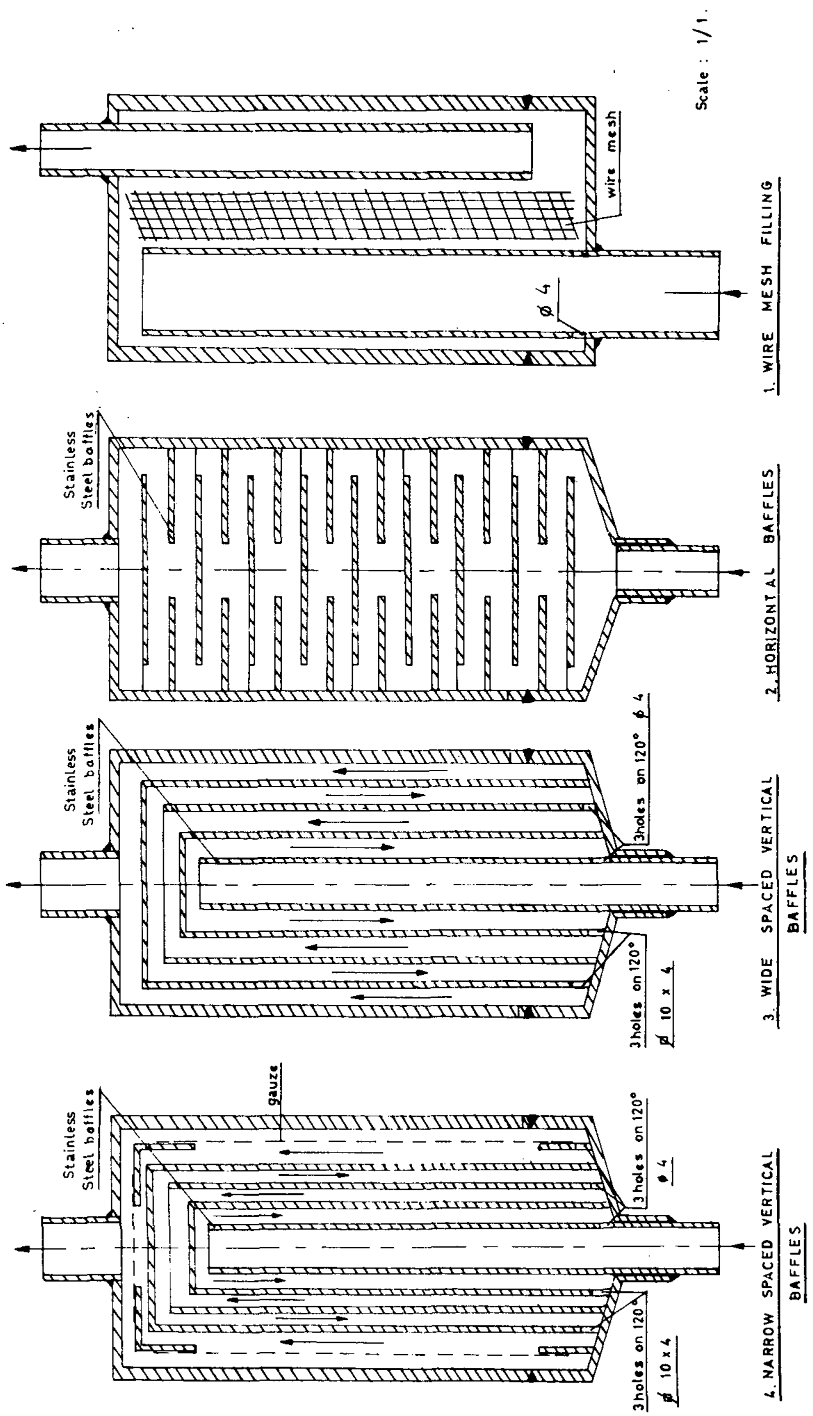

FIG.20. Schematic arrangement of different sodium-vapour overflow traps

The gas storage and evacuation is such that all gas discharge to the exterior must pass along the storage tank. A Geiger counter is installed at the outlet of the tank towards the stack. An electromagnetic valve receiving the signal from the Geiger counter stops the evacuation towards the stack if the activity of the gas measured exceeds the set point.

9. Development of an efficient sodium vapour-overflow trap

The presence of condensed sodium around the snap-tight of the helium duct and the desire to monitor fission gases continuously by sweeping the blanket gas for vented fuel irradiation brought forward the need to develop a more efficient sodium vapour-overflow trap.

Such a trap must have the following characteristics: avoidance of freezing sodium vapour in the trap; provision to condense the maximum possible percentage of sodium vapour to liquid; back flow of condensed sodium to the vapour source; and small size to suit the compact nature of the circuit.

To compare the effectiveness of different vapour-overflow traps a set-up as indicated in Fig. 19 is used. A schematic arrangement of the different vapour-overflow traps is shown in Fig. 20. The performance of the different traps is compared with the performance obtained for an identical wire-mesh-filled trap as used during the first irradiation of the loop. The test conditions are set at three temperature levels: 300°C, 450°C and 600°C, and two helium flowrates: 0.5 l/min and 1 l/min.

Each trap is consecutively operated for one week (half a week at 0.5 l/min and half a week at 1 l/min) at one of the specified temperature levels leading to a total testing time of 12 weeks. For any one of the above specified operations sodium precipitation occurs in the flow restriction around the ball indicator of the rotameter, and water with phenolpthalein indicator colours red when the swept-off gas is bubbled through it. This points out that the vapour removal of a small-sized trap is not very efficient, and that the sodium vapour is quite closely mixed with the blanket gas.

At the 300°C temperature level, apart from the two remarks above, all traps perform well.

At the 450°C level sodium precipitates out above the stopcock of the trap with the narrow-spaced vertical baffles. To maintain a flowrate of 0.5 l/min the pressure increases from 0.1 kg/cm^2 to more than 1 kg/cm^2 in about 8 h time necessitating stopping further testing with this trap. The other traps behave as for the 300°C level case. After cleaning the precipitated sodium the test is repeated, leading to the same results for the trap with the narrow-spaced vertical baffles.

At the 600°C level sodium precipitates out above the stopcock and in the bend just beneath the stopcock for each trap. The trap with the horizontal baffles performs the best, probably because it presents the easiest way to backflow the condensed sodium. Whereas the pressure increases from 0.1 kg/cm^2 to more than 1 kg/cm^2 in about 1 h for the trap with the narrow-spaced vertical baffles, and in about 4 h for the traps with the wide-spaced vertical baffles and the wire mesh filling, an 8 h run for the trap with horizontal baffles could be made, obtaining a 0.5 l/min flowrate for each trap.

Visual inspection of the traps after the tests reveals following points:

The holes provided in the inlet tube of three of the traps for back flow of the condensed sodium to the tank are partially plugged with solidified sodium, indicating that back flow is made more difficult by the upstreaming gas.

Even the inlet tube of the trap with horizontal baffles is partially plugged because the lower baffle is mounted too close to the inlet tube.

On the other parts of the traps a more dense sodium film sticks to the inner baffles than the outer ones. This phenomenon is especially visible on the horizontal baffles where the lower baffles are quite contaminated in comparison with the upper ones.

As a general conclusion, from the tests is can be said that under the test conditions specified a trap with horizontal baffles will perform adequately if the lower baffle is somewhat curved to facilitate sodium back flow and is not mounted too close to the inlet tube; and two traps, of the same size as tested, are placed in series to obtain the necessary condensation surface and to enhance the vapour removal.

IV. DISMANTLING THE FUEL PINS IN THE HIGH-ACTIVITY HOT CELLS

1. General

This section describes the general dismantling procedure followed in the high-activity hot cells to recuperate the fuel pins and to permit adequate evacuation of the sub-assemblies and the scrap.

The primary sodium circuit entirely contained within the envelope is transferred, under water, from the reactor pool through the canal towards the high-activity hot cells connected to the reactor containment building. This is done by placing the envelope in a transfer cask which fits into the reactor transfer chute connecting the pool to the hot cells. In the hot cells the lower part of the envelope tube and the sodium circuit are cut to empty the sodium and to take out the irradiated fuel assembly. The upper and middle portions of the envelope tube and the sodium circuit remain intact while the envelope is closed again and stored under water in the canal for ultimate recuperation of some of the sodium circuit equipment.

The general principles on which the operations are based are the following:

(a) There have been no irregularities with the primary sodium circuit during irradiation, and regular flushing of the helium blanket gas has never indicated any contamination. There is good reason to believe that the fuel cladding is intact at the end of the irradiation campaign. A sodium sample taken after the second cut but before the sodium is emptied from the primary circuit is analysed to verify once more the integrity of the fuel pins.

(b) The dismantling operations in the hot cells do not present any risk of bringing in contact materials which may violently react with sodium.

(c) All delicate operations are done with dummy assemblies beforehand to permit personnel to get acquainted with the different techniques to be employed.

Under these circumstances, the principal operations to be done in the high-activity hot cells are as follows:

(i) Empty the sodium in a dump tank by means of the electrical heaters installed on the primary circuit;

(ii) Cut off the envelope finger containing the fuel assembly and recuperate the pins after cleaning in ethyl alcohol;

(iii) Close the envelope again to store some of the sodium circuit equipment under water in the canal for ultimate recuperation;

(iv) After visual inspection put the fuel pin in the container and transfer cask for return to the experimenter and evacuate the scrap to the "waste".

The preparation of the experiment before doing the above operations is also included in this section.

2. Preparation of the experiment stored in the reactor pool

After the envelope containing the primary circuit has been stored for at least two weeks in the reactor pool to allow for adequate nuclear cooling, the following preparations are done:

(a) All connections grouped in the connection box on top of the envelope and at the pool parapet are loosened to enable the flexible stainless-steel tube with all control cables to be removed.

(b) A new flexible PVC tube, strengthened with a stainless-steel plug at one end and containing the necessary cables for the electrical heaters and thermocouples of the primary circuit, is connected to the connection box on top of the envelope.

(c) The flexible tube for the helium stand-by duct is loosened on top of the envelope and taken away while the duct is strengthened with a stainless-steel cap.

(d) The flexible tube for the normal helium duct is loosened and replaced by a cable of sufficient length for use in the hot cells.

(e) All flexible tubing is wound up round the top of the experiment and fixed to fit inside the storage cask.

(f) The upper part with lifting head is bolted to the storage cask to make the cask ready for transfer through the transfer chute.

3. Manipulations in the high-activity hot cells to prepare the dismantling operations of the experiment

When the experiment is inside the transfer cask of the reactor transfer chute, inclined towards the high-activity hot cells, the following operations are done to prepare the proper dismantling:

(a) The hook from the hot cell is brought into the reactor transfer chute to withdraw the transfer cask;

(b) The transfer cask is lowered into the vertical channel nearest to the transfer chute. To ensure guiding of the transfer cask and to facilitate withdrawal of the experiment the vertical channel is equipped with a special guide at the top and a supporting piece at the bottom;

(c) The lifting head of the transfer cask is taken off and put away on one of the working floors;

(d) The envelope containing the primary circuit is withdrawn from the transfer carrier and positioned in the mandrel of the sawing machine.

(e) The PVC tube with the cables for the electrical heaters and the thermocouples, together with the helium cable, is carried through a special plug fitted in the hot cell wall traverse to be connected to a control panel, an argon supply and a vacuum pump outside the hot cells;

(f) Carried through the same plug are the connections for the pump tank. Special care is taken to place a liquid-nitrogen-cooled charcoal filter with shut-off valves on the vacuum connection to the dump tank inside the hot cells. A Geiger counter placed on the vacuum line at the inlet of the pump outside the hot cells allows any contamination of the off-gas to be detected and the shut-off valves of the charcoal filter to be closed.

At this stage the experiment is manipulated into the proper working position so that the cutting operations can be begun.

4. Cutting operation

To recuperate the fuel pins various cuts are necessary. The sequence of operations is as follows:

(a) First cut.

The first cut is performed on the envelope tube, 44.5/41.5 mm diam. at 260 mm from the bottom.

(b) Second cut.

The second cut is performed on the primary sodium circuit containing solidified sodium, 33/30 mm diam. at 95 mm from the bottom. Only the tube wall is cut with the machine. A knife-cut through the solidified sodium was proposed, but the solidified sodium is already broken away by a small movement of the upper portion of the experiment. At this stage two sodium samples are taken to detect eventual contamination of fission products, further dismantling of the loop being continued only after the qualitative results of the analysed samples are available.

(c) Emptying of the sodium circuit.

To empty the sodium circuit the tube at the lower end, 33/30 mm diam., is joined to the dump tank by means of a flange and an O-ring. The operations performed are: Vacuum is made on the dump tank and on the sodium circuit; the sodium in the circuit is heated up with the electrical heaters and falls by gravity into the dump tank, the level in the tank being observed with spark-plug-type level indicators; after cooling a slightly higher pressure than atmospheric is placed on the circuit, and the dump tank is unbolted from the circuit and the top closed with a blank flange. A schematic arrangement of the set-up in the hot cells for sodium emptying of the circuit is given in Fig. 21.

(d) Third cut.

The third cut is made through the in-core finger at 825 mm above the reference of the first cut. This cut is made through three concentric tubes: envelope tube, 44.5/41.5 mm; outer sodium tube, 33/30 mm; and the central tube, 23/20 mm.

Before cutting a system is provided to prevent the B4C screen and the central tube slipping out by cutting vibrations.

(e) Recuperation of the in-line fuel assembly.

The cut-off part is immersed in a tray containing ethyl alcohol ($C_2H_5OH + Na \rightarrow C_2H_5ONa + \frac{1}{2}H_2$). After the reaction is finished the

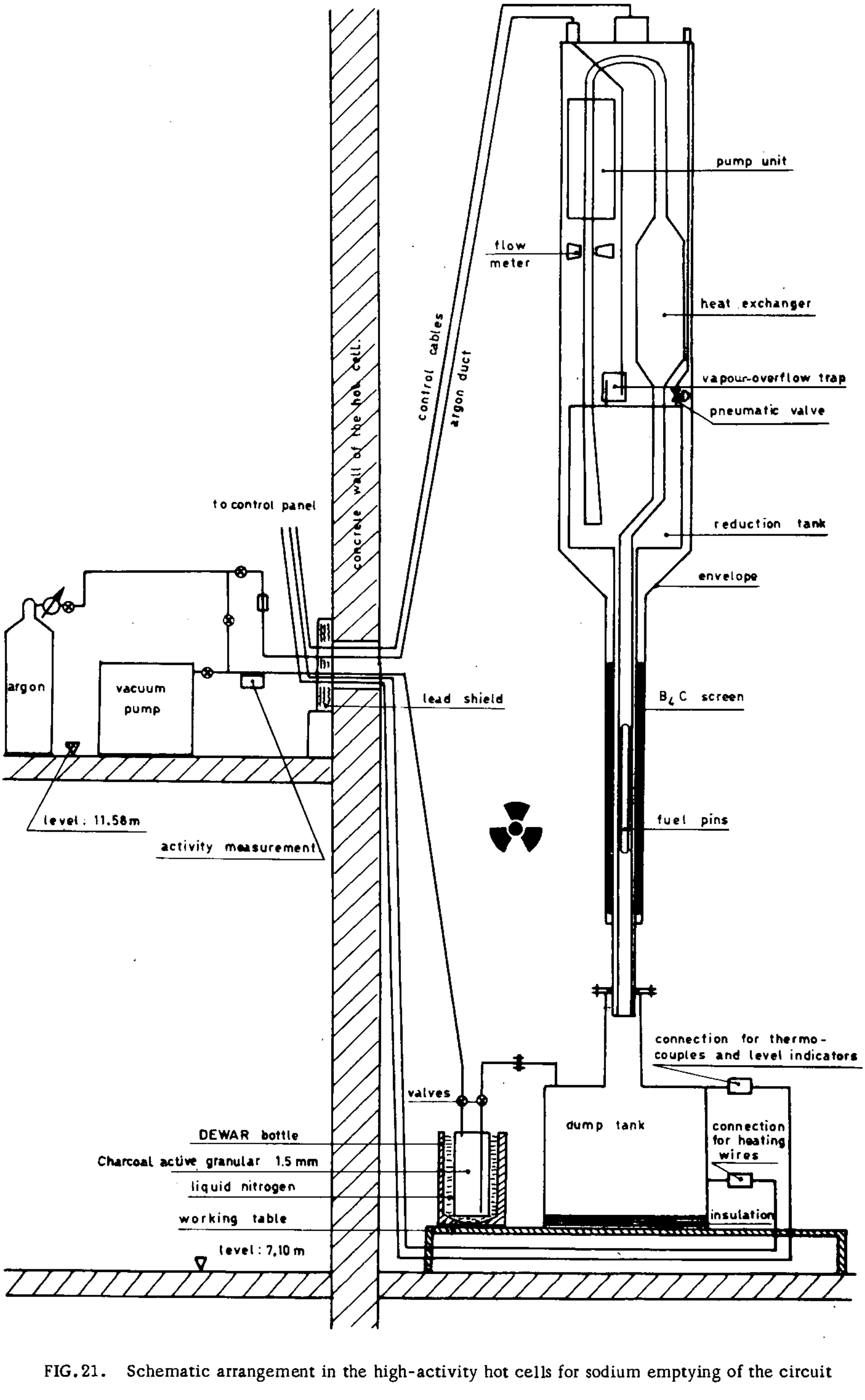

FIG. 21. Schematic arrangement in the high-activity hot cells for sodium emptying of the circuit

cut-off part is immersed in a second tray containing ethyl alcohol plus 10% water ($C_2H_5ONa + H_2O \rightarrow C_2H_5OH + NaOH$). After this cleaning the central tube with the in-line fuel assembly is withdrawn from the cut-off part. The envelope tube with the boron carbide screen is placed apart to be sealed later on in a special container to be stored for further examination.

(f) Recuperation of the flux monitor.

The flux monitor fixed by spot-welded stainless-steel clips at the outside of the central tube along the axial length of the fuel pins is loosened. To familiarize the technician with this technique a test is done beforehand on a dummy monitor.

(g) Recuperation of the fuel pins.

The support ring at the lower extremity of the in-line fuel assembly is welded to the central tube. To withdraw the in-line fuel assembly from the central tube a cut is made at 120 mm from the bottom end of the central tube just above the visible weld on the support ring. The in-line fuel is cut into five parts (two end pieces and three central pieces containing the fuel). The way of cutting the guide pieces is indicated in Fig.4. The central tube serves as guide tube during the cutting.

(h) Encasing of fuel pins and end pieces.

After cutting off the in-line fuel assembly the central fuel pins are encased by welding and the different parts put into a container which is later transferred to the lead-shielded carrier for dispatch to the experimenter for complete examination. Only a visual examination with a check of the fuel diameters of the pins is performed in the high-activity hot cells. To familiarize the technician with this technique a transfer operation of the container is done beforehand.

5. Evacuation of sub-assemblies and scrap

The upper and middle portions of the envelope and the emptied sodium circuit are closed for storage under water in the canal. The closure is done by welding an end cap to the bottom of the envelope finger. To ensure leaktightness the end cap is once more contained in a liquid metal seal.

The scrap is evacuated as follows:

(a) Alcohol: the trays with the reacted alcohol are discharged in the hot cell drains;

(b) Sodium tank: the sodium storage tank is sent to the "waste" following their prescriptions;

(c) Cut-off parts: all cut-off parts are assembled in a container and sent to the "waste" following their prescriptions.

V. VISUAL EXAMINATION OF THE STORED SODIUM CIRCUIT DURING CUTTING: CLEANING WITH ALCOHOL AND RECUPERATION OF SOME EQUIPMENT

This section describes the visual examination of the stored sodium circuit during cutting. The tubes (including pump unit and flowmeter), the heat exchanger, the vapour-overflow trap, the pneumatic valve, the helium ducts, the reduction tank and the expansion bellows are closely examined. Cleaning with alcohol and the recuperation of some equipment is also described.

1. Cutting of the sodium circuit

After under-water storage of the upper and middle portions of the envelope and the emptied sodium circuit in the canal for at least two months, the degree of contamination is such that further dismantling can be done in a limited yellow zone. The ability to perform the dismantling in a yellow zone facilitates the work to such an extent that all instrumentation cables can be detached in about 3 h, and all the different pieces of equipment, pump unit, flowmeter, heat exchanger and reduction tank are cut from the circuit in about 4 h.

Visual examination of the cut pieces reveals the following points:

(a) Tubes (including pump unit and flowmeter).

On the tubes, to which the pump unit and the flowmeter essentially belong if only the sodium passage is considered, there is a thin sodium film visibly sticking to the walls. No other traces of sodium can be found indicating a complete emptying by the dumping method.

(b) Heat exchanger.

In the heat exchanger containing on the sodium side a tube bundle of 61 tubes and two collectors only small traces of sodium are still sticking to the welds of the tube sheets.

(c) Vapour-overflow trap.

The vapour-overflow trap inlet tube is free of sodium. The holes provided in the inlet tube for back flow of the condensed sodium vapour to the reduction tank are plugged, however, with solid sodium, indicating the need for larger holes. Also the wire mesh has been too compact in the trap, and has in some places solid sodium sticking to the mesh. The vapour-overflow outlet tube is partially plugged at the lower edge, which must be due to the insufficient back flow of the condensed sodium through the holes in the inlet tube, as explained above.

(d) Pneumatic valve.

The pneumatic valve on the top cover of the reduction tank is cut to find out why the valve behaved somewhat peculiarly during irradiation. As no sodium traces were found on the bellows assembly of the valve after cutting, it is clear that the behaviour of the valve is not influenced by condensed sodium, as was feared. On the contrary, on examining the casing of the valve, it was found that the guiding length of the casing for the bellows contained a weld which obtruded at some points, preventing from time to time a normal movement of the bellows in the casing to open or close the valve.

(e) Helium ducts.

The helium ducts to the reduction tank over the pneumatic valve and over the vapour-overflow trap did not contain any condensed sodium. However, the helium duct over the vapour-overflow trap was plugged at the snap-tight connection just at the outlet of the envelope. It is likely for precipitation to occur here as it is the first region out of the heating zone, and the first turbulence in the flow pattern round the snap-tight ball restriction.

The presence of condensed sodium round the snap-tight of the helium duct clearly indicates the importance and care that must be paid in the design of an efficient vapour-overflow trap.

Some of the development work done along these lines is explained in Sub-section III. 9.

(f) Reduction tank.

The top cover of the tank is cut to enable a closer look to be given to the inside of the tank. Apart from a thin sodium film on the walls the inside was clean indicating again a complete emptying of the circuit by the dumping method. Only on the top cover of the tank were there some deposits of sodium visible, caused by sodium evaporation.

(g) Expansion bellows.

The expansion bellows Trade BOA, Type Z, with interior guide, are cut to free the interior guide and to examine the quantity of sodium trapped in the undulations of the bellows. Most of the undulations are filled with sodium which explains the stiffness of the bellows and the care one should take in warming up this part of the circuit.

2. Alcohol cleaning

After cutting all pieces are strengthened with rubber bungs or transparent self-adhesive tape. Later they are grouped together to clean with technical ethyl alcohol to solve all sodium traces that apparently contribute the greater part to the degree of contamination. The cleaning is done in a three-step operation. The first step is a batch cleaning with 100% technical ethyl alcohol. The second step is a batch cleaning with technical ethyl alcohol cut with about 50% of water. The third step is a continuous cleaning with streaming water. Only the first-step cleaning leads to a somewhat exothermic reaction by the first contacts. This reaction slows down rapidly giving no more reaction after a quarter of an hour. All effluents from these cleaning operations are sent to the drain for disposal to the waste.

3. Recuperation of some equipment

The pump unit and the flowmeter are decontaminated by the reactor service to the non-active level.

The envelope tube, the heat exchanger, the pneumatic valve, the gamma shields and the vapour-overflow trap are decontaminated to a non-transferable degree. These pieces are put in a plastic bag. Welding, filing, cutting and so on cannot be performed on these pieces without health precautions.

The most valuable of the instrumentation cables, the thermocouples and the disconnectable plugs are found to be non-contaminated and are recuperated.

Of all the other pieces those that are non-contaminated are put to scrap. Those contaminated or active are assembled in a special tank for disposal to the waste.

DISCUSSION

A. G. IOLTUKHOVSKY: What is the maximum temperature of the sodium in your loop, and what is the material of the loop?

A. M. SOENEN: The maximum sodium temperature is 600°C and the material of the loop is AISI 316 stainless steel.

A. G. IOLTUKHOVSKY: Have you envisaged the possibility of material behaviour tests – in particular stress tests?

A.M. SOENEN: The loop was built to test the behaviour of fuels subjected to a fast neutron flux. Material behaviour tests with pressures up to 15 kg/cm^2 could be considered.

E.L. ZEBROSKI: What linear power (peak) can be attained in your loop for a given fuel diameter and enrichment?

A.M. SOENEN: The maximum specific power is 2.2 kW/cm^2.

E.L. ZEBROSKI: What fuel damage do you think would occur if the flow failed while peak power fuel was under irradiation?

A.M. SOENEN: The double containment of the loop is so designed that the fuel section will always remain immersed in sodium, and we therefore think that any damage to the fuel would be limited.

A. BARTHOUX: Have you had any incidents with the fuel which resulted in fission products being released into the sodium? If so, would you care to comment on the measurements that you made?

A.M. SOENEN: Regular flushing has never revealed any activity from fission gases. The active charcoal adsorber is designed to retain all fission gases, even when a complete fuel melt-down occurs.

A.V. CAMPISE: Did you set any particular transient pressure requirement for the internal structure of your loop? For example, in an accident involving flow failure, could the structure of the loop withstand an internal pressure of 500-1000 lb/in^2, resulting from sodium boiling, void formation and mixing of the hot fuel with the sodium coolant?

A.M. SOENEN: No. The loop is designed to withstand 15 kg/cm^2 at 600°C. Transient conditions are very difficult to predict, and no special design for such high internal pressures was considered.

EXPERIENCE IN THE DESIGN AND OPERATION OF HIGH-TEMPERATURE ALKALI METAL SYSTEMS

R.C. WERNER AND R.C. ANDREWS
MSA RESEARCH CORPORATION,
EVANS CITY, PA.,
UNITED STATES OF AMERICA

Abstract

EXPERIENCE IN THE DESIGN AND OPERATION OF HIGH-TEMPERATURE ALKALI METAL SYSTEMS. Our experience with the alkali metals began in 1942, when it became necessary to manufacture potassium as an intermediate step in producing potassium superoxide and oxygen generator chemicals for use in rebreather safety equipment evaluation. Study of the alkali metals has continued to the present with measurement of the physical properties, high temperature heat transfer properties, followed by the development of liquid metal instruments and the design and reliable manufacture of components. The present operation (up to 1200°F) of two sodium systems to study the instream mechanical properties of materials for long periods of time reveals the satisfactory operation of many components and the trouble to be experienced when operation is attempted with impurities added to the sodium.

Cold-trap purification of 1200°F sodium systems is sufficient for low-corrosion operation over a 2-yr period in an AISI, Type 316 stainless-steel system. The adding of new specimens always raises the oxygen level, requiring repurification of the sodium. Some carbon was removed by the cold trap when high carbon-sodium conditions prevailed, but removal is not complete enough for satisfactory operation; therefore great care should be taken in preventing the carbon contamination. Plugging indicators were a good tool for normal operation. Under high carbon conditions the intitial break in the plugging indicator curve can be related to the carburization potential of the sodium. Inert gas lines in sodium systems need to be heated above the melting point of sodium to prevent plugging. However, under high oxygen-sodium conditions, solids deposit in the cover gas regions under ambient temperatures above the melting point of sodium. It is observed that the main difficulty incurred in running with high oxygen-sodium systems is the oxide plugging of small lines. In high carbon sodium systems, the failure of valve bellows by carburization causes operational difficulties.

Stability of magnetic flow meters and reliability of electromagnetic pumps for long-term operation in sodium loops are discussed. In general, these components give excellent performance.

INTRODUCTION

Our first experience in the design and operation of alkali metal systems began in 1942 when it became necessary to manufacture potassium as an intermediate step in the production of potassium superoxide. This latter chemical was needed as the oxygen-generating chemical in rebreather safety equipment.

The process for manufacturing potassium consisted of replacing the potassium in a molten salt, such as potassium chloride, with sodium and distilling over a mixture of potassium and sodium vapors at 1550°F to a condenser. Descriptions of the batch-reaction process, the separation of potassium from sodium by distillation and, later, a combination of the two steps into a continuous process have already been published.[1]

The interest in the use of NaK -- the alloy of sodium and potassium -- as a heat-transfer fluid led to the study of

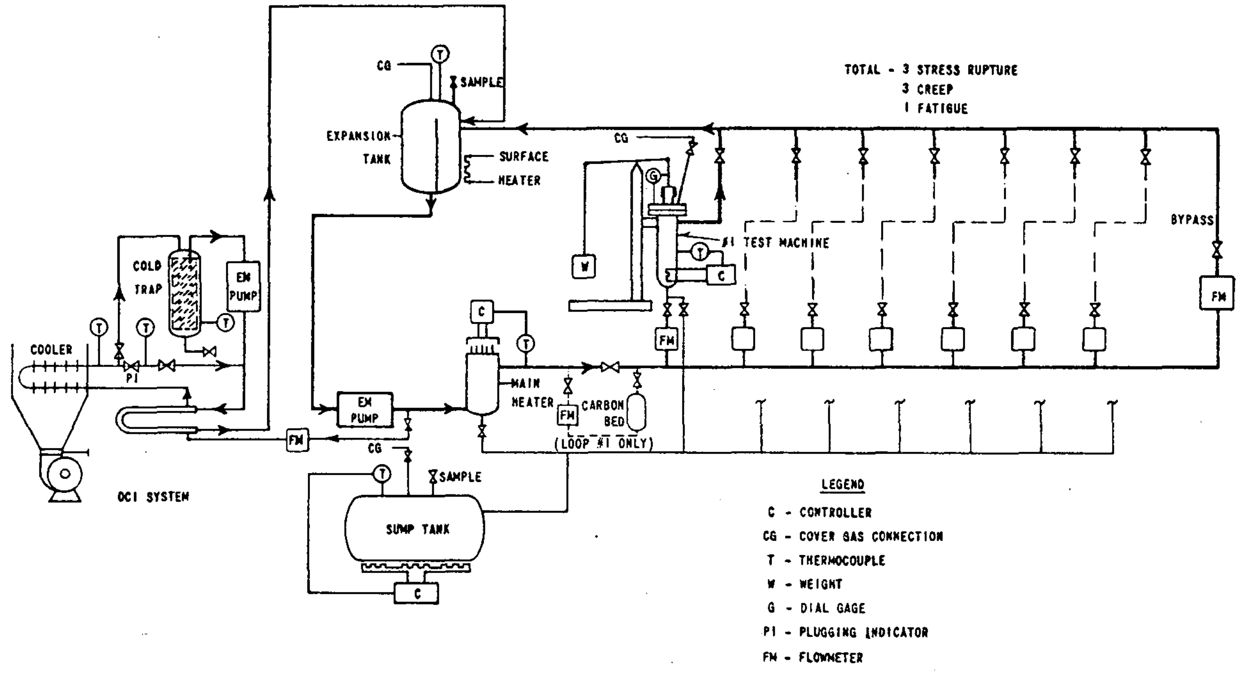

FIG. 1. Mechanical properties test loop schematic: Loop 2, Test 3

its physical properties, such as density, viscosity and specific heat of its heat-transfer properties[2]; and to the development of components, such as flowmeters, pressure transducers and electromagnetic pumps. Many of the results were reported in the first[3] and second[4] editions of the LIQUID METALS HANDBOOK and the Sodium-NaK Supplement[5].

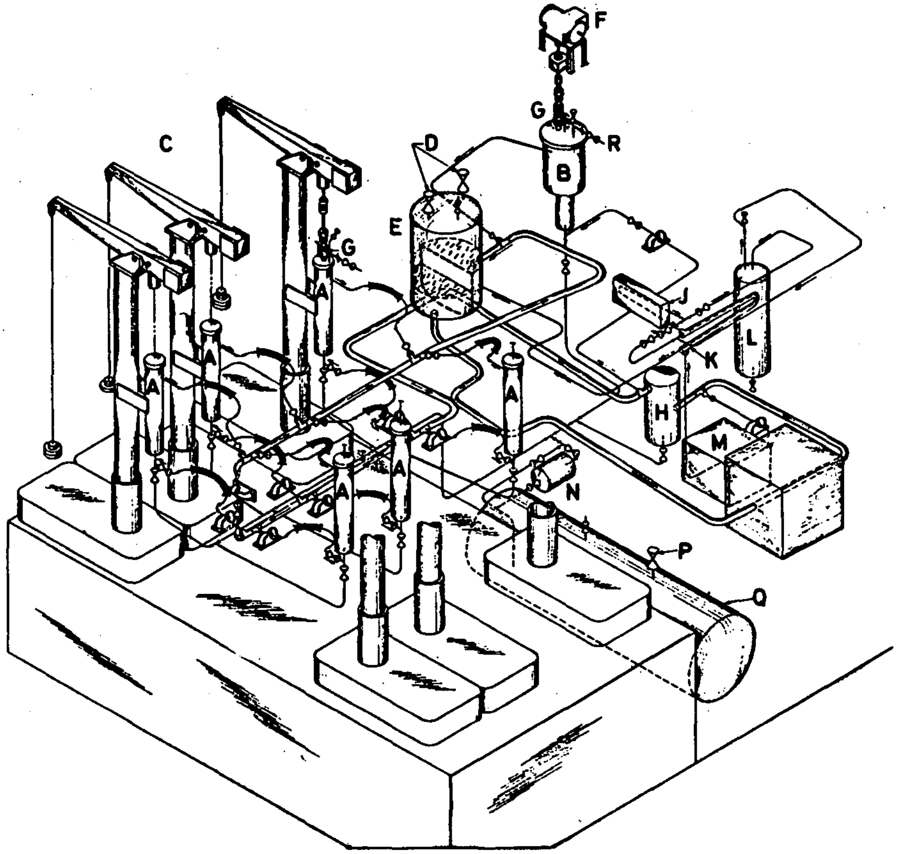

FIG.2. Mechanical properties of materials test loop (Isometric): Loop 2

A	Test units 1-6	F	Motor drive	L	Cold trap
B	Fatigue rest unit	G	Bellows	M	OCI pump
C	Stress machines	H	Heater	N	Filter
D	Sample extraction valves	J	OCI cooler	P	Sample extraction valve
E	Expansion and sampling tank	K	OCI economizer	Q	Sump tank
				R	Cover gas

In order to best set forth some of the useful experience with alkali metal systems, the two mechanical property loop systems which have operated at 1200 F for 33,050 and 31,570 hours respectively in the AEC Mechanical Properties Program will be described. What makes these two systems such outstandingly useful examples has been the requirement that they include operation under extremely dirty conditions so as to hasten any detrimental effects.

DESCRIPTION OF ALKALI METAL SYSTEMS AND FACILITIES FOR MECHANICAL PROPERTIES STUDIES

The two loops are identical in design. A flow sheet layout is shown in Fig. 1 and an isometric view of the piping and components is shown in Fig. 2. Only the Loop No. 2 will be described here.

The loop is designed such that six creep or six creep-to-rupture tests, or any ratio of the two totalling to six, plus one fatigue test, can be run simultaneously and independently. This is accomplished by using seven parallel test circuits, a main system bypass and the oxide control and indicating system.

Sodium is pumped through the main heater into a header system which feeds each of the seven test units. Each unit can be isolated by manually operated bellows-sealed valves located at the inlet and outlet of each test unit. A flowmeter in the inlet line of each test unit monitors the sodium flow rate. Sodium enters the bottom of each test unit and flows up across an electrical immersion heater which adjusts the final temperature of the sodium before passing over the test specimen and out the discharge line. The outlets of the seven test units are joined together by a manifold running to an instream combination expansion and sampling tank. The inlet and outlet lines of the six creep or creep-to-rupture units are flexible stainless-steel hoses which permit a more compact design. Each unit contains a drain line with bellows-sealed valve connecting to a common drain line running to the sump tank. Each test unit can be drained or filled individually and independently.

The bypass circuit containing a liquid metal flowmeter and a bellows-sealed shut-off valve permits the circulation of sodium without going through any of the test units.

The oxide control and indicating (OCI) system is connected in parallel to the main system. The cold trap and oxide indicator permit the purification and measurement of the oxygen in the sodium throughout the operations.

CREEP AND CREEP-TO-RUPTURE TEST UNIT

The design of the Creep-to-Rupture Test Unit is shown in Fig. 3. A 4-in. IPS weld neck flange with a quick disconnect temperature-compensating coupling manufactured by the DSD Manufacturing Company is being used for this service. This device depends upon a clamped band containing Inconel X curled "fingers". These "fingers" work like a bimetal, uncoiling as the temperature increases to grab harder and harder. A seal between the clamped flange is established by a hollow "Toruseal" stainless-steel O-ring.

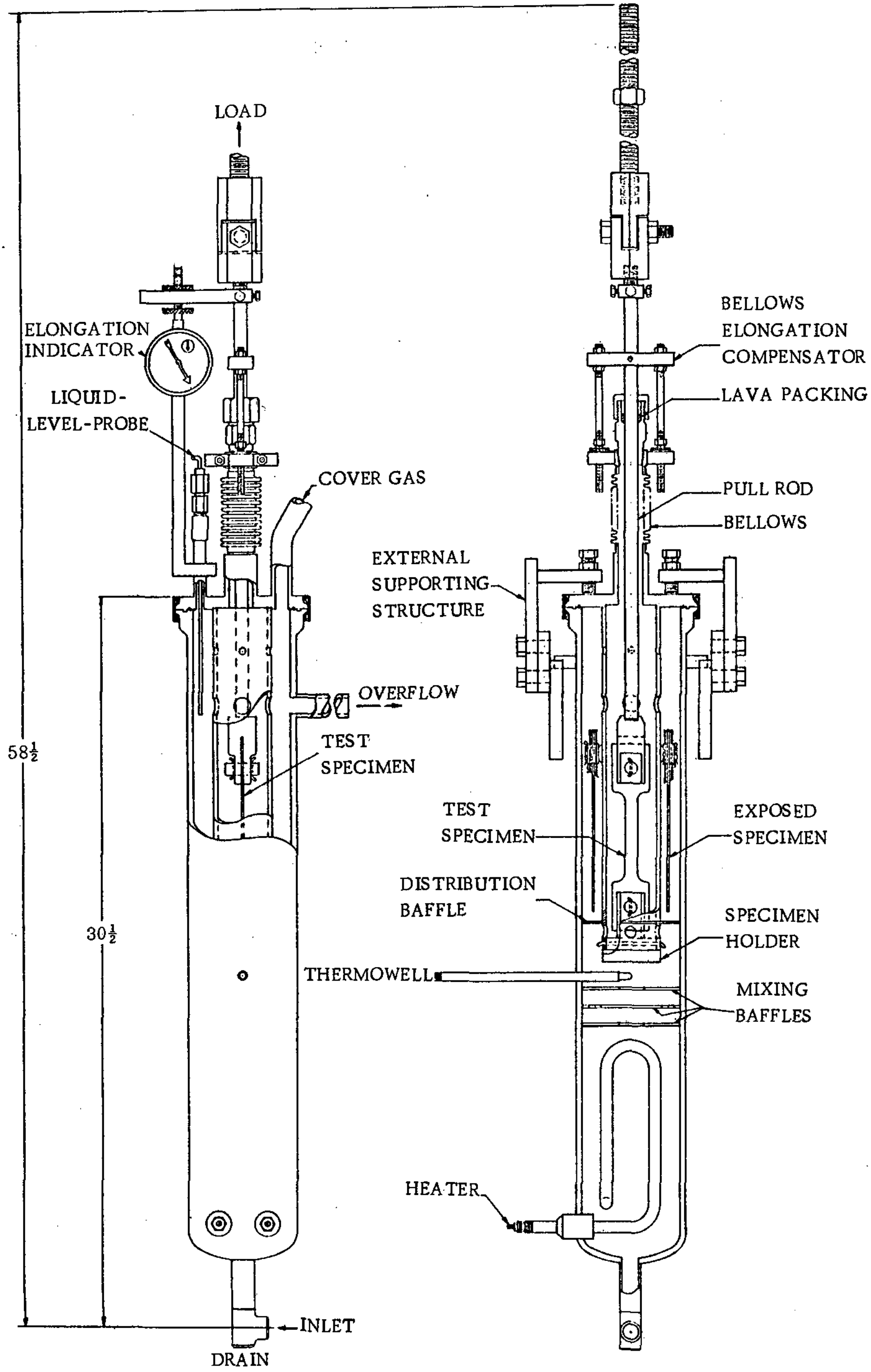

FIG.3. Creep and creep-to-rupture test unit

A 316-ss metallic bellows is used in conjunction with a Conax mechanical packing gland to seal the 1/2-in. diameter pull rod connecting the test specimen through the top of the test unit to the stress machine. The bellows have an averaged spring constant of 100 pounds per inch of travel and, in order to eliminate this force from the pull rod, the elongation of the bellows is measured and the resulting stress compensated for throughout the various tests. During the creep-to-rupture tests, the bellows are readjusted to the neutral point after 1/16 inch of travel. In the case of the creep tests, this compensation is made by periodically adding an appropriate weight to the stress machine. These weights are added in 1/2 pound increments after 1/16 inch of bellows elongation. The maximum error in the applied stress is 2.5% based on the lowest stress test, this being the worst case.

Fully jeweled dial gages mounted externally are being used with a dial range of 0.100 inches divided into 0.001 divisions. Any force transmitted to the test specimen through the pull rod is transmitted back to the blind flange tending to break the seal; therefore, an external support assembly is provided to counteract this force. This assembly is bolted to the test-unit support members and adjustable bolts tightened down against the flange prevent the transmission of the stress from the test machine to the clamp and seal.

A clevis assembly is threaded to the pull rod which permits adjustment of rod length and connection to the lever arm of the test machine. The test pot is supported by means of brackets welded to the column of the test machine.

The test machine itself is a standard Arcweld Model K, 6000-lb capacity creep-rupture machine with a 10:1 ratio lever arm. It is equipped with a load weight elevator for manual operation and a switch assembly for determination of elevator position with respect to load weights. The test machines are calibrated by a factory representative prior to each TEST series.

FATIGUE TEST UNIT

A drawing of the complete fatigue test assembly, as finally conceived and constructed, is shown in Fig. 4.

The heater section is identical to that of the creep-stress rupture pots, except in the orientation of the heater with respect to the inlet and drain nozzles.

The second section contains the test specimen. It is fabricated from a length of 10-in. Sch 40 pipe, a 10-in. butt-weld cap, and a 10-in. I.P.S. weld neck quick-disconnect temperature-compensating coupling. Sodium leaving the heater section passes through a stainless-steel wire screen and over the control thermocouple. The screen is used to prevent pieces of the fatigue specimen from falling into the heater section after fracture. The sodium outlet is located over the baffle in the test section but below the disconnect coupling seal level.

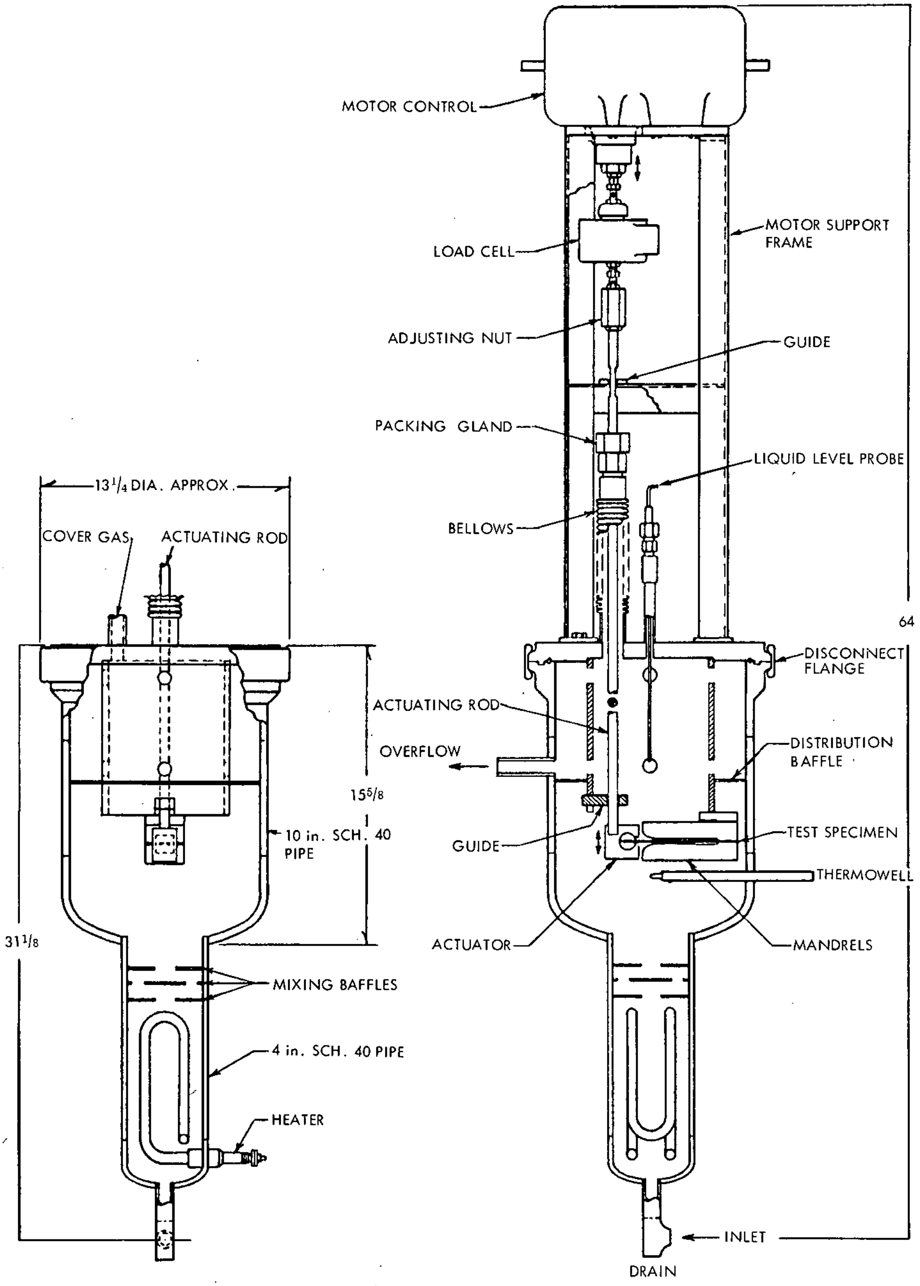

FIG. 4. Fatigue test unit

The third section (test section) is built around the 10-in. blind flange used to seal the pot from the atmosphere. The inner shell welded to the underside of the blind flange is a length of 6-in. Sch 40 pipe with a baffle between the inner and outer shell to insure flow over the test specimen. Sodium outlet holes are provided in this inner shell. The actuator-rod guide, mandrel holder and pins for holding specimens during exposure are welded to the lower section of this inner section. A bellows assembly, welded to the outside of the blind flange, in conjunction with a packing gland seal, permits passage of the actuator rod through the top flange to the motor drive. A probe and cover gas nozzle are also located in the flange. The DSD quick-disconnect flange with the actual test assembly attached to the blind portion of this flange permits removal of the entire mechanical unit for assembly and disassembly.

MAIN HEATER

The main heater unit consists of twelve 1000-watt immersion-type tubular heaters welded to a flat tube sheet. Ferrules are used to permit welding of the thin-walled heaters to the heavier tube sheet. The tube sheet serves as the top of a vertical tank made of 8-in. Sch 40 pipe with a bottom 8-in. Sch 40 pipe cap. One-inch Sch 40 inlet and outlet nozzles are welded into the side of the tank with the outlet nozzles located as close to the tube sheet as fabrication would permit to eliminate a potential gas pocket. A 1/2-in. Sch 40 nozzle is welded into the center of the bottom cap to provide a line for charging and draining.

EXPANSION AND SAMPLING TANK

A tank located in the main stream provides for the volumetric changes of sodium as well as the sampling station for extraction of sodium samples for analysis. Fig. 5 shows a drawing of this tank. The tank is constructed from 1/4-in. plate rolled to an outside diameter of 18 in. Eighteen-inch diameter ASME flanged and dished heads complete the shell of the tank. The interior of the tank is divided into two sections by a vertical baffle set slightly off center. Sodium enters the first section below the top of the baffle and overflows into the second section where the liquid level is maintained below the baffle height. Positive cover-gas pressure is maintained in the gas space common to both sections. One- and one-half inch gate valves located on the top of the tank over each section provide for sampling of each of the two sections. Such a design permits the addition of contaminants into the downstream section without mixing with the upstream section. Samples can then be taken at the contaminant source and of the returning stream prior to mixing.

A second smaller baffle, at right angles to the main baffle, is installed in the downstream section to prevent formation of a vortex at the bottom outlet. Two wells located in the downstream section are used for temperature and liquid-level measurements.

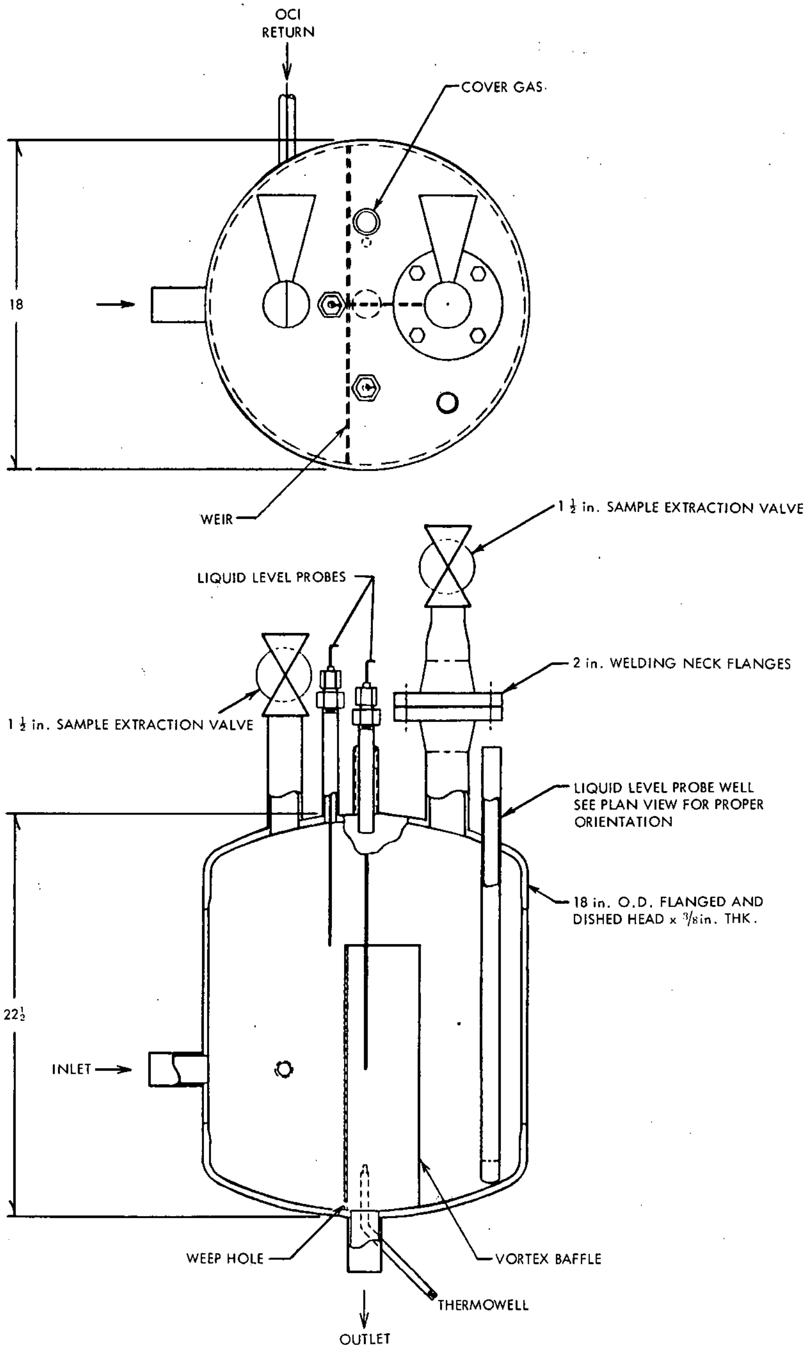

FIG. 5. Expansion and sampling tank

Six 650-watt surface auxiliary heaters connected to give a heat output of 3.9 KW are located on the shell of this tank. They are so placed on the section having the high liquid level to prevent the surface of the tank from overheating.

SUMP TANK

The sump tanks are of sufficient volume to hold the entire loop charge at its operating temperature. The pertinent nozzles on each tank are a liquid level probe nozzle, a thermocouple well, a nozzle for cover gas and a nozzle with a 1 1/2-in. gate valve for taking samples. Both tanks have a 1/2-in. pipe dip leg for charging and draining the test loops and a 1/2-in. drain line on the bottom of the tank. Loop No. 1 sump tank is 24 in. in diameter and 64 1/2 in. long with standard flanged and dished heads, while Loop No. 2 sump tank is also 24 in. in diameter but is only 2 ft long with standard flanged and dished heads. Both tanks are in a horizontal position.

MAIN PUMP

The main pump is an electromagnetic pump designed and constructed by MSAR, as shown in Fig. 6. Electromagnetic pumps have no moving parts and operate on the principle of the "left-hand rule." Alternating current is passed through the liquid metal at right angles to an alternating magnetic field, and the resultant force exerted on the liquid metal causes it to flow through the pump. Control of the pump is accomplished by varying the voltage from 0 to 270 V (not exceeding 28 amps)

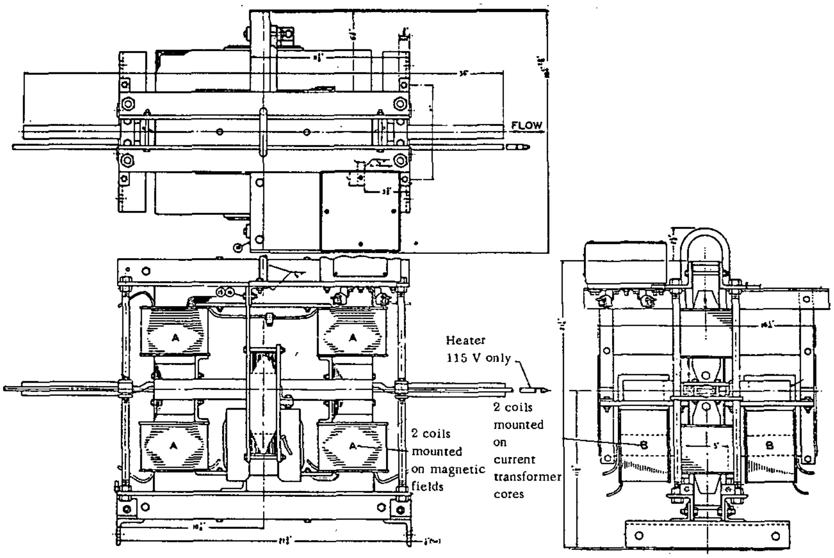

FIG. 6. Electromagnetic pump assembly

through the use of a variable autotransformer. A 7.5-KVA capacitor is connected across the input lines between the transformer and pump to correct the power factor and reduce the line current required to operate the pump. The pump installed has a nominal rating of 25 gpm at 30 psi developed head.

LIQUID METAL FLOWMETERS

Each loop has nine to ten liquid metal flowmeters used for monitoring the sodium flow rates. Their operating principle is based on the flowing sodium stream cutting the lines of force between the poles of a permanent magnet, generating a voltage which is proportional to the flow rate. The voltage is monitored on a standard panel-mounted millivoltmeter. The flowmeters have been calibrated by measuring the magnetic force (Gauss) of the permanent magnet and calculating a conversion curve from the basic equation of generators[6]:

$$E = BVd10^{-8}\left[\frac{2\frac{d}{D}}{1+\left(\frac{d}{D}\right)^2+\frac{pf}{pw}\left[1-\left(\frac{d}{D}\right)^2\right]}\right]$$

where E = output, volts

B = flux density, gauss

V = velocity of fluid, cm/sec

d = inside diameter of pipe, cm

D = outside diameter of pipe, cm

pf = resistivity of fluid

pw = resistivity of pipe wall material

VALVES

There are 26 valves utilized in each loop for isolating and/or throttling the sodium. Each test unit requires two isolation valves and one drain valve. Four valves are needed in the OCI system and one valve on the bottom of the main heater is the main system drain valve. All of these valves are 1/2-in. globe valves, bellows-sealed, Type 316 ss with stellite integral seats and blue African asbestos secondary packing. The valves are manufactured by the Powell Valve Company (Part No. 2475BSF).

SURFACE HEATERS

Preheat for the system is provided for by standard electrical tubular heating elements attached to the surface of heavy wall pipe and tanks. These can be operated with a sheath temperature of 1500°F at their rated watt density but, in most cases, the heaters are limited to a watt density of 20 watts per sq in.

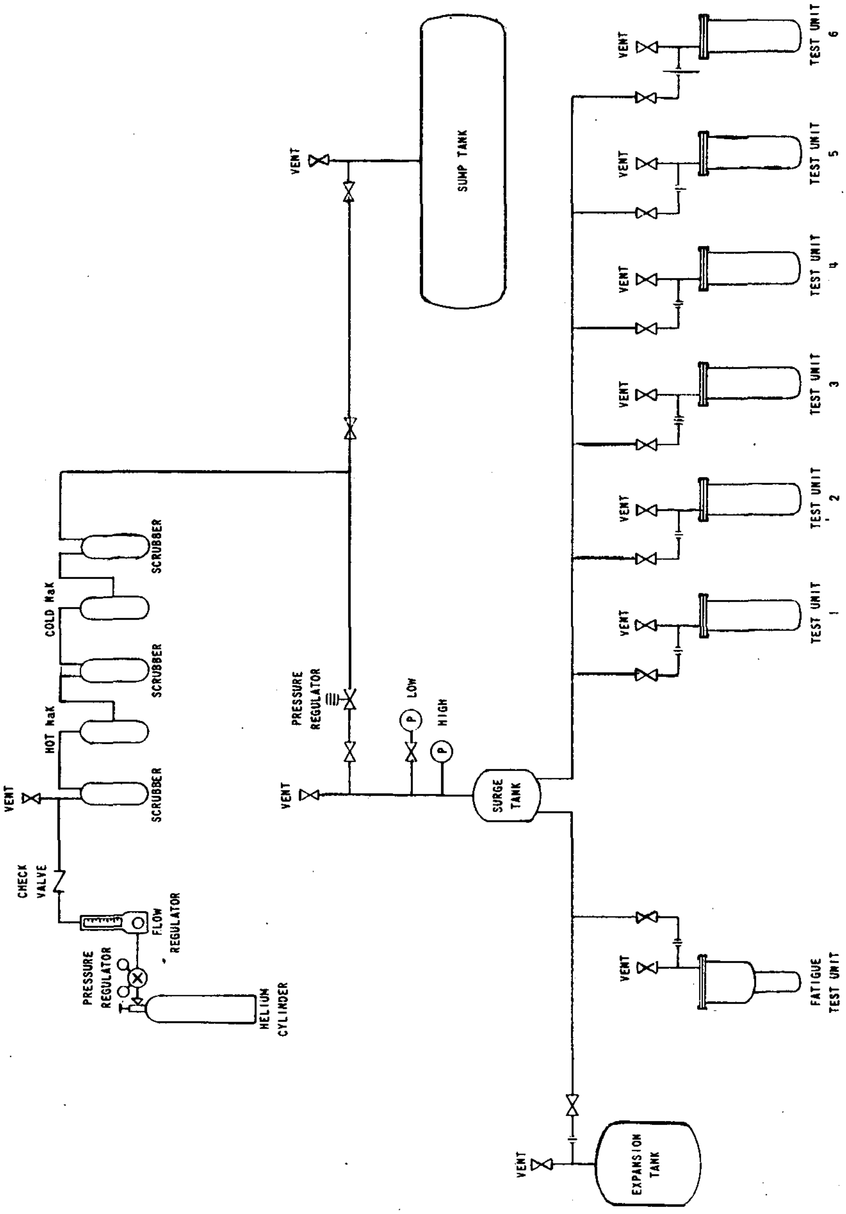

FIG.7. Cover gas schematic

OXIDE CONTROL AND INDICATING SYSTEM

Flow from the main system enters the OCI system through a liquid metal flowmeter to an economizer to minimize the ΔT of the system. Upon leaving the economizer, the sodium is passed through a hairpin-bent finned cooler equipped with a centrifugal air blower where the amount of cooling is regulated by an electrical motorized damper. Upon leaving the cooler, the sodium flow can be split into two parts by control of manually operated bellows-sealed valves.

All or part of the flow can be directed through an isolation valve to the cold trap where further temperature reduction takes place and the oxygen contaminants are removed. Upon leaving the cold trap, the sodium goes through an EM pump which has been added to help overcome the increase in pressure drop as the cold trap becomes filled with oxide. The sodium is returned to the main system through the economizer.

Similarly, all or part of the flow can be directed through the plugging indicator (PI) isolation valve and into the cold-trap discharge line. The plugging indicator is used to determine the system's impurities whose solubilities are dependent upon temperature.

COVER-GAS SYSTEM

A schematic of the helium cover-gas system is shown as Fig. 7. The gas is purchased in commercial, pressurized cylinders. The gas is passed from the cylinder through a regulator that lowers the pressure to 5-10 psi and then to a NaK bubbler purification system.

The bubblers consist of five steel tanks made from 4-in. tubing, 6 in. long, with pipe-cap ends. The first pot is empty; the second pot is packed with stainless-steel mesh and contains NaK which is maintained at 500-600°F; the third pot is empty; the fourth pot is packed with stainless-steel mesh and contains room-temperature NaK; and the fifth pot is packed with mesh.

The piping arrangement between pots is such that if a high volume of gas is put through the bubblers NaK carry-over is caught in the adjacent tank. If this should occur, the NaK is returned to the proper tank simply by reversing flow through the bubblers.

Since the sodium system is made up of a series of test units interconnected through the liquid metal and cover-gas systems, it is important that an equal pressure be maintained between all the test units and main-system expansion tank. Cover-gas differentials between test units will cause corresponding level differentials in these test units. A dampening or surge tank is utilized in the cover-gas system and is located so as to be the distribution header for the supply gas going to each of the separate test units.

From past experience, it is realized that sodium vapors diffuse back into the cover-gas lines, condense and freeze. The resultant plugs would lead to unequal pressures between test units. In order to minimize this possibility, the cover-gas lines are heated above the melting point of sodium back to the surge (distribution) tank.

OPERATIONAL EXPERIENCE

Generally, when the system was clean, with the cold trap operating at 250°F or below, no operational difficulties were experienced. It was necessary, however, to run the cold-trap purification system each time one of the test stations was put on-stream since some air could enter and react with some of the sodium remaining from the previous tests.

However, when the systems were operated dirty -- such as with 300 ppm oxygen in the sodium or with the sodium nearly saturated with carbon -- changes could be noted in the operation of the plugging indicator and in the cover-gas analysis. These results will be discussed in more detail.

THE DOUBLE-BREAK PLUGGING INDICATOR WITH HIGH OXYGEN

Prior to beginning the actual mechanical tests, the usual practice was to charge the loop, then spend some time in operation establishing equilibrium at the actual sodium test conditions. The condition for this particular test was isothermal sodium at 1200 F with an oxygen content of 300 ppm. The oxygen concentration was to be confirmed by both oxygen analyses and plugging-indicator runs. This was, in a way, a recalibration period where the agreement between plugging-indicator and sodium analysis was once again checked. Later, in the course of the actual test period, the plugging indicator would be the main controlling instrument with only periodic analytical checks. It was during this period of preliminary operation for TEST 5 with high oxygen in the sodium that the so-termed double-break plugging indicator runs first appeared with any consistency. The first break generally occurred between 640 and 660°F, with the second break initially occurring between 550 and 560°F and then gradually decreasing to 510°F as length of operation continued. The chemical analyses during this initial period was somewhat scattered, but generally fell between the first and second breaks.

Several studies were made of the plugging indicator versus oxygen analysis and the effects of cold trapping, with relationship to this first and second break in the saturation curve. Various flow rates and rates of cooling were used in making these runs and, although the shape of the curve changed somewhat, the actual breaking points were reproducible. In one case, the cooling rate was greatly reduced following the first break. In this run, the flow fell off continually until complete plugging occurred at 520°F. As proven by runs made before and after, this was still above the second break curves in which the cooling rates were not changed. In these runs, the second break occurred at 510°F.

Fig. 8 is shown to illustrate the reproducibility of the two-break plugging curve, the gradual decrease in the second break with time, and the scatter of the chemical analysis results.

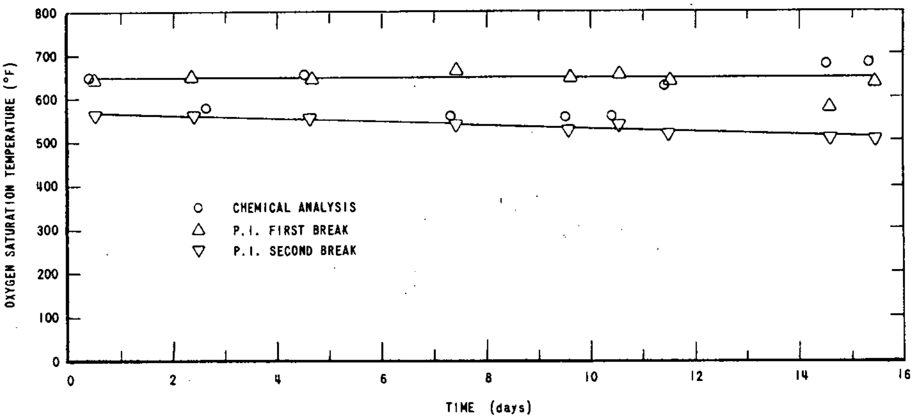

FIG. 8. Test 5: Preliminary operations. Double-break plugging indicator runs versus oxygen analysis

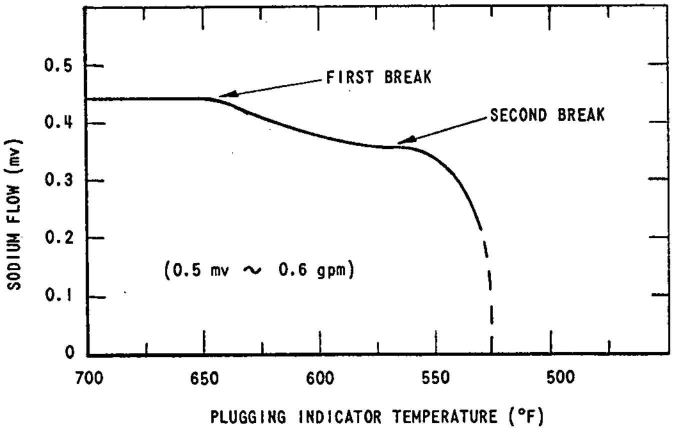

FIG. 9. Test 5: Preliminary operations. Typical double-break PI curve

Fig. 9 shows a typical two-break PI curve during the period shown in Fig. 8.

In trying to eliminate one of the two plugging run "breaks", the system was cold trapped for approximately 19 hours at 500°F, after which plugging runs were made and three sodium samples were taken for chemical analysis. There appeared to be no change in the pattern of either the plugging runs or the chemical analysis.

The cold trap was activated for an additional 18 hours at 500°F and again PI runs were made and sodium samples taken. The first break of the PI curve appeared to be lower (590-600°F compared to the previous 640-660°F range) but there was no change in the 510°F second break. The chemical analysis again fell between the two PI values. If a subtle change did occur in the chemical analysis, it was towards a better agreement between the chemical analysis and the second break following the cold-trapping operations.

To continue the attempt to eliminate one of the two breaks of the PI curve, the cold-trap temperature was reduced and the cold trap was operated intermittently at 400°F with plugging runs being made between operations. After 5.5 hours of operation at a nominal cold-trap temperature of 400°F, the plugging run indicated a single break at 380°F. Fig. 10 is a typical PI single break curve obtained during this period.

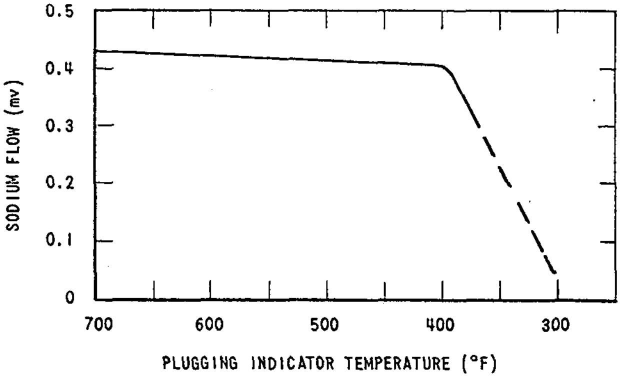

FIG. 10. Test 5: Preliminary operations. Typical single-break PI curve

Fig. 11 illustrates the effects of cold trapping and operating temperature on the plugging curves, the disappearance of the two breaks, and the scattering of the chemical analysis. During subsequent periods of cold trapping and making PI runs, this single break occurred between 390 and 405°F. Three chemical analyses of sodium samples were taken during this period: the first after approximately 56 hours of cold trapping at 400°F; the second after 75 hours; and the third after 102 hours. The first two analyses indicated saturation temperatures approximately 100°F above that indicated by the plugging indicator, while the third analysis was approximately the same as the PI. Each of these samples, after amalgamation, was visibly cleaner than the preceding one. Over a 20-hour period, the cold-trap temperature was gradually increased from 400 to 700°F. At the end of this period, a plugging run was made and a sodium sample taken for chemical analysis. The plugging curve had a single break at 700°F and the analysis gave a saturation temperature of 670°F. Again the residue after amalgamation was dirty and required a larger number of washes. Additional PI runs were made with similar results. A second chemical analysis was in agreement with the PI run made immediately after the same was taken.

The operating temperature of the cold trap was lowered from 700 to 400°F in 25°F steps. At each step, operation of the cold trap was suspended after four hours and a plugging run made. This is shown in Fig. 12. No double-break runs occurred, indicating the contaminant causing the first break of the two-break curve had been removed from the system. The single-break PI curve consistently occurred at a temperature comparative to that of the cold-trap operating temperature.

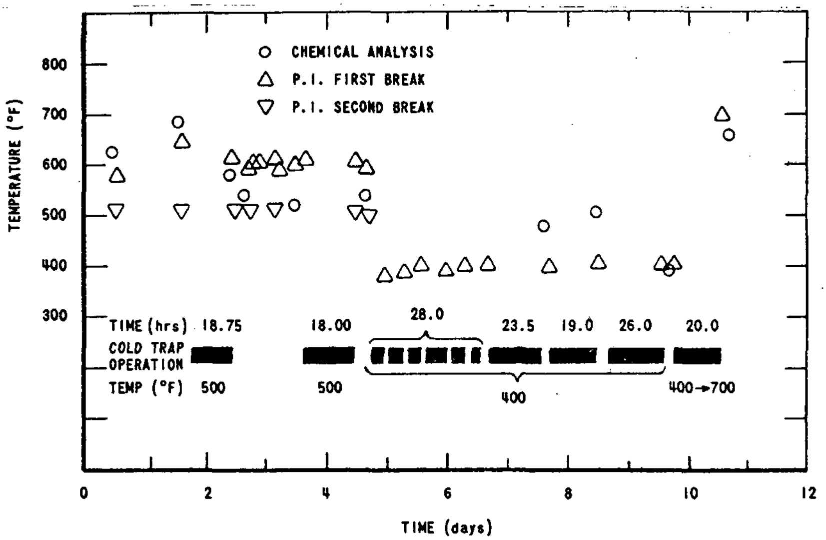

FIG.11. Test 5: Preliminary operations. Effects of cold trapping on double-break PI runs and oxygen analysis

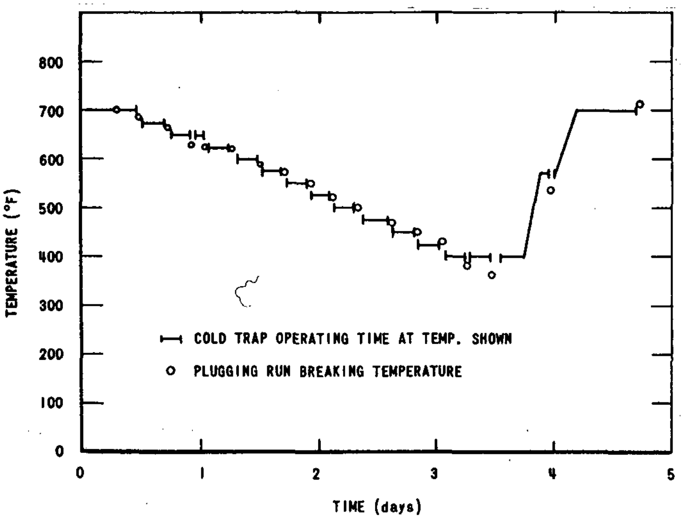

FIG.12. Test 5: Preliminary operations. Plugging run versus cold-trap operating temperature

Again, the operating temperature of the cold trap was increased to 700°F and PI runs made. The single break in the plugging curve continued to agree with the operating temperature of the cold trap.

A sodium sample analyzed for hydrogen after the cold trap had operated for a number of days at 400°F showed 12 ppm H_2. The cold trap was heated to 700°F and the hydrogen content increased to 30 ppm H_2. The cold trap was again cooled to 400°F and, after two hours of circulation through the trap, the hydrogen level was 19 ppm H_2. Upon reheating to 700°F, the hydrogen was increased to 33 ppm H_2. These operations indicated that hydrogen could be added to the system by heating the cold trap.

The results of this study warrant the following conclusions:

1. It is possible to obtain two independent breaks in a plugging curve. The effect is apparently caused by a compound other than sodium oxide.

2. The temperature at which these breaks occur is independent of the flow rate or cooling rate of the run.

3. The plugging meter will eventually plug if held at a temperature between the first and second break temperatures.

4. Chemical analysis is scattered when two breaks do occur and it is sometimes impossible to wash the sample clean of the free sodium during the amalgamation procedure. This situation may not be connected with the two breaks, since the difficulty was also present at high saturation temperatures when only a single break was observed.

5. Cold trapping seemed to minimize the problem of washing samples free of sodium, although the condition seemed to reappear after cold trapping was discontinued.

6. Although scattered, the chemical analysis does favor the second break as the true plugging temperature.

7. The first break can be eliminated by cold trapping at 400°F or lower but not for short times at 500°F or higher. However, for longer periods of time ($\sim$36 hours) cold trapping at 500°F did appear to lower the first-break temperature from $\sim$650°F to $\sim$600°F.

8. The second break, or a single break, agrees with the operating temperature of the cold trap.

DOUBLE BREAK PLUGGING INDICATOR WITH HIGH AVAILABLE CARBON

While operating Loop No. 1 for the purpose of determining a method of operation whereby the oxygen could be controlled low and carbon concentrations could be effectively controlled high without encountering plugging difficulties it was observed that, by cold trapping with the carbon bed isolated, the plugging temperature, representing carbon concentration, of the system could be reduced, and by cold trapping with the carbon bed on-stream the oxygen could be controlled at 30 ppm or less. Fig. 13 shows two typical curves which show the effect of cold trapping and the operation of the carbon bed on the apparent carbon concentration of the system.

The feasibility of successfully conducting TEST 3 was demonstrated by repeating a previous 20-day tab test. During such tests, the oxygen content was to be controlled at 30 ppm or less and the plugging temperature maintained between 750 and 800°F by cold trapping and varying the flow through the carbon bed as required.

The second 20-day tab tests were completed without encountering plugging problems. There were two valve bellows failures during this period, but they did not affect the tests. The carburization potential of the sodium during this series of tests was in close agreement with the first series as determined by the comparison of instream monitoring tabs.

IMPURITIES IN THE COVER GAS DURING HIGH OXYGEN SODIUM RUNS

During preliminary operations of TEST 5 at high oxygen concentrations in the sodium, the helium cover gas in the expansion tank was analyzed by gas chromatography with specific interest in carbon-containing gases. The results are listed as:

Gas	Minimum Limit of Detection (ppm)	Concentration (ppm) (Cold Trap - 700°F)
CO	10	10
CH_4	10	10
C_2H_4	10	10
H_2	5	1.07%, 1.23%*
Ar	5	150
N_2	5	4%

* Concentration was 165 ppm H_2 with a cold-trap temperature of 400°F.

The most likely carbon-containing gases were not found. The presence of Ar and N_2 indicated an influx of air during normal system operation or during charging and extraction of test specimens.

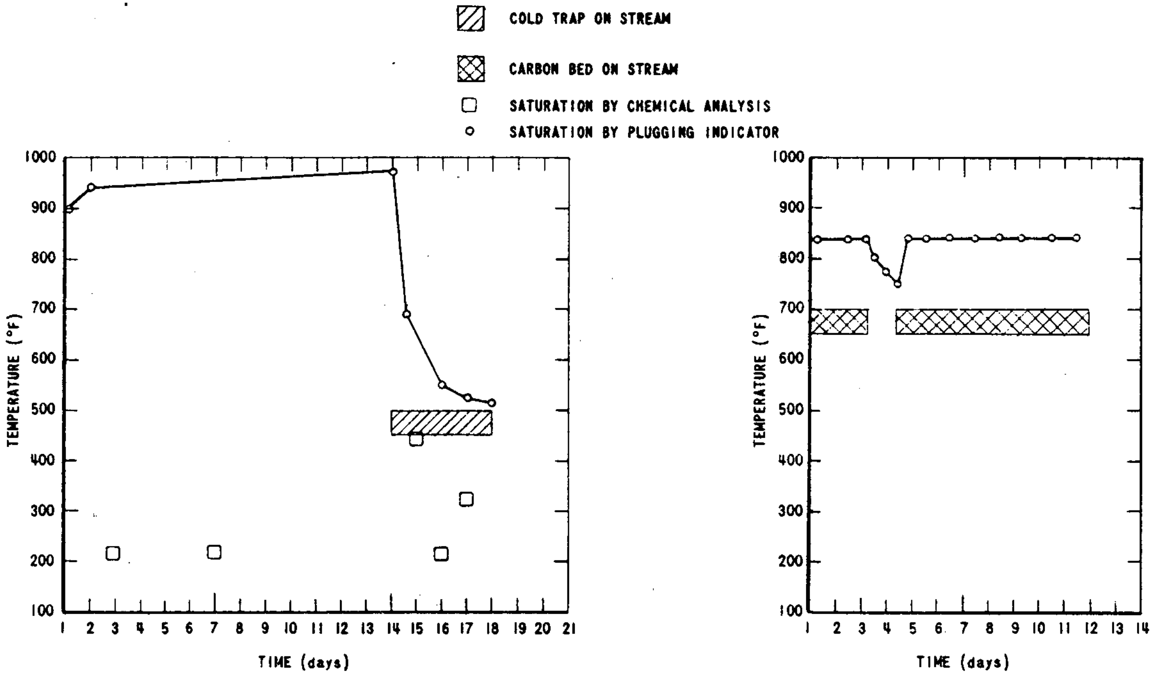

FIG. 13. Effect of cold trapping and operation of carbon bed on plugging temperatures during preliminary operations of Loop 1, Test 3

Later in the test program, these tests were repeated resulting in a value of 1.23% H_2 in the cover gas, giving close agreement with the original figure. [The cover gas from TEST 3 was also analyzed during this period and hydrogen was not found to be above the detection limits of the method (5 ppm). The absence of H_2 in the cover gas of TEST 3 was attributed to the operation of the cold trap at $\lesssim$400°F (with a norm of 250°F) which maintained the hydride content of the sodium at a low value. At this temperature, the hydride concentration of the sodium should be $\lesssim$50 ppm NaH which is $\lesssim$2 ppm H_2.]

It was assumed that the hydrogen in TEST 5 was present in the vapor phase over the sodium because of decomposition of the NaH at 1200°F, the main loop temperature.

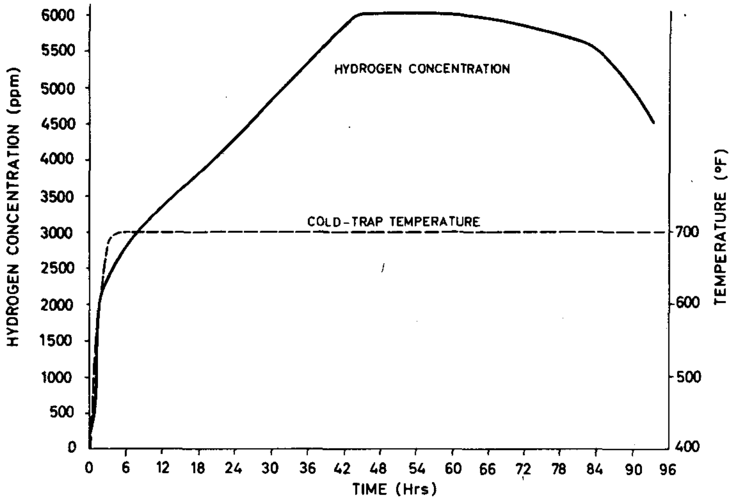

FIG.14. Hydrogen concentration in cover gas as a function of cold-trap temperature and time (Preliminary, Test 5)

To verify whether such was the case, the cold-trap temperature was increased from 400°F to 700°F. During this time, a gas chromatograph monitored the cover gas. The chromatograph was calibrated for hydrogen in argon. (Helium is normally used as the system cover gas, but this was temporarily replaced with argon to increase hydrogen sensitivity.) Fig. 14 shows the data graphically. When the H_2 concentration in the vapor phase exceeded 0.2%, a sample was then taken for mass-spectrometer analysis and showed 0.45% H_2. At the end of the run, another mass-spectrometer sample was taken which indicated 1.07% H_2 in the cover gas. At concentrations up to about 0.3%, the chromatographic results should be the more reliable. Above 0.3%, the mass spectrometer samples are more accurate; however, the chromatographic results do show the trend in concentration during heating.

Hydrogen concentration in the cover gas increased from 110 ppm at a cold-trap temperature of 400°F to 2850 ppm when the cold-trap temperature reached 700°F. After the cold trap reached 700°F, the rate of hydrogen increase in the cover gas decreased, but the concentration continued to rise to an average maximum of 6450 ppm H_2 after 43 hours at 700°F. After this maximum was obtained, a decrease was observed; this likely represents a diffusion of hydrogen through the system walls in conjunction with complete removal of the hydrogen-bearing compound from the cold trap. The concentration of H_2 after 86 hours at 700°F was 4650 ppm.

PLUGGING

Part way through the program of TEST 5 with high oxygen in sodium, the OCI circuit plugged. An increased pressure drop had been observed through this circuit for a considerable period prior to the actual plugging. After unsuccessfully trying to establish flow by increasing heat on several areas of the OCI circuit, it was decided to remove and wash out the economizer. This was the suspected trouble area. The design of this exchanger was a U-shaped single tube-in-shell unit. The outlet end of the inner tube was found to be collapsed, which accounted for the high pressure drop experienced over a several-month period. Only hydraulic forces were available to provide the high pressures needed to collapse this tube. It is therefore postulated that during one of the pre-heating periods, the sodium in the shell side became trapped by plugs of sodium until the shell side pressure increased sufficiently to collapse the tube. A new economizer was fabricated and installed.

While examining the inner tube of the economizer, it was noted that the outside surface was covered by a thin, tightly adhering, dull gray metallic film. This coating appeared to be evenly distributed over the tube except in several locations where the deposits were heavily concentrated and were more crystalline in nature.

While attempting to restart the OCI system, following the repair of the economizer, a leak developed in the return line from the cold trap to the economizer. This section was isolated and cooled to room temperature with no damage to the system. The leaking section was replaced. The leak was located on the underside of a horizontal run of 1/2-in. pipe, adjacent to the electrical preheater, which was not damaged and, when tested, appeared to be electrically sound. It appeared similar to the type of catastrophic oxidation observed in an earlier portion of this program.

Several plugs formed in the OCI section of the system at various times throughout TEST 5. As a result of one of these plugs, it was necessary to remove the OCI pump. During the installation of the pump, following removal of the plug, a flaw was observed in a section of the pipe downstream from the pump. This area of piping did not appear to have been involved in the leak described above, and the flaw has been assumed to be a separate incident. It would appear to be the result of catastrophic oxidation also.

Obtaining a representative sample of a plug with subsequent chemical analysis is always difficult. Four such samples were analyzed and the results of these would indicate that an average plug would show its major constituents to be as follows:

Fe - 5% to base
Cr - 1/2 to 4% (average 1.5%)
Ni - 1 to 4% (average 1.8%)
Mo - 0.5 to 1.5% (average 1.2%)
Mn - 0.5 to 2% (average 0.8%)
Si - widely scattered but $\sim$0.8%
Ti - widely scattered

CONCLUSIONS

In summarizing the operations of TEST 3 in which the reactor grade sodium had carbon introduced as the contaminant while maintaining the oxygen at a low concentration (30 ppm or less), the following statements appear valid:

1. It is possible to operate a 1200°F sodium system with a high carbon content and to maintain a low oxygen (30 ppm or less) concentration.

2. Plugging indicators cannot be used to monitor for oxygen while at the high carbon conditions.

3. The plugging indicator does have some relationship to the carbon concentration, although this relationship was not determined, since it did not fall within the scope of the contract.

4. Carbon can be effectively cold trapped from the sodium. Rates were not determined.

5. The useful life of thin 316 and 304 ss components, such as valve bellows, is greatly reduced in a high carbon sodium environment.

In summarizing the operations of TEST 5, in which the oxygen concentration of the sodium was at approximately 300 ppm, the following statements are valid:

1. It is possible, although difficult, to operate a system at 1200°F with a high (300 ppm) oxygen content.

2. Interpretation of plugging indicator runs becomes more difficult at these conditions and it has been shown that hydrogen (result of the high cold-trap operating temperature) may be a contributing factor.

3. The high oxygen content of the sodium increases corrosion which in turn enhances the formation of plugs.
4. The plugs formed were located in small cross-sectional areas or where there was a sudden increase in flow area.

REFERENCES

[1] JACKSON, C.B., WERNER, R.C., The manufacture of potassium and NaK, Adv. Chem. Ser. 19 (1957) 169.

[2] WERNER, R.C. et al., Heat transfer with sodium-potassium liquid alloy, A.I.Ch.E. annual meeting, Pittsburgh, Pa.

[3] LYON, R.C., Liquid Metal Handbook, U.S. Government Printing Office (1955).

[4] LYON, R.C., Liquid Metal Handbook, U.S. Government Printing Office (1952).

[5] JACKSON, C.B., Liquid Metal Handbook, - Sodium-NaK Supplement, TID-5277, U.S. Government Printing Office (1955).

[6] ELROD, H.G., Jr., FOUSE, R.R., An investigation of electromagnetic flowmeters, Trans. Am. Soc.-mech. Engrs 74 (1952) 589.

DISCUSSION

E. L. ZEBROSKI: Have you tried to identify the composition of the materials forming the first and second plugging temperature breaks?

C. WERNER: No, but the paper does give the results of analysis of four plugs which formed in the oxygen control and plugging indicator system during tests with approximately 300 ppm of oxygen in the sodium, and these results may be of interest to you. These plugs occurred in the high-oxygen sodium system after the disappearance of the two break conditions. You will notice that the analysis given in the paper does not total 100%. The balance is mostly sodium and oxygen.

PROBLEMS OF A SODIUM LOOP DESIGNED TO OPERATE AT TEMPERATURES UP TO 800°C

E. MATYAS, G. RAJAKOVICS AND N. SCHWARZ
ÖSTERREICHISCHE STUDIENGESELLSCHAFT
FÜR ATOMENERGIE G. m. b. H AND
GEBR. BÖHLER & CO. A. G.,
VIENNA, AUSTRIA

Abstract

PROBLEMS OF A SODIUM LOOP DESIGNED TO OPERATE AT TEMPERATURES UP TO 800°C. As a prototype reactor will not be developed in Austria, emphasis is being laid on problems concerning the technology of non-radioactive circuits. The expected late start of the commercial use of nuclear energy in Austria is a recommendation in favour of advanced concepts in nuclear research.

The great importance of liquid metal technology to fast breeder reactors was the reason for the construction of a universal sodium loop at Seibersdorf. Today the maximum coolant temperatures of liquid-metal-cooled reactors reach 600°C. With regard to better power plant efficiency and lower costs of steam generators, higher coolant temperatures would be of interest. Moreover, it is necessary to extend the research somewhat over the expected mean coolant outlet temperature because of, for instance, hot channel factors. Therefore the sodium rig at Seibersdorf is designed for 800-850°C.

The problem of greatest importance in this temperature range is the corrosion resistance of structural materials. Extending corrosion tests on conventional steels to 800°C will make it possible to discern more accurately the influence of the different corrosion variables. Moreover, it may be possible to develop new steels and alloys with better corrosion resistance. Further, it is planned to test minor components for primary and secondary circuits, such as modular heat exchangers and regenerators, compact sodium purification facilities, devices for the measurement of impurities, and others. Heat transfer studies to further component development with the aim of increasing economy are also scheduled.

The design of an experimental facility to serve the above-mentioned aims imposes special problems. With regard to the components, major problems had to be overcome in the design of the heating section, the corrosion test section, the changing system for the samples and the heat exchanger for high temperature.

Further, it was necessary, because of the low strength of steel at design temperature, to install a complicated and precise heating and control system, and to support the components carefully having regard to the high thermal expansion. Finally, the safety problems necessitated extensive precautions, such as, for instance, a complete containment.

The great importance of liquid metal technology to fast breeder reactors was the reason for the construction of a multi-purpose sodium loop at Seibersdorf. Today maximum coolant temperatures of liquid-metal-cooled reactors reach 600°C. From the point of view of more efficient power plant and lower costs of steam-generators higher coolant temperatures would be of interest. It is necessary, moreover, to extend the research some distance beyond the expected mean coolant outlet temperature because of, for instance, hot channel factors and other safety margins. The sodium rig at Seibersdorf is therefore designed for 800-850°C.

The most important problem in this temperature range is the corrosion resistance of structural materials. Extending corrosion tests on con-

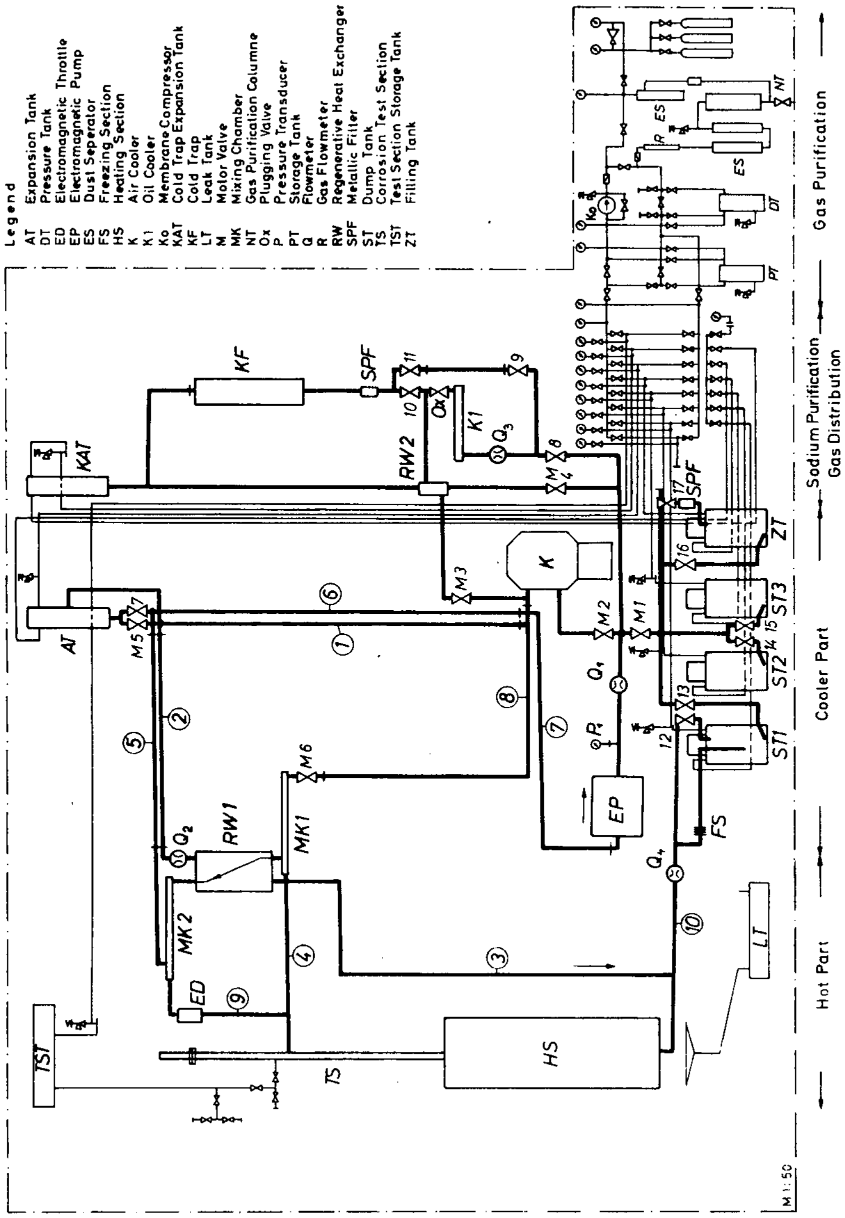

FIG. 1. Disposition of sodium loop

ventional steels to 800°C will make it possible to discern more accurately the influence of the different corrosion variables. Moreover it may be possible to develop new steels and alloys with better corrosion resistance. It is planned further to test minor components for primary and secondary circuits, such as modular heat exchangers and regenerators, compact sodium purification facilities, and devices for the measurement of impurities. Heat-transfer studies to support component development with the aim of increasing economy are also scheduled. For this purpose sensing devices of very small dimensions for operation at these elevated temperatures must be developed. Although it would be of interest to go into details of the experimental programme this paper will be concerned primarily with the special problems which had to be solved in the design of the test rig.

TABLE I. DATA SHEET

Dimension of tubing	25/21 mm
Regenerative heat exchanger coil	25/22 mm
Material: for all parts > 600°C	Böhler * Turbo - therm 1616 M
for all parts < 600°C	Böhler * Antinit SAS 2
Mass flow	20 kg/min
Heater power	28 kW
Over-all heat performance of heat exchanger	60. 000 Kcal/h
Total electrical power including tube heating	80 kW
Heating temperature span (function of flow and max. temperature)	30 degC to 120 degC
Maximum temperature in test section	800°C (850°C)
Cooling temperatures	300°C → 250°C
Total circulated sodium volume including purification plant	130 1
Total sodium volume including storage	200 1
Maximum pressure over atmosphere	3 kg/cm^2

The main data of the loop are shown in Table I.

Figure 1 shows the general disposition of the components. Flow is effected by an electromagnetic pump (EP) circulating the sodium through the main air-cooled heat exchanger (K), the piping system (1) and (2), and to the secondary side of the regenerative heat exchanger (RW1). This point marks the beginning of the high temperature part.

Leaving the heat exchanger by tube (3) the sodium reaches the heater (HS) and the corrosion test section. Flowing through the tube (4) and the

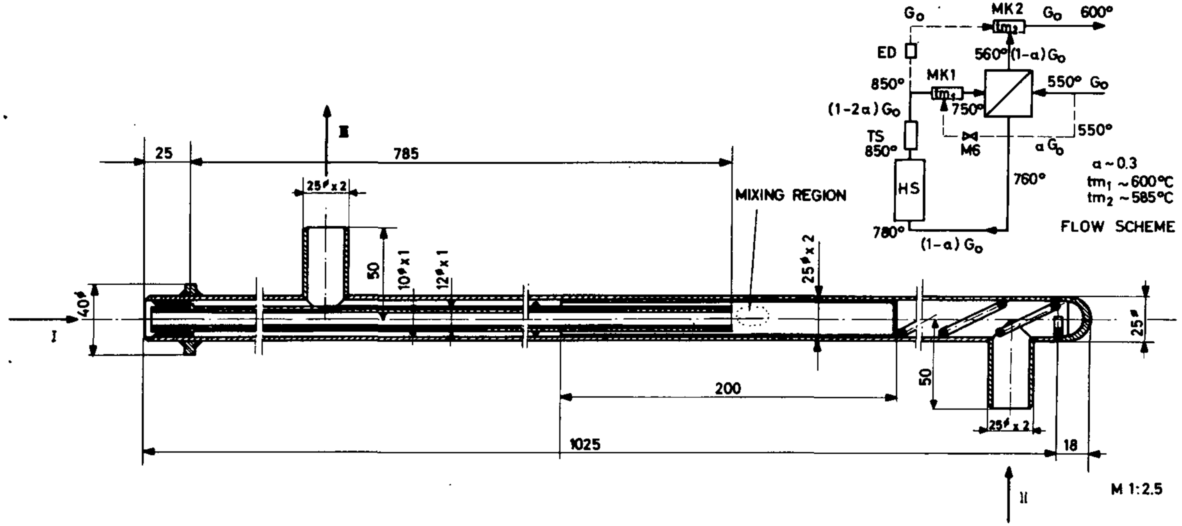

$G_I \sim 540$ l/h $\quad t_{I\,max} = 800°C$

$G_{II} \sim 1260$ l/h $\quad t_{II} \sim 600°C$

$G_{III} \sim 1800$ l/h $\quad t_{III} \sim 660°C$

MATERIAL BÖHLER • TURBOTHERM 1616 M

FIG. 2. Mixing chamber MK

primary side of the heat exchanger it returns to the cold part and enters the pumping section by way of tubes (5), (6) and (7). As the entrance temperature into the heat exchanger would be too high to allow a safe design, a bypass system including two mixing chambers (MK1) and (MK2) is used to lower this temperature. Connected with the main loop is a purification and sampling system. For the cover gas argon is used, purified and stored in a separate system.

The layout of the whole system corresponds to Fig. 1 as the components are erected in a vertical plane. This arrangement is enclosed in a container and the loop is operated from the outside. Owing to the high elongations in the system caused by the high temperature differences severe problems had to be solved in supporting the hot part of the loop.

The extensive heating and electrical surveyance systems for operation with and without personal attendance should also be mentioned. Special features of these hot part components, which were most difficult to design, will be subsequently described.

MIXING CHAMBERS WITH BYPASS FLOWSCHEME

It has been already mentioned that it is necessary to bypass the heat exchanger because of high temperature and temperature gradients resulting in high stresses. A fraction (a) of the incoming flow G_0 is bypassed and returned to the hot flow leaving the test section in mixing chamber (MK1) (Fig. 2). To guarantee a constant temperature gradient in the heat exchanger walls, equal flow has to be maintained. Therefore the same amount of sodium ($a.G_0$) leaves the hot sodium flow after the test section and enters the main flow at the outlet of the heat exchanger in (MK2). In this way the thermal gradient between hot and cold sodium in the heat exchanger is reduced by 10 degC and the problems of high heat flux and resulting stresses are concentrated on the design of a suitable mixing chamber. Flow restriction in the bypasses is effected by means of a regulating valve (M6) and an electromagnetic pump (ED) acting against the direction of flow.

The mixing chamber is made up of a tube with an inner diameter of 21 mm, the hot flow being conducted to the mixing region by means of a smaller tube with an inner diameter of 8 mm (I). The cooler sodium flow reaches this region from the opposite direction (II). The resulting mixture is forced to flow back between the inner and outer tube shell, leaving the chamber at point III. The inner tube acts as an intermediate heat exchanger, considerably diminishing the temperature differences of the mixing sodium flows. Because of high heat transfer rates and resulting high strains the inner tube is made up of two slotted tubes of 1 mm thickness each. To a certain degree corrosion damage does not impair the function of the mixing chamber. Properly arranged thermocouples on the outside of the chamber tube give information when the damage is too great.

HEAT EXCHANGER (RW1)

The exchanger consists of two coaxial cylindrical walls with ring-shaped endplates (Fig. 3). A helicoil tube is placed in the space between the cylinder walls. Through this tube the primary sodium flows upwards (I), being cooled by the counterflow of sodium on the outside. The helicoil tube is held by two opposite tube supports which also function as spacers. Each of these consists of two steel bands surrounding the adjacent tube coils welded together in the intermittent space. They are fixed at the lower end to the inner cylinder wall. This kind of support counteracts the buildup of bending moments and torque induced by the weight of the helicoil. The uppermost coil is left free to take care of the total elongations.

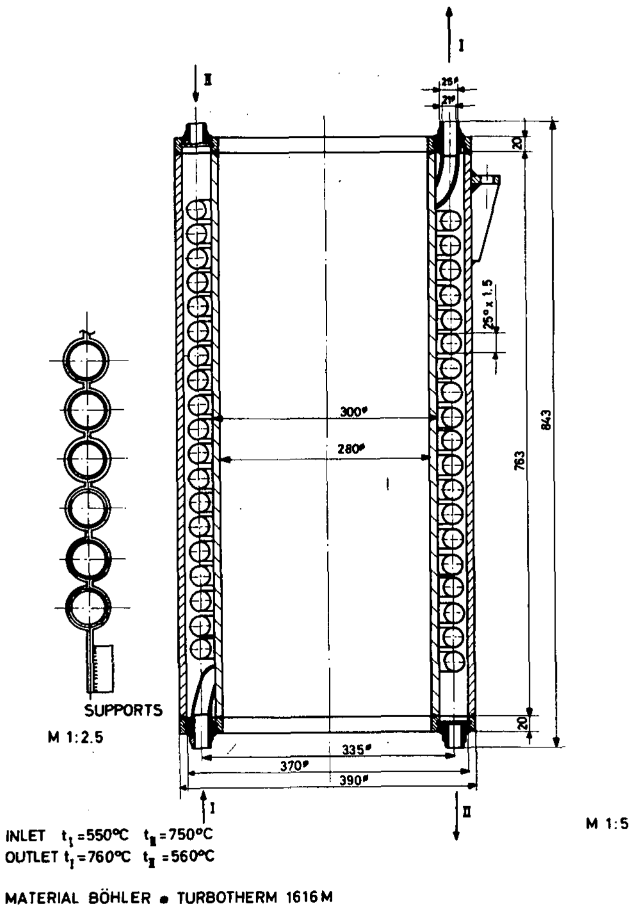

FIG.3. Regenerative heat exchanger RW1

Some difficulties have been encountered in the thermal design of the unit, since the secondary side will have laminar flow conditions. Moreover, theoretical models showed that upward flow by thermal convection may be possible. As a result the dimensions of the heat transfer surface have been made sufficiently large to allow for possible low heat transfer performance.

HEATING SECTION

Many versions of heating the sodium were analysed before it was decided that a set of twenty tubes in parallel heated by radiators from the outside would show optimum performance (Fig. 4). Through a feed pipe the sodium enters a small chamber and is directed outward to a distribution ring by way of five radial tubes. From there the sodium passes through the twenty vertical pipes to an upper collector ring, and through the five radial tubes into the lower end of the test section. To get an even flow distribution the upper and lower radial arms are arranged in a rotated position. Since the internal pressure of the system will be 3 kg/cm^2 the resulting stresses in the tube walls build up to a considerable fraction of the maximum allowable stresses at maximum temperature. As thermal

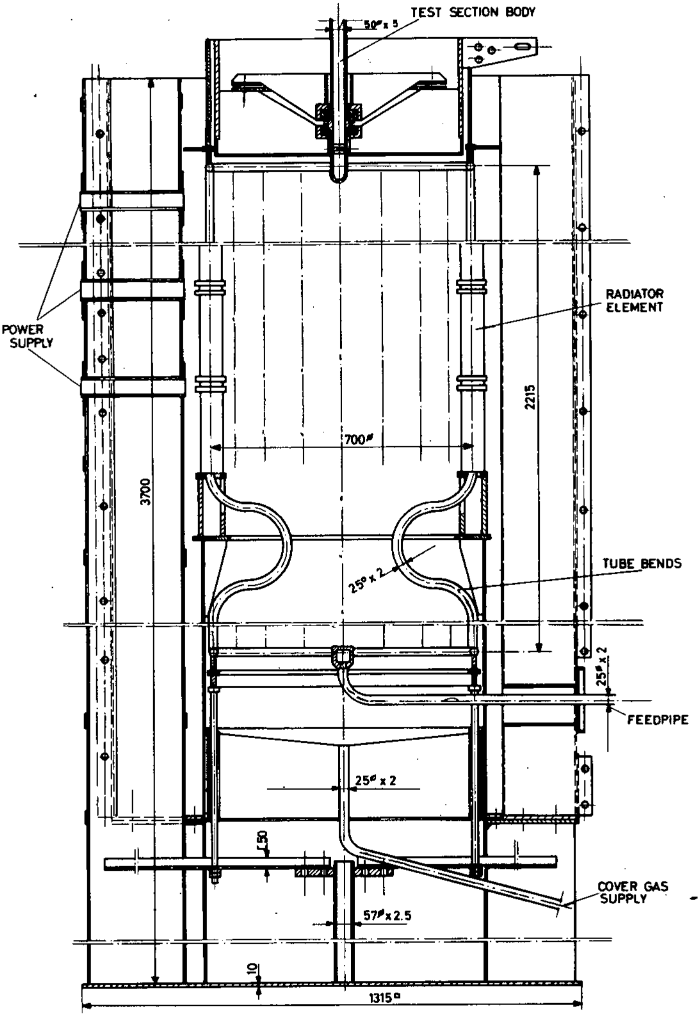

FIG. 4. Heating section

stresses in the heated tubings are a function of the heat rating, it has been necessary to adjust the axial distribution of the heat rating to the temperature distribution along the heating section at which heating takes place. This is effected by dividing the heating section into six horizontal zones, each one supplied with the locally possible heating power, resulting in the heat input being highest at the inlet and lowest at the outlet of the heating section. Differential elongations by unequal heating power in adjoining

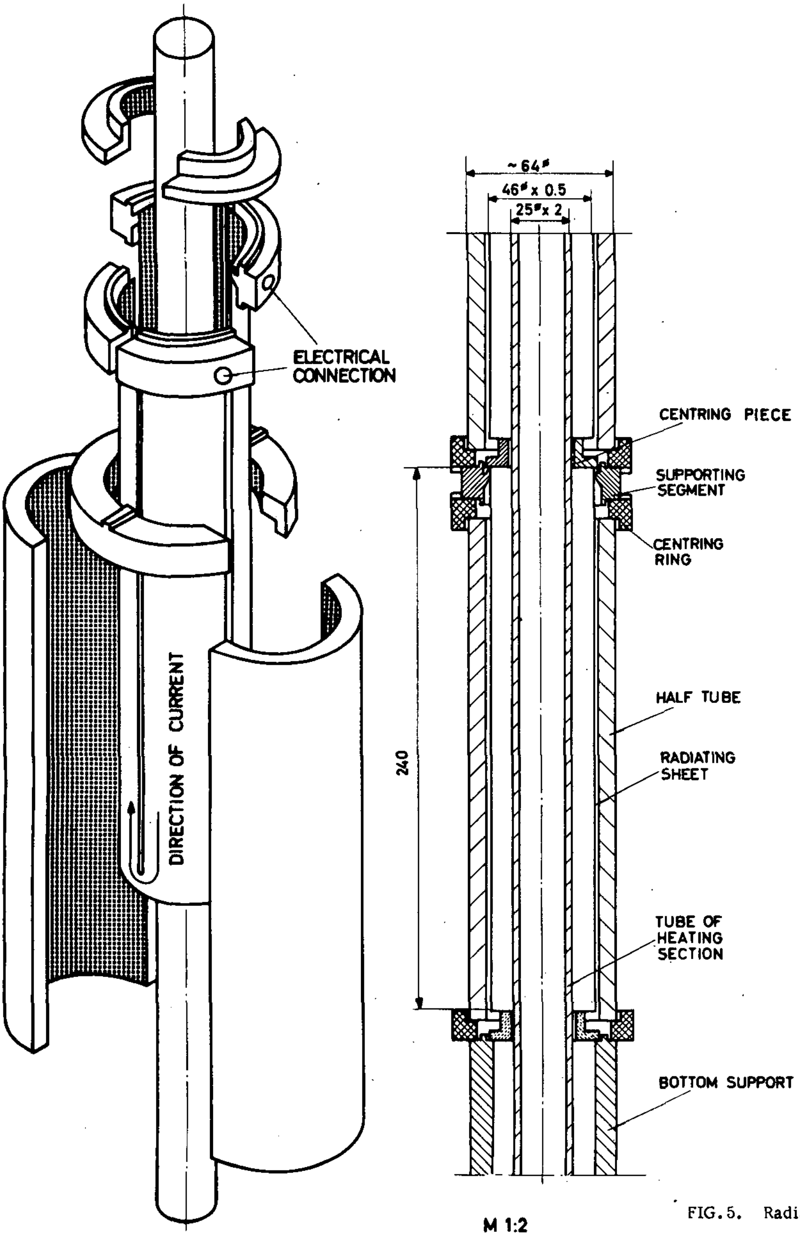

FIG. 5. Radiator element

vertical tubes will be satisfied to a certain degree by an expansion bend in the cooler region of the tubes. These bends also reduce the stresses induced by the welding procedures. The hot part is relieved from its weight by movable counterweights acting upwards on the cooler part of the heating section. The most dangerous accident would be plugging of one vertical tube by corrosion residues. This could cause severe damage, and should lead to immediate shutdown of the plant. Twenty platinum

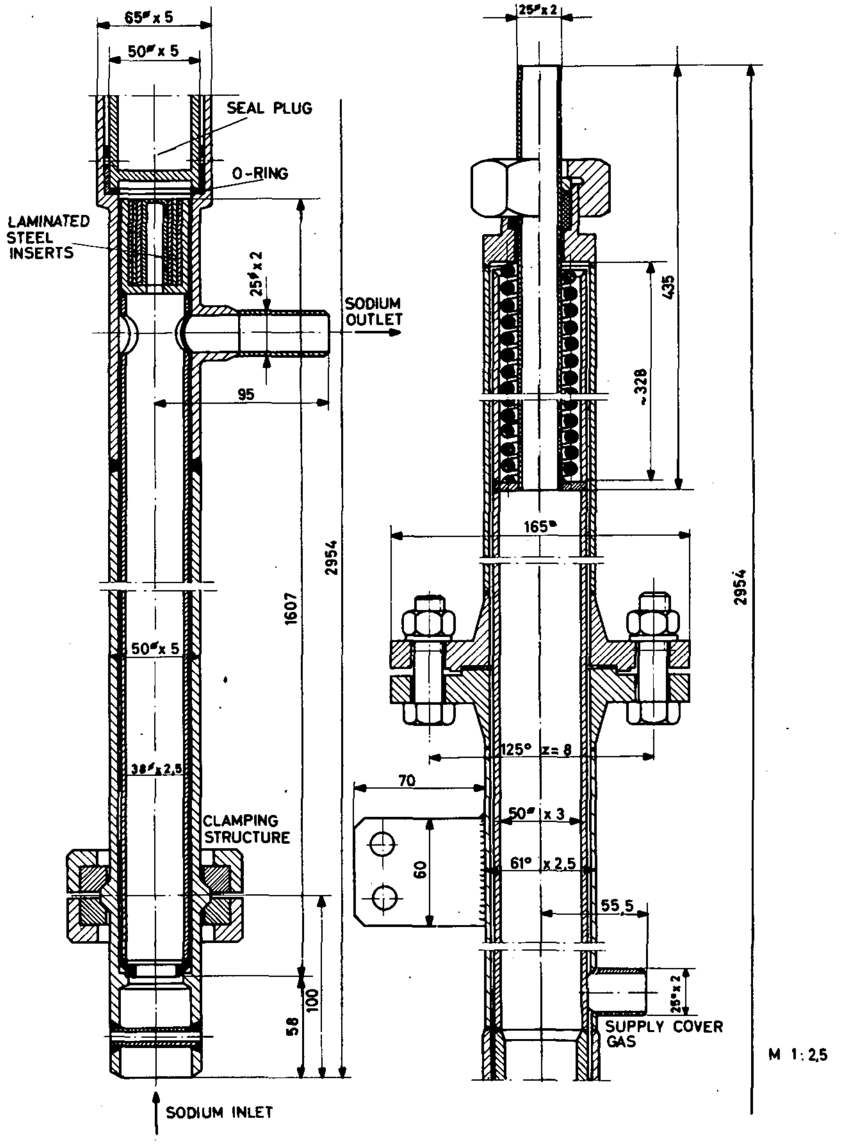

MAX.OPERATING TEMPERATURE 800°C

FIG.6. Test section TS

MATERIAL BÖHLER * TURBOTHERM 1616M; ANTINIT SAS2
TURBOTHERM CN13Co10

resistance thermometers are electrically compared, and a difference of 5 degC indicates the signal for scram.

The radiator elements (Fig. 5) consist of electrically heated 0.5-mm thick NiCr sheets slotted and welded to the two segments of a support ring. Two of these sheets surround the sodium-filled tube and are inserted into a ceramic support structure. All the radiator elements situated in a horizontal plane are connected electrically to form the above-mentioned zones.

CORROSION TEST SECTION AND SAMPLE CHANGING PROCEDURE

The test section (Fig. 6) consists of a container tube with the specimen holder situated on the lower end. This part is purged by the hot sodium and separated from the upper part by a seal plug filled with insulation material. Sealing is effected by a gas-filled O-ring pressed down by a spring at the cold end of the seal plug. An insert of laminated-steel foils protects the seal ring against thermoshock. Thermal gradients around the sealing edge have to be avoided, therefore auxiliary heaters are positioned beyond the sodium seal plug interface. The necessary cooling length is determined by the maximum tolerable temperature of the gate-valve for sample changing. The steps whereby a new sample holder is introduced into the test section are illustrated in Fig. 7. At position 1 the sodium is drained and system temperature reduced. Position 2 shows the insertion of a divided gland. At step 3 the sealing plug is withdrawn as far as it is necessary to be able to close the gate valve (position 4). Step 5

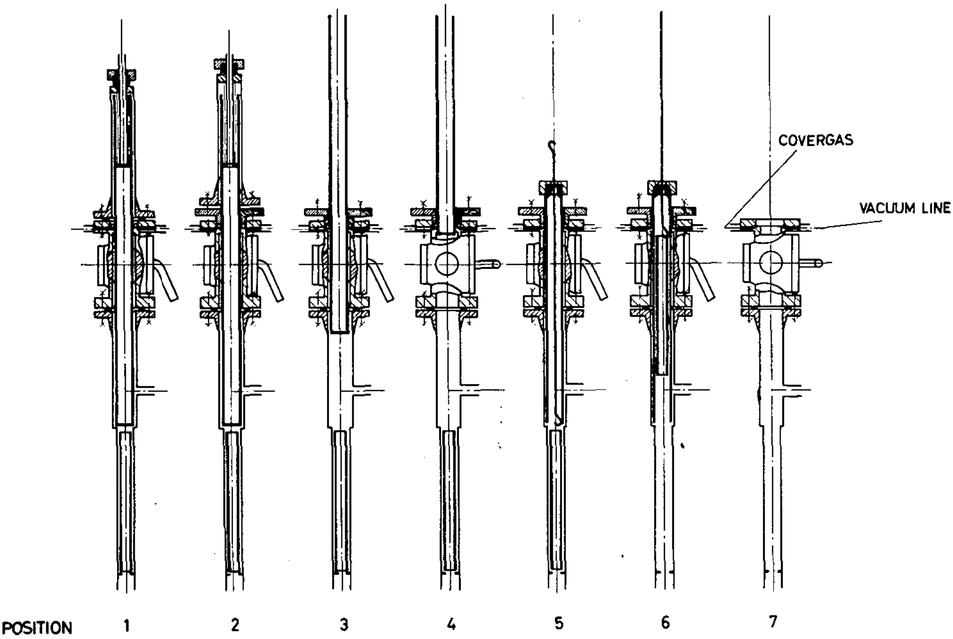

FIG.7. Sample changing procedure

consists of lowering a changing tool. In position 6 the sample is drawn into the changing tool. When both are withdrawn, the gate valve can be closed as in step 4 (position 7). Now the insertion of a new sample can

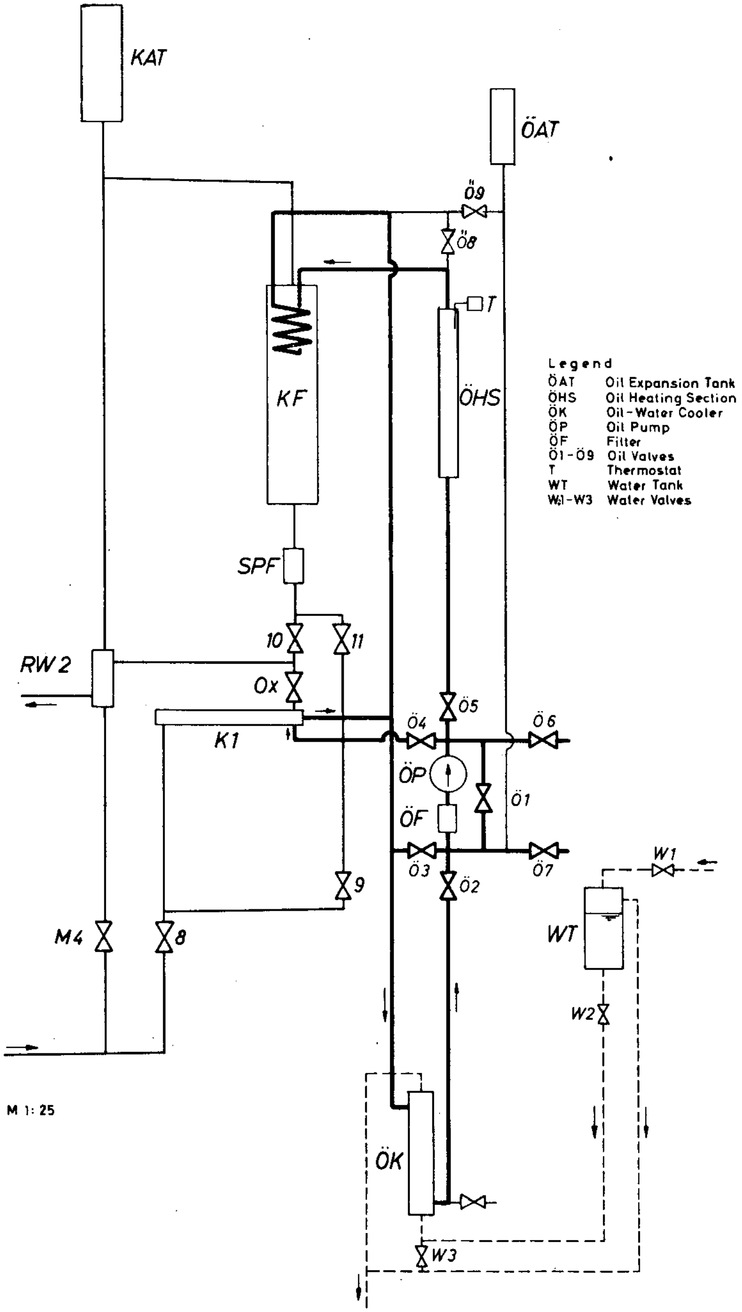

FIG. 8. Auxiliary oil system for sodium purification and plugging meter cooling

be performed in the reverse order. Because of evacuation and purging the gate valve with cover gas at the proper steps no air leaks into the test section, and corrosion tests can be restarted immediately the loop is filled and temperatures are raised.

The test section rests vertically on a clamping structure and is held in position by three steel ropes allowing axial expansion. The strain in the test section outlet tube caused by the friction forces of the different suspensions of the relatively heavy heat exchanger necessitates a special kind of movement control in this hot part region. The movement of the hot end-points of the mixing chambers are guided by rails and roller bearings away from the fixed point of the test section. Assuming equal temperature in this part of the system, bending moments are transformed into axial forces in the system and reaction forces on the rails.

AUXILIARY OIL SYSTEM

Apart from problems of high temperature the decision to instal a separate auxiliary oil system (Fig. 8) seems worthy of mention. The oil is pumped (ÖP) through a heating section (ÖHS) where it is kept at a constant outlet temperature by thermostat. The sodium cold trap (KF) is cooled by the oil in counterflow. The provision of a surplus heat exchange area will result in sodium temperatures near the oil inlet temperature in a wide range independent of mass flow. The heat is removed from the oil by a water cooler outside the containment. The oil system is used also for the cooling of the plugging meter cooler (K1) and a static test facility. Temperature in the oil system will be a few degrees above the melting point of sodium so that freezing can be avoided in any of the heat transfer units.

It has been possible to mention only a few of the numerous and interesting problems which have arisen in aiming to reach 800 (possibly 850)°C with a loop built of conventional austenitic Cr-Ni-steel.

DISCUSSION

J. BEAUFRERE: What is the total pressure drop in your loop?

N. SCHWARZ: The maximum pressure drop will be 3 kg/cm^2 at a flow rate of 20 kg/min; thus if we assume a maximum system pressure of 3 kg/cm^2 the pump will work at 1 kg/cm^2.

J. BEAUFRERE: Have you done any preliminary high-temperature embrittlement tests on your steel, which I see is to operate at 800°C?

N. SCHWARZ: No, but as the steel has a completely austenitic microstructure it will not be susceptible to sigma-phase embrittlement.

J. BEAUFRERE: Are the free-surface level measurements continuous or discrete?

N. SCHWARZ: The free-surface containers are equipped with discrete level indicators.

J. BEAUFRERE: What dimensions are your samples to have, and what will be the maximum sodium velocity?

N. SCHWARZ: The samples will be either cylindrical shells or slotted cylinders, depending on the surface/velocity ratio desired for a particular experiment. The maximum velocity of the sodium will be at least 5 m/s.

A. G. IOLTUKHOVSKY: I should like to say a few things about the design of the apparatus you have just described. As far as I can judge, the high-temperature section is too complex, and this may give rise to difficulties when you come to operate it. The paper which I presented earlier (SM-85/51) describes a unit which has operated at temperatures between 800° and 900°C for several thousand hours with only minor difficulties, and this success is largely attributable, in my opinion, to the simplicity of the design.

Secondly, it seems to me that your inert gas purifier is really a superfluous component. In the Soviet Union, as was reported earlier, we have abandoned argon purification because the gas rarely undergoes any change in the apparatus, and what little contamination it imparts to the sodium is easily removed by the traps.

In conclusion, let me add that I hope your unit is a big success.

J. M. WILLIAMS: What methods are you planning to use, Mr. Schwarz, to determine impurities in your high-temperature sodium loop?

N. SCHWARZ: We shall use a plugging meter, but we also hope to get a more exact indication of the oxide level by the amalgamation method.

E. DUNCOMBE: Going back to Mr. Ioltukhovsky's point about simplicity of design, might I ask why you do not pump each section individually with a small pump and irrigate the sections from a common sodium supply?

N. SCHWARZ. As I have pointed out, this is to be a multi-purpose loop; it could not, unfortunately, be designed to give the optimum conditions for each research programme.

AN INDUCTION HEATER FOR A SODIUM CIRCUIT

E. A. FIELDER AND D. F. DAVIDSON
U. K. ATOMIC ENERGY AUTHORITY,
REACTOR ENGINEERING LABORATORY,
RISLEY, LANCS., UNITED KINGDOM

Abstract

AN INDUCTION HEATER FOR A SODIUM CIRCUIT. The heating of sodium in high-temperature experimental rigs presents problems of reliability of the heater and in the maintenance of a high degree of sodium containment. The problems are particularly severe when the loop is large and non-isothermal, and high heat inputs are required. The Fuel Element Thermal Test Loop at the Reactor Engineering Laboratory of the United Kingdom Atomic Energy Authority, which was designed for fuel element evaluation in sodium at 650°C, makes use of proven pumps of the electromagnetic linear induction type which are limited to a sodium temperature of 375°C. The sodium test section flow of 350 gal/min is raised to 650°C by a 10-MW heat recuperator and a 400-kW electrical heater which replaces the circuit losses.

Experience showed that the use of sheathed mineral-insulated heaters was unsatisfactory for this heater, and an alternative method using mains frequency (50 counts/s) induction was adopted. The heater is in the form of a power transformer, the secondary winding of which is a single short-circuited turn formed by a stainless-steel pipe loop containing the sodium. With suitable lagging and cooling arrangements the iron core and primary windings are maintained at temperatures low enough for normal electrical insulating materials to be used. Conventional methods for the fabrication of the pipe loop circuits are also possible.

The design, construction and operation of the induction heater is described. The design balance between the differing requirements of electrical efficiency, hydraulic pressure drop, and the geometry imposed by the space available in the rig is discussed. Suggestions for improving these factors at the expense of others are given. The performance of the heater is given and compared with the predicted performance.

INTRODUCTION

The heating of sodium in high-temperature experimental rigs presents the dual problems of reliability of the heater and prevention of sodium leaks. These problems are particularly severe when the loop is large and non-isothermal, and large heat inputs are required.

The Fuel Element Thermal Test Loop at the Reactor Engineering Laboratory of the U. K. Atomic Energy Authority [1], designed to investigate the behaviour of fuel elements in flowing sodium at 650°C, posed these problems. The configuration chosen for the loop (Fig. 1) made use of proven components. The prime pumping units were electromagnetic, linear-induction pumps similar to those developed for the Dounreay Fast Reactor, but with improved, high-temperature, electrical insulation which raised their permissible operating temperature to 375°C.

The sodium flow of 350 gal/min was raised in temperature to 640°C by a 10-MW heat recuperator. Though this was of high efficiency, its losses amounted to 400 kW, and this had to be supplied to the sodium leaving the recuperator to raise its temperature to 650°C at entry to the test section.

The heater design first chosen for the rig used stainless-steel sheathed, mineral-insulated heaters immersed directly in the sodium which was in turn contained in a large stainless-steel vessel. These heaters proved unreliable owing to failures in the high-temperature electrical insulation which caused earth faults leading to holes in the heater sheath and consequent sodium leakage.

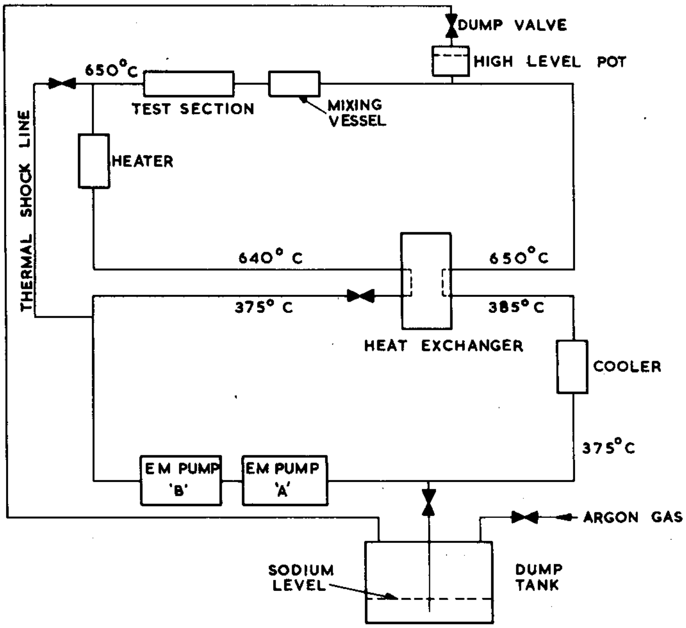

FIG.1. 1. Fuel element thermal test loop

This paper describes the induction heater chosen to replace this unsatisfactory immersion-type resistance heater.

DESIGN

Various forms of heater were considered, including mineral-insulated cable and muffle furnaces [2], but in all such designs heat has to pass through the wall of the vessel before reaching the sodium. The requirement for relatively thick walls to prevent sodium leakage conflicts with the need for thin walls to minimize thermal stresses.

The replacement heater design was based on mains-frequency induction heating [3] using the sodium itself as the shorted secondary turn of a transformer. By generating the heat directly in the sodium, thermal stress problems are minimized and no component is required to operate above the required sodium-operating temperature. No direct electrical connections to the rig pipework are required, and no problems of high temperature electrical insulation arise.

There is a strong cost incentive to use the mains frequency (50 c/s). The penetration of the current is then about 1 in. in sodium and 2 in. in stainless steel, and is therefore adequate for the design considered.

The simplest inductive arrangement in which a coil is wound directly on to a straight pipe has two drawbacks, poor electromagnetic coupling between the coil and the sodium, and the magnitude of the braking effect.

These drawbacks are reduced to acceptable proportions by having a complete laminated iron core linking the energizing winding and a continuous loop of liquid metal. The heater now resembles a transformer with the secondary winding replaced by a single short-circuited turn consisting of a pipe loop containing sodium (Fig. 2a). Geometrical considerations favour a "sandwich" coil construction rather than concentric primary and secondary. Dividing the primary into two halves, one on either side of the secondary, balances the electromagnetic repulsion forces acting on the pipework and improves the magnetic coupling.

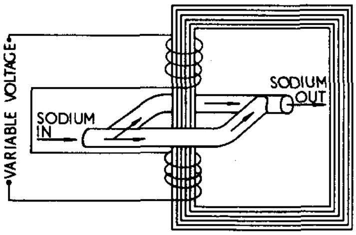

FIG. 2(a). Basic induction heater

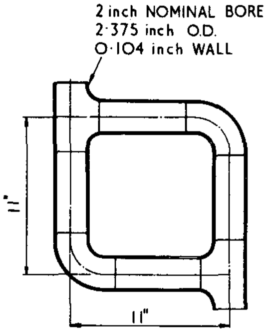

FIG. 2(b). Toroid detail

The space available, the permitted hydraulic pressure drop and the local arrangements of the power supplies made two, 200-kW, three-phase units the desirable choice. Each phase of the heater is based on a toroid (Fig. 2b). This is fabricated from standard pipe fittings and is a compromise between various requirements. For higher power factors and lower capital costs compact units are desirable but these are more difficult to manufacture and inspect, and have higher hydraulic losses than the more open design adopted.

The toroid dimensions chosen are shown in Fig. 2(b) and the general pipework layout for the two heaters is shown in Fig. 2(c). The sizes of the inlet and outlet headers were chosen to bring the over-all pressure drop within the 4 lb/in^2 allowed for the heater. Hydraulic pressure drops can be calculated using conventional methods combining entry, exit and straight pipe losses to the required accuracy. As the pressure drop will usually be a small percentage of the head available, experimental flow checks are not usually necessary. The pipework and toroids are constructed from standard fittings and adequate space is available for full radiography.

Normal transformer design has been followed for the primary windings and the cores though there are some detail points of difference between this heater and a conventional transformer. The equivalent

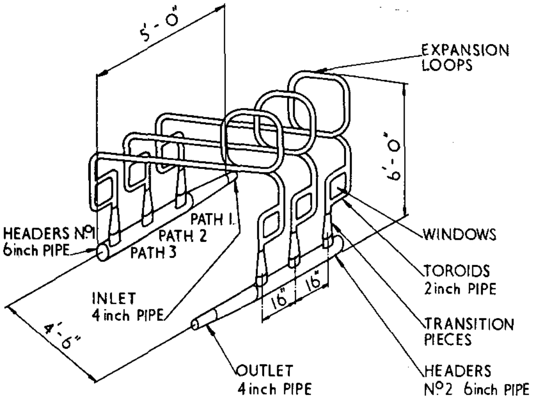

FIG. 2(c). Isometric view of toroid and header assemblies

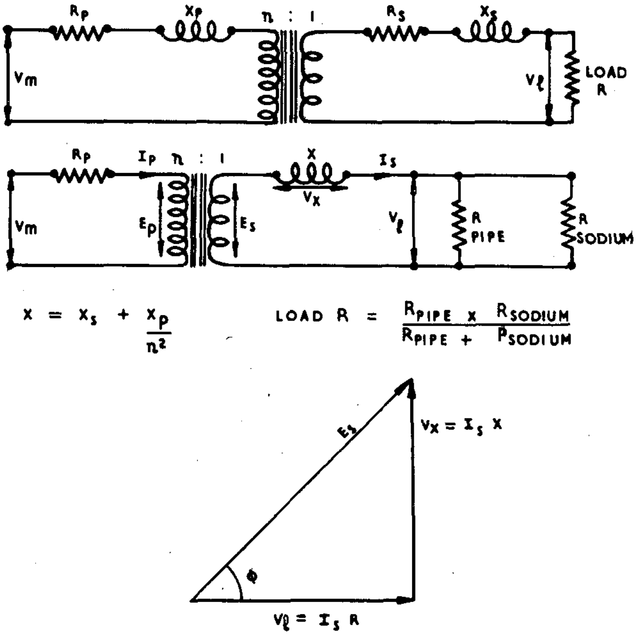

FIG. 3. Equivalent circuits for conventional transformer and heater

circuits for both are given in Fig. 3. No allowance is made for the ohmic resistance power loss of the secondary winding in the case of the heater as this forms part of the useful heat.

Because the sodium circuit operates at 650°C the split primaries are spaced widely enough apart to allow adequate thermal insulation between the coils and the toroids to protect the coil insulation. This spacing leads to a high leakage flux and reactance, degrading the power factor.

Calculations by standard methods predicted a power factor [4] of 0.75 ± 0.05 which, though low, was acceptable. As a check on this calculated value, measurements were made with a model toroid mounted on a laminated core with two split primary coils. The model was manufactured in copper with brass tees, and the equivalent resistance for a sodium-filled stainless-steel toroid at 650°C was obtained by adjusting the temperature. Power factor measurements on this model fell between 0.77 and 0.79. The primary coils were therefore designed for a power factor of 0.77.

For the toroid shape chosen the turns ratio was calculated to be 52 turns per split primary. Each conductor is made up of six layers of high-conductivity copper strip, 3-in. wide by 0.010-in. thick, wound in an Archimedean spiral. These are insulated to Class C standard, using glass tape impregnated with silicone varnish, suitable for operating at 200°C in accordance with B.S. 2757 [5]. Each split primary coil has an outside diameter of 15 in., and inside diameter of $6\frac{1}{2}$ in., and weighs approximately 100 lb.

The heater cores are made of 0.014-in. thick laminations of a standard silicon iron, stepped to approximate to a circular cross-section of 6-in. diameter. The pitch of the limbs is 16 in. and their length is 13 in. The total weight of the laminations for the heater is 1420 lb.

The general arrangement of the heater, with the cooling duct and cover removed, is shown in Figs 4 and 5. The two units of the heater are each inclined at 5° to the horizontal to ensure adequate sodium drainage. The toroids are vertical, aiding drainage and allowing horizontal cores; this eases assembly and enables easier removal of coils for maintenance. The iron cores are supported rigidly to the base plate. The inlet and outlet headers are anchored to avoid transmitting thermal expansion loads to the rest of the components in the rig.

No unusual problems arose in the thermal stress analysis of the heater pipework. The temperature rise across the heater is small and consequently differential expansion in the toroids is limited. Expansion loops are fitted between the two units to reduce the pipe stresses to acceptable values. Differential expansion, affecting the positioning of the cores relative to the toroids, is accommodated by setting the cores some $\frac{3}{8}$ in. off centre in the cold condition. The whole assembly is slid into its position some 25 ft above floor level using guide rails. The heater is finally supported on four suspension rods.

The heater coils and cores together weigh over 1 t and a substantial framework is necessary to support them, resulting in a total heater weight of 3 t, which is significantly greater than the weight of a conventional heater for this rating.

The necessary thermal insulation between the primary coils and the sodium-filled toroids is provided by enclosing the toroids in an aluminium box, suitably slotted to limit circulating currents, and packing this box with mineral insulation to give a minimum radial thickness of $1\frac{1}{2}$ in. The primary windings are fixed on the laminated limbs with wedges of an asbestos-based material, and air is circulated through the $\frac{3}{8}$-in. gap between the insulation box and primary coils. The heat loss from the toroids is 3 kW, and this, combined with the total primary coil losses of 6 kW and the core losses of 1 kW, is removed by a 3000 ft^3/min air blower. The air is ducted to a plenum chamber constructed from 10-gauge

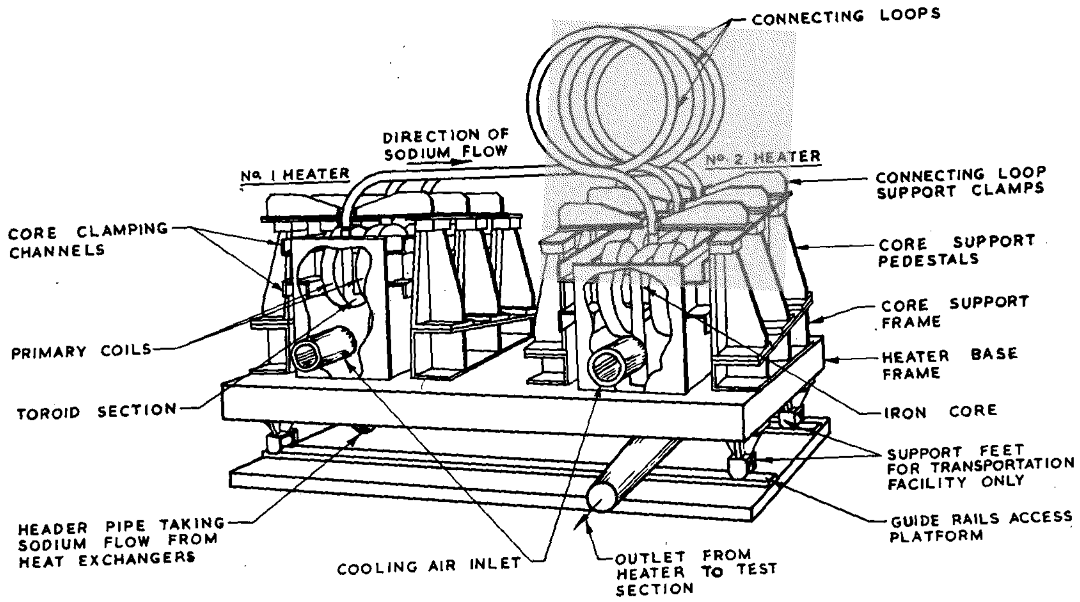

FIG.4. Construction of heater

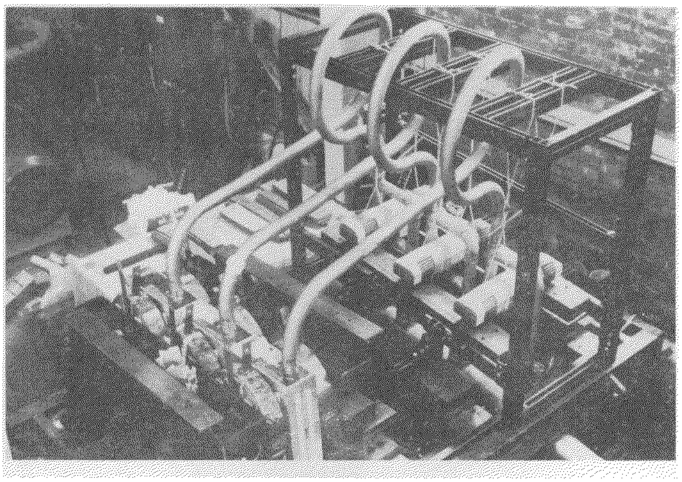

FIG. 5. General view of heater

aluminium sheet. The air enters through a split manifold to the bottom of each of the units, circulates round the coils and is ducted out of the rig cubicle.

CONTROL, INSTRUMENTATION AND PROTECTION

The two heater units are connected via two separate circuits to the 415-V, 3-phase, 50 c/s supply. One unit is controlled by a voltage regulator. The other can be connected directly to the mains supply in either delta or star arrangement to give fixed outputs of 200 kW or 67 kW respectively. Because there is a significant difference in the power induced in the toroid when it is empty and when it is full of sodium, a special arrangement is necessary when heating the rig before filling it with sodium. An additional contactor is used to connect the heaters in parallel to a preset low voltage on the regulator.

The voltage, current and power supplied to each unit are measured. A Chromel-Alumel thermocouple is embedded in each of the twelve primary windings. These are linked via a switch to a temperature indicator. In operation, this is set manually to the highest temperature indicated, and this temperature signal is linked to audible and visual alarms.

The main supply lines are connected via 400-A fuses, and adjustable overload trips are available for each unit. Interlock circuits prevent overheating of the pipework when not filled with sodium. Others ensure that the heater cannot be used without cooling air flowing over the primary windings, or at powers above the pre-heat level unless sodium is flowing through the toroids.

OPERATION

The heater has now been operating in the rig for 2000 h and has performed entirely satisfactorily. Because of the particular experimental programme in progress, the total heater power has not exceeded 260 kW. This has been achieved by operating one heater in star connection with direct on-loading (giving 67 kW) and the other at 194 kW on the regulator control. The flow through the heater has been 240 gal/min and the sodium temperature 650°C.

Typical performance figures for the two heaters are given in Table I.

TABLE I. TYPICAL PERFORMANCE FIGURES FOR THE HEATER

Heater	Voltage	Current (A)	Power (kW)	Primary coil temperature
A	395	351	194	142 - 177°C
B	420	114	67	53 - 73°C

The measured power factor has been 0.81 ± 0.01. This is significantly better than the calculated figure of 0.75 ± 0.05, and the figure of 0.78 ± 0.05 and the figure of 0.78 ± 0.01 measured on the model.

CONCLUSIONS

The principle of using the sodium in a test rig as the single, short-circuited turn of a transformer has been demonstrated in full. The heater is comparable with a conventional power transformer in reliability and life expectation. It is superior to external and immersion-type electrical resistance heaters in that no component is highly stressed mechanically, thermally or electrically, and no component is at a higher temperature than that of the working fluid. Accepted engineering standards are maintained for both the sodium containment and the electrical equipment.

The configuration of the stainless-steel pipe loop introduces a leakage reactance which is large compared with that of a conventional power transformer and this affects the power factor, which must be evaluated with reasonable accuracy to avoid excessive supply installation costs.

ACKNOWLEDGEMENTS

The heater was designed and constructed in the Reactor Engineering Laboratory and many of the authors' colleagues contributed to its successful completion, particularly J. Leece, K. Dickinson, B.J. Maple and D. F. Shipley of the Laboratory, and J. Sillitoe and L. Evans of the Electrical Design Offices, Engineering Group.

REFERENCES

[1] EICKHOFF, K. G., "Engineering development for sodium systems", London Conference on Fast Breeder Reactors (1966).
[2] MAIDMENT, L., Internal document, U. K. A. E. A.
[3] DAVIDSON, D. F., LEECE, J., Mains frequency induction heating of high-temperature flowing sodium, U. K. A. E. A. TRG Rpt 1273(R) (1966).
[4] SAY, M. G., Design and Performance of Alternating Current Machines, Pitman, London (1957).
[5] BRITISH STANDARDS INSTITUTE, B. S. 2757 (1956).

DISCUSSION

W. H. GRAFF: Can the heating system you have described be used for smaller units – say about 30 kW?

E. A. FIELDER: We have made and run a single-phase 5 kW heater operating on the induction principle. This was done primarily to obtain a check value for sodium resistivity at 650°C. We have designed (but not yet made) a 30 kW unit.

The choice of heater will depend on the circumstances in which it is to be used. Resistance heaters are generally simpler to fit to the apparatus, but as they are limited by the safe running temperature of the heater wire, problems are bound to get more serious as the heat sink temperature rises. The induction heater described in our paper has none of these problems.

E. CAMBILLARD: Have you observed in your experiments any pinch effects in the sodium which would alter the pressure drop in the circuit and reduce heating?

E. A. FIELDER: No, the pinch effects are negligible.

E. CAMBILLARD: Has the induction heater been operated at rated power?

E. A. FIELDER: The heater is split into two identical units, each with a design rating of 200 kW. One unit has run under full design conditions (200 kW, 650°C) while the other has supplied the additional 67 kW needed for the particular requirements of our test programme.

G. VANMASSENHOVE: Have you not found any electric currents in the circuit which affect the performance of your instruments (flowmeters or thermocouples for example) or distort their readings?

E. A. FIELDER: No such effect has been observed or measured on the loop instrumentation. The heater loops are essentially equipotential circuits.

G. RAJAKOVICS: I wonder whether a loss of flow, as a result of damage to the pump for example, might not be dangerous in this system since it does not appear to be designed for natural convection.

E. A. FIELDER: The loop is fitted with safety trips, and these are in fact described in the paper. A loss of sodium pump flow or of cooling air flow would trip the heater.

J. S. LINDHE: It strikes me that the alternating current might induce eddy currents, turbulence or high local velocities. Have you, therefore, observed any local corrosion on the inside of the toroids?

E. A. FIELDER: No, we have not examined the heater toroids for corrosion. The mean velocities through the heater are low (less than 1 m/s) compared with the test section, where reactor velocities (about 7 m/s) are simulated. The same temperature and impurity levels apply, and as the test section is safe there seems to be no reason for concern about corrosion in the heater.

COMPATIBILITY OF DIFFERENT BRAZING ALLOYS DURING LONG TIME-EXPOSURE IN SODIUM LOOP*

M. SOENEN
TECHNOLOGY DEPT.,
CENTRE D'ETUDE DE L'ENERGIE NUCLEAIRE,
MOL, BELGIUM

Abstract

COMPATIBILITY OF DIFFERENT BRAZING ALLOYS DURING LONG TIME-EXPOSURE IN SODIUM LOOP. About two years ago, a forced convection sodium loop was added to the existing installations of the Liquid Metal Group at the CEN-MOL Technology Department. Based on five years' experience in the liquid metal field, the conception and instrumentation of the loop is such that it can be used for a great variety of tests, mainly in relation to particular problems connected with in-pile capsules and loops.

One typical test is here analysed with the loop containing an expansion bellows with interior guide, and guided and unguided passages of different mounted types of coaxial wires with different types of brazing alloys. Semi-automatic induction brazing is applied on all passages while development work is carried on to arrive at a complete automatic brazing technique. It is intended, during a long time-exposure test, to examine the behaviour of the bellows and, for each passage, the effects of having guided and unguided stainless-steel bushes with the wires mounted as passing through and as sticking out into the tube.

The first part gives a general description of the loop and some of its applications; the second part describes the tests done with the loop to verify the operating characteristics and some of the security measures. The third part considers more closely the test section and the test sequences; the fourth part describes the operation of the loop with the test section installed, together with the test results and their interpretation. The five brazing alloys selected for testing performed well from 450°C to 600°C and 1 to 0.65 litres/s sodium flow during a 7000-h run. After this period the brazing alloys did not fail for long peak temperatures up to 700°C. Metallographical examination of the brazing alloys is given to compare compositional and structural changes with the existing blanks.

I. GENERAL DESCRIPTION OF THE LOOP

The sodium loop is constructed to be used in a great variety of tests, mainly in relation to particular problems connected with in-pile capsules and loops. The instrumentation and conception of the loop lends itself well for long time-exposure tests. Such a test is analysed with the loop containing an expansion bellows with interior guide and guided and unguided passages of various mounted types of coaxial wires with different types of brazing alloys. A general description of the loop and some of its future applications are presented in the first part of this paper.

1. General disposition of the loop

A schematic disposition of the loop with a typical sodium temperature distribution round the loop is shown in Fig. 1. The disposition fulfils the following objects: Avoidance of gas accumulation during filling, and complete emptying of the loop after operation. To verify these objects a small-scale Pyrex model of the loop was built and operated with water.

---

* Much of this work has been performed by the Association CEN-EURATOM for the exploitation of the BR2 reactor and its auxiliary installations (Contract No. 006-60-5/BRAB).

2. Loop equipment

The principal items of the loop are described below.

2.1. The electromagnetic conduction pump

The electromagnetic conduction pump, Type A6, manufactured by GAAA, France, has a manual transformer and a cosine phi-capacitor. The pump characteristics as measured on the loop, with and without sodium flow, are given in Figs 2-4 for nominal conditions (terminals 1 and 4) and for maximum performance (terminals 3 and 4). The design conditions for the pump are: sodium temperature, up to 400°C; flow, 10 m^3 /h; pressure head, 1.5 kg/cm^2.

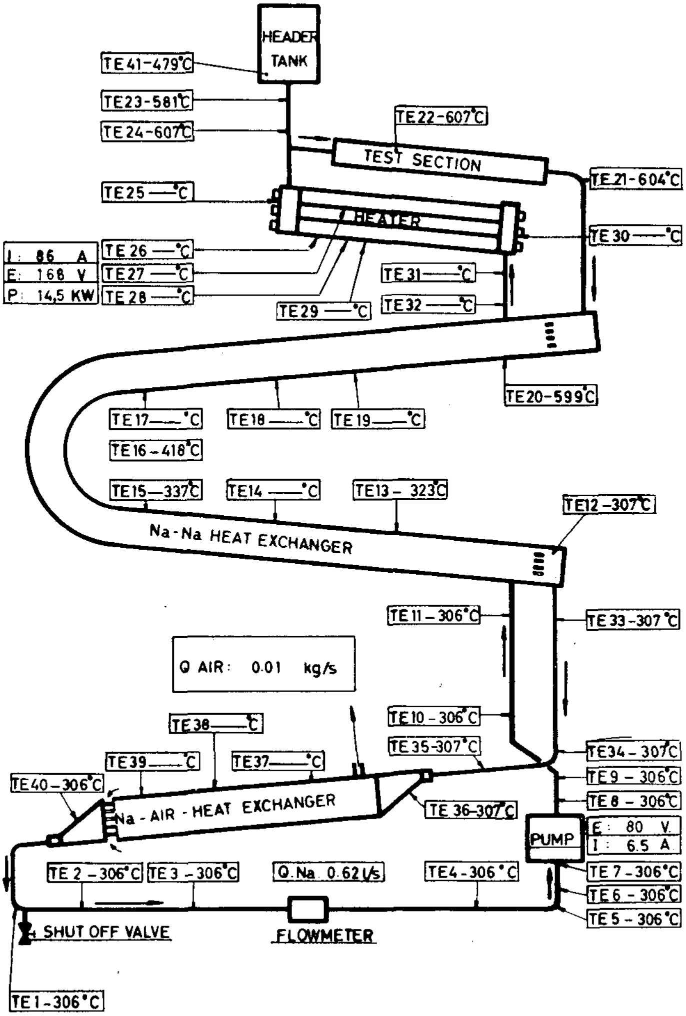

FIG. 1. Schematic disposition of the loop with a typical sodium temperature distribution round the loop

2.2. The sodium-sodium heat exchanger

The sodium-sodium heat exchanger manufactured by Waagner-Biro, Austria, is constructed as a shell and tube counterflow heat exchanger with baffles. It has a U-shape to bring down the dimensions of the loop and to compensate for the different thermal expansions between the shell and the tube. The heat exchanger reduces the temperature at the outlet of the test section to an acceptable value at the pump inlet. The heat is recuperated to raise the temperature of the sodium at the pump outlet.

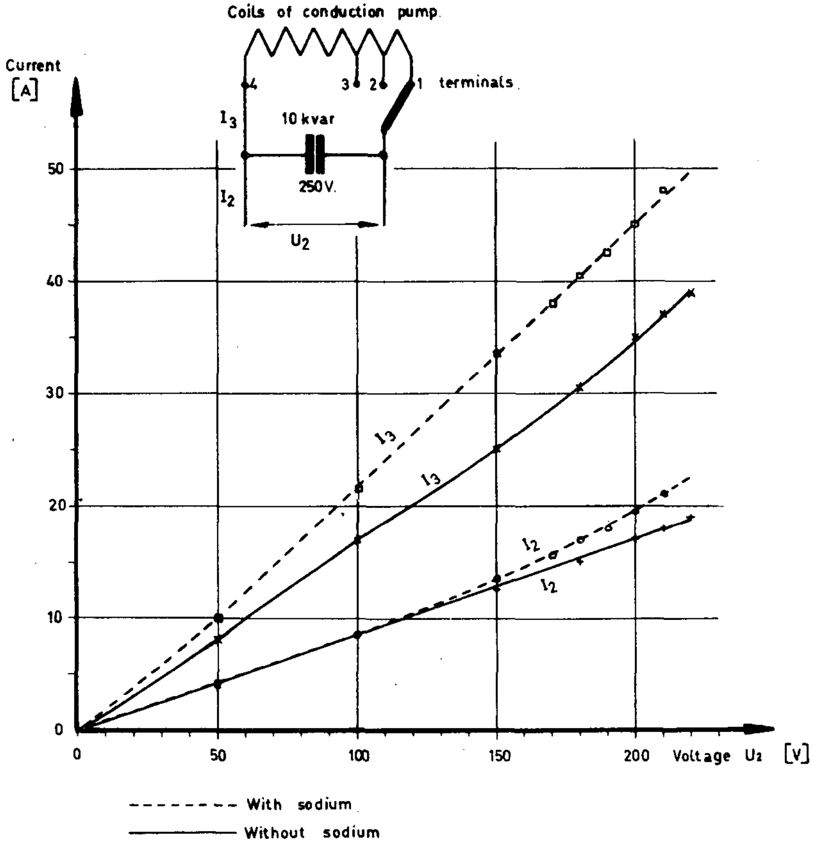

FIG.2. Currents I_2 and I_3, with and without sodium flow, as a function of voltage U_2 between the terminals 1 and 4 (nominal conditions)

2.3. The electrical heater

The sodium flow passes through four parallel tubes heated by electrical resistance elements (kanthall wires). Reassembly of the resistance elements in case of failure is possible without the need of breaking into the sodium circuit. The electrical heater compensates for the heat losses and adjusts the sodium temperature in the test section to the desired temperature. The power input to the electrical heater is adjustable from 0 to 20 kW.

2.4. The sodium-air cooler

The sodium-air cooler is of the shell and tube counterflow type with baffles. The tube bundle and the envelope are straight. To compensate for the different thermal expansions one end of the envelope is not fixed to the tube sheet and is left open to release the air inlet.

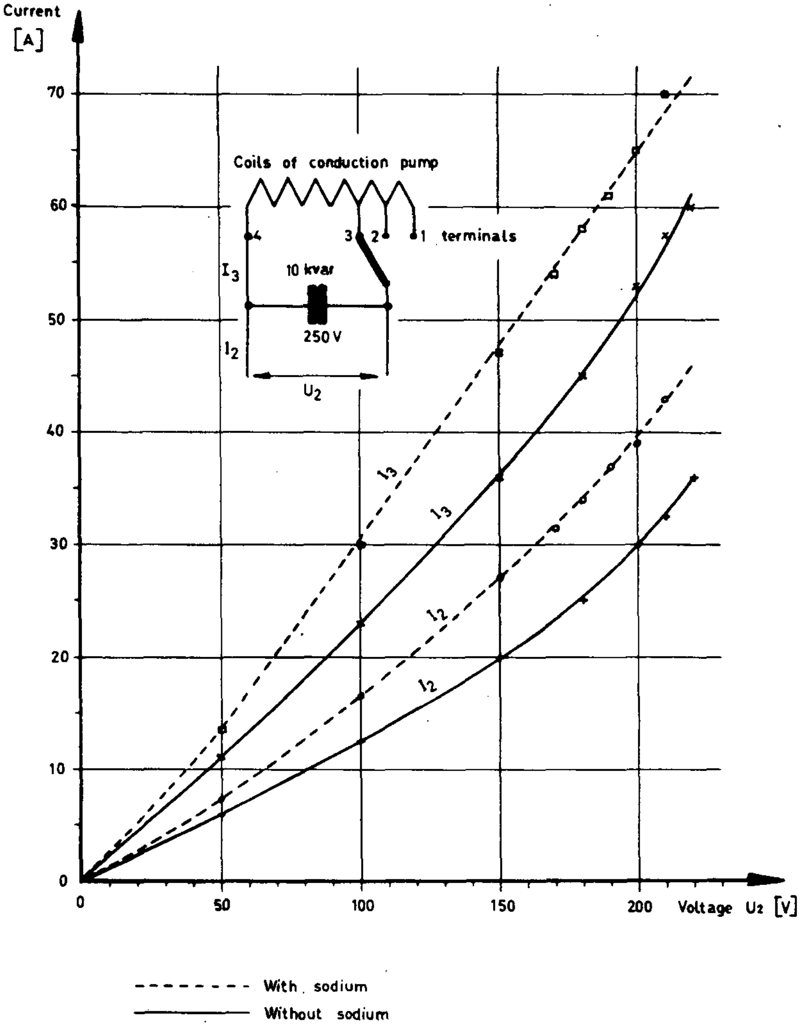

FIG.3. Currents I_2 and I_3, with and without sodium flow, as a function of voltage U_2 between the terminals 3 and 4 (maximum conditions)

The sodium-air cooler brings the sodium temperature down to the desired temperature at the pump inlet, and the temperature in the test section is regulated by air flow through the cooler.

2.5. The electromagnetic flowmeter

The electromagnetic flowmeter manufactured by GAAA, France, is a standard 1-in. unit. Flow as a function of tension is based on a slope of 0.4 m^3/h per mV with a precision of ± 10%.

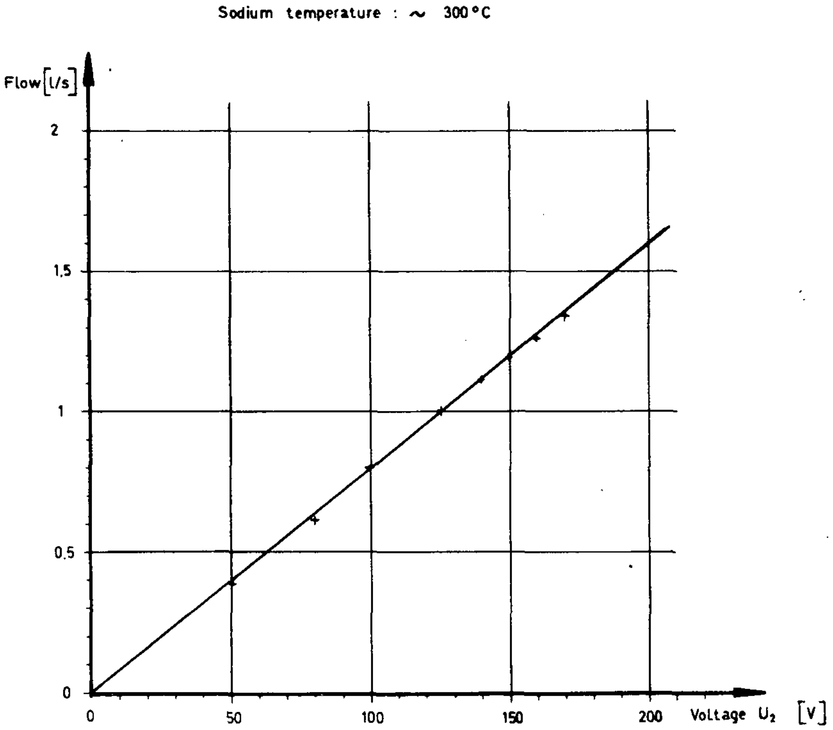

FIG.4. Sodium flow as a function of voltage U_2 between the terminals 1 and 4 (nominal conditions)

2.6. The test section

The test section is installed directly after the electrical heater and before the sodium-sodium heat exchanger. Within the connection to the electrical heater and the sodium-sodium heat exchanger a length (up to 1 m with a diameter up to 100 mm) is available to instal a test section by welding. The maximum flow is limited by the pump to about 10 m^3/h, with no minimum limitation as there is a continuous flow regulation from the pump.

The temperature in the test section is 600°C for a mass flow of 0.65 kg/s at an electrical input of 14.5 kW. More details of this test section are given in Section III below.

2.7. Miscellaneous

The loop is built of 1-in. tubing in stainless-steel AISI 316. A double bellows shut-off valve is installed between the filling system and the loop.

A header tank takes up the sodium volume change on melting. An expansion bellows with interior guide (Trade BOA Type Z) enables part of the test section to be examined.

Electrical heaters are provided in all parts permitting a gradual heating up of the loop. Spark-plug type level indicators detect maximum and minimum sodium levels in the header and the dump tank. All temperatures are recorded by means of Cr-Al thermocouples, spot welded to the tubes and thimble welded in the tanks. The sodium temperature in the test section is measured by one of the thermocouples (protruding junction) in the test section.

3. Auxiliary equipment

The following auxiliary equipment is necessary to enable the loop to be operated.

3.1. A filling system

The filling system contains a melt tank connected to the dump tank of the loop over a coarse filter (metal tissue) and a double bellows valve. The dump tank is connected to the loop over a fine filter (sintered stainless steel) and the double bellows shut-off valve. The dump tank serves from time to time as a cold trap to purify the sodium by effecting a dump-filling operation at different temperatures.

3.2. A ventilator with an adjustable control valve

As explained in Section II, a ventilator that was too powerful was at first installed and a smaller was installed later.

3.3. A vacuum group to out-gas the circuits

3.4. Argon bottles to pressurize the circuits

3.5. A general control panel incorporating all instrumentation

4. Future application

It is planned to make tests with the loop in the near future on the compatibility of a brazing alloy with a platinum-rhodium thermocouple together with three disconnecting devices, the conoseal (Aeroquip) the currujoint seal (Avica Ltd) and the ABF coupling (Braun et fils).

II. OPERATING CONDITIONS

This part of the document describes the tests done with the loop to verify the operating characteristics and the security measures taken before the test section is installed.

1. Setting of operating characteristics

A first series of tests is done with a constant power input of 14 kW to the electrical heater measuring the sodium temperature as a function of sodium flow. The measurements are done with a slightly – and heavily insulated electrical heater. The air cooler is used to limit the pump inlet temperature to 375°C. The results for the sodium temperature obtained, at the pump and at the test section, are shown in Fig. 5.

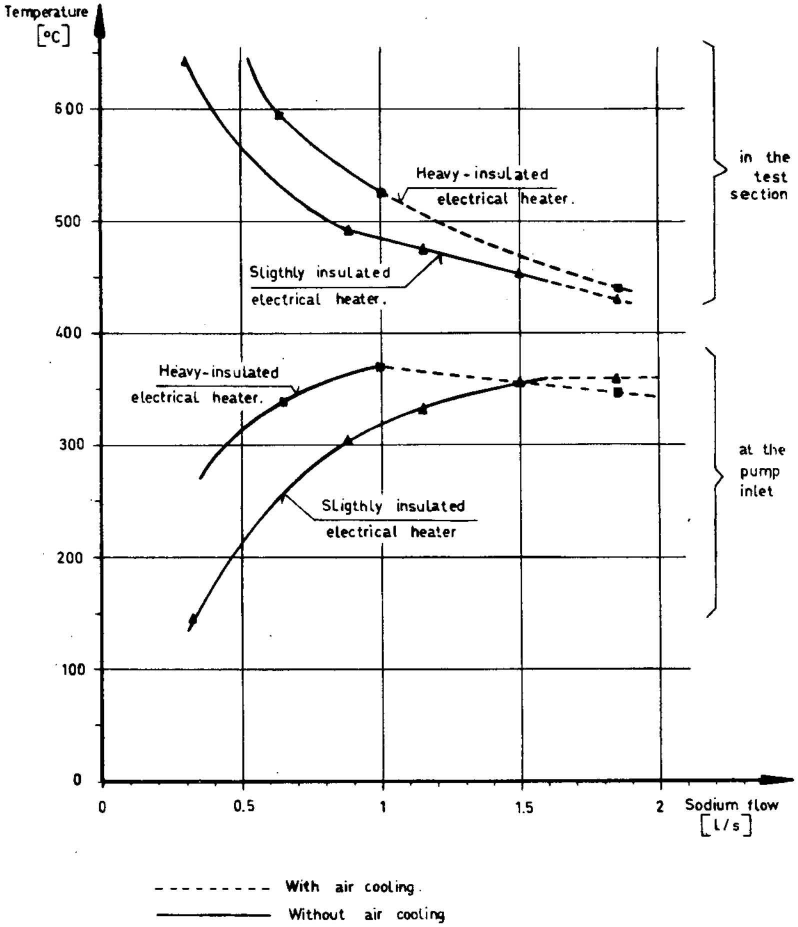

FIG. 5. Sodium temperature, at the pump inlet and at the test section, as a function of sodium flow for a constant 14-kW power input to the electrical heater

A second series of tests is done to verify the automatic regulation of the sodium set point temperature in the test section. The set point temperature is fed into a Leeds & Northrup regulator, acting on a servomotor, who determines the valve opening to control the air flow in the sodium-air heat exchanger. The air flow as a function of the control valve opening is shown in Fig. 6. The presence of the sodium-sodium heat exchanger has a considerable delaying action on the regulation. A temperature change in the test section is delayed by about 50 min compared with a temperature change in the sodium-air cooler. Such a slow action may keep the control valve open too long, leading to sodium solidification in the cooler. To correct for this defect the control valve lever is reduced from 166 mm to 66 mm (70% open) to bring down the air flow to ± one fifth of the total flow (see Fig. 6). The sodium temperatures at the test section and at the pump inlet obtained as a function of the control valve opening (lever reduced to 60 mm), for a constant power input of 12 kW and a sodium flow of 1 litre/s, are shown in Fig. 7.

$$G\,[\mathrm{kg/s}] = 0.01725\,\sqrt{\gamma_D\,[\mathrm{kg/m^3}]\,.\,\Delta p_0\,[\mathrm{kg/m^2}]}$$

$$\gamma_D\,[\mathrm{kg/m^3}] = \frac{P\,[\mathrm{kg/m^2}]}{R\,[\mathrm{m/{}^\circ K}]\,.\,T\,[{}^\circ\mathrm{K}]}$$

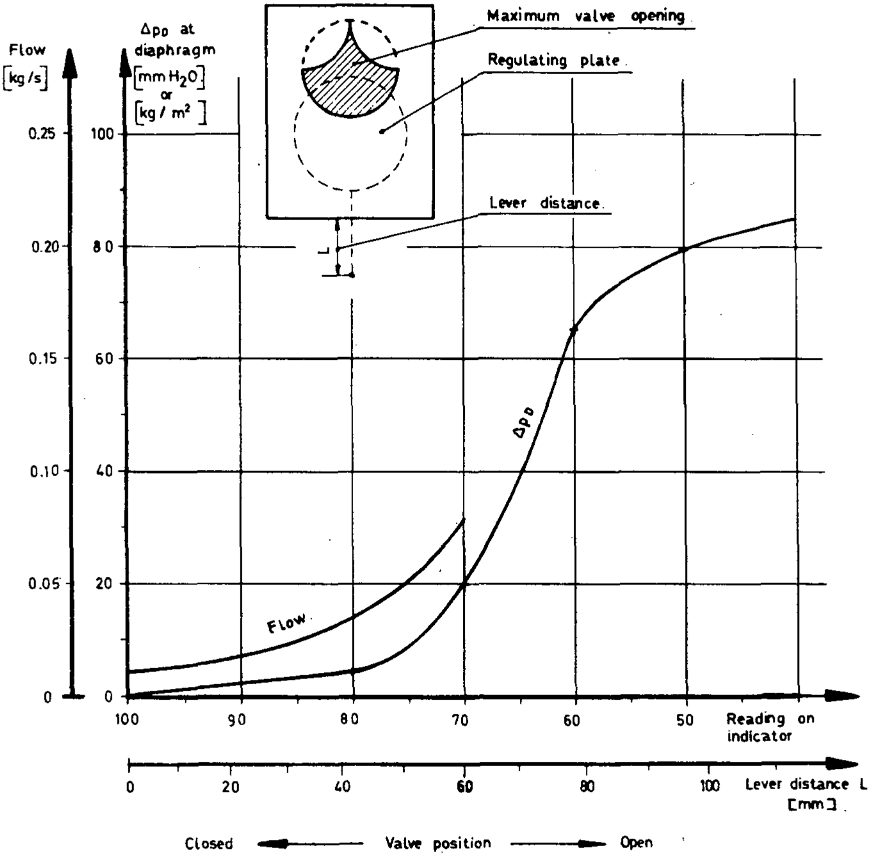

FIG. 6. Air flow as a function of control valve opening

Because the required air mass flow is very small, a smaller ventilator is placed in parallel on the existing one. The sodium temperatures obtained at the test section and at the pump inlet, with the smaller ventilator in service, are shown in Fig. 8 for a constant power input of 14 kW and a sodium flow of 0.62 litre/s.

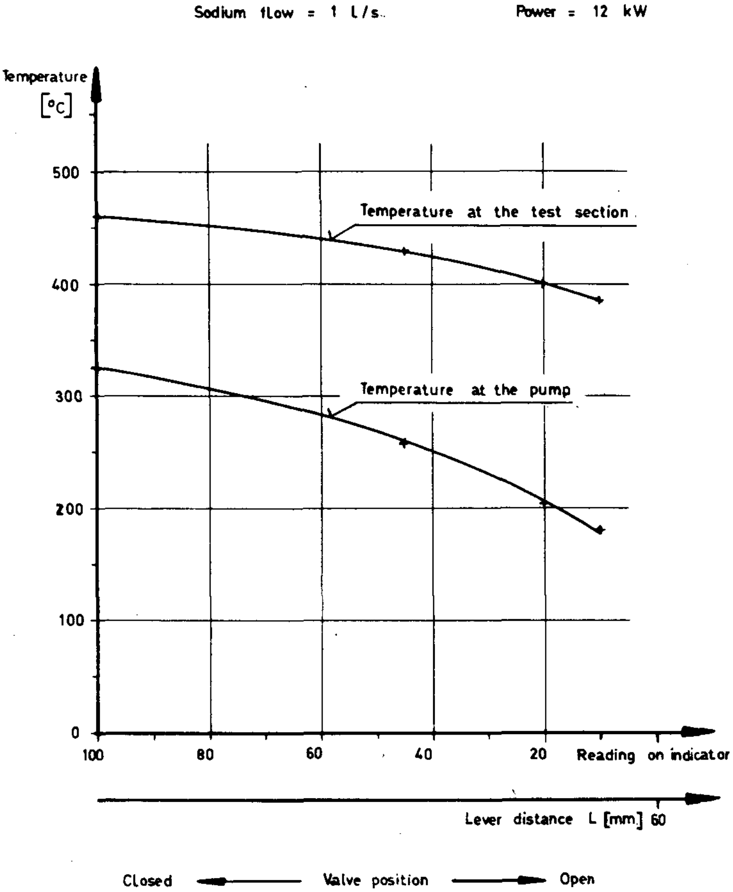

FIG. 7. Sodium temperature, at the pump inlet and at the test section, as a function of the valve opening (lever restricted to 60 mm)

2. Security measures

To ensure the safe operation of the loop a complete electrical shut off of the loop is initiated by one of the following parameters:
(a) maximum sodium temperature in the test section,
(b) maximum sodium temperature at the pump inlet,
(c) minimum sodium flow,
(d) minimum sodium level in the header tank,
(e) power interruption or instrument failure.

Restart of the loop after electrical shut off is only possible by manual intervention of the pilot. If any one of the above parameters comes into operation a visual and sonorous alarm is given outside the liquid metal area to the gate-keeper at the general entrance of CEN, and to the doorman at the entrance of the technology building. In such an event both follow their own instructions.

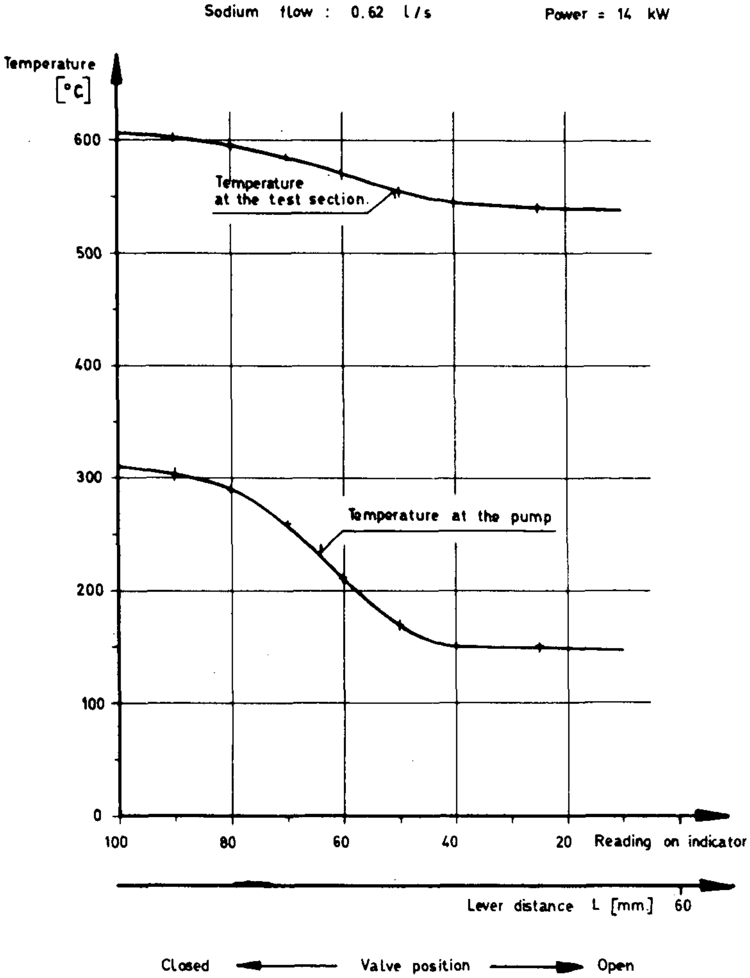

FIG. 8. Sodium temperature, at the pump inlet and at the test section, as a function of the valve opening (lever restricted to 60 mm) with smaller ventilator in service

Malfunction of the loop inside the liquid metal area sets off a visual alarm, and a push-bottom device installed close to the loop warns people outside the area in case of fire. To protect against spills and splashes of burning sodium the loop is built on a framework, with side plates and a perforated bottom plate with small steel trays underneath to catch leaks and to allow fires to be put out easily, should they occur. Two fire extinguishers (Met-L-X dry powder) are on hand to keep the fire under control. First aid equipment consists of liquid oil for burns, absolute alcohol for rapid cleaning and disinfection, boric acid with an eye cup to bathe the eyes, and 5% acetic acid solution for neutralizing caustic on the skin.

III. THE TEST SECTION

1. Test material

The complete test section contains an expansion bellows, Trade BOA, Type Z, with interior guide, undulations and end pieces all in stainless steel, and guided and unguided passages of various mounted types of coaxial wires with different types of brazing alloys (Table I). A schematic disposition of the test section with details of the passages is shown in Fig. 9.

2. Test purpose

During long time-exposure tests the behaviour of the bellows is examined and comparisons are made of the compatibility of various mounted types of coaxial wires with different types of brazing alloys. Induction brazing is applied on all samples using the same brazing tech-

TABLE I. GUIDED AND UNGUIDED PASSAGES OF VARIOUS MOUNTED TYPES OF COAXIAL WIRES WITH DIFFERENT TYPES OF BRAZING ALLOYS

Coaxial wire type	Alloy type	Passage		Mounting	
		guided	unguided	transverse	protruding junction
2 ABAc 20	LM (AMS 4777)	1	1		X
	LC (AMS 4776)	1	1	X	
	30	1	1	X	
	50	1	1	X	
	60	1	1	X	
2 ABAn 20	LM (AMS 4777)	1	1	X	
	LC (AMS 4776)	1	1	X	
	30	1	1	X	
	50	1	1	X	
	60	1	1	X	
1 NcAc 20	LM (AMS 4777)	1	1	X	
	LC (AMS 4776)	1	1	X	
	30	1	1	X	
	50	1	1	X	
	60	1	1	X	

nique throughout. Brazing is done semi-automatically in the Metallurgy Department of CEN. Work is carried out to develop a complete automatic brazing technique. For each passage an examination is made of the effects of guided and unguided stainless-steel bushes passing through the wires, wires mounted as transverse thermocouples, as protruding junction and thermocouples and as transverse heating wires.

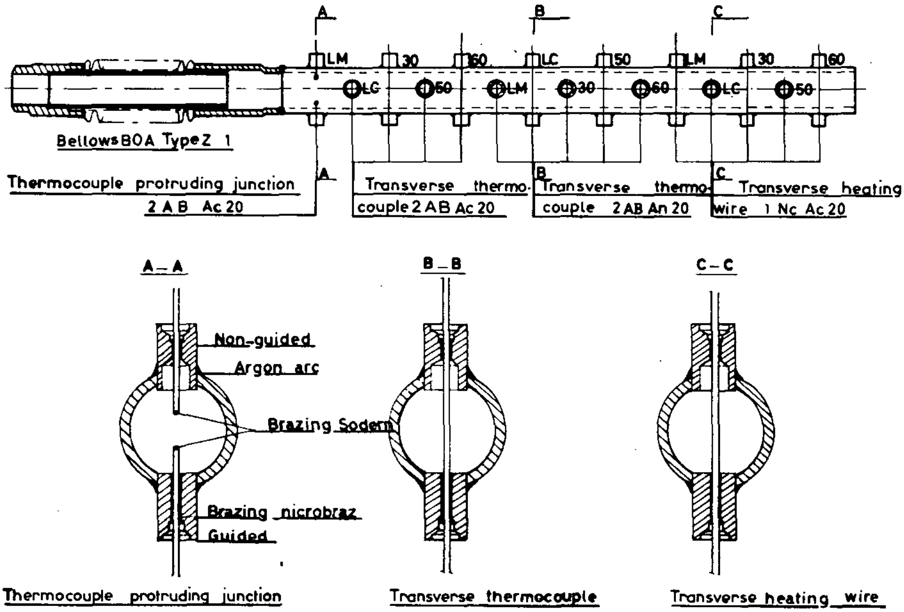

FIG. 9. Schematic disposition of the test section with details of the passages

3. Choice of test material

The coaxial wires chosen for the tests are the types most commonly available. Their designation according to Sodern nomenclature is 2ABAc20 and 2ABAn20 for the thermocouples, and 1NcAc20 for the heating wires.

The symbols indicate:

1 or 2, the number of conductors	
A, B, Nc the nature of the conductors	A alumel B chromel Nc nickel-chrome
An, Ac the nature of the cladding	An stainless steel stabilized with niobium identical to AISI 347 Ac non-stabilized stainless steel identical to AISI 304
20 the outside diameter of the wire expressed in 10^{-1} mm	

The brazing alloys chosen for the tests are two boron-type and three boron-free type alloys. Their designation according to the manufacturer, Wall Colmonoy Corporation, Detroit, Mich., is as follows:

LM nicrobraz (AMS 4776), alloy with the lowest melting point of any chromium-boron-nickel alloy;

LC nicrobraz (AMS 4775), alloy similar to standard nicrobraz (chromium-boron-nickel alloy) except for lower carbon content to minimize carbide formation;
Nicrobraz 30, a silicon-chromium-nickel alloy, boron free;
Nicrobraz 50, a phosphorus-chromium-nickel alloy, boron free;
Nicrobraz 60, a silicon-manganese-nickel alloy, boron free.

The choice for the brazing alloys is based on possible uses for nuclear reactors (boron-free or small boron content), good strength and high-temperature oxidation resistance with liquid metals, and easy brazing technique and availability.

4. Properties of the brazing alloys

4.1. Composition

Table II shows the composition of the brazing alloys.

4.2. Temperature

Table III shows the brazing temperatures of the alloys.

TABLE II. COMPOSITION OF THE BRAZING ALLOYS

Alloy type	Composition (wt. % Ni balance)						
	Cr	Si	P	Mn	C	Fe	B
LM (AMS 4777)	6. 5	4. 5	-	-	0. 15 max.	2. 5	3. 1
LC (AMS 4776)	13. 5	4. 5	-	-	0. 15 max.	4. 5	3. 5
30	19	10	-	-	0. 15 max.	-	-
50	13	-	10	-	0. 15 max.	-	-
60	-	8	-	17	0. 15 max.	-	-

TABLE III. BRAZING TEMPERATURES OF THE ALLOYS

Alloy type	Suggested brazing temperature (°C)	Brazing range (°C)	Solidus (°C)	Liquidus (°C)
LM (AMS 4777)	1038	1010 - 1177	971	999
LC (AMS 4776)	1177	1080 - 1204	971	1077
30	1190	1149 - 1204	1080	1135
50	982	917 - 1038	888	888
60	1121	1038 - 1149	1010	1032

TABLE IV. PROPERTIES OF THE BRAZING ALLOYS

Alloy type	Oxidation resistance (°C)	Ductility (°C)	Typical joint tensile shear strength kg/cm^2 AISI 304 base metal	Microconstituents (before brazing)	Joint corrosion resistance in NaK and high temp. H2O
LM (AMS 4777)	Up to 982	Excellent up to 382	2530	All peritectic	Proved satisfactory
LC (AMS 4776)	Up to 1093	Excellent over 382	4100	Peritectic and solid solution	Satisfactory
30	Up to 1093	Excellent up to 382	4030	Peritectic and solid solution	Proved satisfactory
50	Up to 857	Good 2828	2140	95 to 100% eutectic	Proved satisfactory
60	Up to 927	Excellent up to 382	2340	95 to 100% eutectic	Not known

4.3. Properties

Table IV shows the properties of the brazing alloys.

5. Test sequence

The following tests are done on the brazing alloys:

(a) The alloys are tested for helium leaks on both sides of the stainless-steel bush holding the wire, before and after the test run.
(b) The alloys are visually examined after the test run, in particular for any penetration of the brazing alloys or any macro change.
(c) A metallographical examination is made of the alloys in each passage to compare compositional and structural changes with the blanks made of all passages before the test run.

IV. TEST RESULTS AND INTERPRETATION

The operation of the loop is described with the test section installed, and the test results and their interpretation.

1. Operation of the loop with the test section

During mounting of the test section one end of the heating wire, brazed with the alloy Type 60, broke away. The rupture occurred just above the solder, where the wire is particularly brittle, making it impossible to join the wire with a compensating wire. The heating wire, brazed with the alloy Type LC, fell out from a short cut on the wire after 8 h of service. The heating wires, brazed with the alloys Type 30 and 50, fell out from a short cut on the wires after 3300 h of service. For the complete test run it was possible to keep in service only the heating wire brazed with the alloy Type LM. The test conditions during the long time-exposure run are shown in Fig. 10. They divide mainly into four parts:

From 24 September to 3 November 1965: 425°C, 1 l/s, 9.8 kW, 3A;
From 4 November to 6 December 1965: 500°C, 1 l/s, 12.8 kW, 3.5 A;
From 7 December 1965 to 10 July 1966: 600°C, 0.65 l/s, 14.5 kW, 4 - 13 A;
From 11 July to 15 July 1966: transient conditions up to 700°C.

2. Test results and interpretation

2.1. Visual examination

After cutting the test section from the loop the following observations were made:

(a) General behaviour of the brazing alloys and coaxial wires seemed to be satisfactory up to 700°C.
(b) With the exception of the bellows, which could not be moved because of sodium sticking between the interior guide and the undulations, sodium emptying was complete.

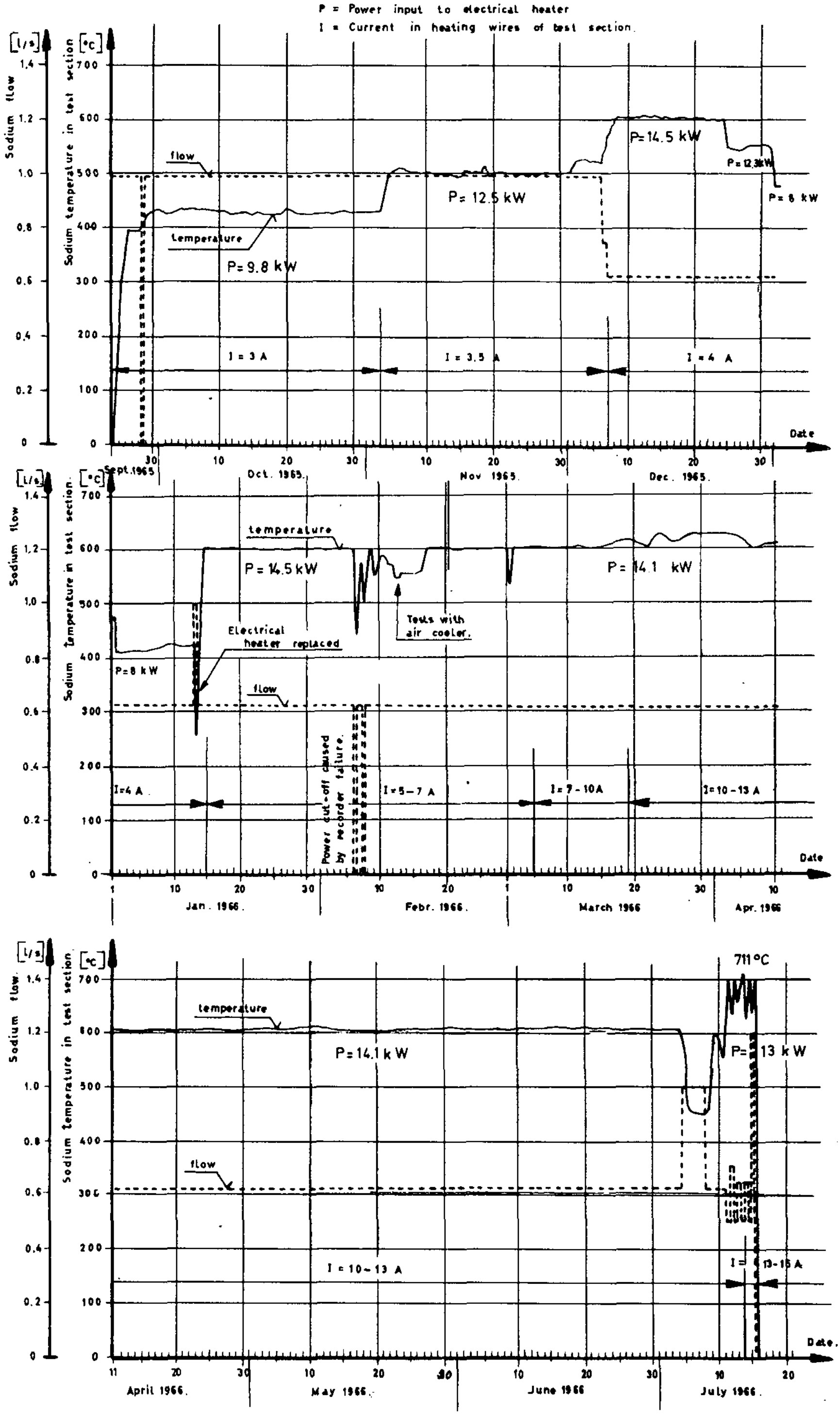

FIG.10. Test conditions during the long time-exposure run

(c) None of the coaxial wires were broken away inside the tube indicating that guided and unguided passages both provided sufficient mechanical strength for the wires.

(d) The breaking-off of one of the coaxial wires in the brazing zone by embrittlement of the cladding, which occurred during mounting of the test section, is a serious problem when using these brazing alloys. To prevent such a breaking-off careful handling of the wire, and possibly a wire support, is necessary.

2.2. He leak test

The complete test section, examined after the test with the helium mass spectrometer, showed the same leak-tightness as before use. To make certain about the bellows an extra leak test is repeated on the bellows alone after they are cut from the test section and all the solidified sodium is solved in alcohol. This test has revealed complete leak-tightness of the bellows. The fact that sodium gets trapped between the interior guide and the undulations requires careful attention when preheating the bellows in the circuit.

2.3. Metallographical examination

2.3.1. Description of photographs. The photographs are indicated by two or three symbols separated by a dash. The first symbol – LM, LC, 30, 50 or 60 – indicates the type of brazing alloy. The second symbol – BL – indicates the blank samples. The numbers – 1, 2 or 3 – indicate

1, guided passage with coaxial wire 2ABAc20;
2, unguided passage with coaxial wire 2ABAn20;
3, guided passage with coaxial wire 1NcAc20.

2.3.2. General remarks. The following remarks on the interpretation of the macro- and micrographs should be borne in mind.

(a) Because of the numerous holes present in the solder and the different types of materials present (coaxial wire, brazing alloy and base material) the samples could not all be etched in the same way. This explains why on some of the macro- and micrographs the structure of the base material is not very clear. Applying a longer etching time in such cases would lead to a less clear over-all picture.

(d) The same brazing alloy may show different effects, which makes an exact interpretation of a metallographical examination difficult. This is caused mainly by the semi-automatic welding method in which all parameters are not unanimously fixed.

2.3.3. Macro-examination (enlargement 4.5 to 10.5). An over-all macro-examination of the blanks 1 (guided passages) (Fig. 11) with the blanks 2 (unguided passages) (Fig. 12) shows that with the semi-automatic welding technique the number of holes in the solder depends on:

(a) The type of passage.

The samples with unguided passages show in general less holes than those with corresponding guided passages.

(b) The type of brazing alloy.

The types arranged by the number of holes in the solder (scarce to numerous) lead to a general classification LM, LC, 60, 30 and 50.

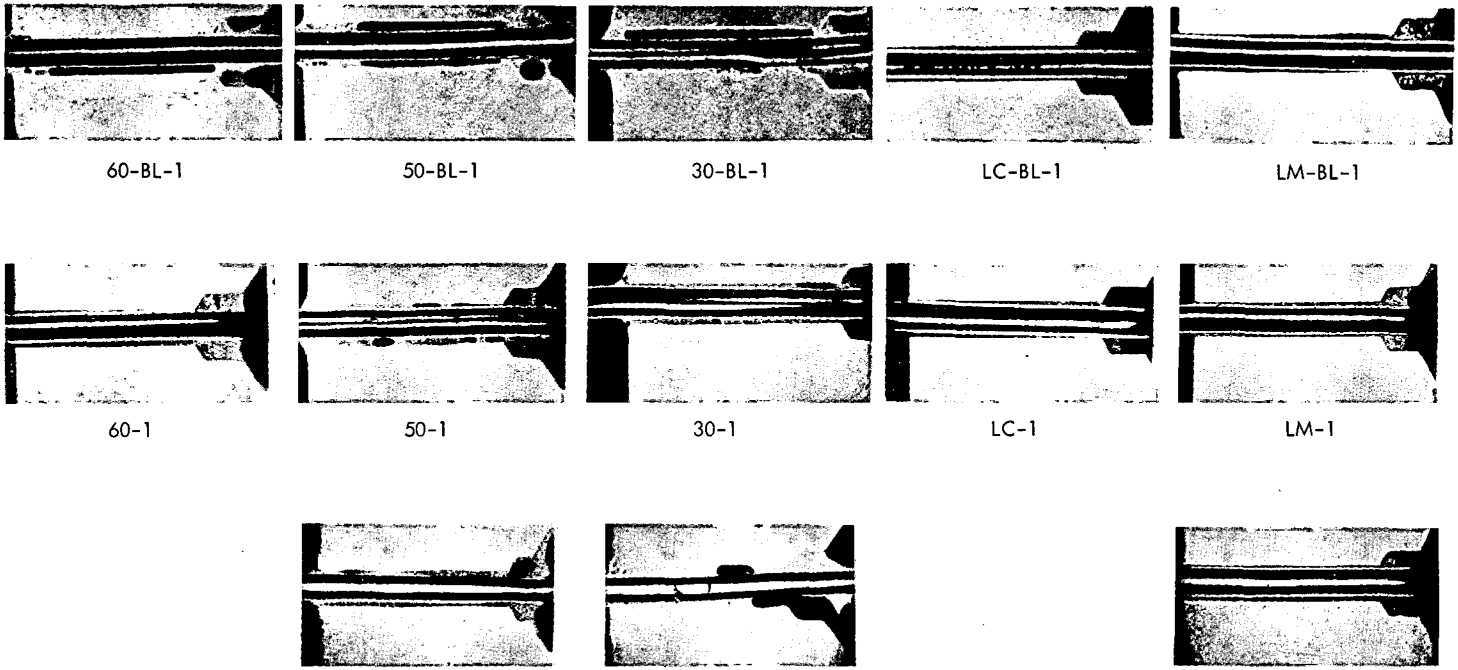

60-BL-1 50-BL-1 30-BL-1 LC-BL-1 LM-BL-1

60-1 50-1 30-1 LC-1 LM-1

50-3 30-3 LM-3

FIG.11. Macrographs: Blanks 1 compared with used samples 1 and 3 (enlargement 4.5)

LM-BL-1	LM-1	LM-3
LC-BL-1	LC-1	
30-BL-1	30-1	30-3
50-BL-1	50-1	50-3
60-BL-1	60-1	

From a comparison of the blank samples with the used ones the following observations can be made:

(i) The cladding on the macrographs 30-3 and 50-3, guided passages with coaxial wires 1NcAc20, has suffered more than the guided and unguided passages with coaxial wires 2ABAc20 and 2ABAn20. The explanation probably lies in the fact that the coaxial heating wire 1NcAc20 has been used up to maximum intensities with high temperatures on the cladding. A closer look at this cladding-attack phenomenon is given in micrograph 50-3.

(ii) The coaxial wire 1NcAc20 on the macrograph 30-3 is burned through in two places by grounding. One of these defects is illustrated more closely in micrograph 30-3.

(iii) The brazing alloy on the macrograph 50-2 seems to be attacked by the sodium. To check such an attack and to judge the difference in corrosion resistance to sodium of the different brazing alloys, micrographs of the blanks and of the alloys in contact with the sodium are jointly examined.

2.3.4. Micro-examination (enlargement 60 to 250. The micrographs reveal the following effects:

(a) Corrosion.

A comparison of the micrographs from some of the blanks 1 and 2 (Fig. 13) with the corresponding used samples 1 and 2, taken at the runouts of the solder to the side of sodium contact, shows that the corrosion resistance of the brazing alloys has been good except for the alloy Type 50. This is not in complete agreement with the properties of the brazing alloys stated in Table IV, where the alloy Type 50 is shown to be satisfactory for joint-corrosion resistance in NaK.

Because of the semi-automatic welding technique applied and the etching difficulties, as explained in the general remarks above, new tests may be required before a classification or more definite statements about corrosion resistance of the alloys can be affirmed.

(b) Cladding attack.

The micrograph 50-3 (75x) (Fig. 14), taken in the zone with a hole in the solder (see macrograph 50-3, Fig. 11), illustrates more closely the cladding attack phenomenon. The cladding has completely disappeared in the zone with the hole in the solder, and is elsewhere severely diffused in the solder.

(c) Structural change.

The micro aspect of LM-BL-1 with LM-3 (250x) (Fig. 15), taken in a sound brazing zone of the corresponding macrographs, does not disclose any compositional change in the structural materials. However, because of the different etching times applied, as explained in the general remarks above, the graphs may clearly show any such a change.

(d) Defect.

The micrograph 30-3 (75x) (Fig. 16) shows in more detail one of the burned through places of the wire by grounding as seen on the corresponding macrograph 30-3. The conductor nickel-chrome is cracked and part of the conductor is projected into the magnesium oxide insulation towards the cladding. The defect is probably due to a burn-through of the cladding followed by a grounding of the conductor.

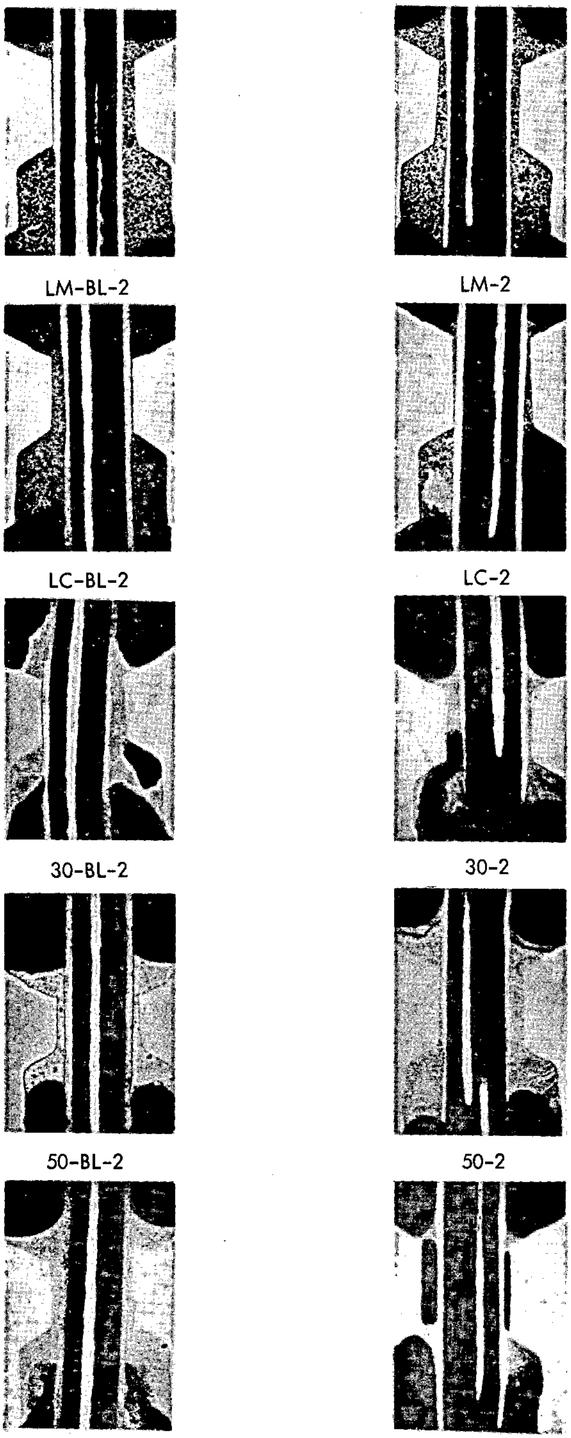

LM-BL-2 LM-2

LC-BL-2 LC-2

30-BL-2 30-2

50-BL-2 50-2

FIG. 12. Macrographs: Blanks 2 compared with used samples 2 (enlargement 10.5)

LM-Bl-2	LM-2
LC-BL-2	LC-2
30-BL-2	30-2
50-BL-2	50-2
60-BL-2	60-2

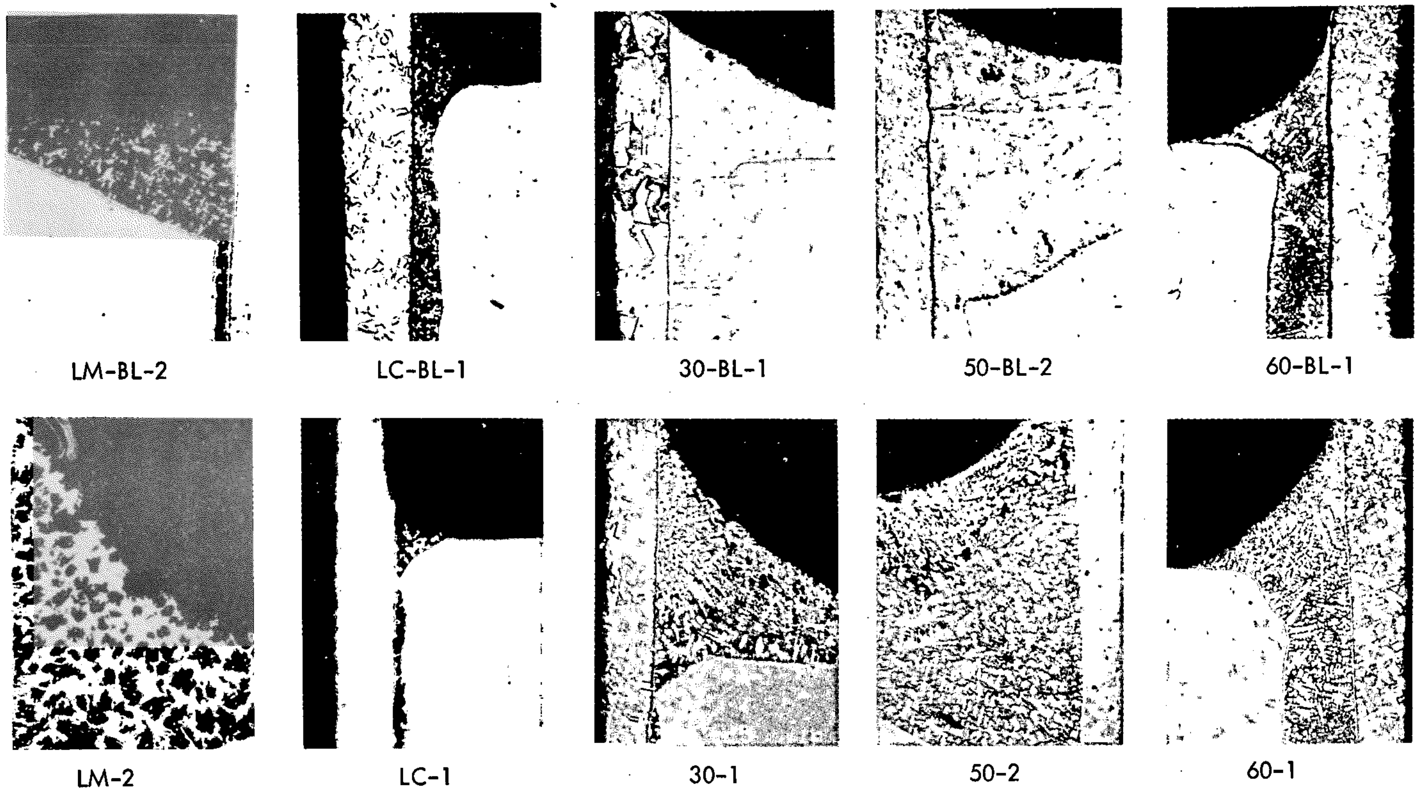
LM-BL-2 LC-BL-1 30-BL-1 50-BL-2 60-BL-1

LM-2 LC-1 30-1 50-2 60-1

FIG.13. Micrographs: Corrosion (enlargement 60)

LM-BL-2	LM-2
LC-BL-1	LC-1
30-BL-1	30-1
50-BL-2	50-2
60-BL-1	60-1

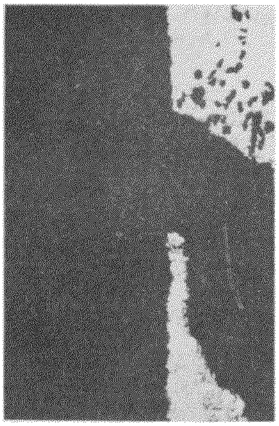

50-3

FIG. 14. Micrograph: Cladding attack (enlargement 75)

50-3

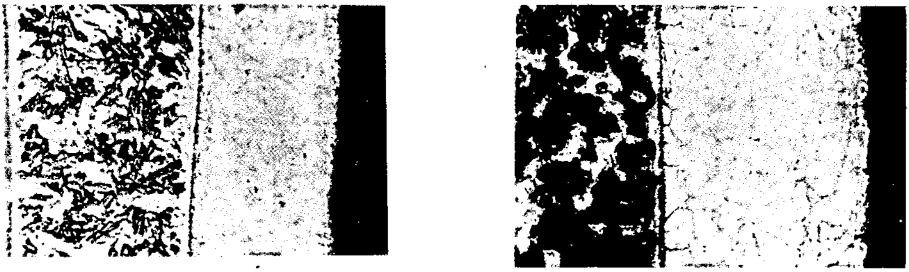

LM-BL-1

LM-3

FIG. 15. Micrographs: Structural change (enlargement 250)

LM-BL-1 LM-3

30-3

FIG. 16. Micrograph: Defect (enlargement 75)

30-3

3. Conclusions and recommendations

3.1. Conclusions

In conclusion the following observations can be made from the long time-exposure run:

(a) Type of passage.
The samples with unguided passages show in general less holes than the corresponding guided passages. Guided and unguided passages both provide sufficient strength to hold the wires.

(b) Type of brazing alloy.
The types arranged by the number of holes in the solder (scarce to numerous) lead to a general classification LM, LC, 60, 30 and 50. Except for the alloy Type 50 the corrosion resistance of the solder to sodium was good. As explained, new tests are required before a classification or more definite statements about corrosion resistance of the alloys can be affirmed.

(c) The embrittlement of the wire in the brazing zone is a serious problem demanding careful handling of the wire and possibly a wire support.

(d) Although the extension bellows behaved well under the test conditions, the fact that sodium is trapped between the interior guide and the undulations requires careful attention when preheating the bellows in the circuit.

A number of shortcomings of the brazing alloys examined can be attributed to the semi-automatic welding technique. Some of these shortcomings could be avoided using a completely automatic brazing technique in which all parameters are fixed. New tests applying such an automatic technique therefore seem necessary before making any firm statements about the corrosion behaviour of the brazing alloys.

3.2. Recommendations

The recommended alloys for use with coaxial wires 2ABAc20 and 2ABAn20 are the Type LM (as boron alloy) and the Type 30 (as boron-free alloy). With the coaxial wire 1NcAc20 intensities up to 13 A are feasible with a breakdown at 15 A. It was possible, for the complete test run, to keep in service only the heating wire brazed with the alloy Type LM, which was the type with the smallest number of holes in the solder.

The unguided passage is recommended as passage for the coaxial wires. It provides sufficient mechanical strength for the wires and leads to less holes in the solder.

DISCUSSION

A. G. IOLTUKHOVSKY: Were the mechanical properties of your brazing alloys studied at high temperatures (~ 500-600°C)?

A. M. SOENEN: No, they were not.

A. G. IOLTUKHOVSKY: Can these alloys be used to join heterogeneous metals, for example steels with refractory metals such as molybdenum, niobium, vanadium and so on?

A. M. SOENEN: I think they could, but we have not tested them for this purpose in sodium.

H. U. BORGSTEDT: I should like to comment on Mr. Ioltukhovsky's second question. At Karlsruhe we have joined refractory metals such as molybdenum, tantalum and niobium to stainless steels with brazing alloys of the type Mr. Soenen has described. These experiments were quite successful.

A. M. SOENEN: Yes, I quite agree that the alloys are suitable for brazing refractory metals, but I would not care to comment on their behaviour in sodium without doing appropriate tests.

A. W. THORLEY: We feel that microprobe analyses must be supplemented by microstructural examinations if we wish to determine the corrosion resistance of brazes in sodium. For example, you say that Nichrobraz 50 is corroded or eroded in sodium whereas the other brazes are not. I think, however, that if you compare Nichrobraz 30, say, with Nichrobraz 50, you will not find much difference in corrosion behaviour – corrosion in this context being considered as the actual removal of metal or material from the surface of the alloy. Even without this, though, the alloy is subject (as is shown by your photomicrographs) to a certain amount of structural modification which, we think, is due to the extraction of phosphorus from the braze. Our results on Nichrobraz 50, together with the results of microprobe analyses reported in our paper (SM-85/18), support this view. Would you therefore care to make any further comment on the actual corrosion resistance of this alloy compared with the others you tested?

A. M SOENEN: I completely agree with you. Before we can reach any firm conclusion about the corrosion resistance of the alloys, there must be further tests with a complete automatic welding technique and microprobe analyses.

W. H. GRAFF: Did you by any chance analyse your sodium for braze constituents after corrosion?

A. M. SOENEN: No, we did not.

EQUIPMENT FOR THE STUDY OF WEAR UNDER CONDITIONS OF OSCILLATORY RELATIVE MOTION IN LIQUID SODIUM

A.W.J. DE GEE, C.P.L. COMMISSARIS,
E.G. CHIRER AND A.J. BOGERS
METAL RESEARCH INSTITUTE TNO,
DELFT, THE NETHERLANDS

Abstract

EQUIPMENT FOR THE STUDY OF WEAR UNDER CONDITIONS OF OSCILLATORY RELATIVE MOTION IN LIQUID SODIUM. Equipment for the study of wear in liquid sodium under conditions of oscillatory relative motion of small amplitude ("fretting") is described in detail.

With this equipment experiments can be performed at temperatures up to 750°C in sodium with controlled oxygen content. The following vibration patterns may be applied: (i) torsional vibration in the plane of contact of two test specimens; (ii) oscillatory motion normal to the plane of contact; (iii) any combination of (i) and (ii).

With this equipment fretting experiments are performed with steel X 8 Cr Ni Mo V Nb 16 13, Inconel 625 and the vanadium alloys V-20 Ti and V-5 Ti-20 Nb, at different levels of temperature and oxygen content.

1. INTRODUCTION

Wear due to small amplitude, high frequency oscillatory relative motion between different constructional elements can be a source of trouble in nuclear reactors and reactor components. This is particularly true for liquid-cooled reactors in which the speed of flow of the coolant can locally exceed 10 m/s, which means that turbulent flow conditions prevail. Under these conditions, vibrational contact may occur, for example between fuel elements and spacers in the reactor core, or tubes and support plates in the steam generator. So far, research efforts in the field of wear in the liquid metal environment have been concentrated upon studies of sliding wear as occurs in a journal bearing. In a recent article, Anderson [1] gives a survey of relevant results. He concludes that, with respect to wear resistance, steels are unsatisfactory at temperatures above about 300°C. The same is true for nickel and nickel alloys and for chromium-tungsten-cobalt alloys. As a matter of fact, the only materials that can be used in the temperature range from 400 to 800°C are tungsten carbide cermets and titanium carbide-tungsten carbide cermets. A pronounced influence of temperature on the wear of materials in liquid metal environments is also found by Roberts [2], who concludes that the wear rate of a variety of materials steadily increases with temperature.

It may well be that the above results are not directly applicable to vibrational contact conditions. Nevertheless, it can be expected that constructional elements which are generally supposed to be excellently compatible with liquid metals of high temperature may be subject to wear when exposed to rubbing under oscillatory motion conditions, even if the normal loads which occur between the contacting surfaces will generally be lower than the load that is transmitted through a journal bearing. On the whole, it is considered to be a worthwhile effort to study the behaviour of a number of potential nuclear reactor structural materials under conditions of vibrational contact, if only to be able to select the best possible material combination under a given experimental condition.

2. EQUIPMENT

The authors believe that a test rig that is to give realistic results should operate under conditions of combined vibration. In the equipment that was eventually designed, the following vibration patterns can be applied:

(1) Torsional vibration in the plane of contact of two test specimens;
(2) Oscillatory motion normal to the plane of contact;
(3) Any combination of (1) and (2).

The frequencies of both torsional and normal vibration can be chosen and kept constant between 10 and 50 c/s. The amplitudes are adjustable between 20 and 100 μm. The maximum normal load that occurs during contact of the vibrating specimens is adjustable between 200 and 500 g. The temperature of the liquid metal in which the experiments are performed can be chosen up to 750°C. Finally, the oxygen content of the liquid metal is adjustable by means of a cold trap described below. Figures 1 and 2 show the implementation of the above. Figure 1 gives the relative position of the principal constructional elements of the test rig. Figure 2 shows a cross-section through the essential part of the machine. In principle, two sepa-

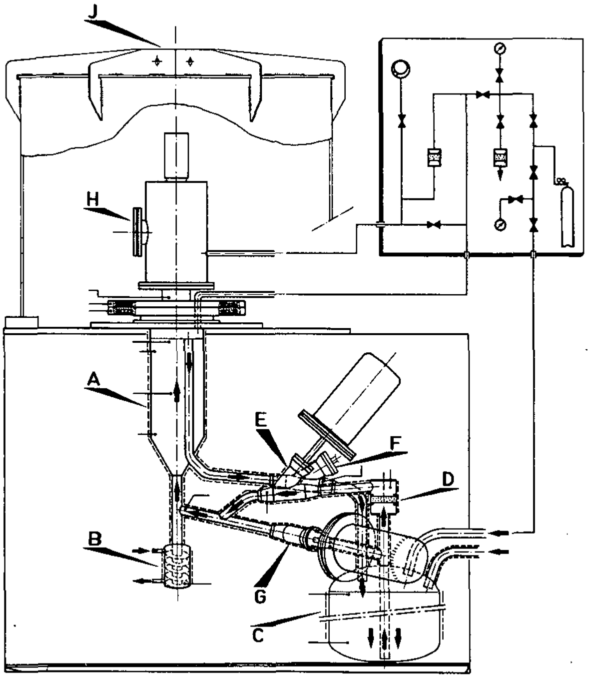

FIG.1. Principal constructional elements of test rig (see text for explanation)

rate parts can be distinguished, viz. a lower part which contains the liquid metal system and an upper part which contains the movement section. The elements of these parts are clearly shown in Fig. 1. In this figure, A is the vessel in which the actual wear experiments take place. Attached to this vessel is a dead-end tube B which can be kept at a relatively low, constant temperature by means of a heating element and cooling air. As during operation of the apparatus this tube has the lowest temperature of the liquid metal system it functions as a cold trap, thereby controlling the oxide content of the liquid metal by diffusion. The other essential elements of the liquid metal system are the liquid metal dump tank C, filling filter D and three remote controlled valves E, F and G. These different elements are suspended on steel wire in a steel frame. Vessel H, which contains the movement system, can be placed on top of vessel A. The elements of the movement system are shown in Fig. 2. The upper specimen holder (1a) is fitted to a vertical shaft (2), which transmits the vibrational movements. The shaft is suspended between two sets of steel wires which can be

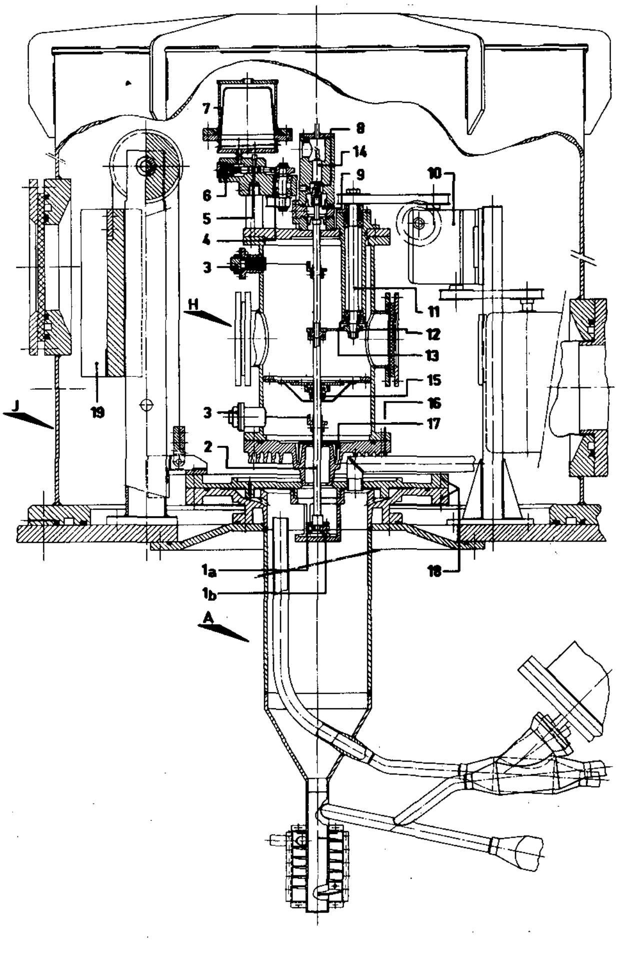

FIG. 2. Cross-section through the essential part of the test rig (see text for explanation)

stretched by adjustable drawsprings, contained in compartments (3). The vertical vibration of the shaft is effected by means of a mixed pneumatic-hydraulic system. This system has the following elements: an eccentric (4) is driven by a motor with adjustable speed (not shown in the drawing). The eccentric drives a piston (5). This piston pressurizes hydraulic oil which is present in compartment (6). This compartment is connected with:

(i) pressurized oil supply tank (7), and
(ii) upper pressure chamber (8).

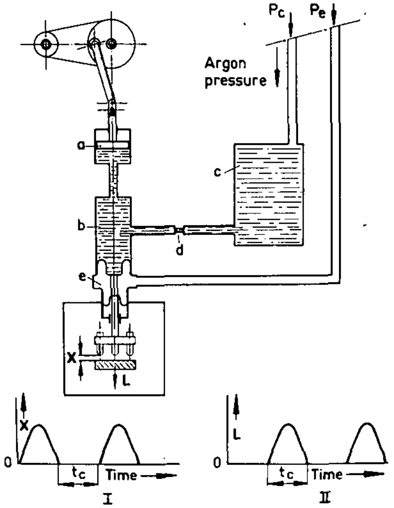

FIG. 3. Schematic diagram of vertical vibrational movement system: displacement-versus-time diagram (I), and normal-load-versus time diagram (II) (see text for explanation)

The connection between compartment (6) and oil supply tank (7) is made by means of a tube with an adjustable orifice. The upper pressure chamber (8) is separated from the lower pressure chamber (9) by means of a roll membrane. The lower pressure chamber can be pressurized with argon. To prevent the penetration of air into the hydraulic system, the driving piston (5) is split into two parts separated by an oil chamber.

To elucidate the working of this driving system, the essential elements are once more presented, in Fig. 3. Sinusoidal vibration of driving piston (a) causes the shaft to which the upper specimen holder is attached to perform a forced normal vibration, shown in Diagram I. As the tube which connects the oil-filled compartment (b) with the pressurized oil supply vessel (c) contains a restricting orifice (d), excess oil pressure is built up between the driving piston and the upper roll membrane, when the driving piston continues to make a downward motion during contact of the test specimens. This causes the normal load between the specimens to vary approximately as shown in Diagram II. Actual diagrams, recorded during performance of a dummy experiment, performed in air, are shown in Fig. 4. The way in which these diagrams were obtained is discussed below. It is seen that the real movement largely approximates the theoretical curves I and II in Fig. 3. A feature of this movement system is that the average distance between upper specimen and lower specimen remains constant, irrespective of the amount of specimen wear. The maximum normal force which is exerted between the test specimens during contact is a function of the pressure difference between the oil supply vessel (c) (Fig. 3) and the lower pressure chamber (e). Thus, by selecting these pressures, the value of the maximum normal load between the specimens can easily be chosen and kept constant.

FIG. 4. Amplitude of normal vibration (a), and normal force between the specimens (b) as a function of time, recorded during actual operation

The rotational vibration of the vertical shaft is effected by means of a mechanical driving system (see Fig. 2). The elements of this system are: a motor (10), which drives a vertical shaft (11) to which an eccentric (12) is attached. This eccentric drives a cam (not shown in the drawing) which is attached to the central shaft by means of a beam (13). The cam is pressed against the eccentric by a spring (not shown in the drawing). The main problem with this system is that wear may occur between the cam and the eccentric, not only because of the rotational movement of the eccentric, but also because of the vibrational movements of the cam. An effective and, up till now, entirely adequate measure has turned out to be the use of salt-bath nitrided steel, Nitralloy 135, as the material for both the cam and the eccentric. Also, before use, the contacting surfaces are lubricated with grease containing molybdenumdisulphide. If, during prolonged use of the test rig, wear between cam and eccentric might occur, the vertical vibration pattern of the shaft will probably be affected. However, this will be observed in time, because the vertical vibration pattern is measured and recorded at given intervals. To make the measurement of the vertical vibration pattern possible, the vertical shaft has an extension in the form of a thin rod which moves within a differential transformer (14). The output of this differential transformer is a measure of the displacement of the shaft versus time (cf. Diagram (a) in Fig. 4). Moreover, when this output signal is fed into a slow recorder with integrating function, information about changes in the average position of the shaft, and thus about specimen wear, is obtained. The amplitude of the rotational vibration is measured and recorded in the following way: an element (15) which contains ten small cylindrical magnets is attached to the shaft. The magnets move inside an electric coil. The voltage drop which is associated with the flow of the induced current through a resistance is fed to an oscilloscope. The lower specimen holder (1b) is mounted in a cage fitted to the upper part of the machine by a screw connection. In dummy experiments, which are performed in the normal laboratory atmosphere, the lower specimen holder can be replaced by a pick-up, which essentially consists of a piëzo-electric bariumtitanate crystal. This crystal responds to a sudden change in normal load (compression or decompression of the crystal) by building up an electric charge. The potential difference which occurs is proportional to the absolute value of the change in normal load. Using this pick-up, a normal load-versus-time diagram can be recorded (cf. Diagram (b) in Fig. 4).

During an experiment, the test specimens are fully immersed in liquid sodium, which may have a temperature of over 700°C. It goes without saying that the upper part of the machine, which contains the movement systems, must be protected against these high temperatures and also against penetration of hot sodium vapours. To keep the temperature down, the bottom of vessel H is provided with cooling ribs (16) along which air can be circulated. Separation between the atmospheres of vessels A and H is effected by means of a liquid seal (17) which is filled with low melting metal. It turns out that even at quite moderate air speeds the temperature of the bottom of vessel H can easily be kept below 105°C, even if the experiment is performed at 750°C. At such a low temperature the vapour pressure of the molten metal in the liquid seal is very low. Therefore, contamination of the different parts of the movement system with condensed metal is kept within bounds.

Vessel H is connected to vessel A by means of a flange (18). If the bolts are removed, the whole upper part of the machine, including the specimen assembly, can be lifted up by means of a lifting tackle with counterweights (19). This is done inside a large glovebox (J), which can be placed over the entire machine. Before the apparatus is opened, the glovebox is evacuated and flushed with pure argon. This argon, which contains less than 3 ppm oxygen, can be introduced into the glovebox as well as into the different parts of the test rig by means of the gas supply system, which is shown schematically in Fig. 1. Flange 18 is sealed by means of a gas-filled metal gasket. In order to prevent sodium from condensing on this gasket, flanges (18) are provided with heating elements; these are shown in Fig. 1.

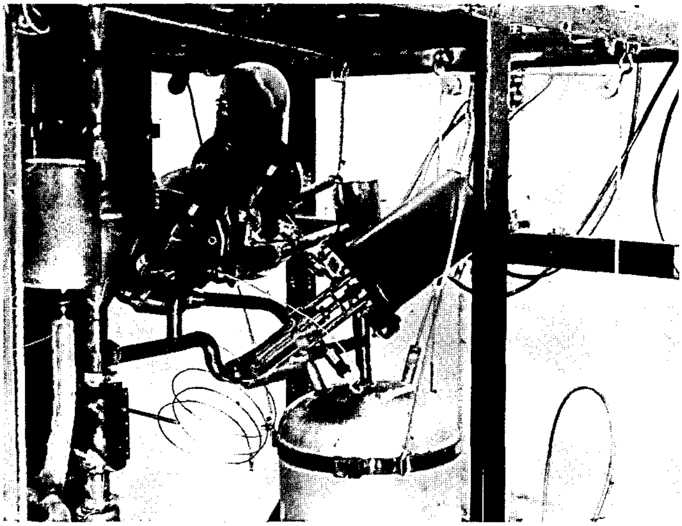

FIG. 5. Liquid sodium system

A photograph of the liquid sodium system is shown in Fig. 5, where the several components discussed above can be seen. The photograph was taken before insulating the different parts. Figure 6 shows the upper part of the test rig (vessel H in Fig. 1). This picture was taken before the constituent parts of the test rig were assembled. Figure 7 shows a magnified picture of the specimen set-up. The upper specimen holder contains three specimens with spherical ends, which vibrate against three flat lower specimens mounted in the cage. Dependent on the difference in coefficient of thermal expansion of the specimen material and that of the material of which the specimen holders are made, the specimens are either clasped in the specimen holders or slipped on pins made of specimen holder material.

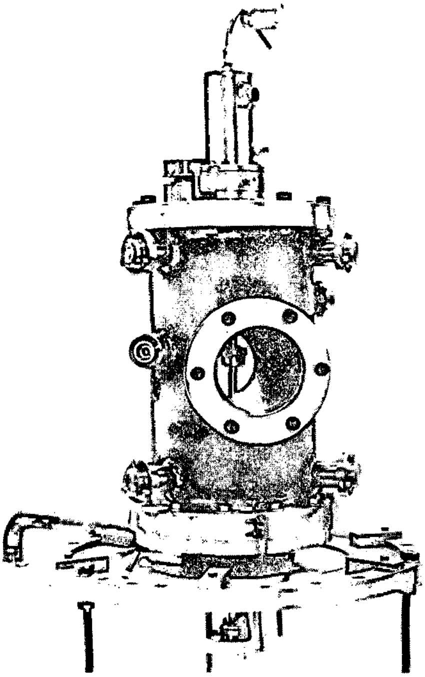

FIG. 6. Upper part of test rig, containing the vibrational movement systems

3. PERFORMANCE OF THE EXPERIMENTS

When an experiment is to be performed, the glovebox (J in Fig. 1) is placed on top of the machine. After the glovebox is evacuated and flushed with argon, the upper part of the machine is lifted up and the specimens are adjusted in the specimen holders. Special care is taken to ensure that the opposite specimens of all three specimen couples are in contact. After the test rig is closed again, the glovebox is removed, and the sodium in the dump tank is melted. The melting procedure can be followed by reading the output of thermocouples which are placed at different heights in the dump tank. In the meantime, the wall of the reaction vessel (A in Fig. 1) is heated up to a temperature of about 275°C. By regulating the cooling air, care is taken that the temperature of the upper part of the machine does not exceed 105°C. Vessel A is provided with three thermocouples. One of these measures the temperature of the wall. The other two thermocouples reach towards the centre of vessel A, one about 1 cm above the upper specimen holder, the other about 1 cm higher. If a wall temperature of 275°C is reached, the lower of these thermocouples reads about

175°C, while the higher thermocouple reads about 135°C. This is because there is a large heatflow to the upper part of the machine. While the melting of the sodium in the dump tank takes place, the other elements of the sodium system (filter, pipes and valves) are heated up to a temperature of approximately 150°C. When the system is in thermal equilibrium, the pressures in vessels A and C are adjusted at respectively 200-mm and 3000-mm water column. Next, the filling valve E (see Fig. 1) is opened and, because of the difference in pressure between dump tank and reaction vessel, the melted sodium is pressed into reaction vessel A. During the filling operation, which lasts about 10 min, the pressures of reaction vessel and dump tank are maintained at their initial values by hand control. Because the sodium level in vessel A rises fairly slowly, the sodium takes up a good deal of heat from the wall of A. It thus reaches the lower thermocouple in vessel A with a temperature of about 225°C. When the sodium touches the thermocouple, its thermovoltage increases sharply. This indicates that there is enough sodium in the reaction vessel. Filling-valve E is closed and overflow-valve F is opened. By this means the pressures of dump tank and reaction vessel are equalized. After the filling procedure is completed, the lower thermocouple in vessel A reads the sodium temperature (about 225°C) while the upper thermocouple in vessel A still reads about 135°C. This indicates that the level of the liquid sodium lies between the upper and the lower thermocouple. Next, the experimental temperature is set by adjusting the power supply of the heating elements which surround vessel A. Also, the temperature of the cold trap (B in Fig. 1) is adjusted. When the latter temperature is constant, the cold trap is allowed 24 h to establish oxygen equilibrium in the system (see also Section 4 below). Finally, the vibrational movements are started.

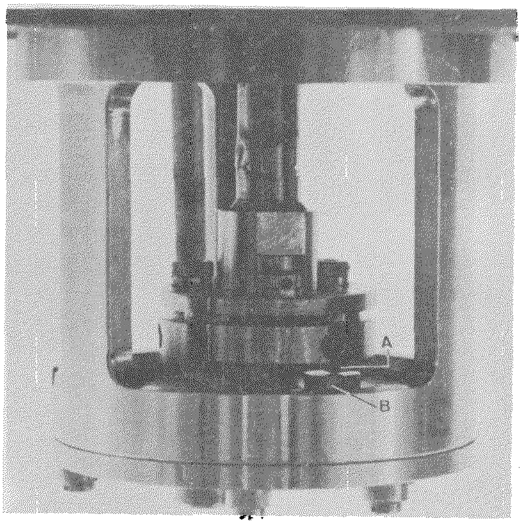

FIG. 7. Specimen set-up
A = upper specimen with spherical end
B = flat lower specimen

The experiments are terminated either when the wear of the specimen assembly reaches a pre-set value, measured by means of the differential transformer (14) in Fig. 2, or when a pre-set experiment duration is reached. If this happens, the vibrational movements are automatically stopped. Finally, the liquid sodium can be dumped from reaction vessel A into the dump tank by opening dump valve G.

4. PRELIMINARY EXPERIMENTS

Experimental conditions

As mentioned in Section 1, the test rig described will be used to perform merit-rating experiments under a variety of experimental conditions. These will probably be long-term experiments, lasting about a month each. In fact, because of the length of time that the experiments are expected to last, the test rig has been made in triplicate.

Nevertheless, the working of the machine was tested by performing a series of 24-h experiments with stabilized austenitic stainless steel X8CrNiMoVNb 16/13. The upper and lower specimens were made from this steel. The experiments were performed under the following experimental conditions:

Frequency of torsional vibration: 35 c/s;
Amplitude of torsional vibration: 50 μm;
Frequency of normal vibration: 40 c/s;
Amplitude of normal vibration (stroke): 60 μm;
Maximum normal load: 250 g;
Sodium temperatures: 450°C and 600°C;
Cold-trap temperatures: 150°C and 280°C.

According to Stang [3], the equilibrium sodium contents that correspond with these cold-trap temperatures are respectively 10 and 100 ppm. Although it is very much a question whether full equilibrium is attained in 24 h, the experimental results presented below indicate that the choice of a 24-h diffusion period may not be too bad.

Results

Figure 8 shows a specimen couple after termination of an experiment performed at a sodium temperature of 600°C and a cold-trap temperature of 280°C. From this figure it is clear that the specimens undergo a certain amount of wear. This wear proceeds by a mechanism of adhesion, small particles of one specimen being transferred to the surface of the opposite specimen by the formation of microwelds between the surfaces. This is clearly shown in Fig. 9, where a cross-section through the lower specimen can be seen. The picture shows a blob of adhering metal that was transferred from the upper specimen to the lower specimen. The weld between the transferred particle and the surface of the lower specimen is nearly perfect. A similar wear mechanism prevails for each combination of experimental temperatures. However, at a cold-trap temperature of 150°C no decrease in height of the specimen assembly, i.e. no volume wear, can be measured during the experiment, irrespective of the sodium temperature applied. This indicates that at 150°C cold-trap temperature (i.e. at a low oxide content) no wear debris is formed, although the contacting surfaces locally deteriorate because adhesion and weld formation occur. On the contrary, at 280°C cold-trap temperature (i.e. at a high

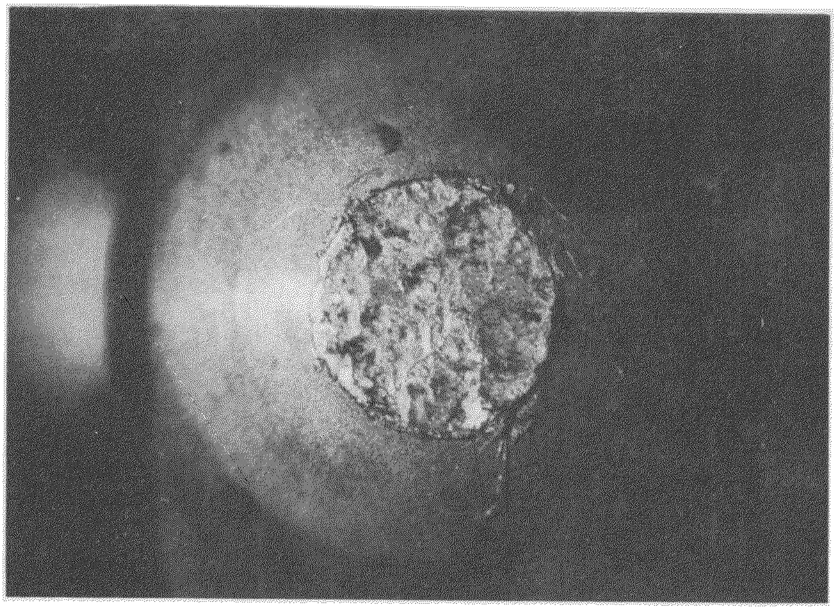

A

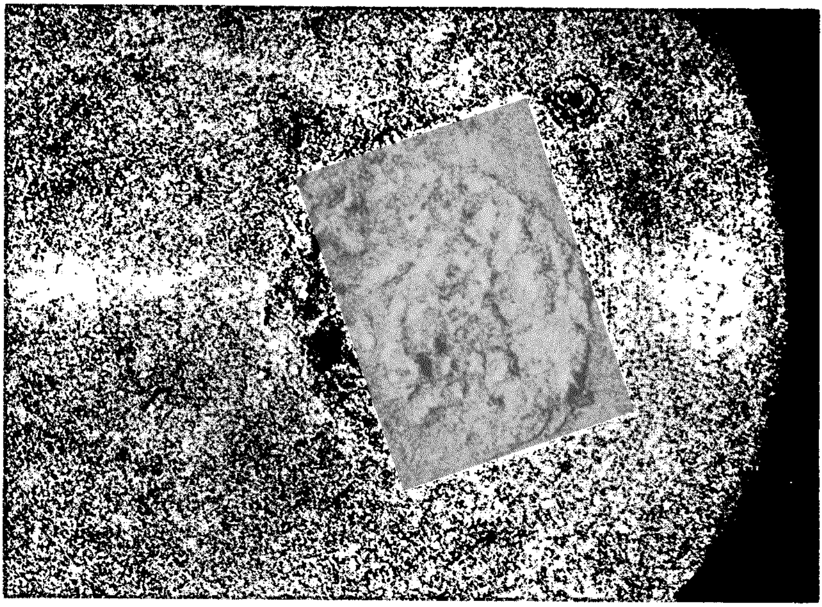

B

FIG. 8. Magnified picture of the opposite components of a specimen couple after termination of an experiment, performed at a sodium temperature of 600°C and a cold-trap temperature of 280°C (Magn. 15x)
A = upper specimen
B = lower specimen

oxide content) a measurable amount of specimen wear occurs. In fact, the total amount of volume wear that could be measured at 450°C, as well as at 600°C sodium temperature, was approximately 7.5×10^{-3} mm^3 in 24 h.

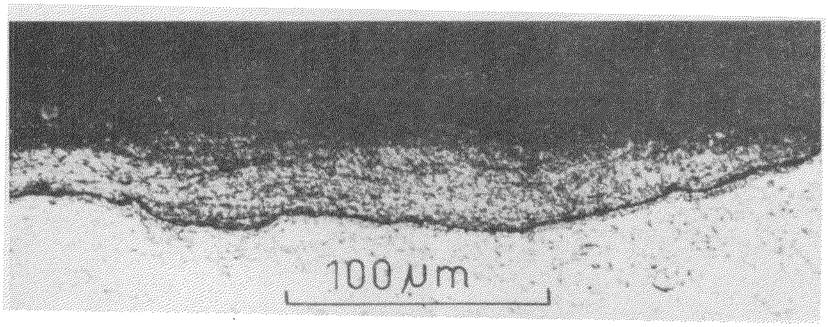

FIG. 9. Cross-section through the lower specimen shown in Fig. 8 (Magn. 350 x)

Discussion

From the above it can be concluded that the cold-trap temperature has an appreciable influence on the wear of stabilized austenitic stainless steel. Undoubtedly, this is due to a difference in oxide content of the sodium. Presumably, at 150°C cold-trap temperature the steel surfaces become completely deoxidized, which results in a very high adhesion at the points of transient contact between the specimens. Under these conditions, small particles are transferred back and forth between upper and lower specimens, without ever becoming loose wear debris. In constructions in which some surface deterioration can be tolerated, this type of "wear" may not be harmful. On the other hand, at 280°C cold-trap temperature, the contacting surfaces are probably never entirely devoid of oxide, which may result in a considerable reduction in "residence time" of the transferred particles, and thus give rise to volume wear.

Apart from the above, the results are indicative of the fact that a diffusion period of 24 h is sufficient to change the oxygen content of the sodium markedly. This is an encouraging finding, especially as reliable measurements of the oxide content of the sodium are extremely difficult, if not entirely impossible.

Somewhat surprisingly, the temperature of the sodium does not seem to influence the wear of the steel to any appreciable extent, which is in marked contrast to the findings of others who performed experiments under conditions of sliding (cf. Refs [1] and [2]). However, more experimental results will be needed to verify this point.

ACKNOWLEDGEMENTS

The work was performed under the auspices of the Association Euratom-TNO/RCN on Fast Reactors, on behalf of the TNO-Neratoom Sodium Technology Project. The authors are indebted to C. Th. M. Koop and C. van der Lingen, who assisted in the design and testing of the apparatus.

REFERENCES

[1] ANDERSON, W.J., "Lubrication of bearings with liquid metals", Advanced Bearing Technology, NASA, Washington, D.C. (1964).

[2] ROBERTS, W.H., Proc. Instn Mech. Engrs Conference on non-conventional lubricants and bearing materials, Manchester (1962).

[3] STANG, J.H., Corrosion by liquid metals, Reactor Mater. 9 1 (1966) 39.

CONTROL, MEASUREMENT AND REMOVAL OF IMPURITIES
(Sessions VI and VII)

A COMPARISON OF THREE METHODS OF OXYGEN CONCENTRATION MEASUREMENT IN SODIUM*

C.C. McPHEETERS AND J.M. WILLIAMS
LOS ALAMOS SCIENTIFIC LABORATORY,
UNIVERSITY OF CALIFORNIA,
LOS ALAMOS, CALIF.,
UNITED STATES OF AMERICA

Abstract

A COMPARISON OF THREE METHODS OF OXYGEN CONCENTRATION MEASUREMENT IN SODIUM. Two electrochemical oxygen meters, an AC resistivity meter, and a vacuum distillation sodium sampler were tested to determine their sensitivities and responses to oxygen concentration changes in sodium. These tests were conducted on an isothermal, forced convection sodium loop of large volume; a bypass cold trap provided for oxygen concentration control. A vacuum distillation analytical technique was used as the primary standard for measurement of the oxygen concentration.

Experimentally determined calibration curves for the electrochemical cells agree closely with the theoretical predictions in the slope, but the EMF values were approximately 85% of theoretical. The low EMF values were probably due to partial electronic conduction in the ceramic electrolyte. Temperature coefficients of the two oxygen meters were found to be 1.15 mV/°C and 1.05 mV/°C.

The AC resistivity meter was calibrated by comparing per cent resistivity with vacuum distillation and analyses. The meter was found to have an oxygen concentration dependence of 0.0070% resistivity change per ppm weight change in oxygen concentration, compared with the predicted value of 0.01%. Later in the experiment this dependence was found to be 0.0139% resistivity change per ppm oxygen. This shift is attributed to the effect of other impurities added to the system.

To determine the response times of the oxygen meters and the resistivity meter, a step change was made in the cold-trap temperature. Within the error of the measurements, all instruments responded in good agreement with the vacuum distillation analyses. The total time elapsed from the beginning of the concentration transient to system equilibrium was 130 ± 10 h.

As a demonstration of engineering use of these instruments, the results of this transient test were used to calculate the efficiency for oxygen addition to the system from the cold trap. This efficiency was found to be 20%.

1. INTRODUCTION

1.1. Objectives

When sodium is used as a coolant in high-temperature nuclear reactors that utilize refractory metals for fuel containment or as structural materials, it is necessary to maintain low oxygen concentration (a few ppm) in the sodium to minimize corrosion of these materials. Oxygen concentration may be controlled at these low levels by various methods for continuous purification of the sodium. The effectiveness of sodium purification systems must be maintained by continuous or periodic measurement devices.

---

* Work performed under the auspices of the United States Atomic Energy Commission, Contract N. W-7405-Eng. 36.

The object of this study was to evaluate two continuous oxygen monitoring devices, the electrochemical cell and the AC resistivity meter. Oxygen concentrations as indicated by these instruments were compared with oxygen concentration determined by the vacuum distillation technique for oxygen in sodium under steady-state and transient conditions.

1.2. Principles of operation

1.2.1. Electrochemical oxygen meter

The oxygen meter is an electrolytic cell that utilizes a ceramic electrolyte and a metal-metal oxide reference electrode [1, 2]. The ceramic electrolyte is immersed in flowing sodium containing dissolved oxygen to be analysed. The EMF produced by the electrolytic cell is proportional to the logarithm of oxygen concentration.

The ceramic electrolyte used in the oxygen meter is ThO_2-$15Y_2O_3$ [3]. This ceramic was chosen because of its high ionic conductivity. (Equations derived to describe the EMF generated by an electrolytic cell neglect electronic conduction. Any electronic conductivity present in the cell will reduce the theoretical EMF.)

Using Cu-Cu_2O powder as the reference electrode the electrolytic cell can be represented by

$$\mathrm{Cu, Cu_2O} \mid \mathrm{ThO_2\text{-}15Y_2O_3} \mid \mathrm{Na_2O, Na} \qquad (1)$$

The EMF produced can be represented by the equation [4]

$$E = E_0 - 0.099\ T \log C/C_0 \qquad (2)$$

where

E = cell EMF, mV

E_0 = standard cell EMF, mV

T = temperature, °K

C = oxygen concentration, ppm by weight

C_0 = saturation oxygen concentration, ppm, at temperature T.

The cell temperature in this experiment was 575°K so that the expression becomes (see Appendix A) in volts

$$E = 1.228 - 0.057 \log C \qquad (3)$$

The expected temperature coefficient of the oxygen meter can be determined by differentiating Eq. (2) with respect to temperature at constant oxygen concentration (see Appendix A)

$$\frac{dE}{dT} = 0.472 - 0.099 \log C \qquad (4)$$

1.2.2. Resistivity meter

Balke [5] predicts that the resistivity of sodium as a function of temperature and impurity concentration can be approximated by the expression

$$\rho = 5.17\ (1 + 0.00263\Delta + 0.0001C)\ \mu\Omega\text{-in.} \qquad (5)$$

where

ρ = the resistivity in $\mu\ \Omega$-in.
Δ = (T - 200) in °C
C = impurity (oxygen) concentration in ppm by weight.

The concentration coefficient of resistivity in this expression of 10^{-4} was empirically estimated and does not imply experimental determination of this parameter in any liquid metal. Equation (5) implies that the change in sodium resistivity due to a 1 deg C change in temperature is equivalent to an increment of 26.3 ppm of impurities (i.e. a sensitivity of 1 ppm requires the temperature to be stable within 0.04°C).

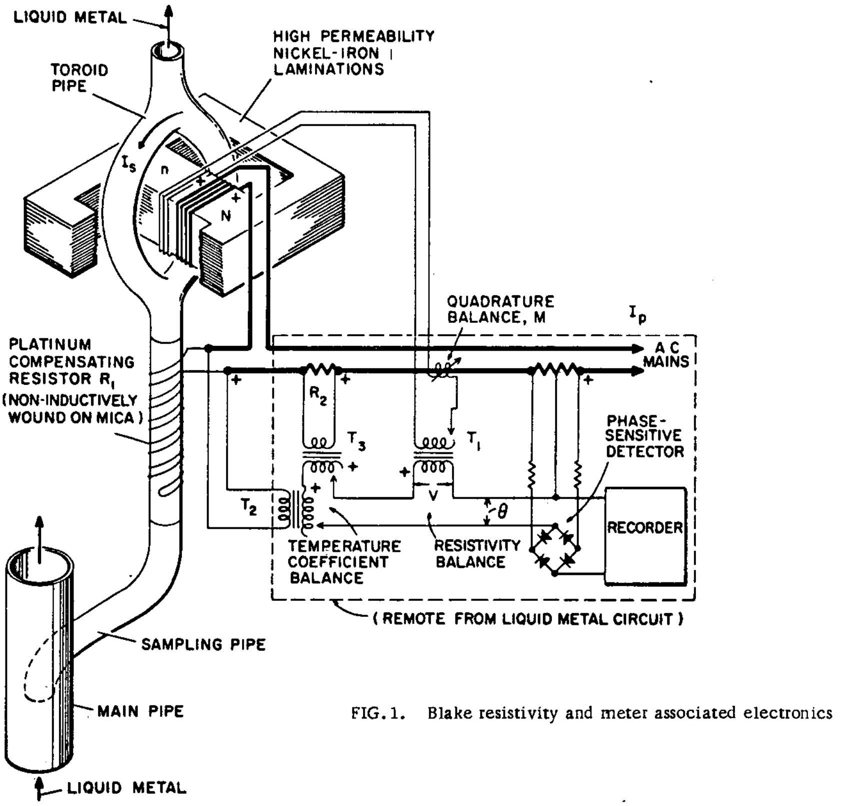

FIG. 1. Blake resistivity and meter associated electronics

The rhometer operates on the principle (discussed thoroughly elsewhere [5-7] of a current transformer in which flowing sodium is coupled with the transformer as shown in Fig. 1. The effect of resistivity change in sodium on transformer characteristics is determined by comparing the phase of alternating current in the secondary winding (probe coil) with the phase of alternating current derived from the primary winding in a phase-sensitive rectifier circuit. The magnitude of the phase shift caused by a change in sodium resistivity is a measure of the change in impurity concentration (or temperature). A judiciously selected resistance that responds to changes in sodium temperature (see Fig. 1) is incorporated into the rhometer circuitry in an attempt to nullify the effect of temperature fluctuations.

Meter readings are expressed as per cent resistivity (%r) and for pure sodium should be 100%r. As will be seen later, the resistivity of pure sodium, as determined by the rhometer used in this study, was ~ 99.85%r. Hereafter in this report, resistivity meter reading as %r is used as distinguished from resistivity, ρ, in Eq. (5).

1.2.3. Vacuum distillation sampler

The vacuum distillation technique is the only method of chemical analysis currently used at LASL for determining oxygen in sodium [8-10]. In this method, a sample of liquid sodium is drawn into a heated cup in a vacuum chamber (see Fig. 2). The sodium metal is evaporated, at a pressure of less than 5 μmHg, from its non-volatile residue, which is subsequently dissolved in an acid solution. This solution is analysed spectrophotometrically for sodium. The amount of oxygen present in the sample (residue) is calculated on the basis that it is all combined as Na_2O with the measured quantity of sodium.

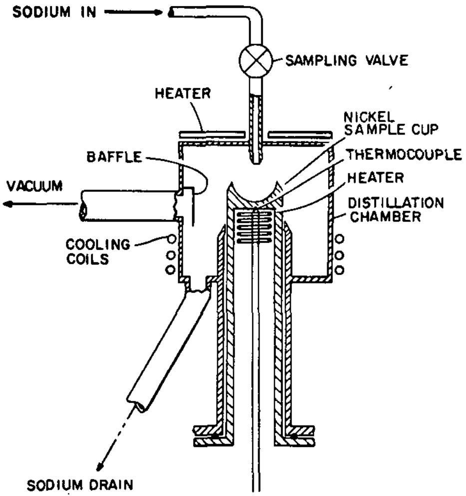

FIG. 2. Vacuum distillation sampler for analysis of oxygen in sodium

The analytical equipment used for these determinations was substantially that described by Humphreys [8]. Vacuum distillation as an analytical technique for oxygen determination in sodium in the 1-10 ppm range is believed to be the most reliable analytical method for oxygen.

2. SUMMARY

Oxygen concentration in a sodium loop was cycled from 1 ppm to 30 ppm to 1 ppm. During this cycle, oxygen concentration measurements were made and the indications of the instruments were compared. Experimentally determined calibration curves for the electrochemical cells agree closely with the theoretical predictions in slope, but the EMF values were approximately 85% of theoretical. The low EMF values were probably due to the effect of partial electronic conduction in the ceramic electrolyte.

Temperature coefficients of the two oxygen meters were 1.15 mV/°C and 1.05 mV/°C. These temperature coefficients are in fair agreement with the 0.94 mV/°C reported by B. Minushkin [2]. The theoretical value was 0.373 mV/°C.

The AC resistivity meter was calibrated by comparing change in sodium resistivity with vacuum distillation analyses. The meter was found to have an oxygen concentration dependence of 0.0070% resistivity change per ppm change in oxygen concentration, compared to the predicted value of 0.01%.

To determine the response times of the oxygen meters and the resistivity meter, a step change was made in the cold-trap temperature from 130°C to 200°C. Within the error of the measurements, all instruments responded in good agreement with the vacuum distillation analyses. The total time elapsed from the beginning of the concentration transient to attainment of system equilibrium was 130 ± 10 h. The results of this transient test indicated that the cold-trap efficiency for oxygen addition to the sodium system was 20%, and the dissolution rate constant for oxygen removal from the cold trap was estimated.

3. THE EXPERIMENT

3.1. Arrangement and procedure

3.1.1. Sodium loop test

Two oxygen meters (designated TP-20 and TP-22), an AC resistivity meter and a vacuum distillation sodium sampler were installed in a large sodium loop, shown schematically in Fig. 3. The loop contained approximately 600 gal of sodium in a carbon steel tank operating at an average temperature of 300°C. An electromagnetic pump provided a nominal 8 gal/min flow to the AC resistivity meter located in the main sodium circuit. The oxygen meters and the distillation sampler were located in series on a 1 gal/min isothermal bypass line.

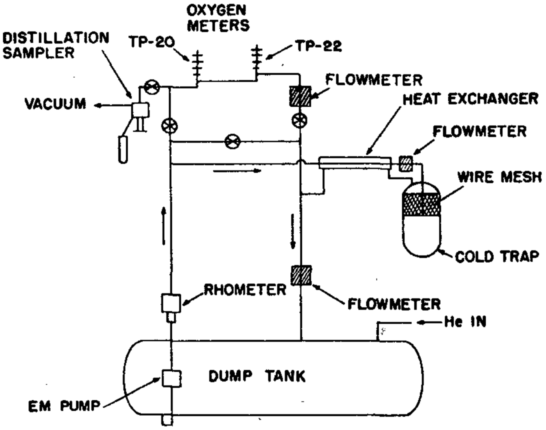

FIG. 3. Schematic of sodium test loop

Oxygen concentration was controlled with a cold trap located in a bypass line at the end of a counter-current heat exchanger. The cold-trap volume was 9.25 gal. At a flow rate through the cold trap of 1.8 gal/min, the residence time in the cold trap was 5 min. Approximately one hundred (100) square feet of stainless-steel surface area in mesh form was located in the top half of the cold trap. Over the 3600 h duration of this experiment, oxygen concentration was maintained at various levels by controlling cold-trap temperature. This method of oxygen concentration control provided a range of concentrations between 1 and 30 ppm oxygen indicating that an adequate supply of oxygen was available in the cold trap.

3.1.2. Electrochemical oxygen meters

The electrochemical oxygen meter consists of a closed end ThO_2-$15Y_2O_3$ ceramic tube inside of which a copper electrode contacts a Cu-Cu_2O powder mixture (see Fig. 4). The ceramic tube is positioned in a stainless-steel pipe cross such that the closed end of the tube is in the approximate centre of the cross. Sodium enters the bottom leg of the cross and exits through a side leg, and the other side leg is blanked off. The ceramic tube is sealed into the sodium with a frozen sodium seal in a finned tube above the stainless-steel cross. The inside of the cell is sealed from the atmosphere with a series of O-rings.

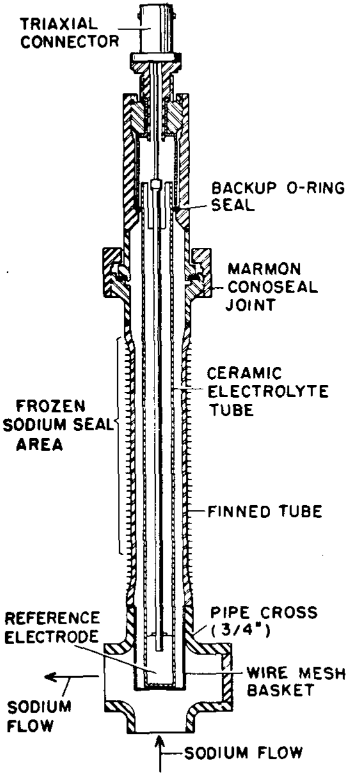

FIG. 4. Electrochemical cell

Two stainless-steel pipe crosses, pre-assembled to the finned tubes, were welded into the sodium loop. Steel rods of the approximate diameter of the ceramic tubes were placed in the finned tubes to create a void when the line was filled; then the line was evacuated, filled with sodium and frozen. The finned tubes were heated and the rods were removed under a flow of argon. While the sodium in the finned tube was molten, the ceramic tubes were lowered into position very slowly to prevent thermal shock to this fragile material. When the tubes were in place and sealed, the sodium in the oxygen meter line was melted and raised to the system temperature at which point flow was initiated. No difficulty was encountered during the oxygen meter installation.

The oxygen meters were maintained at 300°C over most of the testing period, although temperature variations were made at constant oxygen concentration in order to determine temperature coefficients. The EMF readings were made with an instrument package which consisted of a constant voltage source and a voltage divider in conjunction with an electrometer used as a null indicator. The electrometer was equipped with a recorder output for continuous monitoring of the oxygen meters.

3.1.3. Resistivity meter

The resistivity meter used in this experiment was purchased from the Bruce Peebles Co., Ltd. of Edingburgh, United Kingdom, with the following minor modification. Contacts on the temperature compensator and resistivity decade switches were rhodium plated to minimize changes in contact resistance due to oxidation, thus avoiding the necessity for frequent cleaning of contacts. The resistivity meter was installed in the main sodium circuit where it operated with 8 gal/min sodium flow at a nominal temperature of 295°C. The instrument package was set up in accordance with the manufacturer's instructions and the phase-sensitive rectifier was balanced using an oscilloscope to monitor and balance the wave form observed at the output of the phase rectifier. Resistivity readings were obtained by using a potentiometric recorder as a null indicator and adjusting the recorder reading to zero with the decade switches.

3.1.4. Vacuum distillation sampler

The vacuum distillation sodium sampler was located upstream from the oxygen meters. The sample line was a $\frac{1}{4}$-in. O.D. stainless-steel tube with 0.065-in. wall thickness, the inlet of which was positioned in the centre of the flowing stream. The sample tube length was 30 in. Its internal volume was 5.6 cm^3 and that of the sample cup was 5 cm^3. Both were flushed with approximately 50 cm^3 of sodium before collection of the sample; thus, the sodium samples were representative of the sodium stream.

The distillation chamber consisted of a closed stainless-steel cylinder; the sample line entered at the top. A drain line was provided in the bottom and a vacuum line in the side of the chamber. Figure 2 shows the distillation chamber with a sample cup in position. Sodium samples were drawn from the sodium loop into the hot (450°C) sample cup until the cup had overflowed approximately 50 cm^3. At this point, the sample line was valved off and frozen quickly by a water cooling. The sample cup was maintained at a distillation temperature of 400°C and pressure of less than 5 μmHg until distillation was complete. (This was signified by the end of the thermal arrest.) The entire sampler was then cooled to room temperature, and the sample cup was removed while purging with argon to prevent introduction of oxygen into the system. Distillation residues in the cup were dissolved with 0.01 N HCl solution and were analysed spectrophotometrically for sodium content. It is assumed that sodium in the residue was in the form of Na_2O before dissolution and oxygen concentrations were calculated on this basis.

During studies of concentration transients, samples for the distillation analysis were obtained twice daily. The distillation analysis procedure included monitoring on a routine basis for the presence of an analytical blank (or bias). This was accomplished by heating the sample cup in the distillation chamber without drawing or distilling a sodium sample; the cup was then put through the standard residue-dissolving and analytical procedures.

3.1.5. Transient tests

In order to evaluate the response of each instrument to oxygen concentration transients, the concentration was increased by raising the cold-trap temperature to a preselected value. The rate of rise of oxygen concentration was measured by each instrument until steady-state conditions were achieved. The cold-trap temperature change approximated a step function (~ 100°C in 2 h) compared with the change in system concentration of 10 ppm in 5-6 days.

3.2. Results

3.2.1. Electrochemical oxygen meter

Temperature Coefficients. According to Eq.(4) the temperature coefficient of the oxygen meter should be a function of oxygen concentration. However, Minushkin [2] reported that the temperature coefficient was independent of concentration and was constant at 0.94 mV/°C. His value was determined by testing several oxygen meters over a range of concentrations and temperatures. The temperature coefficients of oxygen meters TP-20 and TP-22 were determined by changing their temperatures at constant system oxygen concentration. The temperature coefficients were found to be 1.15 mV/°C and 1.05 mV/°C for TP-20 and TP-22 respectively. Figure 5 shows the data from which these coefficients were determined. Although the coefficients reported are approximately three times the value predicted by theory (0.373 mV/°C), they are in fair agreement with the value reported by Minushkin. In the case of TP-20 (1.15 mV/°C), a temperature change of 10°C causes a voltage change of 11.5 mV, which is equivalent to an indicated oxygen concentration change of ~36%.

Meter Calibration. The nominal operating temperature of the oxygen meters in this test was 300°C. All oxygen meter EMF readings were corrected to this temperature by applying the appropriate temperature coefficients. Meter readings and distillation samples were taken concurrently. Plots of log concentration versus meter EMF are shown in Fig. 6. The least-squares fit of the data for oxygen meter TP-20 is described by the equation

$$E = 1.038 - 0.057 \log C \tag{6}$$

The equation for TP-22 is

$$E = 1.077 - 0.067 \log C \qquad (7)$$

Equations (6) and (7) can be compared with Eq.(3) which describes the theoretical EMF. Meter TP-20 had a calibration curve whose slope was

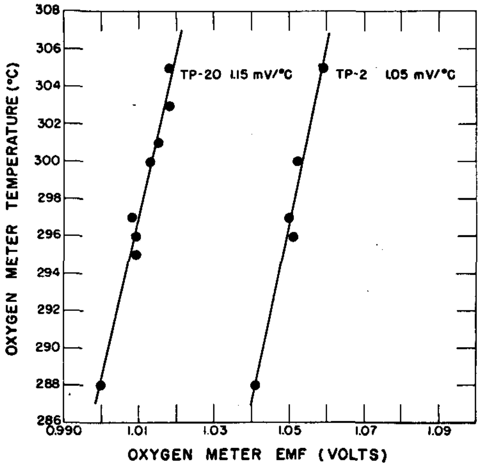

FIG. 5. Oxygen meter temperature coefficients

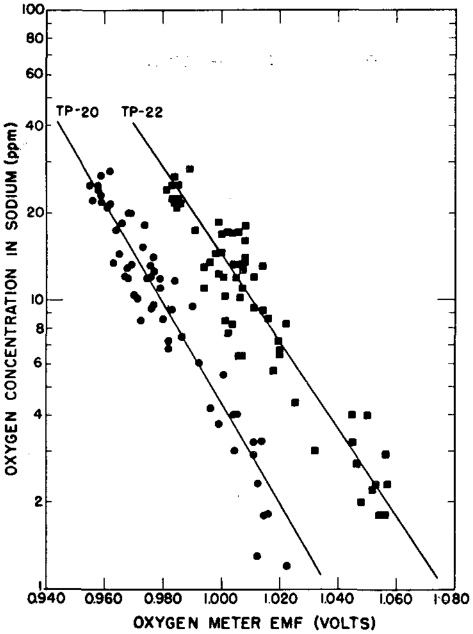

FIG. 6. Oxygen meter calibration curves

in excellent agreement with the theoretical slope and TP-22 had a slope that was 18% greater than theoretical. This deviation from theoretical represents a 30% error in indicated oxygen concentration.

A problem encountered in this test was the apparent dependence of meter EMF upon ambient air temperature. Ambient air temperatures fluctuated at times by as much as ± 17°C, and this variation caused meter EMF fluctuations of as much as ± 8 mV. Low EMF values corresponded to high room temperatures. The ± 8 mV fluctuations correspond to ± 30% fluctuations in indicated oxygen concentrations.

3.2.2. Resistivity meter

Temperature compensator calibration. The temperature dependence of the rhometer was determined by slowly varying loop temperature at a constant cold-trap temperature of 115°C. At each temperature, per cent resistivity was recorded for various temperature compensator settings. The necessary minima were not readily determined in the coarse temperature compensator calibration shown in Fig. 7, but the compensator settings at which more careful data were taken were determined. It was intended that this experiment should be conducted near 300°C (for optimum electrochemical cell operation), and since for this rhometer the temperature compensator range was limited to a maximum setting of 230 × 10^{-5}%r/°C,

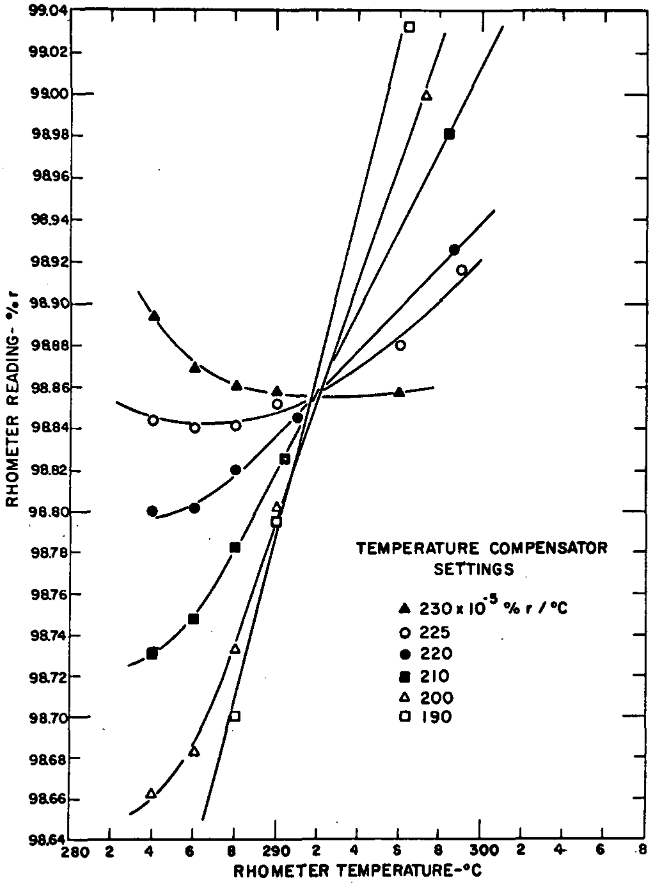

FIG. 7. Preliminary resistivity meter temperature compensator calibration

the temperature calibration was confined to the range between 288 and 298°C. Figure 8 shows the final temperature compensator calibration data and illustrates the precision with which resistivity readings were taken.

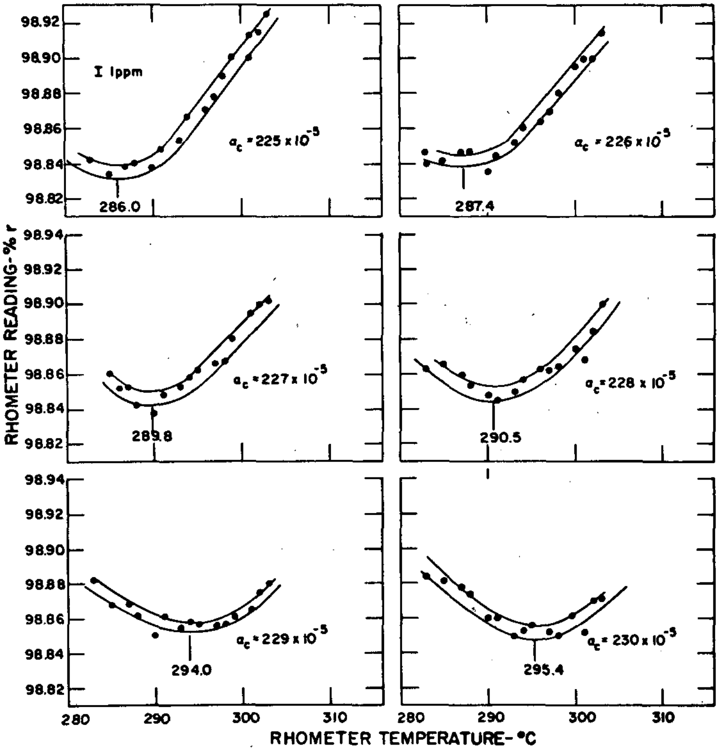

FIG. 8. Final resistivity temperature compensator calibration

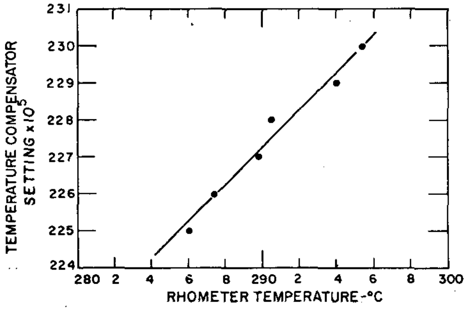

FIG. 9. Rhometer temperature compensator setting as a function of temperature

A plot of idealized temperature compensator setting as a function of rhometer temperature is shown in Fig. 9. A temperature compensator setting of 229 × 10^{-5}%r/°C was used during the experiments reported here.

Resistivity meter calibration. As with the oxygen meter calibration, rhometer readings were taken each time sodium distillation samples were drawn. Over the period of this experiment, a drift in the concentration coefficient of resistivity was observed. The shift in calibration was not sudden, but it appears to have occurred during the time when the system concentration was high. The data were divided into two groups, before and after the high concentration phase of the experiment. A least-squares fit to these data are represented by two equations (see Fig. 10).

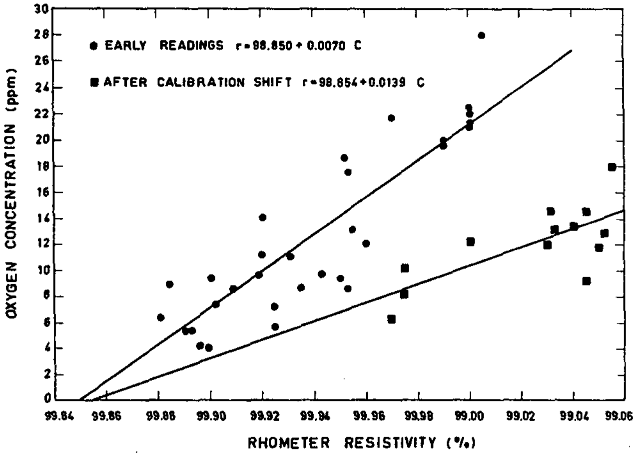

FIG. 10. Rhometer calibration curves

Before high-concentration phase:

$$r = 98.850 + 0.0070\ C \qquad (8a)$$

After high-concentration phase:

$$r = 98.854 + 0.0139\ C \qquad (8b)$$

where

r = indicated resistivity, per cent
C = oxygen concentration, ppm oxygen by weight.

The sensitivity of the rhometer, represented by Eq. (8a), was 0.007%r per ppm oxygen. This compares favourably with a value of 0.0068% per ppm H_2O[1] reported by APDA [7]. The rhometer sensitivity predicted by Blake for any impurity was 0.01% per ppm. The apparent increase in sensitivity described by Eq. (8b) was outside the statistical spread in the data and cannot be discounted. It should be noted here that Eq. (5) can apply to any impurity and that impurities may be additive. The rhometer measures only the net change in total impurities and other methods are required to determine which specific impurities are changing and in what direction. Therefore it is suggested that the observed, apparent increase in oxygen concentration dependence can be attributed to the presence of other impurities (such as iron or its oxides) which appeared during the course of this experiment. The agreement between the

---

[1] APDA quantitatively added H_2O to sodium to study rhometer response. This is assumed equivalent to ppm oxygen.

resistivity of pure sodium (98.850 versus 98.854) implied by Eqs (8a) and (8b) should not be overlooked, although this result may be fortuitous, considering the spread of resistivity data. This agreement lends credence to the hypothesis that the "concentration shift" was a real impurity effect.

3.2.3. Concentration transients

The responses of the instruments to an increase in oxygen concentration are shown in Fig. 11. Figure 12 shows the increase in oxygen concentration as indicated by each instrument on a dimensionless log scale

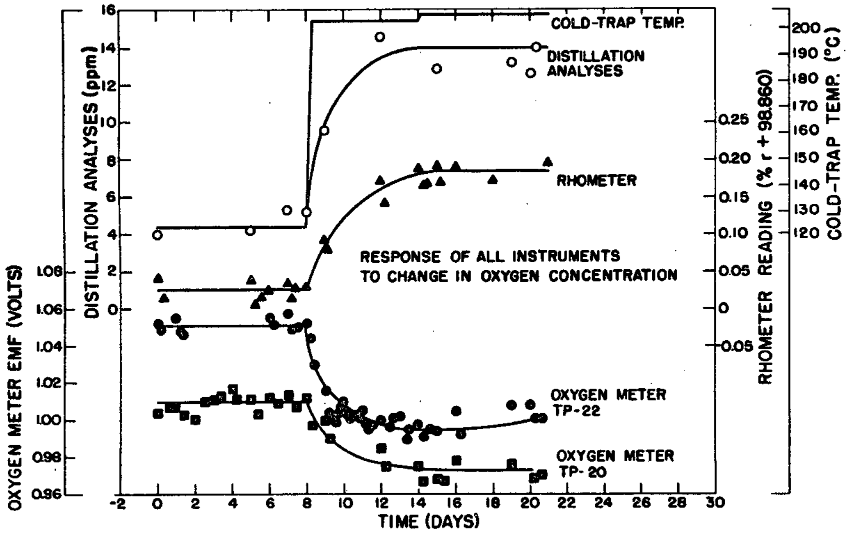

FIG. 11. Response of the rhometer and oxygen meters to a step change in cold-trap temperature

versus time. The dimensionless quantity is $(C-C_0)/(C_f-C_0)$: where C = instrument indication at any time, C_0 = initial instrument indication, and C_f = final instrument indication. Each of these instruments indicated that the new equilibrium was reached in approximately 130 h. It can be said, therefore, that the time constants of these instruments, which were indistinguishable within experimental error, are small compared with the time constant of the sodium system.

As a demonstration of the application of calibrated oxygen monitoring devices, a simple expression for describing transient behaviour of a cold trap was developed (see Appendix B). Results of the theoretically predicted performance of the cold trap used in this experiment appear in Fig. 12. The dissolution constant used was $k = 2.9 \times 10^{-4}$ g Na cm^{-2} s^{-1}.

4. CONCLUSIONS

4.1. Electrochemical oxygen meters

1. The EMF cells used in this study differed slightly in both temperature coefficient and calibration. The slopes of both calibration curves were in good agreement with theoretical values; however, the magnitude of

the EMF's were lower than theory predicts. This deviation from theory is attributed to electronic conduction in the ceramic electrolyte, which partially short-circuited the cell EMF.

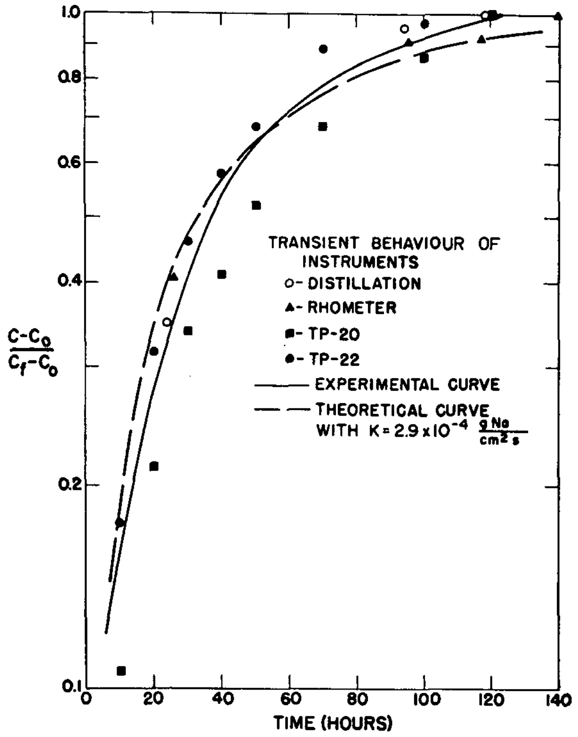

FIG. 12. Comparison of the response shown in Fig. 11 with a theoretically predicted curve

2. Calibrated oxygen meters are capable of measuring oxygen concentration accurately (± 10%) in the range 1-30 ppm oxygen. Uncalibrated oxygen meters may deviate from theoretical predications by as much as 30% of indicated oxygen concentration.
3. Short-term stability of the oxygen meter is limited by its sensitivity to ambient temperature fluctuations. Under controlled ambient conditions the accuracy in conclusion (2) can be realized. During the 3600-h duration of this study no long-term deviations were detected in meter calibration. After 5000 h of continuous operation the oxygen meters appear to be performing satisfactorily.

4.2. Resistivity meter

1. Under ideal conditions, a change in resistivity of 0.01%r (equivalent to ~ 1.4 ppm ΔC in Eq. (8a)) can be detected with the AC rhometer. Over a long term, it is doubtful that resistivity changes below 0.03%r (equivalent to ~ 5 ppm ΔC in Eq. (8a)) could be considered significant. Therefore, it is concluded that the rhometer is of limited value in application as an oxygen monitoring device in typical sodium coolant systems.

2. There is every reason to expect that the presence of a combination of impurities in sodium can result in a spectrum of resistivity readings for a system containing constant oxygen content. The anomalous results from this instrument during two phases of this experiment illustrate this point. The occurrence of mass transfer in a rhometer-monitored sodium circuit could be expected to produce results, which if improperly interpreted, would lead to erroneous conclusions.
3. The major advantage of the rhometer as applied to engineering sodium coolant systems would be as a device for observing transient phenomena. Gas entrainment and particulate entrainment effects are readily apparent in the rhometer signal. The instantaneous response of the rhometer to changes in impurities in the sodium coolant would be particularly useful as an alarm signal.

4.3. Vacuum distillation analysis

As stated earlier, the sampler apparatus used in this study was that described by Humphreys [8]. Major refinements have recently been made in the vacuum distillation analysis technique [9, 10] so that much better results are attainable. With equipment used in this experiment oxygen concentration was measured to within an estimated error of ± 2.5 ppm. Later models of vacuum distillation apparatus are able to reduce this error to ± 0.5 ppm.

APPENDIX A

ELECTROCHEMICAL CELL EQUATIONS

The galvanic cell under consideration can be represented

$$\mathrm{Cu,\ Cu_2O}\,|\,\mathrm{ThO_2 - 15Y_2O_3}\,|\,\mathrm{Na,\ Na_2O,\ dissolved}$$

Cu, Cu_2O is the reference electrode and Na_2O, dissolved, is sodium monoxide dissolved in sodium. The half-cell reactions are

$$\mathrm{O^{2-} + 2\ Na = Na_2O,\ dissolved + 2e^-}$$

and

$$\mathrm{Cu_2O + 2e^- = 2\ Cu + O^{2-}}$$

The voltage generated by this cell is given by the equation

$$E = E_0 - \frac{RT}{nF} \ell n\ K \qquad \text{(A-1)}$$

where

E = cell potential in volts
E_0 = standard potential in volts
R = 8.31 V-C-g-mole^{-1} °K^{-1}
T = absolute temperature, °K

n = 2 g-equivalents-g-mole^{-1}
F = 96 500-C-g-equivalent^{-1}
K = equilibrium constant.

The equilibrium constant, K, can be expressed:

$$K = \frac{\alpha^2_{Cu}\ \alpha_{Na_2O,\ dissolved}}{\alpha^2_{Na}\ \alpha_{Cu_2O}} = \frac{1^2\ \alpha_{Na_2O,\ dissolved}}{1^2\ 1} \qquad \text{(A-2)}$$

Assuming the relationship between dissolved sodium oxide activity and concentration

$$\alpha_{Na_2O,\ dissolved} = \gamma C \qquad \text{(A-3)}$$

where

$\alpha_{Na_2O,\ dissolved}$ = activity of dissolved Na_2O in sodium

γ = activity coefficient

C = concentration of Na_2O in sodium.

If C_0 is the saturation sodium monoxide concentration in sodium at any temperature, T, and since the activity of sodium monoxide in saturated sodium solution is unity, it follows that

$$\gamma = \frac{1}{C_0} \qquad \text{(A-4)}$$

Combining Eqs (A-2), (A-3) and (A-4) in (A-1)

$$E = E_0 - 9.914 \times 10^{-5}\ T \log \left(\frac{C}{C_0}\right) \qquad \text{(A-5)}$$

which is Eq.(2) in the text with units of volts.

The most accurate oxygen solubility data at present available is that of Rutkauskas [10] which is described by the equation

$$\log C_0 = 8.25 - 3499/T \ \text{ppm oxygen in sodium} \qquad \text{(A-6)}$$

The standard potential E_0 can be calculated from the free energies of formation of Cu_2O and Na_2O:

$$E_0 = \frac{\Delta F^f_{Cu_2O} - \Delta F^f_{Na_2O}}{n\underline{F}} \qquad \text{(A-7)}$$

where

ΔF^f_A = free energy of formation of species A at temperature, T(°K)

n = 2-g-equivalents-g-mole^{-1}

$\underline{F}$ = 23 086-cal-g-equivalent^{-1}V^{-1} .

Substituting thermodynamic data from Glassner [11] at 575°K

$$E_0 = \frac{80\,000 - 29\,500}{46\,170} = 1.094\ V$$

Substituting for E_0 and C_0 at 575°K in Eq.(A-5)

$$E = 1.228 - 0.057 \log C \tag{A-8}$$

which is Eq.(3) in the main text.

The temperature coefficient of the electrochemical cell can be estimated by differentiating Eq.(A-5) with respect to temperature at constant oxygen concentration. The result in mV is

$$\frac{dE}{dt} = \frac{dE_0}{dt} - 0.099 \log C + 0.099 \frac{d}{dT}(8.25\ T - 3499) \tag{A-9}$$

Now, $\frac{dE}{dt}$ can be approximated by using Eq.(A-7) as follows

$$\frac{dE_0}{dt} = \frac{E_0(T_1) - E_0(T_2)}{T_1 - T_2} = -0.346 \times 10^{-3}\ \text{V}.$$

The equation for meter temperature coefficient in mV/°C becomes

$$\frac{dE}{dt} = 0.472 - 0.099 \log C \tag{A-10}$$

which is Eq.(4) in this report.

APPENDIX B

COLD-TRAP KINETIC PERFORMANCE PREDICTION

Assume that a cold trap can be represented as a chamber containing a known internal surface area, A, into which sodium containing system-oxygen concentration, C, enters, becomes perfectly mixed, attains the cold-trap concentration, C_c, then leaves the cold trap at C_c; the rate, R, at which oxygen is removed by the cold trap is given by the equations

$$R = kA\ (C_c - C_f) \tag{B-1}$$

$$R = W\ (C - C_c) \text{ and} \tag{B-2}$$

$$R = -M \frac{dC}{dt} \tag{B-3}$$

where

R = oxygen transfer rate, g O/s

k = oxygen dissolution or precipitation rate constant g Na $cm^{-2}\ s^{-1}$

A = internal cold-trap surface area, cm^2

C_f = final (or equilibrium) system oxygen concentration, g O/g Na

C_c = mixed cold-trap oxygen concentration, g O/g Na

C = system oxygen concentration, g O/g Na

W = sodium flow rate in cold trap, g Na/s
t = time from cold-trap temperature change, s
M = system sodium mass, g Na.

Equation (B-1) gives the oxygen transfer rate in terms of the concentration gradient driving force, and Eqs (B-2) and (B-3) are mass balance equations. Combining Eqs (B-1), (B-2) and (B-3)

$$\frac{dC}{dt} = \frac{1}{(W/kA) + 1}\left(\frac{W}{M}\right)(C_f - C) \tag{B-4}$$

which upon integration becomes

$$\ell n(C_f - C) = -\frac{1}{(W/kA) + 1}\left(\frac{W}{M}\right)t + \text{constant} \tag{B-5}$$

Applying the condition that at t = O, $C = C_0$ then the constant becomes $\ell n(C_f - C_0)$. Equation (B-5) then becomes

$$\frac{C_f - C}{C_f - C_0} = \exp\left[-\frac{1}{(W/kA) + 1}\cdot\left(\frac{W}{M}\right)t\right] \tag{B-6}$$

and rearranging

$$\frac{C - C_0}{C_f - C_0} = 1 - \exp\left[-\frac{1}{(W/kA) + 1}\left(\frac{W}{M}\right)t\right] \tag{B-7}$$

Equation (B-7) fits the data shown in Fig. 12 when the exponential term $\frac{1}{(W/kA) + 1} = 0.20$. This term is defined as the cold-trap efficiency. The cold-trap sodium flow rate is known and the internal area can be estimated; therefore, an estimate of the dissolution rate constant, k, can be made. The value for k obtained here was 2.9×10^{-4} g Na cm^{-2} s^{-1}. This constant was determined for dissolution of oxygen from the cold trap; however, the corresponding precipitation rate constant could not be determined.

REFERENCES

[1] HORSLEY, G. W., A possible galvanic cell method for monitoring the activity of oxygen in a hot trapped sodium coolant circuit, Rpt AERE-R-3037 (1961).

[2] MINUSHKIN, B., The liquid metal oxygen meter, United Nuclear Corporation Rpt UNC-MTL-4734 (1965) 7.

[3] MINUSHKIN, B., Electrochemical oxygen meter operating manual, United Nuclear Corporation Rpt UNC-5113 (1965) 7.

[4] STEINMETZ, H., Development of a continuous meter for oxygen in sodium, United Nuclear Corporation Rpt UNC-5032 (1962) 4.

[5] BLAKE, L. R., Resistivity monitor to indicated oxide content of sodium, J. Inst. elect. Engrs, Paper 278M (August 1960).

[6] EAMES, A. R., The rhometer as an impurity indicator for liquid metal circuits, U. K. A. E. A. Rpt TRG-R 337(D) (1962).

[7] Operation of the sodium technology loop for contamination meter evaluations, Atomic Power Development Associates, Inc., Rpt APDA-163 (1954).

[8] HUMPHREYS, J.R., Jr., Sampling and analysis for impurities in liquid sodium systems, Chem. Engng Prog. Symp. Ser. 53 20 (1957) 7-10.

[9] BERGSTRESSER, K.W., WATERBURY, G.R., METZ, C.F., Determination of trace amounts of oxygen added to metallic sodium, Los Alamos Scientific Laboratory Rpt LA-3343 (1965).

[10] RUTKAUSKAS, V.J., Determination of solubility of oxygen in sodium using the vacuum distillation analytical technique, International Symposium on the Alkali Metals, Nottingham, 1966.

[11] GLASSNER, A., The thermochemical properties of the oxides, fluorides and chlorides to 2500°K, Argonne National Laboratory Rpt ANL-5750 (1957).

DISCUSSION

P. MECHELYNCK: I should not think that the observed differences between theoretical and experimental values for the electrochemical cell are entirely due to electrolyte failure. They are probably due in part to the fact that the cell measures oxygen activity, which may be something quite different from the total concentration.

J.M. WILLIAMS: This is in fact an important problem, one which an accurate knowledge of the different oxygen compounds in the sodium would do much to solve.

P. MECHELYNCK: Can you be sure, with the vacuum distillation method of calibration, that all the oxygen in the residue is in the form of Na_2O? If there is any sodium carbonate, is it entirely broken down?

J.M. WILLIAMS: This is a perennial question in distillation analysis. We believe that all the sodium carbonate is broken down at 400°C, which has consistently been our distillation temperature, but no experiment has yet been done to demonstrate the truth of the assumption.

P. MECHELYNCK: Your cell operates, I gather, at 300°C. Can it be used at higher temperatures as, I believe, a similar cell of the United Nuclear Corporation has been?

J.M. WILLIAMS: Our cell has been run at 300°C only, and to our knowledge no cell of its type has been operated at higher temperatures. The problem is one of optimization: one needs a temperature high enough for adequate output yet low enough to allow reasonable lifetimes of the electrolyte in sodium. We have found that at 300°C the lifetime is adequate for our purposes, and we still get sufficient output.

M.N. IVANOVSKY: How much time is required before your electrochemical cell gives a steady reading, for example after an abrupt change in the oxygen concentration of the sodium?

J.M. WILLIAMS: We have observed no time lag in the response of the meter. However, the amount of sodium in the system was such that the cold trap probably controlled the rate of oxygen change, and this gave a longer time constant than we could have measured.

M.N. IVANOVSKY: I have another question. Did you check the concentration of hydrogen and other impurities when you changed the oxygen concentration? Did these other impurities remain constant?

J.M. WILLIAMS: We cannot say whether they remained constant. Hydrogen, in particular, was not measured as a function of time during this experiment. It seems likely that, using a cold trap as a source of oxygen, we were adding hydrogen to the system too, assuming it was present in the cold trap.

M.N. IVANOVSKY: When the temperature is changed while the oxygen concentration remains constant, the amount of sodium monoxide in the solution changes, as does the resistivity; this is because oxides of other metallic impurities are formed. How do you deal with this problem in your temperature compensator calibration?

J.M. WILLIAMS: When we varied the rhometer temperature the cold trap was valved off from the loop. We believe, therefore, that we were not adding or removing impurities as a result of the temperature change.

M.N. IVANOVSKY: I see; but it seems to me that with different oxygen concentrations or a different sodium composition this type of compensation might not be accurate. Did the readings of the electrolytic cells and the rhometer agree well?

J.M. WILLIAMS: This is not a comparison that we can easily make, because we used the oxygen analysis by distillation as our standard, and read resistivity and output.

M.N. IVANOVSKY: One final comment: in our opinion the effect of extraneous impurities is associated not so much with iron as most probably with hydrogen, i.e. with changes in hydrogen content.

L. CHAMPEIX: I understand, Mr. Williams, that you varied the oxygen concentration in the sodium loop between 1 and 30 ppm by changing the temperature of the cold trap. Can you derive an accurate "solubility" curve in this way?

J.M. WILLIAMS: I doubt whether an "accurate" solubility curve could be derived from our cold-trap temperature or from the analytical results because we do not believe that the cold-trap thermocouple measured the coldest point in the system. Furthermore, the plugging temperature did not correspond at any given time to the cold-trap temperature.

L. CHAMPEIX: You used an isothermal circuit at 300°C. Do you think that your calibrations would still be valid for a circuit (a) at high temperature (600°C) and (b) with a temperature gradient? It seems to me that the relationship between activity and concentration would be altered.

J.M. WILLIAMS: Your question brings up a very important point. The oxygen meter, as Mr. Mechelynck has already pointed out, measures oxygen activity, not necessarily the total concentration of oxygen in the sodium. In correlating corrosion data with respect to oxygen concentration, such equilibria as the reaction

$$2e^{-} + Na_2O \rightleftarrows 2Na + O^{=}$$

must certainly be considered. The equilibrium constant for this reaction is a function of temperature, and therefore the oxygen activity in a well-stirred non-isothermal system would probably vary, as you have implied.

DOSAGE DE FAIBLES TENEURS EN OXYGENE, HYDROGENE ET CARBONE DANS LE SODIUM

J. SANNIER ET L. CHAMPEIX
CEA, CENTRE D'ETUDES NUCLEAIRES DE SACLAY, FRANCE

Abstract — Résumé

DETERMINATION OF SMALL QUANTITIES OF OXYGEN, HYDROGEN AND CARBON IN SODIUM. Oxygenated, hydrogenated and carbonated impurities often play a fundamental role in sodium corrosion phenomena even when they are only present in trace amounts in the liquid metal. It is essential therefore to have analytical techniques capable of operating at the sensitivities of the order of a few ppm, and also to be able to identify the different chemical compounds liable to be formed by the oxygen, hydrogen and carbon in the liquid metal.

Oxygen determinations are performed by means of the vacuum amalgamation method. For trace analyses (<10 ppm) a new type of apparatus has been developed. This apparatus removes two causes of pollution: the fixation of oxygen by mercury in the presence of air and the contact between the sodium and the tap grease. The extraction column is not fitted with a tap and the mercury is filled into the apparatus after vacuum distillation without coming into contact with the atmosphere. In addition the column can be entirely oven-dried and the amalgam extraction operation, which is performed by siphoning under a constant mercury flow, does not require any external manipulation or even any particular supervision.

The determination of the dissolved hydrogen or the hydrogen in a hydride state is performed by collecting the gases released during the residue-hydrolysis and amalgamation operation, and by carrying out a quantitative chromatographic analysis of hydrogen present in them. With this extremely sensitive method amounts of hydrogen of the order of 0.1 ppm can be determined. The hydrogen present in the form of hydroxide is analysed by vacuum heating the sodium at 320°C, and by determining the amount of hydrogen released in accordance with the reactions:

$$2\ Na + NaOH \longrightarrow Na_2O + NaH$$

$$NaH \longrightarrow Na + 1/2\ H_2$$

The accuracy is in the ppm range.

The uncombined carbon is also analysed under vacuum by oxidation with van Slykes mixture. The purity of the carbon dioxide collected by pumping is checked by chromatographic analysis. Amounts of carbon of about 5 ppm can be determined with this technique. The carbonate and the carbides are determined by attacking the sodium with acidified water and collecting any carbon dioxide, acetylene and other hydrocarbons that may be formed; these gases are then separated and analysed by chromatography. As the apparatus used is the same for both analyses the carbonate, the carbides (if any) and the free carbon can be determined one after the other with the same sodium sample.

DOSAGE DE FAIBLES TENEURS EN OXYGENE, HYDROGENE ET CARBONE DANS LE SODIUM. Le rôle joué par les impuretés oxygénées, hydrogénées et carbonées dans les phénomènes de corrosion par le sodium est très souvent essentiel même lorsque ces éléments se trouvent à l'état de traces dans le métal liquide. Il est donc indispensable de disposer de techniques analytiques permettant, d'une part, d'obtenir des sensibilités de l'ordre de quelques ppm et, d'autre part, de caractériser les différents composés chimiques que peuvent former l'oxygène, l'hydrogène et le carbone au sein du métal liquide.

Le dosage de l'oxygène est effectué suivant la technique d'amalgamation sous vide. Pour l'analyse des traces (moins de 10 ppm), un nouveau type d'appareillage a été mis au point. Il supprime les deux causes de pollution que peuvent constituer la fixation d'oxygène par le mercure en présence d'air, d'une part, et le contact du sodium avec la graisse des robinets, d'autre part. La colonne d'extraction ne comporte en effet aucun robinet et le mercure, préalablement distillé sous vide, est introduit dans l'appareillage en l'absence de tout contact avec l'atmosphère. De plus, la colonne est entièrement étuvable et l'opération d'extraction de l'amalgame, qui s'effectue par siphonnement sous débit continu de mercure, ne nécessite aucune intervention ni même aucune surveillance particulière.

Le dosage de l'hydrogène dissous ou à l'état d'hydrure est effectué en recueillant les gaz dégagés pendant les opérations d'amalgamation et d'hydrolyse du résidu et en déterminant, par analyse chromatographique, la quantité d'hydrogène présent dans ces gaz. Cette méthode, extrêmement sensible, permet de déterminer des teneurs en hydrogène de l'ordre de 0,1 ppm. Quant à l'hydrogène présent sous forme d'hydroxyde, il est dosé en chauffant le sodium sous vide à 320°C et en déterminant la quantité d'hydrogène alors dégagé suivant les réactions:

$$2\ Na + NaOH \longrightarrow Na_2O + NaH$$

$$NaH \longrightarrow Na + 1/2\ H_2$$

La précision est ici de l'ordre de la partie par million.

Le dosage du carbone non combiné est également effectué sous vide par oxydation à l'aide du mélange de van Slyke. La pureté du gaz carbonique recueilli par pompage est contrôlée par analyse chromatographique. Cette technique permet de déterminer des teneurs en carbone de l'ordre de 5 ppm. Quant au carbonate et aux carbures, ils sont dosés en attaquant le sodium à l'eau acidifiée et en recueillant le gaz carbonique, l'acétylène et les autres hydrocarbures éventuellement formés, ces gaz étant ensuite séparés et dosés par chromatographie. L'appareillage mis en œuvre étant identique pour les deux dosages, il est possible, sur le même échantillon de sodium, de déterminer consécutivement le carbonate, les carbures éventuels et le carbone libre.

I - INTRODUCTION

Les impuretés oxygénées, hydrogénées ou carbonées présentes dans le sodium, même à l'état de traces, interviennent très souvent d'une manière déterminante dans les phénomènes de corrosion des matériaux de structure par ce métal liquide.

Ainsi, la résistance à la corrosion des métaux réfractaires, tels que le niobium [1], le zirconium [2] ou le vanadium [3], dépend essentiellement de la teneur en oxygène du sodium. D'autre part, les propriétés mécaniques des aciers inoxydables peuvent se trouver sévèrement altérées lorsque le sodium renferme du carbone [4] [5]. Quant à l'hydrogène, il peut être responsable de phénomènes de fragilisation importants [6]. En outre, même lorsque le processus de corrosion dépend directement du métal liquide lui-même -c'est le cas du transfert de masse d'un constituant métallique présentant une certaine solubilité dans le métal liquide-, on constate que le phénomène se trouve accéléré par la présence d'impuretés dans le sodium.

Dans ces conditions, pour mener à bien de telles études de corrosion, il convient de disposer de techniques suffisamment sensibles d'analyse de l'oxygène, de l'hydrogène et du carbone, puisque ces éléments peuvent, dans certains cas, intervenir à des concentrations aussi faibles que quelques ppm. D'autre part, leurs rôles respectifs dans les phénomènes de corrosion peuvent être notablement différents suivant la forme sous laquelle ils se présentent. Par exemple, l'influence de l'oxygène ne sera pas nécessairement identique s'il se trouve sous forme d'oxyde ou d'hydroxyde ; de même, la susceptibilité d'un acier à la carburation peut différer selon que le carbone est présent dans le sodium à l'état libre ou sous forme de carbonate.

Nous nous sommes donc efforcés de mettre au point des méthodes d'analyse à la fois sensibles et spécifiques de chaque composé. Elles présentent une caractéristique commune : l'utilisation systématique du vide qui nous paraît plus sûre, du point de vue du risque de pollution, que celle d'une atmosphère inerte ; il est en effet plus facile de contrôler la réalisation d'un bon vide que la pureté d'un gaz inerte. D'ailleurs, la technique de prélèvement utilisée, également commune à toutes ces méthodes, fait elle aussi appel au vide [7].

II - DOSAGE DE L'OXYGENE

Le dosage de cet élément est effectué suivant la méthode au mercure, la quantité d'oxyde résiduel étant déterminée par spectrophotométrie de flamme. La validité de cette méthode, maintenant bien connue, a été démontrée précédemment, tant du point de vue de la reproductibilité que de la justesse : la précision, pour des teneurs inférieures à 10 ppm, atteint 1 à 2 ppm [8] .

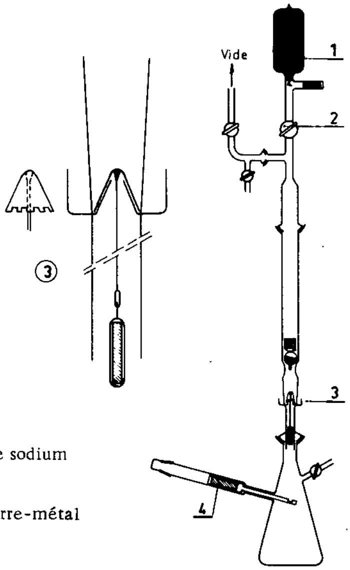

FIG.1. Appareil de dosage de l'oxygène dans le sodium

1 - Réservoir à mercure
2 - Robinet en acier inoxydable avec raccords verre-métal
3 - Siphon
4 - Collecteur de mercure

Cette méthode, utilisée depuis plusieurs années dans deux laboratoires distincts, s'est avérée satisfaisante, les résultats obtenus apparaissant dans l'ensemble reproductibles et concordants. Cependant, quelques résultats difficilement explicables, de même que des différences passagères entre les valeurs obtenues dans les deux laboratoires, nous ont amenés à effectuer un examen critique systématique du mode opératoire, d'où se sont dégagées deux causes principales de pollution possibles :

- le mercure ne se trouvant pas à l'abri de l'air avant son introduction dans la colonne d'extraction et celle-ci s'effectuant à travers un robinet graissé, de l'oxygène ou des traces de graisse pourraient se fixer ou être entraînées dans ce réactif ;

- la réaction d'amalgamation ayant lieu au-dessus d'un robinet graissé, l'amalgame résultant pourrait réagir avec la graisse.

Dans ces deux hypothèses, les résultats sont susceptibles d'être faussés par excès. Un nouveau type de colonne a donc été étudié et mis au point (fig. 1), en vue d'écarter ces risques de pollution.

Principe et appareillage

Le mercure est distillé sous vide dans une ampoule en verre comportant à sa partie inférieure une "queue de cochon". Après scellement sous vide, cette ampoule est soudée à la partie supérieure de la colonne d'extraction. En brisant la queue de cochon à l'aide d'une masselotte, le mercure peut être introduit dans l'appareillage sans qu'il se soit trouvé, à aucun moment, en contact avec l'atmosphère. De plus, afin d'éviter toute possibilité d'entraînement de graisse, son écoulement s'effectue au moyen d'un robinet en acier inoxydable soudé à l'appareillage en verre Pyrex par l'intermédiaire de raccords verre-métal.

La colonne d'extraction comporte, à sa partie inférieure, un siphon constitué par un tube tronconique solidaire de la colonne et par un capuchon amovible maintenu en place au moyen d'un lest ; des crénaux disposés à la partie inférieure de ce capuchon permettent l'écoulement de l'amalgame.

Enfin, l'erlenmeyer servant à recueillir l'amalgame est muni d'un ajutage latéral renfermant un petit collecteur en verre. En déplaçant celui-ci au moyen d'un aimant, il est possible, à la fin de la manipulation, d'effectuer un prélèvement de mercure en vue de déterminer si l'extraction du sodium est bien complètement achevée.

Mode opératoire

Il comporte les étapes suivantes :

- Dégazer l'appareillage sous vide secondaire, la colonne d'extraction étant chauffée à 200°C pendant une heure, afin d'éliminer en totalité la vapeur d'eau adsorbée sur la verrerie. Lorsque le vide s'établit à 2.10^{-6} torr, fermer la vanne d'introduction de mercure et briser la queue de cochon du réservoir à mercure en actionnant au moyen d'un aimant la masselotte prévue à cet effet.

- Remplir le siphon par du mercure et faire solidifier celui-ci en versant de l'azote liquide dans la collerette extérieure. Introduire alors environ 10 cm^3 de mercure, de manière à recouvrir largement le capuchon du siphon.

- Rompre l'ampoule de sodium à l'aide de la deuxième masselotte.

- Faire couler quelques gouttes de mercure, attendre que la chaleur dégagée par la réaction soit dissipée, puis, tout en maintenant solide le mercure du siphon, recommencer ainsi de suite jusqu'à complète amalgamation. Cesser ensuite le refroidissement ; le mercure et une grande partie de l'amalgame s'écoulent alors.

- Solidifier à nouveau le mercure du siphon, amener son niveau à hauteur de l'ampoule, cesser le refroidissement et laisser s'écouler.

- Régler alors goutte à goutte l'écoulement du mercure et parfaire, par siphonnement, l'élimination de l'amalgame. La durée totale de l'opération d'amalgamation et d'extraction est de 4 heures ; elle nécessite l'emploi de 600 à 700 cm^3 de mercure.

- En vue du contrôle de fin d'extraction, prélever environ 1 cm^3 de mercure en déplaçant le collecteur, puis interrompre le débit de mercure, solidifier celui-ci dans le siphon, effectuer la rentrée d'air dans la colonne puis dans l'erlenmeyer, et démonter l'appareillage.

- Recueillir dans un bécher le mercure et l'oxyde présents dans la colonne, y ajouter les 100 cm^3 d'eau distillée utilisés pour le rinçage, acidifier la solution avec quelques gouttes d'HCl 2$\underline{N}$ et doser le sodium par spectrophotométrie de flamme.

- Effectuer la même opération, mais avec 10 cm^3 d'eau, sur le mercure recueilli dans le collecteur, et vérifier l'absence d'ions sodium dans la solution.

- Déterminer le poids de sodium mis en jeu en décomposant l'amalgame avec 100 cm^3 d'HCl 2N, puis en dosant l'acide en excès à l'aide d'une solution de NaOH 2N, en présence de phénol-phtaléine.

Résultats et conclusions

Les résultats obtenus à ce jour en dosant l'oxygène suivant l'ancienne ou la nouvelle technique, dans des échantillons issus du même prélèvement, sont en fait très concordants (tableau I), et ils apportent la confirmation que la première n'introduisait pas d'erreur systématique dans la détermination de la teneur en oxygène.

TABLEAU I. COMPARAISON DES RESULTATS OBTENUS SUIVANT LES DEUX TECHNIQUES

Origine du prélèvement	Teneur en oxygène (ppm)	
	Ancienne technique	Nouvelle technique
Circuit de sodium équipé d'une purification par piège chaud (zirconium à 650°C)	4-6	3-4
Circuit de sodium comportant seulement une purification par piège froid maintenu à 105°C	9-10-10 7-8	7 10

Cependant ces résultats restent certainement trop peu nombreux pour permettre d'imputer définitivement à l'ancienne technique l'obtention de certaines valeurs manifestement erronées par excès. Quoi qu'il en soit, la mise en oeuvre du nouveau type d'extracteur qui vient d'être décrit apporte un perfectionnement appréciable à la méthode d'amalgamation classique :

- elle supprime toute possibilité de pollution liée à la fixation d'oxygène sur le mercure d'une part et à la réaction de l'amalgame avec la graisse d'autre part ;

- elle facilite l'élimination préalable de la vapeur d'eau adsorbée sur la verrerie, le tube à réaction étant entièrement étuvable ;

- enfin, elle rend pratiquement automatique l'opération d'extraction de l'amalgame, puisqu'aucune intervention ni même aucune surveillance particulière ne sont plus nécessaires.

III - DOSAGE DE L'HYDROGENE

Deux méthodes d'analyse ont été mises au point. La première s'applique uniquement à l'hydrogène libre ou sous forme d'hydrure ; la seconde autorise le dosage de l'hydrogène total, les teneurs respectives en hydrure et en hydroxyde étant successivement déterminées. Ces deux techniques, précédemment décrites en détail [9] [10] , seront ici simplement résumées.

1. Dosage de l'hydrogène libre ou sous forme d'hydrure

L'hydrure NaH étant insoluble dans l'amalgame de sodium, la technique d'extraction au mercure précédente peut être mise à profit pour ce dosage, qui s'apparente donc étroitement à celui de l'oxygène, tant par l'appareillage que par le mode opératoire. La réaction d'amalgamation étant exothermique,une partie de l'hydrure est décomposée suivant la réaction :

$$NaH \dashrightarrow Na + 1/2\, H_2$$

L'hydrogène pouvant se trouver à l'état libre doit également se dégager pendant cette opération. Le reste de l'hydrure est ensuite décomposé lors de l'hydrolyse du résidu, suivant la réaction :

$$NaH + H_2O \dashrightarrow Na\,OH + H_2$$

L'hydrogène libéré au cours de ces opérations, toutes deux effectuées sous vide, est recueilli et dosé volumétriquement ; sa pureté est contrôlée par analyse chromatographique.

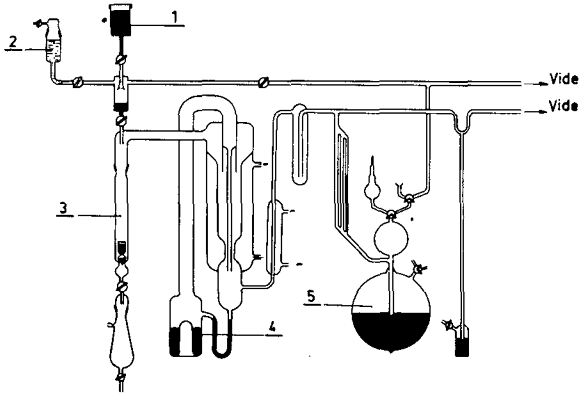

FIG.2. Appareil de dosage de l'hydrogène libre ou sous forme d'hydrure dans le sodium
1 - Réservoir à mercure
2 - Réservoir à eau distillée
3 - Colonne d'extraction
4 - Pompe de transfert à diffusion de mercure
5 - Ensemble pompe Toepler-jauge de MacLeod

L'appareillage comporte essentiellement quatre parties (fig. 2) :

- la colonne d'extraction
- l'ensemble de pompage et de mesure du volume des gaz, composé d'une pompe à diffusion de mercure en verre, d'un piège et d'une pompe Toepler associée à une jauge de Mac Leod
- le système d'introduction du mercure et de l'eau distillée
- le groupe de pompage pour vide poussé.

En raison de la valeur extrêmement réduite du "blanc", cette méthode est très sensible : elle permet de déterminer des teneurs en hydrogène aussi faibles que 0,1 ppm, et ce avec une très bonne reproductibilité. D'autre part, elle est susceptible d'apporter un perfectionnement à l'analyse de l'oxygène, qui peut d'ailleurs être réalisée simultanément. En effet, il s'avère que la totalité de l'hydrogène ne se dégage pas pendant l'amalgamation : en moyenne 30 % de l'hydrure présent ne se décompose que lors de l'hydrolyse. En raison du mode de calcul utilisé, reposant sur la quantité d'ion Na présent dans la solution aqueuse finale, cet hydrure se trouve confondu avec l'oxyde, de sorte que le résultat du dosage de cet élément par la méthode au mercure devient nécessairement erroné si la concentration en hydrure est notable. La détermination de ce composé permet donc d'introduire un terme correctif dans le calcul de la concentration en oxygène du sodium.

2. Dosage de l'hydrogène total

La méthode utilisée repose sur les réactions suivantes :

$$NaH \dashrightarrow Na + 1/2\, H_2 \qquad (I)$$

$$NaOH + 2\, Na \dashrightarrow Na_2O + NaH \qquad (II)$$

Sous vide, la vitesse de la réaction (I) est importante à 280°C, alors que la réaction (II) ne se produit qu'à partir de 300°C [10]. L'échantillon de sodium est donc porté à 280°C sous vide, l'hydrogène provenant de la décomposition de l'hydrure étant recueilli et son volume mesuré. Quand la réaction (I) est achevée, la température est élevée à 320°C ; les réactions (II) et (I) s'effectuent alors consécutivement, et une nouvelle quantité d'hydrogène, provenant de la décomposition de l'hydroxyde, est recueillie et mesurée. Dans les deux cas, la pureté de l'hydrogène est contrôlée par analyse chromatographique.

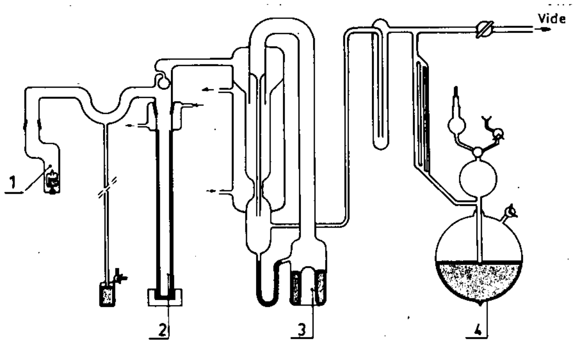

FIG.3. Appareil de dosage de l'hydrogène total dans le sodium
1 - Système d'introduction de l'échantillon
2 - Tube à réaction
3 - Pompe de transfert à diffusion de mercure
4 - Ensemble pompe Toepler-jauge de MacLeod

L'appareillage mis en oeuvre (fig. 3) est d'une conception très voisine de celui utilisé pour le dosage de l'hydrure. La colonne d'amalgamation est simplement remplacée par un tube à réaction en verre, muni d'une chemise en acier inoxydable afin d'éviter la réaction perturbatrice du verre avec le sodium, notable aux températures considérées [10]. De plus, pour la même raison, l'échantillon de sodium est prélevé dans une capsule en nickel, elle-même enfermée dans une ampoule en verre scellée sous vide ; un dispositif particulier permet de séparer la capsule en nickel de son enveloppe, afin d'éviter l'introduction de débris de verre dans le tube à réaction. En raison de la valeur relativement importante du "blanc", due à des dégagements gazeux parasites, cette méthode est moins sensible que la précédente. Elle permet néanmoins de déterminer des teneurs en hydrogène de l'ordre de la ppm, avec une précision d'environ 20 %.

III - DOSAGE DU CARBONE

Deux méthodes de dosage sont utilisées pour la détermination du carbone. L'une s'applique au carbone présent dans le sodium sous forme non combinée ; l'autre permet la détermination du carbonate, et éventuellement du (ou des) carbure(s) de sodium. Si ces deux méthodes mettent en oeuvre des réactions totalement différentes, les techniques opératoires choisies impliquent un appareillage semblable, de sorte qu'il est possible de doser successivement, à l'aide du même appareil, le carbonate, les carbures et le carbone non combiné.

1. Dosage du carbone non combiné

Le principe de la méthode utilisée est le suivant [11]. Après dissolution de l'échantillon de sodium dans l'eau, sous atmosphère inerte, la solution est acidifiée puis portée à l'ébullition afin de détruire les carbonates ayant pu se former pendant la mise en solution. Le résidu est alors introduit dans l'appareil d'analyse où la solution oxydante de VAN SLYKE transforme le carbone en gaz carbonique ; celui-ci est condensé dans un piège à azote liquide puis détendu et dosé par volumétrie, sa pureté étant contrôlée par analyse chromatographique. La manipulation est entièrement effectuée sous vide, ce qui évite les opérations de purification d'un gaz vecteur et simplifie le problème du recueil et de l'analyse du gaz carbonique formé.

L'appareil de dosage (fig. 4) comporte quatre parties :

- un tube à réaction muni d'un rôdage sphérique, permettant la mise en contact du carbone et du mélange oxydant,
- deux pièges pour la condensation successive de la vapeur d'eau et du gaz carbonique,
- une pompe Toepler associée à une jauge de Mac Leod, assurant le recueil du gaz carbonique, la mesure de son volume et le prélèvement d'une éprouvette en vue de l'analyse chromatographique,
- un système de pompage pour vide poussé.

Le "blanc" de cette méthode n'est pas négligeable : sa valeur s'établit à environ 10 μg de carbone, ce qui correspond à une concentration de 10 ppm dans un gramme de sodium. Toutefois, en raison d'une reproductibilité satisfaisante, la sensibilité reste bonne, et il est possible de doser des teneurs en carbone inférieures à 10 ppm avec une précision d'environ 2 ppm.

2. Dosage du carbonate et des carbures

Ce dosage est effectué en faisant réagir sous vide l'échantillon à analyser avec une solution d'acide sulfurique. Dans ces conditions, outre l'hydrogène correspondant à l'attaque du sodium, se dégagent le gaz carbonique, l'acétylène et éventuellement d'autres hydrocarbures provenant des décompositions respectives du carbonate et des carbures de sodium. Ces gaz sont d'abord séparés de l'hydrogène par condensation dans l'azote liquide, puis rassemblés en vue de la mesure de leur volume, et enfin analysés par chromatographie.

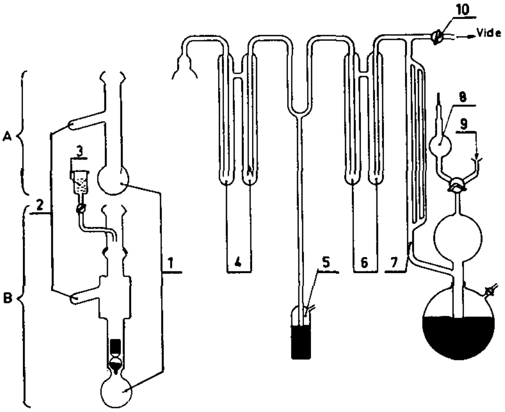

FIG.4. Appareil de dosage du carbone dans le sodium

A - Tube à réaction pour la détermination du carbone non combiné

B - Tube à réaction pour les déterminations successives du carbonate, des carbures et du carbone non combiné

1 - Tube à réaction
2 - Réservoir pour la solution de Van Slyke
3 - Réservoir d'acide sulfurique
4, 6 - Pièges
5 - Manomètre à mercure
7-9 - Ensemble pompe Toepler-jauge de MacLeod
10 - Robinet

Appareillage

Il est identique à celui utilisé pour le dosage du carbone non combiné, exception faite du tube à réaction qui comporte un volume d'expansion d'environ 1 litre (fig. 4). Par ailleurs, une pièce intermédiaire démontable permet d'introduire goutte à goutte la solution d'acide sulfurique au moyen d'un robinet en Téflon.

Mode opératoire

- Un vide d'environ 2.10^{-6} torr étant réalisé dans l'appareil, fermer le robinet ⑩ ; remplir le vase Dewar du piège ④ avec un mélange acétone-carboglace et celui du piège ⑥ avec de l'azote liquide.

- Casser l'ampoule de sodium au moyen de la masselotte et faire couler goutte à goutte la solution d'acide sulfurique $4\underline{N}$.

- Lorsque la pression d'hydrogène atteint environ 10 cm de mercure, arrêter l'attaque et pomper lentement ce gaz (environ 100 cm^3/min) au moyen de la pompe à palettes, par l'intermédiaire du robinet ⑩ .

- Recommencer l'opération jusqu'à dissolution complète du sodium.

- Le robinet ⑩ étant fermé, remplacer le Dewar à azote liquide par un autre contenant de la carboglace et, à l'aide de la pompe Toepler, recueillir la totalité du gaz carbonique et des hydrocarbures dans l'ampoule calibrée ⑧ ; mesurer la pression de ce mélange gazeux à l'aide de la jauge de Mac Leod.

- Transférer ces gaz, au moyen de la pompe Toepler, dans l'éprouvette de prélèvement ⑨ .

- Procéder à l'analyse chromatographique du mélange gazeux sur une colonne de silicagel de longueur 0,5 m maintenue à 70°C, le débit d'hélium, utilisé comme gaz porteur, étant de 30 cm^3 par minute.

Résultats

La validité de cette technique opératoire a été démontrée en ajoutant à du sodium exempt de carbonate et de carbures des volumes connus de gaz carbonique et d'acétylène, qui furent intégralement retrouvés, compte tenu de la précision de la mesure des volumes. En raison d'une part de l'absence totale de "blanc", et d'autre part de la sensibilité de l'analyse chromatographique -1 cm de hauteur de pic correspond à 0,1 mm^3 de CO_2 et à 0,3 mm^3 de C_2H_2-, cette méthode permet de déterminer des teneurs en carbonate et en carbures inférieures à la ppm. Par ailleurs, une fois ce dosage terminé, il suffit de supprimer la pièce intermédiaire servant à l'alimentation en acide sulfurique, d'introduire le réactif de VAN SLYKE dans le réservoir latéral et de remettre l'appareillage sous vide, pour procéder au dosage du carbone non combiné sur le même échantillon.

IV - CONCLUSION

Les méthodes décrites dans cet exposé ne prétendent pas apporter l'unique, ni même la meilleure solution au problème du dosage des impuretés oxygénées, hydrogénées ou carbonées dans le sodium : ainsi, pour la détermination de l'oxygène, la technique de sublimation apparaît à priori tout aussi valable que la méthode au mercure.

Cependant, considérées dans leur ensemble, ces méthodes présentent un certain nombre d'avantages. Elles permettent en effet la détermination sélective des impuretés du sodium avec une excellente sensibilité, la limite de détection n'étant jamais supérieure à quelques ppm, même dans les cas les plus défavorables. D'autre part, elles font appel à des techniques expérimentales semblables : utilisation systématique du vide, analyse chromatographique des gaz recueillis au moyen de pompes Toepler, ce qui simplifie les problèmes d'équipement et facilite la formation des opérateurs. Enfin, le système de prélèvement sous vide dans des ampoules en verre est utilisable dans tous les cas.

REFERENCES

[1] SANNIER, J., CHAMPEIX, L., DARRAS, R., Rapport CEA R-3028 (1966).

[2] CHAMPEIX, L., GRAFF, W., SANNIER, J., C.r. 9^e Colloque de Métallurgie sur la corrosion et la protection du zirconium et de ses alliages, CEN Saclay, juin 1965, Presses Universitaires, Paris (1966) 63.

[3] DARRAS, R., C.r. 3^e Congrès international sur la corrosion métallique, Moscou, mai 1966 (à paraître).

[4] ANDERSON, W.J., SNEESBY, G.V., NAA-SR 5282 (1960).

[5] GILL, J.J., NAA-SR-MEMO 4887 (1961).
[6] THORLEY, A., TYZACK, C., Thermodynamics of Nuclear Materials, IAEA, Vienna (1962) 365.
[7] SANNIER, J., VINGOT, R., Rapport CEA 2369 (1963).
[8] CHAMPEIX, L., DARRAS, R., DUFLO, J., J. nucl. Mater. 2 (1959) 113.
[9] NAUD, G., SANNIER, J., Bull. Soc. chim. Fr. 12 (1963) 2735.
[10] NAUD, G., Thèse, Rennes (1964); Rapport CEA R-2583 (1964).
[11] SANNIER, J., VASSEUR, A., Rapport CEA 2370 (1963).

DISCUSSION

A.M. SOENEN: How do you manage to regulate the drop-by-drop addition of mercury during the amalgamation process?

J. SANNIER: This can be done quite easily with a stainless-steel diaphragm valve.

A.M. SOENEN: Does the addition of mercury proceed in exactly the same way during both the amalgamation and the extraction operations?

J. SANNIER: No, during amalgamation the mercury is added in "instalments" so that the reaction does not become too violent, but during extraction the addition is continuous.

I. SCHREINLECHNER: What is the final step in determining oxygen in sodium by the amalgamation method? Do you titrate NaOH? If so, what sort of indicator do you rely on, and what error would you expect to have in the results from this part of the determination?

J. SANNIER: The quantity of sodium ions in the final aqueous solution is determined by flame spectrophotometry and the oxygen content is calculated on the assumption that all oxygen is in the form of Na_2O. There is no doubt that this assumption does introduce an error when part of the oxygen is present in the hydroxide state – and this is why measurements of total hydrogen are so important.

L.F. EPSTEIN: I should like to ask Mr. Sannier whether he has tried to measure recoveries of carbon by wet oxidation, using refractory carbides. Mr. Dutina of our laboratory has found that heavy metal carbides, those of chromium for example, do not quantitatively decompose or oxidize with the Van Slyke reagent; and very poor recoveries are obtained. This is important, because in the widespread search for the forms of carbon responsible for carbon transport in sodium these heavy metal compounds may prove to be of some significance. But the analytical technique may miss these materials almost entirely.

J. SANNIER: The main purpose of the analytical techniques that we have developed is to get quantitative determinations of the carbon species likely to react with structural or cladding materials. They are probably not applicable to carbon present in the form of very stable carbides, such as chromium carbide; but we feel that in any case carbon in this form will not react with the materials with which we are concerned.

КОНТРОЛЬ ЗА СОДЕРЖАНИЕМ КИСЛОРОДА И ВОДОРОДА В НАТРИИ

В.И.СУББОТИН, Ф.А.КОЗЛОВ, Э.К.КУЗНЕЦОВ,
Н.Н.ИВАНОВСКИЙ
ФИЗИКО-ЭНЕРГЕТИЧЕСКИЙ ИНСТИТУТ, ОБНИНСК
СССР

(Доклад представил М.Н.Ивановский)

Abstract — Аннотация

DETERMINATION OF OXYGEN AND HYDROGEN IN SODIUM. One of the basic problems to be solved when operating sodium-cooled systems is that of checking the amounts of impurities in the sodium, the most common of which are oxygen and hydrogen.

Physico-chemical methods of checking the amounts of oxygen and hydrogen present in the sodium directly in the circulation loop are examined. The amount of oxygen in the sodium is found selectively by the vacuum distillation method, which offers a sensitivity of $(2-5) \times 10^{-4}$% by weight of oxygen. The amount of hydrogen in the sodium is found selectively by using a hydrogen diffusion indicator offering a sensitivity of $(1-2) \times 10^{-4}$% by weight of hydrogen.

There is detailed discussion of the possibility of reliably analysing the amount of impurities in the sodium by means of a plugging meter, ans it is revealed that the plugging meter cannot be used for selective determination of the oxygen and hydrogen concentrations in sodium because the results are affected to an appreciable extent by the combined solubility of oxygen and hydrogen in the sodium. This device is nevertheless useful in practice as it provides a reliable indication of the degree of danger from the total loop contamination caused by precipitation of impurities in the cold sections of the system.

КОНТРОЛЬ ЗА СОДЕРЖАНИЕМ КИСЛОРОДА И ВОДОРОДА В НАТРИИ. Одним из основных вопросов, возникающих при эксплуатации систем с натриевым теплоносителем, является контроль за содержанием примесей в натрии, наиболее распространенными из которых являются кислород и водород.

Рассматриваются физико-химические методы контроля за содержанием кислорода и водорода в натрии непосредственно в циркуляционном контуре. Для селективного определения содержания кислорода в натрии применен метод вакуумной дистилляции. Чувствительность метода составляет $(2 \div 5) \cdot 10^{-4}$вес% кислорода. Для селективного определения содержания водорода в натрии используется диффузионный индикатор водорода, позволяющий контролировать содержание водорода в натрии с чувствительностью $(1 \div 2) \cdot 10^{-4}$ вес% водорода.

Подробно проанализирована возможность достоверного анализа содержания примесей в натрии с помощью пробкового индикатора. Показано, что пробковый индикатор не позволяет селективно определять концентрацию кислорода и водорода в натрии, поскольку на его показания существенное влияние оказывает эффект взаимной растворимости кислорода и водорода в натрии. Тем не менее, этот прибор ценен в эксплуатации, поскольку он надежно показывает, насколько опасен общий уровень загрязненности контура с точки зрения высаждения примесей в холодных участках системы.

Опыт эксплуатации промышленных энергетических установок и экспериментальных стендов, использующих в качестве теплоносителя натрий, показывает, что концентрация примесей в натрии со временем возрастает. Количество примесей, которые могут присутствовать, и их состав определяются интенсивностью и разнообразием источников примесей, имеющихся в системе. Наиболее широко распространенными примесями являются кислород и водород. Опасности, связанные с их появлением, хорошо известны. Они неоднократно обсуждались в литературе [1, 2, 3, 4]. Поэтому одним из основных вопросов, возникающих при эксплуатации систем с натриевым теплоносителем, является вопрос контроля за содержанием окиси и гидрида натрия в натрии.

Контроль за содержанием этих примесей возможен как физико-химическими методами с отбором пробы на вынос, так и специальными приборами, встроенными в систему.

ОПРЕДЕЛЕНИЕ КИСЛОРОДА В НАТРИИ

Для определения кислорода в натрии нами был выбран метод вакуумной дистилляции. Сущность метода заключается в отделении дистилляцией под вакуумом металла от его окислов.

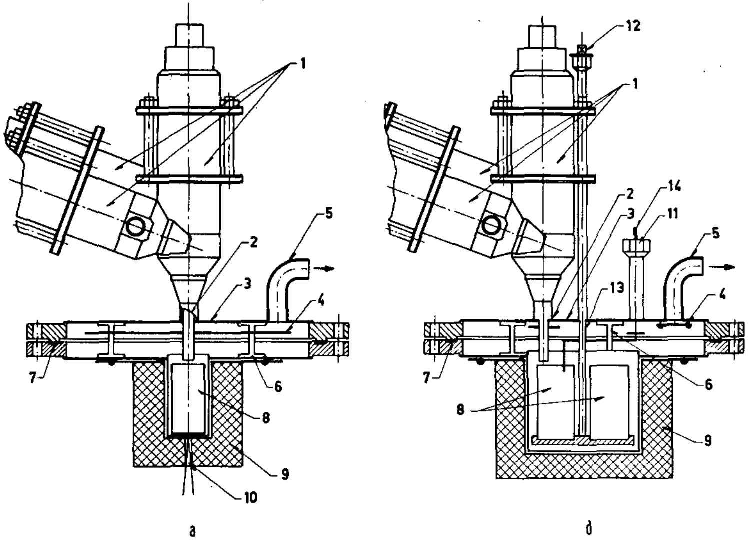

а б

Рис.1. Конструкции пробоотборников-дистилляторов:
1 – вентили для жидкого металла; 2 – съемная сливная трубка; 3 – корпус вакуумной камеры; 4 – отбойник; 5 – линия к вакуумному насосу; 6 – распорки; 7 – уплотнение разъема; 8 – стакан для пробы; 9 – печь; 10 – термопара; 11 – уплотнение подвижного уровнемера; 12 – указатель положения стаканов; 13 – поворотная штанга; 14 – подвижный уровнемер.

Предварительные исследования и анализ литературы показали, что для повышения чувствительности данного метода необходимо увеличить навеску металла и уменьшить загрязнение пробы в процессе ее отбора и подготовки к анализу. Для решения этой задачи были сконструированы специальные пробоотборники-дистилляторы, с помощью которых можно быстро (1 – 2 минуты) отобрать непосредственно из циркуляционного контура пробы натрия и там же вакуумной дистилляцией отделить от него окись.

Оперативный отбор пробы устраняет возможность перераспределения окислов в процессе отбора, а совмещение пробоотбора и дистилляции в одном приборе исключает возможность загрязнения отобранной пробы при подготовке ее к анализу, как это может иметь место при отборе пробы из контура на вынос.

Конструкции пробоотборников-дистилляторов представлены на рис. 1 (а, б). Пробоотборник состоит из трех вентилей и вакуумной камеры. Полость, отсекаемая клапанами вентилей, является тем объемом, из которого происходит отбор пробы. Съемная сливная трубка предотвращает разбрызгивание натрия в вакуумной камере при сливе пробы и упрощает промывку клапанов сливного вентиля.

Температурный режим дистилляции поддерживается с помощью печи с регулируемой мощностью и контролируется термопарой. Пары натрия конденсируются на поверхности отбойника (рис. 1 а) или на верхней крышке вакуумной камеры (рис. 1 б), которая охлаждается воздухом от настольного вентилятора. Для извлечения стаканов с остатком после окончания дистилляции предусмотрен вакуумно-герметичный разъем.

Тарировка. Тарировка пробоотборника осуществлялась на экспериментальном контуре, имеющем холодную ловушку и пробковый индикатор. Перед отбором пробы проводились следующие операции. Тщательно промывались дистиллированной водой и спиртом поверхности вакуумной камеры и стакан для пробы. После сборки камера промывалась аргоном и вакуумировалась до остаточного давления $1 \cdot 10^{-2}$ мм рт. ст.; при температуре 500 ÷ 550°С проводилось обезгаживание стаканов. При обезгаживании через пробоотборник устанавливался расход натрия. При этом циркуляционный контур работал в изотермическом режиме с постоянной прокачкой натрия через холодную ловушку. Отклонение температуры от заданного уровня внутри ловушки не превышало ± 5°С. Проводилось не менее двух определений температуры забивания пробковым индикатором. Если расхождение в температурах забивания не превышало ± 10°С, то прекращали циркуляцию натрия через пробоотборник и отбирали пробу. После этого при заданном температурном режиме и постоянном вакуумировании натрий дистилляцией отделялся от окислов. По окончании дистилляции пробоотборник охлаждался до комнатной температуры, вакуумная камера заполнялась аргоном и разбиралась.

Остаток после дистилляции растворялся в воде и титрованием определялась концентрация щелочи. Зная концентрацию щелочи, объем раствора и навеску пробы, рассчитывали концентрацию окиси в натрии. Вес натрия в пробе определялся взвешиванием конденсата после дистилляции или расчетом при использовании подвижного уровнемера (рис. 1 б). Ошибка в определении веса пробы не превышала 5%.

Результаты опытов. Режим дистилляции должен обеспечить полное удаление металлов из пробы и не допускать существенной потери окислов. Опыты по подбору режима дистилляции проводились при температурах 500, 550, 600°С и времени дистилляции 1 ÷ 40 часов. Концентрация кислорода при этом изменялась от 0,0005 до 0,02 вес %. Результаты приведены в табл. 1. Видно, что при проведении дистилляции проб натрия весом ~100 г из никелевых стаканов диаметром 40 мм при температурах 500 и 550°С в течение 3 ÷ 6 часов достигается хорошая воспроизводимость результатов. При большем времени дистилляции при этих температурах результаты занижаются. При температуре 600°С содержание кислорода в пробе уменьшается пропорционально времени дистилляции. Занижение результатов, вероятно, объясняется как частичной дистилляцией окислов натрия, так и взаимодействием их с материалом стакана. Например, при времени дистилляции 25 ÷ 40 часов при температуре 500°С внутренняя поверхность стакана после дистилляции покрывалась черно-зеленой пленкой, нерастворимой в воде. Расчеты показали, что в наших условиях потеря окислов из "сухого" остатка за счет их

ТАБЛИЦА 1. РЕЗУЛЬТАТЫ ОПЫТОВ ПО ВЫБОРУ РЕЖИМА ДИСТИЛЛЯЦИИ

$t_{дист}$ = 500°C			$t_{дист}$ = 550°C			$t_{дист}$ = 600°C		
Температура забивания, °C	Время дистилляции, часы	Содержание кислорода, вес% 10^{-3}	Температура забивания, °C	Время дистилляции, часы	Содержание кислорода, вес% 10^{-3}	Температура забивания, °C	Время дистилляции, часы	Содержание кислорода, вес% 10^{-3}
218	3,0	2,3	286	5,0	5,7	285	1,0	4,7
222	3,0	1,9	283	5,0	5,3	284	3,0	3,1
225	3,0	1,9	286	7,0	4,6	284	5,0	2,0
212	4,0	1,4	282	10,0	4,6	289	7,0	1,0
212	4,0	1,0						
205	40	1,4	330	3,5	10,0			
			319	3,5	8,9			
284	5,0	5,9	314	5,0	9,6			
281	7,0	4,2	315	6,0	9,0			
286	10,0	3,8	325	7,5	7,7			
335	3,5	20,0	338	10,0	8,1			
338	3,5	19,0						
335	3,5	14,0						
336	6,5	19,0						
335	7,5	16,0						
335	10,0	11,0						
330	25,0	7,2						
336	40,0	6,9						

диссоциации при температурах 500, 550, 600°C приведет к занижению результата анализа соответственно на 10^{-5}, 10^{-4} и $7 \cdot 10^{-4}$ вес%O_2/час.

Учитывая результаты опытов и расчетов, для дальнейших исследований был выбран следующий режим дистилляции: температура 500 ÷ 550°C, время – 5 часов, давление – 10^{-2} мм рт. ст.

Определение потерь кислорода из пробы при проведении вакуумной дистилляции производилось методом "введено-найдено". Дозировка кислорода осуществлялась следующим образом. В чистый стакан вводилось известное количество обезвоженной при температуре 150 ÷ 200°C щелочи. Стакан помещался в вакуумную камеру и в него сливалась проба натрия с собственным содержанием кислорода $(3 \div 8) \cdot 10^{-4}$ вес%. Щелочь реагировала с натрием, образующийся гидрид удалялся при проведении дистилляции, а окислы оставались в остатке. Результаты опытов приведены в табл. 2. Потери кислорода в среднем составляют 14%. Чувствительность данного метода определялась как количество окислов, образующихся на поверхности стакана при выдержке его в парах натрия в условиях выбранного режима дистилляции. При использовании стаканов из никеля чувствительность метода составила $(3{,}4 \div 1{,}4) \cdot 10^{-4}$ вес%, а из молибдена – $(1 \div 0{,}4) \cdot 10^{-4}$ вес% кислорода.

При работе с пробоотборником с четырьмя стаканами пробы, отобранные первыми, в течение длительного времени хранятся в вакуумной камере. Для проверки дополнительного загрязнения натрия кислородом проводились специальные опыты. Они показали, что в течение 9 часов при этом не происходит заметного дополнительного окисления металла.

При выбранной методике время, необходимое для проведения одного анализа, составляло 8 часов при использовании пробоотборников-дистилляторов с одним стаканом и 2 – 3 часа для пробоотборников-дистилляторов с четырьмя стаканами.

ОПРЕДЕЛЕНИЕ ВОДОРОДА В НАТРИИ

Прибором, с помощью которого можно измерять содержание гидрида натрия в натрии, является водородный диффузионный индикатор. В основу работы прибора положен тот факт, что водород способен при повышенной температуре диффундировать с заметной скоростью непосредственно из натрия через конструкционные материалы. Конструкционными материалами, имеющими наилучшую проницаемость при повышенной температуре водорода, являются палладий, никель и железо "армко" [5]. Поскольку палладий несовместим с расплавленным натрием [1], а железо "армко" имеет несколько худшую проницаемость, чем никель, то в качестве конструкционного материала водородного диффузионного индикатора нами был выбран никель. После серии конструктивных переработок и испытаний был сконструирован прибор (рис. 2).

Объем замкнутой камеры (полость Б) определялся тарировкой; давление в камере измерялось вакуумной лампой ЛТ-2. Зная объем камеры и измеряя время, за которое давление в ней возрастает на определенную величину, можно было бы рассчитать количество водорода, продиффундировавшего через никелевую стенку. Неизотермичность камеры учитывалась в расчете. Предварительное разряжение в камере (до величины $5 \cdot 10^{-3}$ мм рт.ст.) создавалось форвакуумным насосом, после чего вентиль закрывался. Показания лампы ЛТ-2 на атмосферу водорода

ТАБЛИЦА 2. РЕЗУЛЬТАТЫ ОПЫТОВ ПО ОПРЕДЕЛЕНИЮ ПОТЕРЬ КИСЛОРОДА ИЗ ПРОБЫ

№ п/п	Количество кислорода в натрии					Найдено количество кислорода (за вычетом глухого опыта) г · 10^{-3} и в %		Потеря кислорода, %
	Введено			Исходное, г · 10^{-3}	Суммарное, г · 10^{-3}			
	Количество NaOH, мл	Нормальность NaOH	Количество кислорода, г · 10^{-3}					
1	5	0,488	39	0,5	39,5	33,7	85	15
2	5	0,488	39	0,6	39,6	34,7	88	12
3	5	–"–	39	0,4	39,4	32,0	81	19
4	1	–"–	7,8	0,6	8,4	7,0	83	17
5	1	–"–	7,8	0,6	8,4	7,0	83	17
6	0,2	–"–	1,56	0,6	2,26	2,0	89	11
7	0,2	–"–	1,56	0,3	1,86	1,4	75	21
8	1	0,099	1,58	0,4	1,98	1,6	81	19
9	0,5	0,105	0,84	0,8	1,64	1,6	98	2,0
10	0,1	0,488	0,78	0,4	1,18	1,1	93	7,0
11	0,1	0,488	0,78	0,7	1,48	1,4	95	5,0

пересчитывались по данным работы [6]. Загрязнение натрия водородом осуществлялось введением в бак насоса через специальное устройство известных количеств водорода или воды. При этом температура натрия в контуре поддерживалась изотермической и равной 400 и 450°С. Чтобы избежать потери гидрида натрия вследствие осаждения его в тупиковых линиях и на поверхности газовой полости бака насоса, были приняты специальные меры: основной контур отключался с помощью двух герметичных вентилей от вспомогательного контура; количество тупиков в основном контуре было сведено к минимуму и их гидродинамика была организована так, что они постоянно промывались потоком натрия; температура газовой полости бака насоса была на 50°С выше температуры циркулирующего натрия. Применение этих мер позволило определять концентрацию гидрида натрия и продуктов взаимодействия натрия с водой расчетом. При этом согласно [4] принималось, что равновесные продукты реакции натрия с водой – окись и гидрид натрия.

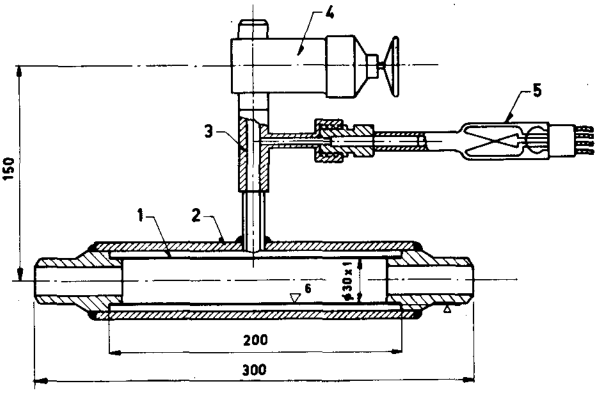

Рис.2. Никелевый датчик в натрии: 1 – никелевая трубка размером 32 × 1 мм; 2 – трубка из сплава Х18Н10Т размером 48 × 4 мм; 3 – тройник; 4 – вакуумный вентиль; 5 – лампа вакуумная.

Эксперименты проводились в следующей последовательности. После монтажа индикатора контур вводился в работу и проводилось длительное обезгаживание прибора. После очистки натрия холодной ловушкой до температуры забивания на пробковом индикаторе 150°С определялась фоновая постоянная прибора. Она соответствовала потоку водорода $<0{,}05$ нсм^3/час.

Специальные опыты показали, что проницаемость водорода при заданной концентрации его в натрии не зависела от того, вводится водород в натрий в виде воды или водорода. В основных опытах загрязнение натрия производилось водой.

Проницаемость водорода через никелевую стенку в вакуум изучалась в зависимости от концентрации гидрида натрия в натрии ($5 \cdot 10^{-5} \div 6{,}5 \cdot 10^{-2}$ вес%), температура натрия ($270 \div 450$°С) и его скорости ($0 \div 1$ м/сек). Результаты опытов по определению проницаемости водорода в зависимости от концентрации гидрида в натрии приведены на рис. 3. В исследуемом интервале концентраций при температурах 400 и 450°С поток водорода через никель прямо пропорционален концентрации гидрида натрия и может быть выражен следующим соотношением:

при $t = 400$°С $I = 0{,}18 \cdot C_{NaH}$ нсм^{3}мм/см^{2}час;

при $t = 450$°С $I = 0{,}31 \cdot C_{NaH}$ нсм^{3}мм/см^{2}час.

Изучение влияния температуры натрия на проницаемость водорода показало, что при температурах ниже 400°С теряется чувствительность за счет снижения проницаемости водорода.

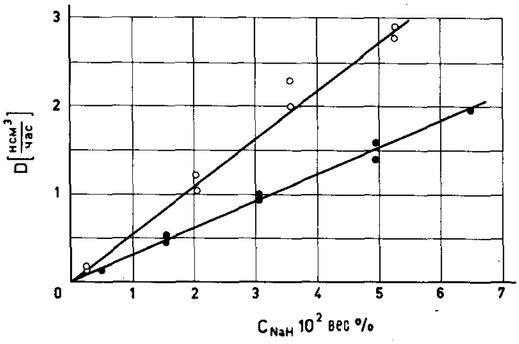

Рис.3. Зависимость проницаемости водорода D от концентрации его в натрии C_{NaH} : o – t = 450°C; ● – t = 400°C.

В наших опытах не было обнаружено влияния скорости натрия на поток водорода. Это свидетельствует о том, что никель составляет основное сопротивление переходу водорода из натрия в вакуум. Диффузия водорода в расплавленном натрии происходит намного быстрее, чем в никеле. Поэтому интенсификация процесса массообмена за счет турбулизации потока натрия не дает ощутимого результата.

ПРОБКОВЫЙ ИНДИКАТОР – ПРИБОР ДЛЯ ОБНАРУЖЕНИЯ ПРИМЕСЕЙ В НАТРИИ

Пробковый индикатор и по настоящее время является прибором, наиболее широко применяемым на установках с жидким металлом для контроля за содержанием примесей.

Принцип работы пробкового индикатора основан на способности выпадающих из раствора при понижении температуры примесей закупоривать проходные сечения. Прибор включает в себя специальное устройство с малым проходным сечением (шайба), теплообменник для охлаждения теплоносителя, регулирующий вентиль или специальный насос для установки необходимого расхода через прибор, расходомер, термопару для определения температуры теплоносителя, протекающего через узкие отверстия.

Конструкция одного из пробковых индикаторов окислов, использованных в данной работе, представлена на рис. 4, характеристика отверстий и теплообменников – в табл. 3.

Рассмотрим, как зависят показания пробкового индикатора от основных параметров. При проведении опыта фиксируется выпадение не первых кристаллов, а тот момент, когда сопротивление прибора из-за высаждения примесей возрастает настолько, что расход через прибор снижается с исходной величины Q_0 до некоторой величины Q_1. В общем случае можно записать:

$$Q_1 = aQ_0, \quad где\ 0{,}9 < a < 1.$$

Время высаждения необходимого количества окислов зависит от конструкции прибора, условий проведения опыта и будет равно некоторой величине τ_3. Поскольку опыт проводится при непрерывном понижении

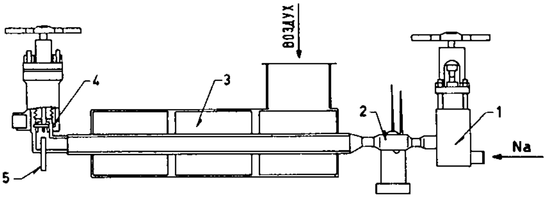

Рис.4. Конструкция пробкового индикатора окислов: 1 – регулирующий вентиль; 2 – расходомер; 3 – теплообменник; 4 – основной вентиль; 5 – карман термопары.

температуры металла, протекающего через отверстия, то температура, фиксируемая в момент снижения расхода через прибор до Q_1, будет ниже температуры насыщения на величину

$$\Delta t = \tau_3 \cdot \frac{dt}{d\tau} \tag{1}$$

При определении зависимости τ_3 от основных параметров прибора и условий проведения опыта будем считать, что:

- перепад давления на приборе при проведении опыта остается постоянным и определяется по формуле Дарси;
- все сопротивление прибора сосредоточено в отверстиях, где поток натрия имеет наинизшую температуру и где происходит высаждение окислов, приводящее к возрастанию гидравлического сопротивления прибора;
- прибор имеет n отверстий диаметром d_0;
- режим течения натрия через отверстия турбулентный, коэффициент сопротивления определяется законом Блазиуса, а поток окиси на единицу поверхности в единицу времени определяется по формуле [7]:

$$j = \sqrt{\frac{\xi}{2}} \cdot \frac{M_{Na_2O} \cdot \gamma_{Na} \cdot \overline{\omega} \cdot z}{100 M_0 \cdot \epsilon \cdot Pr_D^{3/4}} \tag{2}$$

- зависимость пересыщения от времени, концентрации насыщения и скорости понижения температуры металла, протекающего через отверстия, выражается соотношением:

$$z = \frac{dC_H}{dt} \cdot \frac{dt}{d\tau} \cdot \tau \tag{3}$$

- в потоке отсутствуют центры кристаллизации, движущиеся вместе с натрием.

Учитывая эти предположения и используя условие материального баланса, можно показать, что

$$0{,}785\, d_0^2 \left(1 - a^{14/11}\right) \varphi = \pi K_1 \overline{Q}^{0,9} \int_0^{\tau_{заб}} \frac{z}{d^{0,9}}\, d\tau \tag{4}$$

ТАБЛИЦА 3. ХАРАКТЕРИСТИКА ОТВЕРСТИЙ И ТЕПЛООБМЕННИКОВ

№ п/п	Характеристика отверстий			Характеристика теплообменников		
	Размер, мм	Число	Общая площадь, мм^2	Диаметр трубы, мм	Проход. сечение, м^2 · 10^{+4}	Конструкция теплообменника
1	1×1	16	16	30×2,5	4,9	Обребренная труба
2	1×1	16	16	55×3	18,8	То же
3	0,52×0,52	34	~9,2	55×3	18,8	" "
4	0,24×0,31	34	~2,5	55×3	18,8	" "
5	0,29×0,32	64	6	31×2,5	10,6	Змеевик двухзаходный
6	0,31×0,34	16	1,7	–"–	10,6	То же
7	0,52×0,52	16	4,3	–"–	10,6	" "
8	0,87×0,87	16	12	–"–	10,6	" "
9	1×0,75	12	9	20×2	2,0	Змеевик однозаходный
10	0,52×0,52	34	9,2	20×2	2,0	То же
11	0,40×0,50	32	6,4	20×2	10,6	Змеевик двухзаходный

Здесь

$$K_1 = \frac{\gamma_{Na} \cdot M_{Na_2O} \cdot k}{100\gamma_{Na_2O} \cdot M_0 \cdot \epsilon \cdot Pr_D^{3/4} \cdot n^{0,9} \cdot \left(\frac{\pi}{4}\right)^{0,9}}, \qquad (5)$$

а множитель φ учитывает тот факт, что в приборе гидравлическое сопротивление сосредоточено не только в отверстиях. Чем большая доля общего сопротивления прибора сосредоточена вне отверстий, тем φ больше единицы. При учете местных сопротивлений в уравнении (4) выражение в скобках заменится на $(1 - \sqrt{\xi_2 / \xi_1})$, где ξ_1 и ξ_2 полное сопротивление отверстий при расходах Q_0 и Q_1.

Соотношение, описывающее уменьшение размера отверстий во времени из-за высаждения примесей, можно также найти из условий материального баланса. Оно имеет вид:

$$d = \left(d_0^{2,9} - \frac{2,9}{2} K_1 \bar{Q}^{0,9} \cdot \frac{dc}{dt} \cdot \frac{dt}{d\tau} \cdot \tau^2\right)^{1/2,9} \qquad (6)$$

Подставляя (3) и (5) в (4), производя интегрирование и некоторые преобразования с учетом $\bar{Q} = Q_0 (1+a)/2$, получаем

$$\Delta t \simeq 8,7 \sqrt{\frac{M_0 \cdot \gamma_{Na_2O} \cdot d_0^3 \cdot \varphi \cdot \epsilon \cdot n \cdot Pr_D^{3/4} \cdot \frac{dt}{d\tau}\{1 - [1 - \frac{1}{2}(1 - a^{14/11})]^{\frac{2,9}{2}}\}}{M_{Na_2O} \cdot \gamma_{Na} \cdot Q_0 \sqrt{\xi} \cdot \frac{dc}{dt}(1+a)}} \qquad (7)$$

При выводе (7) не было учтено снижение пересыщения из-за кристаллизации примесей на поверхностях теплообменника и трубопровода, соединяющего теплообменник с шайбой. Можно показать, что для большинства реальных конструкций этот эффект будет тем выше, чем больше величина:

$$\frac{dc_H}{dt} \cdot \frac{dt}{d\tau} \cdot \frac{s^{2/3} \cdot v \cdot D^{2/3}}{s_k^{1/3} \cdot Q^{5/3}}. \qquad (8)$$

Оценочные расчеты показывают, что для конструкций приборов, использованных в наших опытах, когда длина трубопровода, соединяющего теплообменник с шайбой, не превышала 0,2 метра, а теплообменник не имел разветвленных поверхностей, снижение пересыщения незначительно. В иных условиях этот эффект может сыграть существенную роль.

Очевидно, что присутствие в натрии центров кристаллизации, движущихся с потоком, будет также приводить к дополнительному занижению показаний прибора.

Из (7) видно: для уменьшения занижения показания прибора необходимо уменьшать размер отверстий шайбы, скорость понижения температура на шайбе и увеличивать расход натрия через прибор; для сохранения постоянства Δt при уменьшении концентрации кислорода нужно или увеличивать расход через прибор или уменьшать скорость охлаждения. Эти положения проверялись экспериментально при загрязнения натрия кислородом.

Зависимость показаний прибора от расхода натрия изучалась на десяти шайбах в различных комбинациях с теплообменниками (см. табл. 3). Уровень концентрации кислорода в натрии при этом изменялся от $2{,}5 \cdot 10^{-2}$ вес% ($t_{\text{заб}} = 400$°С) до $6 \cdot 10^{-4}$ вес% ($t_{\text{заб}} = 150$°С), расход –

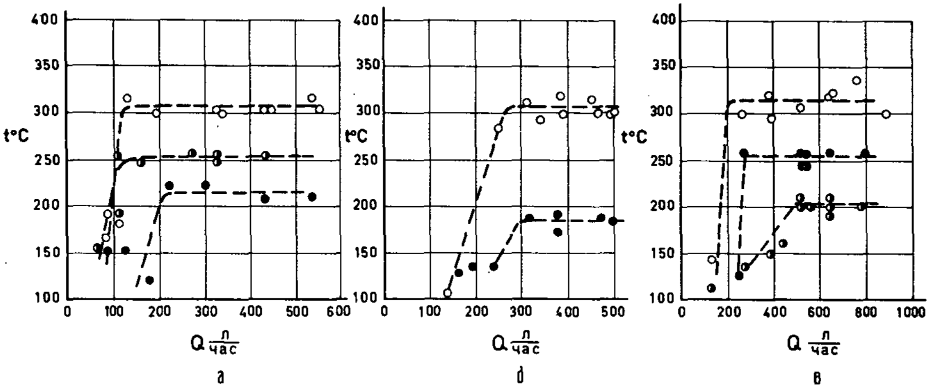

Рис.5. Зависимость показаний приборов от расхода металла: а) индикатор № 5; б) индикатор № 7; в) индикатор № 8.

от 10 до 800 л/час. Некоторые результаты приведены на рис. 5. Общим для всех приборов является тот факт, что с уменьшением расхода натрия ниже определенного уровня показания прибора занижаются, становятся неустойчивыми. Причем, чем ниже концентрация кислорода в натрии, тем при большем расходе прибор начинает давать неустойчивые показания. Увеличение размеров отверстий при неизменной конструкции теплообменника и при постоянной концентрации кислорода в натрии также приводит к увеличению расходов, при которых показания прибора становятся заниженными.

На рис. 6 представлены результаты, характеризующие область устойчивой работы индикаторов. Точками на графиках показаны расходы натрия через прибор, при которых при данной концентрации кислорода в натрии индикаторы занижают результаты. Расчетные оценки показывают, что при уменьшении содержания кислорода в натрии с 0,01 до 0,0005 вес % для обеспечения стабильной работы прибора необходимо увеличить расход в 3,2 раза. При проведении опытов приходилось увеличивать расход в 2 – 3 раза в том же диапазоне концентраций. Учитывая нестабильность параметров (скорость охлаждения, распределение гидравлических сопротивлений в приборе между шайбой и регулирующим вентилем и др.) при определении границы перехода из области I в область II, совпадение эксперимента с расчетом следует считать удовлетворительным. Все дальнейшие эксперименты проводились при расходах, обеспечивающих работу прибора в области устойчивых показаний.

Зависимость показаний прибора от размеров отверстий изучалась методом сравнения показаний двух приборов. Концентрация кислорода при измерениях поддерживалась на заданном уровне с помощью постоянной прокачки натрия через холодную ловушку. Сравнивались показания приборов 4-10, 9-2, 5-7, 3-9 (табл. 3). Усредненные отношения температуры забивания составляли 1,08; 1,03; 1,03 и 1,00 соответственно. Было также замечено, что с ростом концентрации кислорода в натрии

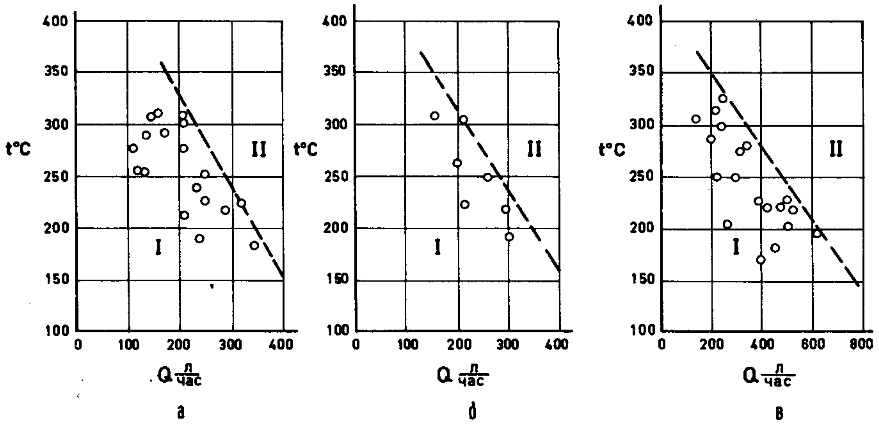

Рис.6. Области устойчивой и неустойчивой работы индикаторов: I – область неустойчивой работы; II – область устойчивой работы: а) индикатор № 5; б) индикатор № 7; в) индикатор № 8.

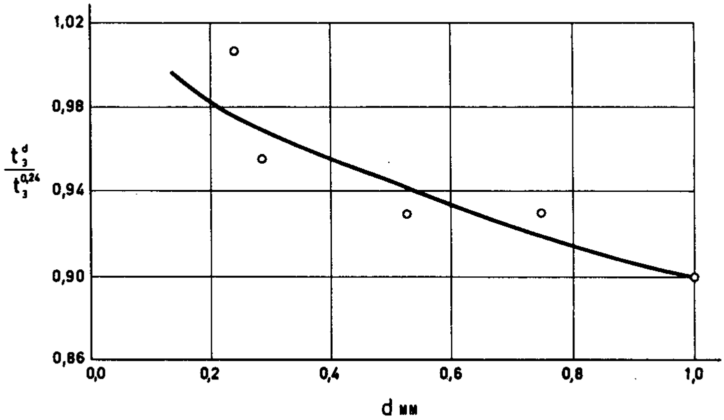

Рис.7. Зависимость показаний пробкового индикатора от размера отверстий.

расхождения в показаниях индикаторов уменьшались. Используя средние значения температур забивания и считая, что

$$\frac{t^2_{заб}}{t^9_{заб}} \cdot \frac{t^9_{заб}}{t^3_{заб}} = \frac{t^2_{заб}}{t^3_{заб}} \quad \text{и т.д.,}$$

высчитали отношение $t^2_{заб}$, $t^3_{заб}$, $t^4_{заб}$, $t^5_{заб}$, $t^9_{заб}$ к $t^4_{заб}$. Зависимость этого отношения от меньшего размера отверстий представлена на рис. 7.

Зависимость показаний прибора от скорости понижения температуры натрия, протекающего через отверстия, изучалась для приборов 1, 2, 3 и 9. Опыты проводились при двух содержаниях кислорода 0,004 и 0,026 вес%. Скорость падения температуры изменялась от 0,3 до 37°С/мин. В пределах точности эксперимента в данном интервале концентраций не было обнаружено зависимости показаний приборов от скорости понижения температуры металла. (При проведении опытов при малых расходах – область 1, рис. 6b, с уменьшением скорости охлаждения занижение показаний прибора уменьшалось). Учитывая результаты экспериментов, а также возможность случайных колебаний расхода через прибор, можно сказать, что нежелательно иметь скорость понижения температуры больше 10°C/мин, так как это может привести к появлению случайной ошибки в определении температуры забивания.

Зависимость температуры забивания от размера отверстий указывала на необходимость проведения тарировочных опытов. Тарировка приборов проводилась по кислороду (прибор 4, табл. 3), водороду и продуктам взаимодействия натрия с водой (прибор 2, табл. 3).

Тарировка по кислороду была проведена двумя методами: сопоставлением температуры забивания с температурой внутри холодной ловушки окислов при длительной ее работе в постоянном температурном режиме и непосредственным анализом натрия на содержание кислорода с помощью пробоотборника-дистиллятора. Результаты тарировки по первому методу показали, что в пределах точности опыта температура забивания совпадала с температурой в холодной ловушке.

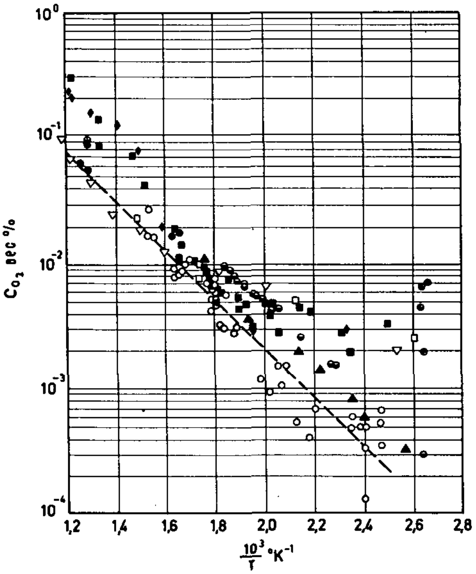

Рис.8. Тарировка пробкового индикатора по кислороду:
♦ □ – данные [1]; ■ – данные [8];
⊕ – данные [9]; ▲ – данные [10];
◒ – данные [11]; ▽ – данные [12];
--○ } – данные авторов.

Результаты тарировки вторым методом представлены на рис. 8. Там же даны результаты некоторых работ по растворимости кислорода в натрии. Разброс экспериментальных данных при концентрациях кислорода, больших $1 \cdot 10^{-3}$ вес% от среднего значения, не превышает 30%. При меньших концентрациях разброс возрастает, так как в этом интервале концентраций величина глухого опыта соизмерима с растворимостью кислорода в натрии. Очевидно, что в пределах указанной точности определение температуры забивания и анализа натрия на содержание кислорода полученные результаты представляют растворимость кислорода в натрии. Они описываются уравнением:

$$\lg C_{O_2} = 1,14 - \frac{1910}{T} . \qquad (9)$$

Тарировка пробкового индикатора по гидриду натрия и продуктам взаимодействия с водой производилась на экспериментальном стенде, описанном в разделе "Определение водорода в натрии".

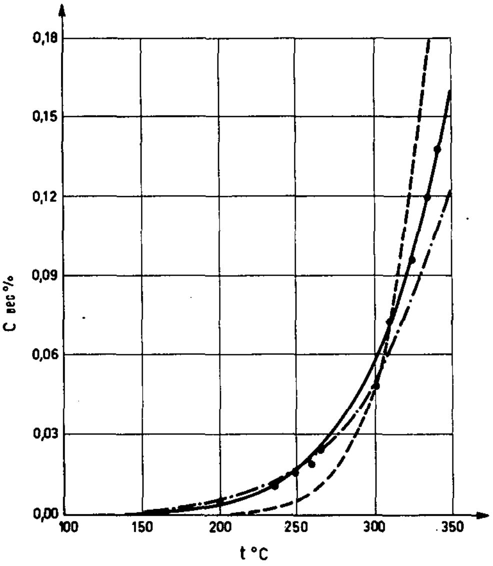

Рис.9. Тарировка пробкового индикатора по гидриду натрия:
----- данные [1]; —·— —·— данные [13];·—— данные авторов (формула 10).

Результаты опытов по тарировке пробкового индикатора на гидрид натрия представлены на рис.9. Линия, усредняющая экспериментальные точки, описывается уравнением:

$$\lg C_{NaH} = 4,36 - \frac{3209}{T} . \qquad (10)$$

Очевидно, что это уравнение с учетом указанных выше допущений описывает растворимость гидрида натрия в натрии. Сравнение наших результатов с данными работ [1, 13] показывает, что они близки к результатам, полученным в последнее время [13].

Результаты опытов по тарировке пробкового индикатора на продукты взаимодействия натрия с водой приведены на рис. 10. На графике концентрация примесей условно представлена в виде окиси натрия, поскольку в настоящее время неизвестно, с окиси или с гидрида натрия начинается кристаллизация. Линия, усредняющая экспериментальные данные, описывается уравнением:

$$\lg C_{Na_2O} = 3,49 - \frac{2650}{T} \qquad (11)$$

Из рис. 10 видно, что растворимость продуктов взаимодействия натрия с водой в несколько раз выше растворимости окиси натрия. Для объяснения этого факта был проведен специальный опыт.

Натрий, находящийся в циркуляционном контуре, очищался холодной ловушкой. За счет подачи в него газообразного кислорода достигалась повышенная температура забивания. Затем порционно подавался газообразный водород. После каждой порции водорода температура забивания понижалась. Это свидетельствовало о том, что растворимость окиси натрия в натрии при введении водорода в систему натрий-кислород увеличивается. Отсюда следует также, что каждому конкретному соотношению между кислородом и водородом в натрии соответствует своя функциональная зависимость растворимости этих примесей от температуры. Полученные нами данные по отношению водорода и кислорода в натрии близки к стехиометрическому составу воды.

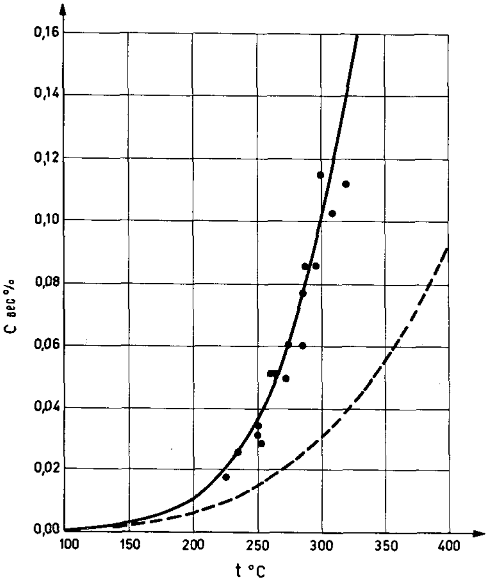

Рис.10. Тарировка пробкового индикатора по продуктам взаимодействия натрия с водой: —— данные авторов (формула 11); ----- данные авторов (формула 9).

ВЫВОДЫ

В результате проведенной работы по обнаружению примесей в натрии можно сделать следующие выводы:

1. Определение концентрации кислорода в пробе натрия методом вакуумной дистилляции является довольно оперативным и чувствительным. Параметры метода, выбранные на основании теоретических соображений и экспериментов, дают хорошую воспроизводимость и относительно малую ошибку. Разработанная методика анализа является в настоящее время наиболее надежной и позволяет определять концентрацию кислорода порядка $(2 \div 5) \cdot 10^{-4}$ вес% в натрии.

2. Обнаружение водорода в натрии и определение его концентрации с помощью диффузионного индикатора водорода является в настоящее

время наиболее чувствительным селективным методом, который позволяет оперативно проводить измерения на работающей установке, что особенно важно в случае обнаружения течи парогенератора "натрий-вода". Чувствительность метода составляет $(1 \div 2) \cdot 10^{-4}$ вес% водорода в натрии.

3. В работе был детально изучен пробковый индикатор, определены оптимальные параметры работы, и показана его работоспособность при определении кислорода, водорода и продуктов взаимодействия натрия с водой. Пробковый индикатор не является селективным прибором, но его показания ценны тем, что он показывает опасную суммарную концентрацию примесей с точки зрения высаждения их в наиболее холодных участках системы. Чувствительность пробкового индикатора при определении концентрации кислорода, водорода и продуктов взаимодействия натрия с водой в натрии следующая:

по кислороду – $5 \cdot 10^{-4}$ вес% O_2 в натрии,

по водороду – $5 \cdot 10^{-5}$ вес% H_2 в натрии,

по продуктам взаимодействия натрия с водой – $5 \cdot 10^{-4}$ вес% в расчете на кислород.

Обозначения

τ	– время	часы;
t	– температура	°С;
Δt	– занижение показаний прибора	°С;
T	– температура	°К;
c	– концентрация примеси в натрии	вес%;
c_H	– концентрация примеси в натрии, соответствующая растворимости при данной температуре	вес%;
$z = c - c_H$	– пересыщение, т.е. избыток концентрации пересыщенного раствора над равновесной	вес%;
a	– коэффициент, учитывающий стабильность расхода через прибор и чувствительность вторичного прибора	
ξ	– интегральный коэффициент сопротивления	
ϵ	– некоторая постоянная порядка единицы	
D	– коэффициент диффузии	м³/час;
$Pr_D = \frac{\nu}{D}$	– диффузионный критерий Прандтля	
M	– молекулярный (атомный) вес	
γ	– удельный вес	кг/м³;
ω	– скорость натрия	м/сек;
s s_k v	– поверхность м², проходное сечение м² и объем участка до шайбы м³, омываемого пересыщенным раствором	

ЛИТЕРАТУРА

[1] Жидкометаллические теплоносители. Перевод под редакцией А.Е.Шейндлина, Изд. ин. литературы, М., (1958).

[2] СУББОТИН В.И., КИРИЛЛОВ П.Л., КОЗЛОВ Ф.А. "Теплофизика высоких температур", 3, 1 (1965) 154 – 63.

[3] СУББОТИН В.И. и др. "Атомная энергия", 19, 3 (1965) 298.

[4] ИВАНОВСКИЙ Н.Н. и др. "Атомная энергия", 17, 5 (1964) 406 – 8.
[5] ДЭШМАН С. Научные основы вакуумной техники, М., 1965 (перевод с англ.).
[6] ХОВКИН Л.П., ЖТФ, XXV, 726 (1955).
[7] ЛЕВИЧ В.Г., Физико-химическая гидродинамика, М., (1959).
[8] McINTOSH A.B. and BAGLEY K.Q. J. Br. Nucl. Energy Conf. 3, 1 (1958) 15 – 40.
[9] БАННЫХ З.С., ФЕФЕЛОВА И.Ф., Труды Уральского научно-исследовательского химического института, вып. 5 (1957 и 1958).
[10] ALLEN T., Nucl. Engng., 7, 76 (1962) 352 – 5.
[11] GREY I.L. et al., Nucleonics, 14, 10 (1956) 34.
[12] WILLIAMS D.D. et al., J. phys. Chem., Ithaca, 63, 1 (1959) 68 – 71.
[13] McCLURE D.W., HALSEY G.D. J. phys. Chem., 69, 10 (1965) 3542.

ИССЛЕДОВАНИЕ ВОЗМОЖНОСТИ КОНТРОЛЯ ПРИМЕСЕЙ В ЖИДКОМЕТАЛЛИЧЕСКИХ ТЕПЛОНОСИТЕЛЯХ ПУТЕМ ИЗМЕРЕНИЯ ЭЛЕКТРОСОПРОТИВЛЕНИЯ

М.Н.АРНОЛЬДОВ, М.Н.ИВАНОВСКИЙ,
В.И.СУББОТИН, Б.А.ШМАТКО
ФИЗИКО-ЭНЕРГЕТИЧЕСКИЙ ИНСТИТУТ, ОБНИНСК
СССР

Abstract — Аннотация

INVESTIGATION OF THE POSSIBILITY OF DETERMINING IMPURITIES IN LIQUID-METAL COOLANTS BY MEASURING ELECTRICAL RESISTANCE. Efforts to determine experimentally the relationship between the specific electrical resistance of molten lithium and sodium, and the amounts of oxygen, nitrogen and hydrogen present, are described. It was found that the results of measurements of the relationship between the electrical resistance of sodium and the hydrogen content are affected by sodium hydride dissociation. Conclusions are drawn on the possibility of determining the amounts of nitrogen and hydrogen in lithium and hydrogen in sodium.

ИССЛЕДОВАНИЕ ВОЗМОЖНОСТИ КОНТРОЛЯ ПРИМЕСЕИ В ЖИДКОМЕТАЛЛИЧЕСКИХ ТЕПЛОНОСИТЕЛЯХ ПУТЕМ ИЗМЕРЕНИЯ ЭЛЕКТРОСОПРОТИВЛЕНИЯ. Излагаются результаты экспериментального определения зависимости удельного электросопротивления расплавленных лития и натрия от содержания примесей кислорода, азота и водорода. Обнаружено влияние диссоциации гидрида натрия на результаты измерения зависимости электросопротивления натрия от содержания водорода. Дается вывод о возможности контроля содержания примесей азота и водорода в литии и примеси водорода в натрии.

Контроль содержания газовых примесей является одним из условий успешной работы ядерных реакторов, охлаждаемых жидкометаллическими теплоносителями.

Известно, что присутствие растворенных примесей в жидком металле отражается на многих физических свойствах металла. Изменение этих свойств может служить сигналом изменения содержания примесей в металле.

Особый интерес представляет контроль содержания примесей путем измерения электросопротивления. Электросопротивление легко поддается измерению с помощью простых методов и аппаратуры. Измерения электросопротивления могут быть автоматизированы и производиться дистанционно.

В литературе описан прибор, основанный на измерении электросопротивления, с помощью которого осуществляется контроль чистоты протекающего в контуре ядерного реактора натрий-калиевого сплава [1]. В работе предполагалось, что изменение электросопротивления жидкого сплава происходит вследствие изменения содержания кислорода, находящегося в сплаве в форме окиси натрия. Влияние температуры на сопротивление исключалось с помощью специальной схемы измерений. Измерение электросопротивления натрий-калиевого сплава производилось при одновременной очистке сплава от примесей с помощью холодных ловушек. Результаты измерения указывают на зависимость электросопротивления сплава от степени его очистки.

Однако в работе [1] не было приведено никаких доказательств того, что изменение сопротивления сплава происходит благодаря изменению содержания кислорода. Не приводится так же и количественной зависимости сопротивления сплава от содержания кислорода или других примесей. Авторы [1] предположили, что зависимость электросопротивления сплава натрия с калием от содержания кислорода аналогична зависимости для некоторых металлов (медь, ниобий).

В дальнейшем появилось сообщение [2], в котором указывается, что наличие зависимости сопротивления от концентрации не специфично для кислорода, растворенного в натрии, а следовательно, и в натрий-калиевом сплаве. Согласно этим данным контроль содержания кислорода в этих жидких расплавах путем измерения электросопротивления невозможен.

Впервые экспериментальные данные по зависимости примесного сопротивления натрия от концентрации кислорода были представлены в [3]. При 350 °С изменение удельного электросопротивления натрия от концентрации кислорода подчиняется зависимости

$$\rho_{350°C} = 0{,}189\ (1+\Delta C_{O_2}) \left[\frac{\text{ом}\cdot\text{мм}^2}{\text{м}}\right]$$

Измерения проводились на циркуляционном контуре с помощью прибора, аналогичного описанному в [1].

Таким образом, в литературе имеются противоположные взгляды на зависимость электросопротивления натрия от содержания кислорода, в то же время там нет сведений о зависимости удельного электросопротивления расплавленного лития от содержания основных газовых примесей кислорода, азота и водорода.

Очевидно, что возможность контроля содержания примесей в расплавленных литии и натрии методом измерения электросопротивления в первую очередь определяется характером зависимости электросопротивления от содержания примесей.

Авторами данного доклада было предпринято измерение удельного сопротивления лития при температуре 300 °С в зависимости от содержания азота, кислорода и водорода, и натрия в зависимости от содержания кислорода и водорода при температуре 350 °С.

Для измерения сопротивления металла использовали двойной мост постоянного тока. Сопротивления лития и натрия измеряли с помощью одной и той же установки. Исследуемый металл находился в измерительной трубке из стали 1Х18Н9Т с наружным диаметром 9 мм и толщиной стенки 0,4 мм. Измерительная трубка подсоединялась к циркуляционному контуру, снабженному насосом для перекачивания металла и устройством для дозированного ввода газов в металл.

Кислород, водород и азот вводили непосредственно в металлы в газообразном виде. Количество введенных газов определялось по изменению их давления в баке известного объема, находящегося при известном давлении и температуре. Кислород в натрий вводился, кроме того, и в виде перекиси натрия. Точность дозировки была не хуже 1%.

Непрерывная циркуляция металла через измерительную трубку обеспечивала постоянство состава металла во время измерения сопротивления. Постоянство температуры металла в измерительной трубке поддерживалось с точностью 0,05 °С с помощью термостата. Конфигурация измерительной трубки полностью исключала утечку тока во внеш-

ТАБЛИЦА. СОСТАВ ПРИМЕСЕЙ В ИСХОДНЫХ ЩЕЛОЧНЫХ МЕТАЛЛАХ (вес %).

Элемент	0	N	H	C	Na	Li	Ca	Ba	Cz	Si	Ni, Mn, Al, Be, Ag, Cu, Ti, Fe
Литий	$1\cdot10^{-2}$	$1\cdot10^{-2}$	$3\cdot10^{-2}$	$5\cdot10^{-4}$	0,5	–	$6\cdot10^{-3}$	$1\cdot10^{-2}$	$3\cdot10^{-2}$	$4\cdot10^{-2}$	$3\cdot10^{-3}$ (кажд.)
Натрий	$5\cdot10^{-4}$	–	$1\cdot10^{-3}$	$5\cdot10^{-2}$	–	10^{-4}	$1\cdot10^{-3}$	–	–	$1\cdot10^{-3}$	$3\cdot10^{-3}$ (кажд.)

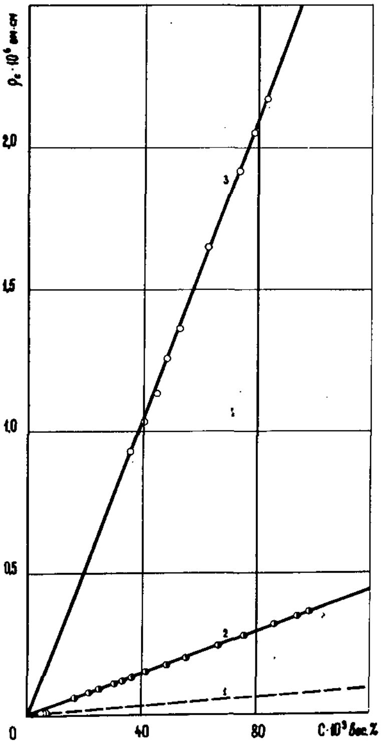

Рис. 1. Зависимость удельного электросопротивления лития от содержания примесей кислорода, азота, водорода при температуре 300°С:
1 – кислород; 2 – азот; 3 – водород.

ний циркуляционный контур. Перед заливкой металла было тщательно измерено электросопротивление пустой измерительной трубки в интервале температур 200 – 350°С. Для исследования применялись металлы, исходное содержание примесей в которых дано в таблице.

Систематически производилось сопоставление количеств введенных газов с результатами химического анализа металлов на содержание введенных примесей. Расхождение между сопротивляемыми величинами не выходило за пределы точности химического анализа и дозировки примеси. Как показал анализ, в процессе ввода одной из примесей содержание остальных примесей (газовых и металлических) оставалось на неизменном уровне, соответствующем данным таблицы.

Данные по зависимости удельного сопротивления лития от содержания кислорода, водорода, азота при температуре 300 °С приведены на рис.1. Каждой прямой на рисунке соответствует изменение лишь данной примеси. Содержание остальных примесей не отличается от данных таблицы.

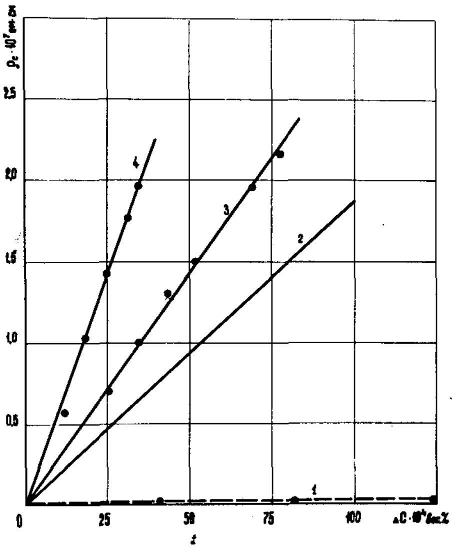

Рис. 2. Зависимость удельного электросопротивления натрия от содержания примесей кислорода и водорода при температуре 350°С:
1 – кислород, данные авторов; 2 – кислород, данные [3]; 3 – водород, данные авторов, отношение объемов металла и газовой полости равно 1; 4 – то же, отношение объемов равно 3.

На рис.2 приведена графически зависимость удельного сопротивления натрия от содержания кислорода при температуре 350 °С. В процессе ввода кислорода не было обнаружено изменения сопротивления измерительной трубки с натрием с точностью до $5 \cdot 10^{-8}$ ом (сопротивление измерительной трубки с натрием при 350 °С равно $5 \cdot 10^{-4}$ ом). Согласно данным [3] изменение электросопротивления трубки при введении такого количества кислорода должно было составить $8 \cdot 10^{-6}$ ом.

Таким образом, полученные нами результаты для кислорода согласуются с данными [2] и расходятся с предположениями, высказанными в [1], и данными [3]. Причины расхождения результатов данной работы и работы [3] не ясны.

Изучение влияния содержания водорода на электросопротивление натрия осложнилось явлением диссоциации гидрида натрия. Как известно, гидрид натрия интенсивно диссоциирует при умеренных температурах (P_{H_2} = 440 мм рт.ст. при 400 °С).

При температурах, когда давление диссоциации становится заметным, щелочные металлы представляют собой равновесные системы, включающие в себя металл, растворенную в металле примесь и свободный газ над поверхностью металла. Равновесие системы, состоящей из металла и газовой полости над ним, определяется уравнением состояния газа, уравнением, описывающим зависимость давления газа от его концентрации в металле и соотношением неизменности количества газа.

В простейшем случае система этих уравнений может быть записана следующим образом:

$$PV = G_г RT \tag{1}$$

$$G_м/G_p = kP^n \exp\left(\frac{Q}{T}\right) \tag{2}$$

$$G_г + G_м = G_0 \tag{3}$$

Формула (2) здесь заимствована из [4], она выражает зависимость концентрации растворенного газа как от давления, так и от температуры. Величина "Q" в ней имеет смысл энергии активации.

Решая совместно уравнения (1, 2, 3), можно получить

$$\frac{(G_0 - G_г)^{1/n}}{G_г} = \beta T \exp\left(\frac{\alpha}{T}\right), \tag{4}$$

где $\beta = \frac{G_p^{1/n} \cdot R\, k^{1/n}}{V}$, $\alpha = \frac{Q}{n}$

Отсюда видно, что равновесие определяется всеми параметрами, характеризующими систему. Изменение любого из параметров (G_p, T, V, G_0) приводит к изменению количества газа, находящегося в газовой полости и в металле. Изменение объема газовой полости может привести к изменению количества газа в ней за счет изменения концентрации примеси в металле. Сброс инертной атмосферы над поверхностью металла, а вместе с ней и свободного газа, так же приводит к уменьшению содержания растворенной в металле примеси за счет восстановления равновесного давления свободного газа в полости.

Нарушение равновесия может возникнуть также вследствие изменения температуры системы. Рассмотрим реакцию системы на изменение температуры с помощью формулы [4]. Продифференцируем формулу [4] по температуре, в результате получим

$$\frac{dG_г}{dT} = -\frac{G_г \cdot \beta (1 - \alpha/T) \exp(\alpha/T)}{\beta T \exp(\alpha/T) + 1/n (G_0 - G\ )^{\frac{1-n}{n}}} \tag{5}$$

Видно, что знак производной определяется лишь знаком сомножителя $(1 - \alpha/T)$, остальные члены формулы (5) сугубо положительны. При высоких температурах $(1 > \alpha/T)$ при увеличении температуры происходит уменьшение количества свободного газа и увеличение газа, растворенного в металле. При низких температурах $(1 < \alpha/T)$, наоборот, повышение температуры должно сопровождаться увеличением доли газа, находящегося в свободном виде.

Эксперименты, проведенные авторами, показали, что в соответствии с формулой (4) результаты измерения электросопротивления расплавленного натрия зависят от размеров газовой полости установки. В этих опытах изучалась зависимость удельного электросопротивления натрия от содержания растворенного водорода, вводимого в натрий в газообразном виде.

На рис.3 приведены записи сопротивления натрия, циркулировавшего через измерительный участок, при вводе в установку водорода. При медленном вводе водорода непосредственно в натрий газообразный водород, не успевая проходить в газовую полость установки, полностью реагировал с натрием, образуя гидрид натрия. В результате сопротивление натрия возрастало. Однако, поскольку содержание водорода в газовой фазе не соответствовало новой концентрации водорода, растворенного в натрии, затем происходила диссоциация части гидрида натрия вплоть до наступления равновесия. В результате этого увеличивалось

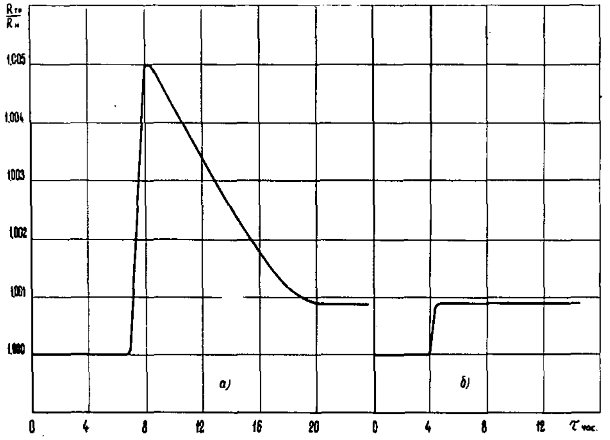

Рис. 3. Изменение электросопротивления натрия при вводе водорода:
а) ввод водорода в металл; б) то же, в газовую полость.

парциальное давление водорода в газовой фазе, а содержание растворенного водорода уменьшалось. Поэтому, после возрастания электросопротивление натрия начинало уменьшаться (рис.3 а). При подаче водорода непосредственно в газовую полость устанавливалось равновесие между свободным водородом и водородом в металле, поэтому концентрация водорода в металле монотонно возрастала со временем (рис.3 б).

На рис.2 приведены зависимости примесной части удельного электросопротивления натрия от общего содержания водорода в системе для двух значений объемов газовой полости при температуре 350°С. Очевидно, наиболее достоверной зависимостью удельного сопротивления натрия от содержания растворенного водорода является зависимость, полученная при минимальном объеме газовой полости, т.к. в этом случае практически весь введенный водород находится в виде раствора в натрии. Равновесное количество водорода в газовом объеме в этом случае не превышает 3% от введенного.

Из приведенных данных видно, что электросопротивление расплавленных натрия и лития существенно зависит от содержания водорода и практически не зависит от содержания кислорода. Сопротивление лития кроме того сильно зависит от содержания азота.

Отсюда следует, что методом измерения электросопротивления можно с высокой чувствительностью контролировать изменение концентрации водорода в натрии, а также водорода и азота в литии. Очевидно, высокочувствительный контроль возможен лишь при термостатировании исследуемых образцов или при компенсации влияния температуры путем введения точных поправок.

Контроль содержания примесей методом измерения сопротивления не является избирательным по отношению к какой-либо одной примеси. Так, сопротивление лития почти одинаково заметно изменяется при изменении содержания как азота, так и водорода. Поэтому эффективный контроль возможен в том случае, если известно, что изменяется содержание определенной примеси.

Обращает внимание весьма слабая зависимость сопротивления лития и натрия от содержания кислорода. Возможно, что это связано с относительно высокой прочностью окисей лития и натрия.

Отличается особенностью контроль содержания водорода в натрии. При измерении электросопротивления натрия, содержащего примесь водорода, следует иметь ввиду, что изменение содержания водорода может произойти вследствие изменения температуры системы, давления или изменения газового объема над поверхностью натрия. По-видимому, такими же особенностями должен отличаться контроль содержания водорода в литии. Однако, поскольку гидрид лития труднее диссоциирует, влияние диссоциации должно оказаться при более высоких температурах, чем для гидрида натрия.

Обозначения

P – давление газа
T – температура
V – объем газовой полости
$G_{\text{г}}$ – количество газа в газовой полости
$G_{\text{р}}$ – количество газа в металле
$G_{\text{м}}$ – количество жидкого металла
ρ – удельное электросопротивление
ρ_C – примесные удельные сопротивления
C – весовая процентная концентрация примесей
n, k – экспериментальные константы.

ЛИТЕРАТУРА

[1] BLAKE, R.N., Nucleonics, 19 (1961) 5.
[2] CLAXTON, K., J. nucl. Energy, Part A/B, 19 (1965) 11.
[3] КОЗЛОВ Ф.А. и др. "Теплофизика высоких температур", 3 (1965) 1.
[4] McCLURE, D. et al., J. phys. Chem., Ithaca, 69 (1963) 10.

DISCUSSION

(on the previous two papers)

P. MECHELYNCK: Does the fact that variations in hydrogen concentration have a marked influence on sodium resistivity, whereas variations in oxygen concentration do not, prove that there is no sodium hydroxide in the sodium, i. e. that the hydrogen is invariably in the form of hydride or dissolved hydrogen, and that the oxygen is always present in the carbonate or oxide form?

M.N. IVANOVSKY: No, it does not. In our experiments the hydrogen was introduced into extremely pure sodium. The oxygen, too, was introduced into sodium containing less than 1 ppm of hydrogen. In an operating circuit both the concentration and the composition of these impurities might be different. But we have shown, in any event, that pure hydride dissolved in sodium has a very powerful effect on resistivity. Pure oxide has virtually no effect on resistivity; but an operating system, again, in which both oxide and hydride are present may well contain hydroxide and other compounds in which hydrogen and oxygen are united.

Therefore, when the loop is contaminated by impurities washed out of the cold trap it does not follow that we are contaminating it with oxide; nor does the correlation between the proton indicator and the rhometer necessarily mean that the rhometer is registering oxygen. We interpret it to mean that the rhometer is reacting to some complex compound which contains, among other things, hydrogen. Dissolved hydrogen, we feel, is likely to be present as a positive ion; in other words it has a powerful effect on resistivity.

J. SANNIER: In the distillation technique that you used at 550°C, is the measurement of oxygen concentration not distorted by carbonate in the sodium?

M.N. IVANOVSKY: Yes, it may be. This is something that has to be taken into account during analysis.

J. SANNIER: I have a second question, concerning the hydrogen detector. Would you not expect the oxide impurities in the circuit to react with the nickel diaphragm, so that in time the response of the instrument would be altered?

M.N. IVANOVSKY: Not really; we have done thermodynamic calculations and tests on the instrument which suggest that nickel is suitable as a diaphragm material.

R.A. DAVIES: In a paper which is to be presented later (SM-85/16) we have shown that up to about 20 ppm of oxygen in sodium the resistivity increases in accordance with the figures Mr. Williams presented earlier in paper SM-85/29, whereas above 20 ppm the increase in resistivity is much smaller. Have you investigated the region below 20 ppm of oxygen?

M.N. IVANOVSKY: Our measurements were carried out at oxygen concentrations above 20 ppm.

R.A. DAVIES: What was the thickness of the nickel diaphragm in the hydrogen detector?

M.N. IVANOVSKY: One millimetre.

K.T. CLAXTON: Your oxygen solubility data suggest a comment or two. In my first review of the data for oxygen solubility (cited by you as

Ref. [2]) I made use of a value of 920°C for the melting point of Na_2O, obtained by Kohlmeyer and his colleagues. Beuaziz and his co-workers have since (in 1966) presented a new value, 1132°C, which has been used to recorrelate the data. The fit of the data in statistical terms is in fact much better, particularly that obtained by Thorley, which is among the best.

I have also analysed the Los Alamos data obtained by Rutkauskas, who used vacuum distillation to separate the sodium from the impurity. It was found that the best means of correlating on a (log) solubility versus temperature $(T°K)^{-1}$ plot was to split the data up into two groups, above and below 215°C. Below 215°C the line obtained gives a heat of solution value of about 8500 cal/mole: this is close to the value obtained by Thorley and other authors for this temperature range. Above 215°C a heat of solution of nearly 10 000 cal/mole was obtained. This change in the slope of the line is the only example that occurs in a given piece of apparatus, and quite clearly it points to a change in the character of the oxygen-bearing species in liquid sodium.

A. HATTERER: The influence of hydrogen and oxygen on the resistivity of caesium at 30°C is at present being studied in our laboratory, and we have observed a marked effect of water traces in the "pure" gases that react with the metal. What was the water content of the gaseous reagents used by the authors in their experiments with lithium and sodium?

M. N. IVANOVSKY: The gases were not analysed for water content. When hydrogen is added to liquid metals water impurities in the gas introduce no error. When oxygen is added no change in resistivity is observed, which suggests that water impurities in the oxygen are negligible for the purposes of our measurements.

EVALUATION OF IMPURITY MONITORING DEVICES TESTED IN A DYNAMIC SYSTEM

J.P. PETREK AND E.C. KOVACIC
ATOMIC POWER DEVELOPMENT ASSOCIATES, INC.,
DETROIT, MICH.,
UNITED STATES OF AMERICA

(Presented by W.L. Chase)

Abstract

EVALUATION OF IMPURITY MONITORING DEVICES TESTED IN A DYNAMIC SYSTEM. Several devices for the detection and monitoring of impurities in sodium are being evaluated in a dynamic test loop. The loop consists basically of a main loop and test loop and is equipped with cold trap, hot trap, plugging meter, sampling station, impurity injection port, and with the various impurity monitoring and purification devices that are being evaluated. Total sodium inventory in the loop is 150 gal. Sodium circulation is 100 gal/min in the main loop and 7.5 gal/min in the test loop. The loop can be operated up to 1000°F.

Three rhometers are being evaluated. In the initial test evaluation of the rhometer, impurities were injected by raising the loop cold-trap temperature, and the impurity level was determined by utilizing plugging temperatures and sodium monoxide solubility data. On this basis, the rhometer response was approximately 0.008% R per ppm of monoxide. Subsequent tests were performed by directly injecting specific impurities including Na_2O, NaOH, NaH, Na_2CO_3 and H_2O into the loop. The rhometer response to the specific impurity injections, except for H_2O, was substantially less than had been previously observed. The rhometer response for Na_2O injection was a factor of 10 less. More recently, evaluations of the meters with sodium monoxide injections tend to confirm the preliminary results.

Four electrolytic oxygen cells are being evaluated in the loop. In the initial semi-quantitative tests, the meters were observed to respond in the predicted direction to specific injections of sodium monoxide and water. The data indicate a large noise-to-signal ratio which primarily has been attributed to changes in ambient temperature. Preliminary tests show that significant step changes in the cell output result from temperature cycling and also from the presence of gamma radiation.

In conjunction with the evaluation of the rhometers and oxygen meters, test programmes are being conducted to evaluate both the plugging meter, and sampling and chemical analysis as means of impurity monitoring. The enclosure of the loop sampling station in an inert-atmosphere glove box has eliminated atmospheric contamination. Segregation of impurities in samples has been definitely established, and the effect has been found to increase with increasing impurity level. A precision of ± 10% has been demonstrated for the determination of sodium monoxide by the amalgamation analysis technique at the 10 ppm level. Plugging meter readings have been demonstrated to be reproducible within ± 10°F in the range 220-300°F.

1. GENERAL

The importance of developing a fast breeder reactor using an alkali metal as coolant is well established. The existing fast breeder reactors such as Experimental Breeder Reactor II and the Enrico Fermi Atomic Power Plant in the United States, the Dounreay Fast Reactor in the United Kingdom, and the Breeder Reactor-5 in Russia have already demonstrated the capability of providing the needed performance using sodium as the coolant. Many other sodium-cooled reactors are in the planning stage and will require more demanding operating requirements. These demands will also require improved control of sodium purity.

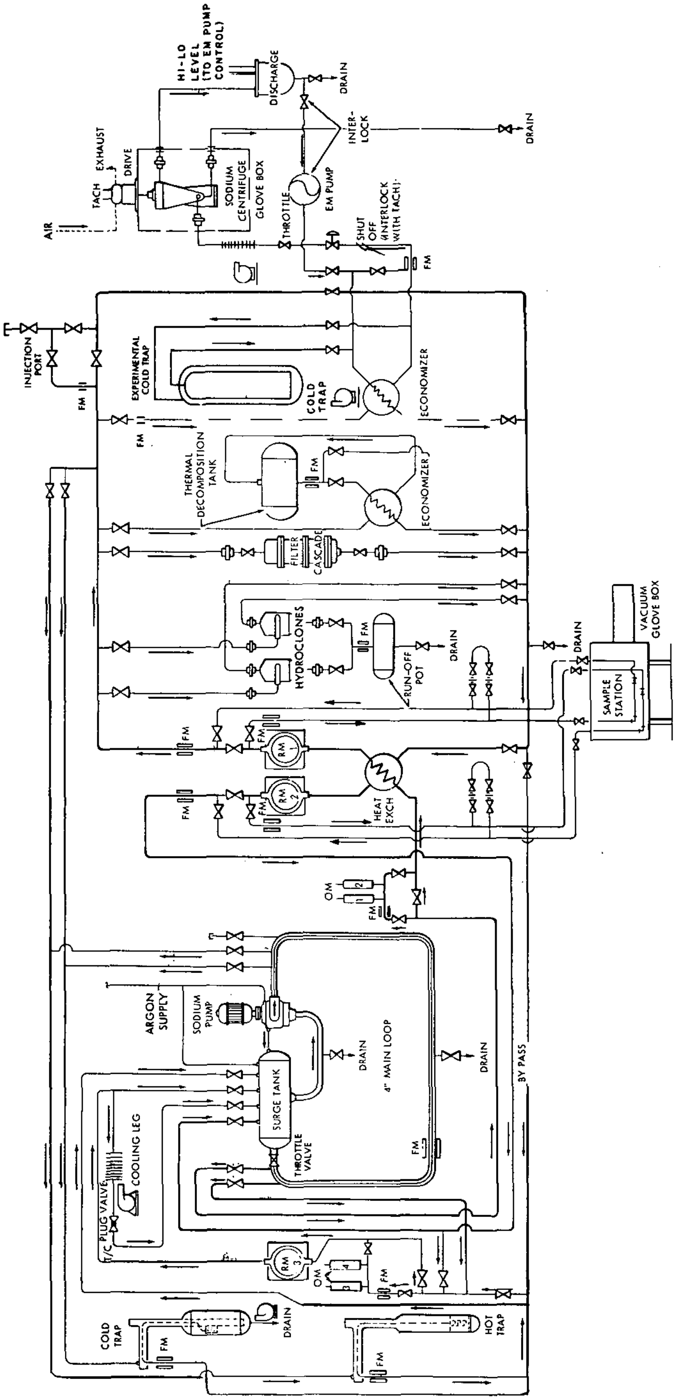

FIG. 1. Schematic of sodium technology showing proposed centrifuge and cold-trap insulation

Generally, the damaging effects of the coolant on reactor materials has been caused by the impurities initially present or inadvertently introduced during operation and not by the alkali metal itself. Impurities such as oxygen, hydrogen, carbon, nitrogen and/or a combination of these elements are considered detrimental to reactor materials when present in sufficient quantities. It becomes important to qualitatively and quantitatively monitor these impurities to achieve a means of controlling the impurities before the system can be harmed.

2. INTRODUCTION

Under the sponsorship of the USAEC, a sodium technology program has been established at APDA to develop and evaluate in-line devices for detecting, monitoring, and controlling impurities in sodium. The program also includes supporting efforts including laboratory analytical techniques and the chemical behavior of impurities in sodium. The discussions in this paper are mainly on the effort to evaluate in-line impurity monitoring devices.

The evaluations are being conducted in a sodium technology loop that was designed and built at APDA specifically for this purpose. This loop permits controlled additions of various impurities into the sodium and provides monitoring and detecting instruments, sampling systems, and clean-up devices to permit a quantitative study of the behavior of these impurities over a range of temperature and concentration.

3. LOOP DESCRIPTION

The sodium technology loop, shown in Figure 1, consists of two Type 304 stainless steel loops: a four-inch main loop and a one-inch test loop. The major components in the four-inch loop include a 200-gallon dump and storage tank, a 200-to 300-gpm Byron-Jackson mechanical pump, a 45-gallon surge tank, a zirconium packed hot trap, and a stainless steel cold trap with economizers and appropriate vent and drain service lines. The active loop inventory is approximately 800 pounds of sodium. The main loop cold trap is air cooled and consists of a 30-gallon vertical tank 14 inches in diameter with a four-inch downcomer inlet; there is stainless steel mesh packing in the tank.

A variable-orifice, air-cooled plugging meter was installed in a side loop of the four-inch loop. The unit consists of a special 1/2-inch bellows-seal globe valve in which the seat is ground to a 15-degree angle for close control of clearance. A special fine thread on the stem and position indicator permits clearance settings to a tolerance of one mil.

The 1-inch test loop connected to the four-inch loop is basically used for installation and testing of impurity measuring instruments and impurity clean-up devices. Presently three Blake resistivity meters and four United Nuclear Corporation oxygen meters are installed in the test loop. Clean-up devices such as a cold trap, hydroclone, filter cascade, and a high-speed centrifuge are installed or will be installed for evaluation studies in the future. The 1-inch loop also contains two 1/2-inch sodium sample lines that pass into a glove box for removing sodium samples from the system under an inert atmosphere before and after a test run.

The sodium circulation in the four-inch loop is approximately 100 gallons per minute and 7.5 gallons per minute in the one-inch loop. The design operating temperature of the entire system is 1000°F. The flow in the one-inch test loop is controlled by a pressure drop across two parallel throttle valves in the four-inch main loop. Tubular, strip, and clamshell heaters provide heat to the system and are controlled by variable transformers.

4. RHOMETERS

4.1 Description

The basic components of the Blake Rhometer, Figure 2, consists of a double loop transformer coil with a primary excitation winding of N turns to produce a constant flux. A single turn toroid pipe, designed to carry the flowing sodium, forms one of the secondary coils and a probe coil of n turns forms the other. The current generated within the toroid constitutes the transformer load. The voltage drop across the primary circuit is a direct reflection of the loading current in the toroid circuit. Since the primary current is very small, a probe coil is provided to amplify the effective voltage generated in the toroid and

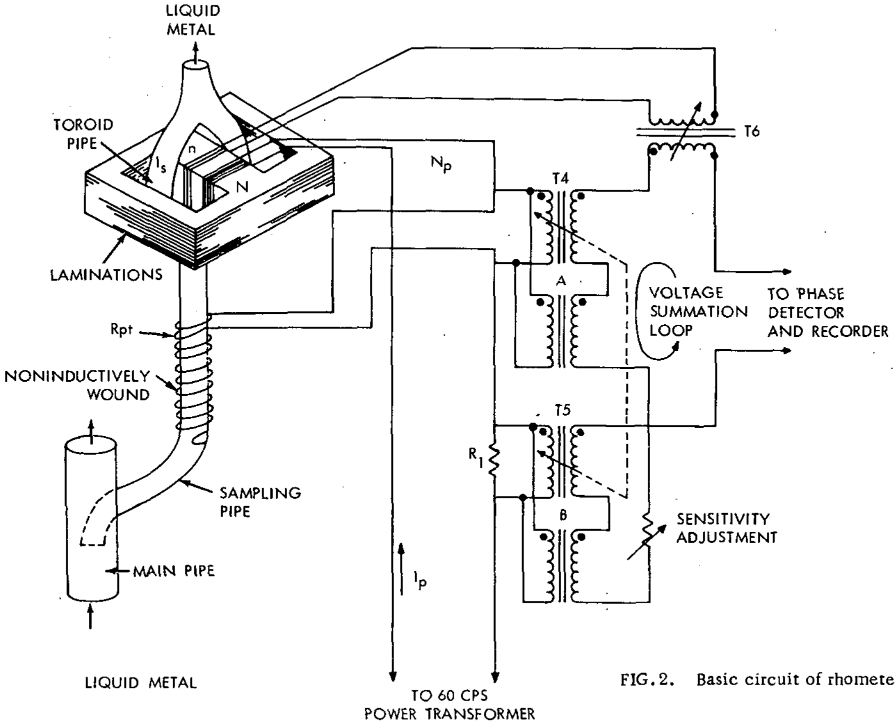

FIG. 2. Basic circuit of rhometer

multiply the effective voltage by n turns. Because sodium has a large temperature coefficient of resistivity, approximately 0.15% R/°F, the Rhometer circuit is provided with a temperature compensator consisting of a platinum wire wound closely around the pipe upstream of the toroid. A close match of compensator coefficient to the thermal coefficient of resistivity of the toroid circuit is obtained over a limited temperature range; thus, in the Mark I Rhometer a temperature change of ± 10°F from the base temperature introduces an error of only ± 0.055%. The electrical system of the Mark I Rhometer was designed to impose an operating temperature limit of 600°F. APDA has modified the Rhometer circuit to increase the range of operation to 1000°F. A new temperature-compensating system is currently being developed and is scheduled for testing in early 1967.

4.2 Preliminary Evaluation of Rhometer Response to Impurities

Evaluation of the Rhometer in terms of its response to changes in impurity concentration has progressed through three phases: response to concentration changes caused by cold trapping and by heat-up of the cold trap, utilizing plugging temperatures and temperature-solubility data as a measure of the concentration change; response to concentration changes caused by injection of measured quantities of specific impurities into a measured quantity of sodium; and response to concentration changes caused by cold trap operation and by injection of specific impurities, utilizing material balance calculations and chemical analysis to determine the concentration change.

In the first phase of testing,(1) evaluation of the Rhometer consisted of injecting and removing dissolved impurities in the sodium by regulating the cold trap temperature in the four-inch loop. Changes in impurity level were determined by measuring the plugging temperature and correlating the results with sodium monoxide solubility data. The results of these tests concluded that the Rhometer response was approximately 0.008% R per ppm change in oxygen which compares closely with Blake's earlier report of 0.01% R per ppm oxygen.(2) The tests were conducted in the temperature range of 400°F to 600°F. There was no observed temperature effect on the meter response per unit change in concentration. During this first phase of testing, response of the Rhometer to gas entrainment also was demonstrated.

In the second phase, the Rhometer was evaluated by injecting known quantities of specific impurities into the sodium: carbon monoxide gas injections and sodium monoxide and sodium carbonate utilizing a tea bag technique.(3) The tea bag, which consisted of a slotted steel tube, was immersed directly into the flowing sodium stream. Prior to injection, the loop was cold-trapped to a freeze-plugging temperature of 215°F; the loop temperature was controlled at various levels in the range of 470°F to 770°F. The results are summarized in Table I. The differences in the average response to the various impurities is significant. The results obtained on Rhometer response to sodium monoxide injections are lower by a factor of 10 than the previous results based on cold trap injections. The differences in the response at different tempera-

TABLE I. RHOMETER RESPONSE TO INJECTION OF SPECIFIC IMPURITIES

Compound Injected	Loop Temperature, °F	Equivalent Concentration, ppm	Rhometer Average Response % R per ppm
Water	470 F	0 - 60	0.00430
	570 F	60 - 160	0.00630
	770 F	160 - 320	0.00430
Sodium Monoxide	770 F	0 - 300	0.00020
	770 F	0 - 500	0.0002
	770 F	500 - 1000	0.00022
Sodium Hydroxide	470 F	0 - 100	0.00180
	570 F	100 - 300	0.00120
Sodium Hydride	570 F	0 - 250	0.00166
	570 F	0 - 250	0.00170
Carbon Dioxide	450 - 720 F	0 - 250	0.00020
	770 F	0 - 400	0.00020

tures is not significant. The response values for carbon dioxide and sodium carbonate injections may be in error because subsequent measurements of the solubility of sodium carbonate in sodium indicate negligible solubility.(4) Chemical analyses were not available for any of these tests.

In these first two phases of testing the qualitative response of the Rhometer to various impurities was demonstrated and some quantitative calibrations were obtained. These tests revealed an apparent discrepancy between Rhometer response to cold-trap impurity injections and to specific impurity injections. In order to permit interpretation of this discrepancy and to improve the quantitative calibration data, the loop was modified to include a sodium-sampling station, and procedures were established to permit analysis of the sodium for oxygen, (5) carbonate carbon,(6) total carbon,(7) nonhydroxide hydrogen, and hydroxide hydrogen.(8) The evaluation of the sampling and analysis procedures and the results of the subsequent Rhometer evaluations will now be discussed.

4.3 Evaluation of Sodium-Sampling Procedures

The chemical analyses of samples obtained from the sampling stations were very erratic, and it was believed that this was the result of sample contamination due to air in-leakage during the sampling operation. To prevent this problem, the sampling stations were completely enclosed within a glove box that was provided with continuously purified argon; preliminary results showed that the incorporation of the glove box considerably reduced the scatter in the chemical analyses. In order to standardize the sampling procedure and to evaluate the combined sampling and analysis procedures, a test was conducted to study various factors that could affect the end result:

(a) the effect of sampling at different sample-station locations
(b) the effect of using nickel versus stainless-steel sample tubes
(c) the effect of analyzing only a portion of the sample, i.e., to determine whether segregation of impurities exists along the length of the tube
(d) the effect of varying sample tube flush time (1 hr, 2 1/2 hrs, and 4 hrs) prior to sampling
(e) to determine whether a statistically significant daily variation exists in samples taken from the loop while it is maintained at essentially constant impurity level.

The test consisted of a two-week run at steady-state conditions, during which the loop was first cold-trapped and then operated at constant conditions of 600 ± 5°F, 7.5 ± 0.2 gpm with no deliberate impurity concentration change; i.e., the cold trap was isolated from the system and no impurity injections were made. During the steady-state test period, one sample was taken every 24 hours from each sample station. After dividing the sample into five equal parts, each sample was analyzed for oxygen by the amalgamation method.(5) Thus, a total of 100 chemical analyses, 50 from each sample station, was performed.

The sample tubes used in the test consisted of a straight section of 0.500-inch OD, 0.055-inch wall thickness, 25-inch long tubes fitted on each end with 1/2-inch Graylok female fittings. The sample tubes were prepared by cleaning, drying and storing, using the following procedure:

(a) Rinse with trichloroethylene to remove grease and other organic residues
(b) Rinse with 5% caustic solution at 70°C to complete the degreasing
(c) Rinse with distilled water and dry with acetone
(d) Vacuum-dry overnight inside the laboratory dry box air lock
(e) Cap the ends with Graylok fittings, seal the tube inside a plastic bag, and remove from glove box.

The sealed sample tubes were then transferred to the loop sample station.

Using the Analysis of Variance Technique, the statistical analysis of the oxygen data led to certain conclusions at the 95% confidence level:

(a) There was no difference in daily results for the four-hour flush time.
(b) At both sample stations, the one-hour flush time samples gave higher oxygen concentrations than either the four-or two and one-half-hour flush time samples.
(c) At one sample station, no difference in daily results was evident when a four-or two and one-half-hour flush time was employed. However, the results for the other sample station did reveal some

difference. Therefore, a four-hour flush time is required at both sample stations to insure consistent results.

(d) The four-hour flush time samples from one station did show a significant site-to-site variation but did not show a significant day-to-day variation. At the impurity concentration level studied, approximately 11-ppm oxygen, the results indicate that if the entire contents of the sample tube are analyzed, the site-to-site variation does not affect the average concentration for the entire tube.

(e) The test revealed that for the four-hour flush time samples the standard deviation for the analysis will not exceed 1.8 ppm more than 0.5% of the time. This means that a single chemical analysis from any site from either sample station will be within 3.5 ppm of the true unknown concentration 95% of the time at the 11-ppm impurity level.

(f) At the conditions of the test the results indicated that there was no difference when using a stainless steel or nickel sample tube.

A similar sodium sampling and analysis test was performed at a high oxygen concentration (47 ppm) to gain confidence in the chemical analysis and sampling procedures at the higher impurity level. A total of 80 chemical analyses, 40 from each sample station, were performed. The loop-operating conditions were similar to those for the test previously described. The conclusions obtained from the statistical analysis at the 95% confidence level are as follows:

(a) There was a statistically significant site-to-site variation at one sample station.

(b) There was no statistically significant sample average variation at either sample station; the range observed was 4 ppm at one station and 8.4 ppm at the other station.

(c) There was no statistically significant difference between the sample averages of the two stations, and the over-all sample averages from the two stations differed only by 1 ppm.

The sampling and analysis tests indicate impurity segregation occurs at one of the stations at both the 11-ppm and 47-ppm levels, and some segregation is indicated at both stations at the 47-ppm level. It is believed that the segregation probably is caused by a nonuniform cooling rate along the length of the sample tubes even though the tubes are horizontally oriented. It is noteworthy that the sample average did not vary significantly at either the low or high oxygen levels and consequently the entire contents of the sample tubes are analyzed to avoid the segregation problem.

4.4 Current Rhometer Test Program

In the current phase of the test program, the principle effort has been directed to an understanding of the difference in Rhometer response to cold trap impurities versus sodium monoxide and also to obtaining a more accurate determination of the response to sodium monoxide injections. In preparation for these investigations, a one-week test was performed to determine the magnitude of the fluctuations in Rhometer signal at steady-state loop operating conditions and to observe whether the meters exhibited statistically significant drift over a one-week test period. The observed fluctuations and drift of the three Rhometers had a maximum range of 0.07% R.

A test also was performed to evaluate the Rhometer response to loop perturbations such as plugging-temperature measurements and sodium sampling with the sodium at constant purity level. Plugging-temperature measurements and sodium sampling were performed daily for a period of two weeks. The results of this test indicated that the Rhometer response did not change by more than 0.01% R and that the plugging temperature and sampling runs do not appreciably affect the Rhometer output. With the establishment of confidence in the sodium sampling and analysis procedures and in the stability of the Rhometer at testing conditions the program proceeded into the sodium monoxide and cold trap injection tests.

4.5 Sodium Monoxide Injections

The sodium monoxide injection tests consisted of three successive injections of an equivalent 25-ppm oxygen each into the loop accompanied with Rhometer, oxygen meter, and plugging-meter response measurements before and after the injections. The injection tube consisted of a straight 30-inch section of Type 304 stainless-steel tubing, 0.0500-inch diameter and 0.035-inch wall thickness, to which 37.1 grams of 60-to 80-mesh sodium monoxide (equivalent to 25-ppm oxygen in the loop) were charged inside of a laboratory glove box. Gross movement of the sodium monoxide out of the tube was prevented by two 70-micron stainless-steel filter frits at the end of the tube. The injection tube was sealed in a plastic bag, transferred into the loop sampling glove box, inserted into one of the sample lines, preheated to 600°F and then held at 600°F with a sodium flow of approximately 0.1 to 0.2 gpm for two days. The Rhometer and oxygen meter response indicated that the sodium monoxide had gone into solution in 4 to 24 hours for each of the three sodium monoxide injections.

Results of the chemical analyses show an increase in the oxygen content of approximately 20 ppm, 12 ppm and 14 ppm, respectively, for the first, second and third sodium monoxide injection. Since 25 ppm oxygen as sodium monoxide were injected in each test, it is concluded that all of the monoxide injected did not remain in solution. The constant response of the Rhometers for the three injections is consistent with the chemical analysis. However, the solubility data for oxygen at 600°F indicate that all the injected sodium monoxide should have gone into solution. The response of each of the Rhometers to each of the three sodium monoxide injections was + 0.06% R, which is equivalent to a sensitivity of approximately 0.0045%R per ppm oxygen injected. This response to sodium monoxide is a factor of 5 times higher than that measured in the preliminary injection tests and is a factor of 2 lower than the preliminary cold trap injection tests.

4.6 Cold-Trap Impurity Injections

Since it was concluded that a cold-trap injection may constitute an injection of various impurities such as hydrogen, carbon, hydroxide and oxygen, sodium samples were taken for total chemical analysis to determine the change in these impurities. Impurity levels were obtained by raising the loop cold-trap temperature to 450°F for a period of 24 hours and then reducing the cold-trap temperature to 220°F for 24 hours. The cold-trap temperature was changed five times during the period of testing and, in each case, the response was reproducible. Prior to each cold-trap temperature change, a sodium sample and a plugging-temperature measurement were taken. A typical response of the Rhometers to the change in cold-trap temperature is shown in Figure 3.

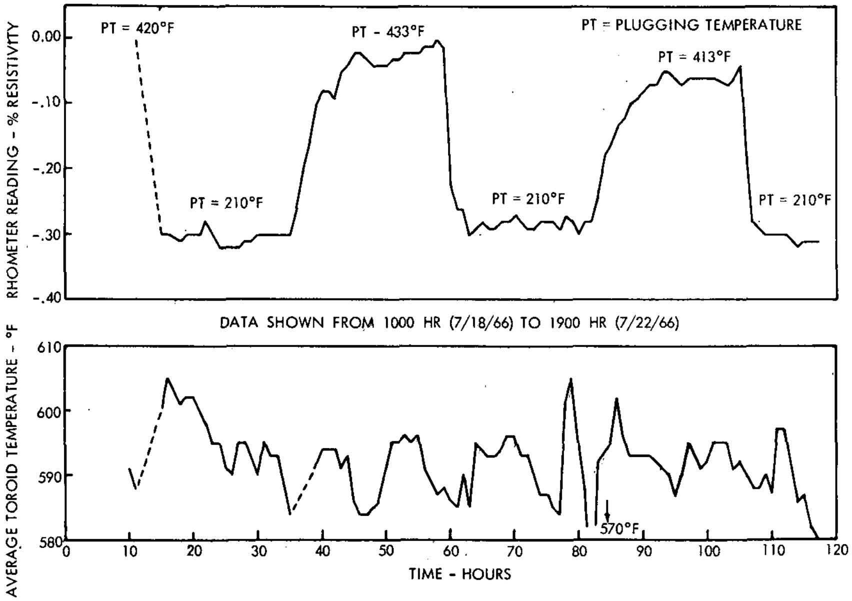

FIG.3. Response of rhometer-3 to variations in cold-trap temperature

The results of the cold-trap injection and clean-up test indicated a Rhometer sensitivity of approximately the same order of magnitude as obtained in the initial cold-trap injection test and the value predicted by Blake (0.01% R per ppm oxygen). From these results it will be noted that if the change in the average Rhometer reading is divided by the change in total alkalinity, expressed as oxygen in sodium monoxide (it is emphasized that the mercury amalgamation technique does not determine either oxygen or monoxide but only total alkalinity), then the concluded Rhometer response is approximately 0.01% R per ppm change in oxygen concentration. This result agrees closely with the earlier work reported by Blake(2) and APDA(1) for cold-trap impurity injections. However, examination of the chemical analysis data in Table II shows the presence of both hydride and hydroxide hydrogen and also shows that the hydroxide content changed during the test. Each of these hydrogen compounds may contribute to the total alkalinity determinations; therefore, it is erroneous to equate the oxygen, or alkalinity, to sodium monoxide. Thus, with the cold-trap injections, firm evidence is presented that impurities other than sodium monoxide are involved, which explains the apparent discrepancy in Rhometer response to cold-trap impurities and to sodium monoxide. It is clear that the Rhometer response to cold-trap impurities represents the net effect of all the impurities--not just sodium monoxide. Another deduction is that the Rhometer response to unit change in impurity content is different from one impurity to another which is to be expected. Finally, it can be deduced that the response per unit change in impurity level is greater for hydroxide than for monoxide.

5. OXYGEN METER EVALUATION

The Rhometer and the plugging meter have responded to all impurities existing in a system. It would be desirable to develop impurity detection and monitoring instruments that would be sensitive to specific impurities. The oxygen meter as developed by United Nuclear Corporation is designed to specifically measure an oxygen activity in a system.(9) It would be very desirable to detect and control the oxygen impurity, since it is felt that its presence greatly affects the corrosion rate of materials.

5.1 Description and Operation of the Oxygen Meter

The oxygen cell basically consists of a reference electrode and a solid electrolyte immersed in liquid sodium (Figure 4). The solid electrolyte is a thoria-15 w/o yttria tube. The cell develops a voltage which is dependent on the oxygen content of the sodium. Within the tube, a reference electrode made of copper-cuprous oxide makes contact with the inside surface of the electrolyte and establishes oxygen activity at this surface. The sodium-containing oxygen forms the second electrode of the cell. An electrical contact is made with the outside of the electrolyte and establishes an oxygen activity which is dependent on the oxygen content of the sodium. A voltage is developed between the sodium and the reference electrode as a result of the difference in oxygen activity at the two electrolyte-electrode interfaces. The change in cell voltage for a given change in concentration is given by

$$\ln \frac{C_1}{C_2} = (K)(E_1 - E_2)$$

where

C_1 = initial oxygen concentration

C_2 = final oxygen concentration

$E_1 - E_2$ = change in cell output signal, in volts, resulting from oxygen concentration change

K = $-36.1 \pm 5.4\ \text{volt}^{-1}$

The meter is designed to operate between 550°F and 650°F; however, the voltage output is strongly influenced by the cell temperature. An

TABLE II. OXYGEN METER AND RHOMETER RESPONSES TO COLD-TRAP IMPURITIES

Change In Plugging Temperature °F	Change in Average Meter Reading			Change In Total Alkalinity Expressed As Oxygen In Na_2O, ppm	Change In Nonhydroxide Hydrogen, ppm	Change In Hydroxide Hydrogen, ppm
	Rhometer-2, %R	Rhometer-3, %R	Oxygen Meter-4, millivolts			
420 → 210	*	*	*	-33	-1.1	-0.5
210 → 433	0.26	0.28	-8.8	27	0.9	0
433 → 210	-0.23	-0.26	20.4	-27	-0.9	-0.1
210 → 413	0.24	0.22	-16.5	19	0.7	0.1
413 → 210	-0.26	-0.24	15.7	-19	-0.7	-0.3

*Data insufficient prior to cold trapping important characteristic of the oxygen meter is its increased sensitivity as the oxygen concentration decreases; thus, it has the potential capability of measuring oxygen concentration at very low levels.

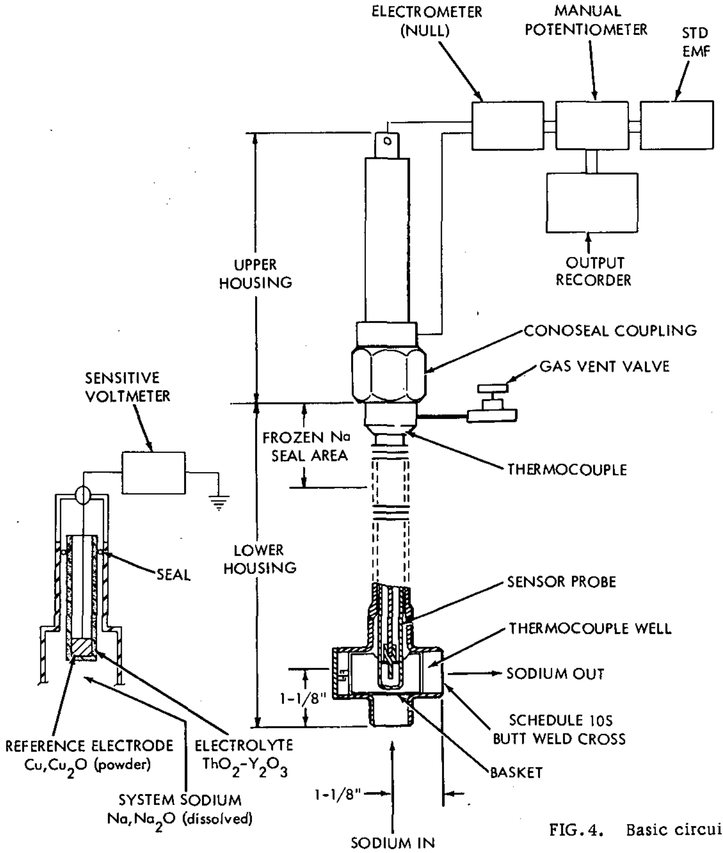

FIG.4. Basic circuit of the oxygen meter

5.2 Oxygen Meter Tests

Four oxygen meters were installed in the loop for evaluation studies. Steady-state tests were initially run to determine meter output stability. The results of these tests produced very erratic readings of the cell output which were attributed to a faulty potential divider switch. The tests to date verify qualitatively the predicted response of the meters; however, quantitative results have been hampered by the large fluctuation in the oxygen meter output. The response of one of the meters during the cold-trap injections is summarized in Table II. It has been noted that the meters are sensitive to ambient temperature effects; the meter output fluctuations were reduced to approximately three millivolts at steady-state conditions after an ambient temperature control device was placed around one of the cells.

The four oxygen meters are read on a single instrument by selectively switching each cell. It was noted that the cell output required approximately 15 minutes to reach a stablized value. It appears that the large noise-to-signal ratio obtained from the meter response data is predominantly caused by the switching from cell to cell, and the data taken may not represent a stabilized meter reading. The cause of this slow response has not been determined; however, indications are that each cell will require individual readout to avoid additional errors.

One of the oxygen cells was purposely exposed to X-ray radiation to study the effect in meter response at constant loop operating conditions of 600°F. The radiation tests consisted of placing a 28-curie source of iridium-192 at various distances for a period of 5 minutes. The results indicate that the cell response was 5 millivolts at a distance of 12 inches, 8.7 millivolts at a distance of 8 inches, and 15 millivolts at a distance of 4 inches. The tests clearly indicate that the response of the oxygen meter will be affected by exposure to radiation, and further evaluation of this significant observation is needed.

6. CONCLUSIONS

6.1 Rhometer

The Rhometer is basically a sound instrument; however, it requires additional development. The instrument is sensitive to a variety of impurities and can detect concentration changes at the 10-ppm level. The meter response is very sensitive to temperature changes, and an automatic temperature compensator is presently being developed to correct for temperatures in the range of 400 to 1000°F. Evaluation of the long-term operating stability of the three Rhometers under test at APDA indicates that the change in phase resistance of the Rhometer response was mostly attributed to the change in platinum compensator resistance. Other effects such as instrument drift, toroid transformer copper losses, poor connections, and changes in flow appear to be having a small effect in the over-all base change in the Rhometer readout.

6.2 Oxygen Meter

Proper interpretation of the oxygen meter response is not clearly understood at this time. The oxygen meter appears to be a good tool for measuring oxygen impurities but requires further development to improve its reliability. Since the oxygen meter response is a measure of oxygen activity in sodium, it is not understood how the oxygen activity is affected by changes in impurities other than oxygen activity or by the presence of other impurities such as hydrogen. Additional testing is required to study the effects of other impurities in sodium and their effect on oxygen activity.

The effect of ambient temperature and the cell-to-cell switching using a common power supply have indicated the need for careful control. Changes in cell temperature due to changes in sodium temperature greatly affect the meter response. It is, therefore, desirable to maintain a constant sodium temperature to maintain minimal effect on oxygen meter response. The long-term operating stability characteristics of the four oxygen meter cells on test at APDA indicated that over a one-year period

(a) the cells were generally unreliable on a day-to-day basis because of short-term temporary changes in output signals and (b) the cells are subject to serious damage in handling, cleaning and installation.

7. TEST PROGRAMS AT APDA

Continued Rhometer and oxygen meter response evaluation tests will be performed to study the effects of various impurities on the meter response. Injection tests with sodium hydride, sodium monoxide, carbon, water and hydrogen will be performed. Various meter sensitivity tests will be conducted to determine possible limitations of the meter. Ultimately, the results of these tests will indicate the reliability in measuring impurities quantitatively and qualitatively using these meters and will suggest certain improvements and modifications to the meters.

REFERENCES

(1) Evaluation of the Blake Sodium Resistivity Meter, APDA-149 (1962).

(2) BLAKE, L. R., Resistivity meter to indicate oxide content of sodium, Paper No. 3278M, Institute of Elec. Engrs. (1960).

(3) Operation of the Sodium Technology Loop for Contamination Meter Evaluations, APDA-163 (1964).

(4) Quarterly Technical Progress Report on AEC-Sponsored Activities APDA-185 (1966).

(5) BOLTZ, D. F., KERMOSHCHUK, J. O., and MEACHAM, S. A., APDA-168 (1965).

(6) BOLTZ, D. F., and MEACHAM, S. A., APDA-166 (1965).

(7) BRADLEY, H., and MEACHAM, S.A., APDA-164 (1964).

(8) HILL, E. F.m and MEACHAM, S. A., APDA-183 (1966).

(9) MINUSHKIN, B., UNC-5113 (1965).

DISCUSSION

M.N. IVANOVSKY: Can the rhometer be used for quantitative measurements of oxygen in sodium?

W.L. CHASE: We do not think so, because it is sensitive to so many things. In fact, we sometimes refer to the rhometer facetiously as the "something meter" since it does respond to so many different impurities.

A. BOGERS (Chairman): I would like to make the point that the electrochemical oxygen meter described by Petrek and Kovacic is essentially the same as the one used in Mr. Williams' tests (paper SM-85/29).

EXPERIENCE D'EXPLOITATION DES INDICATEURS DE BOUCHAGE AUTOMATIQUES

J. P. DELISLE
CEA, CENTRE D'ETUDES NUCLEAIRES DE CADARACHE, FRANCE

(Présenté par J. P. Le Jannou)

Abstract — Résumé

OPERATIONAL EXPERIENCE WITH AUTOMATIC CONTINUOUSLY INDICATING PLUGGING METERS. To provide a permanent check on the purity of sodium in circuits, work has been going on for a number of years on the development of automatic continuously indicating plugging meters.

The experience gained with three such continuously indicating meters used in the experimental circuits of RAPSODIE are described.

The main difficulties encountered so far have arisen in connection with the double plugging temperature. It has also been possible to demonstrate the extremely unfavourable influence of thermal inertia on measurement stability and the considerable improvement that can be achieved by using a constant-pressure sodium feed system.

The automatic equipment used with RAPSODIE was put into service in 1966.

EXPERIENCE D'EXPLOITATION DES INDICATEURS DE BOUCHAGE AUTOMATIQUES. Pour le contrôle permanent de la pureté du sodium dans un circuit, l'auteur a mis au point depuis plusieurs années des indicateurs de bouchage automatiques à mesure continue.

Dans le mémoire, il présente l'expérience acquise avec trois indicateurs continus utilisés sur les circuits expérimentaux de RAPSODIE.

La principale difficulté rencontrée est due au phénomène de double température de bouchage. L'auteur a également mis en évidence l'influence néfaste de l'inertie thermique sur la stabilité de la mesure et l'amélioration importante apportée par un système d'alimentation en sodium à pression constante.

Les appareils automatiques équipant RAPSODIE ont été mis en service en 1966.

I - INTRODUCTION - Historique

Le premier indicateur de bouchage automatique essayé à Cadarache était un appareil à mesure discontinue. Ses essais et son perfectionnement furent rapidement abandonnés devant les premiers résultats beaucoup plus prometteurs obtenus avec un appareil à mesure continue monté sur le circuit secondaire (NaK) 10 MW , en 1962.

Un nouvel appareil plus perfectionné (figure 1 a) fut ensuite construit et installé sur le circuit primaire (Na) 10 MW où il a accumulé depuis 7500 heures de marche. C'est avec cet indicateur que l'on a mis clairement en évidence le phénomène de double température de bouchage sur ce circuit.

Les essais de ces trois appareils expérimentaux ont fait l'objet d'un rapport [1] .

A partir de ces résultats , on a défini les indicateurs de Rapsodie (figure 1 b) et un prototype de ceux-ci a été construit et monté sur le circuit expérimental primaire 1 MW , avec quelques modifications concernant la régulation (figure 1 c). Ses essais ont montré qu'il présentait un défaut important (trop grande inertie thermique) et fonctionnait beaucoup moins bien que l'appareil expérimental initial. Ces résultats sont venus malheureusement trop tard pour permettre de modifier les appareils de Rapsodie qui étaient déjà construits.

La mise en exploitation de ceux-ci en 1966 a permis malgré ce défaut, et après les réglages des appareils, de suivre assez régulièrement l'évolution des températures de bouchage. On a acquis ainsi un début d'expérience de ces appareils sur des circuits montés en propreté nucléaire, et on a pu en particulier constater de nouveau le phénomène de double température de bouchage.

Le premier appareil à mesure continue essayé en 1962 a été modifié d'après les connaissances acquises et on en espère de bons résultats (figure 2).

II - EXPERIENCE ACQUISE SUR LES CIRCUITS EXPERIMENTAUX

1 - Rappel du principe de fonctionnement

Le principe des appareils classiques à mesure manuelle est bien connu.

L'indicateur à mesure automatique discontinue réalise simplement de façon cyclique, et sans intervention de l'opérateur, ce que celui-ci ferait autrement manuellement : refroidissement progressif, détection de la diminution de débit de sodium due au bouchage, réchauffage. Des résultats satisfaisants peuvent être obtenus puisque plusieurs appareils de ce type sont en service continu aux Etats-Unis.

La figure 3 donne un exemple d'enregistrement obtenu sur le circuit 1 MW. On peut lire la température de bouchage (65° dans l'exemple choisi) en regard des amorces de bouchages observées sur la courbe de débit.

La mesure automatique continue est fondée sur un principe légèrement différent : le refroidissement de l'indicateur est asservi par un régulateur au débit de sodium, de manière à maintenir celui-ci à une valeur constante correspondant à un bouchage partiel de l'orifice. Il y a équilibre de dissolution permanent entre le dépôt d'oxyde dans l'orifice et le sodium saturé en oxyde. La température mesurée au niveau de l'orifice est donc en permanence la température de saturation (température de bouchage).

2 - Indicateur monté sur le circuit primaire expérimental 10 MW

2.1. Description

Les essais réalisés avec le premier appareil à mesure continue, sur le circuit secondaire 10 MW, avaient rapidement montré l'intérêt d'une mesure de débit différentielle pour éliminer les perturbations dues aux variations de pression en amont de l'indicateur [1]. La figure 1 a schématise l'appareil équipant le circuit primaire expérimental 10 MW depuis janvier 1963.

Le sodium refoulé par la pompe traverse un filtre à maille de 4/10 mm, et alimente en parallèle avec l'orifice refroidi un tube non refroidi muni d'un diaphragme. La régulation reçoit comme information le rapport R des débits D_1 dans l'orifice et D_2 dans le diaphragme. Ce rapport est voisin de 1 par construction quand l'orifice est débouché. On affiche un rapport de consigne R_0 (par exemple 0,5) au régulateur, et celui-ci commande la vanne d'air de refroidissement pour maintenir $R = R_0$, c'est-à-dire un bouchage partiel. Un régulateur auxiliaire de température entre en jeu, par l'intermédiaire d'un organe de choix, si la température T de l'orifice tend momentanément à descendre au-dessous d'une valeur de consigne T_0, généralement choisie à 110°, pour éviter le gel intempestif du sodium. L'organe de choix maintient toujours en service celle des deux régulations qui demande l'ouverture de vanne la plus faible.

2.2. Résultats d'exploitation

Les essais de cet appareil ont déjà été décrits, ainsi que les observations faites concernant une deuxième température de bouchage [1]. L'expérience de 7500 heures d'exploitation peut se résumer ainsi :

a) - En l'absence d'une deuxième température de bouchage et lorsque les conditions en amont de l'appareil sont stables, le fonctionnement est excellent (voir figure 4). Même en présence de perturbations amont importantes, le fonctionnement reste très acceptable (voir figure 5).

b) - En présence d'une deuxième température de bouchage, le fonctionnement devient plus capricieux, et une certaine habitude est nécessaire pour interpréter les courbes enregistrées. Quand on le met en service, l'appareil peut indiquer la première température de bouchage (correspondant à l'oxyde) mais il a tendance à dériver vers la deuxième température de bouchage, plus élevée, par dépôt progressif de la deuxième impureté remplaçant l'oxyde. Au bout d'un temps très variable (1 heure à 2 ou 3 jours, en fonction de nombreux paramètres) l'appareil finit par réguler sur la deuxième température de bouchage de façon définitive. Les figures 6 et 7 donnent des exemples typiques de courbes obtenues dans ces conditions. La figure 8 montre "l'accrochage" de la régulation sur la deuxième température de bouchage, après que l'appareil a régulé en température pendant 24 heures sur le point de consigne T_0 fixé à 160° pour une première température de bouchage de 140°.

c) - La stabilité de la mesure sur la deuxième température de bouchage est beaucoup moins bonne que sur la première (quand celle-ci est seule). Ceci est attribué à une très faible variation de solubilité de la deuxième impureté en fonction de la température.

d) La deuxième température de bouchage apparaît quand le circuit principal est porté à plus de 400° C et elle croît avec la température du circuit. Elle s'abaisse rapidement après quelques heures de purification si la température du circuit est ramenée à moins de 400° C. Le piège froid collecte efficacement l'impureté correspondante, mais avec un débit faible en regard de sa vitesse de formation dans le circuit si celui-ci est très chaud. Il n'est donc pas possible d'obtenir à l'équilibre, comme avec l'oxyde, des températures de bouchage pratiquement égales à la température du point froid du piège.

On a observé jusqu'à 280° C pour la deuxième température de bouchage, le circuit étant à 550° C, le piège froid et la première température de bouchage à 130° C. On a remarqué une relation entre cette deuxième température de bouchage et la contamination du circuit par une fuite d'huile de la pompe mécanique. Mais aucune détermination quantitative ou analyse chimique n'a pu être établie.

e) - En cas de bouchage progressif complet accidentel de l'orifice, on a toujours pu obtenir le débouchage par simple réchauffage vers 400 à 500° C au moyen d'une résistance chauffante prévue à cet effet.

Si l'on cherche à mesurer la température de congélation du sodium, le débit s'annule de façon quasi instantanée quand on atteint le gel. Ceci permet de contrôler la mesure de température. Le débouchage par refusion du sodium est très facile.

f) - Des perturbations aléatoires et brusques du débit dans l'orifice surviennent parfois, dues certainement à des limailles introduites en aval du filtre lors de modifications de tuyauteries. Malgré cela on n'a pas estimé nécessaire d'étudier un dispositif d'ouverture mécanique de l'orifice, ce qui aurait notablement compliqué l'appareil.

3 - Prototype Rapsodie monté sur le circuit expérimental primaire 1 MW

3.1. Description

Par rapport à l'appareil décrit ci-dessus en 2.1., on a fait les modifications suivantes :

- Carter de refroidissement simplifié : l'air circule parallèlement au tube aileté, dans un simple tube-enveloppe, au lieu de circuler dans une boîte à chicanes perpendiculairement au tube aileté comme dans le premier appareil.

- Economiseur de puissance plus important, pour pouvoir augmenter le débit de sodium (250 litres/heure au lieu de 150). On espérait ainsi augmenter la vitesse de dépôt d'oxyde.

- Orifice percé de 6 trous de 1,5×1,5 mm au lieu de 12 trous de 1 x 1 mm, pour rendre moins probable le bouchage par une limaille accidentelle.

- Schéma de régulation modifié, avec montage "en cascade", le régulateur de rapport commandant le point de consigne du régulateur de température à travers l'organe de choix (voir figure 1 c).

- Pour essai, sur le prototype seulement : débitmètre à double tube dans l'entrefer d'un même aimant, pour annuler l'effet de variations éventuelles de champ magnétique sur le rapport des débits.

3.2. Résultats d'essais

On a constaté :

a) Une amélioration importante de la stabilité en cas de variation rapide de la température du sodium alimentant l'appareil : la perturbation de température est corrigée par le régulateur aval sans qu'il y ait modification du dépôt d'oxyde, elle passe donc inaperçue.

b) Une augmentation très importante du temps de réaction de l'appareil à une modification de la position de la vanne d'air ; ceci est dû à l'inertie thermique de l'ensemble économiseur plus refroidisseur, dont la capacité calorifique a été doublée par les modifications mécaniques.

Ce défaut, dont l'importance avait été sous-estimée à la conception, rend la régulation du rapport molle et la mise en régime très lente. Il oblige de plus, à examiner une assez grande longueur d'enregistrement (plusieurs heures) pour distinguer entre les évolutions intéressantes et celles dues à des perturbations. Celles-ci sont accentuées car l'appareil est lent à les corriger.

c) Pas d'influence notable, semble-t-il, du changement de dimensions de l'orifice car les mesures manuelles se font correctement. On a observé aussi des perturbations brusques dues à des limailles introduites lors d'une modification en aval du filtre. L'agrandissement des trous ne parait donc pas utile.

d) On a pu faire sur ce circuit, contaminé en huile comme le circuit 10 MW, les mêmes observations concernant la deuxième température de bouchage.

La figure 9.1 montre un exemple d'enregistrement obtenu. On observe un "pompage" de la régulation dont les actions sont difficiles à ajuster convenablement.

III - MISE EN SERVICE DES INDICATEURS DE RAPSODIE

1 - Description

Indicateur primaire : il est analogue mécaniquement au prototype mais construit en tube plus épais (21/27 au lieu de 21/25), ce qui augmente encore son inertie thermique. Il y a deux débitmètres séparés. L'ensemble est enfermé dans une "armoire de purification" en azote avec toutes les vannes de la purification primaire.

La régulation est conforme à la figure 1 b.

Indicateurs secondaires : ils sont analogues au primaire, mais sans mesure de rapport : la régulation est faite directement d'après le débit dans l'orifice, comme dans le premier appareil essayé en 1962. On a jugé en effet qu'il n'y aurait pas de perturbations gênantes à cause de la simplicité des circuits de purification secondaires.

2 - Premiers résultats d'exploitation

2.1. Contrairement aux prévisions, les indicateurs secondaires subissent des perturbations importantes dues aux fluctuations de pression dans le circuit principal, surtout lors des changements d'allure de la pompe mécanique.

La figure 9.2 montre en A et B deux exemples de petites perturbations d'origine indéterminée (pompe mécanique à l'arrêt) : en B, on constate l'action momentanée de la régulation de température qui limite celle-ci à 120° pour éviter le gel du sodium.

Lorsque la pompe mécanique tourne au régime nominal, le fonctionnement automatique devient instable. La simplicité recherchée en supprimant le deuxième débitmètre et la mesure de rapport se révèle donc une erreur.

2.2. La grande inertie thermique des appareils entraîne les mêmes défauts que ceux observés sur le prototype.

2.3. Le schéma 1 b apparaît moins bon que les schémas 1 a et 1 c. Il rend la régulation de température généralement moins précise, sans offrir l'avantage signalé en 3.2 a.

2.4. Jusqu'à présent, aucune perturbation brusque pouvant laisser supposer la présence de limaille dans l'appareil n'a été notée.

2.5. Malgré ces défauts, on a pu faire des observations intéressantes pendant la montée en température des circuits jusqu'à 540° C.

a) - Apparition d'une deuxième température de bouchage de 180 à 220° (la première étant inférieure à 180°) pendant la période où le circuit principal était entre 280 et 340°. Cette deuxième impureté a disparu quand on a atteint 350° dans le circuit. Il s'agit peut-être de soude NaOH.

b) - Apparition vers 400° d'une deuxième température de bouchage comme sur les circuits expérimentaux 1 et 10 MW.

La figure 10.1 montre en A et B les décrochements typiques, analogues à ceux des figures 6 et 7, qui se produisent généralement après la mise en régulation de l'indicateur, quand il passe de la première à la deuxième température de bouchage. Une explication possible en a déjà été donnée [1] : on peut penser que la deuxième impureté se dépose de façon superficielle et peu stable sur le dépôt d'oxyde dans les trous de l'indicateur.

c) - La figure 10.2 montre successivement de bas en haut :

A - régulation automatique sur la deuxième température de bouchage,

B - passage en "manuel" avec légère diminution de la température pour mettre en évidence le dépôt de la deuxième impureté ainsi provoqué par l'abaissement au-dessous de sa température de bouchage,

C - mesure de bouchage "manuelle" classique qui fait apparaître en D le début du dépôt de l'oxyde,

F - réchauffage qui provoque la dissolution du dépôt d'oxyde puis de la deuxième impureté à partir de G.

Cette figure montre bien la grande différence entre les vitesses de dépôt et de dissolution de l'oxyde et de la deuxième impureté.

d) - La figure 11 montre, de bas en haut et de droite à gauche, une mesure manuelle (d'ailleurs peu précise à cause du manque d'habitude de l'opérateur) suivie du passage en automatique, puis de la régulation sur la deuxième température de bouchage. Celle-ci baisse lentement, en 12 heures, de 250 à 220° par suite du refroidissement du circuit primaire de 530 à 450°. Un réchauffage manuel provoque ensuite la dissolution du dépôt et le retour au rapport initial (115 %).

2.6. La deuxième température de bouchage observée sur les circuits expérimentaux 1 et 10 MW avait été attribuée à une forte contamination par de l'huile provenant des pompes. L'apparition du même phénomène sur les circuits de Rapsodie repose le problème, de même que les observations faites dans différents laboratoires étrangers.

Des analyses ont été entreprises pour connaître la concentration en carbone du sodium de Rapsodie après cette première montée en température.

IV - ALIMENTATION A PRESSION CONSTANTE

Sur le circuit qui a servi à tester en sodium les pompes de Rapsodie, on a utilisé un indicateur de bouchage manuel alimenté par la différence de hauteur entre le niveau libre du circuit et le réservoir de stockage. La parfaite stabilité du débit obtenue par ce moyen a conduit à imaginer un tube à niveaux constants pour alimenter un indicateur de bouchage automatique. Les perturbations de débit doivent être ainsi éliminées, plus simplement et plus parfaitement que par la mesure de rapport.

La figure 2 schématise le montage effectué sur le circuit secondaire expérimental 10 MW, avec le premier indicateur automatique essayé en 1962. On a modifié légèrement l'appareillage de celui-ci pour utiliser la régulation "en cascade" qui semble intéressante (voir 3.2.a ci-dessus).

Les premiers essais ont montré que les travaux de modification avaient introduit de la limaille entre le filtre et l'orifice provoquant ainsi des variations brusques et aléatoires du débit, rendant la mesure instable. Mais on a pu vérifier que le débit était insensible aux variations de tension de la pompe dans une très large gamme de fonctionnement : il suffit d'assurer la pression suffisante pour que le sodium atteigne le niveau de trop plein.

Le circuit est resté arrêté depuis, et on n'a pas pu poursuivre les essais.

V - CONCLUSION

- Les appareils essayés, bien qu'encore imparfaits, apportent une amélioration intéressante par rapport à la mesure manuelle.

- Le dernier modèle décrit, avec tube d'alimentation à niveaux constants et une faible inertie thermique, doit permettre d'obtenir une bonne stabilité et un faible temps de réponse.

- Il reste à étudier s'il est possible d'améliorer la sensibilité en modifiant la forme de l'orifice ou de l'extrémité du tube.

- En régime permanent, l'appareil n'indique que la température de bouchage la plus élevée. La meilleure solution pour connaître les deux températures de bouchage serait sans doute d'associer deux appareils automatiques, alimentés peut-être par le même tube à niveaux constants : un indicateur continu et un discontinu.

- Il reste encore tout à apprendre concernant la deuxième température de bouchage apparaissant à haute température, sa signification et son importance.

REFERENCE

[1] DELISLE, J.P., LIONS, N., L'instrumentation dans les circuits d'essai Rapsodie 1 et 10 MW: Débitmètres, manomètres, indicateurs de niveau, indicateurs de bouchage, Rapport CEA R 2522 (1964).

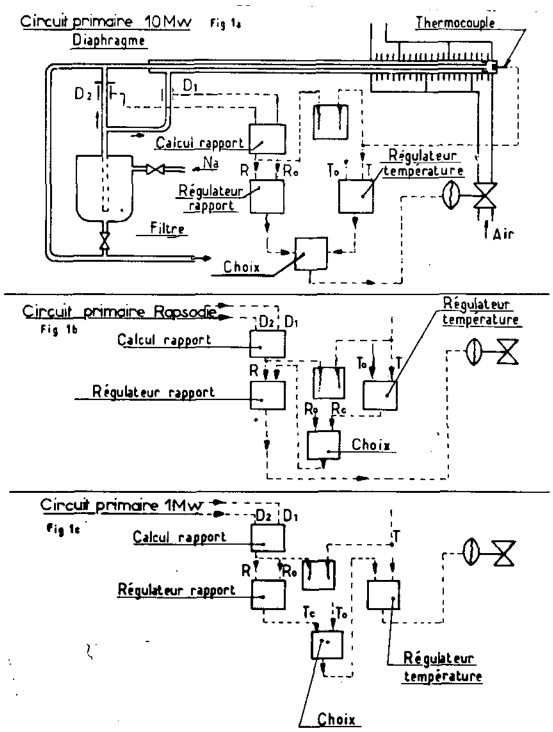

FIG. 1. Indicateur de bouchage automatique à mesure continue

FIG. 2. Indicateur de bouchage automatique à mesure continue alimenté à pression constante

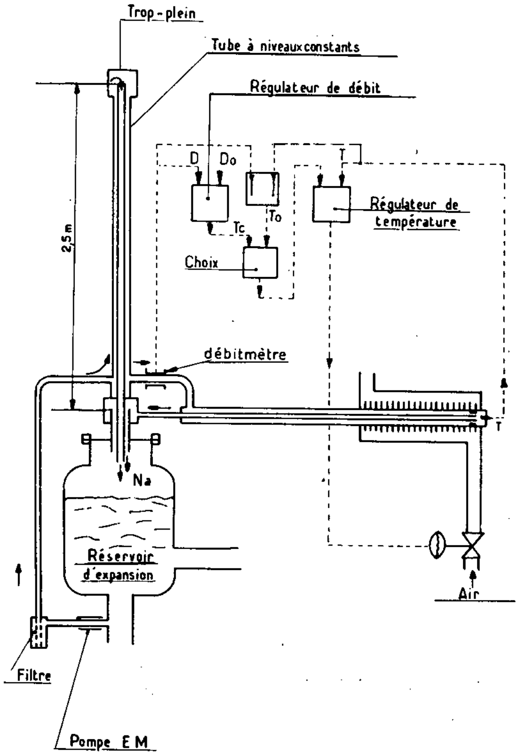

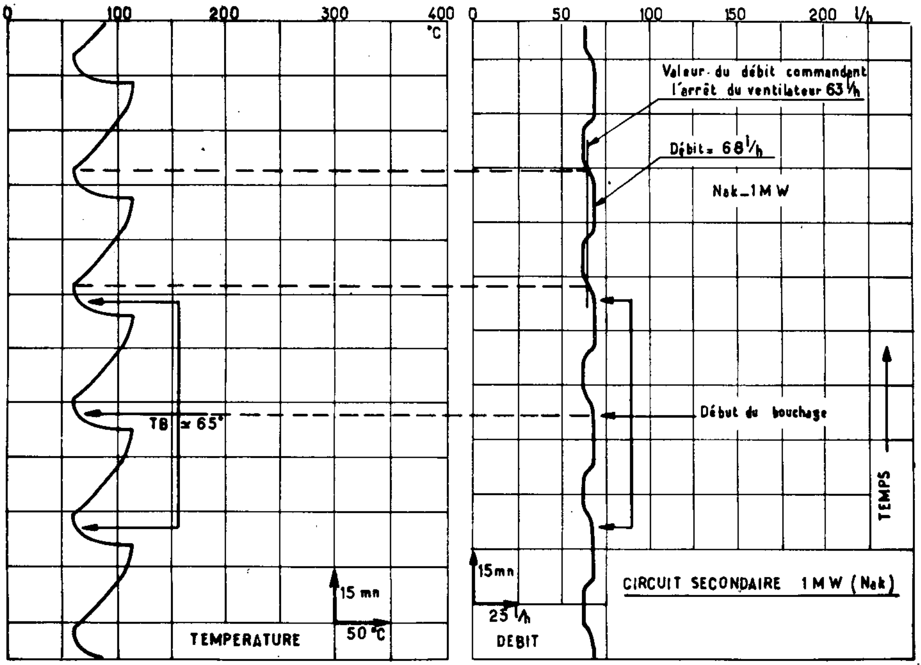

FIG. 3. Enregistrement débit-température en fonctionnement manuel

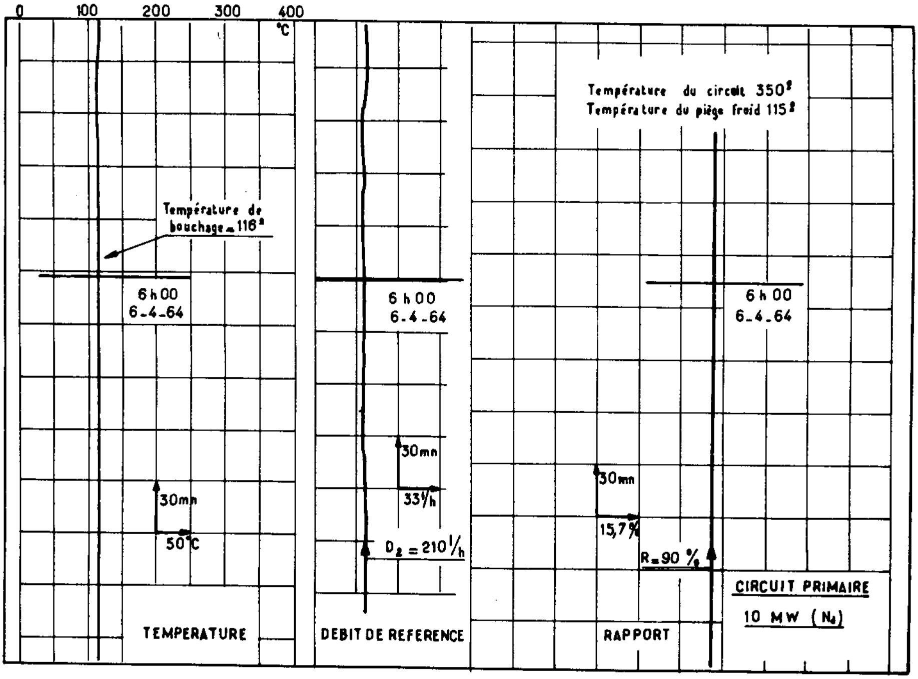

FIG. 4. Enregistrement température, débit et rapport des débits en fonctionnement automatique sans perturbation

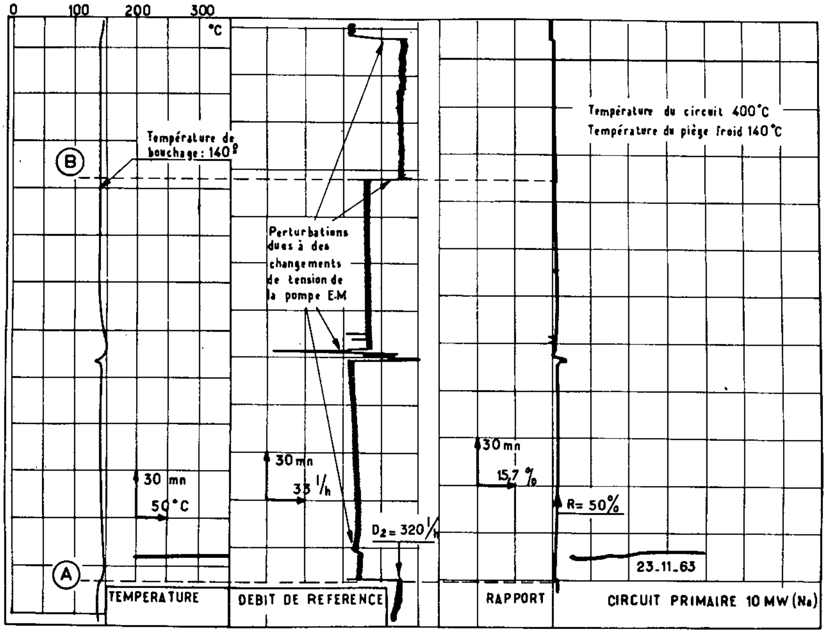

FIG. 5. Enregistrement température, débit et rapport des débits en fonctionnement automatique avec perturbations

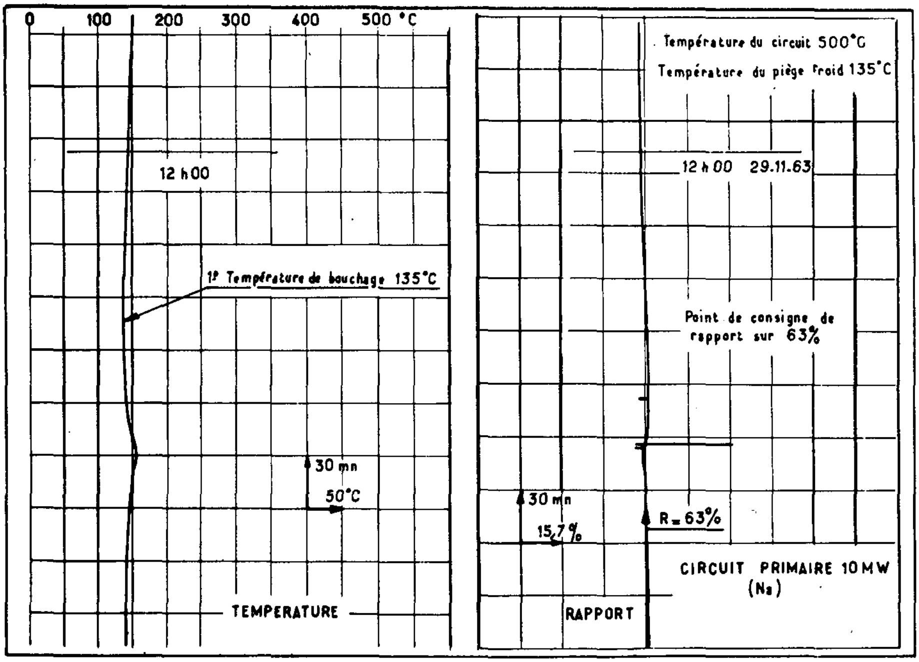

FIG. 6. Dérive lente de la température vers la deuxième température de bouchage

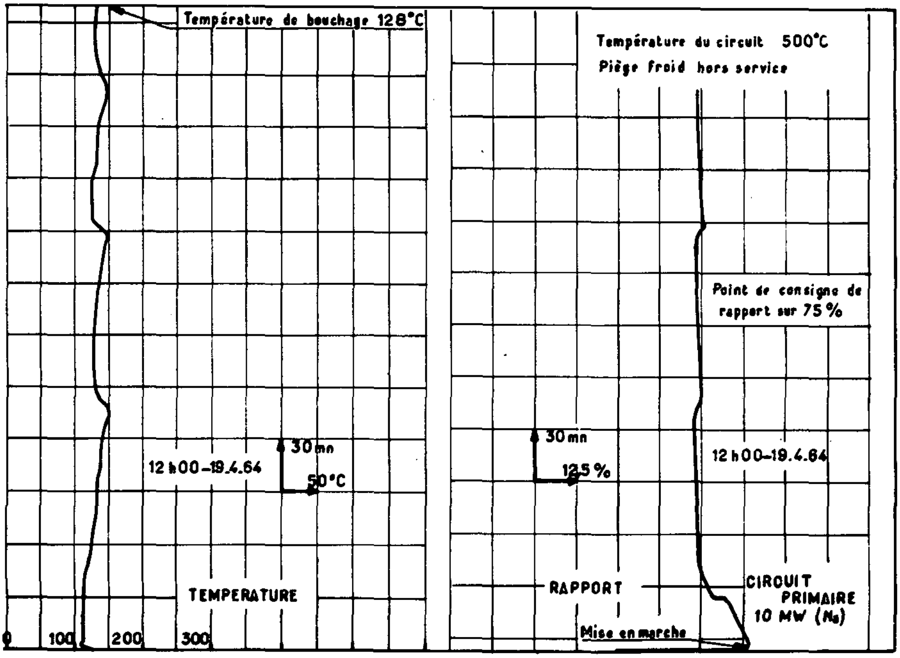

FIG. 7. Dérive lente de la température vers la deuxième température de bouchage

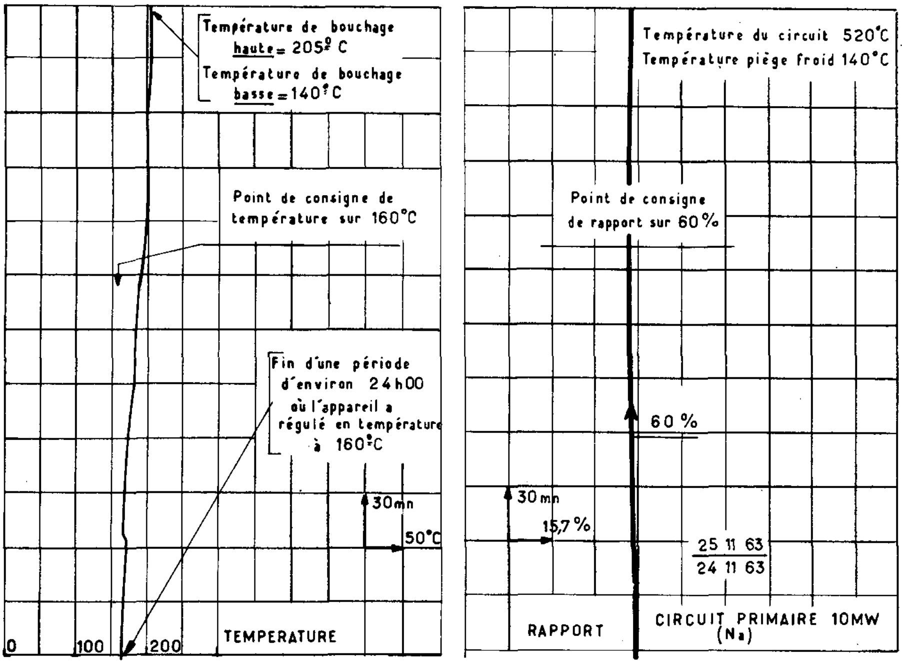

FIG. 8. Accrochage de la régulation sur la deuxième température de bouchage

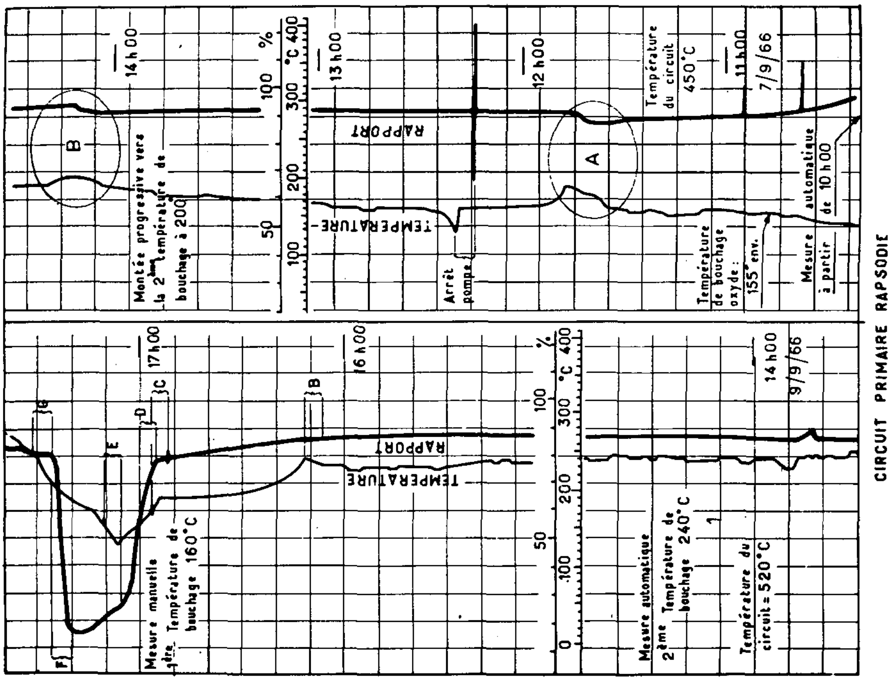

FIG.10.1. Passages à la deuxième température de bouchage

FIG.10.2. Divers types de fontionnement

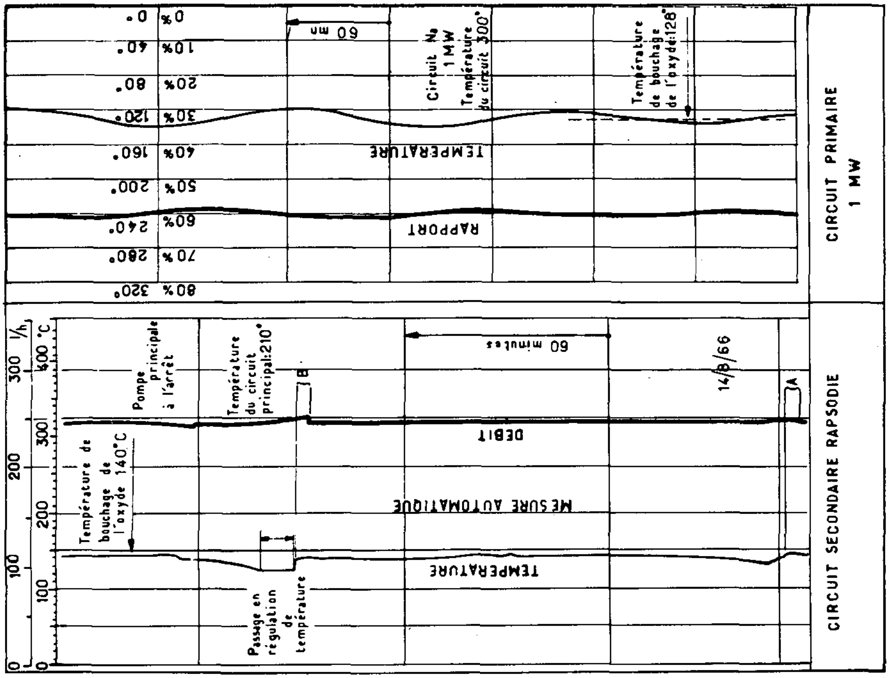

FIG.9.1. Pompage de la régulation

FIG.9.2. Exemples de perturbations indéterminées

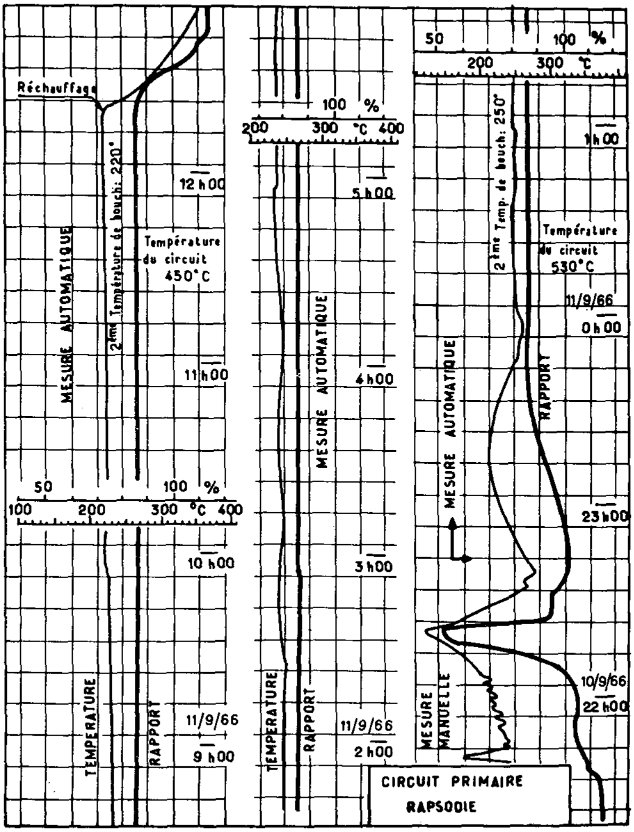

FIG.11. Expérience d'exploitation des indicateurs de bouchage automatiques

DISCUSSION

L.F. EPSTEIN: The composition of the plug material is still a problem. Some 15 years ago Bruggeman at Knolls Atomic Power Laboratories observed a double break on a plugging indicator and attributed it to CaO. We are still attempting to analyse the composition of such plugs in our laboratory, but we have no answer yet.

I wonder whether Mr. Le Jannou knows of any analytical results obtained on these plugs in France, and, in particular, what he thinks of the CaO hypothesis. Or is there anyone else here who has tried to analyse the plugs for material other than sodium and Na_2O?

J.P. LE JANNOU: I am sorry, I cannot answer your question because we have not analysed the impurities in our plugs. We plan to do so but have not yet got round to it.

F.A. SMITH: At Argonne we have tried to analyse the material in plugged valves and in the pipes leading to and from the valves. So far our results indicate that the material is mainly sodium. These measurements are, unfortunately, very difficult.

B. KULPIN: What is the physical significance of the second plugging temperature? Mr. Epstein has mentioned the hypothesis that this second plugging temperature may be due to CaO formation. Have you checked this theory at all?

J. P. LE JANNOU: All we have done so far is to observe and record the second plugging temperature; we have, however, to my knowledge, no special information that could serve as an explanation of the physical phenomenon.

M. N. IVANOVSKY: In experiments on alkali metals we have found that the degree of supercooling required to initiate crystallization on a clean surface depends on the temperature at which the cooling of the metal starts. In our survey paper (SM-85/41) we pointed out that if lithium is cooled from 290°C to about 200°C the supercooling required to initiate crystallization is 20 deg; if the cooling is from 350°C to 200°C, the supercooling required is 30 deg. Have you encountered this phenomenon? If so, how did you calculate the variation in supercooling, and how did you take it into account in graduating your plugging meters? Also, did you study the effect of preliminary coolant heating on the plugging temperature?

J. P. LE JANNOU: So far we have limited ourselves to measuring the temperature at which the plugging occurs, and the results of these measurements are given in the paper. When the temperature of the loop is lowered about 70 deg the plugging temperature drops about 30 deg, and it generally disappears altogether if the loop temperature goes below 350°C. It always reappears, however, when the temperature of the loop is raised again.

M. N. IVANOVSKY: I have no more questions, then. Do you not think that the second plugging temperature might be connected with supersaturation of the solution, with supercooling?

J. P. LE JANNOU: This is a hypothesis that probably ought to be considered but so far we have had no opportunity to verify it.

L. F. EPSTEIN: In connection with Dr. Ivanovsky's very pointed remarks about the possibility of supersaturation I might mention that some years ago we tried to measure the freezing point depression for a series of alkali metals, believing it might provide a useful technique for analysing oxygen and other impurities. We found no evidence of extensive supercooling in sodium, but we did see it in lithium, rubidium and caesium; I cannot remember what the results were for potassium. Of course the degree of supersaturation will also depend on the rate of cooling, agitation, flow rate and similar factors. Perhaps under some circumstances supersaturation can be achieved, but I know of no direct observation of supercooling in sodium systems.

M. N. IVANOVSKY: Have you carried out any experiments which demonstrate more or less conclusively that there is no supercooling in sodium?

L. F. EPSTEIN: The most I can say is that we did not observe it in sodium, and to the best of my knowledge no one else has either.

E. DUNCOMBE: It may be relevant to Dr. Ivanovsky's remarks about supercooling if I point out that with the type of plugging meter used in the United Kingdom it took several hours to establish the initial plug in the orifice, although once it is established the meter controls well. Whether this is due to a supercooling phenomenon or simply to the mechanism of impurity deposition we do not know.

EXPERIENCE WITH IMPURITIES IN A LARGE SODIUM CIRCUIT

E.A. FIELDER, A.N. HAMER, J. HIGSON,
T.E. JENNINGS AND P.A. TREVALION
U.K. ATOMIC ENERGY AUTHORITY,
REACTOR ENGINEERING LABORATORY,
RISLEY, LANCS., UNITED KINGDOM

Abstract

EXPERIENCE WITH IMPURITIES IN A LARGE SODIUM CIRCUIT. In reactors cooled by liquid sodium the impurity level in the coolant must be controlled, to achieve acceptable corrosion rates and avoid circuit blockages. Information on impurity behaviour is required to plan and size the purification system. Information obtained from a large experimental rig of 12 500 litres capacity, operating at 400°C, is reported. The rig, built for testing a sodium pump, was similar to a reactor coolant system in materials, methods of construction and surface area/volume ratio. The results of the investigation are, therefore, applicable to reactor design.

The main impurities considered are oxygen, hydrogen and calcium. It is postulated that these impurities enter the system through the sodium manufacturing process, as contamination in constructional materials and cover gas, and by handling operations. The amounts attributable to each of these routes have been estimated by chemical analysis of the sodium, steels and cover gases, to predict the final impurity level of the sodium charge. This predicted figure is compared with the amounts of impurity which actually entered the rigs, as determined by regular sampling of the sodium during rig commissioning. The specially developed sampling equipment and techniques are described.

The effect on the principal impurities of changing the temperature conditions is assessed. Evidence of the formation of calcium oxide and sodium hydride during initial high-temperature work is reported, and their effect on operations is discussed.

INTRODUCTION

In reactors cooled by liquid sodium, the impurities in the coolant must be controlled to protect the constructional materials against corrosion and embrittlement, and to avoid circuit blockages. Among the principal impurities of concern are sodium oxide, which can accelerate corrosion in stainless-steel circuits [1], and sodium hydride, which can cause serious embrittlement of some reactor materials [2]. Both these impurities can also cause blockages in the reactor-coolant passages.

Before equipment to measure and remove these impurities can be designed, the amounts which are likely to occur in a reactor must be determined. Information about their source and how they will react to varying reactor conditions is also important. This information can be obtained before building a reactor by measuring the impurity during the commissioning of experimental rigs, and this paper describes how such an impurity monitoring programme has been performed on a rig at the Reactor Engineering Laboratory of the U.K.A.E.A.

SOURCE OF IMPURITY

Impurities can enter the reactor through five routes:

(1) As an impurity in the sodium charge;
(2) As a contaminant on the constructional materials;

(3) As a contaminant in the cover gas;
(4) As the result of an operational fault, e.g. accidental admission of atmosphere to the reactor system;
(5) As the result of routine maintenance.

The sodium used in this study was produced by the Downs-cell method [3]; nitrogen was used as the cover gas during manufacture. While the manufacturers do not guarantee to comply with a rigid specification, they generally adhere to a typical analysis, given in Table I. Calcium, potassium metal and sodium oxide are generally the principal impurities at this stage. Carbon can also be expected but a precise figure is not quoted by the manufacturer.

TABLE I. ANALYSIS OF SODIUM AS SUPPLIED (ppm)

Impurity	Manufacturer's typical analysis	Mechanical pump rig supply
Carbon		7
Calcium	500	250
Cobalt		< 1
Copper	1.2	
Chromium		1
Chlorine	14	0.2
Iron	3	5
Magnesium	8	2
Oxygen	60	
Potassium	200	5
Nickel	0.1	
Sulphur	10	0.8
Silicon	16	6

Contaminants will occur on constructional materials as surface films, sorbed gases and possibly as grease and paint, and these will be partially removed by cleaning processes. To estimate the possible oxygen and hydrogen contribution from this source, samples of materials used in the construction of test rig and reactors were analysed by vacuum fusion technique. Samples of 18% Cr, 8% Ni, 1% titanium stabilized austenitic stainless steel and $2\frac{1}{4}$% Cr, 1% Mo ferritic steel were taken from plate and tube stock and analysed ex stock and also after the following stages of cleaning:

(1) Degreasing by trichlorethylene vapour;
(2) Degreasing and acid cleaning by immersion in a solution of 10% concentrated nitric acid, 10% hydrofluoric acid, 80% water; and subsequently vacuum degassing.

The results are given in Table II. They show that with 18/8/1 stainless steel, degreasing removes a significant proportion of the surface oxygen and that subsequent acid cleaning and degassing has little further effect. With $2\frac{1}{4}$ Cr 1 Mo material, however, the full cleaning treatment is necessary to remove a significant amount of the oxygen.

Consideration of the cover gas volumes in rigs and reactors and the normal impurity levels in argon and nitrogen indicate that the cover gas does not contribute a significant amount of impurity to the sodium charge. The analysis of the argon supplied to the experimental rigs in the Reactor Engineering Laboratory is shown in Table III. The oxygen content in the argon cover gas of a typical reactor would raise the level of oxygen in the sodium by less than 1 ppm per hundred changes of cover gas.

TABLE II. TYPICAL OXYGEN AND HYDROGEN CONTENT OF CONSTRUCTIONAL MATERIALS DETERMINED BY VACUUM FUSION ANALYSIS

Material	Cleaning treatment	Oxygen content g/cm² of surface area	Hydrogen content g/cm² of surface area
18/8/1 stainless-steel plate	None	4.0×10^{-5}	0.3×10^{-5}
	Degreased	2.7	0.4
	Full cleaning treatment	2.7	0.44
18/8/1 stainless-steel tube	None	7.0	0.8
	Degreased	1.5	0.4
	Full cleaning treatment	1.5	0.4
18/8/1 stainless-steel weld material (argon arc)	None	19.0	0.18
	Degreased	13.0	0.22
	Full cleaning treatment	11.0	0.17
$2\frac{1}{4}$ Cr-Mo tube	None	62.0	0.22
	Degreased	55.0	0.20
	Full cleaning treatment	30.0	0.15

TABLE III. ANALYSIS OF ARGON

Impurities	ppm (vol.)
Oxygen	3
Nitrogen	30
Hydrogen	1
Carbon dioxide	1
Moisture	1
Hydrocarbons	0.02
Methane	0.02

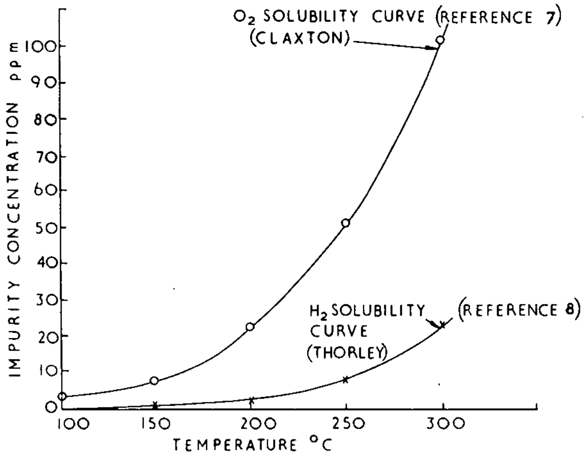

FIG. 1. Solubilities of hydrogen and oxygen in sodium

IMPURITY MEASUREMENT

Impurity levels in the sodium were determined by chemical analysis of samples. Oxygen was determined by using the distillation method [4], and the hydrogen by decomposing samples at 900°C in a wrought-iron can and measuring the diffused hydrogen manometrically [5]. These sample results were supplemented when possible by saturation temperature determinations made by conventional plugging meters [6]. The solubility curves to which the saturation temperatures were referred are shown in Fig. 1 [7, 8].

Three types of sampler were constructed to enable samples to be taken under different conditions. The first was to sample the sodium as supplied from the manufacturer's storage vessel to the transport vessels. To obtain a large representative sample, a small and large vessel were mounted in parallel with the manufacturer's feed pipe. Metered amounts were trapped in the smaller vessel at regular intervals during the transfer operation and stored in the larger vessel. The samples were dispensed from this larger vessel for analysis.

The second sampler, shown in Fig. 2, enabled samples of sodium and surface film to be obtained from rig dump tanks. A glove box was mounted on the dump-tank lid and samples were posted out of this glove box in sealed containers for analysis. Windows for viewing the sodium surface were built into the apparatus, and removable covers and mechanical wipers were provided to keep the glass clear of condensed vapour.

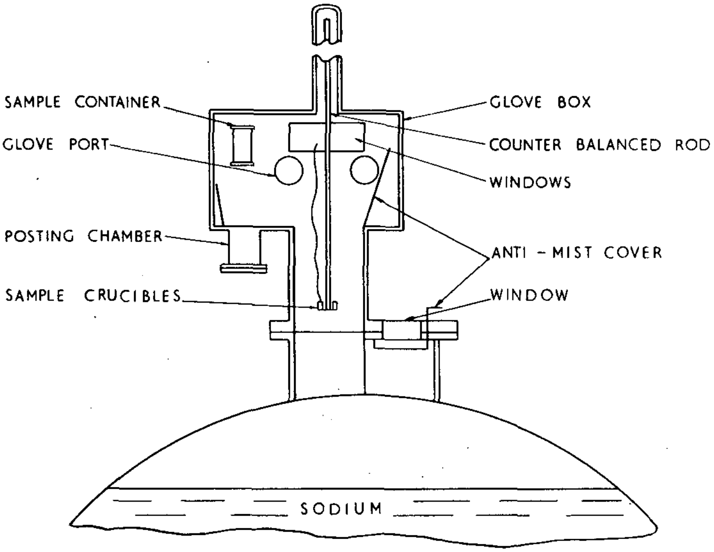

FIG. 2. Dip sampler

To obtain samples after the sodium was charged into the rig, an "in-line" sampler was developed (Fig. 3). A vessel through which the sodium could be circulated was welded into the rig circuit and surmounted by a glove box. Four crucibles were fitted in a holder on the underside of the sample vessel cover and capped by a spring-loaded plate. When the crucibles were completely covered by the sodium this spring-loaded cap was raised by a bellows-sealed actuator rod, thus taking four samples of sodium uncontaminated by any surface film. After the samples had been trapped in the crucibles, the vessel was isolated and drained. The samples were allowed to cool and solidify before being removed from the vessel and posted out of the glove box.

When this apparatus was first used, the samples were often contaminated by moisture present in the glove-box argon, which originated mainly as adsorbed gas on the glove-box walls. Some moisture also entered the box during manual operations in the gloves by perspiration from the operator's hands being transferred through the Neoprene. Effective control of this moisture was obtained by fitting a molecular sieve drier and a simple diaphragm gas circulator directly to the glove box. With a gas flow rate equivalent to 30 box changes per hour, the moisture content of the glove box was reduced from 50 to 5 ppm, which was low enough to prevent measurable contamination of the sample while it was being handled. The moisture content of the box gas was continually monitored by an electrolytic moisture meter. With these precautions an accuracy of better than ± 2 ppm was achieved in measuring oxide at levels of less than 10 ppm. The apparatus has been in regular use since 1964, and more than 5000 samples have been analysed.

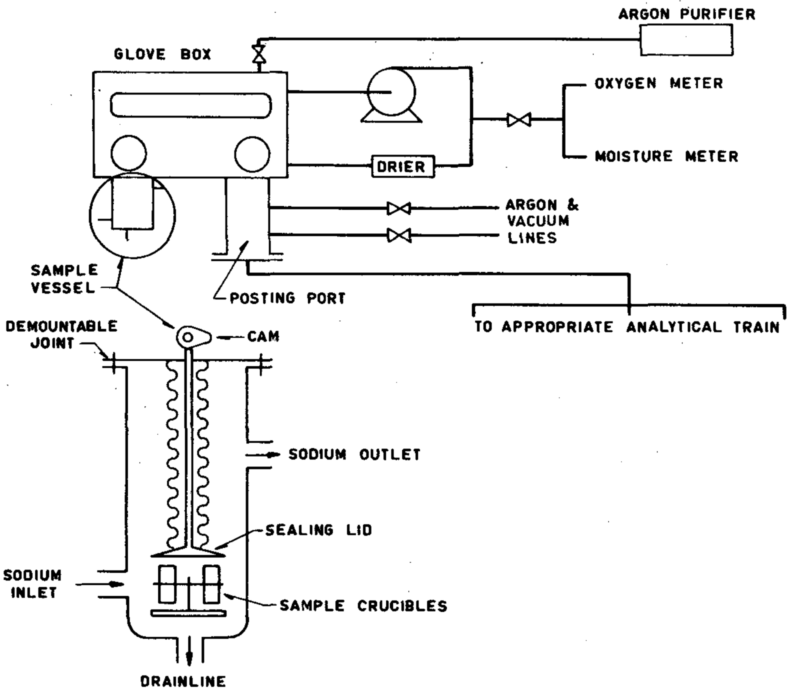

FIG.3. In-line sampler

SELECTION OF EXPERIMENTAL RIGS

The rig to be monitored was selected after comparing a number of U.K.A.E.A. experimental rigs with existing sodium-cooled reactor systems. Information was collected on factors that influence the impurity level in the coolant and the rate at which it is removed from the system. In particular, comparisons were made between materials of construction, the area of constructional materials in contact with the sodium, the volume of sodium in the system, the number of cold traps, and the time required to pass the sodium charge through the cold traps. Results from this survey are given in Table IV.

Small experimental rigs tend to have greater ratios of surface area to sodium volume than large reactor systems, and hence the proportion of impurity arising in such rigs from the constructional materials would be large compared with the proportion brought in by the sodium charge.

The process of dissolution of the impurities from the walls of the rig and their subsequent transfer to the cold trap is complex, possibly involving the diffusion of adsorbed gases through the wall material and a chemical change at the vessel wall. By contrast the removal of impurities brought in with the sodium is more direct. It follows that the behaviour of impurities in small rigs may differ from that in large systems.

In addition, the methods of construction of a rig and the sodium handling operations undertaken in it will be more representative of those employed on a reactor if a large rig is chosen in preference to a small one. Consequently, the Sodium Pump Rig, which was built in the Reactor Engineering Laboratory to obtain experience of operating a large mechanical pump in sodium at 400°C, was chosen for the impurity investigation.

This rig was described [9] at the 1966 London Conference on Fast Breeder Reactors. Its main parameters are listed in Table IV and a simplified flow diagram is shown in Fig.4.

The rig has several features similar to those of reactor practice which made it particularly attractive. While it is mostly constructed in 18/8/1 austenitic stainless steel, the two dump tanks, each of 6250 litres capacity, are made of $2\frac{1}{4}$ Cr-Mo ferritic steel, a possible material for some reactor secondary circuit components. The sodium charge was transported in bulk from the manufacturers, a filling procedure which will be adopted for large reactors. The leak-tightness of the rig was proved by methods which are applicable to reactors and avoided the cleaning effect of vacuum techniques. Dip samplers were fitted to the rig dump tank and the pump tank. An in-line sampler and two plugging meters were fitted in the cold-trap circuit.

The rig was constructed by argon-arc welding and was cleaned to good commercial standards. Stainless-steel components were cleaned by degreasing in trichlorethylene followed by acid wash. The ferritic steel dump tanks were shot-blasted and wire-brushed to remove rust, followed by degreasing. The final closing welds connecting components into the circuit were not cleaned.

From the manufacturer's typical analysis of sodium (Table I) and the measured impurity content of the constructional materials (Table II), the impurity level to be expected in the rig dump tanks and the rig circuit was calculated, and is shown in Table V.

IMPURITY BEHAVIOUR IN THE RIG

Sodium for the rig was obtained by taking the dump tanks to the manufacturers and filling them directly with liquid sodium from the manufacturer's storage vessel. The sodium was allowed to freeze and the tanks were then conveyed to the laboratory where they were connected to the experimental rig. The analysis of this sodium is shown in Table I, which shows that both the calcium and potassium contents were below typical. Because the sampling equipment was not designed to prevent contamination of the sample by air and moisture, neither the oxide nor the hydride content of the sodium was determined at this stage.

Soon after the sodium had been remelted, and when its surface was at 130°C, direct observation through the dip-sampler glove-box ports showed that the surface was covered with a heavy layer of impurity. This was sampled. The analytical results are shown in Table VI; the principal impurities are calcium and sodium oxide. Figures 5 and 6 are photographs of the surface and samples of the impurity layer. Samples were also taken

TABLE IV. COMPARISON OF REACTOR AND RIG PARAMETERS

	Surface parameters				Cold-trap parameters				Impurity parameters	
Facility	Liquid metal volume (m^3)	Surface area of containment (m^2)	Constructional materials	Surface area/ volume ratio (m^{-1})	Number of cold traps	Basket volume per trap (m^3)	Trap residence time (min)	Time for system turnover (min)	Effect of material contamination (ppm)	Effect of rig volume of air (ppm)
Reactors										
D. F. R. (P)[a]	61.2	3840	18/8/1 SS	62	15	0.057	6.2	450	20.5	304
(S)	76.2	6100		80	24	0.057	6.2	350	26.2	304
Enrico (P)	198.0	4970	18/8/1 SS/ 2¼/1 Cr Mo	25	1	1.98	4.3	437	8.9[c]	330
Fermi (S)	127.5	5160		41	1	1.98	4.3	281	14.2	330
Rigs[b]										
Mechanical pump rig	12.5	187	18/8/1 SS 2¼/1 Cr Mo	15	1	0.15	6.6	550	14.0	281
Fuel element thermal test rig	3.7	370	18/8/1 SS	100	1	0.15	6.6	163	30.4	282
Rubbing pair rig	0.034	10.8	18/8/1 SS	32	1	0.008	8.0	275	95.0	277

[a] P = Primary circuit.
S = Secondary circuit.

[b] Described by Eickhoff et al. [9].

[c] 2¼/1 Cr Mo contribution not included.

from below the sodium surface and analysed for sodium oxide: the bulk sodium was found to contain 80 ppm oxygen, which is greater than the solubility value at this temperature. This, added to the oxide in the surface layer, gives a total oxygen content for the sodium charge of 120 ppm, which is in reasonable agreement with the predicted value of 74 ppm (Table V).

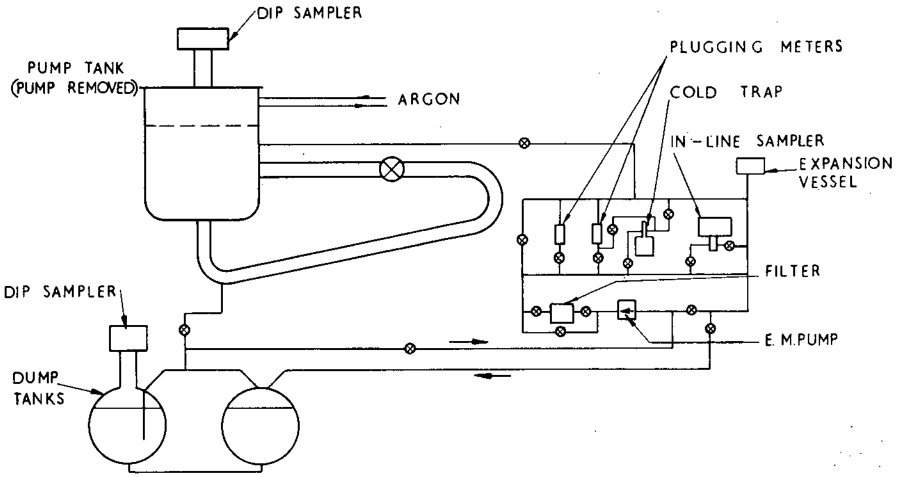

FIG. 4. Mechanical pump rig

TABLE V. ESTIMATED OXYGEN AND HYDROGEN LEVELS (ppm)

	Pump rig dump tanks		Pump rig - circuit	
	O_2	H_2	O_2	H_2
Impurities from sodium charge	60	<1	5	<1
Impurities from materials	14	<1	4	<1
Total	74	<2	9	<2
Estimated from sampling	120	10	No measureable increase	

When the temperature of the dump tanks was increased, the surface layer began to dissolve until at 300°C the surface was completely clear of impurity. Unexpectedly, dip samples taken from the bulk sodium showed that the sodium oxide in solution was also decreasing as temperatures were increased. This effect is shown in Fig. 7.

A possible explanation is that the calcium was reacting with the sodium oxide to form calcium oxide which was collecting as a layer on the walls

TABLE VI. ANALYSIS OF SODIUM SURFACE SAMPLE REMOVED FROM SODIUM PUMP RIG

	Impurities detected
Chromium	70 ppm
Copper	132 ppm
Iron	500 ppm
Magnesium	33 ppm
Manganese	5 ppm
Nickel	100 ppm
Calcium	2.5%
Oxygen	6.5%
Sodium	90.8%

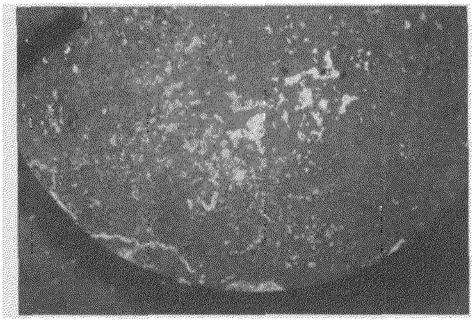

FIG. 5. Sodium surface at 130°C

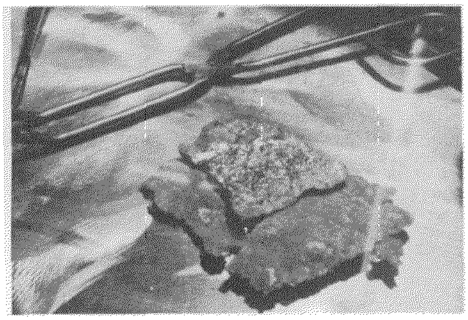

FIG. 6. Sodium surface samples

of the tanks. The sodium analysis (Table I) shows that 250 ppm of calcium were present initially, but with the techniques available at the time it was not possible to prove analytically that this had subsequently combined with the oxygen to form calcium oxide.

The sodium was then circulated through the auxiliary circuit, with the cold trap excluded (Fig. 4), so that samples could be obtained from the in-line sampler and compared with plugging-meter measurements of saturation temperature. The oxygen level was determined as < 10 ppm and the hydrogen level as 8 ppm, the saturation temperature being 235°C.

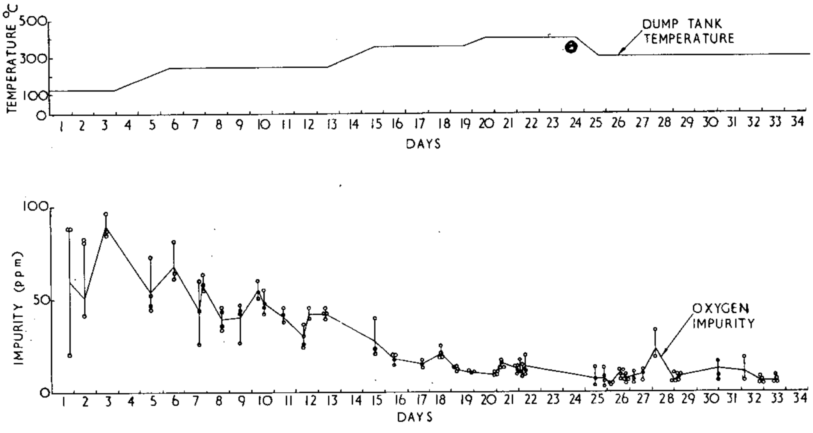

FIG. 7. Sample results from mechanical pump rig dump tanks

Reference to the solubility curves in Fig. 1 shows that the plugging-meter result was probably due to the precipitation of sodium hydride and not sodium oxide.

The hydrogen content was higher than expected, and investigations were made to trace its source. The nitrogen cover gas used at the sodium manufacturers was found to be contaminated with hydrogen and moisture. Examination of the records for the period when the dump tanks were filled showed the hydrogen content of the nitrogen cover gas to be as high as 5% and the moisture content 2000 ppm (vol). It was concluded that this cover gas was the source of the sodium hydride.

An attempt was made to remove the hydrogen from the sodium by heating the dump tanks to 400°C to decompose the sodium hydride and remove the evolved hydrogen by maintaining a continuous purge of argon over the sodium surface. At this temperature the concentration of hydrogen in the cover gas was 1500 ppm (vol.), and when a flow of 140 litres/h was established it fell to an average value of 500 ppm (vol.). The resulting effect on the plugging temperature is shown in Fig. 8: after 40 000 litres of purge gas had been passed over the sodium surface, the hydrogen content had been reduced by about 2 ppm.

The results so far presented were obtained with the cold trap isolated from the circuit. The circuit valves were subsequently arranged so that the cold trap was introduced into a closed loop consisting of a small electromagnetic pump, plugging meters, sampler and expansion vessel. The surface area of the Lessing rings in the cold-trap basket was 74 m^2 and the volume of the subsidiary loop 0.28 m^3, giving an area volume ratio of 260 m^{-1}.

It was expected that when sodium was pumped round this loop sufficient oxygen would be removed from the stainless steel to increase the oxygen content of the sodium to 70 ppm. In the event the impurity level in the sodium after circulating at 330°C for one week was substantially unchanged at 10 ppm oxygen. This result cannot be fully explained at present, but it is possible that some free calcium was present in the sodium and this reacted with the available oxygen.

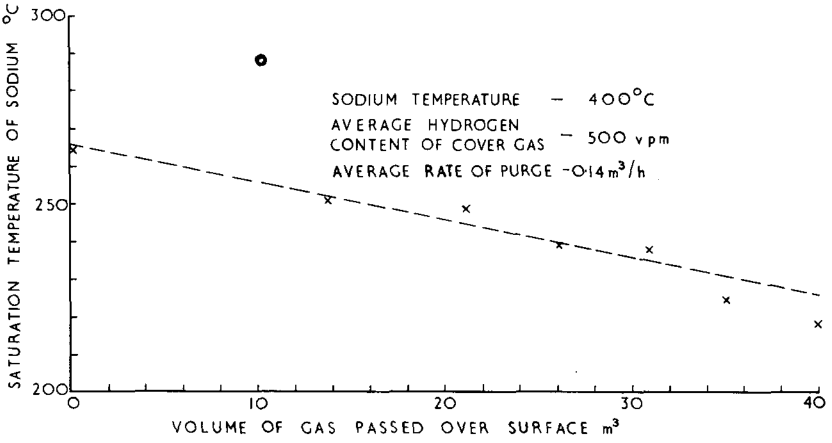

FIG. 8. Effect on saturation temperature of changing the sodium cover gas

After these operations, the sodium was raised into the pump tank and the main loop. During the lifting operation the surface was seen to be bright and highly reflective; it later acquired a very slightly dusty appearance after standing for 24 h at 150°C. This disappeared and the surface returned to its former mirror-like condition when the temperature was raised. Samples of the sodium indicated no significant change in the impurity content.

CONCLUSIONS

The ways in which oxygen and hydrogen can enter a reactor sodium circuit have been investigated; it is concluded that the major proportion of these impurities will enter with the initial sodium charge. Provided that the circuit components are cleaned to good engineering standards, the amount of impurity entering the circuit on the constructional materials will be small.

Apparatus to measure coolant sodium by direct sampling and chemical analysis has been designed and developed, and has been used to monitor the behaviour of oxygen and hydrogen in a large experimental rig containing 10 t of sodium.

The measurements showed an initial oxygen content of 120 ppm and a hydrogen content of 8 ppm. The hydrogen content was unexpectedly high, and was possibly due to cover-gas contamination at the sodium manufacturer's works. There is some evidence that a proportion of the oxygen reacted with free calcium present in the sodium as the rig temperatures were raised, and that some of the sodium hydride dissociated at the higher temperature.

The increase in oxygen and hydrogen content when the sodium was charged from the dump tanks into the main circuit was negligible.

ACKNOWLEDGEMENTS

The authors wish to thank their colleagues at the Reactor Engineering Laboratory, Risley, for their support and assistance in performing the work.

REFERENCES

[1] NETTLEY, P.T., BELL, I.P., BAGLEY, K.Q., HARRIS, D.R., THORLEY, A.W., TYZACK, C., Paper No. 5B/3, British Nuclear Energy Society, London Conference on Fast Breeder Reactors, 1966.

[2] TYZACK, C., THORLEY, A., "The embrittlement of niobium in hydrogen-contaminated NaK", Thermodynamics of Nuclear Materials, IAEA, Vienna (1962) 365.

[3] DOWNS, J.C., U.S. Patent 1 501 756 (1924).

[4] WALKER, J.A.J., FRANCE, E.D., EDWARDS, W.T., Determination of oxygen in sodium, Analyst, Lond. 90 (1965) 727.

[5] WALKER, J.A.J., SEED, H., The determination of hydrogen in sodium, Analyst, Lond. 90 (1965) 19.

[6] BATUTIS, E.F., Operating experiences with oxide monitors for sodium systems, Rpt TID 7568 pt. 2 (1958) 24.

[7] CLAXTON, K.T., Review of solubility data from the liquid sodium-oxygen system, J. nucl. Energy 19 (1965) 849.

[8] THORLEY, A., RAINE, A., Experimental techniques for purifying sodium, U.K.A.E.A. Rpt TRG 1317(C).

[9] EICKHOFF, K.G., ALLEN, J., BOORMAN, C., Paper No. 5B/5, British Nuclear Energy Society, London Conference on Fast Breeder Reactors, 1966.

DISCUSSION

J.P. LAGOWSKI: Did you notice any difference between the sodium impurity levels of dip and in-line samples?

T.E. JENNINGS: Both types of sampling were carried out concurrently after the initial heating of the sodium in the dump tanks, i.e. when the Na_2O level had been reduced to approximately 8-10 ppm. There was no significant difference in the results obtained with the two systems.

L.F. EPSTEIN: I was extremely interested by what you said about calcium oxide. Calcium is always found in sodium because it is normally produced by electrolyzing $NaCl-CaCl_2$ mixtures. It has been found, however, in work carried out under our sodium mass transfer programme that the calcium content of the sodium decreases rapidly with time. We think this is due to the separation and accumulation of the calcium oxide in the cold traps. This would be in line with some results we obtained a few years ago, when we studied the possibility of using calcium and barium as soluble getters to reduce the Na_2O content of the sodium. It was found that these alkaline earth metals tended to form intermetallic compounds with nickel and nickel-bearing alloys like stainless steel. In other words, the calcium content of the system tends to decrease even if there is no oxygen source to convert the calcium to calcium oxide.

E.A. FIELDER: I should like to make a brief comment on our experience in this connection. During the early stages of our development work at the UKAEA Reactor Engineering Laboratory we filled our loop dump tanks at the sodium manufacturers' plant. The impurity level in this sodium was approximately 500 ppm, which is significantly higher than in the case of United States reactor-grade sodium. As the sodium was heated and circulated, we found that the plugging meters indicated a rise in the impurity level. Cold-trapping reduced the saturation temperature indicated by the plugging meter. After a few days no plug could be obtained even when the cold-trap temperature was raised, and we later attributed this to the gettering action of the calcium in the sodium.

I would have thought that this result was at variance with the suggestion made by Mr. Epstein earlier[1] that calcium oxide was a possible cause of the second break phenomena in the plugging meter. I would be interested to hear his comments on this.

L. F. EPSTEIN: This effect you saw, due to the gettering action of the calcium in reducing the Na_2O level, is quite a familiar phenomenon. The idea I put forward earlier is not mine but Mr. Bruggeman's and he suggested it some time ago. He thought that the second break might be due to the fact that some of the calcium, being rather less soluble than the Na_2O, goes into solution after being oxidized to CaO and comes out of solution at a higher temperature. So in fact there is no real inconsistency between what we've both been saying.

---

[1] See discussion of paper SM-85/4.

ОСАЖДЕНИЕ ОКИСЛОВ ИЗ ПОТОКА НАТРИЯ

В.И.СУББОТИН, Ф.А.КОЗЛОВ
ФИЗИКО-ЭНЕРГЕТИЧЕСКИЙ ИНСТИТУТ, ОБНИНСК
СССР

(Доклад представил Б.В.Кульпин)

Abstract — Аннотация

PRECIPITATION OF OXIDES FROM A SODIUM STREAM. In work on the design of cold traps for sodium oxides, it is important to know how the oxides are distributed throughout the trap and the relationship between this distribution and various factors.

By a physical and mathematical analysis the basic parameters governing the mass-transfer processes are determined as well as the nature of the functional dependence of changes in the supersaturation of the solution and thus in the oxide stream on the mass-transfer surface along a cold-trap model, in a case where dt/dx = const. and dt/dx = 0.

The results of an experimental study of oxide precipitation in a cold-trap model are presented, with and without a temperature gradient, and the results obtained with the help of analytical relationships developed in the course of mass transfer investigations are discussed.

On the basis of the results obtained, it is suggested that the low oxide trapping capacity of the trap is attributable to local clogging of its flow-passage cross-sectional area, and methods are recommended for ensuring more even spreading of the precipitated oxides throughout the trap.

ОСАЖДЕНИЕ ОКИСЛОВ ИЗ ПОТОКА НАТРИЯ. При конструировании холодных ловушек окислов натрия важно знать, как распределяются окислы по объему холодной ловушки и как зависит это распределение от различных факторов.

В докладе с помощью физико-математического анализа определяются основные параметры, от которых зависят процессы массообмена, и вид функциональной зависимости изменения пересыщения раствора, а, следовательно, и потока окиси на поверхности массообмена, по длине модели холодной ловушки для случая, когда dt/dx = const и dt/dx = 0.

Описаны результаты экспериментального изучения осаждения окислов в модели холодной ловушки при наличии и отсутствии температурных градиентов. Полученные результаты обсуждаются с привлечением аналитических зависимостей, полученных при решении задач массообмена.

На основании полученных результатов высказываются предположения о том, что низкая емкость ловушки по окислам объясняется локальной закупоркой его проходного сечения. Рекомендуются некоторые пути, обеспечивающие более равномерное заполнение всего объема ловушки высаждающимися окислами.

В настоящее время для очистки натрия от окислов широкое применение получили холодные ловушки. Протекающий через них натрий охлаждается до 110 – 150°С. Раствор окиси натрия становится пересыщенным. Происходит кристаллизация окиси, которая удерживается на специальных фильтрах.

При конструировании холодной ловушки важно знать, как распределяются окислы по ее объему и как зависит это распределение от различных факторов. Это позволит сконструировать холодную ловушку таким образом, чтобы осаждающиеся в ней окислы равномерно распределялись по ее объему, а не скапливались локально, закупоривая преждевременно проходное сечение. Нахождение распределения окислов в холодной ловушке сводится к решению задачи массообмена с учетом конкретных граничных условий. Применение полученных решений требует знания параметров, характеризующих данную систему. Аналитическому и экспериментальному изучению некоторых вопросов, связанных с данной проблемой, посвящена настоящая работа.

ФИЗИКО-МАТЕМАТИЧЕСКАЯ ПОСТАНОВКА ЗАДАЧИ

Решение данной задачи в общем виде весьма сложно. Для нашего случая, когда вследствие осаждения окислов должны изменяться размеры, эти трудности возрастают. Распределение окислов в холодной ловушке определяется их потоком на поверхности массообмена. В общем случае этот поток будет складываться из двух составляющих – потока кристаллизирующего вещества из пересыщенного раствора и потока кристаллов окиси, которые, вообще говоря, могут присутствовать в потоке натрия.

При постановке задачи будем считать, что вторая составляющая (диффузия кристаллов окиси к поверхностям массообмена) пренебрежимо мала по сравнению с первой.

Это предположение, на наш взгляд, является правильным, т.к. коэффициент диффузии кристаллов окиси на один-два порядка ниже, чем коэффициент диффузии окислов, находящихся в растворе [1]. Можно было бы ожидать некоторого увеличения осаждения кристаллов окиси натрия за счет инерционных эффектов. Однако для нашей системы, когда удельные веса натрия и окиси натрия отличаются незначительно, а скорости потока малы, критерий Стокса много меньше единицы ($\sim 10^{-3}$) и, следовательно, инерционное осаждение практически не имеет места.

Вместе с тем, появление кристаллов окиси в потоке приведет к более резкому снижению пересыщения: кристаллизация из пересыщенного раствора будет идти не только на неподвижных центрах кристаллизации, но и на движущихся вместе с потоком кристаллах окиси натрия.

Данное обстоятельство неизбежно приведет к изменению распределения осаждающихся в участке окислов, т.к. высаждение окиси из потока в виде готовых кристаллов характеризуется другими постоянными.

Учитывая реальные условия (наличие центров кристаллизации, не слишком интенсивное перемешивание потока и т.д.), можно сказать, что в нашем случае процесс кристаллизации будет определяться диффузионными процессами, т.е. скорость роста кристаллов в соответствии с [2] описывается уравнением:

$$U_к = \frac{D\,z}{\delta_D \cdot 100} \cdot \frac{M_{Na_2O}}{M_0} \cdot \frac{j_{Na}}{\gamma_{Na_2O}} \qquad (1)$$

Видно, что для нахождения распределения окислов необходимо знать степень пересыщения по длине холодной ловушки и некоторые постоянные, которые для нашей системы неизвестны.

Схематически конструкция холодной ловушки представлена на рис. 1. Там же представлена качественная картина изменения температуры и пересыщения по длине.

Анализ проводился по среднесмешанной температуре, изменение температуры по радиусу не учитывалось. Исходя из материального баланса по кислороду, нетрудно получить:

$$\frac{dz}{dx} + \frac{100}{G_{Na}}\left(j'_{O_2}\,S' + j'_{O_2}\,S''\right) = -\frac{dC_{нас}}{dx} \qquad (2)$$

При решении уравнения (2) необходимо выделить две области: зону, где $dC_{нас}/dx \neq 0$, и участок, где $dC_{нас}/dx = 0$. Для интегрирования уравнения (2) необходимо знать вид функций

$$\frac{dC_{нас}}{dx} = f_1(x); \qquad j'_{O_2} = f_2(z, x); \quad j''_{O_2} = f_3(z, x).$$

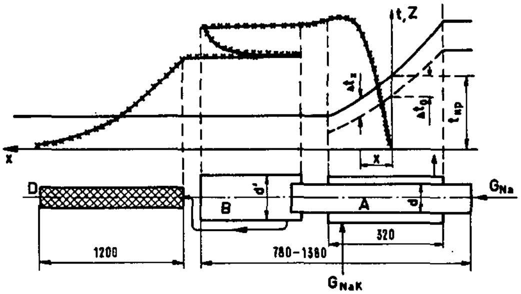

Рис. 1. Схема экспериментального участка: ×××× пересыщение; ——— температура натрия; ----- температура натрия-калия.

В общем случае, когда растворимость кислорода в натрии описывается уравнением вида

$$\lg C_{нас} = A + \frac{B}{T}, \tag{3}$$

а охлаждение натрия происходит в теплообменнике Na – NaK (рис. 1), нами получено выражение для функции $f_1(x)$. Оно имеет вид:

$$f_1(x) = -\frac{2{,}3B}{(273+t_x)^2} \cdot e^{A+\frac{B}{273+t_x}} \cdot \frac{\kappa_x \cdot \Delta t_0}{G_{Na} \cdot C_p^{Na}} \cdot e^{-m\int\limits_0^x \kappa_x dx}, \tag{4}$$

где

$$t_x = t_{кр} - \frac{\Delta t_0}{G_{Na} \cdot C_p^{Na}} \cdot \int\limits_0^x \kappa_x e^{-m\int\limits_0^x \kappa_x dx} \cdot dx,$$

$$m = \frac{1}{G_{Na} \cdot C_p^{Na}} - \frac{1}{G_{NaK} \cdot C_p^{NaK}},$$

$$\kappa_x = \frac{1}{\frac{1}{\alpha_{Na}(x)d_1} + \frac{1}{2\lambda_{ст}}\ln\frac{d_2}{d_1} + \frac{1}{\alpha_{NaK}(x)d_2}}$$

В этом случае вид функции $f_1(x)$ получается довольно-таки громоздким. Однако ее можно существенно упростить, если учесть, что растворимость кислорода в натрии в зависимости от температуры в интервале температур 150 – 350°C можно представить уравнением:

$$C_{нас} = -3 \cdot 10^{-5}t + 1{,}68 \cdot 10^{-7}\,t^2 \tag{5}$$

и принять, что для зоны кристаллизации $dt/dx = \mathrm{const}$. При этих предположениях

$$f_1(x) = \epsilon_1 + \epsilon_2 x, \tag{6}$$

где

$$\epsilon_1 = \frac{dt}{dx}\left(-3 \cdot 10^{-5} + 3{,}36 \cdot 10^{-7} t_{кр}\right), \tag{7}$$

$$\epsilon_2 = \left(\frac{dt}{dx}\right)^2 3{,}36 \cdot 10^{-7} \tag{8}$$

Определение функции $f_2(z, x)$ представляет более сложную задачу. В нашем случае:

$$j'_{O_2} = \alpha_D \cdot z \cdot \frac{\gamma_{Na}}{100} = \frac{Nu_D \cdot z \cdot D \cdot \gamma_{Na}}{100\, d_1} \tag{9}$$

Коэффициент массообмена будет зависеть от "x" не только за счет того, что массообмен происходит на входном участке, при наличии источников кислорода переменной интенсивности по длине, но также и из-за значительного изменения свойств натрия вследствие больших перепадов температур. Так, например, учитывая, что коэффициент диффузии можно представить как $D = \mathrm{const}/\nu$ [1], можно ожидать снижения коэффициента диффузии в $1{,}5 \div 2$ раза.

Для расчета потока на кристаллы окиси натрия, движущиеся вместе с потоком натрия, будем считать, что кристаллы имеют форму шара, а скорость их относительно натрия равна нулю:

$$j''_{O_2} = \frac{D\, z\, \gamma_{Na}}{\bar{d}_k \cdot 100} \tag{10}$$

Тогда:

$$\frac{dz}{dx} + \text{Б}(x)[1 + \varphi(x)]\, Z = -(\epsilon_1 + \epsilon_2 x), \tag{11}$$

где

$$\text{Б}(x) = d_D \frac{S' \gamma_{Na}}{G_{Na}} \tag{12}$$

$$\varphi(x) = \frac{S'' \cdot D}{\bar{d}_к \cdot \alpha_D \cdot S'} \tag{13}$$

Общий интеграл уравнения записывается в виде:

$$z = -e^{-\int_0^x \text{Б}(1+\varphi)dx} \int_0^x [(\epsilon_1 + \epsilon_2 x)\, e^{\int_0^x \text{Б}(1+\varphi)dx}\, dx + C] \tag{14}$$

Учитывая, что при $x = 0$ $z = 0$, получаем $C = 0$.

Для интегрирования уравнения (14) необходимо знать функцию Б$(1+\varphi)$. Будем считать, что кристаллы окиси натрия и другие центры кристаллизации в потоке натрия отсутствуют. При этом условии $\varphi=0$. Далее рассмотрим два случая:

1. Коэффициент массообмена не зависит от длины, т.е. Б = const.
2. Коэффициент массообмена изменяется по длине за счет изменения коэффициента диффузии. Оба случая предполагают, что массообмен происходит в зоне, где процессы гидродинамики, тепло- и массообмена стабилизированы.

Для случая, когда Б = const:

$$z=-\left(\frac{\epsilon_1}{Б}-\frac{\epsilon_2}{Б^2}\right)\cdot\left(1-e^{-Бx}\right)-\frac{\epsilon_2}{Б}x, \tag{15}$$

при $f_1=0$

$$z=z_0\cdot e^{-Бx} \tag{16}$$

Во втором случае в интервале температур 150 – 350°C приближенно зависимость коэффициентов диффузии от x при dt/dx =const может быть представлена прямой линией. Тогда:

$$Б=Б_0-2ax \tag{17}$$

и общий интеграл уравнения (14) запишется в виде:

$$z=\frac{\epsilon_2}{2a}\left(1-e^{-Б_0x+ax^2}\right)-\left(\epsilon_1+\frac{Б_0\epsilon_2}{2a}\right)\cdot\frac{1}{\sqrt{a}}\cdot e^{\left(\sqrt{a}x-\frac{Б_0}{2\sqrt{a}}\right)^2}\cdot\int\limits_{\frac{Б_0}{2\sqrt{a}}}^{\sqrt{a}x-\frac{Б_0}{2\sqrt{a}}}e^{-t^2}dt \tag{18}$$

На практике решениям (15), (16) и (18) ближе всего соответствует случай, когда осаждение окислов происходит при наличии насадки, т.е. гидравлический диаметр мал и зона стабилизации вследствие этого мала. При этом уравнение (15) может быть применено, когда имеется градиент температуры по длине, но изменение коэффициента диффузии при этом незначительно; уравнение (16) применимо для зоны окончательной фильтрации при отсутствии в ней температурных градиентов; уравнение (18) применимо в тех случаях, когда изменение коэффициента диффузии по длине может быть представлено линейной зависимостью.

Поток кислорода на поверхность массообмена в единицу времени на единицу длины может быть рассчитан по уравнению:

$$j_{O_2}=БG_{Na}\frac{z}{100} \tag{19}$$

Количество кислорода, осевшего на поверхность массообмена, расположенную между x_1 и x_2, за полное время эксперимента (τ) – по формуле:

$$P_{O_2}=Б_{cp}G_{Na}\tau_p(x_2-x_1)\cdot\frac{z_{cp}}{100} \tag{20}$$

Здесь $Б_{ср}$ – среднее за время опытов значение для участка массообмена, расположенного между x_2 и x_1; $z_{ср}$ – среднее пересыщение на участке $x_2 - x_1$.

$$z_{ср} = \frac{1}{x_2 - x_1} \cdot \int_{x_1}^{x_2} z \cdot dx.$$

ЭКСПЕРИМЕНТАЛЬНОЕ ИЗУЧЕНИЕ ОСАЖДЕНИЯ ОКИСЛОВ ИЗ ПОТОКА НАТРИЯ

Конструкция экспериментального участка, использованного в данной работе, схематически представлена на рис. 1. Выполненный таким образом рабочий участок представлял модель холодной ловушки: зоны гидродинамической и тепловой стабилизации были совмещены, длина участка теплообмена выбрана короткой ($L/d = 5$).

В участке представлены три основные зоны, имеющиеся в холодной ловушке: охлаждения (А), отстойника (В), фильтрации (Д). Такое построение рабочего участка удобно для изучения распределения окислов между зонами и в каждой зоне. Изучение распределения температур по высоте экспериментального участка производилось продольными передвижными термопарами, которые помещались в карманах, изготовленных из нержавеющей стали $\phi\, 6 \times 0{,}3$ мм. Королек термопар заделывался в медный наконечник, который плотно прилегал к стенкам кармана. Участки также оснащались термопарами, измеряющими температуру натрия и сплава натрий-калий на входе и выходе из рабочего участка.

В одном из экспериментальных участков на расстоянии $L/d = 3{,}2$ была установлена поперечная подвижная термопара.

В качестве дополнительных поверхностей, на которых происходит кристаллизация окислов, нами использовалась нержавеющая стружка толщиной $\sim 0{,}3$ мм и шириной 3 – 5 мм. Набивка выполнялась секционной. Длина каждой секции не превышала 150 мм. Между секциями устанавливались специальные решетки, препятствующие перемещению стружки под действием гидродинамических усилий и перепада давления, возрастающего по мере накопления окислов.

После того как участок был подготовлен к работе, через него в течение 10 – 25 часов прокачивался натрий с расходом $2 \div 3$ м^3/час. Одновременно с этим температура натрия и содержание кислорода в нем доводились до заданного уровня. Затем через экспериментальный участок устанавливали необходимый расход натрия, включали в работу контур сплава и снижали температуру натрия на выходе из рабочего участка. Во время работы участка в режиме осаждения окислов контроль за концентрацией кислорода в натрии на входе в рабочий участок осуществлялся не реже чем через четыре часа. Замер распределения температур по длине рабочего участка производился один раз каждые 8 часов.

Для изучения распределения окислов в рабочем участке после окончания опыта натрий замораживался. Участок с замороженным натрием вырезали из контура, и дистилляционно-газовым методом определяли количество окислов, осевших в разных зонах, и их распределение по длине зон.

Очевидно, что полное количество окислов, осевших в рабочем участке, помимо прочих факторов зависит также и от того количества окислов, которое за все время опыта могло перейти из раствора в кристаллическую фазу.

При обработке экспериментальных данных эта величина определялась нами по формуле:

$$P_{O_2} = \frac{G_{Na}}{100}\int_0^{\tau_p}[C^{вх}(\tau) - C^{вых}_{нас}(\tau)]\,d\tau \qquad (21)$$

Количество окислов, прошедших через отстойник и зону фильтрации, определялось как полное количество окислов, прошедшее через рабочий участок (P_{O_2}), минус количество окислов, осевших в предшествующих зонах. Количество окислов, осевших в каждой зоне, определяли по данным химического анализа.

Расчет средних коэффициентов массообмена для зоны охлаждения производили по формуле (20) методом последовательных приближений: вначале при определении среднего по длине рабочего участка пересыщения считалось, что окислы не осаждаются на поверхностях массообмена; при этом предположении определяли $z^{\circ}_{ср}$; используя $z^{\circ}_{ср}$ и зная количество окислов, осевших в зоне теплообмена, определяли α°_{D}; затем по формуле (18), используя α°_{D}, находили $z'_{ср}$ и соответствующее ему α'_{D} и т.д.

Исходя из соотношений (16) и (20), в зоне окончательной фильтрации следовало ожидать снижение количества окиси при удалении от входа. Причем отношение количества окислов, уловленных в единице объема на расстоянии "L" от входа, к количеству окислов, уловленных в единице объема на входе в зону окончательной фильтрации, должно было зависеть от комплекса "Б" и расстояния пробы от входа. Поэтому приведенные ниже распределения окислов в зоне окончательной фильтрации являются относительными:

$$\frac{C^*_{Na_2O}(L)}{C^*_{Na_2O}(O)} = f(L)$$

Расстояние "L" отсчитывалось от центра "первой" пробы.

Всего было проведено 32 опыта. Из них 24 опыта было выполнено на участке, внутренний диаметр которого равен 66 мм, остальные – на участке с диаметром 31 мм.

Для изучения распределения окислов в экспериментальных участках было проведено около тысячи анализов натрия на содержание кислорода.

При проведении опытов основное внимание было уделено изучению температурных полей в зоне охлаждения и распределению окислов по длине экспериментального участка.

Измерение распределения температур продольными термопарами показало, что в наших опытах при скоростях натрия, больших 15 мм/сек, распределение температур в зоне охлаждения можно считать линейным. Было замечено также, что осаждающиеся в зоне охлаждения окислы заменяют распределение температур по длине и вызывают возрастание разности температур между центром и стенкой.

Более детально распределение температур в рабочем участке изучали с помощью поперечной подвижной термопары. Некоторые результаты этих опытов описаны в [3]. Помимо приведенных в этой работе результатов необходимо отметить следующее.

Было обнаружено возрастание градиента температуры в слое окись натрия – натрий по мере работы участка в режиме накопления окиси, т.е. по мере роста толщины слоя окись – натрий. Поскольку анализ экспериментальных данных показал, что общее изменение теплового потока и его перераспределение по длине зоны теплообмена при нарастании слоя окислов было незначительно (макс. 25%), то увеличение градиента температуры можно объяснить лишь уменьшением теплопроводности слоя. Расчеты, проведенные в предположении постоянства теплового потока, показали, что она снижается более чем в два раза. Это хорошо согласуется с результатами, полученными на таких же экспериментальных участках методом плоского слоя [4].

Снижение теплопроводности слоя по мере его роста можно объяснить лишь увеличением концентрации окислов в слое. Это может происходить по двум причинам: из-за уплотнения слоя под действием гидродинамических сил и из-за непрерывно протекающей перекристаллизации окислов в неподвижном слое [5].

Измерение пульсаций температур на одном и том же тепловом режиме при наличии и отсутствии слоя показало, что в слое окислы – натрий пульсации температур хотя и составляют ощутимую величину, но они заметно затухают.

Распределение окислов по длине экспериментального участка целесообразно рассматривать по трем зонам.

Зона охлаждения. Скорость натрия в опытах изменялась от 5 до 23 мм/сек ($810 \leq \mathrm{Re} \leq 4160$) при диаметре участка 66 мм и от 230 до 810 мм/сек ($17820 \leq \mathrm{Re} \leq 68600$) при диаметре участка 31 мм.

Типичная картина распределения окислов в этой зоне для опытов с малыми скоростями при наличии насадки представлена на рис. 7. Расстояние от начала области кристаллизации до максимума по направлению потока металла составляет ~100 – 130 мм. При наличии насадки (плотность набивки ~100 кг/м^3) в зоне охлаждения удерживается около 24% окислов от полного количества, которое могло перейти в кристаллическую фазу и осесть в зоне охлаждения за время проведения опыта.

При отсутствии насадки при анализе проб натрия дистилляционно-газовым методом имелась возможность визуально наблюдать распределение окислов в пробах после проведения дистилляции (из пробы удалялась основная масса натрия). Типичная картина, полученная в этих наблюдениях, представлена на рис. 2. Видно, как велика роль дополнительных поверхностей в осаждении окислов. Тот факт, что нарастание слоя окислов на центральной термопаре начинается несколько позже, чем на охлаждаемой поверхности, объясняется профилем температуры, существующим в зоне теплообмена [3].

Анализ температурных и кислородных режимов показывает, что осаждение окислов из потока натрия на охлаждаемую и неохлаждаемую (центральная термопара) поверхности начинается практически сразу же, как только раствор становится пересыщенным. Основная масса окислов, осевших в зоне охлаждения, приходится на участок протяженностью 100 – 150 мм. Причем возрастание от нуля до максимальной величины происходит на участке протяженностью 50 – 100 мм. После прохождения максимума количество окислов резко падает.

Доля окислов, удерживаемых в зоне охлаждения при отсутствии набивки, составляет ~4% и не зависит от скорости натрия при изменении ее с 5 до 23 мм/сек. Следует отметить, что параметр Z, характеризующий процессы тепло- и массообмена при совместном действии свободной и вынужденной конвекций, при этом менялся незначительно ~20%. Эта характеристика, полученная в различных опытах при одной и той же скорости и конструкции участка, сильно отличается. Максимальное отклонение от среднего значения составляет более 100%. Оценка ошибки в

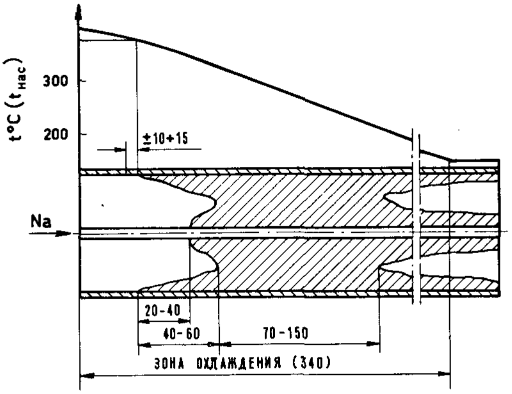

Рис. 2. Качественная картина распределения окислов в зоне охлаждения при отсутствии набивки.

определении доли удержанных окислов показывает, что при наихудших предположениях (точность определения средней за время опыта концентрации кислорода на входе составляет ~50%) она не превышает 70%. Это говорит о том, что имелись какие-то неконтролируемые факторы, влияющие на удержание окислов в зоне теплообмена. Об этом же говорит тот факт, что в трех опытах (из 23) удержание окислов в зоне охлаждения было аномально высоким и составляло 31, 48 и 46% для скоростей 5, 8 и 23 мм/сек соответственно. Анализ условий опытов позволяет сказать, что такие факторы, как температурный режим, загрязнение натрия перекисью, при проведении опыта не могут объяснить повышенное удержание окислов в зоне охлаждения в этих трех опытах. При расчете средних значений доли окислов, удерживаемых в зоне охлаждения, данные этих трех опытов в расчет не принимались.

Коэффициенты массообмена, рассчитанные по экспериментальным данным по описанной выше методике, приведены в таблице. Видно, что при одной и той же скорости натрия они сильно отличаются друг от друга. Это также говорит о том, что в опытах имелись неконтролируемые факторы, которые влияли на осаждение окислов в зоне охлаждения.

Опыты по изучению осаждения окислов при больших скоростях показали, что удержание окислов в зоне охлаждения составляет в среднем 26±3% и практически не зависит от чисел Рейнольдса в указанном выше диапазоне. В этих условиях осаждение окислов на поверхности массообмена начинается как только раствор кислорода в натрии становится пересыщенным. Анализы натрия из зоны охлаждения показали, что максимальная средняя концентрация окислов в пробах составляет ~70% (получено лишь в одном опыте). Концентрации окислов в пробах 60 – 70 вес % встречаются чаще. Максимальная средняя концентрация окислов в зоне охлаждения равна ~37%*.

---

* Здесь и далее под концентрацией окислов в пробах и в участке имеется в виду С*.

ТАБЛИЦА. КОЭФФИЦИЕНТЫ МАССООБМЕНА, РАССЧИТАННЫЕ ПО ЭКСПЕРИМЕНТАЛЬНЫМ ДАННЫМ

Скорость потока натрия, мм/сек	5	8	12	15	23
Коэффициенты массообмена, м/час	0,05 0,2 1,0 0,9	0,008 0,2 0,09 0,3	0,06 0,2 0,7	0,2 0,3 0,5	1,4 0,2 0,5 0,6 0,4

Отстойник. В зависимости от количества уловленных окислов они располагаются в отстойнике двояко: при малых накоплениях (140 – 150 г Na_2O) их концентрация при удалении от дна убывает; при больших накоплениях поддерживается на некотором среднем уровне (приблизительно равном концентрации у дна отстойника), а затем начинает снижаться, как в опытах с малым накоплением. В случае больших накоплений окислов в отстойнике были получены слои, обогащенные окислами до концентрации ~16% высотой ~280 мм (при общей высоте отстойника ~300 мм) и ~600 мм (при общей высоте отстойника 900 мм).

Максимальная концентрация окислов в отстойнике составляет 29 – 24% для большого накопления и ~18% – для малого накопления. В одном из опытов, когда скорость натрия на входе в отстойник была равна 300 мм/сек, была получена концентрация окислов у дна отстойника в 33 вес%.

Анализ распределения окислов по диаметру показал, что максимальная концентрация окислов находится у поверхности трубы.

Удержание окислов в отстойнике составляет 11 и 46% при длине его ~300 и 850 мм соответственно. В опытах, в которых удержание окислов в зоне охлаждения было аномально высоким, было получено и более высокое удержание окислов в отстойнике ~32% при длине его ~300 мм.

Один из рабочих участков работал на контуре в течение нескольких тысяч часов. Максимальная концентрация окислов в одной из проб этого участка составляла ~41%, средняя концентрация окислов в отстойнике – 29%.

Этот факт и то обстоятельство, что максимальная концентрация окислов в отстойнике при больших скоплениях была выше максимальной концентрации окислов при малых скоплениях, показывают, что со временем в отстойнике идут процессы, приводящие к обогащению слоя окислы-натрий окислами. Этими процессами могут быть перегонка более мелких кристаллов на более крупные [5] и действие гидродинамических усилий на слой окислов.

Зона фильтрации. Распределение окислов в этой зоне изучалось в зависимости от скорости натрия, плотности набивки и ее распределения по длине. Скорость натрия в опытах изменялась от 1,8 до 146 мм/сек. Полученные результаты приведены на рис. 3 – 6. Видно, что экспериментальные данные имеют значительный разброс. Это объясняется следующими причинами: смещением набивки вместе с окислами из-за перепада давления; качественными и количественными изменением поверхности массообмена, зависящим от количества окислов, осевших на насадке. Количественный учет этих факторов затруднителен, но очевидно, что они должны приводить к дополнительному разбросу экспериментальных данных.

Из рис. 3 – 5 видно, что расстояние от входа, на котором количество уловленных в единице объема окислов снижается в два раза ($L_{1/2}$),

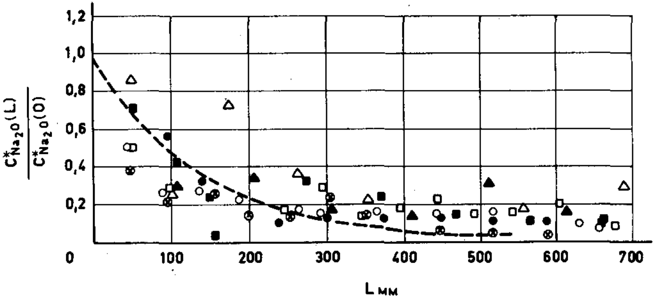

Рис. 3. Распределение окислов в зоне фильтрации при скоростях:

	W мм/сек	γ кг/м³	C* вес %
□	8,2	200	8
■	21	200	45
○	24	120	20
●	9,4	300	36
△	21	300	56
▲	21	100	34
⊗	1,9	100	30

----- $e^{-7,5L\cdot 10^{-3}}$

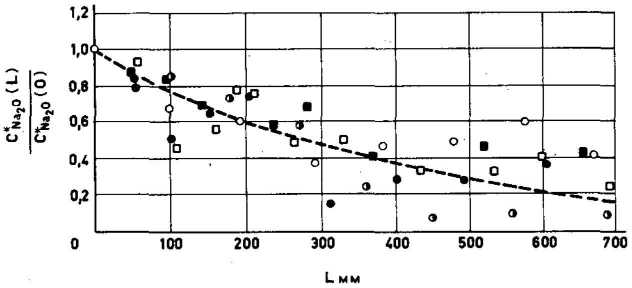

Рис. 4. Распределение окислов в зоне фильтрации при скоростях:

	W мм/сек	γ кг/м³	C* вес %
○	4,6	100	7
●	4,6	200	14,6
◑	4,4	100	9,3
□	5,8	300	22,5
■	10,5	100	14,8

----- $e^{-2,5L\cdot 10^{-3}}$

равно: 50, 300 и 70 мм для скоростей 2; 4,4 – 10,5; 8 – 50 мм/сек соответственно. Это говорит о том, что *при ламинарном режиме обтекания насадки*, $Re = (wd/\nu) \leq 20 \div 50$, с увеличением скорости интенсивность удержания окислов падает, $L_{1/2}$ растет. При появлении турбулентности интенсивность удержания окислов возрастает, $L_{1/2}$ начинает снижаться, достигает некоторого постоянного значения и затем в пределах точности опыта остается постоянным.

Интересно отметить, что в области переходного режима обтекания насадки ($w_{ср}$ ~ 10 мм/сек) при большой плотности набивки (200 ÷ 300 кг/м^3) спад относительной концентрации по длине происходил резче, чем при малой плотности набивки (~ 100 кг/м^3).

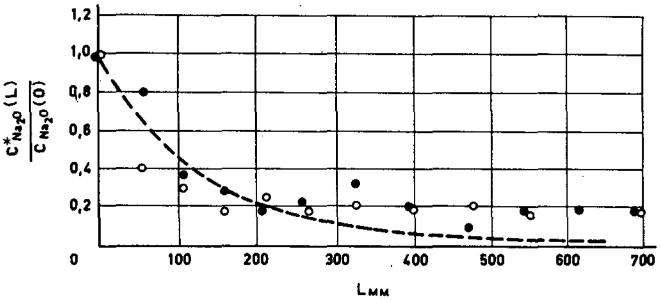

Рис. 5. Распределение окислов в зоне фильтрации при скоростях:

	W мм/сек	γ кг/м^3	C* вес %
○	42	350	26
●	50	350	31

----- $e^{-7,5L\cdot 10^{-3}}$

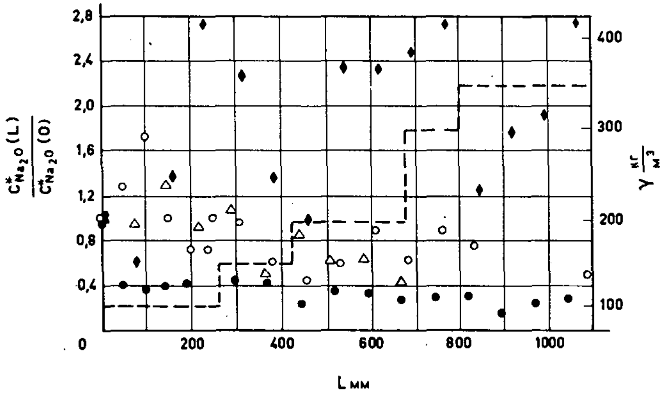

Рис. 6. Распределение окислов в зоне фильтрации при переменной плотности набивки:

	W мм/сек	C* вес %
○	20	9,5
●	21	31,7
△	146	10,6
♦	21	1,6

Из данных, приведенных на рис. 3 – 5, нельзя получить количественной зависимости по влиянию плотности набивки на удержание окислов в зоне фильтрации. Видно лишь, что эта зависимость слабее, чем можно было ожидать на основании соотношений (12) и (20). Расчет относительной доли удержанных в зоне фильтрации окислов при длине ее 1200 – 1300 мм показывает, что с ростом плотности набивки удержание окислов в зоне фильтрации возрастает. Это же видно из опытов, когда плотность набивки была переменной по длине зоны фильтрации (рис. 6); здесь $L_{1/2}$ равно 800 мм.

Особенно наглядно зависимость удержания окислов от плотности набивки видна в опыте с малым накоплением окислов в зоне фильтрации ($C^*_{вх} \sim 1{,}6$ вес%). Здесь при удалении от входа наблюдается не снижение количества окислов, удержанных в единице объема, а возрастание при переходе к зонам с более плотной набивкой. Однако с ростом $C^*_{вх}$ влияние возрастающей по длине плотности набивки уменьшается. Это объясняется изменением геометрии набивки, ее поверхность как бы разветвляется, увеличивается число центров кристаллизации в единице объема, и влияние исходной плотности уже не играет роли.

СРАВНЕНИЕ С РАСЧЕТОМ И ОБСУЖДЕНИЕ РЕЗУЛЬТАТОВ

Согласно соотношениям (16) и (20) для случая, когда $Б = \mathrm{const}$, распределение окислов по длине должно убывать по экспоненте при удалении от входа. Из рис. 3 – 5 видно, что в пределах разброса экспериментальных точек вплоть до расстояний от входа, равных $(3 - 4)L_{1/2}$, это имеет место. При больших расстояниях спад происходит медленнее.

Полученные на основании экспериментальных данных выводы об изменении $L_{1/2}$ с изменением скорости натрия можно понять и объяснить, если учесть, что при ламинарном режиме коэффициент массообмена возрастает пропорционально $\sim w^{1/2}_{ср}$ [1]. Тогда, учитывая соотношение (12), можем сказать, что для ламинарного режима обтекания пластинки $Б \sim w^{-1/2}_{ср}$, т.е. с ростом скорости в ламинарном режиме $L_{1/2}$ должно увеличиваться. Это и наблюдалось в опыте. При появлении турбулентности и дальнейшем ее развитии коэффициент массообмена пропорционален $w^{0,9}$ [1], т.е. $Б \sim w^{0,1}$. Для наших опытов, когда переход к турбулентности наблюдался при скорости $\sim 8 - 10$ мм/сек, а наибольшая скорость в зоне фильтрации при равномерном распределении набивки была равна 56 мм/сек, изменение Б не превышало 20%. Такое изменение из-за разброса экспериментальных данных в наших опытах обнаружить невозможно.

Используя полученные по результатам опытов значения Б, для зоны окончательной фильтрации по формуле (20) рассчитывали количество кислорода, которое должно осесть в пробах. Для расчета было необходимо знать пересыщение на входе в зону фильтрации. Оно определялось расчетом с использованием опытных данных по концентрации кислорода в натрии на входе в рабочий участок при работе его в режиме осаждения окислов и по количеству кислорода, удержанного в предшествующих зонах за время опыта.

Сравнение расчета с экспериментом показало, что количество окислов, найденное в пробах после окончания эксперимента, всегда меньше расчетного. Это обстоятельство, а также тот факт, что спад $C^*_L / C^*_0 = f(L)$ на больших расстояниях от входа происходит медленнее, чем можно было ожидать на основании соотношений (16) и (20), дают основание думать, что сделанное нами предположение об отсутствии (или малой роли $\varphi = 0$) кристаллов окиси в потоке натрия неверно.

Сравнение экспериментальных данных по количеству окислов, уловленных в зоне охлаждения, с расчетом на основании полученных выше соотношений может быть произведено лишь для тех опытов, когда в зоне охлаждения находилась насадка. Для расчета распределения окислов в зоне охлаждения необходимо знать Б. Его значение было определено по экспериментальным данным: максимум уловленного вещества находился на расстоянии ~0,13 м от начала зоны кристаллизации.

В основу расчета было положено значение $Б_0$, полученное из уравнения:

$$\frac{\partial z}{\partial x} Б + \frac{\partial Б}{\partial x} z = 0 \qquad \text{при } x = 0{,}13 \text{ м}$$

Значения dt/dx, $t_{кр}$ и а, необходимые для расчета, были взяты из эксперимента.

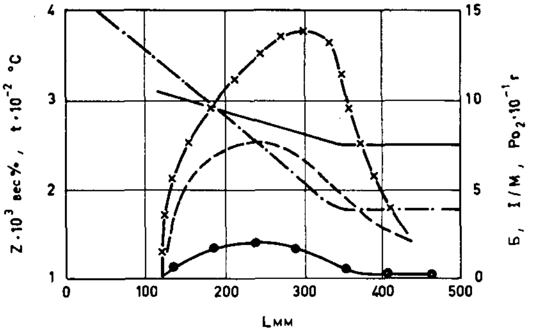

Рис. 7. Сравнение экспериментального и рассчитанного распределения окислов в зоне охлаждения при наличии набивки: —·—·— температура натрия, —●—●— количество кислорода в пробе по данным опыта, – – – – – количество кислорода в пробе по расчету, –x–x–x– пересыщение, ——— коэффициент массообмена.

Результаты расчета представлены на рис. 7. Видно, что количество кислорода, найденного в опыте и полученного расчетом, расходится в несколько раз. Причем расхождение за зоной охлаждения гораздо больше расхождения в зоне охлаждения. Можно указать две причины расхождения результатов эксперимента с расчетом: зависимость Б от x иная, нежели принятая нами в расчете; в потоке натрия имеются кристаллы окиси натрия, на которых идет кристаллизация окислов из пересыщенного раствора.

Первая причина, на наш взгляд, не может привести к столь существенным расхождениям расчета с экспериментом. В пользу этого говорят следующие факторы: при расчетах , не учитывающих зависимость Б от x, расхождение с экспериментом в среднем по зоне охлаждения возрастает незначительно (~15%); в зоне фильтрации, где при кристаллизации из пересыщенного раствора Б постоянно, расчетные количества окислов в пробах также превышают экспериментальные.

Таким образом, мы приходим к выводу, что сделанное предположение об отсутствии кристаллов окиси в потоке натрия неверно, т.е. φ не равно нулю.

Учитывая (13) и делая ряд идеализированных допущений – число кристаллов, приходящихся на единицу длины не изменяется по длине зоны кристаллизации; кристаллы, на которых начинается кристаллизация из пересыщенного раствора, имеют форму шара диаметром $d_к^\circ$; полное снижение пересыщения за счет образования и роста кристаллов составляет $\beta_к z_{max}$, а снижение пересыщения при их образовании $\beta_0 z_{max}$, где $z_{max} = C^{вх} - C^{вых}_{нас}$, – можно показать, что среднее за время роста кристалла значение φ может быть оценено по формуле:

$$\bar{\varphi} = \frac{0{,}29\, D \cdot z_{max}}{Б \cdot Q_{Na}} \left(\frac{d_{уч}}{d_к^\circ}\right)^2 \sqrt[3]{\frac{\beta_0}{\beta_к}} \qquad (22)$$

Значения $\bar{\varphi}$, рассчитанные по уравнению (22) при различных β_0 в зависимости от $d_к^\circ$ в предположении, что $z_{max} = 0{,}009$ вес %; $d_{уч} = 0{,}06$м; $\beta_к = 0{,}4$; $БQ_{Na} = 1$ м^2/час (при наличии насадки в зоне) и $D = 10^{-4}$ м^2/час, приведены на рис. 8. Эти оценки показывают, что φ в уравнении (11) при размерах кристалла ~0,1 мк нельзя пренебречь даже в тех случаях, когда снижение пересыщения при образовании кристаллов, на которых в дальнейшем идет кристаллизация, составляет ~0,02% от полного пересыщения. При увеличении $d_к^\circ$ до 1 мк для сохранения прежнего соотношения потоков на поверхность кристаллов и на неподвижные поверхности снижение пересыщения при образовании кристаллов, на которых в дальнейшем идет кристаллизация, должно возрасти в 25 раз, т.е. составит ~0,5% от полного пересыщения. Для условий наших опытов такое количество кристаллов окиси будет поступать в поток натрия в том случае, когда ~10% окиси натрия, высевшей на стенку, будет сноситься с нее потоком.

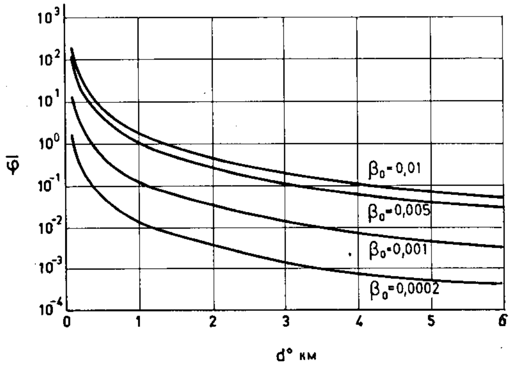

Рис. 8. Соотношение потоков окиси на кристаллы, движущиеся с натрием, и на неподвижные поверхности массообмена.

Можно указать, по крайней мере, на два процесса, за счет которых кристаллы Na_2O могут появляться в потоке: спонтанное зарождение кристаллов из пересыщенного раствора и снос потоком кристаллов окиси натрия, уже образовавшихся на неподвижных поверхностях массообмена.

Распределение окислов в отстойнике можно объяснить на основе опытов по изучению гидродинамики холодных ловушек, проведенных нами. Наибольшая турбулизация потока в отстойнике имела место при повороте струи. В условиях наших опытов поворот струи происходил у дна отстойника. В восходящем потоке по мере удаления от дна турбулентные возмущения затухают. Аналогичным образом должна изменяться интенсивность массообмена по высоте отстойника. Следовательно, количество окислов, осевших в отстойнике, должно быть максимальным у дна и убывать при удалении от него. После скопления на дне отстойника такого количества окислов, через которое не может проходить поток натрия, "дно" отстойника как бы поднимается вверх.

Значения коэффициентов массообмена, полученные на основании опытов по изучению высаждения окислов в зоне охлаждения при отсутствии насадки, позволяют произвести оценку коэффициента диффузии кислорода в натрии. Для этого необходимо знать Nu_D для условий наших опытов. Мы в своих оценках коэффициента диффузии считали $Nu_D \sim 20$. Тогда значения коэффициента диффузии, рассчитанные по минимальному и среднему значениям коэффициента массообмена, равны $8 \cdot 10^{-5}$ и $3{,}2 \cdot 10^{-3}$ см^2/сек.

ЗАКЛЮЧЕНИЕ

Полученные результаты показали, что осаждение окислов из потока натрия является сложным физико-химическим процессом, зависящим от температурных и гидродинамических условий, от распределения поверхностей массообмена и от количества окислов, уже осевших на поверхность массообмена.

В зоне охлаждения при постоянном температурном градиенте и равномерном распределении поверхностей массообмена осаждение окислов происходит неравномерно по длине. Наблюдается локальное скопление окислов, приводящее к закупорке проходного сечения. Для холодных ловушек это означает неравномерное использование их объема, а следовательно, снижение емкости по окислам.

Концентрация окиси в смеси окись натрия-натрий, образующейся в ловушке (участке), зависит от условий ее образования. Температурные градиенты и гидродинамические силы в сочетании с фактором времени способствуют повышению концентрации окиси. Эти факторы показывают трудности конструирования зоны охлаждения холодной ловушки. Из результатов опыта следует, что за счет изотермического отстойника нельзя значительно повысить емкость ловушки по окислам в целом, поскольку его емкость в среднем не превышала 29 вес %.

Зону фильтрации нецелесообразно делать протяженной, т.к. при большинстве режимов основная доля окислов удерживается в ее начале. Увеличение плотности набивки по длине следует считать целесообразным.

Обозначения

Символы

M – молекулярный (атомный) вес
γ – удельный вес (кг/м^3)
C_p – теплоемкость (ккал/кг °С)
λ – коэффициент теплопроводности (ккал/м час °С)
D – коэффициент диффузии (м^2/час)
d – диаметр (м)
P – вес (кг)
δ_D – толщина диффузионного пограничного слоя (м)
S – поверхность массообмена (м)
$C_{нас}$ – растворимость кислорода в натрии (вес %)
$Z = C - C_{нас}$ – пересыщение (вес %)
$C^*_{Na_2O} = \dfrac{P_{Na_2O}}{V_{np} \cdot \gamma_{Na}}$ – емкость по окислам (вес %)
τ_p – время опыта (час)
w – скорость потока натрия (м/час)

G_{Na} – весовой расход натрия (кг/час)
j – поток вещества на единицу поверхности в единицу времени ($\text{кг/м}^2\text{час}$)
$t_{кр}$ – температура начала кристаллизации (°C)
α_D – коэффициент массообмена (м/час)

Индексы

' – относится к неподвижным поверхностям массообмена
" – относится к поверхностям массообмена, движущимся с потоком натрия.

ЛИТЕРАТУРА

[1] ЛЕВИЧ В.Г. Физико-химическая гидродинамика, Москва, 1959.
[2] ТОДЕС О.М. Кинетика процессов кристаллизации и конденсации. Проблемы кинетики и катализа, т.7, Статистические явления в гетерогенных системах, М.-Л., (1949).
[3] СУББОТИН В.И., КОЗЛОВ Ф.А., ИВАНОВСКИЙ Н.Н. "Теплофизика высоких температур", 1, 3 (1963) 409 – 15.
[4] КОЗЛОВ Ф.А., АНТОНОВ И.Н., "Атомная энергия", 19, 4 (1965) 391 – 2.
[5] ТОДЕС О.М., Кинетика процессов коагуляции и укрупнения частиц в золях. Проблемы кинетики и катализа, т.7, Статистические явления в гетерогенных системах, М.-Л. (1949).

DISCUSSION

K. T. CLAXTON: I understood you to say that the average oxide hold-up in the cooling region of the cold trap amounted to 24% and the hold-up in the dump tank averaged 29%. Does this mean that you have an over-all efficiency of over 50% for the whole of the cold-trap region?

B. V. KULPIN: No. These figures relate only to part of the region containing impurities.

K. T. CLAXTON: What was the residence time of the sodium in the cold trap?

B. V. KULPIN: At least 18 min.

K. T. CLAXTON: This seems to be at variance with Bruggeman's data. In investigations carried out by Bruggeman in 1956, a marked increase was observed in cold-trap efficiency when the residence time was raised from $2\frac{1}{2}$ to 5 min but only a slight improvement was found when the time was further increased to 10 min.

B. V. KULPIN: Yes, but in our case an experimental section was involved and not the actual trap. The times are therefore slightly different.

J. P. LAGOWSKI: Can you tell me whether analyses for impurities other than sodium oxide were carried out in these investigations?

B. V. KULPIN: Perhaps Professor Ivanovsky, who works at the institute where this work was done, can tell you.

M. N. IVANOVSKY: As far as I know, other impurities were in fact analysed. The cold trap captures both corrosion and erosion products of the structural materials of the circuit.

J. P. LAGOWSKI: Do you have any quantitative information on, for example, metallic impurities?

M. N. IVANOVSKY: I do not remember the exact figure but it was less than 1%. It was perhaps one tenth or one hundredth of a percent.

ИССЛЕДОВАНИЕ ПРОЦЕССА ОЧИСТКИ НАТРИЯ С ПОМОЩЬЮ ВЫСОКОЭФФЕКТИВНЫХ ХОЛОДНЫХ ЛОВУШЕК ДИФФУЗИОННОГО ТИПА

М.Н.АРНОЛЬДОВ, М.Н.ИВАНОВСКИЙ,
В.И.СУББОТИН, Б.А.ШМАТКО
ФИЗИКО-ЭНЕРГЕТИЧЕСКИЙ ИНСТИТУТ, ОБНИНСК
СССР

Abstract — Аннотация

STUDY OF SODIUM PURIFICATION CARRIED OUT BY MEANS OF HIGH-EFFICIENCY DIFFUSION-TYPE COLD TRAPS. The principles involved in the operation of cold diffusion-type traps used for the purification of liquid-metal coolants are discussed. The results of hydrodynamic studies on diffusion-type traps are given.

Data are also given on investigations on the removal of hydrogen and oxygen from molten sodium, by means of cold diffusion-type traps. It is shown that cold diffusion-type traps offer an effective method of purification under certain conditions. These traps are notable for their ability to trap large quantities of impurities, adequate speed of operation and the thorough purification achieved. In addition, they possess constructional advantages over circulating cold traps, such as simplicity of design and smaller size and weight, and they are also less sensitive to fluctuations in flow rate and the concentration of impurities in the coolant.

ИССЛЕДОВАНИЕ ПРОЦЕССА ОЧИСТКИ НАТРИЯ С ПОМОЩЬЮ ВЫСОКОЭФФЕКТИВНЫХ ХОЛОДНЫХ ЛОВУШЕК ДИФФУЗИОННОГО ТИПА. Излагаются теоретические основы работы холодных диффузионных ловушек, предназначенных для очистки жидкометаллических теплоносителей. Приводятся результаты гидродинамического исследования ловушек диффузионного типа. Приводятся результаты исследования очистки расплавленного натрия от примесей водорода и кислорода с помощью холодных диффузионных ловушек. Показывается, что диффузионные холодные ловушки являются эффективными средствами очистки при соблюдении некоторых условий. Диффузионные ловушки отличаются высокой емкостью по отношению к накапливаемым примесям, достаточной скоростью и глубиной очистки. Вместе с тем они обладают конструктивными преимуществами по сравнению и проточными холодными ловушками – простота конструкции, меньшие размеры и вес, меньшая чувствительность к колебаниям расхода и концентрации примеси в теплоносителе.

Одним из основных средств очистки жидкометаллических теплоносителей от примесей являются холодные ловушки проточного типа. Ловушки этого типа широко применяются на действующих ядерных энергетических реакторах, охлаждаемых расплавленным натрием.

Кроме холодных ловушек проточного типа, известен и другой тип холодных ловушек – диффузионные ловушки.

По сравнению с проточными диффузионные ловушки отличаются простотой конструкции, меньшими размерами и весом, отсутствием необходимости в специальном ответвлении от циркуляционного контура, меньшей чувствительностью к колебаниям расхода и концентрации теплоносителя.

Однако имеется мнение, изложенное в работе [1], согласно которому холодные диффузионные ловушки имеют малую емкость по отношению к примесям и могут использоваться там, где их емкость не имеет большого значения.

По-видимому, в связи с этим холодные диффузионные ловушки не получили распространения в экспериментальных промышленных установках.

Авторами данного доклада были исследованы условия, при которых диффузионные ловушки имеют эффективность, во всяком случае не меньшую, чем проточные ловушки. К параметрам, определяющим эффективность работы ловушки, относятся емкость ловушки по накопляемым примесям, скорость очистки и минимально достижимая концентрация примеси в контуре.

В работе показано, что диффузионные холодные ловушки позволяют организовать процесс очистки таким образом, что достигается практически полное заполнение холодной ловушки примесями. При этом ловушки мало чувствительны к изменениям расхода металла в линиях, на которых они установлены, и не забиваются примесями при любых практически существующих концентрациях примеси на входе в ловушку и при резком изменении концентрации.

1. ТЕОРЕТИЧЕСКИЕ ОСНОВЫ РАБОТЫ ХОЛОДНЫХ ДИФФУЗИОННЫХ ЛОВУШЕК

Холодная диффузионная ловушка представляет собой тупиковую трубку, приваренную к трубопроводу, в котором циркулирует теплоноситель. У открытого в трубопровод конца ловушки устанавливается температура, близкая к температуре циркулирующего металла. Вследствие охлаждения вдоль ловушки устанавливается определенное температурное поле. Температура у холодного конца должна быть близка к температуре плавления теплоносителя. Примеси, растворенные при высокой температуре, поступают вместе с теплоносителем в охлаждаемую часть ловушки и выкристаллизовываются из раствора в количестве, пропорциональном $C_T - C_s$.

Дифференциальное уравнение, описывающее во времени изменение концентрации примеси в теплоносителе, очищаемом ловушкой, есть

$$dC_T = K\cdot(C_T - C_s)\cdot d\tau \qquad (1)$$

Значение коэффициента скорости очистки К в общем случае определяется механизмом переноса примесей в ловушку, кинетикой выкристаллизации примеси из раствора и величиной уноса выкристаллизовавшейся примеси потоком металла. Если выкристаллизация примесей из раствора происходит в одном и том же сечении ловушки (на дне ловушки), и температурное поле ловушки неизменно во времени, решение уравнения (1) получается в виде:

$$\frac{C_T - C_s}{C_T^0 - C_s} = \exp(-K\cdot\tau) \qquad (2)$$

и скорость очистки теплоносителя

$$\frac{dC_T}{d\tau} = -(C_T^0 - C_s)\cdot K\cdot\exp(-K\tau) \qquad (3)$$

Однако концентрирование примесей в одном месте на дне ловушки приводит к тому, что сечение выкристаллизации примесей из раствора перемещается по длине ловушки вместе с перемещением фронта осадка. Величина C_s в соотношении (1) становится переменной величиной, зависящей от температуры в области фронта осадка примеси. Покажем, что в этом случае скорость очистки зависит от характера температурного поля ловушки.

Скорость поступления примесей в ловушку равна $V_\text{т} \cdot \gamma_\text{т} \frac{dC_\text{т}}{d\tau}$,

откуда скорость нарастания объема осадка $\frac{V_\text{т}\,\gamma_\text{т}}{\gamma_\text{п}} \cdot \frac{dC_\text{т}}{d\tau}$ и скорость продвижения фронта осадка от дна ловушки

$$\frac{dx}{d\tau} = -\frac{V_\text{т}\,\gamma_\text{т}}{\gamma_\text{пр}} \cdot \frac{dC_\text{т}}{d\tau} \cdot \frac{1}{F} \tag{4}$$

Величину $\frac{dC_s}{d\tau}$ представим в виде

$$\frac{dC_s}{d\tau} = \frac{dx}{d\tau} \cdot \frac{dC_s}{dx}$$

Сомножитель $\frac{dC_s}{dx}$ определяется формой температурного поля вдоль ловушки. Здесь для упрощения выкладок будем рассматривать такие участки ловушки, где $\frac{dC_s}{dx} = \text{const}$.

Тогда

$$\frac{dC_s}{d\tau} = -\frac{dC_s}{dx} \cdot \frac{V_\text{т}\,\gamma_\text{т}}{\gamma_\text{п} \cdot F} \cdot \frac{dC_\text{т}}{d\tau}$$

и

$$C_s(\tau) = C_s^0 + \int\limits_0^\tau -\frac{dC_s}{dx} \cdot \frac{V_\text{т}\,\gamma_\text{т}}{\gamma_\text{п} F} \cdot \frac{dC_\text{т}}{d\tau} \cdot d\tau$$

Отсюда

$$C_s = C_s^0 + \frac{dC_s}{dx} \cdot \frac{V_\text{т}\,\gamma_\text{т}}{\gamma_\text{п} F} \, (C_\text{т}^0 - C_\text{т}) \tag{5}$$

Подставляя (5) в уравнение (1) и интегрируя, получим:

$$C_\text{т} = \frac{C_s^0 + bC_\text{т}^0}{1+b} + \frac{C_\text{т}^0 - C_s^0}{1+b} \exp\left(-(1+b)\,K\tau\right), \tag{6}$$

где $b = \frac{dC_s}{dx} \cdot \frac{V_\text{т}\,\gamma_\text{т}}{\gamma_\text{п} F}$

Тогда скорость очистки

$$\frac{dC_\text{т}}{d\tau} = -K\,(C_\text{т}^0 - C_s^0) \exp\left(-(1+b)\,K\tau\right) \tag{7}$$

Учет перемещения фронта плотного осадка нерастворенной примеси приводит к уменьшению скорости очистки, что видно из сравнения формул (3) и (7).

Наличие нарастающего осадка выкристаллизовывавшейся примеси приводит к увеличению конечной концентрации примесей в теплоносителе, что следует из (5)

$$\lim_{\tau\to\infty} C_T = C_s^0 + \frac{b\,(C_T^0 - C_s^0)}{1+b} \tag{8}$$

Рассмотрим предельный вид зависимостей (7), (6) и (8). Когда параметр "b" стремится к нулю, формулы (6) и (7) преобразуются к виду (2) и (3). При больших значениях $\frac{dC_s}{dx}$ $(b\to\infty)$, $\frac{dC_T}{d\tau}\to 0$, т.е. очистки практически не происходит. Ловушка с очень большим градиентом температур в зоне выкристаллизации примесей будет быстро терять свою эффективность по мере нарастания слоя осадка в зоне охлаждения.

При выводе предыдущих формул предполагалось, что выпадающая примесь образует плотный осадок, не содержащий избыточного количества металла. Так как практически осадок имеет бóльший объем, эффективность ловушки будет падать с несколько бóльшей скоростью, чем это предсказывали формулы (6) и (7).

Рассмотрим характерные зависимости распределения концентрации насыщения по длине ловушки $C_s = f(x)$, которые имеют место при соответствующих температурных полях.

Выпадающие в ловушке примеси оседают в основном на стенках ловушки, т.к. выкристаллизация примесей происходит преимущественно на охлаждаемых поверхностях. Перемещение осадка, выпавшего на стенках, вглубь ловушки может происходить в основном только путем молекулярной диффузии за счет градиента концентрации насыщения.

Поток примеси в сечении x равен

$$m_x = -\left(D\cdot\frac{dC_s}{dx}\right)_x$$

Воспользовавшись разложением этого соотношения в ряд Тейлора и положив для простоты, что коэффициент диффузии D неизменен по длине ловушки, можно получить

$$\frac{dm}{dx} = -D\cdot\frac{d^2C_s}{dx^2} \tag{9}$$

Из соотношения (9) видно, что скопление примесей на дне ловушки ($(dm/dx) > 0$) будет иметь место тогда, когда $(d^2C_s/dx^2) < 0$. Этому условию соответствует требование $(d^2t/dx^2) < 0$. Если это условие не соблюдается, примеси выкристаллизовываются во входном сечении ловушки, закупоривают вход в ловушку и таким образом существенно уменьшают полезную емкость ловушки.

Однако условию $(d^2t/dx^2) < 0$ соответствует большое значение параметра "b" у дна ловушки. В ловушке с таким температурным полем не будут забиваться входные участки, но она быстрее потеряет свою эффективность по мере накопления примесей в зоне охлаждения у дна ловушки. Для поддержания эффективности работы ловушки на максимальном уровне необходимо поддерживать минимальное значение концентрации насыщения C_s^0, при которой примеси выпадают в осадок, т.е. минимальную температуру в зоне выкристаллизации. Для этого необходимо перемещать сечение с минимальной температурой жидкого состояния теплоносителя вместе с фронтом осадка, растущего от дна ловушки. Скорость перемещения этого сечения должна соответствовать скорости роста осадка в ловушке, выражаемой соотношением (4), или осуществляться периодически по мере ухудшения эффективности работы ловушки.

2. ГИДРОДИНАМИКА ХОЛОДНЫХ ДИФФУЗИОННЫХ ЛОВУШЕК

Гидродинамика теплоносителя в холодных диффузионных ловушках является одним из основных факторов, определяющих скорость очистки теплоносителя.

Процессы переноса жидкости из трубопровода в ловушку примесей, представляющую собой тупиковый отросток, экспериментально и теоретически не изучены. Поэтому нами были проведены эксперименты, позволившие сделать первичные выводы о характере процесса обмена жидкостью между ловушкой и потоком в основном трубопроводе. Эксперименты проводились на подкрашенной воде, циркулировавшей в стеклянной модели участка трубопровода и холодной ловушки в изотермических условиях.

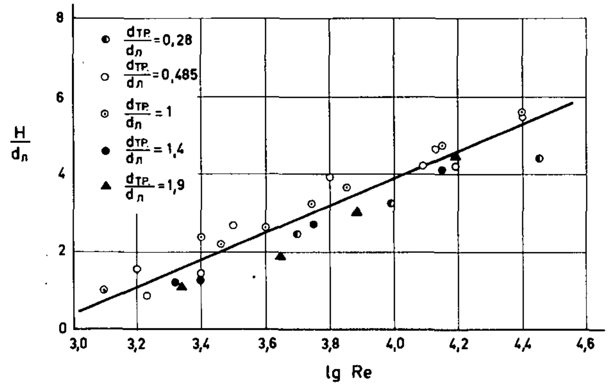

Рис. 1. Зависимость относительной величины зоны перемешивания от числа Рейнольдса.

Как показали эксперименты, между ловушкой и потоком жидкости в трубопроводе осуществляется интенсивный обмен вследствие перемешивания в трубопроводе. Глубина зоны перемешивания зависит от скорости течения жидкости в трубопроводе. Отношение глубины зоны перемешивания к диаметру ловушки пропорционально логарифму числа Рейнольдса потока жидкости в трубопроводе (рис.1).

Как видно из графика на рис.1, относительная глубина перемешивания слабо зависит от соотношения между диаметрами трубопровода и ловушки. Наблюдаемое небольшое расслоение опытных данных для различных значений $d_{тр}/d_л$ возможно зависит от недостаточно точной установки ловушки по отношению к трубопроводу.

При ламинарном режиме течения жидкости в трубопроводе перемешивание жидкости в изотермической ловушке отсутствует. Соответствующая наибольшей практически имеющей место скорости потока в трубопроводе ($Re \simeq 10^5$) глубина перемешивания составляет около 7 диаметров ловушки.

В участке ловушки, расположенном ниже зоны перемешивания, существует застойная зона жидкости. Размеры зоны перемешивания могут быть увеличены путем дополнительной турбулизации потока жидкости в трубопроводе перед ловушкой. Так, установка перед ловушкой шайбы с отверстием, равным 0,6 $d_{тр}$, увеличивает относительную глубину зоны перемешивания при числе $Re \geq 2 \cdot 10^4$ в $2 \div 2{,}5$ раза. Турбулизирующая шайба имеет большее влияние для ловушек с $(d_{тр}/d_л) \geq 1$.

Таким образом, эффективный поднос примесей вместе с потоком жидкости к месту выкристаллизации имеет место лишь при определенных размерах ловушки, зависящих от скорости течения жидкости в трубопроводе. Застойная зона является малоэффективной частью ловушки.

Как уже указано выше, приведенные данные относятся к изотермическому потоку жидкости. В действительности ловушка примесей существенно неизотермична. Поэтому движение жидкости в ловушке является результатом наложения вынужденной конвекции, возникающей в результате турбулентного перемешивания, и естественной конвекции, возникающей вследствие неизотермичности жидкости в ловушке. Однако роль естественной конвекции в движении жидкости в ловушке может оказаться ограниченной, т.к. в ловушках, обычно расположенных вертикально вниз, холодные слои жидкости располагаются под нагретыми.

Эксперименты на стеклянных моделях показывают, что скорость обмена между слоями жидкости в ловушке падает по мере удаления от трубопровода.

Таким образом, проведенные исследования указывают на то, что в диффузионных ловушках может быть осуществлен достаточно интенсивный подвод примесей с конвективным потоком жидкости к зоне выкристаллизации. Основным механизмом подвода примесей к зоне выкристаллизации является турбулентная диффузия, обусловленная перемешиванием жидкости в ловушке вследствие турбулентности потока в трубопроводе. Такие процессы, как молекулярная диффузия примесей в жидкости, термодиффузия и т.п., не имеют значения вследствие весьма малых значений их коэффициентов переноса.

3. ЭКСПЕРИМЕНТАЛЬНОЕ ИССЛЕДОВАНИЕ ПРОЦЕССА ОЧИСТКИ ЖИДКОМЕТАЛЛИЧЕСКИХ ТЕПЛОНОСИТЕЛЕЙ ХОЛОДНЫМИ ДИФФУЗИОННЫМИ ЛОВУШКАМИ

Очистка теплоносителей в холодных ловушках осуществляется в результате последовательного выполнения процесса подвода примеси к зоне выкристаллизации и процесса выкристаллизации.

Выкристаллизовывавшиеся примеси частично удерживаются в зоне выкристаллизации, частично уносятся с потоком жидкости. Значение каждого из процессов в объединенном процессе-очистке зависит от свойств примеси и теплоносителя.

Если наиболее медленным процессом является выкристаллизация примеси, скорость очистки определяется скоростью образования осадка примеси.

Выкристаллизация примесей из металла в процессе охлаждения есть следствие процессов образования зародышей твердой фазы и последующего их роста.

Необходимым условием образования зародышей и их роста является наличие пересыщения. Количественно пересыщение выражается величиной переохлаждения жидкого металла относительно температуры, соответствующей равновесной концентрации насыщения.

Для некоторых систем, например для примеси азота в литии [2], были получены довольно значительные переохлаждения, достигающие 30°С. В подобных случаях выкристаллизация растворенной примеси не следует равновесной кривой растворимости. Концентрация примеси в металле, покидающем ловушку, должна превышать равновесную на величину, соответствующую степени пересыщения.

Однако в диффузионной холодной ловушке имеются более благоприятные по сравнению с проточной ловушкой условия для выкристаллизации примесей ввиду совмещения зон охлаждения и выкристаллизации.

Если выкристаллизация примесей протекает достаточно быстро, скорость очистки определяется результативной скоростью подноса примеси, растворенной в потоке жидкости, и уноса примеси, выпавшей в осадок.

Холодные диффузионные ловушки изучались нами на расплавленном натрии, очищенном от примесей водорода и кислорода.

Контроль концентрации водорода в натрии осуществлялся методом электросопротивления с чувствительностью $3 \cdot 10^{-5}$ вес % H_2. Исследования проводились при температуре натрия в контуре 350°С. Циркуляционный контур из стали 1Х18Н9Т был оборудован двумя диффузионными ловушками, установленными параллельно, системой ввода газообразного водорода в расплавленный натрий и пробоотборником для анализов натрия на водород, кислород и др. примеси. Температура по высоте ловушки измерялась с помощью передвижной термопары, помещенной в чехол.

Эксперименты показали, что при одинаково интенсивном охлаждении всего корпуса ловушки по высоте, т.е. при несоблюдении условия $\partial^2 t/\partial x^2 < 0$. основное количество примеси высаживается во входных участках ловушки. Остальная часть ловушки не использовалась.

В дальнейшем во всех экспериментах поддерживалось распределение температур ловушки в соответствии с условием $\partial^2 t/\partial x^2 < 0$. При этом даже при значительных концентрациях примесей в теплоносителе, превышающих концентрацию насыщения, не наблюдалось закупоривания входных участков ловушки и преждевременного выхода ловушки из строя.

Измерения температурного поля вдоль ловушки, произведенные с помощью передвижной термопары, показали зависимость его формы от числа Рейнольдса расплавленного натрия, протекающего в трубопроводе (см. рис.2). Во время измерений температурного поля тепло снималось с помощью водяной рубашки, расположенной на расстоянии 6 $d_л$ от входа в ловушку. Боковая поверхность ловушки была теплоизолирована.

Температурное поле ловушки отражает изменение эффективного коэффициента теплопроводности натрия вдоль ловушки. Величину эффективного коэффициента теплопроводности жидкого металла в ловушке можно представить следующим образом:

$$\lambda_{\text{эфф}} = \lambda_{\text{турб}} + \lambda_{\text{мол}} = \frac{q}{\operatorname{grad} t} \tag{10}$$

Из рис.2 видно, что температурное поле ловушки распадается на две характерные области. В первой области преобладает турбулентный перенос тепла. В ней $\lambda_{\text{мол}} \ll \lambda_{\text{турб}}$, $\operatorname{grad} t \to 0$. Во второй области перенос тепла осуществляется путем молекулярной теплопроводности. Здесь $\lambda_{\text{турб}} \to 0$.

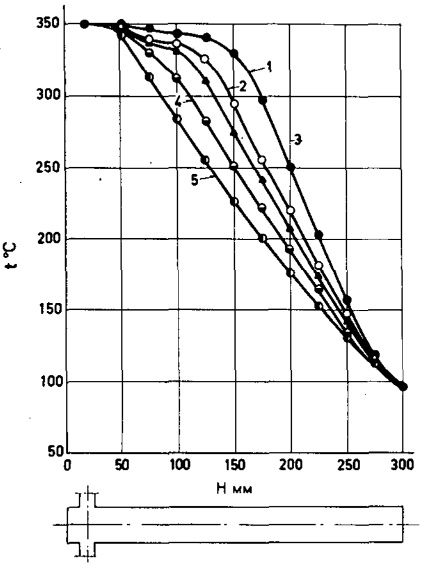

Рис. 2. Температурные поля ловушки при различных числах Рейнольдса потока жидкости: 1 – $\mathrm{Re} = 30\,000$; 2 – $\mathrm{Re} = 22\,000$; 3 – $\mathrm{Re} \doteq 14\,000$; 4 – $\mathrm{Re} = 8000$; 5 – $\mathrm{Re} = 4000$.

Вторая область есть застойная зона, в которой интенсивность движения мала. Очевидно, есть аналогия между переносом тепла в турбулентном потоке жидкости, текущей в трубе, и переносом тепла в холодной диффузионной ловушке. На основании этой аналогии можно предположить, что для ловушек подобного типа

$$\lambda_{\text{турб}} = -C p \gamma_{\text{т}} \overline{V \theta}$$

Отсюда следует, что первая турбулентная область температурного поля должна иметь бóльшую протяженность для жидких металлов, имеющих бóльшую теплоемкость.

Обращает на себя внимание, что при отводе тепла со дна ловушки упомянутое выше требование $\partial^2 t / \partial x^2 < 0$ удовлетворяется автоматически, если зона турбулентного перемешивания занимает достаточную часть ловушки.

На турбулентный характер перемешивания жидкости в ловушке указывают пульсации температуры, обнаруженные при измерениях температурного поля. Зона максимальных амплитуд пульсаций находится в

ТАБЛИЦА. СОСТАВ ПРИМЕСЕЙ В НАТРИИ, ОЧИЩЕННОМ ХОЛОДНОЙ ДИФФУЗИОННОЙ ЛОВУШКОЙ

Элемент	O	H	Ti	K	Fe, Mg, Si, Ca, Al, Ag, Cu, B, Li
Содержание, вес %	$5 \cdot 10^{-4}$	$<10^{-4}$	$1{,}5 \cdot 10^{-3}$	$3{,}7 \cdot 10^{-3}$	$<1 \cdot 10^{-3}$

месте перехода первой области температурного поля ловушки во вторую. Амплитуды пульсаций температуры в остальных частях ловушки существенно меньше.

Исследование режимов очистки при непрерывном контроле концентрации водорода проводились по следующей методике. Натрий предварительно очищался одной из ловушек. При этом другая ловушка была разогрета до температуры 400÷500°С.

Очищенный металл имел содержание примесей, указанное в таблице. Затем работавшая в режиме очистки ловушка отсекалась от системы.

В изотермических условиях при 350°С в натрий вводилось строго дозированное количество водорода. После установления равновесной концентрации водорода в металле на разогретую ловушку подавалось охлаждение. Стационарный температурный режим ловушки устанавливался за 1 – 3 мин.

После проведения опыта ловушка разогревалась до температуры 400÷500°С, и накопленная примесь возвращалась в контур. Устанавливалось новое значение числа Re, или дополнительно передвигался по высоте ловушки водяной холодильник, и опыт повторялся.

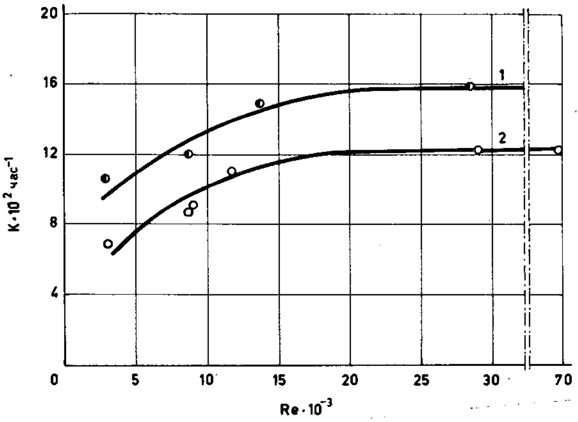

Рис. 3. Зависимость коэффициента скорости очистки K от числа Рейнольдса: $1 - \frac{H}{d_л} = 4{,}3$; $2 - \frac{H}{d_л} = 6$.

На рис.3 приведена зависимость коэффициента скорости очистки K от числа Рейнольдса потока натрия в трубопроводе. Эти данные относятся к ловушке, объем которой составляет 10% от объема всего натрия, циркулирующего в контуре. Видно, что десятикратное уменьшение концентрации водорода в натрии в этих условиях достигается за 15 – 20 часов, т.е. происходит достаточно быстро.

В соответствии с гидродинамическими данными, описанными ранее, при уменьшении числа Рейнольдса наблюдается спад скорости очистки вследствие уменьшения интенсивности переноса примесей к зоне выкристаллизации. При росте числа Re сверх $20 \cdot 10^3$ вплоть до $70 \cdot 10^3$ коэффициент скорости очистки практически не изменяется.

Перемещение холодной зоны в сечение $H/d_л = 4{,}3$ привело к возрастанию коэффициента скорости очистки K в результате увеличения интенсивности перемешивания жидкости в зоне выкристаллизации.

Отметим, что очистка натрия от примеси начинается сразу после установления стационарного температурного режима ловушки. Это свидетельствует об отсутствии заметного влияния процессов выкристаллизации примесей на скорость очистки. На это также указывает зависимость скорости очистки от интенсивности перемешивания жидкости в ловушке.

Химический анализ очищенного с помощью холодной диффузионной ловушки натрия показывает, что в нем содержится водорода не более 10^{-4} вес%.

Отклонения скорости теплоносителя в трубопроводе от номинального значения приводили к несущественным отклонениям концентрации примеси в теплоносителе вследствие незначительных изменений температурного режима ловушки. При этом увеличение или уменьшение скорости теплоносителя в два раза и более не нарушало работоспособности ловушки и не приводило к выбросу осадка из ловушки в контур. Компенсирование изменения температурного режима ловушки, последовавшего за отклонением скорости теплоносителя в трубопроводе, путем изменения интенсивности охлаждения приводило к полному восстановлению первоначальной концентрации примесей в теплоносителе. Поэтому холодные диффузионные ловушки отличаются значительно меньшей чувствительностью к нарушениям режима течения теплоносителя, чем холодные проточные ловушки.

Описанные выше опыты проводились при накоплении малых количеств примесей, практически не изменяющих свойств ловушки. Исследование процесса работы ловушки в режиме накопления значительных количеств примеси водорода производилось при последовательных вводах газообразного водорода в натрий.

В полном соответствии с результатами теоретического анализа работы ловушки наблюдалось изменение свойств ловушки по мере накопления примесей. На рис.4 приведена запись изменения содержания водорода в натрии, очищаемом ловушкой, набравшей значительное количество примеси водорода и потерявшей способность к очистке. Перемещение холодной зоны ловушки из сечений $H/d_л = 6$ в сечение $H/d_л = 4{,}3$ привело, как видно из рис.4, к восстановлению работоспособности ловушки и к дальнейшему снижению концентрации водорода в натрии.

В результате очистки в рабочей зоне холодной ловушки находилось более 30% гидрида натрия. При этом не было препятствий в дальнейшем концентрировании кристаллического гидрида натрия в зоне накопления.

Послойный анализ содержимого ловушек показал, что примеси концентрируются в охлаждаемой зоне в плотный кристаллический осадок Концентрация примеси в осадке превышает 90 вес %.

Холодные диффузионные ловушки способны очищать натрий от примеси кислорода. Анализ натрия, произведенный с помощью дистилляционного метода, указывает на изменение содержания кислорода в натрии в процессе очистки с $1{,}6\cdot10^{-2}$ вес % кислорода до $5\cdot10^{-4}$ вес %. Для очистки натрия от кислорода использовалась та же ловушка, что и для очистки от водорода. Анализ работы ловушки показал, что рабочая зона содержит более 60% окиси натрия. С помощью холодной ловушки осуществляется также и одновременная очистка натрия от водорода и кислорода.

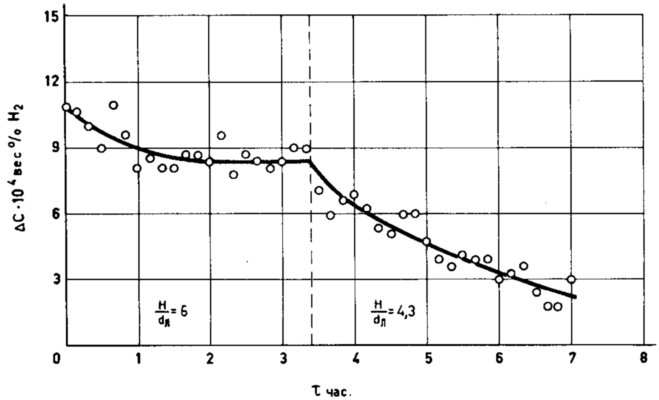

Рис. 4. Изменение содержания водорода в натрии, очищаемом холодной диффузионной ловушкой.

Холодная диффузионная ловушка, установленная на циркуляционных натриевых системах, является местом стока металлических примесей, растворенных в жидком натрии. Химический анализ содержимого ловушки показал присутствие в ней продуктов массопереноса элементов конструкционного материала – железа, никеля, хрома и т.д. Их количество определяется условиями работы жидкометаллического контура – температурой и содержанием примесей.

В одном из экспериментов по очистке намеренно сильно загрязненного неметаллическими примесями жидкого металла было обнаружено, что на дне ловушки концентрация осажденного железа превышает 10 вес %. Очевидно, что холодные диффузионные ловушки в подобных случаях играют положительную роль, заключающуюся в предотвращении закупорки трубопроводов продуктами массопереноса металлических элементов.

ЗАКЛЮЧЕНИЕ

Как следует из приведенных выше материалов, холодные диффузионные ловушки являются эффективным средством очистки жидкометаллических теплоносителей при соблюдении следующих условий:

1. Поле температуры по длине ловушки должно удовлетворять требованию $(\partial^2 t/\partial x^2) < 0$

2. В трубопроводе, к которому подключена ловушка, должен быть турбулентный режим течения.

3. По мере накопления примесей в ловушке должна перемещаться зона охлаждения.

Диффузионные ловушки просты по конструкции и удобны в эксплуатации. Они мало чувствительны к колебаниям расхода и концентрации примеси в очищаемом теплоносителе.

Список обозначений

Символы

C – весовая концентрация примесей
C_p – теплоемкость
K – коэффициент скорости очистки
V – объем
F – сечение
d – диаметр
H – глубина турбулентного перемешивания
x – расстояние вдоль ловушки, отсчитываемое от входа
D – коэффициент диффузии
m – поток примеси (массовый)
Re – число Рейнольдса
τ – время
γ – удельный вес
λ – коэффициент теплопроводности
$\overline{V\theta}$ – пульсационный член

Индексы

0 – начальный момент времени
т – теплоноситель
п – примесь
s – состояние насыщения
x – в сечении
эфф – эффективный
турб – турбулентный
мол – молекулярный
л – ловушка
тр – трубопровод

ЛИТЕРАТУРА

[1] ПАРКИНС В., Экспериментальный натриевый реактор. Доклад № 499 (США) на 1-й Женевской конференции по атомной энергии, Proc. UN Int. Conf. PUAE, 3 (1956) 295.

[2] АРНОЛЬДОВ М.Н., ИВАНОВСКИЙ М.Н., СУББОТИН В.И., ШМАТКО Б.А., Зависимость удельного электросопротивления расплавленных щелочных металлов от содержания примесей. Доклад на Всесоюзной конференции по теплофизическим свойствам веществ в г.Новосибирске, 25 – 30 июля 1966 г.

DISCUSSION

E. L. ZEBROSKI: In your cold-trap analysis did you investigate the chemical form of the iron and chromium oxides that were found?

M.N. IVANOVSKY: No, we only investigated the quantity. We did not study the chemical form of these substances.

E. L. ZEBROSKI: Can you give me some information on the effectiveness of the diffusion trap? Is the removal effectiveness affected by the position of the trap?

M.N. IVANOVSKY: Part of the flow is diverted into the trap and our results show that about 20% of the flow passing through the circuit reaches the precipitation zone. As for the question of position, the trap was placed vertically for the sodium experiments. In our experiments with coloured water, however, we tried out the trap in various positions and this did not appear to influence its effectiveness. I expect that similar results would be obtained with metals.

H.J.K. ALLGEIER: When you use this trap, how do you determine the rate at which the cooling zone has to be moved? Do you do this simply by observing how effectively the trap removes impurities? Can you also tell me how you determine when the trap is filled? Is this also done by observing the effectiveness of the trap? The flow in the main circuit would not give you any indication of this.

M.N. IVANOVSKY: The simplest way of finding out when to move the cooling zone is to observe the changes which occur in the total concentration of impurities in the circuit. We use a device similar to the one described by Blake for checking the concentration of impurities in the circuit. If a minimum concentration (in our case 5×10^{-4} for oxygen) is not reached in a given time, we have to move the zone. It would also be possible to use methods based on the difference in the physical properties of the impurity and the metal.

J.M. WILLIAMS: As I understand it, Eq. (9) in your paper refers to the diffusion coefficient of oxygen in sodium. Have you determined a value for this coefficient or can you infer one from your experiments?

M.N. IVANOVSKY: The equation refers to the effective diffusion coefficient of impurities. It can be worked out on the basis of the experimental data for the purification rates.

J.S. LINDHE: What do you do with the diffusion traps once they are filled? Do you disconnect them?

M.N. IVANOVSKY: The traps we used in our laboratory installations were disconnected and then washed. In some experiments the traps were washed in sodium at high temperatures.

J. BEAUFRERE: Is it possible to trap impurities selectively with this device by utilizing the thermal gradient?

M.N. IVANOVSKY: No.

IMPURITIES IN THE PRIMARY SODIUM AND COVER GAS OF THE ENRICO FERMI ATOMIC POWER PLANT

J.P. LAGOWSKI
ATOMIC POWER DEVELOPMENT ASSOCIATES, INC.,
AND
E. HAVLENA
THE DETROIT EDISON COMPANY,
DETROIT, MICH.,
UNITED STATES OF AMERICA

Abstract

IMPURITIES IN THE PRIMARY SODIUM AND COVER GAS OF THE ENRICO FERMI ATOMIC POWER PLANT. The impurities carbon, hydrogen, oxygen, and nitrogen in sodium are of particular significance in high-temperature, long-life reactor systems. They have a potential for causing or contributing to carburizing, hydriding, nitriding and/or corrosion of structural and fuel clad materials. Clad reactivity effects, plugging of small lines and close tolerance mechanism malfunction are additional potential problems.

The primary sodium and argon cover gas of the Fermi reactor have been monitored for impurities for a number of years. Periodic sodium samples are analysed for carbon, hydrogen, oxygen, iron, and recently for nickel and chromium. A chromatograph is used to monitor the cover gas for hydrogen, oxygen, nitrogen, methane and carbon monoxide.

A typical sodium analysis shows 50 ppm total carbon, 2 ppm carbon as sodium carbonate, 1 ppm total hydrogen, 10 ppm oxygen and 2 ppm iron. Hydrogen, oxygen, methane and carbon monoxide are routinely less than 10 ppm in the cover gas, with nitrogen in the 3000-ppm range. Higher peak values have been experienced, which are dependent in some cases upon plant operating conditions such as primary system temperature and cover gas system operations.

Cold-trap operation has routinely kept oxygen in sodium down to the 10-ppm range, with results obtained as low as 7 ppm. Hydrogen in sodium has been kept in the 1-ppm range using the cold trap. Examination of the first Fermi cold trap shows evidence of removal of nitrogen.

The source of hydrogen in the sodium is believed to be the graphite in the top shield graphite. Several possible sources of the nitrogen in the cover gas have been identified. One, diffusion of nitrogen into the primary system, is of possible significance to sodium-cooled reactors operating in the 900-1200°F range.

Experience with the Fermi reactor indicates the value of monitoring the cover gas and sodium for impurities, and suggests design features of a monitoring nature for future plants.

1. SIGNIFICANCE OF IMPURITIES

The development of reliable sodium-cooled reactors for long life service must reflect an awareness of the importance of impurities in both the primary and secondary coolant systems. In the primary system, the impurities of particular interest at this time are oxygen, carbon, nitrogen, hydrogen, and compounds thereof. These impurities have a demonstrated potential for causing or contributing to corrosion, mass transfer, carburizing, nitriding, and/or hydriding of structural, control, or fuel cladding materials. Reactivity effects associated with hydriding of fuel cladding, plugging of small diameter openings, and close tolerance mechanism malfunction are additional potential problems.

2. FERMI BACKGROUND

In May, 1961, the Fermi primary system was heated to 1000°F for approximately five days in an isothermal nonnuclear test. Subsequent examinations inside the reactor vessel disclosed a substantial quantity of carbonaceous material on the vessel surfaces and floating on the sodium. The source of this material was complex hydrocarbons off-gassed from the carbon blocks in the reactor top shield plug; holes in the plug permit cover gas - shield plug gas communication. Attempts to remove this foreign material by filtration, cold trapping, and hot trapping were not completely successful. This experience, and an increasing awareness of the importance of monitoring to forestall the type of potential problems previously discussed, has led to an improving program of monitoring for impurities in the argon cover gas and sodium of the primary system.

The Fermi plant design has been described in detail.(1, 2) In summary, Fermi is a three-loop, sodium-cooled fast breeder reactor of 430-MW(th) capability, with a corresponding sodium outlet temperature of 900°F. Following completion of a test program to 200 MW(th), now in progress, the reactor will be run at 110 MW(th) as part of a program to extend the first core life until development and purchase of a second core is completed. The core outlet temperature for the 110-MW(th) period will be approximately 565°F. The primary sodium inventory is approximately 340 000 lbs and the argon cover gas volume is approximately 1200 ft^3.

3. COVER GAS IMPURITIES

The argon cover gas is continuously monitored for oxygen, hydrogen, nitrogen, methane, and carbon monoxide, using a commercially available gas chromatograph operating on a 12-minute cycle. The sampling arrangement is shown schematically in Figure 1. Valve adjustments permit sampling the cover gas in the reactor vessel, and the No. 1 and No. 3 primary pump tanks. No provision was made for sampling the cover gas in the No. 2 pump tank, the overflow tank, the three intermediate heat exchangers, or the fuel transfer port. Periodic cover gas grab samples are taken for laboratory analysis to help check the accuracy of the chromatograph. Prior to 1965, grab samples were the only source of cover gas purity information.

Typically, hydrogen, oxygen, and methane are in the 0-to 10-ppm range, carbon monoxide in the 0-to 50-ppm range, and nitrogen in the 3000-to 4000-ppm range. Figures 2 and 3 show these impurities for selected periods during the months of April, May and June, 1966. These figures are representative of cover gas impurity levels for isothermal nonnuclear, and recent nuclear operation up to 100 MW(th). With the exception of nitrogen, offscale readings are not representative of what is occurring in the cover gas, but apparently the result of high pressure in the waste gas collection header.

3.1 Hydrogen in the Cover Gas

The original source of hydrogen is believed to be the carbon blocks in the reactor top rotating shield plug. The 1000°F heatup noted previously resulted in the decomposition of an organic binder used in block manufacture, and the evolution of complex hydrocarbons, some of which are believed to have condensed in the cooler regions of the plug. Subsequent heatup and/or radiation exposure could result in the decomposition of these compounds and their slow release to the cover gas. Laboratory tests of carbon block offgassing clearly showed the evolution of hydrocarbons, nitrogen, carbon monoxide, carbon dioxide, oxygen, hydrogen, and water vapor.

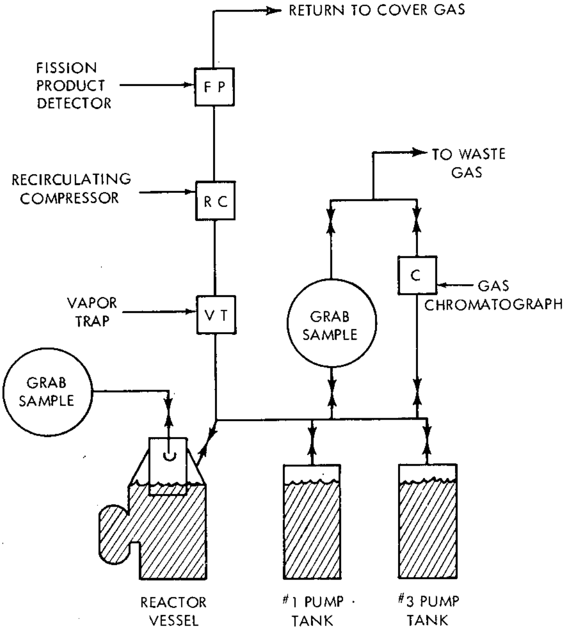

FIG.1. Primary cover gas sampling system simplified schematic

The hydrogen level in Figure 2 shows a peak of approximately 120 ppm during an April,1966,heatup to 650°F. Later heatups to the same temperature show no change in the normally low (0 to 10 ppm) hydrogen level. The reason for this difference is not known. Earlier hydrogen levels during changes in primary sodium temperature, and prior to nuclear operation, are shown in Table I. There were definite trends in cover gas hydrogen content as sodium temperature was changed or held constant following a heatup:

(a) Increases in temperature resulted in an increase in hydrogen content.

(b) Decreases in temperature resulted in a decrease in hydrogen content.

(c) The hydrogen level in the cover gas decreases at a constant temperature after a heatup.

The rate of change in hydrogen concentration during cool-downs or at constant temperature appears to be a function of the initial hydrogen concentration, i.e., the higher the initial concentration, the greater the rate of change.

The primary interest in cover gas hydrogen is its relationship to hydrogen in the sodium, with the possibility of hydriding the zirconium fuel cladding. A fuel assembly removed in 1965 was examined for evidence of zirconium hydriding, and a slight increase in hydriding was found. Additional fuel examinations are planned. The keys to avoiding excessive hydriding are believed to be maintaining low hydrogen in the sodium and the ability of the zirconium oxide surface film to inhibit hydrogen migration. Low hydrogen, approximately 1 ppm, can be maintained by cold trap operation. The extent to which the zirconium oxide film inhibits hydrogen migration in a sodium environment is not clear.

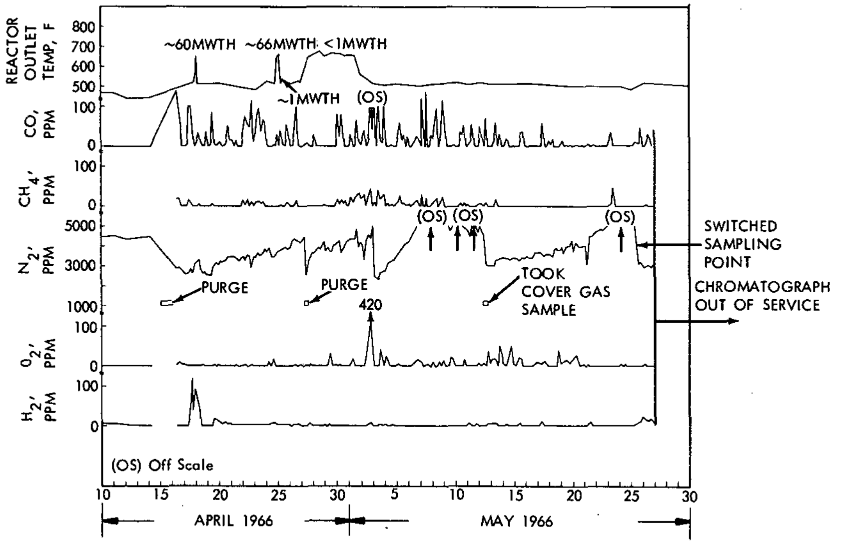

FIG. 2. Cover gas impurities

3.2 Nitrogen in the Cover Gas

Since the first cover gas samples were taken, the nitrogen level has been substantial. The normal range has been 1000 to 5000 ppm with the highest level reported as approximately 9000 ppm in a grab sample. The equilibrium level appears to be 3000 to 4000 ppm. The variation in Figure 2 is typical. Following a cover gas purge with clean argon, the nitrogen level drops, then builds up again at a rate typically in the 20 to 40 ppm/hr range. The Fermi nitrogen experience is qualitatively similar to that at Experimental Breeder Reactor II.

There has been no obvious correlation of the nitrogen with any plant operating condition. Attempts to define the sources of the nitrogen have not been successful. One such attempt is shown in Figure 3 in which the cover gas in the reactor vessel and pump tanks No. 1 and No. 3 were alternately sampled. The difference in nitrogen levels has not been explained, but may be due to back diffusion through a pump seal argon leak(s). The lack of oxygen may be explained by the fact that it combines rapidly with the sodium vapor in the gas space and is not detected by the chromatograph. No significant change in other impurities was noted during this sampling point switching. It should be noted that the cover gas is under a positive pressure and the pump seals are supplied with clean argon. Other possible sources of nitrogen include:

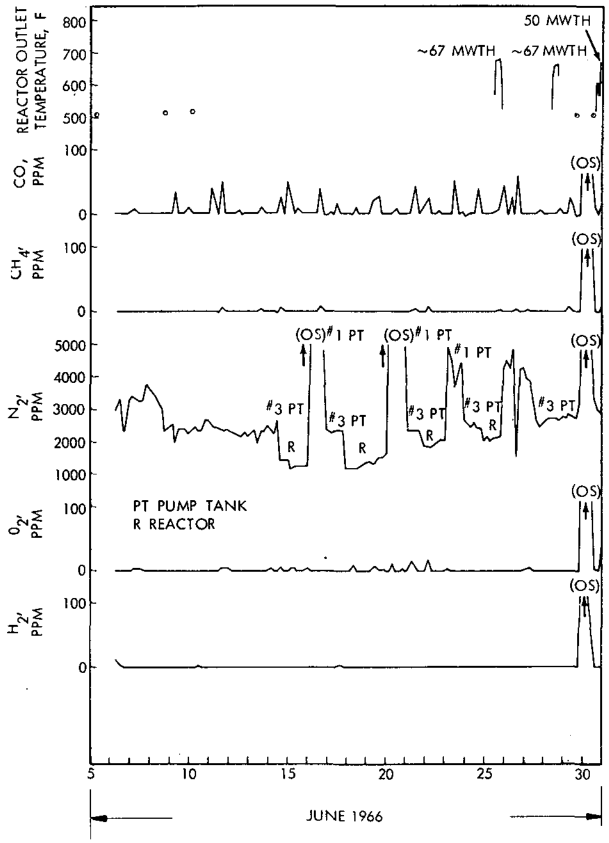

FIG.3. Cover gas impurities

(a) Air leakage or back diffusion into the pressurized cover gas regions through other mechanical seals such as those on the rotating shield plug, overflow pump shafts, and fuel transfer port.

(b) Leakage into the cover gas from the nitrogen-filled primary shield tank surrounding the reactor vessel.

(c) Nitrogen contained in the primary system stainless steel, including surfaces nitrided to obtain better wear and antigalling characteristics. There is some evidence that sodium can deplete nitrogen from the Fe_4N phase of nitrided Type 304 stainless steel.(3) The CrN phase does not appear to be affected.

(d) Diffusion of nitrogen from the nitrogen-filled below-floor region through the stainless-steel walls containing the primary system.

TABLE I. COVER GAS HYDROGEN VERSUS CHANGES IN SODIUM TEMPERATURE

Heatup	T start, °F	T end, °F	H_2 start, ppm	H_2 end, ppm	Time, hrs	Avg. T Change, °F/hr	Avg. H_2 Change, ppm H_2/hr
3-4/62	400	750	40	120	312	+ 1.12	+ 0.26
4-5/63	510	755	100	1400	192	+ 1.28	+ 6.78
6/64	450	750	15	500	168	+ 1.79	+ 2.88
3/65	550	750	105	1250	96	+ 2.08	+ 11.92
11-12/65	515	650	5	160	42	+ 3.2	+ 3.69
Cooldown							
4-5/63	755	525	1400	650	120	- 1.92	- 6.24
6/64	750	450	600	130	168	- 1.79	- 2.80
11-12/65	550	495	120	65	66	- 0.83	- 0.83
Constant Temperature							
3-4/62	750		120	60	120	0	- 0.5
6-7/64	460		130	15	240	0	- 0.49
2/65	550		150	105	48	0	- 0.94
3-4/65	750		1400	975	192	0	- 2.21
4/65	500		74	42	360	0	- 0.09
11-12/65	650		275	110	66	0	- 2.50

The interest in nitrogen as an impurity lies in its demonstrated potential for gas-phase nitriding of stainless steels at temperatures above approximately 900°F; of particular interest are thin members such as sealing bellows. Since Fermi will not operate at this temperature level for several years, adequate time is available to better define the extent of the problem and take corrective action, should this be required.

Based on a suggestion by Los Alamos Scientific Laboratory personnel, a calculation of diffusion of nitrogen from the below-floor region into the primary system stainless steel was made using the data of Ryder.(4) Isothermal system temperatures of 600, 750, and 900°F were used. The results are shown in Figure 4. At 900°F, the diffusion rate and the cover gas nitrogen buildup is approximately 1 ppm/hr. This is a factor of 20 to 40 less than the buildup rates normally experienced. For the nonisothermal reactor operating case, in which a system temperature difference exists, the rate would be well below 1 ppm/hr.

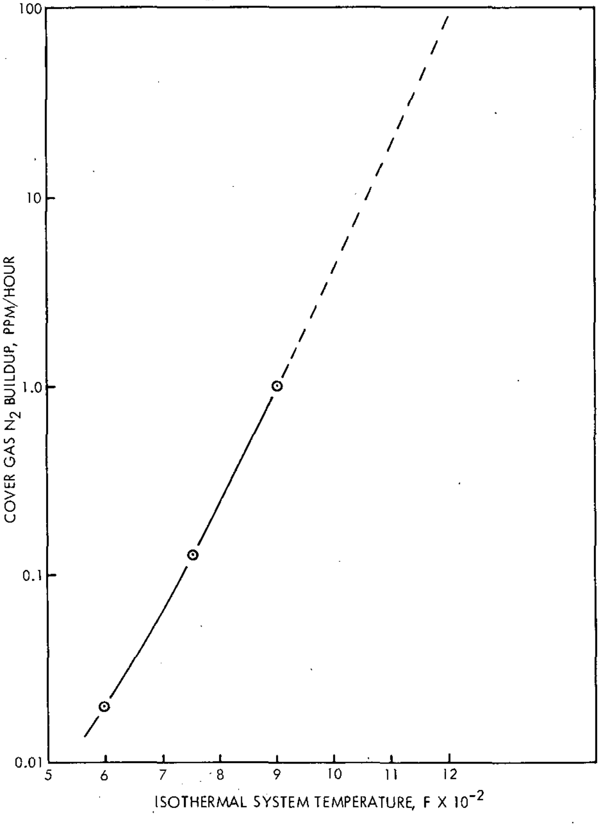

FIG.4. N_2 diffusion through primary system stainless steel

An extrapolation of the points in Figure 4 indicates buildup rates of 5 to 50 ppm/hr for systems operating in the 1000 to 1200°F range. Assuming the primary system stainless-steel surface areas and thickness in the Fermi plant are representative of systems being planned, nitrogen

TABLE II. PRIMARY SODIUM IMPURITIES

Date	Oxygen, ppm	Total Carbon, ppm	Carbonate Carbon, ppm	Nonhydroxide Hydrogen, ppm	Hydroxide Hydrogen, ppm	Fe	Ni	Cr
12/63	25	37	8					
3/64	27	41	3					
6/64	13	43	6		11			
7/64	12	38	7		3			
8/64	10	59	4		7			
9/64	15	43	7		2			
10/64	21	31	8		3			
1/65	16	50	3		4			
2/65	14	40	1		8			
3/29/65	12	48	2		3			
5/20/65	18	33	4	0.1	1.2	1 - 5		
6/65	27	44	5	1.1	2.8			
8/65	10	38-82	-	0.16	1.91			
10/6/65	11	47	2	0.15	0.60			
11/24/65	9	64	1	0.16	0.55			
12/6/65	9	47	2	0.68	0.62			
12/24/65	9	105	1.5	0.6	0.7	2.6		
2/1/66	8	82	1.3	0.3	0.6	2.9		
2/26/66	11	42	2	0.3	0.5	3.0		
3/29/66	9	36	1.3	0.2	0.9			
4/14/66	14	40-77	2	0.3	0.9	3.2	0.1	<0.3
5/66	8	73	2	0.1	0.6	1.9	0.2	<0.3
6/21/66	13	(A)	(A)	(A)	(A)	8.9	1.3	2.0
8/8/66	6	61	1.5	0.1	1.0	0.8	<0.3	<0.1

(A) Insufficient sample

diffusion calculations should be considered for those cases where it is intended to inert piping and equipment vaults with nitrogen.

3.3 Other Cover Gas Impurities

The other three impurities monitored by the chromatograph are oxygen, methane and carbon monoxide.

Oxygen was originally monitored for air in-leakage detection. Later recognition of the possibility of a rapid reaction of oxygen with sodium vapor has resulted in little confidence being placed on oxygen monitoring for small leaks. Oxygen has usually been at the lower limit of detectibility. The occasional peaks in the 20-to 30-ppm range in Figures 2 and 3 have not been explained.

Methane and carbon monoxide are monitored as impurities which can be released to the cover gas from the carbon block region of the reactor top rotating shield plug; both may be sources of carbon in the sodium. Methane is an additional possible source of hydrogen. Figures 2 and 3 indicate measureable quantities of methane and carbon monoxide. The methane buildup that occurred during the sustained April,1966, heatup to approximately 670°F returned to essentially zero, approximately six days after the temperature was reduced to the normal shutdown temperature of approximately 500°F. The lag in methane buildup and decay compared to temperature may be due to the time required to heat the carbon block area in the top shield plug, and for the gas(es) to travel to the argon cover gas. A similar methane buildup was noted in a 2 1/2 day, 100-MW(th) power run at 670°F in early August, 1966. There is no explanation for the apparently erratic carbon monoxide readings, although there appears to be a relationship between methane and carbon monoxide peaks.

For reactor operations through the end of September, 1966, there has been no significant quantity of fission gases as indicated by analysis of grab samples and fission product detector operation.

4. RELATIONSHIP BETWEEN COVER GAS AND PRIMARY SODIUM IMPURITIES

There is an obvious qualitative relationship between cover gas impurities and sodium impurity level. A quantitative understanding of this relationship, however, is essentially impossible with existing information. Meaningful work on the kinetics of reactions of cover gas impurities with sodium vapor and/or sodium has barely begun. The effect of reactor operating conditions involving flow, temperature differences, and a radiation environment add to the confusion. The lack of reliable solubility data, data on the evolution from or absorption of impurities by sodium, and even the extent of compounds which can be formed are examples of the meager state of knowledge on this general subject. For example, a recent reference (5) to cyanide formation in sodium suggests that we may have more to learn before we really understand stainless steel carburization or nitriding in a high-temperature sodium environment.

APDA is now doing work for the United States Atomic Energy Commission on hydrogen solubility in sodium and on the development of an in-line hydrogen meter.

5. SODIUM IMPURITIES

The Fermi primary sodium is periodically monitored for oxygen, carbon, hydrogen, iron, and recently for nickel and chromium. Sodium samples are taken outside the reactor building by means of a sample coil installed in parallel with the primary sodium cold trap. Each time a sodium sample is taken, the cold trap is run for approximately eight hours at 50 to 60 gpm (one sodium inventory turnover) to obtain a representative sample in the sampling coil. The sample coil is cooled in-place, allowed to decay to a point where it can be removed, transported to the APDA laboratory, and analyzed. At present it requires approximately two weeks to complete this process. Improvements are underway which will permit a reduction in this time to approximately one week. The effect of sample coil cooling on sample reliability is not known.

The frequency of sodium sampling has increased from an originally planned once a year in the late 1950's, to the present frequency of approximately once a month. Consideration is being given to increasing this frequency, in addition to improving the timing of sampling, to obtain data which can be more confidently correlated with reactor operation.

The results of all recent primary sodium analyses are provided in Table II. The nonmetallic impurities reported are the average results of three analyses from each sample coil. Total carbon is broken down to include carbon as sodium carbonate. Hydrogen is reported as nonhydroxide hydrogen and hydroxide hydrogen. The hydrogen results prior to the May 20, 1965, sample are known to be high. The apparent abrupt change in hydrogen starting May 20, 1965, reflects the use of an improved analytical technique.(6) The analytical techniques for oxygen and carbon have been reported.(7,8) The analytical technique for iron, nickel, and chromium is based on atomic absorption principles, with an APDA report on this method to be published in the very near future.

Figure 5 shows primary sodium impurities since early May, 1965, together with the periods of cold-trap operation and primary system heatups above the normal shutdown temperature of approximately 500°F. For clarity in presentation, only total carbon and total hydrogen are shown. Nickel and chromium have been omitted for the same reason.

The plugging temperature in the primary system has been below 250°F for the period indicated in Figure 5 and is generally less than 220°F. Plugging indicator runs are made approximately once a week.

5.1 Total Carbon in Sodium

Total carbon has been in the 40-to 60-ppm (by weight) range with correspondingly high and low values of 105 and 32 ppm, respectively. Carbon as sodium carbonate has decreased from an early range of 3 to 8 ppm to an apparent steady-state value of approximately 2 ppm. There is no real explanation for the variation in total carbon content, although the peak of 105 ppm appears to be the result of the nonnuclear heatup to 750°F in November-December 1965. The source of the carbon is believed to be carbon monoxide and possibly methane from the top shield plug, in addition to that remaining as a result of the 1000°F heatup in 1961.

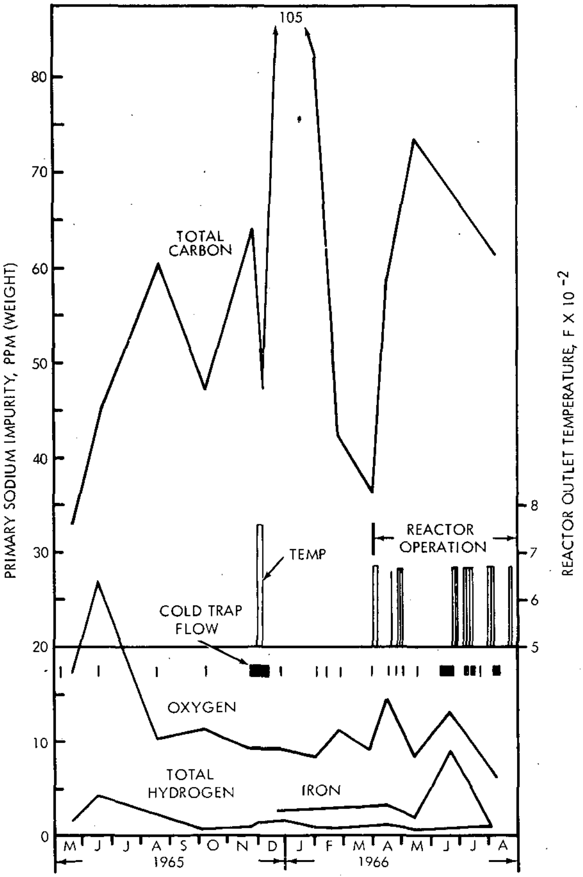

FIG. 5. Primary sodium impurities

5.2 Total Hydrogen in Sodium

For the last year, total hydrogen has been 1 ± 0.4 ppm with non-hydroxide hydrogen from 0 to 12 times lower than hydroxide hydrogen. In a November - December 1965 heatup to 750°F, nonhydroxide hydrogen increased from approximately 0.2 to 0.7 ppm, while hydroxide hydrogen remained essentially constant. During the heatup, the cold trap was in operation and the cover gas was frequently purged. This heatup was part of a test to determine the source of the hydrogen in the cover gas and, therefore, the sodium. Results of this test tended to confirm that the shield plug carbon blocks were the source. Figure 5 indicates that above approximately 10-ppm oxygen, hydroxide hydrogen content may depend upon oxygen content as indicated by the hydrogen and oxygen peak in June, 1965.

5.3 Total Oxygen in Sodium

Total oxygen in the primary sodium has been maintained in the 10-ppm range, with high and low values of 27 and 6 ppm, respectively. The 6 ppm value is the most recent and at the end of the most extensive cold-trapping period to date. Total oxygen is total alkalinity calculated as oxygen in sodium monoxide.(8)

5.4 Metallic Impurities

Iron normally has been in the 2-to 3-ppm range with a June, 1965, peak of 8.9 ppm. This peak is noted to occur at the same time as the oxygen level increased. Both the oxygen and iron increase may be related to the fact that an insufficient sodium sample was obtained. The peaks in hydrogen (hydroxide hydrogen) and iron with oxygen peaks above approximately 10 ppm, suggest the possible presence of an iron hydroxide. Both nickel and chromium increased when iron increased to 8.9 ppm. The 0.8-ppm iron in the last sample is the lowest to date, apparently the result of the recent extensive cold trapping.

5.5 Fission Products in Sodium

Due to the lack of significant fission gas activity through September, 1966, no analysis of sodium for fission products has been performed. Analyses in 1960 and 1961 showed uranium in the sodium to be less than 1 ppm.

6. EFFECT OF TEMPERATURE AND COLD-TRAP OPERATION

There are a number of plant operations which affect the impurity level in the Fermi cover gas and primary sodium. The key ones to date are reactor outlet temperature and cold-trap operation.

There has been no indication to date that reactor power has an effect on impurity content. The longest power run was approximately 60 hours at 100 MW(th) in early August, 1966. The effects of extended operation, if any, remain to be demonstrated. The only known possibility is radiation decomposition of hydrocarbons in the top shield plug and fission product activity.

The reactor outlet temperature is important for a number of reasons:

(a) The lower portion of the top shield plug is in outlet sodium, and carbon block offgassing is temperature dependent.

(b) Temperature increases would result in the increased dissolution of whatever impurities are in the system. The higher the temperature, the higher the impurity equilibrium level, assuming no cold-trap operation.

The original Fermi cold trap was removed in 1963 to permit replacement of this four-year-old unit with a new one prior to the start of nuclear operation. During this period the original cold trap was in operation for approximately 3700 hours at 50 to 60 gpm, processing the equivalent of 160 times the primary sodium inventory. The results of the analysis of the original cold trap contents have been reported.(9)

In summary, the trap contained an estimated 50 pounds of oxygen, 0.9 pounds of carbon, and smaller amounts of carbonate carbon, hydrogen, and nitrogen. The level of these impurities in the stainless steel mesh of the cold trap was:

Oxygen - up to 230 000 ppm
Total Carbon - up to 4300 ppm
Carbonate Carbon - up to 1200 ppm
Hydrogen - up to 10 800 ppm
Nitrogen - up to 102 ppm

Spectrographic analyses for metallic impurities revealed high concentrations of copper and iron. Typical results were:

Copper - up 360 ppm
Iron - up to 165 ppm
Nickel - up to 9 ppm
Chromium - up to 30 ppm
Maganese - up to 12 ppm
Calcium - up to 8 ppm

There was no analyses for specific compounds of any impurity. There is also no explanation for the high copper results.

Cold-trap operation at numerous facilities has been shown to be an effective means of maintaining any oxygen level in the sodium in the 10-ppm range. The last Fermi sodium sample shows 6 ppm, the best to date. The corresponding plugging temperature is less than 220°F. This level is based on intermittent cold-trap operation, as indicated in Figure 5. Some slight improvement might be possible with sustained long-term operation; however this has not been required.

Table II and Figure 5 show that total hydrogen in the primary sodium can be reduced to approximately 1 ppm by means of cold-trap operation. The hydrogen breakdown in Table II indicates that with a plugging temperature of less than 220°F, nonhydroxide hydrogen can be reduced to less than 0.1 ppm and hydroxide hydrogen to 0.5 to 1.0 ppm with a cold trap. Positive confirmation of this indication has recently been provided by APDA laboratory work. Assuming hydroxide hydrogen is present as NaOH, 1-ppm hydroxide hydrogen corresponds to 40-ppm NaOH. This is the equivalent of 8-ppm oxygen as Na_2O.(8) Table II shows 1-ppm hydroxide hydrogen corresponds to approximately 10-ppm oxygen as Na_2O, and suggests the bulk of the oxygen may be present as a hydroxide and not as Na_2O.

7. DESIGN AND DEVELOPMENT SUGGESTIONS

The practical significance of monitoring cover gas and sodium purity depends upon such factors as possible sources and types of impurities; reactor coolant velocity and outlet temperature; and structural, control, and fuel-cladding materials. These factors tend to determine the extent of gas and sodium purity monitoring and cleanup equipment initially installed in a plant. In most cases this is a bare minimum due to capital cost considerations; reactor outlet temperatures to date; and the fact that, with two exceptions, there have been no really serious incidents in sodium-cooled reactors due or related to impurities in the cover gas or sodium. The exceptions are the fuel damage in the Sodium Reactor Experiment in 1959 due to coolant channel blockage with carbonaceous material from an organic cooling line leak, and the Fermi steam generator sodium-water reaction as a result of a tube leak in 1962. It is possible that the consequences of both these incidents could have been minimized by early detection of changes in sodium and cover gas impurity levels. Preventing or minimizing the consequences of one such incident in the lifetime of a plant would pay for the initial installation of a complete cover gas and sodium monitoring system. Later monitoring and cleanup equipment additions to a plant are handicapped by lack of flexibility in design, possible interference with operation, and added costs due to a radiation environment.

The trend to sodium-cooled reactor outlet temperatures in the 1000 to 1100°F range emphasizes the importance of component reliability and plant availability. The inability to define all possible impurity sources, and uses for an adequate monitoring system, suggest as a minimum the following design features for impurity monitoring and cleanup in future plants:

(a) In-line gas chromatographs for both the primary and secondary system cover gas, with sample lines and valving to permit monitoring of all cover gas regions. A better but perhaps more expensive device would be a mass spectrometer.
(b) Heated gas sample lines with sodium vapor traps to minimize or eliminate line plugging.
(c) A capability to obtain frequent, representative sodium samples from both the primary and secondary coolant systems, with shielded space for the possible addition of the in-line sodium impurity monitoring devices now under development.
(d) A capability for the prompt and complete analysis of radioactive sodium samples, including fission product analysis.
(e) The installation of two shielded cold traps in the primary system and individual loop cold traps in the secondary system, with valving and piping to permit the use of a secondary cold trap in another loop for backup purposes.
(f) A capability for continuous cold-trap operation independent of reactor operation.
(g) Plugging meters in each of the secondary loops and at least one in the primary system, preferably two if they are not accessible. Programmed, automatic plugging meter operations are much preferred to manual operations for repeatability and minimum use of manpower.

There are also a number of apparent development needs. In addition to those previously mentioned in the sodium chemistry area, it would be desirable to expand the development of reliable in-line sodium impurity measuring devices for use in the primary and secondary coolant systems. The availability of cold traps from several sodium-cooled reactors suggests that they be examined to determine their over-all performance regarding the quantity and types of impurities removed, with specific emphasis on identification of individual compounds and isotopes.

The ability to obtain timely information on impurities which can affect plant operation and operating costs is easily justified for a high-temperature system designed for a 30-year life.

A sodium and cover gas impurity monitoring capability, based on an adequate sodium chemistry foundation, will contribute to the commercial success of sodium-cooled fast reactors.

ACKNOWLEDGMENT

The authors gratefully acknowledge the assistance of the personnel at the Enrico Fermi Atomic Power Plant and Atomic Power Development Associates, Inc. in the preparation and review of this paper.

REFERENCES

(1) AMOROSI, A., YEVICK, J. G., Proc. 2nd Int. Conf. PUAE 9 (1958) P2427.
(2) IAEA, Directory of Nuclear Reactors, 4 (1962) 319.
(3) PHALEN, D. I., VAUGHAN, D. A., Phase distribution through the case of nitrided Type 304 stainless steel (unpublished), Battelle Memorial Institute.
(4) RYDER, H. M., Elec. J. 17 (1920) 161.
(5) BJORK, R. G., HOBART, E. W., Nuclear Applications, 1 10 (1965) 490.
(6) HILL, E. F., MEACHAM, S. A., APDA-183 (1966).
(7) BOLTZ, D. F., MEACHAM, S. A., APDA-166 (1965).
(8) BOLTZ, D. F., KERMOSHUCK, J. O., MEACHAM, S. A., APDA-168 (1965).
(9) HERB, J., WRIGHT, J. H., WCAP-4321 (1965).

DISCUSSION

M.N. IVANOVSKY: I understood you to say that nitrogen was discovered in the first cold trap. In what form was it found?

J.P. LAGOWSKI: Nitrogen was detected at the maximum level of 102 ppm. The form of the nitrogen, or of any of the other impurities, was not identified.

M.N. IVANOVSKY: How did you analyse the nitrogen in the sodium?

J.P. LAGOWSKI: This was done by carrying out a spectrographic analysis of samples taken at various points in the cold trap.

M.N. IVANOVSKY: What do you think were the main sources of this nitrogen and what was the diffusion rate of the nitrogen through the pipe wall?

J.P. LAGOWSKI: As is pointed out in the paper, we have not really identified the source of the nitrogen in the cover gas. Quite a number of sources are possible, but none have been identified with any degree of certainty. Possible sources are the nitrogen in the steel of the primary system and air inleakage. It has to be remembered also that the nozzles of the fuel sub-assemblies and the region in the core support plate in which they are situated were deliberately nitrided for better wear and anti-galling purposes. In addition, the primary shield tank which surrounds the reactor vessel contains graphite. It is blanketed with nitrogen. Leakage in some form may occur between these two regions although this has not been proved.

As for your second question regarding the diffusion rate of nitrogen through stainless steel, I do not remember the exact value. The appropriate reference is quoted in the paper and you will find this information there.

J. R. WEEKS: According to the data given in Fig. 2 of your paper, the maximum values for oxygen and carbon monoxide, and major peaks for the carbon monoxide and nitrogen traces, occurred several days after the reactor outlet temperature had been lowered. As it is difficult to explain this on the basis of the lower temperature, I wonder whether it was not due to a leak.

J. P. LAGOWSKI: In our opinion these are not real peaks at all. They appear to be due to the fact that the pressure in the waste gas header was maintained at a value above the normal level. This increased pressure would affect gas chromatograph performance, and for most impurities these pressure peaks did in fact correspond to the peaks indicated by the chromatograph.

J. S. LINDHE: Did you try to identify long-chained carbon compounds in the sodium or on surfaces?

J. P. LAGOWSKI: No, we didn't perform any analyses of this sort. I don't think that any reliable techniques have been developed for this type of work.

DETECTION DES GAZ ENTRAINES DANS LE SODIUM AUX SURFACES LIBRES

N. LIONS
CEA, CENTRE D'ETUDES NUCLEAIRES DE CADARACHE,
FRANCE

Abstract — Résumé

DETECTION OF GASES ENTRAINED IN SODIUM AT FREE SURFACES. A method for measuring the gas volume fraction in a homogeneous two-phase flow with two constituents is presented.

The principle employed is based on the measurement of the speed of sound in a flow. For a flow with two given constituents, the latter value is a function of temperature, static pressure, gas volume fraction and average radius of the gas voids. With the exception of the gas fraction and the average radius these parameters can be measured directly. When the average radius exceeds a threshold r_m, the speed of sound varies, in particular with the steric pressure. Use is made of this phenomenon by carrying out sound-velocity measurements in the flow at two different static pressures. This provides information on the order of magnitude of the average radius of the gas voids as well as the gas volume fraction. With this method it is possible to determine the volume fraction in the 10^{-4} -5×10^{-2} range for gas voids with an average radius of $r_m > 10^{-5}$ mm.

Experimental results for water-argon and sodium-argon flows in horizontal geometries are also presented and there is a discussion of the equipment used to measure the gas fraction in the central channel of the RAPSODIE core.

DETECTION DES GAZ ENTRAINES DANS LE SODIUM AUX SURFACES LIBRES. L'auteur présente une méthode de mesure de la fraction volumique de gaz dans un écoulement diphasé homogène à deux constituants.

Le principe de détermination repose sur la mesure de la vitesse du son dans l'écoulement. Celle-ci est fonction, pour un écoulement à deux constituants donnés, de la température, de la pression statique, de la fraction volumique de gaz et du rayon moyen des bulles de gaz. A l'exception du rayon moyen et de la fraction de gaz, les autres paramètres sont directement mesurables. Lorsque le rayon moyen est supérieur à un seuil r_m, la vitesse du son varie notablement avec la pression statique; on met à profit cette propriété en effectuant les mesures de vitesse du son dans l'écoulement à deux pressions statiques différentes. On obtient ainsi un ordre de grandeur du rayon moyen des bulles de gaz, ainsi que la fraction volumique de gaz. Cette méthode permet de déterminer la fraction volumique dans la gamme s'étendant de 10^{-4} à $5 \cdot 10^{-2}$ pour des bulles de gaz de rayon moyen $r_m > 10^{-5}$ mm.

L'auteur présente des résultats expérimentaux obtenus sur des écoulements eau-argon et sodium-argon en géométrie horizontale ainsi que le dispositif de mesure de la fraction de gaz dans le canal central du cœur du réacteur RAPSODIE.

NOTATIONS

Les paramètres affectés au liquide, au gaz et au mélange portent respectivement les indices L, g et m.

a = célérité du son dans l'écoulement diphasé
a_0 = célérité du son dans le liquide
B = inverse du coefficient de compressibilité
D = diamètre intérieur de la tuyauterie
G = glissement
K = coefficient de compressibilité isotherme
P = pression statique
P_g = pression du gaz au sein d'une bulle

Q = débit volumique
r = rayon moyen équivalent d'une bulle de gaz
S = section droite de la tuyauterie
T = tension capillaire de l'interface liquide-gaz
U = vitesse moyenne d'écoulement
U_0 = vitesse du liquide s'écoulant seul dans le canal
V = volume occupé par chacun des constituants ou par le mélange
W = débit massique
x = titre massique du mélange
x_w = titre massique de l'écoulement
α = taux volumique de gaz dans une tranche de l'écoulement (ou fraction de gaz)
α_Q = titre volumique
ρ = masse spécifique
θ = température

La notation d(...) est réservée à des variations infiniment petites du paramètre.

Les notations $\delta(\ldots)$, $\Delta(\ldots)$ sont réservées à des variations d'amplitude finie du paramètre.

1. INTRODUCTION

Le but de cette étude est de définir une méthode de mesure de la fraction de gaz dans un écoulement diphasé à deux constituants.

L'application pratique la plus immédiate, pour laquelle cette étude a été effectuée, est la détermination du taux de gaz dans un écoulement sodium-argon. La technique mise au point a été expérimentée sur les circuits d'essai du réacteur RAPSODIE, elle sera appliquée à l'écoulement dans le cœur de la pile. La méthode de mesure que nous proposons est donc essentiellement adaptée à ces applications.

Les limites que nous fixons portent sur le choix du modèle et sur les hypothèses simplificatrices que l'on est conduit à effectuer pour traiter ce genre de problème.

Parmi les différents types d'écoulement en double phase, nous retenons celui qui est le plus probable dans les circuits thermiques et dans les assemblages du réacteur, à savoir: phase liquide en régime turbulent, et faible taux de gaz.

2. ETUDE THEORIQUE ET PRINCIPE DE LA MESURE

2.1. Définition des principaux paramètres utilisés

Nous rappelons la définition des paramètres qui seront utilisés par la suite:

a) Rayon moyen équivalent: Le rayon moyen équivalent d'une bulle de gaz est le rayon r d'une sphère de même volume que la bulle considérée.

b) Taux volumique de gaz: Dans une tranche du mélange, le taux volumique de gaz est égal au rapport du volume moyen occupé par le gaz au volume total occupé par le mélange

$$\alpha = \frac{V_g}{V_m} = \frac{V_g}{V_L + V_g} \tag{1}$$

c) Glissement: Le glissement est égal au rapport de la vitesse moyenne du gaz à la vitesse moyenne du liquide

$$G = \frac{U_g}{U_L} \tag{2}$$

d) Titre volumique de gaz: Le titre volumique de gaz est égal au rapport du débit volumique de gaz au débit volumique total

$$\alpha_Q = \frac{Q_g}{Q_g + Q_L}$$

Dans un écoulement homogène, où le glissement est constant et égal à l'unité, $\alpha_Q = \alpha$.

e) Masse spécifique d'un mélange homogène: La masse spécifique d'un mélange homogène de liquide et de gaz a pour expression

$$\rho_m = (1 - \alpha)\,\rho_L + \alpha\rho_g \tag{3}$$

ρ_L et ρ_g étant les masses spécifiques respectives du liquide et du gaz à la température et à la pression correspondantes.

f) Titre massique du mélange: Dans une tranche d'un mélange homogène de liquide et de gaz le titre massique a pour expression

$$x = \frac{\alpha\rho_g}{\rho_m} = \frac{1}{1 + \dfrac{1-\alpha}{\alpha} \cdot \dfrac{\rho_L}{\rho_g}} \tag{4}$$

g) Titre massique de l'écoulement: C'est le rapport des débits massiques

$$x_w = \frac{W_g}{W_g + W_L}$$

Dans un écoulement homogène à glissement constant et égal à 1, $x_w = x$.

2.2. Données et hypothèses simplificatrices de base

L'étude s'applique aux conditions suivantes:

- Tuyau indéformable, rectiligne et indéfini, de section constante.
- Ecoulement permanent, turbulent, et adiabatique dans son ensemble. Le nombre de Reynolds utilisé sera celui de la phase liquide que l'on suppose occuper toute la section droite du tuyau.

- Pression statique et taux volumique de gaz faibles, dans tous les cas: $\alpha < 50\%$; $P \leqslant 10$ b; la limite supérieure exacte au-delà de laquelle les hypothèses simplificatrices ne sont plus valables sera définie expérimentalement pour chaque cas particulier.

Les formules théoriques seront établies après avoir fait les hypothèses simplificatrices suivantes:

- L'écoulement a des caractéristiques constantes le long du canal (en particulier le taux volumique de gaz est constant).

- Le glissement est constant et très voisin de 1; nous nous efforcerons de montrer expérimentalement que, dans les limites que nous avons fixées, cette hypothèse est pratiquement vérifiée.

- Les bulles de gaz sont supposées sphériques, de rayons voisins, indépendantes, et uniformément réparties dans toutes les sections droites du tuyau.

- Les pertes de pression sont négligeables dans le tronçon d'essai.

- La solubilité du gaz dans le liquide est négligeable.

2.3. Célérité de l'onde élémentaire de pression

Le principe de la méthode étudiée repose sur la mesure de la célérité du son dans l'écoulement diphasé. Nous étudions donc tout d'abord le phénomène de propagation du son dans l'écoulement.

Considérons un canal dans lequel a lieu un écoulement diphasé satisfaisant aux hypothèses précédentes. La vitesse moyenne du mélange est égale à U_m, la pression statique absolue est P, et ρ_m est la masse spécifique du mélange à la température θ. Nous supposons que le milieu fluide est le siège d'une perturbation de pression d'amplitude infiniment petite, appliquée en un point infiniment éloigné situé en amont ou en aval du tronçon d'essai.

Les conditions expérimentales sont supposées telles que la fréquence de résonance des bulles est très supérieure aux fréquences de travail, de sorte qu'aucun phénomène de résonance ne se manifeste.

D'après les hypothèses que nous avons faites, la perturbation de pression dP se propage dans le milieu par ondes planes avec une célérité a définie par l'expression [1]

$$(a \pm U_m)^2 = \frac{1}{K_m \cdot \rho_m} \qquad (5)$$

où K_m est le coefficient de compressibilité du mélange

$$K_m = \frac{1-\alpha}{B_L} - \frac{\alpha}{V_g}\frac{dV_g}{dP} \qquad (5\text{ bis})$$

En supposant le gaz isotherme au sein du liquide [2-4], la célérité du son a pour expression

$$a \pm U_m = \left[\frac{B_L}{[(1-\alpha)\rho_L + \alpha\rho_g] \left[1 - \alpha + \dfrac{\alpha B_L}{P + \dfrac{4}{3}\dfrac{T}{r}} \right]} \right]^{\frac{1}{2}} \tag{6}$$

ρ_g est la masse spécifique du gaz à la température θ et à la pression

$$P_g = P + \frac{2T}{r} \tag{7}$$

Lorsque le taux de gaz $\alpha < 10^{-1}$ et pour des vitesses d'écoulement $U_m < 5$ m/s, U_m est négligeable devant a. C'est en général le cas dans nos expérimentations; sinon U_L reste une valeur suffisamment approchée de U_m .

Pour chaque valeur de la pression statique P, la célérité du son est une fonction du taux de gaz α et du rayon moyen r des bulles, qui est représentée par un réseau de courbes tel que celui de la figure 1. Ce réseau est tracé dans le cas d'un écoulement eau-argon à 6°C pour $P_1 = 2$ b, $P_2 = 1$ b.

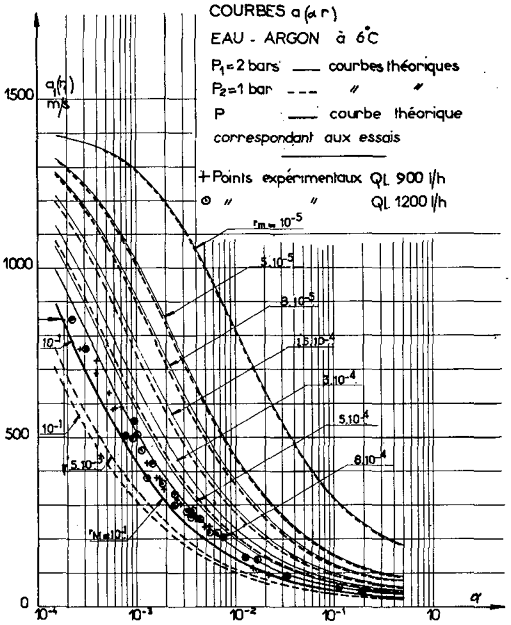

FIG. 1. Etude d'un écoulement eau-argon

D'après les hypothèses que nous avons faites, nous ne considérons que les régions définies par $0 \leqslant \alpha \leqslant 50\%$.

Lorsque $r \to 0$, on voit d'après (6) que a est indépendant de P. En fait, il existe une limite inférieure du rayon moyen des bulles, r_m, en deçà de laquelle la vitesse du son est pratiquement indépendante de la pression statique. La valeur de ce seuil dépend à la fois de la nature des constituants, de la température, et de la gamme de pressions considérée. Dans le cas des écoulements eau-argon et sodium-argon à basse pression $r_m \approx 10^{-5}$ mm.

Par ailleurs, quand le rayon des bulles augmente, il apparaît une limite r_M de r au-delà de laquelle les courbes sont pratiquement indépendantes de r, ce qui est en accord avec l'expression (7). Dans les conditions d'expérience, cela se produit pour $r > 10^{-1}$ mm environ.

2.4. Détermination du taux de gaz

L'examen de l'équation (6) et du réseau de courbes de la figure 1 montre que la mesure de la célérité du son a permet de définir le taux de gaz α, si on connaît B_L, ρ_L, ρ_g, P, T et r. A l'exception du rayon des bulles r, ces grandeurs sont connues ou directement mesurables. Il apparaît donc la nécessité de déterminer un ordre de grandeur du rayon des bulles.

2.4.1. Détermination du rayon moyen des bulles

Cette détermination peut être faite, comme on va le montrer, en effectuant la mesure de la célérité du son dans l'écoulement, à deux pressions différentes P_1 et P_2. Dans ce but, on utilise un canal composé de trois tronçons successifs de même section droite S:

- Un tronçon d'entrée où l'écoulement est défini par θ, P_1, ρ_L, ρ_{g1}, x, r_1, α_1 ; la célérité du son est a_1 ;
- Un tronçon intermédiaire où s'effectue une variation de pression;
- Un tronçon de sortie où les caractéristiques de l'écoulement sont θ, P_2, ρ_L, ρ_{g2}, x, r_2, α_2 ; la célérité du son est a_2.

L'écoulement est supposé constant et homogène dans le tronçon d'entrée, et le tronçon intermédiaire est suffisamment long pour que l'écoulement dans le canal de sortie soit à nouveau constant et homogène. On suppose que les bulles ont un rayon moyen $r > r_m$, sont indépendantes, et qu'il n'y a aucune coalescence.

Parmi les caractéristiques de l'écoulement citées plus haut, pour les tronçons d'entrée et de sortie, on peut facilement mesurer la température θ et les pressions P_1 et P_2. On connaît donc ρ_L. On ne mesure pas U_m car on peut en général le négliger, mais lorsque les conditions expérimentales l'exigent, on calcule U_m en admettant que le liquide occupe toute la section droite du canal. P_{g1} et P_{g2} sont définis par (7), la tension capillaire ne dépendant que de la température; ρ_{g1} et ρ_{g2} sont définis.

L'équation d'état du gaz appliquée à une bulle sphérique donne

$$P_2 r_2^3 + 2Tr_2^2 = P_1 r_1^3 + 2Tr_1^2 \tag{8}$$

La racine positive de cette équation définit r_2 en fonction de r_1. Enfin, la constance du titre massique permet d'écrire

$$\alpha_2 = \frac{1}{1 + \frac{1-\alpha_1}{\alpha_1} \cdot \frac{P_{g2}}{P_{g1}}} \tag{9}$$

Il en résulte que, pour des conditions expérimentales données (θ, P_1, P_2) et pour tout couple fixe de valeurs r_1, α_1, (7) permet de calculer P_{g1}, donc ρ_{g1}, (6) donne alors a_1. On peut ensuite calculer r_2 grâce à (8), P_{g2} donc ρ_{g2} grâce à (7) et α_2 grâce à (9). On obtient alors a_2 en utilisant (6). Donc, pour toutes valeurs de r_1 et de α_1, on peut calculer a_1 et a_2, c'est-à-dire l'écart $\Delta a = a_1 - a_2$. On peut alors déduire de ces résultats le réseau de courbes de la figure 2 où l'on a tracé les variations de Δa en fonction de a_1 pour différentes valeurs de r_1.

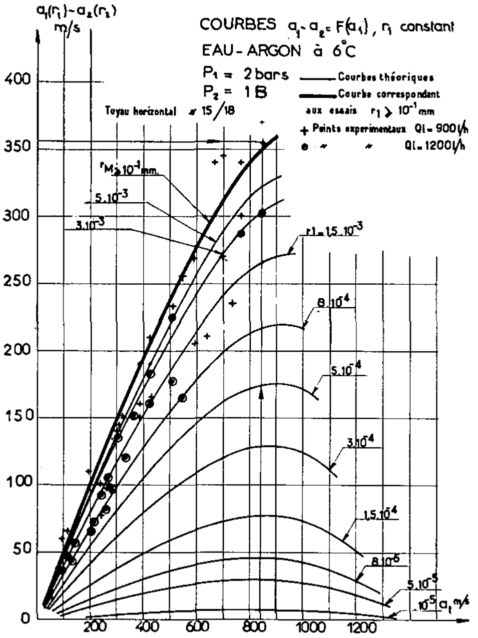

FIG.2. Etude d'un écoulement eau-argon

On peut remarquer que ces courbes présentent un maximum au voisinage de $a_1 = 950$ m/s. On voit également apparaître la limite inférieure $r_m = 10^{-5}$ mm, mentionnée plus haut, au-dessous de laquelle la célérité du son est indépendante de P, ainsi que la limite $r_M = 10^{-1}$ mm. Les courbes de la figure 2 permettent de déterminer la valeur du rayon moyen des bulles r_1 dans le canal d'entrée lorsque l'on a mesuré θ, a_1, a_2 pour un couple de pressions P_1, P_2 connu.

2.4.2. Principe de la mesure du taux volumique de gaz

Le rayon moyen des bulles r_1 ayant été déterminé comme on vient de l'indiquer, le réseau de courbes a_1 (α_1, r_1) de la figure 1 donne le taux volumique de gaz α_1 dans le canal d'entrée.

3. EXPERIMENTATION

Les mesures ont été effectuées sur des écoulements eau-argon et sodium-argon en géométrie horizontale. Elles avaient pour but la vérification des résultats théoriques et la détermination du domaine de validité des hypothèses simplificatrices de base.

3.1. Description des circuits d'essai

3.1.1. Circuit eau-argon

Le schéma du circuit d'essai est représenté sur la figure 3. L'argon est injecté dans l'axe du tuyau par un tube capillaire de 0,5 mm de diamètre. L'injection est faite en amont des tronçons de mesure à une distance voisine de 2 m du tronçon d'entrée. Le passage de la pression P_1 à la pression P_2 est réalisé par la vanne V_1. La célérité du son est obtenue en mesurant la vitesse de propagation d'une onde de pression, réalisée à l'aide d'une électrovanne à fermeture rapide.

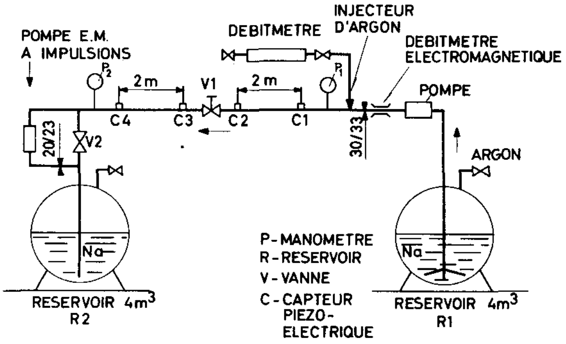

FIG.3. Schéma de principe du circuit d'essai eau-argon

3.1.2. Circuit d'essai sodium-argon

Le schéma de principe du circuit d'essai sodium-argon est représenté sur la figure 4. Le circuit se compose de deux réservoirs de 4 m^3 reliés par une tuyauterie principale de 30/33 mm de diamètre. Le sodium est chauffé et dégazé dans le réservoir R_1, une pompe électromagnétique placée sur la tuyauterie principale permet d'obtenir un débit maximal de sodium de 8 m^3/h. Le saut de pression est obtenu à l'aide d'une pompe électromagnétique à impulsions montée en by-pass sur la vanne V_2.

3.1.3. Mesure de la vitesse du son

La propagation de l'onde de pression est mesurée par des capteurs piézo-électriques disposés suivant le schéma des figures 3 et 4. Les signaux délivrés par ces capteurs sont enregistrés sur un oscilloscope cathodique muni d'un appareil photographique. La mesure du déphasage entre ces signaux permet de déduire la vitesse de propagation du son dans le canal.

3.2. Résultats

3.2.1. Etude d'écoulements eau-argon

Essais préliminaires. A titre d'essai préliminaire, on a contrôlé la distribution des bulles, on a mesuré leur rayon moyen par photographie et on a effectué des mesures de glissement.

Dans ce but, le circuit d'essai eau-argon de la figure 3 est équipé d'un dispositif photographique muni d'une lanterne stroboscopique qui permet de mesurer la vitesse des bulles de gaz, leur distribution, et leur rayon. On a vérifié que, pour des vitesses $U_0 \geqslant 1,4$ m/s et des taux de gaz $\alpha < 10^{-2}$, l'écoulement est pratiquement homogène (glissement voisin de 1) et que les bulles de gaz ont un rayon moyen voisin de celui de l'injecteur ($r \approx 0,25$ mm). Ces limites de U_0 et de α correspondent pratiquement à notre domaine de mesure.

Pour les taux de gaz $\alpha > 5 \cdot 10^{-3}$ le glissement a été mesuré par pesée de la quantité de liquide emprisonné dans un tronçon de tuyauterie isolé par deux électrovannes à fermeture rapide. On a trouvé (fig. 5) que le glissement est d'autant plus voisin de 1 que α est petit et que la vitesse d'écoulement est élevée.

Enfin, on a vérifié expérimentalement les lois et courbes obtenues dans l'étude théorique exposée précédemment, c'est-à-dire la loi $a = f(\alpha)$ dans des conditions de température et pression données, et pour r connu.

Le rayon des bulles était déterminé par examen photographique. On ne mesurait pas α; par contre, la mesure des débits de gaz et de liquide Q_g et Q_L permettait de connaître la qualité volumique α_Q. Or, on sait qu'on peut admettre approximativement $\alpha_Q \approx \alpha$ lorsque le glissement est voisin de 1. Au cours de ces essais, le rayon moyen des bulles était de l'ordre de 0, 25 mm, la qualité volumique α_Q couvrait le domaine $10^{-4} < \alpha_Q < 10^{-2}$.

Avant d'effectuer un essai, le dégazage de l'eau était contrôlé par mesure de la célérité du son dans l'eau; nous avons mesuré $a_0 \approx 1400$ m/s.

La figure 6 donne la courbe théorique de a en fonction de α, déduite de l'équation (6) et correspondant aux conditions expérimentales. Les points expérimentaux sont portés aux coordonnées a, α_Q mesurées. Les écarts entre les points expérimentaux et la courbe théorique peuvent provenir, soit d'erreurs expérimentales (mesures de a et de α_Q), soit du fait qu'on n'a pas rigoureusement $\alpha_Q = \alpha$. On voit sur la figure 6 que ces écarts restent faibles pour $\alpha > 7 \cdot 10^{-4}$: écart moyen de l'ordre de 10%. Pour $\alpha < 7 \cdot 10^{-4}$, la dispersion des points est plus grande, ce qui peut paraître anormal, car il semble que les conditions de l'expérience sont d'autant plus proches des hypothèses simplificatrices de base que la fraction de gaz est faible. Nous attribuons ces dispersions à l'instabilité du débit de gaz injecté, car nous avons constaté expérimentalement qu'il est très difficile d'obtenir dans cet intervalle une qualité volumique vraiment stable.

Détermination du taux volumique de gaz. Il s'agit de déterminer le taux volumique de gaz au moyen de la méthode de mesure exposée au paragraphe 2.4. Les expériences ont été réalisées sur le circuit de la figure 3. Nous présentons deux séries de mesures effectuées dans les conditions définies sur les figures 1 et 2.

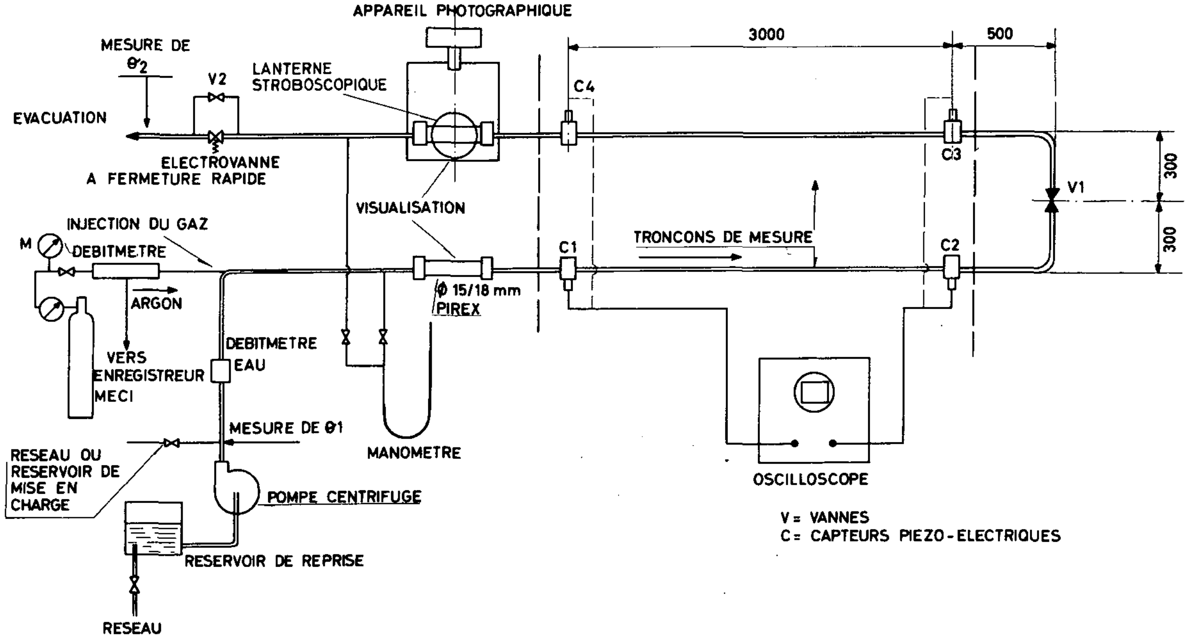

FIG. 4. Schéma de principe du circuit d'essai sodium-argon

La figure 2 permet de déterminer un ordre de grandeur du rayon moyen r_1 d'après les mesures de a_1 et de $\Delta a = a_1 - a_2$. On obtient alors le taux de gaz α_1 d'après les courbes de la figure 1. Le taux de gaz ainsi déterminé a été comparé à la qualité volumique α_{1Q}. Cette comparaison a mis en évidence dans la gamme $\alpha_1 < 3 \cdot 10^{-2}$ un écart relatif moyen de 35%.

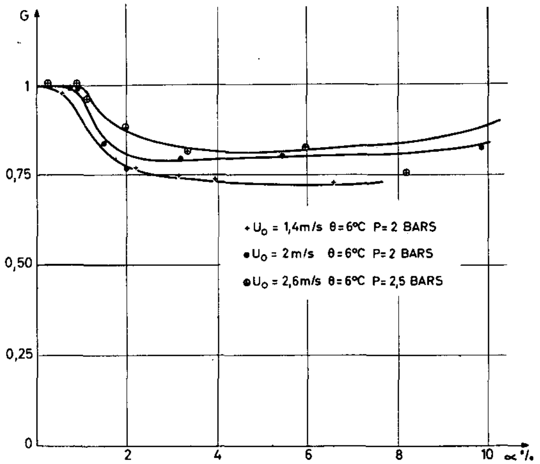

FIG.5. Etude du glissement en fonction du titre volumique et de la vitesse d'écoulement dans un écoulement eau-argon

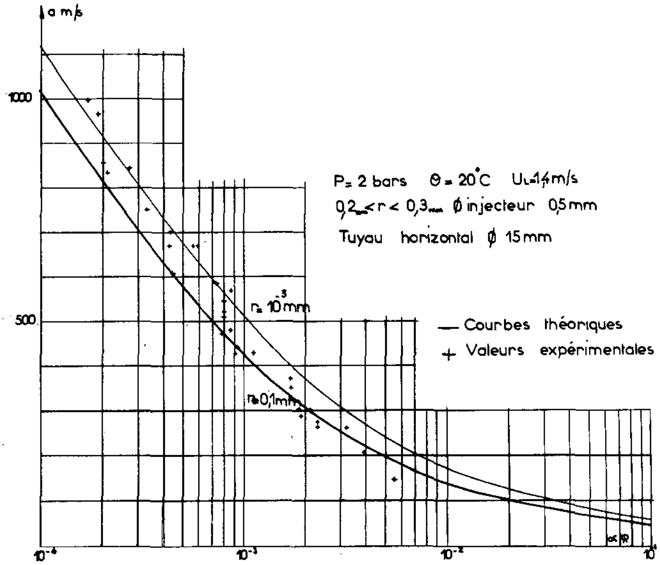

FIG.6. Mesure de la vitesse du son en fonction de la qualité volumique dans un écoulement eau-argon

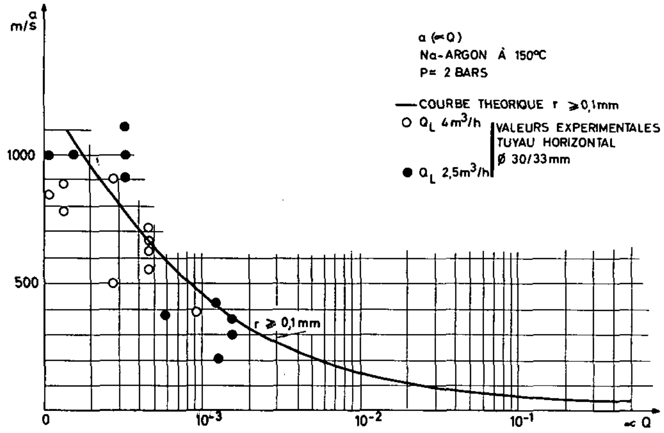

FIG. 7. Mesure de la vitesse du son en fonction de la qualité volumique dans un écoulement sodium-argon

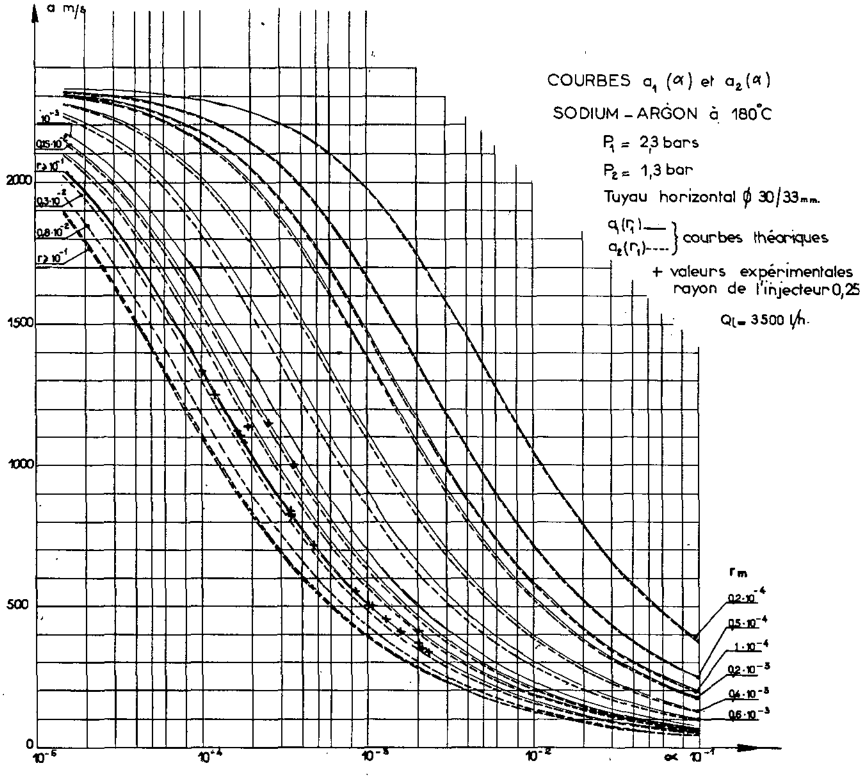

FIG. 8. Mesure du taux de gaz dans un écoulement sodium-argon

3.2.2. Etude d'écoulements sodium-argon

Mesure de la célérité du son en fonction de la pression statique et du titre volumique. Ces mesures ont été effectuées sur le circuit sodium-argon de la figure 4 pour des débits de sodium de 2500 et 4000 litres/h à 150°C. L'injecteur de gaz avait un diamètre intérieur de 0,5 mm; le diamètre moyen des bulles d'argon ne pouvait pas être contrôlé comme dans le cas de l'eau. On a reporté sur la figure 7 les valeurs expérimentales obtenues ainsi que la courbe théorique déduite de (6) pour $r \geqslant 0,1$ mm. On observe une dispersion des points de mesure sensiblement plus élevée que dans le cas de l'eau; nous l'attribuons principalement aux instabilités des débits.

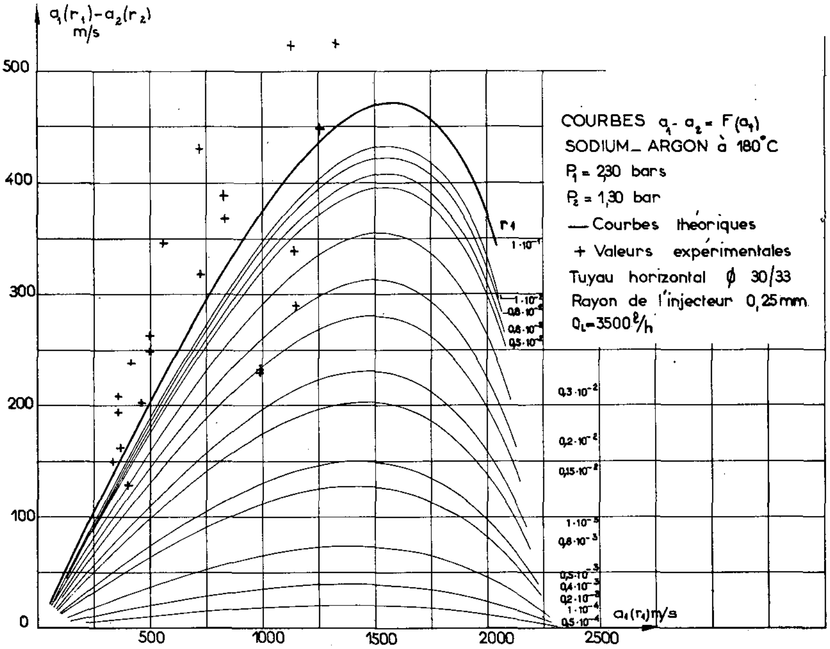

FIG.9. Mesure du taux de gaz dans un écoulement sodium-argon

Détermination du taux de gaz. Nous avons reporté sur les figures 8 et 9 les résultats relatifs à un écoulement sodium-argon à 180°C. Le débit de sodium était de 3500 litres/h et la qualité volumique $10^{-4} < \alpha_{1Q} < 3\cdot 10^{-3}$. Les valeurs de α_1 déduites des mesures de célérité du son aux pressions statiques $P_1 = 2,3$ b et $P_2 = 1,3$ b d'après le principe de détermination du paragraphe 2.4 ont été comparées pour chaque point à la qualité volumique α_{1Q}. On observe un écart relatif moyen du même ordre de grandeur que celui obtenu au cours des essais eau-argon.

3.3. Précision de la mesure

Un calcul d'erreur effectué dans le cas de l'écoulement eau-argon (fig. 1 et 2) pour $\alpha_1 \approx 10^{-3}$ montre que des incertitudes de ± 0,25% sur

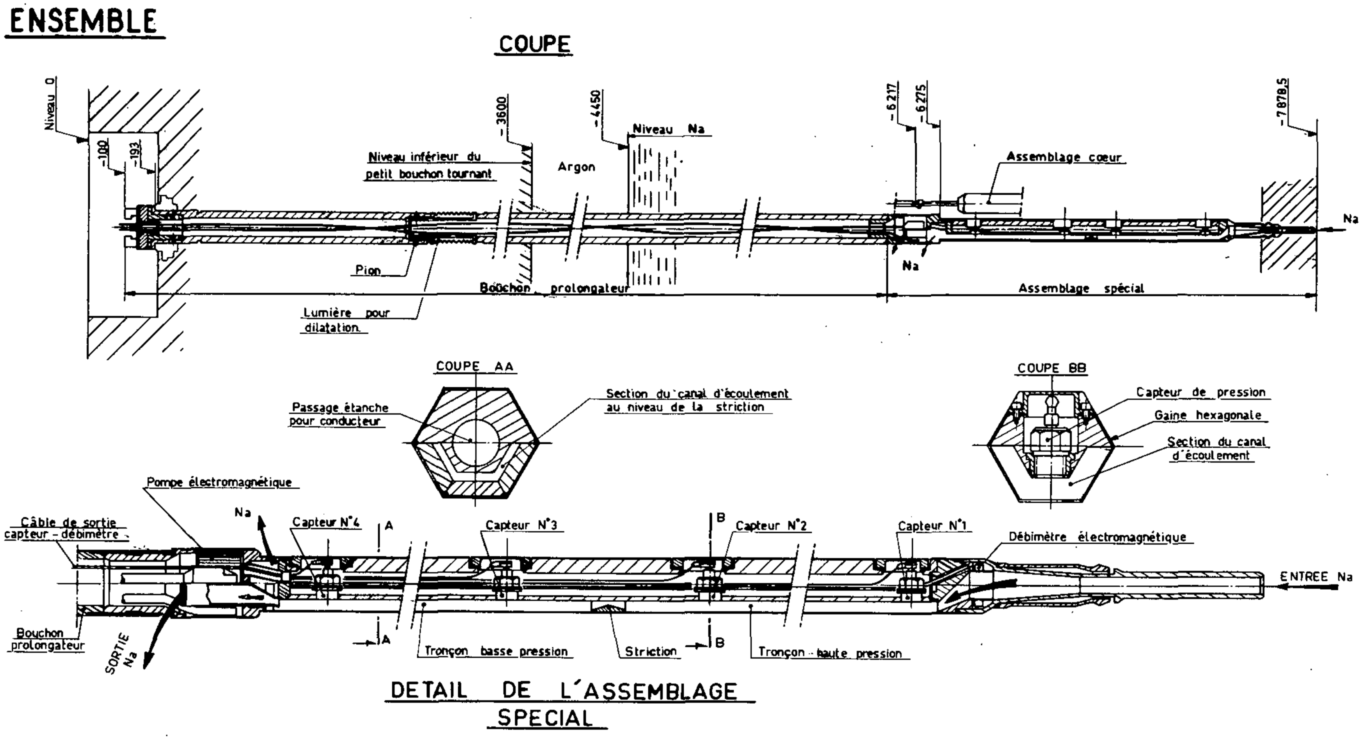

FIG.10. Schéma de principe du dispositif de mesure du taux de gaz dans le cœur de RAPSODIE

les mesures de pression statique et de ± 1% sur la mesure de célérité du son entraînent une erreur de ± 40% sur la détermination du rayon moyen r_1 et de ± 8% sur le taux de gaz α_1. Cette erreur provenant essentiellement de l'erreur de mesure de la célérité du son, il est souhaitable que celle-ci soit faite avec la meilleure précision possible. De plus, les hypothèses simplificatrices qui ont été faites pour mettre le problème en équations introduisent une incertitude qu'il est impossible de chiffrer: finalement les valeurs obtenues expérimentalement pour α diffèrent de 35% environ de α_Q. Rappelons qu'on devrait trouver $\alpha = \alpha_Q$ si on a exactement $G = 1$.

4. MESURE DU TAUX DE GAZ DANS LE CANAL CENTRAL DU CŒUR DE RAPSODIE

Le dispositif de mesure du taux de gaz dans le cœur de RAPSODIE est représenté sur le schéma de la figure 10. Il comprend un assemblage spécial où se trouvent les appareils de mesure et un bouchon prolongateur placé dans le canal central du réacteur. La perte de pression de l'assemblage spécial est identique à celle de l'assemblage du cœur auquel il est substitué. Cet assemblage est composé de trois tronçons: un tronçon haute pression, un tronçon intermédiaire où est placée une striction, et un tronçon basse pression. Les mesures de la célérité du son dans les tronçons haute et basse pression sont effectuées par quatre capteurs piézo-électriques. Le débit de sodium est mesuré à l'entrée du canal haute pression par un débitmètre électromagnétique; la perturbation de pression est obtenue par une pompe électromagnétique à aimant permanent placée en by-pass sur les orifices de sortie du sodium.

Les mesures vont être effectuées très prochainement à 180°C avant la divergence du réacteur; elles seront faites pour plusieurs régimes de fonctionnement des pompes mécaniques et de la pompe auxiliaire des circuits de purification primaires, afin de mettre en évidence les sources possibles d'entraînement d'argon. Ce dispositif est en cours d'étalonnage sur un circuit d'essai.

5. CONCLUSION

Les résultats obtenus en géométrie horizontale avec des tuyaux de 15 et 30 mm de diamètre permettent de penser que, pour des taux volumiques de gaz tels que $10^{-4} < \alpha < 10^{-2}$, les principales hypothèses de base (écoulement homogène et glissement suffisamment voisin de 1) sont pratiquement vérifiées pour des vitesses d'écoulement de la phase liquide supérieures à 1,4 m/s. Les formules théoriques établies en supposant le gaz isotherme au sein du liquide sont assez bien vérifiées par l'expérience et la mesure du taux de gaz est obtenue avec un écart moyen de l'ordre de 35% par rapport au titre volumique.

Pour le but recherché (contrôle de l'absence d'entraînement de gaz dans les circuits primaires de RAPSODIE), la précision obtenue est très largement suffisante.

Dans le cas d'un écoulement contenant une proportion plus importante de gaz ($\alpha > 10^{-2}$), la méthode perdrait de sa sensibilité, mais elle reste parfaitement valable pour obtenir un ordre de grandeur du phénomène.

REFERENCES

[1] BRUN, E.A., MARTINOT LAGARDE, MATHIEU, J., Mécanique des Fluides, Ed. Dunod, Paris.

[2] DIN-YU HSIEH, PLESSET, M.S., On the propagation of sound in a liquid containing gas bubbles, Calif. Institute Technol., Pasadena (Calif.) (19 April 1961).

[3] MARCHAL, R., Sur la stabilité des écoulements dans les tuyauteries parcourues par une émulsion de liquide et de gaz, C. r. hebd. Séanc. Acad. Sci. 254 (1962) 2524.

[4] HETRICK, D.L., Velocity of sound in water containing gas bubbles, Atomics International Technical Data Record, NAA-SR-Memo 3148 (1958).

SOME ANALYTICAL AND PROCESS INSTRUMENTS FOR MEASUREMENTS IN SODIUM

E. DUNCOMBE, D. F. DAVIDSON
U. K. ATOMIC ENERGY AUTHORITY,
REACTOR ENGINEERING LABORATORY,
RISLEY, WARRINGTON, LANCS.,
R. A. DAVIES AND R. DEHN
DOUNREAY EXPERIMENTAL REACTOR ESTABLISHMENT,
THURSO, CAITHNESS, UNITED KINGDOM

Abstract

SOME ANALYTICAL AND PROCESS INSTRUMENTS FOR MEASUREMENTS IN SODIUM. Recent U.K.A.E.A. operating experience and development work on analytical and process instruments are reviewed.

The main experience with analytical instruments has concerned the rhometer and plugging meter. Two mk IA rhometers have been installed on the primary circuit of the Dounreay Fast Reactor and their long-term performances compared with plugging meter indications. Further rhometer studies have included a recalibration of the mk IA instrument against oxygen impurity and the development of a mk II model which also allows for a much wider range of temperature conditions. A continuously indicating plugging meter, using the principle of an orifice automatically maintained in the partially plugged state, has been successfully demonstrated on a sodium loop. Some studies have also been made on measuring oxygen in sodium by EMF methods.

Development in sodium process instrumentation is primarily directed towards solving the problems arising from the large flows and high temperatures in the Prototype Fast Reactor, and in the supporting experimental rigs.

Two general methods of measuring flow in large ducts are being pursued. The first depends on observing the transport time of thermal "noise" between two measuring thermocouples stationed a few diameters apart along the duct. The second is based on the conventional electromagnetic flowmeter but with the permanent magnet system replaced by DC energized coils of "saddle" form applied to either side of the duct. This arrangement avoids the need for massive ferromagnetic items and allows the calibration to be derived with reasonable certainty.

A method of measuring differential pressure, using the reverse head generated by a small DC conductance pump, has been successfully applied to an orifice-plate flow-measuring installation. To measure liquid levels at temperatures up to 700°C, an electromagnetic sensor, bifilar-wound in metal-sheathed, mineral-insulated cable, is being developed. An inductive transducer for monitoring displacements of about 0.5 mm has been operated satisfactorily immersed in sodium at 400°C. The calibrational stability, response speed and reliability of sheathed mineral-insulated Chromel/Alumel thermocouples, directly immersed in flowing sodium, is being studied. The optical absorption of light from a low-pressure sodium lamp by sodium vapour (or dispersion by smoke) is used as the principle of an instrument for leak monitoring on sodium rigs.

1. INTRODUCTION

The analytical and process instrumentation is usually an important part of any reactor coolant system. This is particularly true for sodium systems, where not only are the rates of corrosion and mass transfer of circuit materials affected to a marked extent by small changes in the temperature and flow rate of the liquid metal, and in the amount of impurities in it, but often such changes are also the first indication of fault conditions in some part of the system. It is therefore of considerable interest to review this topic periodically, and in the present paper some of the experience which has been gained and the developments which are under way in the U.K. are outlined. The analytical instruments dealt with are the plugging meter, rhometer (Blake resistivity meter), and oxygen meter; the process instruments discussed are for measuring temperature, flow, level and displacement and for leak detection.

2. ANALYTICAL INSTRUMENTATION

2.1 Plugging Meter

Whilst the plugging meter has been used on a number of loops in the U.K., perhaps the most important application has been on the Dounreay Fast Reactor where it has provided the main operational instrument for measuring the purity of the sodium-potassium coolant in the primary circuit. The instrument used is a manually operated poppet valve with slots cut in the valve poppet. The correlation between the plugging temperature as indicated by this instrument and the corresponding saturation temperature of the NaK was obtained by varying the temperature of the cold-trap. The cold-trap basket temperature at which trapping ceased and oxide started to re-dissolve (detected by changes in the plugging meter indications) was assumed to be the saturation temperature. The difference between the observed plugging temperature and the saturation value was found to depend on the plugging temperature level but the latter was always found to be lower, e.g. a plugging temperature of 130°C corresponding to a saturation temperature of 160°C.

Between the commencement of full-power operation of D.F.R. (July 1963) and shut-down to remove the damaged breeder elements (August 1965) the plugging temperature showed a steady fall from 135°C to about 80°C. Results from chemical analysis of the coolant for oxygen and measurements on the corrosion of the niobium fuel cans confirmed the drop in oxygen content. Sample results of 5-10 ppm oxygen were obtained, and it is generally supposed that at the lower plugging temperatures the oxygen content lay in this range.

On resuming full-power operation, the plugging temperature increased during the first 48 hours' operation whilst the liquid-metal temperature was being raised; after this, it fell fairly steadily until after seven days it was about 80°C. During the initial increase the plugging meter blocked; the highest recorded temperature was 135°C. Figure 1 shows the plugging temperature behaviour during the seven-day run.

Corrosion of the niobium during this period was assessed from two elements discharged at the end of the run, and losses of up to 0.003 in. were obtained. Compared with the value expected from out-of-pile experiments in sodium at oxygen levels equivalent to the saturation temperature during the run, the corrosion was rather larger than was expected, by a factor of two or three. Furthermore, sodium sampling and chemical analysis at the start of the run suggested that the oxygen content was higher than was indicated by the plugging temperature. The discrepancy was most probably due to the presence of sodium hydroxide which had formed as a result of ingress of moisture during the operations to remove the blanket. As the temperature of the coolant was increased on resumption of the power runs, the sodium hydroxide decomposed to sodium monoxide but, until this process was complete, the oxygen content as measured by the plugging meter was lower than the true value.

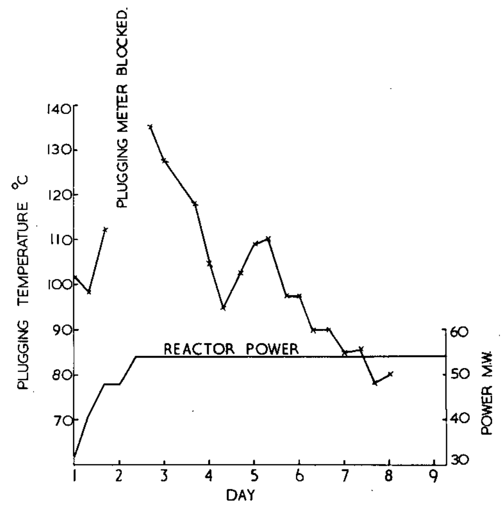

FIG. 1. Plugging-meter temperature after start up of the Dounreay Fast Reactor following removal of breeder elements

Measurements on the elements discharged after the completion of a further operational period showed that the anomalous high corrosion rate did not continue and implied that the sodium hydroxide was completely decomposed within the initial seven-day run. The plugging temperatures suggested in fact that the decomposition occurred after 48 hours, and that a very high corrosion rate existed during this period. The element cans were also embrittled; this would be expected from the presence of sodium hydroxide. The rapidity with which the coolant clean-up occurred was surprising in view of the small throughput to the cold traps; this lends further support to the belief that the uranium fuel plays a significant part in "gettering" the oxygen.

2.2 Automatic plugging meter

Whilst the manually operated cyclic plugging meter has proved to be a reliable device, provided that its limitations are recognised, there is considerable operational advantage in an automatically operated form of instrument of the type described by Delisle, [1] especially for monitoring transient conditions. Four possible modifications to the original Delisle form suggested themselves, viz.

(i) The total sample flow through the instrument should be constant and independent of flow in the loop being sampled.

(ii) To avoid regenerative (positive feed-back) effects in the cooling control system, the flow through the cooler should be constant and unaffected by the degree of plugging at the measuring orifice.

(iii) To reduce thermal lags in the cooling system, the regenerative type of heat exchanger commonly employed on plugging meters should not be used.

(iv) In case of accidental total plug, there should be an ample adjacent flow of sodium to re-dissolve the plug quickly.

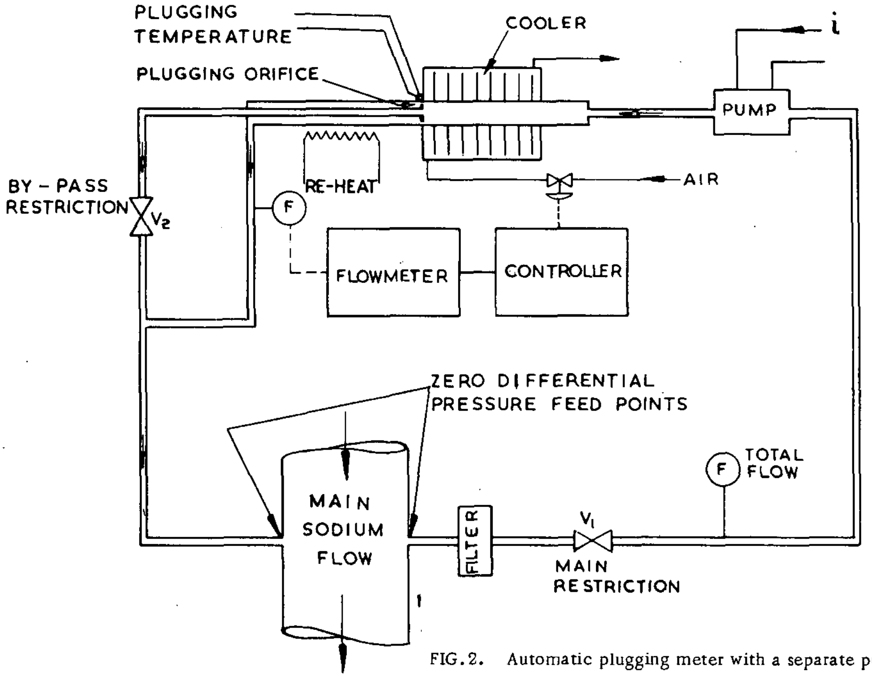

FIG.2. Automatic plugging meter with a separate pump

A design based on these premises[2] is shown in Fig. 2. A small constant-head electromagnetic pump circulates the sample through a high resistance (restriction V1) so that the total sample flow is virtually constant. After the cooler, this flow divides between two branches of low but similar resistance, namely, the plugging orifice and a fixed restriction (valve V2). The proportion of the total sample flow through either of these parallel paths is thus a measure of the flow resistance (i.e. degree of plugging) at the measuring orifice. The signal derived from an electromagnetic flowmeter in the orifice branch is used to control the air supply to a simple counter-flow cooler, and hence the temperature of the sodium at the orifice. The control system seeks (via the rate of cooling) to maintain the orifice flow at the partially-plugged value so that, at equilibrium, the sodium temperature at the orifice is that at which the rates of precipitation and re-solution of impurity are balanced and a stable partial plug exists. This orifice temperature is measured and displayed as the impurity saturation temperature.

The measuring orifice consists of twelve rectangular slots at the periphery of an annular plate (Fig. 2), one side of each flow path so formed being the internal wall of the cooler body. These slots are located at the coldest region of the cooler wall. Electrical re-heat is applied to both flow streams downstream of the cooler to prevent further precipitation of impurity, particularly at the restriction V2.

In practice, the restriction V1 is formed by reducing the throat area of the pump so that, with the circulating flow of $\frac{1}{4}$ gal/min, most of the head loss occurs in the pump itself. To avoid blockage of the pump throat and of the plugging orifices by foreign particles, a wire-mesh inlet filter is included in the instrument.

Satisfactory operation and stable control were obtained with an experimental model installed on a small (150 kg hold-up) loop. A plugging temperature range of 125-280°C was covered in a number of tests, each of several days duration, and good agreement was obtained with the prevailing cold-trap temperatures. Similar performance has also been obtained with a commercially-produced version.

The quality of the control, as might be expected, deteriorates at the lower saturation temperatures because of the decreased rate of mass transport of impurity, which reduces the effective control-loop gain. This results in an increased hunting of indicated plugging temperatures about the equilibrium value. At 125°C, this hunting is about ± 5 deg C, decreasing to about ± 1 deg C at 250°C. Nevertheless, the performance in the 125°C region of plugging temperature (equivalent to about 6 ppm of oxygen) is adequate for reactor use and for most loop purposes.

Anomalous behaviour has, however, been observed with this instrument. A new test section was added to the test loop used, and the loop operating temperature increased to 350°C from the previous 250-290°C working range. Initially, a stable plugging temperature corresponding closely with the cold-trap temperature of 150°C was obtained. This was followed by a very slow increase in indicated plugging temperature up to 300°C. After re-dissolving (with difficulty) the accumulated plug, a similar sequence occurred but with a somewhat lower final temperature. This "second" plugging temperature gradually reduced to below 200°C, and eventually became undetectable, presumably as a result of the continued cold-trapping of the disturbing impurity. With pre-knowledge of the second precipitation temperature, this could be detected, with care, by a manually operated meter.

When controlling at the second impurity temperature, it was noted that the instrument was unduly sensitive to mechanical shocks. Such shocks caused a sharp increase in orifice flow followed by a slow recovery to the controlled value. This effect was almost certainly due to part of the impurity plug breaking away from the orifice. It was also observed that the poor control performance at the second plugging temperature could be improved by reducing the value of the restriction at V2, so reducing the orifice pressure drop. This limited evidence suggests that the rates of precipitation and solution of the second impurity are much lower than those of the usual "oxide" plug and also that the physical properties of the precipitate differ from those of "oxide".

The second plugging temperature effect is similar to that described by Delisle[3] and other workers, and may well be due to hydroxide. The automatic form of instrument tends to reveal such unforeseen effects more easily than the manually operated type and so yields extra (although non-specific) information on sodium conditions and cold-trap performance. Its main virtue, however, remains its operational convenience.

2.3 Rhometer

The rhometer is now a widely known instrument for monitoring the impurity level in sodium and sodium-potassium alloy. It has not, however, found the wide application that might have been expected, and reports on its performance show considerable variations in its response to changes in impurity level. Originally a change in resistivity of 0.01% per ppm of oxygen was claimed[4] but considerable doubt has recently been cast on this value[5] and a much smaller and non-linear response has been quoted (0.0008% per ppm). It was suggested that the earlier value was due to the method of contaminating the coolant, i.e. by incremental unloading of the cold trap, which may have resulted in the presence of more than one impurity.

The installation of rhometers in the D.F.R. primary circuit and further loop studies has enabled the behaviour of this instrument to be re-assessed and its long-term behaviour studied.

2.3.1 Experience with monitoring the D.F.R. primary coolant

Two rhometers were installed in the primary coolant circuit of D.F.R. in 1962. One was installed in the cold-trap loop and one in a by-pass cold trap position. The instrument in the cold-trap loop can only be used for monitoring the reactor coolant when the loop is in operation, but the ability to isolate the loop from the main reactor circuit permits additional experimental work to be done without interfering with reactor operation.

Several series of temperature compensation runs were made on the rhometer in the cold-trap loop with the loop isolated from the reactor. These experiments and the results obtained have been fully described[6].

The main experience of continuous operation has been obtained from the rhometer installed in the bypass cold-trap position. The rate of flow through the instrument has been of the order of 5-6 gal/min (22-27 litres/min) and the liquid-metal temperature has been in the range 215-240°C. Conditions have generally been steady enough to allow the instrument to be used on its most sensitive range (± 0.2% f.s.d.). The instrument has proved stable and has given reliable indications of long-term trends.

The general pattern during a long reactor run has been that the equivalent impurity content indicated would drop from about 20 ppm near the start-up to about 8-10 ppm after the first three of four weeks. It is difficult to follow the lower part of this drop in impurity level with the plugging meter, since there is some doubt about the calibration with plugging temperatures below 100°C.

2.3.2 Out-of-pile experience

In addition to the rhometers installed in the reactor circuit a Mk IA instrument has been installed on a NaK-filled loop, and an experimental programme is being performed to study its response to various impurities and to investigate the possibility of using this instrument to study the interaction of impurities in sodium. Much of the previous work on which the calibration of the rhometer has been based has been done over a very wide range of oxygen levels, whereas under normal reactor operating conditions the oxygen level would be expected to be fairly low, certainly less than 50 ppm and most probably below 10 ppm; the present studies are confined to impurity values of this order.

The loop used in these investigations is a conventional 'figure-of-eight' circuit of 15 litres capacity in $\frac{1}{2}$ in. n.b. pipework. The rhometer is installed in the main circuit and the flow rate through it is $2\frac{1}{2}$ gal/min. Two cold traps have been fitted. The impurity level can therefore be reduced to a low value by cold trapping with one of the traps and, after isolating it from the circuit, the second cold trap can be used to control the level of the added impurity. To avoid the necessity of applying a varying temperature compensation, the rhometer temperature is maintained at (300 + 2)°C with full temperature compensation, and the rig is run under nearly isothermal conditions. The rhometer has been re-calibrated for oxygen using this system. The oxygen is added as sodium peroxide after isolating the initial clean-up cold trap. The calibration was performed by controlling the oxide level with the second cold trap, decreasing the trap temperature from 250° to 140°C.

On completion of this series of runs, the oxide in the cold trap was redissolved. An attempt to calibrate the rhometer with increasing cold-trap temperature was unsuccessful, and it appeared that there was some difficulty in redissolving the contents of the cold trap at the lower temperatures. It was therefore flushed with liquid metal at 300°C and the calibration with decreasing cold-trap temperature was repeated.

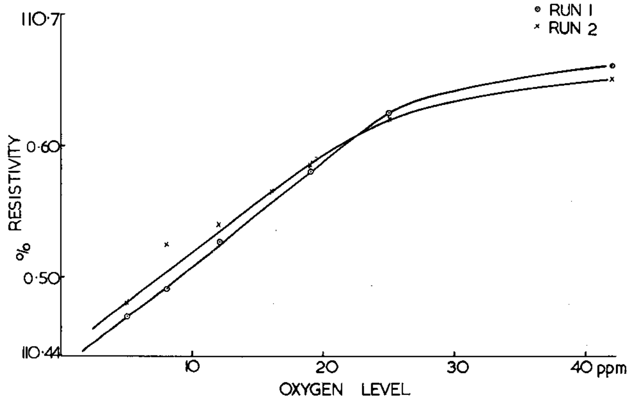

FIG. 3. Rhometer calibration for oxygen

The results from these two calibrations are compared in Fig. 3. The overall change in resistivity agrees fairly well in the two runs but there is some disagreement between the resistivity increments at the lower temperatures. The oxygen content of the NaK was determined by sampling and vacuum distillation. Between 5 and 25 ppm the resistivity change was linear and corresponded to 0.0073% per ppm. This value includes a decrease in resistivity of 0.0005% per ppm oxygen during cold trapping due to the change in NaK ratio caused by removal of sodium as sodium monoxide. The sensitivity appeared to fall off rapidly with increase in oxygen content. This may explain the low sensitivity in the earlier work[5] since this calibration was performed over a much wider range of oxygen level.

A further calibration was made by adding known quantities of sodium peroxide and measuring the change in resistivity caused by the addition. The first addition made at a cold-trap temperature of 140°C gave a resistivity change of 0.06% for 10 ppm whilst a second addition with the cold trap at 300°C gave a change of 0.04%. It is likely that in the second addition the initial oxygen content was already high but not saturated at 300°C and this may account for the lower response. After correcting for the change in NaK ratio the change in resistivity during the first addition was 0.0062% per ppm. The two techniques for oxygen calibration show reasonable agreement.

Whilst the rhometer has operated satisfactorily over long periods and reproducible results have been obtained, occasional anomalous behaviour has been observed on both the loop rhometer and one of the instruments on the reactor. On the loop there have been a number of changes in base-line and the absolute reading on the rhometer has varied by up to 4%. These changes have occurred after dumping and refilling the rig. They may be partly associated with using NaK, since addition of oxygen to the rig changes the Na:K ratio after clean-up. The change in base-line did not appear to alter the incremental change of resistivity with change in oxygen level.

Small negative excursions of the recorded trace have also been observed in one of the instruments in the reactor circuit. These are thought to be caused by mechanical movement of the head of the compensator unit. Such movement may also be a further possible cause of the base-line shift in the rhometer in the test loop.

As a result of operating with the Mk IA rhometer, an improved version (Mk II) has been designed[6]. A Mk II model has been installed on a further test loop and its performance is being assessed.

A particular study is being made of the possibility of using this rhometer to detect small leaks between the sodium and water sides of a secondary heat exchanger, and the test loop has been designed for this purpose. A preliminary experiment in which 0.5 g of water was injected into 70 kg of sodium showed considerable promise. A resistivity change of 0.1% was obtained within one minute of the injection.

2.4 Oxygen meter

The possibility of using a solid oxide electrolyte for measuring the thermodynamic activity of oxygen in sodium was first suggested by Horsley[7]. Since then, further work has been done in the U.K. with the object of setting up a thermodynamically reversible electrode system which would enable the solubility of oxygen in sodium to be determined, in a similar manner to the studies made with liquid lead and tin[8]. Such an electrode system could then be adopted for in-line measurements. Most of these experiments have been based on measurements on the cell configuration: [Me-MeO_2/ThO_2-Y_2O_3/Na_2O(sat.)-Na] where Me-MeO_2 is a reference electrode. The theoretical voltage for this system can be calculated from the standard free energy of formation of the two electrodes. Ni-NiO has been used as a reference electrode in most of the experiments but, ideally, a reference system with an e.m.f. closer to the sodium - sodium monoxide system is desirable, and other possible electrode systems are being studied. Cell voltages close to the calculated values have been obtained, but these have shown considerable instability and drift. It is thought that this may be due to a reaction between the ThO_2-Y_2O_3 electrolyte and sodium monoxide. X-ray examination showed that unidentified compounds are formed on heating ThO_2 or Y_2O_3 with sodium monoxide.

An oxygen meter based on the cell: [Cu-CuO/ThO_2-Y_2O_3/Na O-Na] has been developed by Steinmetz and Minushkin at United Nuclear Corporation, [9] and the performance of this instrument has been, and is still being, examined, particularly in the U.S.A. From the data available it appears that stable e.m.f. values can be obtained and changes in oxygen concentration can be measured. However, the e.m.f.'s produced by two oxygen meters in the same circuit and under seemingly identical conditions do not always agree in magnitude; in addition the slopes of the calibration curves of log concentration against oxygen meter e.m.f. differ. It is therefore necessary to calibrate each electrode by sampling. One of these meters has been installed on a sodium loop at the U.K.A.E.A. laboratories at Culcheth and about five months' operating experience has been obtained. [10]. The first electrode installed was examined at a steady oxygen level of 25-30 ppm with a specimen temperature of 600°C and an electrode temperature of approximately 300°C. Steady readings could not be obtained, but it is now apparent that the probe temperature was not sufficiently constant and was not known accurately enough to make the necessary corrections to the observed readings. This probe was removed from the system after a period of approximately three months because the meter was giving erratic readings, apparently due to probe failure. Examination showed no observable attack. A new probe was installed and a series of test runs was made during which oxygen levels were controlled at three levels by controlling cold-trap temperature. The probe temperature was controlled more closely and measured during these experiments. Over a period of four weeks the meter readings were plotted (after correcting for temperature deviations) against log oxygen concentration in the sodium. A straight line was obtained with a slope of 20.8 $volts^{-1}$. Alteration of cold-trap temperature produced an almost immediate response on the meter, which stabilised after approximately 6-8 hours. This indicated time for the change to be completed is considerably shorter than has previously been thought to apply, using conventional analysis.

The U.N.C. meter represents an important step in the measurement of the oxygen level in sodium but it is obvious that further improvements are required before the full value of such measurements is achieved and the true thermodynamic oxygen activity is measured.

3. PROCESS INSTRUMENTATION

The high levels of temperature and flow in the Prototype Fast Reactor create problems in process instrumentation both in the reactor itself and in the supporting experimental test loops. These require the development of sodium instrumentation techniques for use in temperature ambients of 400-650°C, and, particularly for measurements of flow in large (30 to 58 cm dia.) ducts. Some of this work is concerned with specific problems arising from the reactor layout[11] and only developments likely to be of more general interest are reviewed here.

3.1 Flow measurement in large ducts

Flow-measuring installations of the orifice plate type, especially for larger flow rates, have the advantage of a predictable calibration. The necessary measurement of differential pressure in sodium, however, presents some difficulties and local experience with NaK-filled conventional differential pressure instruments on loops fitted with orifice plates has been far from satisfactory. For this reason, an alternative method of differential pressure measurement has been sought. A promising method depends on the fact that the stalled head generated by a permanent magnet d.c. conduction pump is directly related to the energising current. A small pump and electromagnetic flowmeter are installed in series on a branch coupling the upstream and downstream taps of the orifice installation (Fig. 4A). The value of pump current to reduce the branch flow to zero may then be interpreted in terms of generated pressure (i.e. differential pressure) from the pump characteristic.

This system has been successfully applied to an existing installation. For this purpose a pump of $\frac{1}{4}$-in. throat dimensions and a 6000-gauss gap flux was used, generating a 12-ft head of sodium at 500 amps. The main difficulty experienced was in calibrating this pump in terms of stalled head. This was done using standpipes as manometer legs and inductive search coils to detect liquid-metal levels (see Fig. 4B). Temperature variations along the standpipes created difficulties, but an accuracy of pressure measurement to better than ± 3% was not too difficult to achieve.

The system, although of only moderate accuracy, gives good precision, and is reliable, self-draining and immune to both pressure and thermal shocks. By operating the branch flow at a small fixed positive value, the branch piping temperature may be maintained at a level sufficient to inhibit precipitation of impurities.

Two other methods of flow measurement in large ducts are being investigated for eventual application in the P.F.R.

The primary circuits of the P.F.R. will be totally immersed in a sodium pool at 400°C. The resulting difficulty of access, together with

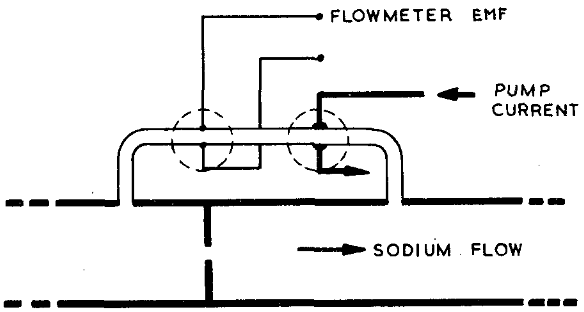

(a)PRESSURE MEASURING ARRANGEMENT

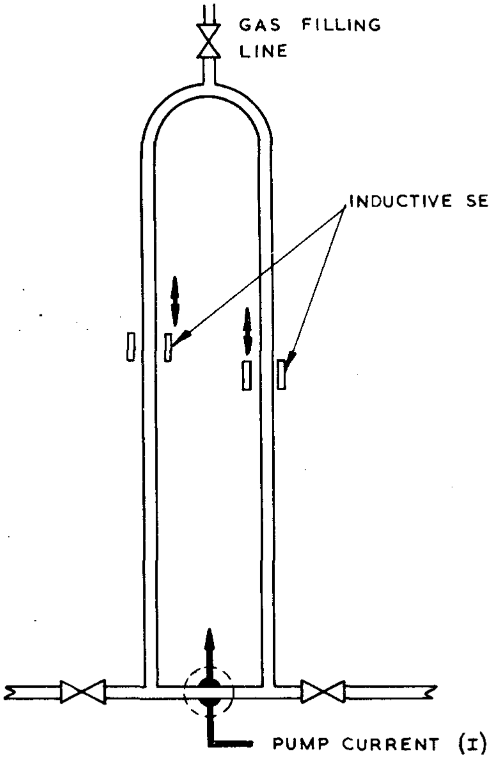

(b) CALIBRATION ARRANGEMENT

FIG.4. Sodium differential pressure measurement using D.C. pump

the short pipe runs between bends, makes the application of conventional flow-measuring techniques virtually impossible. Hence a new technique is being developed. [12] This depends on the fact that the process of heat transfer in fluid streams generates small random temperature fluctuations,i.e. thermal "noise". By measuring the transport time of the noise pattern between two thermocouples sited a few duct diameters apart, the sodium velocity, and hence the mass flow, may be deduced.

The alternating component of the thermocouple signals may be amplified, recorded and subsequently analysed by phase-angle comparison of a single frequency component.

The mean transport time of the thermal signals in the fluid is not substantially influenced by flow profile and thus is reasonable independent of piping layout. Under ideal conditions, the uncertainty of flow estimation is about ± 2%; in the practical case, uncertainties between ± 3% and ± 5% should be obtainable. The method requires elaborate terminal equipment and does not yield an immediate indication. On the other hand, it depends on a reliable and simple sensor. It can be applied to other situations (e.g. in "open" reactor cores) where conventional flow measurement techniques also present considerable difficulty.

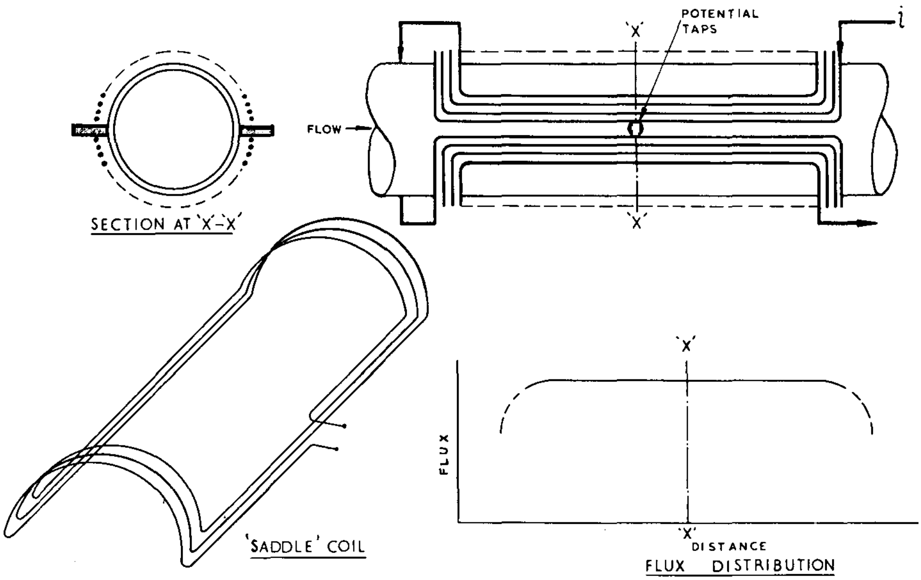

FIG. 5. Saddle coil flowmeter

The second method being investigated is primarily for the secondary circuits of the P. F. R. where access is relatively easy and straight pipe runs are available. An orthodox electromagnetic flowmeter is used, but the permanent magnet is replaced by d. c. energised coils. These coils are wound in a rectangular spiral curved into a "saddle" form (see Fig. 5) and applied to either side of the duct. They are arranged to conform to a cylindrical surface somewhat greater than that of the measured duct and can be applied outside the duct thermal lagging. By suitable choice of dimensions, the field can be made very nearly uniform across the duct and for several diameters along it. This uniform field distribution allows the calibration and corrections [13] to be predicted with reasonable certainty. Under favourable conditions, the calibration can be predicted to ± 3% but, under practical conditions, distortion of flow distribution could degrade the absolute accuracy to about ± 5% of flow. The method has several advantages, such as the ability to correct for spurious thermo-electric signals at the potential electrodes by reversal of the energising current. The principle advantage is the elimination of massive ferro-magnetic components and the associated mounting problems.

These three flow-measuring techniques have been compared on a 12-in. duct on a 6000-gal/min loop. The maximum difference observed between these three measurements was 10% of flow, i.e. within the predicted tolerance for the unfavourable application conditions prevailing.

3.2 Level measurement

Several methods of liquid level measurement have been or are being used, but the type considered to be of almost universal application is that using an inductive sensor inserted into a thimble projecting into the measured vessel. [14] The main problem is to evolve a reliable sensor of up to 5 ft in length capable of continuous operation at temperatures up to 650°C.

A sensor using refractory windings on a ceramic former and capable of operating up to 800°C has been recently described. [15] A more robust form capable of continuous operation at temperatures of at least 700°C is being developed for both reactor and loop applications. The sensor is bifilar-wound using stainless-steel-sheathed mineral-insulated cable of co-axial form. [16] These windings are brazed to a central support tube to give good electrical and mechanical stability. The coil tails may be brazed through a sealing flange to form a secondary containment without employing high-temperature electrical connections.

The power sensitivity of this arrangement is low, but this disadvantage is offset by the fact that the cables, using Nichrome conductors, have excellent high-temperature characteristics so that high energising powers can be used if required. These sensors have a mutual inductance typically of a few microhenries, changing by approximately 25% from the "dry" to the fully immersed state of the thimble at an energising frequency of 2000 c/s. Direct immersion in sodium of the coil system gives a change in mutual inductance approximately three times as great as that when inserted in a pocket. Measurements indicate that linearities within $\frac{1}{2}$% can be achieved over the central 90% of active coil length. A programme of measurements on a calibrating rig is proceeding with the object of producing data to allow the calibration and end-effects to be predicted to an acceptable accuracy, to avoid the need for individual calibrations.

A similar construction has been used for mechanically-traversed short search coils used for detecting small changes in sodium levels.

3.3 Displacement measurement

The drive shafts of the mechanical pumps to be used for P.F.R. will have their lower journal bearings lubricated with sodium. Tests on a 6000 gal/min model pump has required the relative displacement of the shaft in the sodium bearing to be monitored so that the bearing performance could be studied at various speeds and loads. For this purpose a simple inductive transducer has been developed to measure clearance in the range $0-\frac{1}{2}$ mm (see Fig. 6). Four such transducers are mounted in opposing pairs on normal diagonals and supported from the bearing housing. A ferro-magnetic collar is mounted on the pump shaft immediately below the bearing, and the gap between this collar and the transducers is measured (via self-induction changes) as a function of the bearing clearance. The measurements derived at this point may be combined and displayed on a cathode ray tube to give shaft eccentricity and "swash". Each pair of transducers make adjacent arms of an 800 c/s bridge circuit so that the effect of temperature fluctuations on the inductive sensors and their connecting cables is greatly reduced.

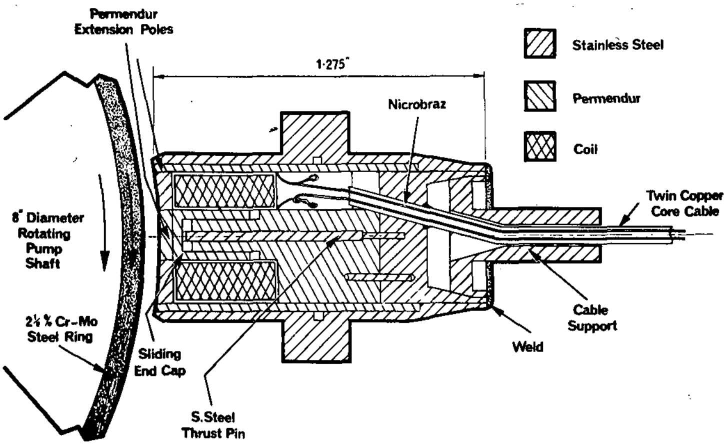

FIG. 6. Bearing clearance transducer

Satisfactory operation has been obtained with these units immersed in sodium at 400°C and in the presence of considerable mechanical vibration for periods exceeding 3000 hours. The construction techniques used have been described elsewhere. [17]

3.4 Temperature measurement

Most temperature measurements on loops are made by Chromel-Alumel thermocouples immersed in pockets, and no special difficulties arise. Sheath corrosion tests on stainless-steel thermocouples directly immersed in sodium flowing at 15 ft/sec at 650°C are proceeding as part of the work to establish the reliability of such thermocouples monitoring channel outlet temperatures above the P.F.R. core. Operation of directly immersed stainless-steel-sheathed mineral-insulated cables down to 0.5-mm dia. at 400°C have given no trouble over a period of several months.

An investigation is proceeding in the out-of-pile calibration stability of Chromel/Alumel thermocouples in the range 500-825°C. For lower temperatures, i.e. up to about 400°C it has been found possible to reduce base-metal thermocouple errors to about $\pm \frac{1}{2}$ deg C by employing suitable preliminary heat treatment and calibration techniques.

The response speeds of thermocouples immersed in flowing sodium in the temperature range 230-370°C have been measured by a technique based on observing the response of the thermocouple to the random thermal noise present in the sodium[18]. It has been shown that the mean dynamic responses of 3-, 1.5-and 1-mm diameter cables directly immersed in flowing sodium are about 700, 150 and 80 m/s respectively. These responses were found not to vary significantly with temperature, and were similar to those measured in flowing water.

3.5 Leakage detection

The detection of sodium leaks usually presents problems and no universal solution seems available. With apparatus contained in an inert atmosphere, simple detectors of the sparking-plug type can indicate quite reliably the presence of liquid metal at suitable collecting points. Most loops, however, operate in air and with lagged pipes, and a leak in a high-temperature region usually results in a concealed fire with release of smoke in varying quantities.

For this particular problem, an instrument depending on the optical absorption by sodium vapour or the scattering by smoke of a light beam from a low-pressure sodium lamp is presently used (Fig. 7). The detecting beam traverses a 20-in. path through the atmosphere of the loop containment. The limiting bulk sensitivities to sodium vapour and smoke are nominally 75×10^{-6} and 1.5×10^{-3} g/m^3 respectively. A reference beam path and a white-light source are used as a self-

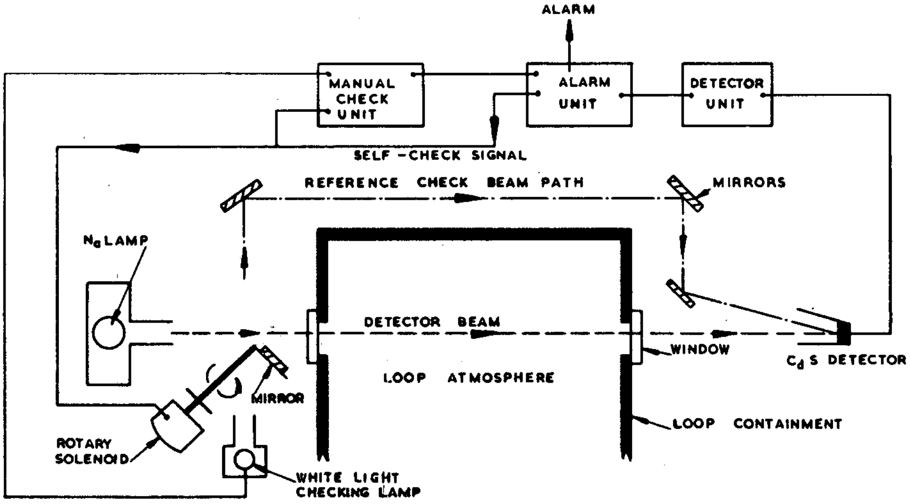

FIG.7. Optical sodium vapour/smoke detector

checking system to differentiate between the presence of vapour and smoke in the measured path and the existence of instrument faults when the alarm circuit is activated.

As an instrument, this equipment functions reliably and well. Its main defect is that it is only of good sensitivity and response speed for leaks in the immediate vicinity of the detecting beam. With a large or complex sodium circuit, many instruments must be used to give satisfactory coverage.

An alternative method being examined is to use a flame photometer, which has an inherent detection limit of the order of 10×10^{-6} g/m^3 for sodium in the form of either vapour or smoke, but yet is insensitive to smoke and vapours arising from external contamination on newly heated sodium installations. It would allow sampling from several points in an installation, and so allow satisfactory and economic coverage from a single instrument. Work to determine the fate of sodium smoke particles in a long sampling line is proceeding.

REFERENCES

[1] DELISLE, J.P., Mesure automatique de la temperature de bouchage du sodium et du NaK , (1963) USAEC Translation TR-6353 .

[2] ROACH, P.F., DAVIDSON, D.F., UK Pat. App. No. 43659/64.

[3] DELISLE, J.P.,(AEC, Caderache, France), Private communication.

[4] BLAKE, L.R., Resistivity monitor to indicate oxide content of sodium , Institution of Electrical Engineers, Proc. A 107 (1960) 383.

[5] ATOMIC POWER DEVELOPMENT ASSOCIATES, Operation of the sodium technology loop for contamination meter evaluation , USAEC Report APDA 163.

[6] DEHN, R., EAMES, A.R., The rhometer. A continuous impurity monitor for liquid metal circuits , Radio & Electronic Eng. 29 (6th June 1965).

[7] HORSLEY, G.W., A possible galvanic cell method for monitoring the activity of oxygen in a hot trapped sodium coolant circuit , UKAEA Report AERE R3037 (1961).

[8] BELFORD, T.N., ALCOCK, C.B., Thermodynamics and solubility of oxygen in liquid metals from e.m.f. measurements,
Pt. I Lead, Trans Farad Soc. (1964) 60 822
Pt. II Tin, Trans Farad Soc. (1965) 61 443.

[9] MINUSHKIN, B., Liquid metal oxygen meter, UNC SPLM 61 (1965).

[10] THORLEY, A., (Reactor Materials Laboratory, UKAEA), Private communication.

[11] EVANS, P.B.F., et al., Control and instrumentation of the prototype fast reactor , Proc. London Conf. on Fast Breeder Reactor P.5A/5 (1966).

[12] BENTLEY, P.G., DAWSON, D.G., Fluid flow measurement by transit time analysis of temperature fluctuations , Trans. Soc. Inst. Tech. 18 3 (Sept. 1966) 183.

[13] SHERCLIFFE, J.A., The Theory of electromagnetic flow-measurement , Camb. Univ. Press (1962).

[14] DAVIDSON, D.F., Measurement of liquid metal levels by the effects of eddy currents on an inductance , UKAEA Report IGR-R/CA-255 (1957).

[15] JOHNSON, T.R., TRATS, F.G., PIERCE, R.D., An induction probe for measuring liquid levels in liquid metals , ANL 7153 (1966).

[16] PETTINGER, D.S., DUNCOMBE, E., HARRISON, E., U.K. Pat. App. No. 20222/64.

[17] DAVIDSON, D.F., DUNCOMBE, E., Some transducer techniques for use at elevated temperatures , Trans. Soc. Inst. Tech. 18 2 (1966) 51.

[18] BENTLEY, P.G., ROWLEY, R., Measurement of the dynamic characteristics of mineral-insulated cables in flowing sodium by analysing their response to random temperature fluctuations , UKAEA TRG Report 1259 (R) (To be issued).

DISCUSSION

J.P. LE JANNOU: I have a question in connection with the plugging meter. We have always had trouble whenever we have used an electromagnetic pump only with this device, and we now use a constant-level feed which provides a completely stable flow. What kind of stability do you get with your device?

E. DUNCOMBE: We use a DC pump with a high-flow resistance at the throat of the pump to obtain a constant-flow system. The pump is supplied from an unstabilized rectified mains supply. We have had no trouble so far with this method, which does away with the need for flow-ratio measurement.

E. CAMBILLARD: Can you tell me what provision has been made to compensate for temperature effects with your induction level indicator? In our case we calculated the exit signal of our continuous induction level indicator. On the basis of these calculations we were able to determine calibration curves as a function of temperature and thus provide for a suitable compensation system.

E. DUNCOMBE: We have not actually measured these effects yet but we shall shortly be obtaining performance data, including data on temperature effects, relating to the diameters of the sensors and thimbles that will be used in the PFR reactor.

E. CAMBILLARD: What is the response time of the flowmeter based on an analysis of the transit time of the temperature fluctuations?

E. DUNCOMBE: This depends on the signal level and the quality of correlation. In the case of a high-level signal and a good system, the interaction time is only a few minutes. In a bad system, it could be as much as several hours.

E. CAMBILLARD: Do you intend to calibrate the electromagnetic flowmeter designed for the secondary circuits of the PFR on a sodium loop or do you think you will be able to set up a magnetic field which is uniform enough to enable you to calculate the EMF-flow constant?

E. DUNCOMBE: One of the purposes of this flowmeter design is to enable us to perform the calibration with a fair degree of certainty and we intend to do this.

N. LIONS: With what sensitivity can flow measurements be made with your diaphragm bypass system of electromagnetic pump and flowmeter?

E. DUNCOMBE: In our present installation we can measure the head with an accuracy of ± 3%. The reason for this poor figure is that temperature control of the calibrating standpipes is difficult to achieve. However, if the design of the system is improved, there is no reason why it should not be possible to obtain long-term calibration with an accuracy of 1-2% of pressure (equivalent of $\frac{1}{2}$-1% of flow). Our experience with DC pumps indicates that these are particularly stable devices.

E. CAMBILLARD: From your experience with the Dounreay reactor have you any information on how flowmeter magnets stand up to gamma radiation?

E. DUNCOMBE: We have not carried out any actual experiments but we do not expect any difficulties in connection with radiation effects on permanent magnets. Work in the United States of America indicates that such effects are very small with "hard" magnetic materials. I wonder whether Mr. Davies has any comments on this.

R.A. DAVIES: We have not encountered any difficulties with the magnetic flowmeters at the Dounreay Fast Reactor.

INSTRUMENTATION DES CIRCUITS DE SODIUM

E. CAMBILLARD
CEA, CENTRE D'ETUDES NUCLEAIRES DE
FONTENAY-AUX-ROSES
ET
N. LIONS
CEA, CENTRE D'ETUDES NUCLEAIRES DE
CADARACHE, FRANCE

Abstract — Résumé

INSTRUMENTATION FOR SODIUM CIRCUITS. Electromagnetic flow meters, level gauges and differential pressure gauges are among the main measurement instruments designed and tested at the Commissariat à l'Energie Atomique (CEA) for sodium reactors.

The main characteristics of the flow meters used with RAPSODIE are indicated. The instruments used in this connection are of the permanent-magnet or electromagnet type (in the primary circuits). A description is given of the calibration methods employed – use is made of diaphragms or Venturi tubes as standard flow meters – and information is given on the results measured for maximum sodium flows of 400 m^3/h.

Three types of continuous level gauge have been studied.

Resistance gauge. Two varieties used for the 1- and 10-MW test circuits of RAPSODIE are described. In one there is a compensation resistance along the whole height of the measuring element (the continuous gauges used with the RAPSODIE reactor are at present of this type). In the other type of gauge a device is incorporated to heat the measurement element and prevent the formation of conducting deposits (prototype sodium tests have been completed).

Induction gauge. This type has two coupled coils and is fitted with a device to compensate for temperature effects. A description is given of a prototype which has been built and the results obtained in the course of sodium tests are described.

Ultrasonic gauge. With this type, a transmitter is fitted on top of the outside of the sodium container; there is also a vertical wave guide, the bottom of which is immersed in the liquid metal and possesses a reflector system which returns the ultrasonic beam towards the surface. Fixed reference marks provide a permanent means of calibration and the whole apparatus is welded. This type of gauge is now being constructed.

The differential pressure gauges that have been built, and used in particular with Venturi tube flow meters, are modified versions of the devices employed with the 1- and 10-MW test circuits of RAPSODIE. A description is given of the modifications carried out in connection with the mechanical zero adjustment and the measurement chain.

INSTRUMENTATION DES CIRCUITS DE SODIUM. Les instruments de mesure qui ont été principalement étudiés et expérimentés au CEA pour les réacteurs à sodium comportent des débitmètres électromagnétiques, des indicateurs de niveau et des manomètres différentiels.

Les auteurs donnent les caractéristiques principales des débitmètres du réacteur RAPSODIE, qui sont à aimant permanent ou à électro-aimant (sur les circuits primaires). Ils décrivent les méthodes d'étalonnage utilisées qui font appel à des diaphragmes ou des venturis comme débitmètres étalons et indiquent les résultats de mesure obtenus pour des débits de sodium maximaux de 400 m^3/h.

Trois types d'indicateurs continus de niveau ont été étudiés:

Indicateur à résistance. Les auteurs décrivent deux variantes équipant les circuits d'essai de RAPSODIE de 1 et 10 MW. L'une comporte une résistance de compensation disposée sur toute la hauteur de l'élément de mesure (les indicateurs continus du réacteur RAPSODIE sont actuellement de ce type). L'autre possède un dispositif permettant le chauffage de l'élément de mesure en vue d'empêcher la formation éventuelle de dépôts conducteurs (les essais en sodium de prototypes sont terminés).

Indicateur à induction. *Il comprend deux bobines couplées et un dispositif permettant une* compensation des effets de température. Les auteurs décrivent le prototype qui a été construit et indiquent les résultats obtenus au cours des essais en sodium.

Indicateur à ultra-sons. Il est caractérisé par l'utilisation d'un transmetteur placé en haut et à l'extérieur de la cuve de sodium, et d'un guide d'ondes vertical dont l'extrémité inférieure plongeant dans le métal liquide possède un système réfléchissant qui renvoie le faisceau ultra-sonore vers la surface. Des repères fixes permettent un étalonnage permanent; l'ensemble de l'appareil est entièrement soudé. Cet indicateur est en cours de réalisation.

Les manomètres différentiels actuellement construits et qui ont servi en particulier sur des débitmètres à venturi sont des versions modifiées des appareils équipant les circuits d'essais de RAPSODIE de 1 et 10 MW. Les auteurs décrivent les modifications qui ont porté sur le réglage mécanique du zéro et sur la chaîne de mesure.

L'instrumentation des circuits de sodium pour les réacteurs nucléaires pose des problèmes encore incomplètement résolus. Pour les installations d'essai de Rapsodie, puis pour le réacteur lui-même, nous nous sommes attachés, au cours des années écoulées, à développer des appareils de mesure de débit, de niveau, et de pression, dont les principes et les premiers résultats de fonctionnement ont été décrits dans des communications antérieures [1] [2] [3] .

On expose ici les caractéristiques des derniers appareils réalisés en insistant sur les méthodes d'étalonnage et la précision obtenue.

MESURES DE DEBIT

Sur le réacteur Rapsodie, ainsi que sur les installations d'essai préalables, les débits de sodium sont mesurés à l'aide de débitmètres électromagnétiques [1] [3] , dont le principe, bien connu, repose sur l'induction d'une force électromotrice dans un conducteur électrique (sodium) qui se déplace dans un champ magnétique.

Pour les circuits du réacteur, on a voulu obtenir des mesures aussi précises que possible, pour qu'elles puissent servir à établir des bilans énergétiques. Dans ce but, on a veillé dans la conception des appareils (figures 1 et 2) à éviter toute cause de perturbation ou d'incertitude dans les mesures, en particulier :

- Les électrodes de mesure sont constituées d'acier inoxydable de même nuance que la canalisation, pour diminuer la force électromotrice thermoélectrique, aux soudures de raccordement [1] .

- Les pièces polaires sont protégées par du calorifuge pour diminuer la température des aimants, et éviter l'évolution corrélative du champ [1] .

- Les débitmètres des circuits principaux, primaires et secondaires, sont munis chacun de trois paires d'électrodes, constituant trois voies de mesure indépendantes.

- Pour assurer une bonne fidélité aux mesures au cours de l'exploitation du réacteur, il a paru essentiel de pouvoir vérifier la permanence de la valeur du champ magnétique, ou d'en mesurer la nouvelle valeur pour corriger la constante d'étalonnage. Les circuits secondaires étant accessibles en marche, le contrôle périodique du champ magnétique dans l'entrefer des débitmètres est possible. Par contre, ces contrôles ne pourront pas être faits sur les débitmètres des circuits primaires, par suite du rayonnement ambiant. C'est pourquoi sur ces circuits des débitmètres à électro-aimant alimenté en courant continu ont été placés en série avec les débitmètres à aimants permanents. Le courant d'excitation est stabilisé à 1 % près, sa valeur étant telle que la culasse se trouve au début de la saturation, le champ magnétique est déterminé avec une précision meilleure que le pour cent. Les bobines des électro-aimants sont fabriquées avec du fil d'aluminium oxydé anodiquement et imprégnées de vernis silicone pour obtenir un isolement qui résiste aux rayonnements gamma émis par le sodium.

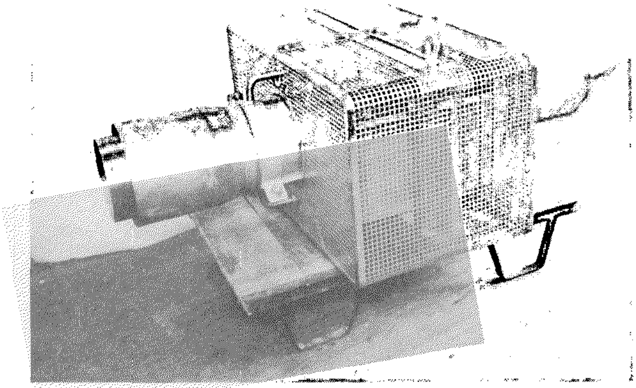

FIG.1. Débitmètre de 200 mm de diamètre à aimants permanents avec double enveloppe

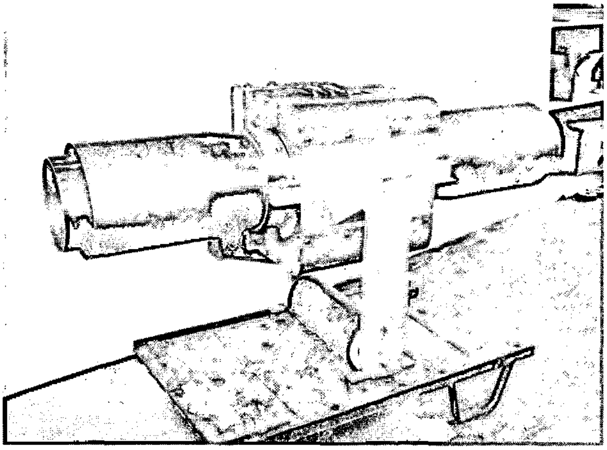

FIG.2. Débitmètre de 200 mm de diamètre à électro-aimant avec double enveloppe

-Tous les débitmètres utilisés sur le réacteur Rapsodie ont subi un étalonnage préalable, les plus petits par mesure directe, les plus gros par comparaison à des appareils déprimogènes.

L'étalonnage direct a été utilisé jusqu'à un diamètre de canalisation de 50 mm (débits inférieurs à 15 m3/h). Le sodium, mis en circulation par une pompe électromagnétique, est transféré d'un réservoir de stockage dans un autre réservoir monté sur une bascule. Le temps de passage est mesuré au chronomètre. La précision obtenue est de l'ordre de ± 2 %.

Les débitmètres d'un diamètre de 50 à 100 mm ont été étalonnés jusqu'à des débits de 100 m3/h sur un circuit comportant trois appareils étalons montés sur deux tuyauteries en parallèle : une tuyauterie de 100 mm équipée d'un venturi et une tuyauterie de 50 mm équipée d'un venturi et d'un débitmètre électromagnétique de référence.

Les mesures de pressions différentielles (pour les venturis) étaient effectuées avec l'appareil décrit plus loin. Les venturis ont été préalablement vérifiés par des essais à l'eau, en similitude de Reynolds ; les résultats d'essais concordent à 1 % près avec les valeurs calculées d'après la norme AFNOR [4].
Le débitmètre électromagnétique de référence avait été étalonné par pesée comme indiqué plus haut. Enfin, on a vérifié que les mesures obtenues par le débitmètre électromagnétique et le venturi montés en série comme indiqué ci-dessus concordaient à ± 2 % près. Les recoupements effectués grâce aux trois appareils de référence ont permis un étalonnage à ± 3,5 % près.

Enfin, les débitmètres des circuits principaux de Rapsodie, d'un diamètre intérieur de 200 mm, ont été étalonnés sur le circuit de sodium construit pour les essais de réception des pompes du réacteur. On a utilisé comme étalon un diaphragme dont les performances calculées ont été préalablement vérifiées à l'eau (écart maximal de 2,5 % avec le calcul). Les mesures de pression différentielle en sodium (sur le diaphragme) étaient effectuées par un manomètre à colonnes de sodium, de 3 mètres de hauteur, constitué par un tube de 100 mm de diamètre placé à l'intérieur d'une chambre cylindrique de 300 mm de diamètre ; des électrodes de niveau donnaient la pression différentielle à ± 0,5 % près au débit nominal de 400 m3/h. Les courbes d'étalonnage ont été obtenues avec une incertitude globale de ± 3,5 %.

La figure 1 montre la photographie d'un débitmètre primaire à aimants permanents. Le diamètre intérieur de la canalisation est de 200 mm. On remarque la double enveloppe qui existe sur l'ensemble des circuits primaires et qui est destinée à canaliser le gaz de préchauffage et à jouer éventuellement un rôle de sécurité. Le capot en tôle d'acier inoxydable ajourée est destiné à protéger les aimants au cours de la manutention et du montage des débitmètres.

La figure 2 donne la photographie d'un débitmètre primaire à électro-aimant. On distingue les trois paires d'électrodes qui aboutissent aux boîtes à bornes.

On notera sur ces photographies la robustesse des appareils.

MESURES DE NIVEAU

Nous n'abordons ici que le problème des indicateurs continus : les indicateurs discontinus à résistance installés sur les circuits de Rapsodie ont été décrits antérieurement et les mêmes appareils ont été utilisés pour Rapsodie. Les indicateurs continus qui ont été mis au point ou qui sont en cours d'étude sont de trois types : à résistance, à induction et à ultra-sons.

Indicateurs continus à résistance

Le principe de fonctionnement est le suivant (figure 3) : un tube d'acier inoxydable est plus ou moins immergé dans le sodium, suivant la position du niveau. On mesure la différence de potentiel définie par la résistance de la partie émergente du tube qui, en première approximation, est fonction linéaire du niveau. Le tube et son support constituent une enceinte étanche contenant les fils d'amenée de courant et les fils de mesure. En fait, la résistance de mesure varie évidemment avec la température : aussi le circuit d'alimentation comprend-il une résistance de compensation, grande par rapport à celle de mesure, destinée à diminuer autant que possible les effets de température. L'indicateur est alimenté sous une tension continue stabilisée.

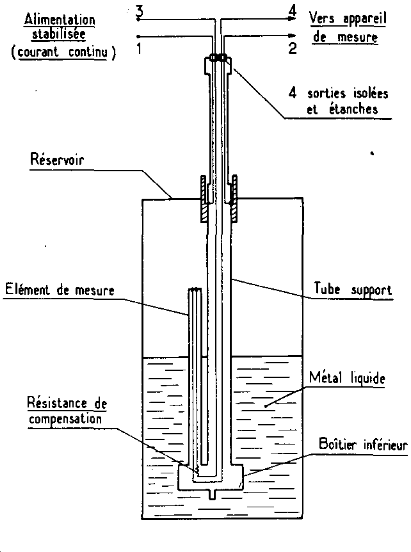

FIG.3. Indicateur continu de niveau à résistance - Schéma de principe

A la suite des essais des premiers prototypes [2] [3], les observations qui sont résumées ci-après ont conduit à des améliorations pratiques de réalisation :

- Pour des appareils de grande longueur (jusqu'à 3,20 m de longueur utile pour Rapsodie), le tube de mesure ne pouvait pas offrir une tenue mécanique suffisante. Pour rigidifier l'appareil, on a été conduit à une réalisation telle que représentée sur la figure 4.

-La résistance de compensation était initialement placée dans le boîtier inférieur de l'appareil et ne donnait qu'une compensation insuffisante : la résistance restait à la température du sodium, même quand l'élément de mesure était peu immergé et se trouvait donc à une température inférieure (courbe 3 de la figure 5). On a amélioré les résultats en enroulant la résistance autour du tube support comme indiqué sur la figure 4. La courbe d'étalonnage est alors la courbe 2 de la figure 5.

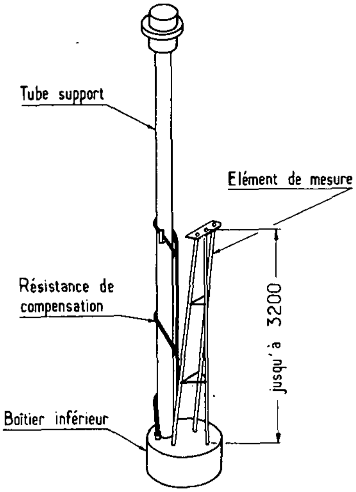

FIG.4. Indicateur continu de niveau avec élément de mesure en trépied

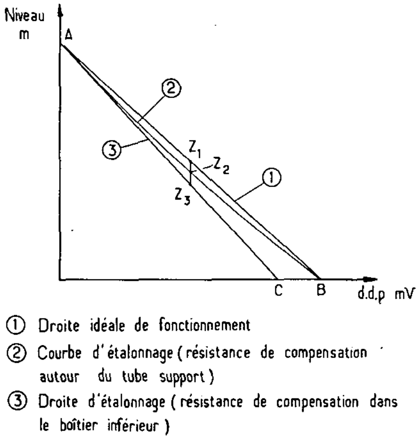

FIG.5. Indicateurs continus de niveau à résistance: courbes d'étalonnage

Cette courbe n'est plus linéaire, contrairement à la courbe 3 précédente. Mais son avantage est que le point B peut être obtenu par une mesure à froid, sans sodium : la courbe de fonctionnement peut donc être tracée en première approximation sans étalonnage en sodium, l'écart Z_1 Z_2 entre les courbes 1 et 2 ne dépassant jamais 1,5 % de la longueur de

l'élément de mesure, soit ± 5 cm au maximum pour les appareils de Rapsodie. Sur Rapsodie, un tracé exact de la courbe d'étalonnage est d'ailleurs obtenu grâce aux indicateurs de niveau discontinus, qui permettent de déterminer deux points à des niveaux connus.
La sensibilité de la mesure est de l'ordre de 140 µV/cm.

-Le fonctionnement des premiers prototypes a été perturbé par des dépôts de sodium plus ou moins oxydé sur l'élément de mesure, qui formaient une couche conductrice et modifiait la résistance.

Pour les appareils de Rapsodie, on a prévu d'y remédier, si besoin est, en élevant périodiquement le niveau de sodium pour dissoudre les dépôts. L'efficacité de cette méthode a été vérifiée expérimentalement.

Depuis, on a mis au point des appareils munis d'un chauffage interne évitant les dépôts de vapeur de sodium sur la partie émergente. Deux thermocouples différentiels montés, l'un dans le boîtier inférieur, l'autre en haut de l'élément de mesure, servent à réguler la puissance de chauffage. Grâce à ce dispositif, l'élément de mesure est pratiquement isotherme et la résistance de compensation peut être placée à la base de l'appareil, tout en donnant une compensation théoriquement parfaite. La courbe d'étalonnage est linéaire.

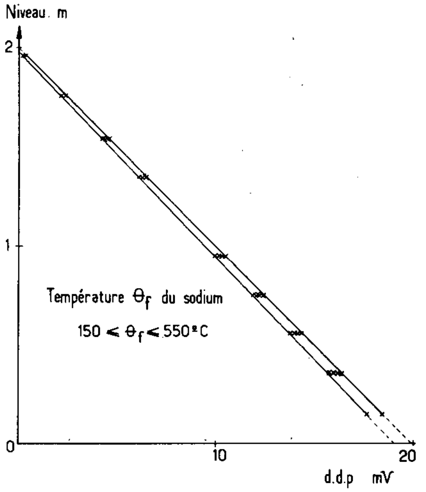

FIG. 6. Indicateur continu de niveau à résistance chauffé: droites d'étalonnage

Les résultats obtenus sont représentés sur la figure 6, pour des températures de sodium variant de 150 à 550° C. Pour un niveau voisin du milieu de l'appareil, soit un niveau de 1 m, l'utilisation d'une courbe moyenne donne une erreur de ± 2,5 cm.

Indicateurs continus à induction

Des indicateurs continus de niveau à bobines couplées ont été étudiés pour Rapsodie afin de disposer d'appareils aisément démontables et peu encombrants. En effet, ces appareils se logent dans un fourreau étanche dont le diamètre extérieur ne dépasse pas 40 mm et d'où ils peuvent être facilement extraits. Un prototype a été essayé et a donné des résultats satisfaisants. Les appareils destinés à Rapsodie seront mis en place au cours de l'année 1967.

Les deux bobines couplées sont disposées dans un fourreau métallique plongeant verticalement dans le sodium et soudé sur le couvercle du réservoir (figure 7). Les bobines sont constituées de fil d'aluminium oxydé pour permettre une utilisation à 550° C. La bobine primaire est alimentée en courant constant à une fréquence de plusieurs kHz. La f.e.m. induite dans la bobine secondaire est fonction du niveau de sodium. La courbe d'étalonnage niveau-f.e.m. induite, est pratiquement une droite.

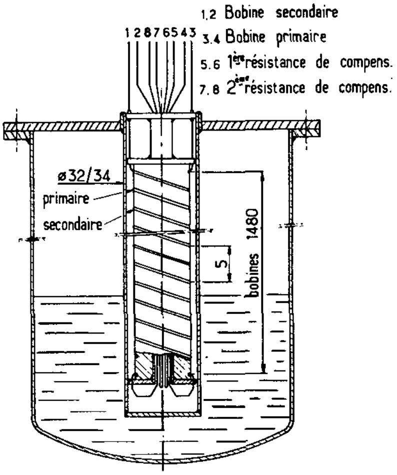

FIG. 7. Indicateur à bobines couplées

On doit utiliser un appareil de mesure à impédance élevée pour s'affranchir des variations de résistance de la bobine secondaire avec la température. Toutefois la courbe d'étalonnage dépend de la température, par l'intermédiaire des résistivités du sodium et du métal du fourreau.

Pratiquement, les variations de la pente et du signal mesuré sont des fonctions linéaires de la température (figure 8).

La compensation de ces effets a été obtenue en deux étapes [5] :

- Un amplificateur dont le gain varie avec la température par l'intermédiaire d'une résistance placée à l'intérieur du fourreau permet de rendre parallèles entre elles les différentes droites d'étalonnage.

- Pour superposer la droite d'étalonnage obtenue à une température θ à celle correspondant à une température de référence θ_0, un pont de résistances dont l'une d'elles est placée dans le fourreau ajoute ou retranche au signal une tension proportionnelle à la différence $\theta-\theta_0$.

Ces deux dispositifs permettent une compensation complète des effets de température (figure 9). L'erreur commise avec un appareil de 1,50 m de longueur n'est plus que de ± 2 cm au lieu de ± 12 cm (figure 8).

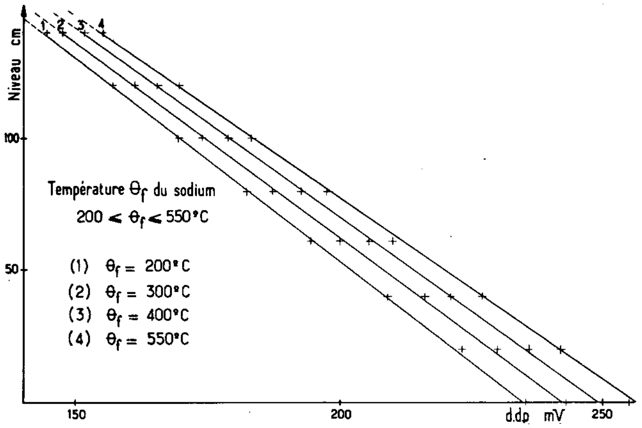

FIG. 8. Indicateur à bobines couplées: droites d'étalonnage sans compensation de température

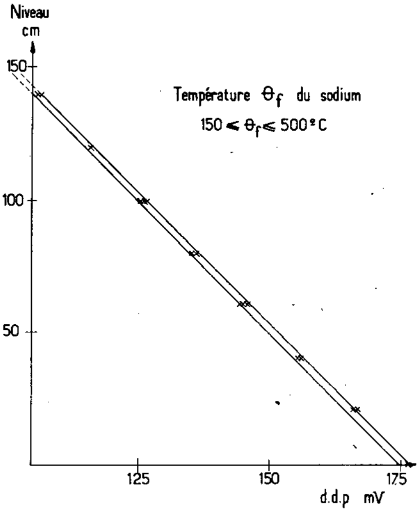

FIG. 9. Indicateur à bobines couplées: droites d'étalonnage avec compensation de température

Indicateurs continus à ultra-sons

L'indicateur de niveau continu à ultra-sons (figure 10) [6]. comporte :

- un émetteur-récepteur ultra-sonore placé à l'extérieur du réservoir de métal liquide,

- un guide d'ondes vertical en forme de tube placé en regard du transmetteur, rempli de sodium-potassium, et fermé par des disques d'extrémité d'épaisseur égale à une demi-longueur d'onde,

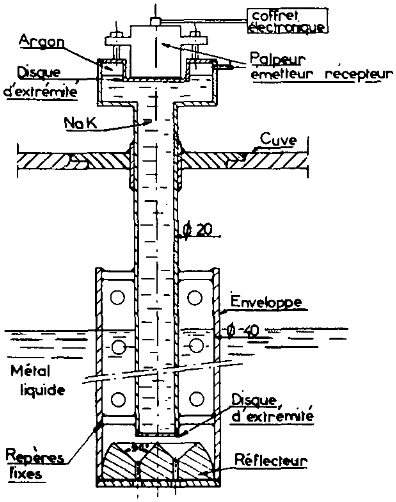

FIG. 10. Indicateur continu de niveau à ultra-sons

- un réflecteur de forme conique, placé dans le métal liquide à l'extrémité inférieure du guide d'ondes et qui réfléchit le train d'ondes en direction de la surface libre. Une enveloppe coaxiale au guide d'ondes tranquillise la surface du métal liquide.

Un appareillage électronique associé permet de connaître le niveau par mesure de l'intervalle de temps compris entre l'émission et la réception d'un train d'ondes allant se réfléchir sur la surface du sodium.

L'appareil est actuellement en cours d'essai à l'eau et l'étude n'est pas suffisamment avancée pour permettre une discussion complète sur les avantages et les inconvénients de ce système.
On peut toutefois signaler que les parties immergées sont simples et présentent des risques de panne très réduits : le palpeur est accessible et peut être facilement contrôlé et remplacé.

MESURE DE PRESSION

Des manomètres différentiels ont été utilisés plus particulièrement sur des venturis, comme il a été indiqué précédemment. Ces appareils sont des variantes de ceux mis au point pour les circuits d'essai de Rapsodie [1] [3] . Les modifications portent sur le réglage mécanique du zéro, l'amélioration de la chaîne de mesure et l'incorporation dans le capteur d'une vanne de liaison entre les chambres haute et basse pression.

Le capteur de pression et le détecteur de force sont représentés sur la figure 11. Le principe de fonctionnement est le suivant : la pression différentielle s'exerce sur le disque auquel est soudé le soufflet 3. L'effort de traction qui en résulte est transmis par une tige au détecteur de force.

On a ajouté au montage initial un ressort placé comme indiqué sur la figure 11. Le but de ce ressort est d'exercer une force de traction constante en l'absence de toute force de pression et de déterminer ainsi avec précision une position zéro.

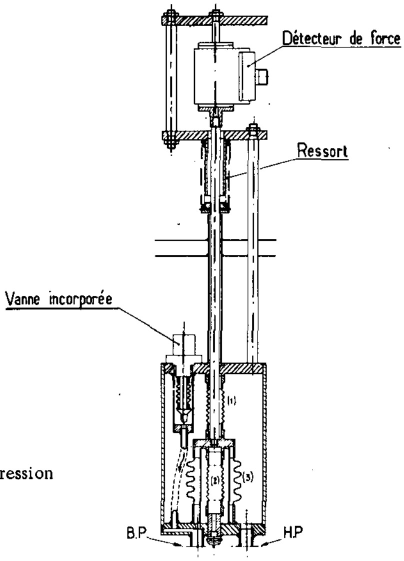

FIG. 11. Manomètre différentiel – Schéma du capteur de pression

La présence du ressort n'a par ailleurs d'autre effet que de modifier la pente de la droite d'étalonnage.

En ce qui concerne la chaîne de mesure, deux modèles de détecteur de force ont été utilisés :

- l'un est composé d'un ressort dynamométrique et d'un transformateur différentiel,

- l'autre est constitué de deux membranes et d'un détecteur inductif utilisant la variation du coefficient de self-induction de deux bobines.

Le détecteur inductif présente l'avantage d'être suivi par un amplificateur dont le gain réglable permet d'obtenir sur l'appareil de mesure la déviation complète pour plusieurs gammes de force. Toutefois, le zéro du système électronique doit être vérifié périodiquement, ce qui nécessite l'arrêt du fonctionnement de l'appareil.

Enfin, on a muni l'appareil d'une petite vanne incorporée qui permet de faire circuler le sodium entre les chambres haute et basse pression (figure 11). On peut ainsi facilement purger l'appareil du gaz emprisonné au moment du remplissage. Cette circulation de sodium peut également être utilisée pour éliminer les dépôts éventuels d'oxydes risquant de boucher les canalisations. Toutefois, avant d'entreprendre de nouvelles mesures après une telle opération, il est important de s'assurer que le capteur est bien isotherme : sa température nominale de fonctionnement est de 300° C.

L'étalonnage de ces appareils a conduit aux précisions suivantes :

- avec le système de mesure inductif : ± 1 % entre 0,5 et 5 bars
  ± 2 % entre 0,25 et 0,5 bar
- avec le système à transformateur différentiel : ± 1,3% entre 1 et 5 bars.

CONCLUSION

On a présenté l'état de notre technique concernant les appareils de mesure à sodium en insistant sur les derniers perfectionnements, sur l'étalonnage et sur les précisions obtenues :

- 2 à 3,5 % pour des débitmètres électromagnétiques de diamètre jusqu'à 200 mm,
- ± 2 à 2,5 cm pour des appareils de mesure de niveau à résistance ou à inductance de 1,50 m à 2 m de long environ,
- ± 1 à 2 % pour des appareils de mesure de pression différentielle dans la gamme de 1 à 5 bars.

REFERENCES

[1] VAUTREY, L., ZALESKI, C.P., "Expériences préliminaires à la construction du réacteur RAPSODIE", Power Reactor Experiments I, IAEA, Vienna (1962) 369.

[2] DELISLE, J.P. et al., Bilan expérimental de certaines installations d'essais pour RAPSODIE, C.r. 8^{e} Congrès nucléaire de Rome, Symposium sur les réacteurs rapides, 17-19 juin 1963 (organisé par le Comitato nazionale per l'energia nucleare).

[3] LIONS, N., L'instrumentation dans les circuits d'essais Rapsodie 1 et 10 MW, Colloque de la Société européenne d'énergie atomique sur les métaux liquides, Aix-en-Provence, 30 septembre-2 octobre 1963.

[4] ASSOCIATION FRANCAISE DE NORMALISATION, Norme NFX 10101, Mesure des débits instantanés des fluides, AFNOR, Paris (septembre 1949).

[5] CAMBILLARD, E. et al., CEA, Brevet n° PV 37 333, Indicateur de niveau à inductances couplées pour métaux liquides, Brevatome, Paris, B 1697. 3 D 2861 (4 novembre 1965).

[6] BUIS, H., CEA, Brevet n° PV 42 455, Dispositif à ultra-sons pour la mesure de la position du niveau d'un liquide, Brevatome, Paris, B 1786. 3 D 2948 (15 décembre 1965).

DISCUSSION

R. RADEBOLD: Why did you not make use of radioactive level control in these investigations?

E. CAMBILLARD: The devices we are studying or which we have already developed are intended for use in reactors as well as test loops. We have not done any development work on continuous level indicators incorporating radioactive sources because meters of this sort cannot be used in reactors.

A.M. SOENEN: You mention in the paper that three pairs of electrodes were used to check the accuracy of your measurements. Where were these electrodes placed?

E. CAMBILLARD: Each of the main primary and secondary circuits of Rapsodie is fitted with three pairs of electrodes and this provides us with three completely independent measurement channels. These channels are used to operate a coincidence system (two signals out of three), which trips the safety devices. For this reason the position of the electrodes has been worked out so that signals may be obtained which are more or less the same though not absolutely identical.

A. HOUTZEEL: Can you give me some idea of the maximum temperatures envisaged with this ultrasonic level indicator?

E. CAMBILLARD: For the transducer, the maximum temperature will be ≤ 250°C.. In the case of the immersed section the value will be ≤ 600°C.

A. HOUTZEEL: Do you plan to cool the transducer?

E. CAMBILLARD: No.

CORROSION BY OTHER ALKALI METALS:
NaK, K, Li, Cs
(Session VIII)

ИССЛЕДОВАНИЕ РАСПРЕДЕЛЕНИЯ ПРИМЕСЕЙ В ТУРБУЛЕНТНОМ ПОТОКЕ ЖИДКОМЕТАЛЛИЧЕСКОГО ТЕПЛОНОСИТЕЛЯ

М.Н.ИВАНОВСКИЙ, Ю.И.ОРЛОВ, В.И.СУББОТИН
ФИЗИКО-ЭНЕРГЕТИЧЕСКИЙ ИНСТИТУТ, ОБНИНСК
СССР

Abstract — Аннотация

DISTRIBUTION OF IMPURITIES IN A TURBULENT LIQUID-METAL COOLANT FLOW. Experimental work is described in which the distribution of undissolved nitrogen impurities in a turbulent lithium coolant flow was studied as a function of various factors: coolant temperature and velocity, the direction of heat flow, and the operating conditions both of the individual units and of the circuit as a whole. The differential material balance equation for the impurity is solved for unit surface area of the contact layer.

ИССЛЕДОВАНИЕ РАСПРЕДЕЛЕНИЯ ПРИМЕСЕЙ В ТУРБУЛЕНТНОМ ПОТОКЕ ЖИДКОМЕТАЛЛИЧЕСКОГО ТЕПЛОНОСИТЕЛЯ. В докладе представлены результаты экспериментального исследования распределения нерастворенных примесей (азота) в турбулентном потоке литиевого теплоносителя в зависимости от различных факторов: температуры и скорости теплоносителя, направления теплового потока, условий работы как отдельных узлов, так и всего циркуляционного контура. Приведено решение дифференциального уравнения материального баланса примеси для единицы поверхности контактного слоя.

При создании ловушек примесей, систем контроля чистоты, насосов и другого оборудования жидкометаллических контуров, при эксплуатации жидкометаллических систем, а также при изучении вопросов коррозии, теплообмена и массообмена необходимо знать и учитывать законы распределения примесей по сечению потока теплоносителя и по отдельным участкам и узлам контура.

При концентрации примесей, превышающей растворимость в заданных температурных условиях, часть примесей находится в теплоносителе в виде взвесей. Кристаллизация примесей из раствора и образование взвесей начинается при достижении определенного пересыщения, часто достаточно малого.

Если в контуре имеются охлаждаемые стенки, то на них происходит накапливание загрязнений за счет кристаллизации. При этом может происходить и перекристаллизация, то есть растворение взвешенных или высевших из потока на стенку мелких кристаллов и рост кристаллов, связанных со стенкой.

При изменении температурного или гидродинамического режима контура может происходить перераспределение примесей. Тупики и узлы контура, служившие ловушками примесей, могут стать их источниками.

Накапливание примесей может происходить не только на охлаждаемых поверхностях и не только за счет кристаллизации. В случае изотермического контура и в случае нагретой стенки часть взвешенных окислов и других примесей может концентрироваться у стенок контура и в застойных зонах с малой скоростью теплоносителя.

Известно, что при отсутствии стоков примесей, взвешенные примеси могут находиться в потоке сколь угодно долго. Расчеты показывают, что при скорости больше 1 мм/сек размер частиц, увлекаемых потоком, составляет десятки микрон. Таким образом потоком могут увлекаться кристаллы примесей практически любых встречающихся размеров.

Взвешенные примеси скапливаются в пристенном ламинарном подслое за счет гидродинамической сепарации в частности, связанной с градиентной коагуляцией частиц примеси [1]. Мелкие частицы примеси, попав в ламинарный подслой и двигаясь в основном вдоль стенки, догоняют частицы, расположенные ближе к стенке и имеющие меньшую скорость. Коснувшиеся частицы слипаются за счет ван-дер-ваальсовых сил, наконец, образуют более крупные частицы – флокулы. Связи между частицами не могут быть разрушены за счет броуновского движения, а турбулентность в ламинарном подслое относительно невелика. Подвижность (диффузия) частиц сильно уменьшается с увеличением их размера. Таким образом ламинарный подслой становится ловушкой для частиц примесей.

Флокулы и кристаллы примесей удерживаются на стенке за счет ван-дер-ваальсовых сил, обуславливающих адсорбцию и др.

Этот пристенный слой примесей будет размываться турбулентным потоком, т.е. будет происходить массообмен между ядром турбулентного потока с концентрацией примесей. Чем выше скорость потока, тем интенсивнее массообмен и меньше пристенный слой примесей повышенной концентрации. Авторами доклада проведено исследование влияния примесей на теплоотдачу при течении в трубах различных щелочнометаллических теплоносителей.

Путем измерения коэффициентов теплоотдачи в процессе очистки и загрязнения металлов примесями [2], путем измерения полей температур в пристенном слое жидкометаллического теплоносителя в статистических условиях и в турбулентном потоке установлено, что нерастворенные примеси концентрируются вблизи горячей стенки и снижают теплопроводность пристенного слоя потока вплоть до величины, примерно соответствующей теплопроводности плотной упаковки твердых кристаллов примеси с порами, заполненными жидким металлом. Пристенный слой примесей растет с увеличением концентрации примесей в контуре, но только до предельного значения, зависящего от скорости потока (критерия Рейнольдса Re). Дальнейшее повышение концентрации примесей в контуре не приводит к увеличению слоя примесей. Минимальные значения теплоотдачи, соответствующие предельной толщине и термическому сопротивлению пристенного слоя примесей соответствуют формуле:

$$\mathrm{Nu} = 3 + 0{,}014\,\mathrm{Pe}^{0{,}8} \qquad (1)$$

На основании данных по теплообмену можно представить физическую модель образования пристенного слоя примесей на горячей стенке, когда нет условий для кристаллизации примесей на этой стенке. Схему возможного распределения объемной концентрации взвешенных примесей в пристенном слое и турбулентном ядре потока можно представить так: примеси образуют плотный слой ($\delta_к$), сцепленный со стенкой, с объемной концентрацией примесей C_0, переходный слой с переменной концентрацией и турбулентное ядро потока с концентрацией C. Представленная схема несколько идеализирована. Так, по-видимому, не существует резкой границы слоя δ_K, и концентрация меняется плавно. Однако, ввиду большой разницы между концентрацией C_0 и C, отличающихся, согласно наших измерений, в десятки тысяч раз, незначительными изменениями концентрации в слое δ_K можно смело пренебречь.

Уравнение материального баланса примеси для единицы поверхности контактного слоя δ_K в единицу времени может быть выражено в следующем виде:

$$C_0\frac{d\delta_K}{d\tau} + W(\delta_K)C_0 = \alpha_D(C_0 - C) \qquad (2)$$

Здесь $W(\delta_K)C_0$ – количество примеси, поступающей в контактный слой со скоростью $W(\delta_K)$; $\alpha_D(C_0 - C)$ – количество примеси, уносимой из слоя за счет массообмена с потоком.

Размер частиц взвешенных примесей мал (порядка нескольких микрон). Скорость движения частиц, согласно закону Стокса, пропорциональна действующей на частицу силе $W = A\ F$.

Силы, связывающие частицу со стенкой, изучены недостаточно. Но эти силы существуют и убывают с увеличением расстояния от стенки, что следует из экспериментальных данных по распределению примесей в потоке и по изменению в зависимости от скорости контактных термических и электрических сопротивлений. Поэтому в общем случае силу можно записать как

$$F = y^{-n(y)}$$

В качестве примера рассмотрим ван-дер-ваальсовское взаимодействие частицы со стенкой. Согласно общей теории ван-дер-ваальсовых сил [3] сила притяжения F между макроскопическими частицами, а также частицами и стенкой, разделенными жидкометаллической прослойкой, убывает с расстоянием по закону y^{-n}. Показатель степени $n = 3$ для расстояний малых по сравнению с микроном и $n = 5$ для расстояний много больших микрона.

Таким образом, выражение для $W(\delta_K)$ можно приближенно записать в виде:

$$W = \frac{b}{y^n} \qquad (3)$$

Подставляя выражение (3) в (2), получим

$$C_0\frac{d\delta_K}{d\tau} + \frac{bC_0}{\delta_K^n} = \alpha_D(C_0 - C) \qquad (4)$$

В стационарных условиях

$$\delta_K = \left(\frac{b}{\alpha_D}\cdot\frac{C_0}{C_0 - C}\right)^{\frac{1}{n}} \qquad (5)$$

Объемная концентрация примеси в пристенном слое C_0 достаточно высока (близка к единице). В потоке же концентрация примеси намного меньше (порядка $1\cdot 10^{-4}$ объемных долей). Отсюда $C \ll C_0$ и можно записать $(C_0/C_0 - C) = 1$.

Коэффициент массообмена α_D при диффузии взвешенных частиц в турбулентном потоке жидкости в различных каналах при больших значениях диффузионных чисел Прандтля может быть взят из решения Левича В.Г. [1].

$$\frac{\alpha_D \cdot d}{D} = Nu_D = K \cdot Re^{0,9} \cdot Pr_D^{0,25}, \tag{6}$$

где D – коэффициент диффузии взвешенных частиц, K – постоянная величина, Pr_D – диффузионное число Прандтля.

Тогда толщина пристенного контактного слоя может быть выражена в виде:

$$\delta_K = \left(\frac{bd}{K \cdot D \cdot Pr_D^{0,25}} \cdot \frac{1}{Re^{0,9}}\right)^{\frac{1}{n}} \tag{7}$$

Как видно из выражения (7) толщина пристенного слоя примесей и, следовательно, контактное термическое сопротивление зависит от скорости потока (критерия Рейнольдса), от коэффициента диффузии D и других параметров. Из решения также следует, что предельная толщина контактного слоя не зависит от концентрации взвеси в потоке. Это объясняет предельный характер формулы (1), обобщающей экспериментальные данные по теплоотдаче к различным, загрязненным примесям, жидкометаллическим теплоносителям, полученные в разное время в условиях, когда не принимались специальные меры по очистке и поддержанию чистоты теплоносителей.

Таким образом, в потоке нерастворенные примеси перераспределяются между пристенным слоем и ядром потока. В каналах сложной формы, например в продольно омываемом пучке стержней, скорость, толщина ламинарного подслоя и толщина пристенного слоя примесей будут неравномерными по периметру канала или по периметру продольно омываемого стержня.

Экспериментальные исследования распределения в турбулентном потоке и в контуре проводились нами на примеси азота в литии. Жидкометаллический теплоноситель циркулировал в контуре, оборудованном системами для дозированного ввода азота и других загрязнений, системами пробоотбора, очистки, контроля.

Содержание других примесей поддерживалось постоянным и существенно меньшим, чем концентрация насыщения при температуре контура.

Для непрерывного контроля содержания азота в потоке использовался электрический индикатор примесей, основанный как и аналогичный прибор [4, 5] на использовании зависимости электросопротивления жидкого металла от количества растворенных в нем примесей. Чувствительность индикатора составляла $1,6\cdot 10^{-4}$ вес % азота на деление шкалы. Температура в индикаторе поддерживалась заведомо более высокая, чем температура насыщения, соответствовавшая суммарной концентрации растворенного и нерастворенного нитрида. Перед поступлением в индикатор жидкометаллический теплоноситель проходил в трубках с нагревателями, обеспечивающими полное растворение нитридов до входа в индикатор. Скорость теплоносителя через индикатор подбиралась так, чтобы дальнейшее уменьшение скорости не приводило к повышению количества растворенного нитрида и, следовательно, к повышению электросопротивления жидкого металла. Отборы потока теплоносителя в индикатор проводились из основного и вспомогательного контуров и из опытного участка, представляющего собой вертикальную трубу внутренним диаметром 90 мм и длиной 3 м. Для исследования распределения примесей по сечению турбулентного потока в этой трубе на расстоянии 33 d_0 от входа навстречу потоку были установлены 3 трубки с внутренним диаметром 6 мм и толщиной стенки 0,3 мм. Входные участки двух трубок, расположенных вблизи стенки, сплющивались и имели размеры 8 × 2 мм. Трубки были установлены в центре, вплотную к стенке и на расстоянии 4,1 мм от стенки. На выходе из опытного участка на каждой трубке установлены вентили. Вентили позволяли поочередно подключать пробоотборные трубки к индикатору примесей и регулировать расход теплоносителя через индикатор. Процесс образования пристенного слоя нерастворенных примесей контролировался с помощью индикатора контактного электросопротивления. Этот индикатор выполнен в виде трубки из стали 1Х18Н9Т с толщиной стенки 0,3 мм. К наружной поверхности трубки по ее образующей на расстоянии 25 мм друг от друга припаяны серебряным припоем два медных электрода диаметром 5 мм. От одного электрода к другому пропускался постоянный ток. Изменение толщины слоя осевших на внутренней поверхности трубы примесей приводило к изменению электросопротивления цепи индикатора. Из соображений безопасности при протекании теплоносителя тонкостенный участок трубы индикатора помещен в герметический кожух. Внутри кожуха установлен электронагреватель. Он предназначен для обогрева медных электродов в тех опытах, когда необходимо создать тепловой поток, направленный от стенки к теплоносителю. Обратный тепловой поток на внутренней поверхности трубки индикатора в месте припайки стержней получался за счет естественного отвода тепла через медные стержни к окружающему воздуху. Температура медных электродов и стенки индикатора контролировались хромель-алюмелевыми термопарами.

Контрольные опыты, проведенные с чистым теплоносителем, при отсутствии взвешенных примесей во всем контуре показали, что, как и следовало ожидать, растворенные примеси распределены равномерно по сечению потока и по всему контуру. Изменение температуры и скорости в отдельных линиях контура не приводит к перераспределению растворенных примесей, так как турбулентная диффузия полностью выравнивает концентрацию.

Для увеличения содержания примесей в проточный бак контура под уровень жидкого металла вводили газообразный азот. Повышение содержания азота в жидком металле контролировали электрическим индикатором примесей и химанализом. При постепенном введении азота малыми порциями показания электрического индикатора примесей возрастали, а показания индикатора контактного электросопротивления оставались неизменными, пока содержание примесей в контуре не превышало предела насыщения.

После достижения насыщения примесь выкристаллизовывалась и дальнейшего повышения электросопротивления теплоносителя не происходило. Появление нерастворенных примесей в контуре обеспечивалось не только введением азота, но в ряде опытов и снижением температуры жидкого металла ниже температуры насыщения примесью. Кристаллизация примесей из раствора и осаждение их из потока на стенки четко фиксировались по показаниям обоих индикаторов.

На внутренней поверхности трубы индикатора контактного электросопротивления в этих опытах поддерживались условия охлаждения теплоносителя. Тепловой поток был направлен от теплоносителя к стенке и отводился за счет охлаждения электродов индикатора естественной конвекцией воздуха. Величина потока в месте припайки электродов составляла примерно 100 000 ккал/м^2 час.

При повышении температуры теплоносителя часть нерастворенных примесей, осевших на стене, растворяется. При этом содержание примеси в потоке увеличивается, а толщина слоя нерастворенных примесей на стенке соответственно уменьшается. В части опытов этот слой растворялся полностью и дальнейшее повышение температуры не приводило к дальнейшему повышению концентрации растворенной примеси в потоке.

Снижение температуры приводило к уменьшению содержания растворенных примесей в потоке и к увеличению толщины пристенного слоя.

На распределение примесей в данном участке контура оказывают влияние условия в других узлах контура. При появлении в каком-либо месте контура более холодной поверхности (например, холодной ловушки примесей, холодильника или другого стока примесей) наблюдался постепенный перенос нерастворенных примесей в эти наиболее холодные участки контура. В том числе перенос наблюдался и из охлаждаемого участка индикатора контактного электросопротивления, что приводило к снижению контактного электросопротивления.

При выключении стока примеси (например, холодильника) нерастворенные примеси, ранее осевшие на сильно охлаждаемых поверхностях, перераспределяются по контуру и часть их осаждается на стенках в новых местах в соответствии с новым распределением температур и скоростей по участкам контура. Перераспределение заканчивается установлением нового стационарного распределения. Даже в случае, когда в контуре имелись интенсивные стоки примесей (включенный водяной холодильник контура), быстрое снижение температуры всего теплоносителя в контуре при отключении нагревателей приводило к появлению в индикаторе и других участках контура пристенного слоя примеси. Затем, за счет переноса в более сильно охлаждаемые участки холодильников, этот слой исчезает. Это показано на рис.1. Снижение показаний индикатора контактного электросопротивления $R_{икс}$ в первый момент связано с некоторым уменьшением электросопротивления электродов индикатора и самого теплоносителя ввиду снижения температуры. Затем видно изменение показаний индикатора, связанное с выпадением нерастворенной примеси из раствора, скоплением ее в потоке и на стенке индикатора и переносом в более холодные участки контура.

Химанализы проб, отобранных из потока теплоносителя при различных температурах, показали, что концентрация примесей в турбулентном потоке примерно соответствует концентрации насыщения при температуре теплоносителя. Так, например, при температуре теплоносителя 232 °С содержание азота в потоке составляло $2{,}5 \cdot 10^{-3}$ вес %, а при температуре 270 °С – $6{,}0 \cdot 10^{-2}$ вес %. При этом общее количество примеси, введенной в контур, было в несколько раз большим. Это указывает на то, что большая часть нерастворенных примесей в стационарном состоянии находится на стенках контура.

Исследование влияния скорости течения жидкого металла на перераспределение взвешенных примесей проводилось в условиях охлаждения и нагревания теплоносителя на внутренней поверхности индикатора контактного электросопротивления. В условиях охлаждения теплоносителя изменение скорости не приводило к изменению толщины пристенного слоя примесей. В этом случае на холодной поверхности индикатора выкристаллизовываются, вырастают из раствора кристаллы или сцементированный слой кристаллов примеси. Такой выкристаллизованный на поверхности слой может разрушаться только за счет растворения, а увеличение скорости потока в данных условиях при относительно низкой температуре и малой истинной скорости реакции растворения мало влияет на суммарную скорость растворения.

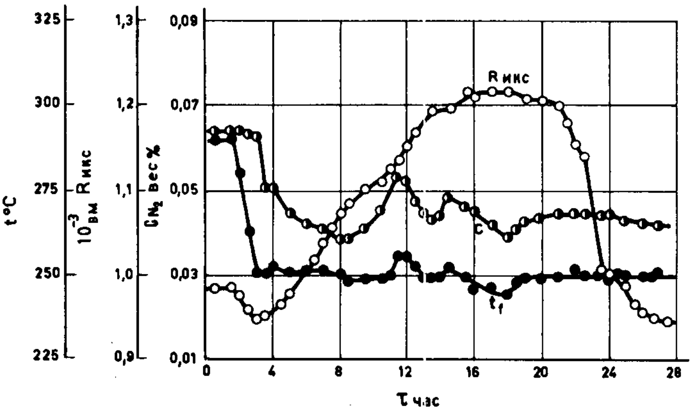

Рис. 1. Изменение концентрации азота в потоке (C) и толщины слоя примесей на стенках индикатора ИКС ($R_{икс}$) при снижении температуры теплоносителя (t_f). (На контуре имеются стоки примесей).

Когда на внутренней поверхности индикатора создавались условия нагревания теплоносителя, было обнаружено влияние скорости потока на толщину пристенного слоя примесей. В этих опытах медные электроды индикатора контактного электросопротивления обогревались электронагревателем, что обеспечивало местный тепловой поток около 50 000 ккал/м^2 час. Сильные стоки примесей на контуре были отключены. Температура теплоносителя поддерживалась постоянной.

В этих условиях изменение скорости теплоносителя приводило к перераспределению взвешенных примесей между стенкой и потоком в соответствии с уравнением (7). С увеличением скорости смывалась и переходила в поток часть кристаллов и флокул примесей, скопившихся на горячей по отношению к потоку стенке. Толщина пристенного слоя примесей при этом уменьшалась до тех пор, пока не наступило новое равновесие сил, связанных с турбулентным массообменом, и сил, удерживающих частицы у стенки. Образец показаний индикатора контактного электросопротивления при повышении скорости, представленный на рис.2, иллюстрирует уменьшение толщины пристенного слоя примесей.

Содержание примесей в потоке теплоносителя при увеличении скорости увеличивается. Это иллюстрировано измерениями концентрации примеси в ядре потока, проведенными с помощью электрического индикатора примесей. На рис.3 видно, что изменение скорости теплоносителя приводит к заметному изменению концентрации примеси в потоке. Тем не менее в широком диапазоне изменения скорости (критерия Re) концентрация взвеси в потоке изменяется крайне мало по сравнению с изменением полной концентрации примеси в данном участке контура при изменении скорости. Смытые со стенок данного участка контура примеси откладываются на стенках в других участках контура и ловушках. В потоке же при изменении критерия Рейнольдса от 7 до 130 тысяч суммарная концентрация взвешенных и растворенных примесей изменяется в потоке менее чем в 2 раза и незначительно превышает концентрацию насыщения.

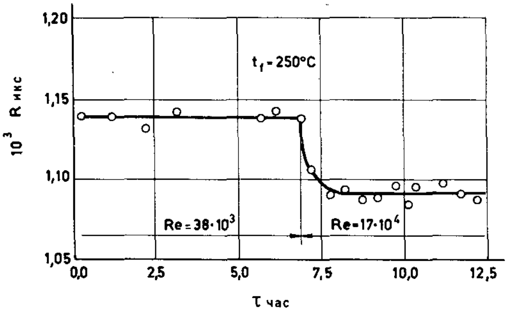

Рис. 2. Изменение толщины пристенного слоя примеси в индикаторе при увеличении скорости теплоносителя. (На стенках индикатора ИКС условия нагревания теплоносителя).

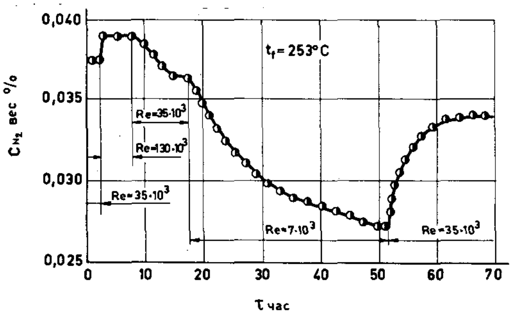

Рис. 3. Изменение содержания азота в потоке в зависимости от скорости теплоносителя. (Содержание примесей в контуре выше предела насыщения).

Сравнение содержания примесей в потоке теплоносителя в различных участках полностью изотермического контура дало такую же картину влияния скорости. При температуре теплоносителя 272 °С содержание азота в потоке в основном контуре (Re = 1500) $5{,}4 \cdot 10^{-2}$ вес %, а в то же время в байпасной линии (Re = 50 000) – $6{,}7 \cdot 10^{-2}$ вес %.

Было проведено измерение распределения взвешенных примесей по сечению турбулентного потока жидкометаллического теплоносителя в трубе диаметром 90 мм. В диапазоне чисел Рейнольдса от 25 до 130 тысяч изменения концентрации примесей по сечению ядра турбулентного потока обнаружено не было. Для взвешенной примеси, имеющей весьма большие диффузионные числа Прандтля, турбулентная диффузия приводит к полному выравниванию концентрации.

ЗАКЛЮЧЕНИЕ

Таким образом, в результате исследований распределения примесей установлено, что в случае, когда примеси полностью растворены в теплоносителе их концентрация постоянна по всему контуру и по всему сечению потока.

При наличии нерастворенных примесей их концентрации в потоке в различных участках циркуляционного контура может быть разной. Различно качество примесей, осевших на стенках, и полная концентрация примесей в различных участках контура. Количество примесей в данном участке контура зависит от температурных и гидродинамических условий в нем и от условий работы других узлов контура. Примеси перераспределяются между всеми участками контура при измерении режима работы всего контура, части контура или отдельного участка контура.

На относительно холодных стенках контура происходит накапливание примесей за счет кристаллизации. При этом, после установления стационарного режима, концентрация примеси в потоке соответствует концентрации насыщения при данной температуре теплоносителя.

Если в контуре включаются стоки примесей (зоны выкристаллизации примесей в холодных ловушках или на сильно охлаждаемых поверхностях), то происходит постепенная очистка теплоносителя. Если при этом отсутствуют источники примесей, то в потоке вначале достигается содержание примесей,близкое к насыщению при температуре в данном участке. После переноса примесей со стенок участков контура в зону выкристаллизации в потоке устанавливается концентрация, соответствующая концентрации насыщения при температуре выкристаллизации.

В случае изотермического контура и в случае, когда отсутствуют стоки примесей или имеются источники примесей, компенсирующие стоки, то в потоке могут постоянно находиться взвешенные примеси. К появлению взвешенных примесей приводит снижение температуры теплоносителя ниже температуры насыщения, диффузия газов через стенки контура, прогрев холодных ловушек и др.

Накапливание примесей может происходить не только на холодных стенках и не только за счет кристаллизации. В случае изотермического контура и в случае нагрева теплоносителя,нерастворенные примеси скапливаются и у горячих стенок, и в застойных зонах с малой скоростью теплоносителя. При этом устанавливается определенное соотношение между количеством примеси в потоке и на стенке. Примеси перераспределяются между турбулентным ядром потока и пристенной областью в зависимости от скорости теплоносителя. Как показали наши измерения и анализы, вблизи стенки примеси скапливаются в слой, представляющий почти плотную упаковку кристаллов примеси. В турбулентном ядре потока концентрация взвешенных примесей невелика и полная концентрация примеси близка к концентрации насыщения.

Увеличение скорости потока теплоносителя приводит к уменьшению слоя осевших на стенке нерастворенных примесей и к уносу их потоком. Унесенные потоком взвеси откладываются в других участках контура пока не наступит новое стационарное распределение примесей между участками контура. Увеличение скорости потока приводит к увеличению стационарного содержания взвешенных в нем примесей.

Пробы жидкого металла, взятые для химанализа из потока теплоносителя, содержащего нерастворенные примеси, имеют концентрацию примесей, близкую к концентрации насыщения при температуре потока и зависящую от скорости потока теплоносителя в участке и от направления теплового потока на его стенке. В действительности полное содержание примеси в участке может быть намного большим (в сотни раз). Анализ теплоносителя, взятый из данного участка контура, может не соответствовать содержанию примесей в других участках, особенно если они отличаются температурой и скоростью теплоносителя в них.

Все это необходимо учитывать при создании представительных методов отбора проб, создании ловушек примесей, при изучении теплоотдачи и ее зависимости от чистоты теплоносителя, при изучении процессов коррозии и массообмена.

Неучет законов распределения примесей приводит к серьезным ошибкам при контроле чистоты теплоносителей, при исследовании коррозии и массообмена, существенно осложняет эксплуатацию установок с жидкометаллическими теплоносителями.

ЛИТЕРАТУРА

[1] ЛЕВИЧ В.Г., Физико-химическая гидродинамика, Физматгиз М., 1959.
[2] СУББОТИН В.И., ИБРАГИМОВ М.Х., ИВАНОВСКИЙ М.Н. и др. Int. J. Heat Mass Transfer 4 (1961).
[3] ДЗЕЛОШИНСКИЙ И.Е., ЛИФШИЦ Е.М., ПИТАЕВСКИЙ Л.П., Общая теория ван-дер-ваальсовых сил. Успехи физических наук, 73, вып.3, (1961) 381.
[4] BLAKE R., Nucleonics, 15, 5 (1961).
[5] КОЗЛОВ Ф.А. и др. "Теплофизика высоких температур", 3, 1(1961).

DISCUSSION

J.R. WEEKS: Would you care to suggest, after these most interesting studies, what might be the best design of a trap for removing impurities accidentally introduced into circuit sodium?

M.N. IVANOVSKY: The design of circulation traps has been extensively considered in the literature. Diffusion cold traps are now, in our opinion, quite efficient enough for the type of work you have in mind, and the design of these is considered in our paper.

K.T. CLAXTON: Have you considered using an ultrasonic attenuation technique to follow the growth of oxide or other impurities present as solid particles?

M.N. IVANOVSKY: No, we have not.

K.T. CLAXTON: I ask this because I have calculated the attenuation for oxide particles of a few hundred molecular diameters at low concentrations and found that satisfactory attenuation occurs only at frequencies greater than about 400 Mc/s. However, it seemed to me that in view of your high boundary-layer concentration of solid material the ultrasonic attenuation technique might be a useful approach.

E.L. ZEBROSKI: First, let me congratulate Dr. Ivanovsky on a most interesting and sophisticated paper. I have two questions. Have you studied the nature of the particles in respect to (a) size distribution, (b) chemical state or solvation, and (c) particle-to-particle forces and particle-to-surface forces? Secondly, what is the effective thermal conductivity of the deposit, or the effective thickness and film coefficient?

M.N. IVANOVSKY: Unfortunately I cannot give a satisfactory answer to the first question because we have made no special study of the properties of the individual particles or of the intermolecular forces between them. In reply to your second question, the thermal conductivity of the wall layer was found to be about seven times less than that of the liquid metal itself; for our experiment this means 6-8 kcal/m.h.degC.

CORROSION OF IRON- AND NICKEL-BASE ALLOYS IN HIGH-TEMPERATURE SODIUM AND NaK*

J.H. DEVAN
OAK RIDGE NATIONAL LABORATORY,
METALS AND CERAMICS DIVISION,
OAK RIDGE, TENN.,
UNITED STATES OF AMERICA

Abstract

CORROSION OF IRON- AND NICKEL-BASE ALLOYS IN HIGH-TEMPERATURE SODIUM AND NaK. Extensive corrosion data on sodium and sodium-potassium alloys have accrued from development studies for aircraft and space-power reactor systems. Such studies at ORNL have included the operation of 61 forced-convection corrosion loops of high-temperature alloys with sodium and NaK at hot-leg temperatures from 1000 to 1650°F. The results of these loop studies are described and a comparison is made of the relative mass transfer rates of nickel-base alloys and austenitic stainless steels in cold-trapped sodium.

All loops were electromagnetically pumped and operated at velocities of 3 to 7 ft/s. Operating times ranged from 500 to 3000 h. Mass transfer rates were determined by gravimetric and metallographic analyses of cold-leg deposits; corrosive attack was monitored by metallographic and chemical examination of loop piping.

The major finding of these loop studies was the strong temperature dependence of mass transfer in Inconel (Ni-15% Cr-6% Fe) and Hastelloy alloys (Ni-26% Mo and Ni-26% Mo-5% Cr) in the range 1000 to 1500°F. In comparative 1000-h loop tests of Inconel, the formation of macroscopic cold-leg deposits was initially observed at 1300°F, and the extent of deposition increased rapidly with increasing hot-leg temperature. The total weight of deposits at 1500°F showed a linear dependence on both flow rate and temperature difference. Changes in the oxygen concentration of sodium from 10 to 500 ppm had little effect on the rate of mass transfer of Inconel. Higher oxygen concentrations increased the mass transfer rate.

Loop tests of austenitic stainless steels between 1500 and 1650°F produced much lower mass transfer rates than nickel-base alloys under comparable temperature and purity conditions. In tests of 18-10 stainless steels (Types 316, 347 and 304) at 1500°F, only trace quantities of cold-leg deposits were measureable after 1000 h. Stainless steels with higher nickel concentrations (Types 310 and 330) and Type 430 stainless steel showed mass transfer rates intermediate between the 18-10 steels and nickel-base alloys.

INTRODUCTION

Liquid sodium and NaK have long been recognized as effective coolants for high-temperature nuclear reactors. Their use in the Aircraft Reactor Experiment [1] and related development programs during the period 1952 to 1956 prompted an extensive corrosion investigation of both coolants in the range 1000 to 1650°F. This report discusses a part of this investigation dealing with the operation of nickel-base and stainless-steel forced-convection loop systems. The objective of the tests was to evaluate the mass transfer resistance of high-temperature alloys in sodium under various conditions of temperature, flow rate, and purity.

---

* Research sponsored by the United States Atomic Energy Commission under contract with the Union Carbide Corporation.

The corrosion program followed earlier screening tests of small static or rocking capsules and thermal-convection loops. Such tests of sodium and NaK at temperatures up to 1500°F for 500 and 1000 hr showed very limited corrosive attack or mass transfer of either nickel-base alloys or austenitic stainless steels. However, as the test time was increased to 1500 hr, thermal-convection loops of nickel-base alloys circulating sodium at a maximum temperature of 1500°F exhibited traces of crystalline deposits in cold-leg regions. These deposits, composed mainly of nickel, decreased in amount as the oxygen content of the sodium was reduced but were detected even in carefully cold-trapped systems (less than 20 ppm O). This apparent tendency at higher temperatures for nickel to deposit across a temperature gradient gave rise to the subject studies with higher velocities and correspondingly greater mass flows.

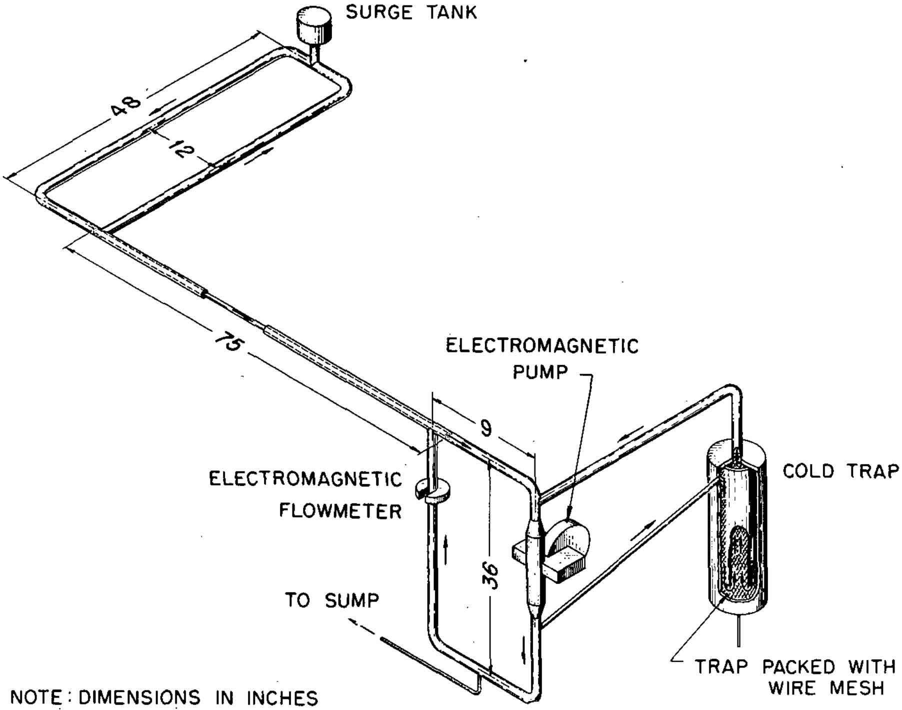

FIG. 1. Forced-convection-test loop

EXPERIMENTAL PROCEDURES

The loop employed for these studies, shown in Fig. 1, was a figure-eight design incorporating an economizer to transfer heat between the hot- and cold-leg sections. The major temperature change in the circulating sodium occurred in the economizer section, and the changes through the hot and cold legs were less than 50°F, respectively. Tubing sizes of the loop components were as follows:

Location	Size
Hot leg, cold leg, economizer shell	3/4-in. OD × 0.065-in. wall
Economizer central tube	1/2-in. OD × 0.020-in. wall
Pump cell	1 1/16-in. OD × 0.065-in. wall

Heat was supplied by Nichrome-wound heaters placed around the economizer and hot-leg sections. The oxygen level of the sodium or NaK was controlled by bypassing approximately one-tenth of the pump flow through a cold trap in parallel with the loop (Fig. 1). The loop was completely closed except at the expansion tank, which was held under a positive pressure of purified helium.

All loop components were fabricated of the same material, and each loop was destructively examined following a single test run. Corrosive attack was monitored by metallographic and chemical analyses of the loop piping. Mass transfer rates were determined by metallographic and gravimetric analyses of cold-leg deposits. The latter analysis entailed dissecting the cold-leg piping into 4-in. segments and mechanically brushing the deposits from each segment. The deposits were then weighed and chemically analyzed.

The alloy designations and compositions of loop materials investigated under this program are listed in Table I. The program chronologically divided into four phases, which are grouped according to test conditions in Table II. Initial loop studies centered around the nickel-base alloy Inconel. Their purpose was to determine the effects of various operating parameters on the mass transfer behavior of this alloy at 1500°F and also to evaluate effects of hog-leg temperature on corrosion in the range 1000 to 1500°F. An additional series of tests on this alloy was completed at 1500°F with 56% K-44% Na in place of sodium. Other nickel-base alloys were evaluated in a series of tests carried out with sodium at 1300 and 1500°F. A final series of loops involved several austenitic stainless steels and one ferritic stainless steel operated with sodium at 1500°F and a single loop at 1650°F.

TABLE I. NOMINAL COMPOSITIONS OF LOOP MATERIALS

Alloy Designation	Composition, wt %							
	C[a]	Fe	Cr	Ni	Mo	Mn[a]	Si[a]	Other
Stainless Steel								
Type 304	0.08	Bal	18	8		2	1	
Type 310	0.25	Bal	24	19		2	1.5	
Type 316	0.10	Bal	16	10	2.5	2	1.5	
Type 330	0.25	Bal	14	33		2	1	
Type 347	0.08	Bal	17	9		2	1	Nb ≥ 10 × C content
Type 430	0.12	Bal	14	0.5[a]		1	1	
Nickel Base								
Inconel	0.15	7	15	Bal		1	0.5	
Hastelloy B	0.05	5		Bal	28	1	1	2.5 Co[a]
Hastelloy W	0.05	5	5	Bal	24	1	0.5	2.5 Co[a]
Inconel X	0.08	7	15	Bal		1	0.5	1 Nb, 2.5 Ti, 0.5 Al

[a] Maximum.

RESULTS OF INCONEL LOOPS CONTAINING SODIUM

Temperature Effects

The effect of sodium temperature on the corrosion and mass transfer behavior of Inconel was evaluated in a series of loops operated between 1000 and 1500°F. The test conditions and results of these loops are

TABLE II. OUTLINE OF SODIUM FORCED-CONVECTION-LOOP PROGRAM AND TEST CONDITIONS

Program Phase	Loop Material	Liquid Metal	Maximum Hot-Leg Temperature (°F)	Temperature Difference (°F)	Flow Rate (gal/min)	Cold-Trap Temperature (°F)	Test Duration (hr)
I	Inconel	Sodium	1000, 1250, 1300, 1350, 1500	300	2.5	300	1000
	Inconel	Sodium	1500	150–400	1.5, 2.0, 3.0	300	500, 1000, 2000
	Inconel	Sodium	1500	300	2.5	[a]	1000
II	Inconel	NaK (56% K–44% Na)	1500	300	2.5	100, 300, 600, 800	1000
III	Hastelloy B	Sodium	1300, 1500	300	2.5	300	1000, 2000
	Hastelloy W, Inconel X	Sodium	1500	300	2.5	300	1000
IV	Type 316 stainless steel	Sodium	1500, 1650	300	2.5	300	500, 1000
	Stainless steel types 304, 347, 310, 330, 430	Sodium	1500	300	2.5	300	1000

[a] Cold-trap temperature was maintained at 300°F except for tests in which sodium purity was the assigned variable. Purity levels in the latter cases were adjusted by (1) direct addition of Na_2O_2 to the sodium, (2) magnesium and barium additions to sodium, and (3) inclusion of titanium or zirconium in hot-leg sections.

listed in Table III. Each loop operated for 1000 hr with a constant flow rate of 2.5 gal/min and with 10% of total loop flow through a bypass cold trap maintained at 300°F. The maximum ΔT (temperature difference) between the hot and cold legs was 200°F in the 1000°F loop test and 300°F in the higher temperature experiments.

As indicated in Table III, the internal surfaces of loops operated at 1000 and 1250°F retained the visual and metallographic appearance of as-received tubing. However, at a maximum temperature of 1300°F metallic crystals were in evidence near the exit of the central economizer tube. Increasing the test temperature to 1500°F greatly increased both the density and range of these deposits. The visual and metallographic appearances of hot- and cold-leg sections of a loop operated at 1500°F are compared in Fig. 2. Note that the mass transfer deposits are distinctly metallic and appear to have been nucleated both on the loop wall and within the sodium. The hot-leg specimen had a distinctly etched appearance and exhibited shallow grain-boundary attack (Fig. 2).

Chemical analysis of cold-leg deposits showed them to be composed primarily of nickel with up to 10% Cr and virtually no iron. The composition varied slightly with the location of the deposit along the cold leg, becoming slightly higher in nickel and lower in chromium in the direction of fluid flow. The particle or crystal size also varied as a function of location. Crystals near the beginning of the cooler were less densely packed and had a rod- or platelike shape. Deposits between the center and the cooler exits, as pictured in Fig. 2, were larger and more equiaxed.

TABLE III. EFFECT OF MAXIMUM SODIUM TEMPERATURE ON HOT-LEG ATTACK AND MASS TRANSFER IN INCONEL FORCED-CONVECTION LOOPS OPERATED FOR 1000 hr[a]

Maximum Hot-Leg Temperature (°F)	Total Weight of Mass-Transfer Deposits (g)	Maximum Deposition Rate (mg/cm^2)	Metallographic Results: Maximum Intergranular Attack (mils)	Metallographic Results: Maximum Deposit Thickness (mils)
1000[b]	c	c	c	c
1250[d]	c	c	c	c
1250[d]	c	c	c	c
1250[d]	c	c	c	c
1300	e	e	1/2	< 1/2
1300	e	e	1/4	2
1350	0.8	5.2	1/2	4
1500	13.1	41.9	2	14
1500	15.0	41.2	1 1/2	18

[a] Cold-trap temperature, 300°F; sodium flow rate, 2.5 gal/min; sodium ΔT, 300°F.

[b] 200°F sodium ΔT.

[c] No evidence of attack or mass-transfer deposits.

[d] Contained beryllium insert at hot-leg exit.

[e] Deposits detected but below measurable limits.

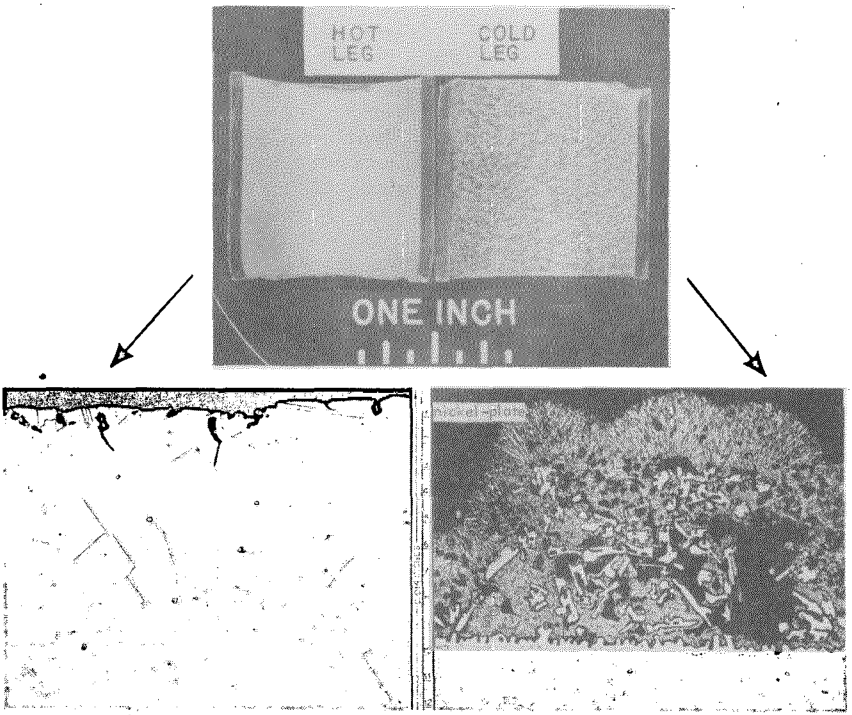

FIG. 2. Visual and metallographic appearance of hot- and cold-leg sections of Inconel loop operated at 1500°F maximum with 300°F ΔT

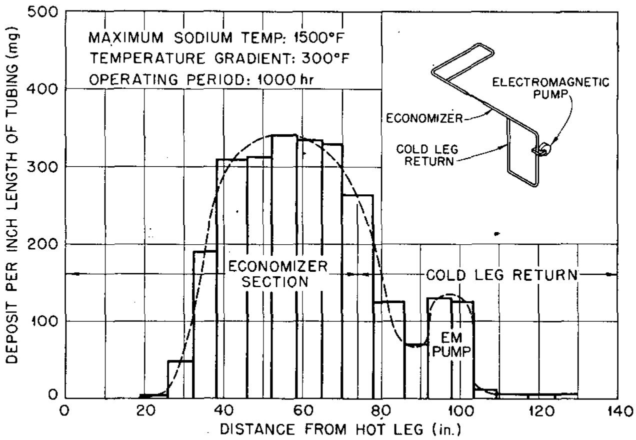

FIG. 3. Profile of mass-transfer deposits in sodium-Inconel forced-circulation loop

The variation in deposit weight as a function of loop position is shown in Fig. 3 for a loop operated at 1500°F. Although the sodium temperature decreased linearly with distance through the economizer, the buildup of deposits was much greater near the middle of the economizer than at the end.

Effects of Operating Time, ΔT, and Flow Rate

The effect of operating time on the buildup of mass transfer deposits in 1500°F loops is shown in Fig. 4. This figure compares the deposit weights produced after 500, 1000, and 2000 hr in loops operated with a 300°F ΔT, a 300°F cold trap, and a flow rate of 2.5 gal/min. The deposit weight increased by a factor of 2 between 500 and 1000 hr but only by a factor of 1.4 between 1000 and 2000 hr.

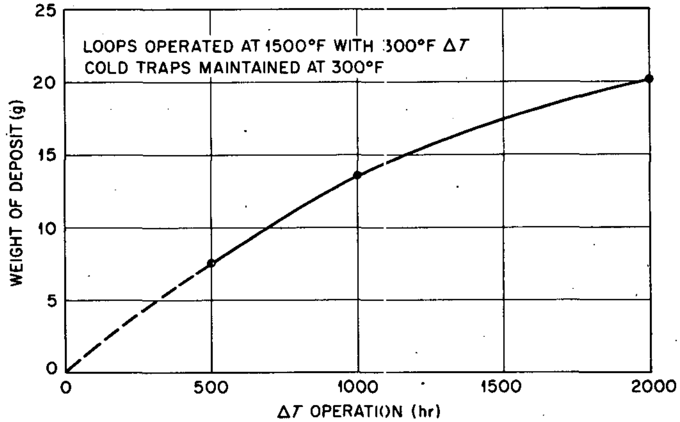

FIG.4. Mass-transfer buildup as a function of time in Inconel-sodium pump loops

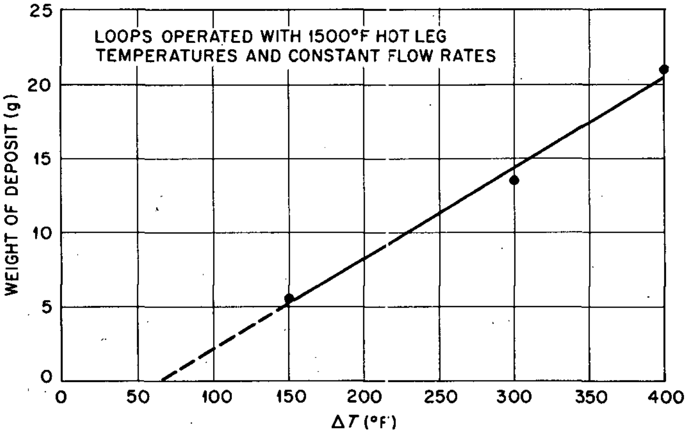

FIG.5. Effect of ΔT on mass transfer in sodium-Inconel pump loops

The effect of ΔT at 1500°F was studied in a series of loops operated for 1000 hr with minimum cold-leg temperatures of 1100, 1200, and 1400°F. The results are shown in Fig. 5. Mass transfer deposits increased by a factor of 4 over the ΔT range studied (100 to 400°F). Assuming the deposit weight to be a linear function of ΔT, extrapolation to zero mass transfer rate gives a threshold ΔT of 60°F (Fig. 5).

The importance of flow rate on mass transfer in the Inconel-sodium system was shown initially by comparing forced- and thermal-convection loop experiments with nearly equivalent ratios of surface area to volume. Circulation of sodium at 1500°F with a 300°F ΔT produced much heavier accumulations of deposits in 500 hr under forced-flow conditions than had been observed in thermal-convection tests even after 2000 hr. Flow-rate effects in forced-convection tests were studied by varying the pumping power to achieve the following sodium flows and velocities:

Flow Rate (gal/min)	Velocity (ft/sec)		
	Hot and Cold Legs	Economizer Annulus	Central Economizer Tube
1.5	1.6	4.6	2.9
2.5	2.7	7.4	4.8
3.0	3.2	9.2	5.8

The extent of deposition in these systems after 1000 hr at a 1500°F hot-leg temperature is shown in Fig. 6. Deposit weight shows roughly a linear variation with flow rate over the ranges studied; however, an extrapolation to no flow and zero mass transfer rate would require the function to depart considerably from linearity.

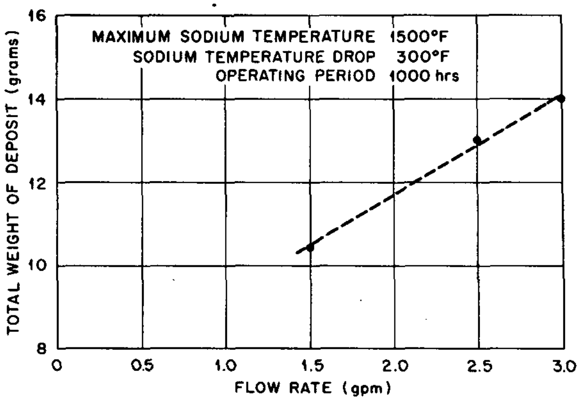

FIG. 6. Effect of flow rate on mass transfer in sodium-Inconel loops

The variations in operating parameters discussed above had essentially no effect on the degree or extent of hot-leg attack observed in these systems. Metallographic examination of the hot-leg region showed no measurable surface changes except for light intergranular penetrations, which ranged from 1 to 2 mils in all of the tests.

Effect of Sodium Purity

It is now well established that the oxygen content of sodium is an important parameter affecting the corrosion of stainless steels by sodium above 900°F. The corrosion rate of ferritic and austenitic stainless steels is reported [2] to have a linear or first-order dependence on oxygen concentration between 1000 and 1300°F. These findings prompted the series of loop experiments shown in Table IV, which were designed to determine the significance of oxygen in Inconel-sodium systems. All loops operated with the same flow rate (2.5 gal/min) and

TABLE IV. EFFECT OF SODIUM PURITY ON MASS TRANSFER IN INCONEL-SODIUM SYSTEMS[a]

Sodium Treatment	Operating Time (hr)	Maximum Intergranular Attack (mils)	Deposit	
			Maximum Thickness (mils)	Weight (g)
Bypass cold trap, 300°F	500	1 1/2	11	7
Bypass cold trap, 300°F	1000	2	11–14	13–15
Reactor grade (no cold trap)	500	1	7	8
0.05% O added as Na_2O_2 (no cold trap)	1000	2	20	15
0.15% O added as Na_2O_2 (no cold trap)	1000	2	30	26
1.0% Ba added (no cold trap)	500	1 1/2	11	7
1.0% Ba added (bypass cold trap)	1000	2	20	13
1.0% Mg added (bypass cold trap[b])	1000	2	14	16
Crystal-bar Ti rod inserted in hot leg	1000	2	23	13
Crystal-bar Zr rod inserted in hot leg	1000	2	14	15

[a] Maximum fluid temperature, 1500°F; ΔT, 300°F; sodium flow rate, 2.5 gal/min.

[b] Cold trap valved off after 50 hr.

temperature conditions (1500°F max). Mass transfer rates were compared against the results of standard loops operated with a 300°F bypass cold trap.

The effect of the before-test sodium purity was evaluated in an otherwise standard cold-trapped loop experiment. The entire loop was precleaned prior to operation by circulating a flush charge of sodium isothermally at 1500°F and draining it at 1000°F. The loop was then recharged with sodium that had been cold trapped in a second loop for over 100 hr at 300°F. No effect on mass transfer rate was found compared to a normally cold-trapped system.

The oxide content was increased relative to the standard loops first by elimination of the bypass cold trap and later by direct additions of Na_2O_2 to the sodium. As shown in Table IV, omission of the cold trap had no apparent effect on mass transfer over a 1000-hr period nor did the addition of 0.05 wt % O to the sodium. However, the addition of 0.15 wt % O doubled the mass transfer rate.

Other experiments to evaluate oxygen effects involved the addition of soluble deoxidants to the sodium and the inclusion of crystal-bar zirconium and titanium inserts in the hot-leg regions of the loops. As seen in Table IV, the mass transfer rates of these "gettered" loop experiments showed no differences from cold-trapped systems.

RESULTS OF INCONEL LOOPS CONTAINING NaK

Further evaluations of the effect of oxygen on the mass transfer of Inconel were made in a series of five loops that circulated the mixture 56% K–44% Na in place of sodium. The loops were operated for 1000 hr with a 1500°F maximum temperature, a 300°F ΔT, and a flow rate of 2.5 gal/min. The oxide content of the NaK was adjusted by (1) varying the minimum cold-trap temperature over the range 100 to 800°F and (2) eliminating the cold trap.

The test results for these NaK loops, shown in Table V, were generally similar to those from sodium loops operated under comparable temperature and flow conditions. Visual and metallographic examination of the economizer and cold-leg sections showed the same range and distribution of metallic deposits as in the sodium tests, although, as noted below, the weight of deposits was lower in the NaK systems. Hot-leg sections, like those in sodium tests, showed no effects other than shallow intergranular attack.

TABLE V. EFFECT OF COLD-TRAP OPERATION ON MASS TRANSFER IN INCONEL-NaK PUMPED LOOPS[a]

Minimum Cold-Trap Temperature (°F)	Total Weight of Mass-Transfer Deposits (g)	Maximum Deposition Rate (mg/cm^2)	Metallographic Results: Maximum Intergranular Attack (mils)	Metallographic Results: Maximum Deposit Thickness (mils)
100	b	b	1 1/2	7
300	b	13.1	1 1/2	12
600	3.86	11.5	1	11
800	6.29	17.6	1 1/2	20
c	b	14.9	1	12

[a] Maximum NaK temperature, 1500°F; sodium ΔT, 300°F; test time 100 hr.

[b] Not recorded.

[c] Loop operated with no cold trap.

Deposits formed in loops having cold-trap temperatures of 100 and 300°F were quite adherent to the loop wall and weight could be determined only for the point of maximum deposition. The maximum deposition rates are seen to be lower by a factor of 3 to 4 than those for equivalent sodium loop experiments (Tables IV, V). In the NaK tests with higher cold-trap temperatures, deposits were composed of larger crystallites and were more easily separated from the loop walls. The total weights of deposits in these latter loops were considerably less than for sodium loops operated with cold-trapped sodium. Despite the relatively large range of cold-trap temperatures covered in these NaK systems, very little change was noted in the maximum rate of deposition and, as judged from metallographic examinations, in the total weight of deposits. Thus, the absence of measurable oxygen effects observed in sodium systems below 0.05 wt % O was qualitatively borne out in these NaK tests.

STUDIES OF OTHER NICKEL-BASE ALLOYS

The mass transfer rates of Hastelloy B, Hastelloy W, and Inconel X were evaluated in cold-trapped sodium loops operated for 1000 hr at a 1500°F hot-leg temperature. Results are shown in Table VI. As in the case of Inconel loops, metallic mass transfer crystals composed predominantly of nickel were observed in the economizer and cold-leg regions in the same general distribution as shown in Fig. 3. The deposit weights ranged from 11 g for the Inconel X test to 20 g for the Hastelloy W test, compared to 13 to 15 g in standard Inconel loops. The maximum deposition rates were also comparable to those of Inconel tests.

A second Hastelloy B loop was operated for 1000 hr at a maximum temperature of 1300°F and a third loop for 2000 hr at 1500°F. The results, shown in Table VI, were generally the same as had been obtained in Inconel loops under comparable conditions.

STUDIES OF STAINLESS-STEEL LOOPS CONTAINING SODIUM

The final series of loop experiments in this program involved the operation of several austenitic stainless steels (types 316, 304, 347, 310, and 330) and one ferritic (type 430) under the following test conditions:

Maximum sodium temperature, °F	1500
Sodium ΔT, °F	300
Sodium flow rate, gal/min	2.5
Cold-trap temperature, °F	300
Test duration, hr	1000

An additional type 316 stainless-steel loop was conducted under the above conditions but with the maximum sodium temperature increased to 1650°F.

The test results for this series are shown in Table VII. All steels showed much lower mass transfer rates than did nickel-base alloys under equivalent test conditions. The steels containing 18% Cr and 10% Ni (types 316, 304, and 347) were the most corrosion resistant of the various types studied. Cold-leg sections from this group exhibited only traces of deposits under the above test conditions. In the case of type 304, deposition rates were below the limit of gravimetric detection. The mass transfer rate of type 316 was a factor of 10 higher at 1650°F than at 1500°F; however, even at this higher temperature the accumulation of deposits was much less than that found in Inconel sytems at 1500°F.

The deposits in these "18-10" stainless-steel tests at both 1500 and 1650°F were composed predominantly of chromium (Table VII). Iron and nickel concentrations, which were approximately equal, were less than 20 wt %. Examinations of hot-leg sections from these tests revealed very little intergranular attack but showed metallurgical changes attributable both to the operating temperature and to the selective removal of alloy constituents. Figure 7 compares photomicrographs taken at the positions of maximum wall temperature of the loops made from types 304 and 347 stainless steel. The martensitic-appearing precipitate evident near the exposed surface of the type 304 stainless-steel specimen is a transformation product that resulted from light cold work received when the specimen was polished for metallographic observation. The product was conspicuously absent near the center of the specimen and indicates that the surface compositional changes were in a direction to promote a ferritic or martensitic structure. The surfaces of the type 304 sample also showed a marked depletion of carbides compared to areas deeper in the sample. The grain boundaries of the type 316 stainless-steel specimen at 1500°F showed a relatively heavy concentration of sigma phase and an apparent depletion of carbide near the exposed surface. A much greater depletion of carbide was evident in the 1650°F specimen.

Although the effect of oxygen was not programmed as a test variable in the stainless-steel loop series, evidence of its importance was provided by a short-time 316 stainless-steel loop which operated without a

TABLE VI. OPERATING CONDITIONS AND RESULTS OF FORCED-CIRCULATION-LOOP TESTS OF HASTELLOY B, HASTELLOY W, AND INCONEL X WITH SODIUM AS THE CIRCULATED FLUID[a]

Loop Material[b]	Maximum Fluid Temperature (°F)	Operating Time (hr)	Maximum Hot-Leg Attack[c] (mils)	Total Weight of Cold-Leg Deposits (g)	Composition of Deposits, wt %			
					Ni	Cr	Mo	Other
Inconel X	1500	1000	1	11.0	85	11	d	0.1 Ti, 0.3 Al
Hastelloy B	1500	1000	2	17.3	94	d	0.6	d
Hastelloy B	1300	1000	2	0.45	94	1.0	1.0	2.0 Fe
Hastelloy B	1500	2000	2	20.6	97	0.5	0.5	d
Hastelloy W	1500	1000	1.50	20.6	92	3.0	0.8	d

[a] Sodium ΔT, 300°F; sodium flow rate, 2.5 gal/min.

[b] Alloy composition listed in Table I.

[c] Attack appeared as surface pits and subsurface voids.

[d] Not determined.

TABLE VII. RESULTS OF STAINLESS-STEEL LOOP STUDIES WITH SODIUM[a]

Type Stainless Steel	Operating Time (hr)	Maximum Temperature (°F)	Total Deposits		Attack (mils)	Deposit Analysis, wt %			
			(g)	(mils)		Ni	Cr	Fe	Other
316[b]	476	1500	0.8	1	2	17, 18	50, 56	20, 19	
316	1000	1500	0.17	1	3/4	> 5, > 5	>> 5, >>5	10, 3	1 Si, 0.02 Mo
316	1000	1650	1.7	5	2(voids)	5, 5	72, 79	22, 16	
304	1000	1500	c	<1	2	c	c	c	
347	1000	1500	0.29	<1	2	3.2	81	3.3	0.5 Nb
310	1000	1500	2.2	3	9	12, 40	82, 60	6, 0.2	
330	1000	1500	3.0[d]	2	2[d]	45, 64	50, 34	4, 2	
430	1000	1500	2.0	5	1	e	e	e	

[a] Sodium ΔT, 300°F; sodium flow rate, 2.5 gal/min.

[b] No cold trap.

[c] Insufficient for analysis.

[d] Some deposit lost during handling.

[e] Not determined.

cold trap. After 475 hr the weight of mass transfer deposits in this loop was four times greater than the 1000-hr cold-trapped loop test of this alloy.

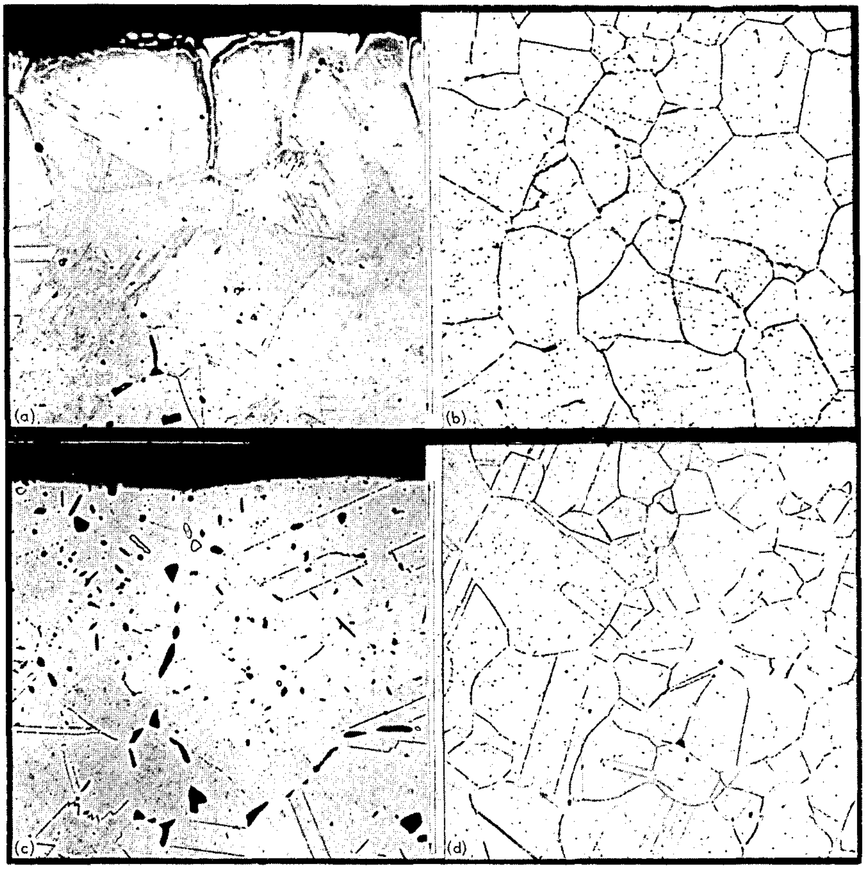

FIG. 7. Metallographic appearance of Types 304 and 316 stainless steel following exposure to sodium — Operating conditions: maximum temperature, 1500°F; ΔT, 300°F; flow, 2.5 gal/min; test time, 1000 h - (a) Type 304 sodium-exposed edge - (b) Type 304 center - (c) Type 316 sodium-exposed edge - (d) Type 316 center

Stainless steels containing greater percentages of chromium or nickel (types 310 and 330) showed correspondingly higher mass transfer rates. Deposit accumulations for these latter alloys were heavier in 1500°F tests than for type 316 stainless steel at 1650°F. The deposits again contained a large percentage of chromium. However, the concentration of nickel and particularly the iron-to-nickel ratio of these deposits was notably higher than for the 18-10 alloys.

A single loop test completed on a ferritic stainless steel (type 430) containing 14% Cr exhibited a mass transfer rate comparable to the higher alloy austenitic stainless steels.

DISCUSSION AND CONCLUSIONS

The relative mass transfer rates for the several alloys evaluated in this study are compared in Fig. 8. The comparison is based on cumulative deposit weights in 1000-hr loop tests. Immediately evident in this figure is the marked temperature dependence of mass transfer in Inconel and Hastelloy B systems between 1200 and 1500°F. Also apparent is the higher mass transfer rate of nickel-base alloys at 1500°F compared to stainless-steel systems under comparable conditions.

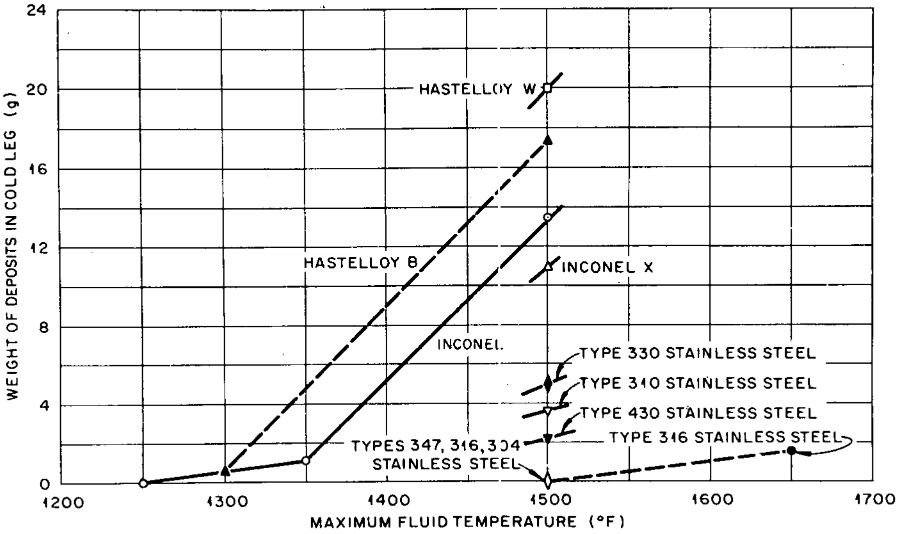

FIG. 8. Comparative mass transfer rates of nickel-base alloys and stainless steels in sodium - Operating conditions: ΔT, 300°F; flow, 2.5 gal/min; test time, 1000 h

Similar findings were noted by Russian investigators [3] in comparative evaluations of high-temperature alloys in cold-trapped sodium between 1300 and 1700°F. Their studies compared the corrosion rates of alloys containing 60 to 75% Ni, 16 to 20% Cr, and various amounts of W, Mo, Al, and Ti with those of a 20% Cr–14% Ni stainless steel. At 1300 to 1400°F, the corrosion rates of the nickel-base alloys over a 300-hr period were relatively low and comparable to those of the stainless steel. Further increases in temperature effected only small weight changes in the stainless-steel samples, while the weight changes of the nickel-base samples increased rapidly at 1500°F and above. They also noted that addition of 3% Al to the nickel-base system noticeably lowered the mass-transfer rate. The present investigation included a nickel-base alloy with 0.5% Al and 2.5% Ti (Inconel X), which also showed the lowest mass-transfer rate among the nickel-base alloys studied.

Despite the relatively high mass-transfer rates of the Inconel and Hastelloy alloys in sodium above 1300°F, the resultant attrition of hot-zone surfaces tended to be quite uniform without serious pitting or intergranular fissuring. Thus, in considering nickel-base systems for sodium containment, the problem of cold-leg flow restriction appears to be more important than that of hot-leg corrosion. For example, in Inconel systems operated for 1000 hr at 1500°F, the maximum deposit thickness reached 14 mils and decreased the flow area of the 1/2-in.-diam economizer by 6%.

Had the total weight of deposit in this loop been contributed by only one-fourth of the hot-leg surface, the corresponding average wall reduction would have been less than 0.2 mil.

Deposits in both the Inconel and Hastelloy systems were enriched in nickel over the base metal. However, the preferential depletion of nickel from hot-leg surfaces resulted in no observable metallographic or density changes, and the most serious corrosive effect was associated with shallow intergranular attack (1 to 2 mils). The depth of intergranular penetration increased only slightly in 1000 hr between 1300 and 1500°F and did not increase measurably in 2000 hr at 1500°F. In a related series of long-term Inconel loops [4], intergranular attack of Inconel at 1500°F reached 5 mils in 4000 hr. However, deposit thicknesses in the same loop exceeded 50 mils.

Another factor of importance to the selection of nickel-base materials for sodium service concerns the effect of oxygen contamination on corrosion. The mass transfer rates of Inconel at 1500°F were not measurably affected by changes in the oxygen content of either sodium or NaK below 500 ppm. This indicates that at normal oxygen levels the transport of nickel involves a nonoxidative solution mechanism and suggests either a higher equilibrium solubility or solution rate for nickel than for the other major alloy components (chromium and molybdenum). It further implies that a greater latitude in sodium purity can be permitted for nickel-base alloys than for stainless steels.

The effects of cold-trapped sodium on stainless steels, in contrast to nickel-base alloys, appear significant in a microscopic rather than macroscopic sense. Both the extent of deposition and degree of wall reduction for steels containing 18% Cr and 10% Ni were quite superficial. However, mass transfer in these systems involved the preferential movement of chromium and carbon which, while minor in terms of material transported, was manifested by significant metallurgical changes in the hot-zone surface. Although the nickel concentration of mass-transfer deposits in these stainless-steel systems increased in proportion to the amount present in the base metal, the ratio of chromium to nickel in these deposits was much higher than in deposits in Inconel systems.

The maximum deposition rates in both the nickel- and iron-base systems occurred midway through the cooler rather than at the coldest point in the loop. In fact, no mass transfer deposits were detected in either the relatively long cold-leg section beyond the pump or in the bypass cold-trap section, where the sodium temperature dropped to 300°F. One possible explanation for this behavior lies in the temperature dependence of the equilibrium concentrations of the affected solute species in sodium. If the dependence is exponential with temperature, less solute would be rejected in the first half of the cooling cycle than in the second half. Another explanation for the observed deposition profile may be found in the effects of temperature on the kinetics of nucleation and growth of the mass-transfer deposits. If the latter processes are diffusion controlled, deposition rates for a given degree of undercooling should fall off exponentially with temperature.

The effects of various operating parameters on the mass transfer behavior of Inconel-sodium systems were analyzed in terms of two possible corrosion models. In the first, the rate of transfer was assumed to be limited by the diffusion of solute through a liquid boundary layer and in the second, by the diffusion of nickel to the solid surface [5]. The first of the proposed mechanisms predicted a mass-transfer rate in 1500°F systems of between 400 and 1000 g for the 1000-hr test, compared with an observed value of 13 to 15 g. Furthermore, the temperature dependence of mass transfer predicted by this mechanism was less than that actually observed. Based on published data for the self-diffusion coefficient of nickel, the second of the proposed mechanisms gave an estimated mass transfer between 2 and 25 g for the 1000-hr operation at 1500°F, in better agreement with observation. Also, the temperature dependence predicted by the wall diffusion mechanism was in fair agreement with that observed above 1350°F. However, the solid-state diffusion mechanism fails to account for the observed dependence on flow rate and time. Both of the assumed mechanisms predicted the observed dependence on ΔT.

We conclude on the basis of these correlations that neither diffusion model by itself could account for the observed behavior. A more satisfactory model can be deduced by assuming one of the diffusion processes to control initially and the other to control at a later stage. Early in the corrosion process, when the nickel concentration of the hot-leg surfaces is relatively high, it seems reasonable that nickel transfer should be relatively rapid and dependent on the diffusivity of nickel in the liquid boundary layer. With preferential removal of nickel, however, the limiting transfer process would eventually revert to slower solid-state diffusion control.

REFERENCES

[1] BRIANT, R.C., WEINBERG, A.M., Nucl. Sci. Eng. 2 (1957) 799.
[2] GOLDMAN, K., MINUSHKIN, B., Reactor technology, selected reviews – 1965, USAEC rep. TID-8541 (1966) 351.
[3] NEVSOROV, B.A., et al., Proc. Intern. Conf. Peaceful Uses At. Energy, 3rd, Geneva, 1964, 9 (1965) 561–569.
[4] DEVAN, J.H., CROUSE, R.S., Metallurgy Div. Ann. Progr. Rep. for Period Ending Oct. 10, 1957, USAEC rep. ORNL-2422, 20–22.
[5] KEYES, J.J., Jr., Some calculations of diffusion controlled thermal gradient mass transfer, USAEC rep. ORNL CF-57-7-115 (1957).

DISCUSSION

J.R. WEEKS: You have shown us some very high concentrations of chromium in mass-transfer deposits in stainless-steel loops. What was the oxygen concentration of the sodium used in these experiments?

J.H. DEVAN: The oxygen concentration was not measured at the time the experiments were run. In our more recent studies on stainless steel we have tried to isolate some of these deposits, and what our analyses have revealed is a combination of metallic and non-metallic deposits. The metallic deposits are consistently high in iron and chromium whereas the non-metallic deposits consist almost entirely of chromium.

E. KRANZ: Did you study carbon mass transfer in your stainless-steel loops, and, if so, did you find any difference in mass transfer rates between the stabilized 347 and the unstabilized 304 and 316 steels?

J.H. DEVAN: No, there was no apparent difference between the three types of steel analysed. Perhaps I should add that I did not elaborate on the problem of carbon transfer because of the following problem: in some of our loops we got no carbon transfer at all but actually saw carburization of almost all the surfaces. Later, other loops showed definite depletion of carbon in the hot zone and enrichment in the cold zone. The problem seems to lie in the control of carbon in the sodium put into these systems: in some cases our sodium obviously must have contained more carbon than in others, so that the picture we get of carbon is incomplete and not entirely reliable. Personally, I am inclined to think that at these temperatures, using sodium very low in carbon, one will get hot-leg depletion with these three 18/8 stainless steels.

E. KRANZ: Did you find any evidence of mass transfer of niobium in your Type 347 stainless steel?

J. H. DEVAN: No. I can show you the analyses of deposits in the Type 347 loop if you wish, but there was very little niobium.

A. G. IOLTUKHOVSKY: Did you not observe an alpha-phase formation in the deeper layers and at the grain boundaries of your 18/8 steel samples after exposure in sodium?

J. H. DEVAN: We found none of the ferrite below about the outer 5 mils[1] of exposed surface. What you have seen in my photomicrograph is typical in that sense. We do, of course, find some sigma-phase formation in our 18/8 stainless steels after such long exposures, particularly in the intermediate temperature positions of the loops.

A. G. IOLTUKHOVSKY: Did you find more sigma-phase formation after exposure to sodium than, say, after high-temperature tests?

J. H. DEVAN: Yes, one effect of sodium exposure, particularly in the case of the Type 316 stainless steel, was a marked increase in sigma-phase formation, especially around the grain boundaries. I have photomicrographs of the 316 specimens that show this very clearly.

A. G. IOLTUKHOVSKY: In your photomicrographs one can see a very sharp boundary between the basic material and the mass transfer products deposited on it. Is it reasonable to assume that there is not interaction between them, and have you checked the deposits to see whether their thickness changes at all?

J. H. DEVAN: This is an interesting question. When I set about writing up the results of these investigations I intended to do a considerable amount of microprobe work on the samples, work that had not been done at the time the tests were run because we had no microprobe at that time. We now have a microprobe, but because of the heavy demands on it I have still not been able to use it on these specimens. I propose to examine as soon as possible both the structure of the hot-leg surfaces and the composition of the deposits, as well as the layer that has plated out on the cold-leg surface.

A. G. IOLTUKHOVSKY: Another question. You did not go into the effects of oxygen on the stability of your steels. Have you found that the effects of oxygen follow a predictable pattern, and would you say that the purification method you described is absolutely essential for stainless steels that are to be used in this temperature range?

J. H. DEVAN: If I understand your question properly, the answer is simply that we did not evaluate oxygen as a variable in our stainless-steel studies; we did not have an opportunity to do so because the programme was concluded immediately after the last series of tests I have described. However, our more recent studies with stainless steel definitely indicate a need for stringent control of oxygen in stainless-steel systems.

I believe I mentioned that the nickel-base alloys seem far less sensitive to oxygen in sodium than the iron-base alloys. We have found cases at these high temperatures where they actually revealed lower mass transfer rates than the iron-base alloys, and in heavily contaminated systems too.

---

[1] 1 mil = 0.001 in.

Where one has to deal with high levels of contamination the nickel-base alloys may prove to be the best alloys after all.

A. G. IOLTUKHOVSKY: In the high-nickel alloys you apparently found that the rate of corrosion diminishes with time. Did you observe the same effect in the steels?

J. H. DEVAN: We have not yet done the type of experiment on stainless steel that would enable us to establish a relationship between corrosion and time. Let me make one point, however: although the corrosion models discussed at this meeting have dealt only with the liquid phase of the diffusion processes, at the same time concentration gradients of material in the hot-leg surfaces have been mentioned. Certainly this suggests that we must consider solid-state diffusion in our corrosion models.

A. G. IOLTUKHOVSKY: One last question. Do you believe, after these investigations, that stainless steels and high-nickel alloys (such as Inconel) could be used for thin-walled structures?

J. H. DEVAN: Here corrosion is only one of many problems that must be considered. The metallurgists at the Oak Ridge National Laboratory feel very strongly that minimum section thicknesses must be maintained at something over 20 mils. Our counterparts at many other laboratories in the United States do not agree. Our conservatism is inspired mainly by the problem of inspection, by the need to avoid defects which could result in damage to thin-walled tubes. You should bear in mind, too, that the types of stainless steel we have been talking about become extremely weak at about 800°C. At such high temperatures their applications would be rather limited.

A. G. IOLTUKHOVSKY: To conclude, I should like to comment briefly on our own work. In experiments similar to yours we have observed alpha-phase formation through the whole cross-section of thin-walled samples (up to 0.5 mm), progressing inward from the surface and following the grain boundaries. This was particularly marked in steels of unstable structure such as the 18/8 steels.

In the Type 316 steels we observed sigma-phase formation, a finely dispersed sigma phase which seemed to follow the alpha phase; in other words the formation of the two was to all appearances related. In zones where no alpha phase was found we observed no sigma phase either. The alpha phase was detected by means of magnetometallography.

BEHAVIOR OF REFRACTORY METALS AND ALLOYS IN BOILING SODIUM AND OTHER BOILING ALKALI METALS*

A. ROMANO, A. FLEITMAN AND C. KLAMUT
BROOKHAVEN NATIONAL LABORATORY,
UPTON, NEW YORK,
UNITED STATES OF AMERICA

(Presented by J. R. Weeks)

Abstract

BEHAVIOUR OF REFRACTORY METALS AND ALLOYS IN BOILING SODIUM AND OTHER BOILING ALKALI METALS. In high temperature Rankine cycle space power systems increasing the radiator temperature results in high thermodynamic efficiency, and more important, a more favourable power-to-weight ratio. Of the alkali metals, sodium has attractive properties for high-temperature operation and caesium has desirable properties for low-temperature service. This study was undertaken to determine whether sodium and caesium (boiling and liquid) can be contained in refractory metal alloys. Other alkali metals were also tested in these alloys to compare their corrosiveness with that of sodium and caesium.

The studies were conducted in reflux capsule tests and in a forced circulation loop. Tests were conducted in high-vacuum chambers operating at 10^{-8} torr to minimize embrittlement and accelerated corrosion occurring when the refractory metals are contaminated with reactive gases.

Seventeen refractory metal alloys such as Nb-1Zr, Nb-10W-1Zr, Nb-10W-10Ta, Ta-10W, Ta-8W-2Hf, etc., were tested in boiling sodium at temperatures up to 1320°C and for as long as 10 000 h. The other alkali metals were Cs, Rb, Li and K. In all the tests, purified alkali metals (by contacting with Zr foil at 650°C) were used.

Of all the refractory metal alloys tested, alloy FS-85 (Nb-27 Ta-10W-1Zr) was the most susceptible to corrosion by sodium; intergranular penetration as deep as 0.05 mm was detected in one test. Several other alloys exhibited very slight transgranular corrosion by sodium but most of the alloys were not attacked. None of the alloys seem to be susceptible to stress-induced corrosion.

The compatibility of two alloys (Nb-1Zr and Nb-10W-1Zr) with Li, Na, K, Rb and Cs was also evaluated. In general, very slight corrosion of Nb-1Zr was detected in these tests, although K seemed to be the least aggressive of the alkali metals. There was no corrosion of Nb-10W-1Zr detected by any of the alkali metals.

Of all the alkali metals, Cs offers the most attractive thermodynamic properties relative to optimum turbine design. The recent drastic reduced cost and availability of Cs have made it attractive for Rankine cycle applications. Molybdenum-base alloys TZM and TZC have been tested under conditions of high-velocity vapour impingement (245 m/s) at 840°C for 1096 h in a forced circulation loop fabricated completely of refractory metals. Caesium is boiled at 960°C, condensed at 650°C, and the mass flow rate is 41 kg/h. Results of this test showed no corrosion or erosion of either of the test materials, but a 0.025 mm thick deposit of Nb was found on each impingement blade.

Introduction

Among the most promising advanced high performance systems for space power applications are the reactor turbo-electric and reactor-thermionic types. To obtain this high performance, liquid metals, and more specifically the alkali metals, must be used.[1] Two basic questions relative to

---

* This work was performed under the auspices of the United States Atomic Energy Commission.

the use of alkali metals are (1) which of the alkali metals should be used to obtain the highest performance, most reliable system, and (2) are there engineering materials available to contain the alkali metals?

A study[1] of these questions concluded that there was not enough information available to single out any one of the alkali metals for intensive investigation. Extensive corrosion studies and engineering development has been done with potassium since it represents perhaps the best compromise of all requirements. However, sodium is the most attractive alkali metal for high thermal efficiency whereas cesium is the best choice for optimum turbine performance.

In this investigation, the compatibility of both Na and Cs with refractory metals and their alloys were studied. Two tests were conducted in order to resolve the question of which of the alkali metals (Li, Na, K, Rb, Cs) was most compatible with the refractory metals in the 1100 °C temperature range.

Sodium Corrosion of High-Strength Alloys

Extensive testing of the refractory metals in Li and K[2-5] showed corrosion to be strongly dependent on oxygen in the system. Our tests indicate the same dependency in the Na-refractory metal systems.[6] These results show that very little corrosion occurs because of simple dissolution of the refractory metals or their alloying constituents. To obtain low corrosion rates, it is necessary to maintain less than 10 ppm oxygen in the Na and incorporate a "getter element" such as Zr, Ti or Hf in the refractory metal alloy. Also, it is necessary to heat-treat the gettered alloys to insure that less than some finite limiting amount of oxygen is in solid solution.[7]

The Nb-1Zr alloy has been extensively tested to determine its compatibility with all of the alkali metals. The program at BNL has shown Nb-1Zr to be an excellent containment material for liquid and boiling Na at temperatures up to 1200 °C for as long as 10 000 hours. Unfortunately the Nb-1Zr alloy does not have adequate creep and rupture strength properties above 1150 °C. Many Nb, Ta and Mo base alloys have been developed or are being developed which do have excellent strength up to 1400 °C.

Several high-strength alloys(a) were tested in purified(b) Na at 1315 °C. In order to minimize the effect of external environment on the corrosion test, all tests were performed in vacuum chambers utilizing sputter-ion pumps nominally operating at 1 x 10^{-8} torr. Results of these tests are summarized in Table II. Initial tests of these alloys were performed on specimens which were inserted into capsules fabricated of alloy D-43. As more material (either in tubes or bar form) became available, the tests were repeated in capsules fabricated entirely of the alloy. These latter tests were run for 6271 hours as compared to 3000 hours for the insert specimen tests. All specimen and capsule internal surfaces were polished to a 1 x 10^{-4} mm rms finish to provide reference surfaces suitable for post-test metallographic corrosion evaluation.

(a) Compositions of alloys tested are shown in Table I.

(b) Hot gettered with Zr at 650 °C for 250 hrs prior to test. Analysis of purified Na by Hg amalgamation procedure indicated O to be <10 ppm.

Table I

Nominal Composition of Alloys Tested in Program

Alloy Designation	Alloying Element, wt %									
	Nb	Ta	Mo	W	V	Zr	Ti	Hf	C	Others
AS-55	Bal			5		1			0.06	0.2Y
B-66	Bal		5		5	1				
Cb-753	Bal				5	1				
Cb-Ti	Bal						10			
D-11	Bal					1				
D-14	Bal					5				
D-43	Bal			10		1			0.1	
F-48	Bal		5	15		1			0.05	
FS-60		Bal		10						
FS-85	Bal	27		10		1				
S-291	Bal	10		10						
T-111		Bal		8				2		
T-222		Bal		10				2.5	0.1	
TZC			Bal			0.35	1.4		1.15	
TZM			Bal			0.08	0.5			
W-26Re				Bal						26Re
X-34	Bal			5		3			0.1	

Table II

Corrosion Results on High-Strength Refractory Metals

Alloys Tested in Na at 1315°C

Alloy Designation	Monometallic Capsule, Test Time 6,271 Hours	Tested as Insert in D-43 Capsule for 3,000 Hours
D-43	No Corrosion	No Corrosion
FS-85	0.05-mm G.B. Attack in Weld Both Liquid and Vapor Regions	0.05-mm G.B. Liquid Region
FS-60	-	No Corrosion
T-111	No Corrosion	0.025 mm G.B. Attack Vapor Region
TZM	0.01-mm G.B. Attack of Weld in Vapor Region	No Corrosion
X-34	No Corrosion	-

Alloy D-43 appeared best, not showing corrosion in either test. Tantalum alloy T-111 and Mo alloy TZM exhibited 0.025 mm or less corrosion. Alloy FS-85 was by far the poorest; metallographic inspection showed as deep as 0.05-mm attack in the insert test and in the capsule test as shown in Figure 1 and Figure 2 respectively. The FS-60 alloy was purposely not tested here as a monometallic capsule since results from other monometallic tests conducted at BNL have shown this alloy corrodes severely if oxygen in the Na is not adequately controlled.[8] These tests also showed increased corrosion with increasing levels of oxygen in the Na. The lack of corrosion of Ta-10W in the insert test is probably due to the D-43 capsule acting as a "getter" thus tying up the oxygen initially present in the Na and maintaining it at a low level during the test.

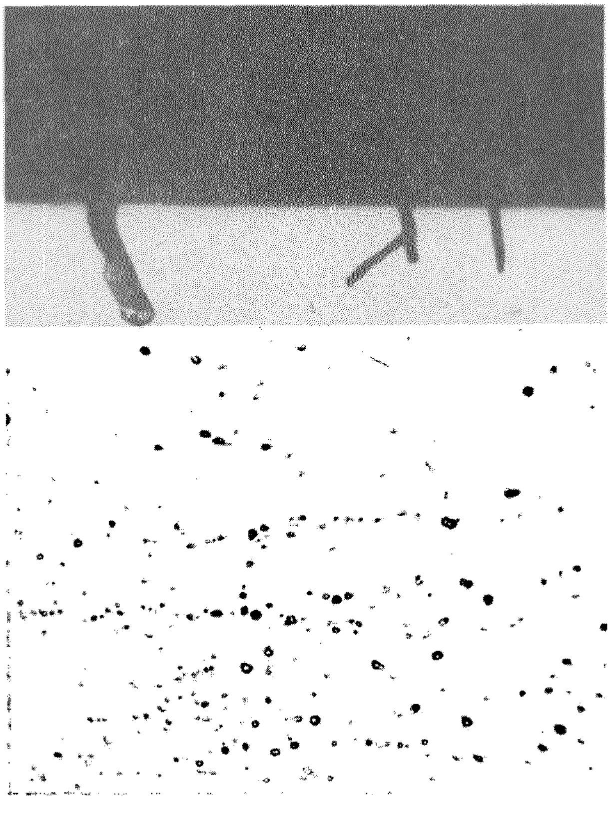

FIG. 1. Grain boundary corrosion (0.05-mm deep) of alloy FS-85 insert after exposure to 1315°C sodium for 3000 h (250X)

Weeks[9] has postulated a possible embrittlement phenomena for alkali metal-refractory metal systems. In order to determine if such an effect were present in Na, sheet specimens of several high-strength alloys were prestrained and tested in purified Na in Nb-1Zr capsules at 1000°C for 2000 hours. A test temperature of 1000°C was selected since it represented a temperature high enough to obtain corrosion and low enough so that rapid stress relief of the specimen did not occur. Results of this test are summarized in Table III.

No cracking was observed to have occurred in any of the samples. These results confirm observations made in similar tests with potassium.[10] Control samples which were exposed at the test temperature in the vacuum chamber but not in the sodium also showed no effect of bending and subsequent thermal aging. Very slight roughening was observed in the TZM and S-291 alloys. However, measurable corrosion (0.02 mm) in the form of grain boundary attack was detected on the FS-85 alloy. This agrees with the tests described above in which FS-85 corroded at higher temperatures. The susceptibility of this alloy to grain boundary attack is not apparent at this time in view of the low O content (140 ppm) and presence of Zr. Interestingly it is the most highly alloyed composition tested.

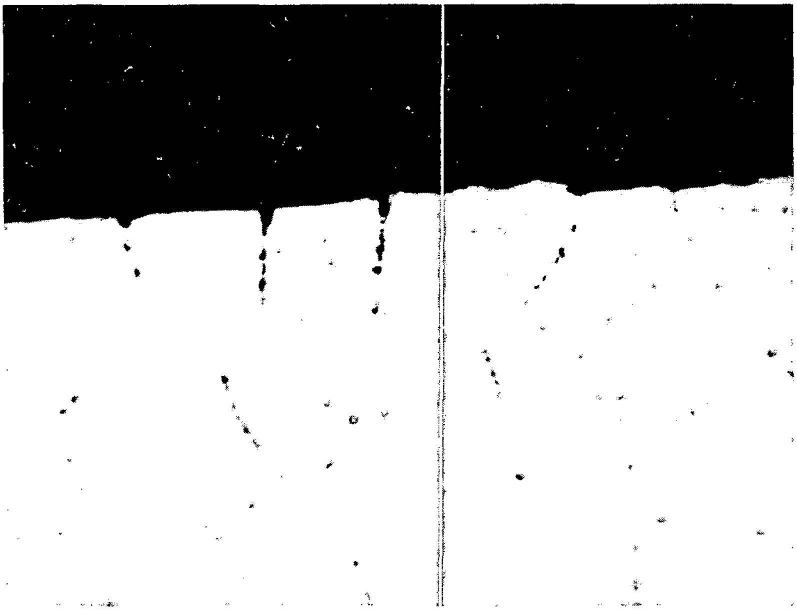

FIG.2. Grain boundary corrosion (0.02-mm deep) of heat-affected zone of weld in alloy. FS-85 capsule after exposure to 1315°C sodium for 6271 h (250X)

Relative Corrosion by Alkali Metals

Experimental results obtained at various laboratories show that under well-controlled conditions any of the alkali metals could be adequately contained in refractory metal alloys.[11] Unfortunately, test parameters varied from laboratory to laboratory so it was difficult, if not impossible, to select which of the alkali metals was least aggressive.

Two tests, one with Nb-1Zr and the other with alloy D-43, with identical capsules containing either Li, Na, K, Rb or Cs, were run at the same temperature for 6000 and 9000 hours respectively. Reflux rates for the various alkali metals increase with increasing atomic weight by a factor of 50 with Cs refluxing at the highest rate and Li the lowest. In this respect, this experiment was a compromise; however, it was felt the relative corrosion rates could be normalized with respect to the relative reflux rates.

Table III

Corrosion Results of Refractory Metal Alloy Pre-Strained Inserts Tested in Na at 1000°C for 2,000 Hours

Alloy Designation	Results of Metallographic Examination
FS-85	0.02 mm grain boundary attack. No cracking
T-111 TZM S-291	Slight transgranular roughening of polished surfaces. No cracking.
AS-55 B-66 Cb-753 Cb-Ti D-11 D-14 D-43 F-48 FS-60 T-222 W-26Re	No corrosion detected on any of these inserts. No cracking.

Table IV

Relative Aggressiveness of Alkali Metals in Refractory Metal Alloys Nb-1Zr and D-43

Alkali Metal*	Capsule Material: Nb-1Zr Temperature: 1150°C Time: 6,000 Hours	Capsule Material: D-43 Temperature: 1205°C Time: 9,437 Hours
Cs	Slight attack at liquid vapor interface	No corrosion
Rb	Slight attack at liquid vapor interface	No corrosion
K	No corrosion	No corrosion
Na	Slight attack at liquid vapor interface	No corrosion
Li	Slight attack at liquid vapor interface	No corrosion

*All alkali metals purified by contacting with Zr at 650°C for 250 hours.

Results of these tests are shown in Table IV. Generally, very little or no corrosion occurred making the selection of the alkali metal showing the least aggressiveness difficult. A very careful metallographic examination of the surfaces was made and on this basis it was judged that Cs, Rb, Na and Li were comparable and K the least aggressive. This is based on the relative post-test surface roughness. No penetrating grain boundary attack was detected in either the Nb-1Zr or D-43 alloy with any of the alkali metal.

On the basis of these tests it appears alkali metal-refractory metal compatibility could not be the criterion for selection of a specific alkali metal.

High-Velocity Cesium Impingement Studies

Sodium was initially chosen for study in this program since it had the most desirable physical properties for advanced high-temperature Rankine cycle power conversion systems. Fuel element and radiator development to date have indicated a major breakthrough in those areas would be necessary to attain the temperatures at which Na could be used.

Recent system design studies[12,13] have favored the use of Cs as the fluid for a Rankine cycle because it represents the preferred alkali metal for optimum turbine performance. Since the turbine appears to be a major problem in Rankine cycle systems there has been renewed interest in Cs. Originally Cs was discounted because of its high cost, but recent advances in the alkali metals industry have reduced the price to $330/kg with a further reduction to $22/kg in 5,000 kg quantities.[14] These developments shifted the emphasis in this program to Cs.

A forced-circulation loop,originally designed to test resistance of materials to Na vapor impingement,was modified to test materials in Cs vapor. The loop is shown schematically in Figure 3. Construction of the loop is entirely of refractory metals with Nb-1Zr the major alloy of construction. Valves fabricated completely of Nb-1Zr were used to regulate flow and isolate the flowing Cs from a dump tank. A General Electric spiral induction pump was used to circulate the Cs at 41 kg/hr. All heat transfer was by radiation. The boiler was heated by a low voltage-high current tungsten mesh heater and the condenser radiated to an air-cooled surface. Pressure transmitters made of Nb-1Zr bodies and Ta diaphragms were used to measure the pressure at the boiler and condenser. Temperatures were measured with W-5Re vs W-26Re thermocouples insulated with high purity alumina. To avoid contamination by oxygen, nitrogen and hydrogen, which could obscure corrosion results or embrittle the refractory metals, the loop was operated in a high-vacuum chamber 3-m high and 1.25 m in diameter. A 1200-liter/sec sputter-ion pump maintained the chamber pressure at $\sim 1 \times 10^{-7}$ torr at loop-operating conditions. The Cs was contacted with Zr chips at 650°C for 250 hours just prior to filling the loop.

The vapor impingement test section consisted of two parallel nozzles and blade sections operating at the same conditions. Both nozzles (fabricated of Nb-1Zr) were of the convergent type having a throat diameter of 1.8 mm. This gave a vapor velocity of 245 m/sec which is 0.7 Mach for Cs vapor. One impingement blade was made of molybdenum alloy TZM and the other TZC, also a molybdenum alloy. Molybdenum alloys were chosen because of their high strength-to-weight ratio and resistance to Cs attack.

Both blades were polished to a 1 x 10^{-4} mm rms finish and weighed before test. Finely polished corrosion specimens were also located in the boiler condenser and superheater coils, and also at the exit of the vapor impingement section.

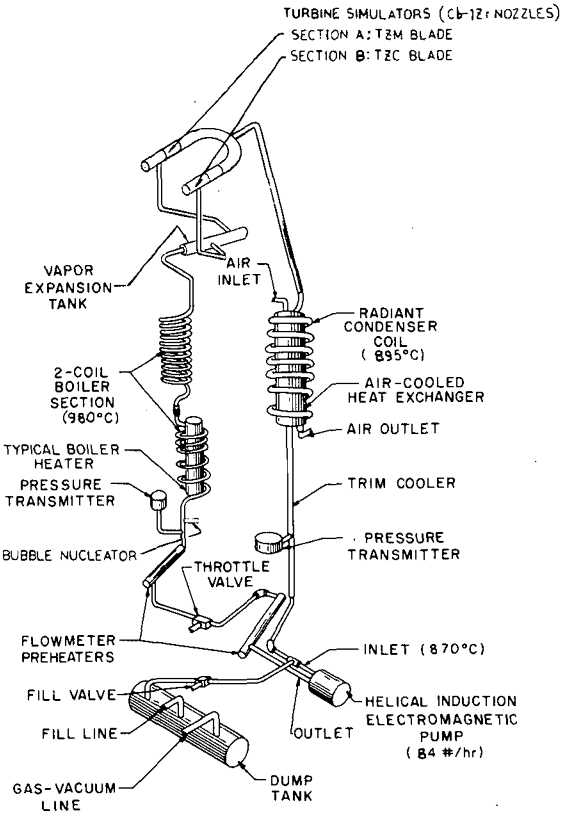

FIG.3. Pumped cesium loop schematic layout

Conditions for the first test run are shown in Table V. Temperatures were measured with thermocouples in wells located at the entrance to the test sections. The vapor quality was estimated to be 80% ± 10% from the known boiling condition by performing a heat balance across the superheater section. These operating parameters were chosen since they represented the wettest stage in a typical Cs turbine which is expected to be the worst condition relative to materials behavior.

The appearance of the blades and nozzles after test are shown in Figures 4 and 5. In Figure 4, the apparent vortexing of the vapor on the back side (downstream side) of the blade is noticeable. Examination of this area indicated the discoloration was merely a stain and no corrosion or deposition occurred. Figure 5 is a photograph of the front or impingement side of the blades showing a definite darkened zone outlining the high velocity vapor impingement area. No evidence of material loss from the blade could be detected by metallographic examination. In fact, post-test weight measurements indicated a weight gain in the order of 1 mg.

Table V

Forced Circulation Boiling Cs Loop
Operating Conditions - Run 1

Materials:	Nozzles (2) - Nb-1Zr Impingement blades (2) - TZM and TZC
Temperatures:	Boiling - 960°C ± 10°C Impingement - 840°C ± 20°C Condensing - 650°C ± 20°C
Vapor Quality:	Impingement - 80% ± 10%
Vapor Velocity:	Impingement - 245 m/sec ± 30 m/sec
Mass Flow Rate:	41 Kg/hr ± 4 Kg/hr
Operating Time:	1096 hours

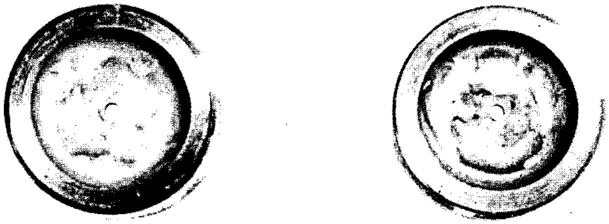

Nb-1Zr NOZZLES

TZC BLADE TZM BLADE

FIG.4. Back side or downstream side of nozzles and blades showing apparent vortexing on blades after 1096-h exposure to 840°C cesium vapor impinging at 245 m/s

The darkened zone on the blade was a metallic deposit with a maximum thickness of 0.025 mm. A photomicrograph of the deposit is shown in Figure 6. Notable in this figure are the excellent condition of the blade surface and the sponginess of the deposits. The deposit, however, was quite adherent. An electron microprobe analysis of this layer indicated the major constituent to be Nb. A similar, but non-adherent deposit, was found in the throat of the nozzles.

Metallographic examination was made of various finely polished test specimens located in the boiler-superheater sections of the loop. No corrosion was detectable by this analysis.

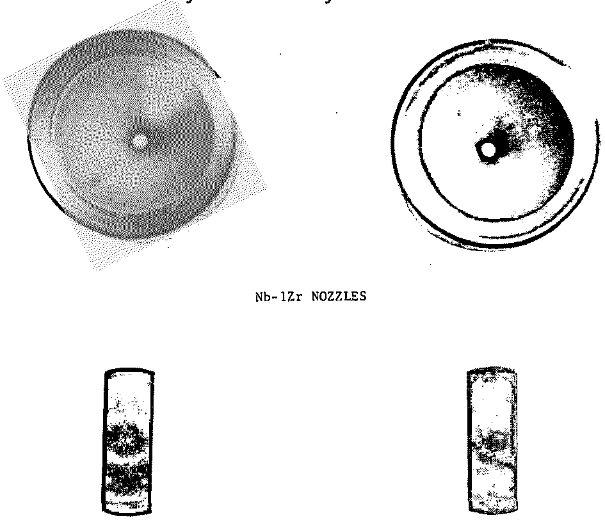

FIG. 5. Front or impingement side of nozzles and blades showing darkened area of deposition on blades

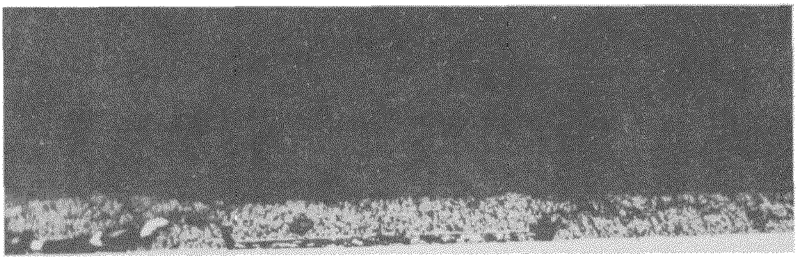

FIG. 6. Photomicrograph of typical impingement blade showing 0.0025-mm deep adherent Nb deposit (250X)

Although no finite corrosion was detected on the Nb-1Zr loop specimen it is expected that some corrosion occurs. Corrosion products are likely to accumulate in the boiler to form particulates which are then carried in a vapor-liquid mixture. Since the superheat condition was not attained in the loop, the liquid droplets remained in the vapor and were accelerated in the nozzles. The high velocity impingement caused the particulates to separate from the liquid and adhere (weld) to the blades.

Summary

Exposure of many high-strength alloys to refluxing Na did not indicate the presence of any stress corrosion effects. However, these tests were performed at a temperature where stress relief begins to occur. Future tests should be conducted at lower temperatures under continued applied stress. These tests did show that of the alloys tested, FS-85 was most susceptible to corrosion.

Tests to compare the relative aggressiveness of the various alkali metals to two Nb base alloys up to 1205°C pointed to the excellent resistance of these alloys to all the alkali metals. There was some slight indication that K may be the least aggressive of the alkali metals.

Niobium-1Zr has shown excellent resistance to Cs liquid and vapor at high velocities. Molybdenum alloys TZM and TZC have demonstrated good resistance to wet Cs vapor impingement at 840°C at 245 m/sec. The results of the test reported here point to the need for system boiler and superheater designs which will generate vapor free of entrained liquid. The presence of these entrained liquids even carrying small quantities of corrosion products could create serious problems in turbines by causing unbalanced wheels rotating at high velocities.

Acknowledgements

The authors would like to thank their project advisor, D. H. Gurinsky, for his guidance during this study.

Special gratitude is extended to the personnel in the various groups who provided invaluable assistance in performing the functions leading to the publication of this paper. The authors would like to thank the Metallography Group and the Reactor Metallurgy Group of the Metallurgy and Materials Science Division, and to the Analytical Chemistry Group of the Hot Laboratory Division.

References

[1] ROSENBLUM, L., The use of liquid metals in space electric power systems, Journal of Metals 15 (1963) 637.
[2] Proc. AEC-NASA Liquid Metals Information Meeting Conf-650411 (1965).
[3] FREED, M. S., Corrosion of columbium base and other structural alloys in high temperature lithium, USAEC Rep. PWAC-355 (1961).
[4] DiSTEFANO, J. R., Corrosion of refractory metals by lithium, USAEC Rep. ORNL-3551 (1964).
[5] DiSTEFANO, J. R. and LITMAN, A. P., Effects of impurities in some refractory metal-alkali metal systems, Corrosion 20 (1964) 12.
[6] ROMANO, A. J., FLEITMAN, A. H., and KLAMUT, C. J., The evaluation of Li, Na, K, Rb, and Cs boiling and condensing in Nb-1%Zr capsules, to be published in Nuclear Applications.
[7] SCHENCK, G. F., Application of internal friction methods to corrosion study in columbium alloys, ASTM Technical Report MP5-1.3 (1965).

[8] ROMANO, A. J., FLEITMAN, A. H., and KLAMUT, C. J., A summary of the high temperature alkali metal corrosion program at Brookhaven National Laboratory, Conf-650411 (1965) 217-234.
[9] WEEKS, J. R., Corrosion mechanisms - panel presentation, Proc. NASA-AEC Liquid Metals Corrosion Meeting - Vol. I, NASA-SP-41 (1963) 97-99.
[10] SCHEUERMANN, C. M. and BARRETT, C. A., Compatibility of columbium and tantalum tubing alloys with refluxing potassium, NASA TN D-3429 (1966).
[11] STANG, J. H. et al., Compatibility of liquid and vapor alkali metals with construction materials, DMIC Rep. 227 (1966).
[12] BLINN, H. O., et al., Space Power Plant Study - Final Report, NASA 5-250 (1963).
[13] GLASSMAN, A. J., and FUTRAL, S. M., Analytical study of turbine geometry characteristics for alkali-metal turboelectric space power systems, NASA TN D-1710 (1963).
[14] TEPPER, F. (Mine Safety Appliances Research) to KLAMUT, C. J. (Brookhaven National Laboratory), Private communication (1965).

DISCUSSION

R. I. HODGE: Do you not think it probable that the vapour in the jet in your impingement tests is completely supersaturated at the plane of the target? This metastable dry state would then account for the lack of erosion on the impact surface, for it seems likely that any liquid phase would cause erosion at such a velocity.

J. R. WEEKS: This is possible. The saturation pressure at the impingement specimens corresponded to some level between the vapour pressure of caesium at the boiling and condensing temperatures. Another possibility is that the boiling process scattered solute-saturated liquid into the vapour zone where it subsequently evaporated, leaving fine particles of niobium which were then carried by the high-velocity vapour into the nozzle, where they collected by impingement on the turbine blade simulator.

LITHIUM AND POTASSIUM CORROSION STUDIES WITH REFRACTORY METALS *

J.H. DEVAN, A.P. LITMAN,
J.R. DISTEFANO AND C.E. SESSIONS
OAK RIDGE NATIONAL LABORATORY,
METALS AND CERAMICS DIVISION,
OAK RIDGE, TENN.,
UNITED STATES OF AMERICA

Abstract

LITHIUM AND POTASSIUM CORROSION STUDIES WITH REFRACTORY METALS. Potassium and lithium are of interest as coolants for high temperature reactor systems. Current corrosion studies of these liquids centre on their compatibility with refractory metals in the range 1100-1400°C. A review is given of the present status of these corrosion studies and compares the effects of contaminants in the two liquids.

The solubilities of refractory metals have been measured in potassium up to 1400°C. Except for tantalum, solubilities were generally less than 100 ppm, but were increased substantially by the presence of oxygen in either the liquid or refractory metals. In the absence of oxygen, alloys of niobium, tantalum or molybdenum have shown little evidence of corrosion or mass transfer in boiling potassium for up to 10 000 h at 1200°C and 5000 h at 1300°C. Simulated nozzle and turbine blades made of Nb-1% Zr, TZM, and Mo-½% Ti showed surprisingly little impingement damage upon exposure to high-velocity vapour for times up to 5000 h at 1000-1200°C.

Capsule tests of refractory metals in lithium have shown relatively low solubilities and negligible attack up to 1320°C. Unlike potassium, oxygen in lithium does not appear to affect the corrosion resistance of refractory metals; however, rapid penetration of tantalum or niobium by lithium occurs if >200 ppm O is present in the solid metal. Most advanced refractory-metal alloys contain an active metal such as hafnium or zirconium which raise the minimum oxygen required for lithium penetration by forming HfO_2 or ZrO_2, thus preventing oxygen from entering into corrosion reactions.

Excellent compatibility of refractory metals with lithium has been demonstrated in thermal- and forced-circulation-loop tests operated for up to 10 000 h at 1200°C. Mass transfer studies at 1200°C have indicated a preferential transfer of zirconium, nitrogen and carbon in niobium-base systems. Further studies of this effect will be required at higher temperatures and flow rates.

The generally good compatibility of refractory metals with both lithium and potassium reported throughout the literature suggest that the useful application of systems involving these materials may be limited by strength rather than corrosion.

INTRODUCTION

Lithium and potassium offer outstanding properties as coolant and working fluid, respectively, for high-temperature heat engines. Current interest in these alkali metals centers on nuclear reactor systems being developed to supply electrical or motive power in aerospace vehicles.

Refractory metals such as niobium, tantalum and molybdenum show low solubilities in both lithium and potassium and, by virtue of their strength at elevated temperatures, are attractive container materials for such systems. The general corrosion properties of refractory metals

---

* Research sponsored by the United States Atomic Energy Commission under contract with the Union Carbide Corporation.

in liquid alkali metals were reviewed in an earlier report [1]. Data at that time, obtained mainly from capsule tests, indicated that, in the absence of oxidizing impurities, there was negligible dissolutive attack of refractory metals by either potassium or lithium up to the maximum temperature investigated, approximately 1200°C. Subsequent corrosion experiments have been conducted to extend both the temperature and velocity ranges of previous investigations as well as evaluate newer refractory metal systems. The present paper reviews the results of these more recent experiments with lithium and potassium and discusses the relative corrosion properties of these two liquid metals, particularly with respect to oxide impurity effects. Compositions of refractory metals reviewed are listed in Table I.

TABLE I. NOMINAL COMPOSITION OF REFRACTORY ALLOYS

Alloy Designation	Composition, wt %									
	Nb	Ta	W	Zr	Mo	V	Hf	Ti	Y	C
Niobium Base										
B-33	Bal					5				
D-14	Bal			5						
SCb-291	Bal	10	10							
AS-55	Bal		5	1					0.3	
D-43	Bal		10	1						0.1
B-66	Bal			1	5	5				
C-129	Bal		10				10			
Cb-752	Bal		10	2.5						
Cb-753	Bal			1.25		5				
FS-85	Bal	28	10	1						
PWC-11	Bal			1						0.1
PWC-33	Bal			3						0.3
PWC-533	Bal			3	5			3		
Tantalum Base										
T-111		Bal	8				2			
T-222		Bal	10				2.5			0.02
Molybdenum Base										
TZM				0.1	Bal			0.5		0.01

POTASSIUM CORROSION STUDIES

Corrosion experiments with potassium continue to show excellent compatibility of refractory metals with potassium liquid and vapor up to 1400°C [2]. The most significant parameters affecting compatibility, aside from temperature, are concentrations of impurities in the system such as oxygen, nitrogen, and carbon. Recent studies have been directed toward understanding the mechanism of corrosion in both liquid and boiling potassium systems when oxygen is present and furnishing quantitative data on the rates of corrosion as a function of temperature, velocity, and impurity content. Since current interest in potassium is primarily as a thermodynamic working fluid, the majority of corrosion studies have involved liquid-vapor systems in refluxing capsules and natural- or forced-circulation loops.

The various types of corrosion observed in potassium systems are consanguineous to sodium and NaK [3]. Virtually no dissolutive attack of refractory metals has been observed in these liquid metals below 1200°C in the absence of oxygen-containing impurities. However, in each of these systems, the presence of oxygen in either the refractory or alkali metal can lead to deleterious corrosion effects [4].

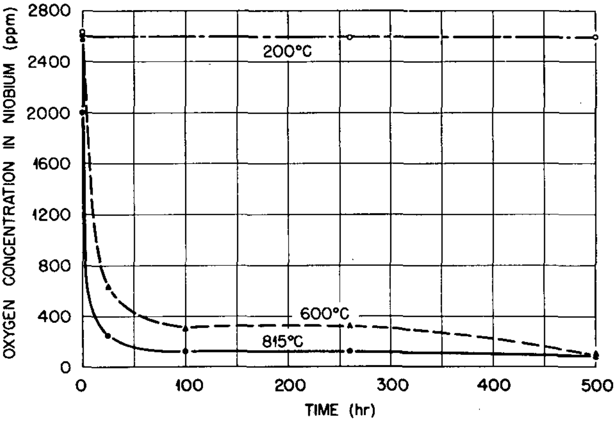

FIG.1. Effect of time on the migration of oxygen from niobium in contact with potassium

A detailed investigation of the oxygen-niobium-liquid potassium system has shown that oxygen is rapidly depleted from commercially pure or oxygen-doped niobium in potassium above 600°C [5]. The rates of depletion, shown in Fig. 1, have been related to the solid-state diffusion of oxygen in niobium [6]. This behavior is in opposition to thermodynamic predictions of oxygen migration based on the relative stabilities of the binary oxides of niobium and potassium and suggests the existence of relatively stable mixed oxides in the system. Characterization of possible complex oxides was attempted by reacting niobium and its oxides with excess potassium [5]. Although, a small amount of $KNbO_3$ was detected in these experiments, it appeared to have formed during cooling to room temperature. Thus, evidence for mixed metal oxides in the niobium-potassium system remains circumstantial. The mixed metal compound theory of attack in oxygenated potassium systems has, nevertheless, found reinforcement in corrosion investigations on molybdenum where K_2MoO_4 was the mixed oxide formed [7,8], on tantalum where $K_2Ta_4O_{11}$ was found [9], and by solubility experiments on very pure and oxygen-contaminated systems, discussed below.

Recent studies of the reactions of very active refractory metals in potassium have centered around zirconium and have emphasized oxygen redistribution. Prior to the formation of a visible oxide scale on the zirconium, the partitioning of oxygen appears to be solid-state diffusion controlled [10]. In capsule tests conducted for 100 hr at

815°C, the weight fraction of oxygen acquired by zirconium from potassium was a reproducible function of zirconium specimen thickness and initial oxygen content of the potassium (Fig. 2). This information has been successfully applied to the chemical analysis of oxygen in potassium in the 100 to 3000 ppm range [10].

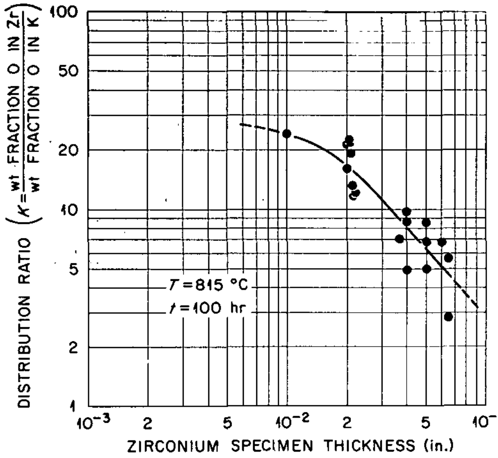

FIG. 2. Distribution ratio for oxygen between zirconium and potassium

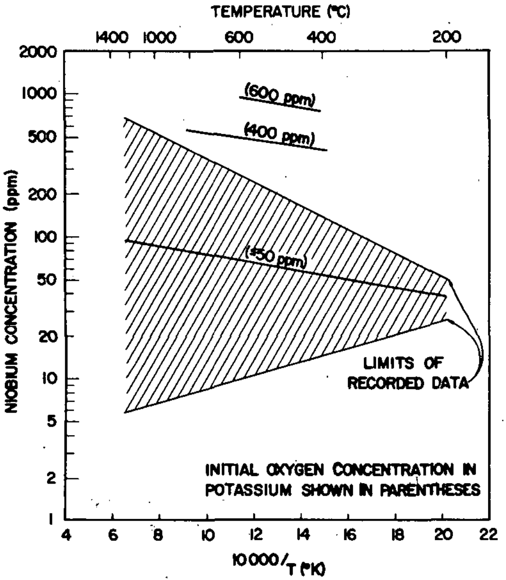

FIG. 3. Solubility of niobium in potassium

Solubility Results

In the past three years, several workers have studied the dissolution of niobium in potassium in solubility or corrosion experiments [5, 7,11,12]. The data from the various investigations are shown in Fig. 3.

Values of the saturation concentration of niobium in high-purity potassium (≤50 ppm O) at temperatures above 1000 °C vary by an order of magnitude. The effect of oxygen as a third component in the system is to increase the dissolution of niobium, as is evident in the figure.

The solubilities of other refractory metals in potassium are summarized in Table II. In general, the reported solubilities in pure potassium have been in the range 10 to 100 ppm, but substantially higher solubilities have resulted when oxygen impurities existed in either the potassium or the container material. In this regard, the solubility of niobium appears to be much lower in the case of alloys containing small zirconium additions than for the zone-refined pure alloy [12].

Refluxing-Capsule Tests

The effect of a two-phase (vapor-liquid) alkali metal environment on container materials is most simply investigated in a refluxing-capsule experiment. In this type of test, liquid is vaporized from a pool at one end of the capsule and vapor is condensed at the other end. The process is continued as the condensate flows down the wall of the capsule back into the liquid. Table III summarizes the results obtained from testing a variety of refractory-metal alloys in refluxing potassium at temperatures up to 1380 °C and for times up to 10 000 hr.

The majority of refluxing capsule tests have involved the alloys Nb–1% Zr and D-43.[1] Weight changes of both materials, determined from tubular insert specimens lining the condenser section, have been relatively small and related principally to the gettering of oxygen by potassium vapor and its subsequent deposition in areas near the liquid-vapor interface. Weight gains as well as weight losses were observed in the condenser section depending on location and the direction of oxygen migration. Despite the high vacuum environment ($<10^{-7}$ torr) used to protect these capsules, oxygen was acquired externally by the container in some of the tests conducted at 1200 °C or higher. The most serious effect of oxygen infusion into the capsules was to decarburize the D-43 alloy by reaction with carbon to form CO. Surface films of ZrO_2 were also found in the boiler region of some capsules, apparently the result of preferential oxygen buildup there. One investigator [9] concluded that alloys containing zirconium or hafnium were more resistant to attack by boiling potassium because of the reaction of these alloying elements with oxygen to form stable oxide precipitates, thus preventing oxygen from entering into corrosion reactions.

Molybdenum-base alloys such as TZM have exhibited good resistance to boiling potassium up to 1260 °C. However, a study in which oxygen was deliberately added to the potassium indicated that oxygen accelerated attack and mass transfer [8]. Two Nb–1% Zr refluxing capsules that contained TZM inserts in the condenser section were operated for 2500 and 5000 hr at 1100 °C [15]. Except for slight decarburization of the TZM, no evidence of activity gradient mass transfer was noted.

Natural- and Forced-Circulation Loop Tests

Liquid and boiling potassium have been studied under nonisothermal, dynamic conditions in both natural- and forced-circulation loops. Results of monometallic and dissimilar alloy natural-circulation tests are summarized in Table IV. In general, they reinforce the findings of refluxing-capsule tests. Weight changes of insert specimens from the condenser and subcooled liquid sections correlated closely with changes

---

[1] Compositions of alloys are listed in Table I.

TABLE II. SOLUBILITY OF SOME REFRACTORY METALS IN POTASSIUM

Solute Element	Temperature (°C)	Equilibration Time (hr)	Measured Solute Concentration (ppm)	Oxygen Concentration in Potassium[a] (ppm)	Reference
Molybdenum	815	100	<10[b]	<1000[c]	5
	<1200	100	<0.2	25	7
	700–1200	100	500	500[c]	7
	1000	4–8	3,4	14	12
	1100	4–8	1,13	14	12
	1200	4–8	13,14	14	12
Tantalum	800	8	413	3.5	12
	900	8	572	3.5	12
	1000	2–8	370–2730	3.5,14	12
	1100	4–8	688,2290	14	12
	1125	6	9	23	11
	1200	4–8	1520,1840,2880	3.5,14	12
	1225	6	8,19	<15	11
	1250	4	10–806	<15	11
	1250	9	52–88	<15	11
	1330	5	5,10,18	<15	11
	1400	7	15,18	<15	11
Titanium	1200	8	61,88,100	9	11
	1300	8	45,131,134	9	11
Zirconium	815	100	<10[d]	<1000[c]	5
	1200	8	39,83,110	9	11
	1300	8	76,77	9	11

[a] Amalgamation method used.
[b] Zirconium present in the system.
[c] Oxygen added as K_2O.
[d] Molybdenum present in the system.

in interstitial concentrations, and no evidence of dissolution and mass transfer of metallic constituents was observed. The magnitude of condenser weight changes was the same as observed in refluxing-capsule tests operated at an equivalent specific condensing rate.

Combinations of niobium- and molybdenum-base alloys tested in D-43 or Nb–1% Zr loops with liquid [18] or boiling potassium [17,19] likewise showed no interactions of the alloys with potassium up to 1200°C.

Space electric power systems are most closely simulated in forced-circulation (pumped) loop tests. These tests contain test sections designed to provide corrosion-erosion data on potential nozzle and turbine-blade materials as a function of vapor temperature, quality, and flow rate. A summary of the test conditions and results from three such tests involving refractory-metal components is presented in Table V. All three loops were constructed of Nb–1% Zr but contained Nb–1% Zr, TZM, and Mo–0.5% Ti in various stages of the test sections. The Nb–1% Zr alloy nozzle and turbine-blade specimens showed no effects on high-velocity potassium except for superficial erosion of a test section in which the temperature was 1032°C and the vapor quality only 83%. No corrosion or erosion was observed in the tests containing the molybdenum-base alloys as nozzles or turbine blades. Mass transfer of metallic constituents was not detected in any of the tests; however, pickup of oxygen occurred along certain internal and external surfaces and was heaviest when argon rather than vacuum was used as the test environment.

In addition to corrosion loop tests, a qualitative assessment of the compatibility of Nb–1% Zr with boiling potassium has been afforded by a 100-kw facility to study heat transfer to boiling potassium at temperatures up to 1150°C [22]. This system has operated for 6200 hr with no evidence of dissolutive attack or mass transfer of metallic constituents.

Effect of Exposure to Potassium on Mechanical Properties

The yield strengths of TZM, PWC-533, and PWC-11 were measured [17] after 3000-hr exposure at 730 to 1070°C in boiling-potassium loops constructed of Nb–1% Zr alloy. The strengths were measured at a temperature equivalent to the exposure temperature of each specimen, and no significant differences were found when compared with argon tests having the same conditions of time and temperature. Creep-rupture tests of TZM and Mo–0.5% Ti in saturated potassium vapor for up to 1539 hr at 1100°C likewise did not indicate any significant effects on the rupture strength of these materials [23]. However, fatigue tests of Mo–0.5% Ti indicated that the endurance limit of this alloy was significantly reduced in potassium vapor compared to vacuum at 1100°C [24]. The reduction was the same in specimens tested for short and long times.

No corrosion was observed in two D-43 capsules biaxially stressed in refluxing potassium for 1000 hr at 1150°C and 2000 hr at 1120°C [25]. However, the extent of creep was measured continuously during the tests and in both tests the creep strength of D-43 was less than that determined by conventional uniaxial methods in the absence of potassium. Since no corrosion effects by the potassium were observed, it is not clear whether the lower creep strength was a result of the test exposure or the fact that D-43 was stressed biaxially rather than uniaxially.

LITHIUM CORROSION STUDIES

Evaluations of refractory metals as containment materials for lithium date from the earliest considerations of this liquid metal as a high-temperature reactor coolant. These early screening studies showed

TABLE III. SUMMARY OF MONOMETALLIC REFRACTORY METAL-BOILING POTASSIUM-REFLUXING CAPSULE TEST RESULTS

Alloy	Temperature (°C)	Maximum Time Tested (hr)	Oxygen Content of Starting Potassium[a] (ppm)	Results		References
				Chemical	Metallographic	
Nb–1% Zr	1000–1200	10 000	<20–72	Oxygen pickup in boiler regions of capsules from external environment. Some transfer of oxygen from vapor to liquid region of capsules.	No attack in most tests. Deposits and gold-colored discoloration in 10 000-hr test. Anomalous intergranular attack in several tests.	9,13,14
D-43	1000–1380	10 000	<20–72	Oxygen pickup and migration similar to Nb–1% Zr tests. Decarburization in areas of high oxygen pickup.	No attack. Film near liquid-vapor interface. ZrO_2 surface layer on end plug weld in boiler region.	9,13,14
AS-55	1100–1200	10 000	<20–72	Oxygen loss in condenser when starting content >400 ppm. Oxygen pickup in boiler.	No attack. Some coalescence of carbides.	9,13
SCb-291	982–1200	1000	<20	Slight increase in oxygen content of capsule.	Intergranular attack to 16 mils.	9
B-33	982–1260	2000	<20	Oxygen pickup at bottom of capsule.	Dissolutive attack to 3 mils.	9
B-66	1200	4000	<20	Oxygen pickup at bottom of capsule.	Dissolutive attack to 0.2 mil. ZrO_2 film at liquid-vapor interface.	9
D-14	1100	4000	<20	Oxygen pickup at bottom of capsule.	No attack. ZrO_2 film at liquid-vapor interface.	9
Cb-752	1200	4000	<20	Oxygen pickup at bottom of capsule.	No attack. ZrO_2 film at liquid-vapor interface.	9

TABLE III (continued)

Alloy	Temperature (°C)	Maximum Time Tested (hr)	Oxygen Content of Starting Potassium[a] (ppm)	Results		References
				Chemical	Metallographic	
C-129	1200	4000	<20	Oxygen pickup at bottom of capsule.	No attack. Film at liquid-vapor interface.	9
FS-85	1200–1300	400	<20	Slight increase in oxygen content of capsule.	No attack. Film at liquid-vapor interface.	9
TZM	815–1260	5000	<20–500	Increase in Ti and Mo concentration in K.	No attack in tests with low-oxygen potassium. Mass transfer deposits of Mo at liquid-vapor interface increasing with increasing oxygen in starting K.	8,13
Ta–10% W	982–1200	110	<20	Slight increase in oxygen content of capsule.	Intergranular attack to 16 mils.	9
T-111	1200–1260	4000	<20	Slight increase in oxygen content of capsule.	No attack. Film at liquid-vapor interface.	9
T-222	982–1300	4000	<20	Large oxygen pickup at bottom of capsule.	No attack; $K_2Ta_4O_{11}$ and WO_3 film at interface	9

[a] Determined by amalgamation analysis.

TABLE IV. SUMMARY OF BOILING POTASSIUM-NATURAL-CIRCULATION-LOOP-TEST RESULTS

Loop Material	Insert Material	Temperature, °C		Time (hr)	Flow Rate (g/hr)	Weight Change (mg/cm^2)	Results		Reference
		Maximum	Minimum				Chemical	Metallographic	
Nb–1% Zr	Nb–1% Zr	1150	650	2800		+0.13 to +0.01	No significant changes detected.	No attack.	16
Nb–1% Zr	Nb–1% Zr	1200	680	1200	2100	+0.7 to –0.2	Increase in oxygen concentration in specimens from subcooled liquid region.	No attack.	13
Nb–1% Zr	Nb–1% Zr PWC-533	1070	870	3000	4540	–0.09 to –3.6	Increase in oxygen, carbon and zirconium in condenser exit specimens. Slight increase in carbon in boiler.	No attack.	17
Nb–1% Zr	PWC-11	1100	700	3000	4100	+0.2 to –0.7	Carbon pickup in PWC-11 specimens in the boiler.	No attack.	17
Nb–1% Zr	Nb–1% Zr TZM 316 stainless steel	1010	680	3000	1000	+0.01 to –0.02 +0.05 to +0.01	Slight increase of molybdenum in Nb–1% Zr specimens.	No attack.	17
D-43	D-43	1200	835	3000	2100	+0.6 to +0.2	Increase in oxygen in specimens from the subcooled liquid region.	No attack.	13
D-43[a]	AS-55	1100	1010	2000	75 000		Oxygen picked up by AS-55 insert in boiler.	Thin film on the AS-55 insert <1 mil thick.	18
PWC-533	PWC-533	1120	870	3000	5450	–0 to –2.2	No significant changes detected.	No attack.	17
D-43	TZM	1250	1000	3000	1320	+0.3 (av)	Some decarburization of TZM inserts. ZrO_2 transferred to subcooled liquid region.	No attack.	19
AS-55[a]	None	1100	1010	2000	75 000		No significant changes detected.	No attack.	18
T-111	T-111	1250	1040	3000	2100	–0.4 to +0.7	Oxygen pickup in boiler and vapor carry-over line.	No attack.	19

[a] Thermal-convection-loop circulating liquid potassium.

TABLE V. SUMMARY OF TEST CONDITIONS AND RESULTS FROM REFRACTORY METAL-FORCED-CIRCULATION LOOP TESTS

Material		Time (hr)	Temperature, °C				Flow Rate		Vapor Quality (%)	Results	Reference
			Liquid		Vapor		Mass	Vapor			
Loop	Nozzles and Turbine Blades		Maximum	Minimum	Maximum	Minimum	(lb/hr)	(ft/sec)			
Nb–1% Zr	Nb–1% Zr	3000	1075	355	1100	690	33	3100–1300	83–96	1-mil erosion in second-stage blade. Slight oxygen pickup in boiler and sub-cooler.	13
Nb–1% Zr	TZM	5000	1040	425	1100	790	20–40	830–1350	88	No significant corrosion, erosion or migration of interstitial impurities.	20
Nb–1% Zr	Mo–0.5% Ti	307	1065	100	1100	960	26–42	1500	80	No significant corrosion or erosion. Oxygen contamination of Nb–1% Zr from external argon environment.	21

that iron-, cobalt-, and nickel-base alloys were subject to excessive mass transfer in lithium above about 600°C, but niobium and molybdenum were quite resistant to dissolutive attack to at least 1000°C [26,27]. Continued studies of refractory metals, however, revealed a corrosion problem associated with the presence of interstitial oxygen in either niobium or tantalum when exposed to lithium above 200°C. This problem was manifested by heavy localized intergranular attack in certain weld areas and by more general intergranular attack occurring in longer term loop studies, in which the refractory metal acquired oxygen from the test environment [27].

Until recently lithium corrosion studies have concerned primarily the effects of interstitial oxygen in refractory metals on attack by lithium. With the advent of improved metal processing techniques and ultrahigh vacuum test environments, the significance of this "oxygen disease" problem has lessened considerably. Furthermore, as discussed below, alloying additions of strong oxide formers such as zirconium and hafnium in most present-day refractory-metal alloys have greatly increased the tolerable level of oxygen in these alloys. Consequently, the emphasis in corrosion tests has currently shifted to the parametric effects of flow rate and temperature on thermal gradient and activity gradient mass transfer in lithium.

When exposed to lithium above 800°C, all but the most reactive refractory metals lose oxygen rapidly to lithium, the rate depending on the exposure temperature. In the case of niobium and tantalum, the movement of oxygen out of the alloy may be accompanied by lithium penetration to form a complex oxide phase along grain boundaries and {110} crystallographic planes adjoining exposed surfaces [27,28]. Lithium penetration occurs only when the oxygen concentration in the refractory metal exceeds a threshold level of 200 to 500 ppm; hence attack occurs only during the time required to reduce the oxygen concentration below this level. Alloying additions such as zirconium, titanium and hafnium significantly increase the threshold oxygen concentration for lithium penetration. Studies of the Nb–1% Zr system indicate that the increased tolerance for oxygen correlates closely with the amount of oxygen removed from solid solution by reaction with the oxide former [29].

Recent studies of developmental niobium and tantalum alloys have verified the effectiveness of both zirconium and hafnium additions for increasing the threshold oxygen level for lithium attack. Niobium-base alloys such as B-66, D-43, FS-85, Cb-752, Cb-753, PWC-11, and the tantalum-base alloy T-111 exhibited essentially the same behavior as Nb–1% Zr when exposed to lithium at temperatures to 1000°C [30–32]. When oxygen was added to these alloys at 1000°C or when they were welded in contaminated atmospheres, all were susceptible to subsequent attack upon exposure to lithium at 1000°C. However, prior heat treatment at 1300 to 1600°C resulted in precipitation of the dissolved oxygen as ZrO_2 or HfO_2. These heat-treated alloys were resistant to lithium attack except where the oxygen atom concentration was over twice the zirconium or hafnium atom concentrations.

Solubility Studies

In contrast with sodium or potassium, the addition of oxygen to lithium (as opposed to the refractory metal) appears to have little effect on either the solubility or dissolution rate of refractory metals. The corrosion and solubility effects of nitrogen, either in the refractory metal or in lithium, have not been resolved. Early solubility data indicated a strong dependence of the apparent solubility of elements such as Fe, Cr, Ni, Nb, and Ti on the nitrogen content of the lithium [33].

However, in more recent tests conducted from 760 to 1425 °C, the apparent solubility of either niobium or molybdenum in lithium was not affected by the addition of up to 10 000 ppm O or 5000 ppm N to the lithium [7].

The solubility of niobium in lithium gradually increased from 760 to 1425 °C according to the expression

$$\log_{10} S \text{ (atom \% Nb)} = 4.77 - 1094/T \text{ (°K)} \text{ [Ref. 7].}$$

The solubility of molybdenum in lithium was reported to be less than 1.0 ppm at temperatures below 1320 °C, and a preliminary test at 1540 °C gave a value of 5.4 ppm. No reliable data are yet available on the solubility of tantalum in lithium, a serious omission in view of the current interest in tantalum-base containment materials.

Capsule Tests

A series of lithium capsules was recently operated to study the dissolutive effects of lithium on refractory metals at temperatures from 1370 to 1650 °C [34]. The capsules in all cases were fabricated of the molybdenum alloy TZM and contained one or more specimens of the following alloys: W–0.9% Nb, W–15% Mo, W–10% Re, W–25% Re, TZM, Mo–50% Re, Re, T-111, Ta–10% W, and B-66. Following exposures of 100 and 1000 hr, tungsten and molybdenum alloys showed generally better compatibility than tantalum and niobium alloys under the test conditions. Metallographic examinations of the tantalum and niobium alloys exposed at temperatures above 1370 °C showed surface reaction layers and subsurface precipitates that were identified as carbides or carbonitrides. The tungsten-base alloys showed no evidence of attack at 1370 °C, but at 1540 and 1650 °C they showed varying degrees of surface dissolution and grain-boundary grooving. The alloys TZM and Mo–50% Re were not attacked up to 1650 °C, even after 1000-hr exposure. However, molybdenum from the TZM capsule was found to transfer to pure rhenium, resulting in the formation of brittle intermetallic molybdenum-rhenium compounds at the rhenium surface.

Additional capsule studies have been concerned with the stability of oxygen, nitrogen, and zirconium in niobium-base alloys in contact with lithium [31]. The studies involved alloys of Nb–1% Zr containing 50 to 100 ppm C and 600 to 1000 ppm C separated by distances of 5 and 30 mils. After exposure for 100 hr at 1200 °C, the alloy containing the higher carbon content exhibited a surface layer of (Nb, Zr) C, which apparently resulted from mass transfer of zirconium from the lower carbon to the higher carbon alloy. Oxygen was depleted from the higher carbon alloy to a much greater extent than the lower carbon material indicating that the effect of zirconium on oxygen activity in niobium is lessened by the presence of carbon. However, the oxygen concentration at which lithium penetration was encountered was comparable for both carbon levels.

Thermal-Convection Loop Tests

Quantitative data on the rate of mass transfer of refractory metals in lithium have been obtained from thermal-convection loop tests [30,35, 36]. Tests were conducted in vacuums of 10^{-8} to 10^{-9} torr and circulated lithium for 3000 hr at a 1200 °C hot-leg temperature. Results are summarized in Table VI. The weight-change profiles of Nb–1% Zr and D-43 monometallic loops are compared in Fig. 4. Dissolution occurred over two-thirds of the loop surfaces, while deposition was confined to a narrower temperature band encompassing the remaining one-third. This indicated that the rate of deposition was considerably faster than that of dissolution for a comparable concentration driving force (i.e., the mass transfer coefficient [3] for the deposition process exceeded that

TABLE VI. RESULTS OF THERMAL-CONVECTION LOOP TESTS OF REFRACTORY ALLOYS IN LITHIUM[a]

Alloy	Inserts	Temperature, °C		Flow Rate (fpm)	Total Weight Loss (mg)	Total Weight Gain (mg)	Results	
		Maximum	Gradient				Chemical	Metallographic
Nb–1% Zr	Nb–1% Zr	1190	110	10.6	99	87	Loss of O in all sections of loop. Transfer of Zr, N and C from hot to cold leg.	No attack. Light ZrN on specimens in cold leg of loop.
D-43	D-43	1200	170	7.5	44	24	Loss of O and C in all sections of loop. Transfer of Zr from hot to cold leg. Gain of N in cold leg.	No attack. No films or deposits.
Nb–1% Zr	TZM Nb–1% Zr	1210	150	7.5	810	626	TZM specimens lost C but picked up Nb and Zr. Nb–1% Zr specimens gained N, C and Mo.	Nb–1% Zr showed irregular surface protuberances in hot leg. ZrC and ZrN deposits on both Nb–1% Zr and TZM in cold leg. Nb crystals on TZM specimens in hot leg.

---

[a] Tests were conducted for 3000 hr.

for dissolution). The weight changes reflected the transport of nitrogen, carbon, and zirconium from hot- to cold-leg regions and the depletion of oxygen in all loop regions.

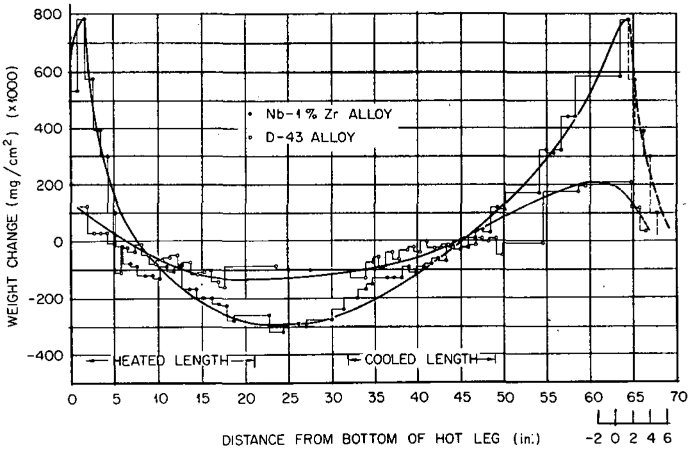

FIG.4. Weight change as a function of distance for Nb-1% Zr and D-43 inserts from lithium thermal-convection loop tests

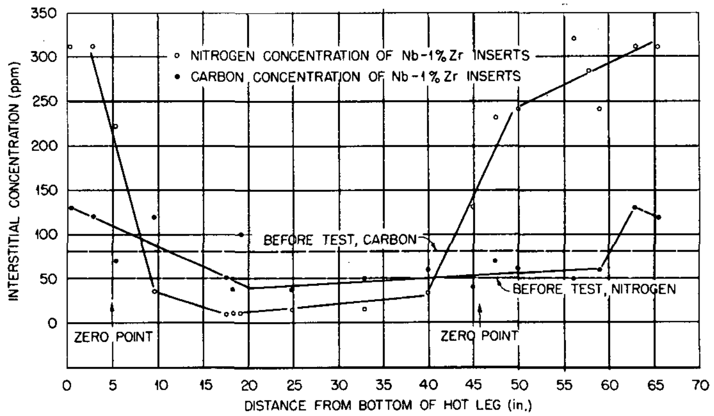

FIG.5. Nitrogen and carbon concentration profile for Nb-1% Zr inserts from lithium thermal-convection loop tests. Zero points refer to positions in the loop where no weight change occurred

Microprobe examinations of hot-leg specimens from both loops revealed a zone depleted of zirconium from 1 to 3 mils below the exposed surface. Cold-leg specimens from the Nb–1% Zr loop exhibited a light gold-colored zirconium-rich deposit identified as predominantly ZrN. Weight changes were nearly equivalent at isothermal points in the hot- and cold-leg regions, indicating that little change occurred in the solute concentration in lithium around the loops. Calculations based on system weight changes indicated a maximum change in solute concentration of the lithium on the order of a few parts per billion.

The nitrogen and carbon concentration profiles in the Nb–1% Zr loop compared closely with the overall weight-change profile, as indicated in Fig. 5; however, the specific role of oxygen and nitrogen in actual mass transfer processes in these systems has not been defined.

TABLE VII. SUMMARY OF REFRACTORY METAL-LITHIUM FORCED-CONVECTION LOOP TESTS

Material	Temperature, °C		Velocity (fps)	Total Accumulated Test Time (hr)	Extent of Attack and Deposition
	Maximum	Gradient			
Titanium	760–816	110	13	1082	Light[a]
Zirconium	816–871	110	13	1070	nil[b]
Tantalum	816–982	110–220	3–13	2261	nil[b]
Vanadium	871	220	13	1194	nil
Mo–0.5% Ti	816	110	13	694	nil
Niobium	816–1093	110–220	10–50	8233	nil[c]
Nb–1% Zr	760–1315	110–540	10–50	>20 000	Light-nil

[a] High nitrogen content in pretest lithium.

[b] Carbide-nitride phase precipitate.

[c] Nitride deposits in early tests containing contaminated lithium.

In a dissimilar metal loop of Nb–1% Zr containing TZM inserts, a much more complicated interchange of chemical species took place. The weight changes of the TZM inserts were approximately eight times that found for Nb–1% Zr in the monometallic loop test. The larger weight changes are attributed to at least three different processes: (1) temperature gradient mass transfer of zirconium, nitrogen and carbon from the hot to the cold leg; (2) activity gradient mass transfer of carbon from TZM to Nb–1% Zr in all sections of the loop; and (3) dissimilar metal interactions resulting in the transfer of zirconium and niobium to TZM and a pickup of molybdenum by the Nb–1% Zr in the hot leg.

Forced-Convection Loops

The corrosion behavior of refractory metals in lithium under forced-flow conditions has been evaluated in three general groups of loop tests: (1) monometallic loops of Ti, Zr, Ta, V, and Mo–0.5% Ti, operated to 815°C [27]; (2) monometallic tests of niobium, niobium-titanium and niobium-zirconium alloys operated to 1300°C [27,37,38]; and (3) a Nb–1% Zr test-bed loop used to evaluate developmental refractory-metal specimens at 1200°C [39].

The majority of these loops operated under cover of a helium or argon atmosphere. Initial test environments were not of sufficient purity to avoid contamination of the loop materials, which in the case of niobium alloys resulted in lithium penetration. Although the magnitude of this problem gradually decreased with further test experience, the use of helium or argon has proved marginal as a protective cover for large-loop installations. More recent studies have shifted to ultrahigh vacuum systems capable of reducing contaminating gases to pressures less than 10^{-10} torr. Alloys tested in these latter systems have shown no significant interaction with the test environment even after 3000 hr at 1300°C.

Table VII lists the test conditions and results of the first two groups of loop studies. Of the various alloy systems evaluated, only titanium showed significant attack or mass transfer. However, light carbide and nitride deposits were observed in the cold legs of certain of the earlier loop systems. These products were attributed to reactions involving either residual contaminants present in the lithium or in the external helium environment.

Extensive forced-convection loop studies of the Nb–1% Zr alloy have confirmed the excellent compatibility of this alloy with lithium up to 1100°C for times as long as 10 000 hr (Table VII). Mass transfer in these systems was limited to a zirconium-rich superficial layer in the colder loop regions and a slight depletion of zirconium from the higher temperature surfaces [37]. Superficial grain-boundary-solution attack was evident in a 10 000-hr, large-loop system at 1100°C and in a 500-hr, 1320°C loop system [31].

The corrosion properties of T-111, FS-85, W–25% Re, PWC-11, and PWC-33 in lithium under forced-flow conditions were evaluated in a Nb–1% Zr loop which operated with a 1200°C maximum hot-leg temperature and a 220°C temperature difference [39]. Tubular specimens of each alloy were inserted sequentially into the surge tank of the loop and were exposed for periods of 200 and 1000 hr to lithium flowing at 0.45 and 0.88 fps. Examinations after test revealed no evidence of solution or grain-boundary attack in any of the specimens. All specimens showed a slight increase in nitrogen concentration, while the PWC-11 and PWC-33 specimens also exhibited a depletion of zirconium and carbon near the surface. Tube-burst tests at 1200°C were conducted on all of the alloys except FS-85. Comparison with control specimens heat treated in argon at 1200 °C showed no changes in stress-to-rupture values except for PWC-11. This alloy, in one case, exhibited a 10 to 15% decrease in rupture strength, which was comparable to the decrease experienced by the argon control sample given an equivalent thermal treatment. A second series of specimens, however, showed a much shorter life than the argon controls.

CONCLUSIONS

The earliest considerations of nuclear reactors for the generation of electric or motive power recognized the unique qualities of liquid metals for achieving high operating temperatures and, therefore, high thermodynamic efficiencies. Until recently, however, this recognition has remained of academic significance because of limitations in the properties of available construction materials. Tantamount were limitations of creep and corrosion resistance at high temperatures.

A breakthrough with respect to both of these basic limitations has occurred with the emergence of commercial refractory-metal-alloy systems. The corrosion testing of refractory metals in lithium and potassium has demonstrated that refractory metals maintain exceptional compatibility with alkali metals at temperatures considerably above 1000 °C. Particularly impressive are relatively long-term forced-convection loop tests (5000 to 10 000 hr) completed with the Nb–1% Zr alloy in both lithium and potassium at 1100 to 1200 °C that show almost negligible effects attributable to liquid metal exposure.

The present base of corrosion information is not yet sufficient to gauge the ultimate temperature ranges that can be achieved practically in a refractory metal—alkali metal system. There is already evidence, however, that the maximum temperatures of potassium systems will be limited by strength rather than corrosion considerations. This is based on the rapid increase in potassium vapor pressure and the decrease in creep strength of all refractory metals with increasing temperature. There is also limited evidence that the creep strength of niobium alloys, specifically D-43, is decreased in potassium vapor compared with vacuum.

In the case of lithium, there is evidence to suggest that 1320 °C may approach the temperature at which corrosion can limit the useful life of alloys like Nb–1% Zr. Forced-convection loops of this alloy, operated under cover of helium, showed the initiation of grain-boundary grooving after 500 hr at 1320 °C. Similarly, specimens of niobium and tantalum alloys showed relatively heavy attack when exposed in lithium-filled TZM capsules at 1400 to 1600 °C. On the other hand, tungsten and molybdenum showed quite limited attack under the same conditions. None of these experiments is completely definitive, however, because of the relatively short time and slightly reactive environment used in the high-temperature loop experiment and dissimilar metal effects in the capsule experiments.

To date there have been few basic studies of the mass transfer processes occurring in high-temperature refractory-metal systems circulating either lithium or potassium. It follows, therefore, that little is known regarding the rate-controlling aspects of either the dissolution or deposition steps. This will remain the case for potassium until models describing the flow of heat and mass in two-phase boiling systems are sufficiently rigorous to enable a boundary value approach to the flow of solute into and out of the potassium.

In the case of lithium, thermal-convection-loop studies have been conducted to establish the mass transfer pattern of niobium alloys operating at 1200 °C. These studies showed that mass transfer was quite selective with respect to the most soluble metallic element in the system – zirconium. A measurable zirconium concentration gradient was noted at those surfaces that lost weight and implied that solid-state diffusion of zirconium was the controlling mode of transport in the dissolution step. Deposition was limited to a relatively narrow temperature region in the coldest part of the loop and occurred at a much faster rate than dissolution with the same concentration driving force. Since the kinetics of the dissolution and deposition steps were in opposite order to their relative temperatures, it was concluded that the precipitation reaction was not the reverse of the solution reaction.

Past discussions of the compatibility of refractory metals with alkali metals have emphasized the importance of interstitial impurities, particularly oxygen, on corrosion behavior. The resistance of niobium and tantalum to attack by lithium is particularly affected by the oxygen concentration of these refractory metals. However, with the advent of ultrahigh vacuum environments and better control of impurities during refractory-metal fabrication, the probability of encountering critical oxygen levels in either tantalum or niobium has greatly diminished. This reduced probability for oxygen contamination will eventually reopen considerations as to the desirability for incorporating zirconium and hafnium additions in refractory alloys for lithium containment. The susceptibility of zirconium in the alloys Nb–1% Zr and D-43 to mass transfer by lithium at 1200°C has been found to be considerably greater than that of the remaining alloy components. Hence, the advantages accruing from hafnium and zirconium additions, in terms of strength and oxygen stabilization, need to be weighed against their mass transfer behavior in high-temperature lithium.

Unlike in lithium, the oxygen effects encountered in potassium–refractory-metal systems derive not only from the refractory metal but also from the liquid metal. Oxygen additions to potassium have been shown to significantly increase the solubilities of refractory metals in potassium. Likewise, the solubilities of tantalum and niobium containing oxygen levels of 100 to 1000 ppm appear to be much higher than electron-beam-melted or zone-refined stock.

An additional problem involving interstitial impurity effects in both lithium and potassium concerns the mass transfer of carbon and nitrogen across a temperature gradient or between dissimilar alloys. Many refractory metals derive strength advantages from the addition of carbon or nitrogen to form dispersions with the more reactive metallic constituents in the alloy. Mass transfer studies of zirconium-containing alloys in lithium have shown a tendency for carbon and nitrogen to be depleted from hot-zone regions and, in the case of carbon, to transfer between alloys with different carbon concentrations tested under isothermal conditions. Additional corrosion studies will therefore be required to determine the stabilities of nitride or carbide phases in dynamic nonisothermal potassium or lithium and the ramifications of interstitial transfer on high-temperature mechanical properties.

REFERENCES

[1] DISTEFANO, J.R., HOFFMAN, E.E., "Corrosion mechanisms in refractory metal–alkali metal systems", Proceedings of an AGARD Conference on Refractory Metals held at Oslo, The Science and Technology of Tungsten, Tantalum, Molybdenum, Niobium and their Alloys, (PROMISEL, N.E., Ed.) Pergamon Press, Oxford, (1964).

[2] STANG, J.H., SIMONS, E.M., DEMASTRY, J.A., GENCO, J.M., Compatibility of liquid and vapor alkali metals with construction materials, US Rep. DMIC-227 (1966) 51–91.

[3] GURINSKY, D.H., WEEKS, J.R., KLAMUT, C.J., ROSENBLUM, K.L., DEVAN, J.H., Corrosion in liquid metal systems, Proc. Intern. Conf. Peaceful Uses At. Energy, 3rd, Geneva, 1964, 9 (1965) 550–558.

[4] DISTEFANO, J.R., LITMAN, A.P., Effects of impurities in some refractory metal–alkali metal systems, Corrosion 20 12 (1964) 392t–399t.

[5] LITMAN, A.P., The effect of oxygen on the corrosion of niobium by liquid potassium, USAEC Rep. ORNL-3751 (1965).

[6] LITMAN, A.P., Diffusion of oxygen in niobium, Phys. status solidi 11 (1965) K-47–K-48.

[7] CLEARY, R.E., BLECHERMAN, S.S., CORLISS, J.E., Solubility of refractory metals in lithium and potassium, USAEC Rep. TIM-850 (1965).

[8] SIMONS, E.M., LAGEDROST, J.F., Mass transfer for TZM alloy by potassium in boiling-refluxing capsules, AEC-NASA liquid metals information meeting held in Gatlinburg, Tennessee, April 21–23, 1965, USAEC Rep. CONF-650411 (1966) 237–271.

[9] SCHEUERMAN, C.M., BARRETT, C.A., Compatibility of columbium and tantalum tubing alloys with refluxing potassium, USNASA Rep. NASA TN D-3429 (1966).

[10] LITMAN, A.P., PRADOS, J.W., The partitioning of oxygen between zirconium and liquid potassium, Electrochem. Technol. 3 9–10 (1965) 228–233.

[11] GINELL, W.S., TEITEL, R. J., Determination of the solubility of transition metals in molten potassium, Douglas Aircraft Rep. SM-48883 (1965).

[12] MCKISSON, R.L., et al. Solubility studies of ultra pure transition elements in ultra pure alkali metals, NASA Rep. AI-65-210 (1966).

[13] DEVAN, J.H., DISTEFANO, J.R., JANSEN, D.H., Compatibility of refractory metals with boiling alkali metals, Trans. Am. Nucl. Soc. 8 2 (1965) 390–391.

[14] ENGEL, L.B., Jr., FRANK, R.G., Evaluation of high-strength columbium alloys for alkali metal containment, USNASA Rep. NASA-CR-54226 (1964).

[15] HOFFMAN, E.E., (Ed.), Potassium corrosion test loop development, USNASA Rep. NASA-CR-54843 (1965).

[16] JANSEN, D.H., HOFFMAN, E.E., Niobium–1% zirconium, natural-circulation, boiling-potassium corrosion loop test, USAEC Rep. ORNL-3603 (1964).

[17] BLECHERMAN, S.S., HODEL, J., The compatibility of structural and turbo-machinery alloys in boiling potassium, USAEC Rep. PWAC-501 (1965).

[18] Proceedings of the NASA-AEC liquid metals corrosion meeting, October 2–3, 1963, Vol. I, loop results, USNASA Rep. NASA-SP-41 (1964) 189–197.

[19] DEVAN, J.H., DISTEFANO, J.R., JANSEN, D.H., Metals and Ceramics Div. Ann. Progr. Rep. June 30, 1965, USAEC Rep. ORNL-3870 (1965) 124–129.

[20] HOFFMAN, E.E. to DEVAN, J.H., Personal communication September 1966 Potassium corrosion test loop development, Space Power and Propulsion Section, Missile and Space Division, General Electric Company, Cincinnati, Ohio, work performed under NASA Contract NAS 3-2547.

[21] KOVACEVICH, E.A., SALLEY, R.L., Mass-transfer tests with two-phase flow, USAF Rep. APL-TDR-64-119 (1964).

[22] JUDGE, J.R., Dynamic liquid-metal plants practical, Missiles Rockets 18 19 (1966) 22.

[23] KELLY, K.J., BLECHERMAN, S.S., HODEL, J.E., Corrosion studies of refractory metal alloys in boiling potassium and liquid NaK, USAEC Rep. CNLM-6246 (1965).

[24] KOVACEVICH, E., SALLEY, R., Materials investigation, SPUR program, part III, fatigue evaluation of Mo + 0.5 wt. % Ti, USAF Rep. ASD-TDR-63-270 (1963).

[25] HARRISON, R.W., The compatibility of biaxially stressed D-43 with refluxing potassium, Gen. Electric Rep. R-665D3010 (1966).

[26] HOFFMAN, E.E. Corrosion of materials by lithium at elevated temperatures, USAEC Rep. ORNL-2674 (1959).

[27] FREED, M.S., KELLY, K.J., Eds., Corrosion of columbium base and other structural alloys in high temperature lithium, USAEC Rep. PWAC-355 (1961).

[28] DISTEFANO, J.R., Corrosion of refractory metals by lithium, USAEC Rep. ORNL-3551 (1964).

[29] CUMMINGS, D., et al. Internal friction study of oxygen and nitrogen interactions with columbium-zirconium alloy, USAEC Rep. PWAC-358 (1961).

[30] SESSIONS, C.E., Corrosion of advanced refractory alloys in lithium, AEC-NASA liquid metals information meeting held in Gatlinburg, Tennessee, April 21–23, 1965, USAEC Rep. CONF-650411 (1966) 143–148.

[31] SNAP-50/SPUR final summary report – coolants and working fluids, USAEC Rep. PWAC-491 (1965).

[32] HARRISON, R.W., The effects of welding atmosphere purity on the lithium corrosion resistance of refractory alloys, Gen. Electric Rep. TIS-R66SD3013 (1966).

[33] LEAVENWORTH, H., CLEARY, R.E., BRATTON, W.D., Solubility of structural metals in lithium, USAEC Rep. PWAC-356 (1961).

[34] DEMASTRY, J.A., GRIESANAUER, N.M., Investigation of high-temperature refractory metals and alloys for thermionic converters, USAF Rep. BMI AFPL-TR-65-29 (1965).

[35] DEVAN, J.H., SESSIONS, C.E., Compatibility of some refractory alloys in flowing nonisothermal lithium, Trans. Am. Nucl. Soc. 8 2 (1965) 394.

[36] DEVAN, J.H., SESSIONS, C.E., Mass transfer of niobium-base alloys in flowing nonisothermal lithium, accepted for publication in Nuclear Applications, February 1967.

[37] BOURDON, P., LYMPERES, C.J., SCHENCK, G.F., Columbium – 1 zirconium alloy lithium corrosion loop tests LCCBK-5, 6, 7, 8 and USAEC Rep. TIM-823 (1965).

[38] HIBBEN, R.D., Lithium test aimed at SNAP-50/SPUR technology, Aviation Week and Space Technology 81 18 (1964) 58–63.

[39] Columbium – 1% zirconium alloy forced convection lithium slave loop test LCCDB-1, USAEC Rep. TIM-898 (1965).

DISCUSSION

C. TYZACK: In the experiment where you found mass loss on the hot leg and deposition on the cold leg, did you discover what the deposit was? Was it metal or complex oxide?

J.H. DEVAN: We see the net result of deposition as a zirconium carbonitride layer. Whether the layer is really deposited in this form, or whether zirconium is deposited alone and followed afterwards by carbon and nitrogen, we are not yet sure.

A.W. THORLEY: In connection with your equilibration studies involving niobium in potassium you mention oxygen levels in the niobium of 0.28 wt.%, i.e. 2800 ppm. This seems extraordinarily high. Is it a homogeneous level through the niobium sample or a surface level?

J.H. DEVAN: This is a very important point. Our specimens were of course doped with oxygen, which was admitted at very low partial pressure, at 1000°C, for approximately 24 h. The specimens were then homogenized at 1200°C, and we ran hardness traverses to satisfy ourselves that the oxygen composition was uniform across them. Our experience is that the pure niobium alloy can be homogenized quite easily, but this is not true of the Nb-1% Zr material, where it becomes a tricky task to get the oxygen homogeneously dispersed through the whole specimen.

A.W. THORLEY: Thank you. This is an important point, as you say, because if an oxygen concentration gradient existed at the surface, surface complexing would occur, the oxygen in the metal matrix would be progressively reduced and, in the final analysis, you would no longer be doing an equilibration study.

J.H. DEVAN: Yes, we worried a great deal about this possibility, but in the end we were satisfied that the oxygen was homogenized. The tests have since been extended to 1200°C and we find exactly the same behaviour: a rapid depletion of oxygen in the matrix. I might mention, too, that we have been able to correlate the rate of oxygen depletion quite nicely with the published diffusion data for oxygen in niobium, a fact which again suggests that our material probably has a uniform oxygen composition from the start. It is curious, however, that we have yet to find a complex in the system when examining it after test operation.

A.G. IOLTUKHOVSKY: Do you set any limit on the oxygen content of your niobium-zirconium alloy in lithium?

J.H. DEVAN: Early studies showed that pure niobium samples containing approximately 200 to 400 ppm of oxygen are rapidly attacked by lithium, which appears to form a complex phase through the alloy. Later work showed, however, that the addition of zirconium sharply reduces this sensitivity to oxygen. In fact, oxygen can be introduced to the point where it stoichiometrically uses up the amount of zirconium present in the alloy. At present we subject our niobium-zirconium alloys to careful heat treatment to tie up any oxygen that may be present in them. We find that we can work with nominal oxygen compositions of 200 to 400 ppm in our alloy without any serious corrosion effects.

A.G. IOLTUKHOVSKY: In your tests on pure niobium I gather you observed the formation of a complex phase between the lithium and the niobium. Did the lithium appear to penetrate the niobium at all? In other words, did this phase form on the surface or within the sample,. and was the lithium distributed evenly over the niobium samples or not?

J.H. DEVAN: This is an interesting reaction in that it takes place very quickly, so quickly in fact that we have never been able to get the material up to temperature and back down again before the reaction was completed.

A. G. IOLTUKHOVSKY: Have you not observed some sort of structural change in the resultant compound with time, in the course of further processing of your niobium samples?

J. H. DEVAN: This question is unfortunately just as difficult to answer as the previous one, simply because we have never been able to isolate any amount of this compound once the loop has been brought back to room temperature. The compound has never been properly identified; certainly it is not stable for long periods in air, even at room temperature.

SPACE-POWER-SYSTEM MATERIAL COMPATIBILITY TESTS OF SELECTED REFRACTORY METAL ALLOYS WITH BOILING POTASSIUM

L. ROSENBLUM, C. M. SCHEUERMANN AND T. A. MOSS
LEWIS RESEARCH CENTER,
NATIONAL AERONAUTICS AND SPACE ADMINISTRATION,
CLEVELAND, OHIO,
UNITED STATES OF AMERICA

Abstract

SPACE-POWER-SYSTEM MATERIAL COMPATIBILITY TESTS OF SELECTED REFRACTORY METAL ALLOYS WITH BOILING POTASSIUM. The compatibility of potential niobium and tantalum tubing alloys with boiling potassium was investigated in the range of temperature representative of the upper operational temperatures of a turbo-electric space power system. Two types of compatibility test were employed: (1) reflux capsule tests for materials screening, and (2) a forced convection two-phase loop test in which power system flow rate and temperature gradient service conditions were simulated.

In the reflux capsule tests, eight alloys were studied: B-33 (Nb-4 V, nominal alloy composition in weight percent); SCb-291 (Nb-10 Ta-10 W); Nb-1 Zr; D-43 (Nb-10 W-1 Zr-0.1 C); FS-85 (Nb-28 Ta-10 W-1 Zr); Ta-10 W; T-111 (Ta-8 W-2 Hf); and T-222 (Ta-9.6 W-2.5 Hf-0.01 C). Many of the alloys were tested in both the as-worked and recrystallized conditions. The initial oxygen content of the alloys was less than 150 ppm and that of the potassium less than 20 ppm. Tests were conducted over the temperature range of 1800° to 2400°F for times up to 10 000 h in vacua of 10^{-7} to 10^{-8} torr. In general, the gettered alloys (i.e. those containing the reactive elements Zr or Hf) were resistant to corrosive attack, while the ungettered alloys all exhibited significant corrosion. Since the presence of oxygen is known to increase alkali metal corrosion (probably via the formation of a soluble alkali-metal container metal - oxygen complex), the observed corrosion resistance of the gettered alloys can be attributed to a reaction of the getter element with available oxygen to form a stable oxide and thereby prevent oxygen from entering into the corrosion reaction. No stress corrosion effects were observed in tests on D-43 and B-33 alloy reflux capsules specially stressed to produce, respectively, 15% and 45% creep strain in sections of the capsule wall.

In the forced convection two-phase loop test, the material of construction was Nb-1 Zr alloy. The loop was run in a vacuum of 2×10^{-8} torr for 5000 h under the following operating conditions: potassium flow rate, 0.1 gal/min; saturation temperature, 1850°F; superheat temperature, 2000°F; condensing temperature, 1425°F; and subcool temperature, 800°F. No measureable potassium corrosion was observed in any portion of the loop.

INTRODUCTION

Interplanetary space travel and longtime orbital and lunar-based manned space stations will require large quantities of electricity for propulsion, communications, and life support equipment. Advanced nuclear turboelectric generator systems in the megawatt range will be needed to provide the electrical power for these operations. Such systems will require containment materials having adequate creep and corrosion resistance under the conditions of space operation at temperatures in the range of 1800° to 2400° F and for times in excess of 10 000 hours. At present, potassium is a favored choice for the system working fluid, and niobium and tantalum alloys are candidates for the containment material.

As part of the NASA technology program for advanced space power systems, studies have been initiated at the NASA Lewis Research Center, Cleveland, Ohio (LeRC) and at the General Electric Laboratory, Cincinnati, Ohio (GE) to determine the compatibility of potential tubing alloys with potassium. Two types of compatibility tests have been employed: (1) a reflux capsule test for material screening (LeRC and Ge) and (2) a forced convection two-phase loop test in which power system fluid flow and temperature conditions are simulated (GE).

Presented herein are initial findings of these tests. Reflux capsule test results are given for 8 niobium- and tantalum-base tubing alloys. The alloys were of both the gettered (i.e., containing hafnium or zirconium) and nongettered varieties: B-33 (Nb-4V, nominal alloy composition in weight percent); SCb-291 (Nb-10Ta-10W); Nb-1Zr; D-43 (Nb-10W-1Zr-0.1C); FS-85 (Nb-28Ta-10W-1Zr); Ta-10W; T-111 (Ta-8W-2Hf); and T-222 (Ta-9.6W-2.5Hf-0.01C). Many of the alloys were tested in both the as-worked and recrystallized conditions. Tests were conducted over the temperature range of 1800° to 2400° F for times up to 10 000 hours. Data from reflux capsule tests to determine the possible effect of stress on corrosion are also presented. In these tests, three niobium-base alloys, B-33, D-43, and FS-85 were tested at 2200° F up to 1000 hours at an initial stress of about 4000 psi. Lastly, results are presented of a test run of a forced convection boiling potassium loop. The loop, constructed of Nb-1Zr alloy, was operated at 1850° F saturation temperature for 5000 hours.

REFLUX CAPSULE TESTS

The corrosion resistance of the potential space-power-system tubing alloys to potassium was determined by means of reflux capsules, the capsule wall serving as the test specimen. In these tests, potassium is vaporized from a pool at the bottom of the capsule, rises, and is condensed near the top of the capsule. Condensate flows down the capsule wall to join the bulk liquid, completing the circuit.

1. PROCEDURE

The potassium used was purified by the hot-getter method [1] to an oxygen level of less than 20 ppm. The alloys, their composition, and their condition are given in Table I. The so-called nongettered alloys, B-33, SCb-291, and Ta-10W, were specifically analysed for the presence of getter-element contaminants, namely, Ti, Zr and Hf. Heats 1, 2 and 3 of the B-33 alloy were found to contain small amounts of Zr.

Capsules of two sizes were used: a small capsule, 1/2-inch outside diameter by $1\frac{3}{4}$-inch by 0.040-inch wall (LeRC), and a large capsule, 1-inch outside diameter by 11-inch by 0.080-inch wall (GE). The choice of capsule size was somewhat arbitrary, reflecting mainly the test preferences and techniques employed by each laboratory. The small capsules were machined from rod stock, while the large capsules were fabricated by roll forming and tungsten-inert-gas welding of 0.080-inch sheet.

To preclude air contamination of the capsules and their contents, capsule loading and sealing were performed in special vacuum facilities, at pressures of about 10^{-5} torr. A volume of potassium equal to about 1/3 the internal volume of the capsule was introduced into each capsule. A cap was placed over the top of the capsule and electron beam welded to the capsule. This procedure is described in detail in the LeRC motion picture

TABLE I. COMPOSITION AND CONDITION OF CAPSULE MATERIALS

Alloy	Heat	Condition	Composition						ppm			
			Weight percent						C	O	N	H
			W	Zr	Hf	V	Nb	Ta				
SCb-291	--	Worked	8.37	----	----	----	Balance	9.69	14	101	119	30
B-33	1	Worked	----	0.02	----	4.88		-----	64	142	52	17
B-33	2	Recrystallized	----	0.05	----	5.14		-----	63	113	57	18
B-33	3	Worked	----	0.19	----	4.24		-----	111	159	77	15
Nb-1Zr	1	Worked	----	0.91	----	----		-----	81	200	75	8
Nb-1Zr	2	Recrystallized	----	1.29	----	----		-----	40	144	28	5
D-43	--	Worked	9.4	1.0	----	----		-----	870	56	44	4
FS-85	--	Worked	8.53	0.80	----	----		26.95	58	148	41	10
Ta-10W	1	Worked	8.09	----	----	----	-------	Balance	41	48	9	15
Ta-10W	2	Recrystallized	9.70	----	----	----	-------		33	37	37	4
T-111	--	Worked	7.87	----	2.31	----	-------		37	25	13	33
T-222	--	Worked	8.45	----	2.31	----	-------		141	48	18	4

(C-241, available on request) entitled Vacuum Handling of Air Sensitive Space-Power-System Materials.

In the small capsule tests, in order that weld material might be exposed to the condensing vapor as well as the boiling potassium liquid pool, some capsules were positioned with the cap weld at the top and others inverted.

Testing was conducted in high-vacuum chambers at pressures in the range of 10^{-8} torr. Heat was supplied to each capsule by a tantalum heater. Electric power to the heaters was regulated by automatic control equipment to maintain a set temperature. Capsule temperatures, measured with platinum - platinum-13%-rhodium thermocouples, were continuously recorded throughout the test duration. Estimates of the condensation rate and condensate film velocity within the large capsules are 1 lb/h and 0.09 ft/sec, respectively.

At the conclusion of a test the capsules were opened and the potassium removed. X-ray, chemical, and metallographic analyses were made on selected capsule sections.

2. RESULTS

Test results are summarized in Table II. Several general corrosion or corrosion-related results can be noted:

1. The alloys containing the gettering elements, zirconium or hafnium, were found to be markedly more resistant to corrosive attack than the nongettered alloys. A typical comparison of corrosion results between gettered and nongettered alloys can be seen in Figures 1 and 2 for niobium- and tantalum-base alloys, respectively.

2. Corrosion attack, when it occurred, was mainly intergranular. However, in the case of B-33, heats 1 and 2, and SCb-291 significant solution attack also was observed. In the case of the alloys tested at the more extreme conditions of temperature and time, a small amount of leaching

or alloying elements from the condensate zone was manifest as a black film deposit in the region below the condensate zone (e.g., FS-85 capsule, Fig. 1).

TABLE II. SUMMARY OF CAPSULE TEST RESULTS

Alloy (heat)	Temperature, °F	Time, h	Number capsules tested	Corrosive attack, (a)	Remarks (b)
SCb-291	1800	1,000	2	Ig, 1.5, W Ig, 6, W(inv.)	P P
	2200	1,000	2	Ig, 16, L; Sol, C	R, D(Nb and W, by X-ray diffraction)
B-33(1)	2200	1,000	2(c)	Sol, 3.5, C	R, G
	2300	380	2(c)	None	R, G
B-33(2)	1800	2,000	2	None	----
	2200	2,000	1	Sol, 1, C	G
B-33(3)	1800	2,000	2	None	R
	2200	2,000	2	None	F, R, G
Nb-1Zr(1)	1800	2,000	2	None	G
Nb-1Zr(2)	2000	10,000	1(d)	None	G, Z, D(Zr, by Electron Beam Probe)
D-43	2200	1,000	2(c)	None	P
	2200	2,000	1	None	F, P
	2300	1,000	2(c)	None	F, P, Z
	2300	2,000	1	None	F, P, Z
	2000	10,000	1(d)	None	-------
FS-85	2200	4,000	2	None	F, R, Z
	2300	1,000	2(c)	None	F, R, Z
	2300	2,000	2	None	F, R, Z
	2400	2,000	1	Ig, <1, C and L	F, R, Z
Ta-10W(1)	1800	110	1	Ig, 16, W	-------
	2200	8	1	Ig, 16, W	-------
Ta-10W(2)	1800	128	1	Ig, 16, W	-------
	2200	8	1	Ig, 17, W(inv.)	-------
T-111	2200	4,000	1	None	F, R
	2300	2,000	2	None	F, R
	2400	2,000	1	Ig, <1, C and L	F, R
T-222	1800	4,000	1	None	----
	2200	4,000	1	None	R, F($K_2Ta_4O_{11}WO_3$, by X-ray diffraction)
	2400	4,000	1	Ig, 3,(e) L	R, Z, F($K_2Ta_4O_{11}WO_3$, by X-ray diffraction)

[a] Corrosion results are presented in the following order: (1) Type: Ig, intergranular; sol., solution. (2) Maximum depth in mils. (3) Location: C, vapor condensation region; L, liquid pool; B, region between C and L; W, weld. Note that normal capsule test position was with weld in region C. Some tests were run with capsule inverted, inv., so that weld was in region L.

[b] The following code is used: D, crystalline deposit at region B; F, film mainly in region B; G, accelerated grain growth, mainly in region C; P, partial recrystallization; R, complete recrystallization; Z, zone at inner edge, mainly in region C, deficient in second-phase precipitates.

[c] One capsule of pair tested for stress corrosion effects.

[d] Large capsule: 11 inches by 1.0-inch diameter by 0.08-inch wall. The initial oxygen content of the Nb-1Zr capsule was <50 ppm.

[e] Penetration was in one highly localized area of bottom corner; no other penetration was found.

3. Grain growth was more pronounced in the top sections of the capsules than in the bottom, even though the capsule temperature was lower at the top than at the bottom.

4. The gettered alloys generally showed less second-phase precipitation in the capsule top section than in the bottom and a precipitate deficient zone along the inner edge of the top sections.

STRESS CORROSION TESTS

1. PROCEDURE

For purpose of stress corrosion testing the standard reflux capsule was altered by machining down the wall thickness just above the midregion, as shown in Fig. 3. Internal pressure in the capsule resulting from the vapor pressure of the capsule imposed an initial hoop stress of about 4000 psi on the thin-wall section, causing it to creep (see Fig. 3). Three

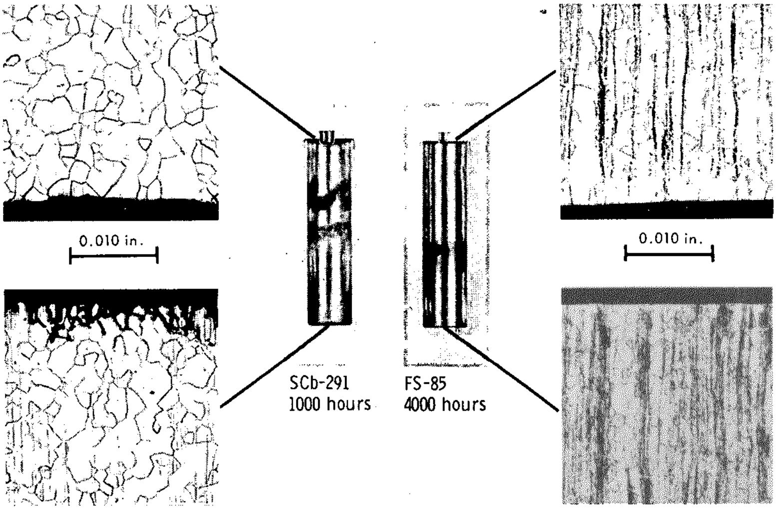

FIG.1. Comparison of ungettered (SCb-291) and gettered (FS-85) niobium-base alloys tested at 2200°F

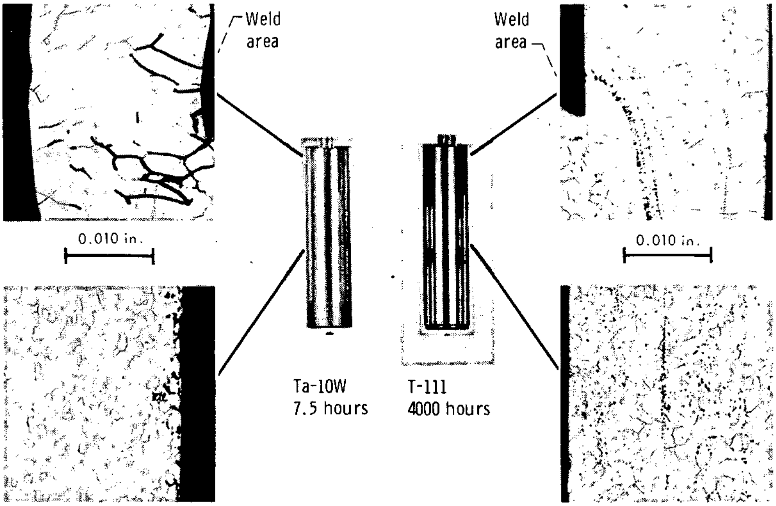

FIG.2. Comparison of ungettered (Ta-10W) and gettered (T-111) tantalum-base alloys tested at 2200°F

niobium-base alloys, B-33, D-43, and FS-85, were tested for stress corrosion at 2200° F for up to 1000 hours. In each stress corrosion test, as a reference, a standard capsule of the same material was tested at the same temperature and time as the stress corrosion capsule.

2. RESULTS

A summary of the test results is included in Table II. In general, no stress corrosion effects were found over the range of conditions tested.

B-33 (heat 1)

The nature and extent of corrosion attack in the stress corrosion capsule test at 2200° F for 1000 hours and 2300° F for 380 hours were the same as in the standard capsule. The 2300° F thin-walled capsule failed by creep rupture at a creep strain of 45%.

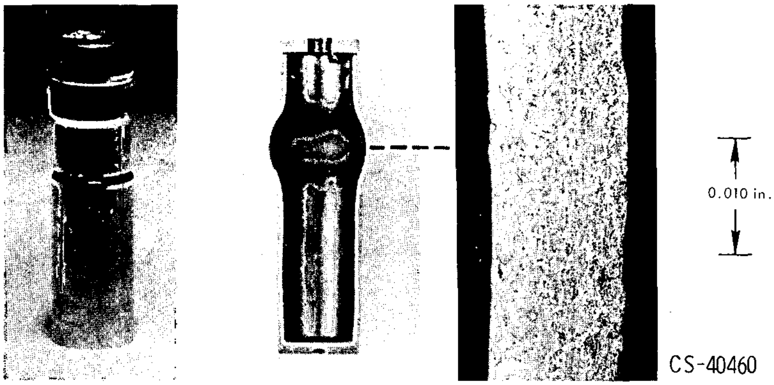

Before test   Sectioned capsule, post test   Photomicrograph of high-stressed region

FIG. 3. Test for stress corrosion in niobium alloy D-43 at 2300°F for 1000 hours

D-43

No effect of stress or corrosion was observed at 2200° F or at 2300° F (Fig. 3) for 1000-hour tests. The 2200° F and 2300° F thin-wall capsules underwent creep strains of 3.5% and 37%, respectively.

FS-85

No stress corrosion effects were seen in the capsule test at 2300° F for 1000 hours and a creep strain of 2.7%.

PUMPED LOOP TEST

The initial screening of potential space-power-system materials is readily accomplished in capsule tests, as previously described. The final materials selection, however, must be made on the basis of proof tests which simulate closely the temperature and flow conditions of an actual power system. Described below is the first of the forced convection two-phase corrosion tests in the NASA's advanced space-power-system technology program.

The prototype test system was fabricated from Nb-1Zr alloy (the only refractory metal alloy available as tubing at the start of the test program in 1963). The composition of the alloy was as follows: 0.87 Zr; 33 ppm C; 260 ppm O; 47 ppm N; 1 ppm H; balance, Nb.

The corrosion test system basically consisted of two liquid metal loops, a sodium heater loop and a potassium boiling and condensing loop, mounted in a vacuum chamber. A vacuum of 2×10^{-8} torr or better was maintained in the chamber during the test duration of 5000 hours.

In the heater loop, sodium, circulated by an electromagnetic pump, was heated by an electric resistance heater. From the heater, the sodium flowed into a tube-in-tube counterflow boiler where heat from the sodium was transferred to the potassium. The sodium loop operated at a maximum temperature of 2130° F, a minimum temperature of 1990° F, and a flow rate of 910 lb/h.

In the second loop, potassium, discharged from an electromagnetic pump, was preheated by an electric resistance heater before entering the boiler. In the boiler, the potassium converted from liquid to superheated vapor. The vapor passed through the turbine simulator (the pressure drop, heat extraction section) and on into the condenser. Condensed vapor then returned through the subcooler to the pump. The operating conditions were as follows: saturation temperature, 1850° F; superheat temperature, 2000° F; condensing temperature, 1425° F; flow rate, 31 lb/h, and liquid velocity in the boiler, 0.8 ft/sec.

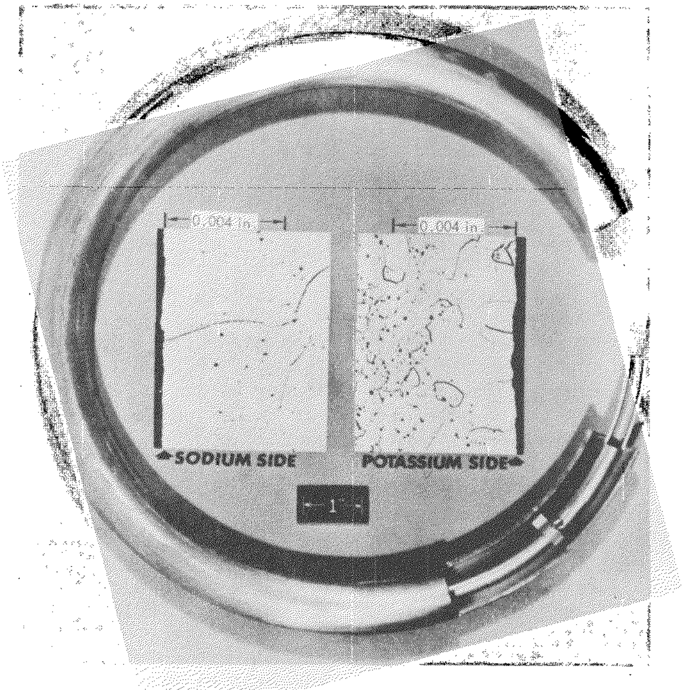

FIG. 4. Post-test view of Nb-1Zr tube-in-tube boiler

Figure 4 shows a view of the tube-in-tube boiler and photomicrograph of a typical section of the tube wall following the 5000-hour test. No corrosion or erosion attack was found in any portion of the potassium loop.

On the sodium side of the boiler a small amount of mass transfer deposit was found on the outside diameter of the inner tube. The deposit was in the relatively short section where the greatest temperature drop in the sodium is estimated to have occurred. The 1/2-mil deposit consisted primarily of zirconium. There were no other manifestations of corrosion in the sodium loop.

DISCUSSION

1. EFFECT OF OXYGEN ON CORROSION

The prominent role of oxygen in the dissolution mass-transfer reactions of alkali metals has been established by previous investigations. It has been found (1) that oxygen enhances the corrosion of various materials by Na and Li [2 to 5] and (2) that the presence of oxygen increases the measured solubility of elements such as Fe, Mo, Ta and Nb in Li, Na and K [6 to 8]. In the corrosion tests reported here, a similar "oxygen effect" is believed to account for the salient test result, namely, the gettered alloys were markedly more resistant to corrosion by potassium than were the nongettered alloys. The effectiveness of the gettered alloys in reducing corrosion appears to stem from the effectiveness of the getter element in scavenging and immobilizing oxygen through the formation of a stable oxide, i.e., ZrO_2 or HfO_2.

It has been suggested that the mechanism of oxygen-enhanced mass transfer involves a container-metal - alkali-metal complex oxide as a reaction intermediate [2,5]. Evidence for the existence of complex oxides has been obtained by Horsley in the Fe-Na-O system [2] and by Tyzack in the Nb-Na-O system [3]. Pertinent to the potassium corrosion tests reported herein are the results of a recent study at LeRC [9] in which tantalum, containing 1200 to 2400 ppm oxygen, was exposed to potassium at 1800° F for 100 hours. In all cases the Ta suffered corrosion and complete oxygen depletion; the corrosion product isolated from the potassium was a white solid characterized as $3K_2O \cdot Ta_2O_5$. These results support the contention that, when oxygen is available, potassium corrosion attack occurs via the formation and subsequent dissolution of a Ta (or Nb) complex oxide.

In potassium corrosion tests reported herein, available oxygen potentially can be found either in the potassium, as K_2O or in the refractory alloy, as refractory metal oxide or as interstitial oxygen Potassium oxide is not considered a prime source of oxygen, since the amount of oxygen present as K_2O accounts for 3% or less of the total available oxygen. The same can be said for the refractory metal oxides, since oxides are not likely to form when the oxygen concentration of the alloy is below the solubility limit. Thus, interstitial (i.e. dissolved) oxygen is the most probable source of available oxygen.

The location and distribution of dissolved oxygen will depend largely on regional differences in solubility and diffusion rates which in turn depend on the temperature and the alloy composition and structure. When oxygen is more or less uniformly distributed throughout an alloy, uniform solution attack (such as exhibited by the B-33 alloys, heats 1 and 2) would be expected. Alternately, oxygen may concentrate in certain preferred regions such as grain boundaries [10], specific crystal planes [11] or lines of dislocations [12]. Corrosion attack, then, would be expected to follow these oxygen enriched paths. Although transgranular attack has been observed in tests of Ta in K [9] and Ta and Nb in Li [4], corrosion of the preferred path type when observed in the tests reported herein was exclusively intergranular.

The results for the two nongettered alloys tested indicated that the sensitivity to intergranular attack, considering time, temperature, and initial oxygen content, is Ta-10W > SCb-291. (The B-33 alloys used in this study cannot be considered as nongettered, since they contained Zr as a fortuitous impurity.) The order of penetration sensitivity of the Ta alloy, Ta-10W, and the Nb alloy, SCb-291, in potassium was the same as that found for Ta and Nb in Li [4]. No explanation can be offered for the difference in sensitivities.

2. GETTER-RELATED CORROSION THRESHOLD

As discussed previously, the corrosion resistance of the gettered Nb- and Ta-base alloys appears to result from the ability of the getter element to scavenge oxygen. If this is the case, a getter-related corrosion threshold should exist which may be defined in terms of the minimum amount of getter required to immobilize the oxygen. An estimate of the minimum amount of getter required to prevent corrosion must necessarily take into account interstitials such as N and C as well as O. The reason for this is the N and C, conceivably, may also react with the getter and thereby compete with O for available getter. (Reaction, as described here, may entail weak association or "clustering" as well as compound formation between getter and interstitials.) Evidence supporting the possibility of competitive reactions of oxygen and other interstitials with the getter element can be found in the results of two pertinent studies. First, internal friction measurements of a Nb-0.9 Zr alloy, containing 0.015% N and <0.07% O, have indicated that all of the O and part of the N are associated with the Zr [13]. Second, in a study of the Nb-Zr-C system, containing <0.015% O, one of the four phases found in the Nb corner of the system was tentatively identified as $Zr_2(OC)$ [14]. Thus, on the basis of the foregoing discussion, the amount of getter required to prevent corrosion should depend (1) on the extent to which the getter is partitioned between oxygen and other interstitials and (2) on the amount of interstitials present.

The premise of a getter-related corrosion threshold can be examined by considering the three heats of B-33 alloys. Each heat, because of a fortuitous presence of Zr as an impurity, contained a small amount of Zr (viz., 0.02%, 0.05%, and 0.19% for heats 1, 2, and 3, respectively). Also, each heat showed a different corrosion response; the order of corrosion attack was heat 1 > heat 2, and no attack was found for heat 3. The previous data show that there is a qualitative relation between Zr content and corrosion. However, to convincingly verify the premise of a getter-related corrosion threshold, a quantitative relation is needed This relation may be achieved by comparing the corrosion results with the actual Zr content of the alloy Zr_A and with the amount of Zr theoretically required to prevent corrosion Zr_{th}. For each heat, Zr_{th} can be calculated from the interstitial composition given in Table I together with an estimate of the partition functions for the Zr-(O,N,C) reactions. (The interstitial H is neglected here because of the instability of pertinent hydrides at the test temperatures.) Since no quantitative information is available for the partition functions, two limiting cases will be considered. In case 1, it will be assumed that all the O, N, and C react to form ZrO_2, ZrN, and ZrC, respectively; in case 2, it will be assumed that only the oxygen reacts and forms ZrO_2. The true value of Zr_{th} is expected to be between the high value of Zr_{th}, case 1, and the low value of Zr_{th}, case 2.

A comparison of corrosion and Zr content for the three heats of B-33 alloy is given in Table III. Shown are the test time, the corrosive attack, Zr_A, and the values calculated for Zr_{th}, cases 1 and 2. These

TABLE III. CORROSION AND Zr CONTENT OF B-33 ALLOYS AT 2200°F

Heat	Test time, h	Corrosion (a)	Zr_A, %	Zr_{th}, %	
				Case 1	Case 2
1	1000	Sol., 3.5, C	0.02	0.12	0.04
2	2000	Sol., 1, C	0.05	0.12	0.03
3	2000	None	0.19	0.18	0.05

[a] Corrosion results are presented in the following order: (1) Type: sol., solution. (2) Maximum depth in mils. (3) Location: C, vapor condensation region.

results generally substantiate the premise of a getter-related corrosion threshold. When $Zr_A < Zr_{th}$ there is corrosion attack which tends to increase as the difference between Zr_A and Zr_{th} increases.

3. CORROSION BY ELEMENTAL DISSOLUTION

If the amount of getter available is greater than the amount of getter required to prevent corrosion, dissolution mass transfer cannot occur through the formation and dissolution of a container-metal complex oxide. Instead, the path of mass transfer attack will be restricted to direct dissolution of container metal in K. The capsule test results suggest that the dissolution potential of the container metal is very much lower than that of the container-metal complex oxide. Even at the upper test temperature of 2400° F, no gross dissolutions was observed.

The only indications of dissolution attack in the getter alloys were (1) the <1-mil-grain boundary penetrations in the 2400° F tests of he FS-85 and T-111 alloys and (2) the black film found on the inner surface at the middle third region of the capsules tested at the more extreme time and temperature conditions. In the former instance, the penetrations may possibly reflect grain boundary grooving arising from surface energy differences between grain and grain boundary at this temperature. In the latter instance, the black film presumably results from deposition of material leached out of the condensation region. The black film in the T-222 capsules was identified as $K_2Ta_4O_{11}$ plus traces of WO_3. In the 10 000-hour Nb-1Zr capsule, the black deposits were identified as predominantly Zr. Analyses were not made of the films found in the remaining capsules. However, in all of the capsules in which films were found, indirect indications of Zr (or Hf) leaching were noted (viz., less second-phase precipitation and acceleration of grain growth at the potassium-refractory alloy interface of the condensing region).

4. EFFECT OF STRUCTURE ON CORROSION

Alloy structure (i.e., worked or recrystallized) did not noticeably influence the gettered-alloy test results. Structure, however, did markedly affect the extent of attack on the ungettered Ta-10W alloy. The worked structure of the Ta-10W, heat 1, tested at 1800° and 2200° F showed no attack, while in the same capsules the recrystallized weld zone exhibited extensive intergranular penetration. The recrystallized Ta-10W, heat 2, tested at 1800° and 2200° F exhibited intergranular attack throughout the entire capsule.

When the mode of corrosion attack is intergranular, it is likely that a worked structure provides corrosion resistance from purely mechanical considerations. Disruption of the original grain boundaries during the process of cold working leads to a discontinuous network of grain boundaries and hence a discontinuous network of potential corrosion paths.

The protection offered by a worked structure is probably quite limited in duration at temperatures of 2000° F and above, since in this temperature range Nb- and Ta-base alloys recrystallize in a relatively short time. For the Ta-10W capsule, failure by grain boundary penetration at the weld occurred so rapidly that there was not time for recrystallization of the worked structure. However, in the case of the SCb-291 alloy, corrosion attack was more moderate, and recrystallization had time to take place. As expected, the initially recrystallized weld zone was deeply penetrated, and the subsequently recrystallized portions of the capsule showed intergranular penetration to a lesser extent.

CONCLUSIONS

The results of the capsule screening tests indicate that the gettered Nb- and Ta-base alloys have excellent corrosion resistance to boiling potassium in the range of temperature and time required in the operation of an advanced space power system. The corrosion resistance of the gettered alloys is attributed to the reaction of the getter element with available oxygen to form a stable oxide and thereby preclude the formation and subsequent dissolution of a potassium - refractory-metal - oxygen corrosion intermediate. It was demonstrated that as long as the amount of getter is greater than the amount needed to tie up all the oxygen present, no significant corrosion will occur.

The negative findings in tests for the possible effect of stress on corrosion are encouraging, inasmuch as thermally and mechanically induced stresses are inherently present in power systems. None of the three Nb alloys tested, B-33, D-43 or FS-85, showed any stress corrosion effects.

The results of the Nb-1Zr loop test support the general findings of the capsule tests concerning the corrosion resistance of gettered alloys. This is all the more significant inasmuch as the loop test conditions were more severe than those imposed on capsule tests, namely, a much larger temperature gradient and ~10 times greater liquid flow velocity. Further, it seems likely, given the low elemental dissolution potential inferred from the gettered alloy capsule results, that the effect of temperature gradient or flow velocity will not be a major problem at temperatures below 2400° F.

REFERENCES

[1] HINZE, R. B., USAEC Rpt NAS-SR-3638 (1959).
[2] HORSLEY, G. W., J. Iron Steel Inst. 182 (1956) 43.
[3] TYZACK, C., Advances in Materials, Interdisciplinary Symposium, Third and Fourth Session, Institute of Chemical Engineers, London (1964) 239.
[4] DISTEFANO, J. R., HOFFMAN, E. E., Corrosion of Reactor Materials II, IAEA, Vienna (1962) 431.
[5] EVANS, J. W., THORLEY, A., U. K. A. E. A. Rpt IGR-TN/C-1019 (1958).
[6] SWISHER, J. H., USAEC Rpt NASA TN D-2734 (1965).

[7] BAUS, R. A., BOGARD, A. D., GRAND, J. A., LOCKHART, L. B., Jr., MILLER, R. R., WILLIAMS, D. D., Proc. UN Int. Conf. PUAE 9 (1955) 356.
[8] CLEARY, R. E., BLECHERMAN, S. S., CORLISS, J. E., USAEC Rpt TIM-850 (1965).
[9] HICKAM, C. W., Jr., Unpub. data (1966).
[10] INOUYE, H., Columbium Metallurgy (DOUGLASS, D. L., KUNZ, F. W., Eds), Interscience Publ., New York (1961) 649.
[11] KOFSTAD, P., J. Less Common Metals 7 (1964) 241.
[12] BAKISH, R., Trans. metall. Soc. A. I. M. E. 212 (1958) 818.
[13] BUNN, P. M., CUMMINGS, D. G., LEAVENWORTH, H. W., J. appl. Phys. 33 (1962) 3009.
[14] CORNIE, J. A., DELGROSSO, E. J., GRANGER, R., USAEC Rpt PWAC-461 (1965).

DISCUSSION

C. TYZACK: What assumptions do you make regarding the action of compounds such as 3 $K_2O \cdot Ta_2O_5$ in your loops? Do you visualize them as taking part in a sort of cyclic process, dissociating at high temperature and reforming at low temperature, or do you think that they are associated with intergranular attack which does not occur in the presence of the stabilizing element (zirconium)?

L. ROSENBLUM: No corrosion of any kind was observed on the potassium loop described. However, I would not expect a cyclic corrosion process involving a tantalate to occur in the once-through loop system I have discussed, mainly because the phase change interrupts the continuity of the liquid, thus separating the high-temperature liquid region from the low-temperature liquid region (condensate). Our observation is that the tantalate is associated with the intergranular attack (or the transgranular attack seen in the case of pure tantalum in potassium).

EXPERIENCE IN INVESTIGATION OF COMPONENTS OF ALKALI-METAL-VAPOR SPACE POWER SYSTEMS

R. E. ENGLISH AND RUTH N. WELTMANN
LEWIS RESEARCH CENTER,
NATIONAL AERONAUTICS AND SPACE ADMINISTRATION,
CLEVELAND, OHIO,
UNITED STATES OF AMERICA

Abstract

EXPERIENCE IN INVESTIGATION OF COMPONENTS OF ALKALI-METAL-VAPOUR SPACE POWER SYSTEMS. *As a preliminary to development* of a reactor-powered alkali metal-vapour turbogenerator power system for use in space, components of such a system have been studied and operated in various alkali metal loops. The observed performance of the components and the experience in operation of the loops are both described. Although the work encompasses both sodium and potassium, the work with potassium is emphasized.

Heat transfer to boiling potassium was investigated in a 300-kW loop of L-605 for temperatures as high as 1750°F, and in a 150-kW loop of Cb-1Zr for temperatures as high as 2100°F. In addition, heat transfer to boiling sodium was investigated in a 500-kW bimetallic loop of Cb-1Zr and 316 stainless steel; the boiling temperature reached 2000°F. Condensation of potassium at temperatures of 1200-1500°F was investigated in two loops of 50- and 150-kW capacity. Wet potassium vapour at 1500°F was produced by a 3-MW gas-fired boiler and supplied to a 2-stage turbine; although the entire loop was built of 316 stainless steel, the turbine rotor blades were of TZC, TZM, and Udimet 700 so that erosion resistance could be compared. The condition of the turbine at the end of an endurance run of 5000 h is described. Alkali metals at 1100° and 1980°F were pumped for several thousand hours by, respectively, a motor-driven centrifugal pump designed for flight and an electromagnetic induction pump; the pump designs are described. Both electrical and magnetic materials for long-time use at 1100°F have been investigated; results of these tests are presented. The methods used for measuring fluctuating pressure in these alkali metal systems are also described.

INTRODUCTION

The investigation of alkali-metal power systems by the National Aeronautics and Space Administration has as its objective long-lived space power systems having electric power outputs of the order of 100 kW to 10 MW. This power might be either for electric propulsion or for powering equipment within the spacecraft. For these high powers, both the area and the mass of the waste-heat radiator are important factors in selection of a Rankine-cycle system operating at high temperature and using an alkali-metal vapor as the working fluid. The considerable experience here on Earth with turbogenerating Rankine-cycle powerplants and the long lives of these powerplants indicate that a similar turbogenerating powerplant might possess a comparable long life in space. Nuclear reactors might provide the required thermal energy with only small additions of mass and volume to the powerplant.

The type of system being investigated is shown in figure 1 and contains four separate fluid loops. The temperatures shown illustrate the levels that might be used; these temperatures, although high, are within the capabilities of the alloy T-111 (Ta-8W-2Hf). The liquid coolant pumped through the reactor flows through the boiler, where its temperature drops

100° to 200° F. One of the main reasons for use of a separate loop for the reactor is to diminish the problems of shielding against nuclear radiation. If some of the reactor fuel elements develop small cracks, the reactor might well be capable of continued operation, but some of the fission products could then leak into the reactor coolant stream. With a separate reactor loop, only the reactor loop need be shielded in order to protect against such fission product leakage. If a separate reactor loop were not used, these fission products would contaminate the entire power loop, and thereby shielding, inspection, and maintenance of the power system would be complicated.

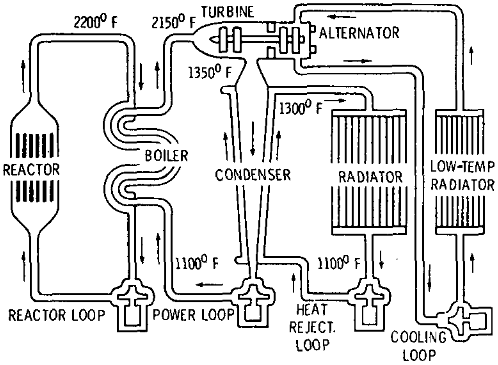

FIG.1. Potassium-Rankine system

For the power loop, potassium is the working fluid. In the counterflow boiler, the maximum temperature at which the potassium may be boiled is approximately the same as the temperature of the reactor coolant as it leaves the boiler. For this reason, some superheating of the resulting potassium vapor is possible, of the order of 50° to 150° F. The turbine outlet temperature of 1350° F produces minimum radiator area per unit power for the specified boiling conditions.

The potassium vapor at the turbine discharge is condensed by transfer of heat to a counterflowing liquid, this liquid then being cooled by means of thermal radiation to space. The condensing and radiating functions are separated for two reasons. First, system weight is reduced if liquid rather than vapor of low density passes through the radiator tubes because the smaller liquid-filled radiator tubes require less armor against meteoroid penetration than do the larger vapor-filled tubes. And second, the design of the power loop is then almost independent of the manner in which the power system integrates with the spacecraft and mission. Radiator geometry can be adapted to each spacecraft and mission with only minor alterations in pumping power.

Such a power system as this has a considerable number of components and a substantial diversity of problems. To this time, various constituent problems of many of these components and the physical properties of potassium vapor and liquid have been investigated both within the NASA laboratories and under contract [1] to [5]. A number of these investigations are described below. For brevity, the discussion is limited to components of the power loop.

HEAT TRANSFER

For design of potassium boilers and condensers, the heat transfer characteristics of the liquid, two-phase, and vapor potassium working fluid have to be known. Many facilities have been developed and operated to test boilers and condensers of different design, to obtain sufficient heat transfer information, and to develop these two components for a space power system [6,7]. Two different types of boiler test facilities were operated to obtain heat transfer information for all conditions of boiling of potassium and for different boiler geometries [8 to 11]. Different boiler geometries are used to improve the heat transfer and obtain once-through boiling; that is, subcooled liquid potassium enters one end of heated tubes and dry, superheated vapor leaves the other end.

Several types of test apparatus were used for investigation of boiling potassium, one rig being shown schematically in figure 2. This apparatus, built of L-605 (Co-20Cr-15W-10Ni, nominal alloy composition in weight percent), was operated for investigation of boiling potassium temperatures up to 1750° F. Heat was added to the boiling potassium by a flowing stream of liquid sodium that itself was heated by a 300-kW gas-fired heater. An air-cooled condenser cooled the potassium, and the potassium and sodium streams were each circulated by an electromagnetic pump. In the potassium boiler, the sodium and potassium flows through concentric tubes, the potassium being in the inner tube. In some tests the sodium and potassium flows were countercurrent with respect to one another, and in other tests cocurrent. Thermocouples spaced axially along the outer sodium tube indicated the axial distribution of heat transferred to the potassium. In some of the potassium boilers, a vortex-generating insert extended the full length of the potassium tube in order to provide high centripetal acceleration for phase separation; thermocouples located in this central body indicated the axial distribution of both the pressure and temperature of the boiling potassium. Potassium pressures at boiler inlet and outlet were measured by means of slack diaphragm transducers. This test apparatus was operated for over 4000 hours.

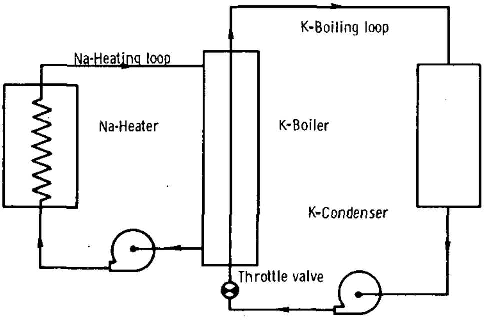

FIG.2. Potassium 300-kW boiler rig

Typical data of local heat flux, quality and heat transfer coefficient along the boiler length are presented for one of the test boilers in figure 3. The local heat flux at the entrance to the boiler is very large (over 200,000 Btu/(hr)-(ft^2)) because the temperature difference between the potassium and the sodium heating fluid is great. Heating the potassium decreases the heat flux because of decreasing temperature difference. The heat flux in the nucleate boiling region increases primarily because of the increased heat transfer coefficient for this mode of heat transfer. At a vapor quality of about 75 percent, the heat flux and heat transfer coefficient begin to decrease, marking the onset of critical heat flux and the beginning of the transition-boiling region. In the superheat region, the heat flux and heat transfer coefficient have fallen to values typical of the heat transfer to gases. In figure 4, the average heat transfer coefficients with and without an insert are compared. The insert was a helix wound on a cylindrical center body that extended radially from the tube wall to the wall of the center body; the pitch of the helix was twice the tube inside diameter. High heat transfer coefficients were obtained at intermediate qualities either with or without the insert. The low heat transfer coefficients at low quality result from low fluid velocities and are readily increased by reduction in flow area. At high vapor quality, the decline in heat transfer coefficient in the transition region is markedly delayed by the presence of the helical insert. With the insert, 200° F of superheat was obtained, but without the insert 100 percent quality was not achieved.

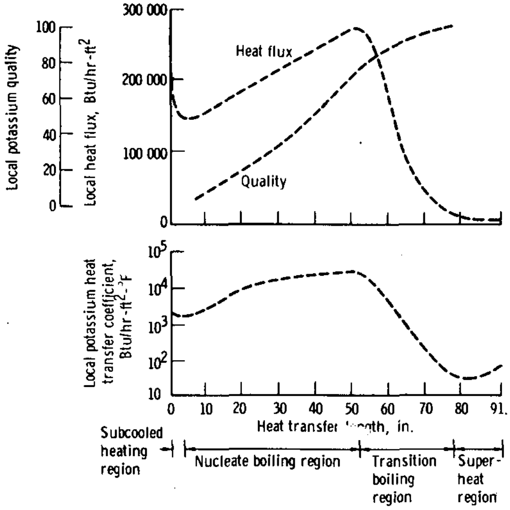

FIG.3. Potassium boiler heat transfer characteristics

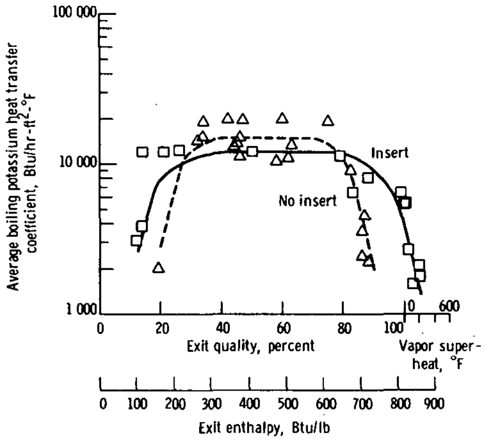

FIG.4. Effect of insert on boiling potassium heat transfer

Boiling of potassium at higher temperatures was investigated in the apparatus shown schematically in figure 5. This apparatus was built entirely of Nb-1Zr and so was capable of boiling potassium at temperatures as high as 2100° F. For protection against oxygen, the loop was contained in a vacuum chamber at 10^{-6} to 10^{-7} torr. The potassium stream was heated electrically in three successive heaters of a maximum capacity of 150 kW. The preheater and the preboiler heat liquid and low-quality potassium, respectively, in order to provide potassium of specified enthalpy at the inlet to the test boiler. The test boiler was heated by thermal radiation from its surrounding electric heater. The resulting vapor was condensed by thermal radiation and then pumped again to the boiler by an electromagnetic pump. The facility was operated in excess of 6000 hours.

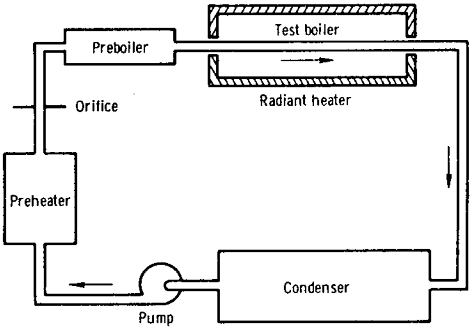

FIG. 5. 150-kW potassium boiler rig

The heat flux for boiling burnout, or critical heat flux, was measured with this apparatus in the following way: The preheater and the test boiler were operated at constant power, and high-speed recordings were made of the potassium flow and of various pressures and temperatures. Preboiler power was then increased. If under such conditions the wall temperature in the test boiler would suddenly rise (perhaps 200° F in 5 sec), the heat flux in the test boiler is the critical heat flux for boiling burnout.

In addition to these investigations of boiling potassium, boiling of sodium at temperatures as high as 2100° F was investigated in a 500-kW test rig, the boiler sections being built of Nb-1Zr and the others of stainless steel. This equipment has accumulated 900 hours of test time.

Condensing of potassium at temperatures from 1100° to 1500° F has been investigated in two rigs. One of these facilities supplied 50 kW of heat to boil potassium in a pot boiler. The potassium vapor was then condensed within a nickel tube by heat rejection to a countercurrent stream of sodium in a surrounding concentric tube. Except for the condensing tube itself, the test apparatus was built of 316 stainless steel and operated in air. Local heat transfer coefficients for potassium condensing at temperatures from 1100° to 1400° F were measured during 1200 hours of operating time [12 to 14].

A second rig for investigation of condensing-potassium heat transfer is shown in figure 6. Heated NaK was used to boil potassium which then flowed to either a radiatively or a convectively cooled condenser, the particular condenser being selected by settings of two shutoff valves. The radiatively cooled condenser was enclosed within a vacuum chamber in order to avoid atmospheric convection, and the other condenser was cooled by circulation of cooled NaK. The 150-kW NaK heater and boiler were L-605 and the remainder of the system was 316-stainless steel. Condensing temperatures to 1500° F have been investigated during 900 hours of rig operation [15].

A convectively cooled condenser is shown in figure 7. Potassium vapor condensed within seven parallel tubes, these tubes being cooled by a counterflow of NaK in a surrounding shell. The condenser had a bend in order to allow for thermal deformations of the tubes and shell. Thermocouples along the condenser shell indicated the temperature and energy content of the NaK and thus, indirectly, the energy content of the potassium. Pressure transducers measured potassium inlet pressure and overall pressure differential.

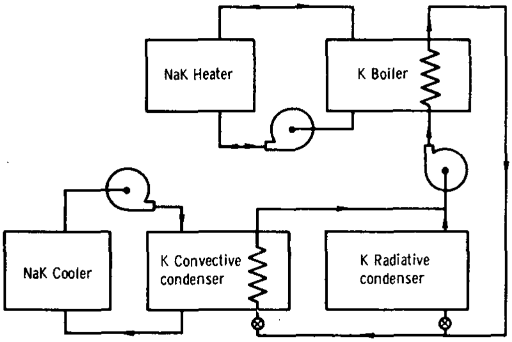

FIG. 6. Potassium condenser-radiator test rig

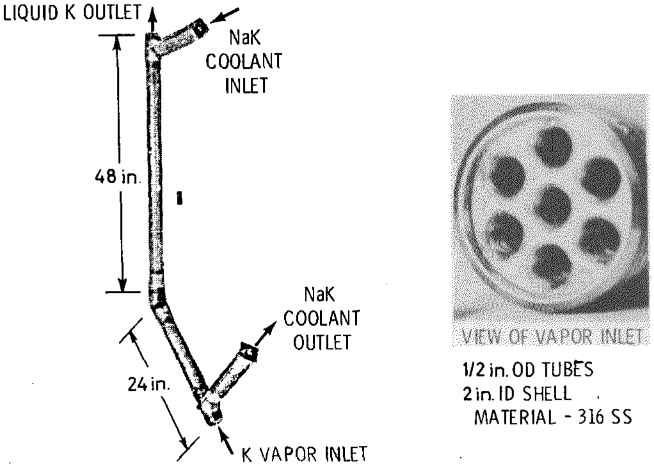

FIG. 7. Seven-tube K-condenser

The general results of these heat transfer investigations of boiling and condensing potassium can be summarized as follows: High heat transfer coefficients in excess of 10^4 Btu/(hr)(ft^2)($^{\circ}$F) are attainable both for condensing potassium and for boiling to intermediate qualities, such as 60 to 70 percent. The transition to the low heat transfer coefficients of gas heat transfer can be delayed until quality is near 100 percent if swirl-producing devices are employed. In general, condensing flows are stable, but boiling flows require some flow-stabilization device such as an orifice, especially in order to fix the zone of transition from all-liquid to boiling.

TURBINE

For turbines having inlet temperatures of 2000° to 2200° F, creep strength of the rotor materials is a crucial question. The high centripetal accelerations imposed on the rotor's parts also make low density highly desirable. On the other hand, weldability and post-weld ductility are not as rigid requirements as for the piping and heat exchangers of the power system. For these reasons, alloyed molybdenum and niobium, which have about one-half the density of tantalum-base alloys, were investigated. The creep characteristics of the alloys TZC(Mo-1.25Ti-0.15Zr-0.12C), Cb-132M(Cb-20Ta-15W-5Mo-2Zr-0.13C) and TZM(Mo-0.5Ti-0.08Zr) are summarized in figure 8, in which the Larson-Miller parameter P relates temperature T (°R) and time t (hr); these data were obtained by tests as long as 10 000 hours at temperatures as high as 2200° F. For the alloy TZC, less than 0.5 percent creep results from a stress of 20,000 lb/in.^{2} at a temperature of 2000° F for a time of 10 000 hours. The TZM was also tested for compatibility with potassium vapor in a refluxing capsule at 2000° F for 5000 hours; there was no evidence of metallurgical attack.

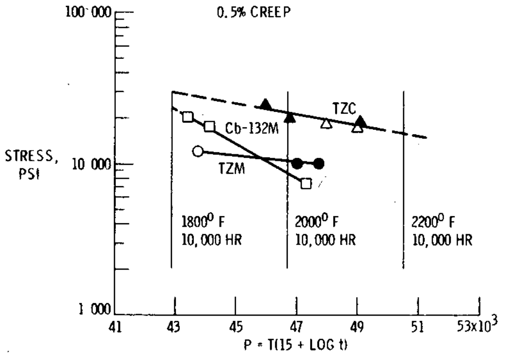

FIG. 8. Strength of turbine alloys

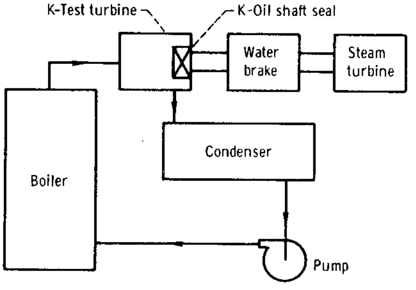

FIG. 9. Potassium turbine test loop

A second crucial question about the turbine is the possibility of turbine blade erosion by liquid potassium droplets. For investigation of blade erosion, a two-stage turbine was designed, built, and tested in the apparatus shown in figure 9 [16 to 22]. The potassium boiler is a gas-fired multitube recirculating unit of three MW capacity. In order for the potassium entering the turbine to be near 100 percent quality, the vapor on leaving the boiler passes first through a wire-mesh demister and then through an inertia type of liquid separator. The turbine rotor is supported by oil-lubricated bearings, and a dynamic shaft seal prevents contact between the potassium and oil. A water-brake absorbs output power, and a steam turbine is used during startup to raise rotational speed to a value at which the dynamic potassium-oil seal functions. Because the entire loop was built of stainless steel, maximum metal temperature during operation is limited to 1600° F and turbine inlet temperature to about 1550° F.

A turbine performance test was completed in May 1965 and a 2000-hour endurance test in December 1965. An additional 3000-hour endurance test was completed in September 1966. Most of the rotor blades from the 2000-hour test were reinstalled in the rotor for the additional 3000-hour endurance test in order to accumulate 5000 hours on these blades.

Initially all of the turbine rotor blades were Udimet 700 (Ni-18Co-15Cr-5Mo-4.5Al-3.5Ti-0.3B). In the second stage, however, eight of the Udimet 700 blades were replaced by two pairs each of blades of TZM and TZC to obtain erosion data on actual candidate rotor blade materials. For the 5000 hours, the turbine was operated on potassium vapor under the following test conditions: inlet temperature, 1500° F; inlet vapor quality, 0.99; second-stage inlet quality, 0.97; rotor tip speed, 770 ft/sec; exit temperature, 1260° F; and exit quality, 0.93. After the test, the second-stage rotor blades were photographed (fig. 10) and weighed. No significant erosion is visible; some of the original machining marks can still be seen. The maximum change in blade weight was only ±0.1 percent; these weight changes indicate that the erosion, if any, was negligible.

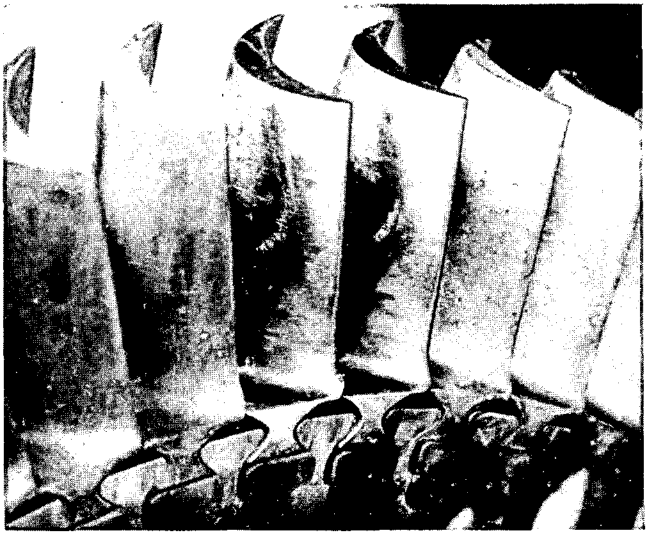

FIG. 10. Second-stage turbine rotor blades after 3000 and 5000 hours of operation with potassium vapor

In order for turbine exit vapor quality to be at least as high as the 0.93 so far investigated, either liquid removal from the vapor stream or reheating is required. A single, direct expansion of the potassium vapor should produce about 0.88 vapor quality at the turbine exit. Turbine exit vapor quality can be increased by addition of a single reheating at an intermediate point in the expansion process or by a combination of liquid separation and reheating. If at one point in the expansion process vapor quality is increased to 100 percent, then minimum vapor quality in the turbines can be increased to 93 percent. Whether or not turbine exit vapor qualities of 0.85 to 0.90 will erode the turbine blades has not yet been investigated for potassium vapor. For investigation of this problem, the present two-stage turbine will be modified by addition of a third stage which will have an exit vapor quality of about 0.88. This three-stage turbine will then be subjected to a performance and endurance test for the same turbine inlet conditions used in endurance test of the two-stage turbine.

PUMPS

For the type of power system being investigated (fig. 1), four pumps are required, one in each of the four loops. A motor-driven centrifugal pump is shown in figure 11; this unit, which is designed for flight, has pumped NaK at 1100° F for 3000 hours. The rotor of the motor is immersed in NaK, and the bearings are lubricated by NaK. Cooling of the motor's stator limits the hot-spot design temperature to 600° F [23]. The NaK temperature limit of 1100° F for this pump is adequate for all but the reactor loop of the potassium-vapor power system. However, the pump has to be redesigned for different flow rate and pressure head requirements.

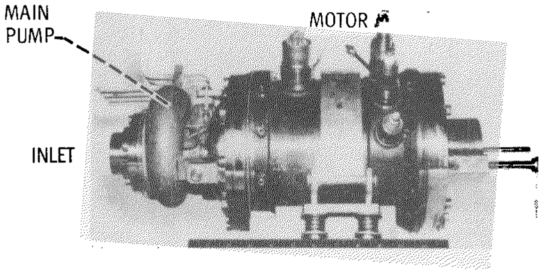

HEAD RISE: 35 PSI
FLOW: 35,300 LB/HR
INPUT POWER: 4.6 KW
OVERALL EFF: 35%
NaK LUBRICATED, TILTING PAD JOURNAL AND THRUST BEARINGS

FIG. 11. NaK pump-motor assembly

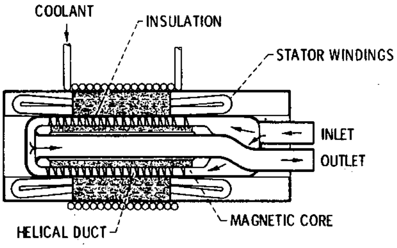

HEAD RISE: 240 PSI
FLOW: 33 GPM
TEMP: 1000° F
EFFICIENCY: 0.20

FIG. 12. EM helical induction pump

As an alternative to a mechanical pump, an electromagnetic helical induction pump is being investigated for space application (fig. 12) [24 and 25]. In this type of pump, a 3-phase alternating current produces a rotating magnetic field that, in turn, produces eddy currents in the annulus of alkali metal. The resulting circumferential motion of the liquid metal creates axial motion as well because of hydrodynamic forces caused by the helical grooves in the flow annulus.

A pump of this type made of Nb-1Zr was used in a pumped loop for investigation of corrosion and in the boiling heat transfer rigs described previously. Although sodium at 1980° F was pumped for 5000 hours, the electrical and magnetic parts of the pump were cooled to 200° C in order that conventional electrical and magnetic materials might be used. These pumps are very inefficient (1 to 2 percent) but very reliable. A similar type of pump is now being investigated as a boiler-feed pump for the advanced potassium Rankine cycle (fig. 12) [26]; this more advanced pump is designed for its electrical and magnetic materials to operate at a temperature of 1000° F while pumping potassium at 1000° to 1400° F. This pump will have an efficiency of about 20 percent.

ELECTRICAL MATERIALS

The pump just described, the turbine driven-alternator, and other electrical components of the power system all benefit from investigation of high-temperature electrical materials. Evaluation of various candidate materials resulted in selection of the following materials for further evaluation in small assembled electrical devices: magnetic material, Fe-27Co; electrical conductor, nickel-clad silver; conductor insulation, Anadur E glass serving plus refractory oxides; interlaminar and slot insulation, alumina; and end-turn potting compound, phosphate-bonded zirconium silicate [27,28]. Three types of electrical device were built for further evaluation of these materials and of their mutual compatibility; these devices were (1) a stator for a 3-phase 15 kVA alternator, (2) two solenoids, and (3) a transformer. These devices were placed in vacuum ovens, electrically energized, and maintained at a temperature of 1100° F for 5000 hours. With the single exception of the transformer, the performance of each device was as good at the end of the test as at the start. During the test, a short circuit occurred in the power supply. Another transformer is being built with some alteration in insulating materials, and this transformer will be subjected to endurance tests.

Materials for the rotor of the alternator have also been investigated, these materials being required to have both good magnetic properties and good strength at temperatures of the order of 1000° to 1100° F. For this reason, the creep strength of Nivco (Co-23Ni-1.1Zr-1.8Ti) was measured at temperatures of 1050° to 1150° F and times to 10 000 hours, the results being presented in figure 13. At 1050° F and 47 000 lb/in.^{2}, Nivco creeps 0.5 percent in 10 000 hours. At this temperature its useful magnetic flux is 10 000 gauss and its permeability 100.

PRESSURE MEASUREMENT

Pressures of liquid, vapor, and two-phase alkali metals have to be measured. These pressures have generally been measured by using a slack diaphragm to isolate a low-temperature transducer from a high-temperature fluid. These devices have slow response and require careful temperature control. Two devices having faster response have been developed to measure pressures in alkali-metal systems.

The efflux pressure-measuring system shown in figure 14 balances the system pressure against a continuous stream of argon gas. Argon flows through a filter, a small metering orifice (0.005 in.), a valve, a vapor trap, and into the flowing alkali-metal vapor. The nearly continuous argon flow prevents alkali-metal vapor from entering the pressure-sensing tube. The argon flow is briefly interrupted, and the pressure in the sensing tube is then measured with a standard transducer. An emergency argon purge valve is connected to the sensing tube in order to flush out any metal vapors inadvertently entering the system [29]. The efflux system has a moderate frequency response but can be used only in systems that tolerate the presence of noncondensible argon in the alkali metal. The efflux measuring system has been used successfully in the NASA turbine test facility.

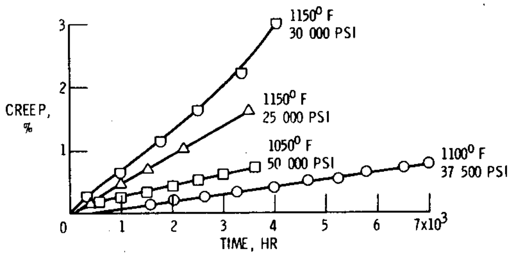

FIG. 13. Creep of Nivco

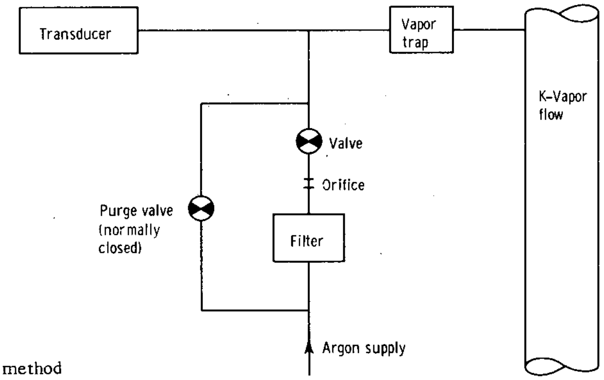

FIG. 14. Efflux pressure-measuring method

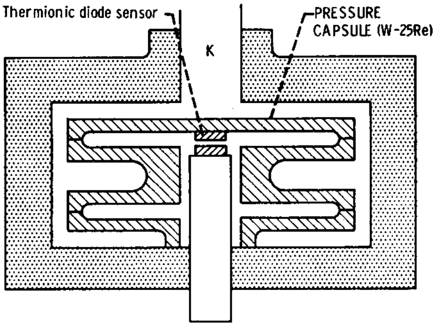

FIG. 15. 1800°F vacuum diode pressure transducer

The other pressure measuring system (fig. 15) uses as the sensing element a W-25Re diaphragm shaped like a 2-convolution bellows. The displacement of the bellows is measured by a thermionic diode operating in the space-charge-limited mode. A second diode is used as a reference for the sensing diode, to linearize the output of the instrument, and to compensate for changes in emitter work function as a result of any emitter poisoning during the life of the instrument. The measuring diode consists of a heated planar circular emitter (cathode) in the center and a planar collector (anode) attached to the diaphragm. The second reference diode consists of a similar planar emitter and second collector a fixed distance from the emitting surface [30]. These pressure instruments have shown feasibility and are in the development stage. They can be used to measure pressures at temperatures up to 1800° F with a frequency response up to 100 cycles per second.

CONCLUDING REMARKS

Although a substantial amount of knowledge has been accumulated on the various constituent problems of the potassium-vapor turbogenerator space power system, a very large amount of work yet remains before a system can be successfully demonstrated. On the bases of corrosion and strength, maximum temperatures of 2200° to perhaps 2400° F appear practical. Satisfactory data on thermodynamic properties of potassium are now available for design of such a powerplant. Knowledge of the heat transfer coefficients and pressure drop of boiling and condensing potassium is adequate to design single-tube boilers typical of a boiler segment for space power systems; multi-tube space boilers have yet to be investigated. The knowledge of boiling stability is advancing. For turbine-exit vapor qualities as low as 93 percent, turbine blade erosion has been acceptable; lower qualities must yet be investigated. In addition, a substantial amount of information is available for design of bearings, seals, pumps, and electrical components.

The program is now changing its general character from the technology and basic design phase to the demonstration of system components. Over the next several years, the major components of such a power system will be investigated.

REFERENCES

General

[1] Space Power Systems Advanced Technology Conference. Lewis Research Center, Cleveland, Ohio, August 23-24, 1966. NASA Special Publication SP-131, 1966.

Properties

[2] Ewing, C. T., Stone, J. P., Spann, J. R., Steinkuller, E. W., Williams, D. D., Miller, R. R., High-temperature properties of potassium, U. S. Naval Res. Lab. Rep. NRL-6233 (1965).

[3] Lemmon, A. W., Jr., Deem, H. W., Eldridge, E. A., Hall, E. H., Matolich, J., Jr., Walling, J. F., Engineering properties of potassium, Battelle Memorial Inst. Rep. BATT-4673-Final (NASA CR-54017) (1963).

[4] Achener, P. Y., The determination of the latent heat of vaporization and vapor pressure of potassium from 1000° to 1900° F, USAEC Rep. AGN-8141 (1965).

[5] Tepper, F., Zelenak, J., Roehlich, F., May, V., Thermophysical and transport properties of liquid metals, MSA Res. Corp. (AFML-TR-65-99, AD-464138)(1965).

Heat transfer

[6] Brooks, R. D., Ed., Alkali Metals boiling and condensing investigati-gations, Vol. I - Experimental program, General Electric Co. (NASA CR-54050) (1964).

[7] Semmel, J. W., Jr., Young, W. R., Kearns, W. H., Alkali metals boiling and condensing investigations, Vol. II - Materials support, General Electric Co. Rep. GE63FPD66 (NASA CR-53406)(1963).

[8] Peterson J. R., High performance once-through boiling of potassium, USAEC Rep. CONF-651026 1 (1965) 357.

[9] Bond, J. A., Peterson, J. R., Tippets, F. E., Heat transfer and pressure drop measurements for high temperature boiling potassium in forced convection, USAEC Rep. ANL-7100 (1965)53.

[10] Peterson, J. R., High performance "once-through" boiling of potassium in single tubes. Topical Report, NASA Lewis Research Center Contract NAS 3-2528. To be published.

[11] Bond, J. A. and Converse, G. L., Vaporization of high-temperature potassium in forced convection. Topical Report, NASA Lewis Research Center Contract NAS 3-2528. To be published.

[12] Sawochka, S. G., Thermal and fluid dynamic performance of potassium condensing inside a tube, USAEC Rep. CONF-651026 1 (1965) 669.

[13] Sawochka, S. G., Measurements of forced convection condensing potassium heat transfer, USAEC Rep. ANL-7100 (1965)97.

[14] Sawochka, F. G., Thermal and fluid dynamic performance of potassium during condensation inside single tubes. Topical Report, NASA Lewis Research Center Contract NAS 3-2528. To be published.

[15] Gutierrez, O. A., Sekas, N. J., Acker, L. W., Fenn, D. B., Potassium condensing tests of horizontal multitude convective and radiative condensers operating at vapor temperatures of 1250° to 1500° F, USAEC Rep. CONF-651026 1 (1965) 694.

Turbine

[16] Rossbach, R. J., Space vehicle Rankine-cycle power plant potassium-turbine development, ASME Paper 63-WA-326 (1963).

[17] Rossbach, R. J., Schnetzer, E., Nichols, H. E., Eckard, S. E., Performance test of a two-stage, 200 horsepower turbine in wet potassium vapor, USAEC Rep. CONF-651026 1 (1965) 521.

[18] Zimmerman, William, and Rossbach, Richard, Metallurgical and fluid dynamic results of a 2000-hour endurance test on a two-stage, 200 horse power turbine in wet potassium vapor. To be presented at Spring ASME Conference in Houston, Texas, March 5-9, 1967.

[19] Rossbach, Richard, and Wesling, Gordon, Two-stage potassium turbine - fluid dynamic design and performance. Topical Report, NASA Lewis Research Center Contract NAS 5-1143. To be published.

[20] Nichols, Herbert, Fink, Roy, Two-stage potassium turbine - mechanical design and development. Topical Report, NASA Lewis Research Center Contract NAS 5-1143. To be published.

[21] Eckard, Spurgeon, Two-stage potassium turbine test facility. Topical Report, NASA Lewis Research Center Contract NAS 5-1143. To be published.

[22] Semmel, J. W., Jr., Zimmerman, W., Hand, Robert, and Engleby, Dudley, Materials support, Vol. II. Topical Report, NASA Lewis Research Center Contract NAS 5-1143. To be published.

[23] Chalpin, E. S., Colker, C. P., Foss, C. L., Design and development of pumps for high temperature NaK service, USAEC Rep. CONF 651026 1 (1965) 186.

[24] Verkamp, J. P., Rhudy, R. G., Electromagnetic alkali metal pump research program, NASA Rep. CR-380 (1966).

[25] Rhudy, R. G., Verhamp, J. P., Electromagnetic pumps for space power systems, USAEC Rep. CONF-651026 1 (1965) 201.

[26] Electromagnetic pumps. Final Report, NASA Lewis Research Center Contract NAS 3-8500. To be published.

Electrical Materials

[27] Kueser, P. E., et al, Magnetic materials topical report, NASA Rep. CR-54091 (1964).

[28] Kueser, P. E., et al, Electrical conductor and electrical insulation topical report, NASA Rep. CR-54092 (1964).

Instruments

[29] Wesling, G. C., Rossbach, R. J., and Shaffernocker, W. M., Development of efflux measuring device for performance evaluation of potassium vapor turbine, USAEC Rep. ANL-7100 (1965) 127.

[30] Cassano, A. J., and Engdahl, R. E., Pressure transducer for liquid metal applications, USAEC Rep. ANL-7100 (1965) 165.

DISCUSSION

K. T. CLAXTON: If the coolant flow were to become blocked adjacent to a fuel element there is some question, I think, whether the heat generated in the fuel could be carried off quickly enough. A possible mechanism for its removal might be boiling heat transfer. My question, then, is whether boiling can occur in liquid potassium (or lithium, if that is to be your coolant) under the influence of nuclear radiation. I am thinking particularly of the fission fragments and heavy alpha-recoils that would be present in the coolant in the event of a fuel can failure, and also of knocked-on atoms of the coolant material.

R. E. ENGLISH: This is a problem we have not considered. In the type of power system we are studying the coolant fluid (probably lithium) within the reactor will be pressurized precisely to avoid boiling. We have not investigated the boiling mechanisms that might prevail during the type of failure postulated in your question; but even if boiling did occur I doubt whether it could serve as an adequate mechanism of heat removal in the conditions of space flight. The absence of acceleration and consequently of any natural convection would probably mean heating, melting and destruction of the reactor fuel elements in the vicinity of the blockage.

J. S. LINDHE: Did you find any deposits in the once-through boiler?

R. E. ENGLISH: No; as the oxygen level was carefully controlled in these systems no attack or deposits should be expected.

BEHAVIOUR OF FISSION PRODUCTS
(Session IX)

FISSION PRODUCT BEHAVIOR IN SODIUM SYSTEMS*

A. W. CASTLEMAN, Jr., I.N. TANG AND
R. A. MACKAY
BROOKHAVEN NATIONAL LABORATORY,
UPTON, NEW YORK,
UNITED STATES OF AMERICA

Abstract

FISSION PRODUCT BEHAVIOUR IN SODIUM SYSTEMS. Three types of data are essential for predicting fission product behaviour in sodium systems. These are (1) the chemical potential of fission products in liquid sodium, (2) their volatility and the extent to which they would be released during the vaporization of sodium, and (3) their chemical state upon release to the vapour phase. Both experimental and theoretical studies to provide such data are currently under way in this Laboratory.

The excess free energies of antimony, barium, caesium, iodine, rubidium, strontium and tellurium in sodium were calculated from existing phase diagrams. Activity coefficients were calculated from these assuming regular solutions. These values, with vapour pressure data, were used to derive equations which express the quantity of each fission product evolved as a function of the percentage sodium vaporized. These are plotted for the temperature range 500° to 1100°K. Experimental results are given for the vaporization of caesium and iodine from sodium, and are compared with the theoretical predictions.

The chemical states of iodine and caesium upon vaporization from sodium are considered in detail. A critical evaluation of existing data for the system caesium-iodine-sodium is given together with the results of transport studies showing the extent of each of the species vaporized from liquid sodium.

Introduction

A knowledge of the behavior of fission products in dilute solutions is of both practical and theoretical interest. From operational and safety points of view, it is important to know the distributions and fates of fission products, either intentionally or accidentally vented to a reactor coolant. Those fission products which are relatively insoluble may deposit throughout the primary system during operation. Others, which remain in solution, may exert large partial pressures at high temperatures so that their potential vaporization becomes a safety hazard. Unfortunately, there are very little data published on the behavior of fission products in alkali metal systems. What little information does exist has been obtained from gross measurements in large-scale systems under poorly defined conditions. These data are of little value in their application to other situation.

From a theoretical standpoint, our understanding of the nature of solutes dissolved in metallic solutions is unsatisfactory. Studies of fission product-sodium systems provide information which furthers our understanding of these solutions. The regions of interest are those below 10^{-5} mole fraction, where solute-solute interactions become negligible.

---

* Work performed under the auspices of the United States Atomic Energy Commission.

Three types of data are essential for predicting fission product behavior in sodium. These are (1) the chemical potential of fission products in liquid sodium, (2) their volatility and the extent to which they would be released during the vaporization of sodium, and (3) their chemical state upon release to the vapor phase. Both experimental and theoretical studies are currently under way in this Laboratory to provide such fundamental data.

This paper is divided into three sections. The first discusses the chemical states of the fission products. Here, the results of our studies on the interactions of iodine and cesium in a sodium environment are presented. The second section contains a discussion of our experimental determination of the excess free energy of mixing of NaI in dilute sodium solutions. Also included are the excess free energies of mixing for Sb, Ba, Cs, NaI, Rb, Sr and Te calculated from existing phase diagrams. The third section deals with fission product vaporization from sodium solutions. Here, activity coefficients, calculated from the excess free energy values, have been combined with vapor pressure data and used to predict fission product vaporization as a function of sodium vaporization.

Chemical States

Two fission products of major interest are iodine and cesium. Castleman, Tang and Munkelwitz[1] have studied the chemical states of these upon release from uranium and uranium monocarbide into helium. These studies show that iodine is released as a uranium iodide and the cesium is transported independently.

A comparison of the estimated standard free energies of formation of the uranium iodides with that of sodium iodide shows that if the uranium iodides enter sodium they will undoubtedly react to form NaI. In considering reactions of iodine with other fission products, compound formation with cesium was found to be among the most probably based on relative concentrations and thermodynamic values. We undertook a complete evaluation of the values which were used to calculate the free energy of formation of CsI as estimated by Brewer.[2] He estimated the original free energy function using aqueous heat of solution information and relatively sparse heat capacity data.

Kayor, Walder, and Smith[3] recently measured the heat capacities over the temperature range 273.15° to 1172°C and the heat of fusion for CsI at its melting point. These authors have tabulated the heat content and entropy values for cesium iodide over this temperature range. Taylor, Gardner, and Smith [4] used an adiabatic calorimeter to measure the heat capacity of cesium iodide from 13° to 300°K. Using values taken from the above, we recomputed the free energy function for the temperature range 298° to 1200°K, and these values are shown in Table I. Combining this free energy function with those for iodine [5] and cesium, [6] gives the required free energy of formation functions (Table I). These values are about 10% lower than those given by Brewer.

Subsequently, we attempted to calculate the cesium iodide to sodium iodide distribution in sodium as a function of composition and temperature. The over-all reaction is given by

$$\mathrm{NaI} + \mathrm{Cs} = \mathrm{CsI} + \mathrm{Na} \tag{1}$$

The standard free energy ΔF^{o} of this reaction can be found using our tabulated free energy of formation function for CsI and the one given in the JANAF tables for NaI. In terms of the chemical activities of the system and the equilibrium constant K, the equilibrium can be calculated from

$$K = \frac{\gamma_{CsI}}{\gamma_{NaI}\gamma_{Cs}} \cdot \frac{X_{CsI}}{X_{Cs}X_{NaI}} = e^{-\Delta F^{o}/RT} \tag{2}$$

where the activity of sodium is taken as unity, and the activities of the other components are expressed as the product of their activity coefficient γ, and mole fraction X. Although sufficient information is available for calculating the activity coefficients for cesium and sodium iodide in sodium, no such data are available for cesium iodide. Therefore, no accurate prediction of the relative distribution can be made. If the activity coefficients for the two salts are nearly equal, the iodide should be nearly 100% NaI for concentrations in the parts per million range and at temperatures above 450°C. At concentrations higher by several orders of magnitude, the percentage of cesium iodide could become nearly equivalent to that of the sodium iodide. However, in general, one would expect cesium iodide to be far less soluble than sodium iodide in sodium, leading to larger activity coefficients and smaller CsI/NaI ratios. In view of the uncertainties in the theroretical calculations, we proceeded to carry out an experimental investigation of the Cs-I-Na system.

A study of the species vaporized from solution proved to be useful for determining the relative importance of NaI and CsI in sodium systems. Since interactions between cesium and iodine might occur, care was taken to assure that the quantity of CsI formed would not be hindered by the reaction kinetics. Therefore, we decided to start with CsI, dissolve it in sodium, and study the vapor species above ths solution.

An unambiguous analysis of systems of very low concentration such as those of fission products in solutions has proved to be a formidable problem for many years. However, Castleman and Tang[7] developed a thermochromatographic technique for studying the states of semivolatile fission product vapor species. Briefly, the method consists of separating the fission products vaporized from a solution by condensing them or their compounds in a tube having a linearly descending temperature profile along the wall. The deposition temperature of the species is determined by the radioactivity distribution in the tube at the completion of an experiment. The behavior of these species is compared with that of standards in much the same manner as done in conventional chromatography.

In these experiments, CsI was dissolved in liquid sodium contained in a stainless-steel boat, and then placed in the thermochromatographic apparatus. Prior to dissolution, the CsI was tagged with Cs^{134} and I^{131}. A thin-walled stainless-steel liner was placed inside the usual quartz deposition tube to eliminate reactions between sodium and quartz. After the apparatus was heated to a predetermined temperature, the boat containing the sample was rapidly introduced into the sample heating zone. The species were released into a helium carrier gas at a fixed temperature and their respective deposition temperatures were measured. The deposition profiles of these species were compared with those of sodium iodide and cesium iodide.

The results of the experiments, carried out over the temperature range 485° to 748°C and with Cs and I concentrations as high as 7.7×10^{-3} mole fraction, are shown in the lower insert of Figure 1. Without exception, these results show that cesium and iodine are independently transported in the vapor phase. The only difference in the experiments carried out at low and high temperatures was the length of run needed to transport a given quantity of material away from the sample boat. The distribution of the product was not affected. It is evident from reaction (1) and the free energy of reaction (shown in Table I) that the lower the concentration of cesium and iodine, the greater the extent of conversion to NaI. Therefore, it is not surprising that no change in the percentage NaI in the vapor was noted in the experiments carried out at lower concentrations.

Other experiments were carried out to prove that CsI is stable under these experimental conditions in the absence of sodium. The results, shown in the center insert of Figure 1, clearly show that CsI is transported and deposited as the compound. Note carefully that these ordinates show the relative counting rates of the two species and do not represent the total quantities of the atoms.

A third set of experiments was performed employing NaI in place of the CsI. NaI was also observed to deposit as the compound. The deposition temperature of pure NaI (465°C) is in good agreement with that of the iodide transported from the CsI-Na solution (475°C). These experiments show that CsI converts to NaI and Cs in a sodium environment.

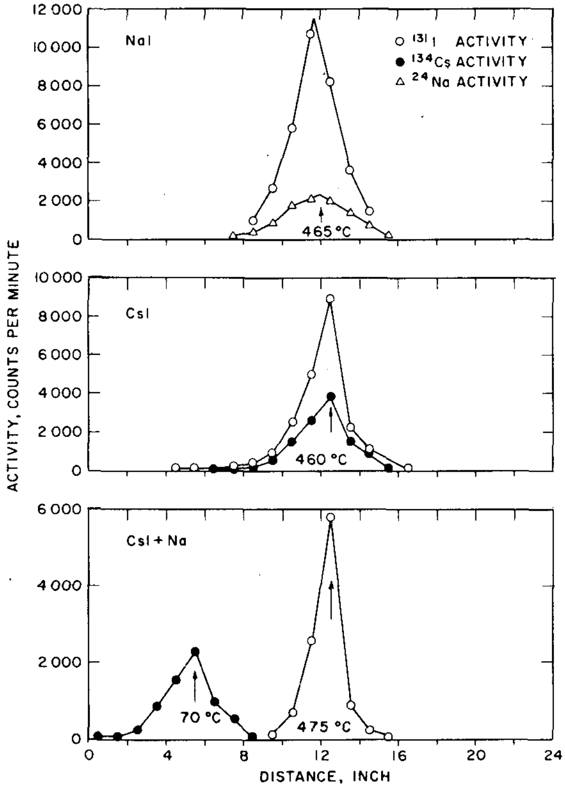

FIG. 1. Thermochromatograms for system Na-I-Cs

Subsequent to these free vaporization experiments, we carried out a similar investigation using a Knudsen cell in place of the open sample boat. Although the pressure range was above that in which transport through an orifice is governed by the equations of molecular flow, the use of the Knudsen cell permitted us to carry out experiments with a steady-state vapor phase above the solution. These experiments, which required about an order of magnitude longer time to complete, showed essentially the same results. Namely, within the limits of detection all the iodine is transported as sodium iodide and the cesium is transported as the pure element. This suggests that the observed vapor species are a result of the instability of CsI in sodium. In any event, however, we have clearly shown that free Cs and NaI are the important species transported from sodium.

TABLE I. THERMOCHEMICAL DATA FOR CsI REACTIONS

T^oK	$-(F^o-H^o_{298})/T$ cal/mole, ^oK	$(\Delta F^o-\Delta H^o_{298})/T$ cal/mole, ^oK	$-\Delta F^o$ kcal/mole**
298 (s)	29.40	21.90	
400	29.92	22.27	11.44
500	30.82	22.56	10.53
600	31.88	22.63	10.32
800	34.04	22.66	9.85
1000 (ℓ)	36.75	22.56	8.96
1200	39.61	22.37	7.73

* Calculated for the reaction: $Cs(\ell) + 1/2I_2(g) = CsI(s,\ell)$ ΔH^o_{298} = 87.96 kcal/mole, taken from NBS Circular 500 and recalculated using ideal gas at 1 atm as standard state for I_2.

** Free energy of reaction for reaction (1) in text.

Solution Thermodynamics

The equilibrium properties of variable composition liquid systems can be accurately calculated employing the methods provided by the classical thermodynamics of solutions. One of the most useful concepts is that of the chemical potential which is the free energy of mixing of component i in a solution.

The excess free energy of mixing, ΔF_i^E, is given by

$$\Delta F_i^E = \Delta F_i^M - RT \ln X_i = RT \ln \gamma_i \qquad (3)$$

where ΔF_i^M is the free energy of mixing, X_i the mole fraction, and γ_i the activity coefficient of component i.

Excess free energies are very difficult to measure at low concentrations and very few methods are available. We have found a variation of the Rayleigh distillation technique provides a useful method for measuring free energies at infinite dilution and have measured values for the NaI-Na system as discussed in a later part. Many metallic solutions often satisfy regular solution restrictions.[8] In theory, the equilibrium data on phase diagrams can be used for calculating activity coefficients for regular solutions and have been employed extensively.[9,10,11,12]

Unfortunately, great practical difficulties are experienced in extrapolating to infinite dilution with the usual methods employed. All methods either assume some particular analytical equation for the variation of activity coefficient with composition, or involve a graphical integration technique employing the Gibbs-Duhem relation. Often these techniques involve a rather uncertain extrapolation to infinite dilution which can introduce large errors.

A combination of the use of the phase diagram for estimating the activity coefficients of the solutes, together with a method proposed by Tang, Castleman and Mackay[13] for extrapolating activity coefficients to infinite dilution, was found to be most satisfactory for many systems.

Cesium-Sodium

The excess free energy of mixing at infinite dilution was calculated from the phase diagram employing two different techniques. The cesium-sodium phase diagram[14] is a relatively simple eutectic, but does show the presence of the intermetallic compound Na_2Cs. The eutectic point is at a composition of 75 mole percent cesium and a temperature of -29^oC. Since the phase diagram shows that there is no solid solubility, the activity of each of the pure components is readily calculated by equating free energy along the tie lines between the pure component and the respective liquidus curve. The resultant equation expresses the activity, a_i, of either component i, from the pure state, up to the eutectic point or the first intersection of the compound-liquidus tie line.

$$\ell n\ a_i = \ell n\ \gamma_i X_i = \int_{Tm}^{T} \frac{\left(H_i^{(1)} - H_i^o\right) - \left(H_i^{(s)} - H_i^o\right)}{RT^2}\, dT \qquad (4)$$

where $\left(H_i^{(1)} - H_i^o\right)$ and $\left(H_i^{(s)} - H_i^o\right)$ are the enthalpy functions for the liquid and solid component i respectively. These enthalpy functions are tabulated for many systems,[15] but can be calculated for others from the appropriate heat of fusion and heat capacity data. Here, the integration is carried out between the melting point of pure component i and temperature T at point X_i on the liquidus curve.

Using Bjerrum's method[16] as a basis, for a binary system, we define the function

$$\xi = \frac{\ell n \gamma_1}{y_2} \qquad (5)$$

where $y_2 = X_2/X_1$. Differentiating this function, introducing it into Gibbs-Duhem relationship, and integrating from infinite dilution for component 2 to some point y_2^*, where γ_2 is known (or can be evaluated from the other side of the phase diagram), gives

$$\ln \gamma_2^o = \ln \gamma_2^* + \xi(y_2^*) + \int_o^{y_2^*} \frac{\xi dy_2}{y_2} \qquad (6)$$

where γ_2^o is the activity coefficient of component 2 at infinite dilution.

This method was shown[13] to give values for $\ln \gamma_2^o$ which are insensitive to the choice of reference temperature. The graphical integration of the function ξ/y_2 converges to a finite value at y_2=0 and does not involve a large extrapolation error.

In those cases where a tie line exists between an intermetallic compound and the liquidus curve, an extrapolation is necessary to obtain a value of $\ln \gamma_2$ at y_2^*. For the cesium-sodium system, an extrapolation of the cesium activity from 75 to 70 mole percent is necessary. A plot of the individual values shows this small extrapolation to be quite satisfactory. The resultant value of ΔF_{Cs}^E at infinite dilution is 2050 cal/mole. This compares favorably with the experimental value of 1900 cal/mole for the heat of solution.[17] Using the van Laar equation[18] to correlate the activities obtained from the phase diagram leads to a ΔF_{Cs}^E of 1920 cal/mole.

Rubidium-Sodium

The rubidium-sodium phase diagram[19] is very similar to that of the cesium-sodium system, showing a simple eutectic at 75.5 mole percent rubidium. There are, however, no intermetallic compounds. The excess free energy of rubidium in sodium at infinite dilution is calculated using the method discussed above. The calculated ΔF_{Rb}^E (1715 cal/mole) compares favorably with the experimental heat of solution (1750 cal/mole)[17]. A value of 1790 cal/mole is obtained for the excess free energy of mixing from the van Laar correlation method.

Strontium-Sodium

The strontium-sodium system[20] exhibits a simple eutectic at 3.2 mole percent strontium. Although no intermetallic compounds exist, the heat difference between the α and β phases of solid strontium must be considered in performing the calculations. This transition temperature is 589°C. For this system, the van Laar method was unsatisfactory since the activity coefficients cannot be represented by a two-parameter equation.

However, our method proved to be very satisfactory. The excess free energy calculated for this system is 2885 cal/mole.

Barium-Sodium

The barium-sodium phase diagram as determined by Kanda et al.[21] was used to calculate the excess free energy of mixing for this system. Here, it was necessary to extrapolate the barium activity from 24 mole percent barium to the eutectic at 5.5 mole percent barium to obtain the required value for $\ln \gamma_2$ at y_2^*. The solid solubility of barium and sodium was considered in calculating the appropriate activities from the phase diagram. Our method was again quite satisfactory for obtaining the excess free energy of mixing. A value of 2450 cal/mole was obtained.

Sodium Iodide-Sodium

The sodium iodide-sodium phase diagram shows a large immiscibility gap[22] throughout nearly the entire range of composition. Consequently, the above methods are unsuitable for estimating the free energies of mixing. Using Wagner's method for immiscible systems, a ΔF^E_{NaI} of 2060 cal/mole is obtained.[23] If we assume Henry's law applies for the metal-rich phase, the ΔF^E_{NaI} becomes 7820 cal/mole at 750°C. Using another method, Pitzer[24] calculated the expression ΔF^E_{NaI} = 14 200-6T for this system. This gives a value of 8060 cal/mole for the excess free energy of mixing at the same temperature.

Experimentally, we find the value to be 9100 ± 400 cal/mole for the temperature range 650° to 830°C. The measurements were made by employing an equilibrium vaporization technique described in the next section. These measurements show the excess free energy of mixing to be substantially temperature independent within the precision of the experiments. This result is to be expected, since the solution approaches regular behavior at infinite dilution.

Antimony-Sodium

This phase diagram[25] shows the existence of the stable compounds Na_3Sb and NaSb. Since none of the above methods is applicable for calculating the excess free energy of mixing, we employed a method used by Pitzer,[24] assuming the solutions to be regular throughout the entire range of composition. The calculated ΔF^E_{Sb} is -6740 cal/mole.

Tellurium-Sodium

This phase diagram[25] shows the existence of the stable compounds Na_2Te and $NaTe_3$. None of the above methods is applicable for calculating ΔF^E_{Te}. For this system a plot of $(RT \ln \gamma_{Te})/X^2_{Na}$ versus X_{Te}/X_{Na} gives a straight line which is easily extrapolated to zero mole fraction tellurium. This amounts to correlating the data with a power series in composition. The excess free energy at infinite dilution is -4050 cal/mole.

Fission Product Vaporization

The vaporization of sodium iodide and cesium from sodium solutions was measured experimentally employing equilibrium vaporization methods. It is well known that equilibrium vaporization follows the Rayleigh equation

$$f_i = 1 - (1-f_j)^A \tag{7}$$

where f_i and f_j are the fraction of species i and j vaporized. Here A is given by

$$A = P_i^o \gamma_i / P_j^o \gamma_j \tag{8}$$

where P_i^o and P_j^o are the vapor pressure of the species i and j and γ_i and γ_j are their respective activity coefficients. If we consider sodium to be component j, Eq. (7) relates the fraction of fission product i vaporized to the fraction of sodium vaporized. Fortunately, in the systems of interest here, $\gamma_j \cong 1$. Therefore γ_i is the appropriate activity coefficient at infinite dilution and a function of temperature only.

An equilibrium distillation apparatus was constructed to measure the relative vaporization of cesium and sodium at constant temperature. The apparatus consists of an isothermal vaporization cell and a condenser connected by a heated transport line. A cesium-sodium alloy, tagged with Na^{22} and Cs^{137}, was introduced into the apparatus under an inert atmosphere. The apparatus was heated to a specified temperature and evacuated. The vaporization of the alloy was continuously monitored with suitable scintillation counting equipment. The experimentally determined vaporization curves are in general agreement with the calculated curves shown in Figure 2. The vaporization curves were calculated using the Rayleigh equation given above, together with the required activity coefficients evaluated from our excess free energy of mixing values.

A Knudsen cell was employed to study the vaporization of sodium-sodium iodide solutions. During the vaporization experiment, the sodium and sodium iodide, tagged with Na^{22} and I^{131} were released into a flowing helium stream maintained at a pressure equivalent to that of the sodium at the experimental temperature. The vaporization of sodium and sodium iodide was continuously followed using a scintillation counting method. Although the equations of molecular flow do not apply in the pressure range employed, this cell did enable us to carry out equilibrium vaporization experiments for a system with components of widely varying volatility. Experiments, carried out at temperatures of 650°, 710° and 830°C, give the excess free

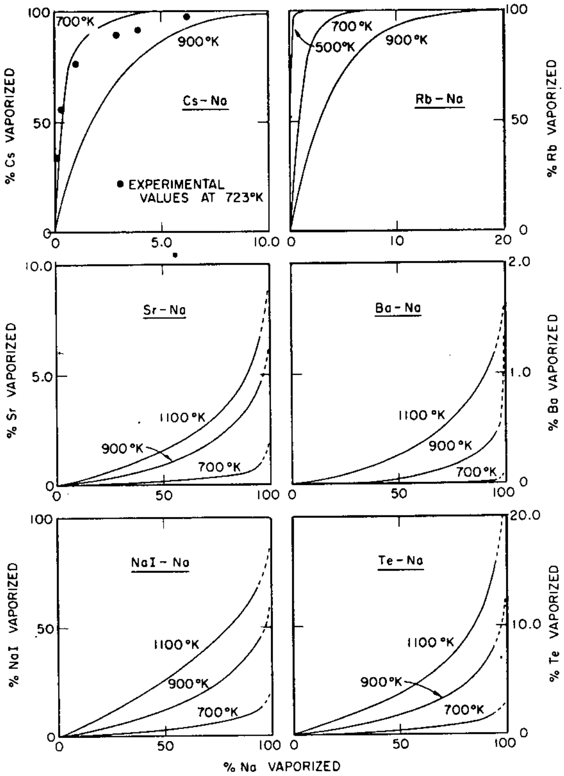

FIG.2. Fission product — sodium equilibrium vaporization

energies 9700, 8950 and 8600 cal/mole respectively. The experimental error is approximately ±4%. Even though these values show the same trend with temperature as those estimated by Pitzer,[24] within the precision of the experiments, we recommend the use of the average value 9100 ±400 cal/mole.

Employing the activity coefficients calculated from this excess free energy, the vaporization curves for the sodium iodide-sodium system were calculated for the temperatures 700°, 900°, and 1100°K. These are also shown in Figure 2.

The equilibrium vaporization curves for the fission products barium, strontium, rubidium and tellurium from sodium are shown in Figure 2 as well. Here, the activity coefficients were calculated from the appropriate free energy of mixing values given above. The vaporization of antimony is negligible ($<10^{-3}\%$ for ≈100% Na vaporized at 1100°K) and is not plotted.

Conclusions

At concentrations equivalent to those expected in a reactor, cesium iodide is not stable in a sodium environment. Free cesium and sodium iodide are the important species vaporized from sodium solutions. The excess free energy of mixing of sodium iodide in sodium at infinite dilution was measured experimentally, yielding the value 9100 ±400 cal/mole. Excess free energies of mixing at infinite dilution, which are generally difficult to obtain experimentally, are readily obtained from equilibrium vaporization techniques. The ξ-function employed by the authors gave satisfactory excess free energy of mixing values for the systems Cs-Na, Rb-Na, Sr-Na and Ba-Na. The excess free energy of mixing values for the systems Sb-Na and Te-Na are somewhat less certain. The vaporization of cesium from sodium is in general agreement with calculated vaporization curves. These studies show that fission product vaporization from sodium can be satisfactorily calculated knowing values of excess free energies of mixing and the appropriate vapor pressures.

Acknowledgments

The authors acknowledge the invaluable assistance of Mr. Harry R. Munkelwitz and Mr. Steven Lewkowitz in performing many of the experiments and calculations.

REFERENCES

[1] CASTLEMAN, A. W., Jr., TANG, I. N., MUNKELWITZ, H. R., Chemical reactions and transport behavior of fission-product iodine," Proc. Intern. Symp. Fission Product Release and Transport Under Accident Conditions, CONF-650407 1, Oak Ridge National Laboratory, Oak Ridge, Tenn. (Apr. 1965) 325.
[2] BREWER, L., BROMLEY, L. A., GILLES, P. W., LOFGREN, N. L., "The thermodynamic properties of the halides," The Chemistry and Metallurgy of Miscellaneous Materials: Thermodynamics, 1st Ed. (L. L. Quill, Ed.), McGraw-Hill Book Co., Inc., New York (1950) 104.
[3] KAYLOR, C. E., WALDEN, G. E., SMITH, D. F., High temperature heat content and entropies of cesium chloride and cesium iodide, J. Phys. Chem. 64 (1960) 276-8.
[4] TAYLOR, A. R., Jr., GARDNER, T. Estelle, SMITH, D. F., Thermodynamic properties of cesium chloride and cesium iodide from 0^{o} to 300^{o}K, U. S. Dept. of the Interior, Bureau of Mines Report 6157 (1963).
[5] STULL, D. R. et al., Janaf Thermochemical Tables, Dow Chemical Co., Midland, Mich. (1965).
[6] STULL, D. R., SINKE, G. C., Thermodynamic Properties of the Elements, No. 18 of Advances in Chemistry Series, American Chemical Society, Washington, D. C. (1956).

[7] CASTLEMAN, A. W., Jr., TANG, I. N., Vaporization of fission products from irradiated fuels. I. Experimental method and general fission product behavior. Submitted to Nucl. Sci. Engng.

[8] HILDEBRAND, J. H., SCOTT, R. L., The Solubility of Non-electrolytes, 3rd Ed., Dover Publications, Inc., New York (1950).

[9] CHU, B., EGAN, J. J., Thermodynamics of molten binary chloride mixtures calculated from the phase diagrams, Ann. N. Y. Acad. Sci. 79 (1960) 908-18.

[10] WAGNER, C., Thermodynamics of Alloys, Addison-Wesley Publishing Co., Inc., Reading, Mass. (1952).

[11] KUBASCHEWSKI, O., EVANS, E. Ll., Metallurgical Thermo-chemistry, Pergamon Press, New York (1958).

[12] LUMSDEN, J., Thermodynamics of Alloys, The Institute of Metals, London (1952).

[13] TANG, I. N., CASTLEMAN, A. W., Jr., MACKAY, R. A., to be published.

[14] HANSEN, M., Constitution of Binary Alloys, 2nd Ed., McGraw-Hill Book Co., Inc., New York (1958) 577.

[15] HULTGREN, R., ORR, R. L., ANDERSON, P. D., KELLEY, K. K., Selected Values of Thermodynamic Properties of Metals and Alloys, John Wiley and Sons, New York (1963).

[16] LEWIS, G. N., RANDALL, M., Thermodynamics, 2nd Ed., McGraw-Hill Book Co., Inc., New York (1961) 263-5.

[17] YOKOKAWA, T., KLEPPA, O. J., Heats of mixing in binary-liquid-alkali-metal mixtures, J. Chem. Phys. 40 (1964) 46-54.

[18] HALA, E., PICK, J., FRIED, V., VILIM, O., Vapour-Liquid Equilibrium, 2nd Ed., Chap. IV, Translated by G. Standart, Pergamon Press, New York (1957).

[19] HANSEN, M., Constitution of Binary Alloys, 2nd Ed., McGraw-Hill Book Co., Inc., New York (1958) 1001.

[20] ELLIOTT, R. P., Constitution of Binary Alloys, First Supplement, McGraw-Hill Book Co., Inc., New York (1965) 651.

[21] KANDA, F. A., STEVENS, R. M., KELLER, D. V., The barium-sodium equilibrium system, J. Phys. Chem. 69 (1965) 3867-72.

[22] BREDIG, M. A., BRONSTEIN, H. R., Miscibility of liquid metals with salts. IV. The sodium-sodium halide systems at high temperatures, J. Phys. Chem. 64 (1960) 64-7.

[23] CASTLEMAN, A. W., Jr., TANG, I. N., Chemical considerations in fast reactor safety," Proc. Conf. Safety, Fuels, and Core Design in Large Fast Power Reactors, ANL-7120, Argonne National Laboratory, Argonne, Ill. (Oct. 1965) 848-54.

[24] PITZER, K. S., Solubility and the nature of binding in fused alkali halide-metal systems, J. Am. Chem. Soc. 84 (1962) 2025-8.

[25] HANSEN, M., Constitution of Binary Alloys, 2nd Ed., McGraw-Hill Book Co., Inc., New York (1958) 1002 and 1006.

COMPORTEMENT DES PRODUITS DE FISSION DANS LE SODIUM LIQUIDE

A. BARTHOUX ET J. SAROUL
CEA, CENTRE D'ETUDES NUCLEAIRES DE CADARACHE,
FRANCE

BEHAVIOUR OF FISSION PRODUCTS IN LIQUID SODIUM. Out-of-pile experiments were performed to study the behaviour of fission products released in sodium during the melting of a specimen of irradiated uranium.

With the experimental rig employed it was possible to heat 250 litres of sodium to a temperature of 550°C and to melt a fuel sample in it containing about 200 mCi of fresh fission products. Samples were taken from the crucible, the sodium and the cover argon to determine the various diffusion coefficients for the fuel in the sodium and the sodium in the argon.

The behaviour and the efficiency of various filters were measured with an argon sampling circuit fitted with a coarse filter for the sodium vapour, a magnetic filter, various iodine traps and a rare-gas trap.

With this experimental rig it is possible to determine the wall contamination rate and to check the efficiency of various decontamination methods.

COMPORTEMENT DES PRODUITS DE FISSION DANS LE SODIUM LIQUIDE. Des expériences hors pile ont pour objet d'étudier le comportement des produits de fission libérés dans du sodium lors de la fusion d'un échantillon d'uranium irradié.

Le dispositif expérimental permet de chauffer 250 litres de sodium jusqu'à une température de 550°C et d'y fondre un échantillon de combustible contenant environ 200 mCi de produits de fission frais. Des prélèvements dans le creuset, dans le sodium et dans l'argon de couverture permettent de déterminer les différents coefficients de passage du combustible dans le sodium et du sodium dans l'argon.

Les auteurs mesurent la tenue et l'efficacité de différents filtres à partir d'un circuit de prélèvement d'argon sur lequel sont disposés un filtre grossier pour vapeur de sodium, un filtre aimanté, différents pièges à iode et un piège à gaz rares.

Le dispositif expérimental permet de déterminer le taux de contamination des parois et de vérifier l'efficacité de différentes méthodes de décontamination.

1. INTRODUCTION

L'évaluation des conséquences radiologiques d'un accident survenant dans un réacteur nécessite une détermination aussi précise que possible du comportement des produits radioactifs dans les différents circuits de l'installation.

Parmi les éléments composant cette contamination, les produits de fission sont souvent les plus importants et doivent faire l'objet d'études approfondies. Les différentes phases de leur cheminement sont les suivantes:
- émission à partir du combustible et passage dans le réfrigérant primaire,
- transport dans ce circuit et passage dans l'atmosphère du bâtiment,
- comportement dans le bâtiment,
- piégeage plus ou moins complet dans les dispositifs filtrants,
- diffusion dans l'atmosphère à l'extérieur du bâtiment.

De nombreuses études ont été entreprises depuis plusieurs années, en particulier aux Etats-Unis [1]. Elles concernent essentiellement la filière des réacteurs refroidis à l'eau. Néanmoins, une grande partie des résultats obtenus concernant la diffusion atmosphérique, l'efficacité des dispositifs de filtration, le comportement dans les enceintes, voire les taux d'émission à partir du combustible, sont applicables à l'étude des réacteurs refroidis au sodium.

Il n'en est pas de même pour le comportement des produits de fission dans les circuits de sodium. Nous avons donc décidé de réaliser un circuit pour l'étude de ces phénomènes.

Nous étions bien conscients, dès le début, que seule une expérience en vraie grandeur pouvait fournir des résultats directement utilisables pour un réacteur donné. Cependant, outre son coût prohibitif, une telle expérience fournit des résultats globaux qui ne permettent guère l'extrapolation à un autre réacteur de la même filière.

Il a donc fallu choisir une échelle intermédiaire entre le montage de laboratoire, commode et peu coûteux mais nécessitant ensuite des extrapolations hardies, et l'expérience sur un réacteur. Le choix de l'échelle doit tenir compte des différents paramètres qui régissent le cheminement des produits de fission:

- la nature du milieu et de ses impuretés,
- la température,
- la pression,
- la géométrie des volumes considérés,
- la concentration des produits de fission.

Nous avons choisi un circuit dont les dimensions et les caractéristiques mécaniques et thermiques sont aussi voisines que possible de celles du cœur d'un réacteur réel. RAPSODIE a été pris comme modèle car on peut espérer vérifier certains résultats de l'expérience hors pile directement sur le réacteur lorsque celui-ci fonctionnera. L'exploitation de cette maquette pendant un an a montré que l'échelle choisie est assez commode. Un rapport publié très récemment à Oak Ridge [2] vient confirmer l'intérêt d'expériences effectuées à échelle intermédiaire voisine de la nôtre.

La simulation de l'accident sur le combustible a été simplifiée, car le but de cette expérience n'est pas de déterminer des taux d'émission. Il serait en effet illusoire de prétendre à une telle détermination hors pile, car les expériences à notre portée ne peuvent simuler convenablement les accidents survenant sur les cœurs réels. D'ailleurs, les constructeurs eux-mêmes ne peuvent décrire à priori, d'une manière suffisamment détaillée, des accidents qui pourront se développer dans le réacteur.

Nous nous sommes donc efforcés de remplir seulement trois conditions:

- les produits de fission seraient produits directement à partir d'uranium irradié;
- ils seraient libérés par fusion de cet uranium dans du sodium liquide de manière à produire de la vapeur de sodium;
- les concentrations en produits de fission dans le sodium seraient aussi élevées que possible, compte tenu des possibilités que nous avions de manipuler des substances radioactives.

La première série d'expériences a été effectuée avec du sodium statique, car il semble à priori possible d'additionner les effets du transport par diffusion dans le milieu et ceux du transport par le milieu lui-même. La deuxième série d'expériences avec du sodium en mouvement doit permettre de vérifier cette hypothèse.

Enfin, l'expérience a été conçue de manière à effectuer certaines déterminations annexes concernant la décontamination des circuits et la tenue de certains types de filtres en présence de vapeur de sodium.

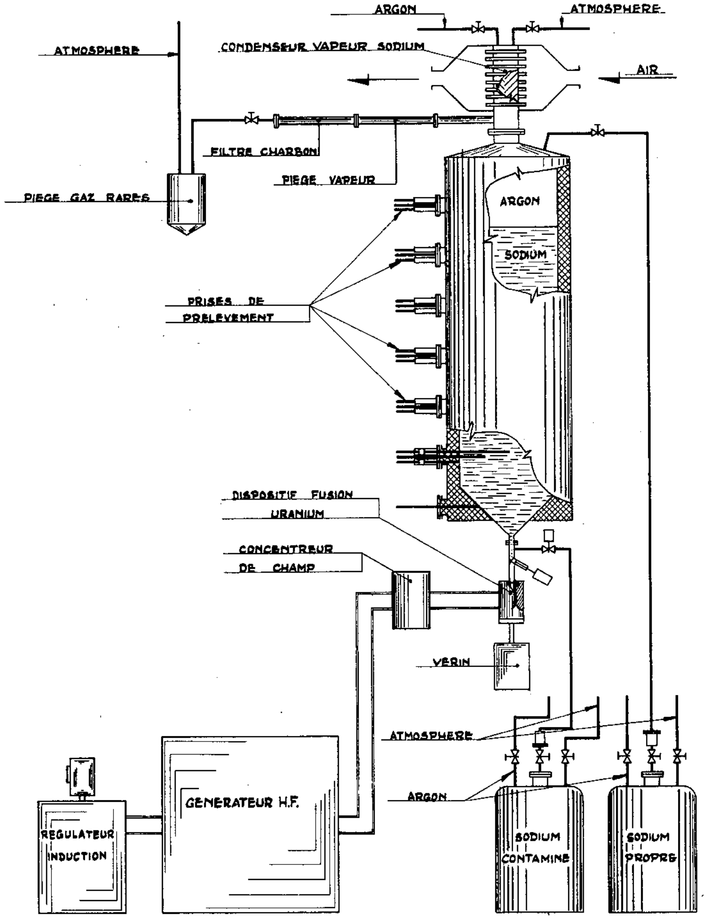

FIG. 1. Schéma PIRANA

2. DESCRIPTION DE L'ENSEMBLE EXPERIMENTAL PIRANA (fig. 1)

La cuve d'expérience, en acier inoxydable, a 2,5 m de hauteur et 0,4 m de diamètre interne. Elle est chauffée et calorifugée pour permettre de maintenir le sodium à 550°C. Cette cuve est, à sa base, reliée au creuset de fusion de l'uranium par l'intermédiaire d'une vanne de sécurité. Ce circuit, qui relie le creuset à la cuve, a une longueur de 40 cm et un diamètre intérieur de 2, 16 cm. Il est lui-même chauffé et calorifugé. Des produits de fission émis par le combustible et circulant dans le sodium rencontrent donc tout d'abord un circuit étroit et assez long qui peut simuler approximativement la traversée de la couverture supérieure du cœur de RAPSODIE. Ils débouchent ensuite dans la cuve proprement dite, dont les dimensions correspondent à celles de la cuve du réacteur, au-dessus du cœur. Un piquage situé sur le circuit d'injection, juste au-dessus du creuset, permet éventuellement d'injecter de l'argon dans le sodium lors de l'émission des produits de fission, de manière à produire un entraînement mécanique. Il sera utilisé ultérieurement pour faire circuler le sodium de bas en haut.

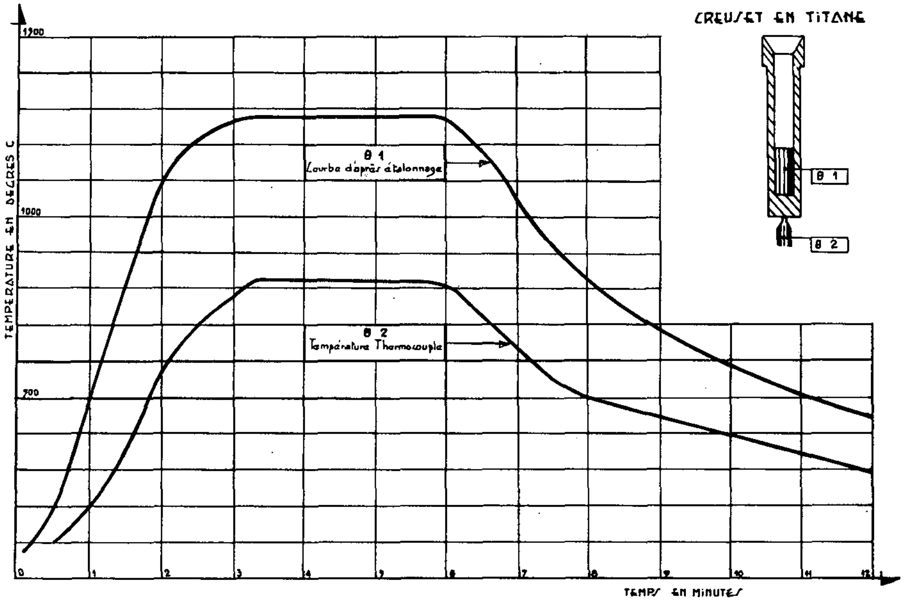

FIG. 2. Fusion d'un échantillon d'uranium en présence de sodium liquide

Le creuset en titane est chauffé par induction. Il élève en 3 ou 4 min la température de l'uranium pendant 2 ou 3 min (fig. 2). Ce creuset est démontable et peut être envoyé au laboratoire pour étude du taux d'émission des différents produits de fission.

L'échantillon d'uranium naturel métallique, gainé d'aluminium, a un diamètre de 1 cm et une longueur de 2 cm; son poids est de 17 g. Il est en général irradié pendant 40 h dans un flux de 2 à 5 · 10^{12} n/cm^2 · s.

Au moment de l'expérience, soit après un temps de refroidissement de 14 j environ, l'activité des principaux produits de fission est, pour un flux de 5 · 10^{12} n/cm^2 · s:

Iode-131	26, 5 mCi
Baryum-lanthane-140	60 mCi
Xénon-133	54, 5 mCi
Césium-137	0, 2 mCi

Dix-neuf prises d'échantillons sont disposées sur les parois de la cuve le long de trois génératrices. Elles permettent d'effectuer des prélèvements à différents niveaux et à différentes profondeurs, sans que la diffusion des produits de fission soit gênée par des éléments métalliques présents dans le sodium au moment de l'expérience. Les volumes prélevés sont d'environ 8 cm^3.

A la partie supérieure de la cuve se trouve le circuit de prélèvement d'argon qui comporte:

- un piège grossier pour la condensation des vapeurs de sodium,
- un filtre inspiré du May-Pack comprenant deux filtres d'amiante et quatre filtres de charbon actif de 1 cm d'épaisseur chacun,
- un piège froid constitué par une couche de 5 cm de charbon actif maintenu à la température de l'azote liquide.

Le débit du balayage d'argon est de 12 à 20 litres/min.

Après l'expérience, la cuve est vidangée dans un réservoir. On peut alors procéder à sa décontamination en injectant successivement des quantités connues d'alcool, d'eau acidulée et d'eau pure.

3. RESULTATS

A ce jour, six essais ont été effectués. Les trois premiers ont surtout permis la mise au point définitive du dispositif expérimental, l'étalonnage des différents appareils de mesure et la détermination de la sensibilité des mesures et des possibilités de manipulation d'échantillons irradiés. Les problèmes les plus délicats à résoudre ont été:

- le réglage des prises d'échantillons de sodium,
- la réalisation de pièges froids pour condenser les vapeurs de sodium en amont des différentes canalisations de gaz.

Les trois derniers essais ont été faits dans les conditions nominales, mais seuls les essais n° 4 et n° 6 ont fourni des renseignements positifs. L'essai n° 5 a néanmoins été intéressant par le côté négatif des enseignements tirés.

3.1. Conditions expérimentales

Les conditions expérimentales sont présentées au tableau I.

3.2. Fusion de l'uranium

Dans tous les essais, le contrôle de la fusion de l'uranium s'est fait par la mesure de la température à la base du creuset. Un étalonnage préalable a permis d'établir la relation entre les températures à l'intérieur et à l'extérieur du creuset, en fonction du temps, pour une puissance de chauffage donnée.

Pour fondre l'uranium, la puissance du four est réglée à son maximum pendant trois à quatre minutes, jusqu'à ce que la température à la base du creuset soit aux environs de 800°C — température à laquelle on doit obtenir la fusion. Elle est ensuite réduite de manière à conserver cette température pendant trois minutes (fig. 2).

TABLEAU I. CONDITIONS EXPERIMENTALES

	C04	C05	C06
Date de l'expérience	1.12.1965	2.6.1966	7.7.1966
Volume de sodium	120 litres	120 litres	120 litres
Hauteur au-dessus du creuset	1,75 m	1,75 m	1,75 m
Température du sodium	550°C	550°C	550°C
Poids de l'échantillon	17 g	17 g	17 g
Durée d'irradiation	39 h	39 h	39 h
Flux	$5 \cdot 10^{-12}$ n/cm$^2 \cdot$ s	$2 \cdot 10^{-12}$ n/cm$^2 \cdot$ s	$2 \cdot 10^{-12}$ n/cm$^2 \cdot$ s
Durée de refroidissement	14 j	14 j	14 j
Durée de la fusion	3 min	3 min	3 min
Conditions d'injection des produits de fission:			
- Longueur du circuit	40 cm	40 cm	40 cm
- Diamètre du circuit (avec rétrécissements aux extrémités)	20 mm	21,6 mm	21,6 mm
- Injection d'argon	non	non	oui

La coupe longitudinale d'un creuset, après fusion dans du sodium liquide d'un échantillon d'uranium non irradié, a révélé une structure très friable de l'uranium après fusion (fig. 3).

3.3. Emission des produits de fission

Les quantités d'iode-131 et de baryum-140 émises lors de la fusion de l'uranium ont pu être déterminées par la différence entre les activités de l'échantillon avant et après fusion. Pour les quatre premiers essais, on a trouvé qu'environ 50% de l'iode-131 et 30% du baryum étaient émis. Ces valeurs ont été adoptées pour les essais suivants.

3.4. Transmission des produits de fission dans le circuit d'injection

Connaissant les quantités d'iode-131 et de baryum-140 émises et celles contenues dans la cuve, on a considéré que la différence se trouvait à l'intérieur du circuit d'injection, soit dans le sodium, soit sur les parois.

Ainsi, dans l'essai C04, le circuit d'injection contenait 73% de l'iode et 97,5% du baryum émis (tableau II). En admettant que la concentration, pour chacun de ces corps, était la même dans tout le sodium de ce circuit et égale à celle du sodium contenu dans le creuset, il est possible d'estimer les quantités piégées dans la masse du sodium et dans le sodium restant fixé sur les parois. Les 105 cm^3 de sodium du circuit contenaient donc 40% de l'iode-131 et 13% du baryum-140 émis, tandis que sur les parois restaient 33% de l'iode-131 et 84,5% du baryum-140 émis (tableau II).

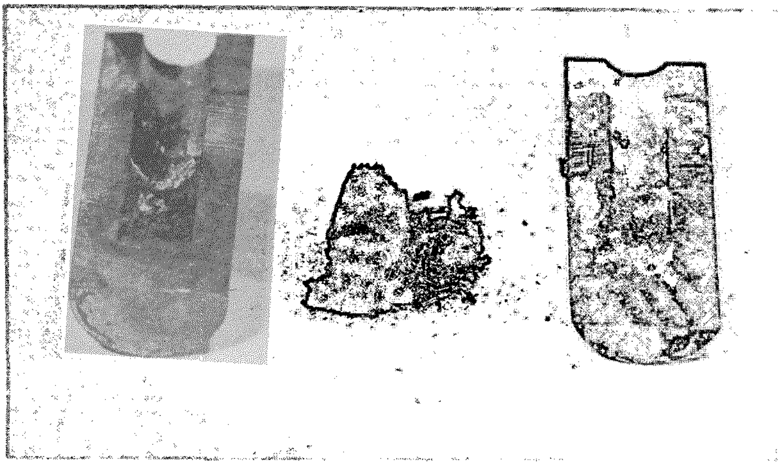

FIG.3. Vue en coupe d'un creuset après fusion de l'uranium

Pour les essais suivants, la section du circuit a été augmentée et le volume intérieur est passé ainsi de 105 cm^3 à 150 cm^3. On pensait à priori que cette augmentation permettrait d'améliorer la diffusion des produits de fission vers la cuve.

L'essai C05, réalisé dans des conditions identiques à celles de l'essai C04, allait nous démontrer le contraire. En effet, aucune activité n'a pu être décelée dans les différents prélèvements de sodium de la cuve. Par conséquent, on peut admettre que pratiquement toute l'activité émise est restée piégée à l'intérieur du circuit d'injection. Ce phénomène pourrait s'expliquer par la condensation plus rapide de la vapeur de sodium dans le circuit d'injection qui contenait une quantité plus grande de sodium liquide.

Pour confirmer cette hypothèse, on a réalisé l'essai suivant, C06, en injectant de l'argon à la base du circuit, juste au-dessus du creuset. Pendant la fusion de l'uranium, le débit était maintenu à 2 litres/min; immédiatement après, il était porté à 12 litres/min pendant une vingtaine de secondes. Tous les prélèvements de sodium de la cuve contenaient de l'iode-131 et du baryum-140 avec des concentrations très homogènes pour chacun de ces corps (tableau III).

En utilisant les mêmes méthodes de calcul que pour C04, on trouve que 93,3% de l'iode-131 et 96,7% du baryum-140 sont restés dans le circuit; 58% de l'iode-131 et 20,6% du baryum se trouvaient dans le sodium; 35,3% de l'iode-131 et 76,1% du baryum-140 sont restés piégés au voisinage des parois (tableau IV).

TABLEAU II. ESSAI C04 – REPARTITION DE L'IODE-131 ET DU BARYUM-140

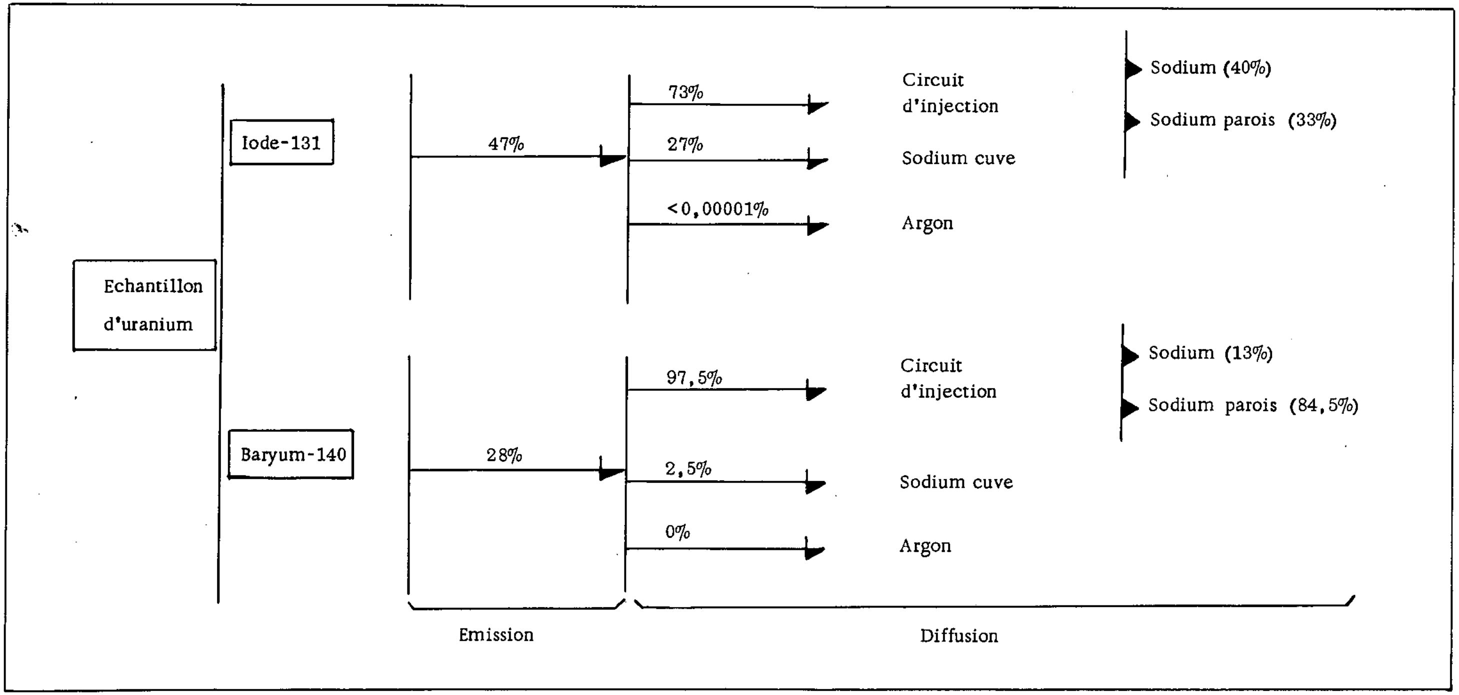

TABLEAU III. ESSAI C06 – RESULTATS EXPERIMENTAUX

	Numéro	Poids (g)	Iode-131		Baryum-140	
			Activité totale (μCi)	Activité spécifique (μCi/g)	Activité totale (μCi)	Activité spécifique (μCi/g)
Echantillon d'uranium avant fusion		17	20 900	1 229	32 600	1 917
Prélèvements de sodium dans la cuve	C06 12	6,5	0,047	0,00721	0,022	0,00341
	C06 21	6,35	0,036	0,00573	0,0165	0,0026
	C06 22	4,80	0,037	0,00775	0,008	0,0017
	C06 23	6,45	0,036	0,00565	0,018	0,0028
	C06 30	8,55	0,045	0,00526	0,019	0,0022
	C06 31	8,8	0,042	0,00480	0,017	0,0019
	C06 32	6,5	0,046	0,0044	0,018	0,0021
Sodium creuset	C06 20		Valeurs de C04			

A la lumière de ces trois essais, il est donc possible d'entrevoir le rôle important que doit jouer une circulation de sodium ou de vapeur de sodium dans la transmission des produits de fission à l'intérieur d'un circuit.

3.5. Concentration et répartition des produits de fission à l'intérieur de la cuve

Dans l'essai C04, il est apparu que la répartition des produits de fission à l'intérieur de la cuve n'était pas homogène. Pour l'iode-131, les concentrations sur l'axe de la cuve, aux différents niveaux, étaient plus faibles qu'au voisinage de la paroi. D'autre part, compte tenu de la forme cylindrique de la cuve, les valeurs des concentrations moyennes, pour tous les niveaux, suivaient très approximativement une loi exponentielle de la forme

$$A_S = A_{S0}\, e^{-3h}$$

où A_{S0} représente l'activité spécifique en μCi/g au niveau 0 (niveau du prélèvement le plus bas) et h la hauteur de sodium en mètres par rapport au niveau 0 (fig.4 et 5, tableau V). Dans le cas du baryum-140, seul le prélèvement le plus bas avait une activité spécifique appréciable. La répartition en fonction du niveau, pour ce corps, décroît donc très rapidement, ce qui s'explique en raison de sa température de fusion

TABLEAU IV. ESSAI C06 – REPARTITION DE L'IODE-131 ET DU BARYUM-140

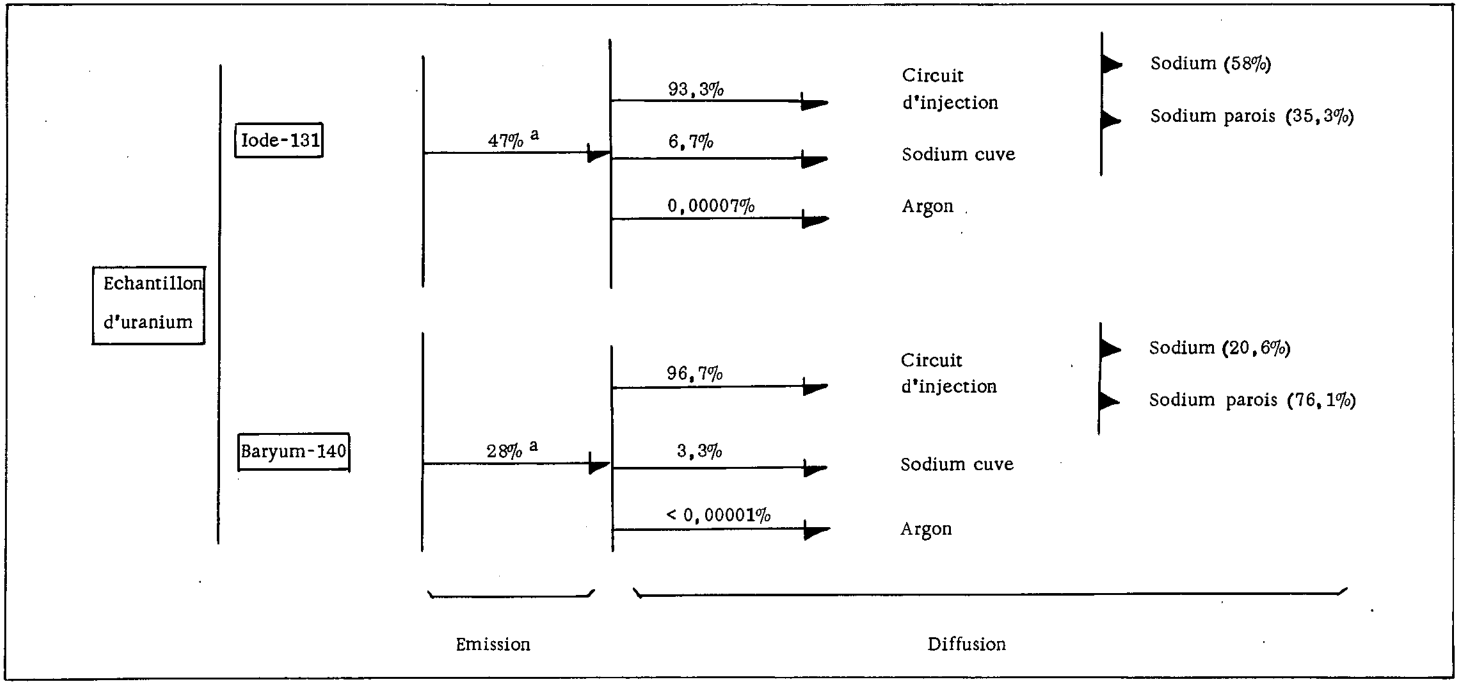

[a] Valeurs de C04.

TABLEAU V. ESSAI C04 – RESULTATS EXPERIMENTAUX

	Numéro	Poids (g)	Iode-131		Baryum-140	
			Activité totale (μCi)	Activité spécifique (μCi/g)	Activité totale (μCi)	Activité spécifique (μCi/g)
Echantillon d'uranium avant fusion		17	24 200	1420	47 500	2 800
Echantillon d'uranium après fusion	C04 01	17	12 800	760	34 070	2 000
Prélèvements de sodium dans la cuve	C04 11	07,4	0,076	0,010	< 0,0002	
	C04 12	07,4	0,067	0,009	< 0,0002	
	C04 13	07,4	0,023	0,003	< 0,0002	
	C04 21	07,4	0,199	0,027	0,0002	0,000027
	C04 22	07,4	0,345	0,047	< 0,0002	
	C0423	07,4	0,046	0,006	< 0,0002	
	C04 30	07,4	0,528	0,071	0,022	0,003
	C04 31	07,4	0,240	0,032	< 0,0002	
Sodium creuset	C04 20	5,4	235	43,5	98	18,2

relativement élevée (850°C). En considérant les activités spécifiques moyennes à l'intérieur de la cuve, on trouve que 27% de l'iode-131 et 2,5% du baryum-140 émis ont diffusé dans le sodium de la cuve.

Dans l'essai C06, où l'on avait procédé à une injection d'argon, la répartition des deux corps considérés s'est avérée homogène. Les quelques fluctuations qui ont pu apparaître ne sont dues qu'à des imprécisions dans les méthodes de mesures (tableau III). Les activités spécifiques moyennes pour l'iode-131 et le baryum-140 étaient respectivement de $5,5 \cdot 10^{-3}$ μCi/g et de $2,5 \cdot 10^{-3}$ μCi/g. Dans ce calcul, on a éliminé les valeurs qui, à priori, étaient entachées d'erreurs.

A partir des valeurs précédentes, et en admettant que les pourcentages d'émission aient été les mêmes que pour C04, on trouve donc que 6,7% de l'iode-131 et 3,3% du baryum-140 émis ont diffusé dans le sodium de la cuve.

3.6. Mesure sur les vapeurs de sodium

Le dispositif de prélèvement d'argon comprenait en série un piège à vapeur de sodium et différents filtres classiques (amiante et charbon).

Après la fusion de l'uranium, on procédait à un balayage d'argon à un débit de 12 litres/min pendant une durée de 30 min.

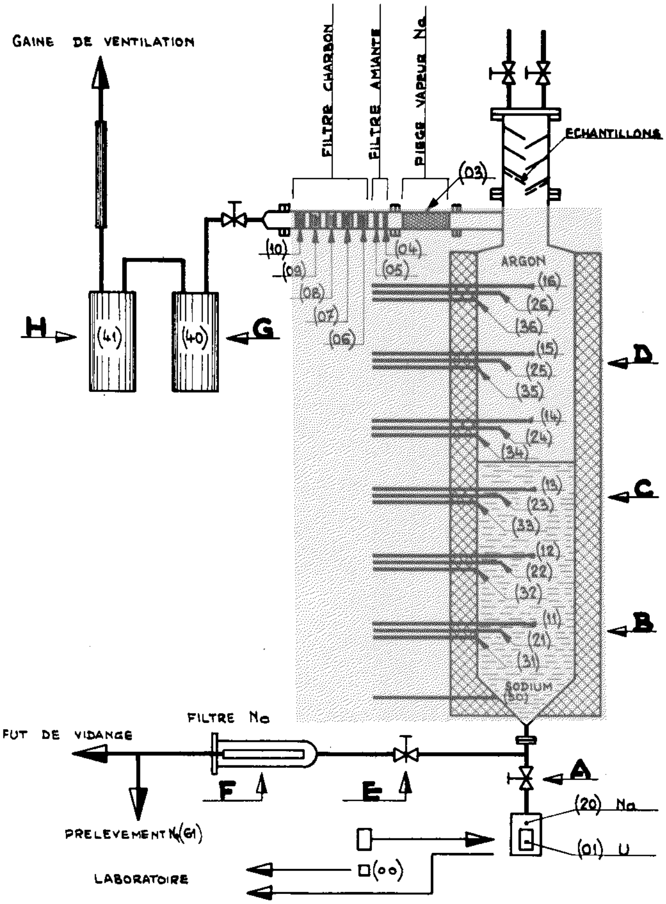

FIG.4. Expérience PIRANA — Analyses et mesures

Dans l'essai C06, la vapeur de sodium condensée dans le piège à vapeur a été pesée et analysée. Ces mesures ont montré que les 25 g de sodium ainsi piégés contenaient $2 \cdot 10^{-2}$ μCi d'iode-131, ce qui représente une activité spécifique de $0,8 \cdot 10^{-3}$ μCi/g. On s'aperçoit donc que cette concentration est du même ordre de grandeur que la concentration moyenne à l'intérieur du sodium ($5,5 \cdot 10^{-3}$ μCi/g).

On peut aussi définir le facteur de transmission de l'iode comme le rapport des activités contenues dans un même volume de sodium et de gaz de couverture. Le facteur de transmission ainsi calculé est pour cette expérience égal à 10^{-5}.

3.7. Mesure sur les filtres

Dans les essais C04 et C05, aucune activité en iode-131 n'a été décelée sur les différents filtres. Par contre, dans l'essai C06, on a déterminé sur le premier filtre amiante, placé juste derrière le piège à vapeur, une activité de 2,6 · 10^{-3} µCi. Sur les filtres suivants, rien n'a pu être décelé. L'activité précédente est donc due très certainement à des dépôts de vapeur de sodium.

Si l'on ajoute cette activité à celle trouvée sur le piège à vapeur, on trouve un facteur de transmission très légèrement supérieur à celui qui a été calculé plus haut. Il serait de 1,1 · 10^{-5} .

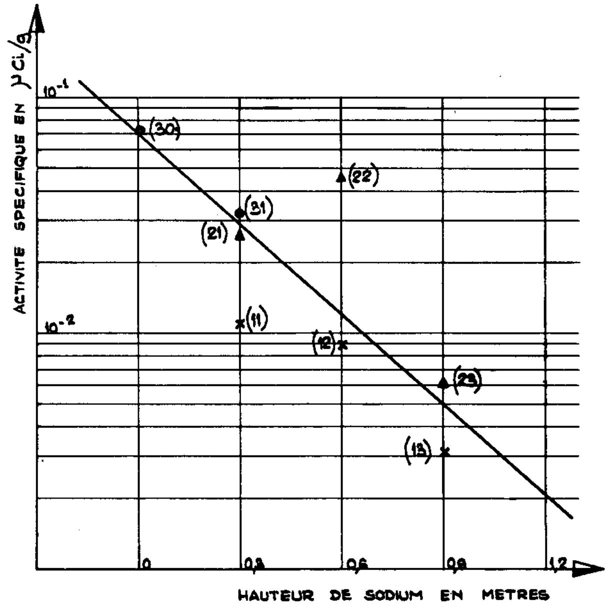

FIG.5. Essai C04 — Activité spécifique des prélèvements de sodium en fonction de la hauteur de sodium

● prélèvement sur la paroi;
▲ prélèvement à mi-profondeur;
× prélèvement dans l'axe de la cuve

Dans les pièges froids, le xénon-133 a été mis en évidence avec certitude. Malheureusement, les moyens de mesure utilisés n'ont pas permis de faire une étude quantitative précise.

3.8. Résultats de la décontamination

Après chaque expérience, la cuve a été décontaminée avec des volumes connus d'alcool, d'eau acidulée et d'eau. Chacune de ces solutions a été ensuite récupérée et analysée. Les résultats suivants ont été obtenus, dans l'essai C06:

	Iode-131	Baryum-140
Alcool	530 µCi	12,5 µCi
Eau acidulée	2 · 10^{-4} µCi	5,2 µCi
Eau	2 · 10^{-4} µCi	10^{-4} µCi

Des mesures directes sur la cuve ont permis de vérifier que la décontamination était correcte. Ainsi, l'activité totale déterminée pour chacun des corps considérés correspond à l'activité qui demeurait sur les parois, essentiellement dans le dépôt de sodium, après la vidange en sodium de la cuve.

4. CONCLUSION

Bien que ces essais ne visent pas la détermination des taux d'émission, ils montrent que, lors d'une fusion de combustible dans le sodium, les gaz rares, les iodes, les baryums seront libérés en grande quantité. Il paraît donc raisonnable, en attendant d'avoir fait des expériences en vraie grandeur en pile, de conserver pour ces corps les hypothèses de 100% d'émission à partir du combustible.

Le transport de la contamination dans le sodium est essentiellement lié aux mouvements de sodium ou de vapeur de sodium. Il importe donc, si l'on veut tirer des conclusions valables, que l'expérience faite simule au mieux l'accident réel. En particulier, il faut que la quantité de vapeur de sodium produite dans la fusion soit représentative et que son cheminement dans les canalisations soit suffisamment semblable à celui qui se produira dans le cœur. Notre expérience ne permet donc pas d'extrapoler à un réacteur réel les valeurs de concentration de produits de fission dans le sodium. Pour cela, il faudrait simuler bien mieux l'assemblage combustible, les vitesses de circulation du sodium et le taux de vapeur de sodium produite. Seule, une expérience de grande dimension peut permettre d'atteindre ce résultat.

La contamination du gaz de couverture est due en partie à la diffusion libre des gaz de fission que nous n'avons pas pu mesurer, en raison d'une cascade d'incidents survenus sur nos dispositifs de prélèvement. On peut à priori penser que cette diffusion est facile. Pour le reste, il s'agit d'un entraînement par les vapeurs de sodium. Il est donc essentiel de connaître la concentration en produits de fission du sodium susceptible de produire ces vapeurs, c'est-à-dire le sodium en contact avec le gaz de couverture. Les résultats obtenus montrent que l'entraînement de l'iode par la vapeur est très important puisque l'on a:

$$\frac{\text{Concentration d'iode dans vapeur}}{\text{Concentration d'iode dans sodium}} = \frac{0{,}8 \cdot 10^{-3}\ \mu\text{Ci/g}}{5 \cdot 10^{-3}\ \mu\text{Ci/g}} = 0{,}16$$

Si l'on raisonne sur les volumes globaux de sodium et de gaz de couverture, on obtient:

$$\frac{\text{Concentration d'iode dans vapeur}}{\text{Concentration d'iode dans sodium}} = \frac{0{,}55 \cdot 10^{-4}\,\mu\text{Ci/l}}{5{,}5\ \mu\text{Ci/l}} = 10^{-5}$$

En ce qui concerne les autres produits de fission présents dans le sodium, nous n'avons pas pu les déceler dans les vapeurs, ce qui correspond à des transmissions inférieures à 0,02 pour les concentrations massiques, et $1{,}3 \cdot 10^{-6}$ pour les concentrations volumiques.

Nous n'avons de même décelé aucune activité d'iode et de baryum-lanthane dans les différents éléments constituant le May-Pack. Il semble donc que, s'il y a des fuites sur le circuit de gaz de couverture d'un réacteur et si les orifices de fuite ont des dimensions faibles, la condensation des vapeurs piégera l'iode. Seuls les gaz rares diffuseront à l'extérieur.

Enfin, la décontamination à l'alcool s'est avérée efficace puisque le facteur de décontamination des parois, mesuré directement par introduction d'une sonde $\beta\gamma$ dans la cuve, est supérieur à 20.

Les prochaines expériences seront faites avec circulation du sodium de bas en haut, pour l'étude de la répartition de l'iode dans la cuve. On placera dans le sodium des plaquettes de métal pour analyser la contamination subsistant éventuellement sur les parois. Enfin, on pense obtenir confirmation d'un taux de transmission élevé pour les gaz rares de fission.

REFERENCES

[1] COTTRELL, W.B. et al., "U.S. Experience on the release and transport of fission products within containment systems under simulated reactor accident conditions" Proc. 3rd UN Int. Conf PUAE 13 (1965) 77.

[2] MILLER, C.E., Jr., BROWNING, W.E., Jr., The adequacy of scale-up in experiments on fission products behavior in reactor accidents, ORNL 3901, Part 1 (1966).

DISCUSSION

A.W. CASTLEMAN: Perhaps Mr. Barthoux could explain the hookup of the induction furnace, as I am not sure I understand how the coupling is arranged. Is the furnace coupled with the crucible, with an outer liner or with the fuel itself?

A. BARTHOUX: It is a little difficult to answer your question because we are not sure how the induction lines are split up between the crucible and the fuel. However, as the distance between the sample and the crucible is very small the heating probably occurs via the crucible, which then transmits the heat by conduction through the sodium to the uranium sample itself.

BEHAVIOUR OF FISSION PRODUCTS IN SODIUM*

J. C. CLIFFORD, J. M. WILLIAMS AND J. C. McGUIRE+
LOS ALAMOS SCIENTIFIC LABORATORY,
UNIVERSITY OF CALIFORNIA,
LOS ALAMOS, N. MEX.
UNITED STATES OF AMERICA

Abstract

BEHAVIOUR OF FISSION PRODUCTS IN SODIUM. The techniques being employed to study the behaviour of mixed fission products in sodium are described and experimental results for ^{137}Cs are presented. The experiments are designed to examine possible methods for controlling fission product activity levels in sodium-cooled fast reactors.

Specimens of a Pu-Co-Ce fuel alloy, irradiated to 10^{19} fissions and cooled for two years, are the source of fission products for behavioural studies in a sodium forced convection loop. Liquid fuel and sodium are contacted at 600°C in one portion of the loop and the remainder of the loop is cycled between 550 and 110°C. The release and distribution of gamma-active species are detected by scanning loop components with a scintillation detector and 400-channel pulse-height analyser. The behaviour of beta-emitters is determined through radiochemical analyses of sodium, metal foils and trapping materials removed at intervals from the loop. Of the long-lived gamma-emitters in the fuel, only ^{137}Cs has been released in a quantity sufficient for detection by gamma scanning. Partition of ^{137}Cs between sodium and cover gas, and between sodium and traps containing stainless steel mesh, carbon and sodium oxide, has been detected.

Trapping techniques that appear promising in the loop experiments are examined in more detail by encapsulating individual gamma-active species with sodium and a collection material. A capsule is arranged so that the fission product source and sink are separated by a static sodium column several inches long. The capsule is heated in the range 150-500°C and the approach to equilibrium is followed using a movable scintillation detector and single channel analyser. In this manner the adsorption of ^{137}Cs on stainless steel, nickel and graphite has been studied. Estimates have been made of the diffusibility of caesium in sodium and the adsorption rates of caesium on stainless steel and graphite.

1. INTRODUCTION

The behaviour of fission products released to sodium coolant from tramp uranium, or from failed or deliberately vented reactor fuel elements, may limit access to the primary coolant system and affect the consequences of a loss-of-coolant incident. Depending on the fission product inventory expected in the primary coolant, it may be desirable to concentrate uranium, plutonium, long-lived energetic gamma-emitting isotopes, and short-lived, biologically hazardous isotopes at specific locations within the primary system.

To this end the interaction of plutonium-based fuels with sodium is being investigated. The release and distribution of fission products from irradiated fuel to sodium, and methods by which this distribution may be altered are included. This paper describes the techniques and preliminary results from a study of the distribution and trapping of long-lived fission

---

* Work performed under the auspices of the United States Atomic Energy Commission, Contract No. W-7405-Eng. 36

+ Present address: Donald W. Douglas Laboratories, Richland, Wash.

products in sodium systems. Results from this study are compared with the behaviour noted after failure of fuel elements in the LAMPRE (Los Alamos Molten Plutonium Reactor Experiment), which was operated at Los Alamos during 1962-1963 [1].

Two types of laboratory experiments are being used: contact of irradiated fuel and sodium in a small forced convection sodium loop; and encapsulation of a single radioisotope, ^{137}Cs, with sodium and a potential adsorber material in small tubes. In both types of experiment, in-situ gamma-ray spectrometry is the principal analytical tool, augmented by wet radiochemical analyses. The loop experiments are used to determine the general distribution of fission products in a sodium system and the relative effectiveness of trapping techniques on this distribution. Trapping techniques that show some merit are examined in the capsule experiments.

2. EXPERIMENTAL APPARATUS AND TECHNIQUES

2.1 Forced convection loop

A schematic representation of the stainless-steel forced convection sodium system is shown in Fig. 1. The loop consists of three vertical legs, an electrical heater, an air heat dump and a regenerative heat exchanger.

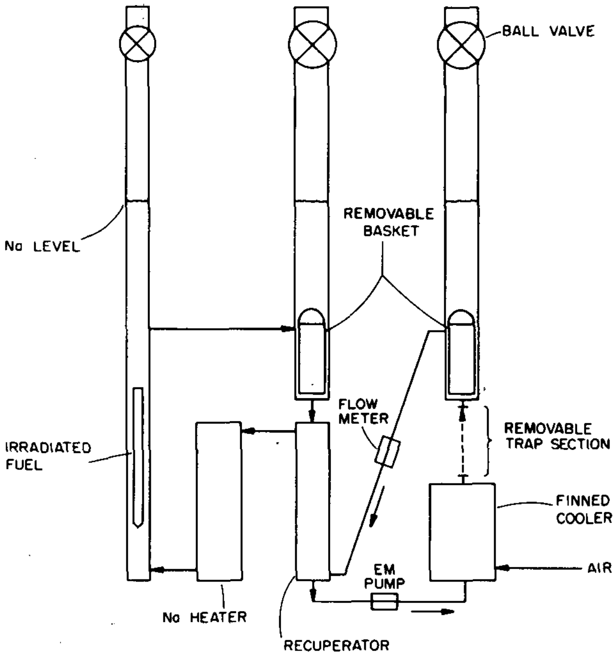

FIG.1. Forced convection sodium loop

The loop contains approximately 1600 cm^3 of sodium flowing at a maximum rate of 170 litres/h. One leg is lead-shielded and holds irradiated fuel in an open-mouth tantalum container. The container and fuel are inserted and removed through a gas lock and shielded handling can at the top of the column. The other vertical legs accept specimens of various materials held in 12.7-cm-long by 2.5-cm-diameter baskets. A section of piping in one vertical specimen leg is removable, allowing insertion of traps into the system.

The vertical leg containing the air cooler (the low-temperature specimen leg) can be scanned using a lead-collimated, lead-shielded, NaI(Tl) scintillation detector and a 400-channel pulse-height analyser.

Although no impurity determinations were made on sodium from this loop, our experience with other zirconium hot-trapped loops of the same size and construction indicates that the oxygen content can be assumed to be below 5 ppm. Typical values for C, H and N are ≤ 15, ≤ 10 and ≤ 3 ppm respectively.

2.2 Capsule experiments

Figure 2 illustrates the arrangement used in the isothermal capsule experiments. The activity sink, consisting of a bed of granulated graphite or a coiled metal screen, is located at the bottom of a stainless-steel capsule. Approximately 2 in. above the sink is suspended a stainless-steel planchet containing 1 mCi of ^{137}Cs deposited as a carrier-free solution of CsCl and evaporated to dryness. The planchet is submerged in a column of sodium containing < 10 ppm O, ≤ 15 ppm C, ≤ 10 ppm H and ≤ 3 ppm N at loading. Capsules are heated with electric mantles, and movement of the gamma activity within a capsule is detected using a shielded, collimated NaI(Tl) scintillation detector and a scaler. Axial scans of a capsule are made by moving the capsule in relation to the detector, with a positioning accuracy of 0.0025 cm.

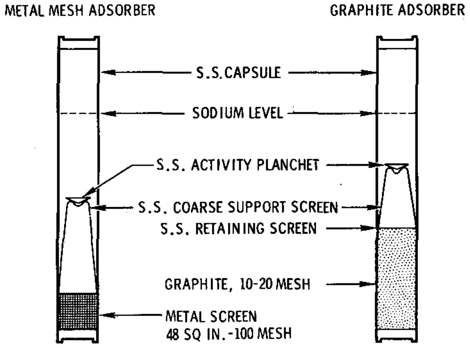

FIG.2. Arrangement of capsule experiments

3. EXPERIMENTAL RESULTS

Five grams of Pu-Co-Ce alloy (34 wt.% Pu), irradiated to a level of 2.5×10^{18} fissions and cooled for $2\frac{1}{2}$ yr, were immersed in the 600°C fuel leg of the forced convection loop. From a consideration of the chemical species involved, and from previous measurements of the distribution of fission products between irradiated liquid Pu-Co-Ce alloy and sodium, it was expected that at least 0.9 of each of the long-lived fission products ^{137}Cs, ^{90}Sr and ^{155}Eu would be extracted into the sodium phase. Of these, ^{137}Cs was identified in the low-temperature specimen leg a few hours after the fuel had been immersed. The others were found in substantial quantity on materials later removed from the system.

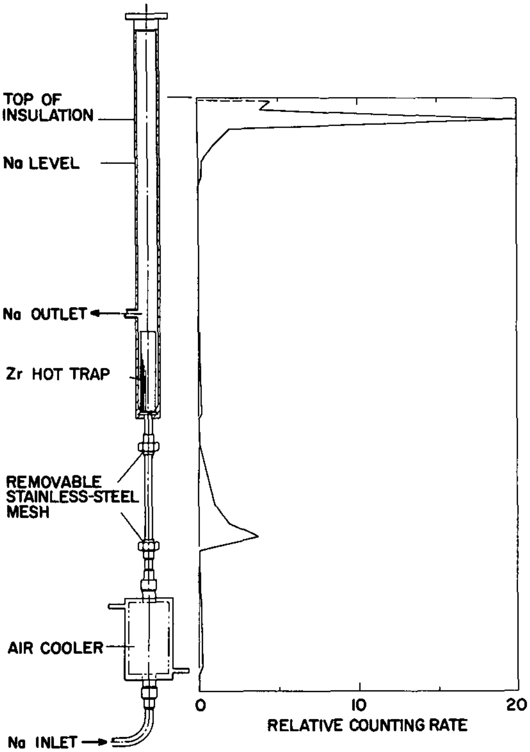

FIG.3. Distribution of ^{137}Cs in low-temperature leg after 145 d

3.1 Behaviour of caesium in hot-trapped sodium

Within 48 h of the fuel addition, the ^{137}Cs activity in the low-temperature (500°C) specimen leg had reached a maximum, decreasing approximately 20% within the next 33 d. The majority of this activity was distributed, non-uniformly, within a 12.5-cm section of tubing packed with stainless-steel wire mesh. The section is identified in Fig. 1 as the "removable trap section".

Attempts were made to influence the distribution of ^{137}Cs by cycling the low-temperature leg between 500°C and 300°C, but the over-all change in activity level and distribution was trivial until the low temperature was maintained for periods longer than two days. After a month at 300°C, the stainless-steel mesh section had lost half its ^{137}Cs activity. The rate of loss was constant over the time period. Figure 3 shows the ^{137}Cs distribution in the low-temperature leg 145 d after the beginning of the experiment. This distribution does not represent an equilibrium condition, but illustrates the direction in which ^{137}Cs is moving. The larger ^{137}Cs deposit appears in a 7.6-cm ring in the helium-filled gas space. The position of peak activity coincides with the top of the thermal insulation. The second ^{137}Cs deposit extends through the 12.5-cm wire mesh section, and its point of maximum activity is the leading, or upstream, edge of the section. Caesium was detected in the finned cooler, in the zirconium hot trap and in the connecting tubing, but at a level that was negligible compared with that in the mesh. The remaining sodium-filled portion of the system showed the same "background" gamma activity levels as had been found in the low-temperature leg. The remaining gas spaces contained 1.3 times as much caesium as had been found in the low-temperature leg gas space.

To provide a quantitative estimate of the ^{137}Cs inventory in various portions of the system, integrated counting rates for gas spaces, stainless mesh and bare tubing were corrected for geometric attenuation, detection efficiency and mass absorption. The results, after 145 d of operation, are shown in Table I along with the original ^{137}Cs inventory in the fuel. Factor-of-two agreement had been anticipated between the activity of the caesium inventory in the fuel and the sum of the activities shown in Table I; the very close agreement is probably fortuitous. The estimates of activity distribution are sufficiently reliable to illustrate the gross behaviour of caesium. Over half of the available activity was concentrated in the gas phase. An additional 31% was distributed through the hot traps and stainless-steel tubing, and the remainder appeared in the stainless-steel mesh. The values in Table I imply that none of the ^{137}Cs detected in the sodium-filled portion of the loop was dissolved in sodium. However, samples of sodium removed from the loop contained 3 parts per thousand million of ^{137}Cs, from which it is estimated that approximately 10% of the

TABLE I. DISTRIBUTION OF ^{137}Cs IN A HOT-TRAPPED Na SYSTEM AFTER 145 d OF OPERATION

Location	Activity (d/m)	Per cent of total	Average activity/ unit surface (d/m/in.^{2})
Gas phase	3.58×10^9	57	3.8×10^8
Stainless-steel mesh	0.77×10^9	12	7.7×10^7
Hot traps and stainless-steel tubing	1.93×10^9	31	4.7×10^6
Total	6.28×10^9		
^{137}Cs inventory in original fuel	6.37×10^9		

activity within the sodium-filled portion was in solution. Neglecting the small correction for this dissolved caesium, the stainless-steel mesh was an average of 16 times more effective (per unit surface) as a caesium collector than the bare tubing. The effectiveness of mesh over tubing as a caesium collector, and the difference in effectiveness among portions of the mesh (Fig. 3), have not been explained satisfactorily.

Additional experiments were conducted in which ^{137}Cs was encapsulated with sodium and stainless-steel mesh. At low temperatures (approximately 200°C) caesium segregated to the mesh surfaces, while at higher temperatures (350°-500°C) it segregated to the gas phase. By cycling the temperature of the capsules between these extremes, it was possible to move caesium rapidly (approximately 50 h) in either direction.

3.2 Behaviour of caesium in sodium containing graphite

The effectiveness of graphite as a caesium collector also was explored in loop and capsule experiments. The zirconium hot traps used during the initial 145 d of loop operation were removed, and a basket containing rods of spectroscopic-grade graphite was placed in the low-temperature leg (Fig. 1). The loop was operated in the 110°-300°C range for 50 d and the migration of caesium was observed. The graphite bed collected caesium at the expense of the stainless-steel tubing and mesh surfaces until the caesium remaining on these surfaces was below the

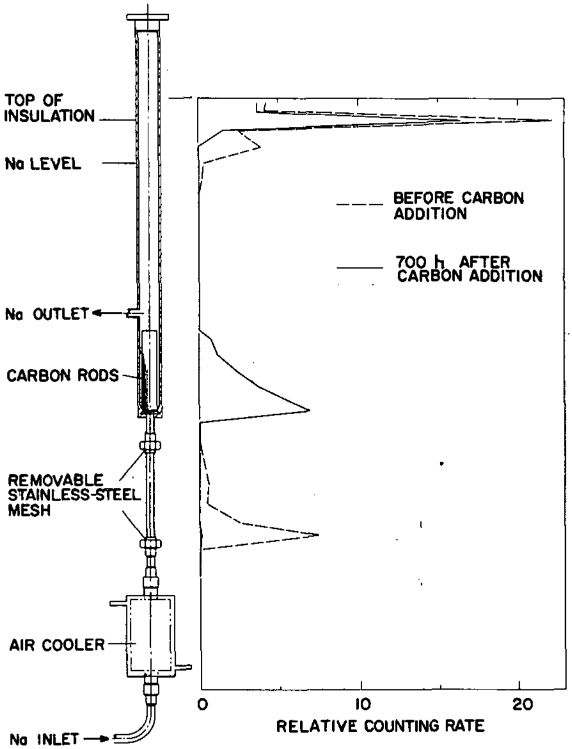

FIG.4. Effect of graphite on the distribution of ^{137}Cs in low-temperature leg

estimated detection limit of approximately 10^6 d/m/in.^{2} (5×10^{-9} g/in.^{2}). During this same period the caesium activity in the gas phase was reduced approximately 40%. Figure 4 shows the activity distribution before graphite addition and 29 d later. Eighty-five per cent of the caesium lost from the gas phase and from the sodium-wet stainless surfaces appeared in the bed. The bed continued to collect activity for the remainder of the 50 d, but redistribution of ^{137}Cs within the bed began after 33 d.

These general observations were confirmed by short (200-h) time capsule tests employing beds of 10-20 mesh spectroscopic-grade graphite, sodium and ^{137}CsCl. During tests in the temperature range 200°-400°C, caesium was quantitatively transferred from the planchet to a narrow band at the sodium/graphite interface. Radiography of the capsule showed that sodium had not penetrated the bed at these temperatures; however, penetration occurred rapidly (in less than one hour) when the capsule was heated to 500°C. The band of caesium activity was then observed to progress slowly into the graphite bed. From the rate of penetration into the bed at 500°C, an apparent caesium diffusivity of 5×10^{-7} cm^2/s was calculated.

3.3 Behaviour of caesium in cold-trapped sodium

The effectiveness of a sodium oxide cold trap as a caesium collector is being studied using a full-flow cold trap inserted in place of the "removable trap section" of Fig. 1. The trap consists of a regenerative cooler and a thin-walled bulb filled with stainless-steel mesh (Fig. 5). With the trap operating at 175°C, oxygen was added to the loop (as NaOH), and the walls in the gas spaces were washed with sodium. Ninety per cent of the ^{137}Cs deposited in the gas spaces during the earlier experiments was returned to the sodium phase, and half of this was deposited in the cold trap. The distribution of this activity within the trap is shown in Fig. 5. This activity was not fixed in the trap but moved slowly to the gas phase without any change in cold-trap temperature.

3.4. Distribution of Pu, ^{90}Sr, ^{155}Eu and ^{106}Ru in hot-trapped sodium

During the initial caesium experiment in the forced convection loop some information was obtained concerning the distribution of other long-lived isotopes. The zirconium hot traps, representing 27% of the system total wetted surface, were removed from the loop and were analysed for ^{90}Sr, ^{137}Cs, ^{144}Ce, ^{155}Eu, ^{60}Co and plutonium. The high-temperature trap had been maintained above 500°C for 75% of the time and the low-temperature trap between 300° and 500°C for 86% of the time. Because the traps were exposed to sodium of varying temperature, only the relative collection efficiencies of stainless steel and zirconium, and the general effect of temperature on activity deposition, were obtained. After traces of sodium had been removed from each trap, the traps were disassembled. Each stainless-steel portion (one-third of the total surface of a trap) and zirconium portion was acid-leached, and the leachings were analysed separately. The results, normalized to unit surface of collector and expressed as multiples of the least effective collector, appear in Table II. Plutonium and strontium were concentrated on the low-temperature stainless-steel surfaces, while europium was uniformly distributed over the low-temperature trap. Ruthenium appeared only in the hot leg, and at levels suggesting that the fraction of the inventory released from the fuel was negligible. Neither ^{144}Ce nor ^{60}Co was detected in either trap.

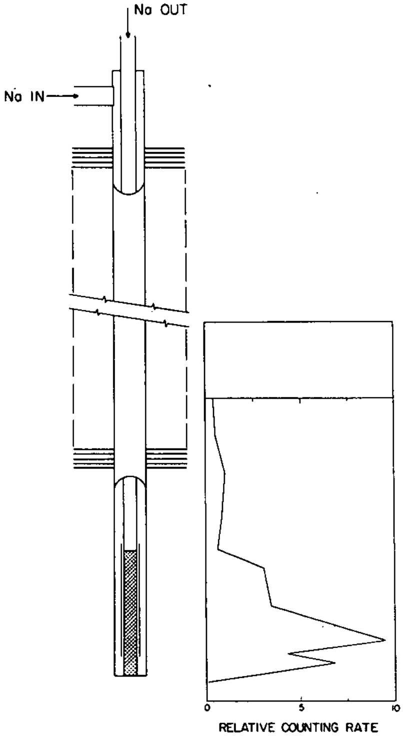

FIG. 5. Distribution of ^{137}Cs in cold trap

TABLE II. FIXED ACTIVITY RECOVERED FROM Zr HOT TRAPS

	Activity/unit surface of collector, normalized to the least effective collector			
	"High-temperature" trap		"Low-temperature" trap	
Species	Zr	S. S.	Zr	S. S.
^{90}Sr	1	1.2	31	52.5
^{106}Ru	2.8	1	Below detection	Below detection
^{115}Eu	6.5	1	29.2	31.4
Pu	3	1	3	24

Based on the ^{90}Sr levels in the traps and the ^{90}Sr levels in sodium samples removed at the same time as the traps were removed, the total ^{90}Sr "fixed" on loop surfaces and the total ^{90}Sr in "solution" were estimated. The quantity in solution was 2% of the total, or approximately 0.05 parts per thousand million ^{90}Sr in sodium.

4. CAESIUM IN LAMPRE-I

The behaviour of caesium in the forced convection loop and in the capsule tests agrees with previous observations of caesium distribution in the sodium-cooled LAMPRE-I experiments. A breach of the tantalum containment of three liquid plutonium fuel elements in LAMPRE resulted in the release of approximately 130 g of plutonium and fission products from approximately 10^{22} total fissions. A survey of caesium deposition in reactor components revealed ^{136}Cs and ^{137}Cs concentrations in the gas phase of the sodium system surge tank which contained 500°C sodium during normal operations. The presence of ^{136}Cs, which is a direct yield fission product, infers that caesium probably transfers through the sodium as the metallic species. This tendency to segregate to the gas phase at high temperatures is in agreement with results of this study.

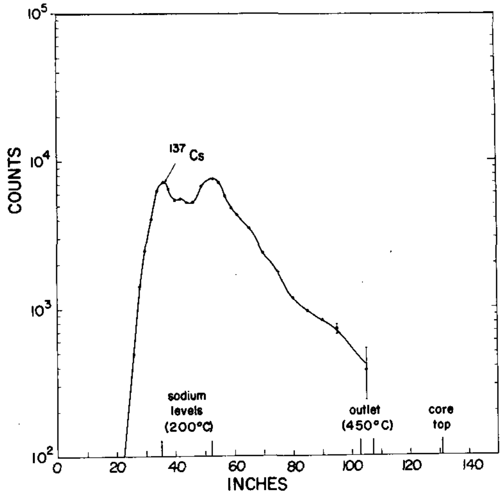

FIG.6. Distribution of ^{137}Cs in LAMPRE fuel rod handles

Caesium was further observed to deposit in a static temperature gradient which existed in the bundle of fuel rod handles directly above the outlet plenum from the core. Figure 6 shows the increase in ^{137}Cs activity deposited on the surface of a 17-4 PH steel rod handle along a temperature gradient which decreased from 500°C at outlet plenum to 200°C at the sodium/cover gas interface. This profile is probably caused by diffusion and deposition (possibly co-precipitation) on to a cold solid surface, and constitutes qualitative agreement with laboratory experiments.

5. CONCLUSIONS

The behaviour of ^{137}Cs in the small-scale experiments and in LAMPRE present a qualitatively consistent picture of elemental caesium as a mobile and volatile species. Caesium appears to be only weakly adsorbed on metal surfaces and, over long periods of time, it migrates to cool gas spaces. The presence of a sodium oxide cold trap in the flow circuit appears to have little effect on this behaviour. Caesium forms lamellar compounds with graphite (C_8Cs, $C_{24}Cs$), so the effectiveness of graphite surfaces over metal surfaces as caesium collectors is not entirely unexpected. However, the desirability of placing large surfaces of graphite in a sodium system, and the long-time effectiveness of graphite as a caesium scavenger, are doubtful. These uncertainties do not preclude the use of a graphite bed in the vapour phase.

The temperature-dependent fractionation of plutonium, ^{90}Sr, ^{155}Eu, and ^{106}Ru observed in the forced convection sodium system, while not impressive in terms of coolant decontamination, suggests that selective concentration of some fission products may be possible. The factors of 20-50 difference in species activity levels between high- and low-temperature zirconium traps might be increased another factor of 5 or 10 by the use of extended surface metal adsorbers within the system.

In interpreting these observations it should be remembered that the source of activity was, for the most part, a liquid metal in which all fission product species very likely existed in the fully reduced state. Transfer of these species from fuel to sodium was probably a simple solution step. Departures from this condition, brought about by substitution of oxide and carbide fuels for the liquid Pu-Co-Ce alloy, have not been considered.

REFERENCES

[1] LAMPRE-I final design status report, Rpt LA-2833, Los Alamos Scientific Laboratory, Los Alamos, N. Mex. (1963).

DISCUSSION

J.S. LINDHE: I should just like to ask Mr. Williams whether the fuel was molten, since most of the caesium (to judge by the figures in Table I) appears to have escaped from it.

J.M. WILLIAMS: Yes, the Pu-Co-Ce alloy is a eutectic that melts just above 400°C. The fuel in our loop ran between 500° and 600°C.

R. A. DAVIES: I assume that the cobalt in your Pu-Co-Ce eutectic must have been irradiated. Did you find any deposits of irradiated cobalt on the pipe-work, and were you able to reach any conclusion regarding the effect of temperature on cobalt deposition?

J.M. WILLIAMS: No, we found neither cobalt nor cerium deposited on the pipe-work of our system.

R.A. DAVIES: Did you measure the plutonium content of the sodium?

J.M. WILLIAMS: Yes, we measured it when trying to determine the solubility of plutonium in sodium. In general, the plutonium levels have been below 1 ppm. We have, however, observed plutonium plated out on the metal surfaces of our system.

J.R.B. HUGO: In the last paragraph of your paper you say that "all fission product species very likely existed in the fully reduced state", by which I assume you mean the metallic state. Is there any evidence to show that the fission products that plated out in the system were in the metallic state? I ask this question because oxygen and other non-metallic substances were present in the sodium.

J.M. WILLIAMS: I cannot really say, because we did not try to identify these species. We assume that the caesium, in the concentrations observed, was in the metallic state.

GENERAL DISCUSSION

C. DESCAMPS: We have heard from United States and French participants about studies of fission product distribution in molten sodium. This amounts, of course, to an analysis of accident conditions. The hypothetical accident can be taken further, however; one can well imagine a circuit rupture that would result in a violent reaction between the contaminated sodium and air. For a case like this it would be useful to know not only the distribution of fission products in the sodium but also the chemical form in which they are likely to spread through the surrounding atmosphere. My question, then, is whether anyone here is familiar with research on this type of problem, whether there are any programmes under way, and whether any results have yet been achieved.

A. W. CASTLEMAN: Without trying to give a complete answer to Mr. Descamps' question, I should like to make one or two comments. We have examined the behaviour of iodine in sodium during oxidation, and our findings were reported in 1965[1]. I cannot describe them in detail now as too much time would be needed. Suffice it to say that we plan to study the behaviour of other fission products in sodium undergoing oxidation, though so far we have examined only iodine.

J. R. WEEKS (Chairman): I believe there are research programmes concerned, in a general way, with the behaviour of fission products during a reactor incident. Whether the specific question raised by Mr. Descamps has been covered I cannot say. In any case it is a subject more fit for a whole new conference than for a symposium on alkali metal coolants.

J. P. LAGOWSKI: After our recent experience of fuel damage in the Enrico Fermi reactor we located three sources of information (in addition to Los Alamos and Brookhaven work) on the general subject of fission products in sodium. These are (1) the SRE fuel damage report, (2) the BR-5 experience, reported in the proceedings of the last Geneva Conference, and (3) work undertaken by Atomics International for the USAEC, some of which has been completed and published and some is still in progress. This last includes a study on the release of fission products during a sodium fire.

A. BARTHOUX: I, too, will attempt to give Mr. Descamps a short answer. We are at present doing some experiments on sodium fires – fires involving sodium contaminated first by fission products and afterwards by plutonium. The main object of this work is to find out how the building filters would react during an incident of this kind.

---

[1] Castleman, A. W., Jr., Tang, I. N., in "Chemical considerations in Fast Reactor Safety", Proceedings of a conference on safety, fuels and core design in large fast power reactors, ANL-7120 (Argonne National Laboratory), October 1965, 848.

SYMPOSIUM ON ALKALI METAL COOLANTS

HELD IN VIENNA, 28 NOVEMBER - 2 DECEMBER 1966

CHAIRMEN OF SESSIONS

Session I	E. DUNCOMBE	U.K.A.E.A., Risley
Session II	L.P. VAUTREY	Centre d'études nucléaires de Saclay, Gif-sur-Yvette
Session III	M. IVANOVSKY	Institute of Physics and Power, Obninsk
Session IV	H.O. BÖHM	Gesellschaft für Kernforschung, Karlsruhe
Session V	V. ŠULC	Atomic Energy Research Institute, Řež, Prague
Session VI	A.J. BOGERS	Metaalinstituut TNO, Delft
Session VII	F. HECHT	Analytisches Institut der Universität Wien, Vienna
Session VIII	J. PLANQUART	Centre d'étude de l'energie nucléaire, Mol
Session IX	J.R. WEEKS	Brookhaven National Laboratory, New York

SECRETARIAT OF THE SYMPOSIUM

Scientific Secretaries:	A. PUSHKOV	Division of Nuclear Power and Reactors, IAEA
	J. SPITALNIK	Division of Nuclear Power and Reactors, IAEA
Administrative Secretary:	P. GHELARDONI	Division of Scientific and Technical Information, IAEA

Editor:	SHELAGH M. FREEMAN	Division of Scientific and Technical Information, IAEA
Records Officer:	S. A. EDMINSTER	Division of Languages, IAEA

LIST OF PARTICIPANTS

AUSTRIA

Clausen, H.D.	Institut für angewandte Mathematik, Technische Hochschule Graz, Steyrergasse 17, 8010 Graz
Hecht, F.	Analytisches Institut der Universität Wien, Währingerstaße 38, 1090 Vienna
Janitschek, F.	Draukraftwerke AG, Anzengruberstraße 50, Klagenfurt
Matyas, E.	Österreichische Studiengesellschaft für Atomenergie, Lenaugasse 10, 1080 Vienna
Nentwich, A.	Österreichische Elektrizitäts- wirtschafts AG, Am Hof 6A, 1010 Vienna
Obermair, G.	Bundesministerium für Verkehr und verstaatlichte Unternehmungen, Section IV, Schwarzenbergplatz 1, 1010 Vienna
Rajakovics, G.	Gebr. Böhler & Co. AG, Kapfenberg, Styria
Schreinlechner, I.	Österreichische Studiengesellschaft für Atomenergie, Lenaugasse 10, 1080 Vienna
Schwarz, N.	Österreichische Studiengesellschaft für Atomenergie, Lenaugasse 10, 1080 Vienna

BELGIUM

Descamps, C.	BelgoNucléaire, 35 rue des Colonies, Brussels I
Michel, A.	BelgoNucléaire, 35 rue des Colonies, Brussels I

Planquart, J.	Centre d'étude de l'énergie nucléaire, Mol
Soenen, A.M.	Centre d'étude de l'énergie nucléaire, Mol
Vanmassenhove, G.	Centre d'étude de l'énergie nucléaire, Mol

CANADA

Hodge, R.I.	Chalk River Nuclear Laboratories, Chalk River, Ontario

CZECHOSLOVAKIA

Ilinchev, G.	Research Institute of Protection Materials, U mestanskeho provimru 4, Prague 7
Šulc, V.	Atomic Energy Research Institute, CSAV, Řež, near Prague

FRANCE

Barthoux, A.	CEN de Cadarache, BP n° 1, St. Paul-lez-Durance
Beaufrère, J.	Electricité de France, Direction des études et recherches, 12 Place des Etats-Unis, Paris 16^{e}
Cambillard, E.	CEN de Fontenay-aux-Roses, BP n° 6, 92 Fontenay-aux-Roses
Champeix, L.	CEN de Saclay, BP n° 2, 91 Gif-sur-Yvette
Decroix, J.H.	Aciéries électriques d'Ugine, 73 Ugine
Eude, J.C.	CEN de Saclay, BP n° 2, 91 Gif-sur-Yvette

Graff, W.H.	Société d'électrochimie d'Ugine, 10 rue du Général Foy, Paris 8^{e}
Hatterer, A.	Ecole supérieure de chimie, 3 rue A. Werner, 68 Mulhouse
Le Jannou, J.P.	CEN de Cadarache, 13 St. Paul-lez-Durance
Kessler, H.	Ecole supérieure de chimie, 3 rue A. Werner, 68 Mulhouse
Lions, N.	CEN de Cadarache, 13 St. Paul-lez-Durance
de Mazancourt, R.	CEN de Fontenay-aux-Roses, BP n° 6, 92 Fontenay-aux-Roses
Parrot, R.R.E.	CEN de Saclay, Services de physique appliquée, BP n° 2, Gif-sur-Yvette
Sannier, J.	CEN de Saclay, BP n° 2, 91 Gif-sur-Yvette
Traxler, A.M.	Groupement Atomique Alsacienne Atlantique (GAAA), 104 Av. Edouard Herriot, 91 Le Plessis Robinson
Vautrey, L.P.	CEN de Saclay, BP n° 2, 91 Gif-sur-Yvette

GERMANY, FEDERAL REPUBLIC OF

Armbruster, H.	Kernkraftwerks Betriebsgesellschaft, Karlsruhe
Baerlecken, E.	Thyssen Röhrenwerke AG, August Thyssenstraße 1, Düsseldorf
Böhm, H.O.	Gesellschaft für Kernforschung, Weberstraße 5, Karlsruhe
Borgstedt, H.U.	Gesellschaft für Kernforschung, Weberstraße 5, Karlsruhe
Brudermüller, G.	Gesellschaft für Kernforschung, Weberstraße 5, Karlsruhe

Büscher, E.	Interatom, Bensberg/Cologne
Dreissigacker, H. L.	Bundesministerium für wissenschaftliche Forschung, Bad Godesberg
Frees, G.	Gesellschaft für Kernforschung, Karlsruhe
Grosser, E. D.	Interatom, Bensberg/Cologne
Henzel, N.	Battelle Institut e. V., Wiesbadenerstraße, Frankfurt/Main
Köhler, M. J.	Interatom, Bensberg/Cologne
Kranz, E.	Thyssen Röhrenwerke AG, August Thyssenstraße 1, Düsseldorf
Laue, H. J.	Gesellschaft für Kernforschung, Weberstraße 5, Karlsruhe
Marth, W.	Gesellschaft für Kernforschung, Weberstraße 5, Karlsruhe
Peppler, F. W.	Gesellschaft für Kernforschung, Weberstraße 5, Karlsruhe
Radebold, R.	AEG Forschungsinstitut Berlin, Technische Universität Berlin, Marchstraße 17-20, D-1000 Berlin
Rühle, M.	Metallgeselschaft AG, Reuterweg 14, Frankfurt/Main
Stieding, L.	Siemens AG, Zentrale Entwicklung und Forschung, Erlangen
Vetter, H.	Technischer Überwachungsverein Baden e. V., Richard Wagnerstraße 2, Mannheim
Wagner, K.	Technische Universität Berlin, Institut für Kerntechnik, Marchstraße 17-20, Berlin

ITALY

Bruschetti, S.	Ansaldo, Piazza Carignano 2, Genoa
Bruzzi, L.	CNEN, Via Mazzini 2, Bologna
Canali, A.	CNEN, Via Belisario 15, Rome
Perona, G.	CISE, Via Redecesio 12, Segrate (Milan)
Sala, L.	CNEN, Via Belisario 15, Rome

LUXEMBOURG

Houtzeel, A.	S.A. Gradel, Steinfort, Luxembourg

NETHERLANDS

Bogers, A.J.	Metaalinstituut TNO, Rotterdamseweg 139, Delft
de Gee, A.W.J.	Metaalinstituut TNO, Rotterdamseweg 139, Delft
Koppes, P.	Natriumtegnologie TNO, Den Haag
Nieuwenhuijs, A.	Kon. Mach. Fabriek, Gebr. Storken Co., Hengelo
Wisman, H.	Comprimo N.V., James Wattstraat 77, Amsterdam
de Wringer, P.	Reactor Centrum Nederland, Petten

SOUTH AFRICA

Hugo, J.R.B.	South African Atomic Energy Board, Private Bag 256, Pretoria

SPAIN

Carreira-Vazquez, M.	Junta de Energía Nuclear, Ciudad Universitaria, Madrid (3)
de la Torre-Cabezas, M.	Junta de Energía Nuclear, Ciudad Universitaria, Madrid (3)

SWEDEN

Lindhe, J.S.	AB Atomenergi, Studsvik, Nyköping
Ljungberg, L.G.F.	AB Atomenergi, Studsvik, Nyköping

SWITZERLAND

Fuchs, H.	Swiss Federal Institute for Reactor Research, Würenlingen

UNION OF SOVIET SOCIALIST REPUBLICS

Ioltukhovsky, A.G.	State Committee for Atomic Energy, Staromenetny pereulok 26, Moscow
Ivanovsky, M.	Institute of Physics and Power, Obninsk
Kulpin, B.	N.I.I.O.R., Melekess

UNITED KINGDOM

Board, J.	Atomic Power Construction Ltd., Crawford Lane, Hounslow, Middlesex
Claxton, K.T.	A.E.R.E., Harwell, Didcot, Berks.
Davies, R.	U.K.A.E.A., Dounreay Experimental Reactor Establishment, Thurso, Caithness
Duncombe, E.	U.K.A.E.A., Reactor Engineering Laboratory, Reactor Group, Risley, Warrington, Lancs

Fielder, E.	U.K.A.E.A., Reactor Engineering Laboratory, Reactor Group, Risley, Warrington, Lancs.
Hargreaves, K.	U.K.A.E.A., Reactor Engineering Laboratory, Reactor Group, Risley, Warrington, Lancs
Jennings, T.E.	U.K.A.E.A., Reactor Engineering Laboratory, Reactor Group, Risley, Warrington, Lancs.
Sutherland, K.S.	Nuclear Chemical Plant Ltd., St. James Ave., London, W.13
Thorley, A.W.	Reactor Materials Laboratory, U.K.A.E.A., Wigshaw Lane, Culcheth, Lancs
Tyzack, C.	Reactor Materials Laboratory, U.K.A.E.A., Wigshaw Lane, Culcheth, Lancs

UNITED STATES OF AMERICA

Bauer, A.A.	Kernforschungszentrum Karlsruhe, Federal Republic of Germany
Castleman, A.W.	Brookhaven National Laboratory, Upton, New York 11973
Campise, A.V.	Atomics International, 8900 Desoto, Canoga Park, Calif.
Chase, W.L.	Atomic Power Development Associates, 1911 First Street, Detroit, Mich. 48226
Devan, J.	Oak Ridge National Lab., Oak Ridge, Tenn.
English, R.	National Aeronautics and Space Administration (NASA), 21000 Brookpark Rd., Cleveland, Ohio 44135

Epstein, L. F.	Vallocitos Nuclear Center, General Electric Co., Pleasanton, Calif. 94566
Greenberg, S.	Argonne National Laboratory, Argonne, Ill.
Horton, E.	USAEC, Fuels and Materials Branch, Reactor Development Division, Washington, D.C., 20545
Killias, H.R.	General Electric Co., Research and Development Center, Pelikanstraße 37, CH-8001 Zurich
Lagowski, J.	Atomic Power Development Associates, 1911 First St., Detroit, Mich.
Rosenblum, L.	National Aeronautics and Space Administration (NASA), 21000 Brookpark Rd., Cleveland, Ohio 44135
Semmel, J.W.	Space Power and Propulsion Section N-20, General Electric Co., Cincinnati, Ohio
Simons, E.M.	Battelle Memorial Institute, Columbus, Ohio 43201
Smith, F.A.	Argonne National Laboratory, Argonne, Ill.
Tetenbaum, M.	Argonne National Laboratory, Argonne, Ill.
Weeks, J.R.	Brookhaven National Laboratory, Upton, New York 11973
Werner, C.	MSA Research Corp., Evans City, Pa. 16033
Williams, J.M.	Los Alamos Scientific Laboratory, Los Alamos, N.Mex. 81544

Zebroski, E. L.	General Electric APO, 310 Deguigne Dr., Sunnyvale, Calif. 94086

EURATOM

Allgeier, H.J.K.	European Atomic Energy Agency, 51-53 rue Belliard, Brussels
Marchandise, H.	European Atomic Energy Agency, 51-53 rue Belliard, Brussels
Mechelynck, P.	European Atomic Energy Agency, 51-53 rue Belliard, Brussels

AUTHOR INDEX

(including Participants in Discussions)

The numbers underlined indicate the first page of a paper by an author; other numbers denote the page numbers of discussion comments. Literature references are not indexed.

IAEA SALES AGENTS

Orders for Agency publications can be placed with your bookseller or any of our sales agents listed below :

ARGENTINA
Comisión Nacional de
Energía Atómica
Avenida del Libertador
General San Martin 8250
Buenos Aires - Suc. 29

AUSTRALIA
Hunter Publications,
23 McKillop Street
Melbourne, C.1

AUSTRIA
Georg Fromme & Co.
Spengergasse 39
A-1050, Vienna V

BELGIUM
Office international de librairie
30, avenue Marnix
Brussels 5

BRAZIL
Livraria Kosmos Editora
Rua do Rosario, 135-137
Rio de Janeiro

Agencia Expoente Oscar M. Silva
Rua Xavier de Toledo, 140-1° Andar
(Caixa Postal No. 5.614)
São Paulo

BYELORUSSIAN SOVIET SOCIALIST REPUBLIC
See under USSR

CANADA
The Queen's Printer
Ottawa, Ontario

CHINA (Taiwan)
Books and Scientific Supplies
Service, Ltd.,
P.O. Box 83
Taipei

CZECHOSLOVAK SOCIALIST REPUBLIC
S.N.T.L.
Spolena 51
Nové Město
Prague 1

DENMARK
Ejnar Munksgaard Ltd.
6 Nörregade
Copenhagen K

FINLAND
Akateeminen Kirjakauppa
Kesküskatu 2
Helsinki

FRANCE
Office international de
documentation et librairie
48, rue Gay-Lussac
F-75, Paris 5^e

GERMANY, Federal Republic of
R. Oldenbourg
Rosenheimer Strasse 145
8 Munich 8

HUNGARY
Kultura
Hungarian Trading Co. for Books
and Newspapers
P.O.B. 149
Budapest 62

ISRAEL
Heiliger and Co.
3 Nathan Strauss Street
Jerusalem

ITALY
Agenzia Editoriale Internazionale
Organizzazioni Universali (A.E.I.O.U.)
Via Meravigli 16
Milan

JAPAN
Maruzen Company Ltd.
6, Tori Nichome
Nihonbashi
(P.O. Box 605)
Tokyo Central

MEXICO
Librería Internacional
Av. Sonora 206
Mexico 11, D.F.

NETHERLANDS
N.V. Martinus Nijhoff
Lange Voorhout 9
The Hague

NEW ZEALAND
Whitcombe & Tombs, Ltd.
G.P.O. Box 1894
Wellington, C.1

NORWAY
Johan Grundt Tanum
Karl Johans gate 43
Oslo

PAKISTAN
Karachi Education Society
Haroon Chambers
South Napier Road
(P.O. Box No. 4866)
Karachi 2

POLAND
Ośrodek Rozpowszechniana
Wydawnictw Naukowych
Polska Akademia Nauk
Pałac Kultury i Nauki
Warsaw

ROMANIA
Cartimex
Rue A. Briand 14-18
Bucarest

SOUTH AFRICA
Van Schaik's Bookstore (Pty) Ltd.
Libri Building
Church Street
(P.O. Box 724)
Pretoria

SPAIN
Librería Bosch
Ronda de la Universidad 11
Barcelona

SWEDEN
C.E. Fritzes Kungl. Hovbokhandel
Fredsgatan 2
Stockholm 16

SWITZERLAND
Librairie Payot
Rue Grenus 6
1211 Geneva 11

TURKEY
Librairie Hachette
469, Istiklâl Caddesi
Beyoğlu, Istanbul

UKRAINIAN SOVIET SOCIALIST REPUBLIC
See under USSR

UNION OF SOVIET SOCIALIST REPUBLICS
Mezhdunarodnaya Kniga
Smolenskaya-Sennaya 32-34
Moscow G-200

UNITED KINGDOM OF GREAT BRITAIN AND NORTHERN IRELAND
Her Majesty's Stationery Office
P.O. Box 569
London, S.E.1

UNITED STATES OF AMERICA
National Agency for
International Publications, Inc.
317 East 34th Street
New York, N.Y. 10016

VENEZUELA
Sr. Braulio Gabriel Chacares
Gobernador a Candilito 37
Santa Rosalía
(Apartado Postal 8092)
Caracas D.F.

YUGOSLAVIA
Jugoslovenska Knjiga
Terazije 27
Belgrade

IAEA publications can also be purchased retail at the United Nations Bookshop at United Nations Headquarters, New York, at the news-stand at the Agency's Headquarters, Vienna, and at most conferences, symposia and seminars organized by the Agency.

In order to facilitate the distribution of its publications, the Agency is prepared to accept payment in UNESCO coupons or in local currencies.

Orders and inquiries from countries where sales agents have not yet been appointed may be sent to:

Distribution and Sales Group, International Atomic Energy Agency,
Kärntner Ring 11, A-1010, Vienna I, Austria

INTERNATIONAL
ATOMIC ENERGY AGENCY
VIENNA, 1967

PRICE: US $16.00
Austrian Schillings 414,-
(£5.13.0; F.Fr. 78,40; DM 64,-)